

5-1995

ThermalHydraulics Analysis of the Unit-Cell Nuclear Light Bulb Rocket Engine

Vojislav Banjac

Follow this and additional works at: https://digitalrepository.unm.edu/ne_etds



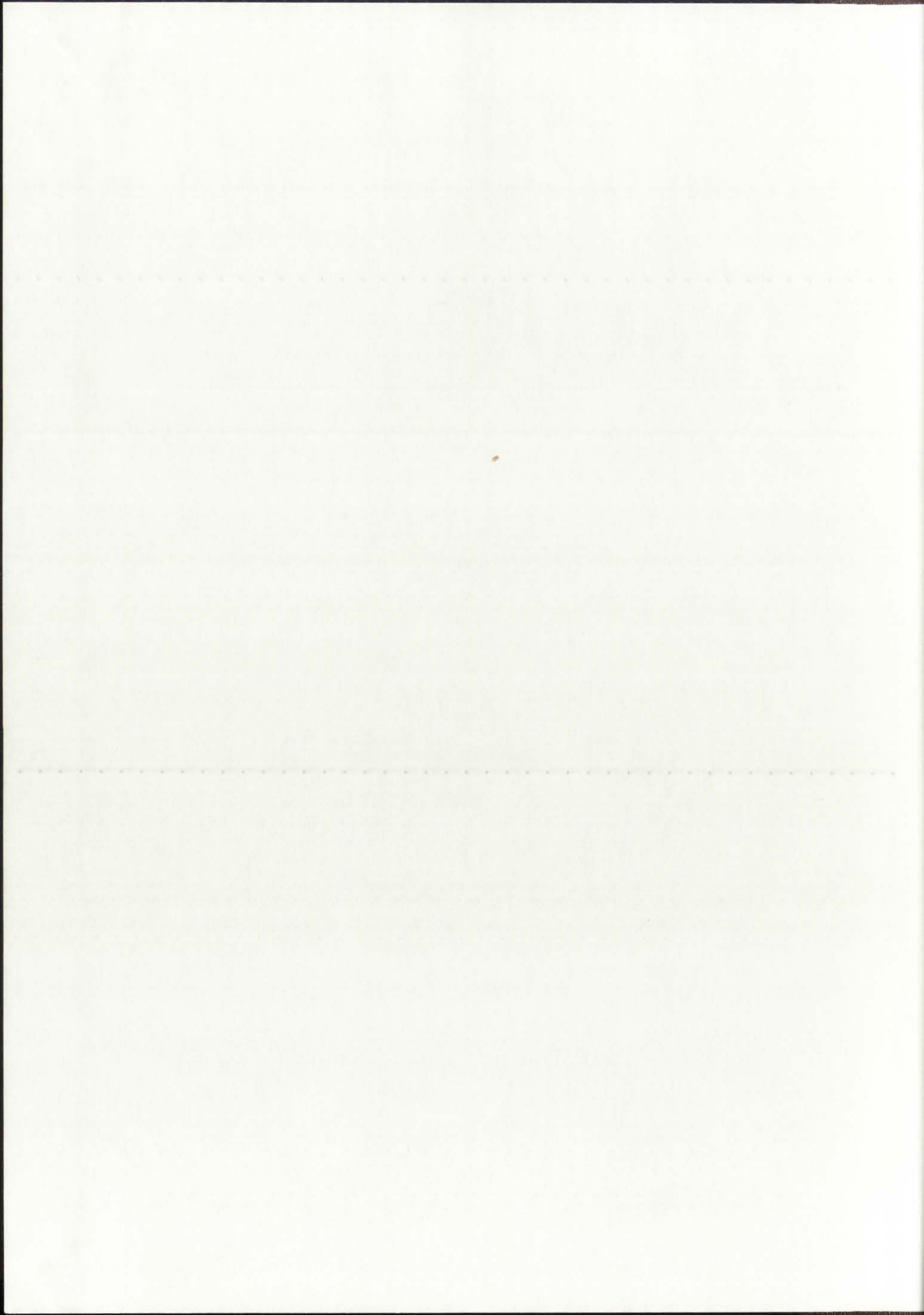
Part of the [Nuclear Engineering Commons](#)

Recommended Citation

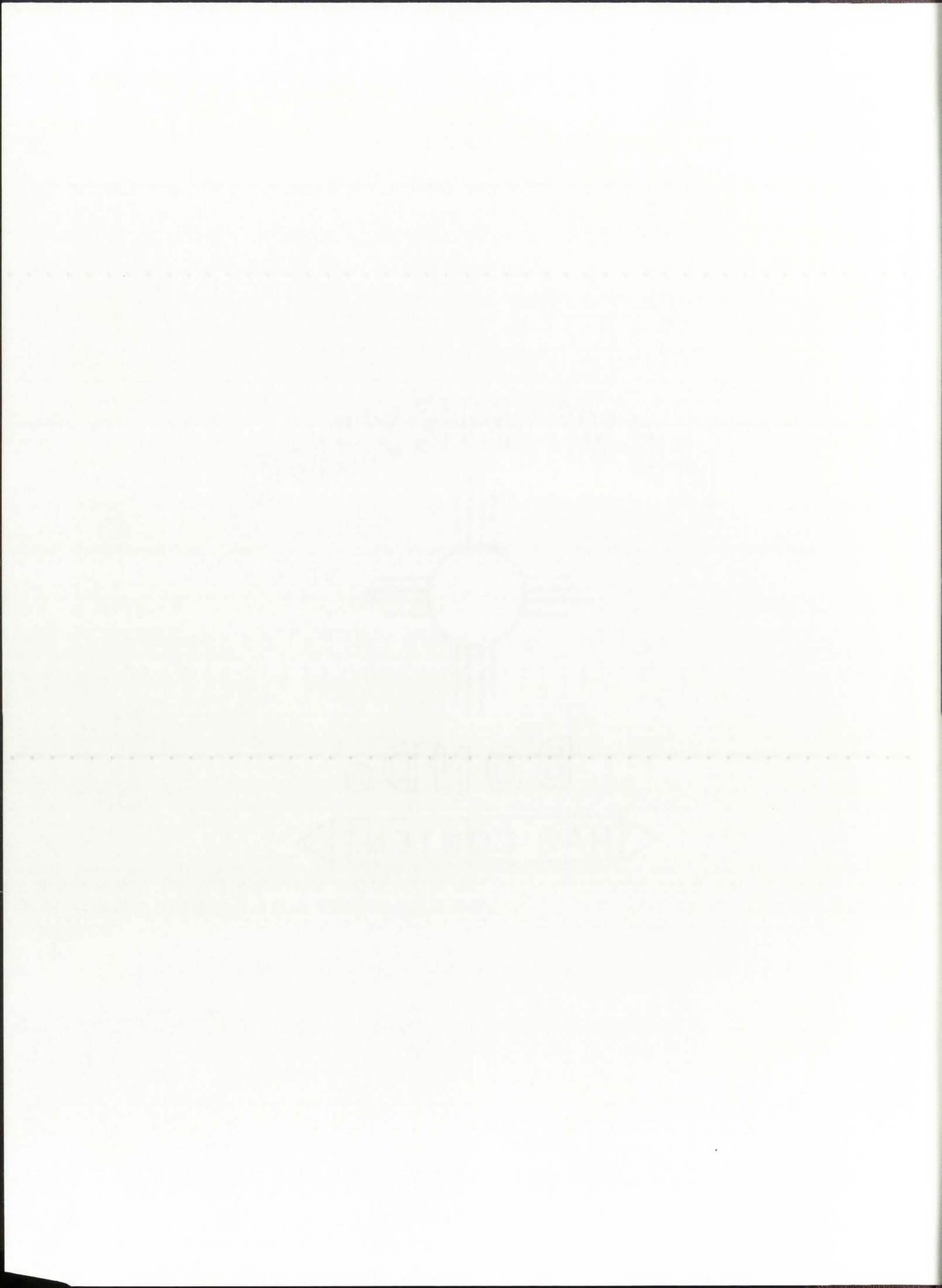
Banjac, Vojislav. "ThermalHydraulics Analysis of the Unit-Cell Nuclear Light Bulb Rocket Engine." (1995).
https://digitalrepository.unm.edu/ne_etds/79

This Dissertation is brought to you for free and open access by the Engineering ETDs at UNM Digital Repository. It has been accepted for inclusion in Nuclear Engineering ETDs by an authorized administrator of UNM Digital Repository. For more information, please contact disc@unm.edu.

A14416 543807



ZIM
LD
3783
C34
1995
B36



THE UNIVERSITY OF NEW MEXICO
ALBUQUERQUE, NEW MEXICO 87131

POLICY ON USE OF THESES AND DISSERTATIONS

Unpublished theses and dissertations accepted for master's and doctor's degrees and deposited in the University of New Mexico Library are open to the public for inspection and reference work. *They are to be used only with due regard to the rights of the authors.* The work of other authors should always be given full credit. Avoid quoting in amounts, over and beyond scholarly needs, such as might impair or destroy the property rights and financial benefits of another author.

To afford reasonable safeguards to authors, and consistent with the above principles, anyone quoting from theses and dissertations must observe the following conditions:

1. Direct quotations during the first two years after completion may be made only with the written permission of the author.
2. After a lapse of two years, theses and dissertations may be quoted without specific prior permission in works of original scholarship provided appropriate credit is given in the case of each quotation.
3. Quotations that are complete units in themselves (e.g., complete chapters or sections) in whatever form they may be reproduced and quotations of whatever length presented as primary material for their own sake (as in anthologies or books of reading) ALWAYS require consent of the authors.
4. The quoting author is responsible for determining "fair use" of material he uses.

This thesis/dissertation by Vojislav Banjac has been used by the following persons whose signatures attest their acceptance of the above conditions. (A library which borrows this thesis/dissertation for use by its patrons is expected to secure the signature of each user.)

NAME AND ADDRESS	DATE
_____	_____
_____	_____
_____	_____
_____	_____
_____	_____

THE UNIVERSITY OF NEW BRUNSWICK
ALBANY, NEW BRUNSWICK

LIBRARY ON LIST OF JOURNALS AND DISSERTATIONS

The following list of journals and dissertations is prepared for your library. It is based on the information in the University of New Brunswick Library and is intended to assist you in the selection and purchase of new titles. It is also intended to assist you in the selection of titles for purchase from other sources. The list is based on the information in the University of New Brunswick Library and is intended to assist you in the selection and purchase of new titles. It is also intended to assist you in the selection of titles for purchase from other sources.

The following list of journals and dissertations is prepared for your library. It is based on the information in the University of New Brunswick Library and is intended to assist you in the selection and purchase of new titles. It is also intended to assist you in the selection of titles for purchase from other sources.

1. The following list of journals and dissertations is prepared for your library. It is based on the information in the University of New Brunswick Library and is intended to assist you in the selection and purchase of new titles. It is also intended to assist you in the selection of titles for purchase from other sources.

2. After a list of two years, the list of journals and dissertations may be revised when specific titles are added or deleted. The list of journals and dissertations provided is based on the information in the University of New Brunswick Library and is intended to assist you in the selection and purchase of new titles. It is also intended to assist you in the selection of titles for purchase from other sources.

3. Quotations that are longer than one line should be indented. The list of journals and dissertations provided is based on the information in the University of New Brunswick Library and is intended to assist you in the selection and purchase of new titles. It is also intended to assist you in the selection of titles for purchase from other sources.

4. The following list of journals and dissertations is prepared for your library. It is based on the information in the University of New Brunswick Library and is intended to assist you in the selection and purchase of new titles. It is also intended to assist you in the selection of titles for purchase from other sources.

The following list of journals and dissertations is prepared for your library. It is based on the information in the University of New Brunswick Library and is intended to assist you in the selection and purchase of new titles. It is also intended to assist you in the selection of titles for purchase from other sources.

NAME AND ADDRESS
DATE

Vojislav Banjac

Candidate

Department of Chemical and Nuclear Engineering

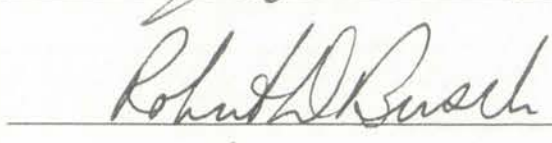
Department


This dissertation is approved, and it is acceptable in quality and form for publication on microfilm:

Approved by the Dissertation Committee:

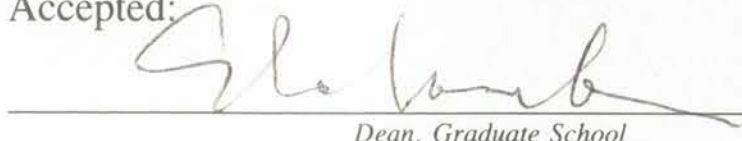
 , Chairperson








Accepted:



Dean, Graduate School



Date

EMERALD BRAND

MADE IN U.S.A.

100% COTTON

EMERALD BRAND

**THERMALHYDRAULICS ANALYSIS OF THE UNIT-CELL
NUCLEAR LIGHT BULB ROCKET ENGINE**

BY

VOJISLAV BANJAC

B.S., Nuclear Engineering, University of New Mexico, 1991

M.S., Nuclear Engineering, University of New Mexico, 1992

DISSERTATION

Submitted in Partial Fulfillment of the
Requirements for the Degree of
Doctor of Philosophy in Engineering

The University of New Mexico
Albuquerque, New Mexico

May 1995

NUCLEAR LIGHT BULB ROCKET ENGINE
THERMAL ANALYSIS AND DESIGN OF THE LIGHT-BULB

BY

WALTER B. BARNARD

U.S. Nuclear Engineering University of New Mexico, 1961
M.S. Nuclear Engineering University of New Mexico, 1961

DISSERTATION

Submitted in Partial Fulfillment of the
Requirements for the Degree of

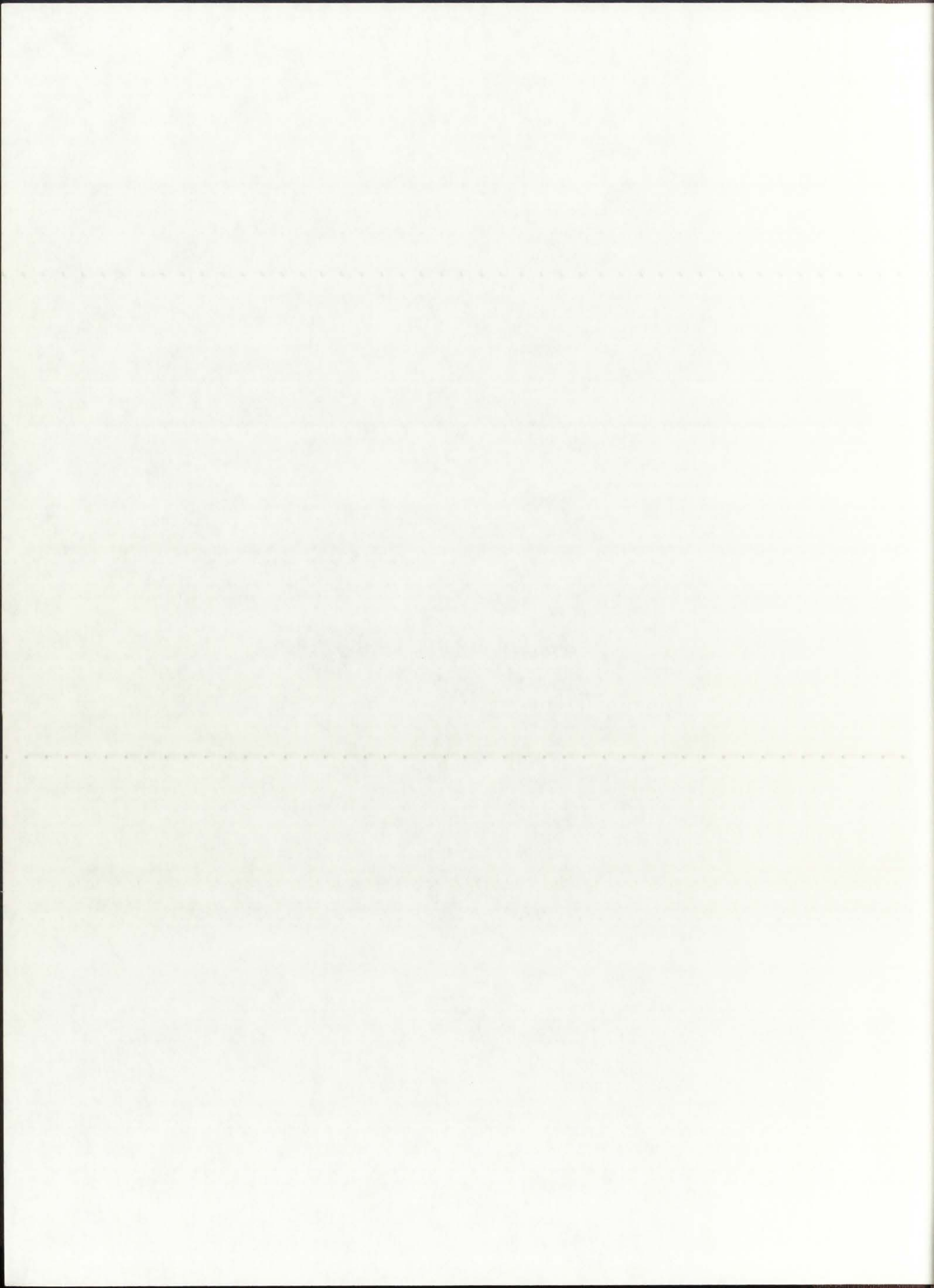
Doctor of Philosophy in Engineering

The University of New Mexico

Albuquerque, New Mexico

May 1962

© Copyright V. Banjac and A.S. Heger, 1995



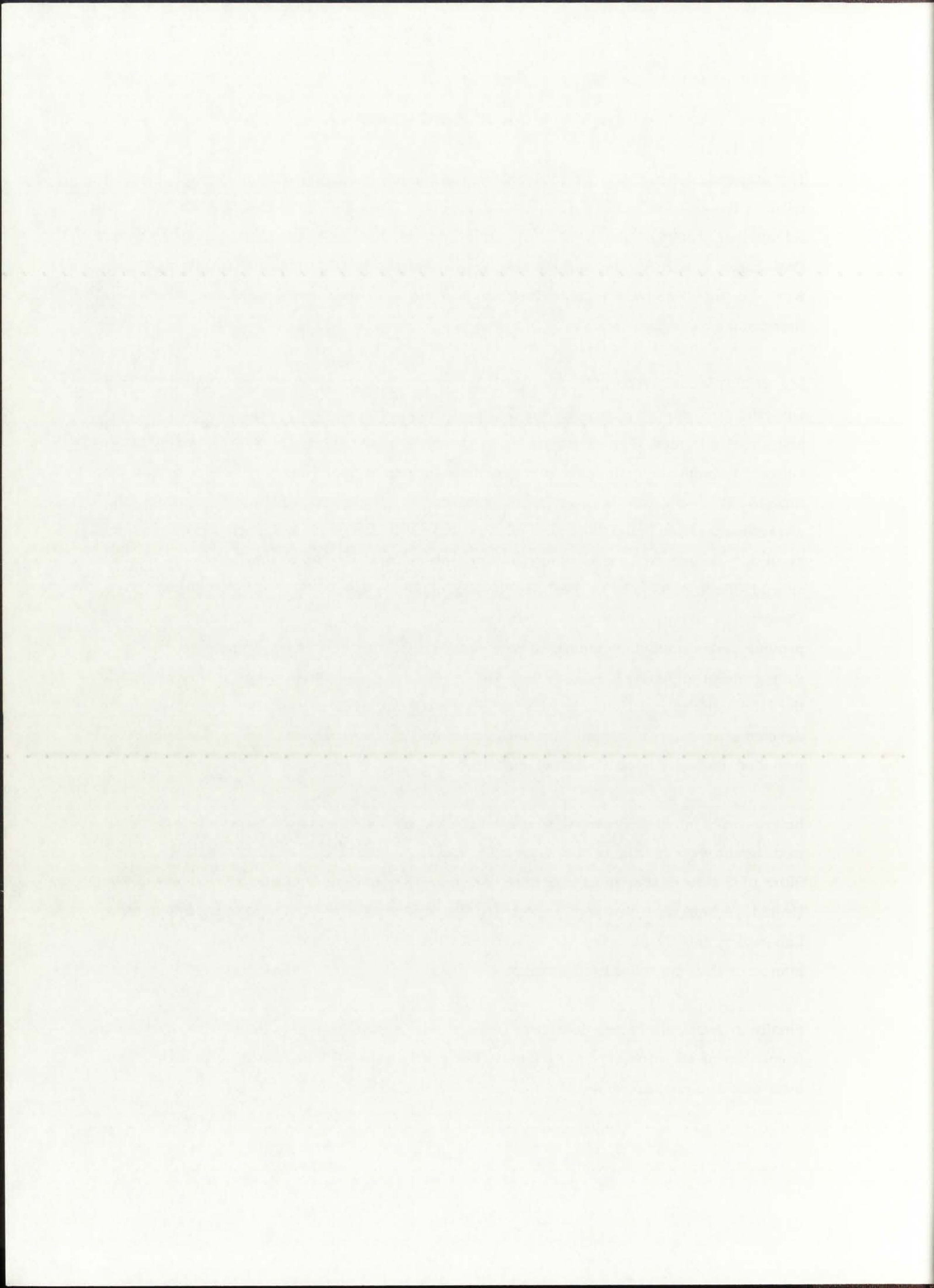
ACKNOWLEDGEMENTS

This academic document, and the research work contained within, would not have been possible without the assistance of a large number of people. The one who should, by all rights, be acknowledged first is Prof. A. Sharif Heger, my advisor and Dissertation Committee chairman. Prof. Heger unselfishly devoted his time, experience, and finances to unilaterally support my work. For that, I am very much indebted to him. He will always remain, first and foremost, a friend and a colleague to me.

My gratitude and recognition also goes out to the official and unofficial members of my Dissertation Committee. Prof. Robert D. Busch, as always, provided advice and comments on just about all areas of research. He was available and always ready to help, and has now suffered through yet another one of my monster documents. Prof. Norman F. Roderick took the time to review all aspects of my work, from the very beginnings of my Ph.D. studies, and always managed to patiently explain what I could not understand. I look back with admiration at all our discussions on everything from propulsion concepts to heat transfer theory. A very special "thank-you" goes to Prof. Arsalan Razani, who was provided a 400-page draft of my Dissertation barely 3 weeks before my defense, and yet managed to comprehend the concept and provide very stimulating comments. Besides the official members of my Committee, I am also very grateful to Albert C. Marshall of Sandia National Laboratories, who initially proposed the NLB topic to me. I went to him looking for a space nuclear power topic; he unselfishly devoted many hours to our joint meetings, introduced me to numerous scientists in the field, and provided me with a large amount of information.

Justice would not be fully served if I did not at least mention by name the others who helped me in different ways to achieve this degree: Dr. Randall Gauntt, Dr. Gary Harms, and Dr. Steven Slutz of Sandia National Laboratories; Dr. Ward Roman and Dr. Richard Rodgers of the United Technologies Research Center; Dr. Bruce Schnitzler of Idaho National Engineering Laboratory; and Dr. Nicholas Morley of the Air Force Phillips Laboratory. It was a pleasure to interact with scientists of such a calibre.

Finally, I would like to veer to a more personal level and acknowledge the love, support, and friendship of all members of my family. Every single one of them, at some point in time, motivated and encouraged me to persevere. Thank you all very much!



**THERMALHYDRAULICS ANALYSIS OF THE UNIT-CELL
NUCLEAR LIGHT BULB ROCKET ENGINE**

BY

VOJISLAV BANJAC

ABSTRACT OF DISSERTATION

Submitted in Partial Fulfillment of the
Requirements for the Degree of
Doctor of Philosophy in Engineering

The University of New Mexico
Albuquerque, New Mexico
May 1995

NUCLEAR LIGHT BULB ROCKET ENGINE
THERMAL-HYDRAULIC ANALYSIS OF THE WWT-CUT

BY

JOSEPH W. BARNARD

ABSTRACT OF DISSERTATION

Submitted in Partial Fulfillment of the

Requirements for the Degree of

Master of Science in Engineering

The University of New Mexico

Albuquerque, New Mexico

May 1962

THERMALHYDRAULICS ANALYSIS OF THE UNIT-CELL NUCLEAR LIGHT BULB ROCKET ENGINE

Vojislav Banjac

B.S., Nuclear Engineering, University of New Mexico, 1991

M.S., Nuclear Engineering, University of New Mexico, 1992

Ph.D., Engineering, University of New Mexico, 1995

This Dissertation presents a detailed thermalhydraulics analysis of the unit-cell derivative of the Nuclear Light Bulb (NLB) rocket engine. The NLB engine is a gas core nuclear rocket first proposed in the 1960's by the then-United Aircraft Research Laboratories (UARL); its unit-cell derivative consists of a low-temperature moderator/reflector as well as segmented propellant channels, both proposed with the intent of increasing the k_{eff} of the system.

The results of this work can be grouped into two major areas: (1) thermal and neutronics analysis of the engine, and (2) investigation of the feasibility of the engine over a wide range of operating conditions. This work is believed to comprise the first comprehensive analysis of the unit-cell NLB derivative. The unit-cell derivative, although first proposed in the early 1970's, has never been analyzed in detail, and most associated parameters are based on an assumed thermal and neutronics behavior of the engine. No significant work has been performed with regard to the engine since termination of gas core research efforts in 1973, so the feasibility of the concept was never proven.

The research work is based on an analysis of the unit-cell for three thermal power configurations: 500 MWth, 5 MWth, and 50 kWth. For each thermal power configuration, a total of three operating pressure cases are analyzed: 250, 500, and 1,000 atm. The thermal analysis of the engine in (r) geometry, along with determination of rocket performance parameters, is performed by GNRATR-1D, a FORTRAN 77 code developed by the author. The main purpose of GNRATR-1D is to provide an *uncooled* temperature distribution $T(r)$ across the rocket engine, as well as major rocket performance parameters.

THEORETICAL ANALYSIS OF THE UNIT-CELL NUCLEAR LIGHT BULB REACTOR SYSTEM

John E. ...

Ph.D. Thesis, Department of Nuclear Engineering, University of New Mexico, 1972
M.S. Thesis, Department of Nuclear Engineering, University of New Mexico, 1972
Ph.D. Thesis, University of New Mexico, 1972

This dissertation presents a detailed theoretical analysis of the unit-cell behavior of the Nuclear Light Bulb (NLB) reactor system. The NLB system is a gas core nuclear reactor first proposed in the 1950's by the United States Atomic Energy Commission (USAEC) as an alternative concept of a low-temperature moderator/reflector as well as a potential propellant channel. Both proposed with the intent of increasing the life of the system.

The results of this work can be grouped into two major areas: (1) thermal and neutronic analysis of the engine, and (2) investigation of the possibility of the engine over a wide range of operating conditions. This work is believed to comprise the first comprehensive analysis of the unit-cell NLB derivative. The unit-cell derivative, although first proposed in the early 1970's, has never been analyzed in detail and most associated parameters are based on an assumed thermal and neutronic behavior of the engine. No significant work has been performed with regard to the engine since termination of gas core research efforts in 1973, so the feasibility of the concept was never proven.

The research work is based on an analysis of the unit-cell for three thermal power configurations: 500 MWth, 2 MWth, and 50 kWth. For each thermal power configuration, a total of three operating pressure cases are analyzed: 250, 500, and 1,000 atm. The thermal analysis of the engine is performed by along with determination of inlet performance parameters is performed by GMATR-1D, a FORTRAN IV code developed by the author. The main purpose of GMATR-1D is to provide an analytical temperature distribution. (1) across the reactor engine, as well as major reactor performance parameters.

Based on the temperature distribution provided by GNRATR-1D, appropriate atomic densities of the materials in the engine are calculated, and then provided to the neutron transport code ONEDANT for determination of the actual volumetric heat generation rate $Qg'''(r)$ and k_{eff} .

The thermalhydraulics analysis, conducted by coupling GNRATR-1D and ONEDANT, indicates that the unit-cell NLB rocket engine is feasible in the 50 kWth configuration. The physical properties calculated for that configuration, such as fuel and propellant temperature, exit velocity, and specific impulse, are in very good agreement with the properties that the original UARL designers were expecting. Thus, the results of this Dissertation work can be used to validate the assumptions and expectations of the original designers, who were never able to complete their work due to termination of funding.

The 50 kWth configuration is taken as the baseline configuration for detailed analysis, as it is considered both potentially feasible as well as corresponding to the original UARL designers' goals for NLB engine technology. The temperatures characteristic of the 50 kWth configuration correspond to those proposed by the original UARL designers for NLB applications; the 5 MWth and 500 MWth configurations were incorporated to investigate resultant NLB parameters over a wide range of temperatures. The uncooled $T(r)$ results indicate the need for incorporation of cooling mechanisms in the silica wall and moderator/reflector regions. Silica wall melting could be prevented by a combination of film cooling from the buffer gas and propellant sides, and internal cooling of the wall with less than 1.0 kg/s mass flow rate. The solid moderator/reflector would be maintained below melting by film cooling at the propellant/moderator interface.

A comprehensive set of temperature distributions, $Qg'''(r)$, and rocket performance parameters are provided for all nine thermal power/pressure combinations. Thrust is found to decrease with thermal power, while specific impulse increases. The calculated thrust for all three thermal power configurations is approximately 1 kN, due primarily to the very low propellant channel cross-sectional area.

The geometric analysis of the multi-cell NIS engine relies on two different models of electrostatic fields: the 1-D (EDAT) and the 2-D (EDAT2) models. The 1-D model is used as a reference while the 2-D model is compared with a temperature-dependent 2-D (EDAT2) group library derived from the MATS2 (MDS2-V) theory. The latter was included in the analysis as a secondary reference for the 2-D model. The analysis is performed in order to compare the secondary reference to the temperature (100 K) as proposed by the original designer.

With respect to the 1-D calculation, the model is found to be identical to the original 1-D model since the process of the EDAT2 is to analyze in detail the original 1-D design. An attempt is made to modify the cell. Thus, the thermally dynamic analysis is performed for the original design with a sufficient number of iterations for achieving stability for a given set of a standard engine as included as part of the analysis.

Comparison of the Hanen-Roch and MDS2-V 1-D results does not validate the expectation of the original designer regarding the possible electrostatic potential effects of the low-temperature electrodes and reflector. Although this research work included the existence of a 0.500 eV scattering cross-section cutoff in peripheral, a correlation could not be found between the original 1-D model and a similar process in the 2-D model. In particular, the 2-D model is held constant.

The comparison of the research work indicates that the core technology and the multi-cell NIS engine in particular, is feasible provided a number of engineering issues are addressed. Overall, it does seem that the operating temperature and other performance parameters characteristics of the core technology are somewhat lower than one might expect. For the case of the multi-cell NIS engine, a cell temperature of 20.00-25.000 K corresponding to a thermal power of roughly 20 MW, most probably indicates the upper limit of feasibility. This conclusion supports the procedure proposed by the original 1-D design as being achievable by the use of NIS technology.

CHAPTER 1

CHAPTER 2

CHAPTER 3

CHAPTER 4

CHAPTER 5

CHAPTER 6

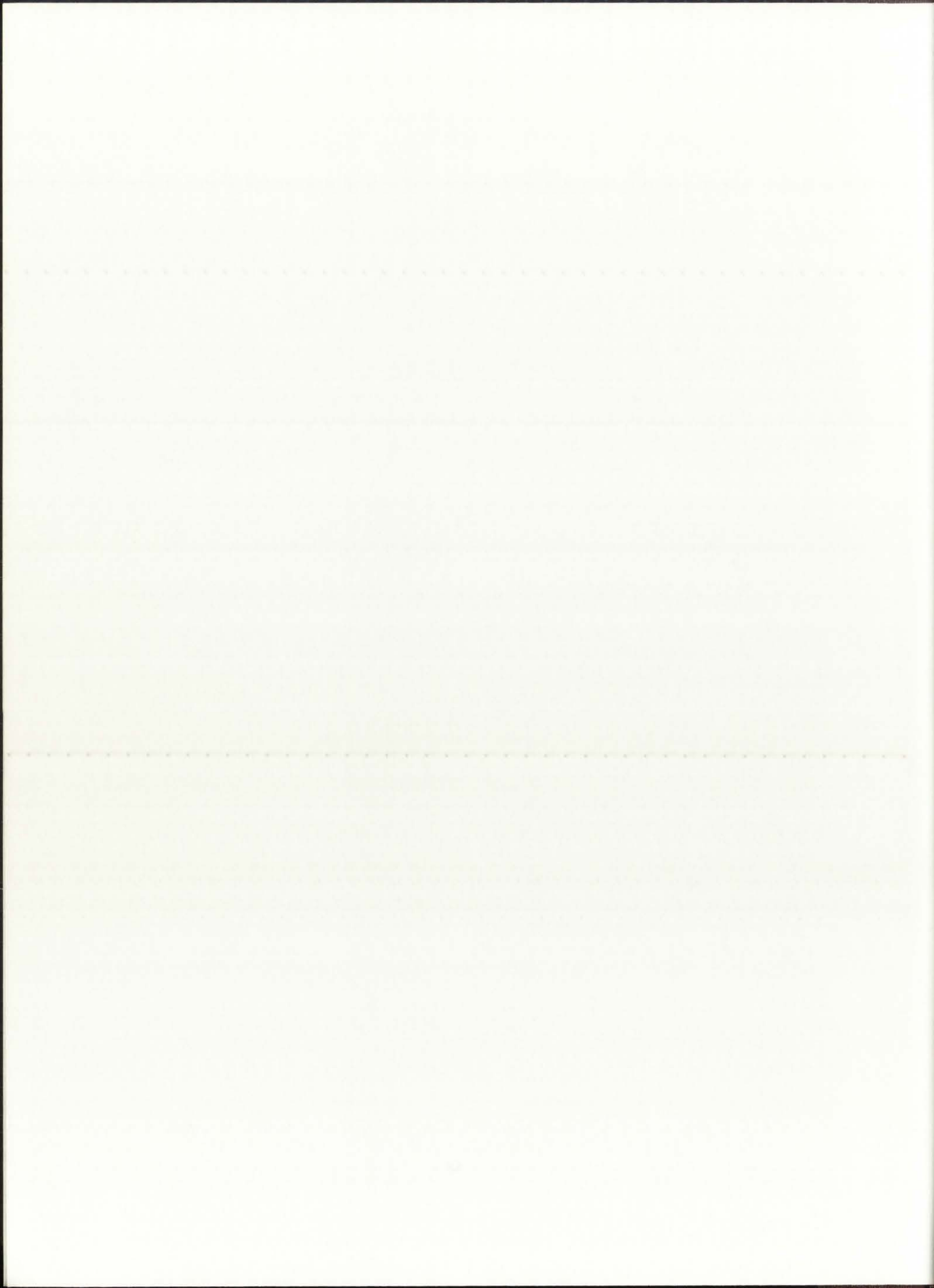


TABLE OF CONTENTS

	<u>Page</u>
CHAPTER 1 - INTRODUCTION AND DISSERTATION OVERVIEW	1
1.1. Introduction	1
1.2. Space Nuclear Power and Propulsion	3
1.2.1. Nuclear Thermal Propulsion (NTP)	4
1.3. Space Nuclear Thermal Propulsion Research	5
1.4. Focus of the Dissertation	5
1.5. Structure of the Dissertation	6
CHAPTER 2 - THE NUCLEAR LIGHT BULB ROCKET ENGINE	7
2.1. The Gaseous Core Reactor Concept	7
2.2. NLB Rocket Engine Background	7
2.3. The NLB Rocket Engine	8
2.4. NLB Rocket Engine Layout	10
2.5. NLB Performance Data	15
2.6. Experimental and Theoretical Validation	17
2.7. Progress of NLB Research Work	19
2.8. Current Status of the NLB Rocket Engine	22
CHAPTER 3 - THE UNIT-CELL ROCKET ENGINE - TECHNICAL BACKGROUND	23
3.1. Introduction	23
3.2. The Unit-Cell Test Reactor	24
3.3. Performance Analysis of the Unit-Cell Reactor	25
3.3.1. Preliminary Criticality Calculations	29
3.4. Summary of UARL Research Work	33
3.5. Current Status of the Unit-Cell Reactor Concept	34
3.6. Motivation for this Dissertation Research Work	34
CHAPTER 4 - RESEARCH GOALS AND BASIS FOR ORIGINALITY	36
4.1. Introduction	36
4.2. Literature Survey	36
4.3. Research Goals	38
4.4. Basis for Originality	42
CHAPTER 5 - PROPOSED METHODOLOGY OF ANALYSIS	44
5.1. Introduction	44
5.2. Top-level Design Specification	44
CHAPTER 6 - HEAT TRANSFER THEORY	50
6.1. Introduction	50

TABLE OF CONTENTS

Page

1	CHAPTER 1 - INTRODUCTION AND ORIENTATION OVERVIEW	
2	1.1 Introduction	
3	1.2 Space Vehicle Power and Propulsion	
4	1.2.1 Nuclear Thermal Propulsion (NTP)	
5	1.2.2 Space Vehicle Thermal Propulsion Research	
6	1.3 Focus of the Dissertation	
7	1.4 Structure of the Dissertation	
8	CHAPTER 2 - THE NUCLEAR LIGHT-BULB ROCKET ENGINE	
9	2.1 The General Gas-Generator Concept	
10	2.2 NLE Rocket Engine Background	
11	2.3 The NLE Rocket Engine	
12	2.4 NLE Rocket Engine Layout	
13	2.5 NLE Performance Data	
14	2.6 Experimental and Theoretical Validation	
15	2.7 Progress of NLE Research Work	
16	2.8 Current Status of the NLE Rocket Engine	
17	CHAPTER 3 - THE UNIT-CELL ROCKET ENGINE - TECHNICAL BACKGROUND	
18	3.1 Introduction	
19	3.2 The Unit-Cell Test Reactor	
20	3.3 Performance Analysis of the Unit-Cell Reactor	
21	3.3.1 Thermodynamic Calculations	
22	3.4 Summary of UARC Research Work	
23	3.5 Current Status of the Unit-Cell Reactor Concept	
24	3.6 Motivation for the Dissertation Research Work	
25	CHAPTER 4 - RESEARCH GOALS AND BASIS FOR ORIGINALITY	
26	4.1 Introduction	
27	4.2 Literature Survey	
28	4.3 Research Goals	
29	4.4 Basis for Originality	
30	CHAPTER 5 - PROPOSED METHODOLOGY OF ANALYSIS	
31	5.1 Introduction	
32	5.2 Top-level Design Specification	
33	CHAPTER 6 - HEAT TRANSFER THEORY	
34	6.1 Introduction	

TABLE OF CONTENTS (cont'd)

	<u>Page</u>
6.2. Thermal Power-related Feasibility Problems	50
6.3. Governing Energy Balance Equations	51
6.4. Governing Modes of Heat Transfer	52
6.4.1. Fuel/Buffer Gas Mixture and Fuel Regions	54
6.4.2. Buffer Gas and Propellant Regions	54
6.4.3. Silica Wall	54
6.4.4. Moderator, Reflector, and Pressure Vessel	55
6.4.5. Ambient Space	55
6.4.6. Summary	56
6.5. The Theory of the Modes of Heat Transfer	57
6.5.1. Heat Generation	57
6.5.2. Thermal Radiation	58
6.5.2.1. Optically Thick Regions	59
6.5.2.2. Optically Thin Regions	60
6.5.3. Convection	63
6.5.4. Conduction	65
6.6. Application of the Derived Heat Transfer Theory	66
6.7. Additional Heat Transfer Theory - Film Cooling	66
 CHAPTER 7 - NEUTRONICS THEORY	 67
7.1. Introduction	67
7.2. The Volumetric Heat Generation Rate	67
7.3. Geometry and Material Composition	71
7.4. Cross-section Libraries	73
7.4.1. The Hansen-Roach Library	74
7.4.2. Temperature-dependent ENDF/B-V Library	77
7.5. Criticality	81
 CHAPTER 8 - ROCKET PROPULSION THEORY	 82
8.1. Introduction	82
8.2. Rocket Performance Parameters	82
8.3. Thermophysical Properties	84
8.4. Axial Dependence	88
 CHAPTER 9 - THE GNRATR-1D THERMAL ANALYSIS CODE	 89
9.1. Introduction	89
9.2. The GNRATR-1D Thermal Analysis Code	89
9.3. The Equation Structure of GNRATR-1D	92
9.3.1. Within-region, generation/radiation eqns.	94
9.3.2. Within-region, radiation/convection eqns.	95

TABLE OF CONTENTS (cont'd)

50	6.3. Thermal Transfered Particle Problems
51	6.2. Governing Energy Balance Equations
52	6.1. Governing Equations of Heat Transfer
54	6.4.1. Fuel-Derived Gas Motion and Heat Transfer
54	6.4.2. Fuel Gas and Radiative Heating
54	6.4.3. Solid Wall
55	6.4.4. Molecular Reflection and Emission Yield
55	6.4.5. Assumed Spots
56	6.4.6. Summary
57	6.5. The Theory of the Modes of Heat Transfer
57	6.5.1. Heat Conduction
58	6.5.2. Thermal Radiation
59	6.5.2.1. Optically Thick Regions
60	6.5.2.2. Optically Thin Regions
63	6.5.3. Convection
63	6.5.4. Conduction
65	6.6. Application of the Derived Heat Transfer Theory
66	6.7. Additional Heat Transfer Theory - Film Cooling
67	CHAPTER 7 - NEUTRONIC THEORY
67	7.1. Introduction
67	7.2. The Volumetric Heat Generation Rate
71	7.3. Geometry and Material Composition
73	7.4. Cross-section Libraries
74	7.4.1. The Hansen-Rauch Library
77	7.4.2. The ENDF/B-4.3 and ENDF/B-V Libraries
81	7.5. Chemistry
81	CHAPTER 8 - ROCKET PROPELLION THEORY
81	8.1. Introduction
82	8.2. Nozzle Performance Parameters
84	8.3. Thermophysical Properties
88	8.4. Axial Gradients
89	CHAPTER 9 - THE CUBAT-1D THERMAL ANALYSIS CODE
89	9.1. Introduction
89	9.2. The CUBAT-1D Thermal Analysis Code
91	9.3. The Equation Structure of CUBAT-1D
94	9.3.1. Wall-weighted generation/conversion rates
97	9.3.2. Wall-weighted radiation/conversion rates

TABLE OF CONTENTS (cont'd)

	<u>Page</u>
9.3.3. Within-region, radiation/conduction eqns.	96
9.3.4. Within-region, conduction eqns.	97
9.3.5. Within-region, radiation equation	98
9.3.6. Interface Conduction Equation	99
9.4. The Structure of GNRATR-1D	101
9.5. Summary of GNRATR-1D Features	103
9.6. Verification and Validation of GNRATR-1D	104
9.6.1. Verification	104
9.6.2. Validation	106
9.6.3. Conclusions	108
 CHAPTER 10 - THERMAL & NEUTRONICS ANALYSIS RESULTS	 109
10.1. Introduction	109
10.2. Breakdown of the Analysis	109
10.3. The 500 MWth Configuration	114
10.3.1. Hansen-Roach Library	115
10.3.2. ENDF/B-V Library	122
10.4. The 5 MWth Configuration	130
10.4.1. Hansen-Roach Library	130
10.4.2. ENDF/B-V Library	137
10.5. The 50 kWth Configuration	143
10.5.1. Hansen-Roach Library	143
10.5.2. ENDF/B-V Library	149
10.6. Variation of T(r) for Fixed Operating Pressures	154
10.7. Thermophysical and Rocket Performance Results	161
10.8. Baseline 50 kWth, P=250 atm, Configuration	172
10.8.1. Baseline Configuration Thermal Analysis	174
10.8.1.1. Combination I	174
10.8.1.2. Combination II	176
10.8.1.3. Combination III	179
10.8.2. Effects of Fuel Temperature on k_{eff}	182
10.9. Accuracy of the (r) Geometry Model and Associated Assumptions	184
10.9.1. (r- θ) Analysis of $Qg'''(r)$	184
10.9.2. (r- θ) Analysis of the Neutron Flux $\Phi(r)$	185
10.9.3. Neutron and Gamma Energy Deposition	187
10.9.4. Criticality Search	189
10.10. Conclusions	190

TABLE OF CONTENTS (cont'd)

Page

9.3.3. With-in-region radiation contribution equation 95
 9.3.4. With-in-region contribution eqn. 97
 9.3.5. With-in-region radiation equation 98
 9.3.6. Inverse Contribution Equations 99
 9.4. The structure of GCRAT-1D 101
 9.5. Summary of GCRAT-1D Features 103
 9.6. Verification and Validation of GCRAT-1D 104
 9.6.1. Verification 104
 9.6.2. Validation 105
 9.6.3. Conclusions 108

CHAPTER 10 - THERMAL & NEUTRONIC ANALYSIS RESULTS

10.1. Introduction 109
 10.2. Breakdown of the Analysis 109
 10.3. The 300 MWth Configuration 114
 10.3.1. Hansen-Roads Library 115
 10.3.2. ENDF/B-V Library 117
 10.4. The 2 MWth Configuration 120
 10.4.1. Hansen-Roads Library 120
 10.4.2. ENDF/B-V Library 127
 10.5. The 50 kWth Configuration 143
 10.5.1. Hansen-Roads Library 143
 10.5.2. ENDF/B-V Library 149
 10.6. Variation of T₁ for Fixed Operating Pressures 154
 10.7. Thermodynamic and Kinetic Performance Results 161
 10.8. Summary of With-in-region Contributions 172
 10.9. 10.9.1. Reaction Contribution Thermal Analysis 174
 10.9.2. Condition I 174
 10.9.3. Condition II 175
 10.9.4. Condition III 179
 10.9.5. Effect of Fuel Temperature on k_{eff} 182
 10.9.6. Accuracy of the 1D Geometry Model and Associated Assumptions 184
 10.9.7. Analysis of Q₁₀ 184
 10.9.8. Analysis of the Neutron Flux etc) 185
 10.9.9. Neutron and Gamma Energy Deposition 187
 10.9.10. Chemistry Search 189
 10.10. Conclusions 190

TABLE OF CONTENTS (cont'd)

	<u>Page</u>
CHAPTER 11 - SPECTRAL ANALYSIS OF RADIATIVE HEAT TRANSFER IN THE SILICA WALL	192
11.1. Introduction	192
11.2. Methodology of Analysis	193
11.3. Spectral Radiative Heat Transfer Theory	194
11.3.1. The Transmission Cutoff (TC)	196
11.3.2. The Absorbed Fraction (AF)	198
11.3.3. Silica Wall Temperature	201
11.3.4. Internal Cooling Mass Flow Rate	204
11.4. Conclusions	212
CHAPTER 12 - FILM COOLING ANALYSIS OF THE MODERATOR/ REFLECTOR REGION	213
12.1. Introduction	213
12.2. Methodology of Analysis	214
12.3. Results of Film Cooling Analysis	215
12.4. Conclusions	221
CHAPTER 13 - CONCLUSIONS	222
13.1. General Conclusions on Feasibility	222
13.2. Feasibility of the Unit-Cell NLB Concept	223
13.3. Conclusions	224
CHAPTER 14 - RECOMMENDATIONS FOR FUTURE WORK	226
14.1. Summary of Recommendations	226
REFERENCES	228
APPENDIX A - GNTRATR-1D.f Source Code Listing	240
APPENDIX B - 500 MWth Configuration: Input and Output Files	279
B.1. ONEDANT Input Files (HR)	280
B.2. GNRATR-1D Summary Output Files (HR)	284
B.3. TRANSX Input Files (ENDF/B-V)	291
B.4. ONEDANT Input Files (ENDF/B-V)	295
B.5. GNRATR-1D Summary Output Files (ENDF/B-V)	299
APPENDIX C - 5 MWth Configuration: Input and Output Files	306
C.1. ONEDANT Input Files (HR)	307

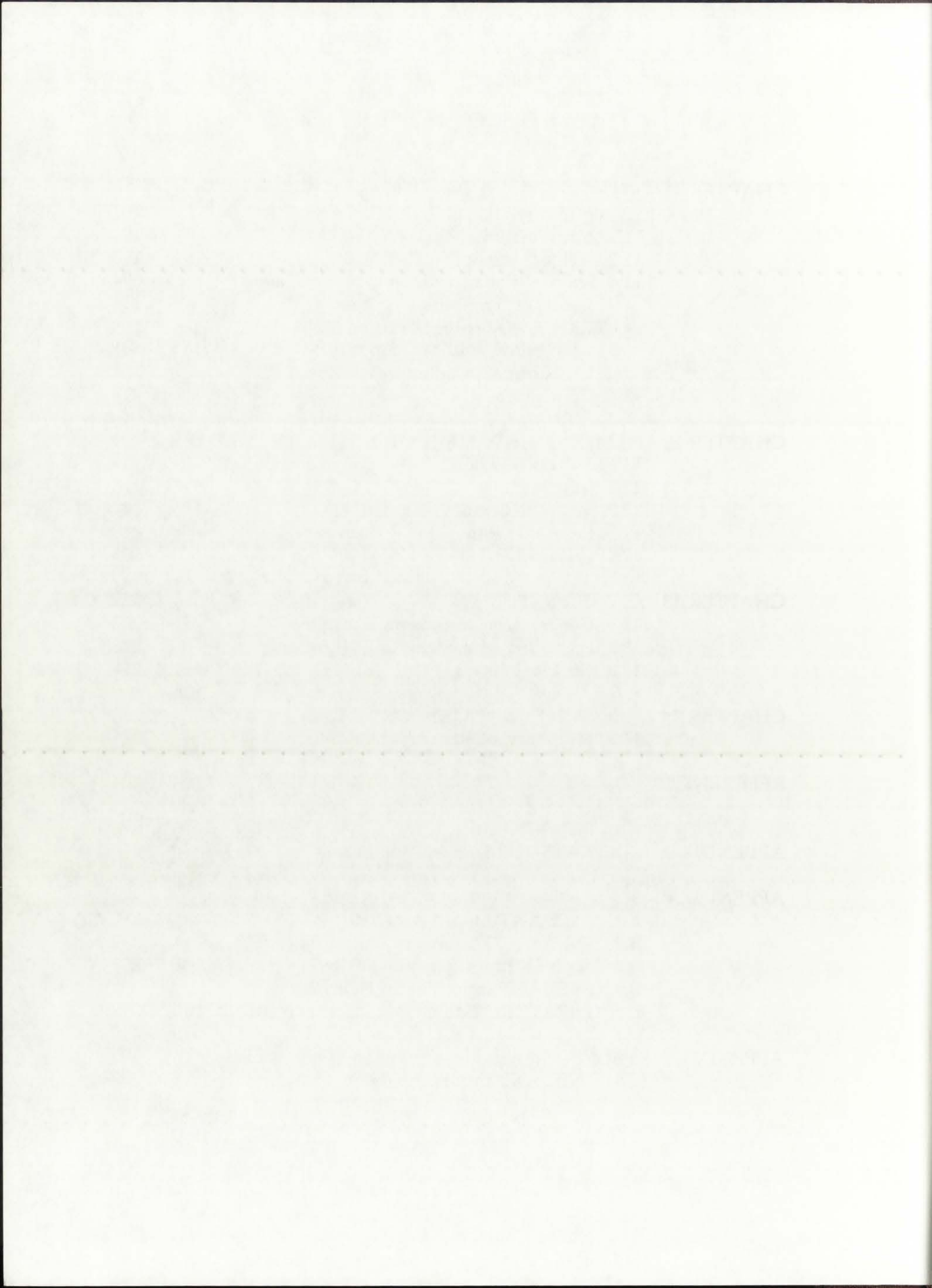
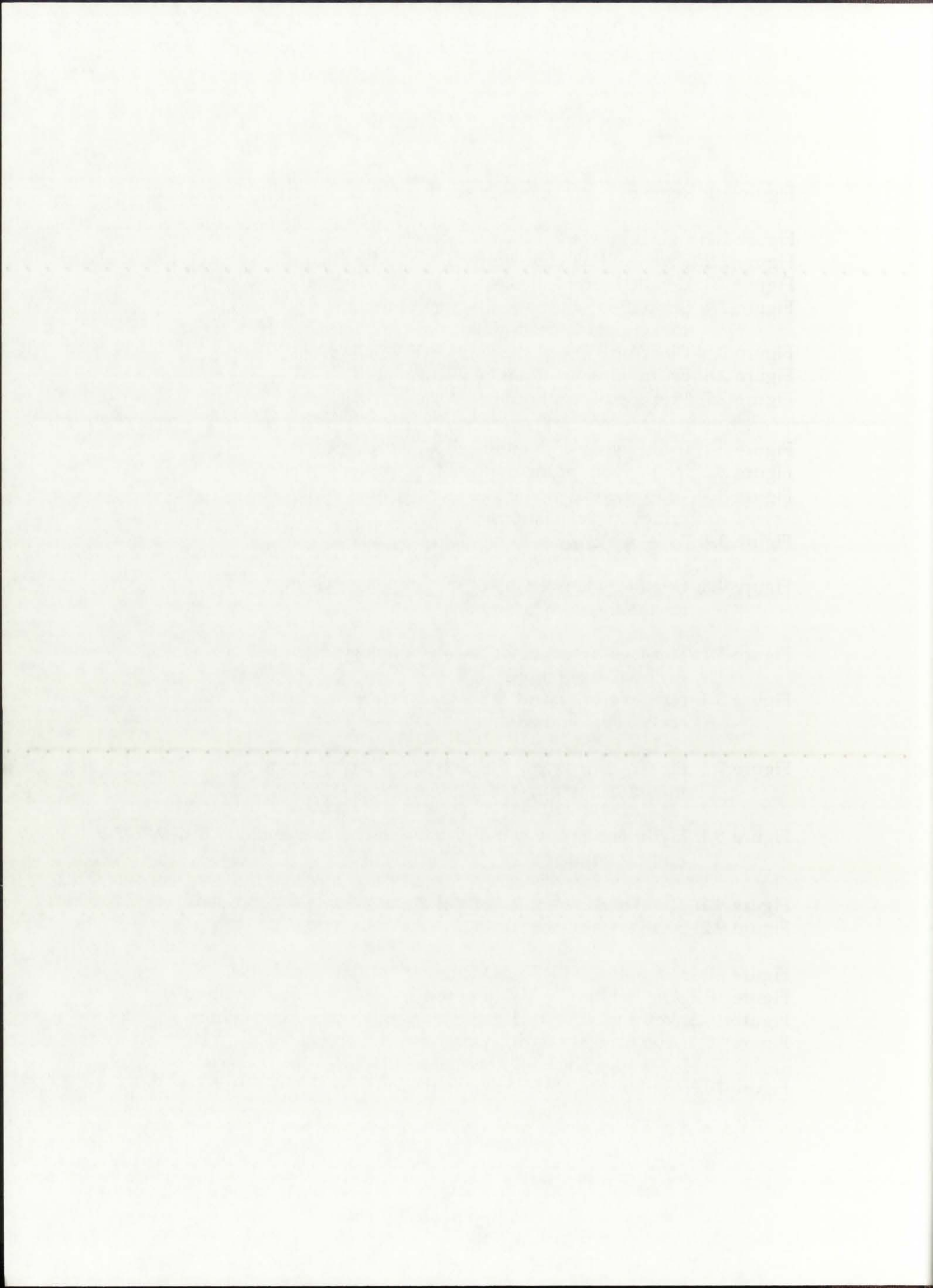


TABLE OF CONTENTS (cont'd)

	<u>Page</u>
C.2. GNRATR-1D Summary Output Files (HR)	311
C.3. TRANSX Input Files (ENDF/B-V)	318
C.4. ONEDANT Input Files (ENDF/B-V)	322
C.5. GNRATR-1D Summary Output Files (ENDF/B-V)	326
APPENDIX D - 50 kWth Configuration: Input and Output Files	331
D.1. ONEDANT Input Files (HR)	332
D.2. GNRATR-1D Summary Output Files (HR)	336
D.3. TRANSX Input Files (ENDF/B-V)	343
D.4. ONEDANT Input Files (ENDF/B-V)	347
D.5. GNRATR-1D Summary Output Files (ENDF/B-V)	351
APPENDIX E - 50 kWth, 250 atm, Combination I	358
E.1. Combination I	359
E.2. Combination II	366
E.3. Combination III	373
APPENDIX F - 50 kWth, 250 atm Baseline Configuration - Fuel Temperature Coefficient of Reactivity	380
F.1. TRANSX Input Files	381
F.2. ONEDANT Input Files	387
APPENDIX G - WVLENABS.f Code Listing	389
APPENDIX H - Mathematica Analysis Listing	393
APPENDIX I - SIWALL.f Code Listing	407
APPENDIX J - FILMCOOL.f Code Listing	411
APPENDIX K - BBC Code Sample Input File	415
APPENDIX L - TRANSX Code Sample Input File	417

LIST OF FIGURES

	<u>Page</u>
Figure 1.1: Regimes of space power applicability.	2
Figure 2.1: General layout of the NLB concept.	9
Figure 2.2: Seven-cell baseline design of the NLB engine.	11
Figure 2.3: Detailed technical sketch of the NLB engine.	12
Figure 2.4: Simplified schematic diagram of the unit-cell NLB rocket engine cooling loops.	13
Figure 2.5: Close-up view of the seven-cell NLB engine.	14
Figure 2.6: Enlarged view of one NLB engine cell.	16
Figure 2.7: Proposed layout of the in-ACRR experiment.	21
Figure 3.1: (r- θ) Layout of the unit-cell NLB rocket engine.	26
Figure 3.2: (r-z) Layout of the unit-cell NLB rocket engine.	27
Figure 3.3: 1-D spherical model used for preliminary UARL criticality calculations.	30
Figure 3.4: Low-energy Be scattering cross-sections.	32
Figure 4.1: Geometry conversion of the propellant channel for the (r)-geometry model.	39
Figure 5.1: Top-level structure of the methodology discussed in this Dissertation.	46
Figure 5.2: Nine-region layout of the (r)-geometry unit-cell NLB rocket engine model.	47
Figure 7.1: Eleven-zone layout of the (r)-geometry neutronics model of the unit-cell NLB engine.	72
Figure 8.1: Hydrogen propellant ionization fraction vs temperature and pressure.	87
Figure 9.1: The two different layouts of a unit-volume about a node.	93
Figure 9.2: Software structure of the GNRATR-1D code.	101
Figure 10.1: Sample GNRATR-1D summary output file.	113
Figure 10.2: $Qg'''(r)$ for 500 MWth power level (Hansen-Roach library).	116
Figure 10.3: k_{eff} for 500 MWth configuration (Hansen-Roach library).	118
Figure 10.4: $T(r)$ for 500 MWth, Hansen-Roach library, comprehensive thermal analysis.	120
Figure 10.5: $Qg'''(r)$ for 500 MWth power level (ENDF/B-V library).	123



LIST OF FIGURES (cont'd)

	<u>Page</u>
Figure 10.6: keff for 500 MWth configuration (ENDF/B-V library).	125
Figure 10.7: T(r) for 500 MWth, ENDF/B-V library, comprehensive thermal analysis.	127
Figure 10.8: Qg'''(r) for 5 MWth power level (Hansen-Roach library).	131
Figure 10.9: keff for 5 MWth configuration (Hansen-Roach library).	133
Figure 10.10: T(r) for 5 MWth, Hansen-Roach library, comprehensive thermal analysis.	135
Figure 10.11: Qg'''(r) for 5 MWth power level (ENDF/B-V library).	138
Figure 10.12: keff for 5 MWth configuration (ENDF/B-V library).	139
Figure 10.13: T(r) for 5 MWth, ENDF/B-V library, comprehensive thermal analysis.	141
Figure 10.14: Qg'''(r) for 50 kWth power level (Hansen-Roach library).	144
Figure 10.15: keff for 50 kWth configuration (Hansen-Roach library).	146
Figure 10.16: T(r) for 50 kWth, Hansen-Roach library, comprehensive thermal analysis.	147
Figure 10.17: Qg'''(r) for 50 kWth power level (ENDF/B-V library).	150
Figure 10.18: keff for 50 kWth configuration (ENDF/B-V library).	151
Figure 10.19: T(r) for 50 kWth, ENDF/B-V library, comprehensive thermal analysis.	152
Figure 10.20: T(r) for p=250 atm, Hansen-Roach library, comprehensive thermal analysis.	155
Figure 10.21: T(r) for p=500 atm, Hansen-Roach library, comprehensive thermal analysis.	156
Figure 10.22: T(r) for p=1,000 atm, Hansen-Roach library, comprehensive thermal analysis.	157
Figure 10.23: T(r) for p=250 atm, ENDF/B-V library, comprehensive thermal analysis.	158
Figure 10.24: T(r) for p=500 atm, ENDF/B-V library, comprehensive thermal analysis.	159
Figure 10.25: T(r) for p=1,000 atm, ENDF/B-V library, comprehensive thermal analysis.	160
Figure 10.26: Centerline fuel temperature.	163
Figure 10.27: Edge-of-fuel temperature.	163
Figure 10.28: Propellant bulk temperature.	164
Figure 10.29: Silica wall mean temperature.	164
Figure 10.30: Solid region reflective liner temperature.	165
Figure 10.31: Hydrogen dissociation fraction.	165
Figure 10.32: Propellant total molecular weight.	167
Figure 10.33: Propellant mass flow rate.	167
Figure 10.34: Nozzle exit velocity.	168

LIST OF FIGURES (cont'd)

	<u>Page</u>
Figure 10.35: Specific Impulse.	168
Figure 10.36: Thrust.	170
Figure 10.37: T(r) for Combination I.	175
Figure 10.38: T(r) for Combination II.	177
Figure 10.39: T(r) for Combination III.	180
Figure 10.40: T(r) for Combination III, with varying propellant velocity.	181
Figure 10.41: Effect of fuel temperature on the k_{eff} of the rocket engine.	183
Figure 10.42: Comparison of (r- θ) slide $Qg'''(r)$ vs. 1-D approximation.	186
Figure 10.43: Comparison of (r- θ) slide $Qg'''(r)$ vs. 1-D approximation.	186
Figure 10.44: Ratio of ENDF/B-V subthermal-to-Total neutron flux.	188
Figure 10.45: Search for criticality: 50 kWth configuration.	190
Figure 11.1: Variation of $e_{\lambda}(\lambda, T)$ with wavelength and temperature.	195
Figure 11.2: Variation of λ_{max} with temperature.	197
Figure 11.3: Spectral transmissivities of several glass compounds.	199
Figure 11.4: Spectral transmissivity of Suprasil 300 silica.	200
Figure 11.5: Calculated AF values for three silica compounds.	202
Figure 11.6: Calculated wall temperatures for three silica compounds.	205
Figure 11.7: Coolant mass flow rates for three silica compounds.	208
Figure 12.1: Interdependence of film heat transfer coefficient and Rosseland mean opacity.	218
Figure 12.2: Interdependence of film mass flow rate and Rosseland mean opacity.	219
Figure 12.3: Interdependence of film axial velocity and Rosseland mean opacity.	220

LIST OF FIGURES (contd)

163	Figure 10.25: Specific losses
170	Figure 10.26: η_{sp}
171	Figure 10.27: η_{sp} for Condition I
177	Figure 10.28: η_{sp} for Condition II
180	Figure 10.29: η_{sp} for Condition III
181	Figure 10.30: η_{sp} for Condition III with varying procedure in body
181	Figure 10.41: Effect of fuel temperature on the η_{sp} of the rocket engine
186	Figure 10.42: Comparison of (a) η_{sp} vs. 1-D approximation
186	Figure 10.43: Comparison of (a) η_{sp} vs. 1-D approximation
188	Figure 10.44: Ratio of EMD-VI-V subsonic-to-total weight flow
190	Figure 10.45: Effect of velocity on η_{sp} vs. 1-D approximation
195	Figure 11.1: Variation of η_{sp} with weight flow and temperature
197	Figure 11.2: Variation of η_{sp} with temperature
199	Figure 11.3: Spectral power density of several glass compounds
200	Figure 11.4: Spectral transmissivity of several glass compounds
202	Figure 11.5: Calculated η_{sp} values for three glass compounds
205	Figure 11.6: Calculated wall temperatures for three glass compounds
208	Figure 11.7: Calculated mass flow rates for three glass compounds
210	Figure 11.8: Interdependence of film heat transfer coefficient and mass flow rate
219	Figure 11.9: Interdependence of film mass flow rate and mass flow rate
219	Figure 11.10: Interdependence of film axial velocity and mass flow rate

LIST OF TABLES

	<u>Page</u>
Table 2.1: Estimated NLB rocket engine power levels and performance parameters.	18
Table 3.1: UARL-estimated critical U-235 density as a function of moderator/reflector.	28
Table 3.2: 17-group neutron cross-section library used by UARL for cavity reactor criticality calculations.	31
Table 7.1: Emitted and recoverable energies for fission in U-235.	70
Table 7.2: 118 Nuclide Hansen-Roach cross-section library.	75
Table 7.3: Hansen-Roach cross-section library energy group structure.	76
Table 7.4: 127 Nuclide MATXS7 cross-section library.	78
Table 7.5: MATXS7 Cross-section library energy group structure.	79
Table 10.1: Parameters available for user specification in GNRATR-1D.	110
Table 10.2: Summary of the comprehensive thermal analysis results (500 MWth configuration, Hansen-Roach library).	121
Table 10.3: Summary of the comprehensive thermal analysis results (500 MWth configuration, ENDF/B-V library).	128
Table 10.4: Summary of the comprehensive thermal analysis results (5 MWth configuration, Hansen-Roach library).	136
Table 10.5: Summary of the comprehensive thermal analysis results (5 MWth configuration, ENDF/B-V library).	142
Table 10.6: Summary of the comprehensive thermal analysis results (50 kWth configuration, Hansen-Roach library).	148
Table 10.7: Summary of the comprehensive thermal analysis results (50 kWth configuration, ENDF/B-V library).	153
Table 10.8: Three combinations of heat transfer modes used for the baseline configuration.	174
Table 11.1: Calculated AF values for three silica compounds.	203
Table 11.2: Calculated wall temperatures for three silica compounds.	206
Table 11.3: Coolant mass flow rates for three silica compounds.	209
Table 11.4: Maximum feasible coolant mass flow rates.	211
Table 12.1: Parametric analysis of the film cooling parameters for 50 kWth, 250 atm	217

LIST OF TABLES

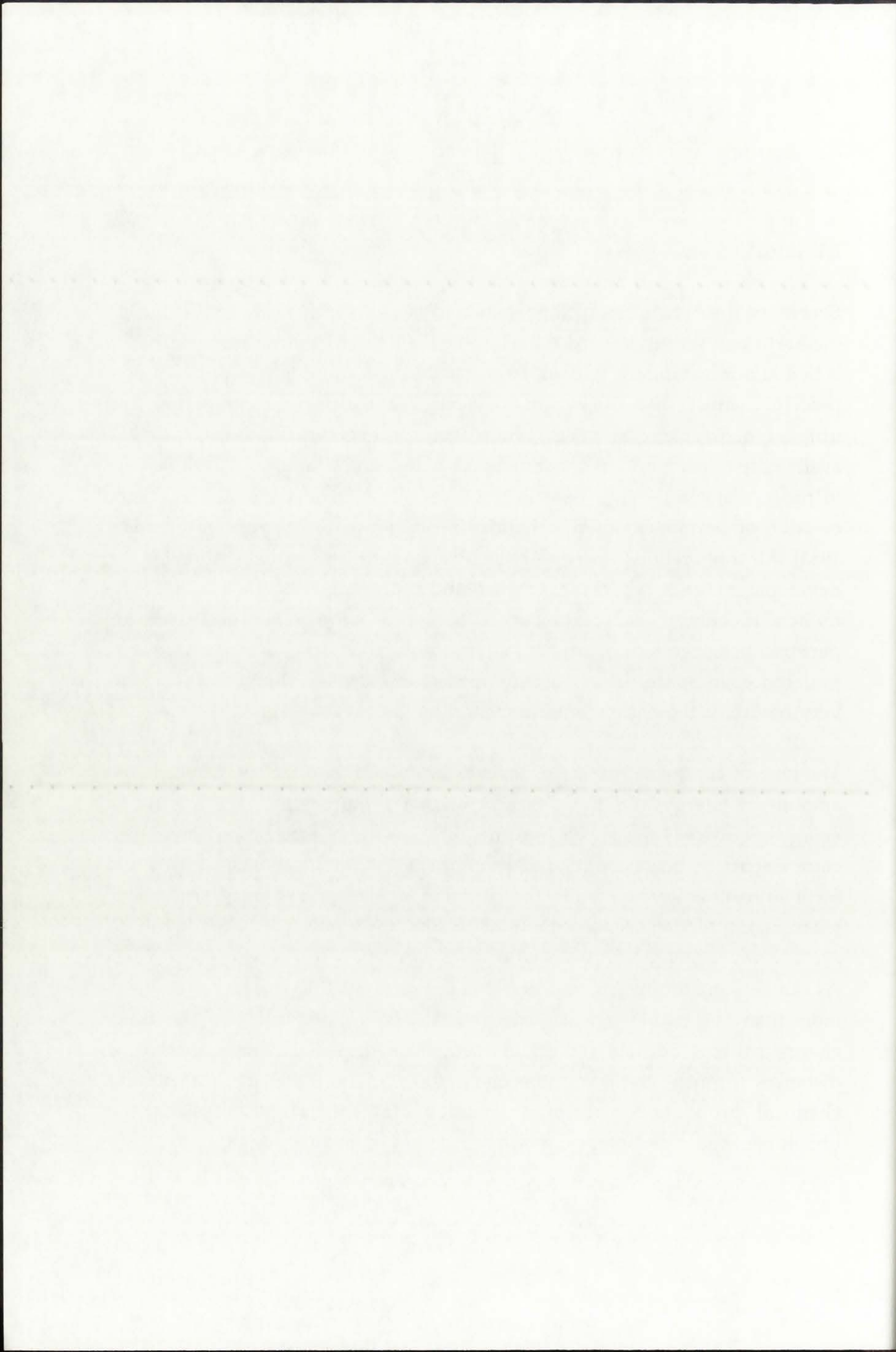
100	Table 11: Estimated β values for the power law fit and performance parameters.
99	Table 10: Estimated critical UDS density as a function of moderator temperature.
97	Table 9: 17-group neutron cross-section library used for UARL for cavity reactor criticality calculations.
96	Table 8: Evaluated and re-evaluated reaction rate factors in U-235.
95	Table 7: 118-group Hansen-Koch cross-section library.
94	Table 6: 118-group Hansen-Koch cross-section library energy group structure.
93	Table 5: 132-group Hansen-Koch cross-section library.
92	Table 4: MATXS2 cross-section data energy group structure.
91	Table 3: Parameters available for user specification in GREAT-1D.
90	Table 2: Summary of the comparative thermal analysis results (200 MWth configuration, Hansen-Koch library).
89	Table 1: Summary of the comparative thermal analysis results (200 MWth configuration, ENDF-B-V library).
88	Table 10: Summary of the comparative thermal analysis results (200 MWth configuration, Hansen-Koch library).
87	Table 9: Summary of the comparative thermal analysis results (200 MWth configuration, ENDF-B-V library).
86	Table 8: Summary of the comparative thermal analysis results (200 MWth configuration, Hansen-Koch library).
85	Table 7: Summary of the comparative thermal analysis results (200 MWth configuration, ENDF-B-V library).
84	Table 6: Three configurations of test reactor nodes used for the baseline configuration.
83	Table 5: Calculated β values for three different configurations.
82	Table 4: Calculated wall temperatures for three different configurations.
81	Table 3: Coolant mass flow rates for three different configurations.
80	Table 2: Maximum feasible coolant mass flow rates.
79	Table 1: Parametric analysis of the film cooling parameters for 20 MWth 235U.

1. Introduction

The first part of the book is devoted to a general discussion of the theory of the firm. It begins with a review of the classical theory of the firm, which is based on the assumption of perfect competition and profit maximization. This theory is then extended to the case of imperfect competition, where the firm's behavior is determined by its market power. The second part of the book is devoted to a detailed analysis of the theory of the firm in the case of imperfect competition. It begins with a review of the theory of the firm in the case of imperfect competition, which is based on the assumption of imperfect competition and profit maximization. This theory is then extended to the case of imperfect competition, where the firm's behavior is determined by its market power.

The third part of the book is devoted to a detailed analysis of the theory of the firm in the case of imperfect competition. It begins with a review of the theory of the firm in the case of imperfect competition, which is based on the assumption of imperfect competition and profit maximization. This theory is then extended to the case of imperfect competition, where the firm's behavior is determined by its market power. The fourth part of the book is devoted to a detailed analysis of the theory of the firm in the case of imperfect competition. It begins with a review of the theory of the firm in the case of imperfect competition, which is based on the assumption of imperfect competition and profit maximization. This theory is then extended to the case of imperfect competition, where the firm's behavior is determined by its market power.

The fifth part of the book is devoted to a detailed analysis of the theory of the firm in the case of imperfect competition. It begins with a review of the theory of the firm in the case of imperfect competition, which is based on the assumption of imperfect competition and profit maximization. This theory is then extended to the case of imperfect competition, where the firm's behavior is determined by its market power. The sixth part of the book is devoted to a detailed analysis of the theory of the firm in the case of imperfect competition. It begins with a review of the theory of the firm in the case of imperfect competition, which is based on the assumption of imperfect competition and profit maximization. This theory is then extended to the case of imperfect competition, where the firm's behavior is determined by its market power.



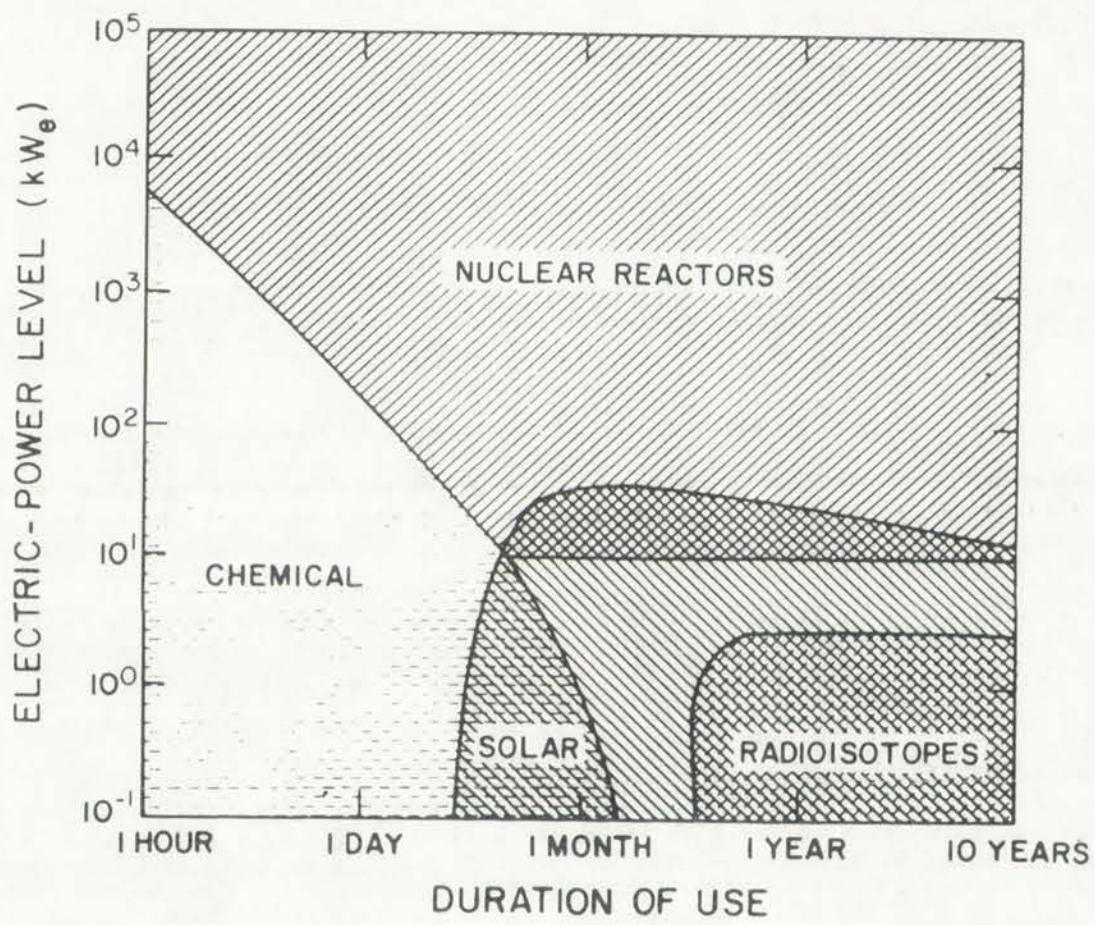


Figure 1.1: Regimes of space power applicability [Angelo and Buden, 1985].



Figure 1: Regions of space over which investment is profitable (Lambert and Budnik, 1981)

Thus, nuclear energy is really the only source that can provide the required power levels and long durations that would be characteristic of manned bases, journeys of exploration, and commercial endeavors in space.

1.2. Space Nuclear Power and Propulsion

The use of nuclear energy in space involves utilization and conversion of the thermal energy liberated by nuclear reactions. This is the mainstay of the benefits of nuclear power in both terrestrial and space applications - more energy (millions of times more) is liberated and placed at our disposal by nuclear reactions than by any other form of energy. The large amounts of thermal energy are released during the splitting of heavy nuclei such as U-235 or U-238 in a fission reaction, or during the formation of light He-3 or He-4 nuclei in a fusion reaction. The fission reaction is currently the better understood and more feasible of the two, so it forms the basis for nuclear reactors in space.

Nuclear energy has been of most interest in two areas of application: power generation and propulsion. Both utilize the thermal energy liberated in a fission reaction and convert it to a second, more desirable form of energy. Power generation involves conversion of the thermal energy into electric energy (electricity) which can be used to provide power for the spacecraft instrumentation and appliances, provide life-support functions to the astronauts, or just be stored in batteries until the need arises for large amounts of energy (for example, during an expedition to a planet's surface). Thus, power generation enables the normal functioning of the spacecraft throughout its journey.

Propulsion, on the other hand, can best be characterized as enabling the spacecraft to get to its destination; it provides the spacecraft with motion and enables its movement forward, backward, or sideways. Two different modes of nuclear propulsion are known and understood today: Nuclear Thermal Propulsion (NTP) and Nuclear Electric Propulsion (NEP). Both rely on nuclear fission to provide the primary source of energy. NTP involves

These nuclear energy is used to heat the water providing the required power for the long distance that would be the transport of nuclear power. The technology of experimental and theoretical advances in space nuclear power.

1.2. Space Nuclear Power and Applications

The use of nuclear energy in space involves utilization and conversion of the nuclear energy provided by nuclear reactions. This is the primary of the power of nuclear power in both terrestrial and space applications - more energy available of these power is provided and placed as per required by nuclear reactions that by the other form of energy. The large amounts of thermal energy are released during the splitting of heavy nuclei such as U-235 or U-238 in a fission reaction or during the fusion of light nuclei such as D-2 and T-3 in a fusion reaction. The fission reaction is currently the power technology and more feasible of the two as it does not require the nuclear reaction to occur.

Nuclear energy has been of great interest in the area of applied nuclear power generation and propulsion. Both utilize the thermal energy liberated in a fission reaction and convert it to a second, more desirable form of energy. Lower generation involves conversion of the thermal energy into electric energy (generators) which can be used to provide power for the spacecraft. This conversion and application provides the support functions to the spacecraft or just be used in fission or fusion power for large amounts of energy (for example during an expedition to a planet's surface). These power generation enables the normal functioning of the spacecraft throughout its journey.

Propulsion on the other hand, can not be characterized as enabling the spacecraft to get to its destination. It provides the spacecraft with motion and enables its movement forward, backward, or sideways. Two different modes of nuclear propulsion are fission and fusion today. Nuclear Thermal Propulsion (NTP) and Nuclear Electric Propulsion (NEP). Both rely on nuclear fission to provide the primary source of energy. NTP involves

conversion of the thermal energy released in fission directly into mechanical energy, namely the provision of thrust. NEP involves conversion of the thermal energy into electrical energy, which is then used to accelerate ionized particles across a voltage gap. This Dissertation concentrates on the principles and theory behind NTP; a detailed discussion of NEP concepts can be found in [Sutton, 1992] and [Hill & Peterson, 1992].

1.2.1. Nuclear Thermal Propulsion (NTP)

Based on Newton's third law of motion - "for every action there exists an equal and opposite reaction" - thermal propulsion involves the ejection of a hot propellant (gas) through a rocket nozzle, which acts on the spacecraft with an equal but opposite force, thus sending the spacecraft in a certain direction. The effectiveness of a propulsion system is expressed by the "rocket equation" [Sutton, 1992]:

$$v_{\text{exit}} = \sqrt{\frac{2\gamma RT_{\text{chamber}}}{(\gamma - 1)M_w}} \quad (1.1)$$

where v_{exit} represents the nozzle exit velocity of the propellant [m/s], M_w the propellant molecular weight [g/g-mol], γ the ratio of specific heats, and T_{chamber} the propellant chamber temperature [K]. Thus, a higher propellant exit velocity (and therefore a higher spacecraft velocity) is achieved with higher T_{chamber} and lower M_w .

The lowest possible value of M_w is associated with the lightest element, hydrogen (H_2). Hydrogen, which is in gaseous form even at room temperature, has been widely used as the propellant of choice in both operating chemical rockets (where it is in the form of liquid hydrogen - LH_2) as well as in nuclear rocket engines. The main difference is that in nuclear rockets, H_2 is the only required propellant, whereas in chemical rockets the additional requirement of the oxidizer results in a much larger M_w than for nuclear systems. The limiting factor on the performance of rocket engines to date, however, has been the magnitude of T_{chamber} . This value, which cannot

... ..

3.2.1. Rocket Thrust Equation (TE)

Based on Newton's third law of motion - for every action there exists an equal and opposite reaction - thrust propulsion involves the ejection of a hot propellant (gas) through a rocket nozzle which acts on the spacecraft with an equal but opposite force, thus causing the spacecraft to accelerate. The effectiveness of a propulsion system is measured by the "thrust equation" (Bertone 1997):

$$F_{thrust} = \dot{m} v_{exhaust} + (p_{nozzle} - p_{ambient}) A_{nozzle} \tag{3.1}$$

where $v_{exhaust}$ represents the nozzle exit velocity of the propellant [m/s], \dot{m} the propellant mass flow rate [kg/s], p_{nozzle} the nozzle exit pressure [Pa], and $p_{ambient}$ the ambient pressure [Pa]. Thus, a higher propellant exit velocity (and therefore a higher specific impulse) is achieved with lighter T_{comb} and lower M_{air} .

The lowest possible value of M_{air} is associated with the lightest element hydrogen (H₂), which is in gaseous form even at room temperature. Hydrogen has been widely used as the propellant of choice in both operating chemical rockets (where it is in the form of liquid hydrogen - LH₂) as well as in certain rocket engines. The main difference is that in rockets, H₂ is the only regulated propellant whereas in chemical rockets the additional requirement of the vehicle results in a much larger M_{air} due to other system. The limiting factor on the performance of rocket engines is T_{comb} , however, has been the magnitude of T_{comb} . This value which cannot

exceed the reaction temperature, has been on the order of 2,500-4,000 K for chemical propellants [Sutton, 1992]. Nuclear reactors, depending on their design, have been associated with potential propellant chamber temperatures of 3,000-100,000 K [Angelo and Buden, 1985; Bennett, 1990; Bennett *et al.*, 1994]. Thus, the use of nuclear reactors for space applications is extremely interesting in the field of space propulsion, where they can provide significant performance benefits over even the best chemical propulsion systems [Borowski, 1990; Borowski, 1991].

1.3. Space Nuclear Thermal Propulsion Research

The research area of application of nuclear reactors for space propulsion is relatively new in terms of visibility and development of systems. Nuclear propulsion research was initiated in the 1950's [Alperin and Sutton, 1959; Penner, 1961; USAEC, 1967], but due to a never established long-term space exploration goal (where nuclear propulsion would provide the greatest advantages) and without a commitment to a mission, no actual application of space nuclear propulsion reactors ever materialized. The fascinating subject of designing nuclear reactors to provide propulsion, as well as the inherent possibility of very high performance parameters, has kept the research alive; new propulsion reactor designs have been proposed, widening the possibilities for space exploration. The work presented in this dissertation attempts to contribute in a small way to that goal - furthering the knowledge base related to NTP.

1.4. Focus of this Dissertation

This Dissertation focuses on analyzing the feasibility of one particular NTP concept: the gaseous core Nuclear Light Bulb (NLB) rocket engine. Emphasis is placed on analyzing the thermalhydraulics characteristics of the unit-cell NLB engine, consisting of a single reactor cavity surrounded by segmented propellant channels and a low-temperature moderator/reflector.

...the reactor... the use of nuclear reactors for space applications is extremely... significant performance benefits over even the best chemical propulsion... systems [Bowers, 1980; Bowers, 1971].

1.3 Space Nuclear Thermal Propulsion Research

The research area of application of nuclear reactors for space propulsion is relatively new in terms of visibility and development of systems. Nuclear propulsion research was initiated in the 1950's [Lichten and Gifford, 1952; Farnes, 1961; US AEC, 1971] but due to a near existential long term space exploration goal (where nuclear propulsion would provide the greatest advantages) and without a commitment to a mission, no actual application of space nuclear propulsion reactors was materialized. The fascinating subject of designing nuclear reactors to provide propulsion, as well as the inherent possibility of very high performance parameters, has kept the research alive. New propulsion reactor designs have been proposed, widening the possibilities for space exploration. The work presented in this dissertation attempts to contribute to a small way to that goal - gathering the knowledge... also related to NTP.

1.4 Focus of the Dissertation

The Dissertation focuses on analyzing the feasibility of one particular NTP concept: the gas-core core Nuclear Light Bulb (NLB) reactor engine. Emphasis is placed on analyzing the thermodynamic characteristics of the engine. The engine consists of a single reactor cavity surrounded by asymmetric propellant channels and a low temperature helium reflector.

Since the majority of NLB-related research work was carried out in the 1960's and was terminated prior to final design and development, a comprehensive analysis of the concept was never performed [Clark and McLafferty, 1970]. This became the motivation behind the research work presented in this Dissertation. The goal is to present a comprehensive thermalhydraulics analysis of the unit-cell NLB engine and indicate whether the concept is feasible with today's technology.

1.5. Structure of the Dissertation

This Dissertation is structured to facilitate reader insight into the technical and historical background of the NLB concept and also of the methodology of analysis developed by the author. The Dissertation starts with Chapter 1, which contains an introduction to NTP and summarizes the focus and structure of the Dissertation. Chapter 2 presents the NLB rocket engine in its baseline configuration, and outlines the original designers' ideas. Chapter 3 focuses specifically on the unit-cell NLB engine and identifies the original assumptions which were the motivating factor for the in-depth analysis performed here. Chapter 4 presents the basis for originality of this research and outlines the research goals. Chapter 5 presents the proposed methodology of analysis. Chapters 6 and 7 provide the heat transfer and neutronics theory pertinent to this research. Chapter 8 presents the pertinent rocket propulsion theory. Chapter 9 discusses the structure and features of the GNRATR-1D thermalhydraulics code. The results of the thermalhydraulics analysis in (r) geometry are given in Chapter 10. Chapter 11 provides the results of the spectral analysis of radiative heat transfer in the silica wall. Chapter 12 provides the results of a film cooling analysis of the solid moderator/reflector regions. The conclusions of this research work, including a feasibility assessment of the unit-cell NLB engine, are presented in Chapter 13, while the author's recommendations for any potential future work are given in Chapter 14.

A series of Appendices (A-L) to this Dissertation provide listings of pertinent computer programs and associated input/output files.

From the analysis of the literature, it was found that the majority of the research work in this area has been carried out in the field of internal combustion engines and the use of a computer-aided analysis of the engine was found to be a promising area for research. The aim of the research was to provide a comprehensive theoretical analysis of the engine and to provide a computer-aided analysis of the engine. The goal is to provide a comprehensive theoretical analysis of the engine and to provide a computer-aided analysis of the engine. The goal is to provide a comprehensive theoretical analysis of the engine and to provide a computer-aided analysis of the engine.

1.2. Structure of the Dissertation

The Dissertation is structured as follows: Chapter 1 contains the introduction to the research and the objectives of the study. Chapter 2 contains the literature review and the theoretical background of the research. Chapter 3 contains the description of the engine and the test conditions. Chapter 4 contains the description of the test rig and the test results. Chapter 5 contains the description of the test results and the comparison with the theoretical results. Chapter 6 contains the description of the test results and the comparison with the theoretical results. Chapter 7 contains the description of the test results and the comparison with the theoretical results. Chapter 8 contains the description of the test results and the comparison with the theoretical results. Chapter 9 contains the description of the test results and the comparison with the theoretical results. Chapter 10 contains the description of the test results and the comparison with the theoretical results. Chapter 11 contains the description of the test results and the comparison with the theoretical results. Chapter 12 contains the description of the test results and the comparison with the theoretical results. Chapter 13 contains the description of the test results and the comparison with the theoretical results. Chapter 14 contains the description of the test results and the comparison with the theoretical results.

A table of Contents (A-1) to the Dissertation provides details of the structure of the Dissertation. The table of Contents is given in the following table.

CHAPTER 2

THE NUCLEAR LIGHT BULB ROCKET ENGINE

2.1. The Gaseous Core Reactor Concept

The concept of the Gaseous Core Reactor (GCR) was first proposed in the mid-1950's in conjunction with studies on advanced missile concepts. The possibility of using GCR technology was first seriously discussed at Los Alamos Scientific Laboratory (LASL) [Everett and Ulam, 1955; Longmire *et al.*, 1958]. The possibility of virtually unlimited fuel and propellant exit temperatures was the motivating factor behind all GCR research work.

The principle behind the GCR is relatively simple: suspend a gaseous highly enriched uranium fuel cloud in a critical configuration, and pass hydrogen propellant in close proximity to maximize heat transfer. Fluid mechanic confinement, i.e., circulation of a light gas around the uranium core, is used to maintain the very hot fuel in a critical configuration and away from the solid walls. The light gas can either be the hydrogen propellant itself, or an intermediate (chemically inert) buffer gas such as neon or argon [Latham and Rodgers, 1972b]. The former arrangement, which allows for physical contact between the fuel and the propellant, is referred to as an open-cycle GCR, while the latter, enhanced with some additional features, is generally referred to as a closed-cycle GCR. The flow profile of a closed-cycle GCR is generally referred to as "vortex-stabilized," as the fuel is intended to be suspended within a buffer gas vortex.

2.2. NLB Rocket Engine Background

The closed-cycle Nuclear Light Bulb (NLB) rocket engine is based on an idea developed at the United Aircraft Research Laboratories - UARL (now the United Technologies Research Center - UTRC) by G.H. McLafferty during the late 1950's. The actual research work started in 1959, and consisted of investigating the characteristics of generalized vortex-stabilized engines, with

CHAPTER 1 THE NUCLEAR LIGHT BULB ROCKET ENGINE

1.1 Introduction

The concept of the Nuclear Core Reactor (NCR) was first proposed in the mid-1950s in conjunction with studies on advanced nuclear concepts. The possibility of using NCR technology was first seriously discussed at Los Alamos National Laboratory (LANL) by Lewis and Henry [1] in a report of 1956. The possibility of directly utilizing fuel and propellant as components was the motivating factor behind all NCR research work.

The objective behind the NCR is to directly utilize a gaseous fuel, which is contained in a fuel tank, in a hot cell configuration, and pass hydrogen produced in close proximity to maximize heat transfer. Fuel molecules are contained in a chamber of a light gas toward the reaction zone in order to maintain the very hot fuel in a critical configuration and away from the solid walls. The light gas can either be the hydrogen propellant itself or an intermediate chemically inert buffer gas such as neon (Latham and Rodgers [2]). The burner arrangement which allows for physical contact between the fuel and the propellant is referred to as an open-cycle NCR while the burner chamber with some additional features is generally referred to as a closed-cycle NCR. The flow pattern of a closed-cycle NCR is generally referred to as "reverse-diffusion," as the fuel is intended to be suspended within a buffer gas vortex.

2.1.1 Nuclear Core Reactor

The closed-cycle Nuclear Light Bulb (NLB) rocket engine is based on an idea developed at the United States Atomic Energy Commission - LANL, now the United States Atomic Energy Commission - LANL, during the late 1950s. The actual research work started in 1957, and consisted of investigating the characteristics of gas-phase nuclear-fueled engines with

the work later expanding to include NLB-related research. The bulk of the work concentrated on the fluid mechanics investigation of vortex flow, since this was judged to be the primary potential show-stopper for both GCR concepts.

From 1967 onward all work was shifted to the NLB design, since it was determined through experimental and theoretical work that the fuel retention characteristics of the vortex-stabilized open cycle concept were lower than would be required with respect to economical considerations [McLafferty and Bauer, 1967]. The NLB design thus became the focus of the UARL gaseous core nuclear rocket program, and numerous experimental and theoretical results were obtained. A baseline configuration for the NLB rocket engine was assumed, and a wide range of parameters were derived for the assumed configuration [McLafferty and Bauer, 1967].

2.3. The NLB Rocket Engine

The NLB concept relies on the transfer of energy from a fissioning uranium fuel to hydrogen propellant by way of a buffer gas and a transparent fused silica wall. The proposed layout of the NLB concept, shown in Figure 2.1, involves fluid mechanic confinement of the uranium fuel by a vortex flow of buffer gas such as neon or argon. The buffer gas is injected from the transparent wall with an axial and tangential velocity component; it swirls around the fuel and ultimately passes along the axial centerline into a recirculator. The mixture of buffer gas, uranium fuel, and any fission products is then cooled by heat exchange with low-temperature bypass buffer gas [Rodgers and Latham, 1972].

As a result of the cooling, the nuclear fuel is condensed, centrifugally separated from the buffer gas, and collected in a fuel crucible zone. The fuel is then processed and prepared for re-injection into the cavity. The buffer gas component is cooled by rejection of heat to the primary hydrogen propellant, and is then pumped back into the transparent wall to drive the vortex. The heat-exchange loops of the NLB engine are discussed in more detail in Section 2.4 of this Dissertation.

The work done regarding the design of the engine is described in the following sections. The first part of the work is concerned with the design of the combustion chamber. The design of the combustion chamber is described in the following sections. The design of the combustion chamber is described in the following sections. The design of the combustion chamber is described in the following sections. The design of the combustion chamber is described in the following sections.

2.1. The HLB System

The HLB concept is based on the transfer of energy from a hydrogen stream to a hydrogen stream by way of a buffer gas and a transparent wall. The proposed layout of the HLB concept is shown in Figure 2.1. The HLB concept consists of the injection of a vortex flow of buffer gas such as neon or argon. The buffer gas is injected from the transparent wall with an axial and tangential velocity component. It swirls around the fuel and ultravioletly irradiates the axial combustion into a radiator. The volume of buffer gas remains fuel and any excess products is then cooled by heat exchange with low-temperature gases before the hydrogen and helium. (Latham 1971)

As a result of the swirling, the nuclear fuel is condensed centrifugally separated from the buffer gas and collected in a fuel injection zone. The fuel is then processed and prepared for injection into the cavity. The buffer gas component is cooled by injection of fuel to the primary hydrogen propellant and is then prepared for the transparent wall to drive the vortex. The heat exchange aspect of the HLB engine are discussed in more detail in Section 1.4 of the Dissertation.

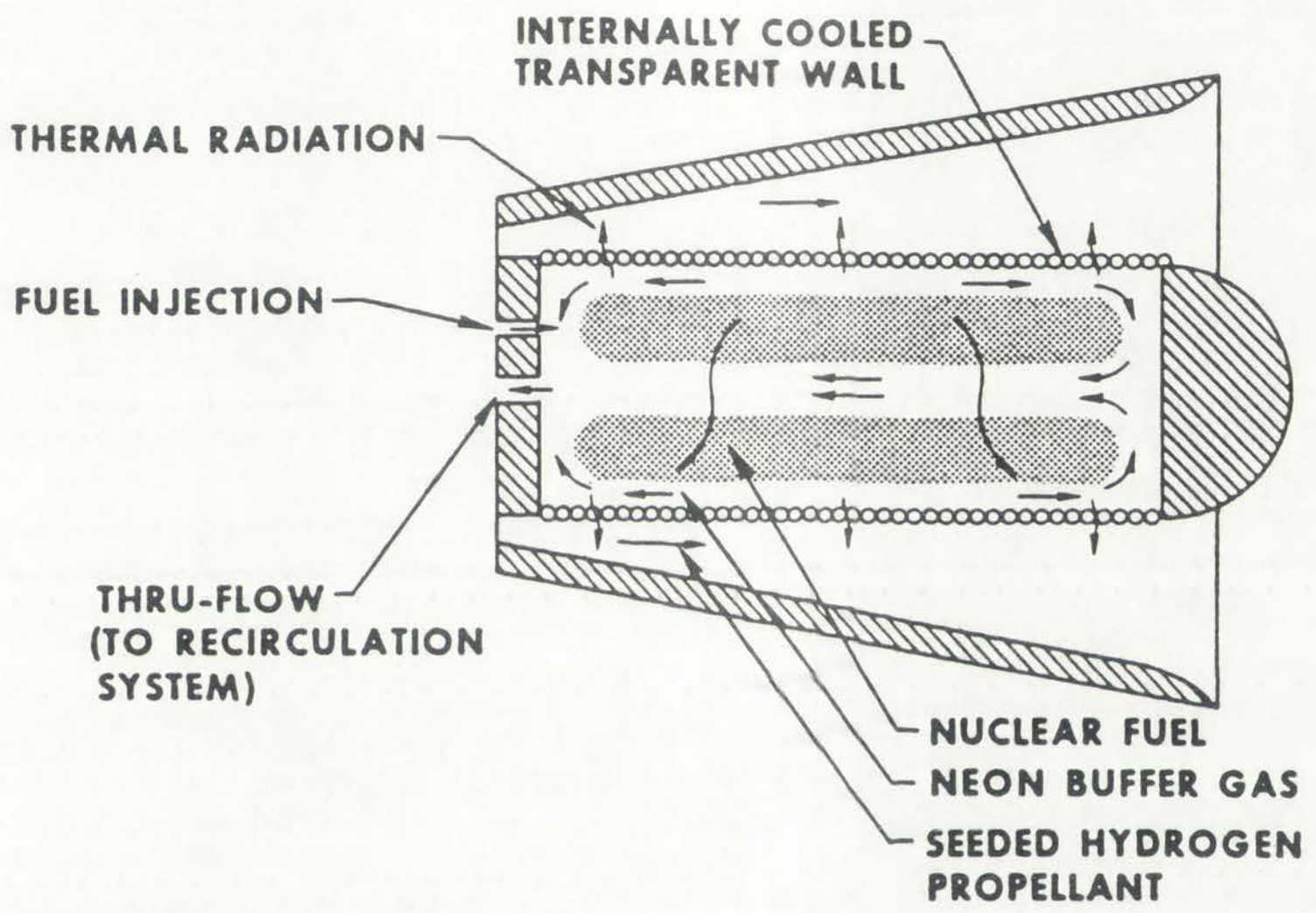


Figure 2.1: General layout of the NLB concept [Latham, 1990].

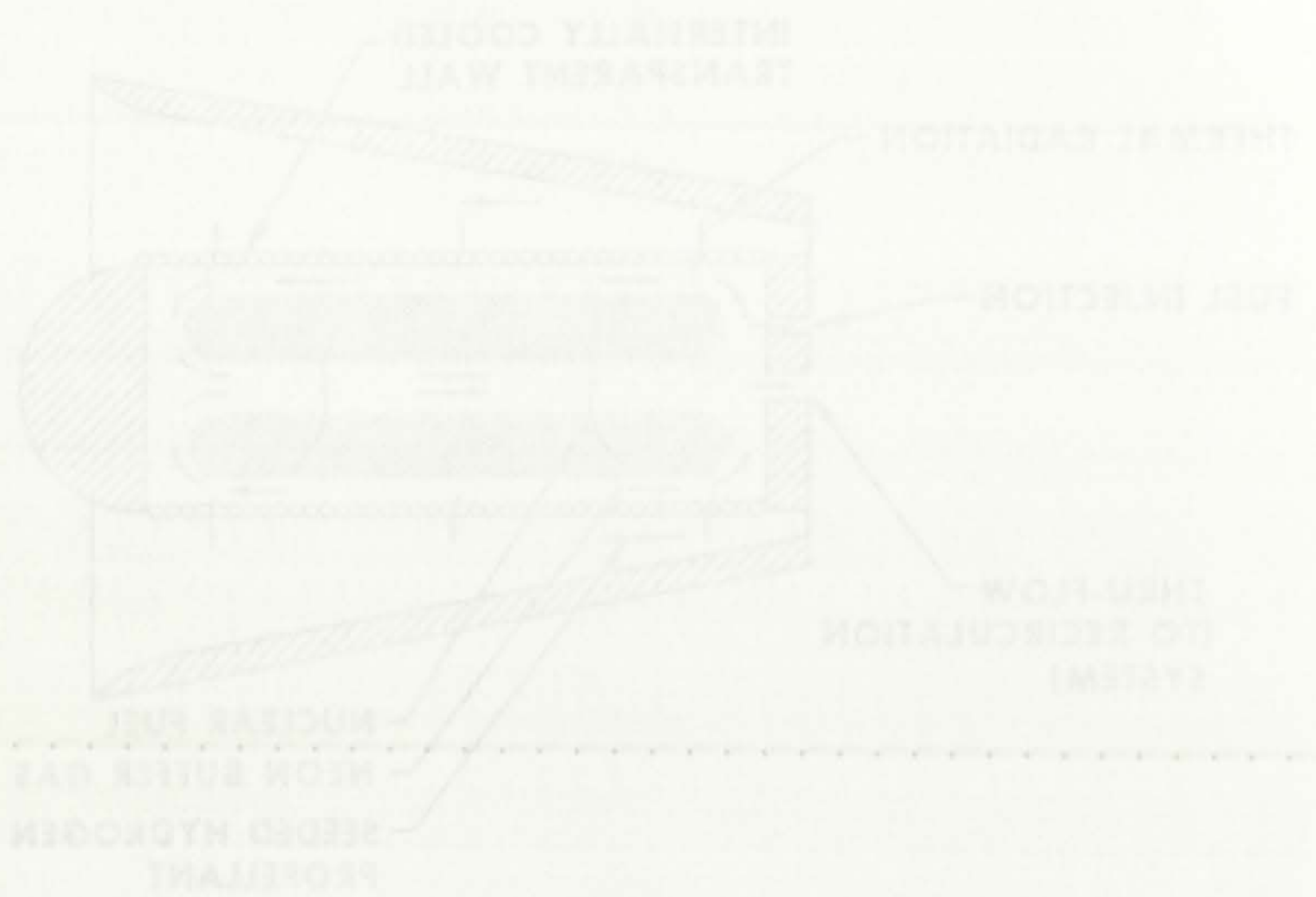


Figure 5.1. General layout of the NFB concept [Latham, 1990]

As a result of the recirculation of the fuel/buffer gas mixture, the NLB engine is intended to utilize only fresh fuel at any given time, thus reducing the amount of fission product poisons and minimizing the beginning-of-life (BOL) fuel mass. In addition, removal of the highly radioactive fission products from the reactor cavity could potentially reduce the consequences of a reactor accident either in Earth or other planetary orbit [Latham, 1990; Gauntt, 1992a].

2.4. NLB Rocket Engine Layout

Based on the layout shown in Figure 2.1, UARL developed a reference NLB rocket engine design. The design consisted of seven reactor cells, each with a separate fissioning core, transparent silica wall, and hydrogen propellant channel. The seven-cell design is shown in Figure 2.2, with cutaway views of the whole engine and of one cell. The forward portion of the engine would house the necessary heat exchangers, plumbing, pumps, and fluid separators, while the rear portion would contain the seven reactor "unit cells" immersed in a BeO moderator matrix and surrounded by a graphite reflector region. The choice of seven cells, as well as the dimensions of the NLB engine, was a "more-or-less arbitrary" decision [McLafferty and Bauer, 1967].

A more detailed technical drawing of the NLB engine is presented in Figure 2.3. The main heat exchangers are the H₂-buffer gas exchanger, facilitating the rejection of heat by the cavity-recirculated neon to the primary hydrogen propellant, and the H₂-H₂ exchanger, which facilitates heat rejection by the secondary H₂ loop (used to cool the transparent wall) to the primary H₂ loop (the propellant). A detailed flowchart for the various coolant, buffer gas, and fuel loops, heat exchangers, and pumps is shown in Figure 2.4 [Latham, 1990].

A close-up view of the seven-cell NLB engine is shown in Figure 2.5 [McLafferty and Bauer, 1967]. The cells are spaced relatively close together to reduce the total neutron leakage while at the same time allowing moderation of the neutrons leaving an individual cell [McLafferty and Bauer, 1967].

As a result of the investigation of the NLB engine, it is intended to make one last test at sea from this engine, the removal of piston product, valves and maintaining the performance (FCI) fuel water. In addition, removal of the highly radioactive products from the reactor core could potentially reduce the consequences of a reactor accident either in terms of environmental impact (Kumar, 1995).

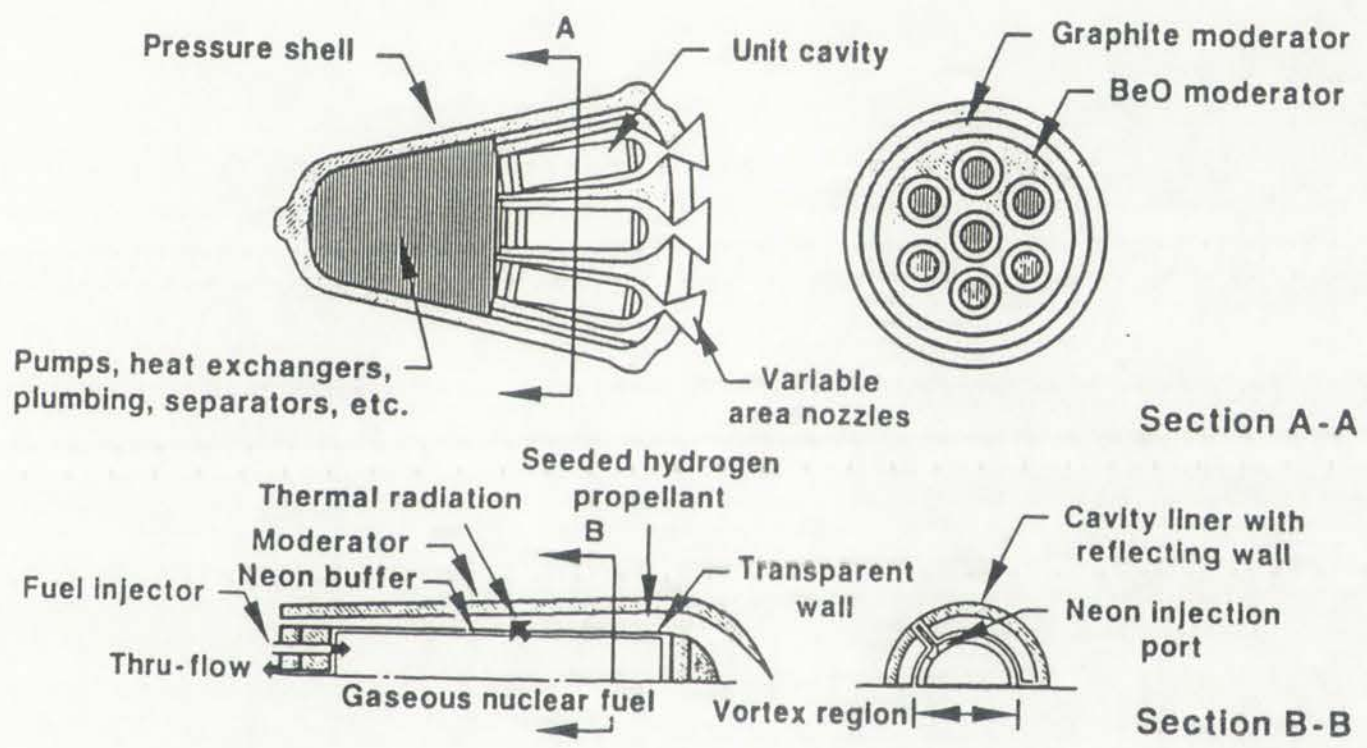
Figure 10

2.4 NLB Reactor Core Layout

Based on the layout shown in Figure 11, IAEA developed a reactor NLB reactor core design. The design consisted of seven reactor cells, each with a separate fueling core treatment area wall, and hydrogen propellant channel. The core cell design is shown in Figure 12, with various views of the whole engine and of core. The forward portion of the engine would house the necessary heat exchangers, pumps and fluid expansion while the rear portion would contain the seven reactor core cells immersed in a 100 rock salt matrix and surrounded by a graphite reflector region. The choice of rock salt, as well as the dimensions of the NLB engine, was a "one-of-a-kind" design (Mishra and Baur, 1997).

A more detailed technical drawing of the NLB engine is presented in Figure 13. The main heat exchangers are the H₂ boiler gas exchanger, facilitating the rejection of heat by the cavity vented from the primary hydrogen propellant and the H₂ gas exchanger which facilitates heat rejection by the secondary H₂ loop (and to cool the transport wall) to the primary H₂ loop (the propellant). A detailed layout for the various coolant buffer gas and fuel loop heat exchangers and pumps is shown in Figure 14 (Mishra, 1997).

A close-up view of the seven-cell NLB engine is shown in Figure 15 (Mishra and Baur, 1997). The cells are spaced relatively close together to reduce the total neutron leakage while at the same time allowing moderation of the neutrons leaving an individual cell (Mishra and Baur, 1997).



RB2738TX.002

Figure 2.2: Seven-cell baseline design of the NLB engine [Latham, 1990].

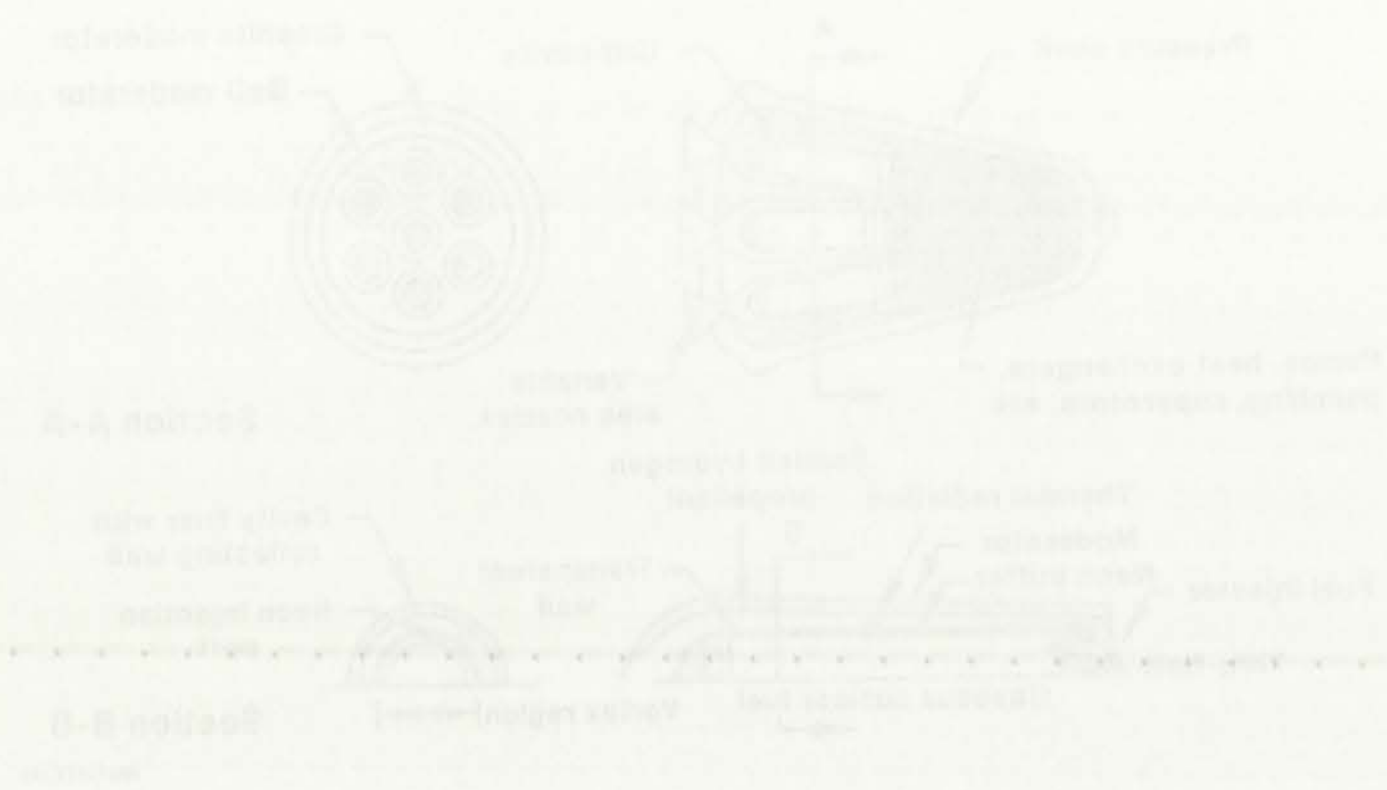


Figure 2. General design of the NLS engine (Latham 1991)

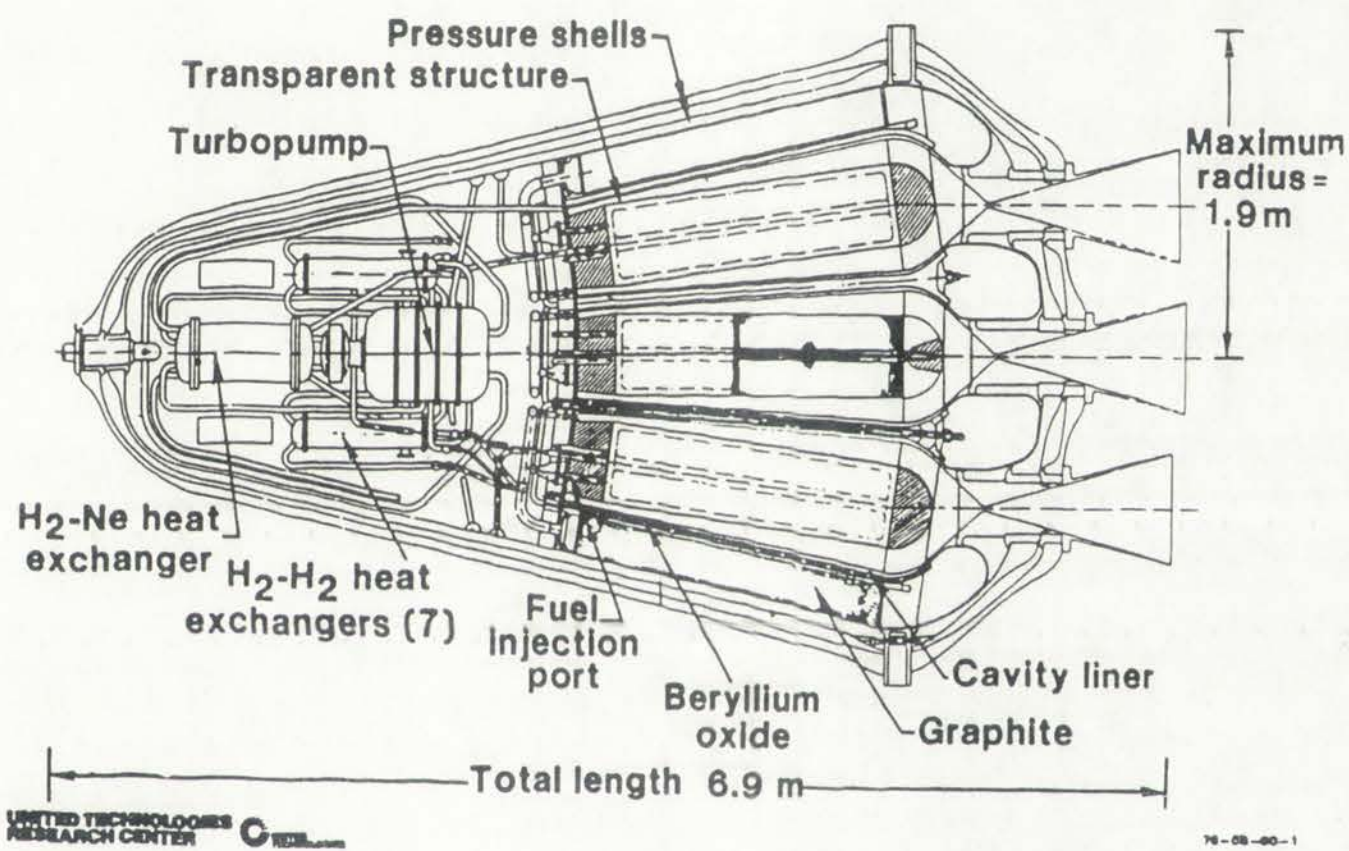
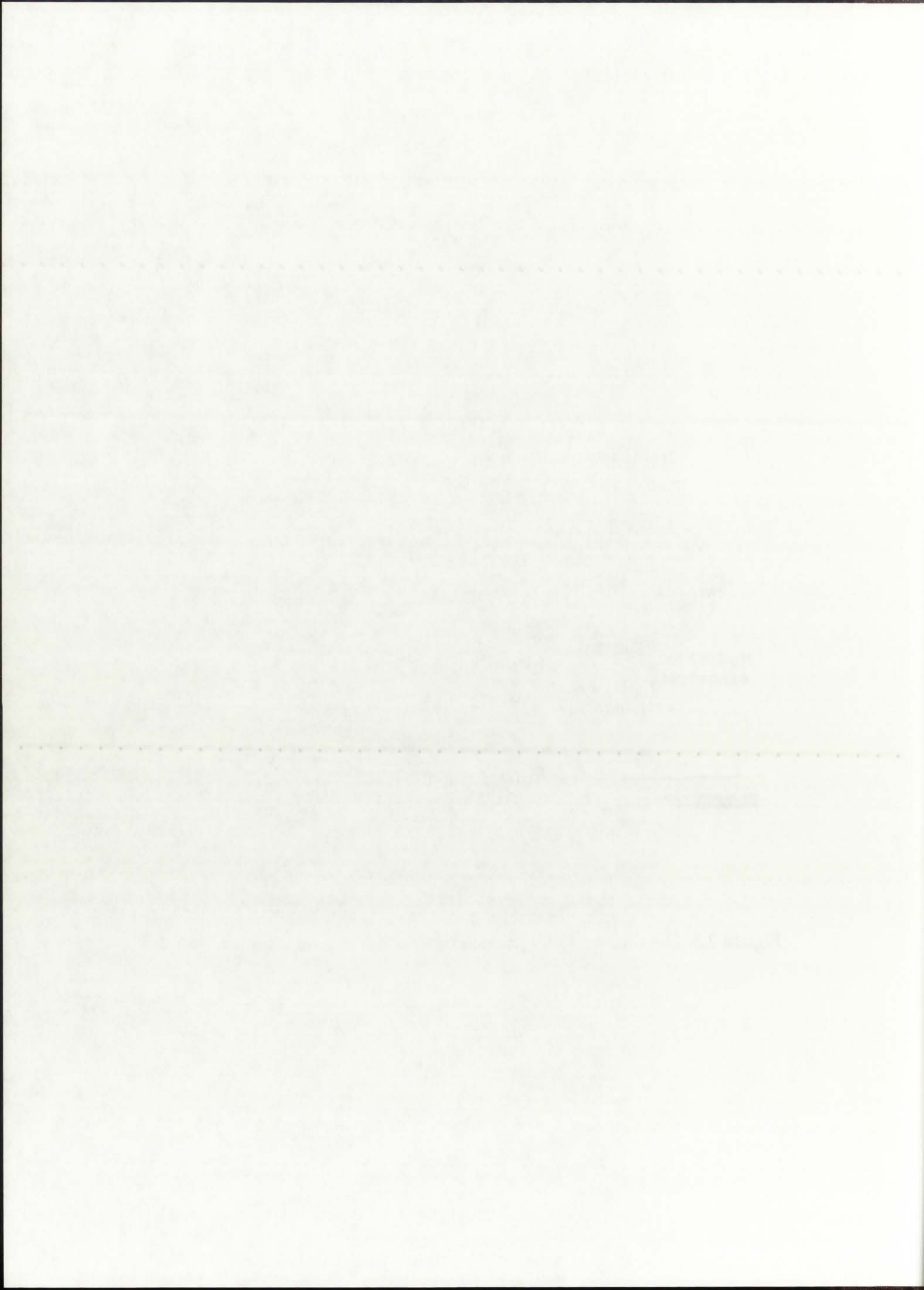


Figure 2.3: Detailed technical sketch of the NLB engine [Latham, 1990].



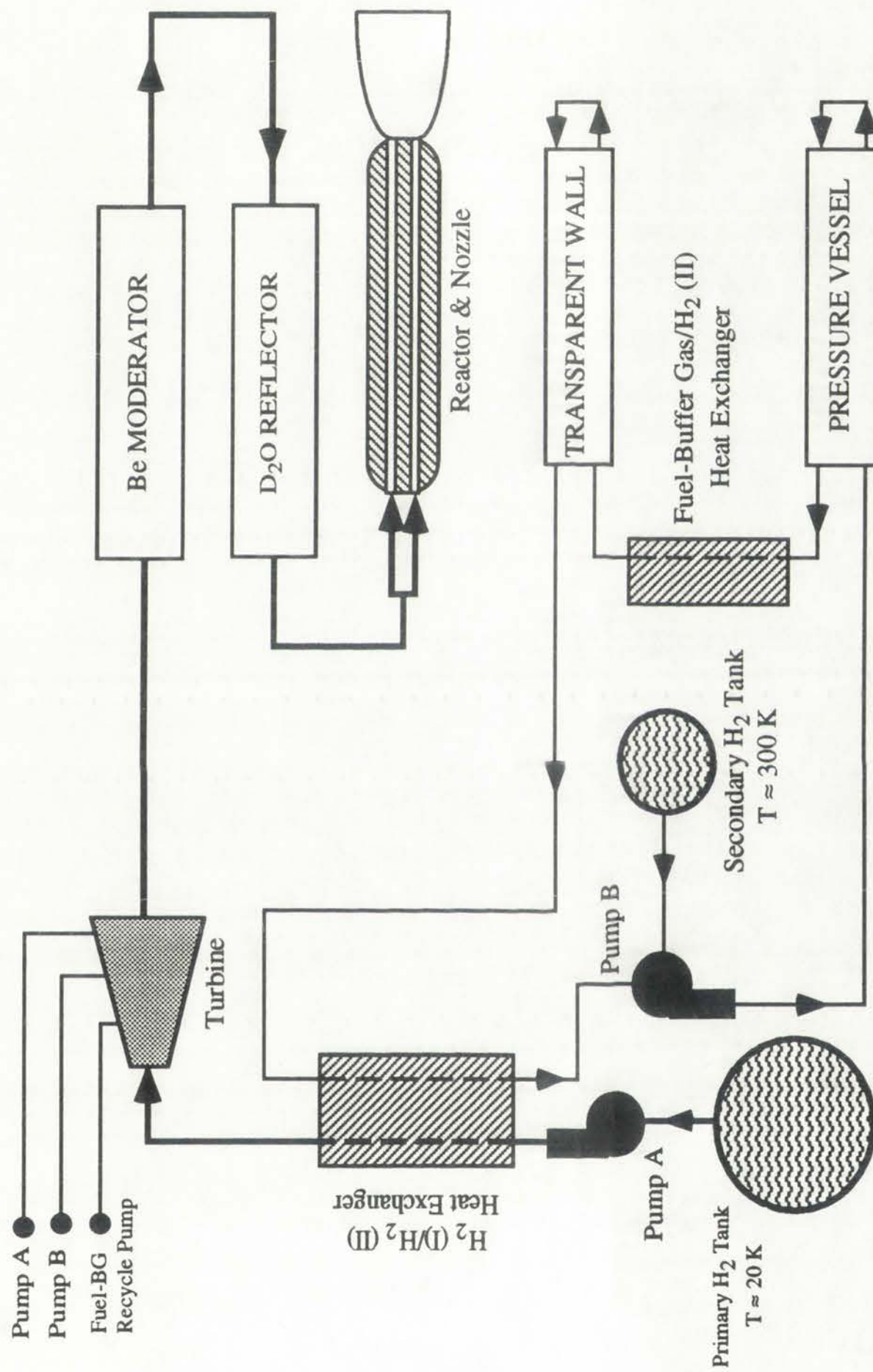


Figure 2.4: Simplified schematic diagram of the unit-cell NLB rocket engine cooling loops.

Figure 2: Schematic diagram of the proposed hybrid MEMS-based system for vibration measurement.



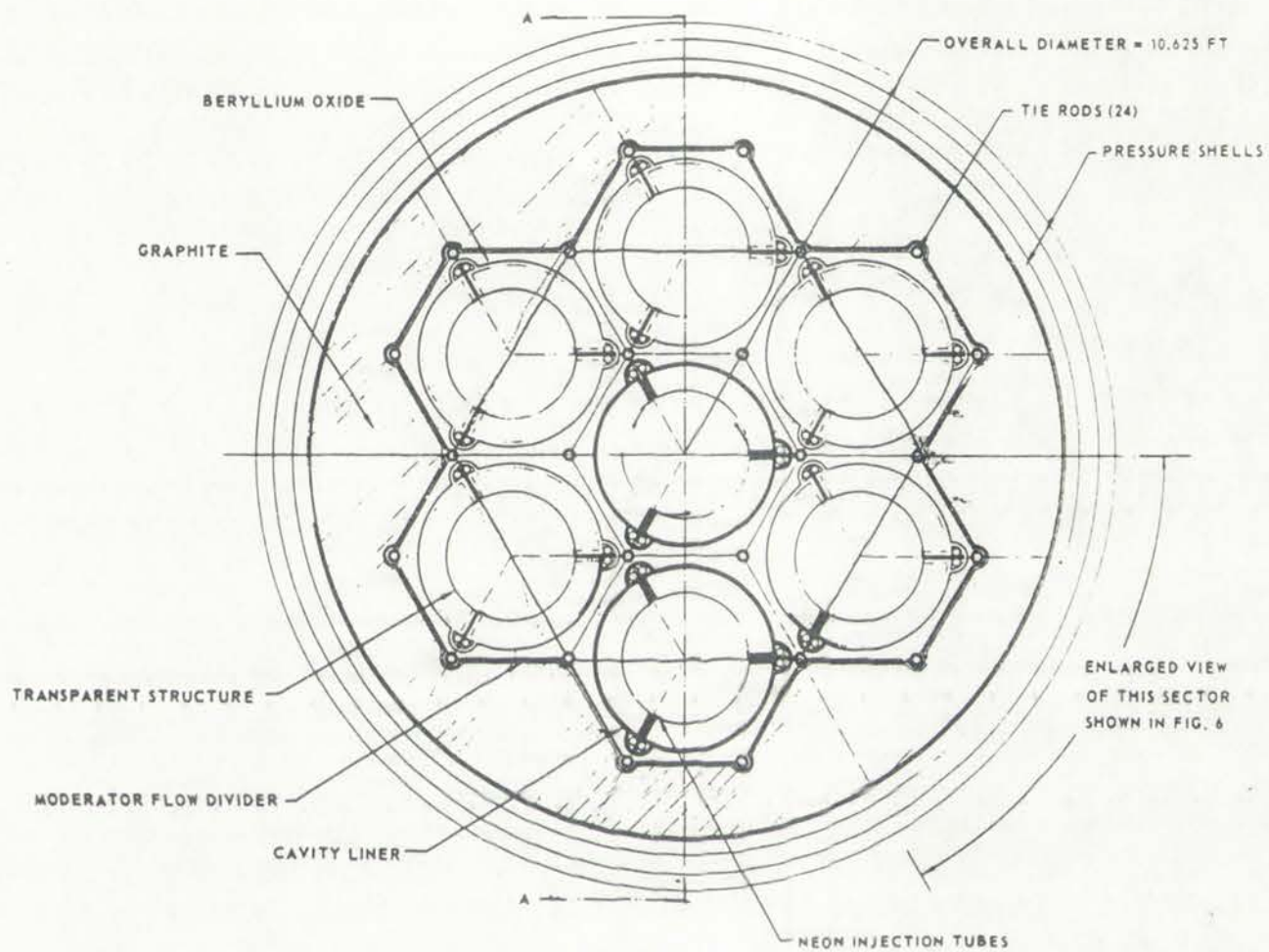


Figure 2.5: Close-up view of the seven-cell NLB engine
 [McLafferty and Bauer, 1967].



Figure 2-3 Close-up view of the combustion chamber of a four-cylinder internal combustion engine. [McLain and Jones, 1997]

Each of the seven cells of the baseline NLB engine is contained in a hexagonal matrix of BeO, with tie rods at each apex for structural strength. The seven cell hexagons are surrounded by a graphite reflector region. An enlarged view of one hexagonal cell is shown in Figure 2.6. This "slice" view corresponds to one-sixth of the total (r- θ) layout of the NLB engine, and shows in detail the components of the cell and the enclosed fuel cavity. The cell consists of three 120° segments joined together with three struts. The struts contain radial tubes which transport the buffer gas from the axially-oriented feeder tubes to the injection pipes inside the fuel cavity. The propellant cavity is lined with thin beryllium tubes coated with aluminum to maximize the reflectivity [McLafferty and Bauer, 1967].

2.5. NLB Performance Data

The intent of the NLB engine was to provide large specific impulse and high thrust, which would enable fast transit times to the Moon or Mars. The engine was designed to be boosted to high earth orbit (HEO) by a Saturn I-C chemical rocket and then started up to achieve the necessary escape trajectory [McLafferty and Bauer, 1967]. Because of the lack of computing capability, all of the performance parameters associated with the NLB were derived from a set of *assumed* baseline values which are discussed in the following paragraph. It is also important to note here that an NLB engine was never developed; the design features of the NLB discussed here were, for the most part, never verified or proven.

The performance data was derived from an *assumed* fuel radiating temperature of 8,333 K and an *assumed* propellant exit temperature of 6,667 K (assumed equal to 80% of the fuel temperature) [McLafferty and Bauer, 1967]. Based on an *assumed* fuel temperature of 8,333 K and an *assumed* fuel surface area of 16.6 m², a baseline thermal power of 4,600 MW_{th} was derived. Using the total thermal power and the hydrogen enthalpy at the assumed exit temperature, a hydrogen flow rate of 2.72 kg/sec per cell was derived [McLafferty and Bauer, 1967]. Propellant inlet and exit velocities were derived in a similar manner (all based on assumed baseline parameters).

The inlet of the MFB engine was to provide large specific impulse and high thrust which would enable fast transit time to the Moon or Mars. The engine was designed to be located in high earth orbit (HEO) by a Saturn V C-2 stage and was intended to achieve the necessary specific impulse, thermal shock and high thrust to achieve the necessary specific impulse, all of the performance parameters associated with the MFB were derived from a set of assumed baseline values which are discussed in the following paragraph. It is also important to note here that an MFB engine was never developed; the design features of the MFB discussed here were for the most part never verified in practice.

3.2 MFB Performance Data

The performance data was derived from an assumed fuel venting temperature of 3000 K and an assumed propellant exit temperature of 2000 K (assumed equal to IEP of the fuel injector) (McLachlan and Baines, 1967). Based on an assumed fuel temperature of 3000 K and an assumed fuel surface area of 100 cm², a baseline thrust power of 2000 MW_{th} was derived. Using the total thermal power and the hydrogen enthalpy of the assumed exit temperature a hydrogen flow rate of 2.72 kg/sec was derived. (McLachlan and Baines, 1967). Propellant inlet and exit velocities were derived in a similar manner (all based on assumed baseline parameters).

The performance data was derived from an assumed fuel venting temperature of 3000 K and an assumed propellant exit temperature of 2000 K (assumed equal to IEP of the fuel injector) (McLachlan and Baines, 1967). Based on an assumed fuel temperature of 3000 K and an assumed fuel surface area of 100 cm², a baseline thrust power of 2000 MW_{th} was derived. Using the total thermal power and the hydrogen enthalpy of the assumed exit temperature a hydrogen flow rate of 2.72 kg/sec was derived. (McLachlan and Baines, 1967). Propellant inlet and exit velocities were derived in a similar manner (all based on assumed baseline parameters).

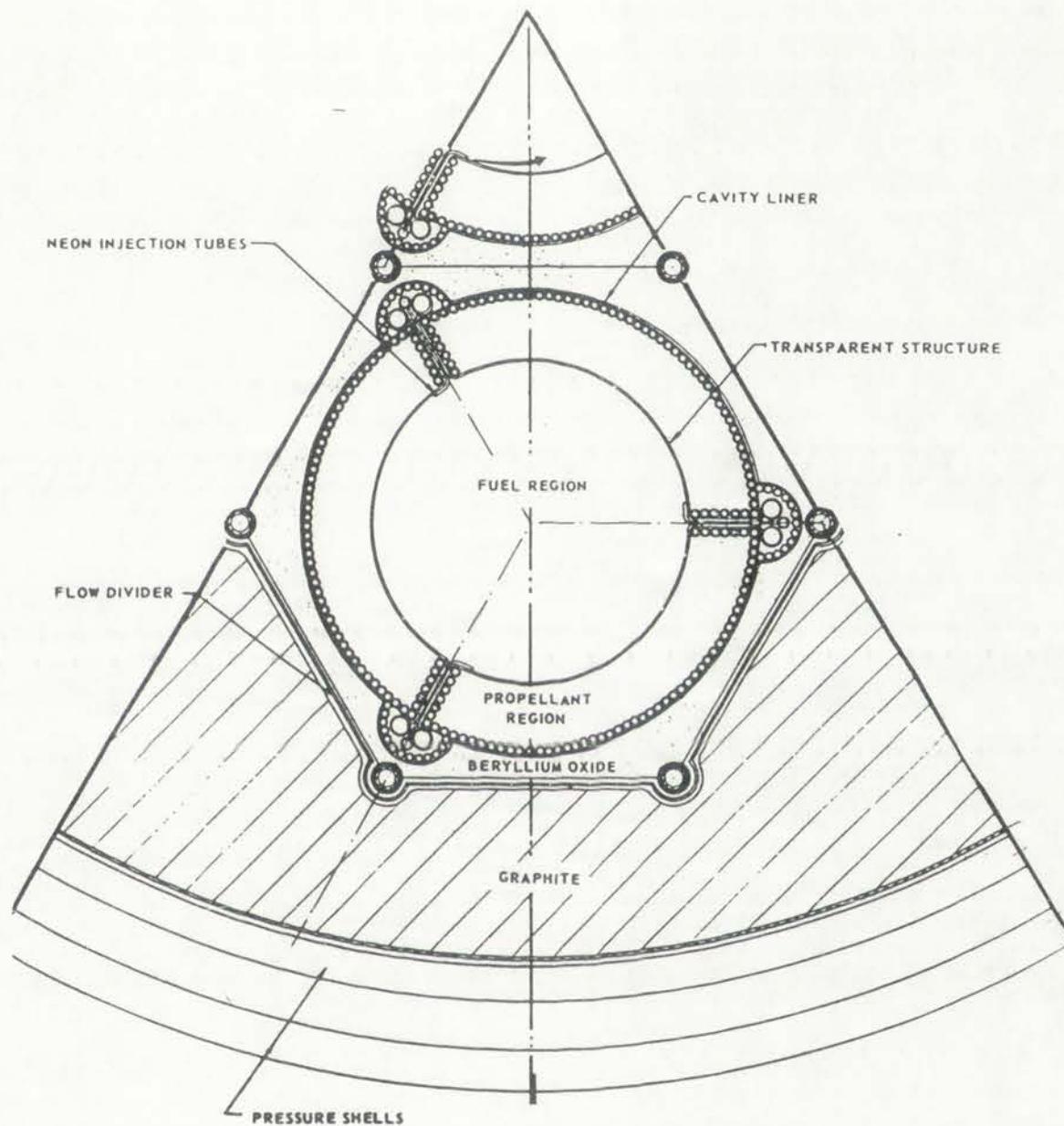
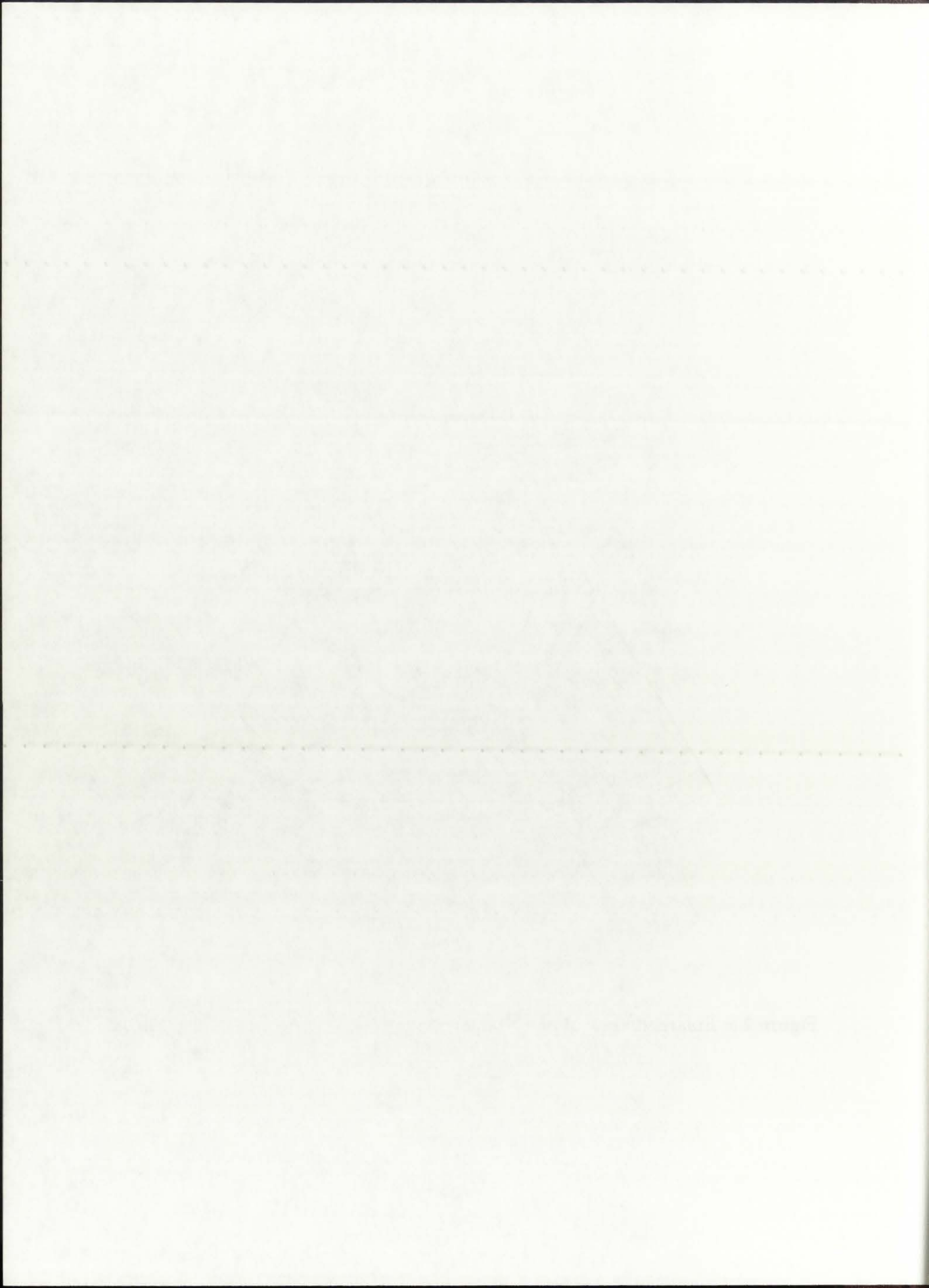


Figure 2.6: Enlarged view of one NLB engine cell [McLafferty and Bauer, 1967].



The specific impulse of the engine was derived to be approximately 1,870 sec, with a thrust of 409,000 N (92,000 lb_f). For all the UARL calculations, a uniform operating pressure of 50.65 MPa (500 atm) was *assumed*. Along with the reference engine characteristics, a set of parametric analyses was performed at UTRC to evaluate a range of performance characteristics. Power levels between 730 and 160,000 MW_{th} were proposed, as shown in Table 2.1, providing calculated specific impulses of 3,100 sec and thrusts of 9,500,000 N. The data, however, is based on *assumed* fuel and propellant temperatures, operating pressures, and dimensions, and therefore serves more as an illustration of the designers' goals than an accurate indicator of NLB performance characteristics. One needs to keep in mind that the fuel radiating temperatures were assumed first, and then were used in a simple correlation to calculate the total thermal power of the engine. In addition, specific impulse and thrust were calculated on the basis of limited hydrogen data.

2.6. Experimental and Theoretical Validation

The NLB concept is an extremely complex system which even today poses numerous engineering and technical challenges in terms of design and development. During the 1959 - 1973 period, UARL concentrated on proof-of-concept studies to determine the feasibility of the design and identify any potential "show-stoppers." The studies consisted of experimental and theoretical analyses, and concentrated mostly on the fluid mechanics aspects of gas confinement by vortices, which were judged to be the most important problems associated with the NLB concept.

Analytical studies and small-scale experiments began in the early 1960's and involved cold flow (fluid mechanics only) and hot flow (coupling of heat transfer to fluid mechanics) demonstrations. A simulated fuel gas, UF₆, was injected into an argon (Ar) vortex and fuel partial pressures, velocities, and densities were measured. Tests were also performed using radio frequency (RF) heating which achieved simulated fuel temperatures of 9,500 K and at the same time provided adequate fluid mechanic confinement of the simulated fuel by Ar buffer gas [Gauntt *et al.* 1992b].

The specific purpose of the engine was defined to be approximately 1000 hp with a thrust of 40,000 N (9000 lbf) for all the UARL calculations. A common operating condition of 50.0 MPa (720 atm) was assumed. Along with the various engine characteristics, a set of geometric angles was generated as UARL to obtain a range of performance characteristics. Power levels between 200 and 180,000 MW were proposed as shown in Table 2.1, providing various specific purposes of 0.100 sec and thrust of 2,000,000 N. The data however is based on assumed fuel and propellant temperatures, operating pressure, and dimensions and therefore errors more as an illustration of the design's goals than an accurate indicator of NLS performance characteristics. One needs to bear in mind that the fuel velocity temperatures were assumed 300 K and that there was a simple correlation to calculate the total thrust power of the engine. In addition, specific impulses and thrust were calculated on the basis of liquid hydrogen data.

2.1 Experimental and Theoretical Validation

The NLS concept is an extremely complex system which even today poses numerous engineering and technical challenges in terms of design and development. During the 1950 - 1970 period, UARL concentrated its effort on concept studies to determine the feasibility of the design and identify any potential "show-stoppers". The studies consisted of experimental and theoretical analyses and concentrated mostly on the fluid mechanics aspects of gas confinement, vortex which were judged to be the most important problems associated with the NLS concept.

Analytical studies and small-scale experiments began in the early 1960's and involved cold flow (fluid resistor only) and hot flow (loading of heat transfer to fluid mechanics) experiments. A simulated fuel gas, UFG, was injected into an axial (A) vortex and fuel partial pressures, velocities and densities were measured. Tests were also performed using radio frequency (RF) heating which achieved simulated fuel temperatures of 2,000 K and at the same time provided adequate fluid mechanic confinement of the simulated fuel by a buffer gas (Lund et al. 1982).

TABLE 2.1
 Estimated NLB rocket engine power levels and performance parameters
 [Latham, 1990]

Thermal Power [MWth]	Fuel Temperature [K]	Isp [sec]	Thrust [kN]
730	5,000	1,120	98
2,500	7,000	1,570	245
4,600	8,333	1,870	410
10,000	10,000	2,150	785
22,000	12,000	2,500	1,470
51,000	15,000	2,700	3,140
160,000	20,000	3,100	9,420

NOTE: The reference NLB parameters (i.e., encountered most often in literature) are highlighted in boldface.

TABLE 1
 Performance parameters of the engine at various operating conditions

Operating Condition	Thermal Efficiency (%)	Specific Fuel Consumption (g/kWh)	Specific Power (kW/kg)
1000 RPM	28.5	200.0	1.425
1500 RPM	29.0	180.0	1.611
2000 RPM	29.5	160.0	1.875
2500 RPM	30.0	140.0	2.143
3000 RPM	30.5	120.0	2.500
3500 RPM	31.0	100.0	2.857
4000 RPM	31.5	80.0	3.214
4500 RPM	32.0	60.0	3.571
5000 RPM	32.5	40.0	3.929

NOTE: The values are for a standard day (15°C, 101.3 kPa, 24.45% humidity) and are based on the manufacturer's data.

Experiments like the ones mentioned previously were deemed as demonstrating that a plasma with temperatures in excess of 9,500 K could be confined by a vortex flow. Altogether, approximately 200 experiments of all kinds were performed at UARL, most of them geared toward the fluid mechanic confinement proof-of-concept [Latham, 1990; Gauntt et al., 1992b].

In addition to the fluid mechanics experiments and theoretical validation, significant results were obtained in the area of determining the thermo-optical properties of the materials involved in the NLB design. Data for fuel, buffer gas, transparent wall, propellant, and seed opacities was presented in numerous UARL reports. Since most of the work was performed in the late 1960's and early 1970's, the methodology used generally consisted of simple zero-dimensional calculations, as evidenced in [McLafferty and Bauer, 1967]. The underlying goal, however, was to establish a proof-of-concept and validate the feasibility of the NLB engine; the research work was planned to take as much time as needed, and future advances in computational capabilities, as well as materials science, were counted on to solve any significant problems [Latham and Rodgers, 1972].

2.7. Progress of NLB Research Work

The bulk of NLB-associated research was carried out at UARL between 1959 and 1973. During that time, the concept was introduced, preliminary studies were performed, and numerous experimental validations were carried out. A number of the experiments were carried out at UARL facilities (the DC- and arc-heater assemblies) while others were performed at the Los Alamos Scientific Laboratory (LASL) - the latter involving subcritical UF₆. Along with the experimental and theoretical validation of the NLB concept, numerous studies were conducted involving parametric analysis of engine performance, its comparison to open-cycle concepts, and possible variations to the reference NLB engine. Full-flowing critical tests were planned for mid- to late-1970's, with engine development in the 1980's [McLafferty and Bauer, 1967].

Experiments like the one described previously were found as the most promising for a study with implications in a range of 0.300 X could be followed by a series of 100 experiments approximately 100 experiments or all trials were performed at UARL, most of them given toward the final mechanical studies in the field of control (Latham, 1990; Latham et al., 1973).

In addition to the field mechanical experiments and theoretical validation algorithms results were obtained in the area of describing the three-optimal properties of the instabilities involved in the VLS design. Data for fuel buffer gas management, wall properties and wall position was provided in numerous IARL reports. Some part of the work was performed in the late 1950's and early 1970's, the methodology used generally consisted of simple two-dimensional calculations as outlined in [McLain and Baker, 1957]. The underlying goal however was to establish a good-of-concept and validate the feasibility of the VLS engine. The research work was planned to take as much time as needed and future advances in computational capabilities as well as materials science were counted on to solve any significant problems (Latham and Rodgers, 1973).

2.2. Progress of VLS Research

The bulk of VLS research research was carried out at UARL between 1950 and 1970. During that time the concept was introduced, preliminary studies were performed and numerous experimental verifications were carried out. A number of the experiments were carried out at UARL facilities (the DC and arc-heater experiments) while others were performed at the Los Alamos Scientific Laboratory (LASL) - the latter involving technical staff. Along with the experimental and theoretical validation of the VLS concept numerous studies were conducted involving practical analysis of engine performance. The comparison to open cycle concepts and possible variations to the reactor VLS engine. Fuel-burning engine tests were planned for mid to late 1950's who engine the document is the 1950's [McLain and Baker, 1957].

The critical, full-flowing tests were viewed as the intermediate step toward the development and ground testing of a full-scale NLB engine. A major portion of 1971 and 1972 was spent at UARL outlining and organizing for the critical tests, which were planned to be carried out within the cavities of existing research reactors. A summary of the then-planned tests is the subject of the introductory sections of Chapter 3.

The planned NLB concept tests never materialized, because in 1973 the space nuclear propulsion program was terminated as a result of restructuring of the nation's space exploration goals. Emphasis was shifted from long-term, long-range planetary exploration and colonization to Earth-orbit flights -- namely the reusable Space Shuttle launch vehicle. This resulted in the termination of all GCR design and experimental work. A small portion of NLB-associated research was maintained as a result of a Congressional initiative toward application of gaseous core technology for terrestrial power generation, but even this ended in 1976 [Latham, 1990]. With that came the end of NLB research; a total of 165 technical reports were issued, most of them authored by UARL [Latham, 1990].

Research on the NLB concept was dormant until 1989, when President George Bush initiated the Space Exploration Initiative (SEI). With the envisioned journey to Mars in the period 2010-2020, the original NLB research team at UARL (now UTRC) revived the NLB studies. A number of workshops were held between 1990 and 1992 concentrating on advanced concepts for space nuclear propulsion, and the NLB engine again became of interest to NASA and the Department of Energy (DOE) [Borowski, 1991]. In 1991, UTRC and Sandia National Laboratories (SNL) proposed "in-reactor" testing of the NLB, with the goal of continuing where the original research left off in 1973 and conducting a series of critical, flowing experiments at Sandia facilities [Gauntt, 1992a]. To that end, analytical approximations of the fluid mechanics, neutronics, and heat transfer parameters were carried out in preparation for the actual experiments [Gauntt *et al.*, 1993]. The experiments were planned to take place in the SNL Annular Core Research Reactor (ACRR); a proposed layout of the experimental assembly is depicted in Figure 2.7 [Gauntt, 1992a].

The initial, preliminary work was done at the University of Michigan for the development and testing of a full scale MFB reactor. A major portion of 1971 and 1972 was spent at UACI, with the major portion of the critical tests which were planned to be carried out within the context of existing research reactors. A summary of the theoretical work in the subject of MFB reactors appears in Figure 1.

The present MFB reactor was never established because in 1973 the space reactor program was terminated as a result of reevaluation of the nation's space exploration goals. However, the initial work was done in the area of plasma physics and ionospheric research in the laboratory of the University of Michigan. The results of the MFB reactor design and experimental work. A small portion of MFB reactor research was terminated as a result of a Congressional initiative toward reduction of space program and research for terrestrial power generation, but even the end of 1974 (Lathrop, 1980). With that case the end of MFB reactor, a total of 15 technical reports were issued, most of them authored by UACI (Lathrop, 1980).

Research on the MFB concept was dormant until 1982, when President George Bush initiated the Space Exploration Initiative (SEI). With the renewed journey to Mars in the period 2010-2020, the original MFB research team at UACI (now URC) revived the MFB studies. A number of workshops were held between 1980 and 1982 concentrating on advanced concepts for space reactor propulsion, and the MFB engine again became of interest to NASA and the Department of Energy (DOE) (Bowers, 1981). In 1981, UTIC and Sandia National Laboratories (SNL) proposed a reactor study of the MFB with the goal of establishing where the original research lab is in 1981 and conducting a series of critical flow, experiments at Sandia facilities (Gandy, 1982). To that end, analytical experiments of the full reactor for momentum and heat transfer problems was carried out in preparation for the recent experiments (Gandy et al., 1982). The experiments were planned to take place in the SNL Auxiliary Core Research Reactor (ACRR); a proposed layout of the experimental assembly is depicted in Figure 2 (Gandy, 1982).

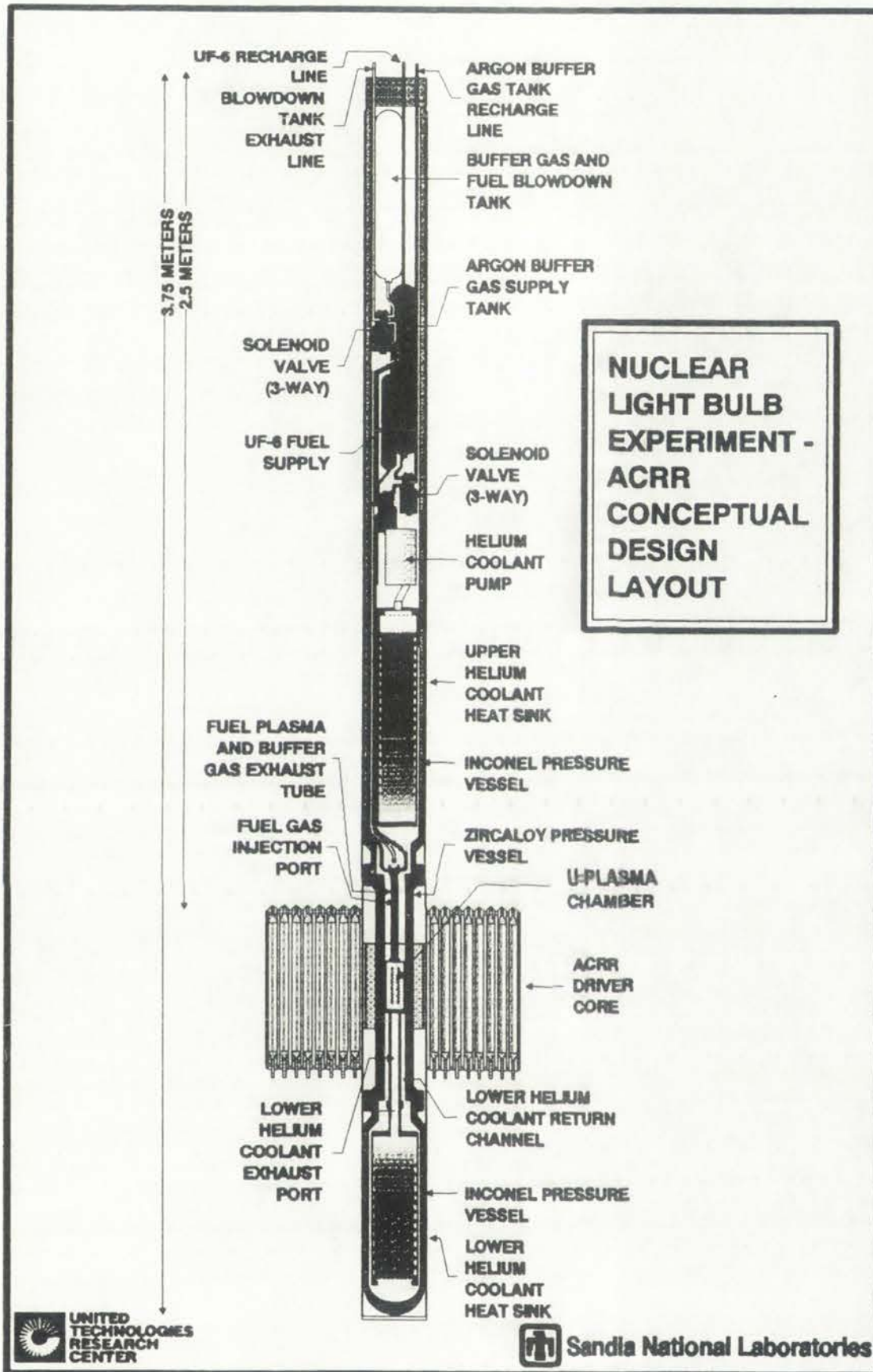


Figure 2.7: Proposed layout of the in-ACRR experiment [Gauntt, 1992a].



Figure 2.7. Geological layout of the Iqaluk segment (from 1992).

The goal of the SNL/UTRC in-ACRR experiments was to determine the feasibility of fissioning plasma confinement; a cloud of UF_6 plasma was to be suspended in an argon flow, with the ACRR providing the "driver" flux. Cooling of the vertical test assembly was to be provided by axial helium flow.

2.8. Current Status of the NLB Rocket Engine

Research into the NLB concept was restarted in 1991 in the form of UTRC/SNL co-operation; by 1994, however, due to the demise of the SEI and termination of the NASA Nuclear Propulsion Office, no organized research effort remained. The planned SNL/UTRC in-ACRR tests were postponed indefinitely. As of this writing, the work presented in this Dissertation comprised the only active (albeit very small-scale) NLB-related effort. In terms of a feasible space nuclear propulsion design, the NLB engine still requires significant amounts of research and experimental validation, which will inevitably require large amounts of funding and a clearly defined mission. At this time, neither funds nor missions are in abundant supply, but this should not preclude further analysis of the NLB concept. Any additional insight into the engineering feasibility of the NLB will either mean fewer obstacles toward a full-scale flight-capable engine, or will point out important feasibility problems related to the design. To that order, a particular derivative of the NLB engine is introduced in the next chapter, and a methodology to analyze its thermalhydraulics behavior and determine the feasibility of such a concept is introduced in the following chapters.

The goal of the NRC/UTRC to-ARJIS experiments was to determine the feasibility of designing a reactor core for the NRC/UTRC to-ARJIS reactor. The design was to be a reactor in an engine form with the ARJIS providing the "drive" flux. Cooling of the vertical test assembly was to be provided by axial natural flow.

The NRC/UTRC to-ARJIS Experiment

Research into the NRB concept was initiated in 1991 in the form of UTRC/ARJIS cooperation by 1994. However, due to the demise of the ARJIS and termination of the NASA Nuclear Propulsion Office, no organized research effort resulted. The NRC/UTRC to-ARJIS tests were postponed indefinitely. As of this writing, the work presented in this Dissertation comprised the only active (albeit very small-scale) NRB-related effort in terms of a technical space nuclear propulsion design. The NRB engine still requires significant amounts of research and experimental validation, which will inevitably require large amounts of funding and a clearly defined mission. At this time, neither funds nor mission are in abundant supply, but this should not preclude further analysis of the NRB concept. Any additional insight into the engineering feasibility of the NRB will either mean fewer obstacles toward a full-scale light-reactor engine, or will point out important feasibility problems related to the design. To that end, a particular objective of the NRB engine is introduced in the next chapter, and a methodology to analyze its thermodynamic behavior and determine the feasibility of such a concept is introduced in the following chapter.

CHAPTER 3

THE UNIT-CELL ROCKET ENGINE - TECHNICAL BACKGROUND

3.1. Introduction

UARL-conducted research into the gaseous core NLB rocket engine had achieved significant progress during the late 1960's and early 1970's; numerous research efforts underway at UARL demonstrated the engineering feasibility of fluid mechanics confinement at high temperatures, and experimental and theoretical studies provided new data on the thermophysical and thermo-optical properties of the materials involved. All the experiments until then, however, had been performed with subcritical UF_6 assemblies and with external heating. The next phase of research was intended to involve small-scale nuclear tests with fissioning uranium plasmas, which would validate the thermal radiation characteristics of the uranium fuel as well as validate the predicted neutronics and criticality behavior of the rocket engine [Bogart and Lantz, 1962].

The nuclear tests were intended to be carried out within the core of then-existing large experimental reactors, which would provide the driver neutron flux and allow for control of the chain reaction until the uranium plasma achieved criticality. Four experimental reactors, in addition to the already utilized Nuclear Furnace at LASL, were identified as potential test-beds for the "in-reactor" testing: the High Flux Isotope Reactor (HFIR), the Kinetic Intense Neutron Generator (KING), the NASA-Lewis Fission Uranium Plasma Facility (FUPF), and a unit-cell test reactor proposed by UARL [Latham and Rodgers, 1972a].

The planning and design of the in-reactor tests were carried out during 1972, at which time only the Nuclear Furnace and the HFIR were operational reactors. The startup of the other three candidate reactors was then estimated to fall in the 1975-1980 period [Latham and Rodgers, 1972a]. Since termination of all space nuclear propulsion research and development efforts occurred in

CHAPTER 2 THE WINDTUNNEL ROCKY ENGINE - TECHNICAL BACKGROUND

2.1 Introduction

UAKI-conducted research into the gaseous core NLS rocket engine had achieved significant progress during the late 1960's and early 1970's. Numerous research efforts underway at UAKI demonstrated the engineering feasibility of liquid mechanical containment at high temperatures, and experimental and theoretical studies provided new data on the thermophysical and thermo-oxidic properties of the materials involved. All the experiments until then, however, had been performed with substantial UTK assistance and with external funding. The next phase of research was intended to involve small-scale nuclear tests with circulating uranium plasma, which would allow the thermal behavior characteristics of the uranium fuel as well as validate the predicted neutronic and radiolytic behavior of the rocket engine [Hogan and Latta, 1961].

The nuclear tests were intended to be carried out within the core of the existing large experimental reactor, which would provide the driver neutron flux and allow for control of the chain reaction and the uranium plasma achieved critically. Four experimental reactors, in addition to the already utilized Nuclear Furnace at UAKI, were identified as potential test-beds for the "in-reactor" testing: the High Flux Isotope Reactor (HFIR), the Kinetic Isotope Reactor Generator (KIRG), the NASA Lewis Fusion Uranium Reactor Facility (FURF), and a wind-tunnel reactor proposed by UAKI [Latta and Rogers, 1972].

The planning and design of the in-reactor tests were carried out during 1972 at which time only the Nuclear Furnace and the HFIR were operational reactors. The setup of the other three candidate reactors was then estimated to fall in the 1973-1980 period [Latta and Rogers, 1972]. Since verification of all space nuclear propulsion research and development efforts occurred in

1973, none of the proposed in-reactor experiments ever took place. The bulk of the nuclear propulsion work was shelved; no advancement in the proposed in-reactor experiments occurred beyond the conceptual phase.

The technical background related to the unit-cell test reactor, as summarized in this Chapter, represents the status of this concept upon its termination in 1973. Information and all pertinent data were retrieved from two available publications related to that particular derivative of the NLB rocket engine: UARL Technical Report L-910900-17: "*Analytical Design and Performance Studies of Nuclear Furnace Tests of Small Nuclear Light Bulb Models*," [Latham and Rodgers, 1972a], and AIAA Paper No. 72-1093: "*Small Nuclear Light Bulb Engines with Cold Beryllium Reflectors*," [Latham and Rodgers, 1972b].

3.2. The Unit-Cell Test Reactor

One of the five experimental reactors intended for the in-reactor testing phase was proposed at UARL, and involved a more complex design than the others. Initially termed the Unit-Cell Test Reactor, the design was to be utilized for experimental verification of the reference NLB concept; toward the end of the NLB research effort, however, it was discussed as a possible rocket engine concept with potential benefits over the reference NLB design.

The reasoning behind the unit-cell reactor was that, in general, gaseous core nuclear rocket engines are inherently large high-pressure devices for two reasons: (1) a requirement for adequate critical fuel density, and (2) the need for a very high fuel temperature to radiate the required heat fluxes to the hydrogen propellant [Latham and Rodgers, 1972a]. A proposed procedure for reducing the critical fuel density, and thereby the reactor cavity size and operating pressure, was to improve (increase) the neutron flux density into the cavity; this was to be achieved by embedding segmented propellant channels along portions of the cavity surface, and by choosing a moderator with a very low thermal neutron scattering cross-section [Latham and Rodgers, 1972a].

1973) some of the proposed in-reactor experiments were not done. The bulk of the reactor program work was shifted to advancement in the proposed in-reactor experiments toward beyond the conceptual phase.

The technical background related to the unit-cell test reactor as summarized in this Chapter, comprises the status of the unit-cell test reactor in 1973. Information and all pertinent data were obtained from two available publications related to that particular derivative of the NLR rocket engine (AARL Technical Report L-8184-B-17, "Analytical Design and Performance Studies of Rocket Engine Test of Small-Nucleon Light-Bit Models," [Latham and Hodgson, 1972a] and AARL Report L-8184-B-17, "Small-Nucleon Light-Bit Engines with Cold-Gasoline Systems," [Latham and Hodgson, 1972b]).

3.2 The Unit-Cell Test Reactor

One of the five experimental reactors intended for the in-reactor testing phase was proposed as UARL and involved a more complex design than the others. Initially termed the Unit-Cell Test Reactor, the design was to be utilized for experimental verification of the reference NLR concept toward the end of the NLR contract effort; however, it was discarded as a possible rocket engine concept with potential benefits over the reference NLR design.

The reasoning behind the unit-cell reactor was that in general, gaseous core nuclear rocket engines are inherently large high-pressure devices for two reasons: (1) a requirement for adequate critical fuel density, and (2) the need for a very high fuel temperature to realize the required heat fluxes to the hydrogen propellant [Latham and Hodgson, 1972a]. A proposed procedure for reducing the critical fuel density, and thereby the reactor cavity size and operating pressure, was to improve (increase) the neutron flux density into the cavity; this was to be achieved by embedding segmented propellant channels along portions of the cavity surface and by choosing a moderator with a very low thermal neutron scattering cross-section [Latham and Hodgson, 1972a].

Segmenting the propellant channels, as opposed to a circumferential propellant channel characteristic of the reference NLB rocket engine, was intended to reduce the thermal neutron diffusion barrier effects of hydrogen; with a smaller hydrogen propellant surface area, a larger thermal neutron flux would be expected into the fuel region, thus reducing the total fuel density requirements [Latham and Rodgers, 1972a]. With a smaller hydrogen surface area, a reduction in the influence of the propellant thermal motion on the neutron scattering rate was also anticipated [Latham and Rodgers, 1972a]. As will be discussed later in this Dissertation, however, a reduction in the propellant surface area also results in the moderator/reflector regions being located closer to the fuel and subjected to higher temperatures.

Due to its low thermal neutron scattering cross-section at low temperatures, beryllium was chosen as the moderator material. UARL studies had determined that beryllium, cooled to temperatures below 100 K, has a very low scattering cross-section for thermal neutrons below 0.006 eV [Latham and Rodgers, 1972a]. An estimate of an order of magnitude reduction in the critical fuel density requirements by using a cold beryllium reflector over room temperature beryllium was obtained [Latham and Rodgers, 1972a]. It was assumed that the beryllium reflector could be maintained in a supercooled state by a refrigeration cycle or low-temperature heat exchanger.

The layout of the unit-cell test reactor is depicted in Figures 3.1 and 3.2, based on the original concept proposed at UARL in 1972. The segmented propellant channels were assumed to cover between 10-25% of the total cavity radial surface area as stated in [Latham and Rodgers, 1972a], an estimate later amended to between 10-40% [Latham and Rodgers, 1972b].

3.3. Performance Analysis of the Unit-Cell Reactor

A comparison of the UARL-estimated critical fuel density requirements for graphite, beryllium, and heavy water is shown in Table 3.1, based on data presented in [Latham and Rodgers, 1972a].

Separating the propellant channels as opposed to a circumferential
propellant channel structure at the entrance of the reactor was
examined in terms of the axial neutron flux distribution of hydrogen
with a fixed hydrogen-to-oxidant ratio and a fixed thermal neutron
flux would be expected to be low region than without the fuel bed
design. Theoretical studies and calculations were made by
Latham and Rodgers, 1972a, in the presence of the propellant thermal neutron
on the reactor walling and was also suggested Latham and Rodgers,
1972a. As will be discussed later in this Discussion, however, a reduction in
the propellant surface area also results in the production of higher neutron
flux density than in the case of a fixed axial neutron flux distribution.

The axial neutron flux distribution was examined at low temperatures
and the results were shown as the moderator mixture (Latham and
Rodgers, 1972a) and the results are shown in Figure 10. A very
low axial neutron flux density was observed for the axial neutron flux
distribution. A neutron flux density of the order of magnitude reduction in the
axial neutron flux density was observed by a low axial neutron flux density
over the temperature region was observed Latham and Rodgers, 1972a. It
was assumed that the axial neutron flux density would be maintained in a
superheated state by a temperature of low-temperature heat exchanger.

The layout of the nuclear test reactor is depicted in Figures 11 and 12. Part
of the original design proposal as shown in Figure 13. The segmented propellant
channels were assumed to cover between 10-15% of the total cavity radial
surface area as stated in Latham and Rodgers, 1972a. An axial neutron
flux density of between 10-15% (Latham and Rodgers, 1972a).

3.1.1. Axial Neutron Flux Density

A comparison of the axial neutron flux density requirements for
axial neutron flux density and how they relate to those in Table 3.1 based on data
presented in Latham and Rodgers, 1972a.

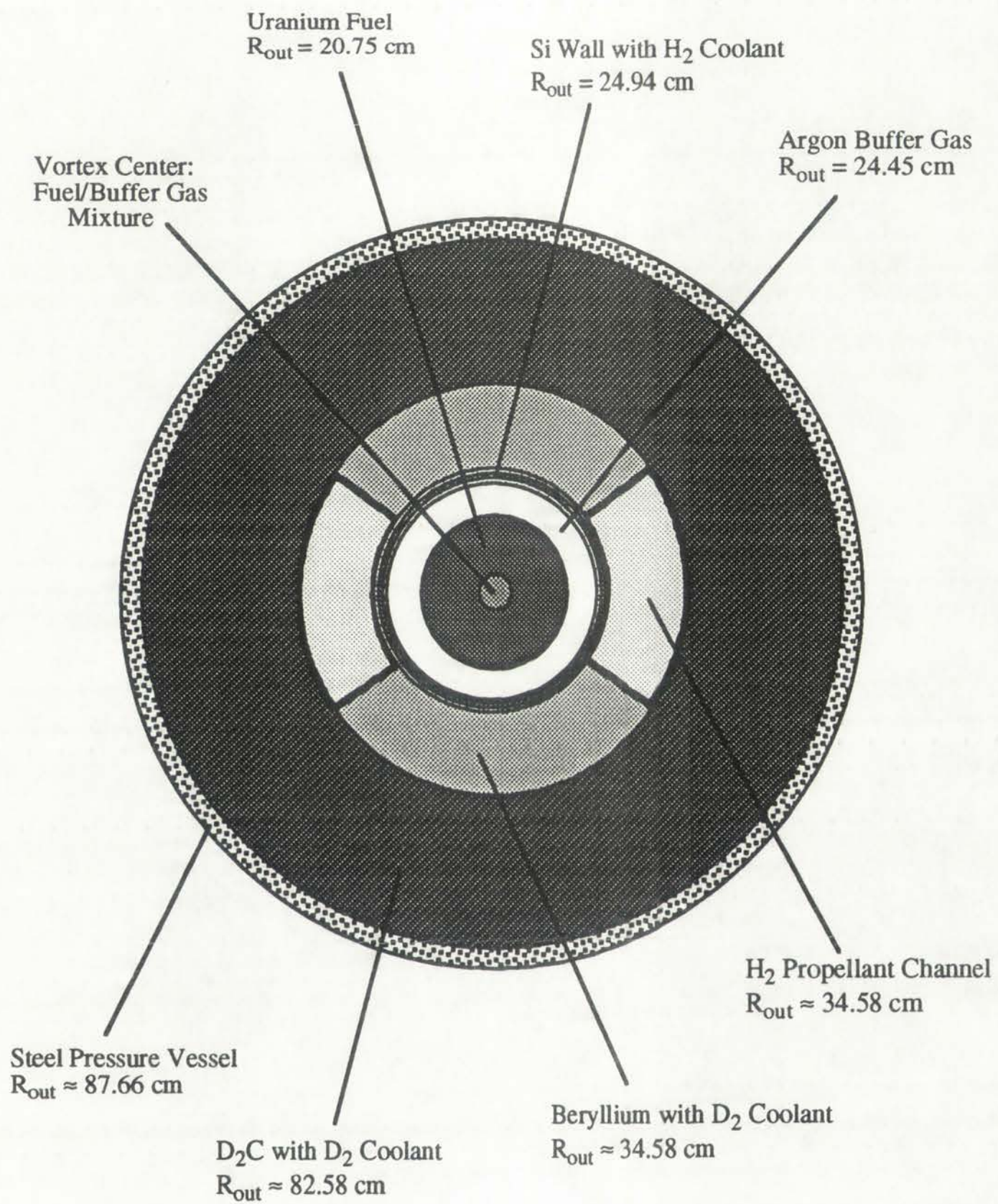


Figure 3.1: (r- θ) Layout of the Unit-Cell NLB rocket engine.



Figure 2.1 (a) Diagram of the cell wall and organelles.

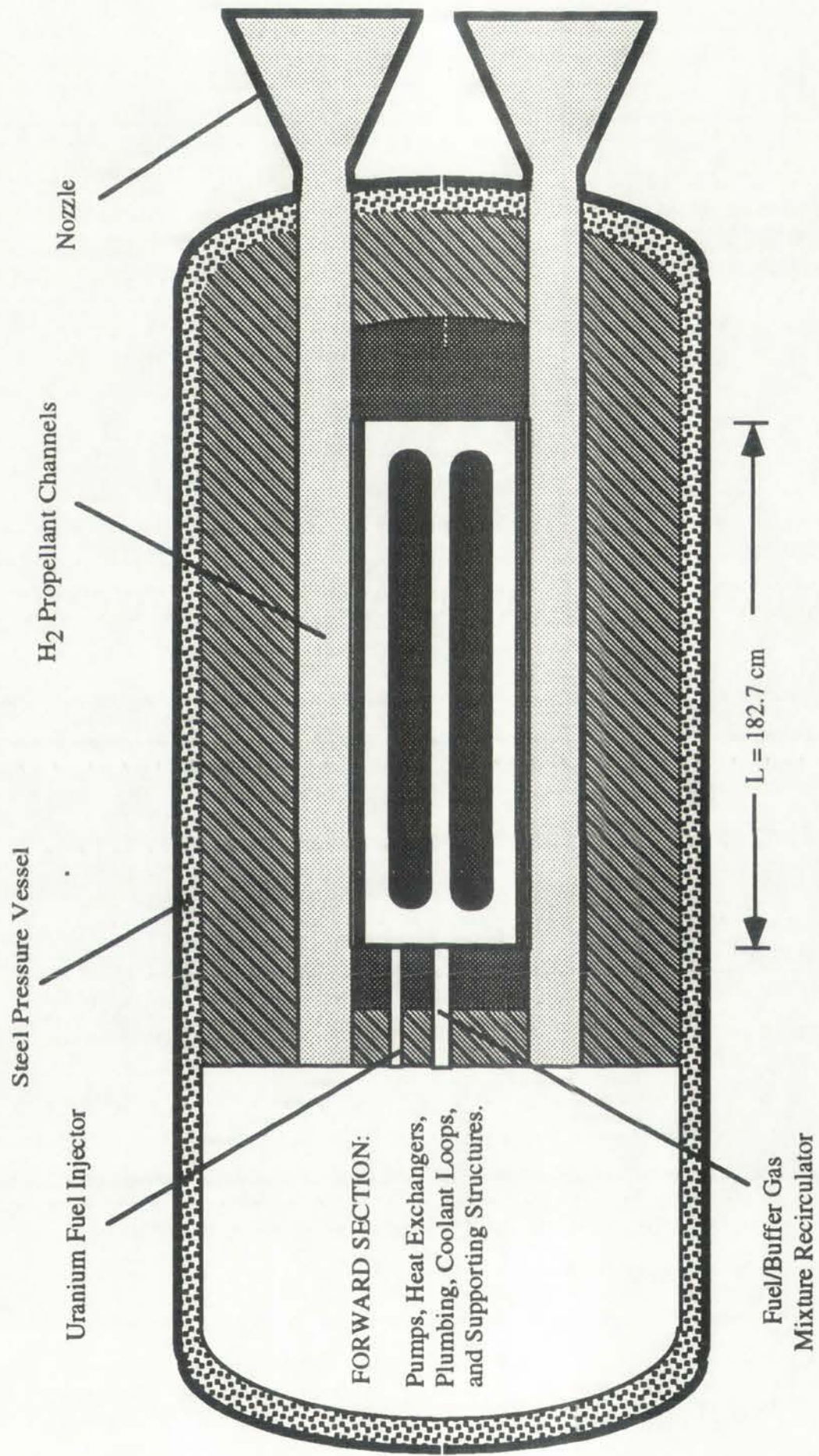


Figure 3.2: (r-z) Layout of the Unit-Cell NLB rocket engine.

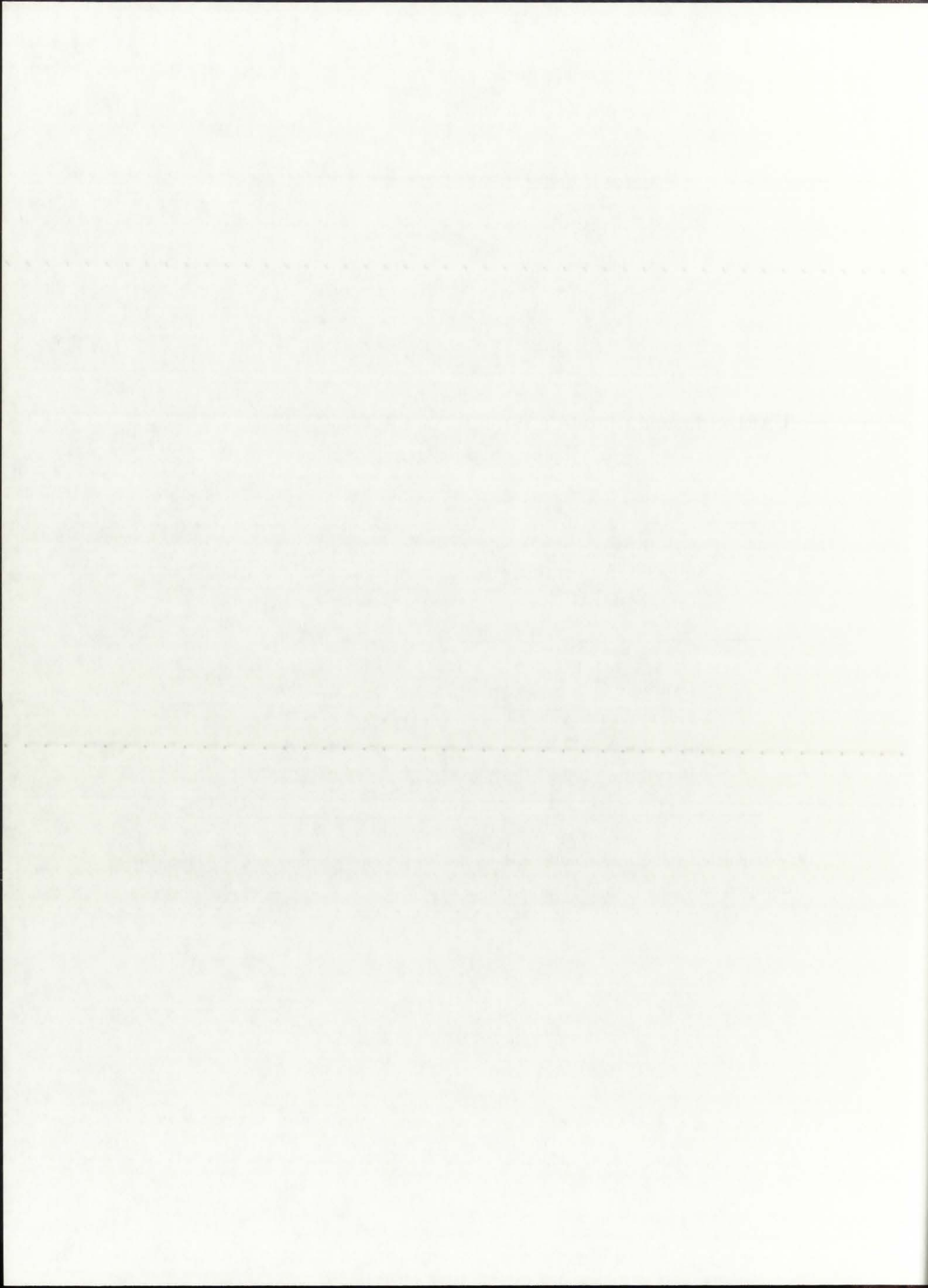
Figure 2.3 (4-5) Front of the CHU-1000 robot car.



TABLE 3.1
 UARL-estimated critical U-235 density as a function of moderator/reflector
 [Latham and Rodgers, 1972a]

Reflector/Moderator Material	Estimated U-235 Critical Density, [atoms/cm ³]
Graphite (300 K)	1.0e19
Heavy Water (300 K)	3.5e18
Beryllium (300 K)	1.2e18
Beryllium (100 K)	2.0 - 4.0e17 #

#: extrapolated value, based on the ratio of the 300 K-to-100 K square root of neutron age to transport mean free path [Latham and Rodgers, 1972a].



Beryllium, supercooled to below 100 K, was recommended as a good moderator for reducing the critical fuel density; the leakage of thermal neutrons from the outside of such a reflector, however, was anticipated to be very large unless the reflector material is backed by a good thermal neutron scattering material. Deuterium compounds, such as frozen heavy water (D_2O) or deuterium carbide (D_2C), were suggested for use in the outer reflector region [Latham and Rodgers, 1972a].

3.3.1. Preliminary Criticality Calculations

A series of multigroup neutron transport calculations were performed at UARL during 1972; comprising only the initial step in a planned detailed neutronics analysis, these calculations focused on simple configurations. The unit-cell reactor was modeled as a one-dimensional spherical cavity equal in volume to the cavity of a reference NLB engine unit cell; this layout is depicted in Figure 3.3, based on data from [Latham and Rodgers, 1972a; and Latham and Rodgers, 1972b]. The criticality analysis was performed with ANISN, a one-dimensional neutron transport code coupled to a 17-group cross-section library developed at UARL. The cross-section library, shown in Table 3.2, contained five energy groups in the thermal range below 1.125 eV, with two groups below the 0.006 eV energy cutoff for low-energy elastic scattering in beryllium [Latham and Rodgers, 1972b]. The behavior of beryllium scattering cross-sections for the lower thermal energy range, $E \leq 0.006$ eV, is shown in Figure 3.4 [Lazo, 1993].

A uniform operating pressure of 250 atm was assumed across the reactor cavity for the purposes of calculating gas densities [Latham and Rodgers, 1972b]. Temperature values were assumed for each region in the model, ranging from 35,000 K in the fuel to 40 K in the supercooled beryllium and deuterium compound regions. Two separate preliminary analyses, based on the same overall structure of the 1-D spherical model (Figure 3.3), were performed at UARL. The first, reported in [Latham and Rodgers, 1972a], utilized a deuterium carbide (D_2C) reflector; the second analysis, described in detail in [Latham and Rodgers, 1972b], utilized a heavy water (D_2O) reflector.

hydrogen, supported in form of a gas moderator for slowing the initial fast neutrons from the outside of each reflection toward the center of the core. The moderator is made of a good thermal neutron scattering material, such as heavy water (D₂O). The moderator is supported in the central region [Latham and Rodgers 1973].

3.1. Preliminary Criticality Calculations

A series of multigroup neutron transport calculations were performed at UARL during 1972, comprising only an initial step in a planned detailed neutronic analysis. These calculations focused on simple configurations. The neutron vector was modeled as a one-dimensional spherical cavity equal in volume to the cavity of a cylinder. The neutron vector cell, the layout is depicted in Figure 3.2, based on data from [Latham and Rodgers 1973] and [Latham and Rodgers 1973]. The criticality analysis was performed with AMISW, a one-dimensional neutron transport code coupled to a 17-group cross-section library developed at UARL. The cross-section library, shown in Table 3.2, contained five energy groups in the thermal range below 1.125 eV, with two groups below the 0.025 eV energy cutoff for low-energy elastic scattering in hydrogen [Latham and Rodgers 1973]. The moderator of hydrogen scattering cross-sections for the lower thermal energy range (0.025 eV) is shown in Figure 3.4 [Latham 1973].

A uniform operating pressure of 250 atm was assumed across the reactor cavity for the purposes of calculating gas densities [Latham and Rodgers 1973]. Temperature values were assumed for each region in the model ranging from 2500 K in the fuel to 40 K in the supercooled paraffin and deuterium compound regions. Two separate preliminary analyses based on the same overall structure of the 1-D spherical model (Figure 3.3) were performed at UARL. The first, reported in [Latham and Rodgers 1973], utilized a deuterium oxide (D₂O) reflector; the second analysis, described in detail in [Latham and Rodgers 1973], utilized a heavy water (D₂O) reflector.

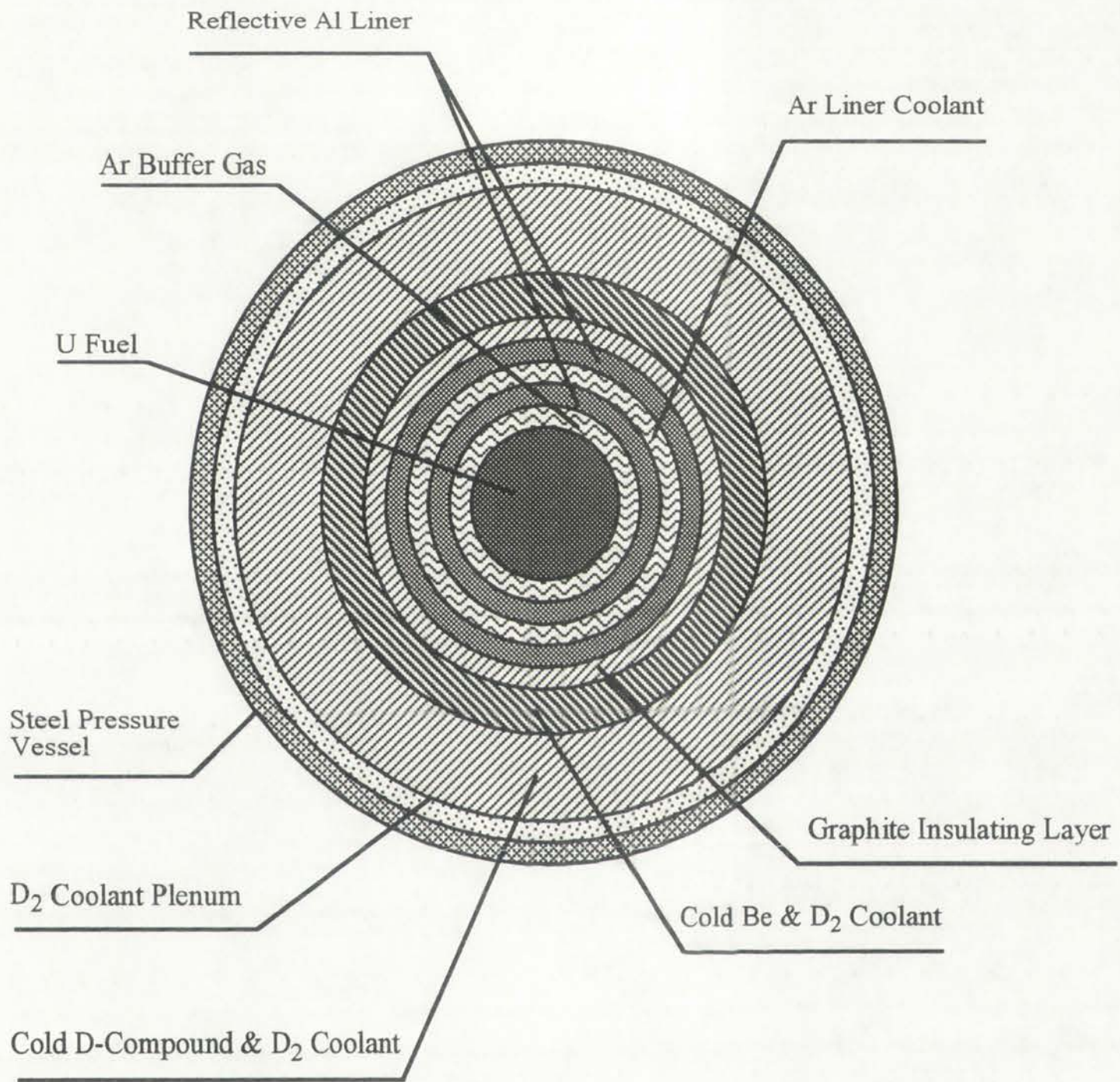


Figure 3.3: 1-D spherical model used in UARL criticality calculations.

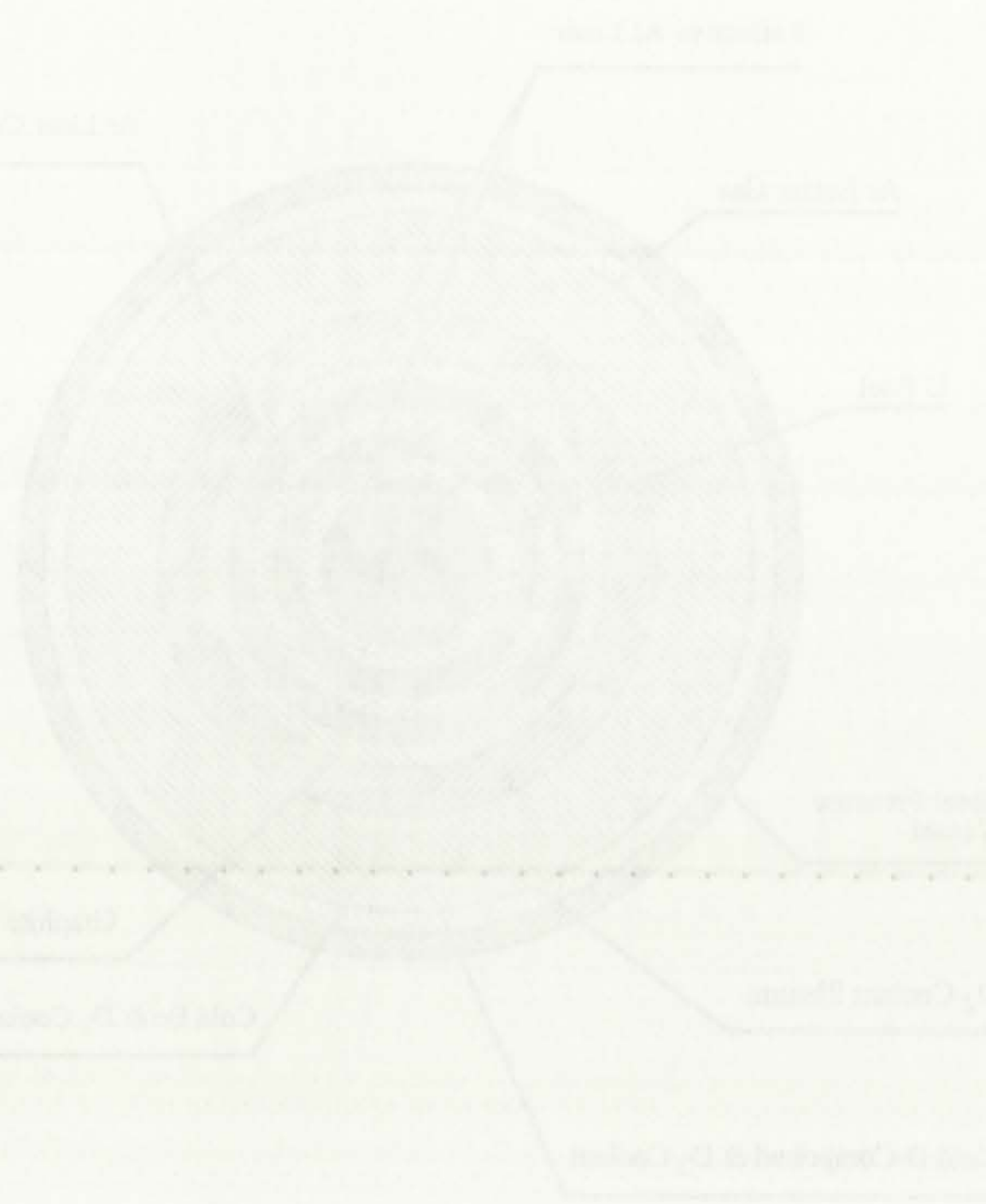


Figure 1: A cross-sectional model of a planet showing various layers and features.

TABLE 3.2
 17-group neutron cross-section library used by UARL
 for cavity reactor criticality calculations
 [Latham and Rodgers, 1972a]

Energy Group	Energy Range			
1	2.865	-	10	MeV
2	1.35	-	2.865	MeV
3	0.821	-	1.35	MeV
4	388	-	821	keV
5	111	-	388	keV
6	15	-	111	keV
7	3.35	-	15	keV
8	0.583	-	3.35	keV
9	101	-	583	eV
10	29	-	101	eV
11	8.32	-	29	eV
12	1.125	-	8.32	eV
13	0.414	-	1.125	eV
14	0.025	-	0.414	eV
15	0.006	-	0.025	eV
16	0.00175	-	0.006	eV
17	0.0	-	0.00175	eV

TABLE 3
 Energy Group Energy Range
 for energy reactor efficiency calculations
 (Latham and Roberts, 1973)

Energy Group	Energy Range
1	0.0000 - 0.0005 MeV
2	0.0005 - 0.0010 MeV
3	0.0010 - 0.0020 MeV
4	0.0020 - 0.0030 MeV
5	0.0030 - 0.0040 MeV
6	0.0040 - 0.0050 MeV
7	0.0050 - 0.0075 MeV
8	0.0075 - 0.0100 MeV
9	0.0100 - 0.0150 MeV
10	0.0150 - 0.0200 MeV
11	0.0200 - 0.0300 MeV
12	0.0300 - 0.0500 MeV
13	0.0500 - 0.1000 MeV
14	0.1000 - 0.2000 MeV
15	0.2000 - 0.5000 MeV
16	0.5000 - 1.0000 MeV
17	1.0000 - 2.0000 MeV

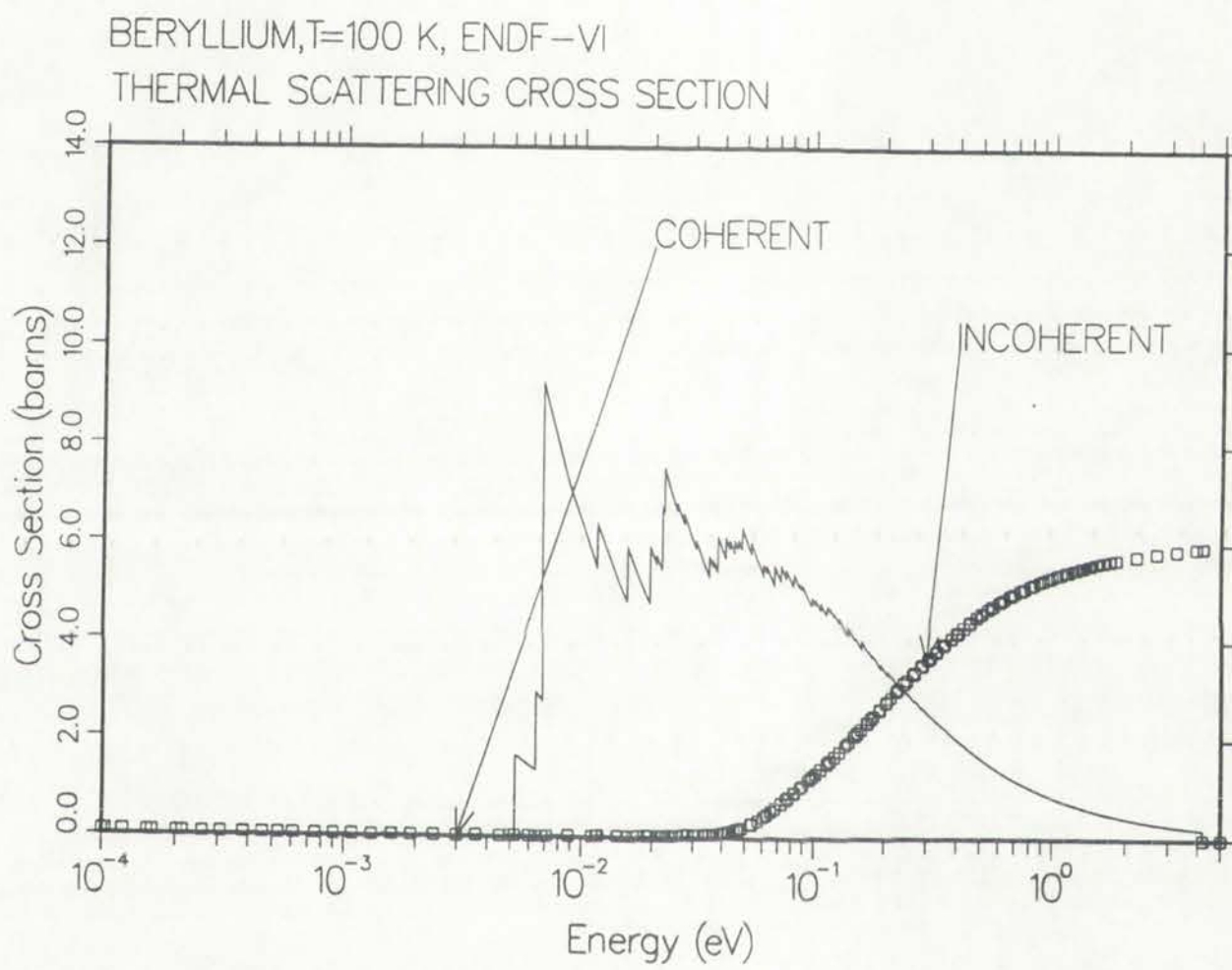


Figure 3.4: Low-energy Be scattering cross-sections [Lazo, 1993].



Figure 2: The change in relative concentration (Lacey 1991)

Although not specifically stated, it can be inferred from the UARL discussion that their two models corresponded to a critical ($k_{\text{eff}}=1.000$) assembly.

The two UARL models were found to differ significantly in their reported U-235 mass density, with the first reporting $5.80 \times 10^{-5} \text{ g/cm}^3$ and the second reporting $4.1 \times 10^{-3} \text{ g/cm}^3$. A series of criticality calculations were thus performed by the author at the onset of this Dissertation work, with the goal of determining the k_{eff} values associated with the two UARL models. The models were analyzed with the neutronics code ONEDANT, conserving all UARL-reported dimensions and material densities. K_{eff} values of 0.037 and 0.604 were obtained for the first and second model, respectively, indicating significant discrepancies between them. Thus, looking back at the preliminary UARL criticality analyses involving the unit-cell reactor, it is unclear as to the purpose of the 1-D spherical model and the reported fuel densities. It does seem, however, that the unit-cell reactor would have been subcritical using the 1-D model of Figure 3.3, and that an external "driver" reactor would need to have been used to prove the initial feasibility of the unit-cell reactor.

3.4. Summary of UARL Research Work

UARL research on the unit-cell reactor concept outlined the general layout of the reactor and the physical reasons behind the anticipated benefits. Termination of the space nuclear propulsion research in 1973, however, shelved the concept and canceled all the planned engineering analyses. Thus, the only available UARL results originate from 1-D calculations, which were in turn based on numerous estimates and assumptions. Potential neutronics benefits of using a supercooled beryllium moderator were discussed, but no detailed analysis with respect to the unit-cell reactor was performed. The criticality analyses were performed with an assumed spherical assembly, and discrepancies between the two models presented in [Latham and Rodgers, 1972a] and [Latham and Rodgers, 1972b] can be found. Performance parameters such as thrust or specific impulse, pertaining to the unit-cell reactor, were never discussed in detail. A thermal analysis to determine the feasibility of the supercooled regions was planned as future work.

Although not explicitly stated in the 1973 report, the JARR documents
that these two models were developed to a level of 1000 dollars.

The two JARR models were found to differ significantly in their response to
the same domain, with the first model of 1973 giving a different
response to a 1000 dollar change in the same calculation area than
provided by the model of the second of the JARR model with the goal
of determining the key values associated with the two JARR models. The
models were analyzed with the nonlinear code GUESS, comparing all
JARR-related dimensions and output changes. Key values of 1000 and
5000 were obtained for the first and second model respectively, indicating
significant differences between them. This finding back at the preliminary
JARR analysis earlier involving the unit-cell reactor is noted as the
purpose of the 1-D spectral model and the 1-D spectral model. It does
not appear that the unit-cell reactor would have been fabricated using
the 1-D model of 1973 and that an earlier "three" reactor would not
to have been used to cover the total capacity of the unit-cell reactor.

3.4 Summary of JARR Research Work

JARR research on the unit-cell reactor concept outlined the general report as
the reactor and the physical reactor behind the unit-cell reactor.
Formulation of the unit-cell reactor proposal research in 1973, however,
showed the concept and canceled all the planned engineering analysis. This
is the only available JARR research originates from 1-D calculations, which was
in turn based on numerous estimates and assumptions. Potential outcomes
before of using a spectroscopic method analysis was discussed, but no
detailed analysis with respect to the unit-cell reactor was performed. The
criticality analyses were performed with an assumed spherical geometry, and
discrepancies between the two models presented in [Latham and Rodgers,
1973] and [Latham and Rodgers, 1973] can be found. The differences
parameters such as initial or specific isotopes pertaining to the unit-cell
reactor were never discussed in detail. A formal analysis to determine the
feasibility of the spectroscopic reactor was planned as future work.

Overall, the the unit-cell reactor concept never got past the first phase, where it was deemed of interest due to its potential critical mass benefits. In conclusion, then, research on the unit-cell reactor never progressed beyond the preliminary conceptual phase, and no detailed theoretical nor experimental validation of the concept was carried out. The concept itself has been regarded with interest, but no research work to determine its feasibility and/or thermalhydraulics behavior has ever been performed.

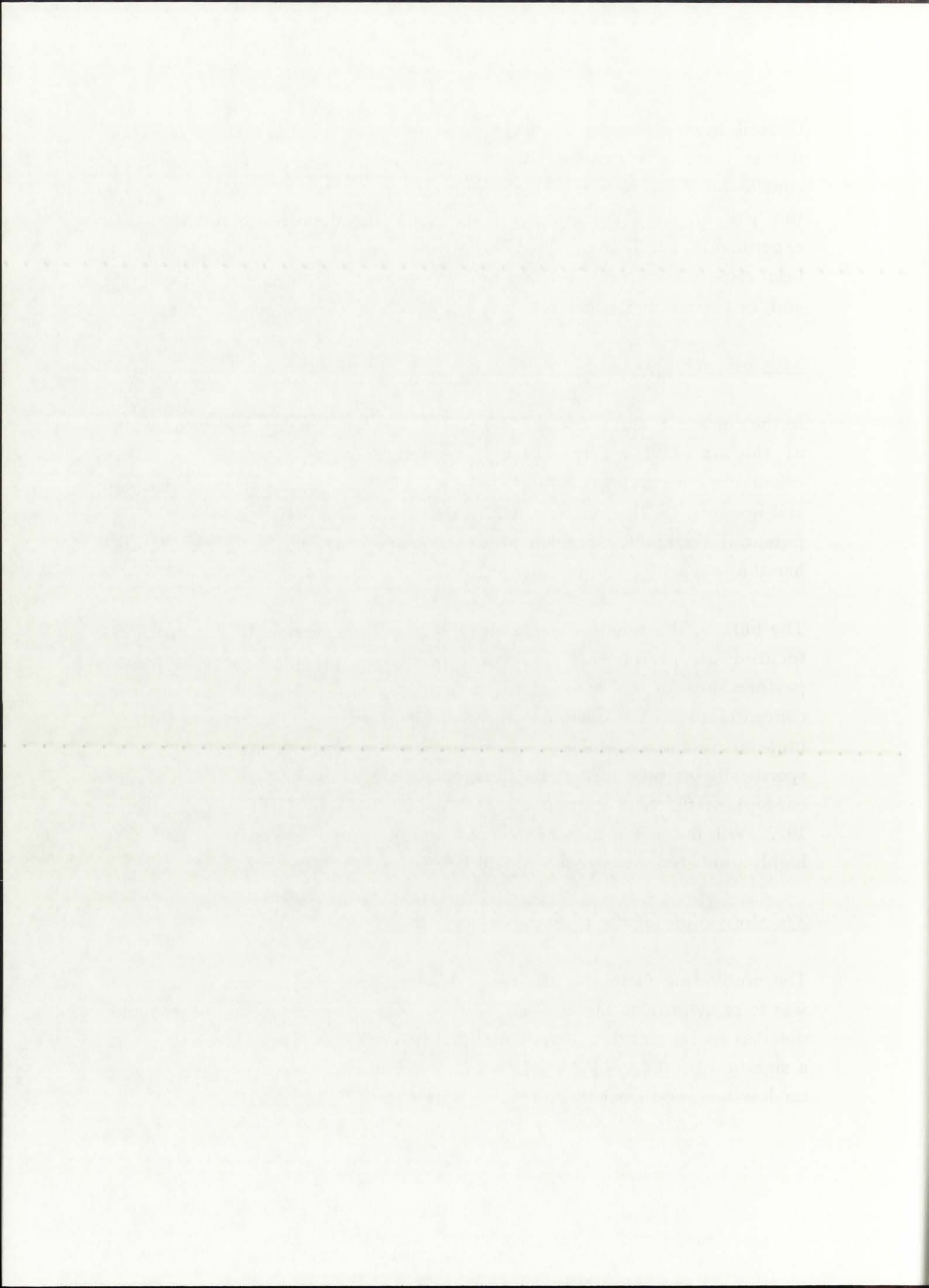
3.5. Current Status of the Unit-Cell Reactor Concept

In the context of the proposed SNL/UTRC in-ACRR testing, a brief overview of the unit-cell reactor was presented. Some preliminary criticality calculations involving the "unit-cell rocket engine," as reported in [Latham and Rodgers, 1972], were revisited by SNL, and the unit-cell was identified as a potential test facility which would demand smaller propellant exhaust handling capacity [Gauntt *et al.*, 1992b].

The bulk of the renewed research effort, centered around UTRC and SNL, focused on preliminary analytical prediction of the thermalhydraulic performance of an in-reactor gas core assembly. No specific analysis concentrated on the design features and performance characteristics of the unit-cell reactor rocket engine. To date, there has not been any research work specifically oriented toward the detailed analysis of the unit-cell rocket engine concept, or the NLB in general, since the preliminary UARL calculations in 1972. With the termination of the space nuclear propulsion effort in 1994, it is highly unlikely that the concept will be analyzed in the near future.

3.6. Motivation for the Dissertation Research Work

The motivating factor for the research work presented in this Dissertation was to re-investigate the unit-cell reactor rocket engine concept and focus on a detailed analysis of its thermalhydraulic characteristics. The concept proposed a significantly different design than the reference NLB rocket engine, relying on low-temperature beryllium and heavy water. The potential benefits of



using such a configuration, as well as the relatively unexplored area of heat transfer and neutronics in the multi-region, non-isothermal reactor, prompted this research work.

Since the initial unit-cell NLB engine design had already been proposed by UARL in 1972, the goal of this research was to expand on the preliminary, assumption-reliant calculations and generate a series of more detailed thermalhydraulics and rocket performance parameters. By focusing on the detailed analysis of a proposed but never validated concept, a level of originality is characteristic of this research work. With that, the author hopes that in a small way the understanding of the behavior of gas core propulsion concepts will have been advanced.

The next Chapter discusses the basis for originality of the research work presented in this Dissertation and outlines the planned research goals. Chapter 5 presents in detail the methodology of analysis employed in this work.

being such a contribution as well as the highly advanced state of the
science and technology in the field of the study and the
importance of the research work.

Since the final draft of the thesis has already been prepared by
the author, the aim of the work was to provide for the
comprehensive and detailed examination and generate a series of more detailed
thermodynamic and other performance parameters by focusing on the
detailed analysis of a proposed but never validated concept. A level of
originality is characteristic of this research work. With that the author hopes
that in a small way the understanding of the behavior of gas turbine
engines will have been advanced.

The next chapter discusses the data for originality of the research work
presented in this dissertation and outlines the planned research goals.
Chapter 2 presents in detail the methodology of analysis employed in this
work.

CHAPTER 4

RESEARCH GOALS AND BASIS FOR ORIGINALITY

4.1. Introduction

The unit-cell NLB rocket engine concept was chosen as the focus of this Dissertation research due to the numerous nuclear engineering-associated challenges that could be analyzed to yield original contributions. The basis of the design, consisting of the gaseous fuel and the silica wall, involves extremely large heat fluxes and associated temperatures, posing the need for a comprehensive thermal (heat transfer) analysis. The original intent of using a low-temperature Be moderator and D₂O reflector was to maximize the thermal neutron flux, thereby minimizing the critical fuel density and reactor critical size; to verify this hypothesis, a neutronics analysis involving very low-energy cross sections was needed.

The challenges associated with the unit-cell NLB rocket engine, then, are twofold: (1) to develop a methodology for analyzing the thermalhydraulics behavior of the engine, and (2) to use the methodology to perform a feasibility analysis of the concept. The following Sections, respectively, present a chronological summary of the initial phases of this research: Literature Survey, delineation of Research Goals, and statement of the Basis for Originality. Such a structure was intended to illustrate to the reader the development of the idea of analyzing the unit-cell engine, and also to provide a justification for the methodology of analysis. A detailed presentation of the methodology of analysis is presented in Chapter 5.

4.2. Literature Survey

The initial phase of the research work presented in this Dissertation concentrated on a thorough literature survey. Even though it was immediately obvious that the NLB concept contained numerous topics suitable for a detailed doctoral research, significant familiarization with the

CHAPTER 1 RESEARCH GOALS AND BASIS FOR ORIGINALITY

1.1 Introduction

The unit-cell MLB model engine concept was chosen as the focus of this Dissertation research due to the numerous needed engineering-associated challenges that could be analyzed in this original contribution. The basis of the design, counting of the engine heat and the alloy wall involves extremely large heat flows and associated temperature forcing the need for a comprehensive thermal heat transfer analysis. The original intent of using a low-temperature ice moderator and D_2O reflector was to maximize the thermal neutron flux thereby enhancing the criticality. Kinetic and reaction criticality were to verify this hypothesis, a numerical analysis involving very low-energy neutrons was needed.

The challenges associated with the unit-cell MLB model engine that are included (1) to develop a methodology for analyzing the thermohydraulic behavior in the engine and (2) to use the methodology to perform a feasibility analysis of the concept. The following sections respectively present a chronological summary of the initial phases of this project. Literature Survey, delineation of Research Goals and assessment of the basis for Originality. Such a structure was intended to illustrate to the reader the development of the idea of analyzing the unit-cell engine, and also to provide a justification for the methodology of analysis. A detailed presentation of the methodology of analysis is presented in Chapter 2.

1.2 Literature Survey

The initial phase of the research work presented in this Dissertation concentrated on a thorough literature survey. Even though it was immediately obvious that the MLB concept contained numerous topics worthy for a detailed doctoral research, significant familiarization with the

concept was needed to understand it. The use of gaseous fuel, fluid mechanics confinement, coupled multi-mode heat transfer, and non-isothermal neutronics conditions were all new research areas for the author.

The bulk of the NLB-related literature was obtained at the onset of research via the kind courtesy of the SNL staff associated with the proposed in-reactor testing. This literature consisted of approximately 75 original UARL technical reports and papers, spanning 12 years; it provided the author with insight into the origin of all the NLB parameters, assumptions, and methods of analysis. Studying the assumptions and methods used by UARL resulted in the identification of potential original contributions by the author and formulation of the methodology of analysis.

Additional NLB- and general NTP-related information was obtained from approximately 300 Conference, Meeting, and Workshop papers. These scientific gatherings, spanning almost 25 years, provided a wealth of historical data as well as modern views on the NLB concept and its application to NTP.

Another source of NLB and GCR information were the numerous NASA and national laboratory technical reports and documents, issued between the mid-1950's and the present. Within this source are also classified personal communications and direct interaction with the staff at those institutions.

A separate source of information were the publications not specifically related to the NLB concept, but needed for the understanding of rocket engine, heat transfer, and neutronics fundamentals. More than 50 textbooks, handbooks, reference literature, and software manuals were accumulated to assist in the development of this Dissertation.

In summary, then, approximately 500 documents were used at one time or another to understand the NLB concept and develop the methodology for its analysis. Most, if not all, of the 500 documents are and will remain in the possession of the author, facilitating the research work.

...in the field of... the author...

The bulk of the... the methodology of analysis...

Additional... information was obtained from...

Another source of... information were the documents...

A separate source of... information were the publications...

In summary, this... documents were used at one time or...

4.3. Research Goals

The goals of this research were to answer the two challenges discussed before: (1) develop a methodology for analyzing the thermalhydraulics behavior of the unit-cell NLB engine and (2) use the methodology to perform a feasibility analysis of the concept. The thermalhydraulics behavior of the engine was decided to be analyzed in (r) geometry to allow for successful and timely completion of the research work. The reasoning behind this decision lay in the layout of the unit-cell NLB engine, presented previously in Figures 3.1 and 3.2. With a height-to-radius (H/r) ratio of 10, the engine could be modeled as an infinite cylinder with little loss of accuracy.

To perform an accurate analysis of the unit-cell NLB engine in (r) geometry, it was necessary to take into account the particular features of the (r- θ) geometry. The radial distances shown previously in Figure 3.1 were conserved; it was also necessary, however, to translate the propellant channel annular segments from a value of 40% of the annular region area in (r- θ) geometry [Latham and Rodgers, 1972b] to a corresponding fraction of the radial thickness in (r) geometry. The radial fraction, of course, is not equal to 40%, and must be calculated by finding an "equivalent outer radius," such that the total propellant annular region area is conserved.

The conversion from (r- θ) geometry to (r) geometry and the equivalent outer radius, R_2' , is shown in Figure 4.1. Since both cases involve the infinite cylinder assumption, the value of R_2' can be obtained by equating the annular region area occupied by the segmented propellant channels to a full circumferential annular region area:

$$A_{\text{segm}} = A_{\text{equiv, circumf}} \quad (4.1)$$

This equation can be written in terms of the inner (R_1) and outer (R_2) radius of the annular region and the equivalent outer radius (R_2'):

$$0.4(R_2^2 - R_1^2)\pi = (R_2'^2 - R_1^2)\pi \quad (4.2)$$

The basis of the present work is an analytical study of the flow of a fluid through a duct of arbitrary cross-section. The duct is assumed to be of uniform thickness and the flow is assumed to be steady and incompressible. The velocity profile is assumed to be parabolic and the temperature profile is assumed to be linear. The analysis is carried out in two parts. In the first part, the velocity profile is determined and the flow rate is calculated. In the second part, the temperature profile is determined and the heat transfer rate is calculated.

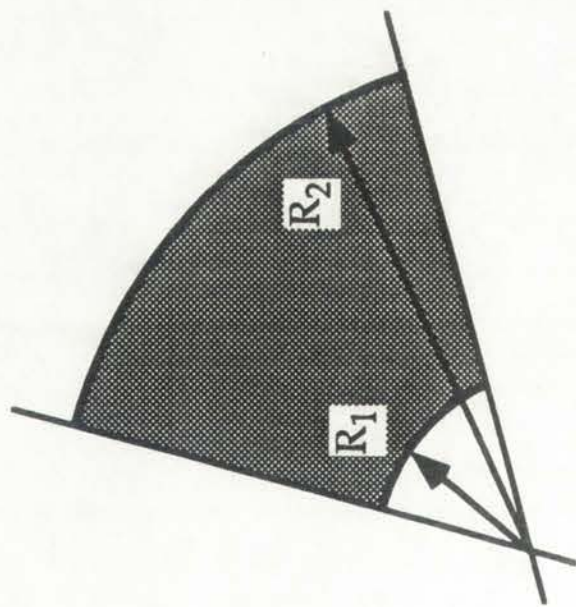
To perform an accurate analysis of the internal flow in a duct, it was necessary to take into account the parabolic features of the velocity profile. The radial distances shown previously in Figure 2.1 were corrected and it was also necessary, however, to transfer the parabolic features from a value of 40% of the radius region and in (2.2) geometry. (Latham and Rodgers, 1975) to a corresponding section of the radial thickness in (c) geometry. The radial thickness of course is not equal to 40% and must be calculated by finding an "equivalent outer radius" such that the total equivalent annular region area is conserved.

The conversion from (a) geometry to (c) geometry and the equivalent outer radius, R_0 , is shown in Figure 2.1. Since both cases involve the same velocity distribution, the value of R_0 can be obtained by equating the annular region area occupied by the equivalent parabolic channels to a full characteristic annular region area.

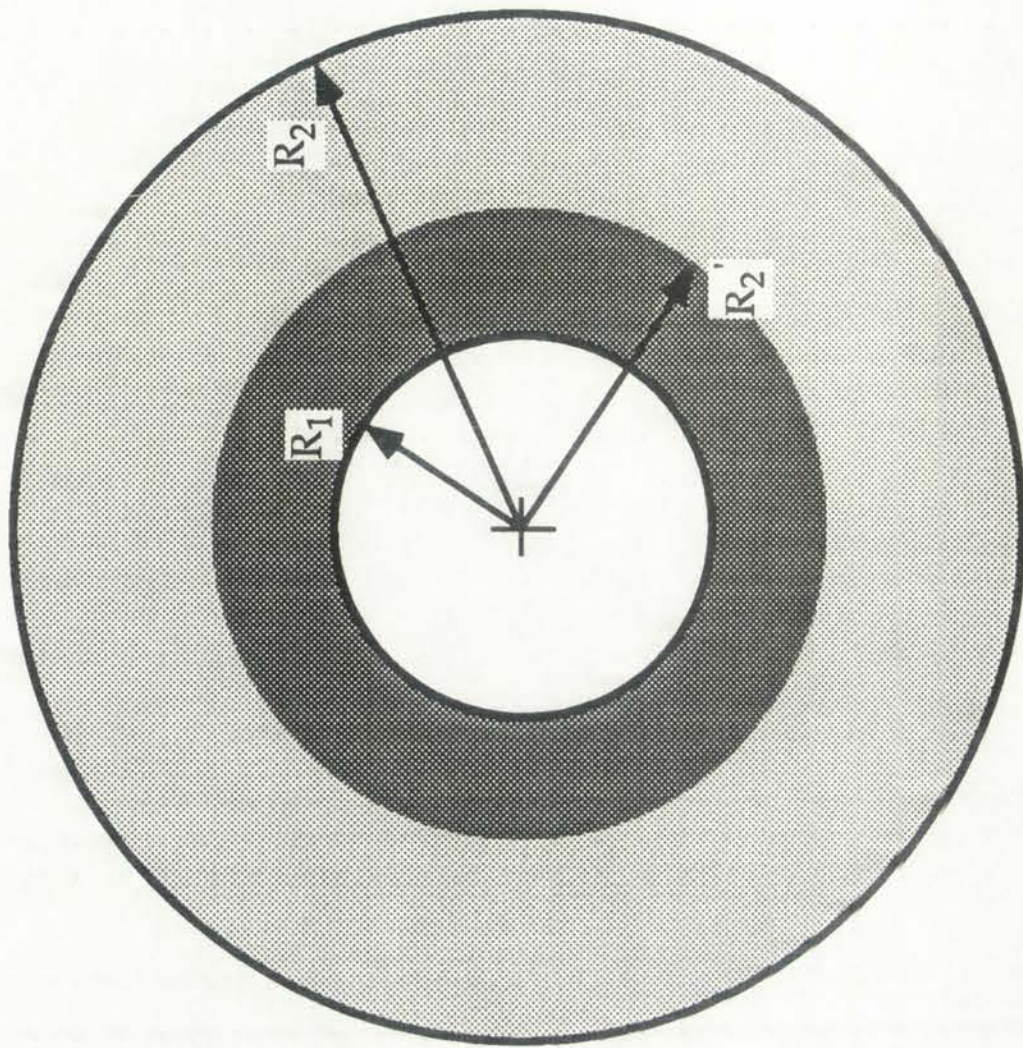
$$A_{annular} = \pi(R_0^2 - R_i^2) = \pi(R_o^2 - R_i^2) \quad (2.1)$$

This equation can be written in terms of the inner (R_i) and outer (R_o) radius of the annular region and the equivalent outer radius (R_0):

$$R_0^2 - R_i^2 = R_o^2 - R_i^2 \quad (2.2)$$



($r-\theta$) geometry: 40° Annular Segment Region



(r) geometry: Circumferential Annular Region

Figure 4.1: Geometry conversion of the propellant channel for the (r) geometry model.

1) $\frac{1}{2}$ of the circle is shaded. What fraction of the circle is not shaded?

2) $\frac{1}{4}$ of the circle is shaded. What fraction of the circle is not shaded?



3) $\frac{1}{3}$ of the circle is shaded. What fraction of the circle is not shaded?

4) $\frac{1}{5}$ of the circle is shaded. What fraction of the circle is not shaded?



From the above equation, a general expression can be derived for the equivalent outer radius, as a function of the inner and outer annular region radii and the fraction of the total annular region area subtended by the propellant channels:

$$R_2' = \sqrt{0.4(R_2^2 - R_1^2) + R_1^2} \quad . \quad (4.3)$$

Using the values of $R_1 = 24.94$ cm and $R_2 = 34.58$ cm from Figure 3.1, the equivalent outer radius for the propellant region modeled in (r) geometry is equal to 29.18 cm. Therefore, the radial thickness of the equivalent propellant region in (r) geometry is 4.24 cm, equal to 44% of the total radial thickness between R_1 and R_2 . Even though the 44% fraction is quite close to the 40% value for (r- θ) geometry, it indicates the need for conservation of dimensions when converting from a two-dimensional to a one-dimensional model. The calculated equivalent propellant region thickness of 4.24 cm was used throughout the (r) geometry analysis.

Taking into account the conservation of dimensions from the (r- θ) geometry to the (r) geometry model, it can be stated that the (r) geometry analysis represents a "best-case" scenario in terms of feasibility assessment because it assumes a propellant region in front of the solid moderator/reflector regions over the whole circumference of the engine. In the actual (r- θ) layout, the solid regions are directly exposed to the fuel, and also nearer to the fuel by 9.64 cm, in more than 40% of the circumference.

It should be noted here that the previous discussion indicated that the (r) geometry model involves positioning the propellant region closer to the fuel, with the Be-moderator region behind it. The (r) geometry model, therefore, provides an approximation of the behavior of such parameters as the neutron flux, volumetric heat generation rate, and temperature, all of which vary both in (r) and (θ). To ascertain that the (r) geometry approximation does not deviate significantly from the (r- θ) behavior, a series of comparative analyses was performed as part of this research work. The comparative analyses are included in Chapter 10 along with the other obtained results.

From the above equation a general expression can be derived for the equivalent zone radius as a function of the inner and outer radii regions and the fraction of the total available region size subtended by the propellant channels:

$$R_e = \frac{R_1^2 + R_2^2 + 2R_1R_2 \frac{V_p}{V}}{2(R_1 + R_2) \frac{V_p}{V}} \quad (2)$$

Using the values of $R_1 = 24.94$ cm and $R_2 = 21.58$ cm from Figure 2, the equivalent zone radius for the propellant region modeled in (1) geometry is equal to 22.18 cm. Therefore, the radial thickness of the equivalent propellant region in (1) geometry is 4.24 cm, equal to 47% of the total radial thickness between R_1 and R_2 . From Figure 2, the 47% fraction is quite close to the 40% value for (2-3) geometry. It will save the need for construction of dimensions when comparing with a two-dimensional model. The calculated equivalent propellant region thickness of 4.24 cm was used throughout the (1) geometry analysis.

Taking into account the construction of dimensions from the (2-3) geometry to the (1) geometry model, it can be stated that the (1) geometry analysis represents a "best case" scenario in terms of feasibility assessment because it assumes a propellant region in front of the solid moderator, reflects regions over the whole circumference of the region. In the actual test, however, the solid region is already exposed to the fuel and also needs to be fuel by 3.64 cm in more than 50% of the circumference.

It should be noted here that the previous discussion indicated that the (1) geometry model is not providing the propellant region closer to the fuel with the Be-moderator region behind it. The (1) geometry model, therefore, provides an approximation of the behavior of such parameters as the neutron flux, volumetric heat generation rate, and temperature, all of which vary both in (1) and (2). It is certain that the (1) geometry approximation does not deviate significantly from the (2-3) behavior, a series of comparative analyses was performed as part of the research work. The comparative analyses are included in Chapter 13 along with the other obtained results.

A breakdown of the research goals for this Dissertation work is presented below, with emphasis on three issues: (1) thermal analysis, (2), neutronics analysis, and (3) rocket performance. These three were deemed most representative of a thermalhydraulics analysis of a nuclear rocket engine.

DISSERTATION RESEARCH GOALS

Thermal Analysis:

- Compile a set of baseline thermophysical data for use in this analysis, and document them so as to provide a basis for any future gas-core rocket research;
- Develop a methodology for solving the heat transfer problem within the complete rocket engine, driven by the fission power;
- Determine the temperature distribution in the (r) direction of the rocket engine;
- Determine the atomic and mass densities of the gases in the engine and use them in the neutronics analysis.

Neutronics Analysis:

- Determine the volumetric heat generation rate as a function of radial distance and rocket engine thermal power;
- Determine the k_{eff} of the rocket engine baseline configuration, in both isothermal and supercooled configurations;
- Based on the results of the above task, delineate any potential benefits of using a supercooled moderator/reflector assembly.

Rocket Performance:

- Determine the feasibility of the concept, based on thermal and neutronics analysis, identify all engineering problem areas, and delineate the potential benefits (if any) of developing gas-core rocket technology for space exploration;
- Determine the Specific Impulse of the unit-cell rocket engine as a function of thermal power, assuming that the problem areas could be solved in the future;
- Determine the Thrust of the unit-cell rocket engine as a function of thermal power, assuming that the problem areas could be solved in the future.

A breakdown of the report goals for this Dissertation will be presented below with emphasis on three items: (1) thermal analysis, (2) performance analysis, and (3) rocket performance. These three items represent most representative of a thermodynamic analysis of a rocket engine engine.

DISSERTATION RESEARCH GOALS

- Thermal Analysis**

 - Obtain a set of baseline thermodynamic data for use in this analysis and document them so as to provide a basis for any future engine design work.
 - Develop a methodology for determining the heat transfer problem within the combustion chamber, nozzle, and nozzle throat.
 - Determine the temperature distribution in the (a) chamber and (b) nozzle.
 - Determine the chamber and nozzle wall heat fluxes and the heat transfer rates and use them in the engine design.
- Performance Analysis**

 - Determine the volumetric heat generation rate as a function of axial distance and rocket engine thrust power.
 - Determine the β_{eff} of the rocket engine nozzle configuration in both chamber and nozzle throat regions.
- Rocket Performance**

 - Determine the feasibility of the engine based on thermal and structural analysis, identify the engineering problem areas, and determine the potential benefits of using the developed technology for space exploration.
 - Determine the specific impulse of the engine based on a function of thrust power, chamber and nozzle throat area, and nozzle exit area.
 - Determine the thrust of the engine based on a function of thrust power, chamber and nozzle throat area, and nozzle exit area.

4.4. Basis for Originality

The research work discussed in this Dissertation is required to conform to the general guidelines set forth by the University of New Mexico for Ph.D.-level work; namely, the research has to be an original contribution to the scientific community, and the quality of the work needs to be such that it would warrant publication in a refereed scientific journal. A discussion of the merits of this research, which the author believes satisfy the above two criteria, is presented in the following paragraphs.

The vast majority of NLB-related research was carried out at UARL, and it consisted mostly of experimental modeling and proof-of-concept of the fluid mechanics behavior. The reason for that lay in the belief (most probably correct) that if there was a significant show-stopper, it would be the fluid mechanics confinement of the fissioning uranium gas. As discussed in Section 2.5 of this Dissertation, because of the lack of computing capability, all of the performance parameters associated with the NLB were derived from a set of assumed baseline values. Thus, the specific impulse of 1,870 sec, thrust of 409,000 N, thermal power of 4,600 MW_{th} and all temperatures associated with the NLB rocket engine are *assumed* values; the same is true for the NLB performance parameters shown previously in Table 2.1. All these factors pointed to a need for a comprehensive thermalhydraulics analysis to provide an accurate set of parameters and determine the feasibility of the concept.

The thermalhydraulics analysis was intended to analyze the unit-cell NLB rocket engine in the configuration proposed by the original UARL designers. Thus, the results obtained from the analysis could be used to ascertain the nature and magnitude of any necessary modifications to the original design. Such modifications, once implemented, could result in a feasible and operational engine which could proceed to ground testing and development.

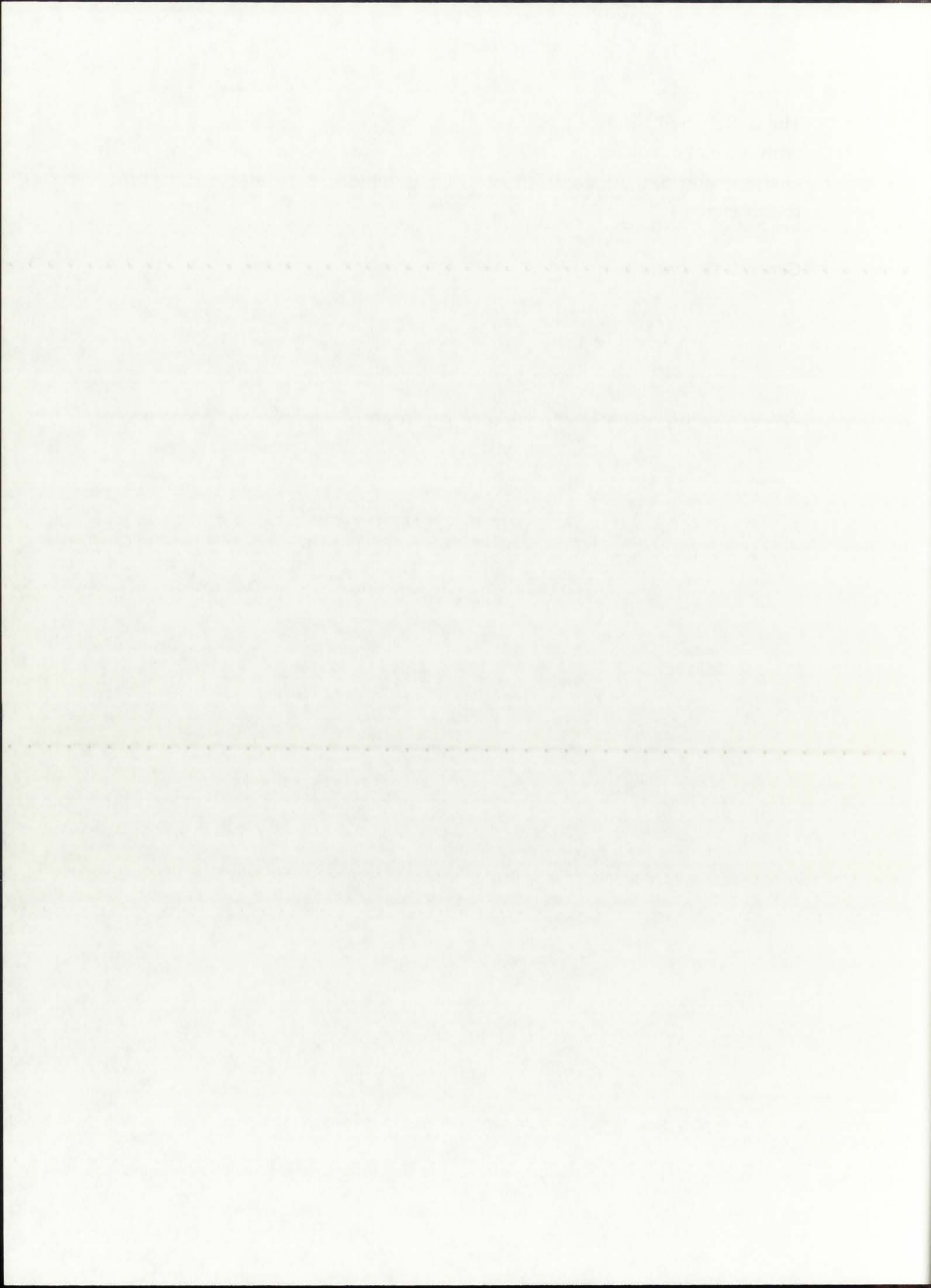
The anticipated original contributions of this research are presented below, with a breakdown into a *General Contribution* (related to a methodology of analysis) and *Specific Contributions* (related specifically to the unit-cell NLB rocket engine).

General Contribution:

- Develop a defensible and reproducible methodology for analyzing the heat transfer and neutronics in a closed-cycle GCR and determine the feasibility of such a concept.

Specific Contributions:

- Analyze the unit-cell NLB concept, determine its feasibility, identify all problem areas in the concept.
- Determine potential benefits (if any) of the low temperature moderator/reflector on the critical size and mass.



CHAPTER 5

PROPOSED METHODOLOGY OF ANALYSIS

5.1. Introduction

The most important aspect of this research work pertains to the methodology chosen to solve the heat transfer and neutronics problems. All other information --assumptions, baseline data, and results-- hinge on the methodology. To facilitate readers' understanding, a top-level design specification is presented in this Chapter, outlining the various components of the methodology and the proposed path from start to completion. The pertinent theory and assumptions used in the heat transfer and neutronics analyses are presented in detail in Chapters 6 and 7, respectively. The pertinent rocket propulsion theory is presented in Chapter 8.

5.2. Top-level Design Specification

The goal of this research work, as stated previously, is to analyze the thermalhydraulics behavior of the unit-cell NLB rocket engine and use the obtained results to determine the feasibility of the concept. Within the scope of thermalhydraulics, the thermal and neutronics behavior are inherently coupled, because the fission reaction is the driver behind heat transfer from the fuel to the rest of the rocket engine, and conversely, the temperature distribution influences fuel density and criticality. To allow for the coupled thermal and neutronics analysis, a number of initial assumptions are required, pertaining to the fluid mechanics aspect of the rocket engine. For the purposes of this analysis, the following assumptions will be used:

- Fluid mechanic confinement has been achieved, resulting in a laminar and well-defined boundary between the gaseous fuel and buffer gas;
- The radial dimensions of the gaseous and solid regions, as well as the cavity length, are equal to the only set of dimensions proposed by UARL.

CHAPTER 2 PROPOSED METHODOLOGY OF ANALYSIS

2.1 Introduction

The most important aspect of this research work pertains to the methodology chosen to solve the heat transfer and neutron problems. All other information—assumptions, boundary data and results—hinge on the methodology. To facilitate readers' understanding a top-level design philosophy is presented in this Chapter, outlining the various components of the methodology and the proposed path from start to completion. The neutron theory and transport used in the heat transfer and neutron analyses are presented in detail in Chapter 5 and 6, respectively. The pertinent nuclear engineering theory is presented in Chapter 8.

2.2 Fuel Element Design Philosophy

The goal of this research work as stated previously, is to analyze the thermally-mechanical behavior of the salt-cooled MTR fuel element and use the obtained results to determine the feasibility of the concept within the scope of thermally-mechanical, the thermal and neutron behavior and integrity. In doing so, the design philosophy is the driver behind heat transfer from the fuel to the rest of the reactor system and conversely, the temperature distribution influences fuel density and thermal expansion. To allow for the coupled thermal and neutron analysis a number of initial assumptions are required, pertaining to the fluid mechanics aspect of the reactor system. For the purposes of this analysis, the following assumptions will be used:

- * Fuel rod thermal conductivity has been selected, resulting in a laminar and well-defined boundary between the gaseous fuel and buffer gas.
- * The radial dimensions of the gaseous and solid regions, as well as the cavity length, are equal to the outer diameter proposed by IAEA.

These values were previously given in Figures 3.1 and 3.2. The segmented propellant channels are represented by an equivalent outer radius, as discussed previously in Section 4.3;

- The operating pressure is equal to 250 atm as initially proposed by UARL for the unit-cavity NLB rocket engine [Latham and Rodgers, 1972a];
- The buffer gas axial velocity corresponds to the only value proposed by UARL, and is approximately equal to 2.0 m/s [McLafferty and Bauer, 1967].

The above assumptions provide a set of baseline assumptions and reference data that will be used to evaluate the thermal and neutronics characteristics of the engine. Some of the data, such as the reactor thermal power and operating pressure, can be open to parametric analysis.

A top-level structure of the proposed methodology of analysis is depicted in Figure 5.1. The methodology consists of two major parts: (1) the heat transfer model and (2) the neutronics model. Analysis commences with UARL dimensions and fluid mechanics parameters (pressure and velocities), and an assumed average volumetric heat generation rate in the fuel $Q_{g,avg}'''(r)$. The above data are used by the heat transfer model to calculate a converged temperature distribution within the nine regions in (r) geometry, as shown in Figure 5.2. The same general nine-region model is used for the neutronics analysis.

As part of the neutronics analysis, two separate neutron cross-section libraries are used: (1) Hansen-Roach and (2) Temperature-dependent ENDF/B-V data. The Hansen-Roach library is used to provide a reference mass and size for the baseline configuration, and also to gauge any potential neutronics benefits of using the supercooled moderator/reflector. It has been widely used in criticality safety analysis and is the standard cross-section library provided with the ONEDANT/TWODANT package of neutron transport codes [O'Dell, 1989; LANL, 1993].

These values were previously given in Figure 2.1 and 2.2. The
assumed geometric shapes are shown in an equivalent circuit
in Figure 2.3. The values are given in Section 2.3.

The operating pressure is equal to 100 atm as initially proposed by IARI.

The buffer gas inlet velocity corresponds to the only value proposed by
IARI, and is approximately equal to 50 m/s. The inlet and outlet
diameters are

The above assumptions provide a set of realistic transport and reaction
data that will be used to evaluate the thermal and chemical characteristics of
the engine. Some of the data such as the reactor thermal power and operating
pressure will be used to generate the engine.

A top level description of the proposed methodology of analysis is shown in
Figure 2.1. The methodology consists of two major parts: (1) the heat transfer
model and (2) the reaction model. Analysis commences with IARI
data and this includes reaction parameters (pressure and velocity) and an
assumed average volumetric heat generation rate in the fuel. The
above data are used by the heat transfer model to calculate a proposed
temperature distribution within the tube region. It is assumed, as shown in
Figure 2.2, the entire general algorithm model is used for the numerical
analysis.

As part of the numerical analysis, the input data are cross-section
data: (1) H₂-O₂ and (2) temperature dependent IARI-V data.
The H₂-O₂ data library is used to provide a reference mass and size for the
reactant configuration, and also to give the potential reaction kinetics of
using the supercritical molecular weight. It has been widely used in
other work and is the standard cross-section library provided
with the CHEMICAL THERMODYNAMIC package in routine transport codes (IARI).

1987 JAN 1988

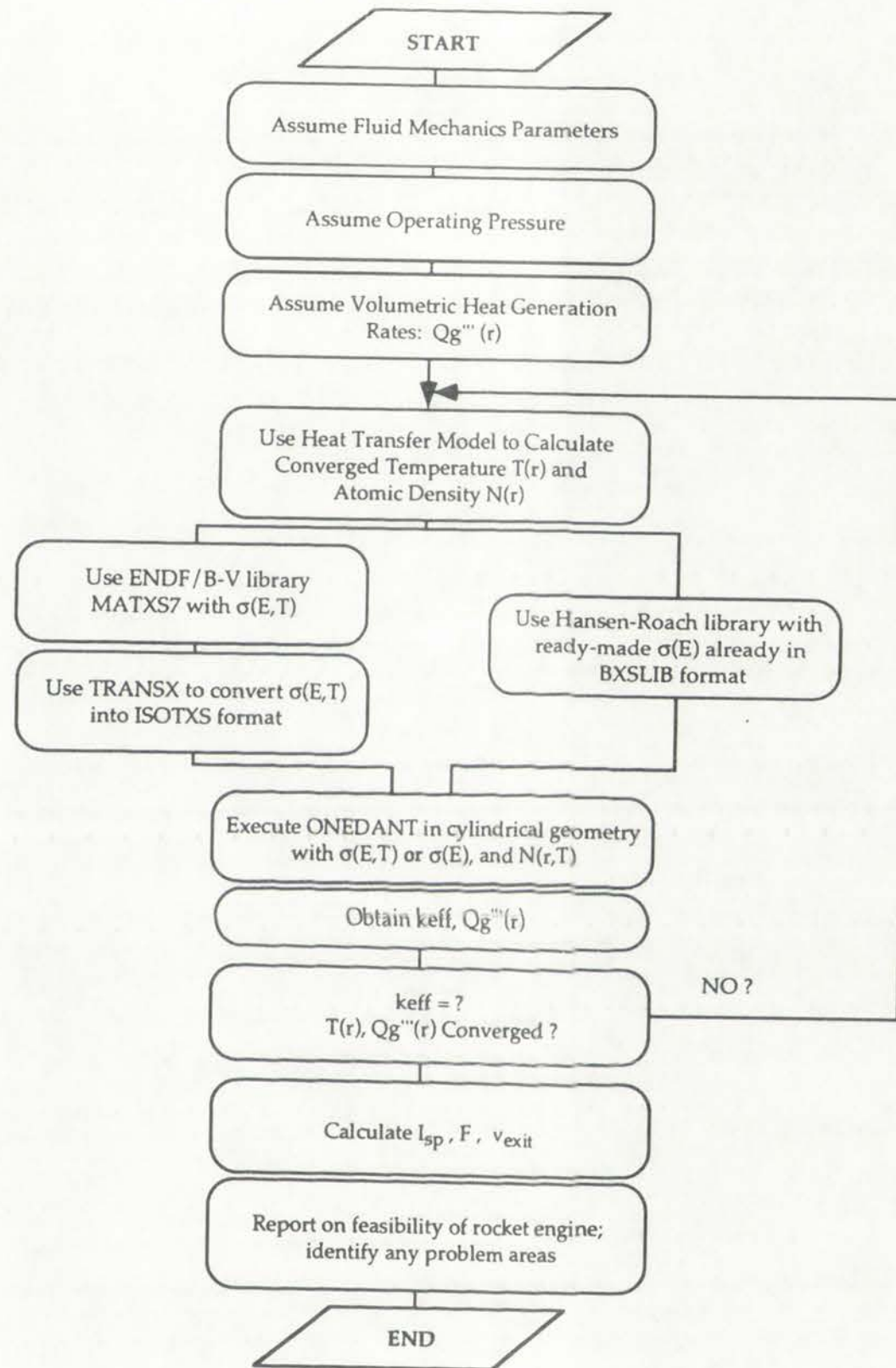
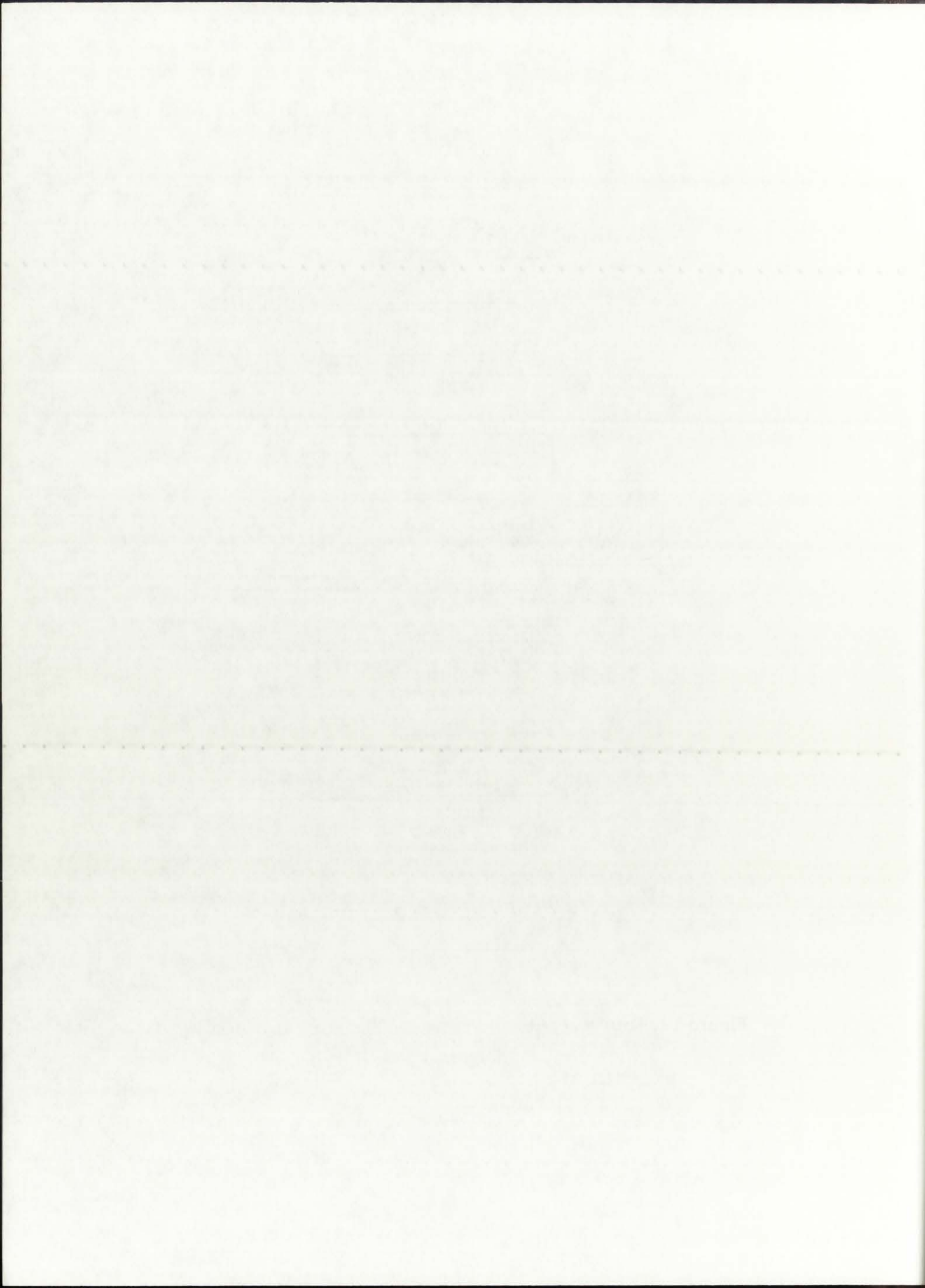


Figure 5.1: Top-level structure of the methodology discussed in this Dissertation.



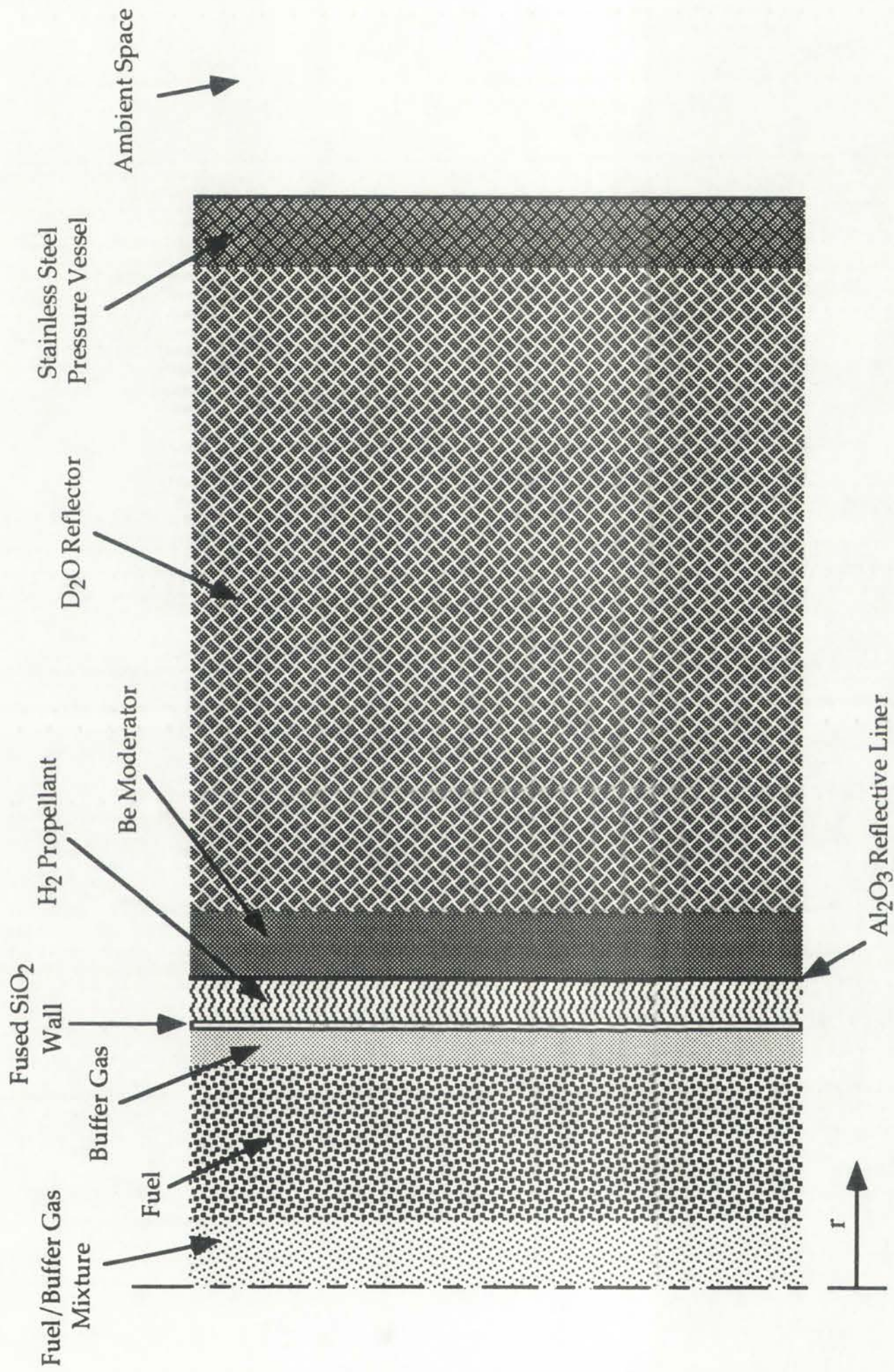


Figure 5.2: Nine-region layout of the (r) geometry unit-cell NLB rocket engine model.

Figure 2.3: Schematic diagram of the layered structure of a typical fiber optic cable. The layers are labeled as follows: Core, Cladding, Buffer, and Jacket.



The Core is the central part of the fiber that carries the light signal. The Cladding surrounds the Core and reflects the light back into the Core. The Buffer is a protective layer that surrounds the Cladding. The Jacket is the outermost layer that provides mechanical protection to the fiber.

The temperature-dependent ENDF/B-V library is constructed from baseline ENDF/B-V neutron data for the nine regions shown in Figure 5.2, and incorporates temperature-dependent microscopic cross-sections. This allows a more accurate modeling of the actual neutronics characteristics inside the NLB engine and accounts for the significant difference between the temperatures of each region. In addition, the energy group structure of the ENDF/B-V library can account for the very low thermal energy neutrons (below 0.025 eV) resulting from the low-temperature moderator/reflector.

For each of the nine regions of the thermalhydraulics model, a set of microscopic cross-sections is provided through the usage of the TRANSX nuclear cross-section processing system [MacFarlane, 1993], with the cross-sections evaluated at the representative temperatures. A 127-nuclide binary-format ENDF/B-V cross-section library, MATXS7, is processed by the TRANSX code to provide a 9-nuclide, temperature dependent cross-section library in binary ISOTXS format.

The cross-sections for the nine regions in binary format, either TRANSX-processed (ISOTXS) or from the readily available Hansen-Roach library (BXSLIB), are provided as a library to the neutronics code ONEDANT [O'Dell *et al.*, 1989]. Also provided as input to ONEDANT are the radial dimensions and atomic densities $N(r)$ of the nine regions. Using the cross-sections, radial dimensions, and representative atomic densities of the nine regions, ONEDANT determines the effective multiplication factor (k_{eff}) of the unit-cell NLB rocket engine and the volumetric heat generation rates $Q_g'''(r)$ in the fuel.

Successful completion of the coupled thermal/neutronics analysis occurs when the ONEDANT-calculated $Q_g'''(r)$ are equal to those provided to the heat transfer model within the same iteration. This provides a set of converged $Q_g'''(r)$, $T(r)$, and k_{eff} . If the execution of the coupled analysis is part of a parametric study on thermal power generation or operating pressure, for example, then the whole process can be repeated to obtain results for varying thermal powers or varying pressures.

The program dependent LIBRARY library is distributed with the
EMC 3.0 source files for the nine regions shown in Figure 3.1 and
includes the program dependent program dependent. The library
more accurate modeling of the actual nuclear cross-sections. It
with regard and accounts for the significant difference between the
cross-sections at each region. In addition, the energy groups are all
ADP/EMC library can account for the very low thermal energy neutrons
below 0.025 eV) resulting from the low temperature moderator/reflector.

For each of the nine regions of the thermal-hydraulic model, a set of
nuclear cross-sections is provided through the code of the EMANX
nuclear cross-section processing system [Mehrtens, 1971] with the cross-
sections evaluated at the appropriate temperatures. A 12x-nucleus energy-
group EMANX 3.0 cross-section library, EMANX, is processed by the
EMANX code to produce a 7-nucleus energy-dependent cross-section
library in binary BOSTX format.

The cross-sections for the nine regions in binary format either EMANX
processed (BOSTX) or from the ready-to-use Hansen-Roch library
(BOSTL) are provided as a library to the computer code ORBITANT [O'Dell
et al, 1981]. Also provided as input to ORBITANT are the radial dimensions
and axial densities (kg/m³) of the fuel regions. Using the cross-sections, radial
densities, and representative axial densities of the nine regions,
ORBITANT determines the effective multiplication factor (k_{eff}) of the nine-
cell 1D reactor and the relative fuel rod power $Q_{rod}(z)$ in the
fuel.

Successful completion of the coupled thermal-hydraulic analysis occurs
when the ORBITANT-calculated $Q_{rod}(z)$ are used to heat provided to the
heat transfer model within the same location. This provides a set of
coupled $Q_{rod}(z)$ (Eq. 4-1) if the location of the coupled analysis is part
of a transient study on thermal power generation or operating pressure. For
example, when the whole system can be modeled to obtain results for varying
thermal power of varying pressure.

Once all desired parametric analyses have been completed, the actual rocket performance parameters are reported: specific impulse (I_{sp}), thrust (F), and exit velocity (v_{exit}). Finally, based on the results of the thermal analysis, a conclusion is reached as to the engineering feasibility of the concept. Any problem areas associated with the concept are reported and possible ways to solve them are proposed as recommendations for future work.

In conclusion, then, a significant number of NLB engine parameters can be obtained as a result of the research work presented in this Dissertation. The baseline engine parameter was chosen to be the total thermal power. Three power levels are analyzed in this Dissertation --500 MWth, 5 MWth, and 50 kWth-- but emphasis is placed on the 50 kWth configuration, as it most closely matches the 8,333 K fuel temperature envisioned by the original UARL designers as obtainable from the NLB engine.

Once all desired parameters have been established, the actual engine performance characteristics are determined. The engine performance characteristics are determined by the engine design parameters. The engine performance characteristics are determined by the engine design parameters. The engine performance characteristics are determined by the engine design parameters.

In conclusion, the significant number of engine parameters can be obtained as a result of the research work presented in this literature. The engine performance characteristics are determined by the engine design parameters. The engine performance characteristics are determined by the engine design parameters. The engine performance characteristics are determined by the engine design parameters.

UNIVERSITY OF CALIFORNIA, BERKELEY

CHAPTER 6

HEAT TRANSFER THEORY

6.1. Introduction

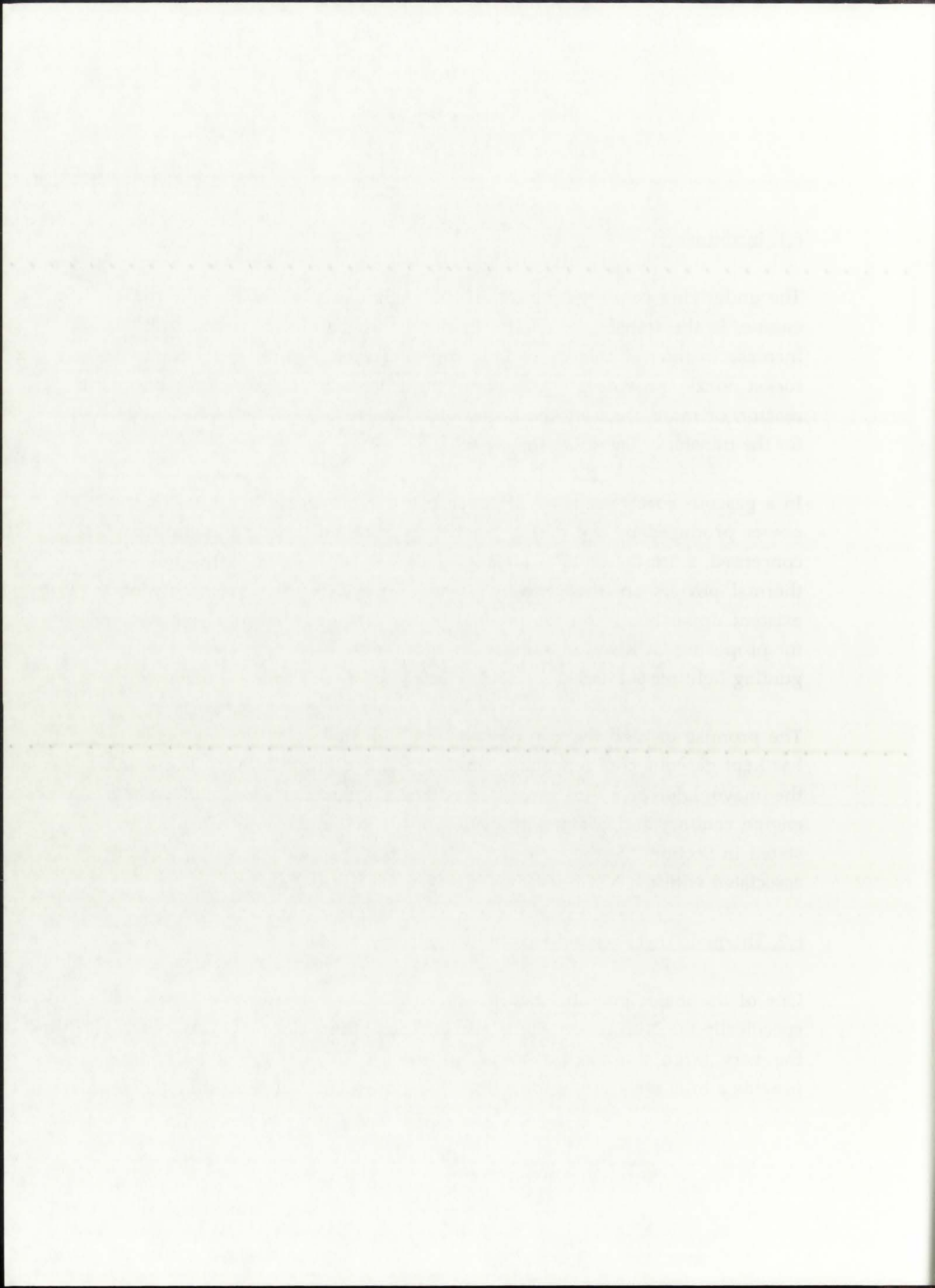
The underlying concept behind the NLB engine, as well as any other rocket engine, is the transfer of energy to the working fluid, or propellant. The increase in internal energy of the propellant results in its ejection out the rocket nozzle, providing movement to the spacecraft. The role of the nuclear reactor, or more precisely the nuclear reaction, is to provide the heat source for the transfer of energy to the propellant.

In a gaseous core reactor (GCR), such as the NLB engine, the total thermal power produced by the fission reaction is not limited as far as the fuel is concerned; since the latter is already in a gaseous phase, virtually unlimited thermal powers are theoretically possible in a GCR. This seemingly non-existent upper bound on the thermal power provided the initial motivation for proposing GCR rocket engines for space propulsion. It has also been the guiding light for continued research efforts into gaseous core technology.

The promise of high thermal powers and high fuel operating temperatures has kept gaseous core technology in the spotlight. From the very beginning, the unavoidable problems associated with this technology --fuel confinement, engine cooling, and complexity of design-- were assumed solvable. As was stated in Section 2.5, the majority of "reference" parameters now commonly associated with the NLB rocket engine were actually assumed values.

6.2. Thermal Power-related Feasibility Problems

One of the major potential benefits of all gaseous core rocket engines, and specifically the NLB rocket engine, is also one of the major practical obstacles: the very large thermal power of the reactor. The following paragraphs provide a brief walk-through the underlying causes of such a condition.



Because of the complexity of its design, the GCR becomes interesting only if it can provide significant performance increases over solid core reactor (SCR) technology. This, translated in performance terms, means that GCR research and development is justified only if it can prove the feasibility of propellant temperatures well in excess of 3,000 K. Such a propellant temperature could undoubtedly be achieved in a GCR, and it would probably be classified as a "lower limit." If one were only concerned with heat transfer from the fuel to the propellant, there would really be no limit to propellant temperatures. The problem, however, is that according to the laws of conservation of energy, the very hot propellant gas will in turn heat its surroundings, namely the moderator, reflector, and structural regions of the rocket engine. In order for the rocket to function, those solid regions must be maintained below their melting temperature. This is precisely where a detailed thermal analysis of the engine is needed: *to determine the temperature distribution within such an engine and indicate the feasibility (or lack thereof) of certain power levels.*

The goal of the thermal analysis presented here is to determine the feasibility of the unit-cell NLB rocket engine from the standpoint of thermal integrity of the solid regions. Because prior work was based on assumed fuel temperatures, thermal powers, and propellant temperatures, the research presented here is believed to constitute the first comprehensive NLB-related thermal analysis. The results of this research are intended to determine the feasibility of the unit-cell NLB rocket engine, as well as present the methodology for performing a general GCR thermal analysis.

6.3. Governing Energy Balance Equations

The heat transfer within the NLB engine is "driven" by the reactor thermal power, i.e. the generation of heat associated with the fission reaction. At any location, or node, in the (r) direction within the engine, the following governing energy balance equation is valid:

$$Q_g + Q_{in} + Q_{out} = 0 \quad . \quad (6.1)$$

process of the synthesis of the design, the GCM (Generalized Control Method) can provide significant performance benefits. This method is particularly useful in the design of control systems for systems with multiple inputs and outputs. The GCM is a powerful tool for the design of control systems for systems with multiple inputs and outputs. The GCM is a powerful tool for the design of control systems for systems with multiple inputs and outputs. The GCM is a powerful tool for the design of control systems for systems with multiple inputs and outputs.

The goal of the thermal analysis presented here is to determine the feasibility of the use of the GCM for the design of control systems for systems with multiple inputs and outputs. The GCM is a powerful tool for the design of control systems for systems with multiple inputs and outputs. The GCM is a powerful tool for the design of control systems for systems with multiple inputs and outputs. The GCM is a powerful tool for the design of control systems for systems with multiple inputs and outputs.

2.1. Generalized Control Method

The first transfer within the GCM engine is driven by the vector thermal power. In the generation of heat associated with the fusion reaction. At any location or time, in the (x) direction within the engine, the following governing energy balance equation is valid:

$$\rho c_p \frac{dT}{dt} + \rho c_p v \frac{dT}{dx} = \rho c_p \frac{dT}{dx} + \rho c_p v \frac{dT}{dx} \quad (2.1)$$

for steady-state operating conditions. Q_g , Q_{in} , and Q_{out} correspond to the total heat generation rate, the total heat transfer into that node, and the total heat transfer out of that node, respectively; all have units of Watts [W]. Since the actual direction of heat flow (i.e., into or out of a particular node) is often unknown, it has been suggested to formulate the energy balance equation with the assumption that all the heat flow is into the node [Incropera and DeWitt, 1990]. Such a condition, although realistically impossible, results in the correct temperature distribution if the condition is diligently applied to each node of the system being analyzed. Thus, the general energy balance equation can be expressed as:

$$Q_g + Q_{in} = 0 \quad . \quad (6.2)$$

Appropriate derivatives of eqn. (6.2) are applicable for any given node in the (r) direction of the unit-cell NLB engine. Thus, for the fuel and fuel/buffer gas mixture, the appropriate energy balance equation consists of both the generation and transfer terms:

$$Q_g + Q_{in} = 0 \quad . \quad (6.3)$$

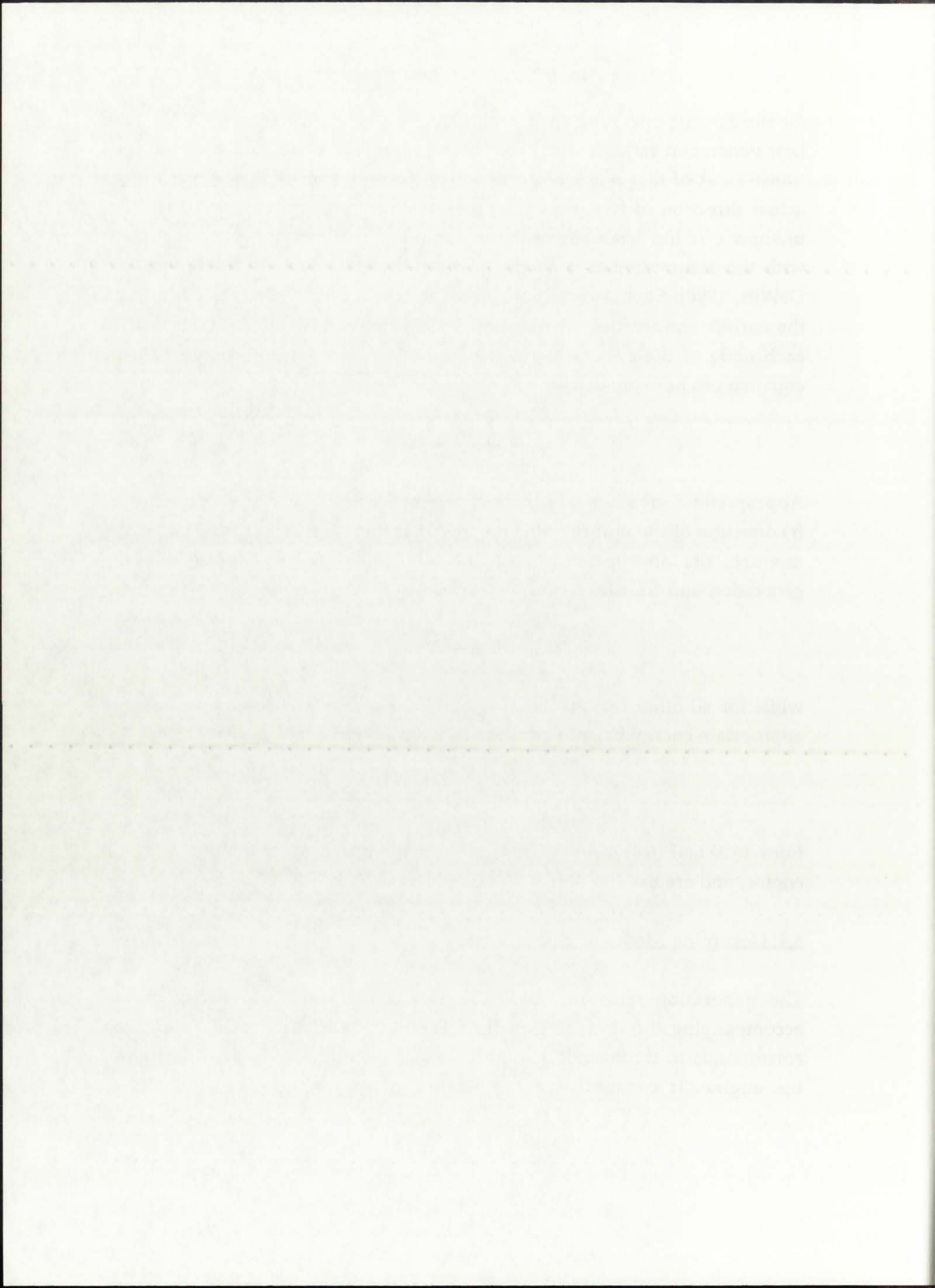
while for all other regions, because of the absence of any fissioning fuel, the appropriate energy balance equation contains only the heat transfer term:

$$Q_{in} = 0 \quad . \quad (6.4)$$

Eqns. (6.3) and (6.4) form the basis of the thermal analysis of the unit-cell NLB engine, and are used to derive all subsequent expressions.

6.4. Governing Modes of Heat Transfer

The generation term in eqn. (6.3), Q_g , is the result of energy release accompanying the fissioning of fuel. The heat *transfer* term Q_{in} , however, corresponds to the overall amount of heat transferred in the (r) direction of the engine. It consists of a combination of conduction, convection, and

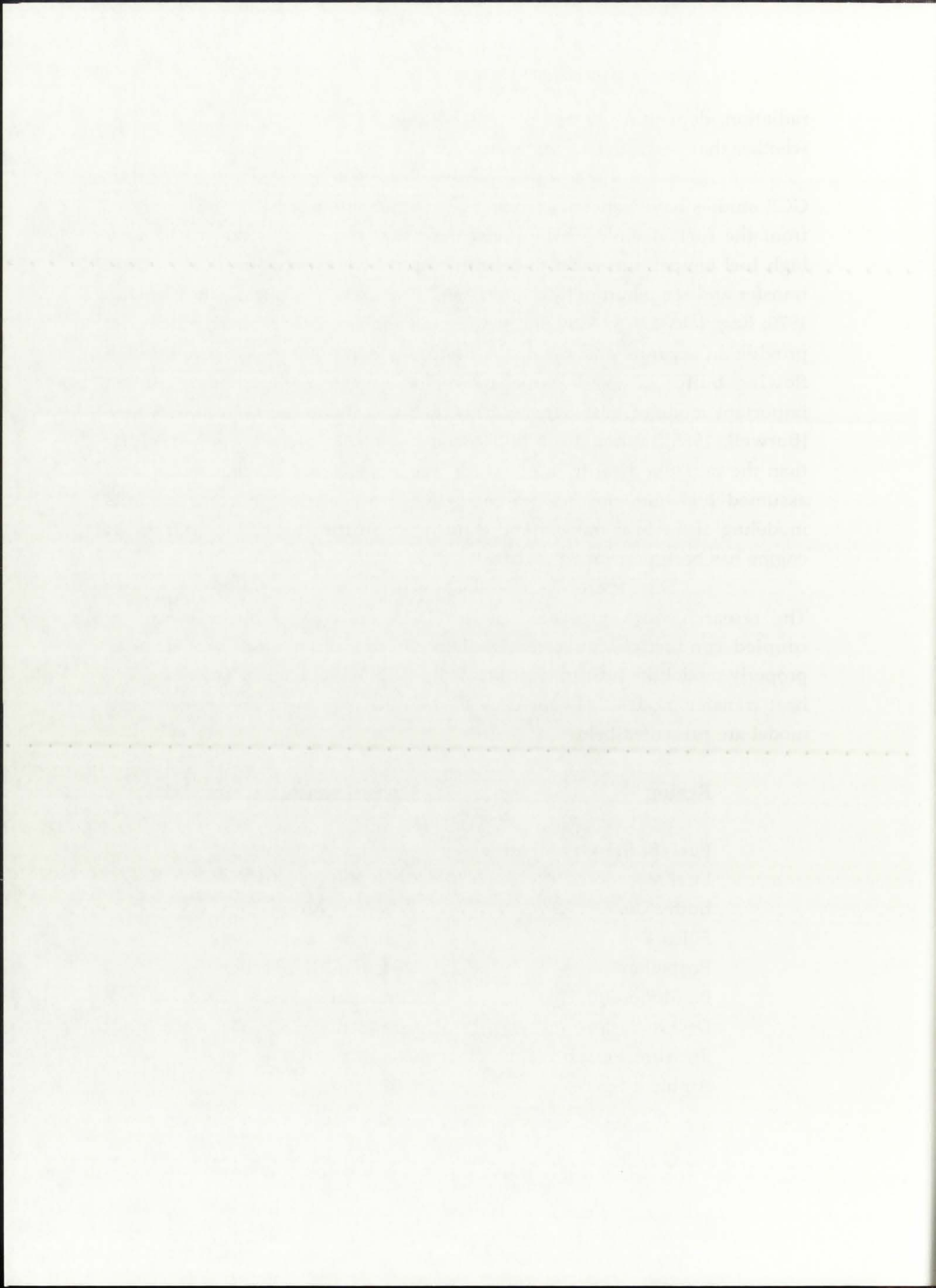


radiation, depending on the physical state of the particular region and also whether that particular region is engaged in bulk fluid motion.

GCR studies have generally focused on estimating the radiative heat transfer from the fuel, deeming it the most important component due to the very high fuel temperatures and the fourth-power relation between radiative heat transfer and temperature [McLafferty and Bauer, 1967; Schwenk and Franklin, 1970; Ragsdale, 1970]. Although that postulate cannot be disputed, it does not provide an accurate analysis of the heat transfer conditions, especially in the flowing buffer gas and propellant regions, where convection is also an important mode of heat transfer. This condition was recognized at that time [Burwell, 1965], although no NLB-associated results were presented. Other than the radiative heat transfer, which was in itself used in conjunction with assumed fuel temperatures, no comprehensive analytical or computational modeling of the heat transfer and temperature distribution in the NLB rocket engine has been performed to date.

The research work presented in this Dissertation work utilizes directly coupled conductive/convective/radiative heat transfer modes in order to properly model the heat transfer across the NLB rocket engine. The respective heat transfer modes used for each of the nine regions of the (r) geometry model are presented below.

<u>Region</u>	<u>Mode(s) of heat transfer</u>
Fuel/Buffer Gas Mixture	Generation, Radiation
Fuel	Generation, Radiation
Buffer Gas	Radiation, Convection
Silica Wall	Radiation, Conduction
Propellant	Radiation, Convection
Be Moderator	Conduction
D ₂ O Reflector	Conduction
Pressure Vessel	Conduction
Ambient Space	Radiation



6.4.1. Fuel/Buffer Gas Mixture and Fuel Regions

Radiation was assumed as the only mode of heat transfer in the fuel/buffer gas mixture and the fuel because, historically, only radiative properties of high-temperature fuel have been available. No information was available on such properties as fuel thermal conductivity, viscosity, and Prandtl number, all needed for convective analysis. Most important of all, no data was available on the fluid dynamic characteristics of the fuel flow (such as axial velocity or mass flow). Because of the lack of data in those two major areas, it was decided, rather than to completely assume such values or engage in speculative extrapolation, to include only radiation as a mode of heat transfer in the fuel. This does not affect the accuracy of the temperature distribution inside the fuel region because generation is the dominant factor, and also because the region is extremely opaque to thermal radiation; as a result of the latter, heat transfer occurs only between adjacent nodes and there is no significant additional contribution from convection.

6.4.2. Buffer Gas and Propellant Regions

Both radiation and convection were included in the buffer gas and propellant regions because of the inherent axial flow profile of both media. In addition, a radiation-only assumption can potentially lead to underestimates of their local temperatures due to the fact that both are relatively transparent to thermal radiation. Inclusion of convection is absolutely necessary in those two regions, both to properly account for the local temperatures and also to accurately model the heat transfer from these two regions to the silica wall and the solid moderator and reflector [Kelm and Peschka, 1970].

6.4.3. Silica Wall

Heat transfer in the silica wall was never analyzed in great detail; [Klein, 1970; Krascella, 1970; Schwenk and Franklin, 1970; Mensing *et al.*, 1990; and Gauntt *et al.*, 1992b] all indicated potential difficulties with maintaining the wall in such a high-temperature environment, but specified only the need for highly

The first part of the document discusses the importance of maintaining accurate records of all transactions. It emphasizes that every entry should be supported by a valid receipt or invoice. This ensures transparency and allows for easy verification of the data.

In addition, it is crucial to review the records regularly to identify any discrepancies or errors. This proactive approach helps in catching mistakes early and prevents them from escalating into larger issues. Consistent monitoring also aids in understanding the overall financial health of the organization.

The second section focuses on the role of technology in modern accounting. It highlights how software solutions can streamline the recording and analysis of financial data. Automation reduces the risk of human error and saves valuable time, allowing accountants to focus on more strategic tasks.

Furthermore, the use of cloud-based systems facilitates real-time access to financial information. This enables stakeholders to make informed decisions quickly. Security features are also a key consideration, ensuring that all data is protected against unauthorized access and cyber threats.

Finally, the document concludes by stressing the importance of ongoing education and training for the accounting staff. The field is constantly evolving, and staying up-to-date with the latest regulations and technologies is essential for success. Continuous learning ensures that the team remains competent and effective in their roles.

In summary, a combination of diligent record-keeping, the strategic use of technology, and a commitment to professional development are the keys to successful financial management. These practices not only ensure compliance but also provide a clear and accurate picture of the organization's performance.

transparent fused silica compounds. [Gauntt *et al.*, 1992b] discussed the possibility of employing free-standing diamond structures, but did not enter into a thermal analysis. [McLafferty and Bauer, 1967] assumed that 5% of the thermal radiation emitted from the fuel will be absorbed in the wall, and concluded that the wall mean temperature would not exceed the melting temperature of the silica, tabulated at 1,883 K [Ultramet, 1992]. The problems with the above approach are twofold: (1) the 5% absorption fraction was an assumption, and (2) the fuel temperature was in itself an assumption, as discussed previously in Section 2.5.

Because the silica wall is one of the most crucial components of the NLB concept, both radiation and conduction were included in the work presented in this Dissertation. That approach, in conjunction with the convection on both sides of the wall, provides the means for analyzing as accurately as possible the true condition of the silica wall inside the NLB engine.

6.4.4. Moderator, Reflector, and Pressure Vessel

Conduction was included in the moderator, reflector, and pressure vessel, as appropriate for solid regions. No cooling was assumed in either of the three regions, both due to lack of information on the layout and dimensions of the cooling system, as well as due to the one-dimensional *r*- geometry analysis.

6.4.5. Ambient Space

The ambient space surrounding the engine acts as an infinite heat sink, and is characterized by a temperature of approximately 200 K [Angelo and Buden, 1985; Morley, 1993]. The analysis presented in this Dissertation treats ambient space as a participating medium in order to obtain a temperature distribution outside of the rocket engine, too. For the purposes of analysis, a distance of 1.0 m from the outer boundary of the engine was assumed to correspond to the infinite heat sink at a temperature of 200 K. The 1.0 m region between the engine boundary and the infinite sink was assumed to be subject to thermal radiation.

temperature field using computer (Ghani et al., 1992) discussed the possibility of employing heat-conducting diamond windows but did not give into a thermal analysis (Kochenderfer and Berman, 1987) assumed that 92% of the thermal radiation emitted from the hot wall is absorbed in the wall and concluded that the wall mean temperature would not exceed the melting temperature of the diamond (3550 K) (Ghani et al., 1992). The analysis with the above approach are provided (1) the 2D absorption function was an absorption, and (2) the hot temperature was in fact an absorption, as discussed previously in Section 2.2.

Because the silica wall is one of the most critical components of the NTR concept, both radiation and conduction were included in the work presented in this literature. That approach, in conjunction with the convection on both sides of the wall, provides the means for analyzing as accurately as possible the true condition of the silica wall inside the NTR engine.

4.4.4. Moderator, Reflector, and Control Rods

Conduction was included in the moderator, reflector and control rod as appropriate for solid regions. No cooling was assumed in either of the three regions due to lack of information on the layout and dimensions of the control system as well as due to the complexity and a separate analysis.

4.4.5. Air Heat Sink

The ambient space surrounding the engine was an infinite heat sink and is characterized by a temperature of approximately 300 K (Ayres and Borden, 1992; Borden, 1993). The analysis presented in this literature treats ambient space as a participating medium in order to obtain a temperature distribution outside of the reactor engine, too. For the purpose of analysis, a distance of 1.0 m from the outer boundary of the engine was assumed to correspond to the infinite heat sink at a temperature of 300 K. The 1.0 m region between the engine boundary and the infinite sink was assumed to be subject to thermal radiation.

6.4.6. Summary

As discussed above, all four modes of heat transfer are selectively used in the thermal analysis. Eqns. (6.3) and (6.4), with the generic Q_{in} term expanded to include the specific heat transfer modes, now have the following form for each of the nine regions in the model:

Fuel/Buffer Gas Mixture and Fuel Regions

$$Q_g + Q_{rad} = 0 \quad . \quad (6.5)$$

Buffer Gas and Propellant Regions

$$Q_{rad} + Q_{conv} = 0 \quad . \quad (6.6)$$

Silica Wall

$$Q_{rad} + Q_{cond} = 0 \quad . \quad (6.7)$$

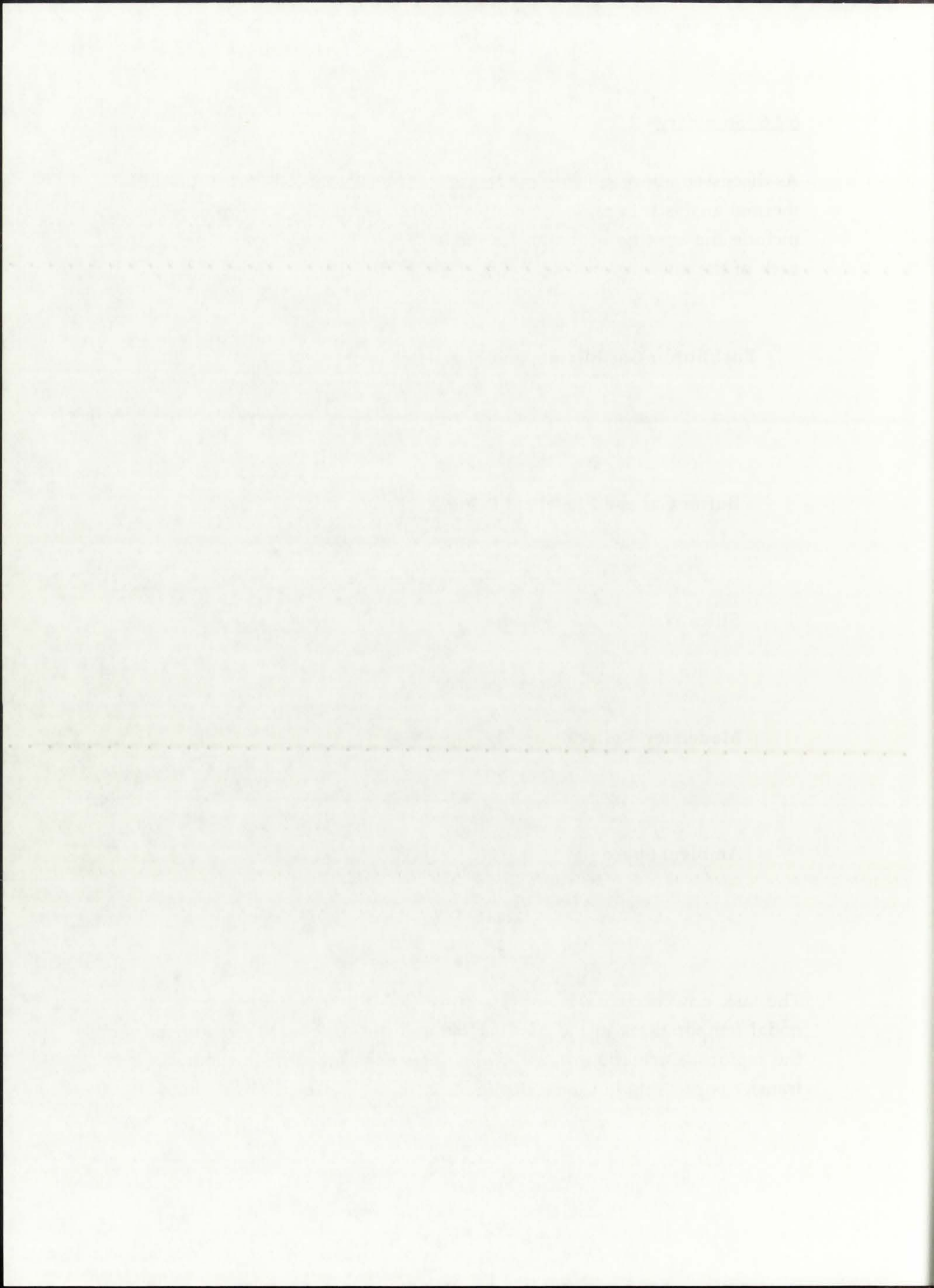
Moderator, Reflector, and Pressure Vessel

$$Q_{cond} = 0 \quad . \quad (6.8)$$

Ambient Space

$$Q_{rad} = 0 \quad . \quad (6.9)$$

The task now becomes to express eqns. (6.5) through (6.9) in terms of the nodal temperatures in the (r) direction and the corresponding properties of the regions. Derivation of the explicit equations for all four modes of heat transfer is presented in the following Section.



6.5. The Theory of the Modes of Heat Transfer

Each of the four modes of heat transfer present in eqns. (6.5) through (6.9) is a function of the nodal temperatures and the region physical properties at those nodes. It is thus necessary to derive the complete expressions and also to develop each expression to account for the cylindrical (r) geometry.

6.5.1. Heat Generation

The generation term in eqn. (6.5) is equal to the volume integral of the volumetric heat generation rate Q_g''' [W/m³] expressed in cylindrical geometry:

$$Q_g = \int_V Q_g'''(r,z,\theta) r dr dz d\theta \quad . \quad (6.10)$$

For an infinite cylinder, a unit-height in the (z)-dimension is assumed, which results in the following expression:

$$Q_g = \int_{r_1}^{r_2} \int_{\theta_1}^{\theta_2} Q_g'''(r,\theta) r dr d\theta \quad . \quad (6.11)$$

The above expression can easily be shown to reduce to the following, for an (r) geometry condition:

$$Q_g = Q_g'''(r) \pi (r_2^2 - r_1^2) \quad , \quad (6.12)$$

where r_1 and r_2 correspond to the inner and outer radii of the unit volume about a particular node, respectively.

Eqn. (6.12) can be directly applied to a heat transfer model in (r) geometry; the volumetric heat generation rate $Q_g'''(r)$ can be obtained from the neutronics code ONEDANT, and r_1 and r_2 are independent variables that correspond to

... of the heat source of heat transfer ...
... of the heat transfer and the region ...
... It is then necessary to derive the ...
... for the cylindrical geometry ...

3.1.1.1. Cylindrical Geometry

The geometry is ... in eqn. (2.1) ...
... cylindrical heat conduction ...
... geometry

(2.10)
$$Q = \int_{\Omega} Q(x, y, z) dx dy dz$$

For an infinite cylinder, a unit length in the z-direction is assumed, which results in the following expression:

(2.11)
$$Q = \int_{\Omega} Q(x, y) dx dy$$

The above expression can easily be shown to reduce to the following for an (i) geometry condition:

(2.12)
$$Q = \int_{\Omega} Q(x, y) dx dy$$

where r_1 and r_2 correspond to the inner and outer radii of the tube volume about a particular axial position.

Eqn. (2.12) can be directly applied to a heat transfer model in (i) geometry; the volumetric heat generation rate Q''' can be obtained from the non-linear ... and it can be independent variables but corresponds to

the outer boundaries of a node in the model. From the thermal analysis point of view, $Q_g'''(r)$ is an independent variable; the method of calculating $Q_g'''(r)$ is discussed as part of the neutronics theory in Chapter 7.

6.5.2. Thermal Radiation

Thermal radiation corresponds to the continuous emission of electromagnetic energy by some matter, by virtue of its internal energy [Siegel and Howell, 1992]. In the case of the unit-cell NLB rocket engine, thermal radiation occurs in each region which in some way transmits electromagnetic energy: the gaseous fuel, fuel/buffer gas mixture, propellant, (assumed) solid silica wall, and the near-vacuum of ambient space. In addition, the solid surfaces of the moderator and pressure vessel both radiate energy toward the fuel and ambient space, respectively.

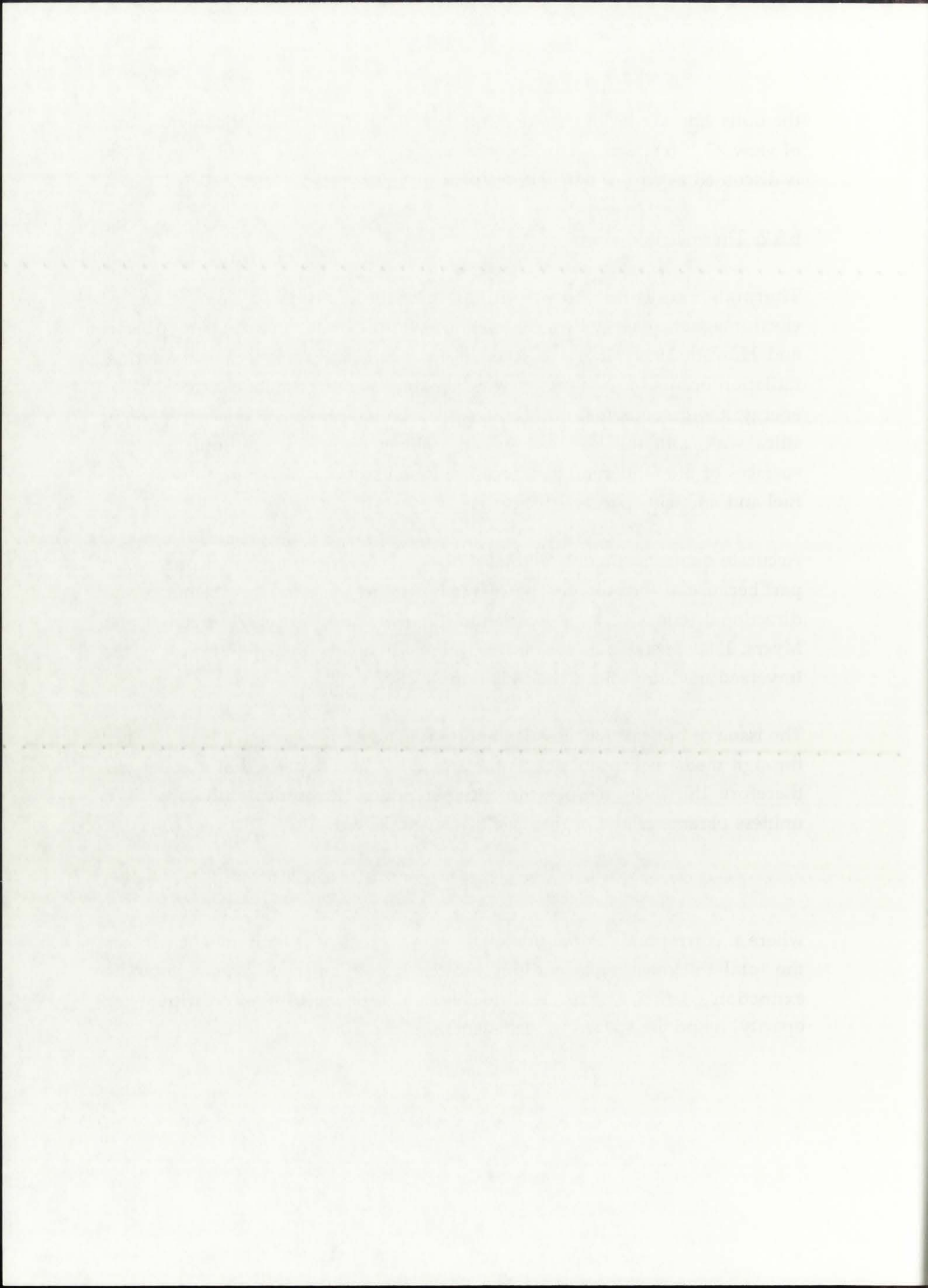
Accurate quantification of thermal radiation is a very complicated process, in part because of the complex thermal (temperature), spectral (wavelength), and directional (emissive angle) variation [Sparrow and Cess, 1978; Bennett and Myers, 1988; Siegel and Howell, 1992]. In addition, the optical thickness of the traversed medium affects the radiation flux.

The issue of optical thickness is important in analyzing radiative heat transfer through media because it affects the amount of heat deposited at a node, and therefore the local temperature at that node. The optical thickness is a unitless parameter and is given as [Siegel and Howell, 1992]:

$$\delta = \kappa \Delta r \quad , \quad (6.13)$$

where κ corresponds to the total extinction coefficient [1/cm] and Δr denotes the total thickness of a medium subjected to thermal radiation [cm]. The extinction coefficient κ is equal to the sum of the absorption coefficient (or opacity) a and the scattering coefficient σ_s :

$$\kappa = a + \sigma_s \quad . \quad (6.14)$$



The scattering coefficient σ_s is generally assumed to be equal to zero because of the strong dominance of absorption (opacity) on the total extinction coefficient [Siegel and Howell, 1992]. The absorption coefficient a is generally associated with the spectral-averaged Rosseland Mean Opacity a_R , a quantity that has been extensively tabulated for gaseous fuels, buffer gases, and propellants as part of the studies into the physical properties of radiating plasmas conducted during the 1960's and early 1970's [Kesten and Kinney, 1965; Kinney, 1966; Krascella, 1971]:

$$\kappa = a_R \quad (6.15)$$

6.5.2.1. Optically Thick Regions

An optically thick region, then, is defined as one in which $\delta \gg 1$, that is, one which either has a very large opacity or is very large in dimension. Conversely, an optically thin region is one in which $\delta \ll 1$. An optically thick medium would predominantly absorb thermal radiation, while an optically thin medium would predominantly transmit thermal radiation.

The assumption of optically thick media has been used in virtually every GCR-related study conducted to date, both in regard to open-cycle and closed-cycle concepts. [McLafferty and Bauer, 1967; Gauntt *et al.*, 1992b; Gauntt *et al.*, 1993; Poston and Kammash, 1994; Tanner, 1994] all use that assumption to simplify the method of calculating the temperature distribution. The assumption is generally quite valid for fuel regions and mixture regions where the fuel is the dominant species in terms of the mass fraction; for example, at a temperature of 15,000 K, $a_R(\text{uranium}) \approx 1,415 \text{ 1/cm}$ and for a representative fuel region $\Delta r = 15 \text{ cm}$, the optical thickness of the fuel is approximately 28,000!

The thermal radiation diffusion method is widely used for the solution of radiative heat transfer problems in optically thick regions. It is conceptually based on Fourier's Law and has the form [Kesten and Kinney, 1965; Siegel and Howell, 1992]:

The scattering coefficient σ_s is generally assumed to be equal to two portions of the energy distribution of absorption (opacity) in the total extinction coefficient (Holt 1971). The absorption coefficient κ is generally associated with the spectral-weighted Rosseland Mean Opacity $\bar{\kappa}$, a quantity that has been extensively discussed for various fluid buffer gases, and is presented in Fig. 10. The total extinction coefficient is the sum of the absorption and scattering coefficients. The data for σ_s and $\bar{\kappa}$ are taken from the work of Kinney and Kinney (1972, Kinney 1975, Kinney 1977).

(11)

$$\kappa = \bar{\kappa} + \sigma_s$$

3.2.1. Optically Thick Regions

An optically thick region is defined as one in which $\tau \gg 1$, that is one which either has a very large opacity or is very large in dimension. Conversely, an optically thin region is one in which $\tau \ll 1$. An optically thick region would predominantly absorb thermal radiation, while an optically thin medium would predominantly transmit thermal radiation.

The assumption of optically thick media has been used in virtually every GCE-related study conducted to date, both in regard to open cycle and closed cycle engines (McLellan and Jones 1967, Grant et al. 1972). Kinney et al. (1977, Kinney and Kinney 1977, Kinney 1977) all use that assumption to simplify the method of calculating the temperature distribution. The assumption is generally quite valid for hot regions and mixture regions where the fuel is the dominant species in terms of the mass fraction, for example at a temperature of 2500 K, $\rho = 0.1415 \text{ kg/m}^3$ and for a representative fuel region 5-15 cm the optical thickness of the fuel is approximately 25,000.

The thermal radiation diffusion method is widely used for the solution of radiative heat transfer problems in optically thick regions. It is conceptually based on Fourier's Law and has been used (Kinney and Kinney 1972, Singh and Howell 1972).

$$Q_{\text{rad}} = -k_{\text{rad}}A_{\text{cs}}\text{grad}T \quad , \quad (6.16)$$

where A_{cs} corresponds to the cross-sectional area for heat transfer [m^2] and k_{rad} denotes the effective radiative thermal conductivity [$\text{W}/\text{m}\cdot\text{K}$]:

$$k_{\text{rad}} = \frac{16\sigma T^3}{3a_{\text{R}}} \quad . \quad (6.17)$$

In the above equation, σ denotes Stefan-Boltzmann's constant ($5.67\text{e-}8 \text{ W}/\text{m}^2\cdot\text{K}^4$) and T corresponds to the local temperature [K]. Combining eqns. (6.16) and (6.17) yields the following expression for thermal radiation heat transfer in (r) geometry:

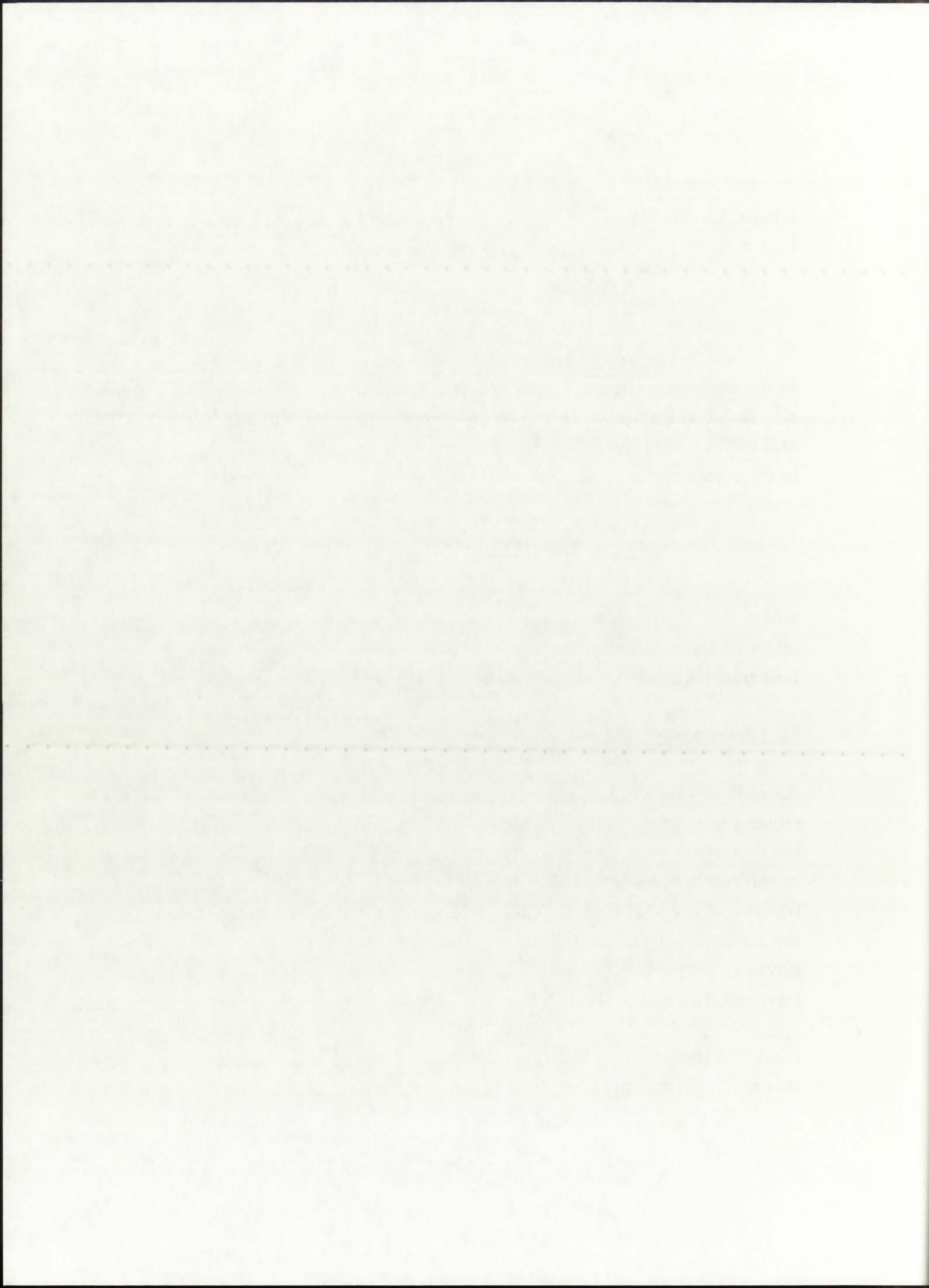
$$Q_{\text{rad}} = k_{\text{rad}}2\pi r \frac{\Delta T}{\Delta r} \quad . \quad (6.18)$$

where the "-" sign has been neglected due to the assumption of all heat flow into a node, as stated in Section 6.3. As can be seen from eqn. (6.18), the rate of heat transfer can be directly related to the temperature at a particular node.

6.5.2.2. Optically Thin Regions

An optically thin region is defined as one in which $\delta \ll 1$, that is, one having either a very low opacity or very small in dimension. In such a region, only a fraction of the heat flow traversing the plane of a node results in an increase in the internal energy of the medium at that node; in simpler terms, only a fraction of the heat flow is available to increase the temperature of the node - the majority of the heat flow is transmitted without any influence on the physical properties at that node. An analogy can be found in gamma-ray traversal through media [Chilton *et al.*, 1984].

Heat transfer through optically thin regions is the most complex aspect of thermal radiation analysis, and is most often ignored by assuming that all



regions are optically thick. It is also often referred to as “radiation transfer through semi-participating media” [Siegel & Howell, 1992]. On the basis of the partially-absorbing and partially-transmitting characteristics of the media, it lies in-between the extreme assumption of fully-participating media (as in the case of fuel) and non-participating media (as in the case of radiation exchange between two surfaces or between the Sun and Earth, for example, where the vacuum of space is assumed not affected by the radiative flux). Both extreme conditions are treated in detail in thermal radiation texts [Bird, Stewart, and Lightfoot, 1960; Sparrow and Cess, 1978; Angelo & Buden, 1985; Bennett and Myers, 1988; Siegel & Howell, 1992; and others], but little emphasis is placed on the derivation of suitable expressions for semi-participating media. Transmittance through semi-transparent media, such as windows, is discussed in [Siegel and Howell, 1992], but emphasis is placed on directional and spectral effects rather than the determination of local temperatures in the transmitting media.

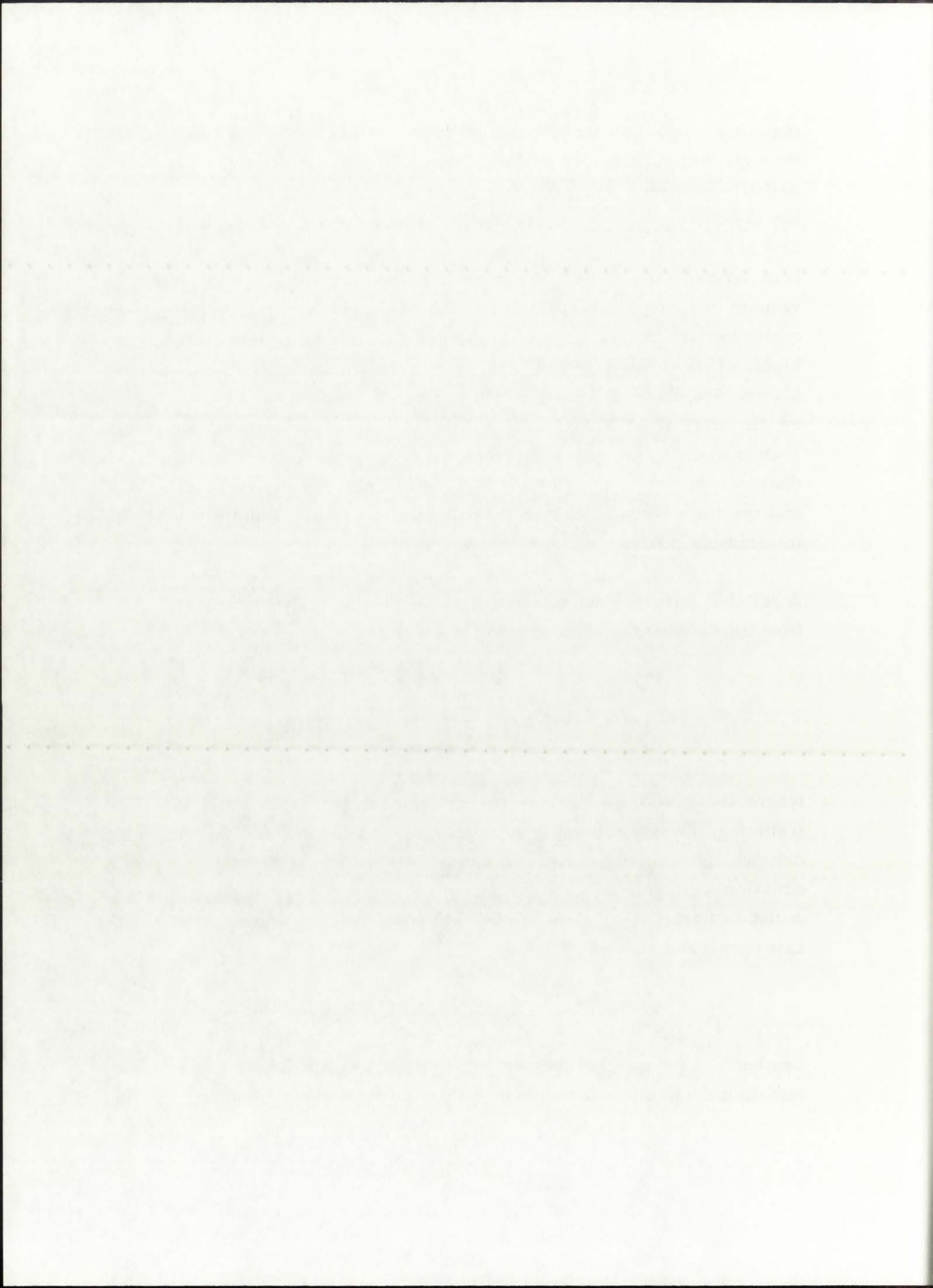
A suitable derivation for semi-participating media can, however, be obtained from the baseline radiation transport equation [Siegel and Howell, 1992]:

$$\frac{dQ_{\text{rad}}}{dr} = -\kappa Q_{\text{rad}}(r) + a_R Q_{\text{rad}}(r) + \frac{\sigma_s}{4\pi} \int_{\omega=0}^{\omega=4\pi} Q_{\text{rad}}(r) \Phi(\tau \rightarrow \omega) d\omega \quad , \quad (6.19)$$

where the first term denotes the combined loss due to absorption and scattering, the second term denotes the gain by emission, and the third term denotes the gain by scattering, respectively. Since scattering as well as emission can generally be neglected in comparison to absorption, the radiation transport equation can be reduced to the form known as Lambert’s Law [Siegel and Howell, 1992]:

$$Q_{\text{rad}}(r) = Q_{\text{rad}}(0)e^{-\kappa r} \quad . \quad (6.20)$$

Lambert’s Law can be interpreted as expressing the fraction of thermal radiation originally emitted at $r=0$ that traverses a path length r ; in that



respect, it also denotes the relation between the transmitted component of the thermal radiation and the total amount of thermal radiation, for the case of thermal radiation traversal of a path length r :

$$\frac{Q_{\text{trans}}(r)}{Q_{\text{total}}} = \frac{1}{e^{\kappa r}} \quad (6.21)$$

The above ratio has been referred to as the Transmission Fraction (TF). For a very low bounding value of κ in the traversed medium, $TF \approx 1.0$ and the medium is considered non-participating, reducing the problem to one of thermal radiation exchange between surfaces. For a very high bounding value of κ , $TF \approx 0$ and the medium is considered fully participating, thus allowing the use of the diffusion method expressed in eqn. (6.18).

For a scenario of $0 < TF < 1.0$, it is necessary to relate the actual temperature, resulting from only a fraction of the total heat flux, to the temperature that would occur if the entire heat flux were to affect the temperature (as in the case of fully participating medium). Denoting the fraction of heat flux influencing the local temperature as Q_{abs} , the following relation can be used:

$$\frac{Q_{\text{abs}}(r)}{Q_{\text{total}}} = \frac{1 - Q_{\text{trans}}(r)}{Q_{\text{total}}} = 1 - TF(r) \quad , \quad (6.22)$$

and assuming that the total path length in the medium, r , is not significant, the following expression can be derived to approximate the bulk (mean) temperature in a semi-participating medium:

$$\frac{T_{\text{abs}}(r)}{T_{\text{total}}} \approx \sqrt[4]{1 - TF(r)} \quad , \quad (6.23)$$

where T_{abs} corresponds to the bulk (mean) temperature of a semi-participating medium with thickness r , T_{total} denotes the temperature if all the heat flux were absorbed in the medium, and $TF(r)$ denotes the thermal radiation transmission fraction for the medium of thickness r . A physical

... is also ... the ...
 ... the ...
 ... of ...

The above ... has been ...
 ... of ...
 ...
 ...
 ...

For a ... of ...
 ...
 ...
 ...
 ...

$$\frac{Q_{\text{total}}}{Q_{\text{total}}} = \frac{Q_{\text{total}} - Q_{\text{total}}}{Q_{\text{total}}} = 1 - T_{\text{total}}$$

and assuming that the total path length in the medium ...
 the following expression can be derived to approximate the total ...
 temperature in a ...

$$\frac{Q_{\text{total}}}{Q_{\text{total}}} = \frac{Q_{\text{total}}}{Q_{\text{total}}} = 1 - T_{\text{total}}$$

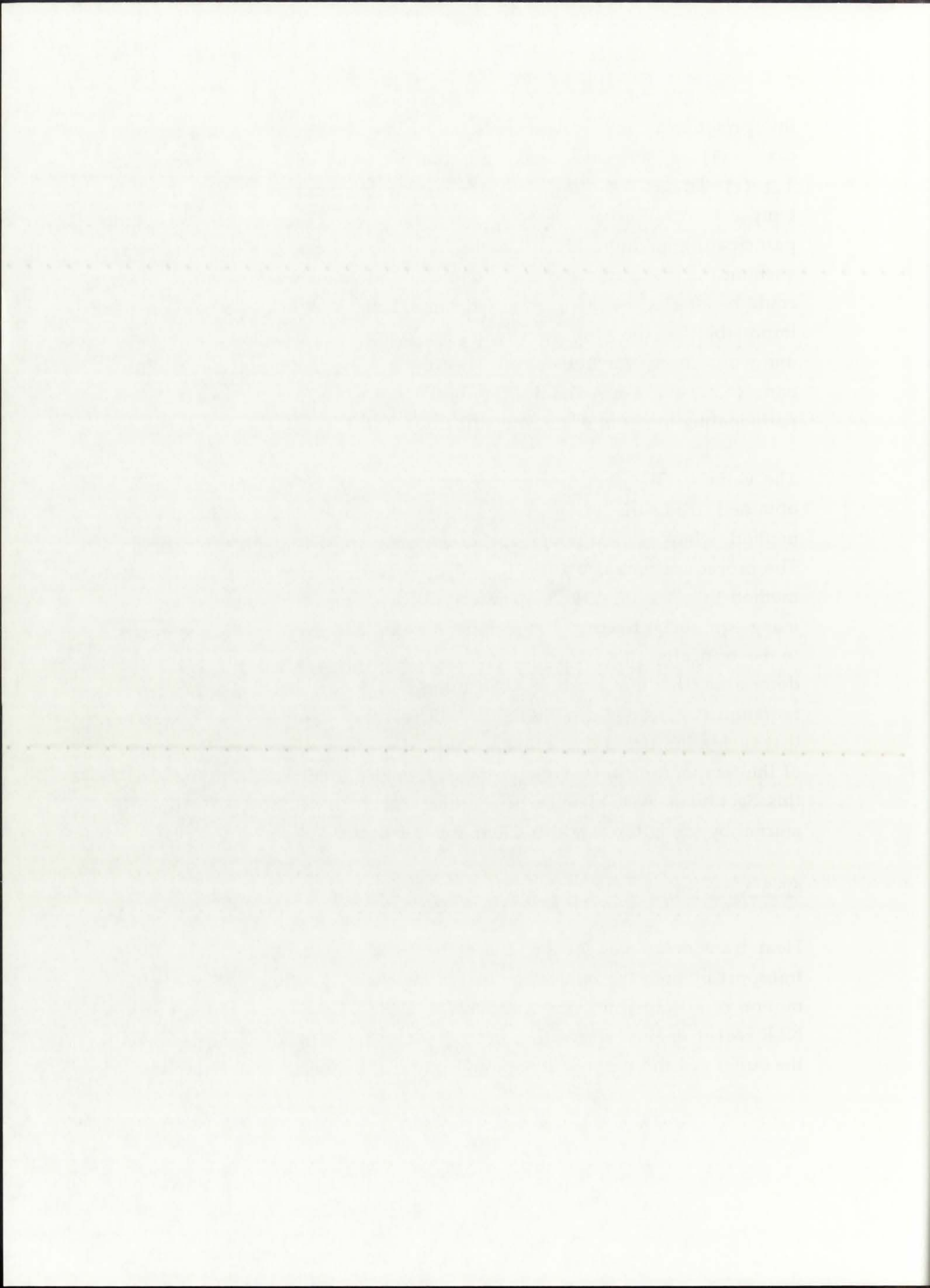
where T_{total} corresponds to the total ...
 participating medium with thickness ...
 the total flux was absorbed in the medium and ...
 reduced transmission fraction for the medium of thickness ...

interpretation of the above expression can be performed for two bounding cases: (1) in the case of a fully participating medium, $TF(r)=0$ and $T_{abs}(r)=T_{total}$, denoting that the actual temperature is equal to the temperature for a case of no transmission, and (2) in the case of a non-participating medium, $TF(r)=1.0$ and $T_{abs}(r)=0$, which would denote a perfect vacuum (i.e. the absence of any molecules and atoms whose internal energy could be affected by the thermal radiation). Both cases, of course, are physical impossibilities; the first one would occur for $\kappa=\infty$ or $r=\infty$, while the second one would occur for $\kappa=0$ or $r=0$. They do, however, indicate the validity of eqn. (6.23) to approximate the bulk (mean) temperature of a semi-participating medium of thickness r .

The value of T_{total} , corresponding to the case of no transmission, can be obtained from the temperature distribution provided by the diffusion method, which is used in conjunction with the optically thick approximation. The procedure for calculating T_{abs} , then, consists of employing the diffusion method to determine the temperature distribution in (r) geometry, and then using eqn. (6.23) to correct the temperature in those media which are known to be optically thin. This procedure provides a very simple method to determine the temperature distribution in media where only thermal radiation is considered, although it will be shown later in this Dissertation that such a limitation (i.e., radiation-only) does not provide a realistic picture of the temperature distribution in a GCR engine. The procedure outlined in this Section is part of an article prepared for presentation in a scientific journal by the author and his Committee Chairman.

6.5.3. Convection

Heat transfer by convection arises from the aggregate effects of energy transport by both the random motion of molecules in a fluid and by the bulk motion of a fluid [Incropera and DeWitt, 1990]. For the case of the unit-cell NLB rocket engine, convection in (r) geometry is primarily associated with the buffer gas and propellant regions, because of the axial tendency of flow.



A general expression for convective heat transfer is the following:

$$Q_{\text{conv}} = hA_{\text{cs}}(T_{\infty} - T_x) \quad , \quad (6.24)$$

where h denotes the heat transfer coefficient [$\text{W}/\text{m}^2\text{-K}$], A_{cs} corresponds to the cross-sectional area to heat transfer [m^2], and T_{∞} and T_x denote the local fluid temperature [K] and the boundary temperature [K], respectively. In cylindrical (r) geometry, eqn. (6.24) can be written as:

$$Q_{\text{conv}} = h2\pi r\Delta T \quad . \quad (6.25)$$

Both the buffer gas and propellant flow conditions correspond to a general internal flow scenario, in which the heat transfer coefficient is expressed as:

$$h = \frac{[\text{Nu}]k}{D_h} \quad , \quad (6.26)$$

where $[\text{Nu}]$ denotes the dimensionless Nusselt number, k the thermal conductivity of the fluid [$\text{W}/\text{m-K}$], and D_h corresponds to the mean hydraulic diameter for internal flow in non-circular tubes [Incropera and DeWitt, 1990]. The latter is defined as the ratio of the cross-sectional area for fluid flow, A_{csf} [cm^2], and the wetted perimeter of the tube, P [cm]:

$$D_h = \frac{4A_{\text{csf}}}{P} \quad , \quad (6.27)$$

and, for the unit-cell NLB rocket engine layout presented in Figure 3.1 (with the segmented propellant channels represented by an equivalent outer radius in (r) geometry), is equal to 8.48 cm.

The thermal conductivity is a baseline property of the fluid and is either obtained from tabulated data or estimated; the Nusselt number, however, must be calculated. Numerous correlations based on experimental data can be found in published texts that are applicable to the particular conditions of buffer gas and propellant flow in the unit-cell NLB engine [El-Wakil, 1984;

A general expression for convective heat transfer is the following:

$$Q_{conv} = hA_s(T_s - T_f) \quad (22)$$

where h denotes the heat transfer coefficient [W/m²·K], A_s corresponds to the cross-sectional area [m²], T_s and T_f denote the solid and fluid temperatures [K] and the boundary temperature [K], respectively. In cylindrical (r) geometry, Eq. (22) can be written as:

$$Q_{conv} = hA_s(T_s - T_f) \quad (23)$$

Both the inlet gas and peripheral flow conditions correspond to a general internal flow geometry, in which the heat transfer coefficient is expressed as:

$$h = \frac{k}{D_h} Nu \quad (24)$$

where $[Nu]$ denotes the dimensionless Nusselt number, k the thermal conductivity of the fluid [W/m·K], and D_h corresponds to the mean hydraulic diameter for internal flow in non-circular tubes (Peterson and Daly, 1990). The latter is defined as the ratio of the cross-sectional area A_c [cm²] and the wetted perimeter of the tube P [cm]:

$$D_h = \frac{4A_c}{P} \quad (25)$$

and for the ducted MJP rocket engine layout presented in figure 4, (with the equivalent properties of a duct represented by an equivalent outer radius to (r) geometry), is equal to 2.68 cm.

The thermal conductivity is a material property of the fluid and is either obtained from tabulated data or estimated; the Nusselt number, however, must be calculated. Numerous correlations based on experimental data can be found in published texts that are applicable to the particular conditions of buffer gas and peripheral flow in the ducted MJP engine (Peterson, 1984).

Bennett and Myers, 1988; Incropera and DeWitt, 1990; Munson *et al.*, 1990]. The correlation chosen for this analysis was that of Dittus-Boelter [Incropera and DeWitt, 1990]:

$$[\text{Nu}] = 0.023[\text{Re}]^{4/5}[\text{Pr}]^n \quad , \quad (6.28)$$

where [Re] and [Pr] denote the dimensionless Reynolds and Prandtl numbers, respectively. The exponent n on the Prandtl number is equal to 0.4 for heating (i.e., $T_x > T_\infty$) and to 0.3 for cooling ($T_x < T_\infty$). Since this analysis is based on the assumption of all heat flow into a particular node, $n=0.4$ was chosen.

The dimensionless [Re] and [Pr] values are calculated with the following expressions:

$$[\text{Re}] = \frac{\rho v D_h}{\mu} \quad , \quad (6.29)$$

and

$$[\text{Pr}] = \frac{C_p \mu}{k} \quad , \quad (6.30)$$

where ρ , μ , C_p , and v correspond to the fluid density [kg/m^3], viscosity [$\text{kg}/\text{m}\cdot\text{s}$], specific heat capacity at constant pressure [$\text{J}/\text{kg}\cdot\text{K}$], and the fluid axial velocity [m/s], respectively. The initial convective heat transfer eqn. (6.24), then, can be expressed in terms of the node temperatures and a set of baseline physical properties, making it possible to determine the temperature distribution in the fluid regions.

6.5.4. Conduction

Heat transfer by conduction is probably the simplest of the four modes of heat transfer incorporated into the thermal analysis model of the unit-cell NLB rocket engine. It is the result of lattice vibrations within a solid material and occurs when a temperature gradient is applied between two portions of a solid [Incropera and DeWitt, 1990]. Conductive heat transfer obeys Fourier's Law:

Prater and Wright (1987) and Prater and Wright (1990) showed that the correlation chosen for the analysis was that of Prater and Wright (1990).

$$[7] \quad \ln \left(\frac{C_{10}}{C_0} \right) = \frac{v}{D} x$$

where C_0 and C_{10} denote the initial and final concentrations, x is the distance from the inlet to the point of sampling, and v is the velocity of the fluid flow. The velocity of the fluid flow is assumed to be constant and is equal to 0.4 for heating and to 0.3 for cooling. From the analysis it is seen that the correlation of all fluid flow into a particular node will be chosen.

The dimensionless $[R]$ and $[T]$ values are calculated with the following expressions:

$$[R] = \frac{C_{10} - C_0}{C_0} \quad (8)$$

$$[T] = \frac{v}{D} t \quad (9)$$

where C_0 and C_{10} are the initial and final concentrations, x is the distance from the inlet to the point of sampling, and v is the velocity of the fluid flow. The velocity of the fluid flow is assumed to be constant and is equal to 0.4 for heating and to 0.3 for cooling. From the analysis it is seen that the correlation of all fluid flow into a particular node will be chosen.

3.2.1. Conduction

The heat transfer by conduction is probably the simplest of the four modes of heat transfer. It is the result of lattice vibrations within a solid material and occurs when a temperature gradient is applied between two portions of a solid. Prater and Wright (1990) conducted heat transfer experiments (Prater and Wright, 1990).

$$Q_{\text{cond}} = -k_{\text{cond}}A_{\text{cs}}\text{grad}T \quad , \quad (6.31)$$

where k_{cond} denotes the thermal conductivity [W/m-K] and A_{cs} , again, the cross-sectional area for heat transfer. In (r) geometry, eqn. (6.31) has the form:

$$Q_{\text{cond}} = k_{\text{cond}}2\pi r \frac{\Delta T}{\Delta r} \quad , \quad (6.32)$$

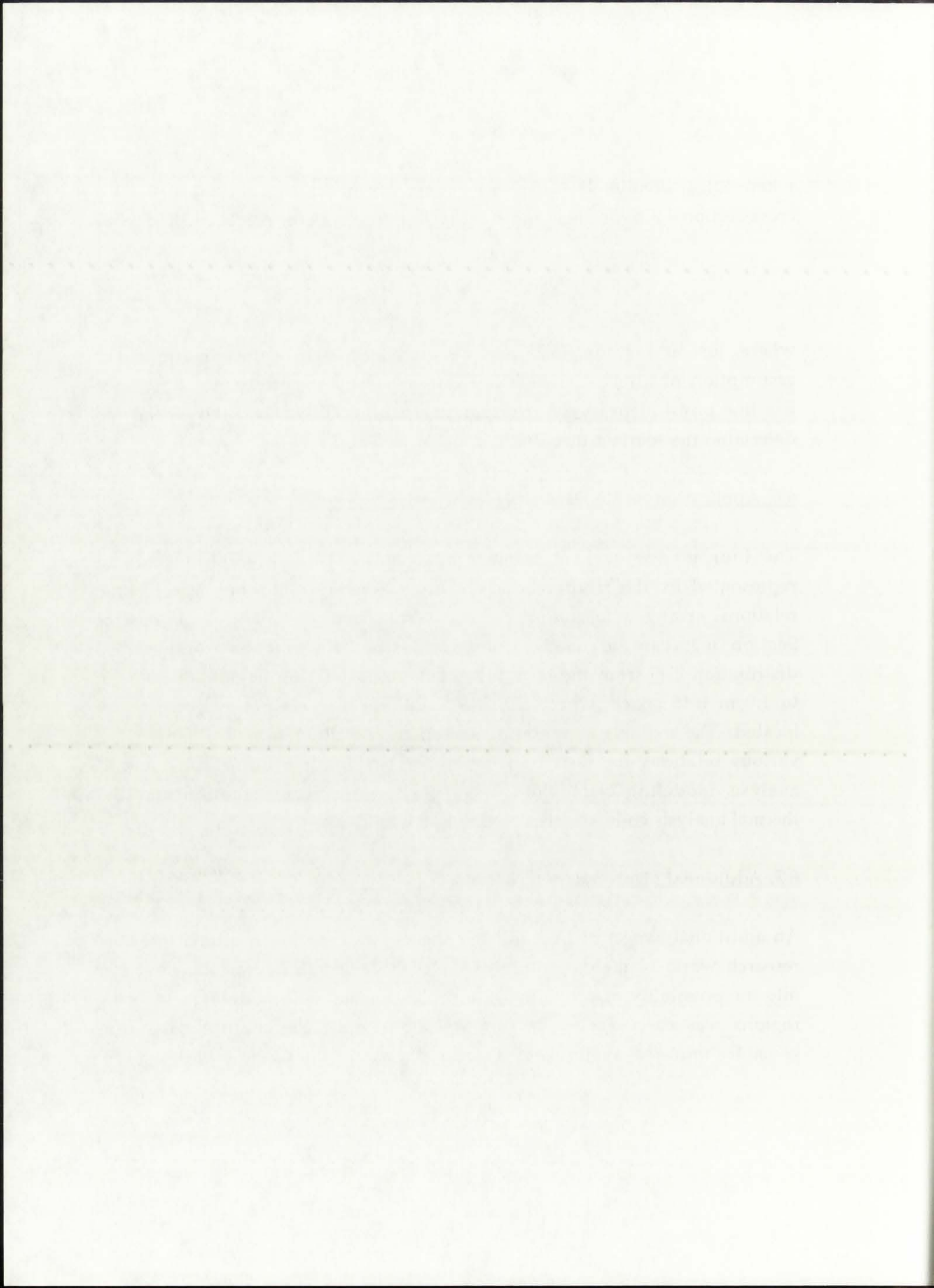
where, just as for eqn. (6.18), the “-” sign has been neglected due to the assumption of all heat flow being into a particular node. Since k_{cond} is a baseline physical property of a material, eqn. (6.32) can be used directly to determine the temperature distribution in the solid regions.

6.6. Application of the Derived Heat Transfer Theory

The four modes of heat transfer analyzed in this Dissertation can be represented by the relations derived in Sections 6.5.1. through 6.5.4. These relations, arranged to comprise the governing energy balance equations of Section 6.3, can be used to determine the (r) geometry temperature distribution $T(r)$ from the centerline of the unit-cell NLB engine all the way to 1.0 m into space, where the 200 K infinite heat sink is assumed to be located. The explicit temperature equations, resulting from combining the various relations for heat transfer modes, are used to develop a thermal analysis modeling code. Both the explicit temperature equation and the thermal analysis code are discussed in detail in Chapter 9.

6.7. Additional Heat Transfer Theory - Film Cooling

An additional aspect of heat transfer theory has been incorporated into this research work. Namely, because of the high values of $T(r)$, an investigation into the possibility of providing film cooling of the solid moderator/reflector regions was carried out. As this work postceded the comprehensive (r) geometry *uncooled* analysis, it is discussed separately in Chapter 11.



CHAPTER 7 NEUTRONICS THEORY

7.1. Introduction

As mentioned in the introduction to Chapter 6, the underlying concept behind the NLB engine is the transfer of energy to the working fluid. The driving force behind the transfer of energy is the thermal power generated in the reactor as a result of the fissioning of the fuel atoms. The thermal power, or more precisely the volumetric heat generation rate Qg''' [W/m^3], is in itself dependent on the geometry, material composition, and k_{eff} of the GCR. Analysis of the three latter variables is the domain of the neutronics theory. The comprehensive neutronics analysis discussed in this Chapter is based on the execution of the ONEDANT code in cylindrical (r) geometry.

7.2. The Volumetric Heat Generation Rate

The importance of the heat generation and thermal power inside a reactor is expressed very well in the following quote [El-Wakil, 1981]:

“the rate of heat release and consequently power generation in a given reactor core is limited by thermal rather than nuclear considerations. There is no limit to the neutron flux attainable in a reactor core, but the heat generated must be removed.”

The above statement illustrates the specific characteristics of nuclear fission heat: with only a slight available excess reactivity, criticality can be achieved for any desired thermal power level. Only a small portion of this source of energy can be utilized, however, because of the thermal considerations. To be able to safely and continuously operate a nuclear reactor, removal of the fission heat must be provided (i.e., the reactor must be cooled). In the absence of adequate fission heat removal, the reactor would self-destruct as a result of the enormous amounts of energy that would be built up within the fuel.

CHAPTER 2 NEUTRONICS THEORY

2.1 Introduction

As mentioned in the introduction to Chapter 1 the underlying concept behind the MTR engine is the transfer of energy to the working fluid. The driving force behind the transfer of energy is the thermal power generated in the reactor as a result of the fissioning of the fuel atoms. The thermal power, or more precisely the equivalent heat generation rate Q_{th} [W/m³], is a function dependent on the geometry, material composition, and size of the core. Analysis of the three major variables in the domain of the neutron theory. The comparative neutron analysis discussed in this Chapter is based on the evaluation of the GEOMETRIC and MATERIAL parameters.

2.2 The Neutron Balance (Heat Generation Rate)

The importance of the heat generation and thermal power inside a reactor is expressed very well in the following quote [F-Walt, 1981]:

The rate of heat release and consequently power generation in a reactor core is limited by thermal rather than nuclear considerations. There is no limit to the neutron flux available in a reactor core, but the heat generated must be removed.

The above statement illustrates the specific characteristics of nuclear reactors. Heat which may be slightly excessive or less desirable, cannot be removed for any desired thermal power level. Only a small portion of this source of energy can be utilized, however, because of the thermal considerations. To be able to utilize and continuously remove a nuclear reactor, removal of the heat must be provided (i.e., the reactor must be cooled). In the absence of adequate heat removal, the reactor would subside as a result of the enormous amounts of energy that would be built up within the fuel.

The total thermal power, or the reactor heat generation rate, was previously expressed for a cylindrical configuration as:

$$Q_g = \int_V Q_g'''(r,z,\Theta) r dr dz d\Theta \quad . \quad (7.1)$$

It can be seen from the above equation that it is the volumetric heat generation rate Q_g''' [W/m³] that is the independent variable in the thermal analysis; it also determines the total thermal power of the GCR. A major goal of the neutronics analysis, then, is to quantify $Q_g'''(r)$ for the (r) geometry and provide these values for the completion of the thermal analysis.

The total volumetric heat generation rate at a location r is equal to the integral over all neutron energies E of the neutron energy-dependent rates, as expressed below:

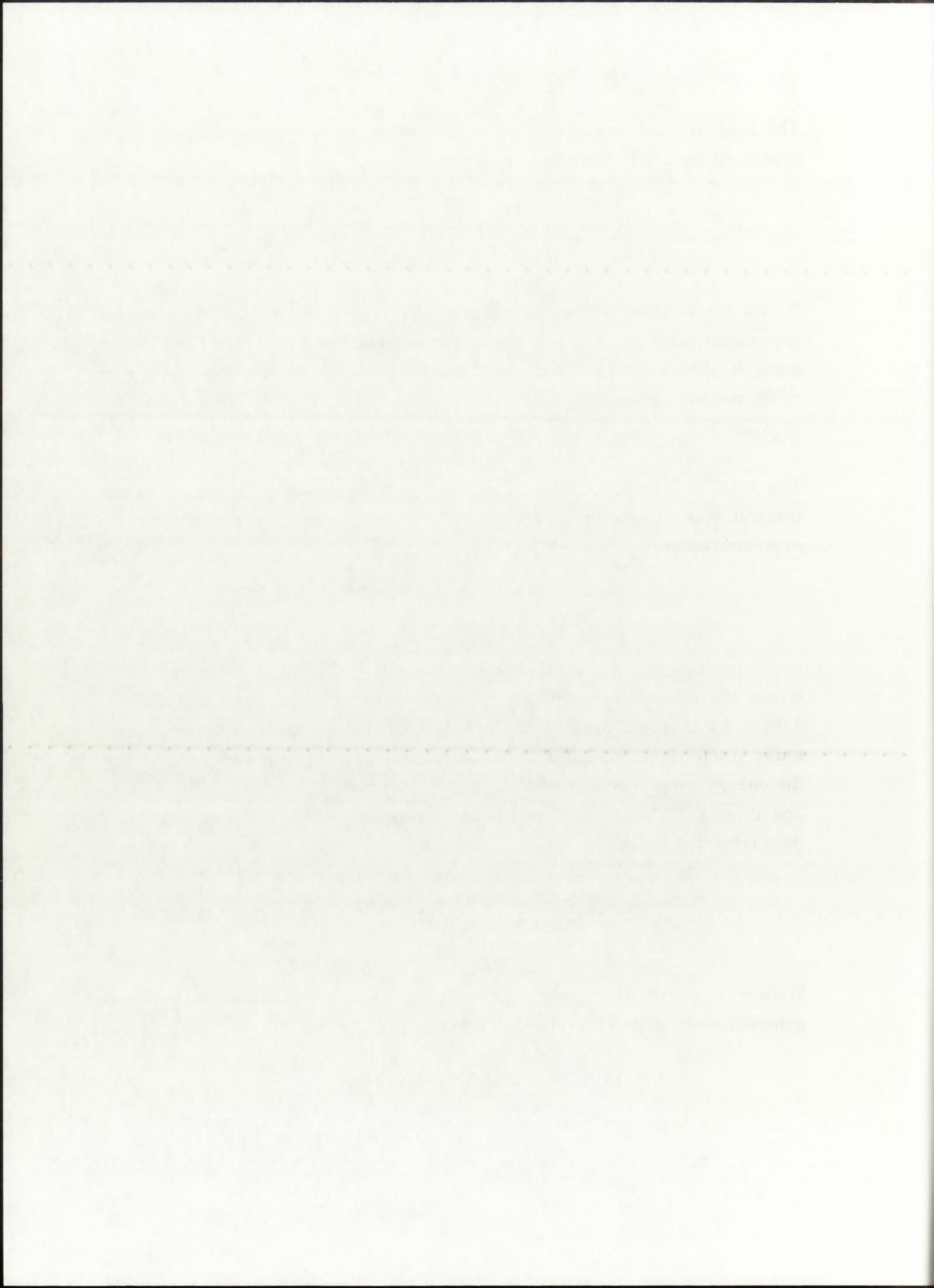
$$Q_g(r) = \int_E Q_g'''(r,E) dE \quad , \quad (7.2)$$

where the integral accounts for all the possible fissions occurring between $0 \leq E \leq \infty$. As an approximation to the indefinite integral, most neutronics codes today (including ONEDANT) use a neutron energy group structure, where the energy range consists of N_g number of groups [Lamarsh, 1983; Pruvost and Prueitt, 1988; and Duderstadt and Hamilton, 1990]. Therefore, eqn. (7.2) then takes the form:

$$Q_g(r) = \sum_{i=1}^{N_g} Q_g(r,E) \quad . \quad (7.3)$$

Within a particular energy group, the energy-dependent volumetric generation rate is given as [El-Wakil, 1981]:

$$Q_g(r,E) = E_R N_{\text{fuel}} \sigma_f(E) \Phi(r,E) \quad , \quad (7.4)$$



where, in the previous expression, E_R corresponds to the recoverable energy released per fission [MeV], N_{fuel} denotes the total fissioning fuel atomic density [atoms/barn-cm], and σ_f and Φ represent the microscopic fission cross-section [barns] and the neutron flux [$1/\text{cm}^2\text{-sec}$], respectively. In the case of a multi-component fuel, as is the case for the unit-cell NLB rocket engine which utilizes highly enriched uranium (96% U-235 and 4% U-238 by mass) [McLafferty and Bauer, 1967], the energy-dependent volumetric generation rate is the sum of the i -component rates:

$$Q_g(r,E) = E_R \Phi(r,E) \sum_{i=1}^2 N_{\text{fuel},i} \sigma_{f,i}(E) \quad (7.5)$$

The recoverable energy per fission is given in Table 7.1 as referenced from [Lamarsh, 1983]. For a GCR concept, it can be assumed that, due to the very low density of the fuel, only the fission fragments and fission product β -decay energies contribute to the recoverable energy per fission, resulting in a value $E_R=176$ MeV. This is consistent with the published recommendation of 180 MeV for quantifying heat generation in the fuel region [El-Wakil, 1981].

The fissioning fuel atomic density N [atoms/barn-cm] is dependent on the mass density of each component i , according to the following relation:

$$N_{\text{fuel},i} = \frac{\rho_i N_A}{M_{w,i}} \quad (7.6)$$

where ρ_i is the component mass density [g/cm^3], N_A denotes Avogadro's Constant [$0.6022 \text{ atoms-cm}^2/\text{barn-mol}$] and $M_{w,i}$ corresponds to the molecular weight of the component [$\text{g}/\text{g-mol}$]. Since the component mass density can be found in tabulated format as a function of temperature, and the molecular weight is a constant value, the fissioning fuel atomic density can be calculated from baseline data, as a function of temperature, and provided to the neutronics code as part of the input file.

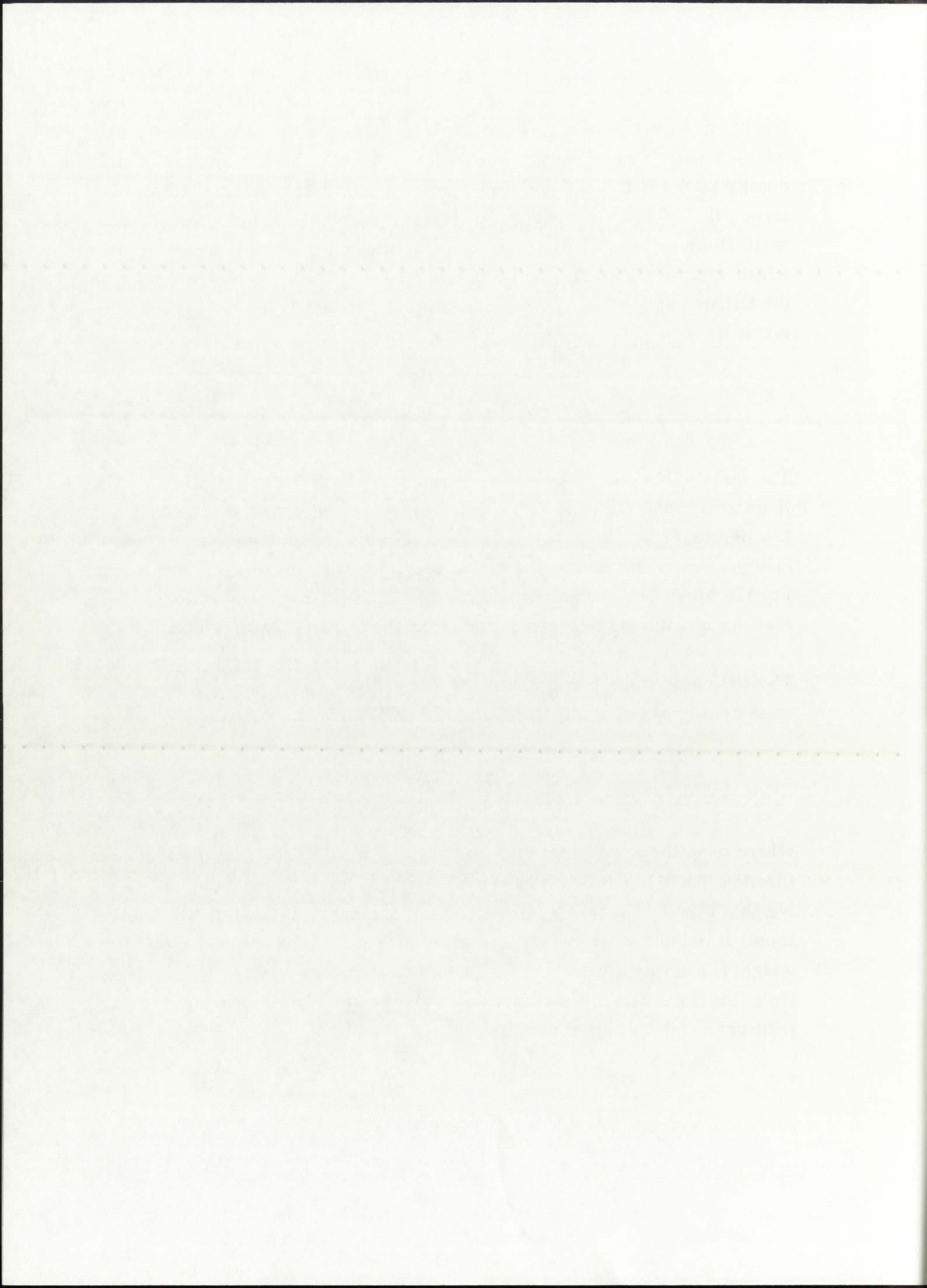
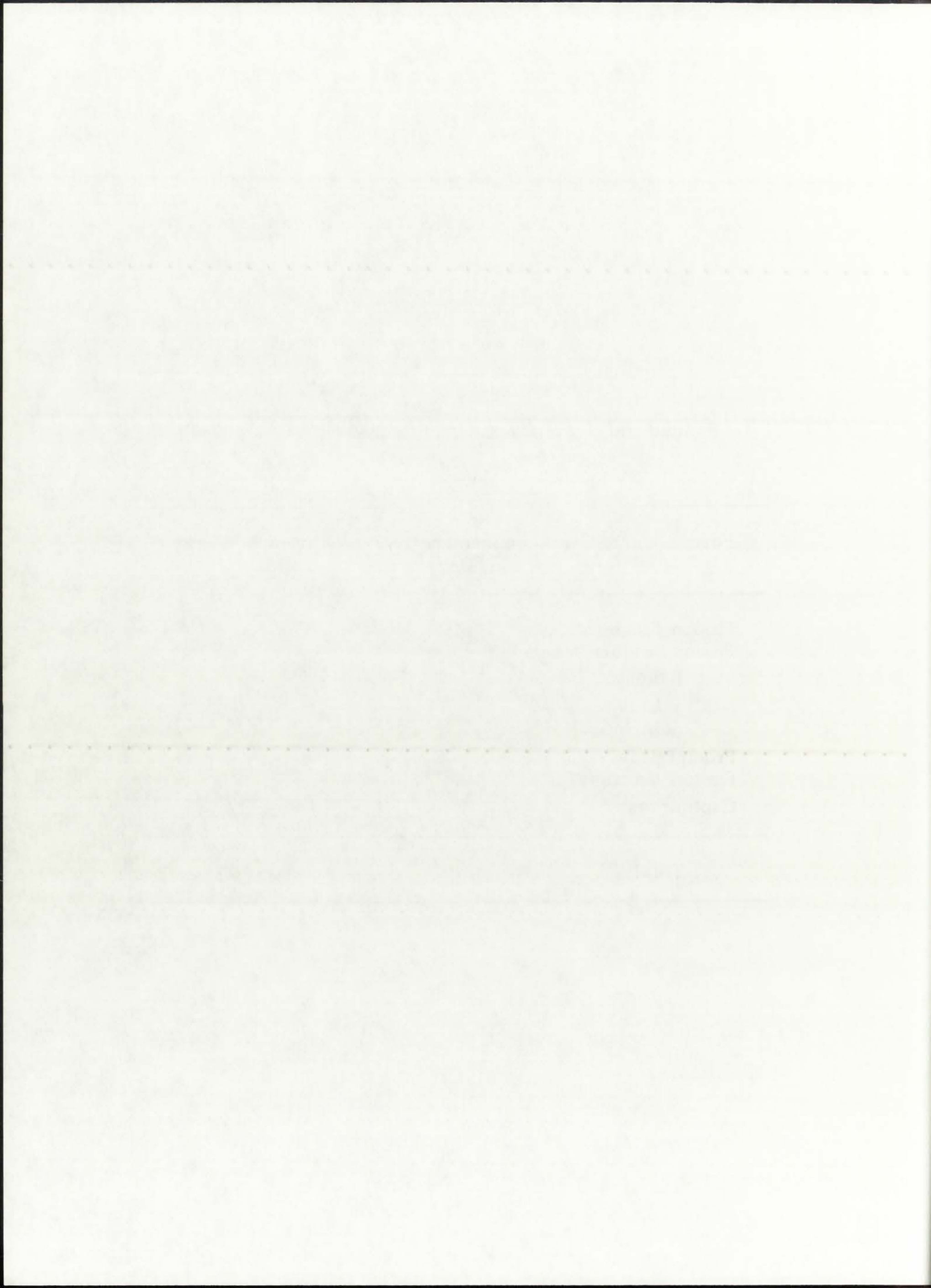


TABLE 7.1
Emitted and recoverable energies for fission [Lamarsh, 1983].

Form	Emitted Energy, [MeV]	Recoverable Energy, [MeV]
Fission Fragments	168	168
Fission Product Decay:		
β -decay	8	8
γ -decay	7	7
neutrinos	12	-
Prompt γ -rays	7	7
Fission neutrons	5	5
Capture γ -rays	-	3-12
Total	207	198-207



The energy-dependent microscopic fission cross-sections are obtained by the neutronics code from an available cross-section library, so they are readily accessed by the code and do not require user manipulation in any way. The energy-dependent neutron fluxes are calculated by the code as part of its overall neutronics calculations, and are used, in conjunction with the user-specified fuel densities and recoverable energies per fission, by the code to calculate the values of $Q_g'''(r,E)$ and ultimately $Q_g'''(r)$.

In summary, then, the neutronics code uses user-specified densities and recoverable energies per fission together with a pre-provided cross-section library to calculate energy-dependent volumetric heat generation rates, which it then sums up over all energy groups to obtain the volumetric heat generation rate at a location r . These values can then be taken from the neutronics code output file and provided as input to the thermal analysis code, according to the procedure discussed in Section 6.5.1.

7.3. Geometry and Material Composition

The (r) geometry neutronics model corresponds to the nine-region model shown previously in Figure 5.2. The model extends from the centerline ($r=0.0$) out to 1.0 m from the outer boundary of the engine (a total of 187.6 cm), and consists of nine distinct regions. The (r) dimensions of the model correspond to those presented in Figure 3.1. To account for the temperature-dependent density variations, the fuel region (total $\Delta r=14.75$ cm) and the D₂O region (total $\Delta r=48.0$ cm) were each split up into two neutronic homogeneous zones. The other regions were represented with only one zone each due to the insignificant temperature variations across those regions. The eleven-zone neutronics model is shown in Figure 7.1.

A total operating pressure for the baseline configuration of 250 atm was assumed within the unit-cell cavity. This value is based on the UARL-proposed unit-cell NLB engine operating pressure, and corresponds to the total pressure in the propellant, buffer gas, and fuel regions, due to the assumed homogeneous nature of those gaseous regions.

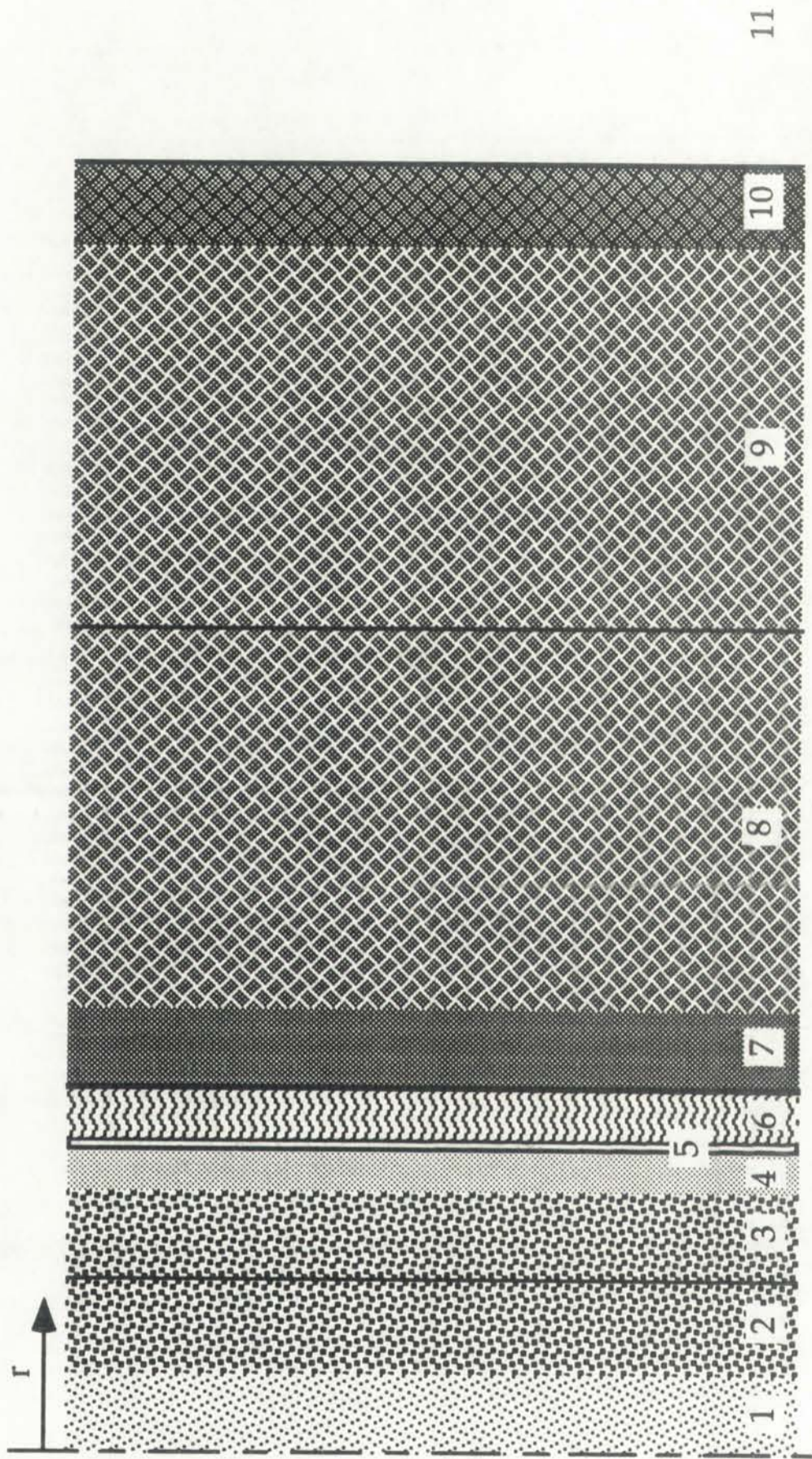
The energy-dependent properties of the cross-sections are obtained by the
method of the code from an available cross-section library. The total
cross-section is the sum of the elastic and inelastic cross-sections. The
energy-dependent neutron flux is calculated by the code as part of its
overall numerical calculation, and is used in conjunction with the
grouped cross-sections and reaction rates to calculate the values of $\Sigma_{f, g}$ and $\Sigma_{a, g}$.

In summary, then, the numerical code uses user-specified domain and
reaction rate energy per fission together with a provided cross-section
library to calculate energy-dependent volumetric fission and absorption rates, which
it then sums up over all energy groups to obtain the volumetric fission
rate at a location. These values are then fed into the thermal analysis
numerical code-output for and provide an input to the thermal analysis
code according to the procedure detailed in Section 2.2.

2.3 Geometry and Material Composition

The (1) geometry numerical model corresponds to the nine-region model
shown previously in Figure 2.2. The model extends from the centerline
($x=0$) out to 1.5 m from the outer boundary of the engine (a total of 3.0 m),
and consists of nine distinct regions. The (2) diameter of the fuel
corresponds to those presented in Figure 3.1. To account for the temperature-
dependent density variations, the fuel region (total 0.41475 m) and the UO₂
region (total 0.418 m) were each split up into two subregions,
homogeneous matter. The other regions were represented with only one
region each. The material composition and density values for each region are
shown in Table 2.1. The material composition is shown in Figure 2.1.

A total operating pressure for the particle configuration of 200 atm was
assumed within the fuel cell cavity. This value is based on the UAR-
project fuel cell NTP engine operating pressure, and corresponds to the
total pressure in the propellant buffer gas and fuel regions, due to the
assumed homogeneous nature of these regions.

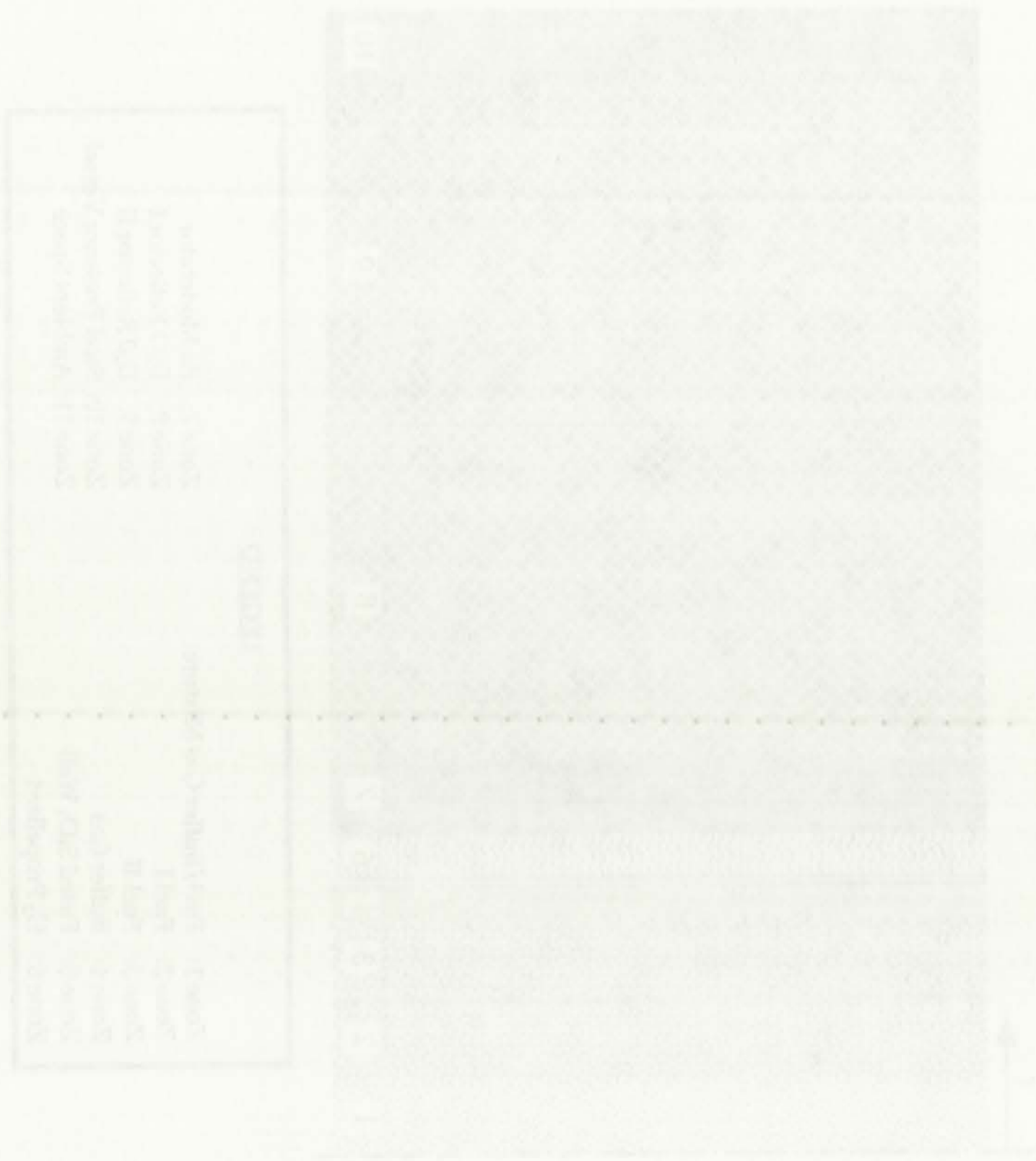


LEGEND

Zone 1:	Fuel/Buffer Gas Mixture	Zone 7:	Be Moderator
Zone 2:	Fuel I	Zone 8:	D ₂ O Reflector I
Zone 3:	Fuel II	Zone 9:	D ₂ O Reflector II
Zone 4:	Buffer Gas	Zone 10:	Steel Pressure Vessel
Zone 5:	Fused SiO ₂ Wall	Zone 11:	Ambient Space
Zone 6:	H ₂ Propellant		

Figure 7.1: Eleven-zone layout of the (r) geometry neutronics model of the unit-cell NLB engine.

Figure 2.1: Diagram of the two-dimensional coordinate system for the two-dimensional case.



The fuel/buffer gas mixture located around the centerline of the reactor, however, contains entrained fuel within the buffer gas flow; Dalton's Law of Partial Pressures can be applied in the form [Hill and Peterson, 1992]:

$$P_{\text{total}} = \sum_{i=1}^N P_{p,i} \quad , \quad (7.7)$$

which signifies that the partial pressure of the uranium fuel and the partial pressure of the buffer gas are additive. Based on the fluid mechanics assumptions associated with the recirculating flow [McLafferty, 1963; Krascella, 1969; and Kendall, 1972], a uniform and equal partial pressure for both uranium and buffer gas was assumed in the mixture region, thereby resulting in a total region pressure of 250 atm.

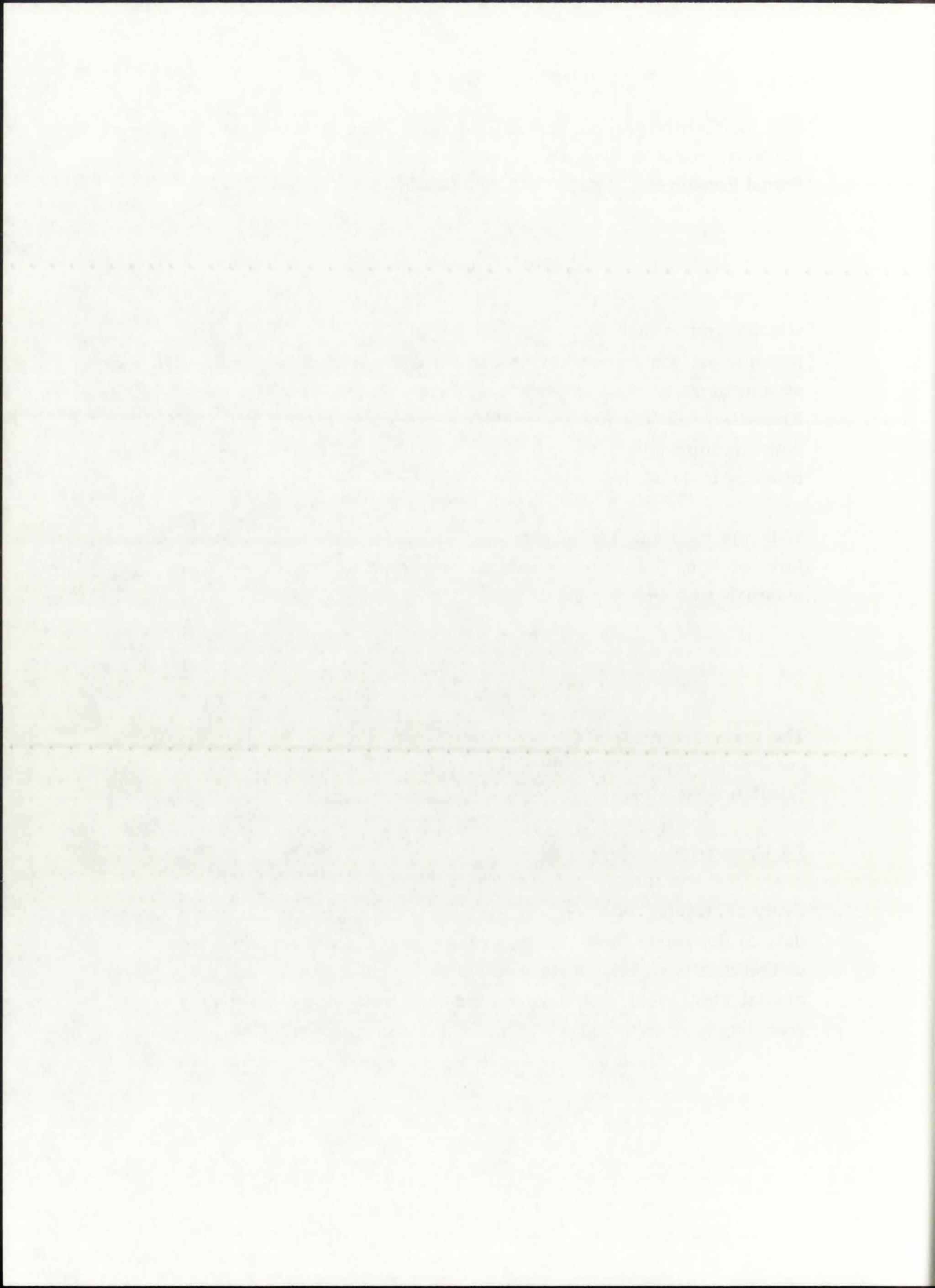
With the total and partial pressures determined for each region, a general form of eqn. (7.6) can be used to determine the atomic densities of all materials i within a region:

$$N_i = \frac{\rho_i N_A}{M_{w,i}} \quad . \quad (7.8)$$

The mass densities as a function of temperature and pressure for all the constituent materials of the nine regions can then be updated for each calculation iteration.

7.4. Cross-section Libraries

Every neutronics code needs to have accessible a set of nuclear cross-section data to determine the neutronics characteristics of an assembly. The cross-section data is generally contained within a cross-section library, and consists of total, absorption, scattering, and fission microscopic cross-sections arranged according to an energy group structure [Pruvost and Prueitt, 1988].



As part of the neutronics work discussed in this Dissertation, two cross-section libraries were utilized: (1) the standard Hansen-Roach 16-group library provided with ONEDANT, and (2) a temperature-dependent very low-thermal energy library generated from baseline ENDF/B-V data.

7.4.1. The Hansen-Roach Library

The Hansen-Roach 16-group cross-section library was first made available in 1961, and has since then been widely used in the field of nuclear criticality safety [Pruvost and Prueitt, 1988]. The library contains data on 118 nuclides. Each nuclide can be referenced either by number or by name, as shown in Table 7.2.

The Hansen-Roach library encompasses a broad energy range, from room-temperature thermal (0.025 eV) up to infinity (∞ MeV), as shown in the group structure in Table 7.3. It is an isothermal cross-section library, i.e., the cross-section data are all evaluated at the same (room) temperature over the whole energy range. This characteristic is generally satisfactory for analyzing critical assemblies and even reactors. In the case of the unit-cell NLB rocket engine, however, it may not accurately account for the effects of the very high-temperature fuel and propellant and the low-temperature Be and D₂O moderator and reflector, respectively.

Use of the Hansen-Roach library is justified for the purposes of determining any potential neutronics benefits of the low-temperature state of the moderator and reflector, as well as any potential neutronic benefits/detriments of the very high-temperature fuel and propellant. Reliance on the Hansen-Roach library, namely, provides the $Q_g'''(r)$ and k_{eff} for an isothermal (i.e. room temperature) condition of the unit-cell NLB rocket engine. This condition is generally as far as any previous NLB-related neutronics analyses were performed, and this data was used to point toward the neutronic feasibility of the NLB concept.

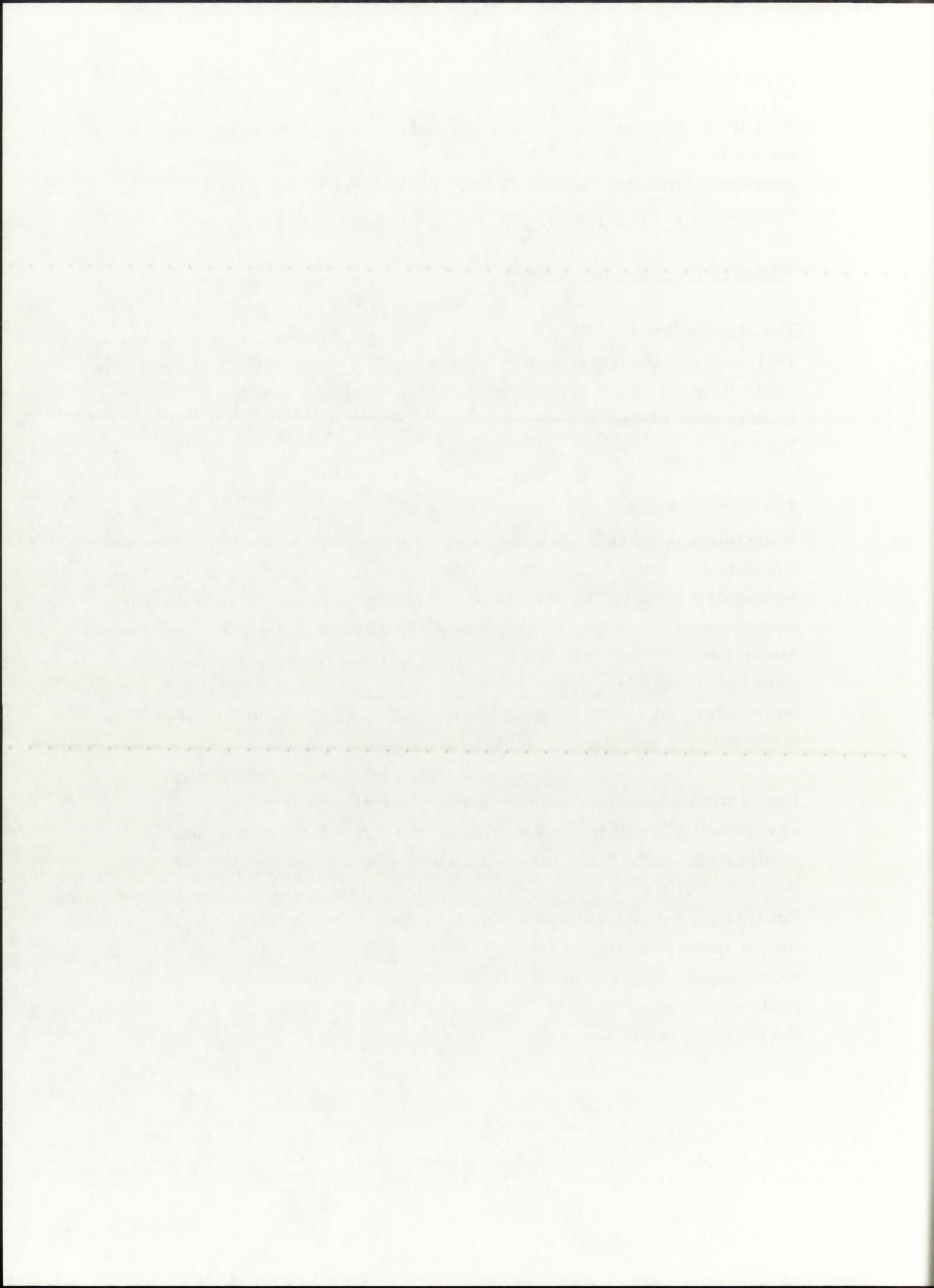


TABLE 7.2
118-nuclide Hansen-Roach cross-section library

<u>Number</u>	<u>Name</u>	<u>Number</u>	<u>Name</u>	<u>Number</u>	<u>Name</u>	<u>Number</u>	<u>Name</u>
1	a l	31	240-12	61	233-6	91	235-8r
2	b	32	240-13	62	233-7	92	235-9r
3	be	33	240-14	63	233-8	93	23510r
4	c	34	240-15	64	233-9	94	238-1r
5	cd	35	240-16	65	233-10	95	238-2r
6	cl	36	240-17	66	233-11	96	238-3r
7	ga	37	240-18	67	233-12	97	238-4r
8	f19	38	239-1	68	u235	98	238-5r
9	fe	39	239-2	69	u238	99	238-6r
10	h	40	239-3	70	u238y	100	238-7r
11	k	41	239-4	71	238-8	101	ce
12	li6	42	239-5	72	238-9	102	co
13	li7	43	239-6	73	238-10	103	ta
14	mo	44	239-7	74	238-11	104	23511r
15	na	45	239-8	75	238-12	105	23512r
16	ni	46	239-9	76	238-13	106	238-0
17	o16	47	239-10	77	238-14	107	cr
18	pu239	48	239-11	78	238-15	108	d
19	pu240	49	239-12	79	238-16	109	pb
20	240-1	50	239-13	80	zr	110	pu241
21	240-2	51	239-14	81	n	111	copper
22	240-3	52	239-15	82	nb	112	ti
23	240-4	53	239-16	83	235-yr	113	mg
24	240-5	54	th	84	235-1r	114	sulfur
25	240-6	55	u233	85	235-2r	115	w
26	240-7	56	233-1	86	235-3r	116	ta-1
27	240-8	57	233-2	87	235-4r	117	si
28	240-9	58	233-3	88	235-5r	118	ca
29	240-10	59	233-4	89	235-6r		
30	240-11	60	233-5	90	235-7r		

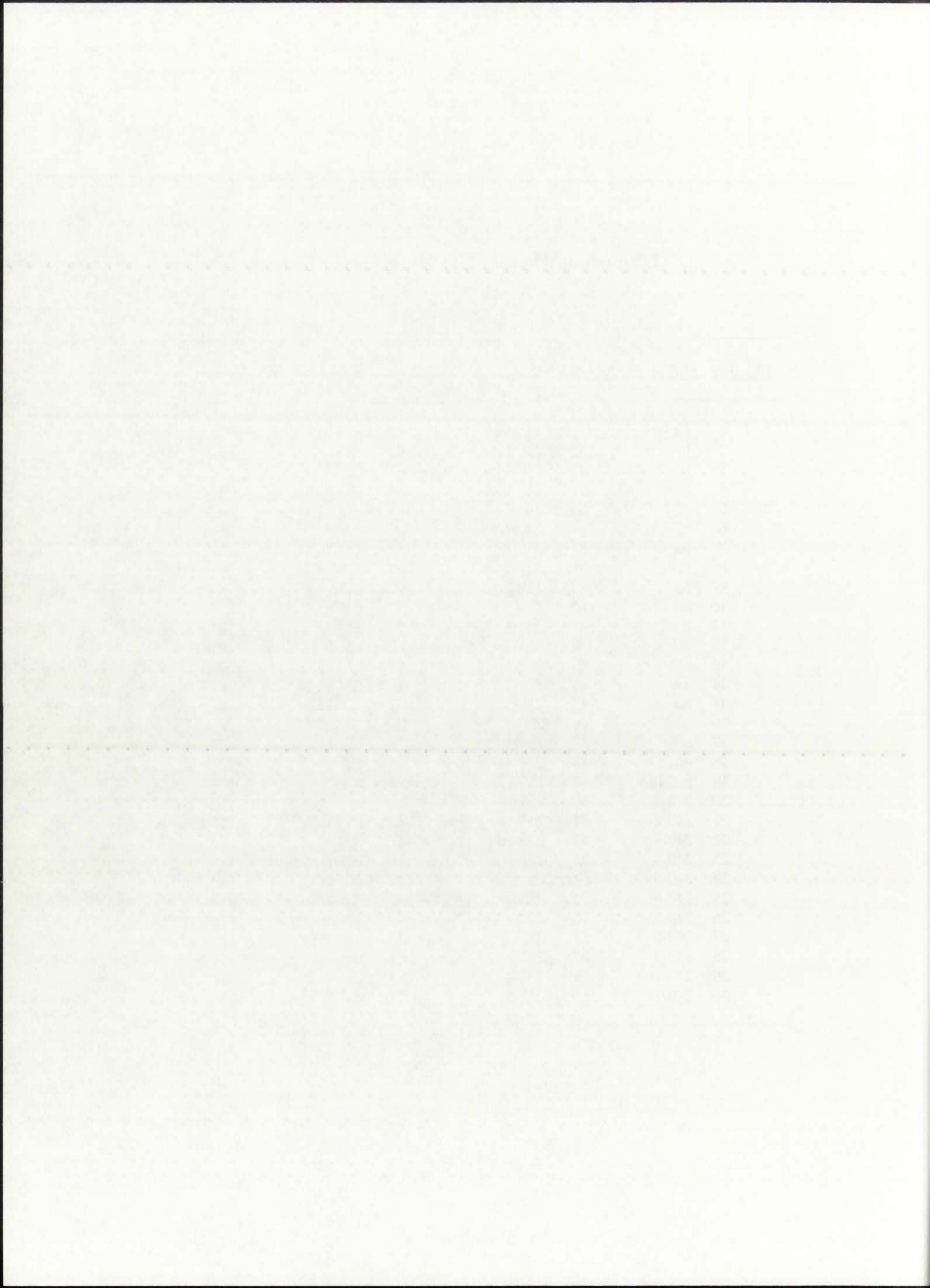
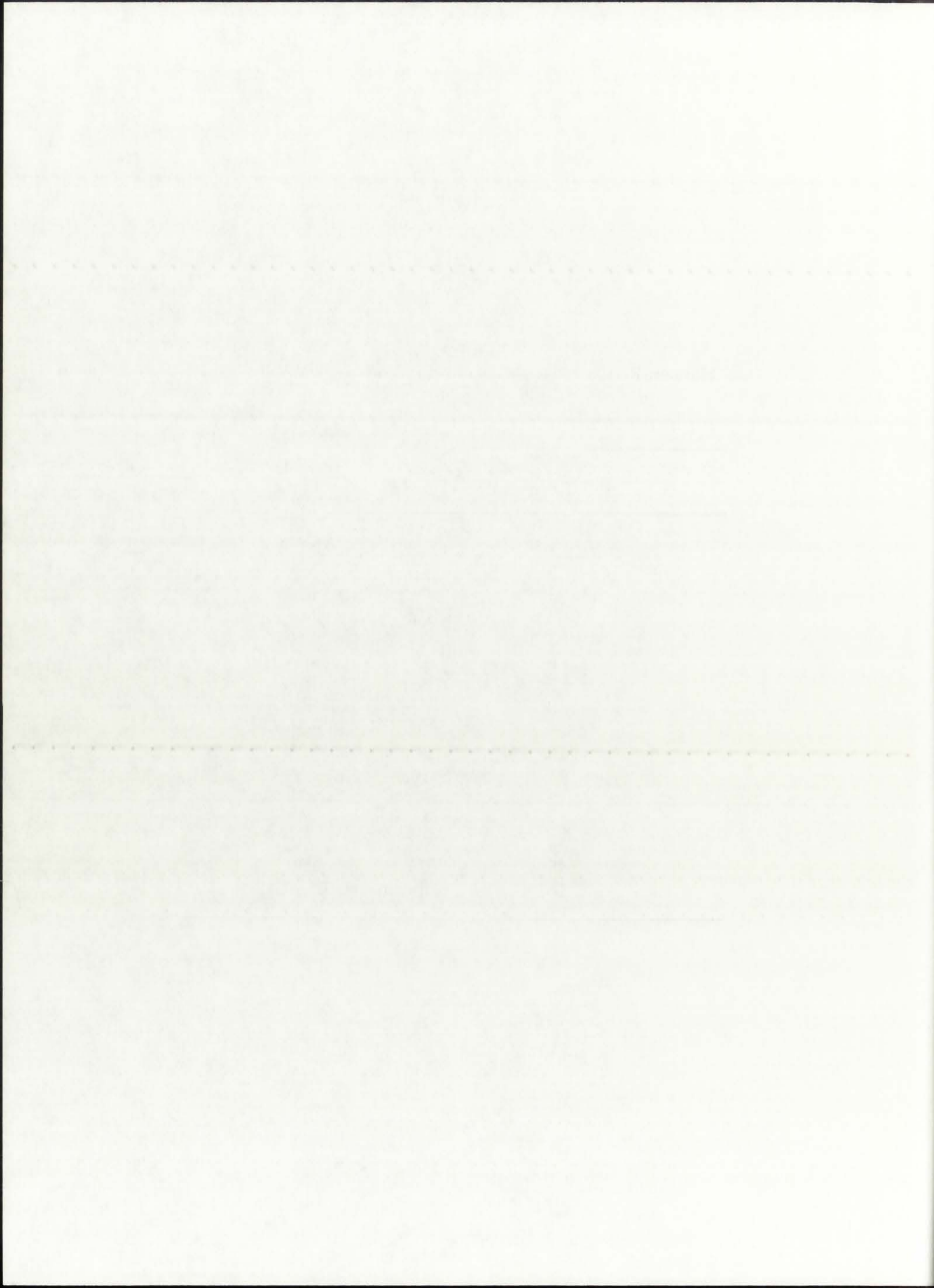


TABLE 7.3
Hansen-Roach cross-section library energy group structure

Energy Group	Energy Range
1	3.0 - ∞ MeV
2	1.4 - 3.0 MeV
3	0.9 - 1.4 MeV
4	0.4 - 0.9 MeV
5	0.1 - 0.4 MeV
6	17 - 100 keV
7	3 - 17 keV
8	0.55 - 3 keV
9	100 - 550 eV
10	30 - 100 eV
11	10 - 30 eV
12	3 - 10 eV
13	1 - 3 eV
14	0.4 - 1 eV
15	0.1 - 0.4 eV
16	thermal (0.025 eV)



For the purposes of the work presented in this Dissertation, the neutronics results obtained using the Hansen-Roach library are intended to serve as reference data. They are used to compare the results obtained with the ENDF/B-V temperature-dependent cross-sections and, based on that comparison, to delineate any benefits of using the low-temperature moderator/reflector with respect to critical mass and dimensions. It is also possible to determine the effects of the very high-temperature fuel and propellant on the critical mass and dimensions.

7.4.2. The Temperature-Dependent ENDF/B-V Library

As mentioned in the previous Section, the Hansen-Roach library assumes isothermal conditions with respect to the microscopic cross-sections. This may not provide accurate results for the unit-cell NLB rocket engine, which is characterized by very large temperature differences: over a radial distance of less than 87 cm, the temperature can potentially range from approximately 90,000 K in the fuel down to 100 K in the moderator/reflector (e.g., for a potential 500 MWth engine configuration).

To account for the large temperature differences present in the NLB engine, a new cross-section library based on baseline ENDF/B-V nuclear data needed to be used. The appropriate temperature-dependent library used for neutronics analysis in this Dissertation was obtained from Los Alamos National Laboratory, Group T-2 of the Theoretical Physics Division. The library, called MATXS7, consists of 69 neutron groups and comprises a total of 127 nuclides [McFarlane, 1992; McFarlane, 1993]. It allows for temperature dependence over a wide range [McFarlane, 1993] and also incorporates five energy groups below the standard room-temperature 0.025 eV cutoff, down to 1.0e-5 eV. This very low energy structure allows for full investigation of any potential benefits of the 0.006 eV scattering cutoff in beryllium. The nuclide content of MATXS7 is given in Table 7.4. The energy group structure of MATXS7 is given in Table 7.5.

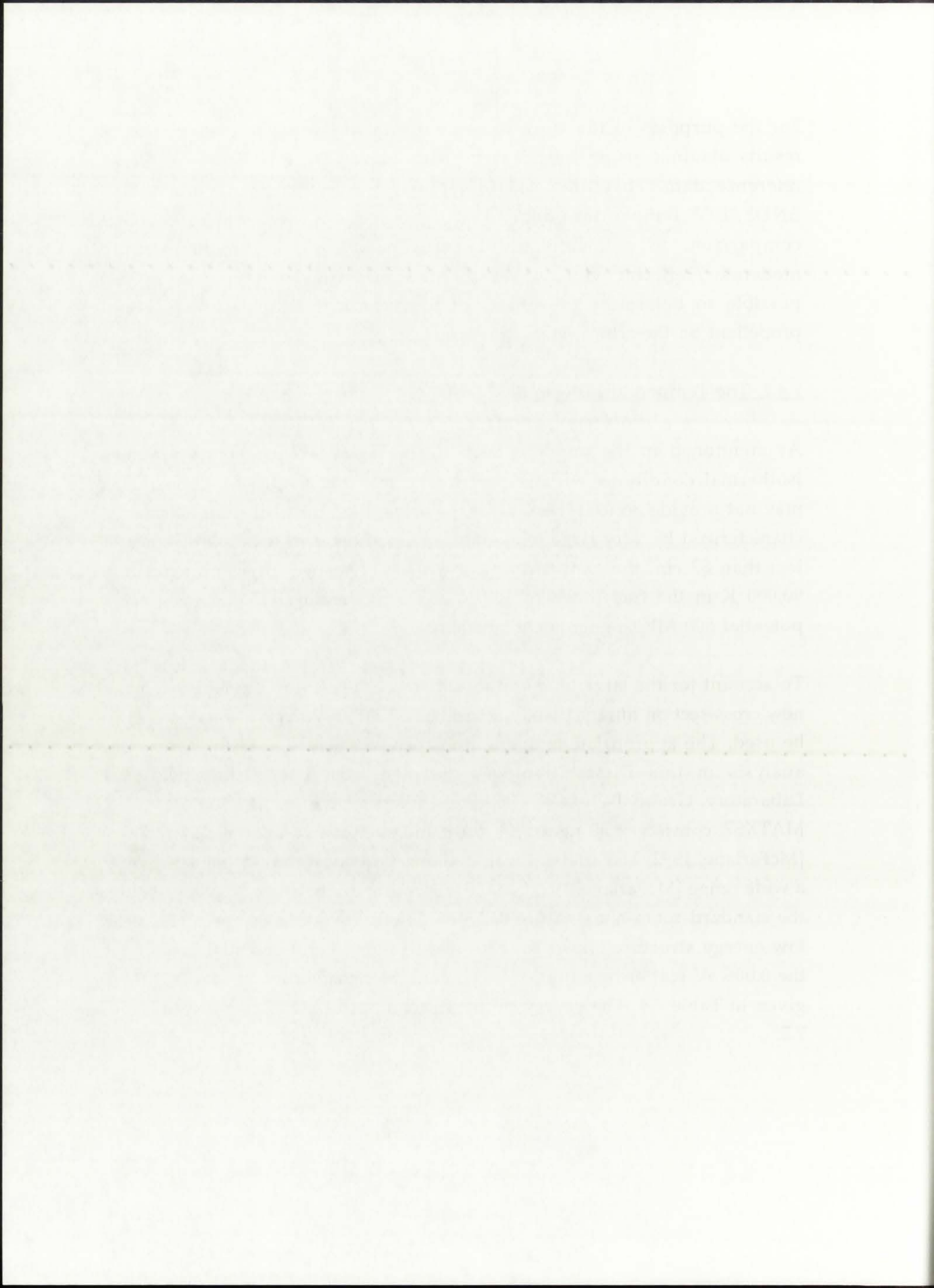


TABLE 7.4
127-nuclide MATXS7 cross-section library [McFarlane, 1993]

<u>Number</u>	<u>Nuclide</u>	<u>Number</u>	<u>Nuclide</u>	<u>Number</u>	<u>Nuclide</u>	<u>Number</u>	<u>Nuclide</u>
1	h1	33	zrnat	65	pm151	97	pbnat
2	h2	34	zr93	66	sm147	98	bi209
3	he3	35	nb93	67	sm149	99	th232
4	he4	36	monat	68	sm150	100	pa233
5	li6	37	mo95	69	sm151	101	u233
6	li7	38	tc99	70	sm152	102	u234
7	be9	39	ru101	71	eu151	103	u235
8	be9l	40	ru103	72	eu152	104	u236
9	b10	41	ru105	73	eu153	105	u238
10	b11	42	rh103	74	eu154	106	u239
11	cnat	43	rh105	75	eu155	107	np237
12	n14	44	pd105	76	eu156	108	np238
13	o16	45	pd108	77	eu157	109	np239
14	f19	46	ag109	78	gd152	110	pu238
15	na23	47	cdnat	79	gd154	111	pu239
16	mgnat	48	snnat	80	gd155	112	pu240
17	al27	49	i135	81	gd156	113	pu241
18	sinat	50	xe131	82	gd157	114	pu242
19	snat	51	xe133	83	gd158	115	pu243
20	clnat	52	xe135	84	gd160	116	pu244
21	arnat	53	cs133	85	tb159	117	am241
22	knat	54	cs134	86	tb160	118	am242
23	canat	55	cs135	87	dy160	119	am242m
24	tinat	56	pr141	88	dy161	120	am243
25	vnat	57	pr143	89	dy164	121	cm242
26	crnat	58	nd143	90	lu176	122	cm243
27	mn55	59	nd145	91	hfnat	123	cm244
28	fenat	60	nd147	92	ta181	124	cm245
29	co59	61	pm147	93	w182	125	cm246
30	ninat	62	pm148	94	w183	126	cm247
31	cunat	63	pm148m	95	w184	127	cm248
32	kr83	64	pm149	96	w186		

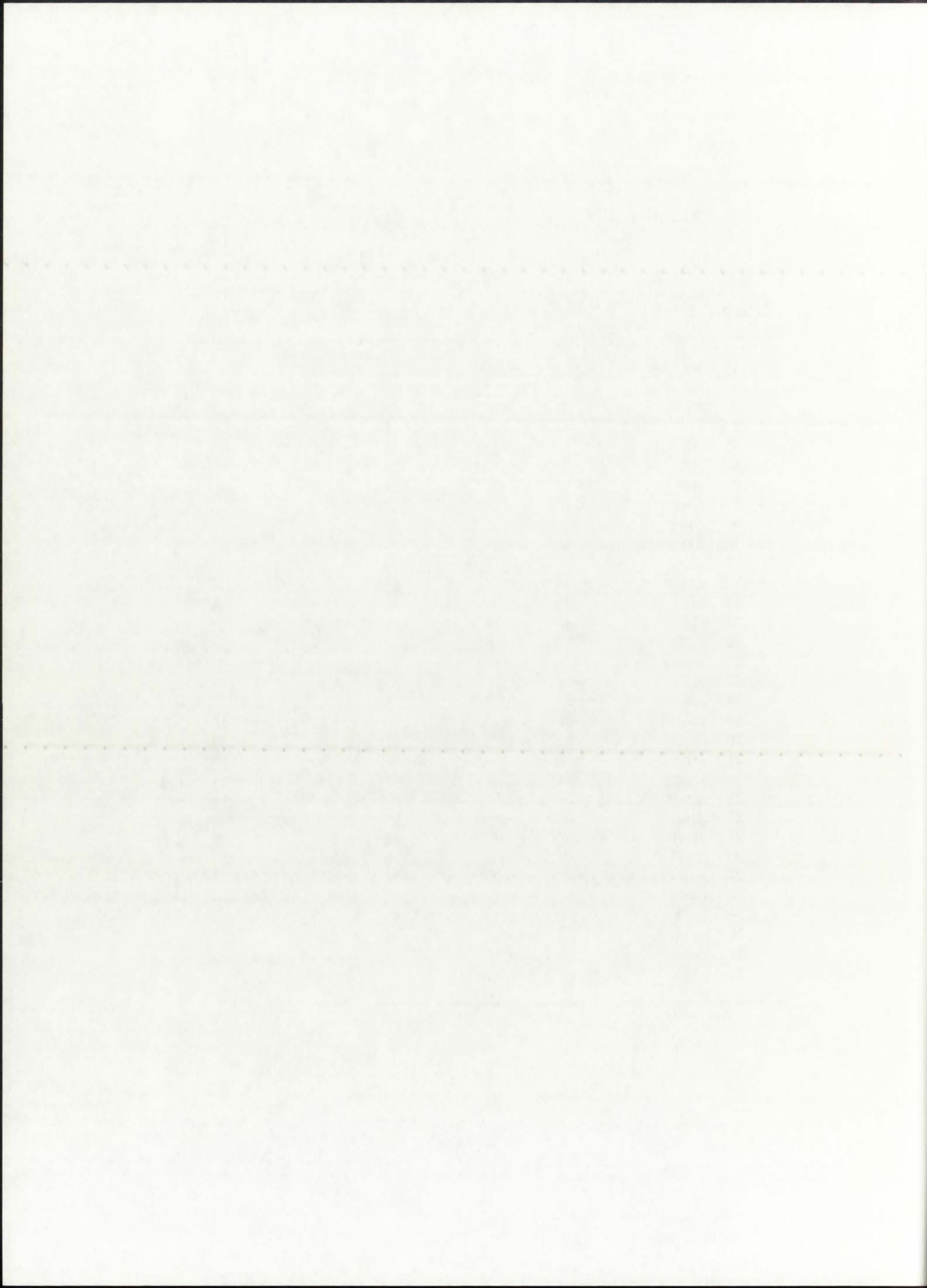
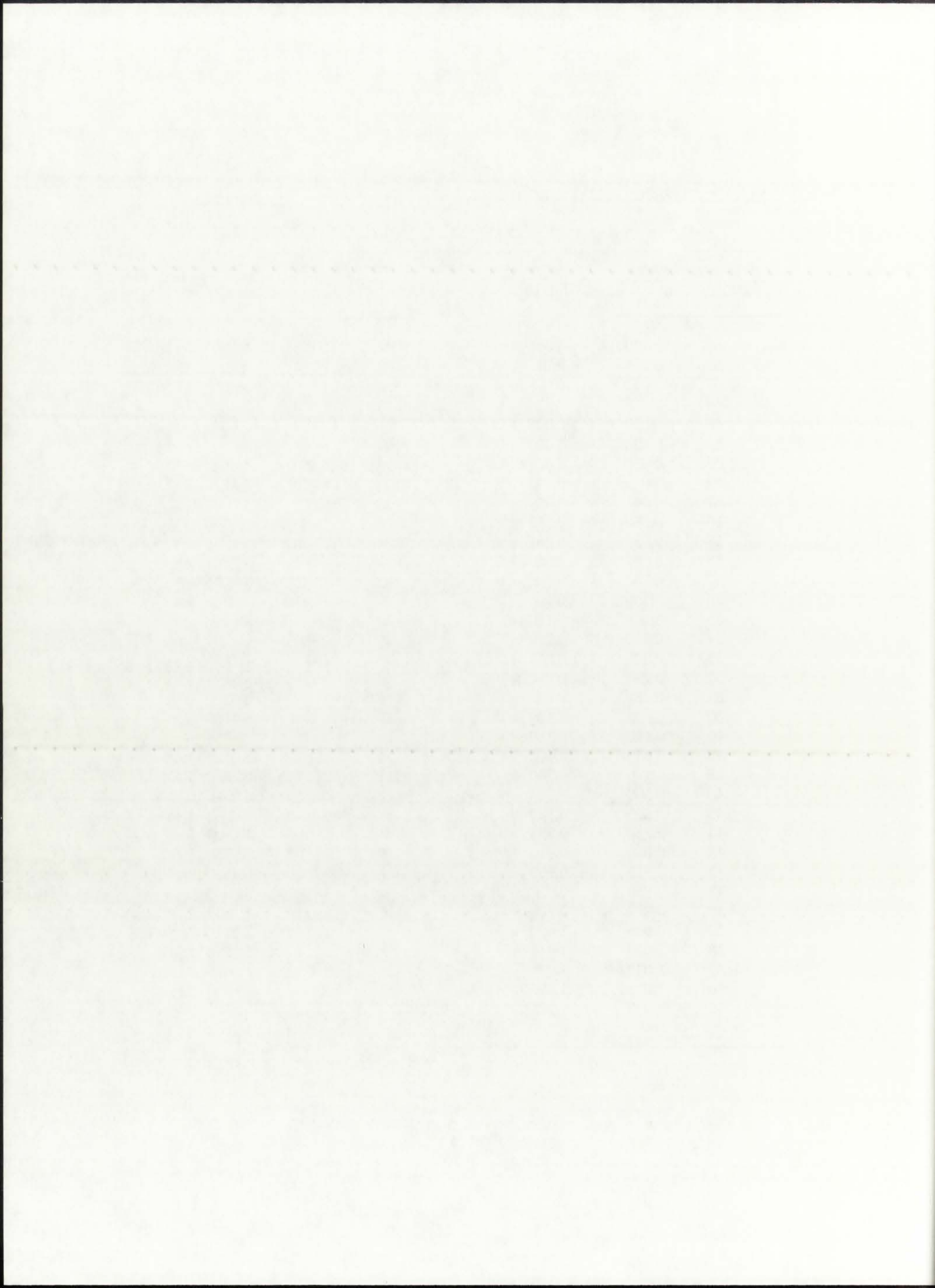


TABLE 7.5
 MATXS7 cross-section library energy group structure [McFarlane, 1992]

<u>Energy Group</u>	<u>Energy Range</u>	<u>Energy Group</u>	<u>Energy Range</u>
69	0.00001 - 0.005 eV	34	1.123 - 1.150 eV
68	0.005 - 0.01 eV	33	1.150 - 1.300 eV
67	0.01 - 0.015 eV	32	1.300 - 1.500 eV
66	0.015 - 0.020 eV	31	1.500 - 2.100 eV
65	0.020 - 0.025 eV	30	2.100 - 2.600 eV
64	0.025 - 0.030 eV	29	2.600 - 3.300 eV
63	0.030 - 0.035 eV	28	3.300 - 4.000 eV
62	0.035 - 0.042 eV	27	4.000 - 9.877 eV
61	0.042 - 0.050 eV	26	9.877 - 15.968 eV
60	0.050 - 0.058 eV	25	15.968 - 27.700 eV
59	0.058 - 0.067 eV	24	27.700 - 48.052 eV
58	0.067 - 0.080 eV	23	48.052 - 75.501 eV
57	0.080 - 0.100 eV	22	75.501 - 148.73 eV
56	0.100 - 0.140 eV	21	148.73 - 367.26 eV
55	0.140 - 0.180 eV	20	367.26 - 906.90 eV
54	0.180 - 0.220 eV	19	0.9069 - 1.4251 keV
53	0.220 - 0.250 eV	18	1.4251 - 2.2395 keV
52	0.250 - 0.280 eV	17	2.2395 - 3.5191 keV
51	0.280 - 0.300 eV	16	3.5191 - 5.5300 keV
50	0.300 - 0.320 eV	15	5.5300 - 9.1180 keV
49	0.320 - 0.350 eV	14	9.1180 - 15.030 keV
48	0.350 - 0.400 eV	13	15.030 - 24.780 keV
47	0.400 - 0.500 eV	12	24.780 - 40.850 keV
46	0.500 - 0.625 eV	11	40.850 - 67.340 keV
45	0.625 - 0.780 eV	10	67.340 - 111.00 keV
44	0.780 - 0.850 eV	9	111.00 - 183.00 keV
43	0.850 - 0.910 eV	8	183.00 - 302.50 keV
42	0.910 - 0.950 eV	7	302.50 - 500.00 keV
41	0.950 - 0.972 eV	6	500.00 - 821.00 keV
40	0.972 - 0.996 eV	5	0.8210 - 1.3530 MeV
39	0.996 - 1.020 eV	4	1.3530 - 2.2310 MeV
38	1.020 - 1.045 eV	3	2.2310 - 3.6790 MeV
37	1.045 - 1.071 eV	2	3.6790 - 6.0655 MeV
36	1.071 - 1.097 eV	1	6.0655 - 10.000 MeV
35	1.097 - 1.123 eV		

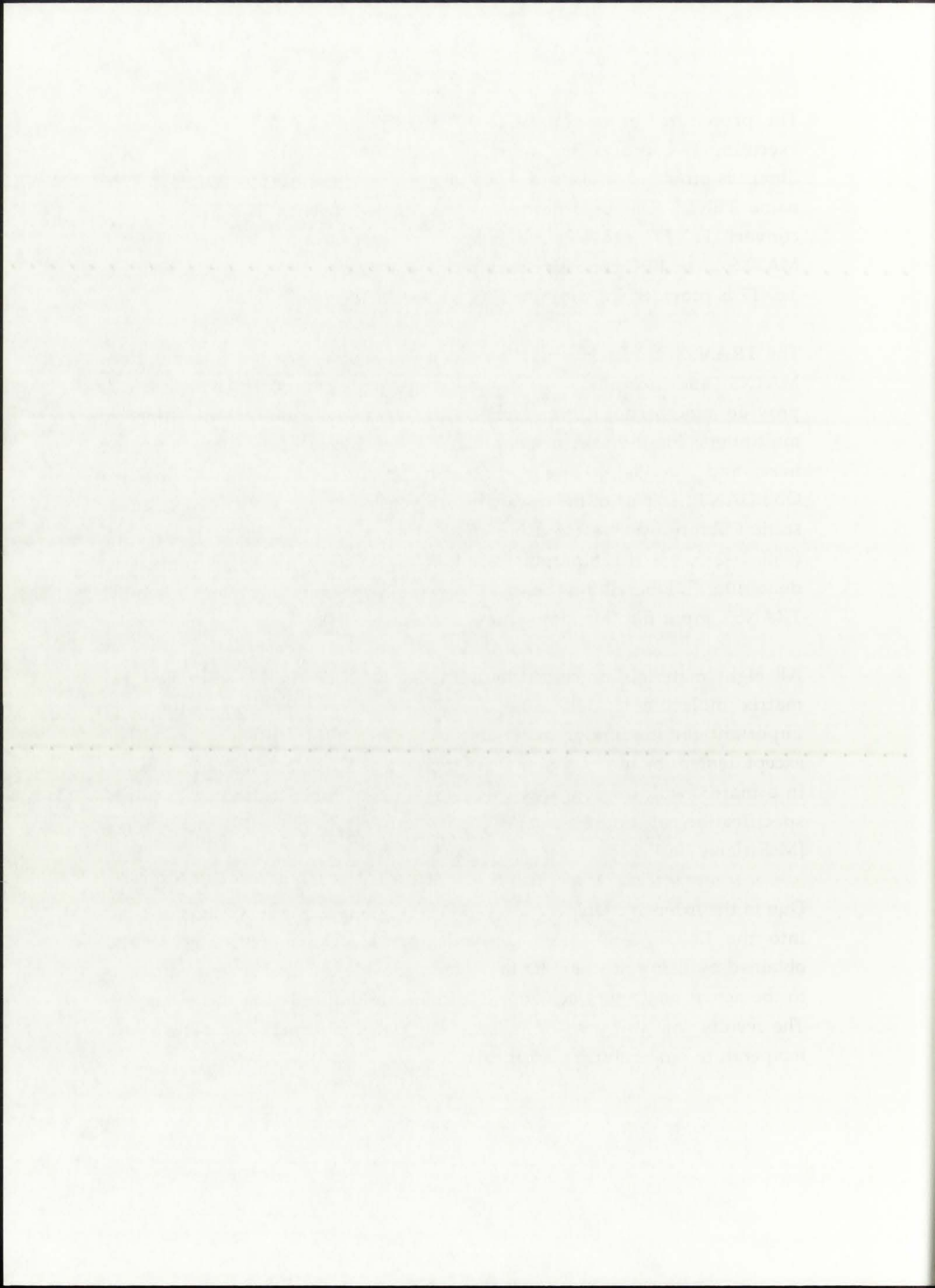


The procedure for making MATXS7 accessible to TWODANT consists of executing two processing codes: BBC and TRANSX. The actual MATXS7 library is provided to users on 1/4" magnetic tape, in ASCII format, under the name TEXT7. The BBC processing code supplied with TEXT7 is used to convert TEXT7 into a machine-specific binary format and to name it MATXS7. The BBC code is relatively simple to use; an input file pertaining to TEXT7 is provided in Appendix K.

The TRANSX processing code is used to extract the required nuclides from MATXS7 and incorporate the desired temperature effects. TRANSX can also provide macroscopic cross-sections by the inclusion of atomic density multipliers; for the sake of simplicity, however, this feature was not used here, and nuclide mixing and density specifications were confined to ONEDANT. As part of the research work presented here, a microscopic cross-section library was created using TRANSX for a total of eight materials: fuel (96% U-235, 4% U-238), argon (Ar), silicon (Si), oxygen (O), hydrogen (H), deuterium (D), beryllium (Be), and steel (Fe). Appendix L contains a sample TRANSX input file (for room temperature materials).

All eight materials processed by TRANSX required the specification of a matrix molecule to determine the self-shielding effect, generally most important for moderator materials [McFarlane, 1993]. Thus, all materials except deuterium and beryllium were specified as "free gas"; deuterium, being in a matrix with oxygen, was specified as "d2o" while beryllium required specification of both inelastic ("be") and elastic ("be\$") components [McFarlane, 1993].

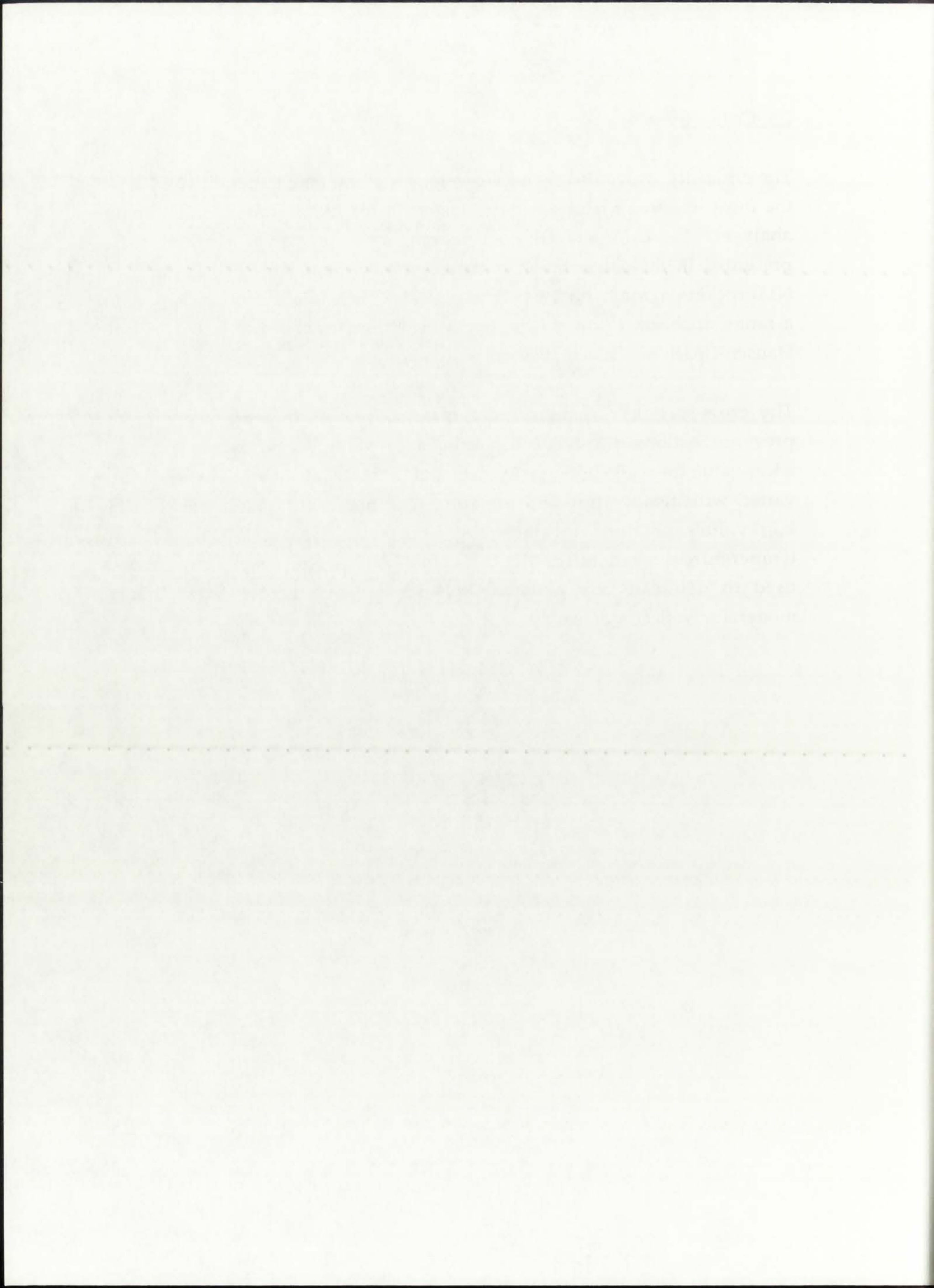
Due to the extensive temperature and energy group dependence incorporated into the ENDF/B-V library derived from MATXS7, neutronics results obtained by using this new library should provide the closest approximation to the actual neutronics behavior of a full-scale unit cell NLB rocket engine. The results will also indicate whether any potential benefits of using a low temperature moderator/reflector exist.



7.5. Criticality

The criticality issue, along with the volumetric heat generation rate $Qg'''(r)$, is the most important neutronics parameter related to the unit-cell NLB engine analysis. The complete coupled thermal and neutronics research work presented in this Dissertation is based on determining the k_{eff} for unit-cell NLB rocket engine, with the original UARL dimensions and composition, for a range of thermal powers and operating pressures and also based on both Hansen-Roach and ENDF/B-V cross-section data.

The cross-sections, geometry, and material composition discussed in the previous Sections all serve to determine a k_{eff} value. As part of the search for a k_{eff} value for a given thermal power and pressure, the atom densities can be varied with temperature and pressure. A comparison is made between the k_{eff} values obtained for both the isothermal (Hansen-Roach) and the temperature-dependent (ENDF/B-V) cross-sections; the results can then be used to delineate any potential benefits of using the low temperature moderator/reflector assembly.



CHAPTER 8 ROCKET PROPULSION THEORY

8.1. Introduction

The nuclear reactor is an integral part of the unit-cell NLB rocket engine; its main function is to provide a source of thermal energy for transfer to the propellant. As such, it is very similar to all other heat sources used for propulsion in that the rocket engine performance parameters can be derived from basic rocket propulsion theory. This Chapter provides an overview of the applicable theory and presents the methodology for estimating rocket performance parameters, such as exit velocity, specific impulse, and thrust, which would be characteristic of the unit-cell NLB engine.

8.2. Rocket Performance Parameters

Evaluation of the pertinent rocket performance parameters is necessary in order to justify any future development of GCR technology in general, and the unit-cell NLB engine in particular. The main motivating factor for continued research in the area of GCR technology has been the potential for rocket performance parameters in excess of SCR and chemical propulsion systems. As part of a feasibility study into the unit-cell NLB engine, then, it is necessary to determine a set of associated performance parameters and conclude whether the concept is justified for further research work.

The most important performance parameters associated with space propulsion concepts are the Specific Impulse (I_{sp}) [sec] and the Thrust (F) [N]. The thrust corresponds to the total reaction force on the spacecraft due to the ejection of the propellant and for an ideal rocket configuration is given as [Sutton, 1992]:

$$F = \dot{m} v_{\text{exit,max}} \quad , \quad (8.1)$$

CHAPTER 1 ROCKET PROPULSION THEORY

1.1 Introduction

The rocket motor is an integral part of the unit-cell MFB rocket engine. Its main function is to provide a source of thermal energy for transfer to the propellant. As such, it is very similar to all other heat sources used for propulsion in that the rocket engine performance parameters can be derived from basic rocket propulsion theory. This Chapter provides an overview of the applicable theory and presents the methodology for estimating rocket performance parameters, such as exit velocity, specific impulse, and thrust, which would be characteristic of the unit-cell MFB engine.

1.2 Rocket Performance Parameters

Evaluation of the pertinent rocket performance parameters is necessary in order to justify any future development of OER technology in general and the unit-cell MFB engine in particular. The main motivating factor for continued research in the area of OER technology has been the potential for rocket performance parameters to exceed those of SR and chemical propulsion systems. As part of a feasibility study into the unit-cell MFB engine, it is necessary to determine a set of associated performance parameters and conclude whether the concept is justified for further research work.

The most important performance parameters associated with space propulsion concepts are the specific impulse (I_{sp}) and the Thrust (T). The thrust corresponds to the total reaction force on the spacecraft due to the ejection of the propellant and for an ideal rocket configuration is given as [Sutton, 1999]

$$T = \dot{m} v_{ex} + p_e A_e \quad (1.1)$$

where \dot{m} and $v_{\text{exit,max}}$ correspond to the propellant mass flow rate [kg/s] and the nozzle exit ideal velocity [m/s], respectively. The specific impulse is defined as the thrust per unit weight flow of propellant, and is given as [Sutton, 1992]:

$$I_{\text{sp}} = \frac{F}{\dot{m} g_0} \quad , \quad (8.2)$$

where g_0 corresponds to the gravity acceleration constant, nominally taken to be 9.807 [m/s²]. To calculate the thrust, both the propellant mass flow rate and the velocity at the rocket nozzle exit are needed. The ideal exit velocity, representing the maximum possible velocity that can be attained for a given set of engine parameters, was previously given in eqn. (1.1):

$$v_{\text{exit,max}} = \sqrt{\frac{2\gamma RT_{\text{chamber}}}{(\gamma-1)M_w}} \quad , \quad (8.3)$$

where γ represents the ratio of specific heats, R denotes the universal gas constant of 8.314 [J/g-mol-K], M_w denotes the molecular weight of the propellant [g/g-mol], and T_{chamber} corresponds to the bulk propellant temperature [K] at the exit of the propellant channel. The propellant mass flow rate can be calculated from the appropriate axial channel exit conditions:

$$\dot{m} = A_{\text{cs,exit}} v_{\text{exit}} \rho_{\text{exit}} \quad , \quad (8.4)$$

where $A_{\text{cs,exit}}$ denotes the channel exit cross-sectional area [m²], and v_{exit} and ρ_{exit} denote the propellant velocity and bulk density [kg/m³] at the axial channel exit. Since this research focuses on determining the characteristics of the unit-cell NLB rocket engine in (r) geometry, all the above parameters will be evaluated as characteristic of the channel exit conditions. The value of $A_{\text{cs,exit}}$ will therefore be taken as the cross-sectional area of a propellant channel, and ρ_{exit} will be evaluated at the bulk propellant temperature determined by the heat transfer model.

The first part of the report is a general introduction to the project. It describes the objectives of the study and the scope of the work. The second part of the report is a detailed description of the methodology used in the study. This includes a description of the data collection methods and the statistical analysis techniques used. The third part of the report is a discussion of the results of the study. This includes a comparison of the results with the objectives of the study and a discussion of the implications of the findings. The final part of the report is a conclusion and a list of references.

The methodology used in this study was a combination of qualitative and quantitative methods. The qualitative methods included interviews with experts in the field and a review of the literature. The quantitative methods included a survey of a large number of respondents. The data collected from these methods were analyzed using a variety of statistical techniques, including regression analysis and factor analysis. The results of the study show that there is a strong relationship between the variables studied. The implications of these findings are discussed in detail in the discussion section of the report.

The results of the study indicate that there is a significant positive correlation between the variables studied. This suggests that as one variable increases, the other variable also tends to increase. The implications of these findings are discussed in detail in the discussion section of the report. The study also identified several limitations and areas for future research. These include the need for a larger sample size and the need to explore the relationship between the variables in more detail.

The study was limited by several factors, including the sample size and the methods used. The sample size was relatively small, which may have affected the generalizability of the findings. The methods used were also limited in their ability to capture the complexity of the relationships between the variables. Future research should aim to address these limitations by using a larger sample size and more sophisticated methods. The study also identified several areas for future research, including the need to explore the relationship between the variables in more detail and the need to investigate the underlying mechanisms of the relationships.

8.3. Thermophysical Properties

Eqns. (8.3) and (8.4) are functions of a total of three thermophysical properties of the propellant: γ , M_w , and ρ_{exit} . Each of the three properties are heavily dependent on the bulk propellant temperature and pressure and need to be evaluated on the basis of the results from the heat transfer model. The propellant density is generally obtained from tabulated data; for the purposes of this research work, $\rho(p,T)$ was obtained from recent NASA sources [Walton, 1992] and incorporated into the heat transfer model. Since the propellant used in the unit-cell NLB engine is hydrogen (H_2), a diatomic gas, the ratio of specific heats and the molecular weight are both dependent on the degree of dissociation of the hydrogen.

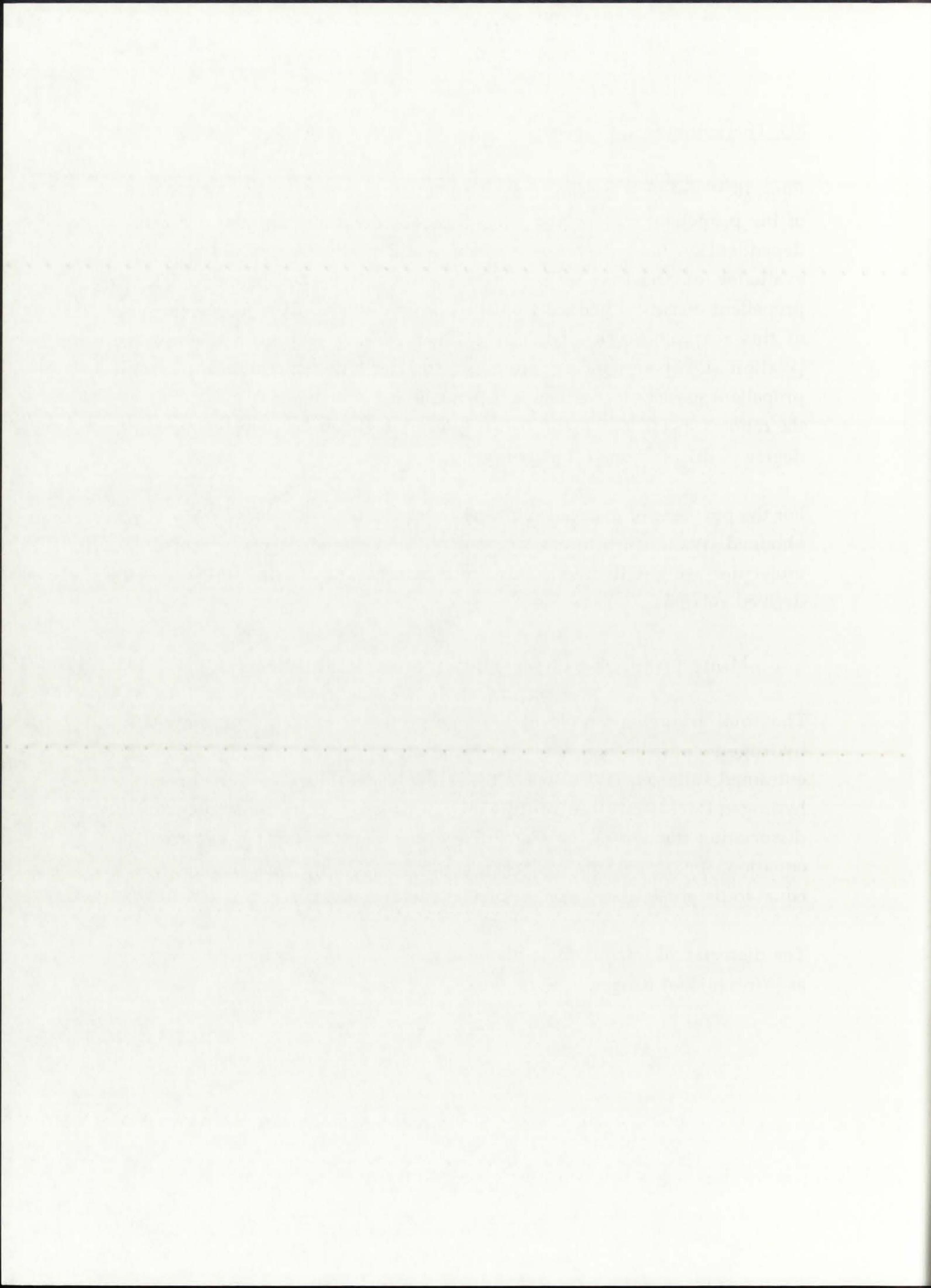
For the purposes of this research work, a set of tabulated values for $\gamma(p,T)$ was obtained [Walton, 1992] and incorporated into the heat transfer model. The molecular weight had to be determined separately, using the following derived relation:

$$M_w(\text{propellant}) = 0.97(\alpha^* M_w(H) + (1-\alpha^*) M_w(H_2)) + 0.03 M_w(W^{\text{nat}}) \quad (8.5)$$

The total propellant molecular weight consists of 97% by composition hydrogen contribution, and 3% by composition contribution from the entrained tungsten (W^{nat}) seeds that are intended to increase the opacity of hydrogen [McLafferty and Bauer, 1967]. In the above equation, α^* denotes the dissociation fraction of the diatomic hydrogen gas; as can be seen from the equation, for $\alpha^*=0.0$, the hydrogen contribution to the molecular weight is equal to the molecular weight of diatomic hydrogen (H_2).

The dissociation fraction for a diatomic propellant such as hydrogen is given as [Vincenti and Kruger, 1965]:

$$\alpha^* = \sqrt{\frac{\Psi(T,p)}{1 + \Psi(T,p)}} \quad (8.6)$$



where $\Psi(T,p)$ has the form:

$$\Psi(T,p) = \frac{e^{-\frac{\Theta_d}{T}}}{2p} \left[\left(\frac{\pi m_{\text{atom}} k T}{h^2} \right)^{1.5} k^{\Theta_R} (1 - e^{-\frac{\Theta_V}{T}}) \frac{(Q_{\text{el}}^{\text{atom}})^2}{Q_{\text{el}}^{\text{molec}}} \right] \quad (8.7)$$

Parameters Q_d , Q_R , and Q_V denote the characteristic hydrogen propellant temperatures for dissociation (4.477 eV or 51,956 K), rotation (85.7 K), and vibration (5,980 K); $Q_{\text{el}}^{\text{atom}}$ and $Q_{\text{el}}^{\text{molec}}$ denote the electronic partition functions for the hydrogen atom and molecule; and k and h correspond to the Boltzmann (1.3806×10^{-23} J/K) and Planck (6.6262×10^{-34} J-s) constants [GE, 1989].

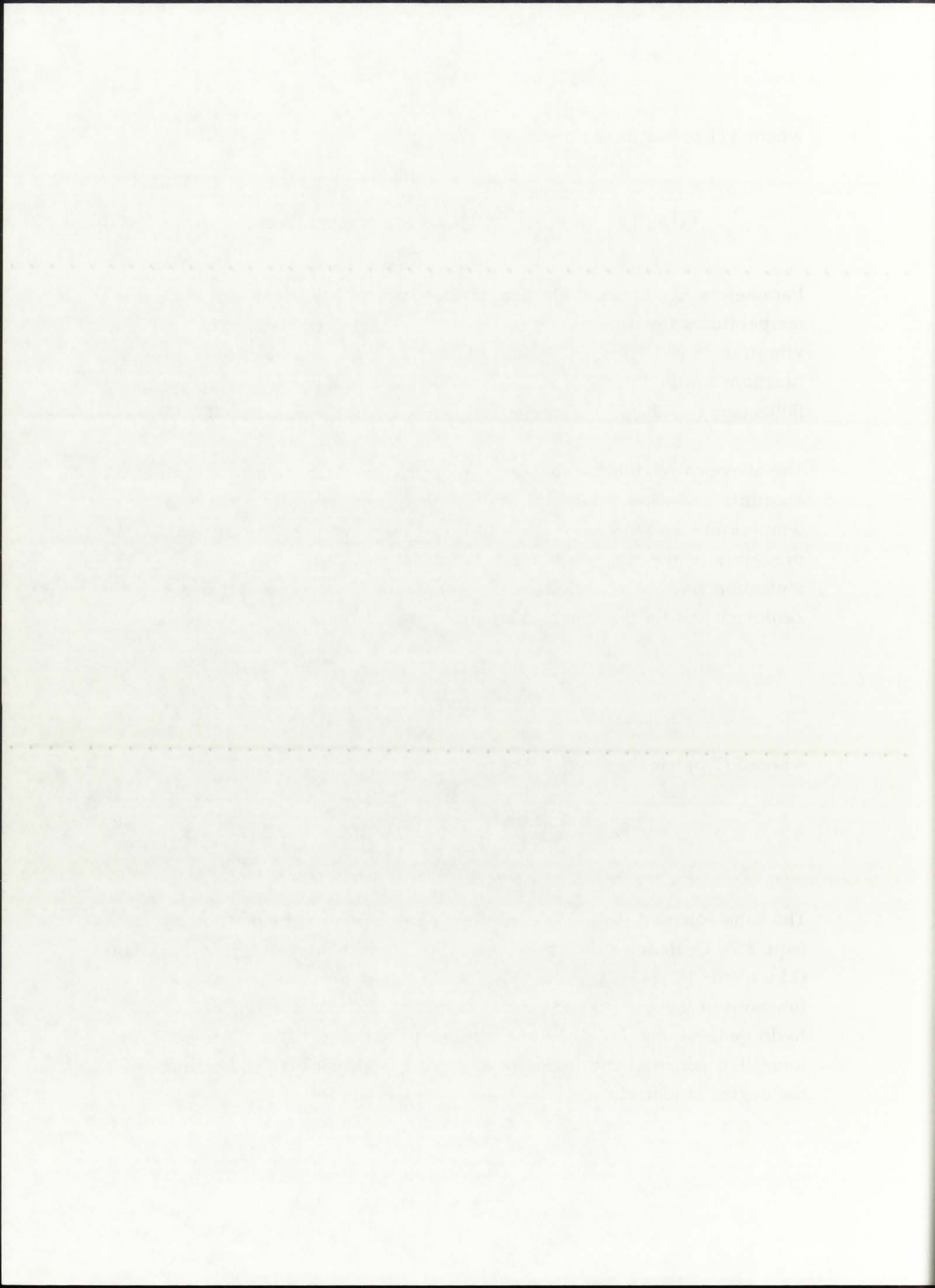
The above correlation for the dissociation fraction of the hydrogen propellant accounts for the rotational, vibrational, and translational effects of temperature and pressure; an additional effect at high temperatures and pressures is the degree of ionization. The procedure for calculating the ionization fraction relies on the Saha equation [Vincenti and Kruger, 1965; Zeldovich and Raizer, 1966], where the degree of ionization δ^* is given as:

$$\delta^* = \sqrt{\frac{\Xi(T,p)}{1 + \Xi(T,p)}} \quad (8.8)$$

where $\Xi(T,p)$ has the form:

$$\Xi(T,p) = \frac{e^{-\frac{\Theta_i}{T}}}{p} \left[\left(\frac{2\pi m_{\text{el}}}{h^2} \right)^{1.5} (kT)^{2.5} \frac{2 \prod_{\text{int}} Q_{\text{int}}^{z+}}{\prod_{\text{int}} Q_{\text{int}}^z} \right] \quad (8.9)$$

The Saha equation (eqn. 8.9) is similar to the molecular dissociation equation (eqn. 8.7); Q_i denotes the characteristic hydrogen temperature for ionization (13.6 eV or 157,842 K), while Q_{int}^{z+} and Q_{int}^z denote the internal partition functions of the ionized and neutral atom, respectively. It is a helpful fact that hydrogen, having only one electron in the orbiting cloud, has only one ionization potential and therefore allows a straight-forward determination of the degree of ionization.



To illustrate the behavior of the degree of ionization for hydrogen, as a function of temperature and pressure, δ^* is plotted in Figure 8.1. The data points correspond to combinations of three propellant temperatures resulting from three thermal power levels (50 kWth, 5 MWth, and 500 MWth) and three operating pressures (250 atm, 500 atm, and 1,000 atm). It can be seen that the degree of ionization δ^* is negligible ($\approx 10^{-6}$) for hydrogen temperatures less than 10,000 K; for temperatures greater than 20,000-30,000 K, ionization becomes an important issue and must be addressed to obtain accurate thermophysical and thermo-optical data for hydrogen. For complete ionization (i.e., $\delta^* \approx 1.0$), the total pressure in the propellant region would consist of equal parts of the ionized hydrogen atoms (H^+) and the stripped electrons (e^-), so the actual hydrogen pressure would equal only 50% of the total operating pressure in the propellant region.

The above discussion on ionization was included for the purposes of familiarization with the possible physical processes that need to be accounted for in the case of very high temperatures and operating pressures. The degree of hydrogen ionization δ^* , although calculated as part of this Dissertation, was not utilized, as the sources of both the hydrogen thermophysical [Walton, 1992] and thermo-optical [Krascella, 1963; Kesten and Kinney, 1965] properties reported ionization accounted for in their calculations.

8.4. Axial Dependence

As mentioned previously in this Chapter, in order to correctly determine $v_{\text{exit,max}}$, I_{sp} , and F , it is necessary to evaluate all pertinent parameters at the axial exit of the propellant channel. Since the thermal analysis model incorporates only (r) geometry dependence, the propellant bulk temperature calculated by the model must correspond to the bulk temperature of the propellant at the channel exit. To achieve this, it is necessary to estimate analytically the magnitude of the channel exit propellant temperature. This is done by modifying the uniform axial power density correlation derived in [Hill and Peterson, 1965], originally applied to the problem of convective heating of propellant from the outside of a cylindrical tube:

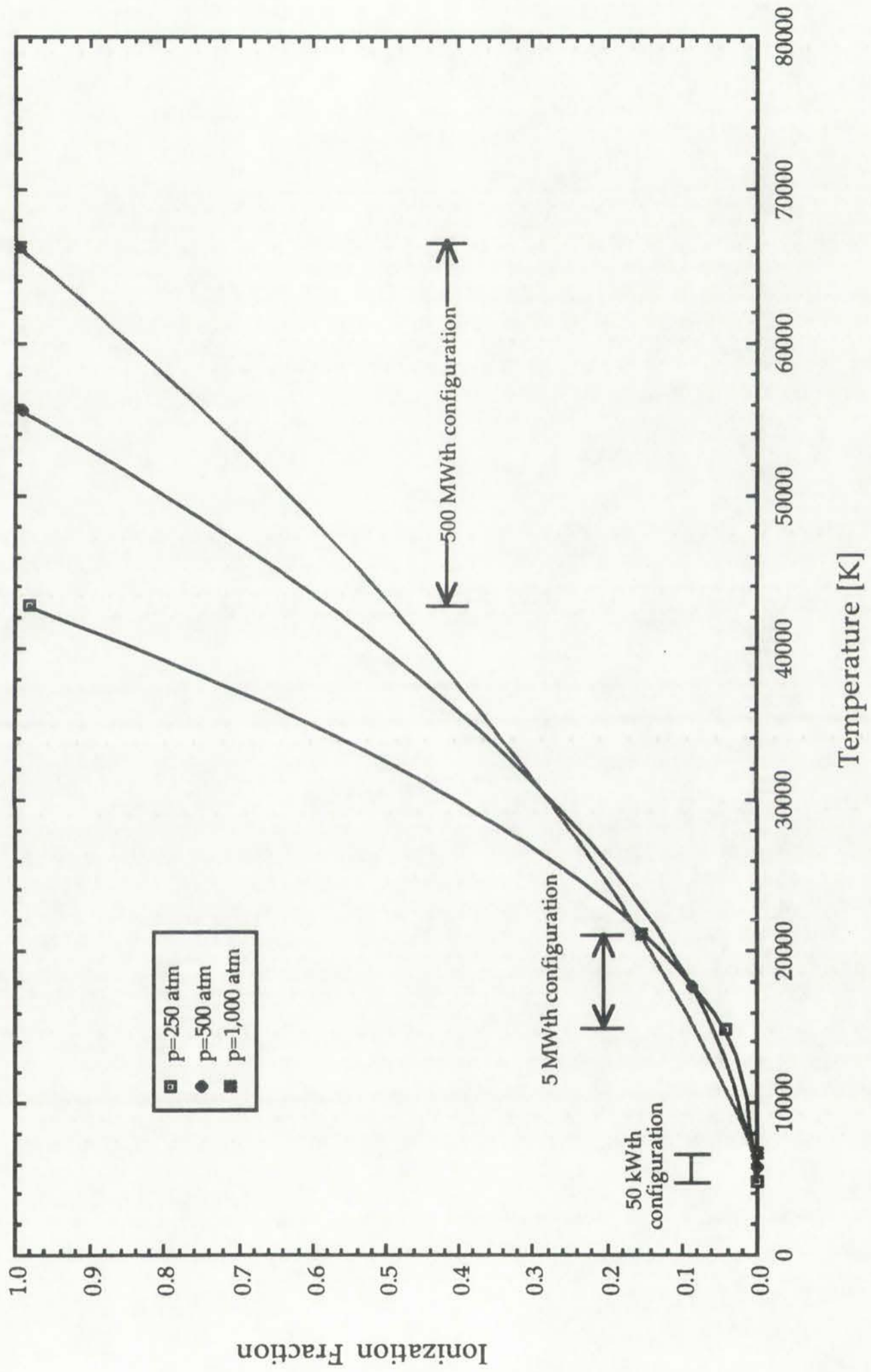
The behavior of the degree of ionization for hydrogen as a function of temperature and pressure is shown in Figure 4. The data points reported in this paper are for temperatures ranging from 10,000 K to 20,000 K and pressures from 0.1 to 1.0 atm. It can be seen that the degree of ionization is a function of both temperature and pressure. For temperatures greater than 10,000 K, the degree of ionization is greater than 0.5 for pressures less than 1.0 atm. For temperatures less than 10,000 K, the degree of ionization is less than 0.5 for pressures less than 1.0 atm. The degree of ionization is a function of both temperature and pressure. For temperatures greater than 10,000 K, the degree of ionization is greater than 0.5 for pressures less than 1.0 atm. For temperatures less than 10,000 K, the degree of ionization is less than 0.5 for pressures less than 1.0 atm.

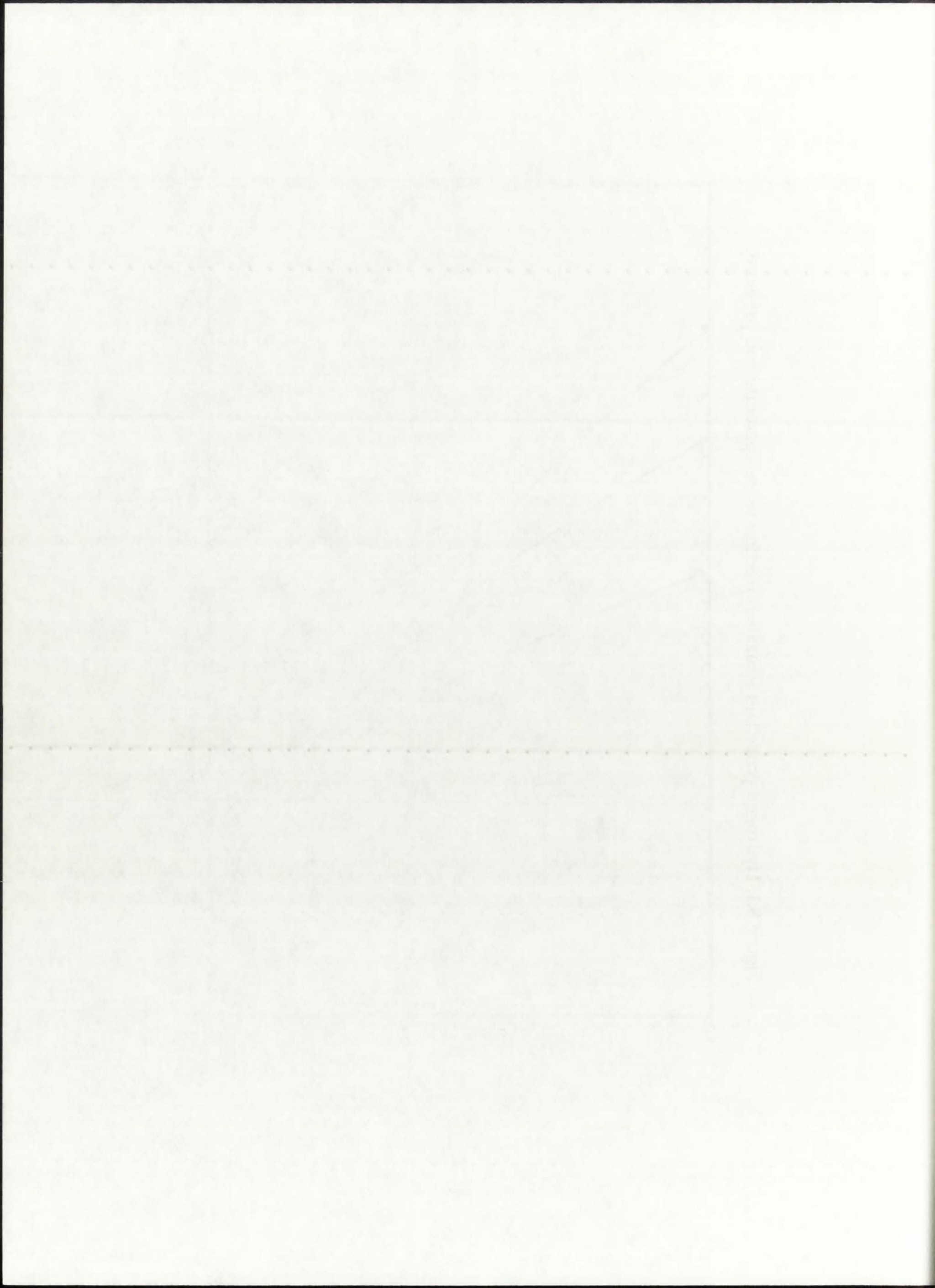
The above discussion on ionization was included for the purpose of comparison with the kinetic physical process that need to be considered in the case of very high temperatures and operating pressure. The degree of hydrogen ionization α , although calculated as part of the Dissertation, was not utilized as the source of both the hydrogen thermochemical [Walton, 1987] and thermo-optical [Krauss, 1987; Kesten and Kinney, 1987] properties reported in this Dissertation are in their calculations.

4.4. Axial Propagation

As mentioned previously in this Chapter, in order to correctly determine the axial propagation of the laser beam, it is necessary to evaluate all pertinent parameters at the axial end of the propellant channel. Since the thermal analysis model considers only (1) geometry dependent on the propellant bulk temperature calculated by the model must correspond to the bulk temperature of the propellant at the channel end. To achieve this it is necessary to estimate analytically the magnitude of the channel end propellant temperature. This is done by studying the nature and power density variation derived in [Hill and Peterson, 1986], originally applied to the problem of convective heating of propellant from the surface of a cylindrical tube.

Figure 8.1: Hydrogen propellant ionization fraction vs. temperature and pressure.





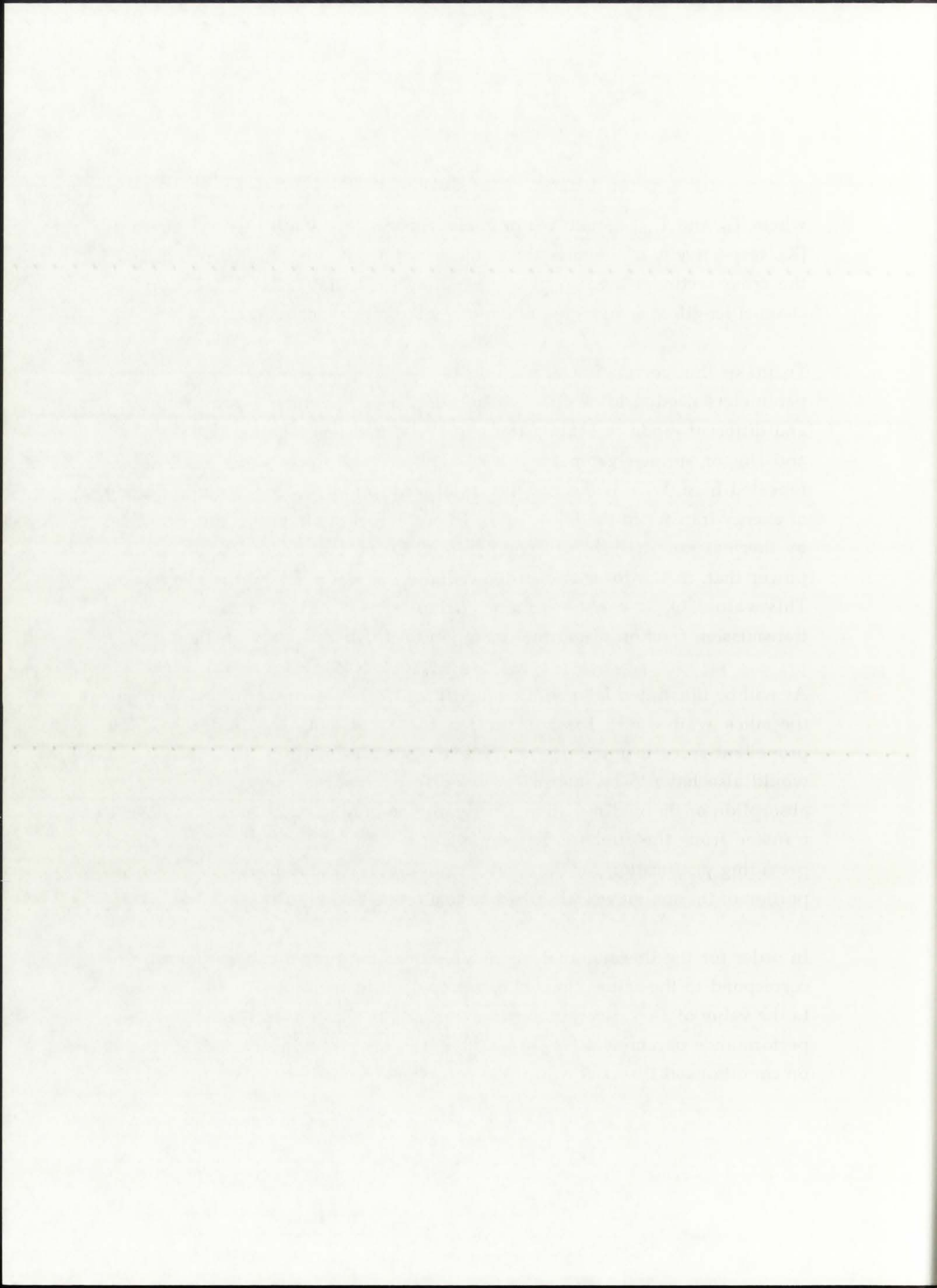
$$T_{\text{out}} - T_{\text{in}} = \frac{A_{\text{CS}} q''}{\dot{m} c_p} \left(\frac{4L}{D_H} \right), \quad (8.10)$$

where T_{in} and T_{out} denote the propellant channel inlet and exit temperatures [K], respectively, q'' denotes the radial heat flux [W/m²], A_{CS} corresponds to the cross-sectional area to propellant flow [m²], and L and D_H denote the channel length and mean hydraulic diameter [m], respectively.

To make this correlation applicable to the (r) geometry NLB mode, three parameters needed to be changed to reflect the different geometry (annulus) and different mode of heating (radiative heat transfer). The derivation of A_{CS} and D_H for annular geometry is a straight-forward process, and need not be repeated here. With respect to the radial heat flux q'' , as the dominant mode of energy transfer in the NLB engine from the fuel to the propellant would be by thermal radiation, q'' is actually equal to the portion of engine thermal power that, in the form of thermal radiation, is absorbed by the propellant. This value, Q_{abs} , can be obtained from eqn. (6.22) by determining the transmission fraction of thermal radiation for the hydrogen propellant.

As will be illustrated later in Chapters 10 and 11, in an operating NLB engine the silica wall would have to be film cooled on both the buffer gas and propellant sides to minimize convective heat transfer from these gases, and would also have to be internally cooled to remove the energy deposited by absorption of thermal radiation. Therefore, the only possible means of energy transfer from the fuel to the propellant would be by thermal radiation, providing justification for the representation of the radial heat flux q'' by the portion of thermal power absorbed by the propellant, Q_{abs} .

In order for the thermal analysis model-calculated propellant temperature to correspond to the actual channel exit propellant temperature, it must be equal to the value of T_{out} determined from eqn. (8.10). This ensures that the rocket performance parameters ($v_{\text{exit,max}}$, I_{sp} , and F) are properly determined, based on conditions at the axial exit of the propellant channel.



CHAPTER 9

THE GNRATR-1D THERMAL ANALYSIS CODE

9.1. Introduction

This Chapter describes the thermal analysis code GNRATR-1D, developed as part of the Dissertation research work. The GNRATR-1D code employs the theoretical concepts outlined in Chapters 6,7, and 8 to perform an (r) geometry thermal analysis of the unit-cell NLB rocket engine. The GNRATR-1D results stem from the research goals discussed in Chapter 4; follow the methodology of analysis presented in Chapter 5; and are based on the application of theory given in Chapters 6, 7, and 8.

9.2. The GNRATR-1D Thermal Analysis Code

As depicted previously in Figure 5.1, this Dissertation work comprising this consists of two parts: (1) thermal analysis, and (2) neutronics analysis. The parts are directly coupled - the results of the thermal analysis are used to perform the neutronics analysis, whose results are then incorporated back into the thermal analysis. It has already been stated that the neutronics analysis relies on the ONEDANT neutronics code and a cross-section library, and provides a set of $Qg'''(r)$ and the k_{eff} of the system. A thermal analysis model was therefore needed to make use of the theory presented in Chapter 6 and calculate the temperature distribution $T(r)$.

The inherent coupling of the modes of heat transfer, as well as the need for temperature-dependent properties, necessitated the use of a numerical solution --a computer code. After some searching, it was determined that no single code available today could be easily modified to perform the task of analyzing the NLB rocket engine. This was primarily due to the high-temperature gaseous condition of five out of the nine regions in the engine, and the different modes of heat transfer that occur. In addition, utilization of the available physical properties of the gaseous regions (such as opacity and

CHAPTER 3 THE GREAT-TO-THERMAL ANALYSIS CODE

3.1 Introduction

The Chapter describes the thermal analysis code GREAT-3D, developed as part of the Great-to-Thermal analysis work. The GREAT-3D code employs the thermal analysis outlined in Chapter 6, and 8 to perform a (a) geometry thermal analysis of the wall-to-wall (b) factor engine. The GREAT-3D results stem from the thermal analysis outlined in Chapter 4, follow the methodology of analysis presented in Chapter 2, and are based on the application of theory given in Chapter 6.5, and 8.

3.2 The GREAT-3D Thermal Analysis Code

As detailed previously in Figure 3.1, the Great-to-Thermal work comprises the analysis of two parts: (1) thermal analysis and (2) neutron analysis. The parts are directly coupled - the results of the thermal analysis are used to perform the neutron analysis whose results are then incorporated back into the thermal analysis. It has already been stated that the neutron analysis relies on the GREAT-3D neutron code and a cross-section library and provides a set of $\Sigma(T)$ and $\Sigma_0(T)$ for the system. A thermal analysis model was therefore needed to make use of the theory presented in Chapter 6 and calculate the temperature distribution $T(x)$.

The inherent coupling of the model of heat transfer, as well as the need for temperature-dependent properties, necessitated the use of a numerical solution - a computer code. When some searching it was determined that no single code available today could be easily modified to perform the task of analyzing the HLB reactor engine. This was primarily due to the high temperature gas flow conditions of five out of the nine regions in the engine and the different nature of heat transfer that occurs. In addition, calculation of the available physical properties of the various regions (such as opacity and

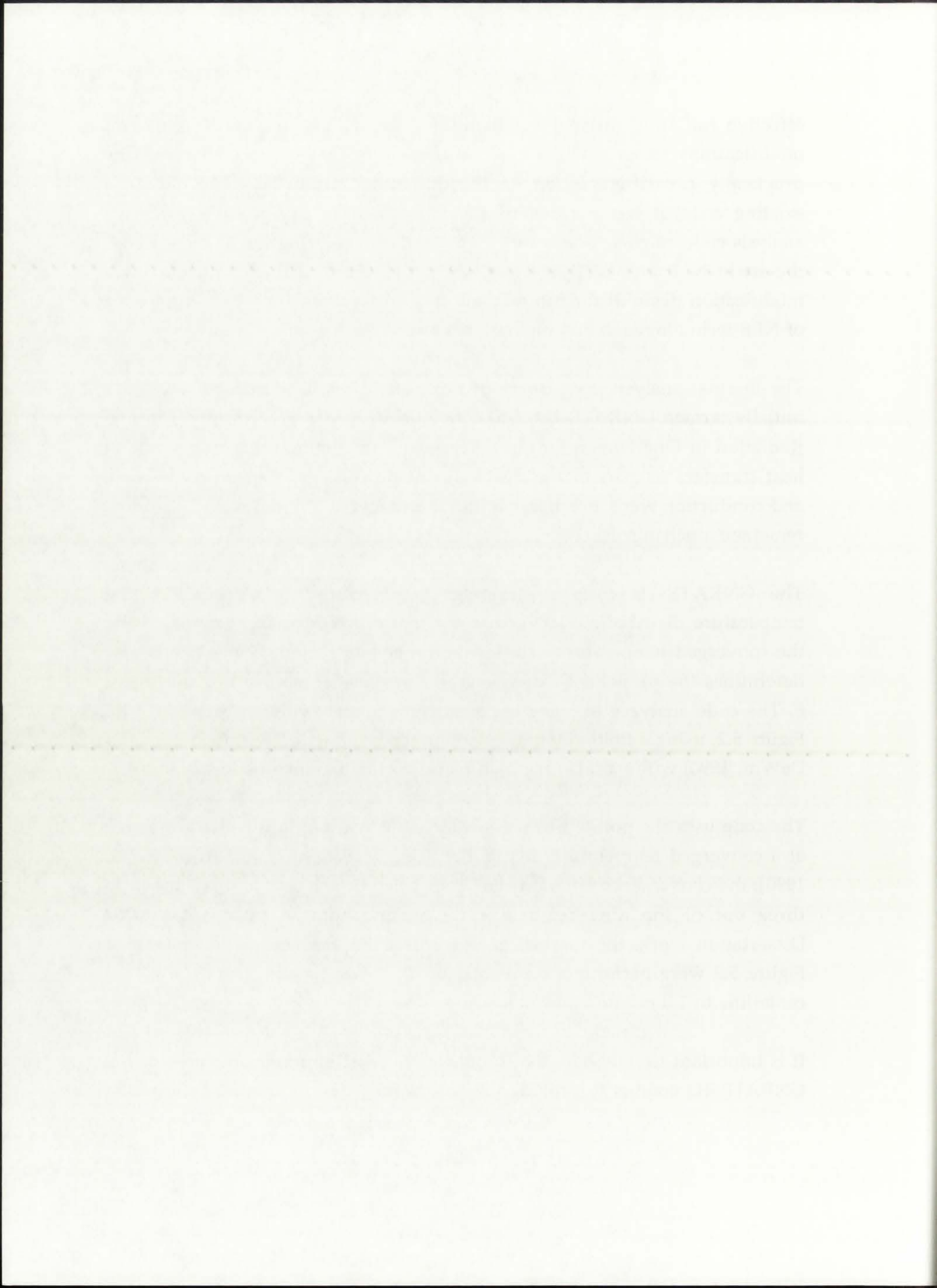
effective radiative thermal conductivity) would have required significant modifications to an existing code to the extent that it would have to be practically re-written. Based on the difficulties predicted in utilizing an existing code, it was decided to develop a dedicated NLB engine thermal analysis code. Such a code would be a significant contribution to the state-of-the-art in NLB and GCR analyses, and would be available (with whatever modification desired) for future analysis and development work in the area of NLB technology (should interest ever re-emerge for such a technology).

The thermal analysis code developed as part of this Dissertation work was initially termed GNRATR-1D (Gas core Nuclear Rocket Analysis by Thermal Radiation in One Dimension) in deference to the main anticipated mode of heat transfer. As part of the development process, generation, convection, and conduction were incorporated into the code; the original name, however, remained unchanged.

The GNRATR-1D code is designed to calculate the *uncooled* radial temperature distribution $T(r)$ across the unit-cell NLB rocket engine. Using the converged temperature data for the propellant region, GNRATR-1D also determines the propellant exit velocity v_{exit} , specific impulse I_{sp} , and thrust F . The code analyzes the nine regions of the engine as shown previously in Figure 5.2, using a finite-difference solving scheme [Riggs, 1988; Incropera and DeWitt, 1990] with variable region dimensions and variable node spacings.

The code uses the pointwise Gauss-Seidel iterative solution method to arrive at a converged temperature distribution [Riggs, 1988; Incropera and DeWitt, 1990]; the convergence criterion can be specified by the user and is applied to three out of the nine regions of the model. For the purposes of this Dissertation work, the thermal analyses used for the nine-region model of Figure 5.2 were performed for a total of 37 nodes, ranging from the model centerline to 1.0 m into ambient space.

It is important to note here that probably the most important purpose of the GNRATR-1D code is to provide the temperature distribution $T(r)$ under the



assumption of *no cooling of the solid regions*. In such a case, the $T(r)$ represents a worst-case scenario and is generally considered to be the most complex part of rocket engine thermal analysis. Once the uncooled $T(r)$ within a region is known, then it can be correlated to the maximum allowable temperature for that region (generally the melting temperature) to obtain the ΔT needed for the engine to function. With a known ΔT , it is a straight-forward matter to determine the necessary coolant flow rate for either internal, film, or regenerative cooling of the solid regions.

The original UARL designers did not investigate the unit-cell NLB concept to the extent of providing a detailed analysis of the cooling schemes for the two solid regions: silica wall and moderator/reflector. Thus, the final decision on the most appropriate cooling mechanism for these regions will be left open; should the unit-cell NLB engine ever be analyzed for a potential mission, the results of this Dissertation work will provide the answers to the *uncooled* temperature distribution. In order to complete the thermalhydraulics analysis of the NLB engine, though, two methods of cooling are suggested and analyzed in some detail in this Dissertation: (1) internal cooling for the silica wall, and (2) film cooling for the moderator/reflector regions. Both methods are suggested in response to the obtained uncooled $T(r)$, and are intended only to reduce the region temperature to below melting. At this point in time, the precise methods of maintaining the moderator/reflector region at 100 K are not well understood; although the region will be assumed to be at 100 K for the purposes of the neutronics analysis, maintaining of such a low temperature is still questionable.

GNRATR-1D is written in FORTRAN 77 and compiled on an Apple Macintosh computer using Macintosh Programmers Workshop and Language Systems Fortran [Language Systems, 1992]. Execution time for a convergence criterion of 0.001 K and 2,300 iterations is approximately 5 minutes on a Macintosh Quadra 700 computer. The GNRATR-1D code is not limited by the number of iterations; a specific value can be pre-set by the user, or the code can be instructed to march out in iterations until the required convergence criterion is satisfied.

assumption of an empty cylinder in such a case. The
assumes a constant velocity and is usually assumed to be the
computer program which calculates the velocity. One of the
with a region of flow, that it can be compared to the
allowable temperature for that region (given by the cooling
which is the case for the case of a cylinder with a mean
straightforward matter to determine the necessary coolant flow rate for
either lateral flow or regenerative cooling of the solid region.

The original U.S. design did not investigate the only NLD concept in
the case of providing a detailed analysis of the cooling scheme for the
solid region, since wall and moderator/reflector. Thus, the final design on
the most appropriate cooling mechanisms for these regions will be left open.
should the rod-cool NLD engine ever be analyzed for a potential solution, the
results of the Discussion will provide the answers to the questions
temperature distribution. In order to complete the thermohydraulic analysis
of the NLD engine, though, two methods of cooling are suggested and
analyzed in some detail in this Discussion: (1) internal cooling for the
wall and (2) film cooling for the moderator/reflector regions. Both methods
are suggested in response to the obtained results (1) and are intended
only to reduce the region temperature to below melting. At this point in time,
the precise methods of maintaining the moderator/reflector region at 300 K
are not well understood, although the region will be assumed to be at 300 K
for the purpose of the thermohydraulic analysis. Maintaining of such a low
temperature is still questionable.

CONTRACT 10 is written in FORTRAN 77 and compiled on an IBM
Mainframe computer using Martin's Fortran 77 Preprocessor. No special
Language System Fortran Language System (1977) execution time for a
convergence criterion of 0.001 K and 1000 iterations is approximately 5
minutes on a Multihouse Quadra 700 computer. The CONTRACT 10 code is not
limited by the number of iterations; a specific value can be given by the user
of the code can be instructed to mesh out in iterations until the required
convergence criterion is satisfied.

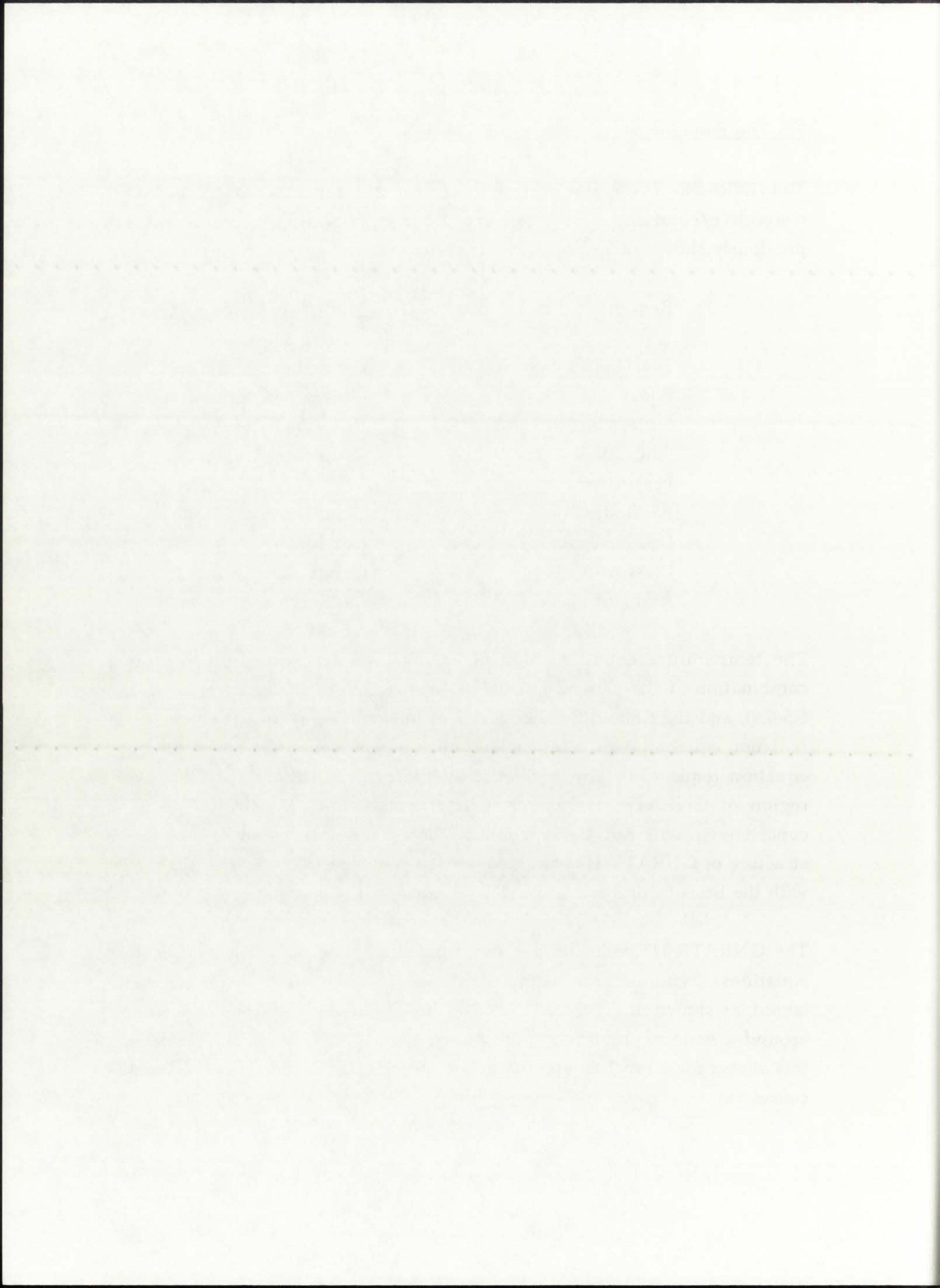
9.3. The Equation Structure of GNRATR-1D

The GNRATR-1D thermal analysis code analyzes directly coupled radiative/convective/conductive modes of heat transfer, according to the breakdown previously shown in Section 6.4 and reproduced below:

<u>Region</u>	<u>Mode(s) of heat transfer</u>
Fuel/Buffer Gas Mixture	Generation, Radiation
Fuel	Generation, Radiation
Buffer Gas	Radiation, Convection
Silica Wall	Radiation, Conduction
Propellant	Radiation, Convection
Be Moderator	Conduction
D ₂ O Reflector	Conduction
Pressure Vessel	Conduction
Ambient Space	Radiation

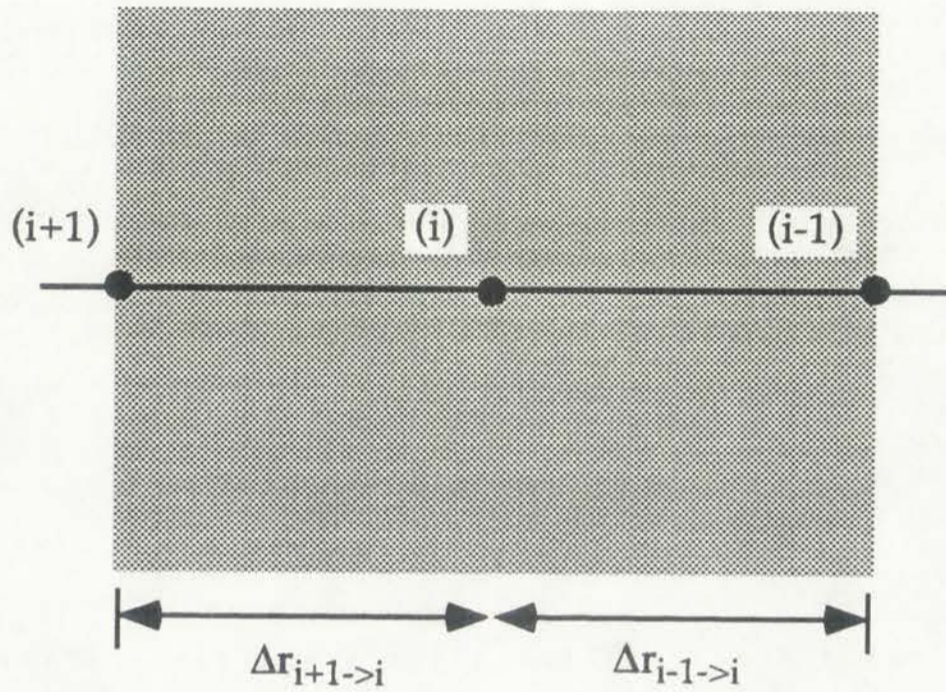
The temperature equations that GNRATR-1D solves are derived from a combination of the general energy balance equations for each region (eqns. 6.5-6.9), and the finite-difference forms of the generation equation (eqn. 6.12), radiation equation (eqn. 6.18), convection equation (eqn. 6.25), and conduction equation (eqn. 6.32). The derivation of the exact equations used for every region of GNRATR-1D is a very long process and, for the purposes of conciseness, will not be reproduced here. A summary of the equation structure of GNRATR-1D will, however, be provided to familiarize the reader with the basis behind the GNRATR-1D-calculated temperatures.

The GNRATR-1D code utilizes two fundamental forms of energy balance equations: "within-region" and "interface." The two differ in the geometry layout, as shown in Figure 9.1. For a within-region equation, the unit-volume around a node is uniform in both directions, i.e., $\Delta r_{i+1 \rightarrow i}$ is equal to $\Delta r_{i \rightarrow i-1}$; this allows for a much simpler equation structure at that node, since the Δr 's cancel out.



"Within-region" Condition

$$\Delta r_{i+1 \rightarrow i} = \Delta r_{i-1 \rightarrow i}$$



"Interface" Condition

$$\Delta r_{i+1 \rightarrow i} \neq \Delta r_{i-1 \rightarrow i}$$

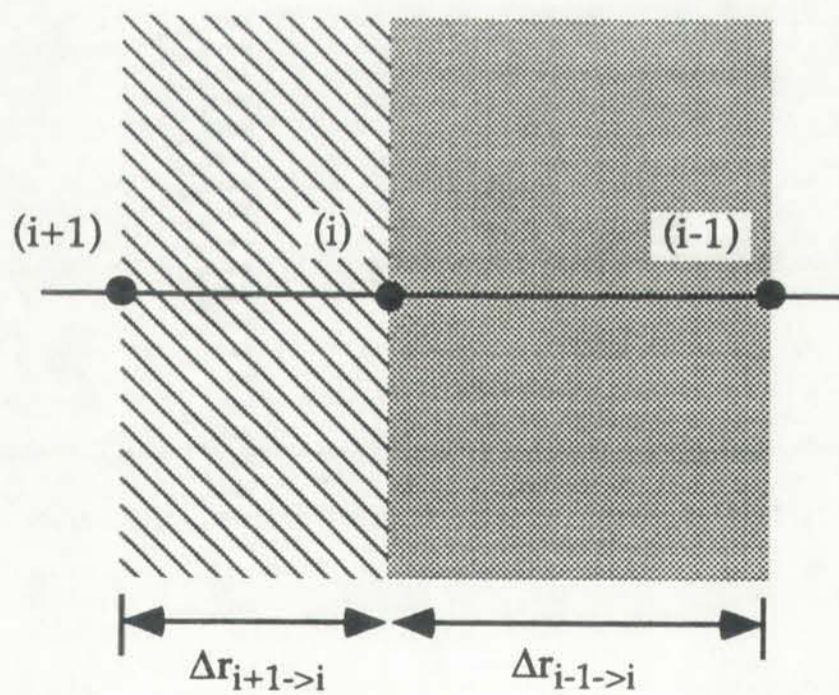
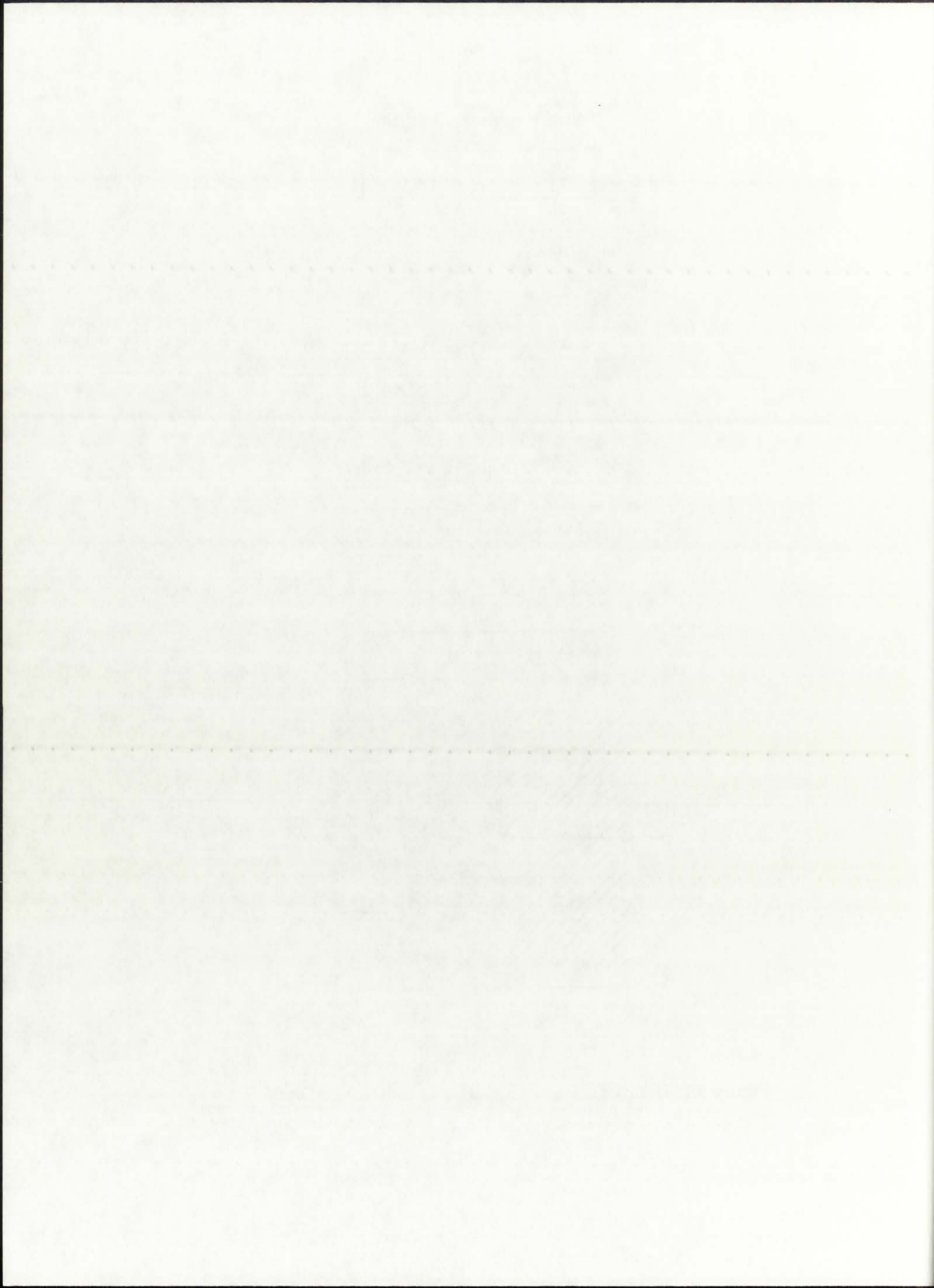


Figure 9.1: The two different layouts of a unit-volume about a node.



For an interface equation, however, it is necessary to include both Δr 's since they can be very different. An interface equation, thus, tends to be longer and more complicated. Within-region equations for the five heat transfer mode combinations are given in the following five Sections. An example of one interface equation is given in Section 9.3.6.

9.3.1. Within-Region, Generation/Radiation Equations

The coupled generation/radiation equations are used for the Fuel/Buffer Gas Mixture and the Fuel regions. The governing energy balance equation for these two regions is eqn. (6.5):

$$Q_g + Q_{rad} = 0 \quad , \quad (9.1)$$

which, in finite-difference form, is written as the rate of heat transfer from the (i+1) and the (i-1) nodes to the (i) node:

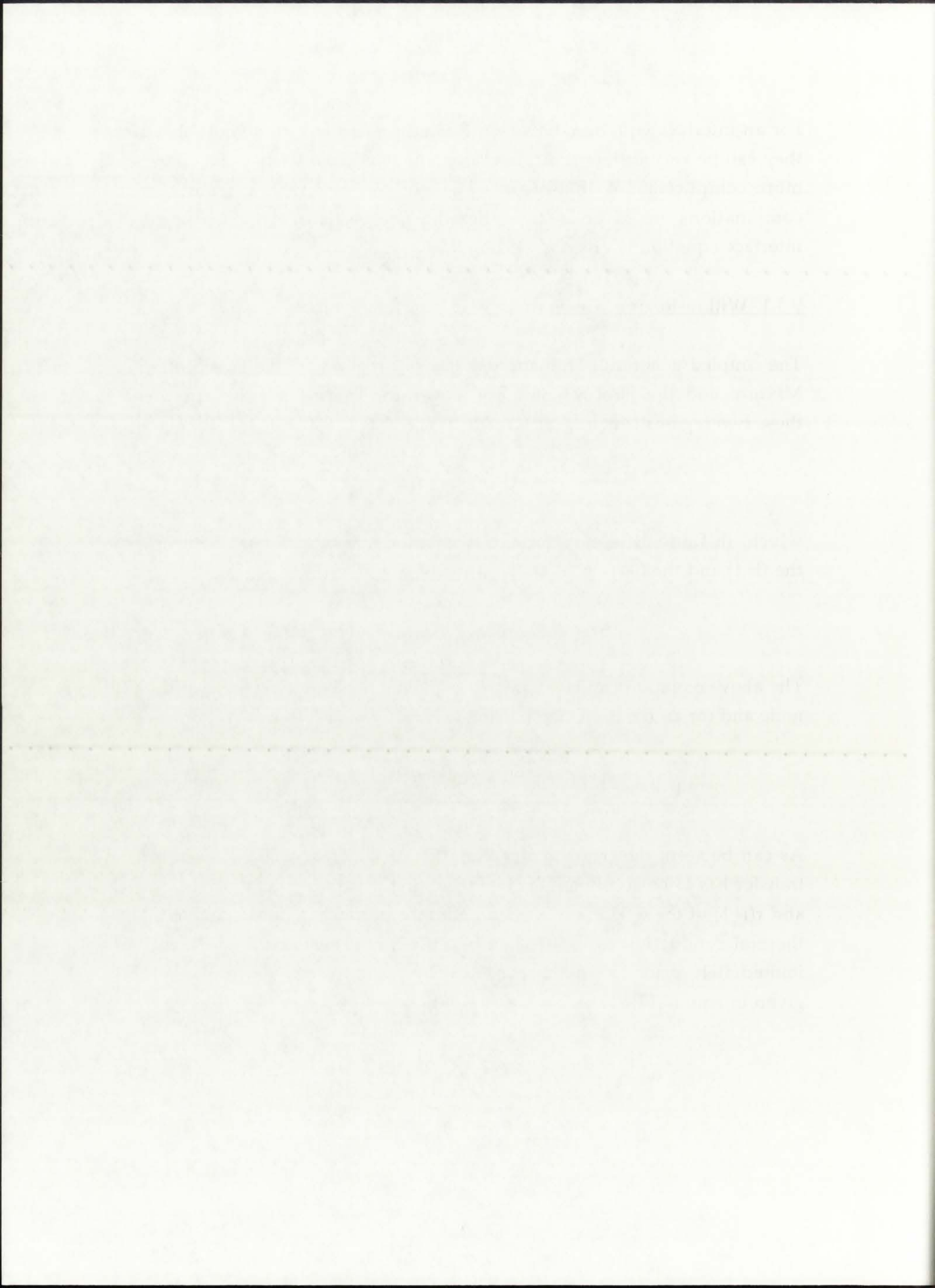
$$Q_g(i) + Q_{rad,(i-1 \rightarrow i)} + Q_{rad,(i+1 \rightarrow i)} = 0 \quad . \quad (9.2)$$

The above equation can be expressed explicitly for the temperature at the (i)th node and for an iteration step t, using eqns. (6.12) and (6.18):

$$T(i,t) = \frac{k_{rad(i-1)}r(i-1)T(i-1,t) + k_{rad(i+1)}r(i+1)T(i+1,t-1) + Q_g(i)r(i)\Delta r^2}{k_{rad(i-1)}r(i-1) + k_{rad(i+1)}r(i+1)} \quad . \quad (9.3)$$

As can be seen, the (r) geometry variation of the cross-sectional area to heat transfer has to be accounted for by including the varying radial distances $r(i-1)$ and $r(i+1)$ of the (i-1)th and (i+1)th nodes, respectively. The effective radiative thermal conductivities $k_{rad(i-1)}$ and $k_{rad(i+1)}$ are calculated by GNRATR-1D immediately prior to solving eqn. (9.3) by using the relationship previously given in eqn. (6.17). Thus, for the (i-1)th node:

$$k_{rad(i-1)} = \frac{16\sigma T^3(i-1,t)}{3a_R(T(i-1,t))} \quad , \quad (9.4)$$



and for the (i+1)th node, because of the marching-out iteration method, the (t-1)th iteration is used:

$$k_{\text{rad}(i+1)} = \frac{16\sigma T^3(i+1,t-1)}{3a_R(T(i+1,t-1))} \quad (9.5)$$

The baseline temperature-dependent Rosseland Mean Opacity a_R is calculated by a subroutine function, called prior to solving for eqn. (9.3). The structure of the GNRATR-1D code, including the various subroutines, is discussed in Section 9.4.

9.3.2. Within-Region, Radiation/Convection Equations

The coupled radiation/convection equations are used for the Buffer Gas and the Propellant regions. The governing energy balance equation for these two regions is eqn. (6.6):

$$Q_{\text{rad}} + Q_{\text{conv}} = 0 \quad , \quad (9.6)$$

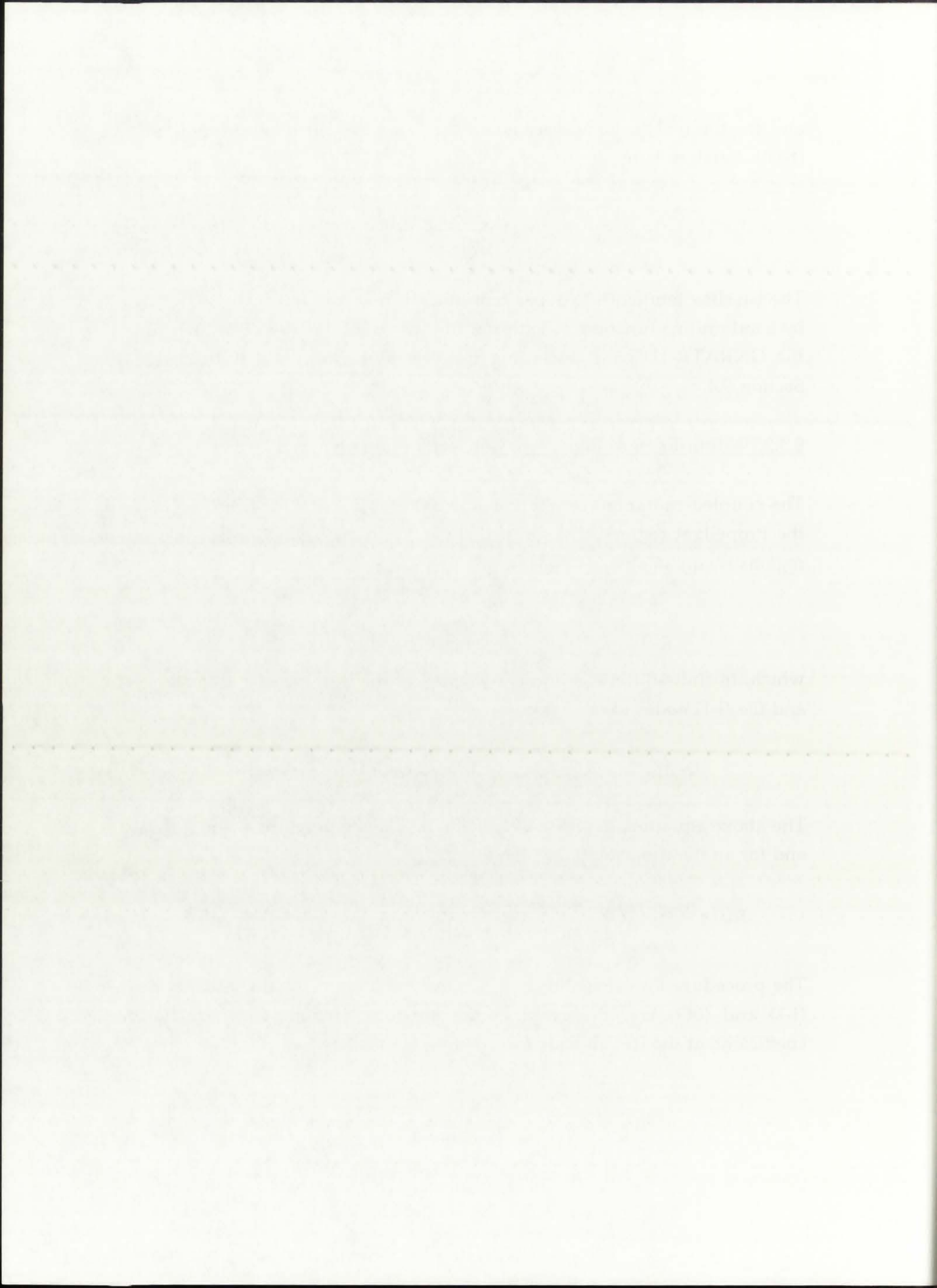
which, in finite-difference form, is written as the heat transfer from the (i+1) and the (i-1) nodes to the (i) node:

$$Q_{\text{rad,(i-1) \rightarrow i}} + Q_{\text{conv,(i-1) \rightarrow i}} + Q_{\text{rad,(i+1) \rightarrow i}} + Q_{\text{conv,(i+1) \rightarrow i}} = 0 \quad (9.7)$$

The above equation, expressed explicitly for the temperature at the (i)th node and for an iteration step t , has the form:

$$T(i,t) = \frac{[k_{\text{rad}(i-1)}r(i-1)+h(i-1)r(i-1)\Delta r]T(i-1,t)+[k_{\text{rad}(i+1)}r(i+1)+h(i+1)r(i+1)\Delta r]T(i+1,t-1)}{[k_{\text{rad}(i-1)}r(i-1)+h(i-1)r(i-1)\Delta r]+[k_{\text{rad}(i+1)}r(i+1)+h(i+1)r(i+1)\Delta r]} \quad (9.8)$$

The procedure for calculating the effective radiative thermal conductivities at (i-1) and (i+1) was discussed in the previous Section. The heat transfer coefficient, at the (i+1)th node for example, is calculated as:



$$h(i+1) = \frac{[\text{Nu}(T(i+1,t-1))]k(T(i+1,t-1))}{D_h} , \quad (9.9)$$

where the Nusselt number is calculated as:

$$[\text{Nu}](T(i+1,t-1)) = 0.023[\text{Re}]^{4/5}(T(i+1,t-1))[\text{Pr}]^{0.4}(T(i+1,t-1)) . \quad (9.10)$$

In the above equation, [Re] and [Pr] denote the Reynolds and Prandtl numbers, respectively. As mentioned before, all the temperature-dependent properties, such as a_R , k , [Re], and [Pr], are calculated by subroutine functions, called prior to solving for eqn. (9.8).

9.3.3. Within-Region, Radiation/Conduction Equation

The coupled radiation/conduction equation is used for the Silica Wall region. The governing energy balance equation for this region is eqn. (6.7):

$$Q_{\text{rad}} + Q_{\text{cond}} = 0 , \quad (9.11)$$

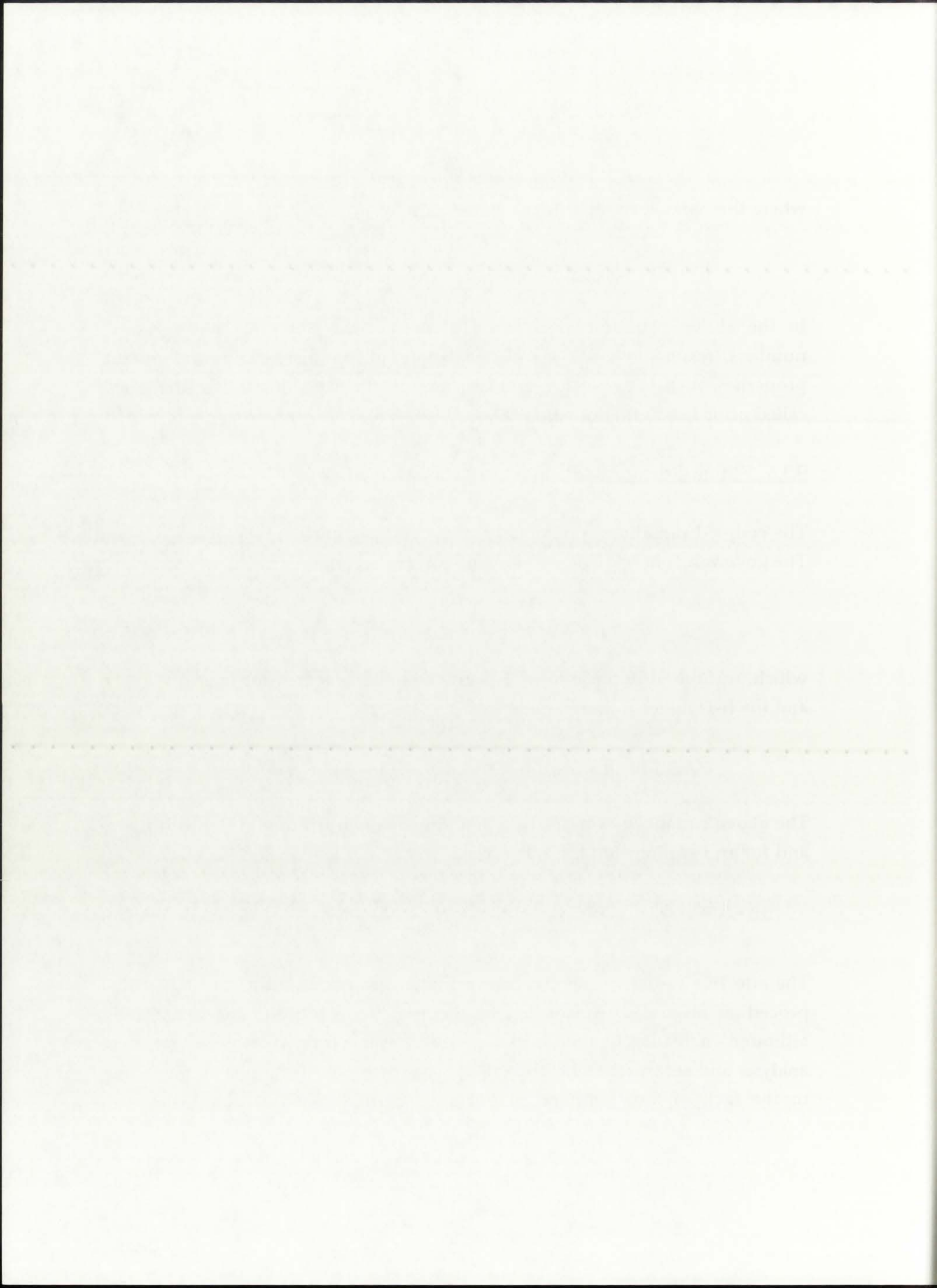
which, in finite-difference form, is written as the heat transfer from the (i+1) and the (i-1) nodes to the (i) node:

$$Q_{\text{rad,(i-1)} \rightarrow \text{i}} + Q_{\text{cond,(i-1)} \rightarrow \text{i}} + Q_{\text{rad,(i+1)} \rightarrow \text{i}} + Q_{\text{cond,(i+1)} \rightarrow \text{i}} = 0 . \quad (9.12)$$

The above equation, expressed explicitly for the temperature at the (i)th node and for an iteration step t , has the form:

$$T(i,t) = \frac{[k_{\text{rad}}(i-1)r(i-1) + k_{\text{cond}}(i-1)r(i-1)]T(i-1,t) + [k_{\text{rad}}(i+1)r(i+1) + k_{\text{cond}}(i+1)r(i+1)]T(i+1,t-1)}{[k_{\text{rad}}(i-1)r(i-1) + k_{\text{cond}}(i-1)r(i-1)] + [k_{\text{rad}}(i+1)r(i+1) + k_{\text{cond}}(i+1)r(i+1)]} . \quad (9.13)$$

The effective radiative thermal conductivities are calculated according to the procedure discussed previously; the thermal conductivity of the silica wall, although in reality temperature-dependent, was assumed constant for this analysis and set equal to 4.00 [W/m-K]. The reason for using this value is due to the lack of any temperature-dependent properties (including thermal



conductivity) above approximately 1,500 K; 4.00 [W/m-K] is the last tabulated value. Since silica has a melting temperature of 1,883 K [CRC, 1990; Incropera and DeWitt, 1990; Ultramet, 1992] and a boiling temperature of 2,863 K [CRC, 1990], all published silica applications focus on temperature ranges from room temperature to about 1,500 K.

9.3.4. Within-Region, Conduction Equations

The conduction equation is used for the Be Moderator, D₂O Reflector, and Pressure Vessel regions. The governing energy balance equation for these regions is eqn. (6.8):

$$Q_{\text{cond}} = 0 \quad , \quad (9.14)$$

which, in finite-difference form, is written as the heat transfer from the (i+1) and the (i-1) nodes to the (i) node:

$$Q_{\text{cond},(i-1) \rightarrow i} + Q_{\text{cond},(i+1) \rightarrow i} = 0 \quad . \quad (9.15)$$

The above equation, expressed explicitly for the temperature at the (i)th node and for an iteration step t, has the form:

$$T_{(i,t)} = \frac{k_{\text{cond}(i-1)}r(i-1)T_{(i-1,t)} + k_{\text{cond}(i+1)}r(i+1)T_{(i+1,t-1)}}{k_{\text{cond}(i-1)}r(i-1) + k_{\text{cond}(i+1)}r(i+1)} \quad . \quad (9.16)$$

The thermal conductivities of the three solid regions, although in reality almost certainly temperature-dependent, was assumed constant for this analysis and set equal to 78.7, 0.37, and 34.0 [W/m-K] for Be, D₂O, and steel, respectively. The reasoning behind such an approach has been explained in the previous Section: the last tabulated value of thermal conductivity for the above materials is available for a temperature of 1,500 K [CRC, 1990; Incropera and DeWitt, 1990]. Rather than extrapolating to significantly higher temperatures and trying to predict the temperature-dependent physical

conductivity above approximately 1500 K (W/m-K) is the last tabulated value. Since steel has a melting temperature of 1810 K (CRC, 1990; Ingersoll and Dewitt, 1997; Dittmer, 1982) and a boiling temperature of 2853 K (CRC, 1990), all published data applications falls on temperature ranges from room temperature to about 1500 K.

3.1. Finite-Difference Conduction Equations

The conduction equation is used for the Be Modexon, D90 Reactor and Pressure Vessel regions. The governing energy balance equation is then written in the form

$$\rho c_p \frac{dT}{dt} = \nabla \cdot (k \nabla T) + \dot{q} \quad (3.1)$$

which in finite-difference form is written as the last term in Eq. (3.1) and the ρc_p term is the product of the mass and specific heat of the material.

$$\rho c_p \frac{dT}{dt} = \nabla \cdot (k \nabla T) + \dot{q} \quad (3.2)$$

The above equation, expressed explicitly for the temperature at the (i,j) node and for an iteration step n , has the form

$$\rho c_p \frac{dT_{i,j}^{n+1}}{dt} = \nabla \cdot (k \nabla T) + \dot{q} \quad (3.3)$$

The thermal conductivities of the three solid regions, although in reality almost certainly temperature-dependent, were assumed constant for this analysis and set equal to 76.3, 82.7, and 51.0 (W/m-K) for the D90, and steel, respectively. The reasoning behind such an approach has been explained in the previous section: the last tabulated value of thermal conductivity for the above materials is available for a temperature of 1500 K (CRC, 1990; Ingersoll and Dewitt, 1990). Rather than extrapolating to significantly higher temperatures and trying to predict the temperature-dependent physical

properties of molten and vaporized materials, it was decided to use the highest-temperature tabulated (i.e., defensible and reproducible) values.

9.3.5. Within-Region, Radiation Equation

The radiation equation is used for the Ambient Space region. The governing energy balance equation for this region is eqn. (6.9):

$$Q_{\text{rad}} = 0 \quad , \quad (9.17)$$

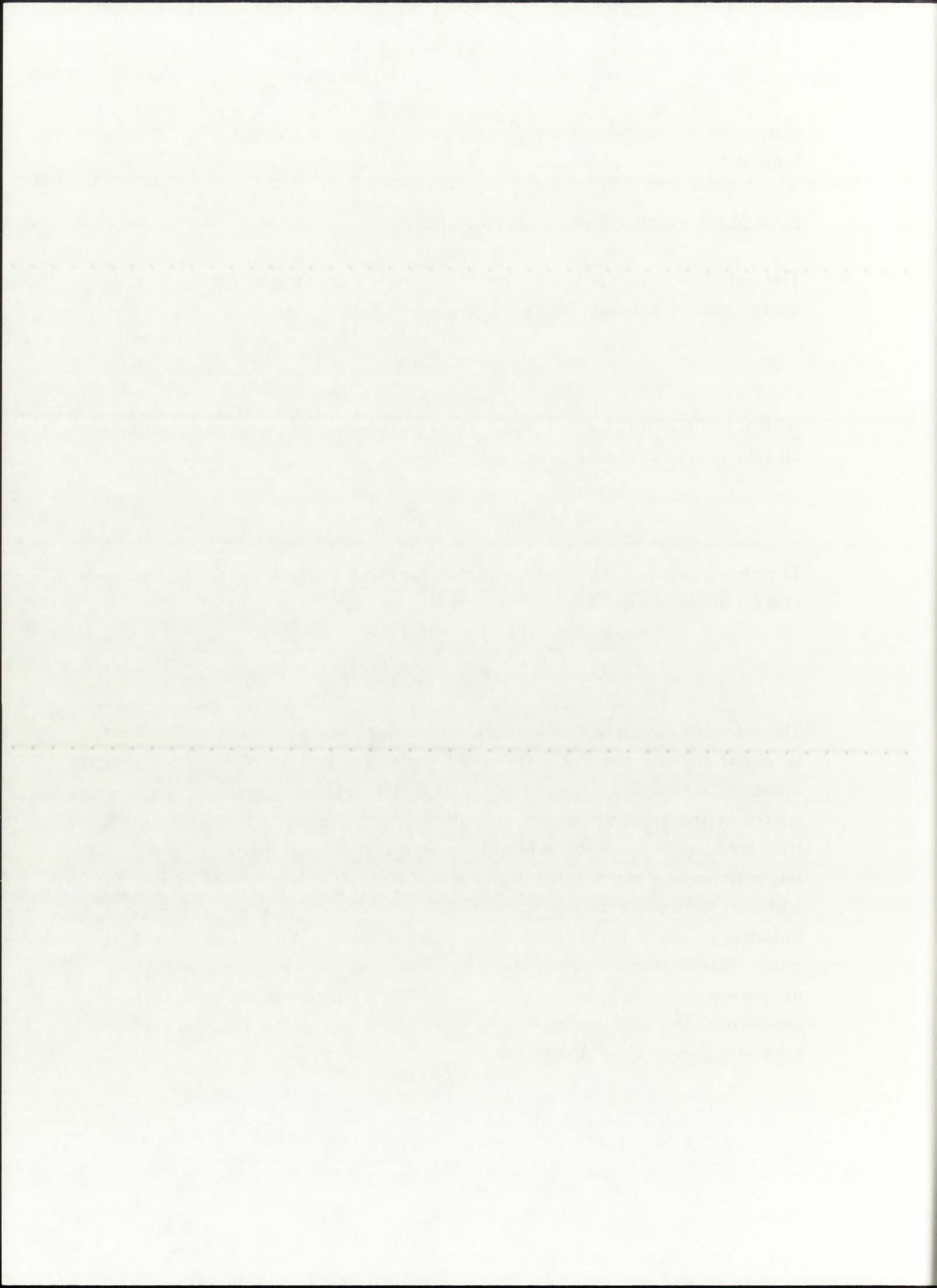
which, in finite-difference form, is written as the heat transfer from the (i+1) and the (i-1) nodes to the (i) node:

$$Q_{\text{rad},(i-1) \rightarrow i} + Q_{\text{rad},(i+1) \rightarrow i} = 0 \quad . \quad (9.18)$$

The above equation, expressed explicitly for the temperature at the (i)th node and for an iteration step t, has the form:

$$T(i,t) = \frac{k_{\text{rad}}(i-1)r(i-1)T(i-1,t) + k_{\text{rad}}(i+1)r(i+1)T(i+1,t-1)}{k_{\text{rad}}(i-1)r(i-1) + k_{\text{rad}}(i+1)r(i+1)} \quad . \quad (9.19)$$

The effective radiative thermal conductivity for ambient space was assumed to equal that of air: 0.022 [W/m-K] [Incropera and DeWitt, 1990]. This assumption was made due to the lack of detailed physical properties of space; space, in the capacity of a heat sink, is a compendium of radiation heat transfer targets (planets, asteroids, and space debris) and it is therefore impossible to determine a uniform radiative conductivity of space. In addition, the spacecraft mission profile would also determine the actual radiative conductivity of space -depending on whether it is a Lunar, Mars, or outer Solar System mission. For all these reasons, the radiative conductivity of space was assumed to equal that of air. Since both are relatively poor heat conductors, this assumption is not a significant influence on the calculated (r) geometry temperature distribution.



9.3.6. Interface Conduction Equation

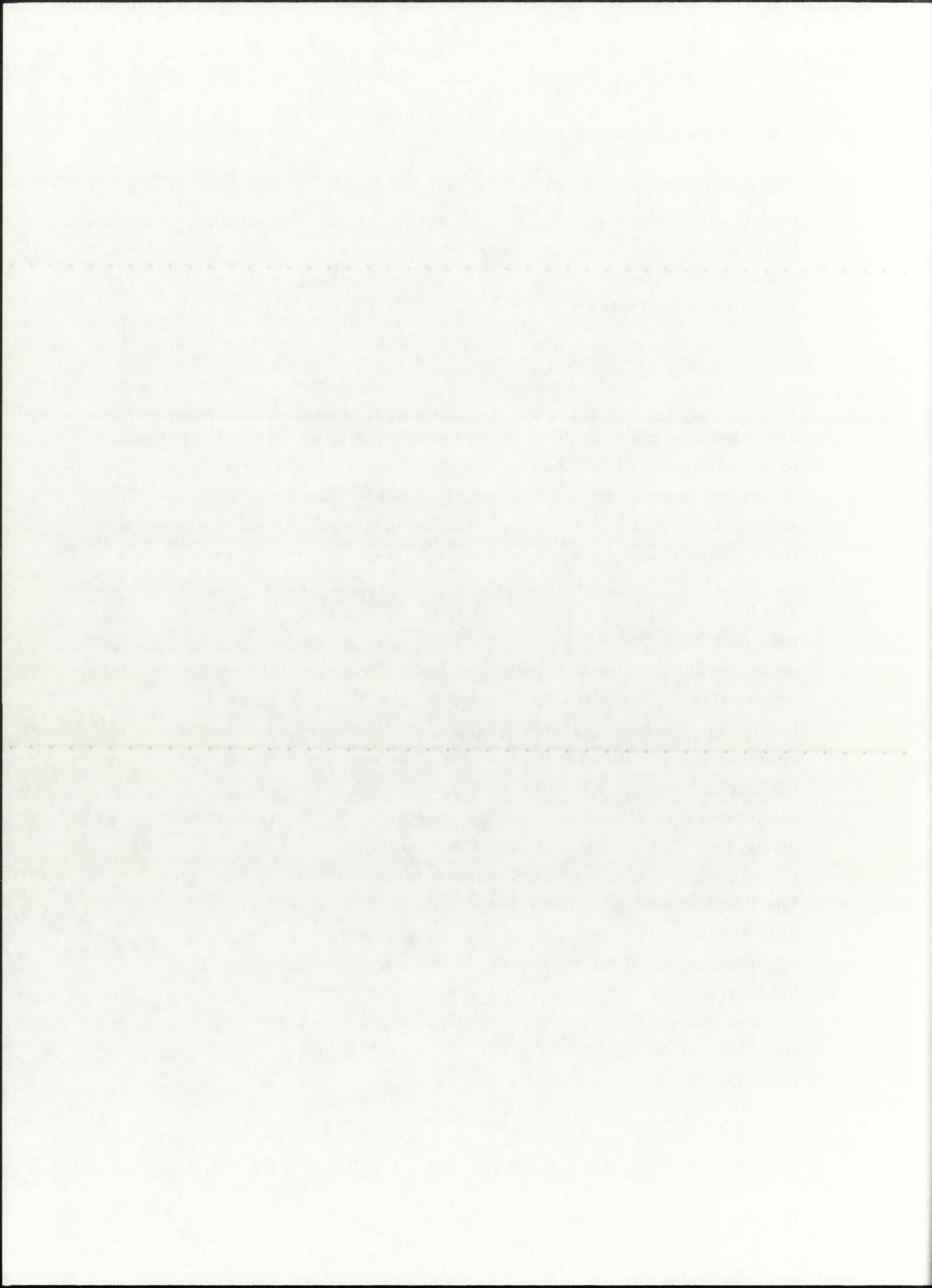
The interface equations are essentially generalized versions of the within-region equations, where the Δr 's of the adjacent nodes are different and therefore do not cancel out. Using as an example the conduction regions, discussed in Section 9.3.4, the Be/D₂O interface node (i) temperature equation would have the form:

$$T_{(i,t)} = \frac{\Delta r_{D_2O} k_{cond(i-1)} r_{(i-1)} T_{(i-1,t)} + \Delta r_{Be} k_{cond(i+1)} r_{(i+1)} T_{(i+1,t-1)}}{\Delta r_{D_2O} k_{cond(i-1)} r_{(i-1)} + \Delta r_{Be} k_{cond(i+1)} r_{(i+1)}} \quad (9.20)$$

The interface equations, therefore, include the two different Δr 's for the nodes to the left and to the right of the interface node (i). This simple modification, of course, is valid only for an interface where both adjacent regions are subjected to the same mode(s) of heat transfer, as is the case for the solid and fuel-containing regions.

The interface equations for the Fuel/Buffer Gas, the Buffer Gas/Silica Wall, the Silica Wall/Propellant, and the Propellant/Be Moderator interfaces are more complicated due to the different modes of heat transfer in the adjacent regions. These equations will not be given here for the purposes of clarity and brevity; an interested reader is invited to derive the appropriate equations by applying energy balances to each interface and, following the procedure outlined in Sections 9.3.1-9.3.6, arrive at an explicit temperature expression. The derived equations can also be accessed from the GNRATR-1D code listing, provided as Appendix A to this Dissertation document.

The interface equation at the Propellant/Be Moderator interface is slightly different from the others, due to the incorporation of a transmission fraction which accounts for the balance of the radiative heat flux incident on the Be Moderator which does not get reflected off the reflective liner. This transmission fraction ($trans_{Be}$) is user-specified and corrects for the radiative contribution to the total heat flow into the moderator region. The Propellant/Be Moderator interface equation has the form:



$$T(i,t) = \frac{\Delta r p k_{\text{cond}}(i-1)r(i-1)T(i-1,t) + [\text{transBe}\Delta r_{\text{Be}} k_{\text{rad}}(i+1)r(i+1) + \Delta r_{\text{P}}\Delta r_{\text{Be}}h(i+1)r(i+1)]T(i+1,t-1)}{\Delta r p k_{\text{cond}}(i-1)r(i-1) + [\text{transBe}\Delta r_{\text{Be}} k_{\text{rad}}(i+1)r(i+1) + \Delta r_{\text{P}}\Delta r_{\text{Be}}h(i+1)r(i+1)]}, \quad (9.21)$$

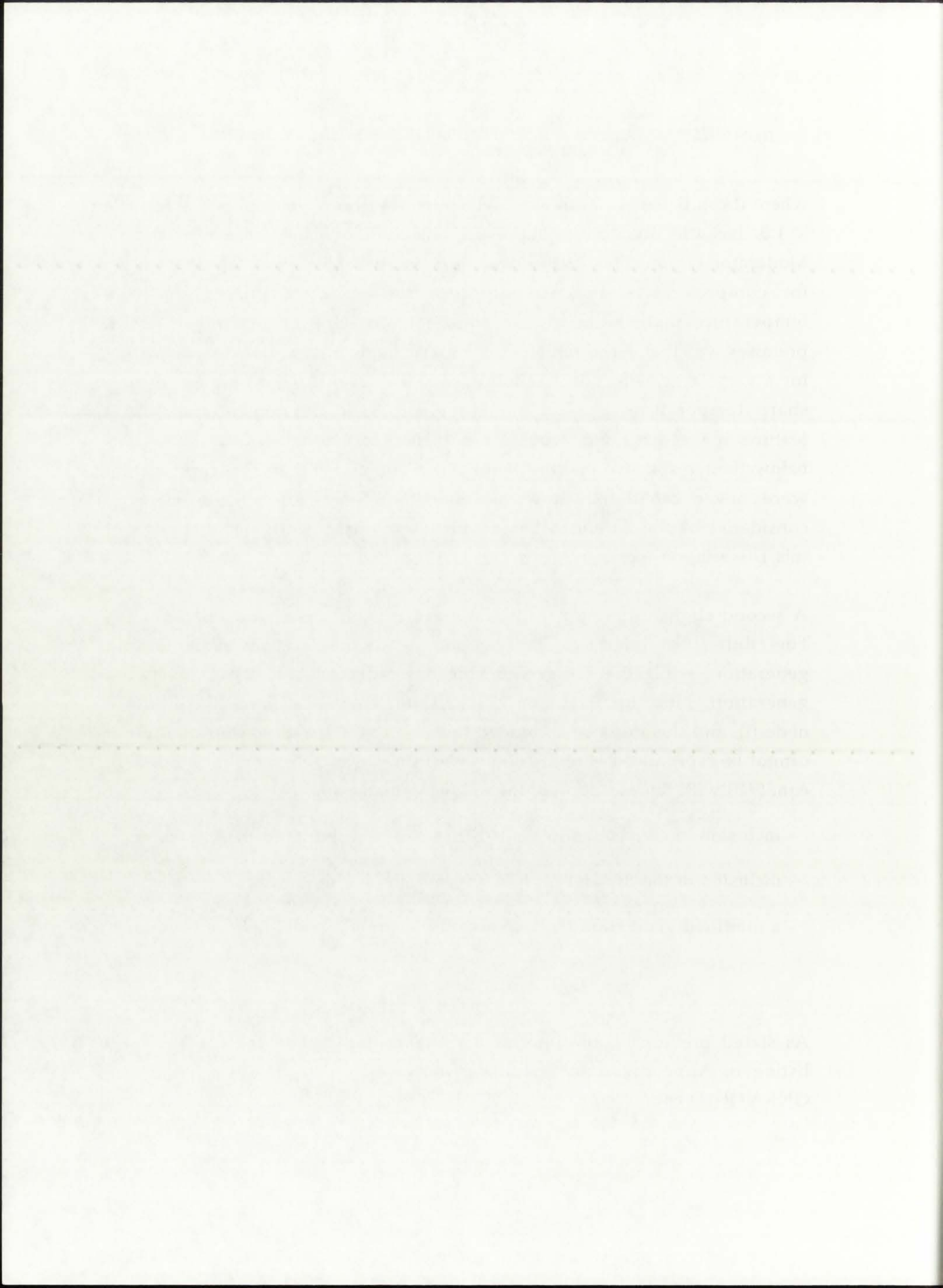
where it can be seen that transBe , which the user can specify to be $0 \leq \text{transBe} \leq 1.0$, has the function of suppressing the radiative heat flux into the Be Moderator region. This feature was incorporated into GNRATR-1D to allow for comprehensive analysis into how the reflective liner affects the temperature distribution in the solid regions. One of the major UARL premises was that, since radiation is a major mode of heat transfer, providing for a very large reflection fraction (i.e., 0.90 or even 0.99) would result in a sharp temperature drop at the Propellant/Be-Moderator interface. This feature, it was assumed, would be sufficient to maintain the solid regions below their respective melting points. The actual results of this combination were never calculated, however, and therefore such a calculation is considered by the author to be part of the original scientific contribution of this Dissertation work.

A second slight difference in the interface equations is characteristic of the Fuel/Buffer Gas interface. The Fuel side of the interface has radiation and generation, while the Buffer Gas side has radiation and convection. Fuel generation, thus, occurs in only a half-unit-volume around the interface node (i), and this must be accounted for. Due to the length of the equation, it cannot be reproduced here; it is, however, similar to the generation/radiation eqn. (9.3) with the exception of the following features:

- inclusion of convection in the (i-1)th node contribution to heat transfer,
- inclusion of the Δr_{F} and Δr_{BG} as appropriate into the heat transfer terms,
- a modified generation term, to account for only a nodal half-unit-volume:

$$Q_{\text{g}}'''(i)2\pi r(i)\Delta r_{\text{F}}\Delta r_{\text{BG}}\left(\frac{\Delta r_{\text{F}} + \Delta r_{\text{BG}}}{2}\right)$$

As stated previously, the interested reader is directed to the GNRATR-1D listing in Appendix A for a full version of all the equations used in the GNRATR-1D code.



9.4. The Structure of GNRATR-1D

The GNRATR-1D thermal analysis code consists of a MAIN program and six ancillary subroutines: RMO, HTCP, HTCBG, ROCKET, HYDROGEN, and TRANSMIT. The structure of the code, as well as the data exchange between the modules, is illustrated in Figure 9.2.

The MAIN program solves all the explicit temperature equations, prints out the 37-node temperature distribution for every iteration (onto the screen and into a comprehensive iteration history output file), and determines how many test nodes have converged for every iteration; following convergence, it prints the summary converged temperature distribution and proceeds to calculate the rocket performance parameters based on the bulk propellant temperature.

Prior to solving for the temperature at a given node, MAIN calls an appropriate subroutine to determine the thermophysical properties at that node (i) and the adjacent nodes ($i-1$) and ($i+1$). Thus, to calculate the Rosseland Mean Opacity a_R , MAIN invokes subroutine RMO, which receives as input a node temperature: $T(i-1,t)$, $T(i,t-1)$, or $T(i+1,t-1)$, as applicable. Subroutine RMO matches the node temperature to a 16-temperature group a_R library (with a range of 3,500 - 110,000 K) and determines the corresponding a_R value for the propellant, silica wall, buffer gas, fuel, or fuel/buffer gas mixture. The respective temperature-dependent a_R is then returned to MAIN to use in the temperature calculation.

Subroutine HTCP is invoked to calculate the heat transfer coefficient for the propellant. It is provided a node temperature and pre-set propellant axial velocity and hydraulic diameter. It then determines the heat transfer coefficient by matching the node temperature to a 16-temperature group mass density, $[\mu]$, viscosity, and hydrogen thermal conductivity library (with an effective range of 3,000 - 30,000 K). The respective propellant heat transfer coefficient is then returned to MAIN to use in the temperature calculation.

The *TEMPERATURE* program is a FORTRAN program which
calculates the temperature distribution in a rocket motor
and the thrust. The structure of the code as well as the data exchange between
the program and the user is shown in Figure 2.1.

The *TEMPERATURE* program solves all the explicit temperature equations first on
the 37 node temperature distribution for every iteration on the screen and
into a comprehensive report about output files and distances from
some and nodes have been computed for every iteration following convergence.
It prints the necessary computed temperature distribution and proceeds to
calculate the total performance parameters based on the bulk propellant
temperature.

After the user has entered the input data, the program calls
the *TEMPERATURE* program to solve for the temperature at a given node. *TEMPERATURE*
proceeds to determine the thermophysical properties at that
node *i* and the adjacent nodes *(i-1)* and *(i+1)*. Then, to calculate the
nodal mass flow rate, *TEMPERATURE* invokes routine *RMF*, which receives
as input a node temperature *T(i)*, *T(i-1)* or *T(i+1)* as applicable.
TEMPERATURE receives the node temperature to a 16-character group as
input with a range of 1.000E-10 to 1.0000E+10 and determines the corresponding
value for the propellant mass flow rate, gas fuel or fuel/oxidizer gas
mixture. The respective temperature-dependent is then returned to *TEMPERATURE*
to use in the temperature calculation.

Subroutine *HTCP* is invoked to calculate the heat transfer coefficient for the
propellant. It is provided a node temperature and gas or oxidant axial
velocity and hydraulic diameter. It then determines the heat transfer
coefficient by searching the node temperature to a 16-character group mass
density [g/cm³] velocity and hydraulic thermal conductivity data with an
effective range of 1.000E-10 to 1.0000E+10. The respective propellant heat transfer
coefficient is then returned to *TEMPERATURE* to use in the temperature calculation.

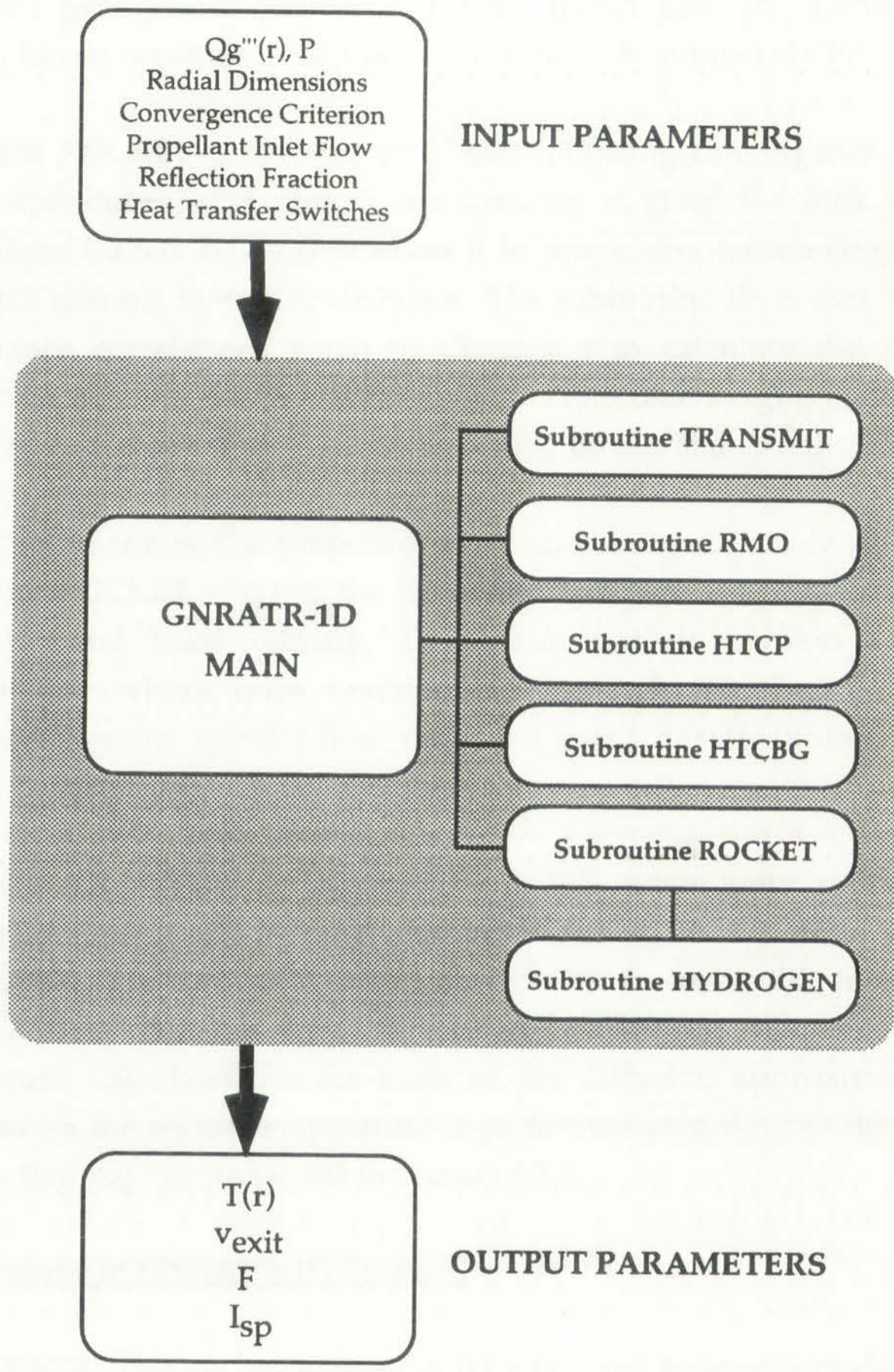
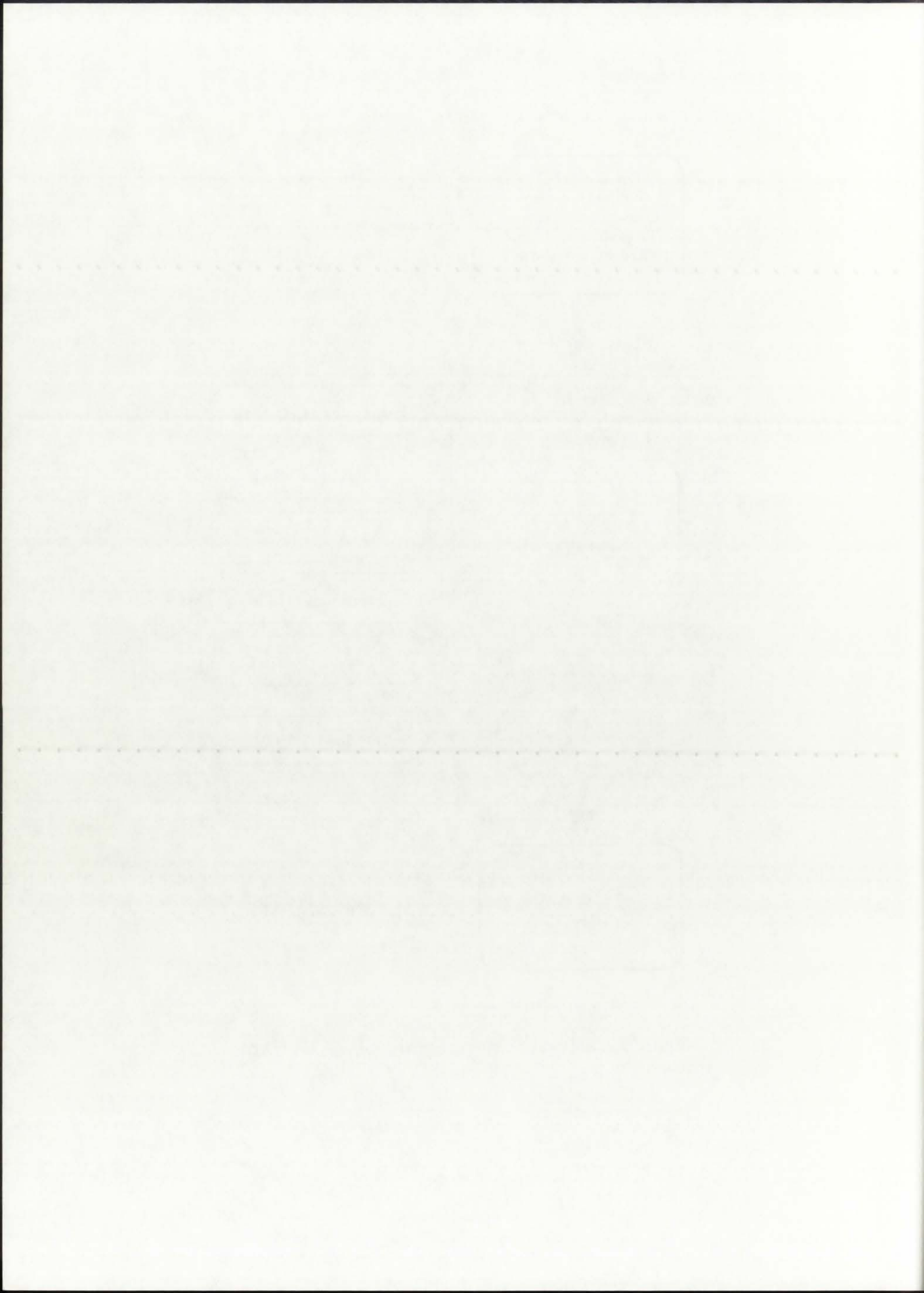


Figure 9.2: Software structure of the GNRATR-1D code.



Subroutine HTCGBG performs the same function as HTCP, except it provides MAIN the heat transfer coefficient for the buffer gas. Its thermophysical property library structure is identical to that for subroutine HTCP.

Subroutine ROCKET is invoked by MAIN following convergence of the 37-node temperature distribution. The subroutine is given the bulk propellant temperature (called T_{chamber} to relate it to propulsion terminology) and the propellant channel hydraulic diameter. The subroutine then uses the rocket performance correlations given in Chapter 8 to calculate the propellant dissociation fraction, the propellant average molecular weight, cross-sectional flow area, nozzle exit velocity, mass flow rate, thrust, and specific impulse.

In order to determine the propellant mass flow rate and nozzle exit velocity, subroutine ROCKET requires the temperature-dependent propellant specific heat ratio and mass density. To obtain that, it invokes subroutine HYDROGEN, whose only function is to match the T_{chamber} to a 16-temperature group specific heat ratio and mass density library (with an effective range of 3,000 - 30,000 K).

Subroutine TRANSMIT is invoked by MAIN when only radiative heat transfer is specified in any combination of the buffer gas/silica wall/propellant regions. TRANSMIT corrects for the transmission effects in a radiative heat transfer-only region by modifying the mean region temperature, calculated on the basis of the diffusion approximation. The correction on the region temperature is performed according to the theory of optically thin regions presented in Section 6.5.2.2.

9.5. Summary of GNRATR-1D Features

The GNRATR-1D code calculates the (r) geometry temperature distribution, $T(r)$, across the unit-cell NLB rocket engine based on an input set of heat generation rates, $Q_g'''(r)$, and an engine operating pressure. On the basis of the calculated $T(r)$, it also estimates the propellant nozzle exit velocity, thrust, and specific impulse. GNRATR-1D provides the user the option of varying almost

Subroutine HICG performs the same function as HIC, except it provides
MAY the fuel tank position for the fuel gas in thermodynamic
property density structure is located to fuel subroutines HIC.

Subroutine HICKIT is invoked by MAY following convergence of the 50
node iterations. It is used to calculate the average fuel tank position
property density structure T_{avg} to relate it to population (thermodynamic) and the
propellant density structure. The subroutine then uses the propellant
performance correlations given in Chapter 5 to calculate the propellant
density structure. The propellant density molecular weight structure
then uses molecular weight, mass flow rate, and specific impulse.

In order to determine the propellant mass flow rate and specific heat
subroutine HICKIT requires the temperature-dependent propellant specific
heat rate and mass density. To obtain that it invokes subroutines
HIDROGEN whose only function is to match the T_{avg} to a 15-
temperature group specific heat rate and mass density library (with an
effective range of 3000 - 20000 K).

Subroutine TRANSMIT is invoked by MAY when only reflective heat
transfer is specified in any combination of the fuel gas and
wall propellant regions. TRANSMIT corrects for the temperature effects in a
reflective heat transfer region by modifying the mean region
temperature calculated on the basis of the diffusion approximation. The
correction on the region temperature is performed according to the theory of
optically thin regions presented in Section 6.2.2.

3.2. Subroutine GEAR-1D Program

The GEAR-1D code calculates the (a) geometry, propellant distribution
(b) mass flow rate and MIB mass flow rate based on an input set of heat
generation rate Q_g and an input operating pressure. On the basis of the
calculated T_p it also calculates the propellant mass flow rate and
specific impulse. GEAR-1D provides the full data output of varying amount

any thermophysical property or parameter. One of its primary features is the incorporation of a reflection fraction off the reflective Be-moderator liner, which can be used to determine the effects of thermal radiation on the solid regions. GNRATR-1D relies extensively on temperature-dependent thermophysical properties to arrive at the most accurate possible (given the available material properties) thermal characteristics of the unit-cell NLB rocket engine. The code was designed to have an extremely simple structure, which allows for future modification and augmentation.

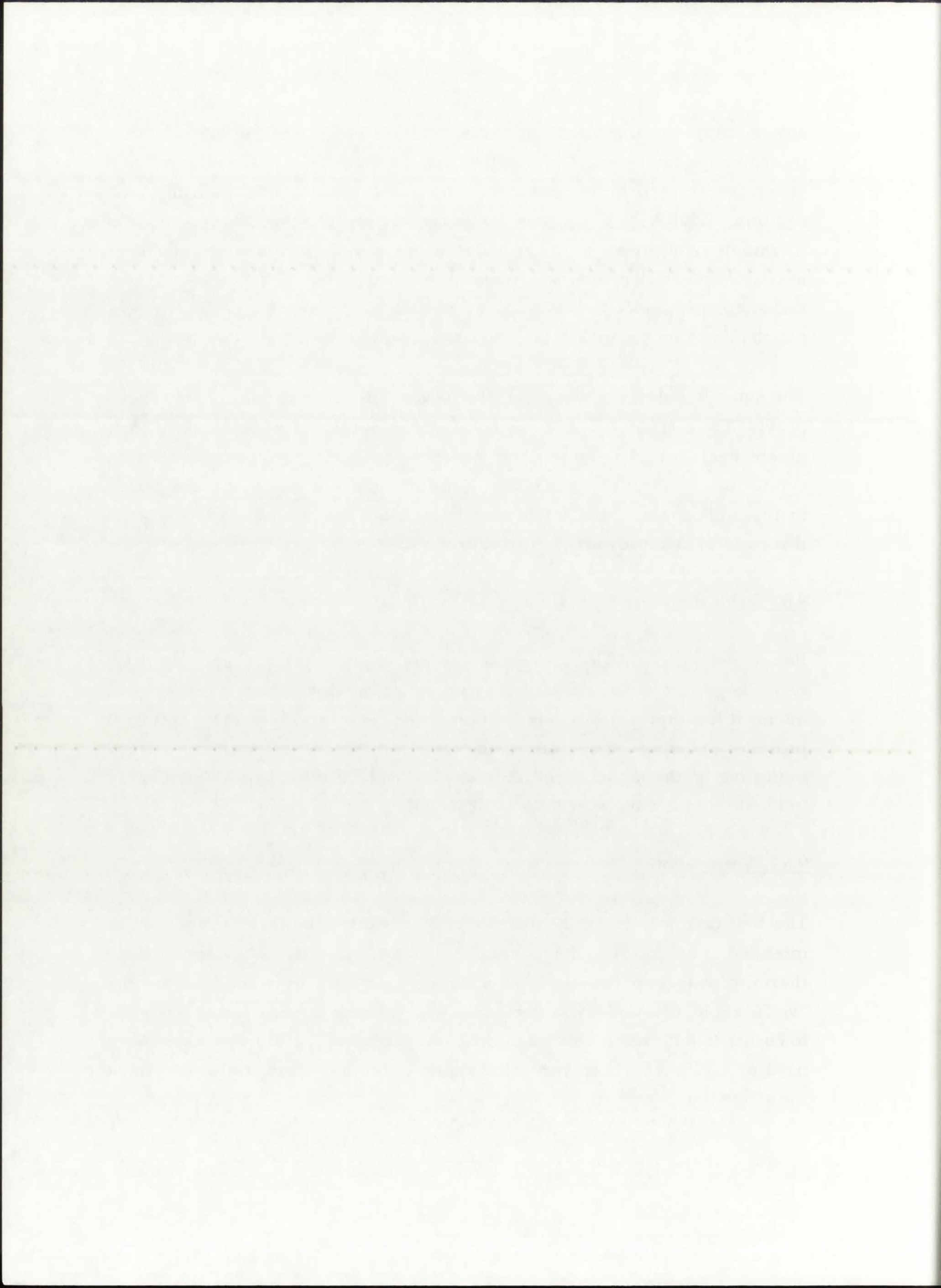
The energy balance "roots" of the GNRATR-1D temperature equations provide the user with a powerful and flexible tool to "switch on and off" any given heat transfer mode and thereby quantify the contribution of conduction, convection, generation, and radiation to the temperature profile in the NLB engine. This "switching on and off" feature of GNRATR-1D is discussed in detail as part of the results in Chapter 10.

9.6. Verification and Validation of GNRATR-1D

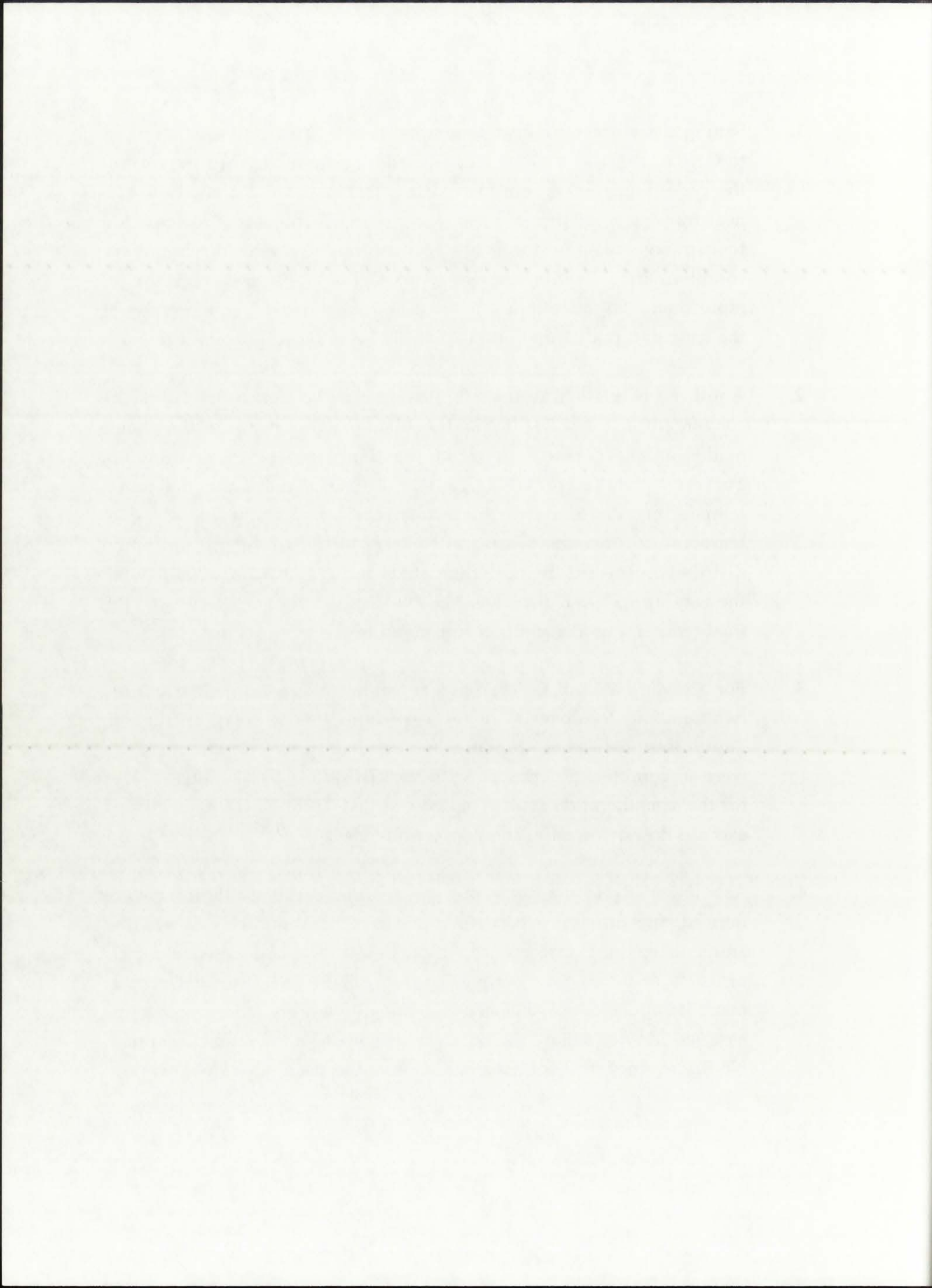
Before using GNRATR-1D for the thermal analysis of the unit-cell NLB rocket engine, it was necessary to ascertain: a) that it performs the task it was intended for appropriately (verification of the code), and b) that the results it provides, whether they follow the outlined theory or not, are indeed indicative of the actual conditions inside the NLB engine, if a functioning full-scale engine were ever to be built (validation of the code).

9.6.1. Verification

The first task was to verify that the code performs the thermal analysis as intended, i.e., follows the equation structure and uses the appropriate thermophysical properties. This task, generally referred to as the "verification" of a code, was performed shortly after the first full compilation to ensure that no errors existed in the code. A total of four different tests were used on GNRATR-1D to verify the code's execution. These tests comprised the following:



1. Setting the volumetric heat generation rate $Q_g'''(r)$, provided as input to GNRATR-1D, to zero at all fuel nodes and tracking convergence of the code. Since no generation existed, there was no "driver" for the heat transfer, and therefore the temperature distribution was expected to converge to a uniform 200 K, conformant to the far boundary condition at 1.0 m into ambient space. GNRATR-1D was tracked over more than 2,000 iterations, and in each case a distinct convergence of the temperature distribution to a flat 200 K profile was obtained.
2. Another postulate was that, for the case of no heat generation, the converged temperature distribution should not depend on the choice of the initial ("guessed" or zeroth-iteration) temperature distribution. To verify compliance, GNRATR-1D was executed for varying initial temperature distributions; for a total of 37 nodes, the initial nodal temperature increment was varied from 0.1 K (i.e., giving an initial distribution toward the centerline of 200.0, 200.1, 200.2, ..., 203.7 K) all the way up to 100 K (i.e., 200, 300, 400, ..., 2900 K). For every case, the final temperature distribution converged to the same set of values.
3. For a given value of $Q_g'''(r)$ and an initial temperature distribution, two iteration steps over 37 nodes were duplicated by hand calculation. The process took about 8 hours, and resulted in two iterations, which were in complete accord with the GNRATR-1D-calculated values for the same iteration steps. This proved that GNRATR-1D does indeed execute the equations in the manner intended.
4. As GNRATR-1D marched out in iterations, no oscillations were noticed; the difference between successive iterations became smaller and smaller until convergence was achieved for a convergence criteria of 0.01% or 0.1 K, for example. To track GNRATR-1D results over as many iterations as possible, convergence criteria were reduced to as low as $1.0e-7$ K, well below the accuracy provided by the 32-bit computer. No discrepancy or inconsistency was found in the GNRATR-1D results.



Based on the tests performed on GNRATR-1D, it was concluded that the code does indeed perform the thermal analysis as desired. The next step was to validate the code, that is, ascertain that the code can provide an accurate estimate of the actual thermal conditions inside a unit-cell NLB engine.

9.6.2. Validation

The best possible way to verify a code is to compare it to the actual conditions that would occur in the system that the code is designed to model. In the case of nuclear rockets, and gaseous nuclear rockets in particular, the technology is so advanced that not even computer codes exist to model the system, let alone the system itself. Thus, it becomes necessary to gauge or "benchmark" a new code with another independently-developed code. An indication of the new code's correctness of results would be if the two completely different codes provide good agreement on the results.

A thorough literature search was conducted to identify a code, preferably developed for analysis of GCR concepts, that could be used to validate GNRATR-1D. Unfortunately, one of the reasons behind the originality of GNRATR-1D also means that there is no existing code that incorporates the methodology of GNRATR-1D. The best candidate code was determined to be that developed by Poston and Kammash [Poston and Kammash, 1994a and 1994b] at the University of Michigan. The author had the pleasure of meeting David Poston at the 11th Symposium on Space Nuclear Power Studies in Albuquerque, held in January 1994. Their code is similar in structure to GNRATR-1D in that it receives as an input set the $Q_g'''(r)$ values, and uses them to determine the temperature distribution inside the fluid region of a coaxial-flow open-cycle GCR. The layout of the open-cycle engine is different than that for the NLB, but the existence of the fuel and propellant regions allows for approximate cross-comparison of the calculated temperatures.

The Poston-Kammash code (unnamed by the authors) analyzes the temperature distribution only in the fluid region of the rocket engine; in addition, it assumes a constant wall temperature of 2,200 K (as will be shown

... the ... of ...
... the ... of ...
... the ... of ...

... the ... of ...
... the ... of ...
... the ... of ...

... the ... of ...
... the ... of ...
... the ... of ...

... the ... of ...
... the ... of ...
... the ... of ...

... the ... of ...
... the ... of ...
... the ... of ...

in the research results discussed in Chapter 10, this parameter is extremely important and needs to be calculated as part of the analysis). Its resultant temperature distribution in the fuel region, though, can be used to cross-compare with GNRATR-1D because the fuel temperatures are primarily influenced by the "driver" fission heat generation rate.

The Poston-Kammash code was executed for a thermal power of 500 MWth and a cavity pressure of 101.3 MPa (1,000 atm). The solution method relied on a direct-matrix solver, and incorporated fluid mechanics as well as heat transfer parameters. The total fuel-bearing region volume was approximately 3.0 m^3 , resulting in an average power density (or volumetric heat generation rate) of approximately $1.65 \times 10^8 \text{ W/m}^3$. This resulted in a bulk fuel centerline temperature of 50,000 K (the temperatures were presented in contour, as opposed to discrete, form).

The Poston-Kammash average power density of $1.65 \times 10^8 \text{ W/m}^3$ was provided as input to GNRATR-1D. The convergence criteria was set to 0.001 K to maximize the number of iterations. For the given power density, GNRATR-1D calculated a (discrete) fuel centerline temperature of 45,000 K. The 10% discrepancy in the results was deemed very acceptable, given the differences in the two codes' structures and methods of analysis.

Additional comparisons (based on exit velocity, propellant mass flow rate, specific impulse, and thrust) with the Poston-Kammash code were performed with respect to calculated rocket performance results. These comparisons, discussed in detail in Section 10.7 of this Dissertation, indicate very good agreement between the results obtained from the GNRATR-1D code and those obtained with the Poston-Kammash code.

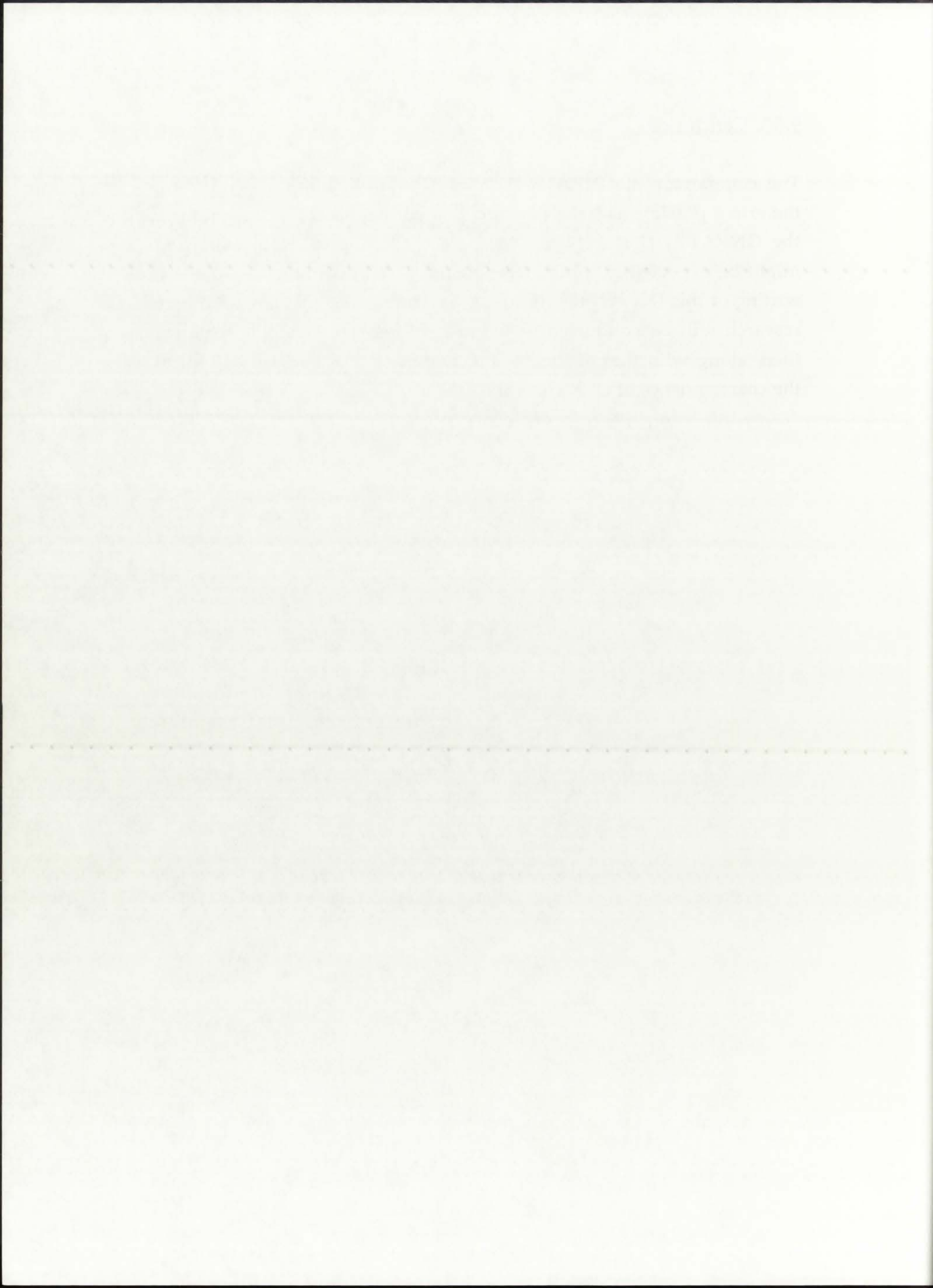
The first part of the report is a general introduction to the subject of the study. It discusses the importance of the study and the objectives of the research. The second part of the report is a detailed description of the methodology used in the study. This includes a description of the data sources, the sampling method, and the statistical methods used to analyze the data.

The third part of the report is a discussion of the results of the study. This section presents the findings of the research and discusses their implications. The fourth part of the report is a conclusion and recommendations. This section summarizes the main findings of the study and provides recommendations for future research. The fifth part of the report is a list of references. This section lists the sources of information used in the study.

The sixth part of the report is an appendix. This section contains supplementary information that is not included in the main body of the report. The seventh part of the report is a list of figures and tables. This section lists the figures and tables included in the report and provides a brief description of each. The eighth part of the report is a list of abbreviations. This section lists the abbreviations used in the report and provides a brief description of each.

9.6.3. Conclusions

The comparison of GNRATR-1D to the Poston-Kammash code indicated, to the extent possible as far as gas core thermal analysis codes are concerned, that the GNRATR-1D results provide a reasonable estimate of conditions that might be expected in a high-temperature GCR rocket engine. At the time of writing of this Dissertation, it does not seem possible that any additional GCR research will be conducted in the near future. The results of this research, then, along with that of Poston and Kammash, can be used as indicators of the characteristics of GCR concepts.



CHAPTER 10

THERMAL AND NEUTRONICS ANALYSIS RESULTS

10.1. Introduction

This Chapter presents the results of the thermal and neutronics analyses performed for the unit-cell NLB rocket engine. The neutronics analysis was based on the use of: (1) the Hansen-Roach isothermal cross-section library and (2) the temperature-dependent ENDF/B-V cross-section library. With the use of these two neutronics libraries, it is possible to account for the temperature effects on the neutronics behavior of the engine, and also to account for the beryllium microscopic scattering cutoff at 0.006 eV. The work presented in this Chapter encompasses the complete methodology of the work for this Dissertation: complete thermal analysis, coupling of thermal and neutronics results, comprehensive parametric studies, delineation of rocket performance parameters, and conclusions on the feasibility of the NLB rocket engine.

10.2. Breakdown of the Analysis

The two main sources of the thermal and neutronics results presented in this Chapter are the GNRATR-1D code (uncooled $T(r)$ and rocket performance parameters) and ONEDANT ($Qg'''(r)$ and k_{eff}). Due to the large number of parameters incorporated into GNRATR-1D, it is possible to vary each one and thus provide an exhaustive analysis of the NLB engine. A list of parameters that could be varied within GNRATR-1D is given in Table 10.1. For the purposes of this research work, it was decided to analyze three thermal power configurations: 500 MWth, 5 MWth, and 50 kWth. With four orders of magnitude, these configurations provide sufficient insight into the characteristics of the NLB engine to warrant a discussion on its feasibility. The 500 MWth configuration was chosen as the upper limit due to the very high associated temperatures [Poston and Kammash, 1994a], while 50 kWth was chosen as the lower limit due to the proximity of the associated temperatures to the lower bounds of the gaseous state of uranium.

CHAPTER 10 THERMAL AND NEUTRONIC ANALYSIS RESULTS

10.1 Introduction

This chapter presents the results of the thermal and neutronic analyses performed for the initial NLS rocket engine. The neutronic analysis was based on the use of (1) the Hansen-Ross technical cross-section library and (2) the temperature-dependent ENDF-V cross-section library. With the use of these two technical libraries it is possible to account for the temperature effects on the neutronic behavior of the engine and also to account for the partial neutronic scattering ratios at 0.02 eV. The work presented in this Chapter encompasses the complete methodology of the work for the comparison with the thermal analysis coupling of thermal and neutronic results, comprehensive parametric studies, definition of rocket performance parameters, and discussion on the feasibility of the NLS rocket engine.

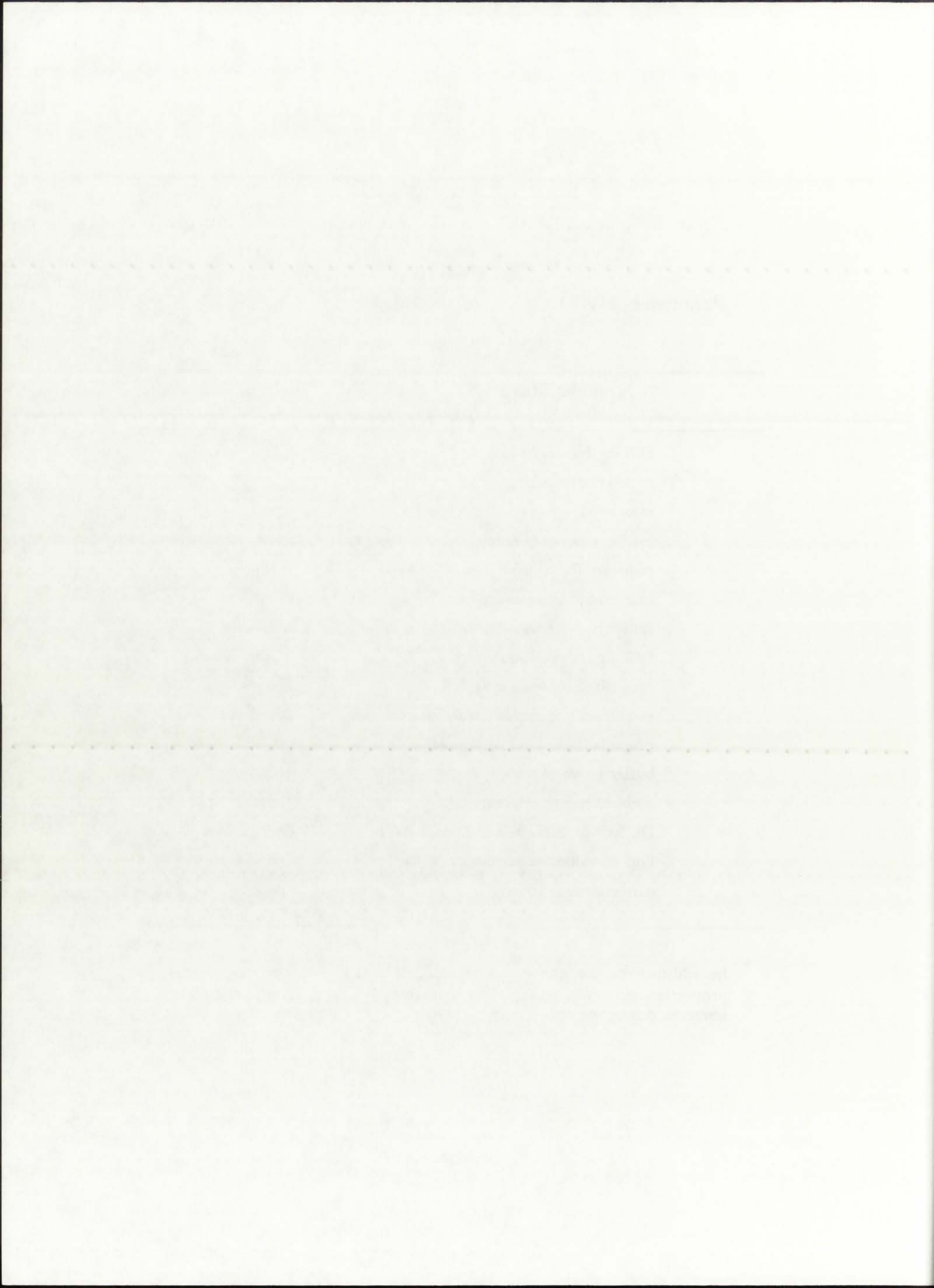
10.2 Description of the Analysis

The two main sources of the thermal and neutronic results presented in this Chapter are the STAR and GIBBY codes. The STAR code (developed by the University of Michigan) and GIBBY (developed by the University of Michigan) are the two main codes used in this analysis. The STAR code provides an extensive analysis of the NLS engine. A list of parameters that could be varied within STAR-10 is given in Table 10.1. For the purpose of this research work it was decided to analyze three thermal power configurations: 300 MWth, 2 MWth, and 20 MWth. With four orders of magnitude, these configurations provide sufficient insight into the characteristics of the NLS engine to warrant a discussion on the feasibility. The 300 MWth configuration was chosen as the upper limit due to the very high associated temperatures (Foster and Johnston, 1994), while 20 MWth was chosen as the lower limit due to the proximity of the associated temperatures to the lower limits of the power state of matter.

TABLE 10.1
Parameters available for user specification in GNRATR-1D *

Nomenclature	Symbol
all 9 region widths [m]	t__
region nodal spacings	n__
max. solid region conductivities [W/m-K]	kcond__
total number of iterations	iters
radiative flux reflection fraction	reflBe
total operating pressure [atm]	P
radiative heat transfer switch	rad=.true.
buffer gas convection switch	BGconv=.true.
propellant convection switch	Pconv=.true.
propellant channel hydraulic diameter [m]	Dhydraul
propellant axial velocity [m/s]	vP
buffer gas axial velocity [m/s]	vBG
ambient space temperature [K]	Tspace
Qg'''(r) values for non-fuel nodes [W/m ³]	Qg(i), 1 ≤ i < 30
Qg'''(r) values for fuel nodes [W/m ³]	Qg(i), 30 ≤ i ≤ 37
convergence criterion	eps

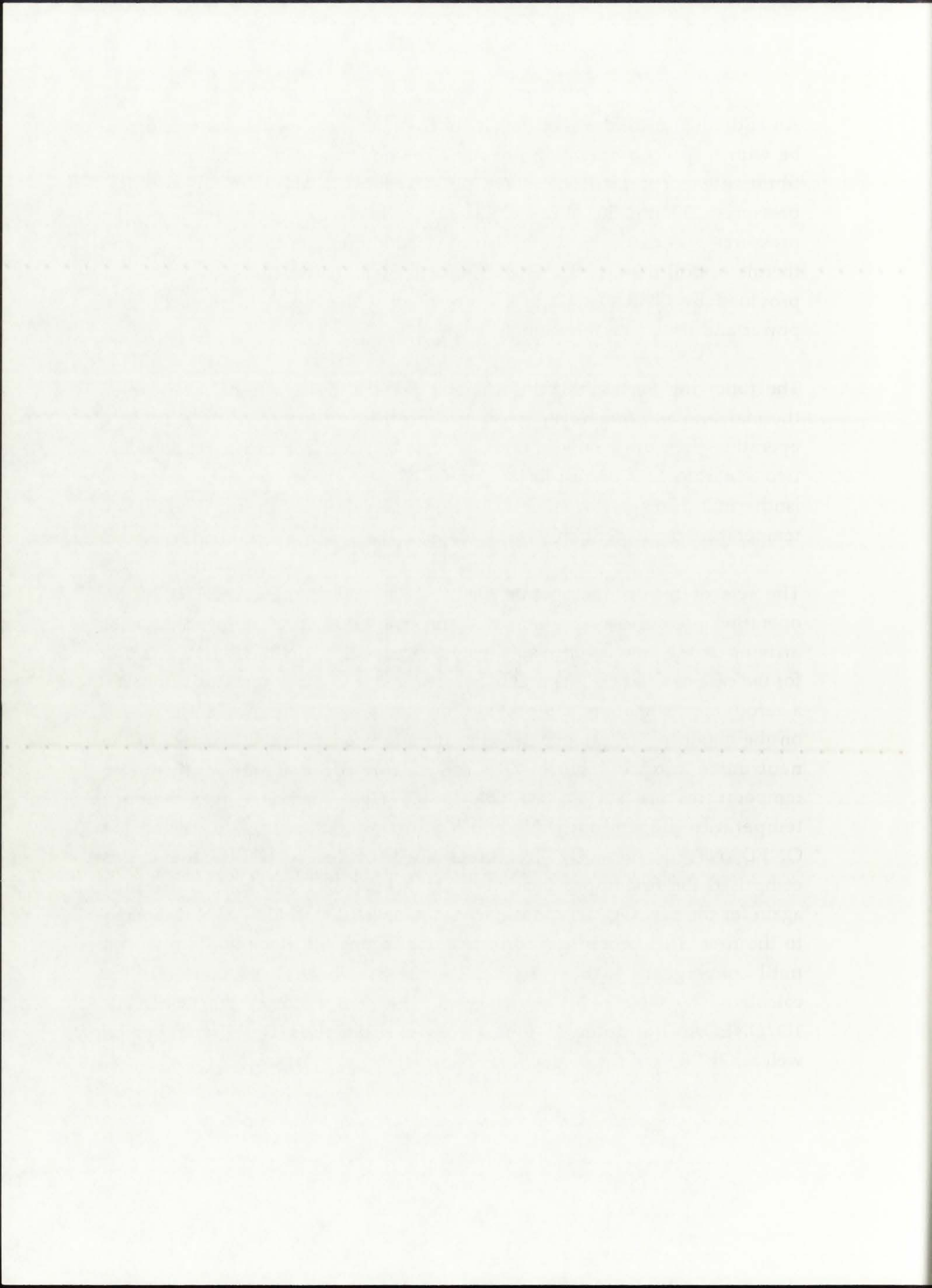
* In addition to the above parameters, all optical and thermophysical properties, currently arranged in temperature- and pressure-dependent libraries, can be varied.



An additional breakdown of the GNRATR-1D analysis results was decided to be with respect to operating pressure. The optical and thermophysical data libraries incorporated into GNRATR-1D allow analysis of up to three pressures: 250 atm, 500 atm, and 1,000 atm. The choice of the three particular pressures was made on the basis of available uranium thermophysical and thermo-optical data [Parks, 1968]. As part of this Dissertation, thus, the data provided by GNRATR-1D is broken down with respect to three thermal power and three pressure configurations.

The following Sections of this Chapter present the results of the coupled thermal and neutronics analyses, for the three thermal power and three operating pressure configurations discussed before. For each configuration, two separate sets of results are provided: one for the analysis with the isothermal Hansen-Roach cross-sections, the other with the ENDF/B-V temperature-dependent cross-sections.

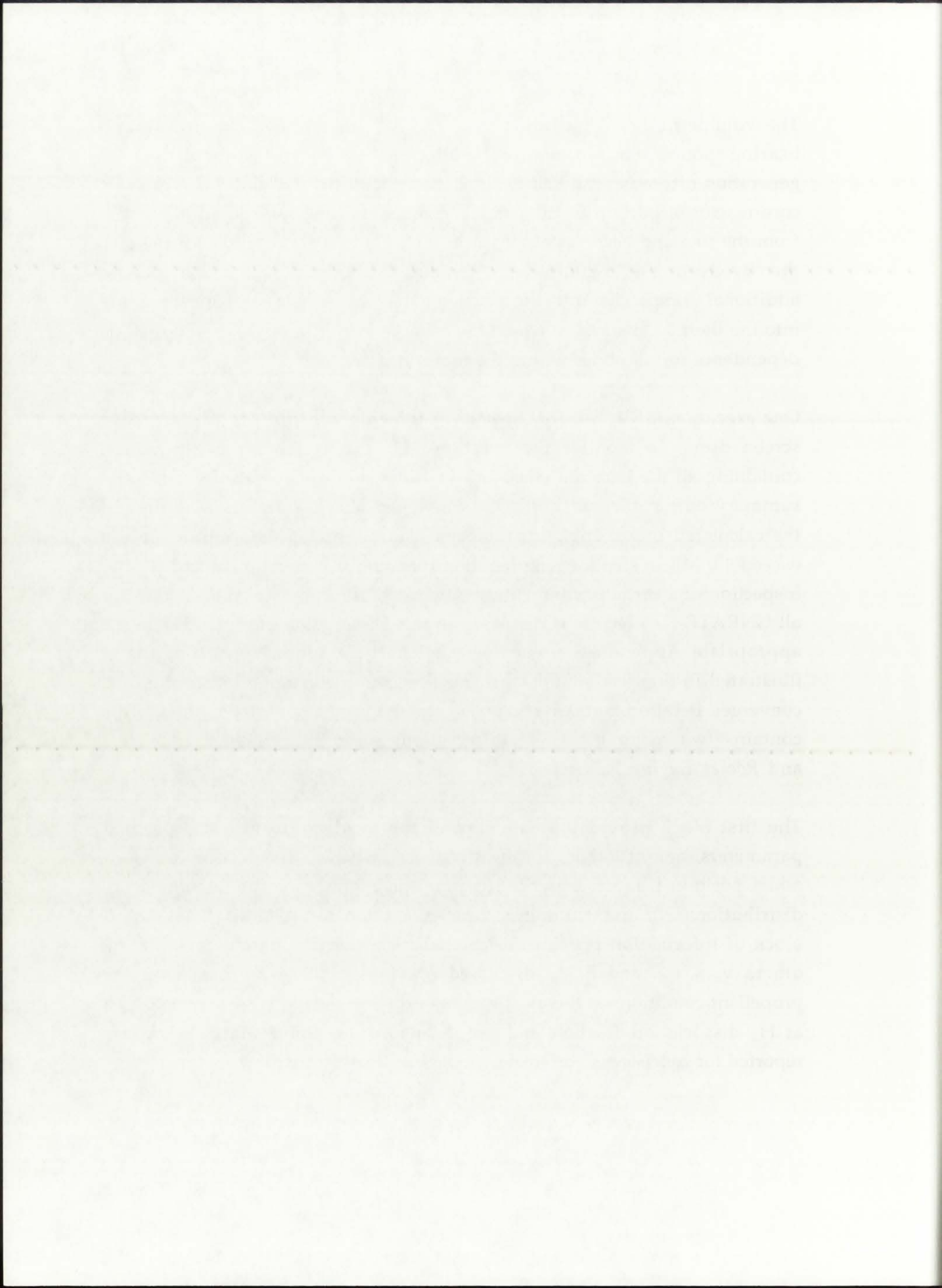
The sets of results incorporate $Qg'''(r)$, k_{eff} , and the *uncooled* $T(r)$, all for operating pressures of 250 atm, 500 atm, and 1,000 atm. The procedure for arriving at the converged results commences with a GNRATR-1D execution for the case of a flat $Qg'''(r)$ profile, where $Qg'''(r) = Q_{total}/V_{fuel}$. This comprises a zeroth approximation, and provides the first temperature profile $T(r)$. Based on the obtained $T(r)$, atomic densities for all materials in the 11 zones of the neutronics model (Figure 7.1) are calculated, and the appropriate temperatures are set in TRANSX for all eight materials, to provide a temperature-dependent ENDF/B-V library. Following execution of ONEDANT, the new $Qg'''(r)$ values are provided to GNRATR-1D; this comprised the first approximation of $Qg'''(r)$. GNRATR-1D is then executed again for the new $Qg'''(r)$ and the second temperature profile $T(r)$ is compared to the first. This procedure, corresponding to one full iteration, is repeated until convergence in both $T(r)$, calculated by GNRATR-1D, and $Qg'''(r)$, calculated by ONEDANT, is achieved. The final result of the GNRATR-1D/ONEDANT coupling is then a converged *uncooled* $T(r)$ distribution as well as $Qg'''(r)$ and the overall k_{eff} .



The volumetric heat generation rates $Qg'''(r)$ are provided for the 7 fuel-bearing nodes. For all non-fuel nodes, naturally, the volumetric heat generation rate was set equal to zero. It can be postulated that for a gaseous core reactor, a portion of the emitted gamma and neutron radiation escapes from the fuel and becomes absorbed in the solid moderator/reflector regions, thereby creating a "pseudo-source" in the solid regions. So as not to include additional complexity into the problem, this feature was not incorporated into the thermal analysis; it would be a simple matter, though, to add $Qg'''(r)$ dependence for all nodes within the rocket engine.

One execution of GNRATR-1D results in three output files: (1) an interactive screen dump to monitor the iterations, (2) a comprehensive output file containing all the iteration steps and the final summary of results, and (3) a summary output file containing the converged temperature distribution and the calculated rocket engine parameters. The comprehensive output file can exceed 1.0 MB in size for long iteration runs and is generally discarded after inspection of a certain run; for those interested, the summary output files for all GNRATR-1D executions discussed in this Dissertation are included in the appropriate Appendices. A sample GNRATR-1D summary output file is illustrated in Figure 10.1; this particular execution corresponded to the final converged iteration for 50 kWth, $P=250$ atm. As can be seen, the summary file contains two major blocks of information: *Summary of Converged Values and Rocket Engine Parameters*.

The first block provides a summary of the most pertinent user-specified parameters, among others the heat transfer switches, and also a listing of nodal position i , radial distance $r(i)$ from the engine centerline, temperature distribution $T(i)$, and volumetric heat generation rate $Qg'''(i)$. The second block of information provides calculated rocket engine parameters, among others v_{exit} , I_{sp} , and F . As discussed previously, these are based on the propellant conditions at the axial channel exit. The auxiliary parameters, such as H_2 dissociation fraction and propellant average molecular weight, are reported for conciseness and to aid debugging, if necessary.



----- SUMMARY OF CONVERGED VALUES -----

This Case Executed for: REFLBe = 0.00000
 Pressure = 250.0 atm

Modes of Heat Transfer: Radiation in BG,SiW, and P = .on.
 Convection in BG = .on.
 Convection in P = .on.

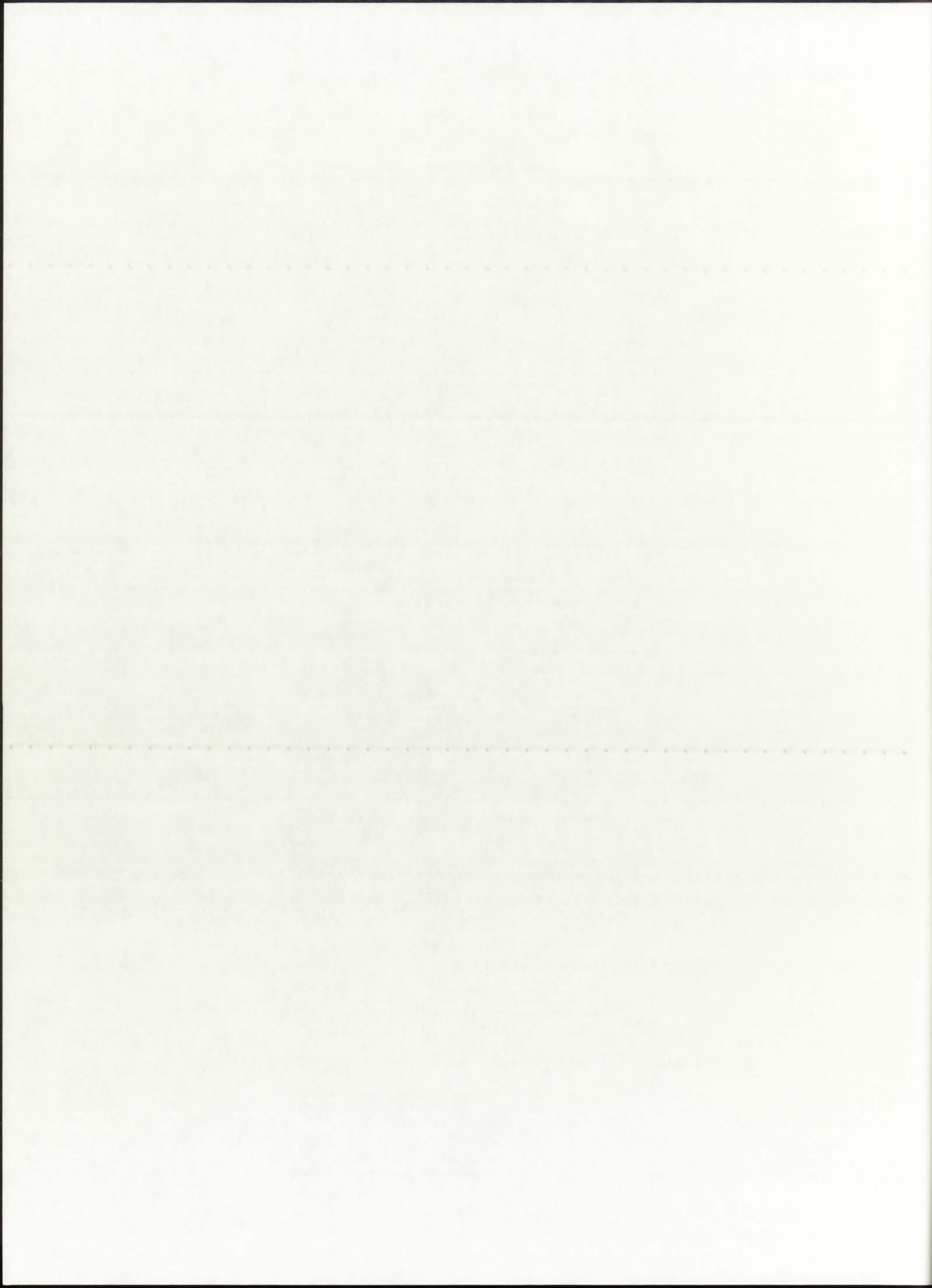
i	r(i)	T(i)	Qg(i)
37	0.000	8559.5	0.6274E+05
36	0.019	8559.5	0.6195E+05
35	0.039	8554.6	0.1255E+06
34	0.059	8539.8	0.1358E+06
33	0.096	8444.1	0.1920E+06
32	0.133	8228.3	0.2300E+06
31	0.170	7820.5	0.3447E+06
30	0.207	4833.2	0.0000E+00
29	0.225	4833.2	0.0000E+00
28	0.244	4833.2	0.0000E+00
27	0.246	4833.2	0.0000E+00
26	0.249	4833.1	0.0000E+00
25	0.268	4833.1	0.0000E+00
24	0.287	4833.0	0.0000E+00
23	0.307	4830.7	0.0000E+00
22	0.326	4828.7	0.0000E+00
21	0.345	4827.0	0.0000E+00
20	0.405	3881.5	0.0000E+00
19	0.465	3179.9	0.0000E+00
18	0.525	2638.7	0.0000E+00
17	0.585	2208.6	0.0000E+00
16	0.645	1858.7	0.0000E+00
15	0.705	1568.6	0.0000E+00
14	0.765	1324.3	0.0000E+00
13	0.825	1115.7	0.0000E+00
12	0.851	1114.9	0.0000E+00
11	0.876	1114.4	0.0000E+00
10	0.976	937.5	0.0000E+00
9	1.076	793.7	0.0000E+00
8	1.176	674.7	0.0000E+00
7	1.276	574.6	0.0000E+00
6	1.376	489.2	0.0000E+00
5	1.476	415.5	0.0000E+00
4	1.576	351.2	0.0000E+00
3	1.676	294.7	0.0000E+00
2	1.776	244.7	0.0000E+00
1	1.876	200.0	0.0000E+00

----- ROCKET ENGINE PARAMETERS -----

The H2 dissociation fraction is: 0.0891
 The H2 average molecular weight is: 1.9262 g/gmol
 The propellant molecular weight is: 7.3839 g/gmol
 The cross-sectional flow area is: 0.0721 m2
 The propellant mass flow rate is: 0.10 kg/s

 The chamber temperature is: 4833.1 K
 The calculated exit velocity is: 7903.5 m/s
 The calculated thrust is: 0.8 kN
 The calculated specific impulse is: 805.9 s

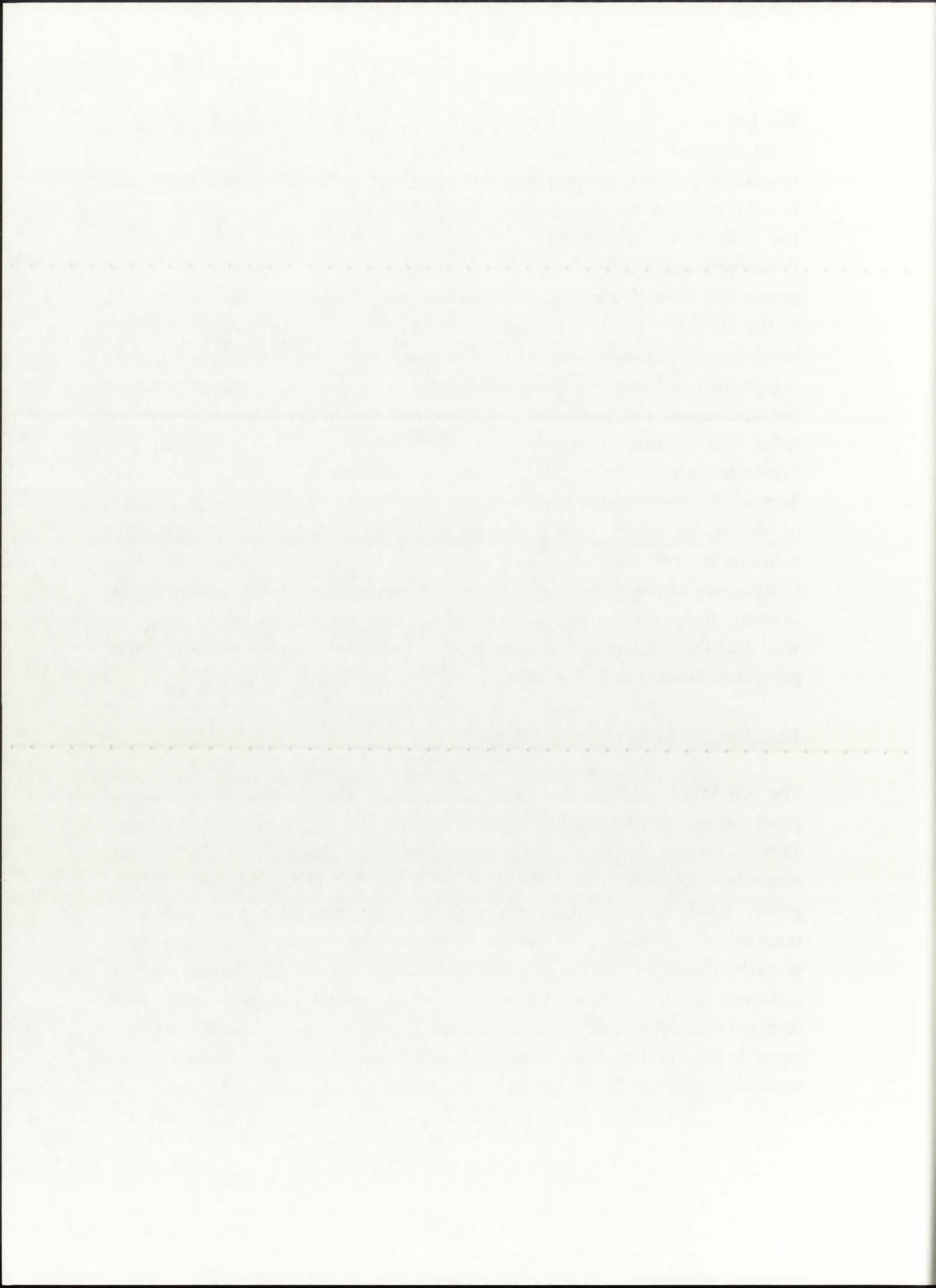
Figure 10.1: Sample GNRATR-1D summary output file.



The following three Sections discuss the GNRATR-1D results obtained for a fixed thermal power (500 MWth, 5 MWth, and 50 kWth configurations, respectively), varying operating pressure, and both the Hansen-Roach and ENDF/B-V cross-section libraries. Section 10.6 discusses the variation of $T(r)$ for a fixed operating pressure. Section 10.7 provides a compilation of thermophysical and rocket performance results, as functions of both thermal power and operating pressure. A baseline configuration, chosen to correspond to the 50 kWth, $P=250$ atm case, is discussed in detail in Section 10.8. This baseline configuration was analyzed in much more detail, with varying solid region liner reflection fractions ($reflBe$) and switching on/off of convection in the buffer gas, convection in the propellant region, and conduction in the silica wall. In addition, the baseline configuration was used as a test-bed to investigate any potential effects of fuel temperature on the k_{eff} of the system. Section 10.9 comprises of series of analyses aimed at investigating the accuracy of the (r) geometry model and its associated assumptions. The Section contains an (r- θ) analysis of both $Qg''(r)$ and the neutron flux $\Phi(r)$ and their comparison to the (r) geometry "smeared" results, a criticality search, and an investigation into the neutron and gamma energy deposition in the silica wall and the moderator/reflector region. The conclusions to Chapter 10 are presented in Section 10.9.

10.3. The 500 MWth Configuration

The 500 MWth configuration was chosen as the upper limit on the thermal power range. Recent published work [Poston and Kammash, 1994a; Tanner, 1994] as well as preliminary analyses performed for this work, indicated a fuel centerline temperature of approximately 50,000-100,000 K associated with that power level; in such cases, and especially for even higher temperatures, removal of the fission heat becomes practically impossible and the feasibility of such concepts becomes only theoretical. The iterative solution procedure, outlined in the previous Section, was applied for the 500 MWth configuration. An initial volumetric heat generation rate of $2.03 \cdot 10^9$ [W/m³], equal to the quotient of the total thermal power and the fuel volume, was set at all seven fuel nodes. Based on the temperatures calculated by GNRATR-1D,



appropriate atomic densities were provided to ONEDANT. The resultant volumetric heat generation rates $Qg'''(r)$ were then provided to GNRATR-1D, for a new temperature distribution. This procedure was carried out separately for both the Hansen-Roach cross-sections and the ENDF/B-V cross-sections. The results of these analyses are presented in the following two subsections.

10.3.1. Hansen-Roach Library

The first set of analyses involving the 500 MWth configuration were performed with the Hansen-Roach cross-section library accessed by ONEDANT. The converged $Qg'''(r)$ distribution for the seven fuel nodes, ranging from the engine centerline ($r=0$) to the edge-of-fuel node ($r=20.7$ cm), for the 500 MWth configuration and three operating pressures, $P=250, 500,$ and $1,000$ atm, is presented in Figure 10.2. Observation of Figure 10.2 indicates that the bulk of the volumetric heat generation, and therefore the bulk of the fissions, occurs in the region between $r=4$ cm and $r=17$ cm. The relatively flat and wide profile of $Qg'''(r)$ indicates that the mean free path of neutrons is comparable to the dimensions of the fuel region; in other words, the fuel density [atoms/barn-cm] is low enough so that the rate of fission is constant almost along the whole radial length of the fuel region.

The ONEDANT input files for this configuration are provided in Appendix B.1. The appropriate fuel atomic densities are on the order of 10^{-6} - 10^{-7} [atoms/barn-cm], which are very low; the main reason for such a condition, of course, is the high temperature of the fuel. Noticeable between the three operating pressure conditions is the increase in $Qg'''(r)$ of the outer fuel nodes, i.e. a shift in $Qg'''(r)$ toward the outer edge of the fuel with increasing pressure. To conserve the total thermal power generated in the fuel, the increase in $Qg'''(r)$ at the outer edge is accompanied by a decrease in $Qg'''(r)$ at the nodes close to the centerline. This trend is due to the increase in fuel density as a result of increasing pressure; the increase in fuel density, along with an appropriate increase in the macroscopic fission cross-section, at the outer edges provides for a greater fission rate and greater $Qg'''(r)$ at that location.

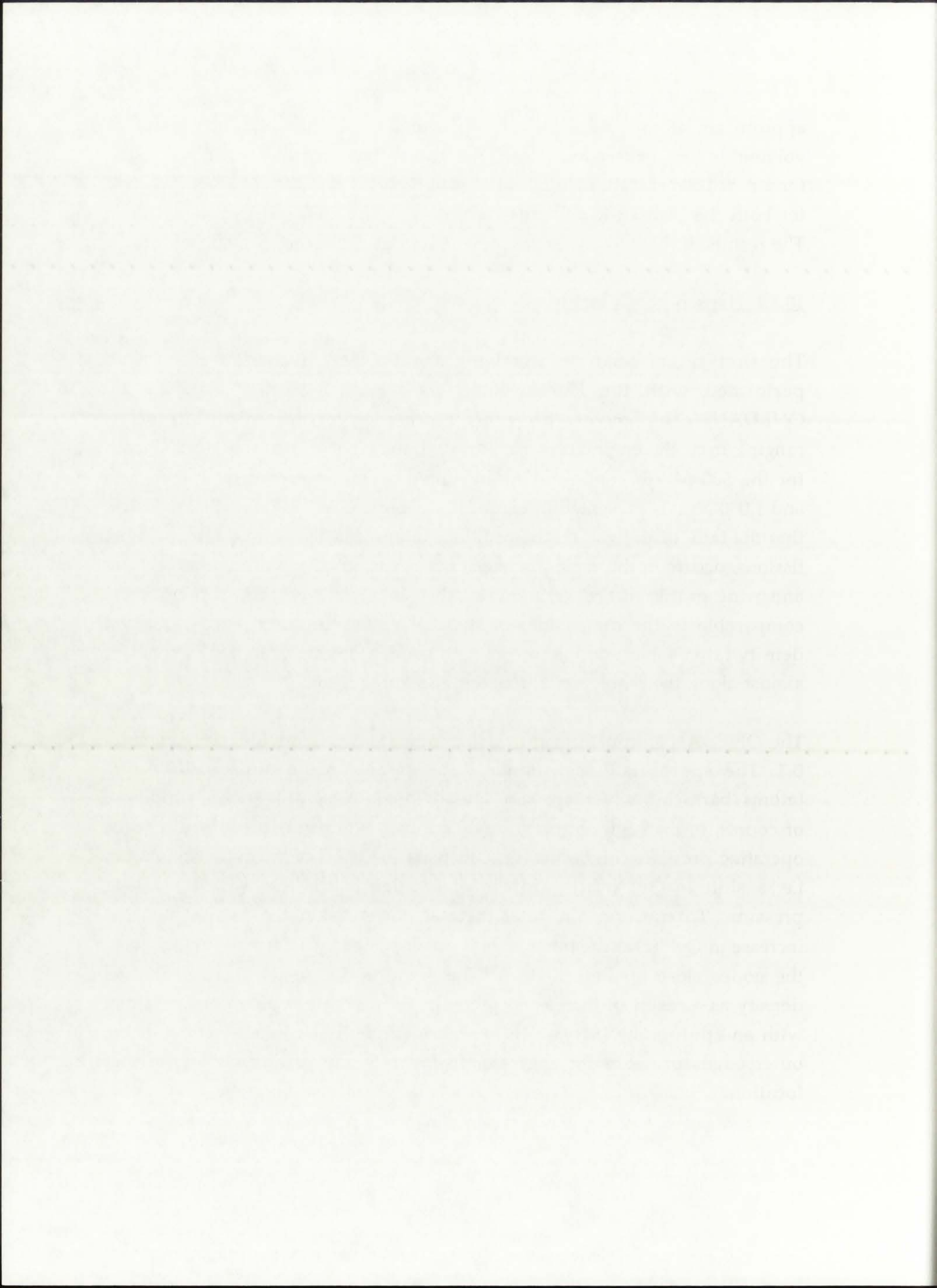
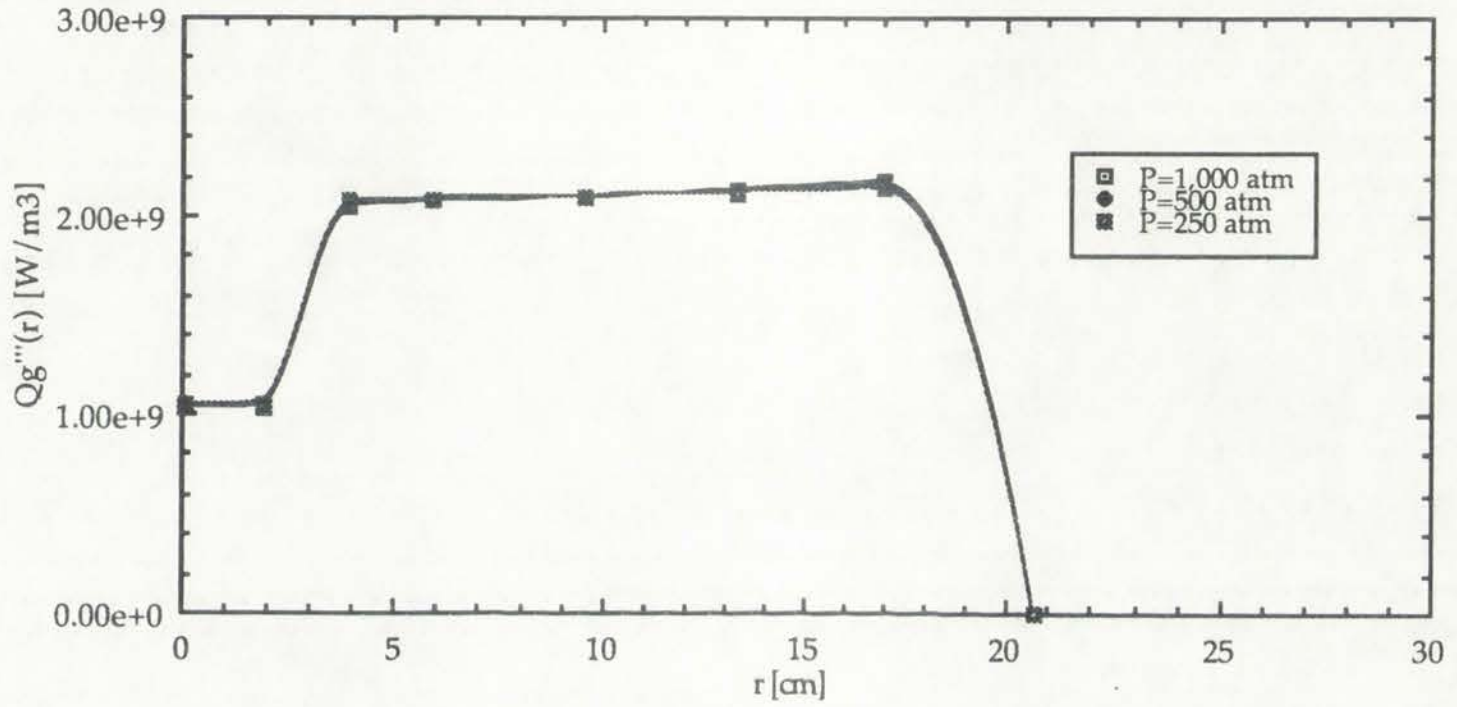
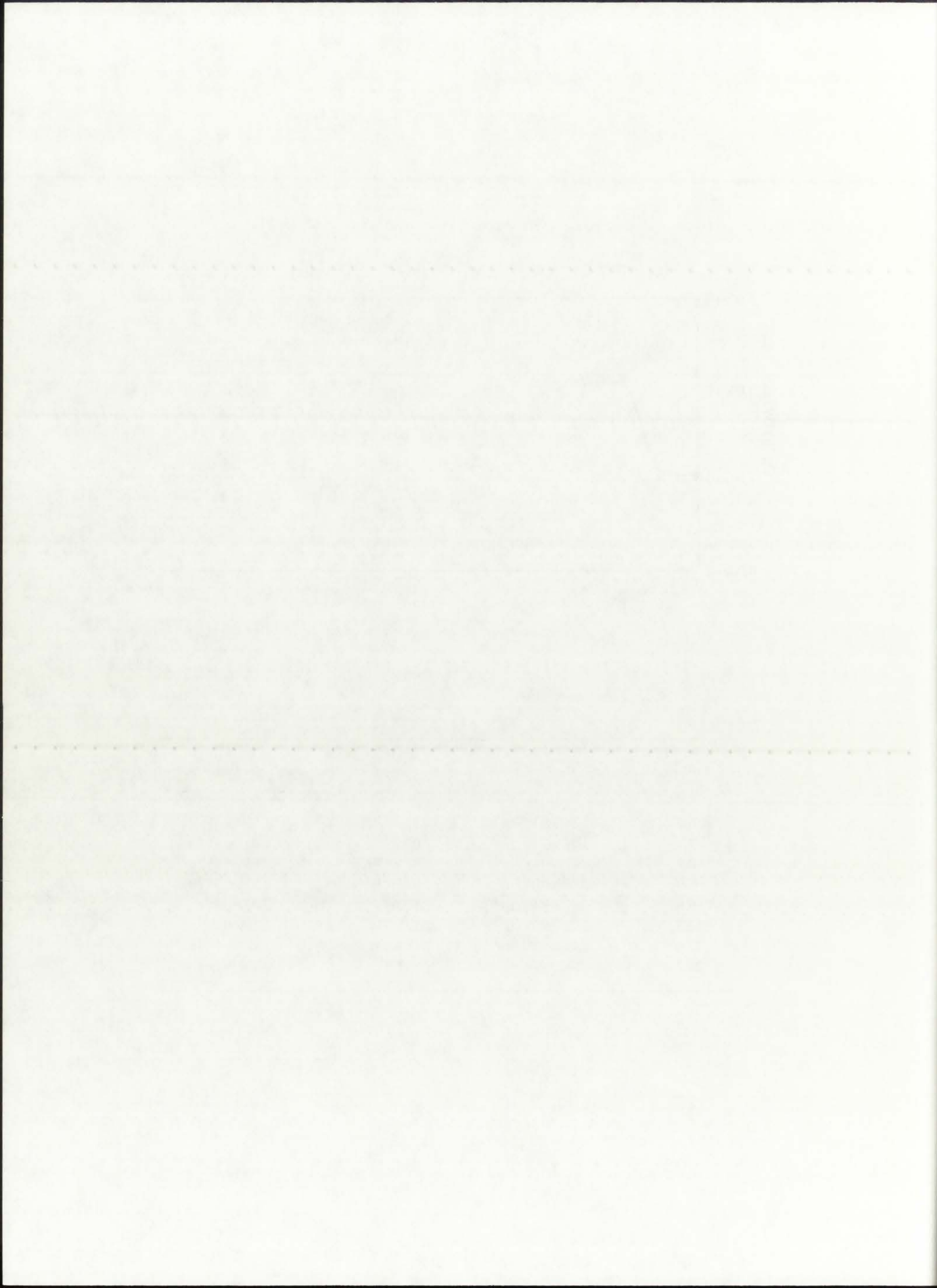


Figure 10.2: $Qg'''(r)$ for 500 MWth power level (Hansen-Roach library).



r [cm]	$Qg'''(r)$, P=250 atm	$Qg'''(r)$, P=500 atm	$Qg'''(r)$, P=1,000 atm
0.0	1.049e9 W/m ³	1.046e9 W/m ³	1.039e9 W/m ³
1.9	1.043e9 W/m ³	1.038e9 W/m ³	1.031e9 W/m ³
3.9	2.079e9 W/m ³	2.071e9 W/m ³	2.056e9 W/m ³
5.9	2.089e9 W/m ³	2.083e9 W/m ³	2.074e9 W/m ³
9.6	2.102e9 W/m ³	2.100e9 W/m ³	2.097e9 W/m ³
13.3	2.120e9 W/m ³	2.123e9 W/m ³	2.129e9 W/m ³
17.0	2.144e9 W/m ³	2.154e9 W/m ³	2.173e9 W/m ³
20.7	0.0 W/m ³	0.0 W/m ³	0.0 W/m ³



The calculated k_{eff} values of the 500 MWth configurations are shown in Figure 10.3. The k_{eff} of the baseline design is low, due mainly to the low fuel density. With increasing pressure, the k_{eff} increases due to a larger fuel density, but is still significantly subcritical. An additional analysis was incorporated at this point, in conjunction with ideas initially posed by the UARL designers. Namely, an important issue put forth by UARL with respect to the unit-cell NLB engine was the segmenting of the propellant channels to reduce the thermal neutron diffusion barrier of hydrogen. Reducing the barrier was intended to increase the flow of neutrons into the fuel region and thereby achieve a higher k_{eff} with the same fuel density. This idea was analyzed here by taking the baseline ONEDANT cases and setting the hydrogen propellant atomic density to zero, thereby creating a vacuum zone in place of the hydrogen. No detrimental effects of the absence of the hydrogen moderator were foreseen as the bulk of the moderation is provided by the combined 54 cm of beryllium and heavy water, both with significantly higher atomic densities.

The resultant k_{eff} values of the modified baseline design are also shown in Figure 10.3. As can be seen, for the extreme case of no propellant present, the increase in k_{eff} is approximately 10-15%. Therefore, there is credibility to the idea of the original UARL designers to reduce the hydrogen propellant cross-sectional area to neutron flow. For the case of the actual unit-cell NLB rocket engine, where the propellant channels were intended to subtend 40% of the total annular surface area, the increase in k_{eff} over the 100% subtending would be significantly less than 15%.

Segmentation of the propellant channels, then, could not be relied on to provide a noticeable increase in k_{eff} for the same operating conditions and dimensions. In order to significantly increase the k_{eff} of the original unit-cell NLB engine for the 500 MWth configuration, it would be necessary to either increase the operating pressure beyond 1,000 atm (and therefore increase the fuel density) or increase the size of the fuel region. Both scenarios involve complex calculations and parametric analyses and would essentially require a major redesign of the original unit-cell NLB rocket engine.

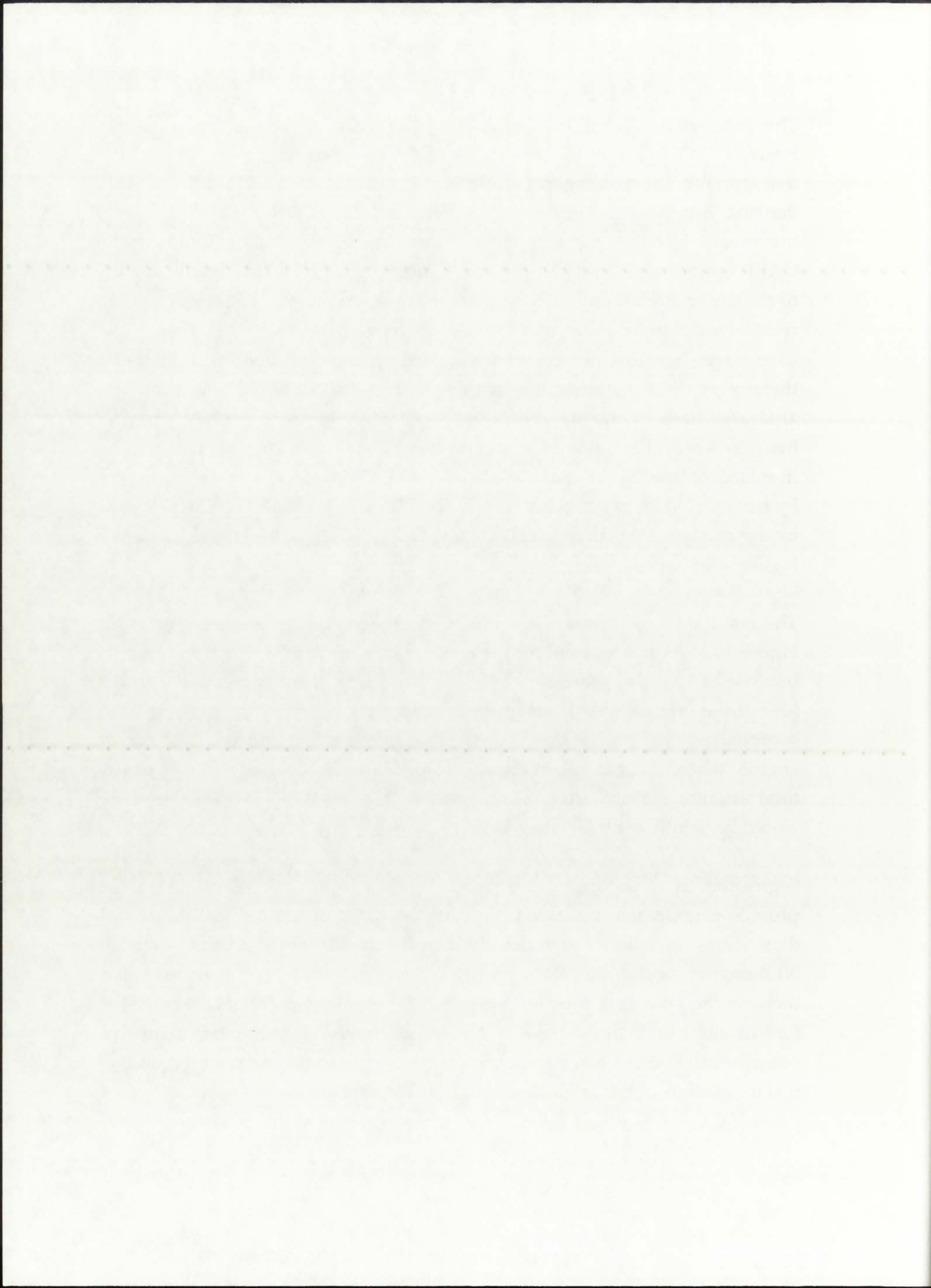
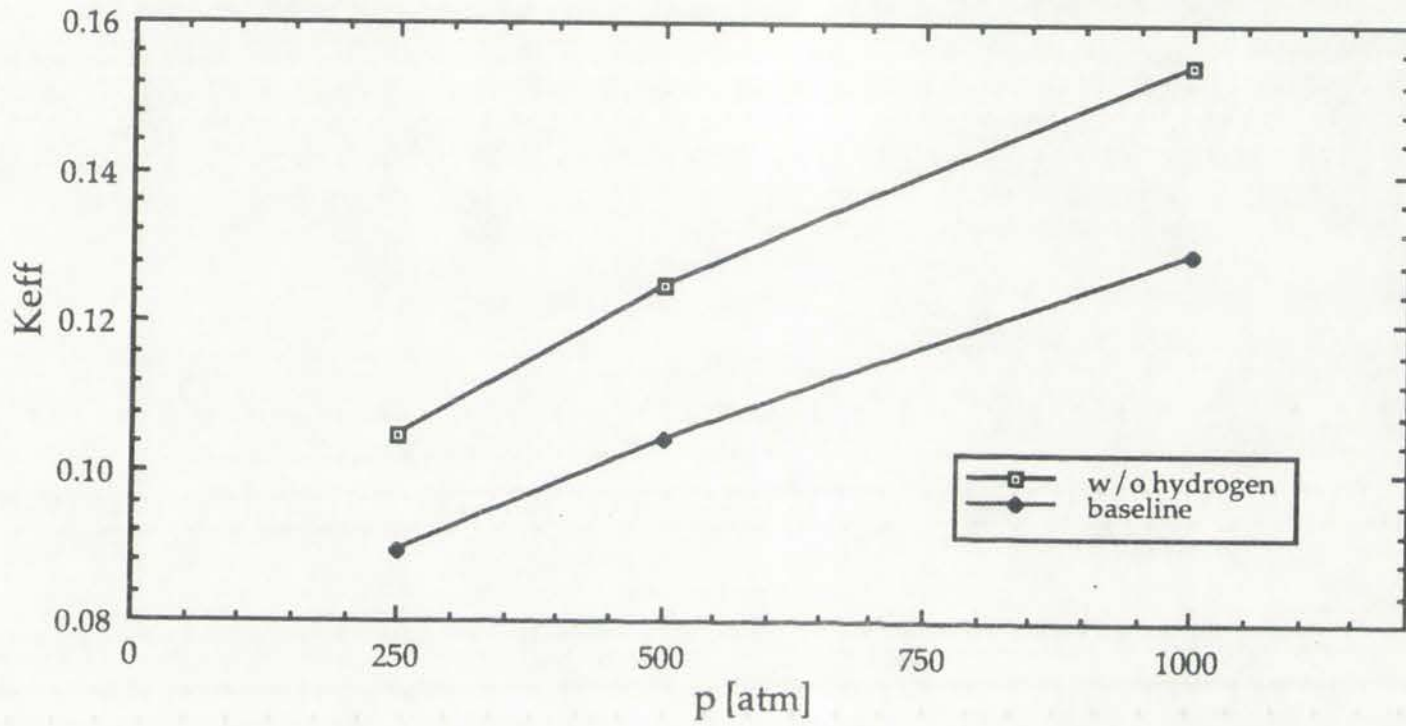
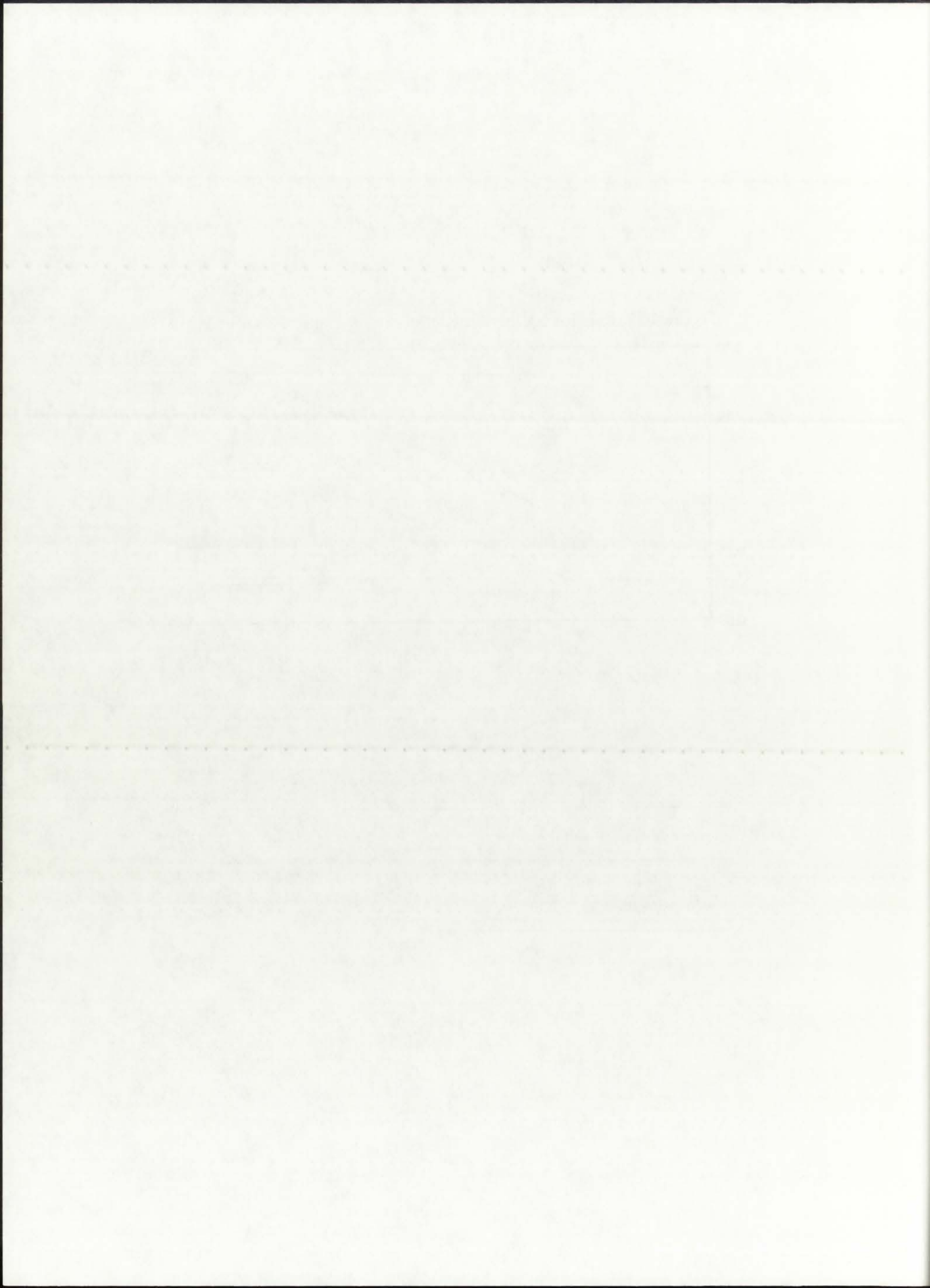


Figure 10.3: K_{eff} for 500 MWth configuration (Hansen-Roach library).



engine design	k_{eff} , P=250 atm	k_{eff} , P=500 atm	k_{eff} , P=1,000 atm
baseline	0.0894	0.1042	0.1294
w/o hydrogen	0.1046	0.1250	0.1543



Based on the $Qg'''(r)$ values in the fuel region, a converged $T(r)$ distribution was determined by GNRATR-1D for each of the three operating pressures, as shown in Figure 10.4. Radiation, convection, and conduction were accounted for in the non-fuel gaseous regions; in addition, a conservative condition of 0% reflection off the solid regions' reflective liner ($reflBe=0\%$) was assumed. As can be seen, the general shape of $T(r)$ is similar for all three operating pressures; the temperature is highest at the centerline and decreases toward the edge of the fuel. The behavior and general shape of $T(r)$ as well as $Qg'''(r)$ in the fuel region of a GCR is in accordance with previous studies performed on the open-cycle concept [Thom, Schneider, and Schwenk, 1974; Schnitzler, 1988; Poston and Kammash, 1994] and with anticipated behavior within the closed-cycle NLB engine [Latham, 1990].

The centerline-to-edge of fuel temperature ratio is approximately constant at 1.8 for the three operating pressures. This characteristic of gas core nuclear reactors has been previously observed; Robert Ragsdale, of NASA-Lewis, introduced an analogy with the temperature distribution within the Sun, where the centerline-to-edge of plasma temperature ratio is equal to 1.5 on the average [Ragsdale, 1970]. The behavior of GNRATR-1D data indicates very good agreement with the current understanding of the temperature distribution within gaseous heat sources, specifically the predicted behavior within the gaseous fuel region of a gas-core nuclear rocket.

The calculated temperature values for the major regions within the unit-cell NLB engine model are given in Table 10.2. Because of the very low overall thermal resistance of the buffer gas, silica wall, and propellant regions, the temperature distribution across those three regions is virtually flat. That profile corresponds to the temperature plateau of Figure 10.4. In the regions of high thermal resistance, such as the fuel and D_2O , the temperature drop is pronounced and significant.

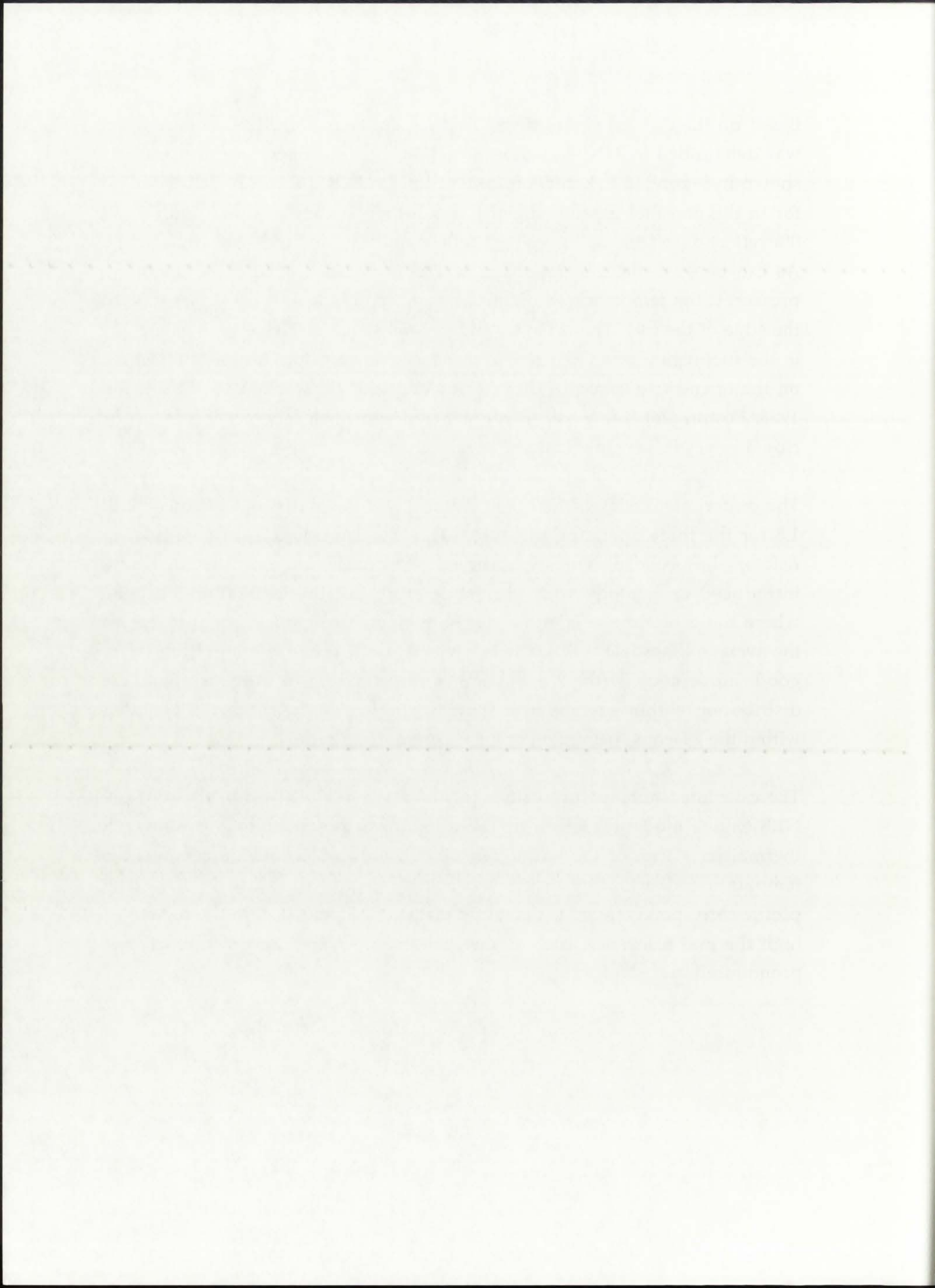
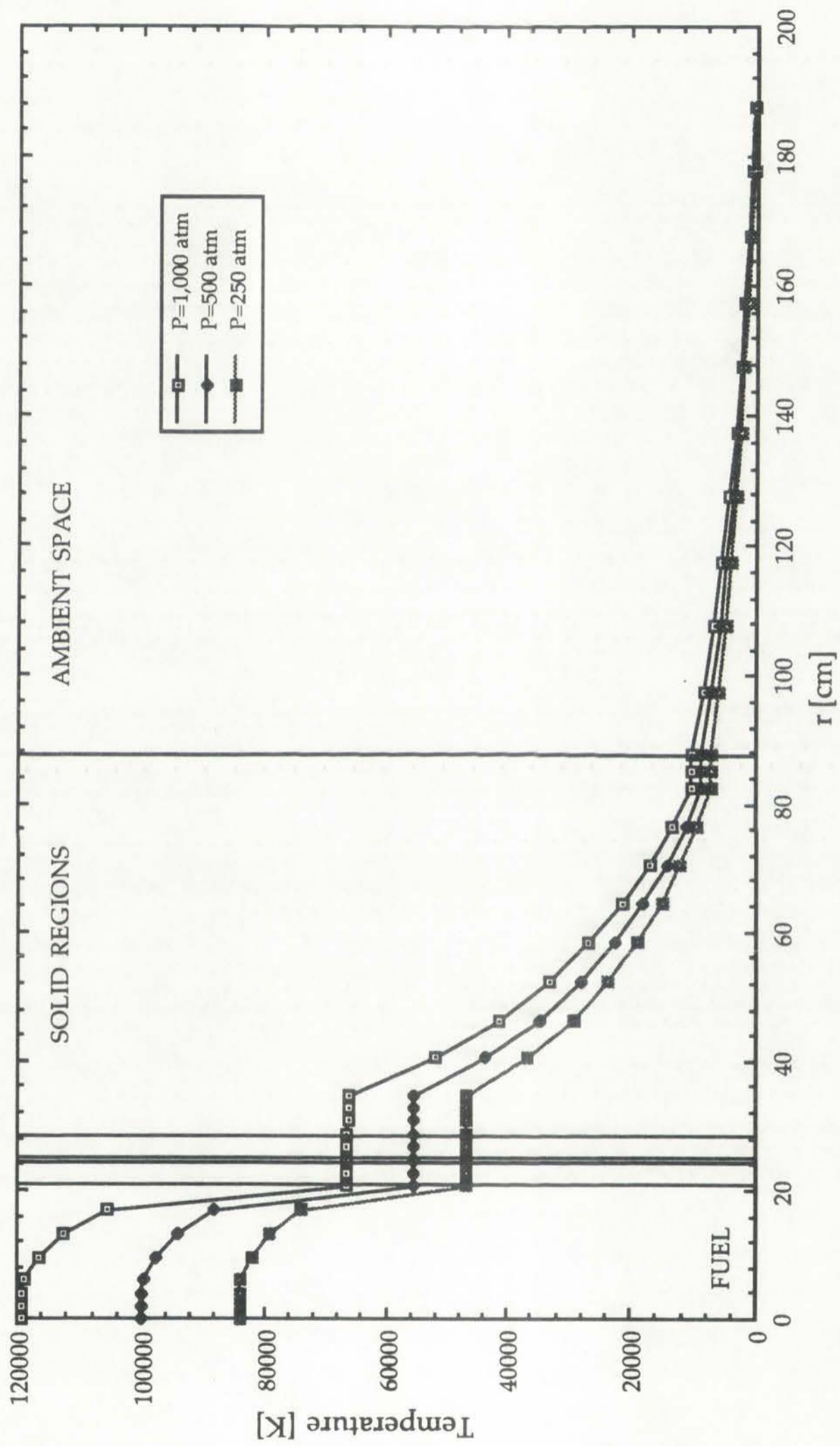


Figure 10.4: $T(r)$ for 500 MWth, Hansen-Roach library, comprehensive thermal analysis.



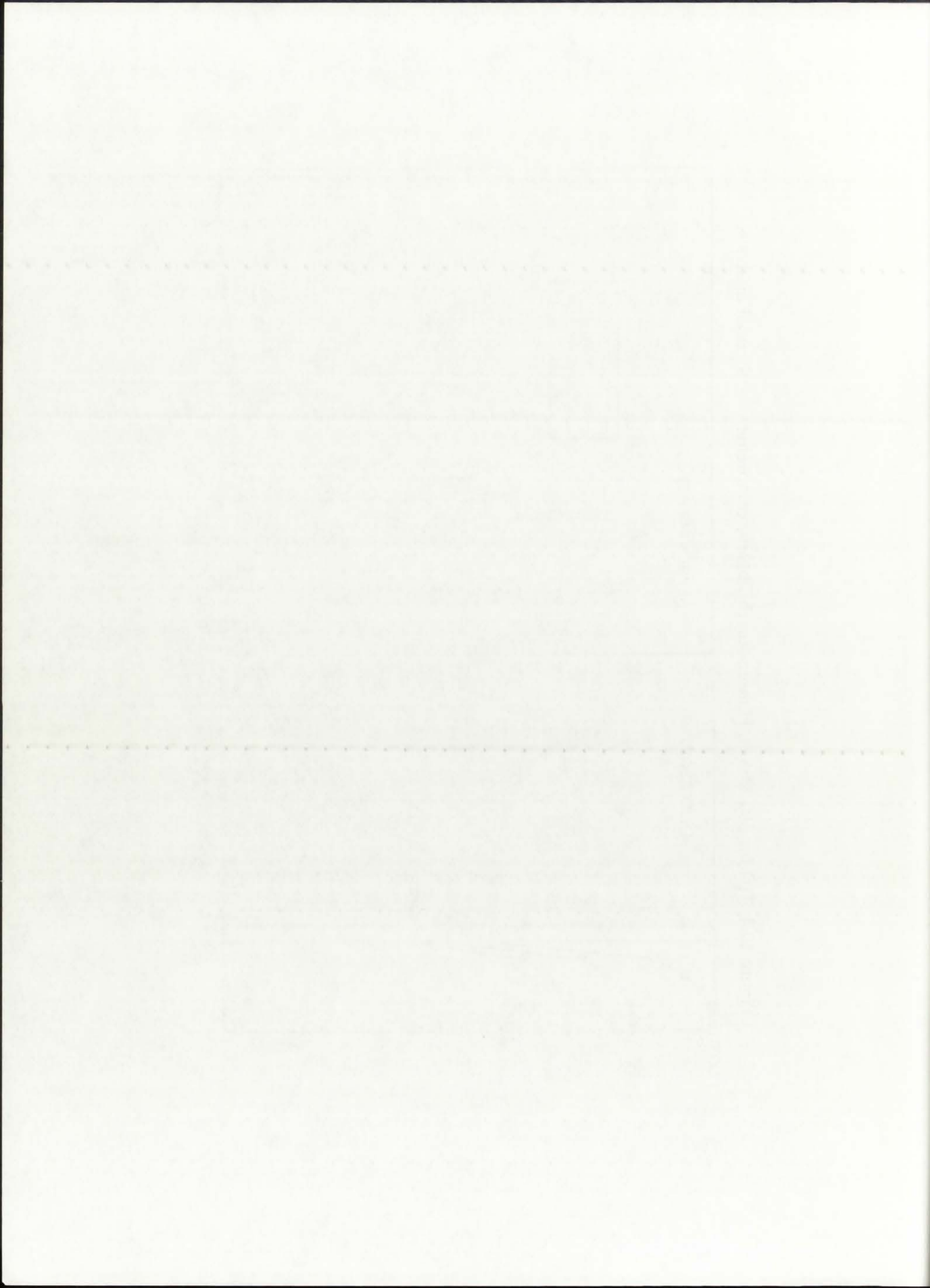


TABLE 10.2
 Summary of the comprehensive thermal analysis results
 (500 MWth configuration, Hansen-Roach library)

P=250 atm

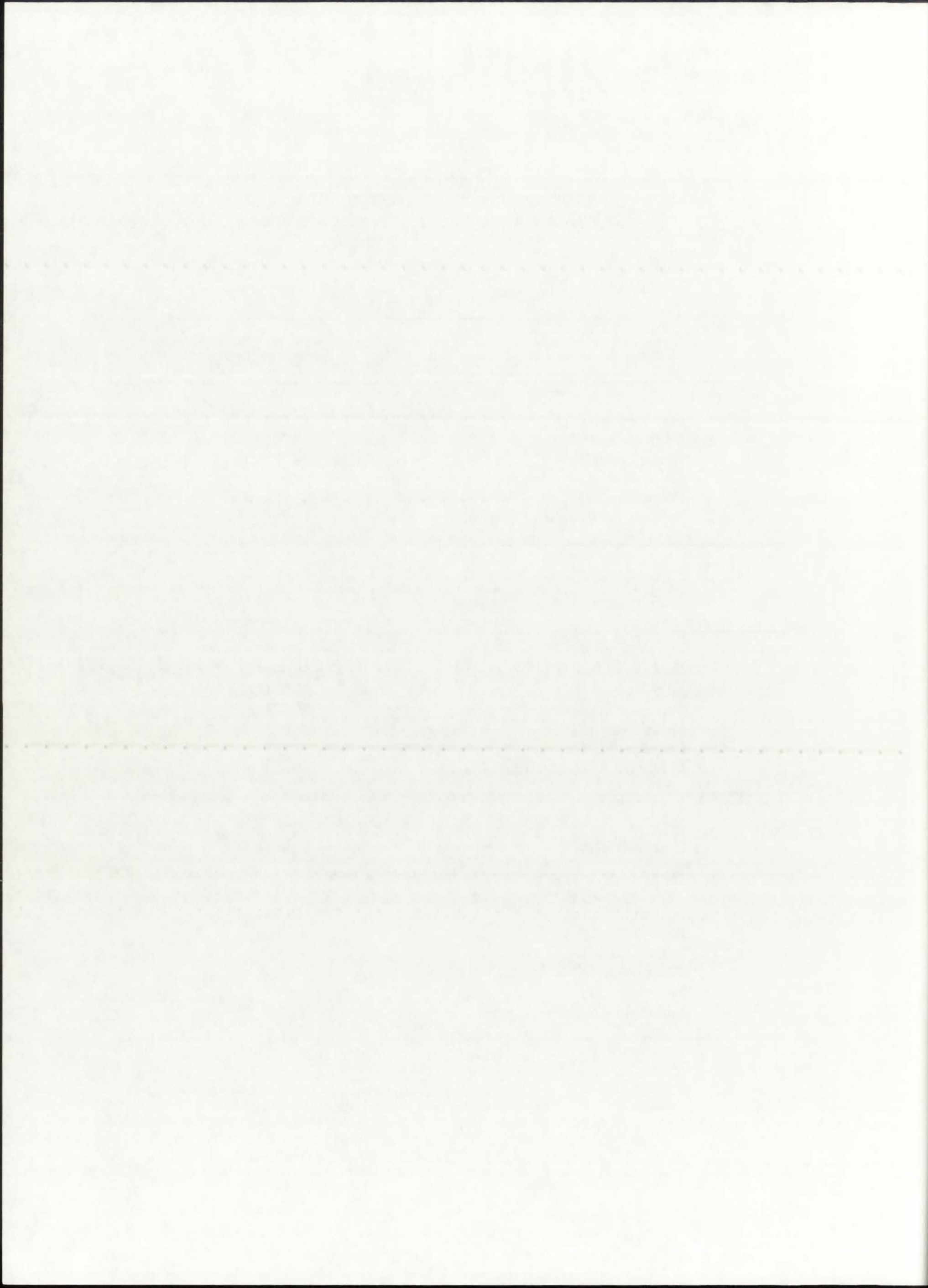
NLB engine region	Temperature
Fuel Centerline [K]	83,970
Edge-of-Fuel [K]	46,757
Buffer Gas [K]	46,756
Silica Wall [K]	42,756
Propellant [K]	42,756
Moderator/Reflector Liner [K]	42,732

P=500 atm

Fuel Centerline [K]	99,891
Edge-of-Fuel [K]	55,574
Buffer Gas [K]	55,573
Silica Wall [K]	55,573
Propellant [K]	55,573
Moderator/Reflector Liner [K]	55,545

P=1,000 atm

Fuel Centerline [K]	119,360
Edge-of-Fuel [K]	66,320
Buffer Gas [K]	66,320
Silica Wall [K]	66,320
Propellant [K]	66,320
Moderator/Reflector Liner [K]	66,286



The feasibility of the NLB concept in 500 MWth configuration can be discussed on the basis of the data shown in Figure 10.4 and summarized in Table 10.2. If it were possible to have only radiation heat transfer in the gases and conduction in the silica wall, with an ideal reflective liner on the solid regions (i.e., $\text{reflBe}=100\%$), a 500 MWth configuration would probably encounter a problem with maintaining the silica wall below melting temperature. Since convection is also present in both the buffer gas and propellant regions, two major problem areas arise: (1) melting of the silica wall, and (2) melting of the entire solid moderator/reflector assembly. In light of the extremely high temperatures calculated for the silica wall and the solid regions, it is unlikely that any cooling method currently available would be able to maintain either of the regions below their respective melting points.

On the basis of the available results, it can be concluded that the 500 MWth configuration of the NLB engine would not be feasible due to the extremely high temperatures within the silica wall and solid moderator/reflector regions. The GNRATR-1D summary output files for the 500 MWth executions can be found in Appendix B.2.

10.3.2. ENDF/B-V Library

The second set of analyses involving the 500 MWth configuration were performed with the temperature-dependent ENDF/B-V cross-section library. The converged $Qg'''(r)$ distribution is presented in Figure 10.5. Observation of Figure 10.5 indicates that the bulk of the volumetric heat generation, and therefore the bulk of the fissions, occurs in the region between $r=4$ cm and $r=17$ cm, similar to the Hansen-Roach case. The difference in magnitude of $Qg'''(r)$ between the Hansen-Roach and ENDF/B-V cases is very small, approximately 0.5%. The ENDF/B-V case results in a slightly greater $Qg'''(r)$ at the outer edge of the fuel; this could possibly be due to the lower thermal neutron energy cutoff of the ENDF/B-V library, which could allow for a larger fission cross-section for the sub-0.025 eV neutrons and therefore effectively increase the rate of fission at the outer edge of the fuel.

The first part of the report deals with the general situation in the region of the ...

The second part of the report deals with the specific situation in the region of the ...

The third part of the report deals with the specific situation in the region of the ...

The fourth part of the report deals with the specific situation in the region of the ...

The fifth part of the report deals with the specific situation in the region of the ...

The sixth part of the report deals with the specific situation in the region of the ...

The seventh part of the report deals with the specific situation in the region of the ...

The eighth part of the report deals with the specific situation in the region of the ...

The ninth part of the report deals with the specific situation in the region of the ...

The tenth part of the report deals with the specific situation in the region of the ...

The eleventh part of the report deals with the specific situation in the region of the ...

The twelfth part of the report deals with the specific situation in the region of the ...

The thirteenth part of the report deals with the specific situation in the region of the ...

The fourteenth part of the report deals with the specific situation in the region of the ...

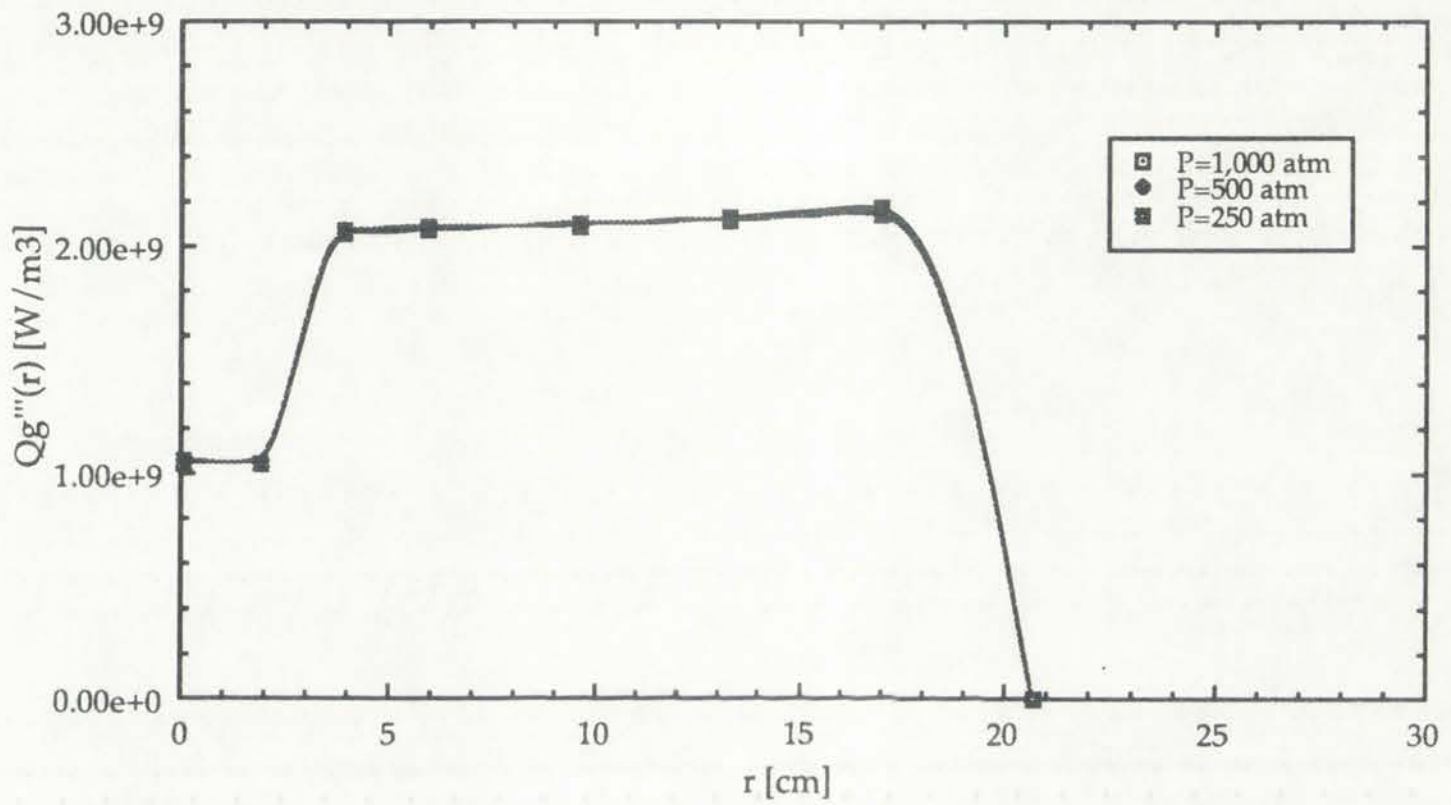
The fifteenth part of the report deals with the specific situation in the region of the ...

The sixteenth part of the report deals with the specific situation in the region of the ...

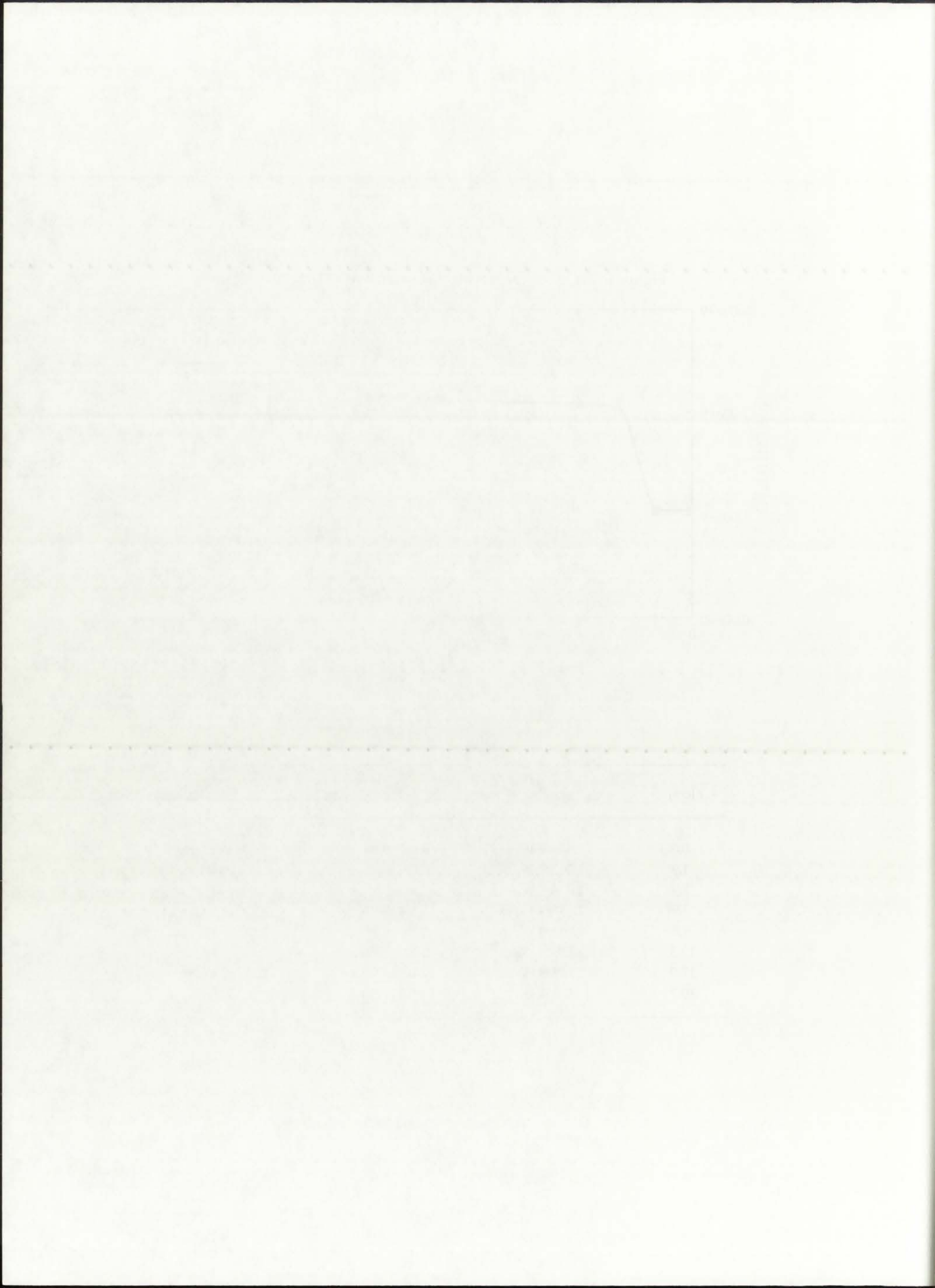
The seventeenth part of the report deals with the specific situation in the region of the ...

The eighteenth part of the report deals with the specific situation in the region of the ...

Figure 10.5: $Qg'''(r)$ for 500 MWth power level (ENDF/B-V library).



r [cm]	$Qg'''(r)$, $P=250$ atm	$Qg'''(r)$, $P=500$ atm	$Qg'''(r)$, $P=1,000$ atm
0.0	1.046e9 W/m ³	1.043e9 W/m ³	1.038e9 W/m ³
1.9	1.042e9 W/m ³	1.038e9 W/m ³	1.031e9 W/m ³
3.9	2.077e9 W/m ³	2.069e9 W/m ³	2.055e9 W/m ³
5.9	2.087e9 W/m ³	2.082e9 W/m ³	2.073e9 W/m ³
9.6	2.100e9 W/m ³	2.099e9 W/m ³	2.095e9 W/m ³
13.3	2.119e9 W/m ³	2.122e9 W/m ³	2.127e9 W/m ³
17.0	2.149e9 W/m ³	2.159e9 W/m ³	2.177e9 W/m ³
20.7	0.0 W/m ³	0.0 W/m ³	0.0 W/m ³



The TRANSX input files for the ENDF/B-V cases of the 500 MWth configuration are provided in Appendix B.3. The ONEDANT input files are provided in Appendix B.4. As with the Hansen-Roach case, the appropriate fuel atomic densities are on the order of 10^{-6} - 10^{-7} [atoms/barn-cm], due to the high temperature of the fuel. The increase in $Qg''(r)$ of the outer fuel nodes, i.e. a shift in $Qg'''(r)$ toward the outer edge of the fuel with increasing pressure, is noticeable as in the case of the Hansen-Roach data. The increase in fuel density, along with an appropriate increase in the macroscopic fission cross-section, at the outer edges provides for a greater fission rate and greater $Qg'''(r)$ at that location. The slight increase in $Qg'''(r)$ of the ENDF/B-V case compared to the Hansen-Roach case was discussed previously.

The calculated k_{eff} values of the 500 MWth configurations are shown in Figure 10.6. As with the Hansen-Roach case, the k_{eff} of the baseline design is low, due mainly to the low fuel density. With increasing pressure, the k_{eff} increases due to a larger fuel density, but is still significantly subcritical. As before, the baseline ONEDANT cases were modified by setting the hydrogen propellant atomic density to zero, thereby creating a vacuum zone in place of the hydrogen. The resultant k_{eff} values of the modified baseline design are also shown in Figure 10.6. As can be seen, for the extreme case of no propellant present, the increase in k_{eff} is approximately 10-15%. These increases in k_{eff} are in line with the behavior indicated by the Hansen-Roach library, and definitely provide credibility to the idea of the original UARL designers to reduce the hydrogen propellant cross-sectional area to neutron flow. Because the actual unit-cell NLB rocket engine would have propellant channels occupying 40% of the annular surface area, though, the increase in k_{eff} over the 100% subtending would be very small.

Comparison of the k_{eff} values provided by the Hansen-Roach and ENDF/B-V libraries indicate strong similarity, and thereby verify each other. By using the very-low energy group structure of the ENDF/B-V library, along with incorporation of temperature dependence through TRANSX processing, it has not been possible, however, to validate the expectation of the original UARL designers regarding the possible neutronicly beneficial effects of the

The first part of the report is devoted to a general survey of the situation in the country. It is followed by a detailed analysis of the economic and social conditions. The report concludes with a series of recommendations for the future.

The second part of the report is devoted to a detailed analysis of the economic and social conditions. It is followed by a series of recommendations for the future.

The third part of the report is devoted to a detailed analysis of the economic and social conditions. It is followed by a series of recommendations for the future.

The fourth part of the report is devoted to a detailed analysis of the economic and social conditions. It is followed by a series of recommendations for the future.

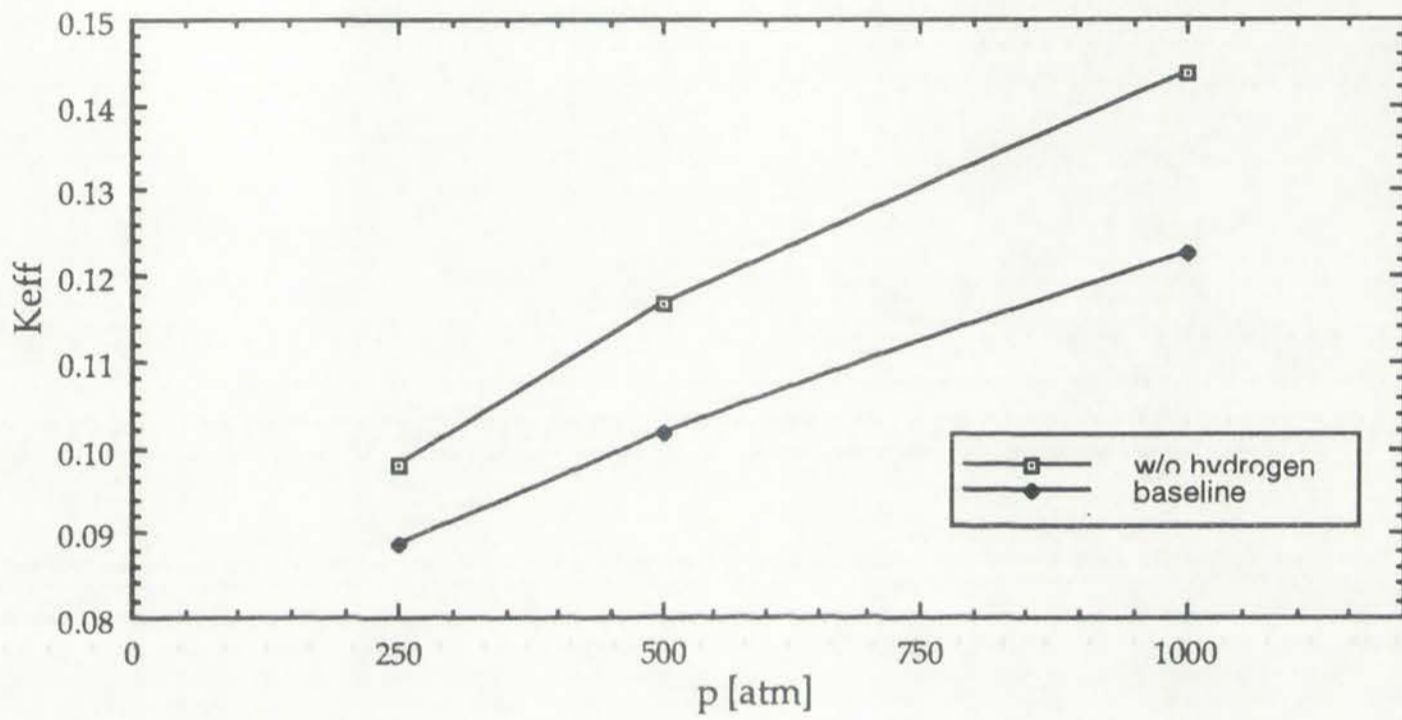
The fifth part of the report is devoted to a detailed analysis of the economic and social conditions. It is followed by a series of recommendations for the future.

The sixth part of the report is devoted to a detailed analysis of the economic and social conditions. It is followed by a series of recommendations for the future.

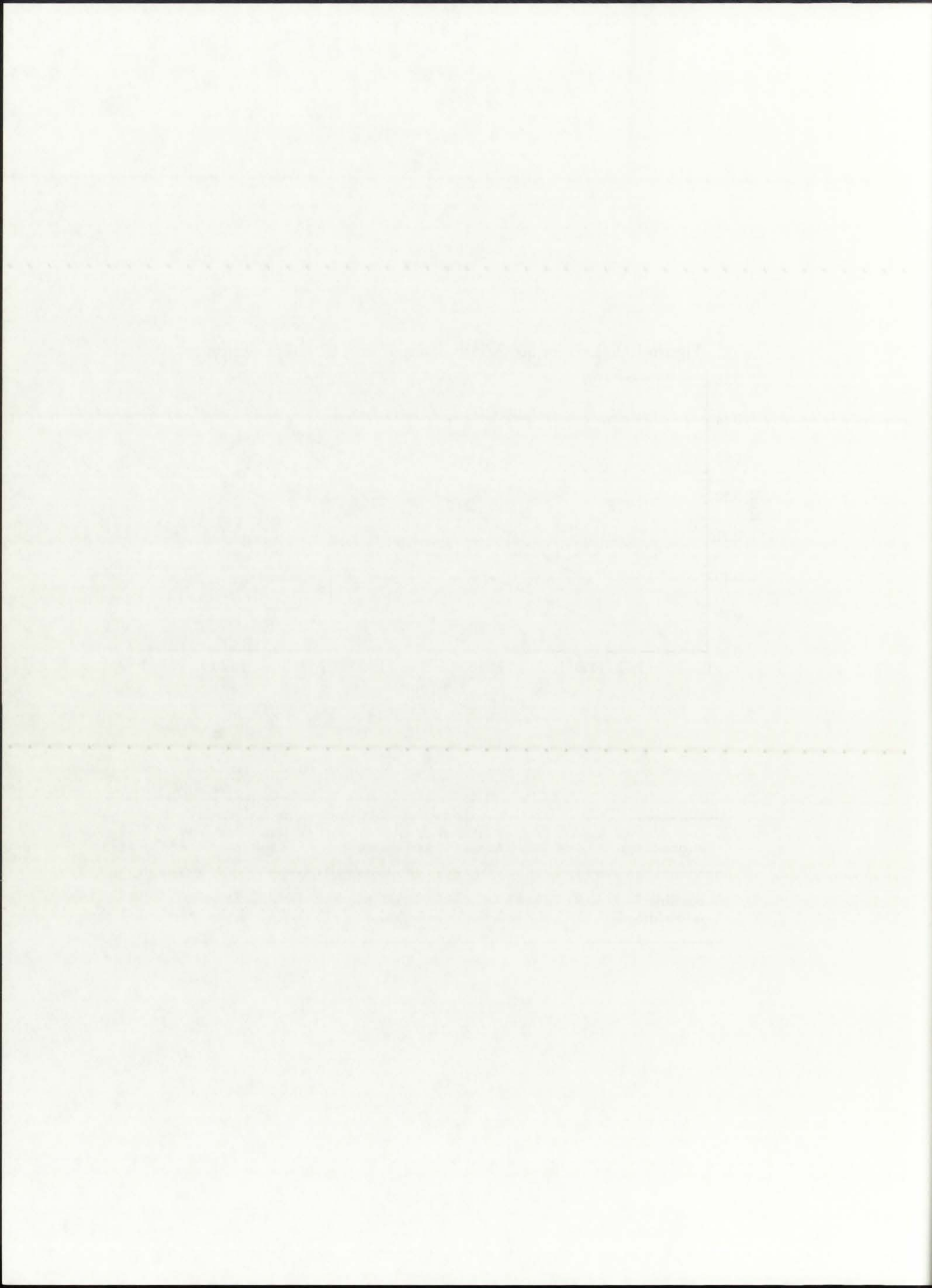
The seventh part of the report is devoted to a detailed analysis of the economic and social conditions. It is followed by a series of recommendations for the future.

The eighth part of the report is devoted to a detailed analysis of the economic and social conditions. It is followed by a series of recommendations for the future.

Figure 10.6: K_{eff} for 500 MWth configuration (ENDF/B-V library).



engine design	k_{eff} , $P=250$ atm	k_{eff} , $P=500$ atm	k_{eff} , $P=1,000$ atm
baseline	0.0886	0.1018	0.1226
w/o hydrogen	0.0978	0.1167	0.1436



low-temperature moderator and reflector. There does not seem to be any correlation between the existence of a 0.006 eV scattering cross-section cutoff in beryllium and a significant increase in the k_{eff} of the system, all other things held constant. This conclusion is based on the comparison of the k_{eff} values of the "baseline" designs using Hansen-Roach and ENDF/B-V libraries. One could ostensibly argue that the neutronic "transparency" of beryllium at $E \leq 0.006$ eV is effectively overshadowed by the thermal neutron diffusion barrier in the propellant; for that reason, both the Hansen-Roach and ENDF/B-V cases were also analyzed with a vacuum substituting for hydrogen in the propellant region. In both the Hansen-Roach and ENDF/B-V cases, slight increases in k_{eff} were evident, but not nearly significant enough to warrant special reliance on the low-temperature moderator/reflector.

In addition, segmentation of the propellant channels could not be relied on to provide a noticeable increase in k_{eff} for the same operating conditions and dimensions. By observing results for both the Hansen-Roach and ENDF/B-V cases, it can be concluded that in order to significantly increase the k_{eff} of the original unit-cell NLB engine for the 500 MWth configuration, it would be necessary to either increase the operating pressure beyond 1,000 atm (and therefore increase the fuel density) or increase the size of the fuel region. Neither segmentation of the propellant channels nor the incorporation of a low-temperature moderator/reflector assembly would increase the k_{eff} by much more than 10-20% over the baseline design (i.e., one with a 100% subtended annular propellant region and room-temperature or higher moderator/reflector).

Based on the $Qg'''(r)$ values, a converged $T(r)$ distribution was determined by GNRATR-1D for each of the three operating pressures, as shown in Figure 10.7. Radiation, convection, and conduction were accounted for in the non-fuel gaseous regions and a conservative condition of 0% reflection off the solid regions' reflective liner ($\text{reflBe}=0\%$) was assumed. As can be seen, the general shape of $T(r)$ is similar for all three operating pressures, and is similar in magnitude to the $T(r)$ obtained with the Hansen-Roach library. The latter, of course, is due to the very similar $Qg'''(r)$ distribution.

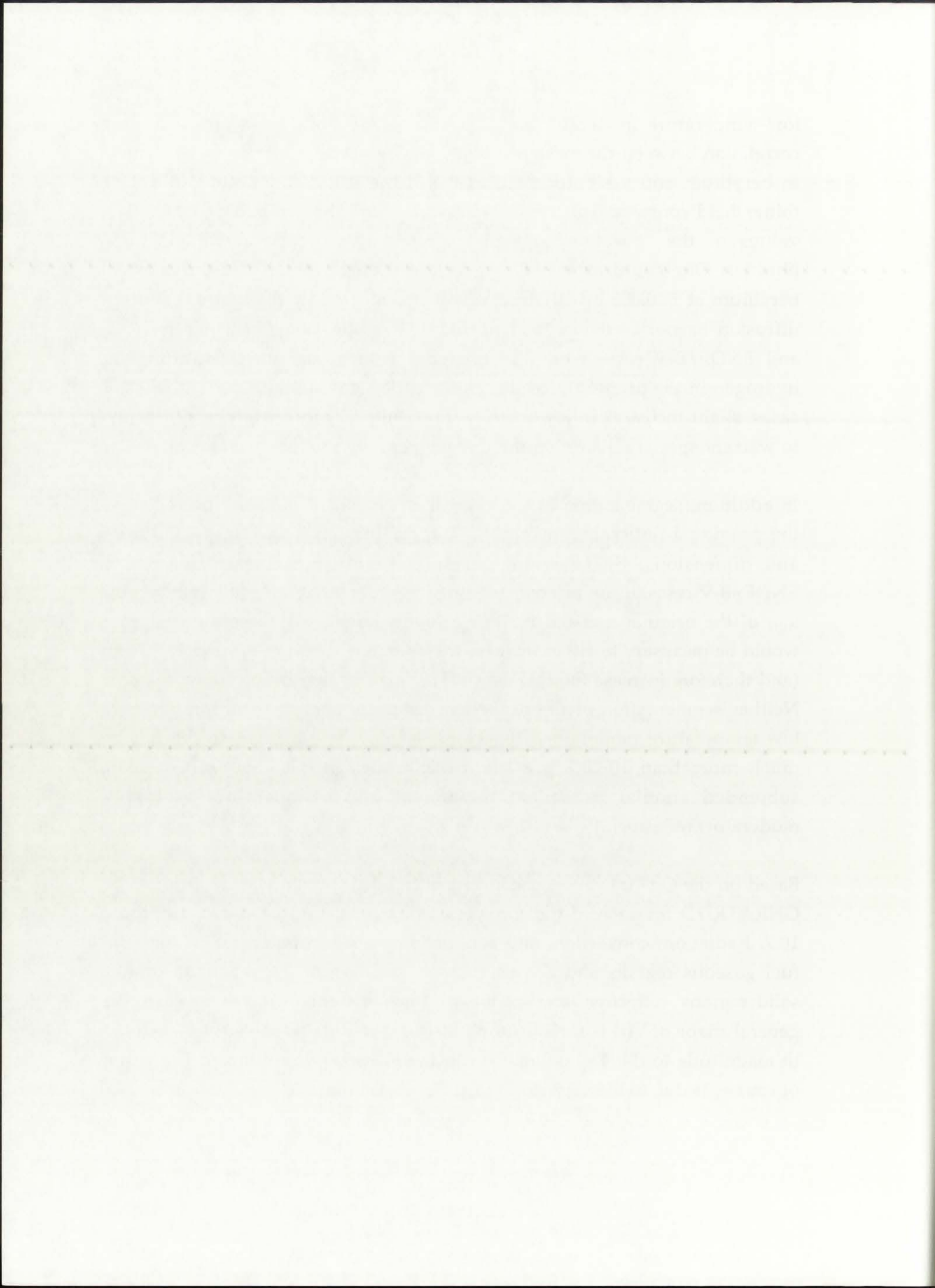
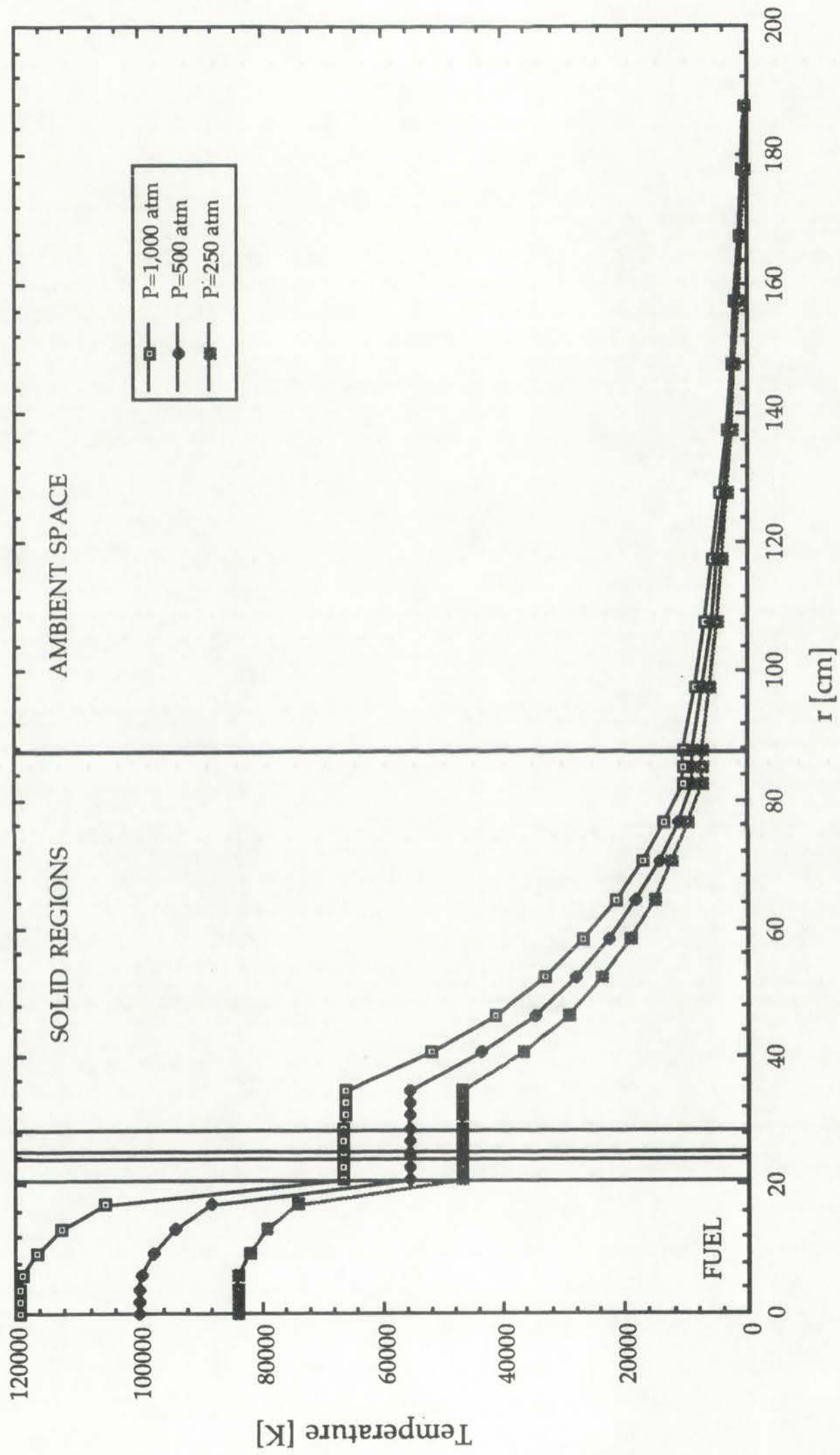


Figure 10.7: $T(r)$ for 500 MWth, ENDF/B-V library, comprehensive thermal analysis.



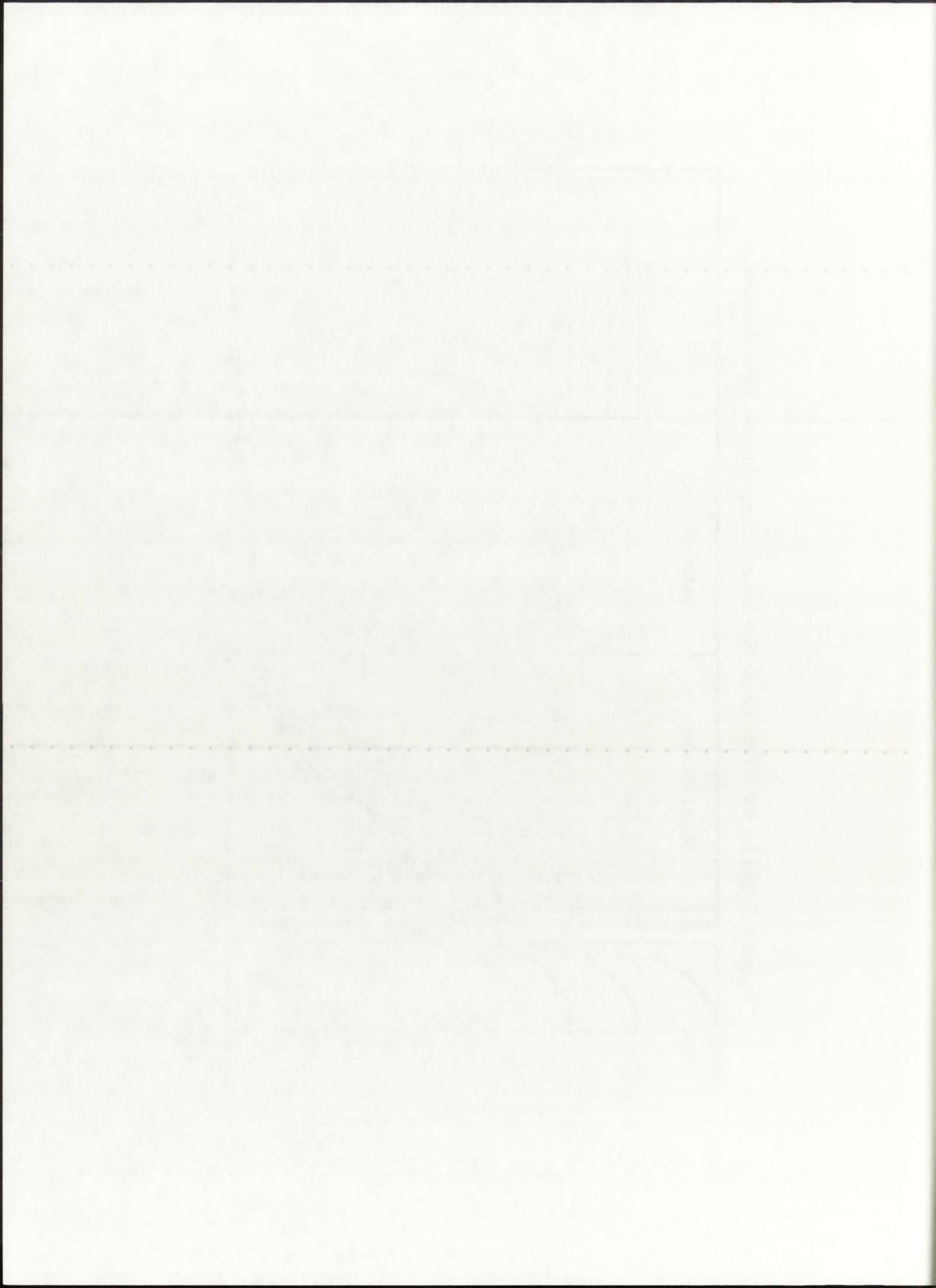


TABLE 10.3
Summary of the comprehensive thermal analysis results
(500 MWth configuration, Hansen-Roach library)

P=250 atm

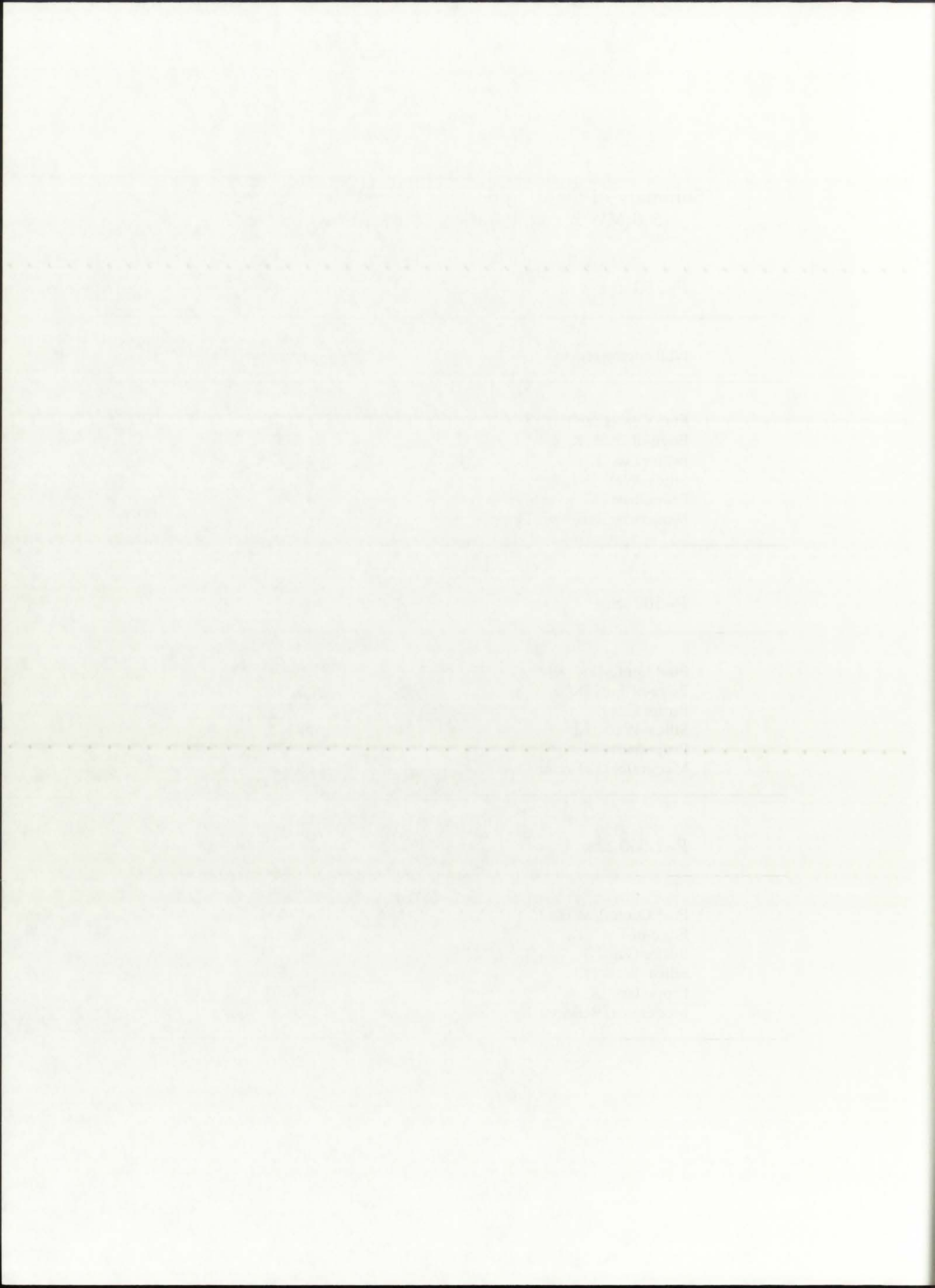
NLB engine region	Temperature
Fuel Centerline [K]	83,970
Edge-of-Fuel [K]	46,757
Buffer Gas [K]	46,757
Silica Wall [K]	42,757
Propellant [K]	42,757
Moderator/Reflector Liner [K]	42,733

P=500 atm

Fuel Centerline [K]	99,897
Edge-of-Fuel [K]	55,574
Buffer Gas [K]	55,573
Silica Wall [K]	55,573
Propellant [K]	55,573
Moderator/Reflector Liner [K]	55,545

P=1,000 atm

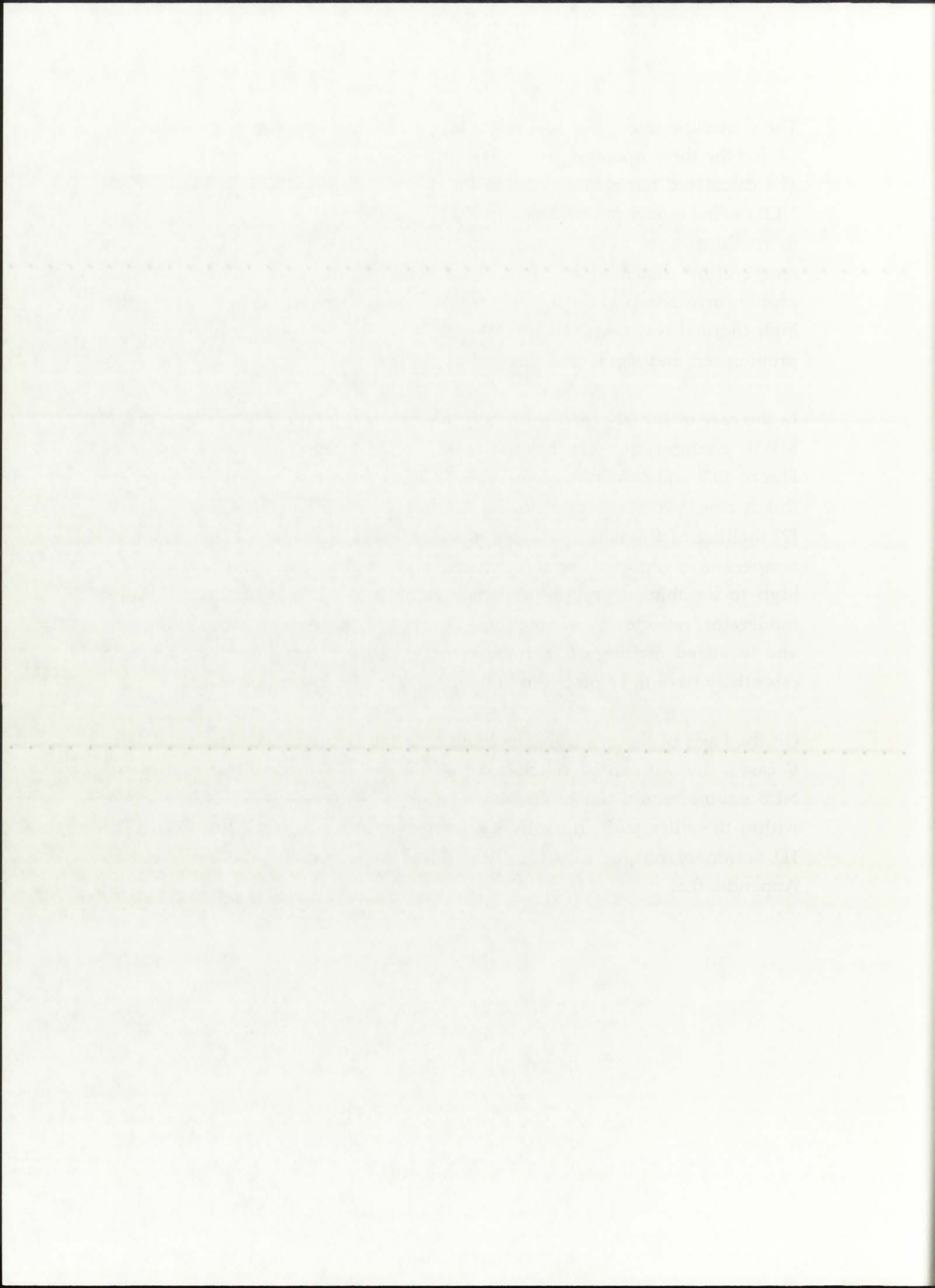
Fuel Centerline [K]	119,354
Edge-of-Fuel [K]	66,320
Buffer Gas [K]	66,320
Silica Wall [K]	66,320
Propellant [K]	66,320
Moderator/Reflector Liner [K]	66,286



The centerline-to-edge of fuel temperature ratio is approximately constant at 1.8 for the three operating pressures, again similar to the Hansen-Roach case. The calculated temperature values for the major regions within the unit-cell NLB engine model can be found in Table 10.3. Because of the very low overall thermal resistance of the buffer gas, silica wall, and propellant regions, the temperature distribution across those three regions is virtually flat. That profile corresponds to the temperature plateau of Figure 10.7. In the regions of high thermal resistance, such as the fuel and D₂O, the temperature drop is pronounced and significant.

In the case of the ENDF/B-V library, the feasibility of the NLB concept in 500 MWth configuration can be discussed on the basis of the data shown in Figure 10.7 and summarized in Table 10.3. As was discussed for the Hansen-Roach case, two major problem areas arise: (1) melting of the silica wall, and (2) melting of the entire solid moderator/reflector assembly. The very high temperatures reported for the *uncooled* solid regions are most probably too high to be able to provide adequate cooling so as to maintain the entire moderator/reflector below melting. To prevent the appearance of hot-spots and localized melting of the moderator/reflector, that whole region would essentially have to be placed in motion, i.e., act as its own coolant.

On the basis of the available results in both the Hansen-Roach and ENDF/B-V cases, then, it can be concluded that the 500 MWth configuration of the NLB engine would not be feasible due to the extremely high temperatures within the silica wall and solid moderator/reflector regions. The GNRATR-1D summary output files for the 500 MWth executions can be found in Appendix B.5.



10.4. The 5 MWth Configuration

The 5 MWth configuration was chosen as a mid-point, two orders of magnitude less than the upper-limit 500 MWth, and two orders of magnitude greater than the lower-limit 50 kWth. This power level was not identified as having been analyzed as part of any previous published work, so there is an added interest in determining the thermal and neutronics parameters associated with the 5 MWth power level.

The iterative solution procedure was applied for the 5 MWth configuration in the same manner as for the 500 MWth configuration. An initial volumetric heat generation rate of 2.03×10^7 [W/m³] (two orders of magnitude less than for the 500 MWth level) was set at all seven fuel nodes. Based on the temperatures calculated by GNRATR-1D, appropriate material atomic densities were provided to ONEDANT. The resultant volumetric heat generation rates $Qg'''(r)$ were then provided to GNRATR-1D, for a new temperature distribution. This procedure was carried out separately for both the Hansen-Roach cross-sections and the ENDF/B-V cross-sections. The results of these analyses are presented in the following two subsections.

10.4.1. Hansen-Roach Library

The first set of analyses involving the 5 MWth configuration were performed with the Hansen-Roach cross-section library accessed by ONEDANT. Following completion of the iterative solution procedure, a converged set of $Qg'''(r)$, $T(r)$, and k_{eff} values were obtained. The converged $Qg'''(r)$ distribution for 5 MWth and three operating pressures, $P=250, 500,$ and $1,000$ atm, is shown in Figure 10.8. The particular values of $Qg'''(i)$ for the seven fuel nodes are also provided in tabular format as part of Figure 10.8. Observation of Figure 10.8 indicates that a more significant fraction of the heat generation, and therefore the rate of fission, takes place on the outer edge of the fuel region. An almost-flat $Qg'''(r)$ profile still exists between $r=4$ cm and $r=17$ cm, but a reduction in $Qg'''(r)$ near the centerline is offset by a pronounced peak in $Qg'''(r)$ between $r=15$ cm and $r=18$ cm.

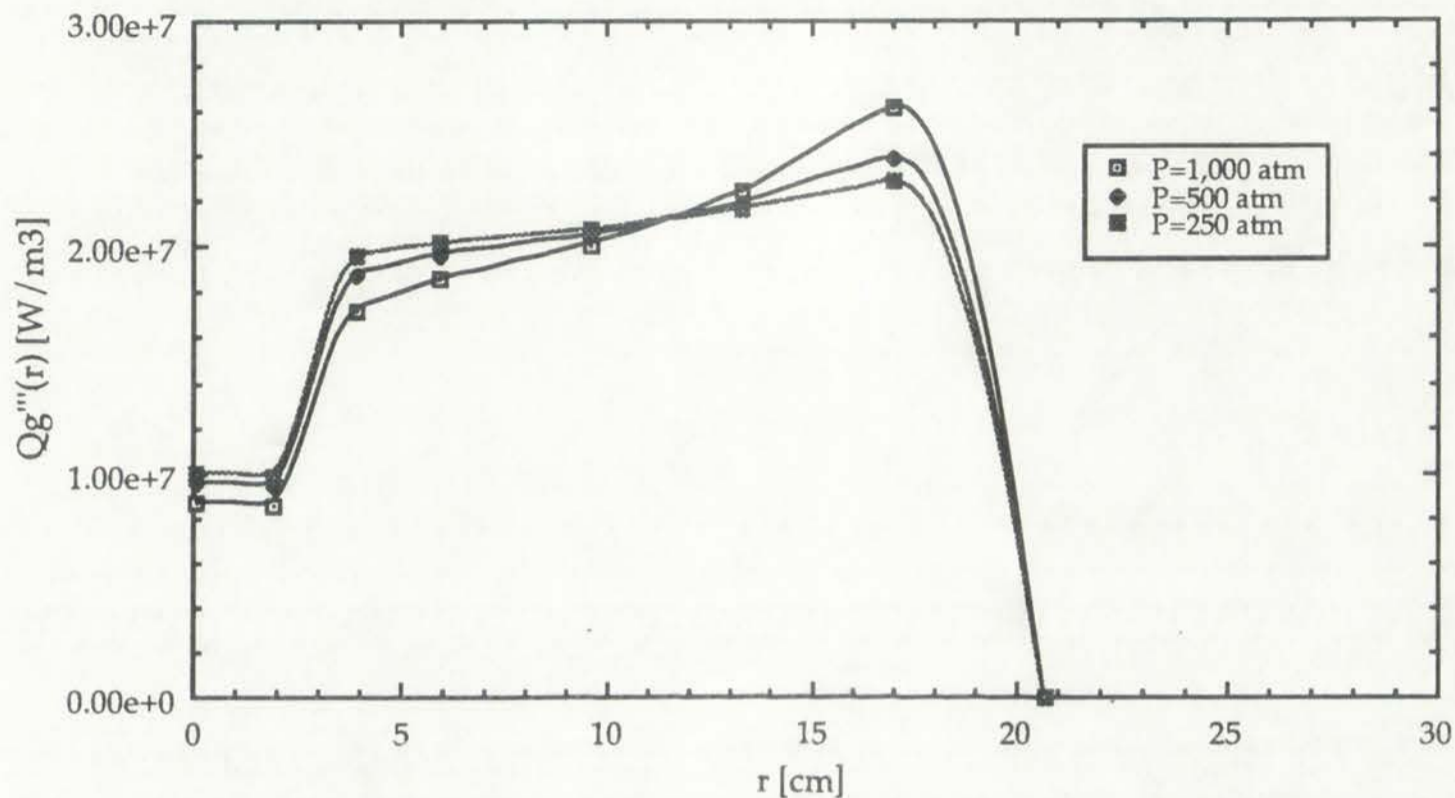
THE HISTORY OF THE

The history of the world is a long and varied one, and it is not possible to give a full account of it in a few pages. The world has been the scene of many great events, and it has been the home of many great men. The history of the world is a story of progress and of struggle, of triumph and of defeat. It is a story of the human race, and of the things that it has done and that it is doing. The history of the world is a story of the human mind, and of the things that it has thought and that it is thinking. The history of the world is a story of the human heart, and of the things that it has felt and that it is feeling. The history of the world is a story of the human soul, and of the things that it has done and that it is doing. The history of the world is a story of the human race, and of the things that it has done and that it is doing. The history of the world is a story of the human mind, and of the things that it has thought and that it is thinking. The history of the world is a story of the human heart, and of the things that it has felt and that it is feeling. The history of the world is a story of the human soul, and of the things that it has done and that it is doing.

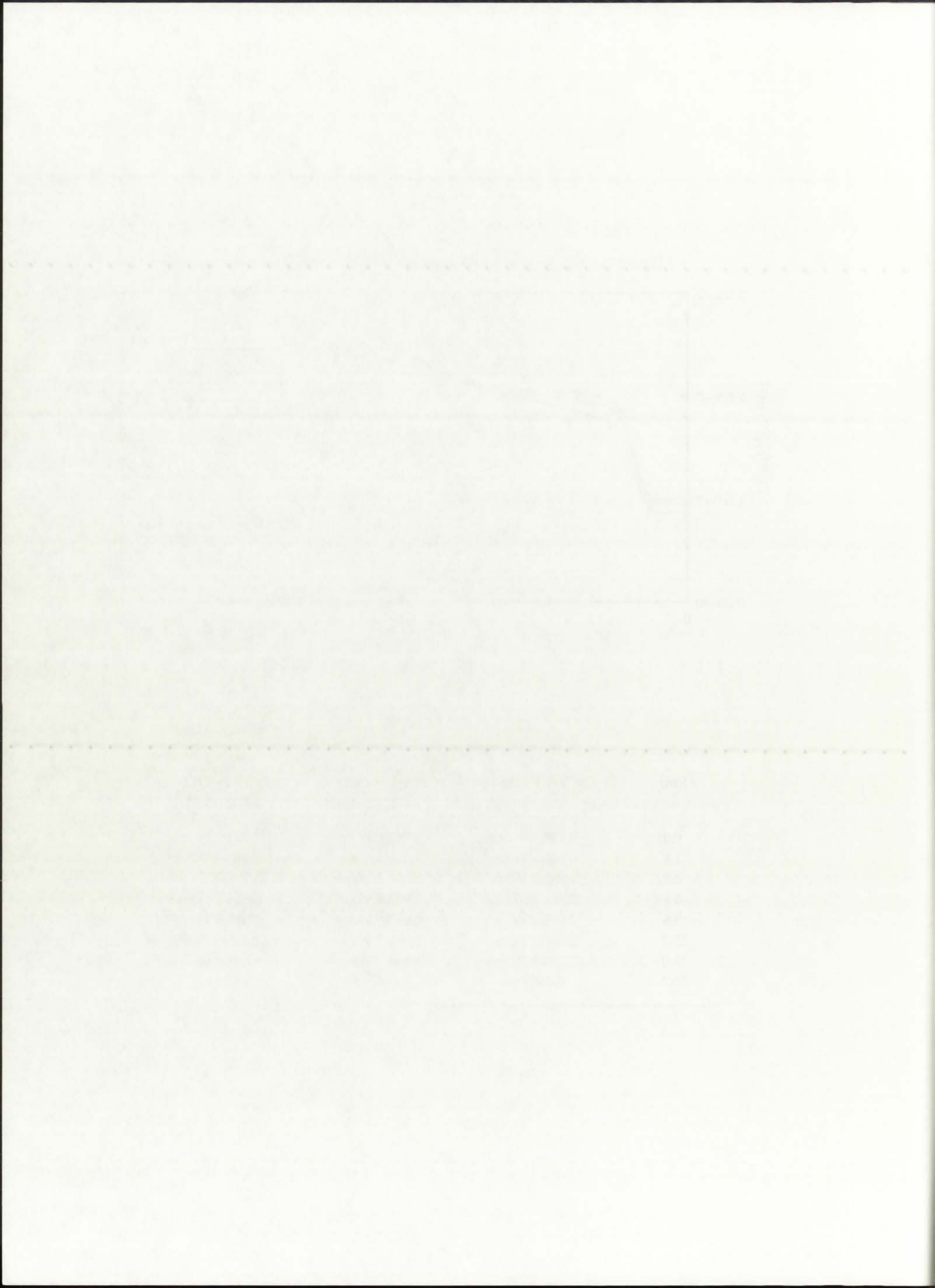
THE HISTORY OF THE

The history of the world is a long and varied one, and it is not possible to give a full account of it in a few pages. The world has been the scene of many great events, and it has been the home of many great men. The history of the world is a story of progress and of struggle, of triumph and of defeat. It is a story of the human race, and of the things that it has done and that it is doing. The history of the world is a story of the human mind, and of the things that it has thought and that it is thinking. The history of the world is a story of the human heart, and of the things that it has felt and that it is feeling. The history of the world is a story of the human soul, and of the things that it has done and that it is doing. The history of the world is a story of the human race, and of the things that it has done and that it is doing. The history of the world is a story of the human mind, and of the things that it has thought and that it is thinking. The history of the world is a story of the human heart, and of the things that it has felt and that it is feeling. The history of the world is a story of the human soul, and of the things that it has done and that it is doing.

Figure 10.8: $Qg'''(r)$ for 5 MWth power level (Hansen-Roach library).



r [cm]	$Qg'''(r)$, $P=250$ atm	$Qg'''(r)$, $P=500$ atm	$Qg'''(r)$, $P=1,000$ atm
0.0	$9.984e6$ W/m ³	$9.587e6$ W/m ³	$8.739e6$ W/m ³
1.9	$9.840e6$ W/m ³	$9.418e6$ W/m ³	$8.566e6$ W/m ³
3.9	$1.964e7$ W/m ³	$1.883e7$ W/m ³	$1.726e7$ W/m ³
5.9	$2.014e7$ W/m ³	$1.962e7$ W/m ³	$1.856e7$ W/m ³
9.6	$2.077e7$ W/m ³	$2.057e7$ W/m ³	$2.011e7$ W/m ³
13.3	$2.164e7$ W/m ³	$2.193e7$ W/m ³	$2.243e7$ W/m ³
17.0	$2.288e7$ W/m ³	$2.396e7$ W/m ³	$2.617e7$ W/m ³
20.7	0.0 W/m ³	0.0 W/m ³	0.0 W/m ³



The appearance of a peak in $Qg'''(r)$, as compared to the 500 MWth configuration, is due to the increase in fuel density as a result of a decrease in fuel temperature. For the 5 MWth configuration, the fuel density [atoms/barn-cm] is high enough that a significant amount of fissions occurs in the outer edges of the fuel region. Since the units of $Qg'''(r)$ are energy rate per unit volume, the total number of fissions occurring at the outer edges of the fuel region is actually much greater than depicted by the peak in Figure 10.8, because the volume of the annular regions of the fuel increases with increasing radial distance from the centerline (i.e., from $r=0$ to $r=20.7$ cm). The ONEDANT input files for the Hansen-Roach cases of the 5 MWth configuration are provided in Appendix C.1. Noticeable between the 500 MWth and the 5 MWth configurations is the pronounced decrease in $Qg'''(r)$ near the centerline as a function of operating pressure, for the 5 MWth configuration. This, again, is due to the conservation of total thermal power generated in the fuel, so that the decrease in $Qg'''(r)$ near the centerline accompanies the pronounced $Qg'''(r)$ peak at the outer edges of the fuel, with increasing operating pressure.

The calculated k_{eff} values are shown in Figure 10.9. The k_{eff} of the baseline design is definitely subcritical, although significantly greater than for the corresponding operating pressure of the 500 MWth engine. The increase in k_{eff} between the two power levels is primarily due to the increase in fuel density, resulting from a lower fuel temperature. For the modified baseline design, with a vacuum in place of the hydrogen, the increase in k_{eff} is approximately 10%, similar to the 500 MWth configuration. It can therefore be postulated that reduction of the hydrogen propellant surface area, and thus the cross-sectional area to neutron flow, definitely increases the k_{eff} of a given system. Unfortunately, due to the principal intent of the reactor, which is to transfer energy to a flowing propellant, the hydrogen propellant surface area must be significant in order to maximize heat transfer from the fuel. Therefore, the neutronics benefits of segmented propellant channels in an actual rocket engine would be far less pronounced than in this ideal analysis, probably increasing the k_{eff} by a few percent over the baseline 100% subtended channel design.

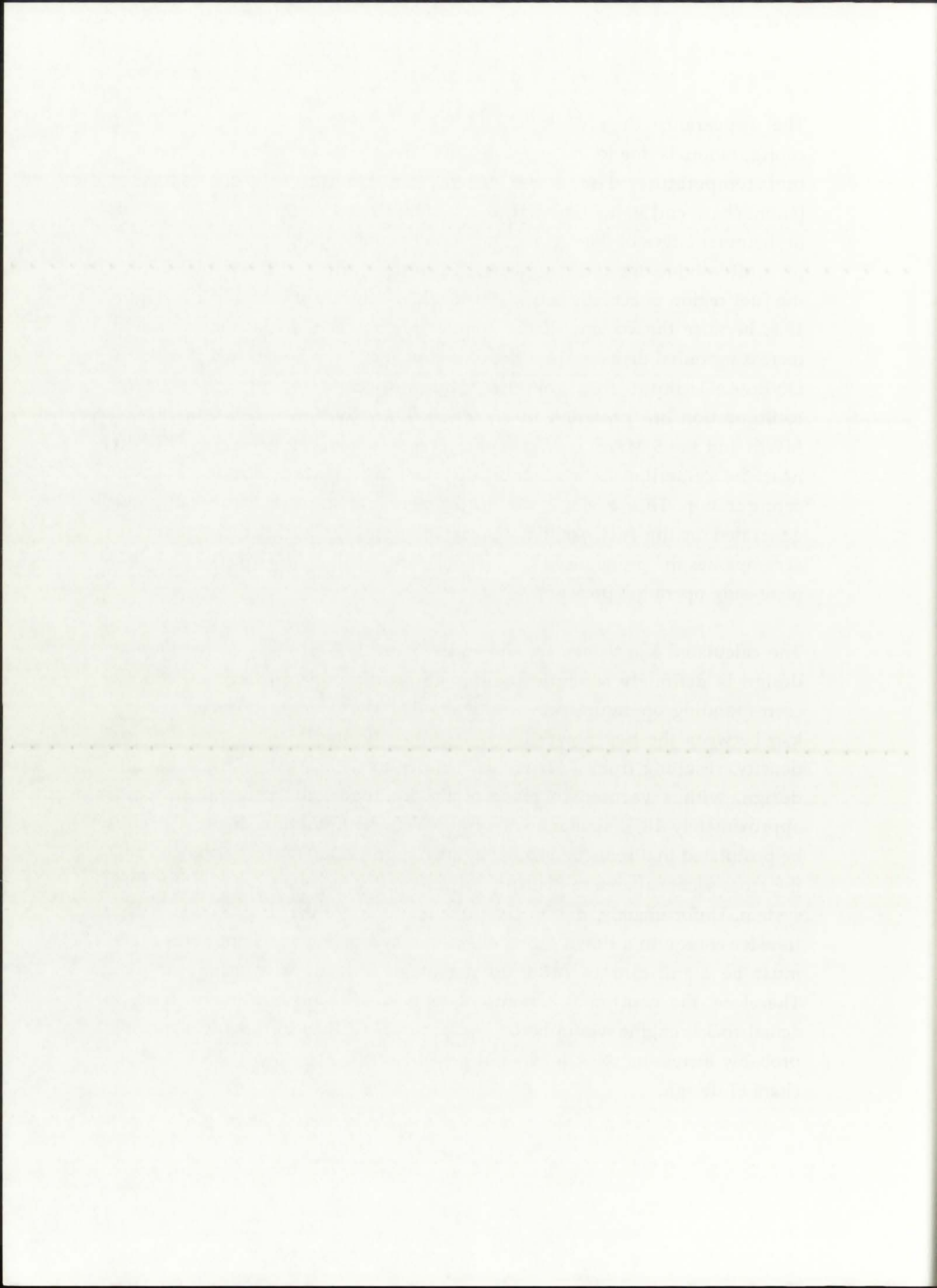
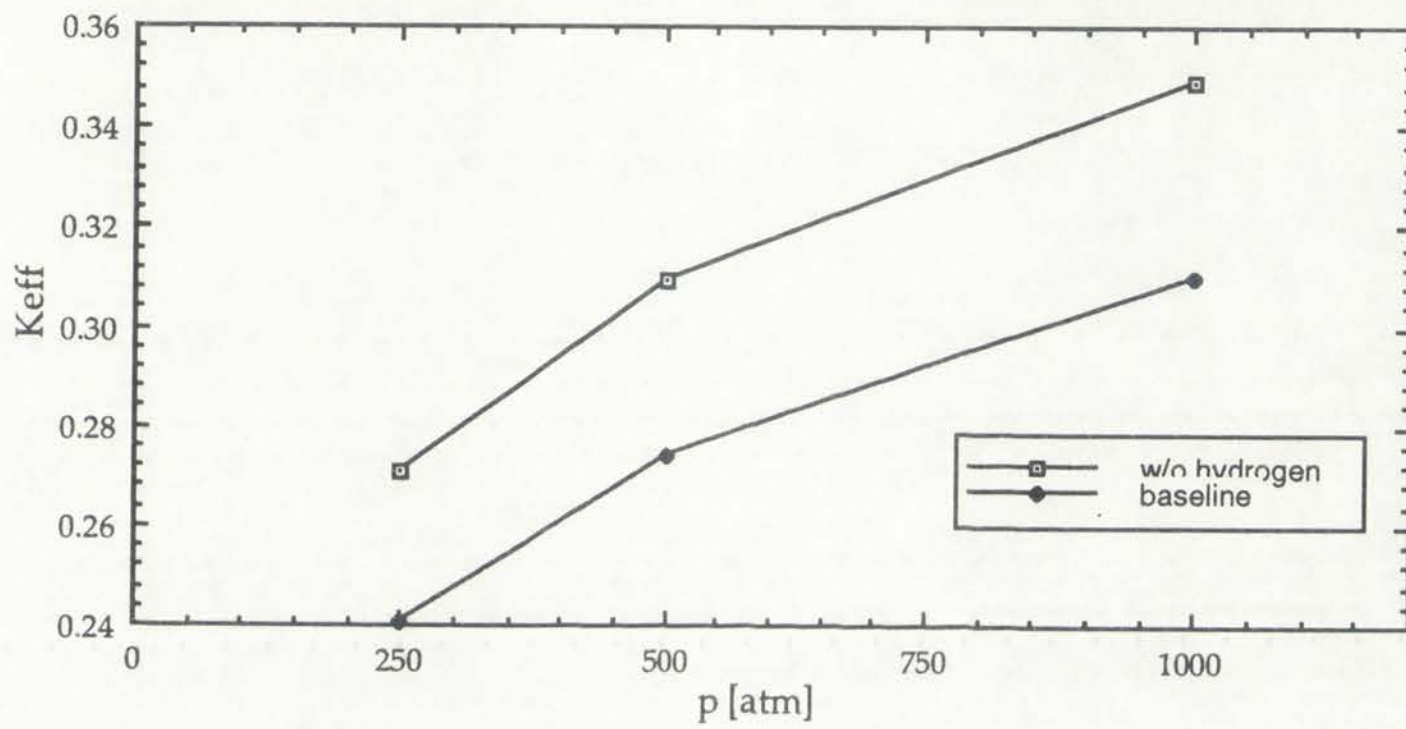
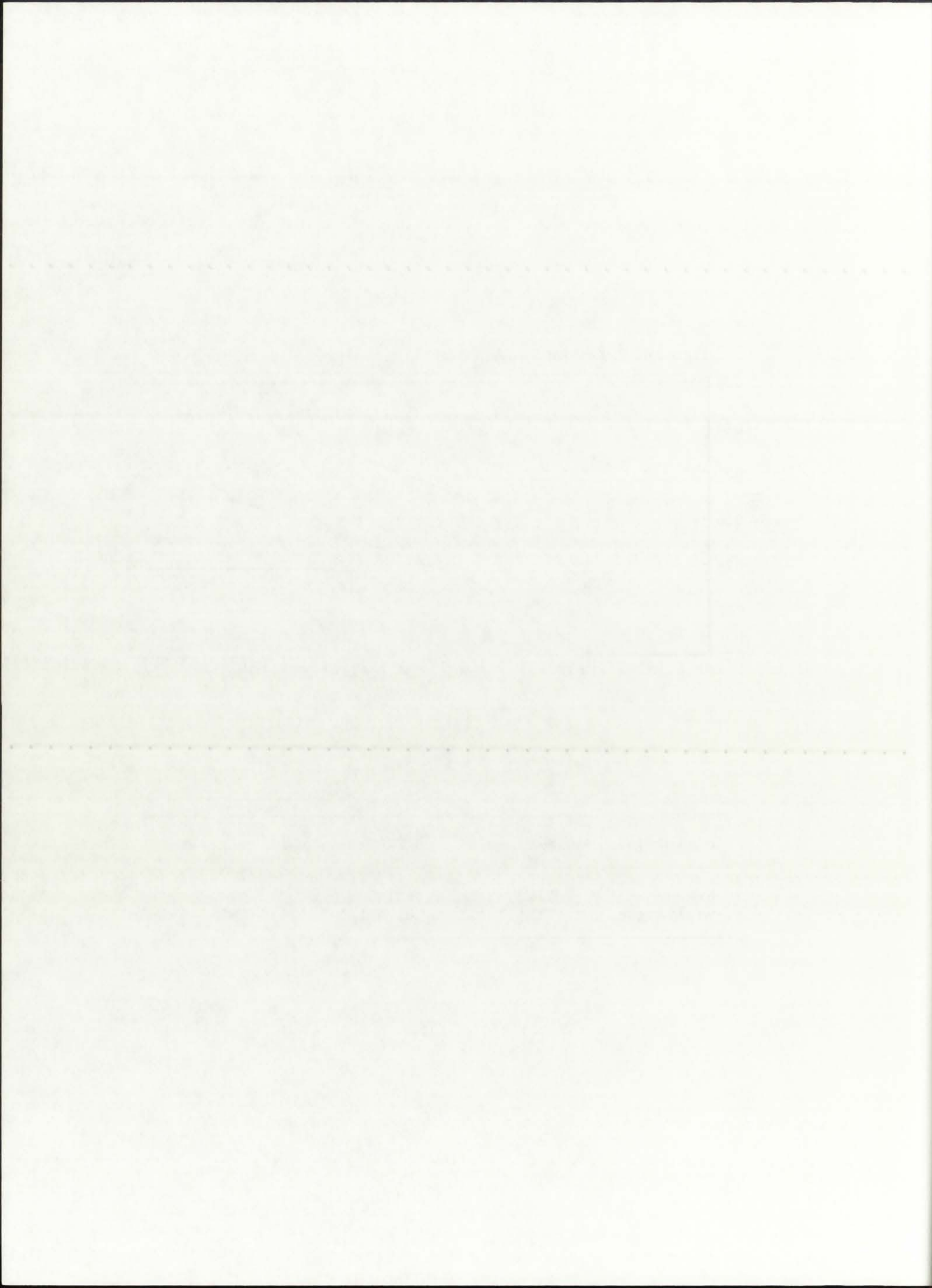


Figure 10.9: K_{eff} for 5 MWth configuration (Hansen-Roach library).



engine design	k_{eff} , P=250 atm	k_{eff} , P=500 atm	k_{eff} , P=1,000 atm
baseline	0.2406	0.2737	0.3099
w/o hydrogen	0.2708	0.3096	0.3489



In both the 500 MWth and 5 MWth configurations, then, segmentation of the propellant channels could not be relied on to provide a noticeable increase in k_{eff} for the same operating conditions and dimensions. In order to significantly increase the k_{eff} of the original unit-cell NLB engine for either the 500 MWth or the 5 MWth configuration, it would be necessary to either increase the operating pressure beyond 1,000 atm or increase the size of the fuel region. For either configuration/scenario combination, a major redesign of the original engine would therefore be necessary.

Based on the $Qg'''(r)$ values in the fuel region, a converged $T(r)$ distribution was determined by GNRATR-1D for each of the three operating pressures, as shown in Figure 10.10. Radiation, convection, and conduction were accounted for in the non-fuel gaseous regions, along with a conservative assumption of 0% reflection off the solid regions' reflective liner ($\text{reflBe}=0\%$). The fuel temperatures, naturally, are lower than for the 500 MWth configuration. Assuming that the rate of heat transfer in the fuel varies approximately as the fourth power of the temperature:

$$Q \approx T_{\text{fuel}}^4 \quad (10.1)$$

it can be stated that for a factor of 100 decrease in thermal power, the fuel temperature should be approximately 3.2 times less. This is almost exactly the ratio of the 500 MWth to 5 MWth fuel temperatures for a given operating pressure (3.15 on the average), confirming again the correctness of GNRATR-1D calculated data.

The calculated temperature values are given in Table 10.4. The temperature distribution across the buffer gas, silica wall, and propellant regions is virtually flat due to the very low overall thermal resistance of these three regions. The major component of the overall thermal resistance is the effective radiative conductivity, which is very large due to both the low opacity of these regions and the high temperature. The combination of radiative, convective, and conductive heat transfer through the three regions causes the resultant $T(r)$ shown in Figure 10.10 and Table 10.4.

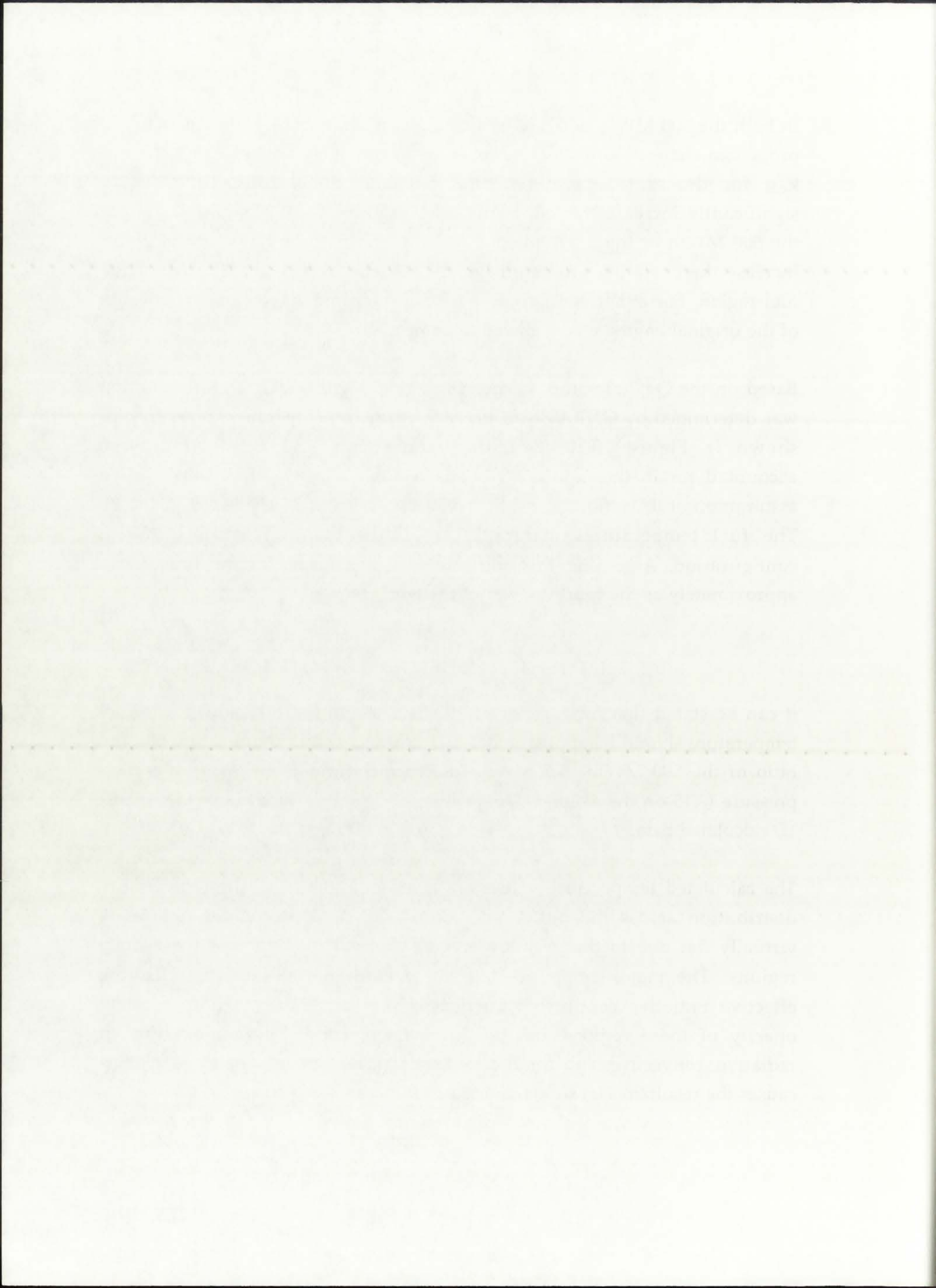
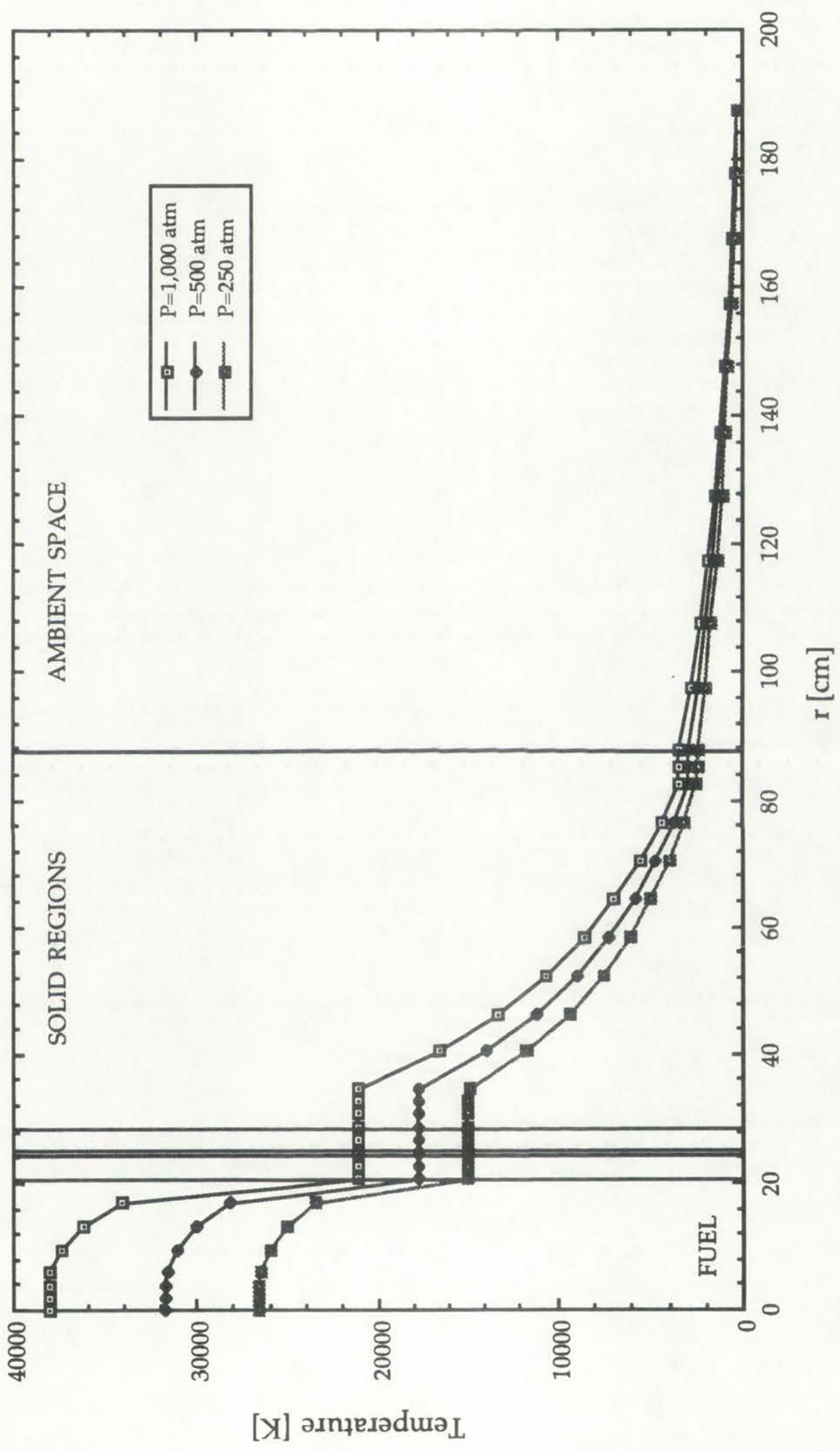


Figure 10.10: $T(r)$ for 5 MWth, Hansen-Roach library, comprehensive thermal analysis.



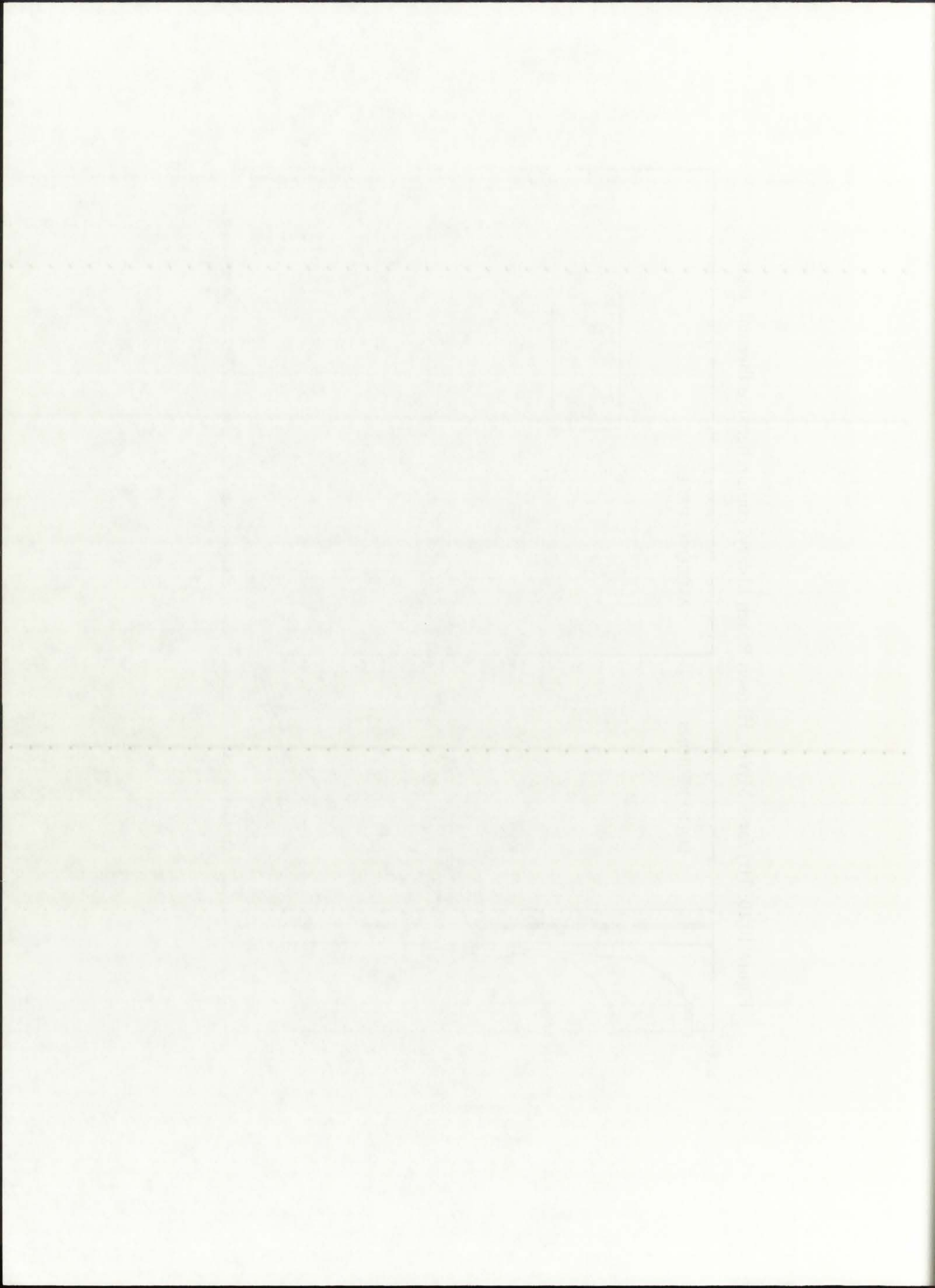


TABLE 10.4
 Summary of the comprehensive thermal analysis results
 (5 MWth configuration, Hansen-Roach library)

P=250 atm

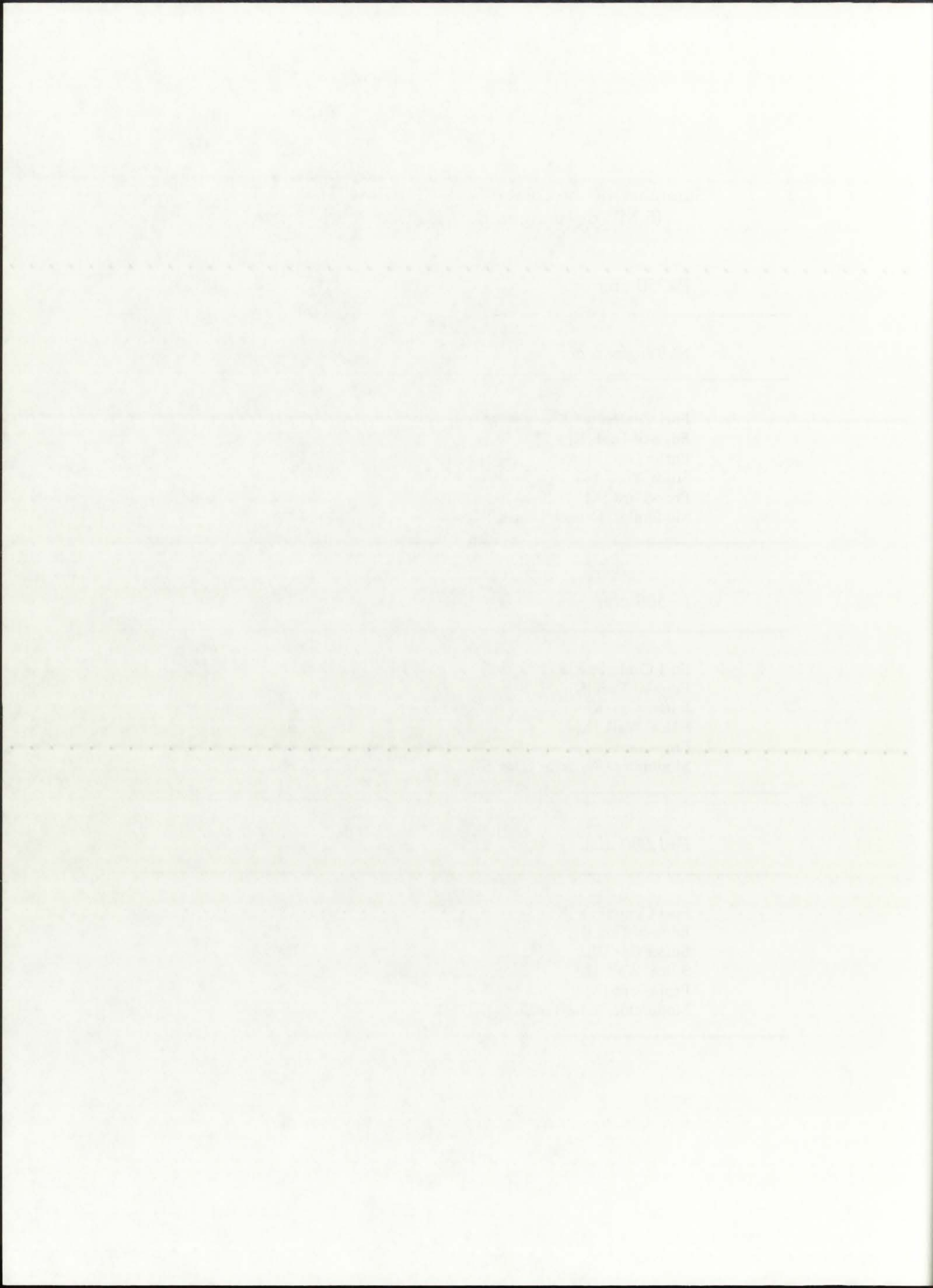
NLB engine region	Temperature
Fuel Centerline [K]	26,598
Edge-of-Fuel [K]	14,903
Buffer Gas [K]	14,902
Silica Wall [K]	14,902
Propellant [K]	14,902
Moderator/Reflector Liner [K]	14,895

P=500 atm

Fuel Centerline [K]	31,726
Edge-of-Fuel [K]	17,689
Buffer Gas [K]	17,688
Silica Wall [K]	17,688
Propellant [K]	17,688
Moderator/Reflector Liner [K]	17,680

P=1,000 atm

Fuel Centerline [K]	38,097
Edge-of-Fuel [K]	21,085
Buffer Gas [K]	21,085
Silica Wall [K]	21,085
Propellant [K]	21,085
Moderator/Reflector Liner [K]	21,074



The centerline-to-edge of fuel temperature ratio is approximately constant at 1.8 for the three operating pressures, similar to the ratio for the 500 MWth configuration. This is consistent with previously mentioned published research [Ragsdale, 1970]. Based on the results shown in Figure 10.10 and Table 10.4, it can be concluded that the 5 MWth configuration, too, would most probably result in temperatures within the silica wall and solid moderator/reflector regions that would be too high to reasonable expect the regions to be maintained in a solid state, regardless of the cooling scheme applied to them. The GNRATR-1D summary output files for the 5 MWth executions can be found in Appendix C.2.

10.4.2. ENDF/B-V Library

The second set of analyses involving the 500 MWth configuration were performed with the temperature-dependent ENDF/B-V cross-section library accessed by ONEDANT. The converged $Qg'''(r)$ distribution is presented in Figure 10.11. The values of $Qg'''(i)$ for the seven fuel nodes are also provided in tabular format as part of Figure 10.11. The behavior of $Qg'''(r)$ as a function of radial distance from the centerline for the ENDF/B-V case is similar to the Hansen-Roach case, as was concluded previously for the 500 MWth configuration. The difference in magnitude of $Qg'''(r)$ between the Hansen-Roach and ENDF/B-V cases is again small, on the order of 1% or less. The ENDF/B-V case results in a slightly greater $Qg'''(r)$ at the outer edge of the fuel; as discussed previously, this could possibly be due to the lower thermal neutron cutoff of the ENDF/B-V library (0.00001 eV versus 0.025 eV for Hansen-Roach), which could allow for a larger fission cross-section for the sub-0.025 eV neutrons and therefore effectively increase the rate of fission at the outer edge of the fuel.

The TRANSX input files for ENDF/B-V cases for 5 MWth configuration are provided in Appendix C.3. The ONEDANT input files are provided in Appendix C.4.

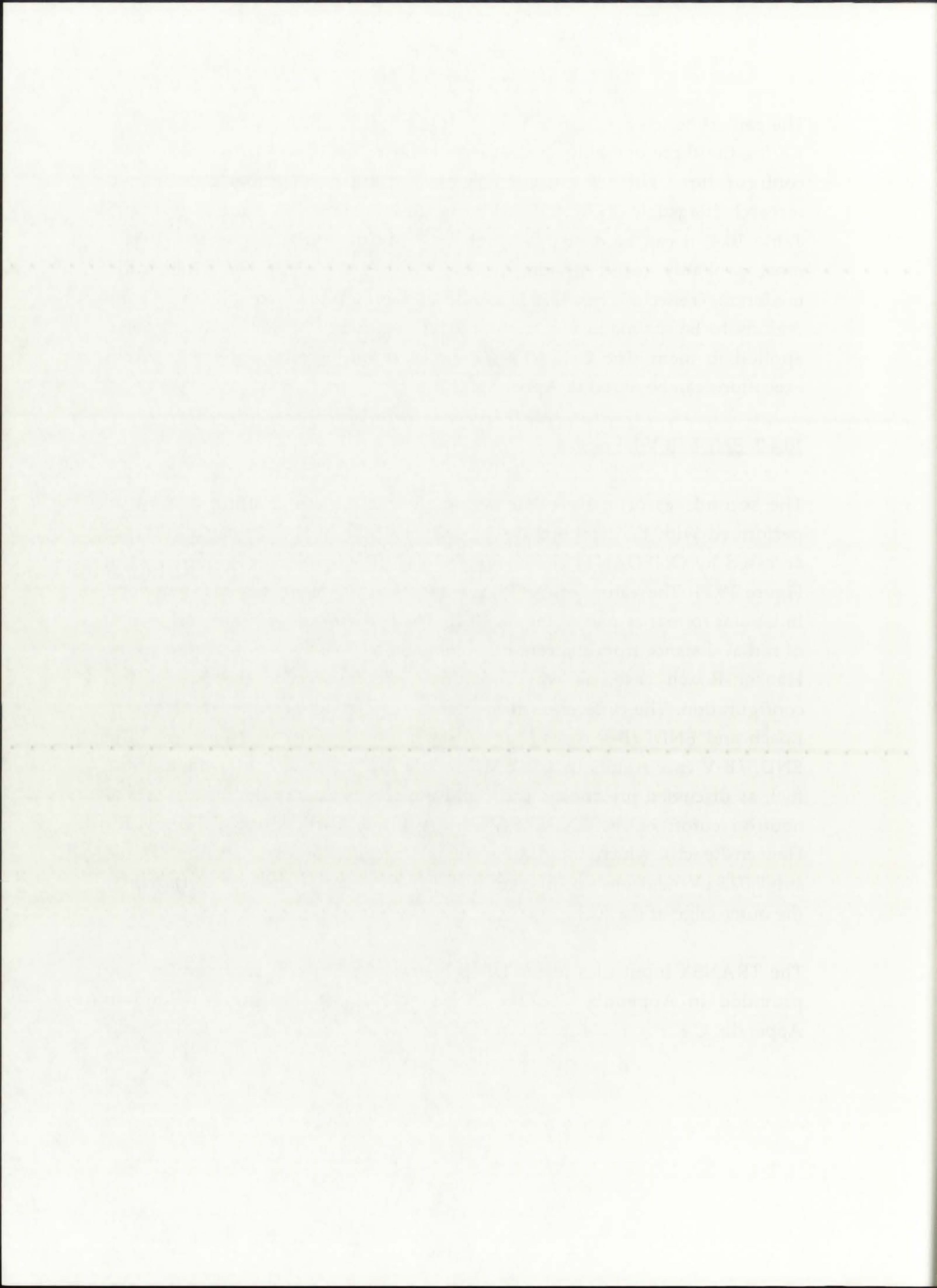
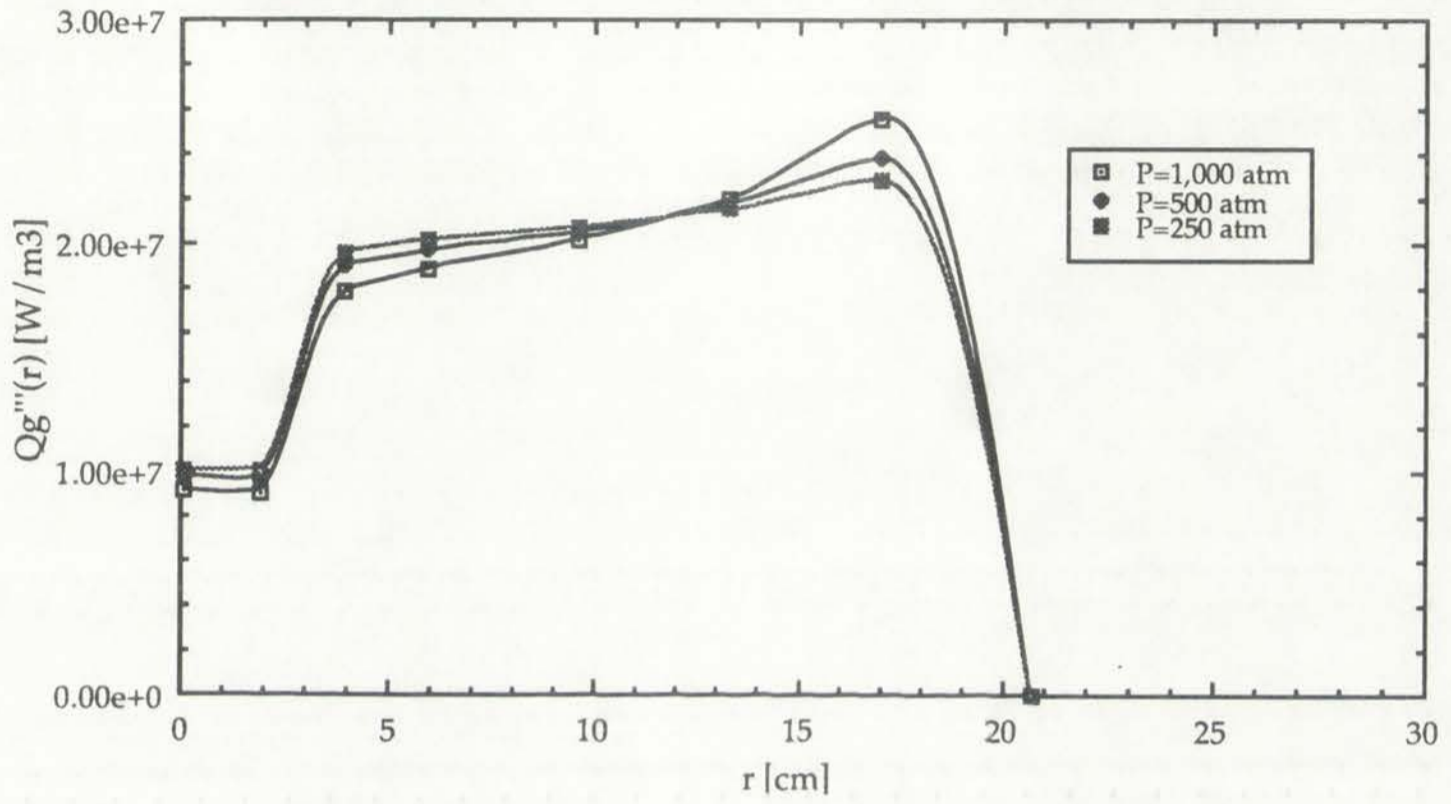


Figure 10.11: $Qg'''(r)$ for 5 MWth power level (ENDF/B-V library).



r [cm]	$Qg'''(r)$, $P=250$ atm	$Qg'''(r)$, $P=500$ atm	$Qg'''(r)$, $P=1,000$ atm
0.0	9.978e6 W/m ³	9.653e6 W/m ³	9.039e6 W/m ³
1.9	9.882e6 W/m ³	9.545e6 W/m ³	8.922e6 W/m ³
3.9	1.967e7 W/m ³	1.904e7 W/m ³	1.787e7 W/m ³
5.9	2.015e7 W/m ³	1.971e7 W/m ³	1.889e7 W/m ³
9.6	2.074e7 W/m ³	2.055e7 W/m ³	2.018e7 W/m ³
13.3	2.156e7 W/m ³	2.175e7 W/m ³	2.202e7 W/m ³
17.0	2.295e7 W/m ³	2.388e7 W/m ³	2.566e7 W/m ³
20.7	0.0 W/m ³	0.0 W/m ³	0.0 W/m ³

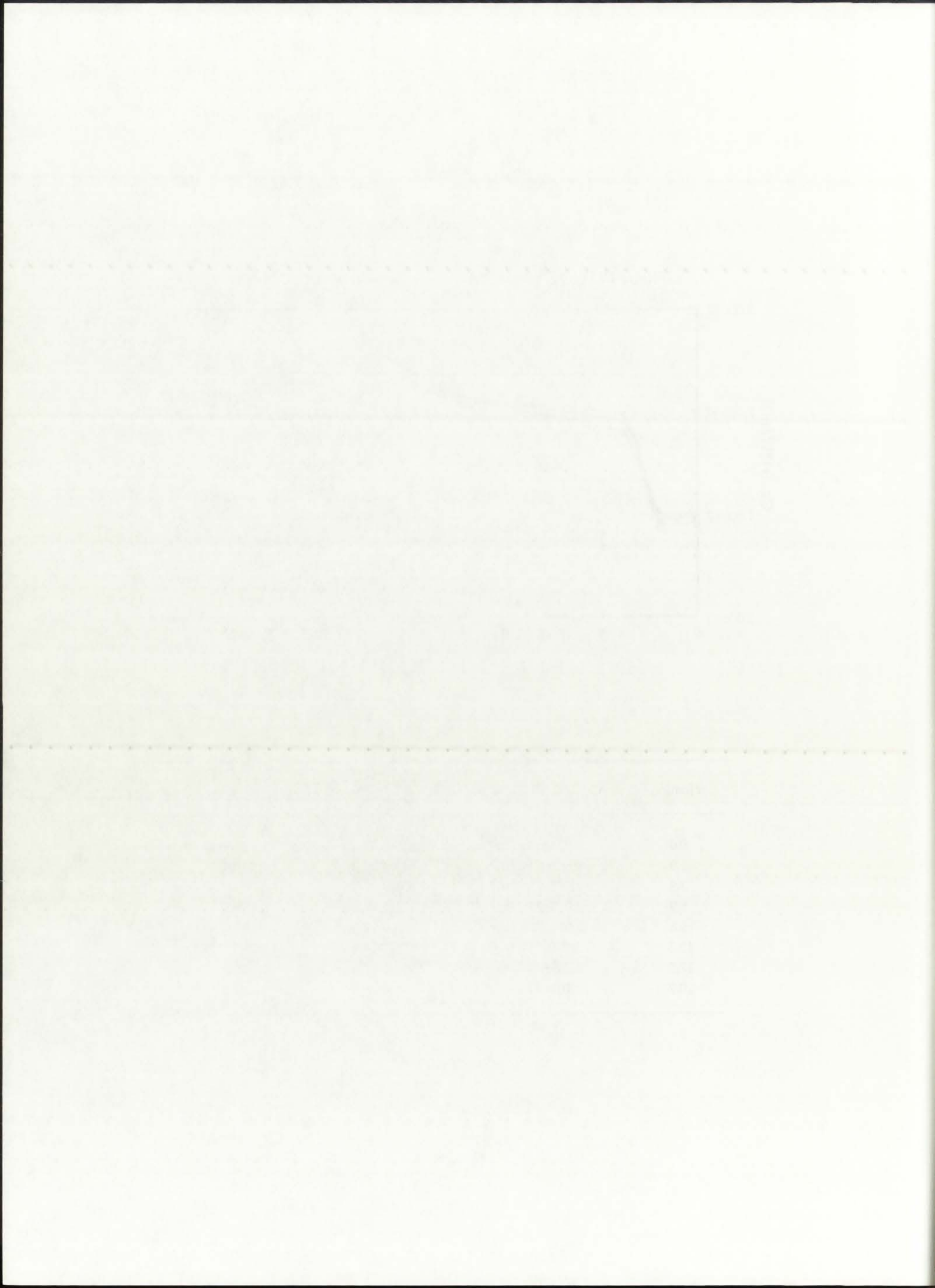
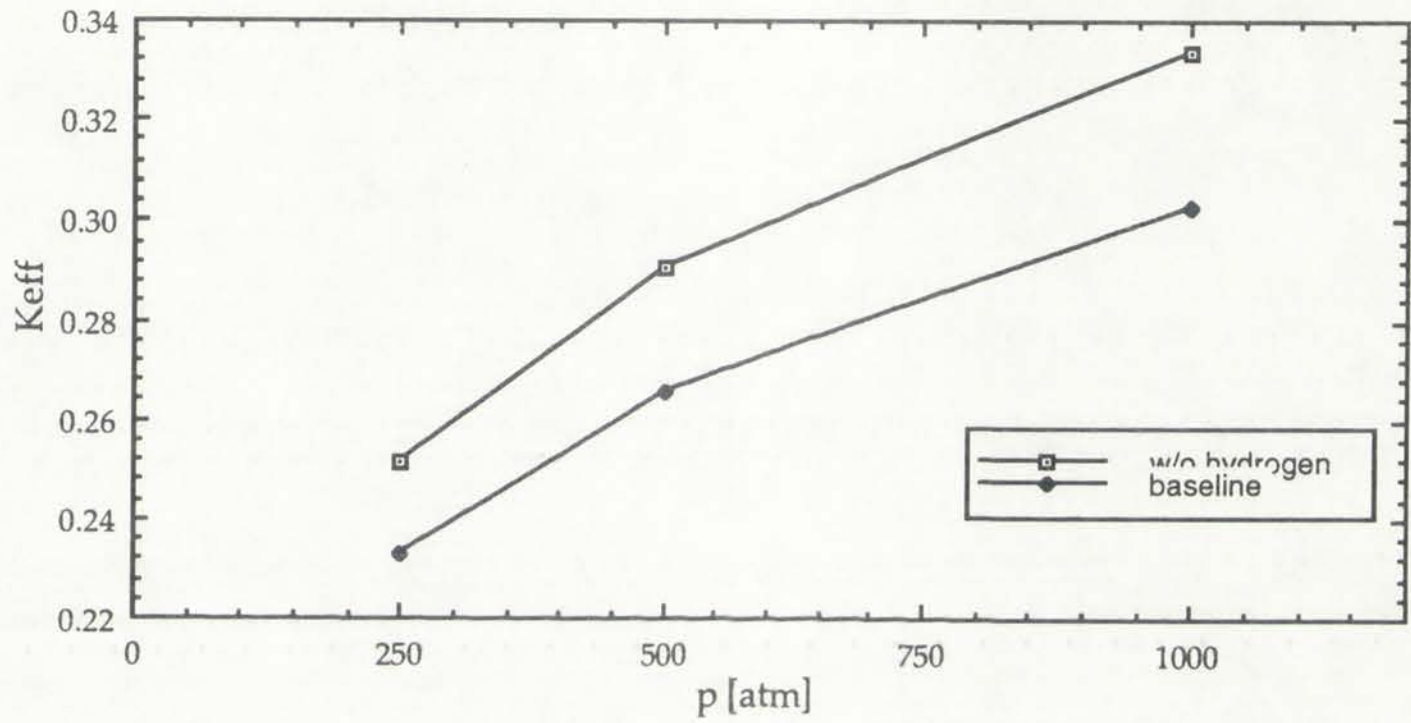
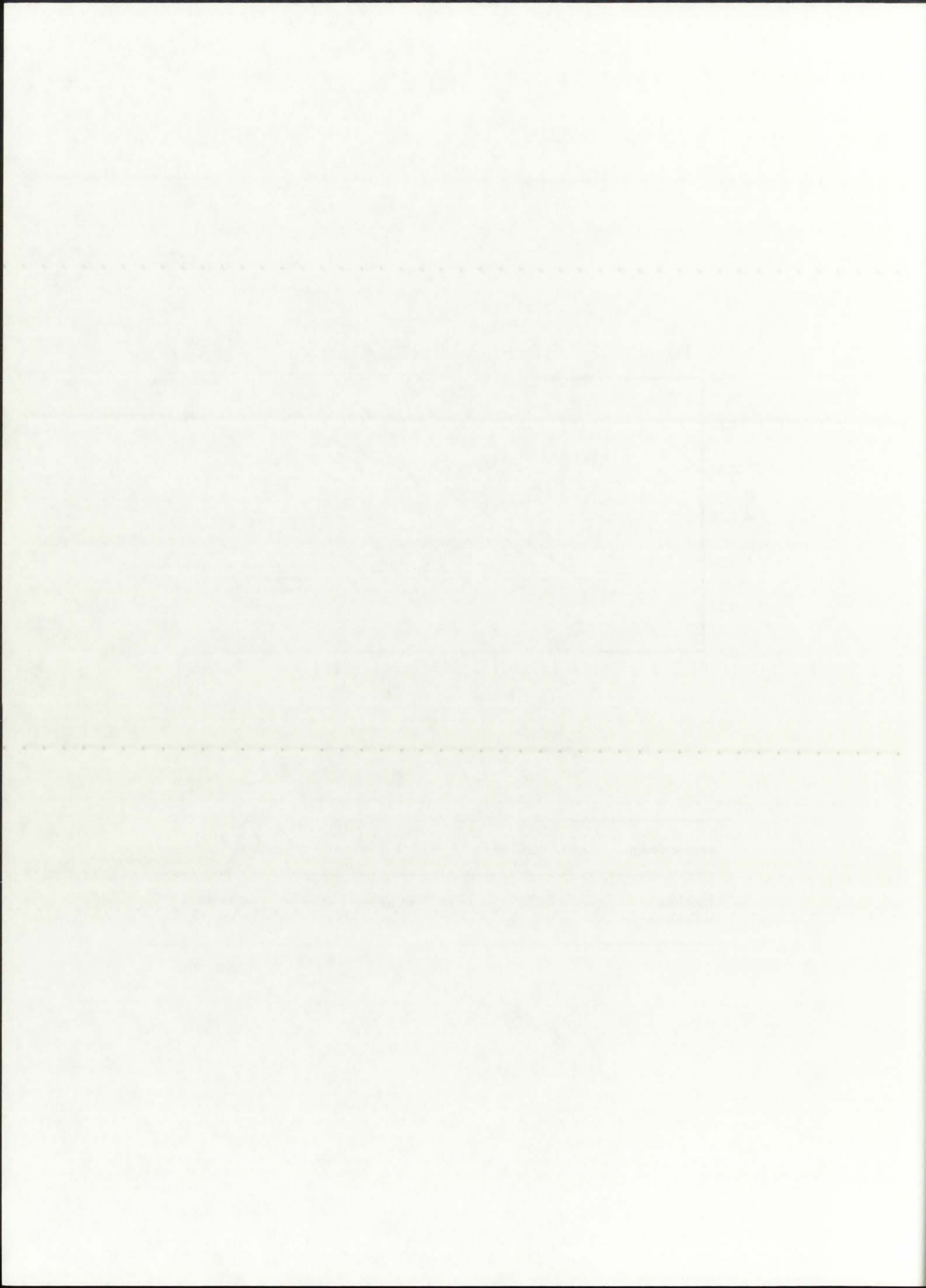


Figure 10.12: K_{eff} for 5 MWth configuration (ENDF/B-V library).



engine design	k_{eff} , P=250 atm	k_{eff} , P=500 atm	k_{eff} , P=1,000 atm
baseline	0.2330	0.2657	0.3027
w/o hydrogen	0.2514	0.2908	0.3334



The calculated k_{eff} values of the 5 MWth configurations are shown in Figure 10.12. As with the Hansen-Roach case, the k_{eff} of the baseline design is subcritical. The modified cases with a vacuum zone in place of the hydrogen propellant are also shown in Figure 10.12. As can be seen, for the extreme case of no propellant present (0% subtending of the propellant channel), the increase in k_{eff} is approximately 10%.

Comparison of the k_{eff} values provided by the Hansen-Roach and ENDF/B-V libraries indicate strong similarity, and thereby verify each other. Again, it has not been possible to validate the expectation regarding possible neutronic beneficial effects of the low-temperature moderator/reflector. There does not seem to be any correlation between the existence of a 0.006 eV scattering cross-section cutoff in beryllium and a significant increase in the k_{eff} of a system, all other things being constant. As discussed before, the argument regarding possible neutronic transparency of beryllium at $E \leq 0.006$ eV being overshadowed by the hydrogen diffusion barrier can be countered by comparison of the baseline and no-hydrogen cases' k_{eff} values.

The converged $T(r)$ distribution is shown in Figure 10.13. The centerline-to-edge of fuel temperature ratio is again approximately constant at 1.8 for the three operating pressures, in line with published data [Ragsdale, 1970]. The calculated temperature values for the major regions of the NLB engine model are given in Table 10.5.

In the case of the ENDF/B-V library analysis of the 5 MWth configuration, the familiar two problems arise with respect to feasibility of the NLB engine at that power level: (1) melting of the silica wall, and (2) melting of the entire solid moderator/reflector assembly. On the basis of the available results in both the Hansen-Roach and ENDF/B-V cases, it can be concluded that the 5 MWth configuration of the unit-cell NLB engine would most probably not be feasible due to the high temperatures within the silica wall and solid moderator/reflector regions. The GNRATR-1D summary output files for the ENDF/B-V case of the 5 MWth configuration can be found in Appendix C.5.

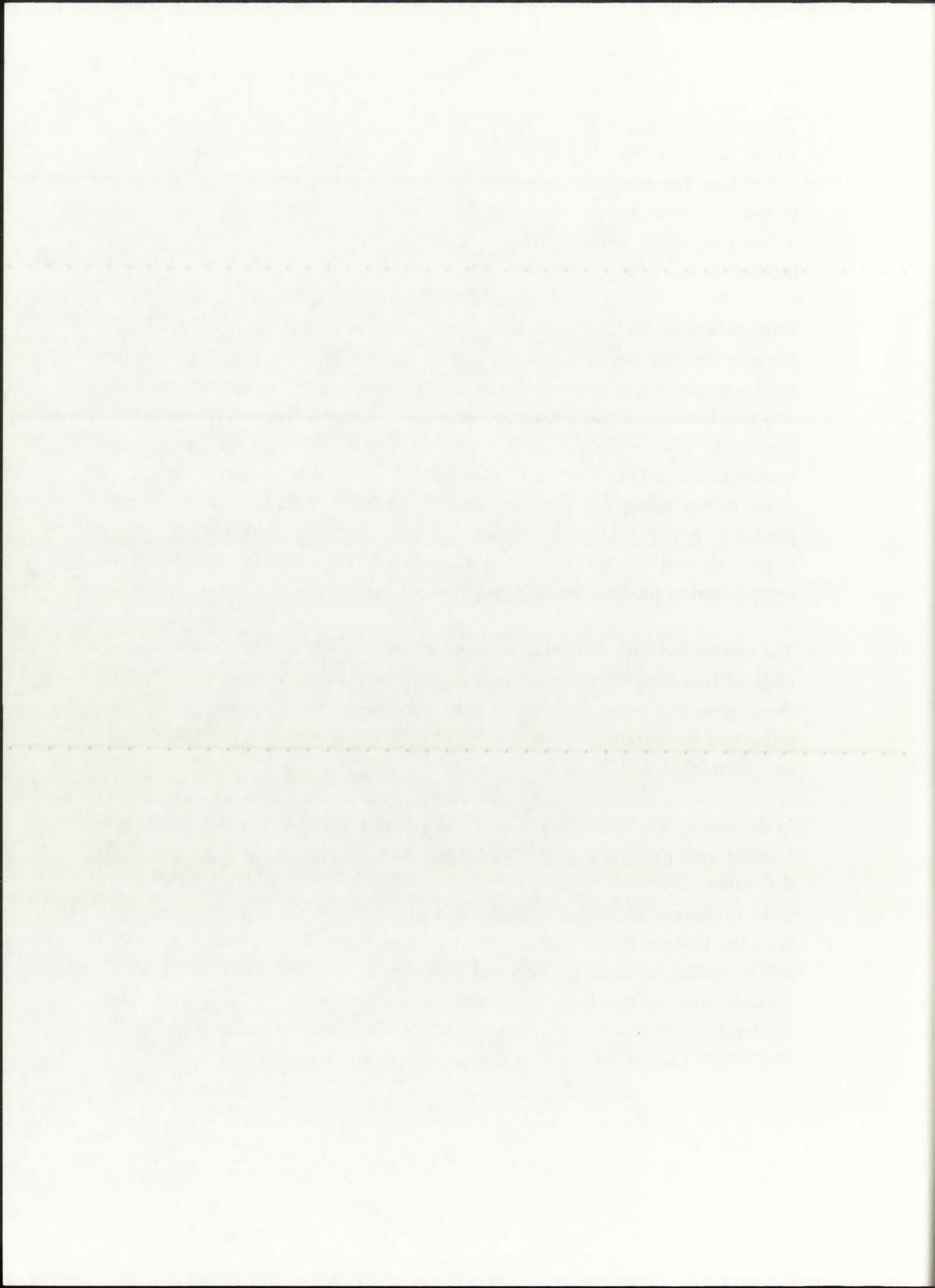
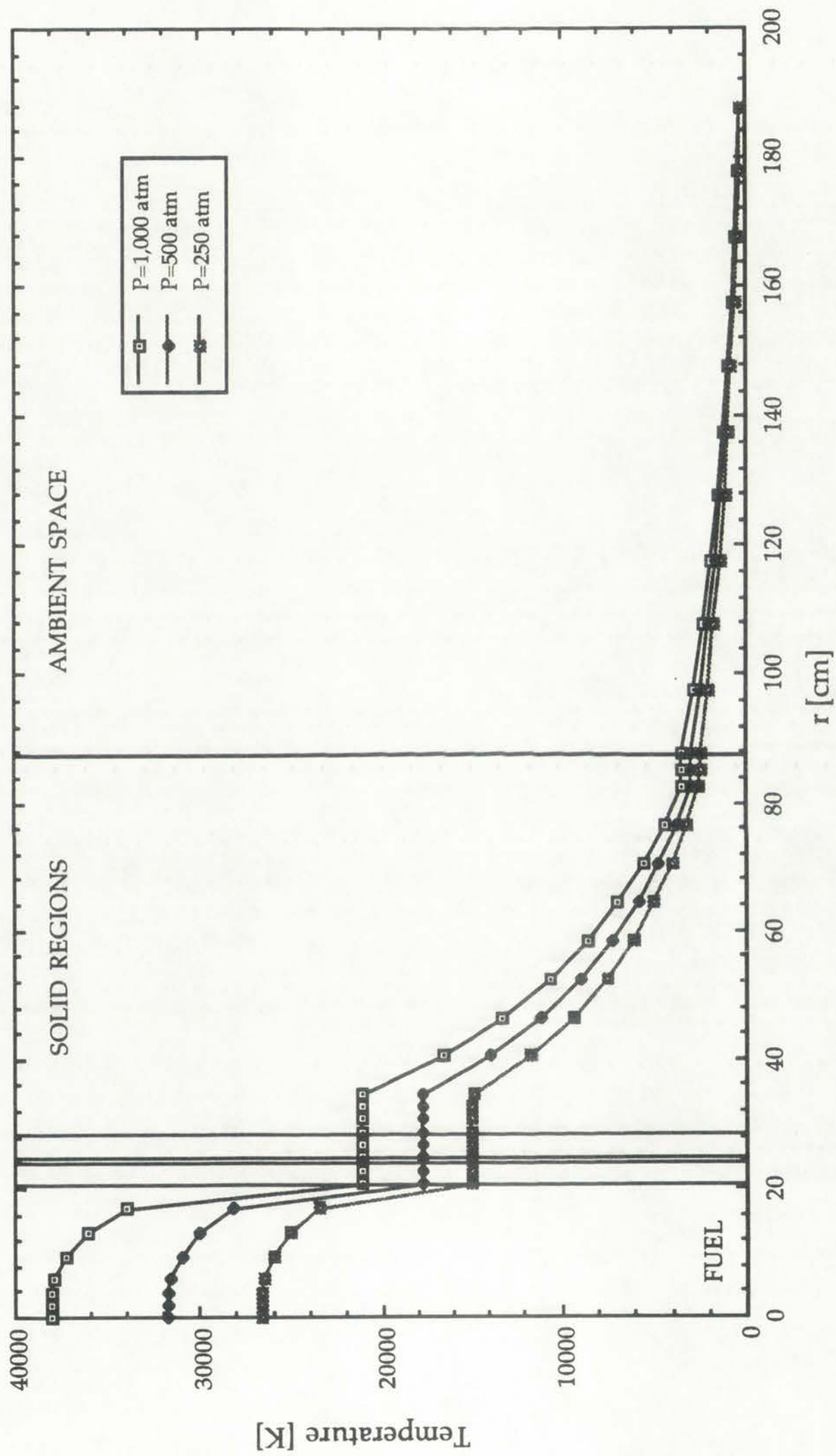


Figure 10.13: $T(r)$ for 5 MWth, ENDF/B-V library, comprehensive thermal analysis.





Vertical text label, possibly 'Vertical Section'.

Vertical text label, possibly 'Vertical Section'.



Vertical text label, possibly 'Vertical Section'.

Small text label, possibly 'Section'.

Small text label, possibly 'Section'.

TABLE 10.5
 Summary of the comprehensive thermal analysis results
 (5 MWth configuration, ENDF/B-V library)

P=250 atm

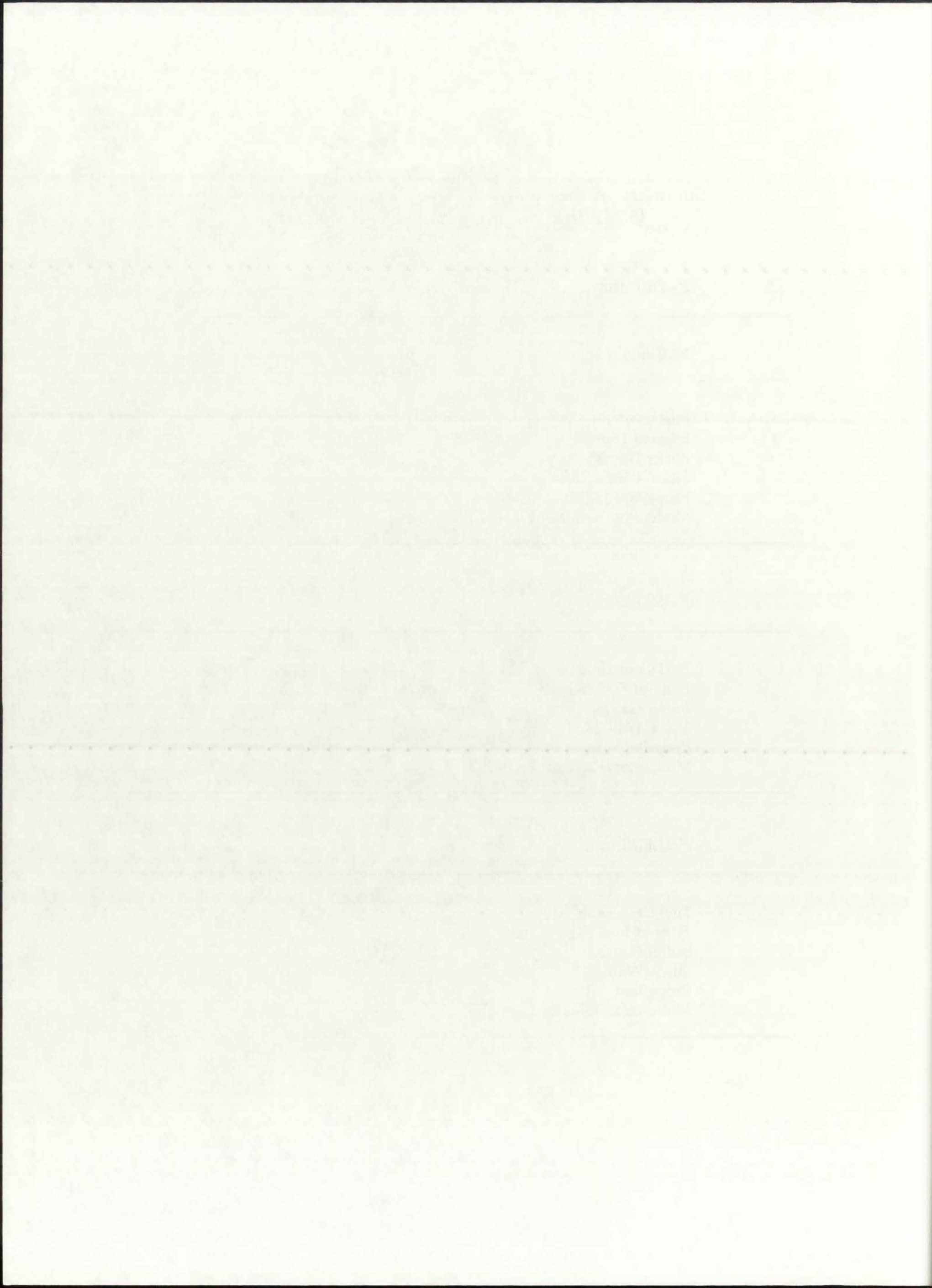
NLB engine region	Temperature
Fuel Centerline [K]	26,594
Edge-of-Fuel [K]	14,903
Buffer Gas [K]	14,902
Silica Wall [K]	14,902
Propellant [K]	14,902
Moderator/Reflector Liner [K]	14,895

P=500 atm

Fuel Centerline [K]	31,702
Edge-of-Fuel [K]	17,689
Buffer Gas [K]	17,688
Silica Wall [K]	17,688
Propellant [K]	17,688
Moderator/Reflector Liner [K]	17,680

P=1,000 atm

Fuel Centerline [K]	38,012
Edge-of-Fuel [K]	21,085
Buffer Gas [K]	21,085
Silica Wall [K]	21,085
Propellant [K]	21,085
Moderator/Reflector Liner [K]	21,074



10.5. The 50 kWth Configuration

The 50 kWth configuration was chosen as the lower limit for the thermal power, as it results in fuel temperatures in the low range of the gaseous state (i.e., near the boiling point of elemental uranium). This power level has never been analyzed as part of any previous published work; in reality, however, it will be seen further on in this Section that the temperatures associated with this relatively low power level allow for proper cooling and therefore indicate a potential feasibility of the unit-cell NLB rocket engine.

The iterative solution procedure was applied for the 50 kWth configuration in the same manner as previously discussed. An initial volumetric heat generation rate of 2.03×10^5 [W/m³] was set at all seven fuel nodes. Based on the temperatures calculated by GNRATR-1D, appropriate material atomic densities were provided to ONEDANT. The resultant volumetric heat generation rates $Qg'''(r)$ were then provided to GNRATR-1D, for a new temperature distribution. The iterative procedure was carried out separately for both the Hansen-Roach and ENDF/B-V cross-sections.

10.5.1. Hansen-Roach Library

The converged $Qg'''(r)$ distribution for 50 kWth is shown in Figure 10.14. It can be seen that the 50 kWth configuration is characterized by the most prominent peak in $Qg'''(r)$ at the outer edge of the fuel region, compared to the 500 MWth and 5 MWth configurations. The fuel density [atoms/barn-cm] at the temperatures associated with 50 kWth is almost 100 times greater than the fuel density at 500 MWth, and almost 10 times greater than the fuel density at 5 MWth. The significant increase in fuel density provides for a much higher macroscopic fission cross-section, which in turn results in the majority of the fissions occurring at the outer edge of the fuel region. As can be seen, the peak in $Qg'''(r)$ occurs between $r=15$ cm and $r=19$ cm; to conserve the total thermal power generated in the fuel, $Qg'''(r)$ decreases sharply as r approaches $r=0$ (centerline). The profile of $Qg'''(r)$ is no longer flat in the intermediate region of the fuel, but instead decreases continuously.

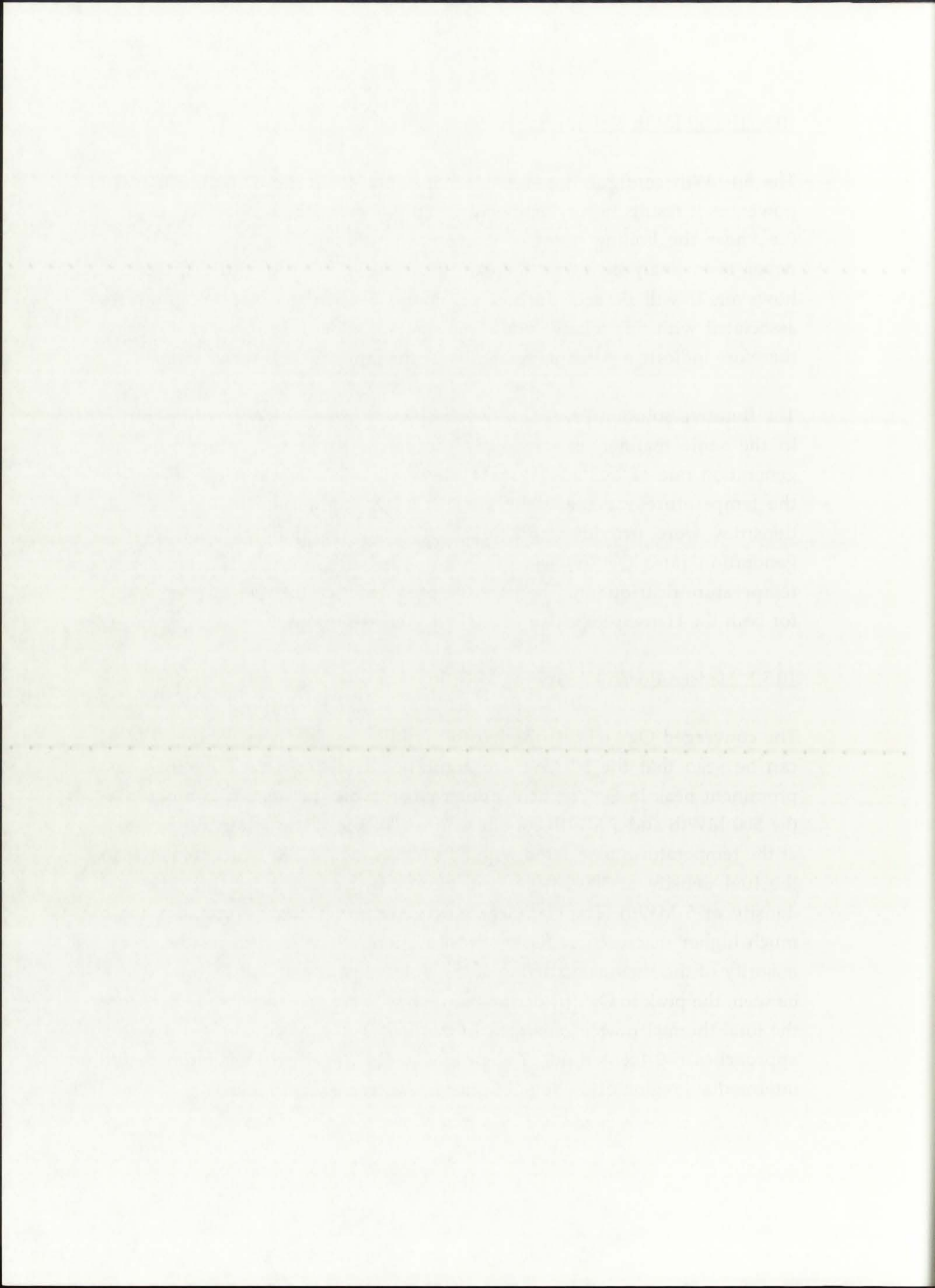
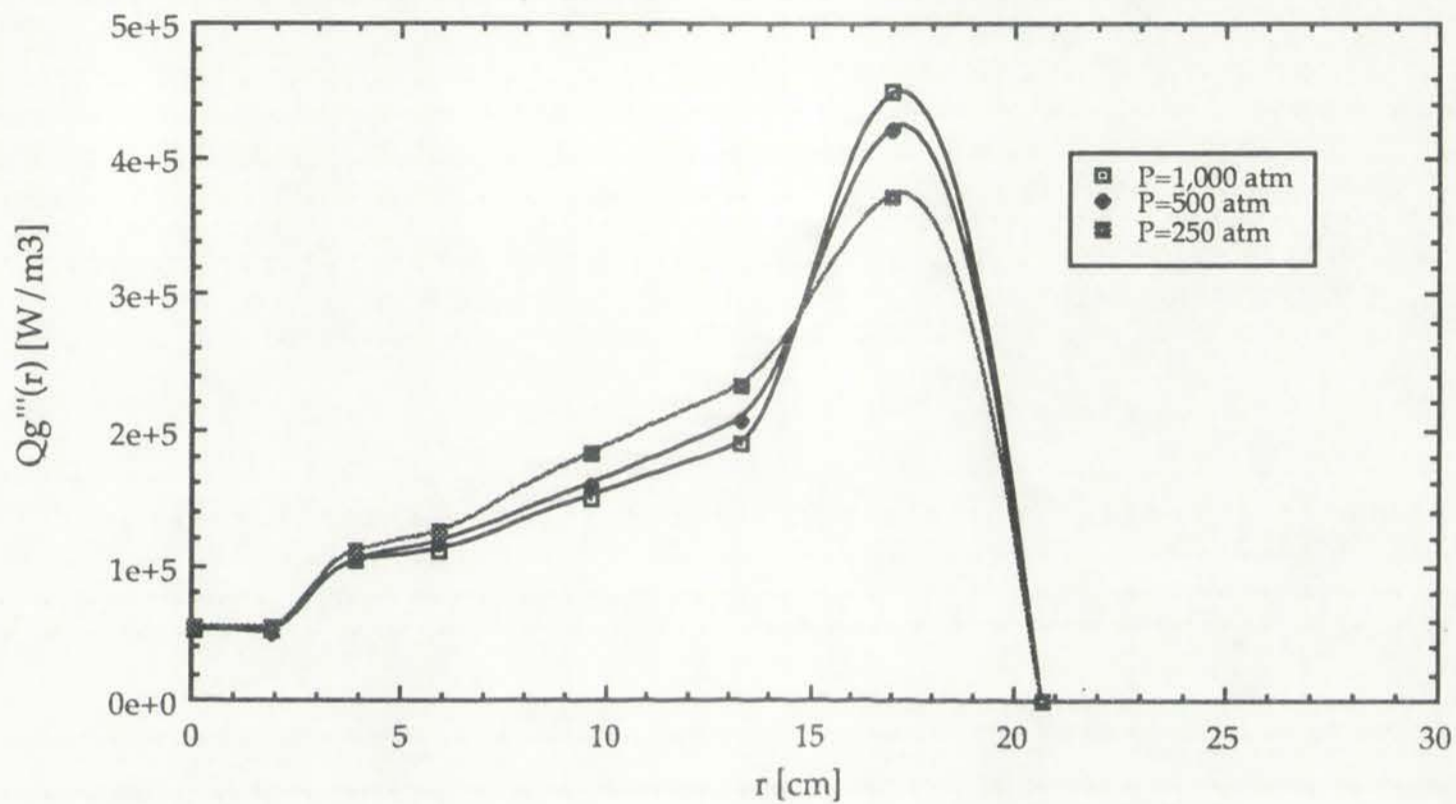
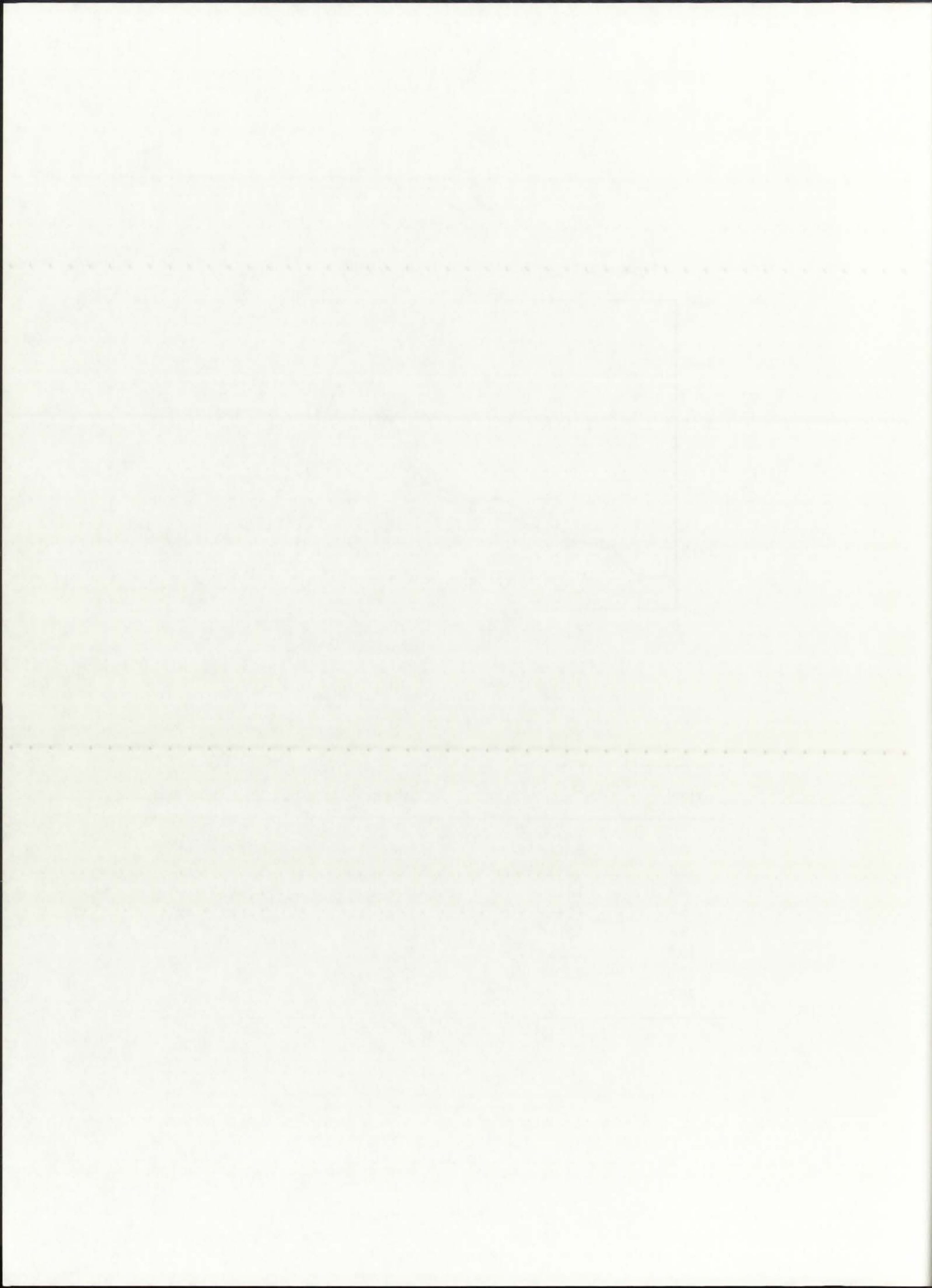


Figure 10.14: $Qg'''(r)$ for 50 kWth power level (Hansen-Roach library).



r [cm]	$Qg'''(r)$, $P=250$ atm	$Qg'''(r)$, $P=500$ atm	$Qg'''(r)$, $P=1,000$ atm
0.0	$5.447e4$ W/m^3	$5.118e4$ W/m^3	$5.147e4$ W/m^3
1.9	$5.370e4$ W/m^3	$5.085e4$ W/m^3	$5.123e4$ W/m^3
3.9	$1.110e5$ W/m^3	$1.052e5$ W/m^3	$1.044e5$ W/m^3
5.9	$1.244e5$ W/m^3	$1.171e5$ W/m^3	$1.112e5$ W/m^3
9.6	$1.816e5$ W/m^3	$1.597e5$ W/m^3	$1.500e5$ W/m^3
13.3	$2.326e5$ W/m^3	$2.069e5$ W/m^3	$1.895e5$ W/m^3
17.0	$3.729e5$ W/m^3	$4.224e5$ W/m^3	$4.492e5$ W/m^3
20.7	0.0 W/m^3	0.0 W/m^3	0.0 W/m^3



The calculated k_{eff} values for the 50 kWth configurations are shown in Figure 10.15. The k_{eff} of the 50 kWth engine is significantly higher than the corresponding value for either the 500 MWth or 5 MWth configuration, but is still subcritical. The increase in k_{eff} with decreasing thermal power (and therefore, decreasing fuel temperature), and also with increasing operating pressure, indicates that the predominant neutronics parameter is the fuel density. The ONEDANT input files for the Hansen-Roach cases for 50 kWth are provided in Appendix D.1.

Overall, the unit-cell NLB engine, in its original design, is probably over-moderated; this is evidenced by the beneficial effect on k_{eff} of the total removal of hydrogen from the propellant region, shown in Figure 10.15 and previously in Figures 10.9 and 10.3. Therefore, a potential increase in k_{eff} could be achieved by reducing the volume of the moderator/reflector region and/or optimizing the hydrogen propellant channel volume. In order to design a critical and also feasible NLB engine, it would be necessary to invest a lot of time and effort and essentially start from the bottom up, selecting the appropriate thermal power, operating pressure, propellant channel geometry, as well as fuel, propellant, and moderator/reflector dimensions.

Based on the $Qg''(r)$ values in the fuel region, a converged $T(r)$ distribution was determined by GNRATR-1D for each of the three operating pressures, as shown in Figure 10.16. The fuel temperatures, naturally, are lower still than for the 5 MWth case. The calculated temperature values are also given in Table 10.6. Assuming again that the rate of heat transfer in the fuel varies approximately as the fourth power of the temperature, the fuel temperature for the 50 kWth case should be approximately 3.2 times less than the fuel temperature for the 5 MWth case. Comparison of the 5 MWth and 50 kWth fuel temperatures determined by GNRATR-1D indicate a ratio equal to 3.17.

Based on the results shown in Figure 10.16 and Table 10.6, it can be concluded that of all the three thermal power cases analyzed, the 50 kWth case is closest to being feasible. The GNRATR-1D summary output files for the 50 kWth cases can be found in Appendix D.2.

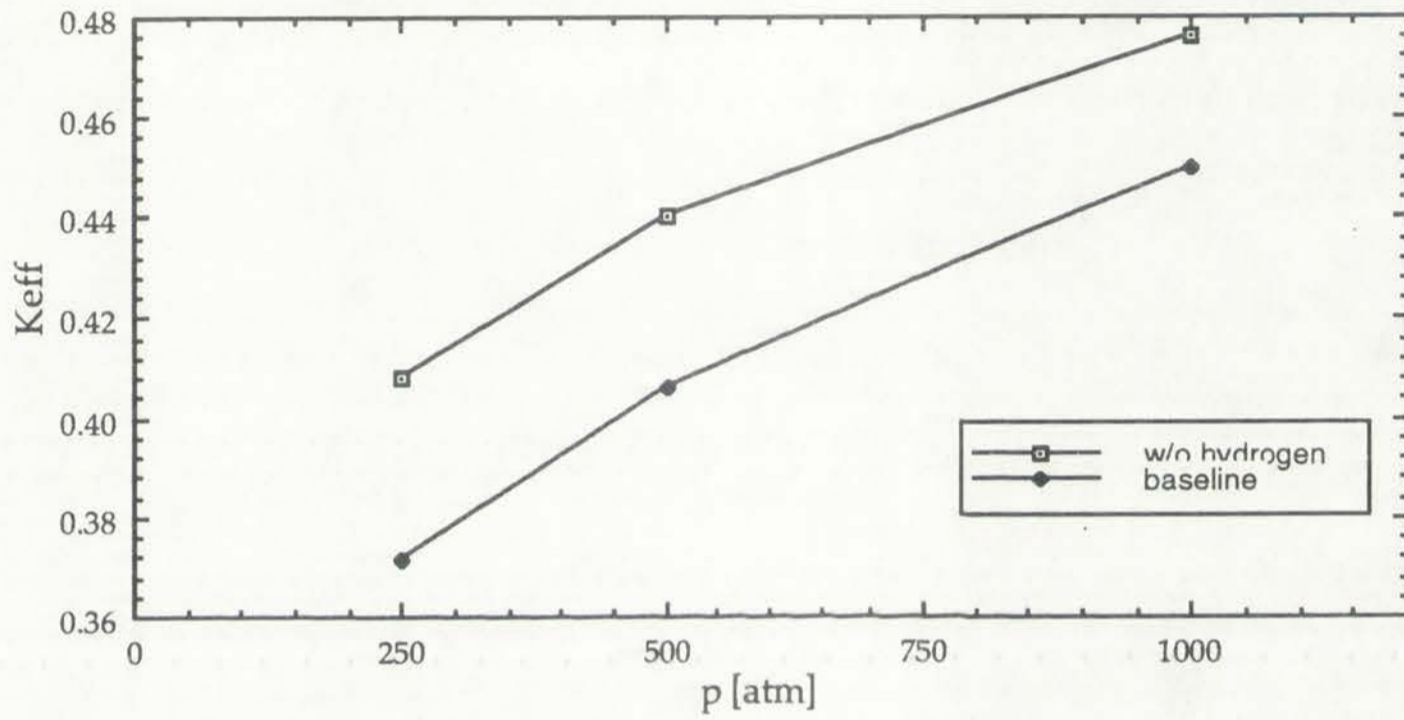
The calculated U_g values for the 50 kWth configuration are shown in Figure 10.15. The U_g of the 50 kWth engine is consistently higher than the corresponding values for either the 5 MWth or 2 MWth configurations, but is still substantial. The increase in U_g with decreasing thermal power (and therefore decreasing fuel temperature) and also with increasing operating pressure indicates that the predominant radiation parameter is the fuel density. The ONEDANT input data for the Hanson-Roch case for 50 kWth are provided in Appendix D.

Overall, the nuclear NLE engine in its original design is probably over-engineered; this is evidenced by the beneficial effect on U_g of the total removal of hydrogen from the propellant region, shown in Figure 10.15 and previously in Figures 10.3 and 10.5. Therefore, a potential increase in U_g could be achieved by reducing the volume of the moderator/reflector region and/or optimizing the hydrogen propellant channel volume. In order to design a critical and also feasible NLE engine it would be necessary to invest a lot of time and effort and essentially start from the bottom up, selecting the appropriate thermal power operating pressure, propellant channel geometry, as well as fuel propellant and moderator/reflector dimensions.

Based on the U_g values in the fuel region, a conserved $T(r)$ distribution was determined by GNRATR-1D for each of the three operating pressures, as shown in Figure 10.16. The fuel temperatures, T_{fuel} , are lower still than for the 2 MWth case. The calculated temperature values are also given in Table 10.4. Assuming again that the rate of heat transfer in the fuel varies approximately as the fourth power of the temperature, the fuel temperature for the 50 kWth case should be approximately 2.1 times less than the fuel temperature for the 2 MWth case. Comparison of the 2 MWth and 50 kWth fuel temperatures determined by GNRATR-1D indicates a ratio equal to 4.15.

Based on the results shown in Figure 10.15 and Table 10.4, it can be concluded that of all the three thermal power cases analyzed, the 50 kWth case is closest to being feasible. The GNRATR-1D summary output files for the 50 kWth case can be found in Appendix D.

Figure 10.15: K_{eff} for 50 kWth configuration (Hansen-Roach library).



engine design	keff, P=250 atm	keff, P=500 atm	keff, P=1,000 atm
baseline	0.3716	0.4063	0.4498
w/o hydrogen	0.4080	0.4401	0.4761

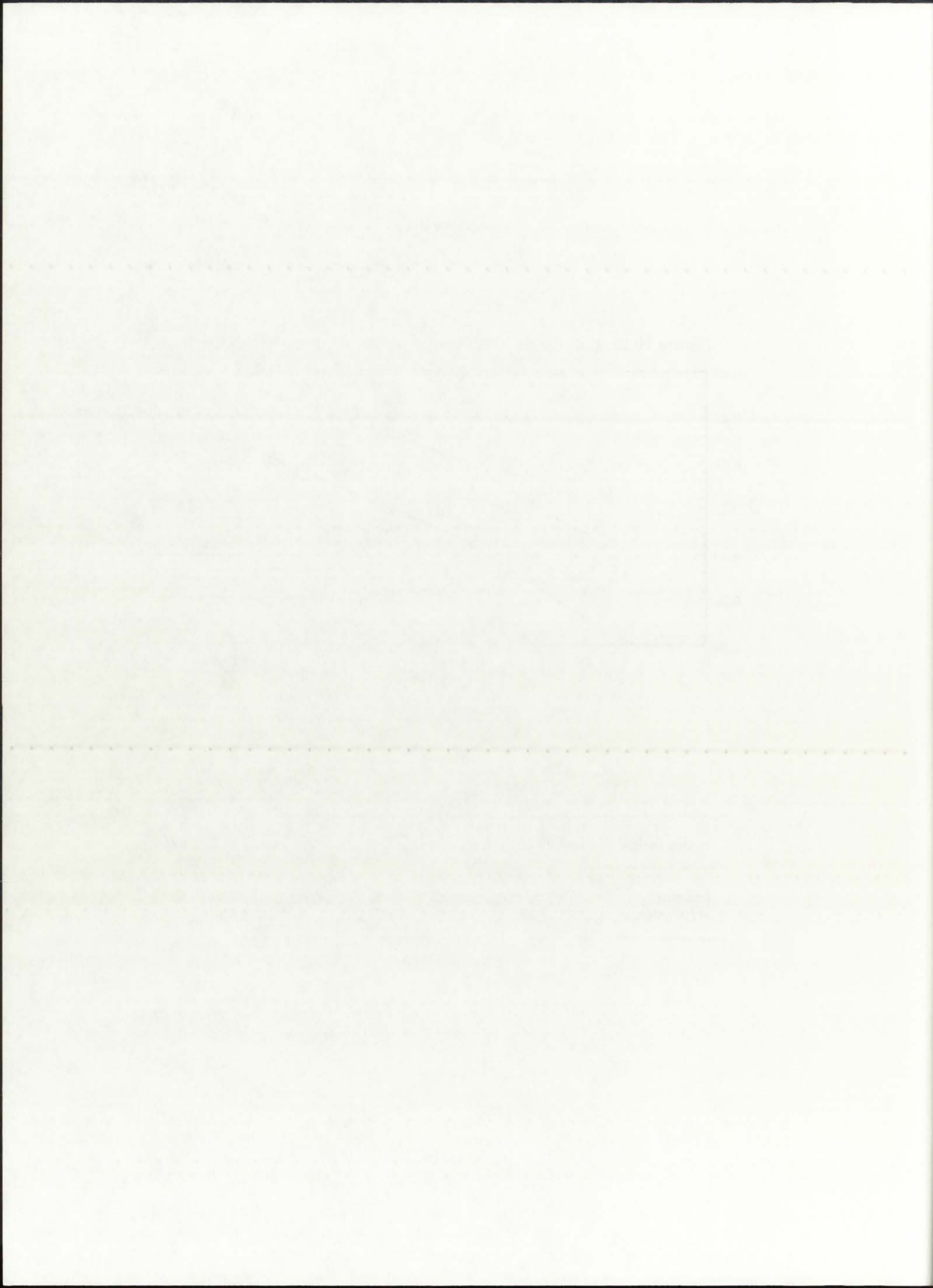
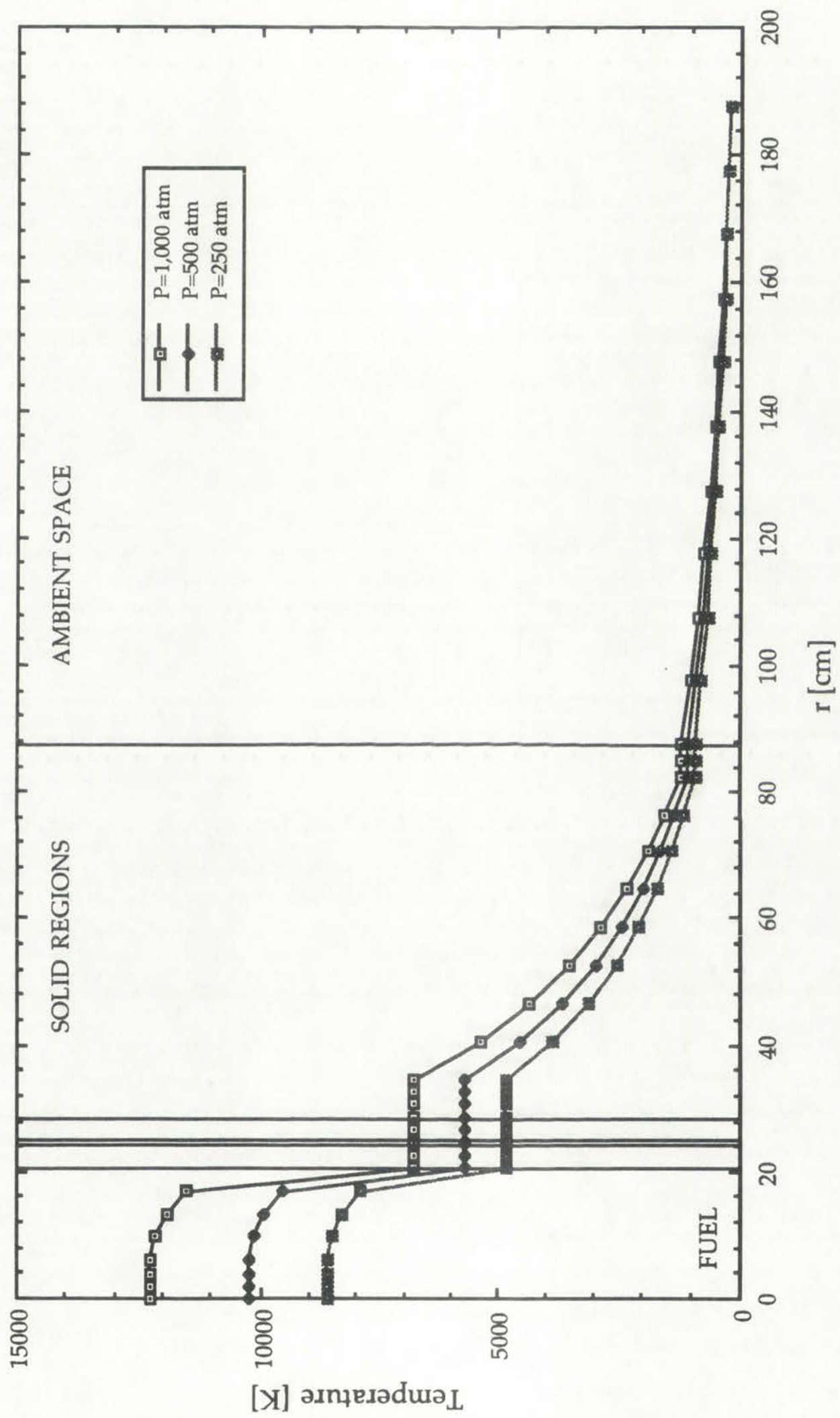


Figure 10.16: $T(r)$ for 50 kWth, Hansen-Roach library, comprehensive thermal analysis.



THE UNIVERSITY OF CHICAGO LIBRARY

TABLE 10.6
 Summary of the comprehensive thermal analysis results
 (50 kWth configuration, Hansen-Roach library)

P=250 atm

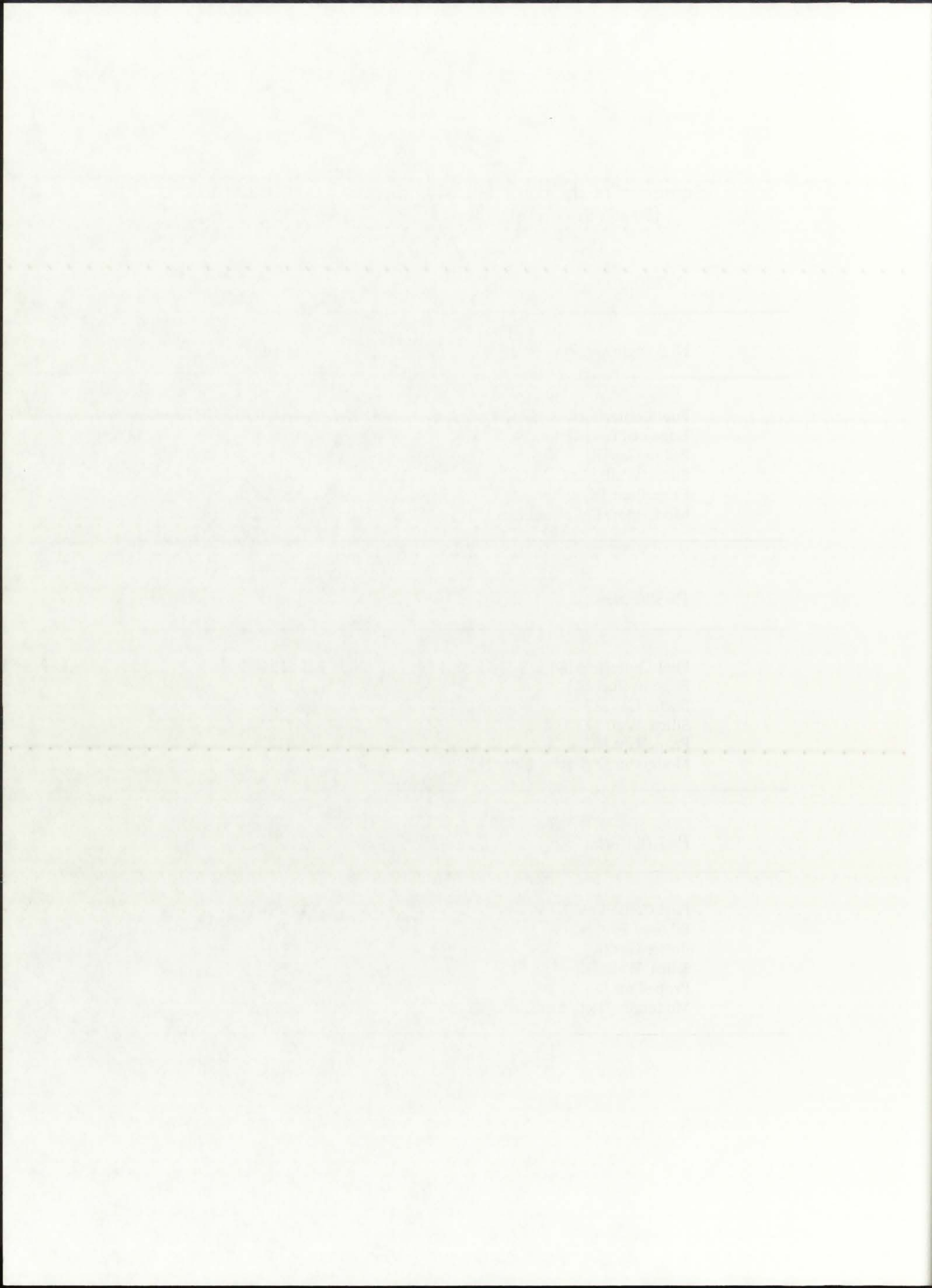
NLB engine region	Temperature
Fuel Centerline [K]	8,604
Edge-of-Fuel [K]	4,833
Buffer Gas [K]	4,833
Silica Wall [K]	4,833
Propellant [K]	4,833
Moderator / Reflector Liner [K]	4,831

P=500 atm

Fuel Centerline [K]	10,252
Edge-of-Fuel [K]	5,717
Buffer Gas [K]	5,717
Silica Wall [K]	5,717
Propellant [K]	5,717
Moderator / Reflector Liner [K]	5,714

P=1,000 atm

Fuel Centerline [K]	12,265
Edge-of-Fuel [K]	6,791
Buffer Gas [K]	6,791
Silica Wall [K]	6,791
Propellant [K]	6,791
Moderator / Reflector Liner [K]	6,788



10.5.2. ENDF/B-V Library

The converged $Qg'''(r)$ distribution for 50 kWth and three operating pressures, using the ENDF/B-V library, is shown in Figure 10.17. The behavior of $Qg'''(r)$ is similar to that for the Hansen-Roach case, with the most prominent peak in $Qg'''(r)$ at the outer edge of the fuel region, compared to the 500 MWth and 5 MWth configurations. The peak in $Qg'''(r)$ occurs between $r=15$ cm and $r=19$ cm; to conserve the total thermal power generated in the fuel, $Qg'''(r)$ decreases sharply as r approaches $r=0$ (centerline).

The calculated k_{eff} values for the 50 kWth configurations are shown in Figure 10.18. The results are similar to the Hansen-Roach case, with the k_{eff} of the 50 kWth engine being significantly higher than the corresponding value for either the 500 MWth or 5 MWth configuration, but still subcritical. As for the 500 MWth and 5 MWth configurations, it is not possible to validate the potential neutronicly beneficial effects of the low-temperature moderator and reflector. The TRANSX input files for the ENDF/B-V cases of the 50 kWth configuration are provided in Appendix D.3. The ONEDANT input files are provided in Appendix D.4.

Based on the $Qg'''(r)$ values in the fuel region, a converged $T(r)$ distribution was determined by GNRATR-1D for each of the three operating pressures, as shown in Figure 10.19. The fuel temperatures are similar to the Hansen-Roach case, due to the similarity in $Qg'''(r)$. The centerline-to-edge of fuel temperature ratio is approximately constant at 1.8. The calculated temperature values are also given in Table 10.7.

Based on the results shown in Figure 10.19 and Table 10.7, as well as the results from the Hansen-Roach analysis for 50 kWth, it can be concluded that of all the three thermal power cases analyzed, the 50 kWth configuration is closest to being feasible. This configuration will be analyzed in detail in subsequent Sections of this Dissertation, with numerous parameters varied. The GNRATR-1D summary output files for the 50 kWth cases can be found in Appendix D.5.

APPENDIX B

The first part of the appendix contains a list of the names of the persons who were interviewed for the purpose of this study. The names are listed in alphabetical order of their last names.

The second part of the appendix contains a list of the names of the persons who were interviewed for the purpose of this study. The names are listed in alphabetical order of their last names.

The third part of the appendix contains a list of the names of the persons who were interviewed for the purpose of this study. The names are listed in alphabetical order of their last names.

The fourth part of the appendix contains a list of the names of the persons who were interviewed for the purpose of this study. The names are listed in alphabetical order of their last names.

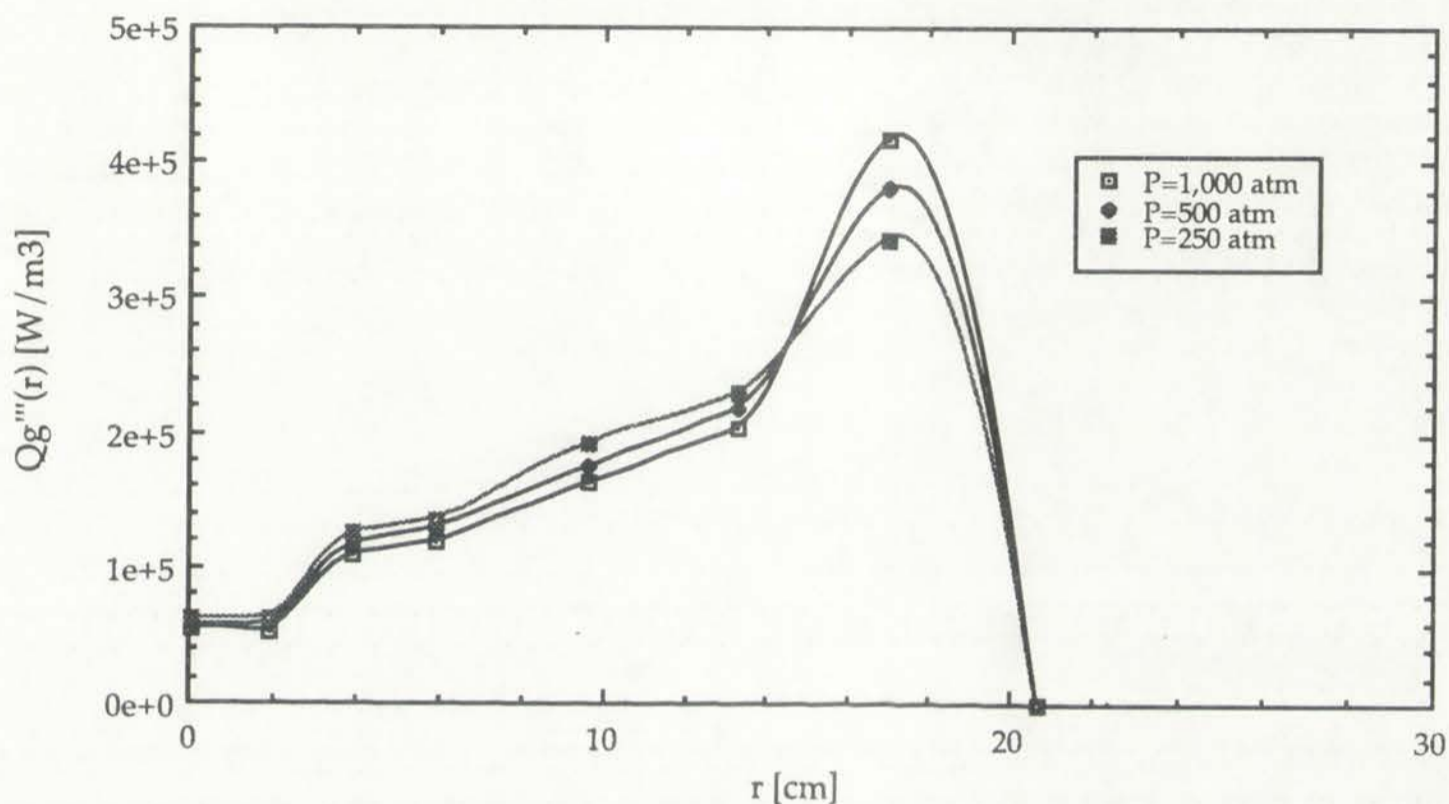
The fifth part of the appendix contains a list of the names of the persons who were interviewed for the purpose of this study. The names are listed in alphabetical order of their last names.

The sixth part of the appendix contains a list of the names of the persons who were interviewed for the purpose of this study. The names are listed in alphabetical order of their last names.

The seventh part of the appendix contains a list of the names of the persons who were interviewed for the purpose of this study. The names are listed in alphabetical order of their last names.

The eighth part of the appendix contains a list of the names of the persons who were interviewed for the purpose of this study. The names are listed in alphabetical order of their last names.

Figure 10.17: $Qg'''(r)$ for 50 kWth power level (ENDF/B-V library).



r [cm]	$Qg'''(r)$, P=250 atm	$Qg'''(r)$, P=500 atm	$Qg'''(r)$, P=1,000 atm
0.0	$6.274e4 W/m^3$	$5.751e4 W/m^3$	$5.350e4 W/m^3$
1.9	$6.195e4 W/m^3$	$5.705e4 W/m^3$	$5.327e4 W/m^3$
3.9	$1.255e5 W/m^3$	$1.170e5 W/m^3$	$1.091e5 W/m^3$
5.9	$1.358e5 W/m^3$	$1.289e5 W/m^3$	$1.185e5 W/m^3$
9.6	$1.920e5 W/m^3$	$1.749e5 W/m^3$	$1.624e5 W/m^3$
13.3	$2.300e5 W/m^3$	$2.180e5 W/m^3$	$2.040e5 W/m^3$
17.0	$3.447e5 W/m^3$	$3.815e5 W/m^3$	$4.178e5 W/m^3$
20.7	$0.0 W/m^3$	$0.0 W/m^3$	$0.0 W/m^3$

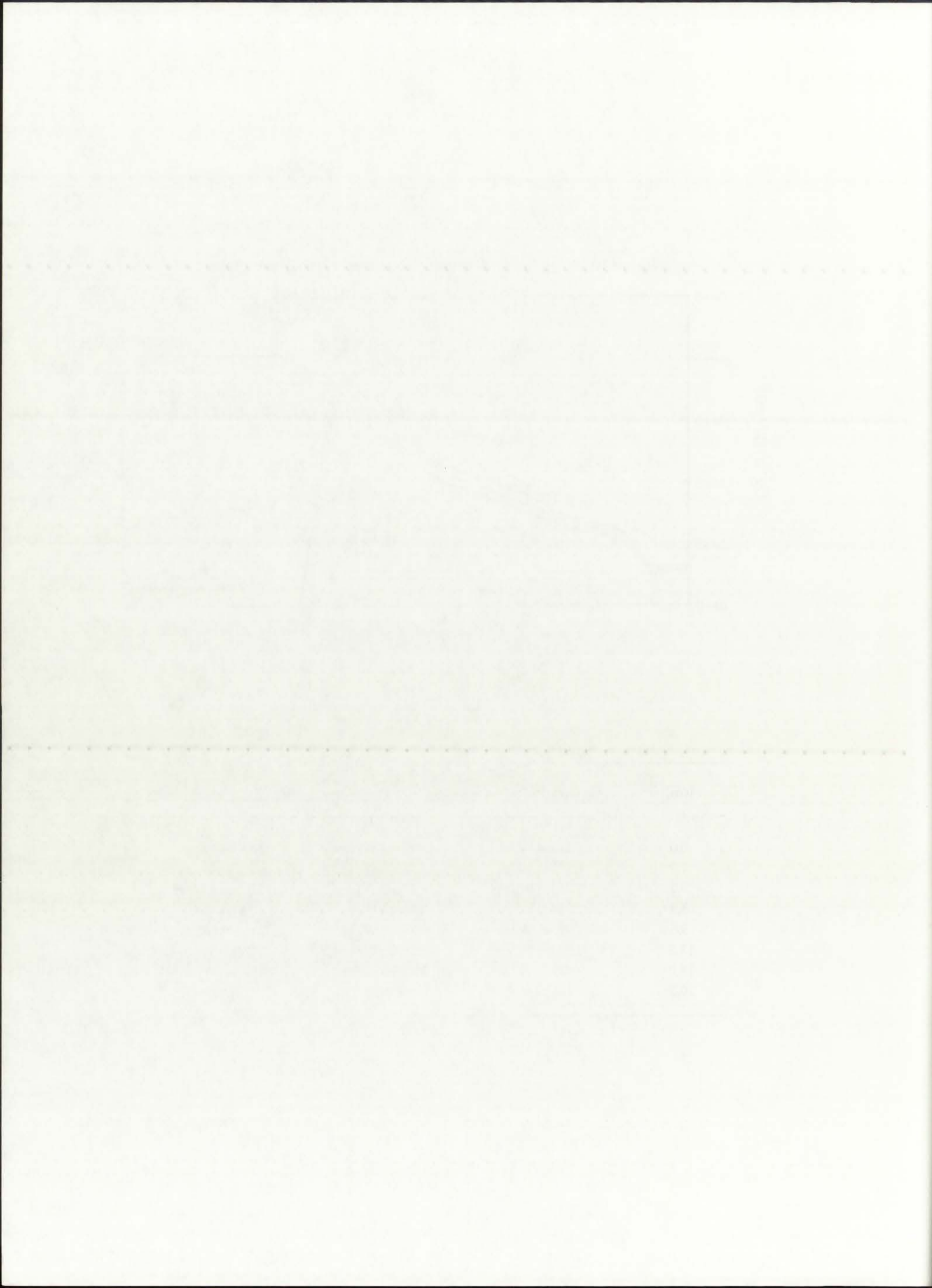
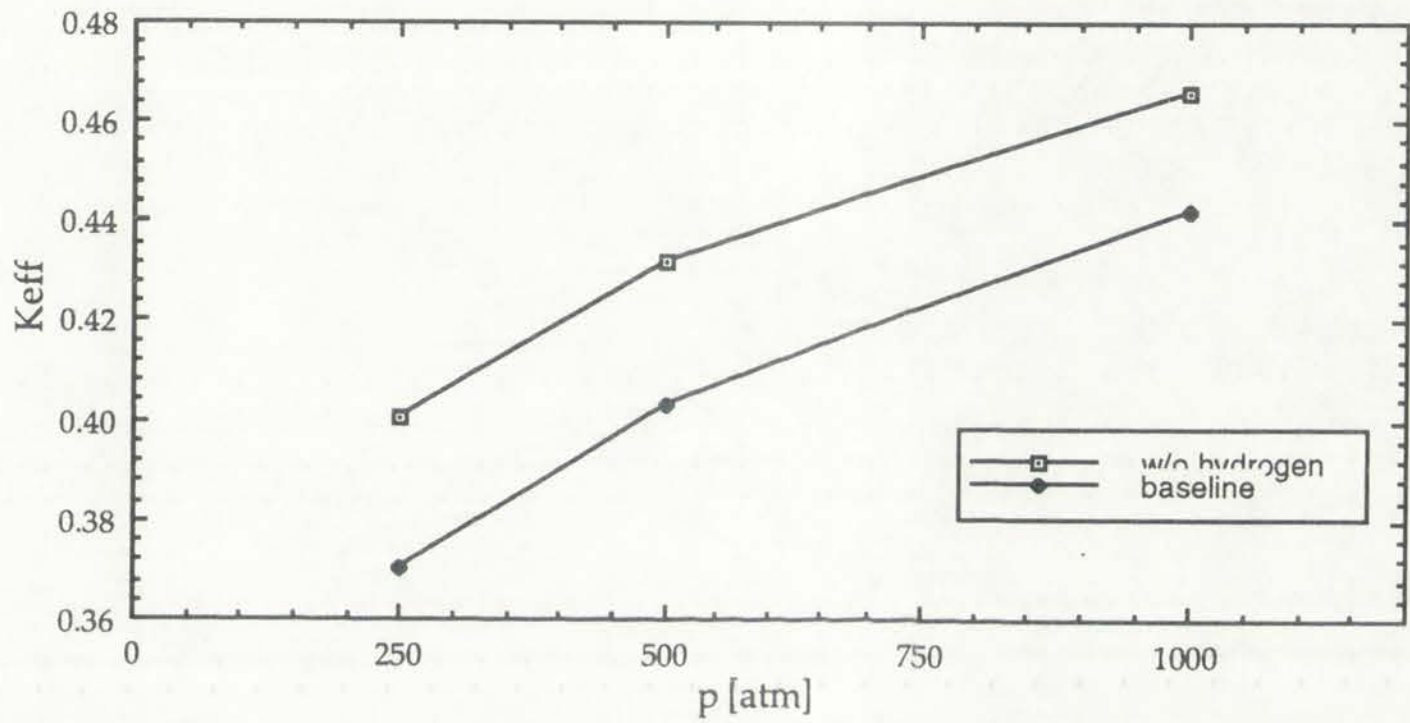


Figure 10.18: K_{eff} for 50 kWth configuration (ENDF/B-V library).



engine design	k_{eff} , P=250 atm	k_{eff} , P=500 atm	k_{eff} , P=1,000 atm
baseline	0.3704	0.4032	0.4419
w/o hydrogen	0.4003	0.4321	0.4659

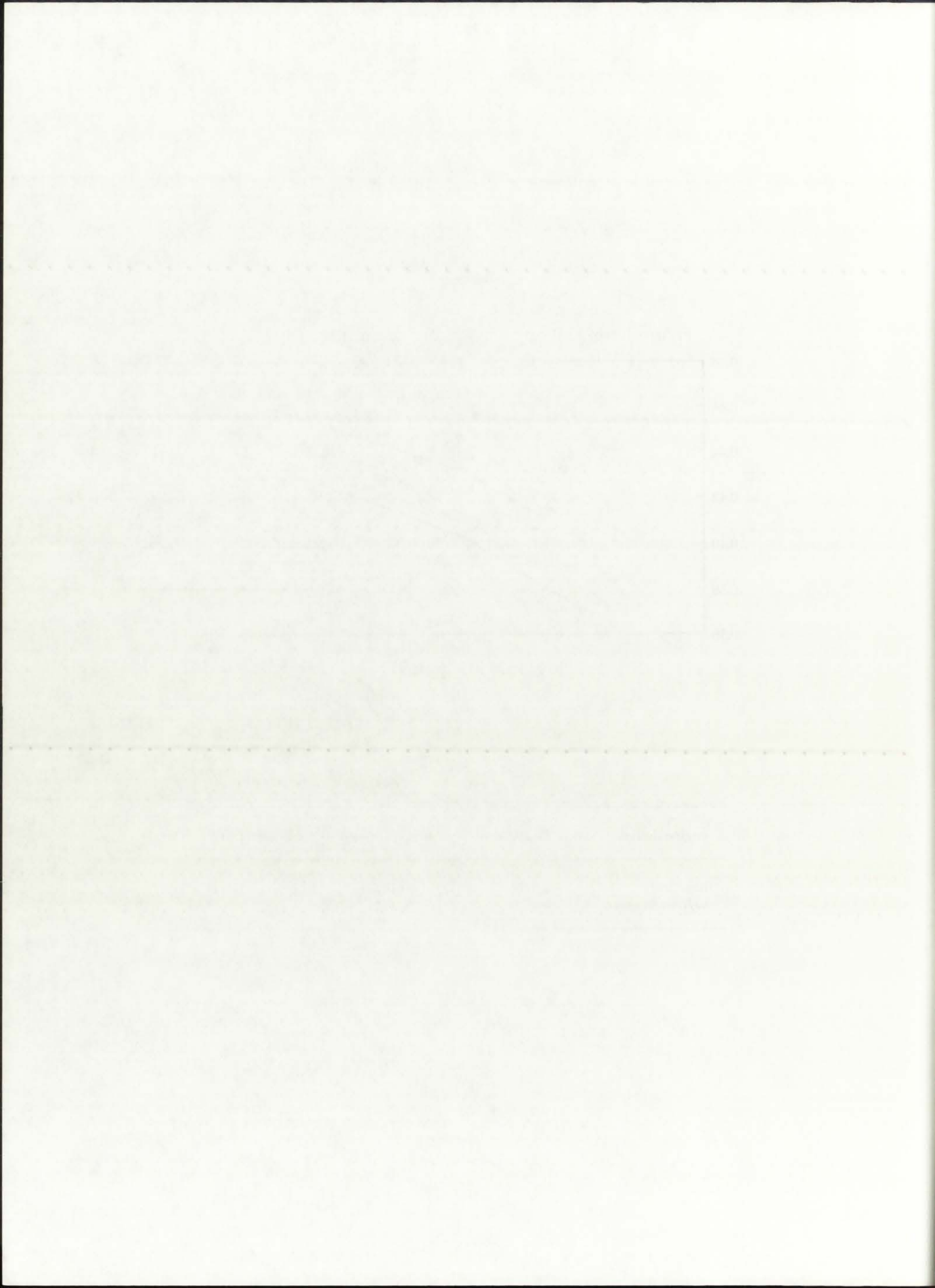


Figure 10.19: $T(r)$ for 50 kWth, ENDF/B-V library, comprehensive thermal analysis.

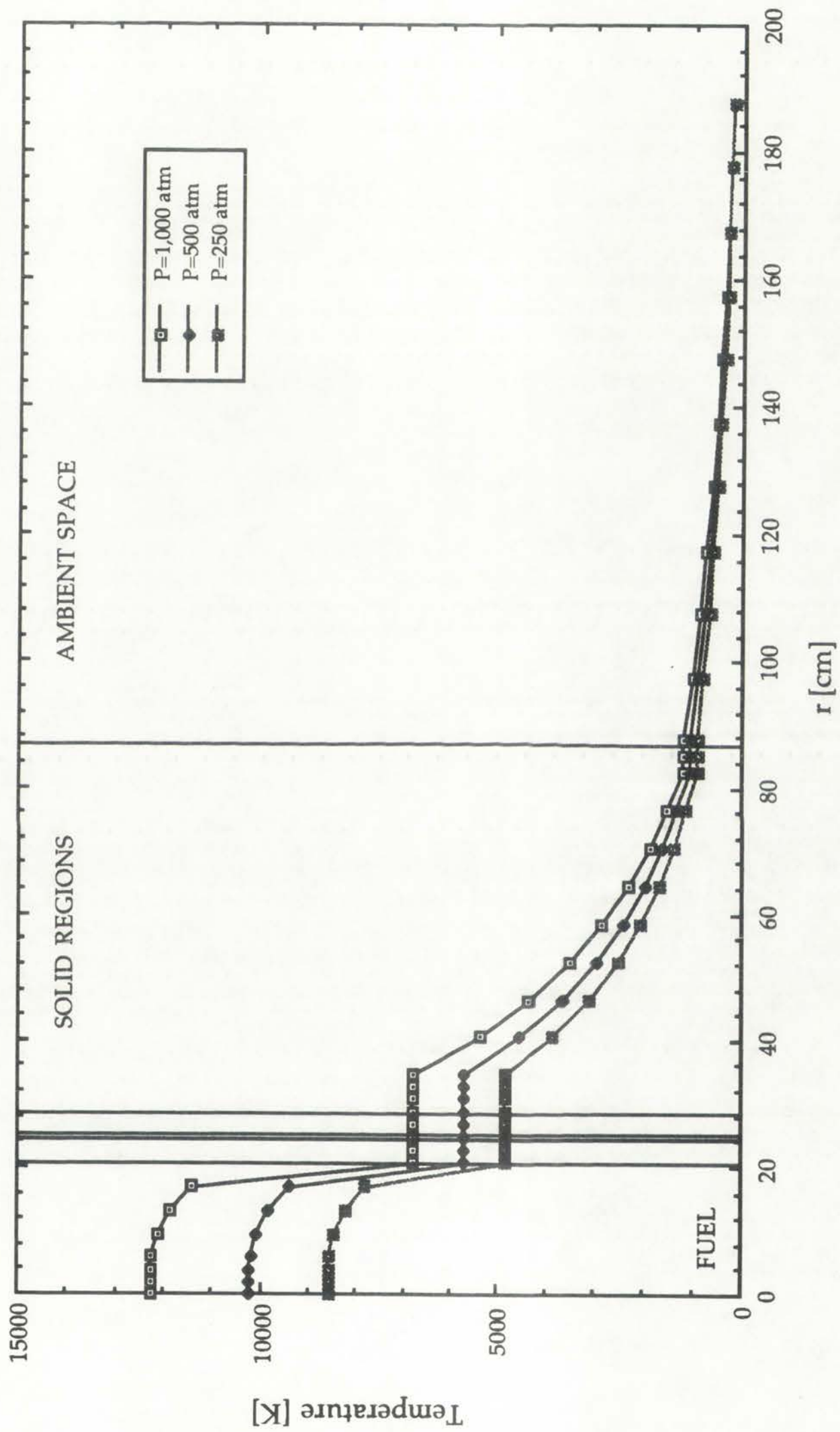




Figure 1: A step function with a jump discontinuity at $x=1$.



Figure 2: A smooth curve representing a continuous function.

Figure 1: A step function with a jump discontinuity at $x=1$. Figure 2: A smooth curve representing a continuous function.

TABLE 10.7
 Summary of the comprehensive thermal analysis results
 (50 kWth configuration, ENDF/B-V library)

P=250 atm

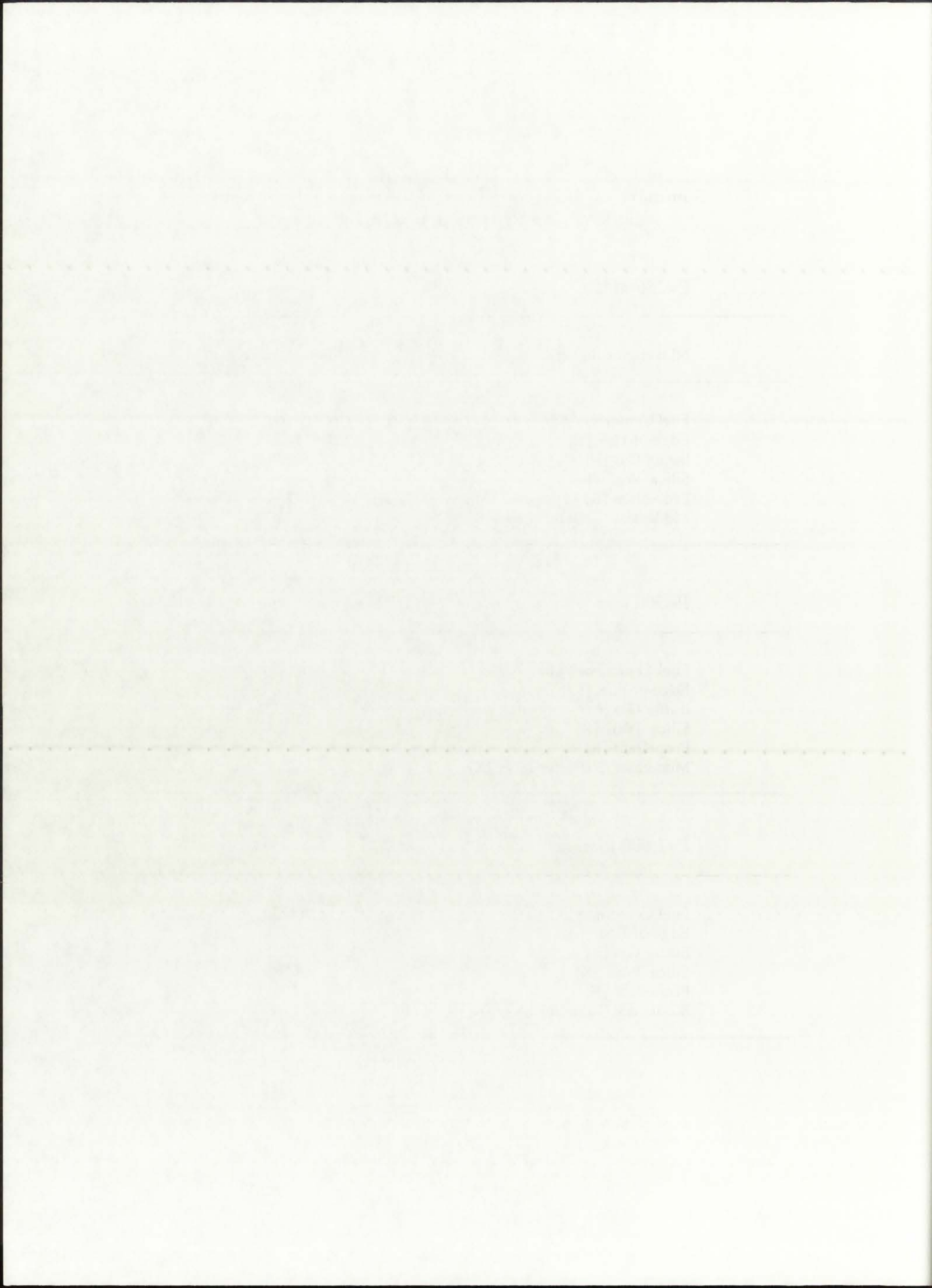
NLB engine region	Temperature
Fuel Centerline [K]	8,560
Edge-of-Fuel [K]	4,833
Buffer Gas [K]	4,833
Silica Wall [K]	4,833
Propellant [K]	4,833
Moderator/Reflector Liner [K]	4,831

P=500 atm

Fuel Centerline [K]	10,212
Edge-of-Fuel [K]	5,717
Buffer Gas [K]	5,717
Silica Wall [K]	5,717
Propellant [K]	5,717
Moderator/Reflector Liner [K]	5,714

P=1,000 atm

Fuel Centerline [K]	12,248
Edge-of-Fuel [K]	6,791
Buffer Gas [K]	6,791
Silica Wall [K]	6,791
Propellant [K]	6,791
Moderator/Reflector Liner [K]	6,788



10.6. Variation of $T(r)$ for Fixed Operating Pressures

In addition to analyzing the dependence of $T(r)$ on the operating pressure for a given thermal power, it is also of interest to determine the effects on $T(r)$ of varying the thermal power within a fixed pressure. Thus, the $T(r)$ data generated for the three thermal power configurations (500 MWth, 5 MWth, and 50 kWth) and discussed in the previous three sections has been arranged with respect to operating pressure. $T(r)$ data based on Hansen-Roach cross-sections for $P=250, 500,$ and $1,000$ atm is plotted in Figures 10.20, 10.21, and 10.22, respectively. $T(r)$ data based on the TRANSX-processed ENDF/B-V cross-sections for $P=250, 500,$ and $1,000$ atm is shown in Figures 10.23, 10.24, and 10.25, respectively.

In each of the graphs it is evident that, for a constant pressure, an increase in thermal power by a factor of 100 results in an increase in the fuel temperature of a factor of 3.2. The increase in fuel temperature as a result of increased pressure, for a fixed thermal power, also needs to be explained. The GNRATR-1D results indicate that, at any given point within the engine for a fixed thermal power, the local temperature $T(r)$ increases with increasing operating pressure. This behavior is the result of a decrease in the effective radiative conductivity within the gases, which in turn is tied to an increase in the opacity of the gases with increasing pressure. Namely, between $P=250, 500,$ and $1,000$ atm, the opacity of the uranium gas increases approximately proportional to the pressure [Krascella, 1963; Parks, 1968; and Patch, 1970]; thus, the opacity at $P=1,000$ atm is approximately double that at $P=500$ atm, which in turn is approximately double that at $P=250$ atm.

If we assume that the total heat transfer from the fuel is constant, then from eqn. (6.18) the following relation can be derived:

$$Q_{\text{total}} \approx \frac{T_{f,\text{new}}^4}{a_{R,\text{new}}}, \quad (10.2)$$

where T_f and a_R denote the fuel temperature [K] and Rosseland opacity [$1/m$].

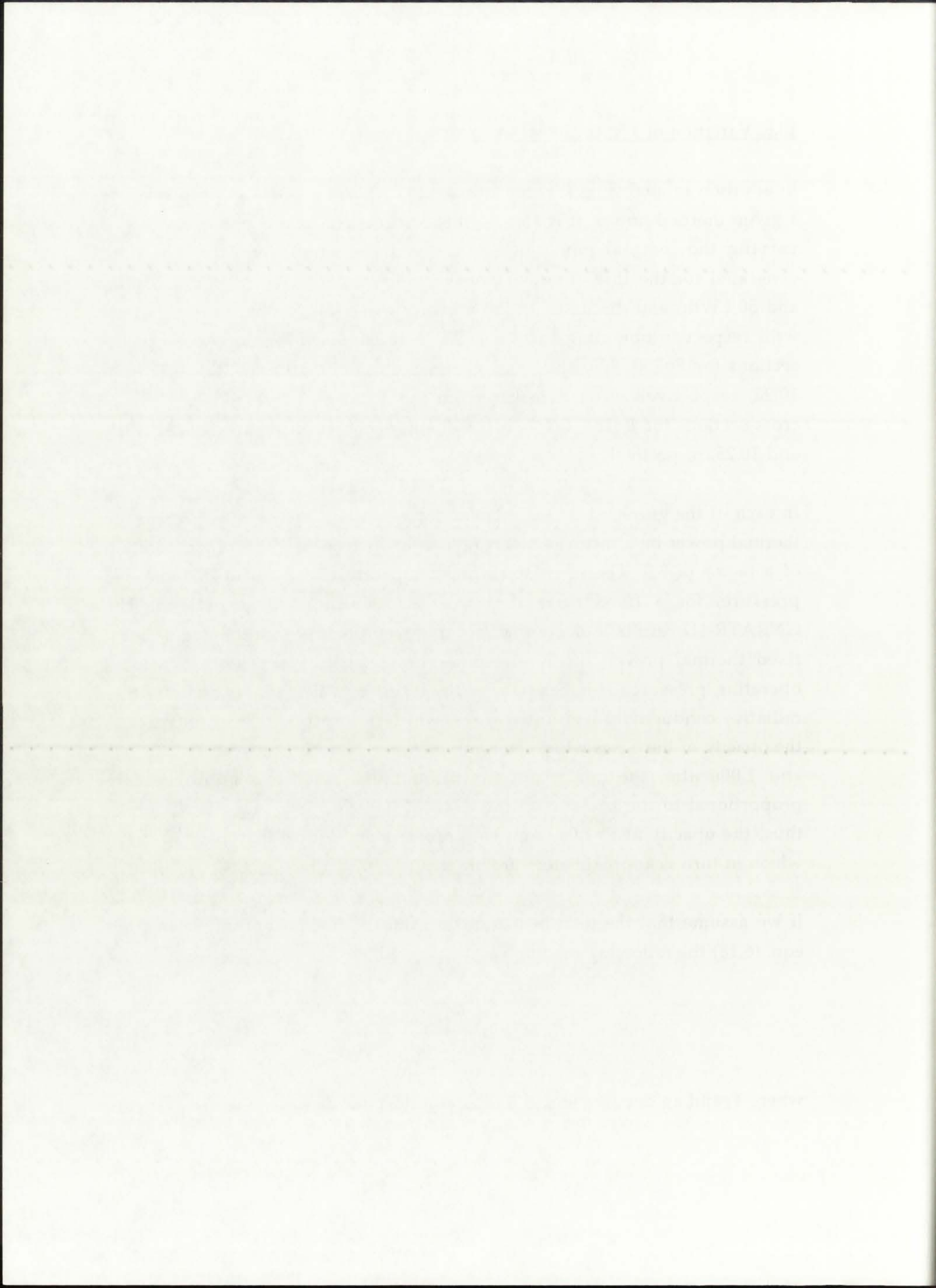
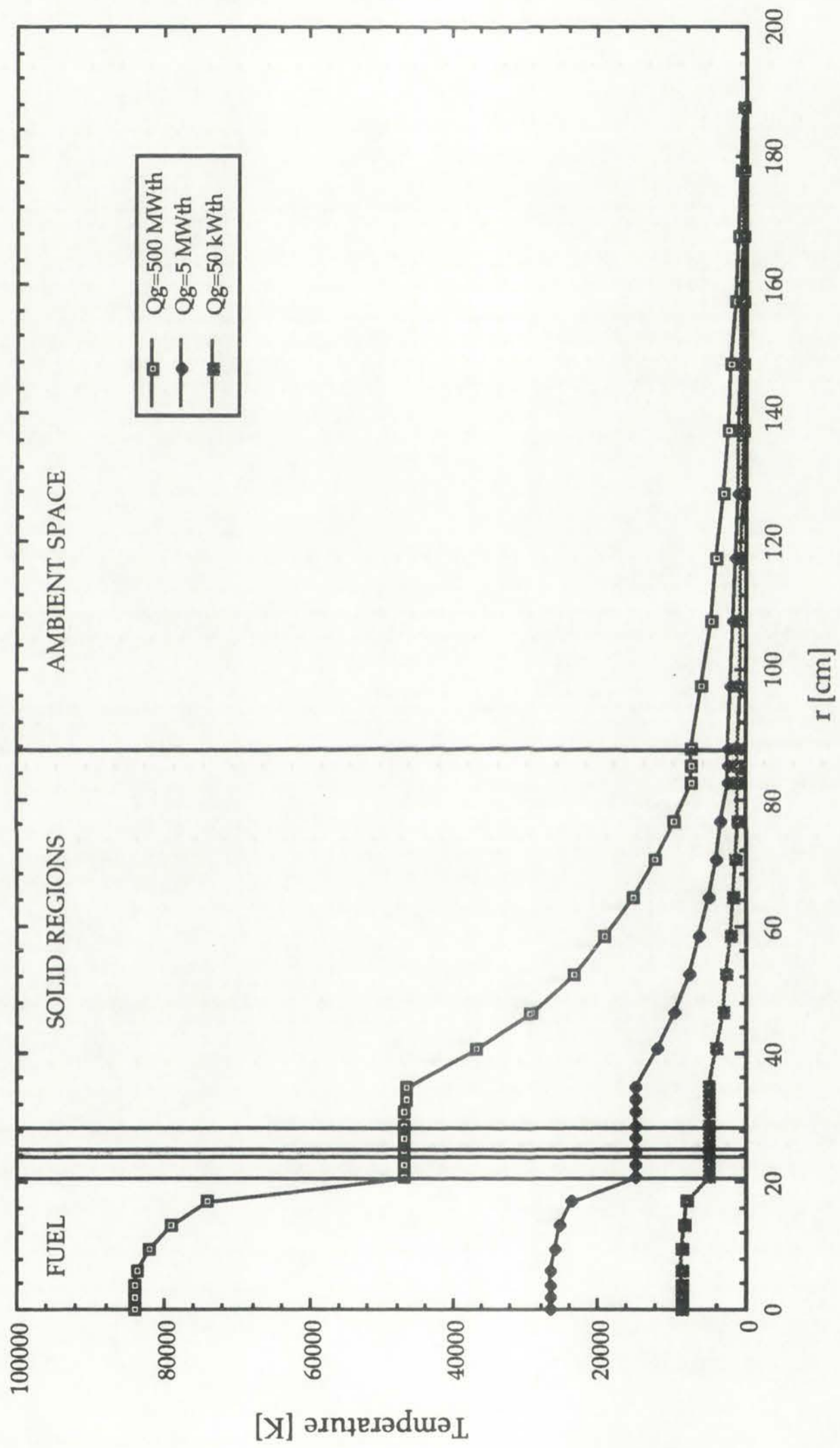


Figure 10.20: $T(r)$ for $p=250$ atm, Hansen-Roach library, comprehensive thermal analysis.



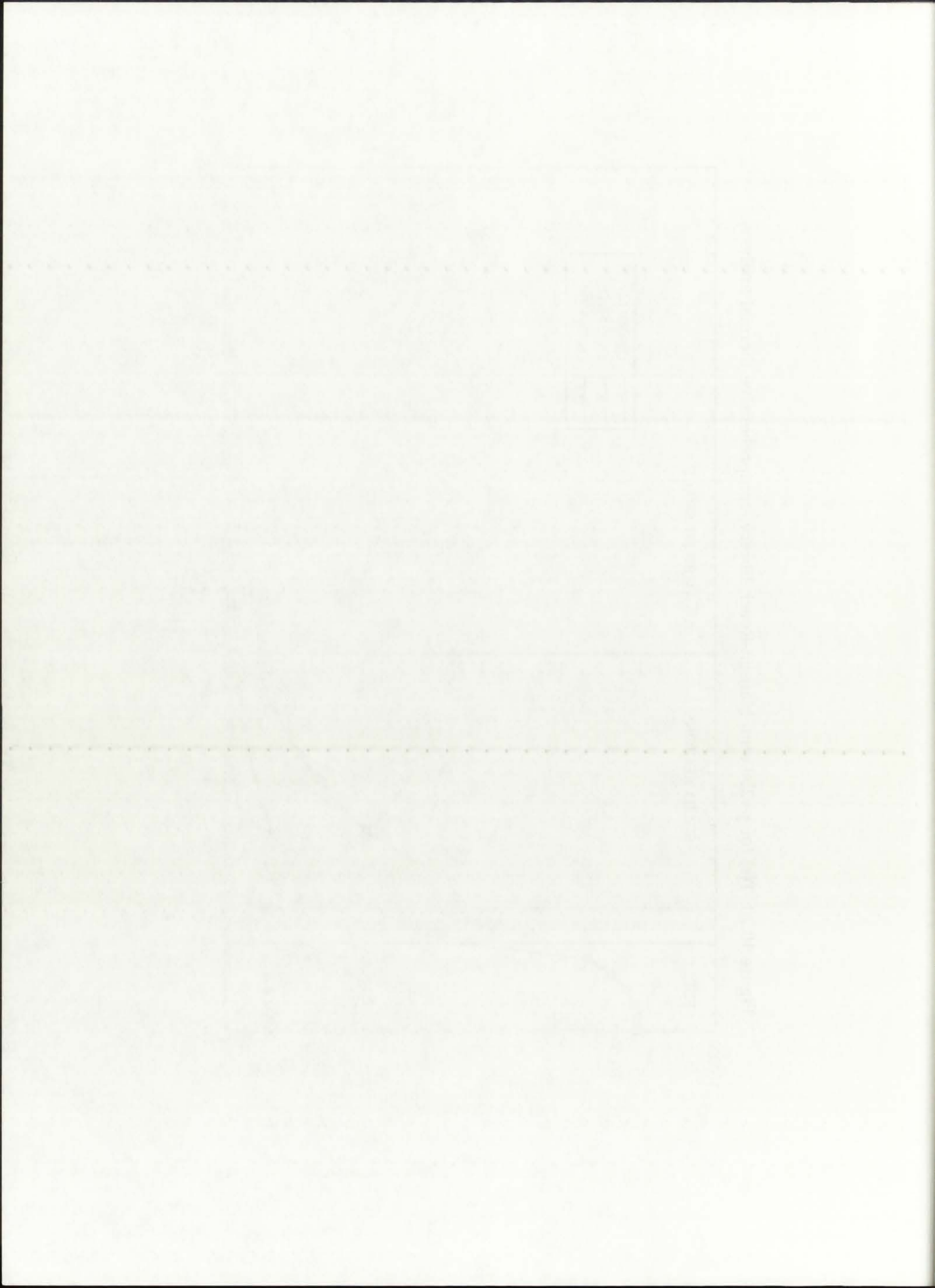
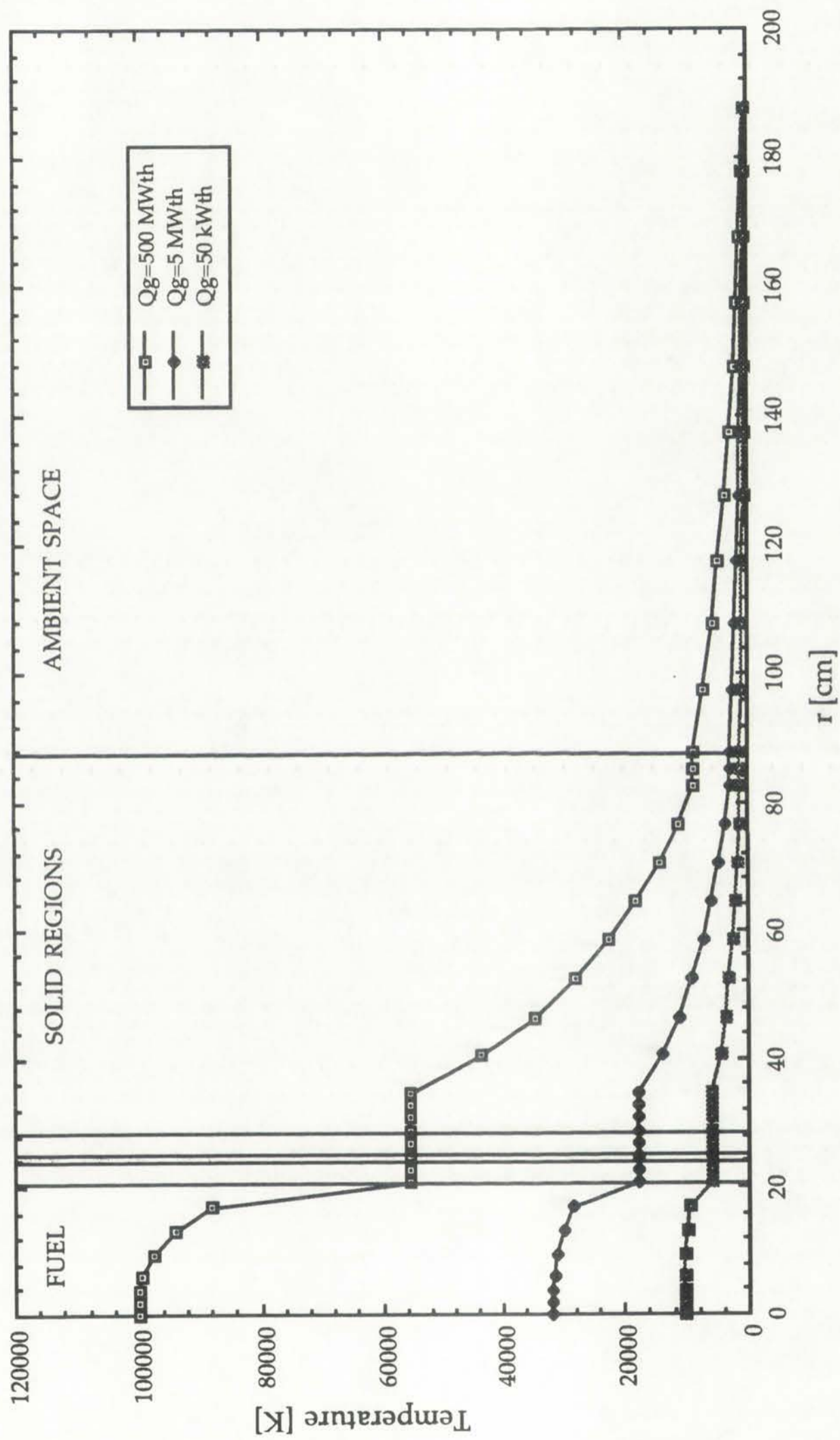


Figure 10.21: $T(r)$ for $p=500$ atm, Hansen-Roach library, comprehensive thermal analysis.



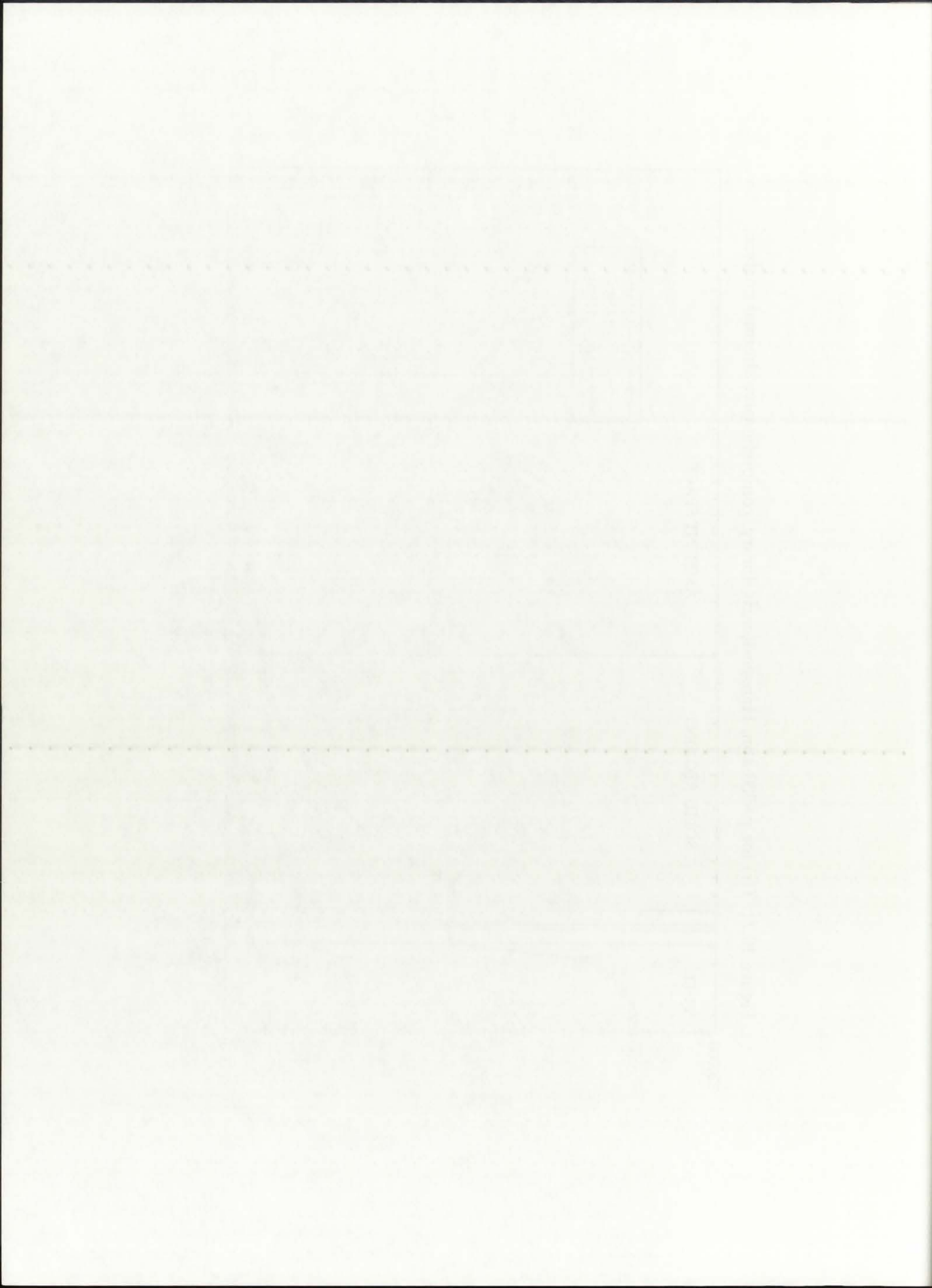
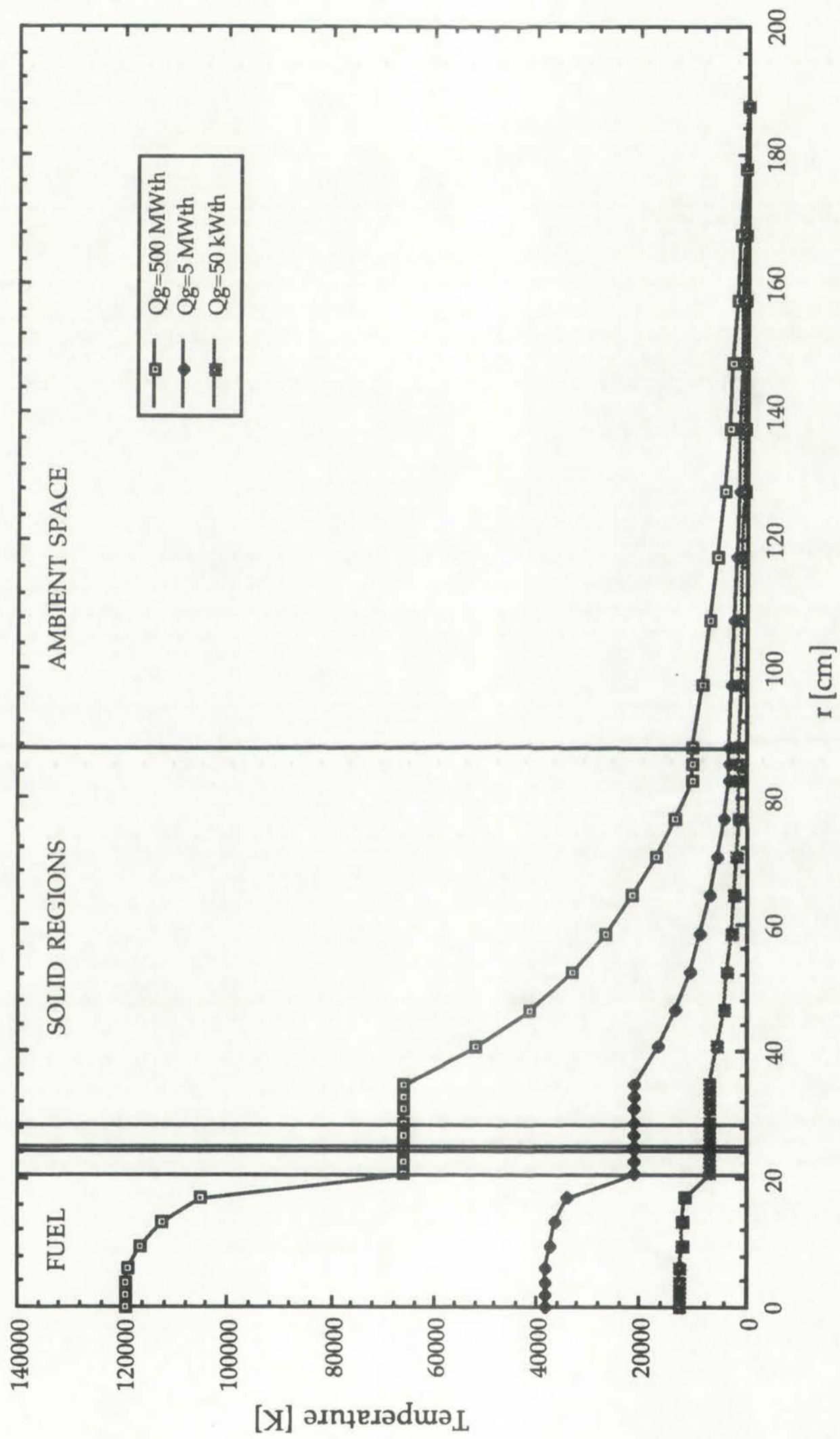


Figure 10.22: $T(r)$ for $p=1,000$ atm, Hansen-Roach library, comprehensive thermal analysis.



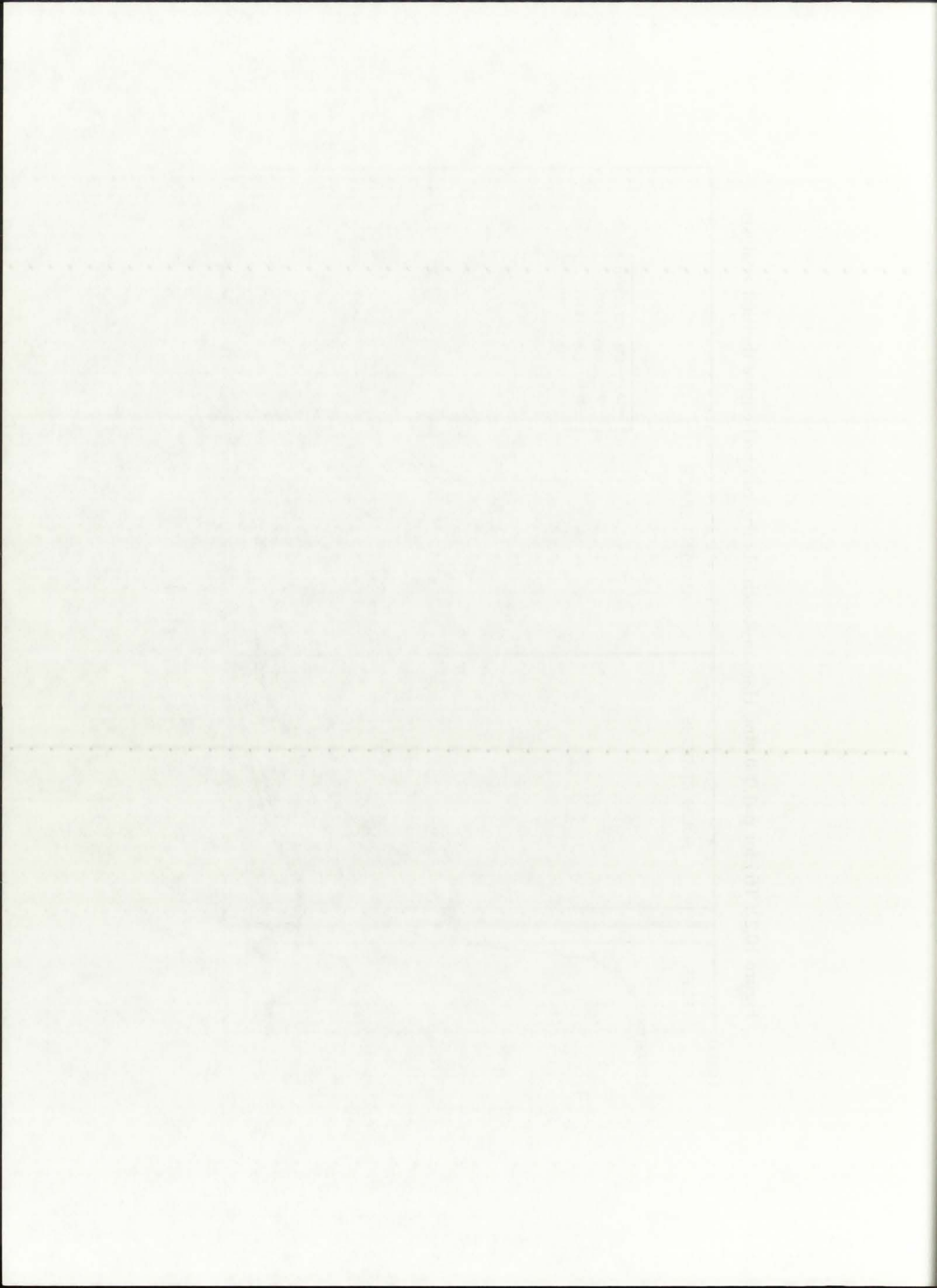
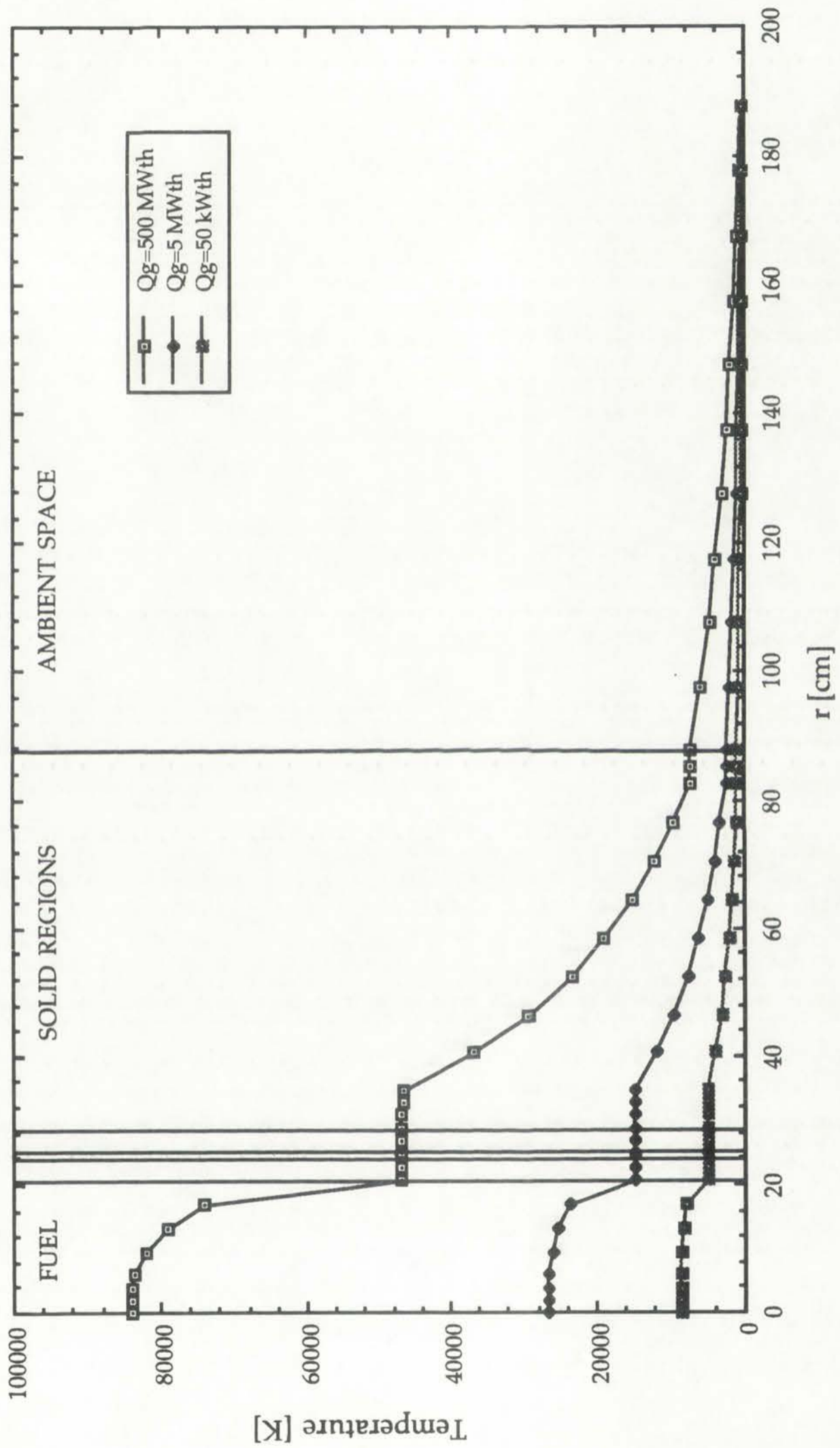


Figure 10.23: $T(r)$ for $p=250$ atm, ENDF/B-V library, comprehensive thermal analysis.



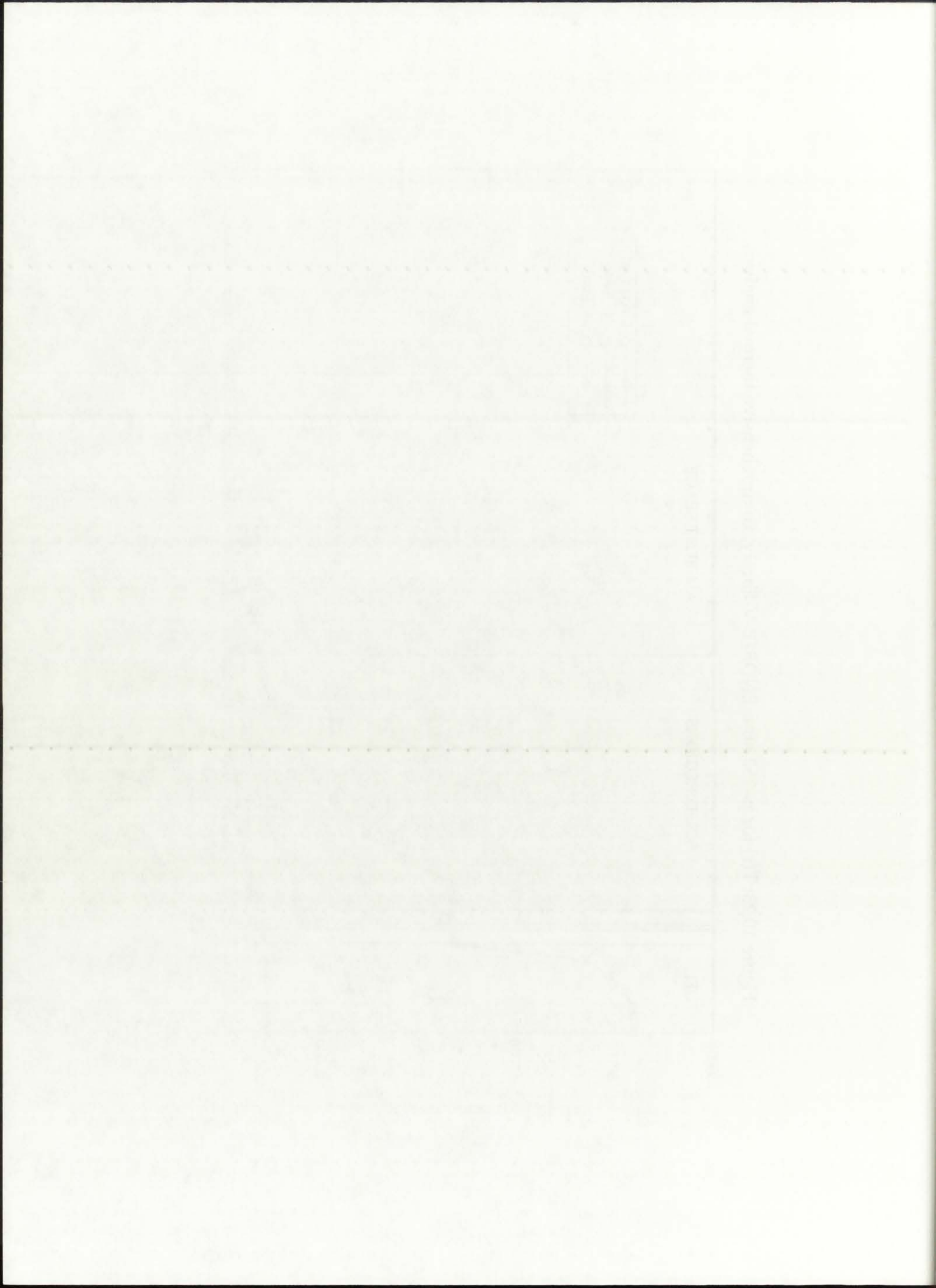
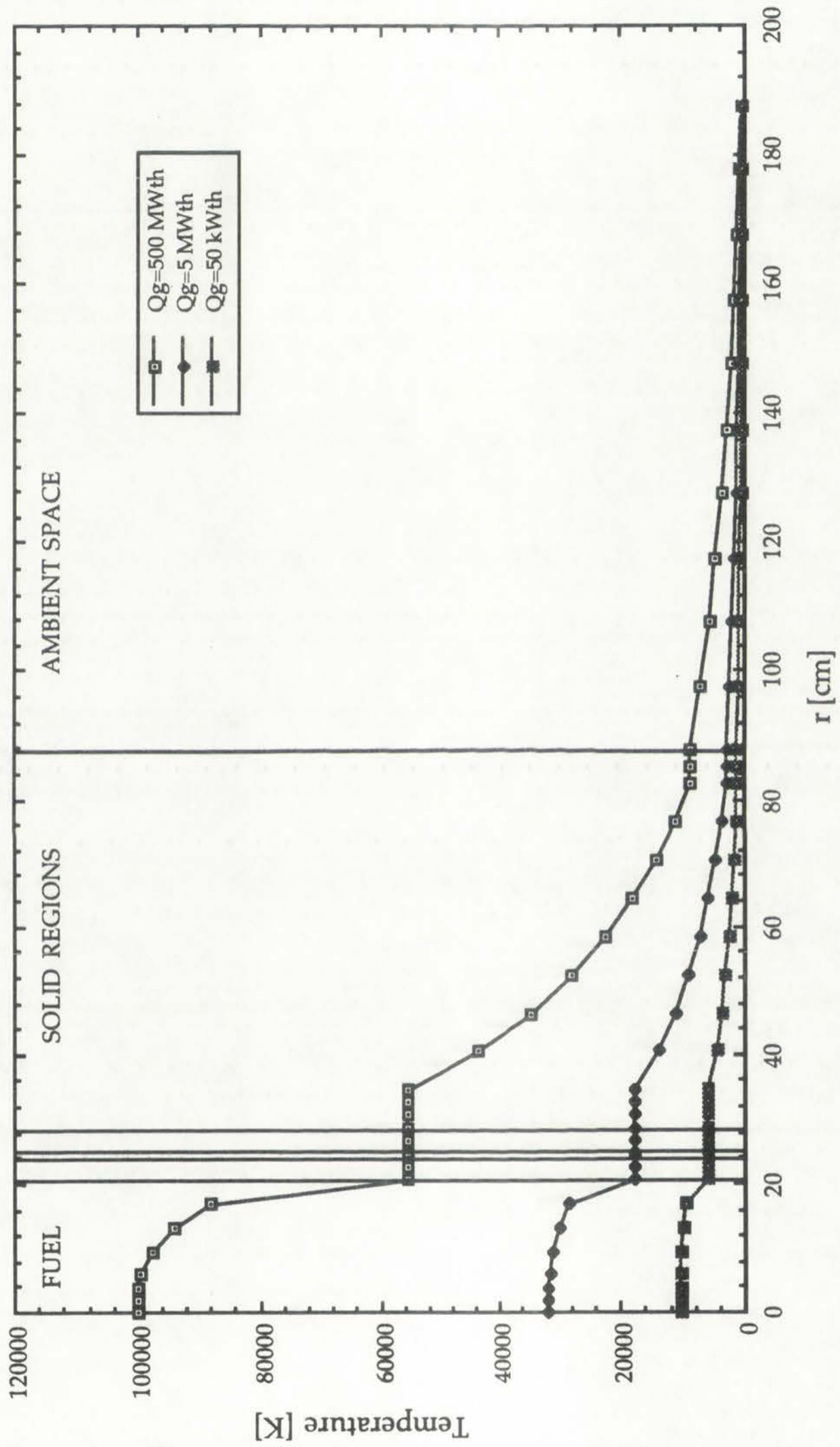


Figure 10.24: $T(r)$ for $p=500$ atm, ENDF/B-V library, comprehensive thermal analysis.



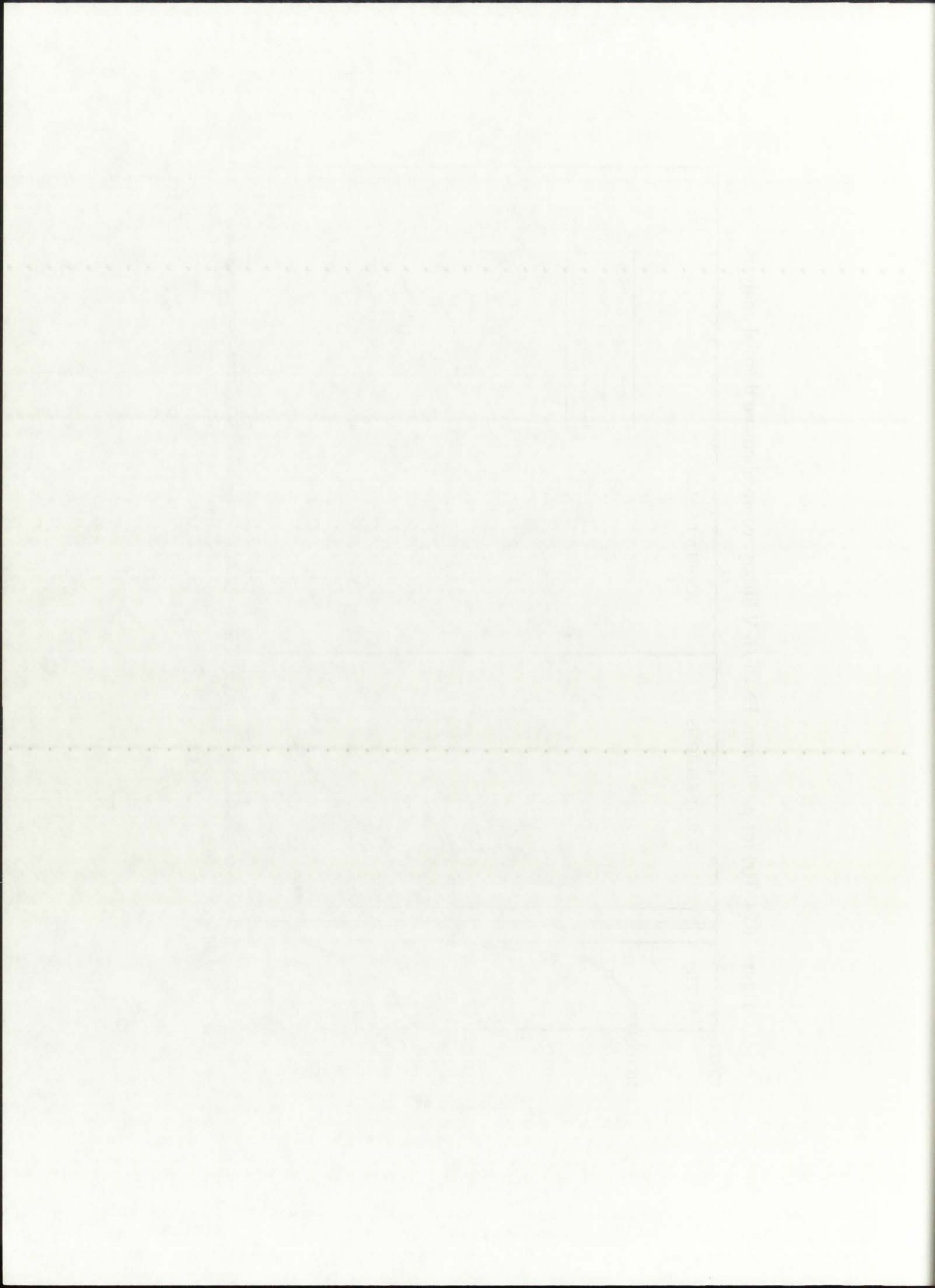
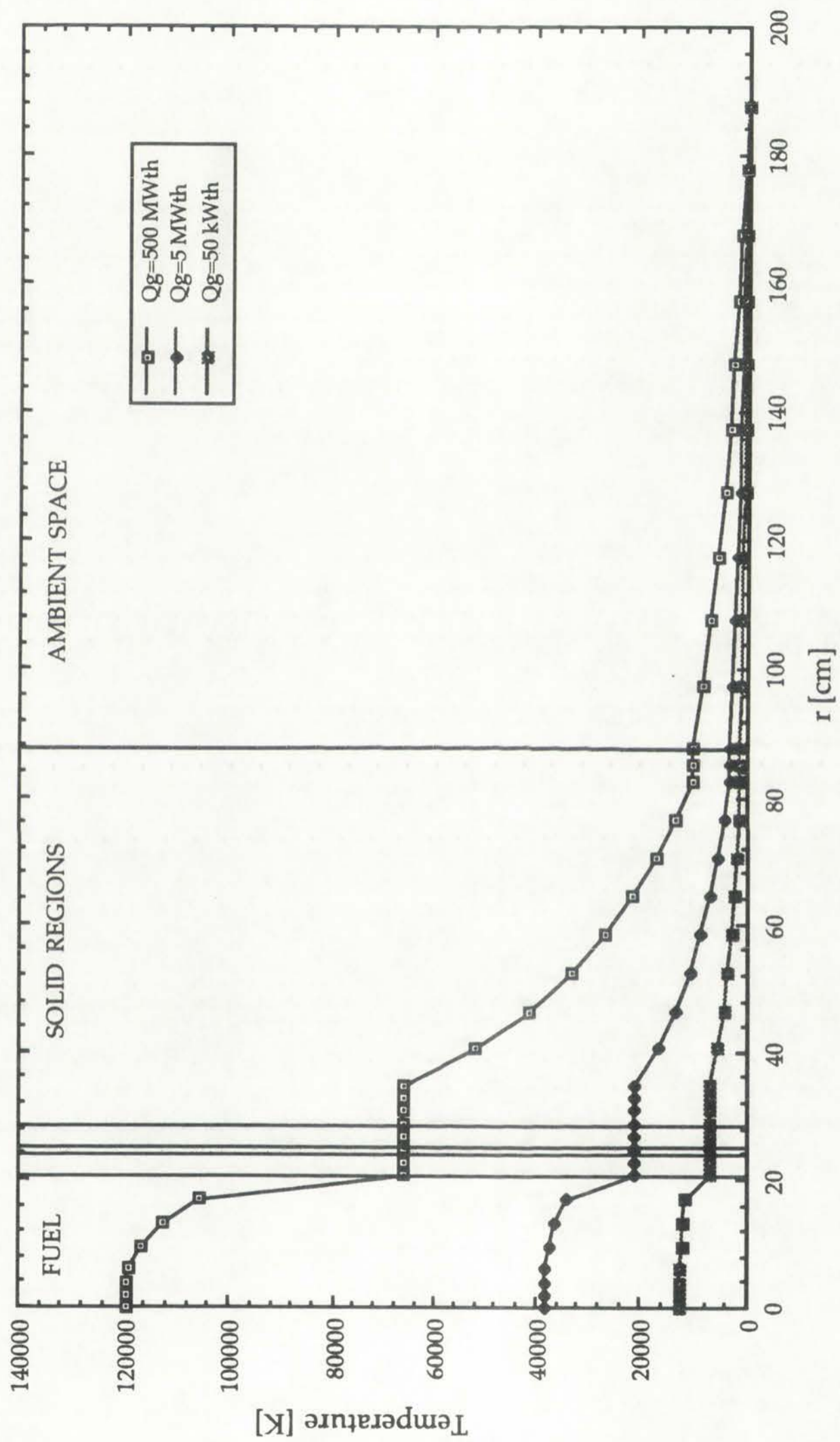
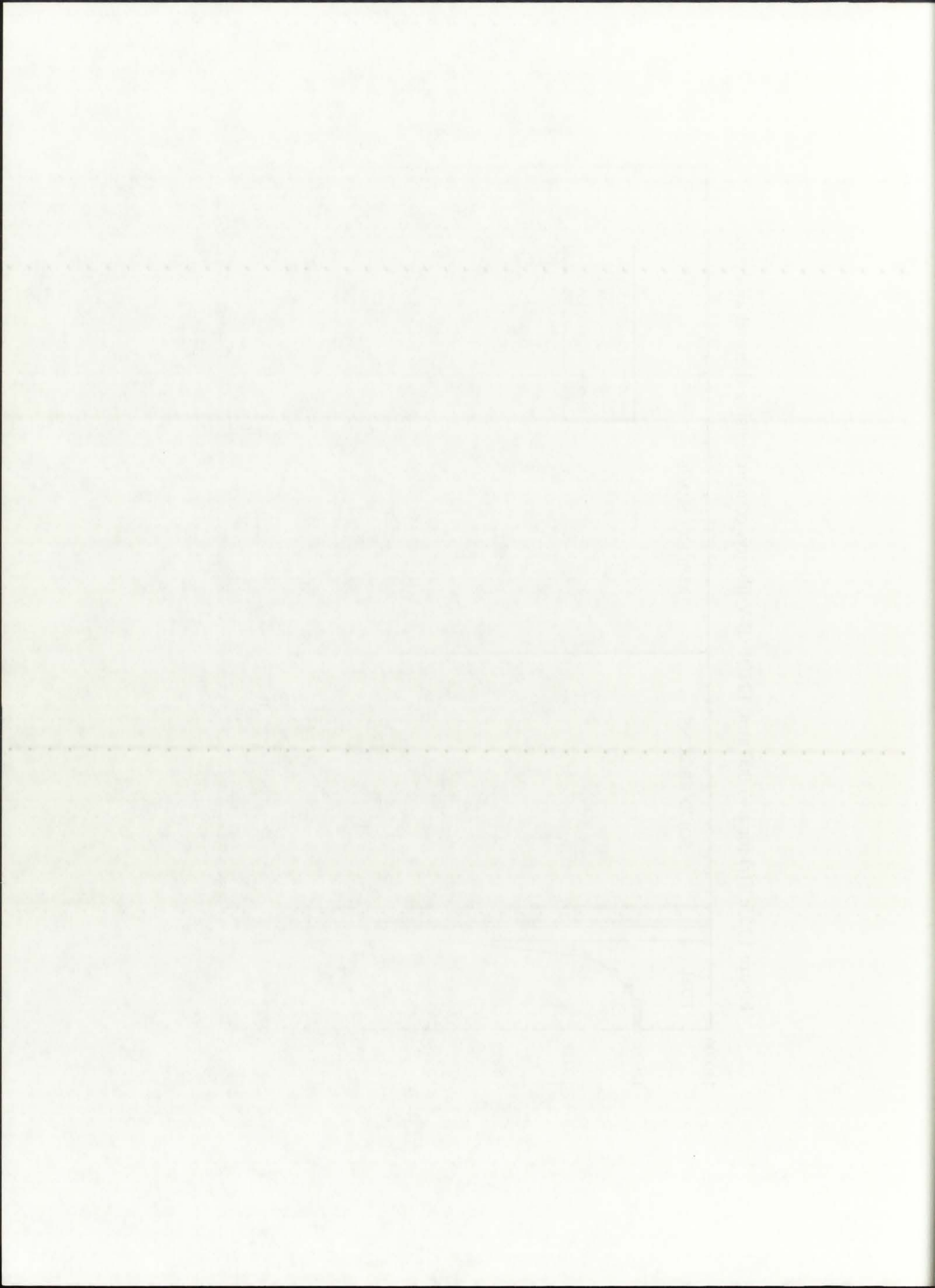


Figure 10.25: $T(r)$ for $p=1,000$ atm, ENDF/B-V library, comprehensive thermal analysis.





In the case of a doubling of the operating pressure (i.e. when comparing the 250 to 500 atm, and 500 to 1,000 atm cases), the fuel opacity approximately doubles, too. For an approximate doubling of the opacity, then, the fuel temperature T_f will increase by a proportional value x :

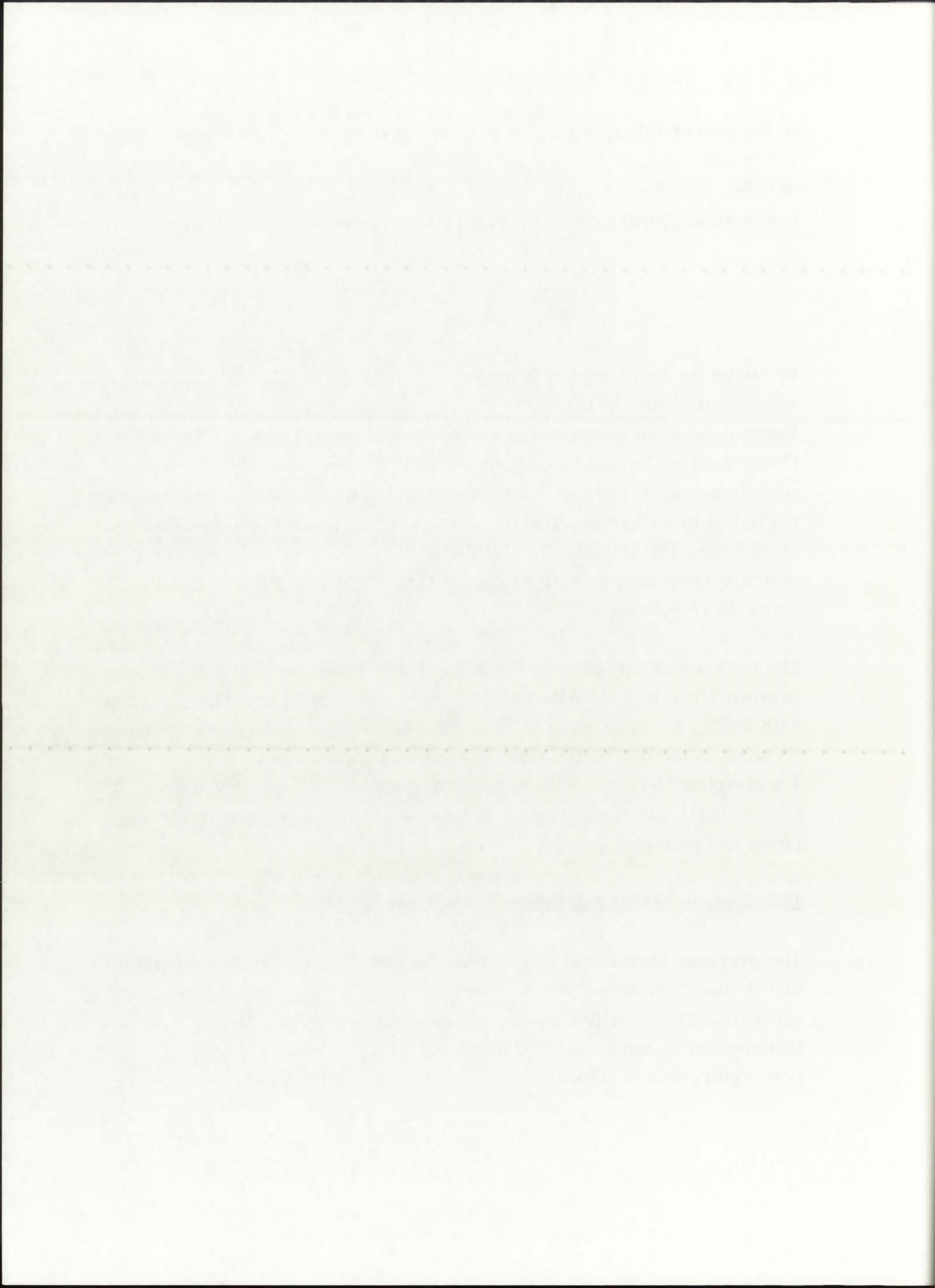
$$\frac{T_{f,new}^4}{a_{R,new}} \approx \frac{(xT_{f,old})^4}{2a_{R,old}} \rightarrow x = \sqrt[4]{2} . \quad (10.3)$$

By taking the fourth-root of 2, x can be found to be equal to 1.19. Using this approach to verify the GNRATR-1D data, and taking the $Q=50$ kWth, Hansen-Roach case as an example, the fuel centerline temperature for $P=250$ atm ($T=8,604$ K) multiplied by 1.19 gives 10,239 K, very close to the calculated centerline temperature for $P=500$ atm ($T=10,252$ K). The latter value, in turn, multiplied by 1.19 gives 12,184 K, in very good agreement with the calculated temperature for $P=1,000$ atm ($T=12,265$ K). The same brief calculational exercises have been performed on the $Q=5$ MWth and 500 MWth cases to verify the correctness of GNRATR-1D calculated data.

The behavior of $T(r)$ in the r -direction of the engine, as well as differences between $T(r)$ calculated with Hansen-Roach cross-sections and $T(r)$ calculated with ENDF/B-V cross-sections, have been discussed in detail in the previous Sections; as the data is the same, the discussions will not be repeated here. The complete $T(r)$ data can be found in Appendices B, C, and D in the form of GNRATR-1D summary output files for a given combination of thermal power and pressure.

10.7. Thermophysical and Rocket Performance Results

The previous four sections, 10.3-10.6, focused on the overall temperature distribution $T(r)$ across the NLB engine, for a given thermal power and pressure. This section is aimed at comparing the more specific thermophysical and rocket performance parameters with respect to thermal power and pressure. These parameters, although not the most crucial players



in determining the feasibility of the concept, serve to indicate what one could expect if the concept were to be made feasible under the specified thermal power and pressure conditions. These parameters also provide insight into the potential capabilities of the unit-cell NLB engine, namely its strengths and weaknesses as a proposed space propulsion system.

Figures 10.26-10.30 illustrate the dependence of fuel centerline, edge-of-fuel, propellant, silica wall, and reflective liner temperatures on the thermal power and operating pressure. Radiation, convection, and conduction are present as part of the comprehensive thermal analysis, and the results are based on a conservative assumption of 0% reflection off the solid regions' reflective liner. To reduce the amount of data and graphs presented in this particular Section, only the region temperatures obtained with the ENDF/B-V cross-sections have been plotted. The Hansen-Roach library-based results were only intended to be used for the purposes of comparison, so results based on ENDF/B-V should be taken as more accurate in this case. In addition, since both sets of results turned out very similar, no confusion should arise for the reader.

As shown previously in Table 10.1, GNRATR-1D allows the user to specify a large number of input parameters; based on such parameters, it provides the user with a comprehensive set of rocket performance results. The user can directly read the results off the summary output file, as was shown before in Figure 10.2. Observation of Figures 10.26-10.30 indicate that temperature is directly proportional to both thermal power and pressure; as was shown previously in the case of the fuel centerline, temperature increases roughly by a factor equal to the fourth root of both the increase in thermal power and the increase in operating pressure.

The next set of figures is devoted to rocket performance parameters, which generally depend on the thermophysical properties of the propellant at the axial channel exit location and are irrespective of the source of energy. Figure 10.31 shows the hydrogen propellant dissociation fraction, calculated in GNRATR-1D by application of eqns. (8.6) and (8.7).

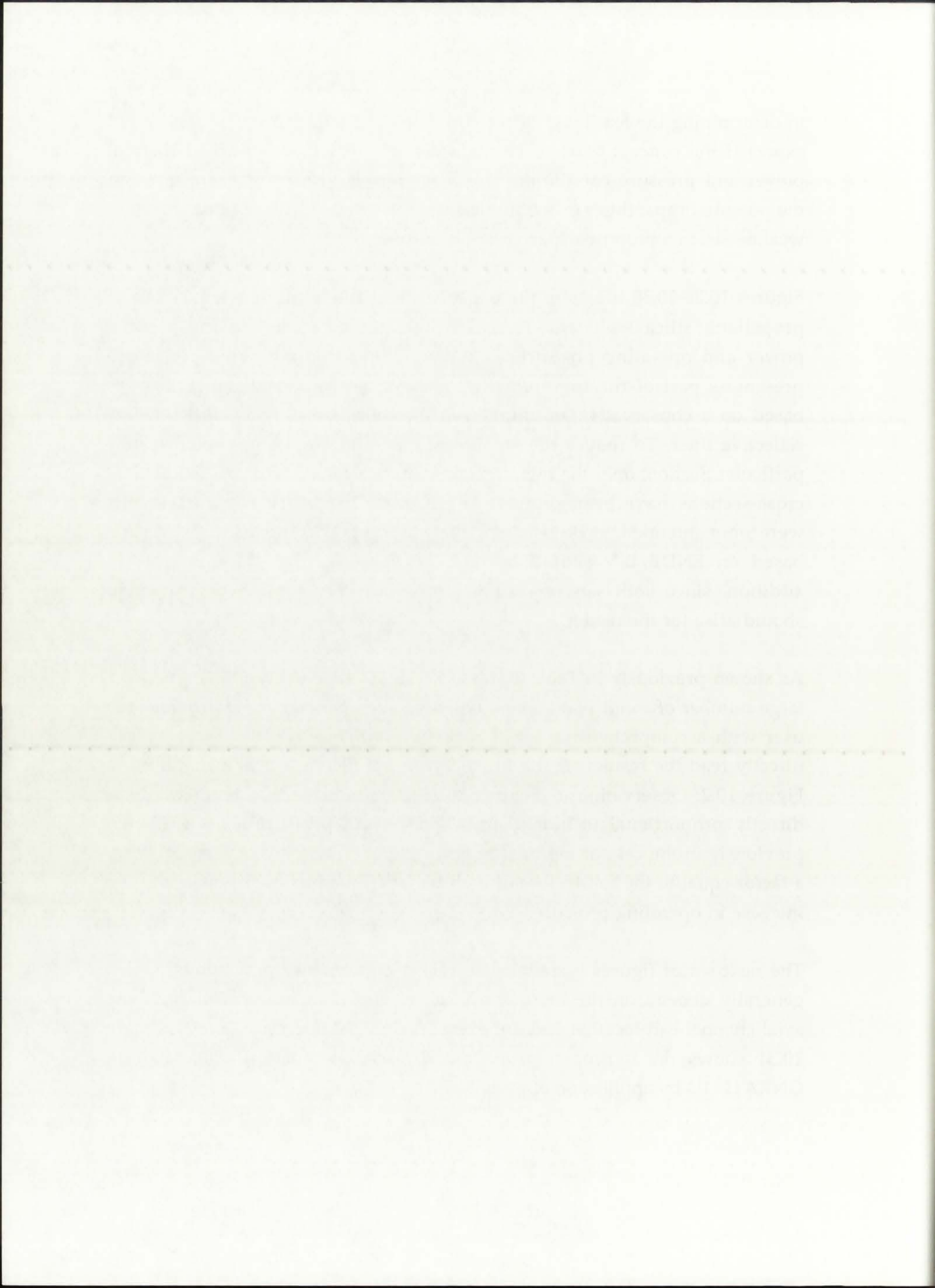


Figure 10.26: Centerline fuel temperature.

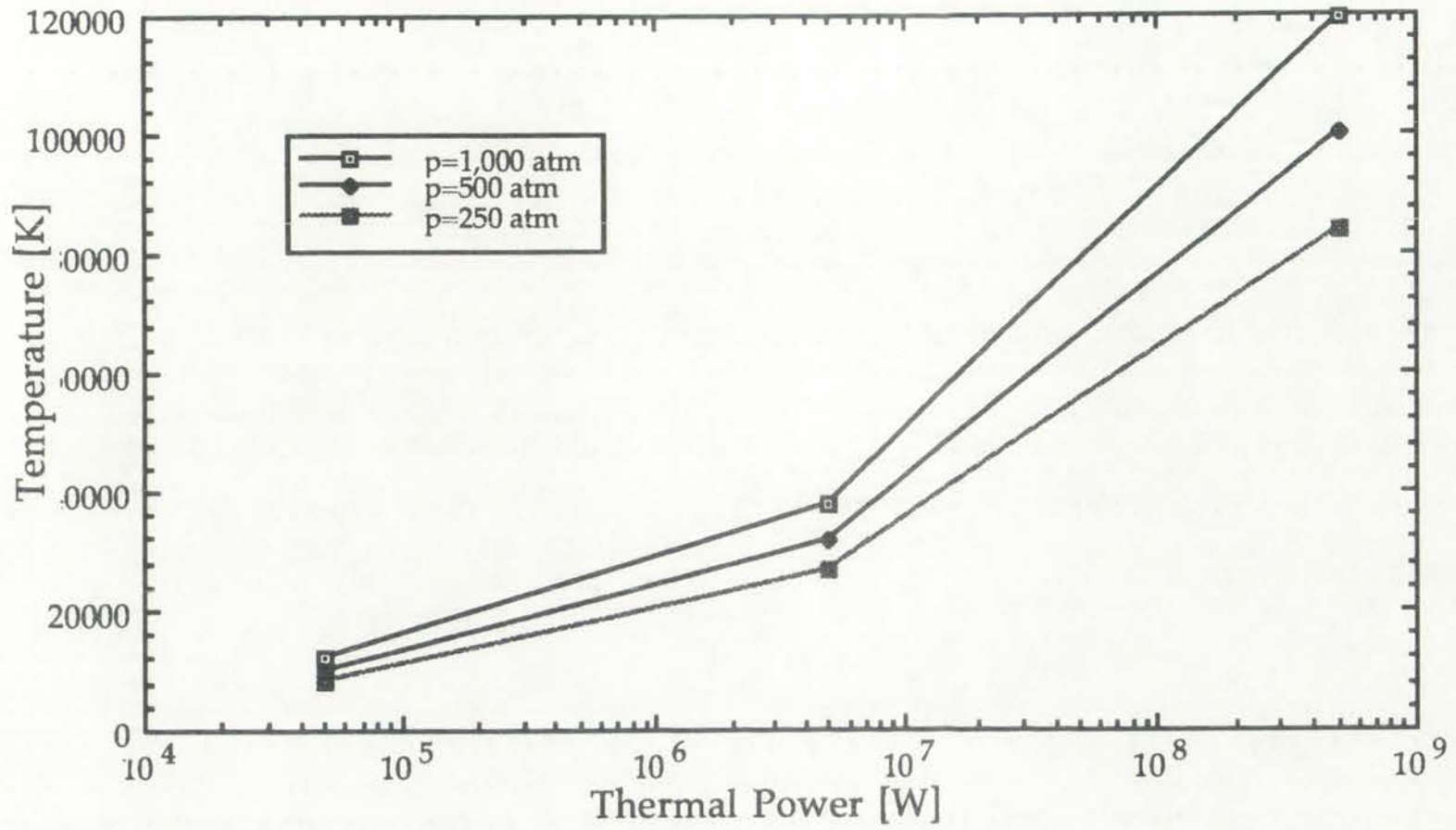


Figure 10.27: Edge-of-fuel temperature.

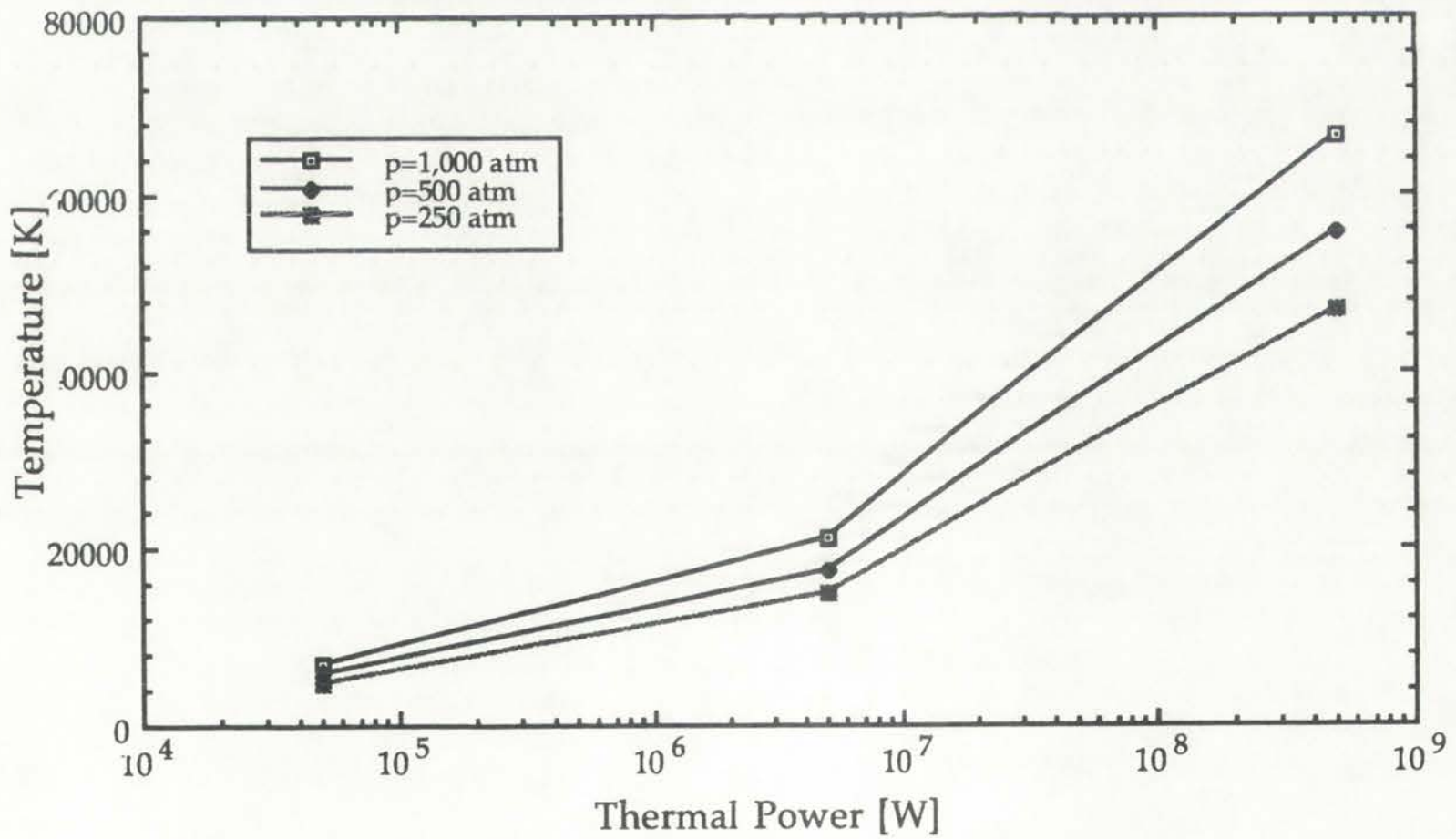


Figure 1

1000
800
600
400
200
0



Figure 2

1000
800
600
400
200
0



Figure 10.28: Propellant bulk temperature.

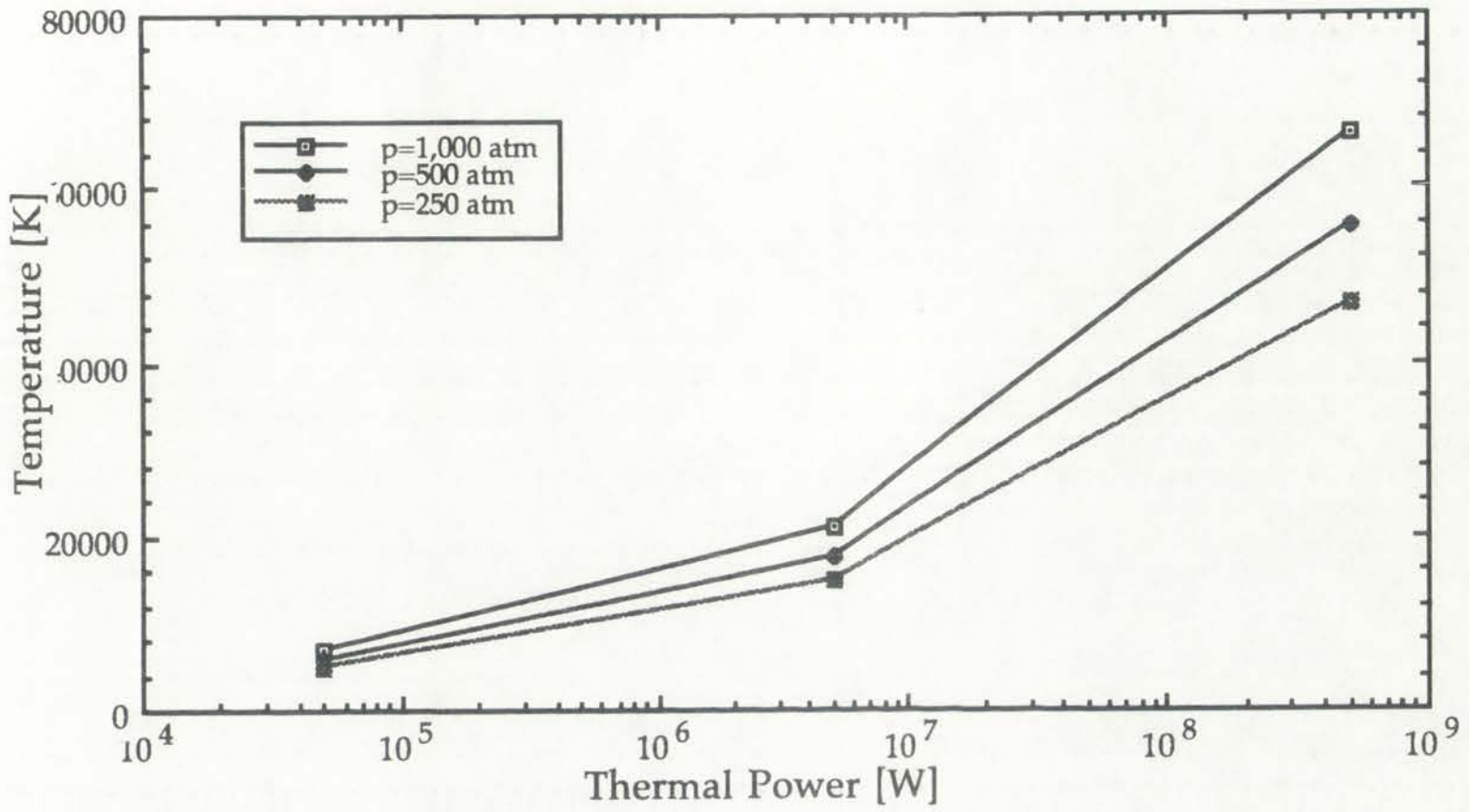
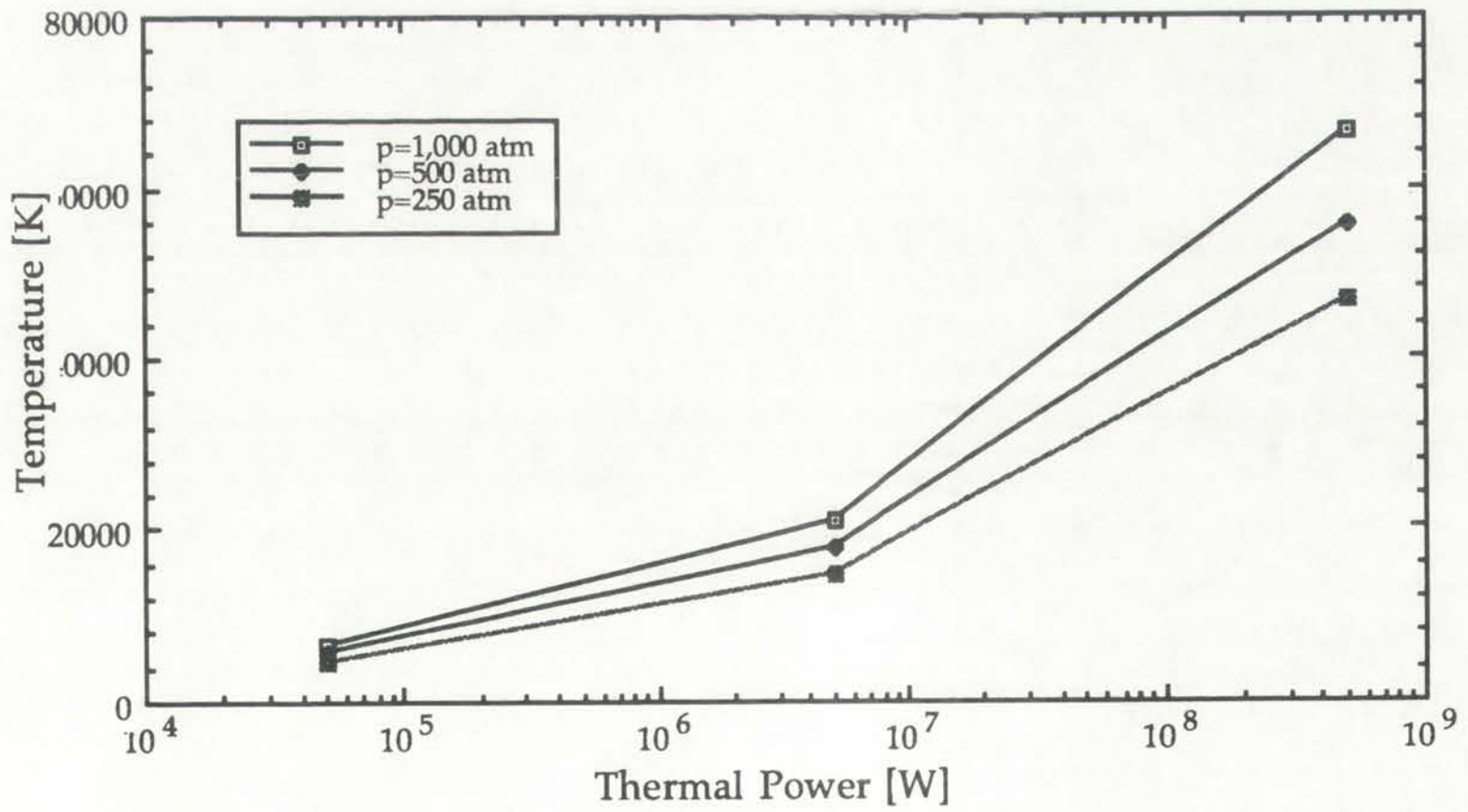


Figure 10.29: Silica wall mean temperature.



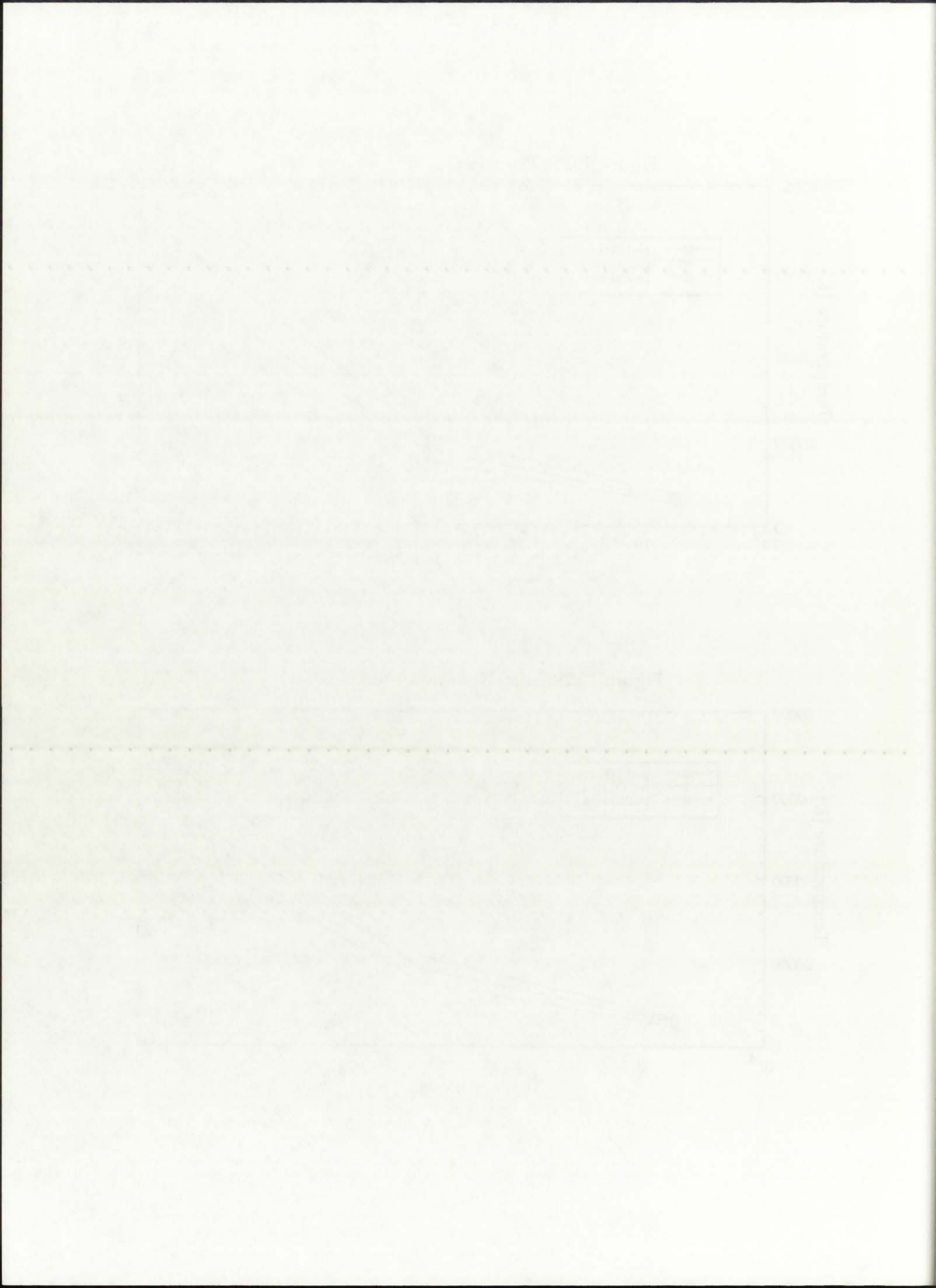


Figure 10.30: Solid region reflective liner temperature.

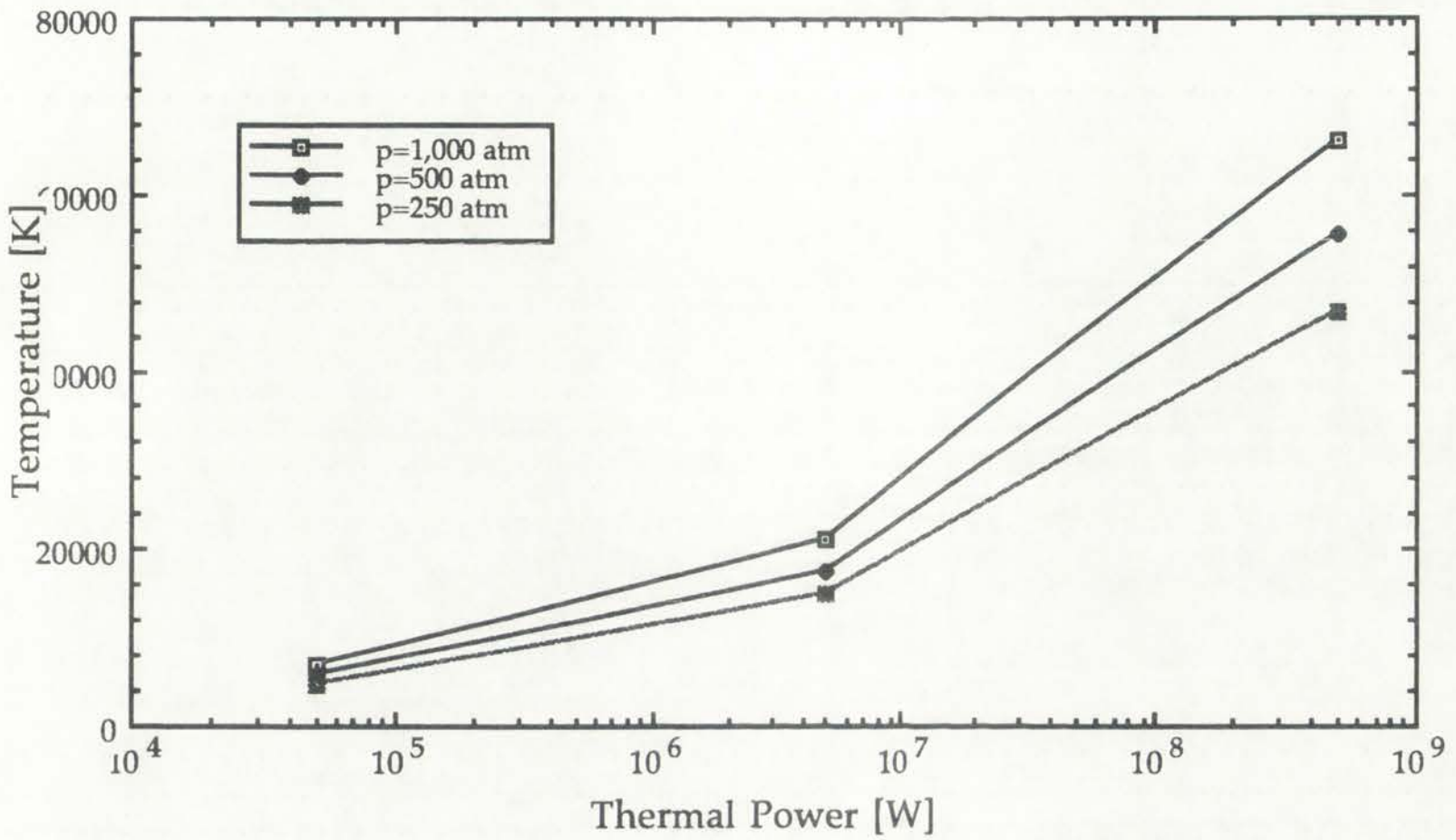
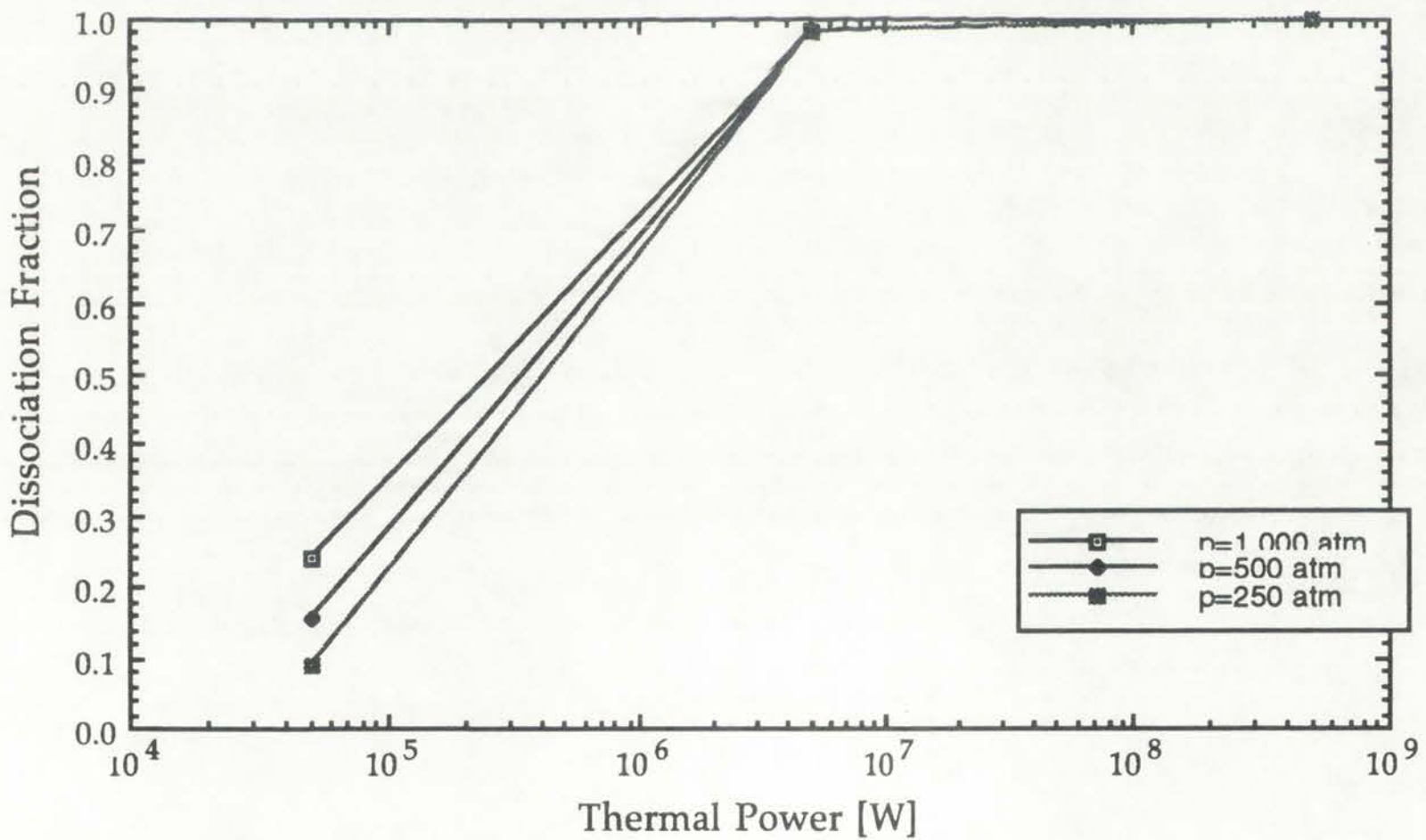


Figure 10.31: Hydrogen dissociation fraction.



100
90
80
70
60
50
40
30
20
10
0

100
90
80
70
60
50
40
30
20
10
0

100
90
80
70
60
50
40
30
20
10
0

It can be seen that the dissociation fraction increases with both thermal power and operating pressure; even though strictly speaking it is inversely proportional to pressure, the dissociation fraction is shown to be affected more by the propellant bulk temperature (which increases with pressure) than the pressure. For the MWth-range, the dissociation fraction is very close to 1.0, indicating an almost completely monatomic hydrogen-composition of the propellant. The GNRATR-1D analysis did not account for possible recombination of the propellant atoms in the nozzle of the rocket; due to the very high dissociation fractions characteristic of this engine concept, recombination is not expected to significantly influence the performance parameters.

The total propellant molecular weight is shown in Figure 10.32. Since the propellant consists of hydrogen gas and tungsten seeds, the bulk of the total molecular weight is due to tungsten (approximately 3% by composition). Thus, even though the molecular weight of hydrogen changes significantly between 50 kWth and 5 MWth, its effect is not as pronounced on the total propellant molecular weight.

Figure 10.33 shows the variation of propellant mass flow rate with thermal power and operating pressure. The mass flow rate is a direct product of the flow cross-sectional area (constant), propellant axial channel velocity, and propellant density, as given in eqn. (8.4). The decrease in propellant density is the primary reason that the mass flow rate becomes inversely proportional to thermal power.

The bulk propellant temperature and the propellant molecular weight (and thus, to a small extent, the hydrogen dissociation fraction) influence the propellant nozzle exit velocity as shown in Figure 10.34. Because of the high temperature and monatomic nature of the propellant, very high ideal exit velocities are calculated. As the variations in propellant temperature are greater than the associated variations in dissociation fraction, the propellant exit velocity curve has a shape similar to the propellant temperature curve.

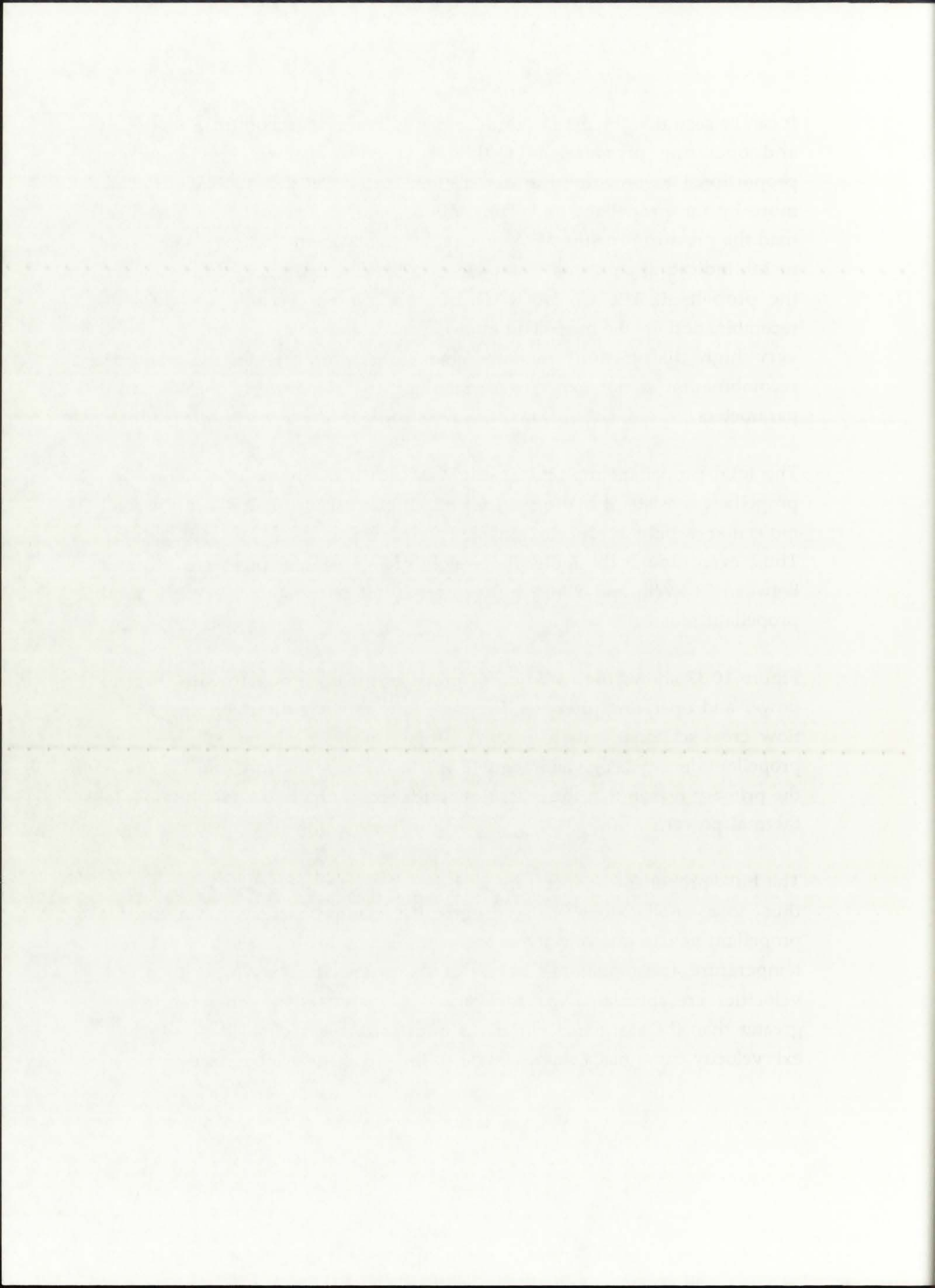


Figure 10.32: Propellant total molecular weight.

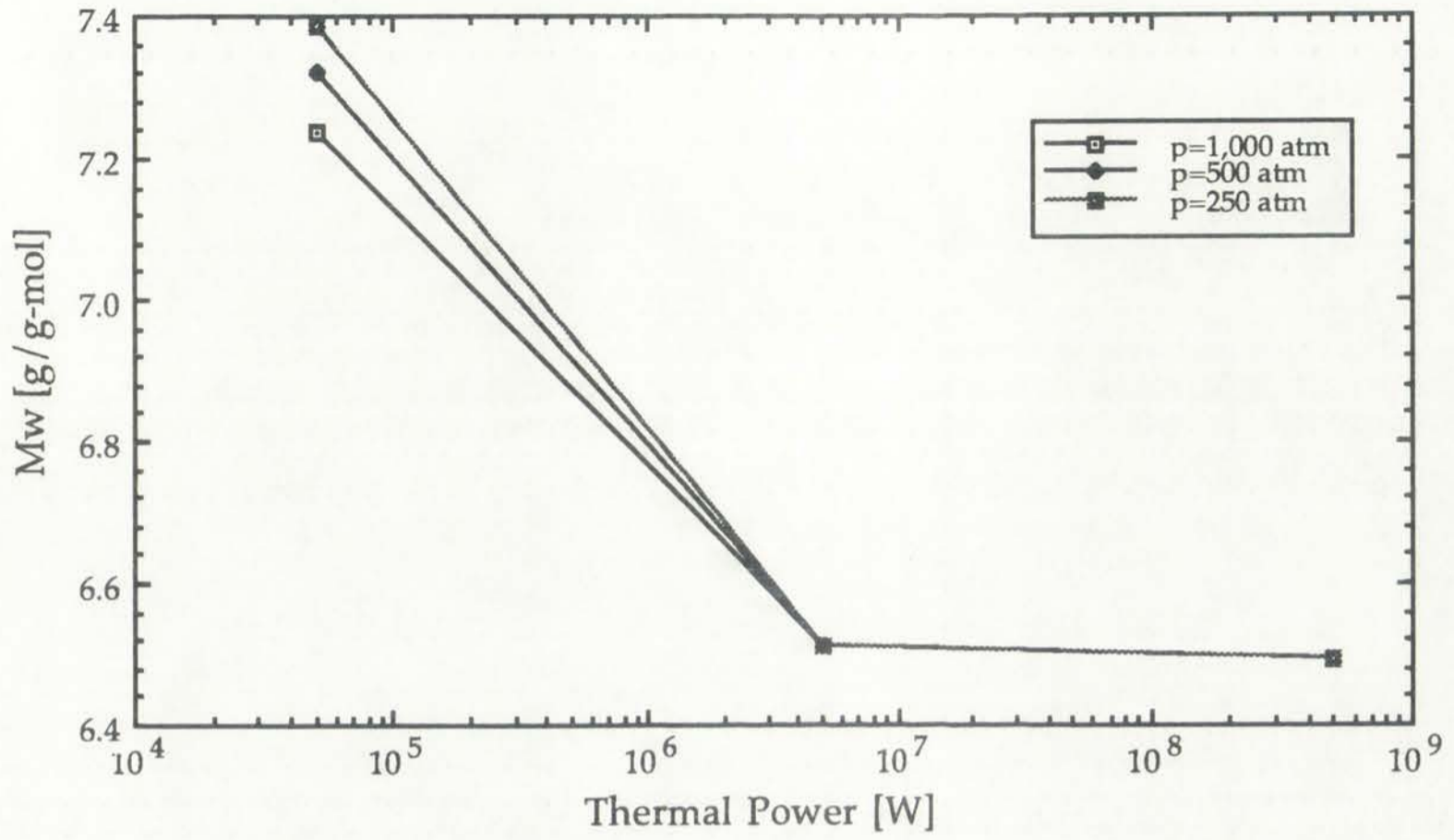
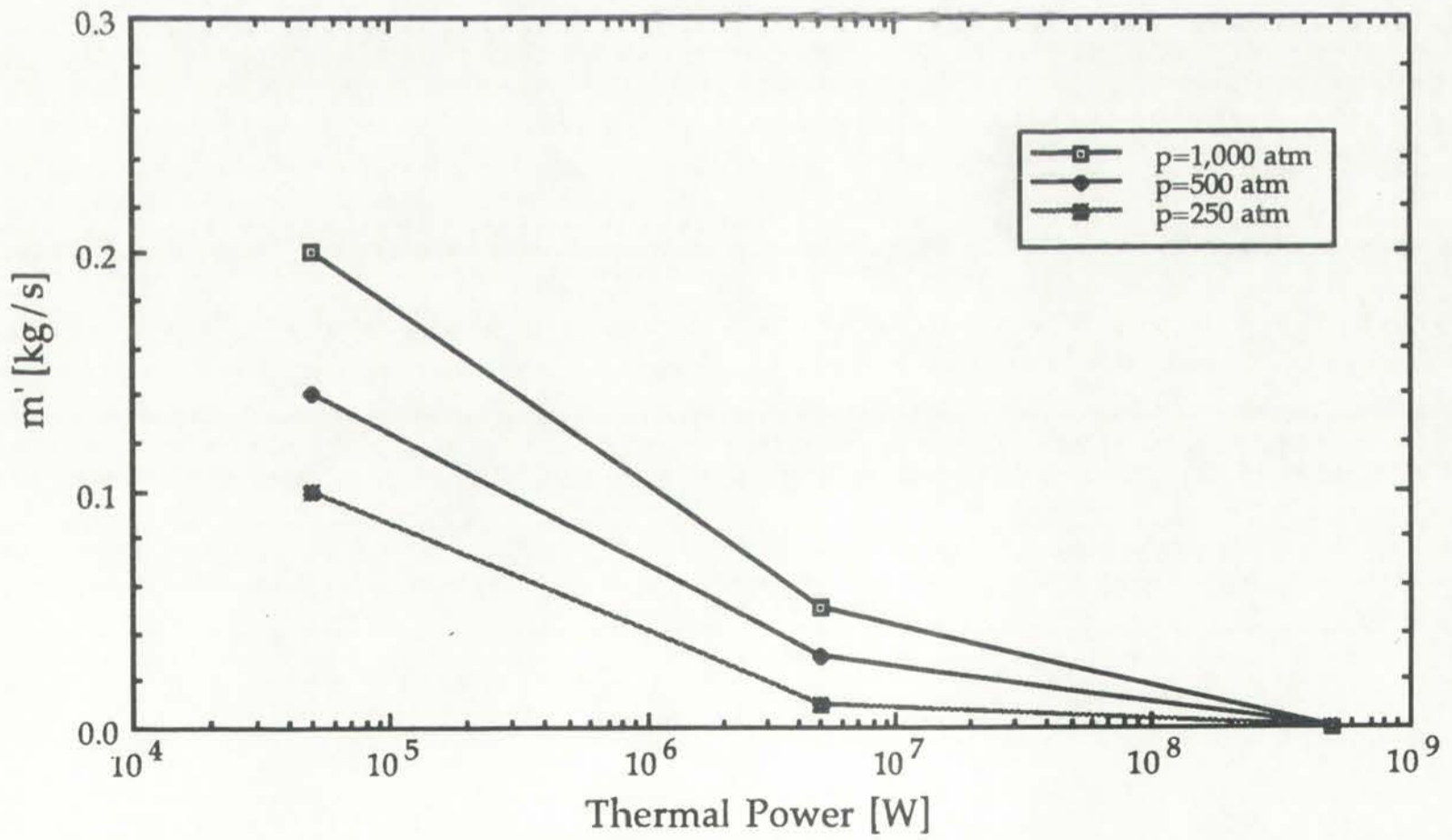
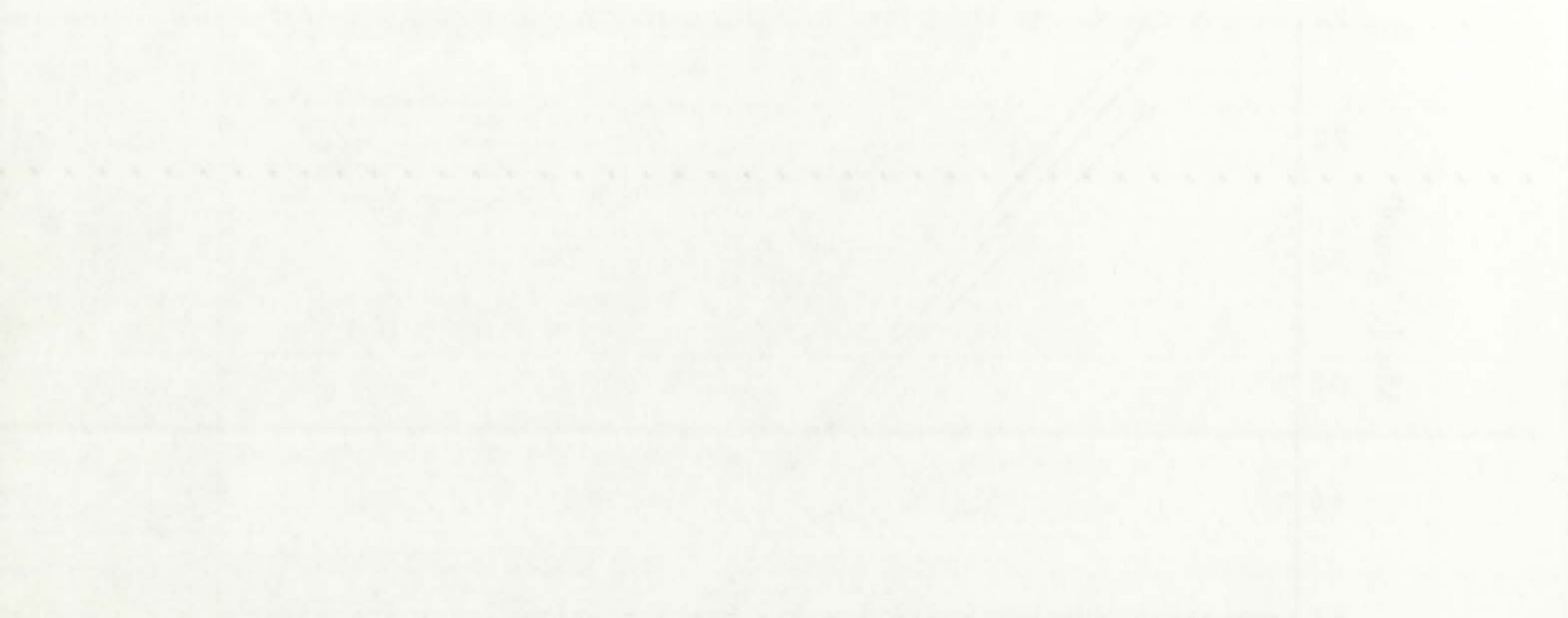


Figure 10.33: Propellant mass flow rate.



1950



1960



1970

Figure 10.34: Nozzle exit velocity.

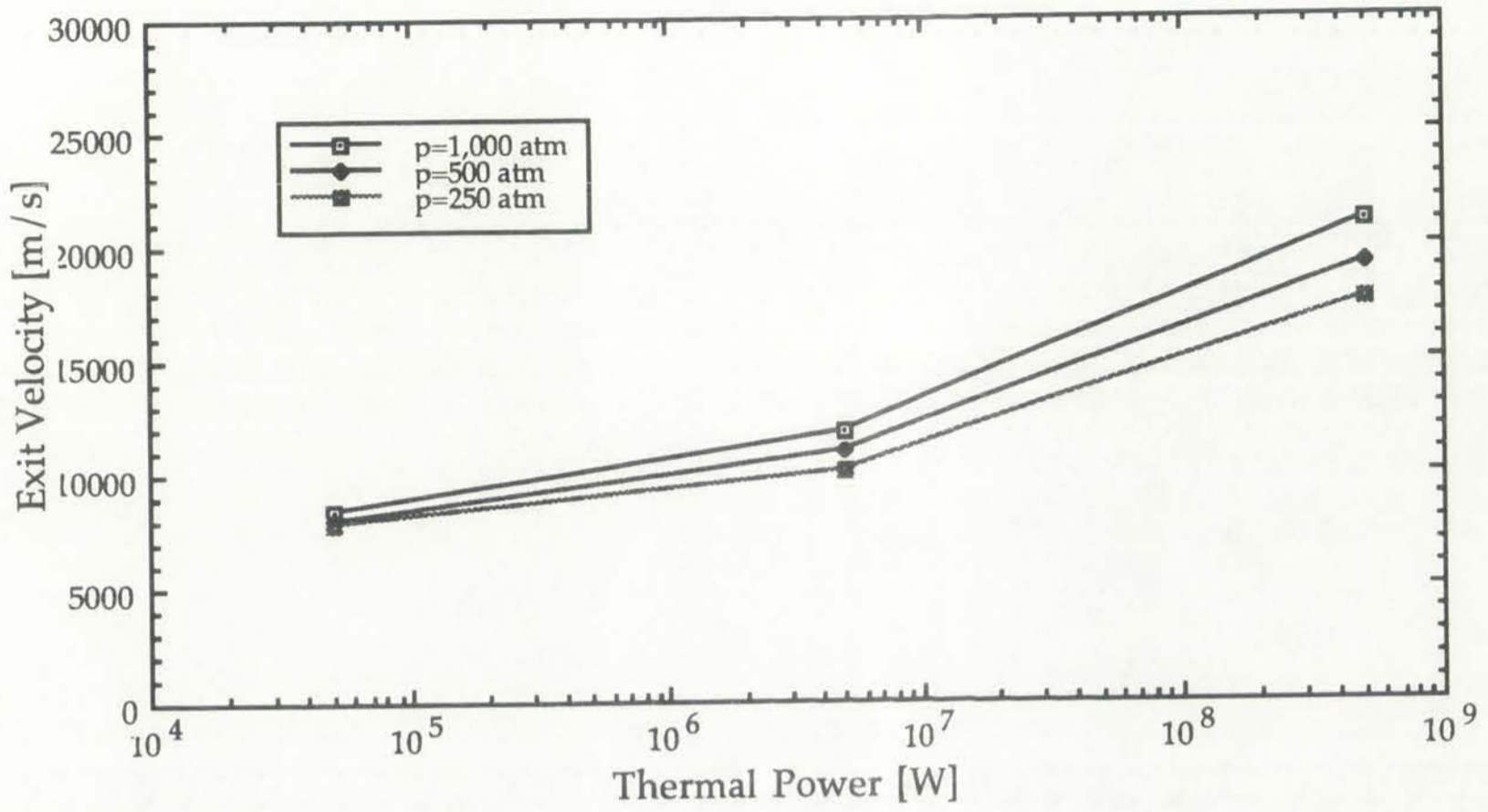
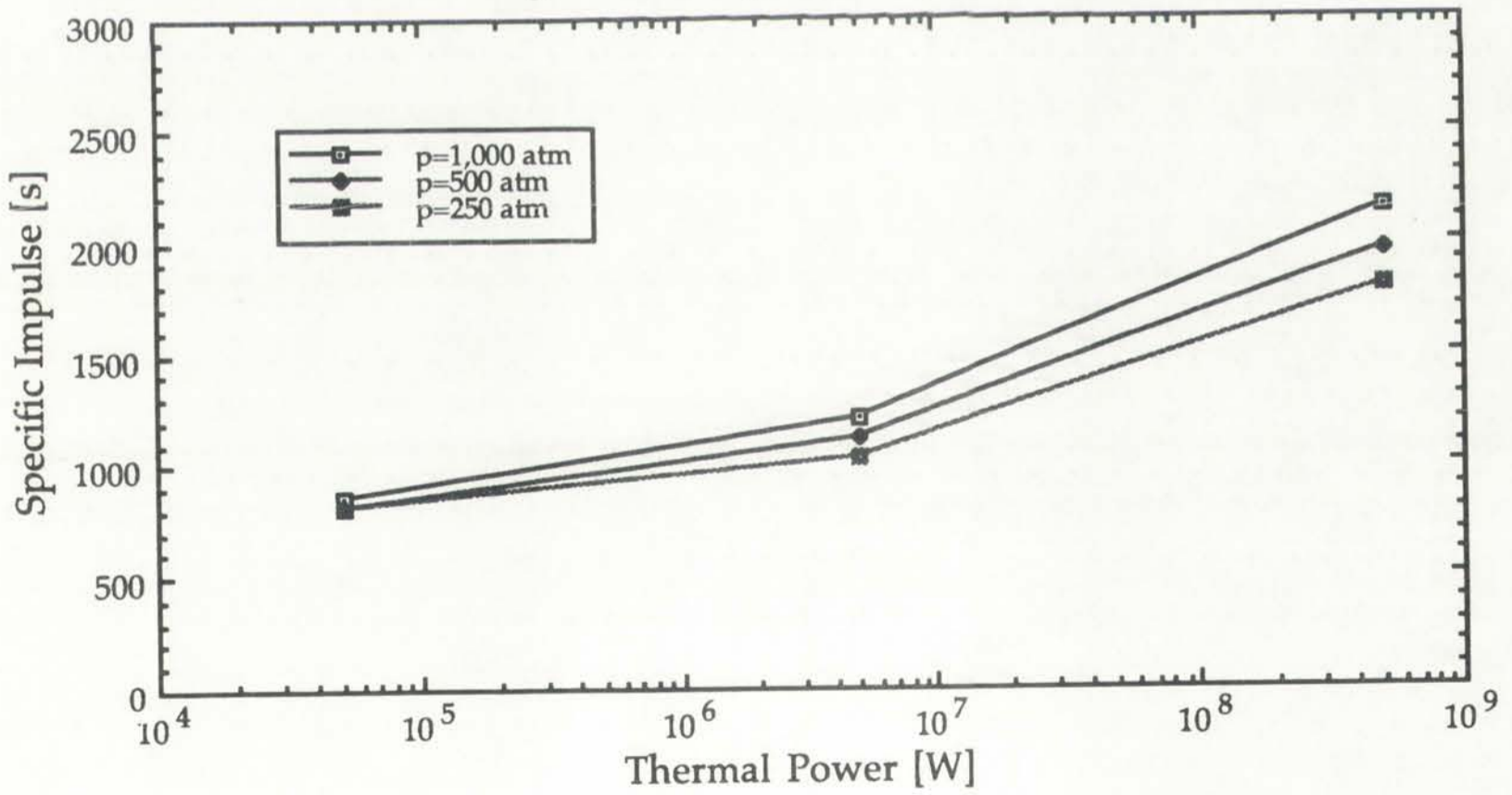
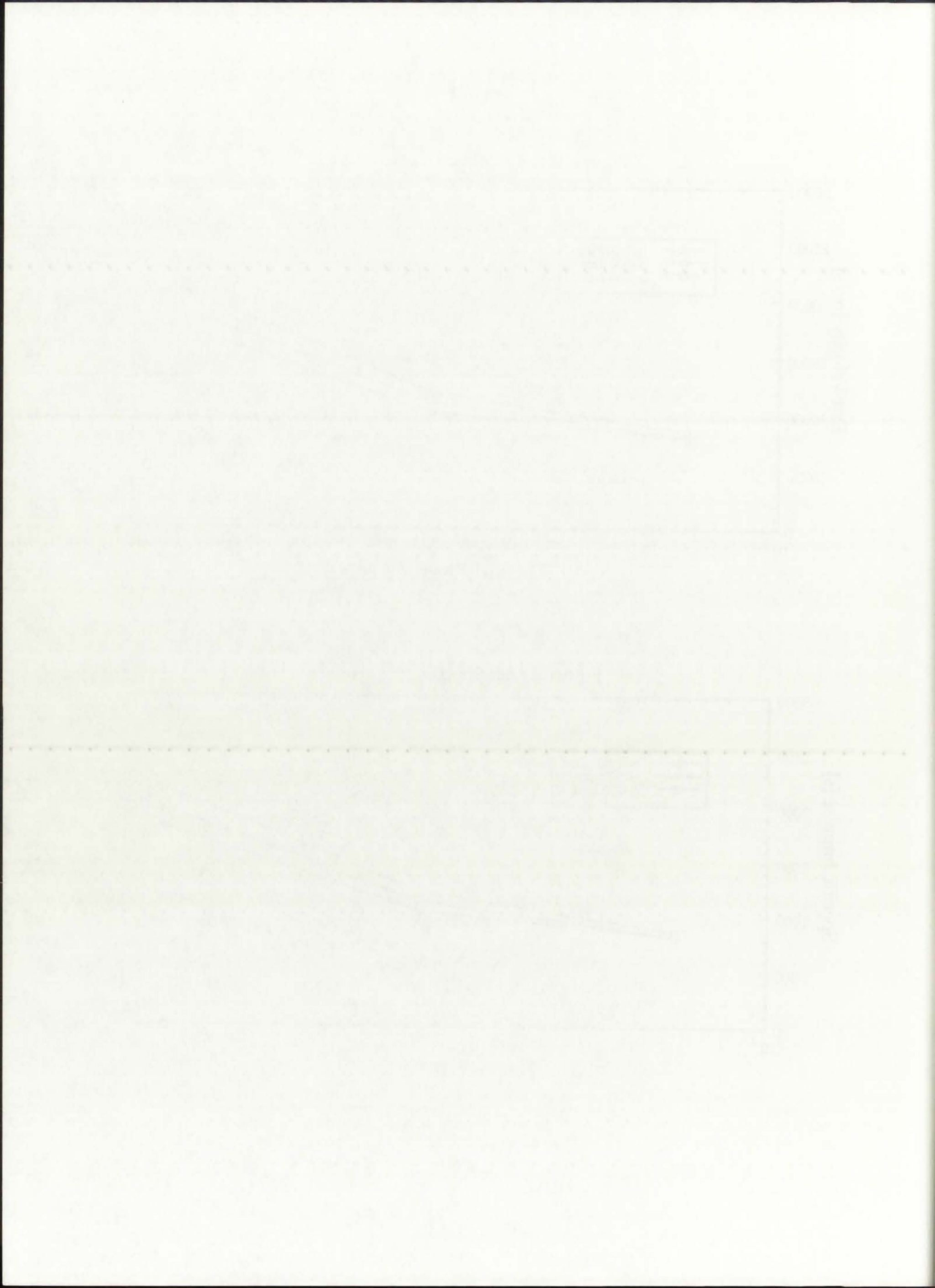


Figure 10.35: Specific Impulse.





The rocket engine specific impulse, one of the two major parameters in rocket propulsion theory, is shown in Figure 10.35. Defined in eqns. (8.1) and (8.2), the specific impulse is primarily dependent on the nozzle exit velocity, and exhibits the same behavior. Just like the velocity, specific impulse is an increasing function of propellant pressure and temperature.

The ideal thrust of the rocket engine is equal to the product of the propellant mass flow rate and nozzle exit velocity. As shown in Figure 10.36, the thrust decreases with increasing thermal power. This is due to the sharp inverse proportionality of the mass flow rate to thermal power, as was shown previously in Figure 10.33. Even though the propellant velocity is a constantly increasing function of thermal power and pressure, the same two parameters act to sharply reduce the propellant density. Figure 10.36 indicates a performance limitation associated with a very large reactor thermal power. Although the promise of gas core technology has always focused around higher and higher temperatures, it is shown here that undesirable reductions in performance occur as a result of very high temperatures.

Figures 10.35 and 10.36 indicate that for very large thermal powers, gas core rocket engines develop only meager thrust, albeit with high specific impulse. In the 1960's, optimistic assumptions of specific impulses of 2,000-6,000 s and thrusts of 100-10,000 kN were put forth; the results presented here, as well as those published previously [Poston and Kammash, 1994b; Tanner, 1994] indicate an upper bound on the specific impulse of approximately 2,000 s and on the thrust of approximately 100 kN. The specific impulse values are formidable, and approximately double those currently thought obtainable from solid core rockets [Angelo and Buden, 1985]. The thrust values, though, are quite low; the NERVA/Rover solid core nuclear rocket, developed and tested in the 1960's, achieved a thrust of 337 kN (Angelo and Buden, 1985), while the Saturn V rocket's main F-1 engines each developed approximately 5,600 kN.

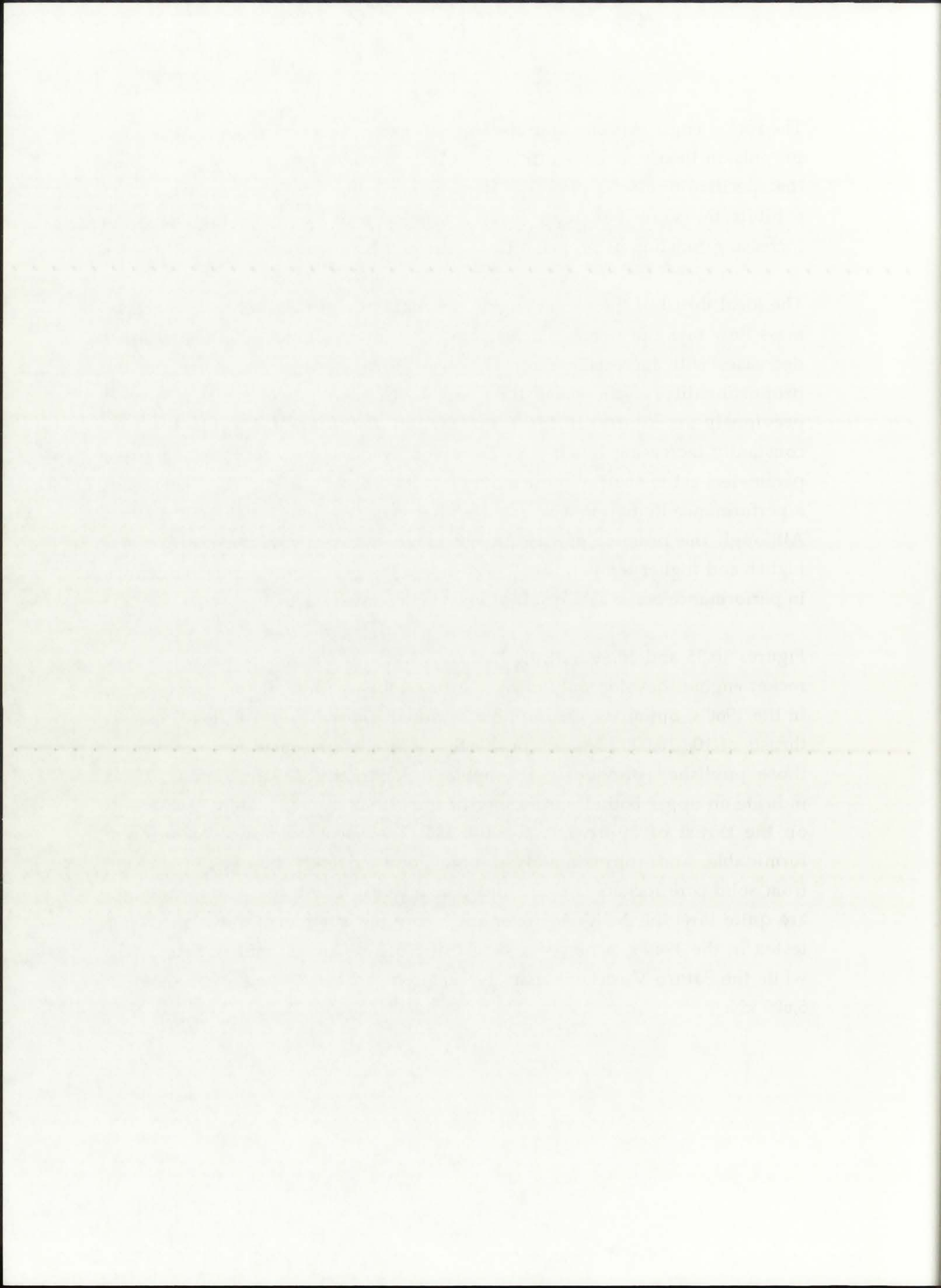
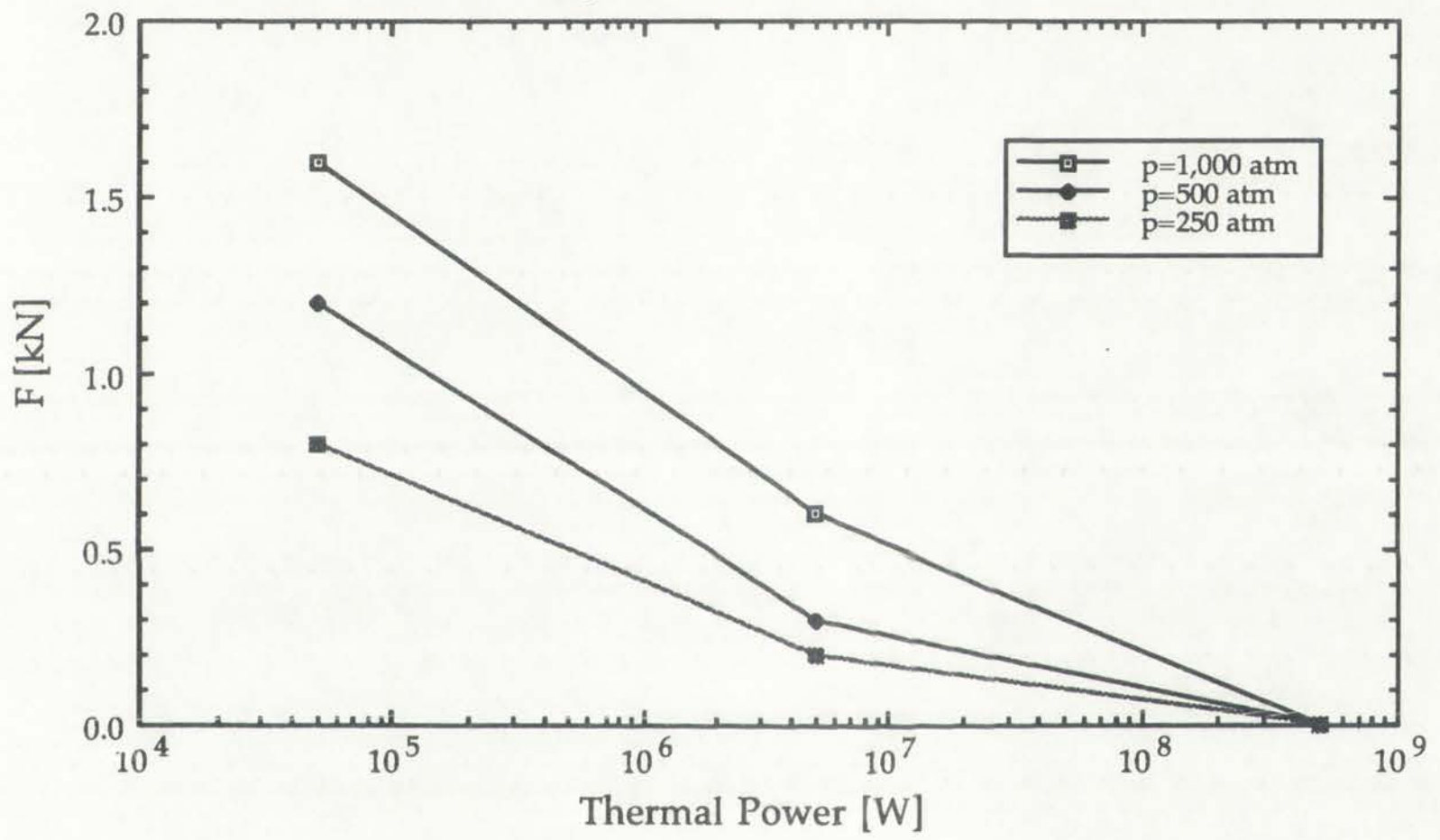
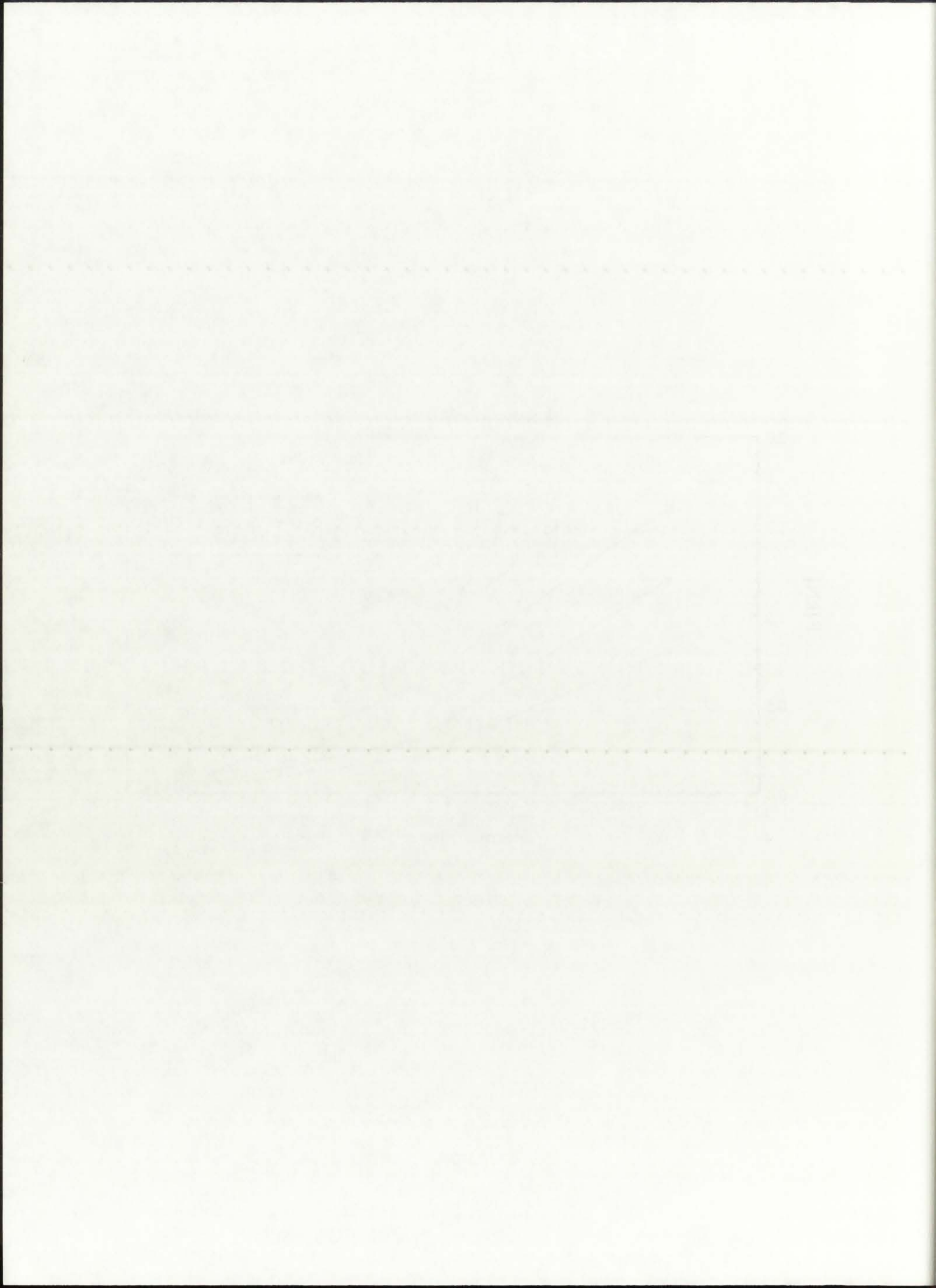


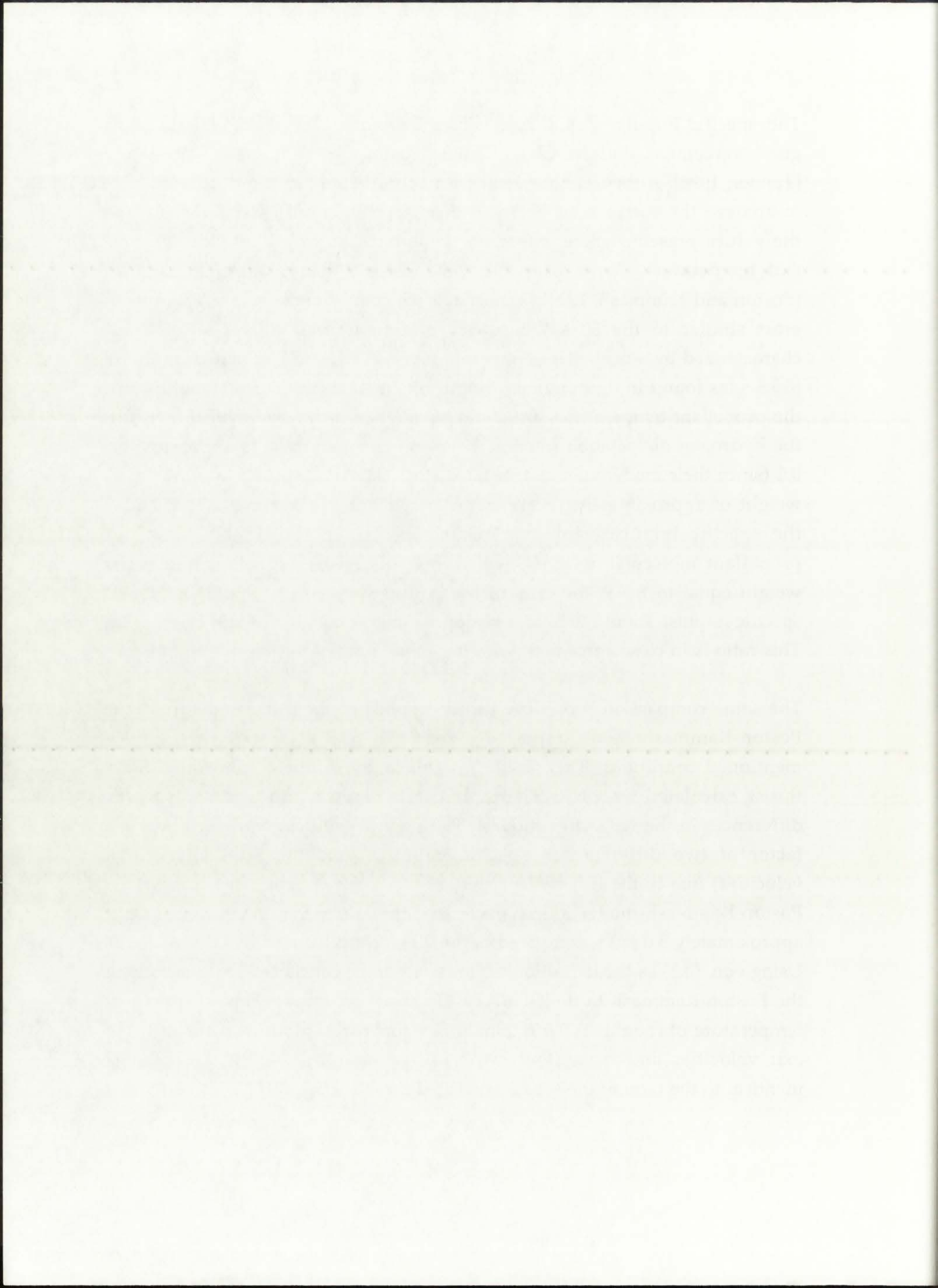
Figure 10.36: Thrust.





The specific impulse and thrust values determined by GNRATR-1D show good agreement with results of both [Poston and Kammash, 1994] and [Tanner, 1994]. Although both dealt with very different concepts, it is possible to analyze the correlations between their specific impulses and thrusts and the values presented here, based on the applicable propellant axial channel exit temperature. For a propellant channel exit temperature of 5,611 K, [Poston and Kammash, 1994b] report a specific impulse of 1,421 s. This case is most similar to the 50 kWth, $p=500$ atm configuration of GNRATR-1D, characterized by a propellant temperature of 5,717 K and a specific impulse of 815.3 s (as found in the summary output file in Appendix D.5). Assuming that the propellant temperatures are about equal, then it can easily be shown that the hydrogen dissociation fraction of Poston and Kammash is approximately 0.2 (since their model assumed $p=1,000$ atm), thereby resulting in a molecular weight of approximately 1.8. With the propellant temperatures about equal, the specific impulses are then related as the inverse of the respective propellant molecular weights; with the GNRATR-1D propellant molecular weight equal to 7.319, the ratio of the Poston-Kammash to the GNRATR-1D specific impulse should therefore be approximately equal to $(7.319/1.8)^{0.5} \approx 2.0$. This ratio is in close agreement with the actual ratio of the specific impulses.

The same comparison procedure can be applied to the calculated thrust; the Poston-Kammash model reported a thrust of 55.7 kN for the previously mentioned conditions. This value is significantly different from the 1.2 kN thrust calculated by GNRATR-1D, but it is necessary to also analyze the differences in the respective models. The previous discussion determined a factor of two difference in specific impulses (and therefore nozzle exit velocities) due to the different propellant molecular weights; in addition, the Poston-Kammash model was characterized by a propellant mass flow rate of approximately 3.0 kg/s, compared to the 0.14 kg/s calculated by GNRATR-1D. Using eqn. (8.1) as the definition of thrust, it can be concluded that the ratio of the Poston-Kammash to the GNRATR-1D thrust for a propellant channel exit temperature of roughly 5,700 K should be equal to the product of the ratios of exit velocities and mass flow rates, or approximately 43. This is almost identical to the ratio of the actual calculated thrusts, $(55.7 \text{ kN}/1.2 \text{ kN}) \approx 46$.

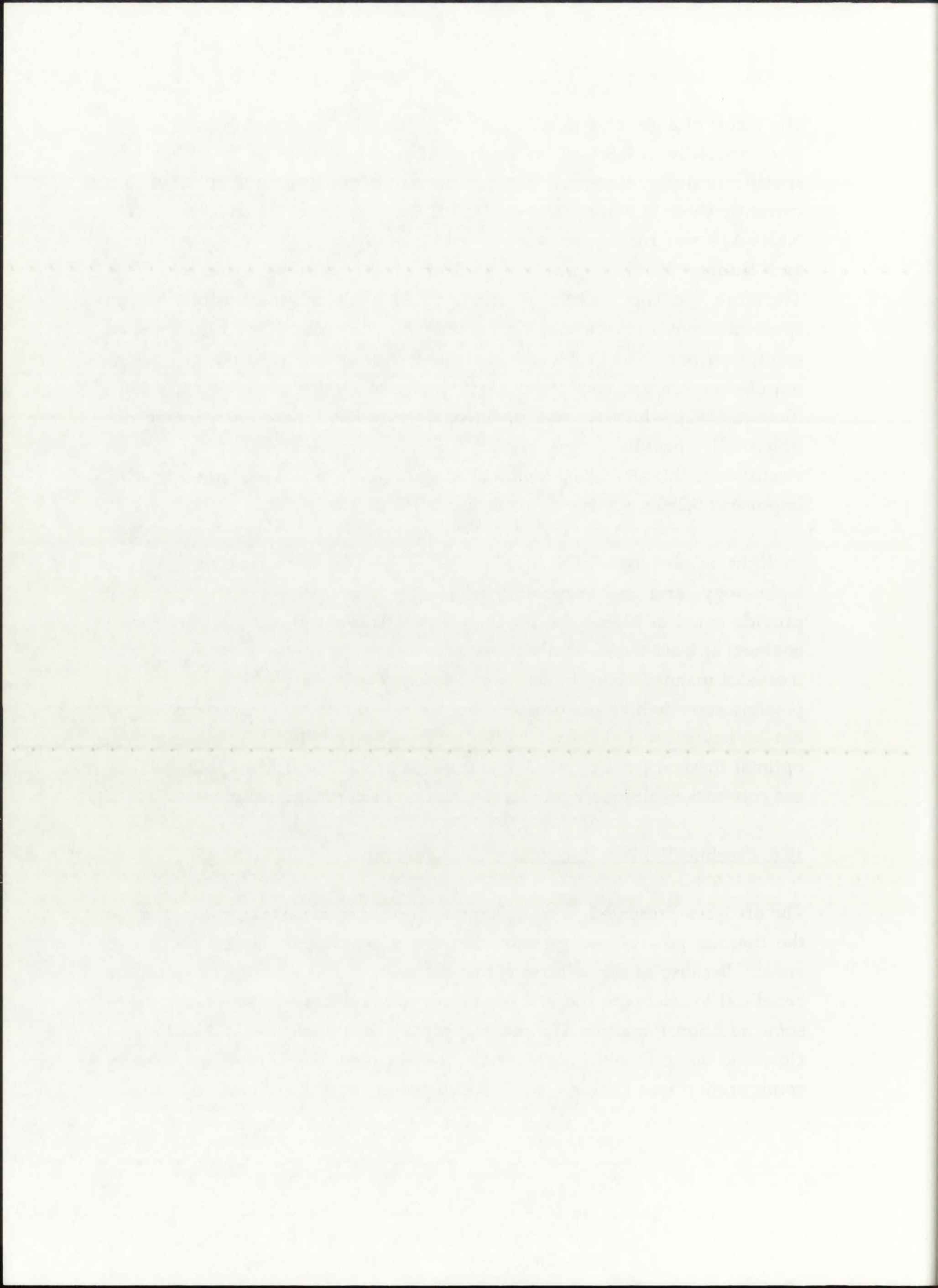


The thrust of a gas core nuclear rocket can therefore be stated as being rather low, especially in light of the high expectations put forth in the 1960's. The specific impulse, however, is significant and approximately double that currently thought achievable with solid core nuclear rocket technology. The NERVA/Rover rocket, for example, had a specific impulse of 824 s [Angelo and Buden, 1985], approximately half of the values discussed above. Therefore, gas core rocket technology could potentially find application in space missions where a high specific impulse is needed, such as unmanned cargo transport. The problem is that the feature of low thrust/high specific impulse makes gas core technology similar to electric propulsion systems [Sutton, 1992], which are well understood, currently in development, and can potentially provide even greater specific impulses. For example, an electrostatic thruster using xenon as a working fluid can provide a specific impulse of 3,250 s, while only requiring 195 W of power [Sutton, 1992]!

In light of the extremely high projected development cost of gas core technology, and the availability of electric propulsion systems that can provide equal or higher specific impulses, it is doubtful that gas core rocket engines, at least the currently proposed concepts, will ever provide a viable means of manned space travel. In conclusion, then, gas core technology *could* possibly provide high performance, but the benefits of such technology would not be based on higher and higher thermal powers and temperatures. An optimal thermal power and temperature range will need to be found where gas core rockets uniquely provide the highest performance parameters.

10.8. Baseline 50 kWth, P=250 atm. Configuration

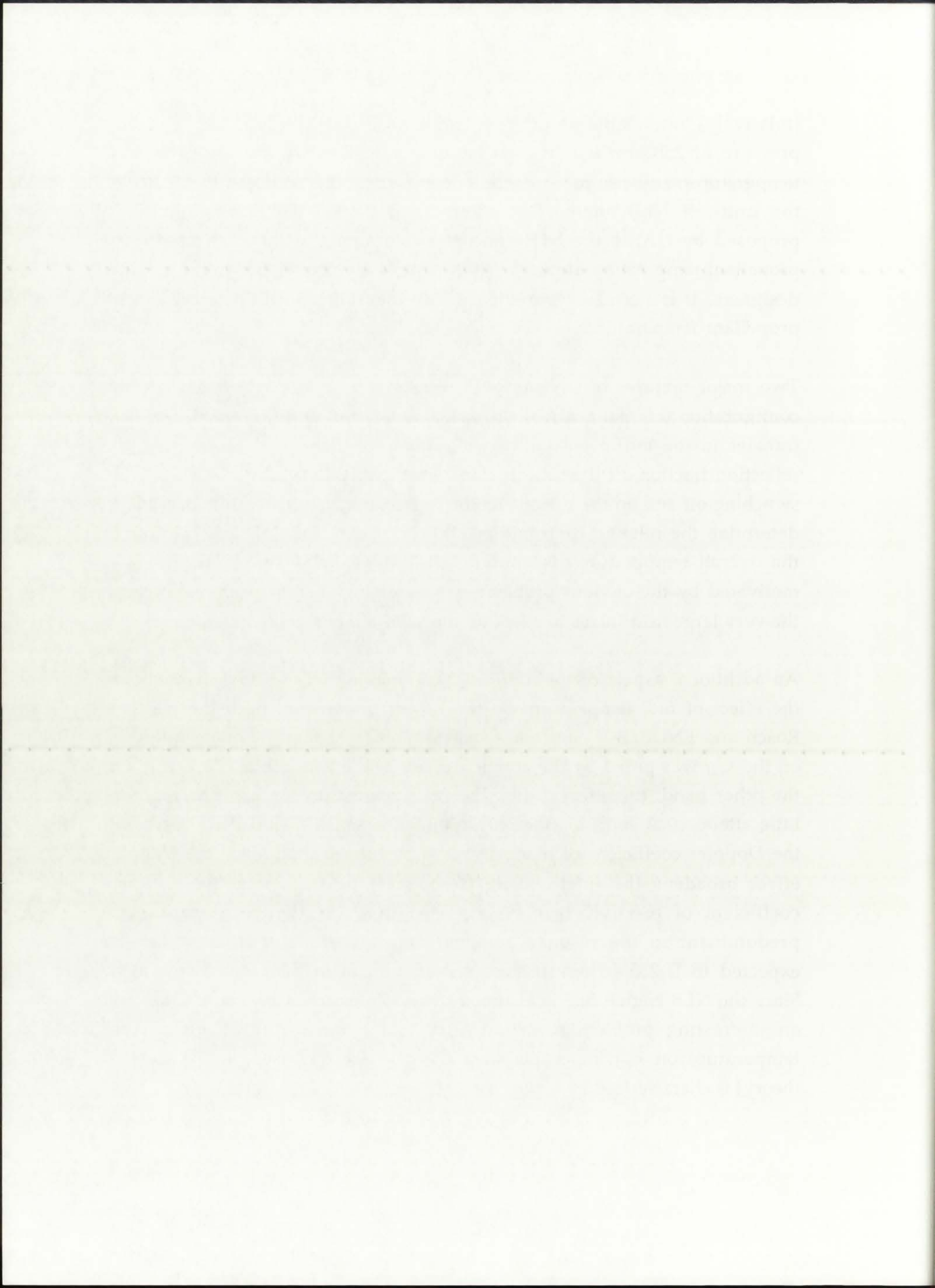
The analyses presented in this Chapter up to now consisted of determining the thermal power- and pressure-dependent behavior of the unit-cell NLB engine. Because of the still-conceptual nature of the NLB design, it would be beneficial to select one thermal power/pressure combination and submit it to some additional analysis. The power/pressure combination should be the one closest to being feasible; based on that requirement, the 50 kWth, p=250 atm configuration was chosen. The 50 kWth power level was chosen due to the



(relatively) reasonable associated temperature distribution; an operating pressure of 250 atm was chosen because it resulted in the lowest overall temperatures, and also to match the operating pressure proposed by UARL for the unit-cell NLB engine [McLafferty and Bauer, 1967]. When initially proposed by UARL, the NLB concept was assumed to have an associated propellant temperature around 6,000 K, so to truly give justice to the original designers, it is necessary to choose a configuration resulting in a similar propellant temperature.

Two major features of GNRATR-1D were exercised as part of the baseline configuration thermal analysis: (1) switching off and on of the modes of heat transfer in the buffer gas, silica wall, and propellant, and (2) varying the reflection fraction off the solid regions' liner (variable reflBe). By selectively switching off and on the various modes of heat transfer, it could be possible to determine the relative contribution of a particular mode of heat transfer to the overall temperature distribution. Utilization of the second feature was motivated by the obvious problem area involving GCR concepts in general: the very large heat fluxes incident on the solid moderator/reflector regions.

An additional aspect of the unit-cell NLB engine that was investigated was the effect of fuel temperature on the k_{eff} of the system. Both the Hansen-Roach and ENDF/B-V neutronics analyses indicated that the major influence on the k_{eff} was posed by the atomic density of the fuel [atoms/barn-cm]. On the other hand, the effect of just the fuel temperature on k_{eff} has received little attention. A short discussion can be found in [El-Wakil, 1981] regarding the Doppler coefficient of reactivity; it is postulated that, since the Doppler effect broadens the intermediate (resonance) peaks, a negative Doppler coefficient of reactivity can be expected in U-238 (where absorption is predominant in the resonance range) and a positive coefficient can be expected in U-235 (where fission is predominant in the resonance range). Since the NLB engine fuel is assumed to be 96% enriched uranium, it became an interesting problem to actually try and quantify the effects of fuel temperature on k_{eff} , especially since the gas core rocket engine (at least in theory) is characterized by a wide range of possible fuel temperatures.



10.8.1. Baseline Configuration Thermal Analysis

The thermal analysis involving the 50 kWth, 250 atm baseline configuration consisted of varying three reflection fractions (reflBe) --100%, 99%, and 0%-- and three combinations of heat transfer modes in the buffer gas, silica wall, and propellant. The three combinations are given in Table 10.8 below.

TABLE 10.8
Three combinations of heat transfer modes used for the baseline configuration

<u>No.</u>	<u>BUFFER GAS</u>	<u>SILICA WALL</u>	<u>PROPELLANT</u>
I	conv, rad	cond, rad	conv, rad
II	rad	rad	rad
III	conv	cond	conv

It should be noted here again that of the three combinations, only combination I is generally indicative of the actual conditions inside the NLB engine. The other two are included for the purpose of determining the effects of each particular mode of heat transfer on the region temperatures.

10.8.1.1. Combination I

The temperature distribution for combination I is shown in Figure 10.37. The graph is essentially the same as the one for $Q=50$ kWth, $p=250$ atm with ENDF/B-V cross-sections, previously shown in Figure 10.19. The added feature shown in Figure 10.37 is the variation in reflBe. This variation was included in order to determine the effect on the temperature distribution within the solid moderator/reflector of the aluminum reflective liner coating these regions.

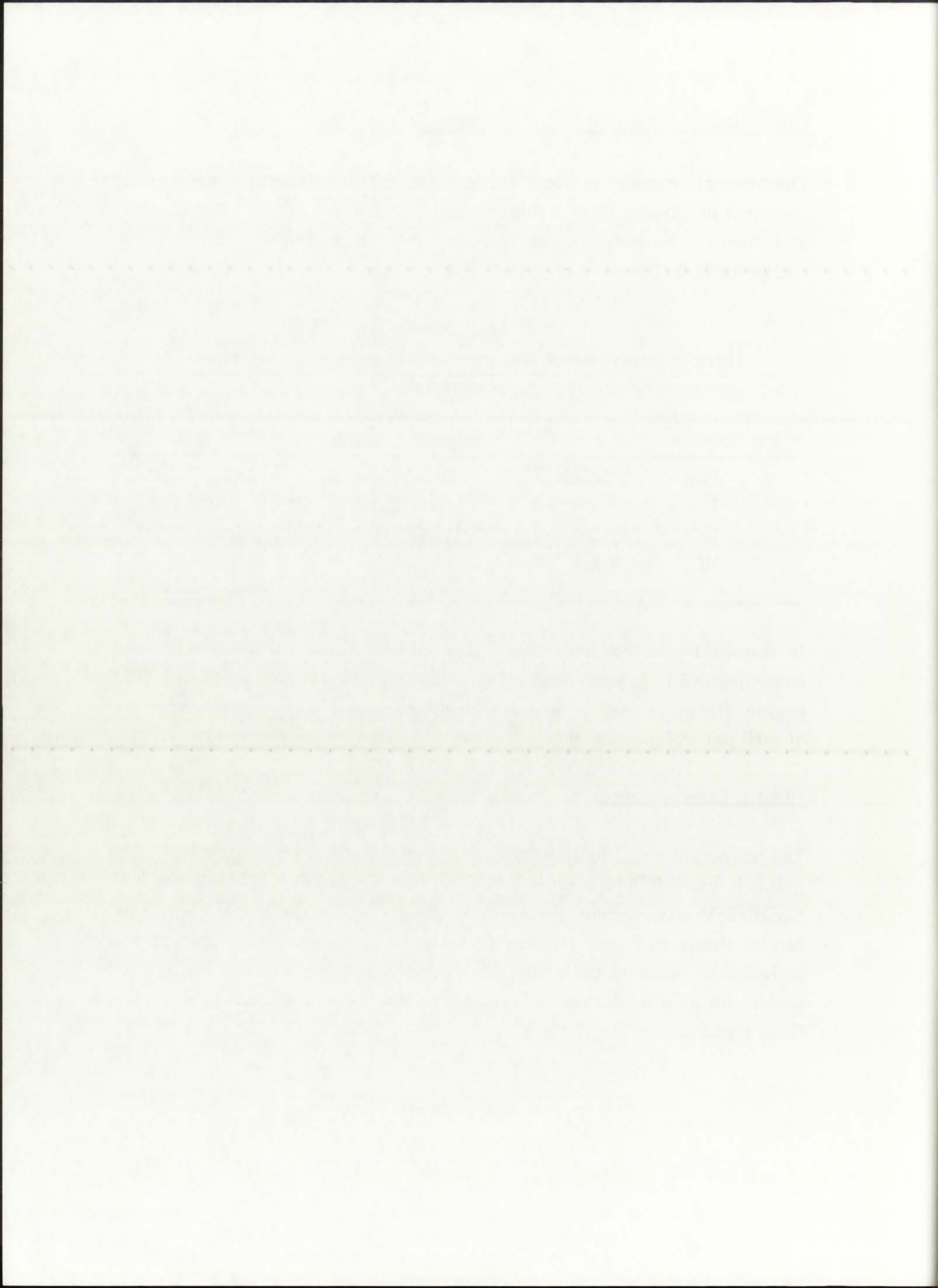
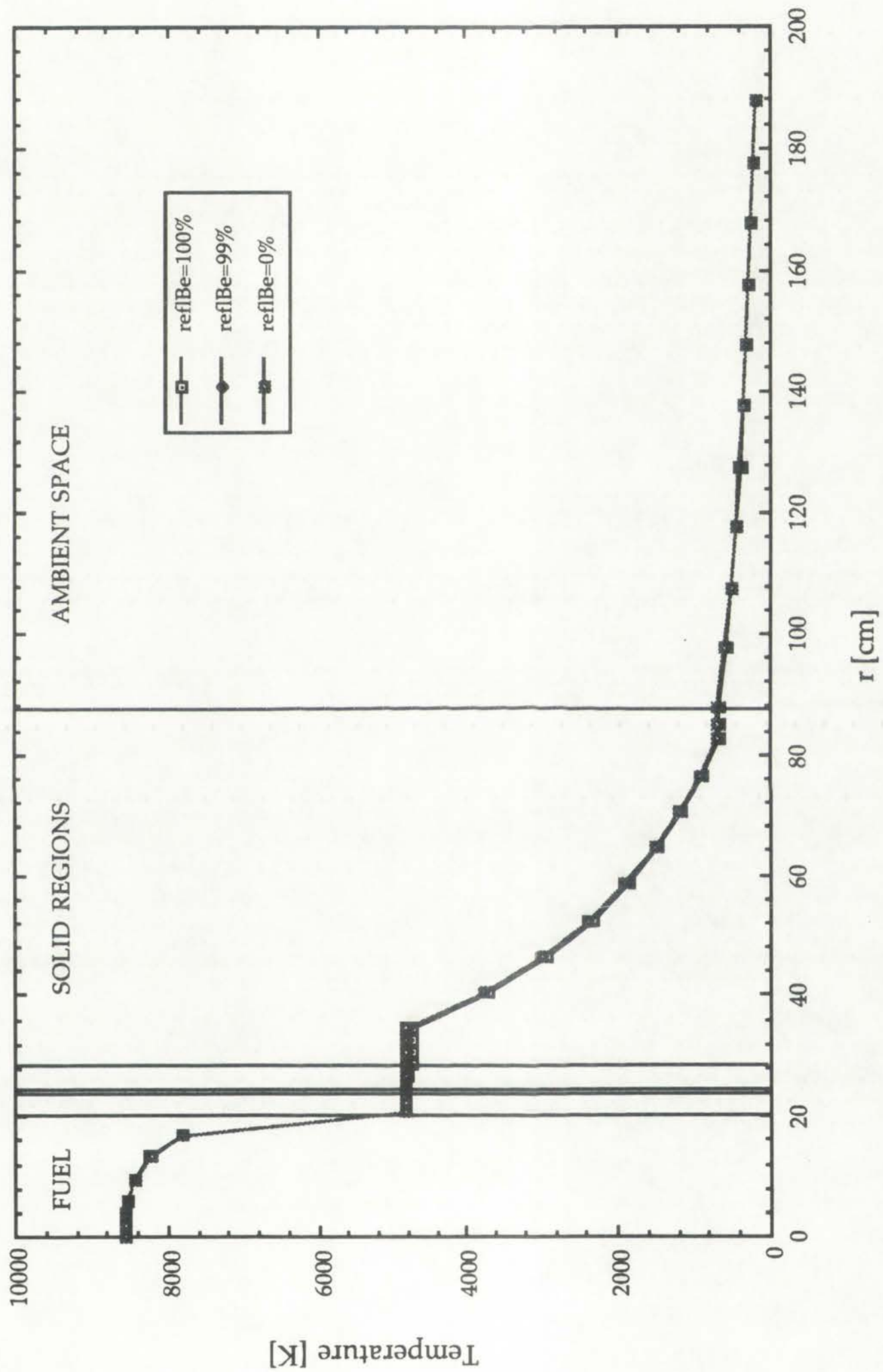
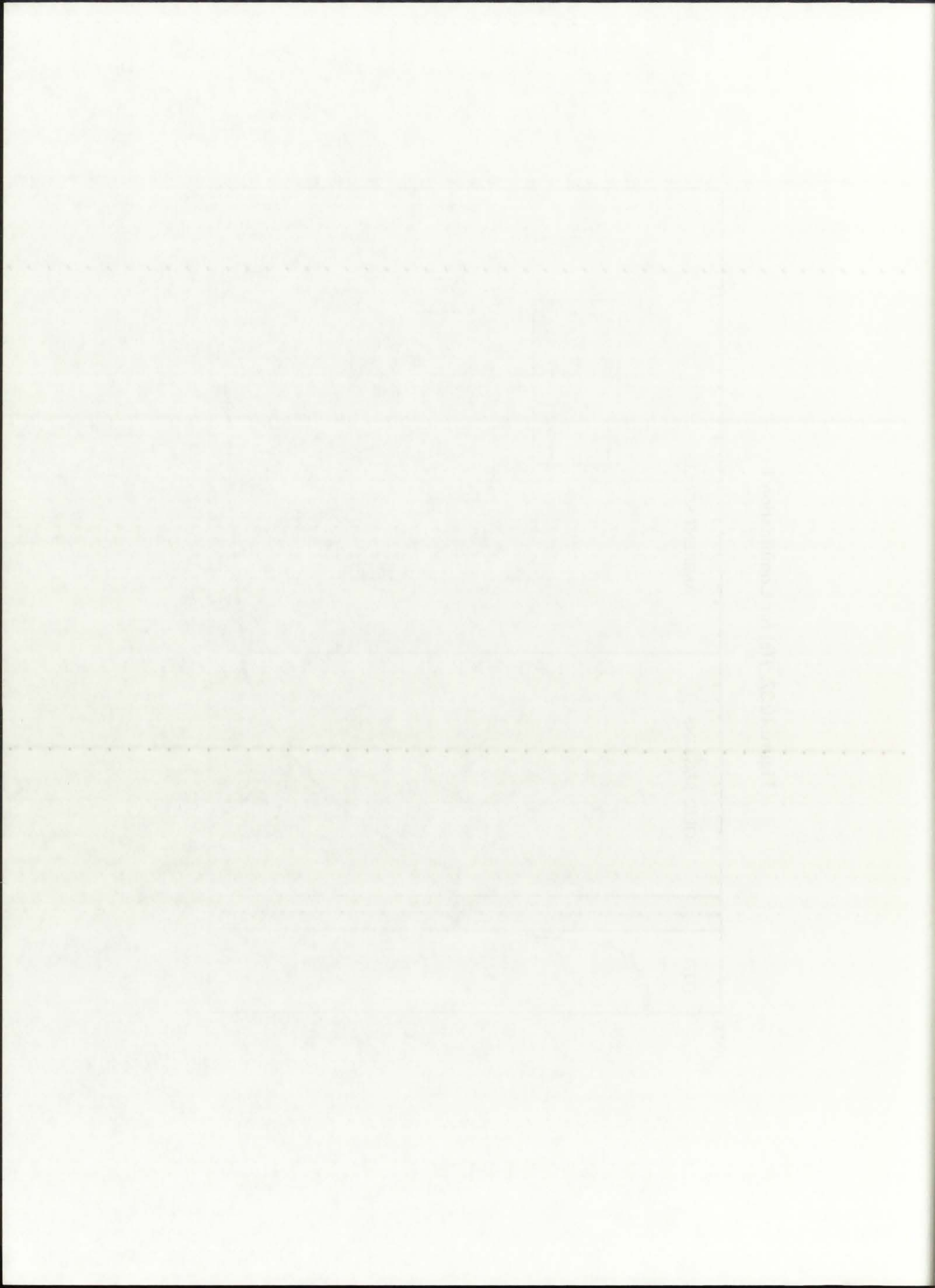


Figure 10.37: $T(r)$ for Combination I.





As can be seen, the reflective liner in actuality has only a small impact on the temperature within the moderator/reflector regions, and then only for the case of $\text{reflBe}=100\%$ (i.e., complete reflection of the incident radiative heat flux off the liner). For that ideal case, heat transfer from the propellant boundary layer (adjacent to the solid regions) to the moderator/reflector occurs by convection; since the bulk of the propellant is at 4,833 K and because of the significant heat transfer coefficient in the boundary layer, the temperature drop across the layer is not very large, resulting in a moderator/reflector temperature of approximately 4,740 K. This, of course, is well above the melting temperature of the solid regions (1,278 K for beryllium), indicating that the reflective liner would not contribute noticeably to maintaining the solid moderator/reflector region below melting temperature for the 50 kWth, 250 atm baseline configuration. Thus, an active cooling method would be needed to effect a necessary ΔT prior to the moderator/reflector region. The listing of GNRATR-1D output files for Combination I is given in Appendix E.1.

10.8.1.2. Combination II

The temperature distribution for combination II is shown in Figure 10.38. Since only radiation heat transfer is taken into account for the gaseous regions and the silica wall, only the $T(r)$ in the solid regions varies appreciably with reflBe . It can be seen that for $\text{reflBe}=100\%$, no heat is transferred to the solid regions, which are characterized by an equilibrium temperature of 200 K (i.e., in equilibrium with the 200 K constant-temperature ambient space boundary condition). Because of the magnitude of the heat flux as well as the fourth-power dependence of temperature on heat flux, even a slight reduction in the reflection fraction from 100% to 99% results in a significant increase in the $T(r)$ in the solid regions. The bulk temperature in the buffer gas, silica wall, and propellant regions is, naturally, dependent on the fraction of the incident heat flux that is absorbed locally. This condition corresponds to the case of optically thin media and was discussed in Section 6.5.2.2.

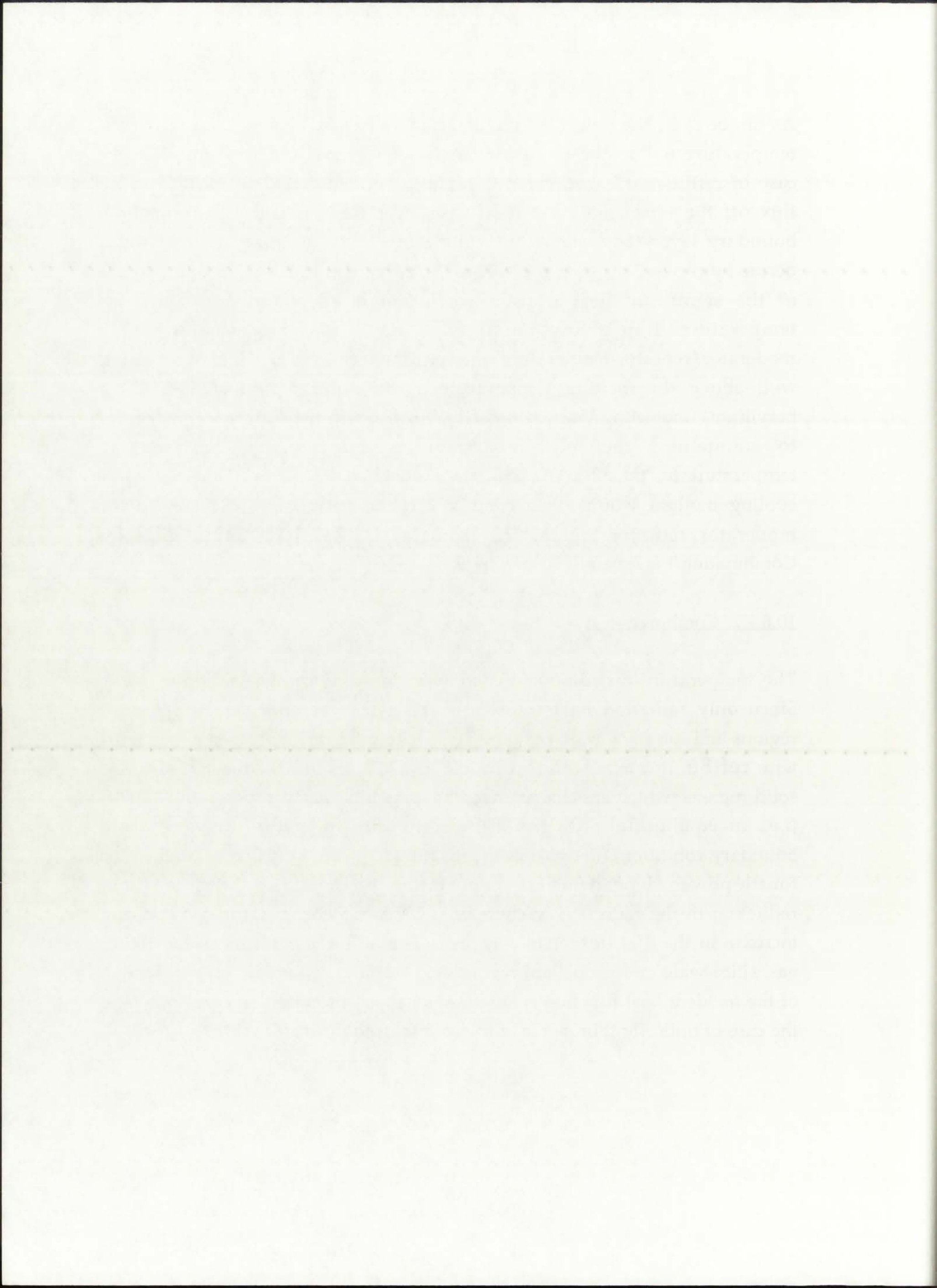
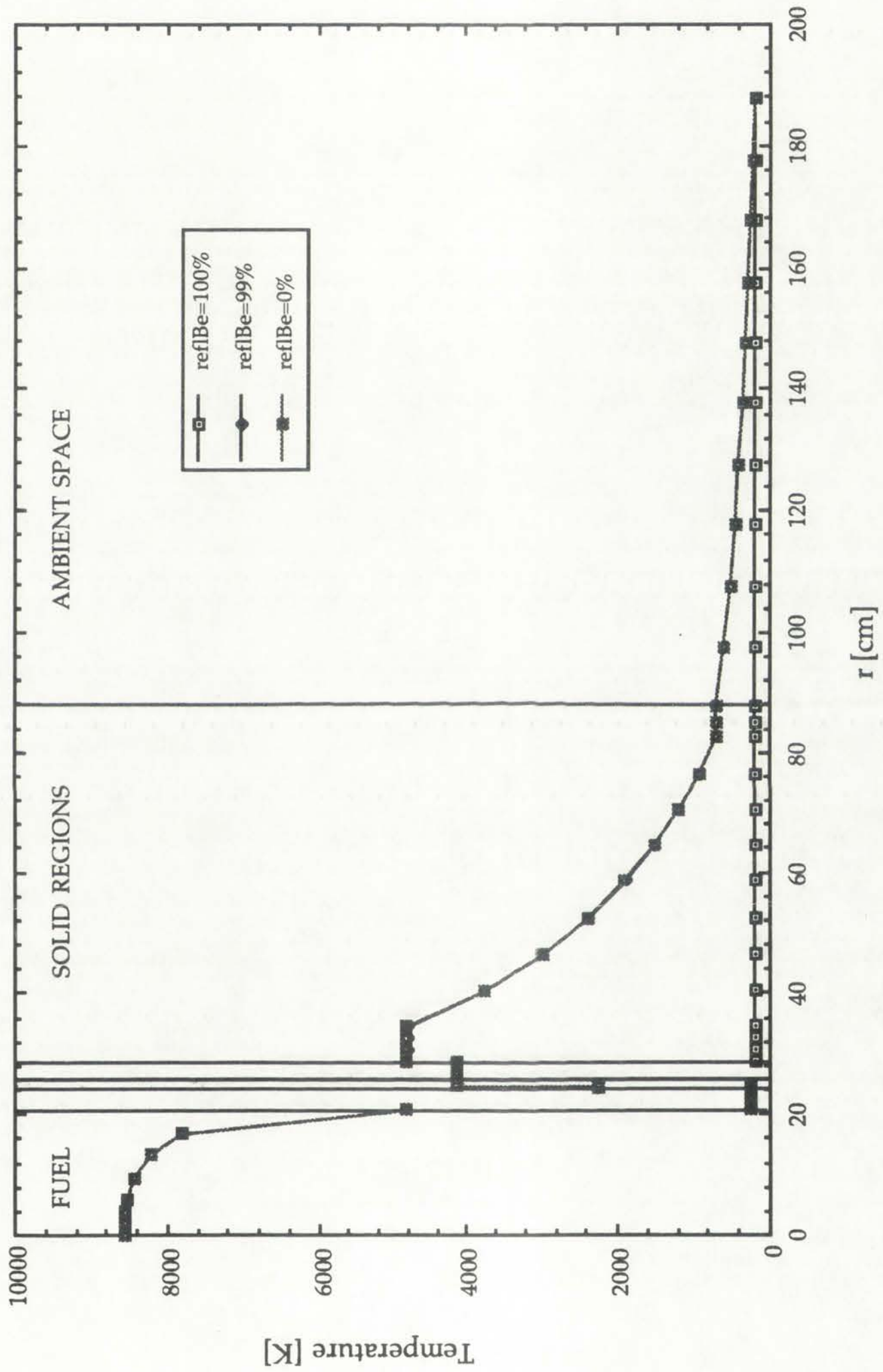
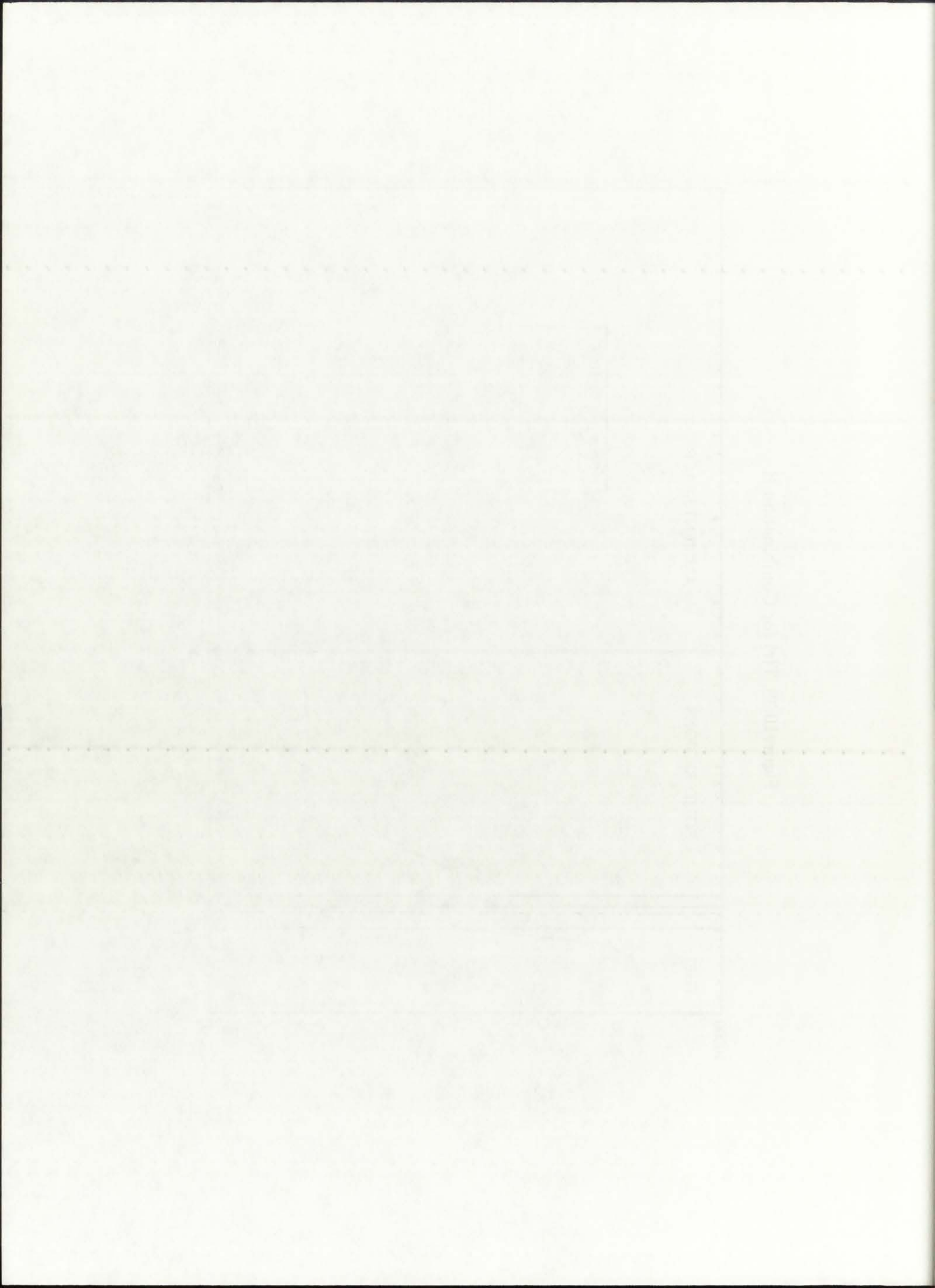


Figure 10.38: $T(r)$ for Combination II.



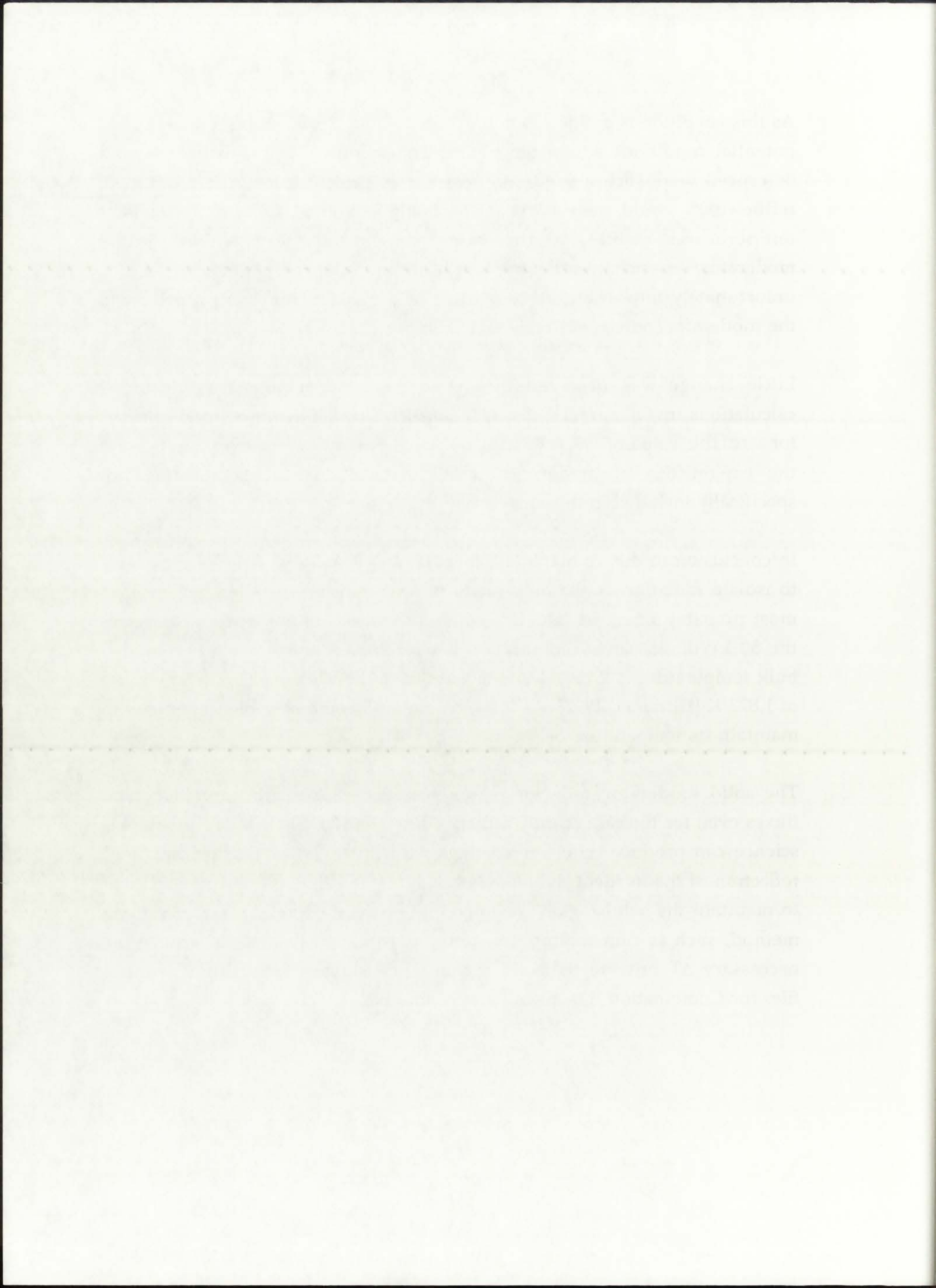


As this condition is an idealization, it cannot be taken as representative of the potential conditions within the engine. The reflective liner, however, would be crucial were such a condition possible; as shown in the Figure, an ideal $\text{reflBe}=100\%$ could then allow for virtually unlimited fuel and propellant temperatures, while at the same time completely shielding the moderator/reflector from the incident heat flux. Such an operating scenario is unfortunately impossible, as convective heat transfer from the propellant to the moderator/reflector is unavoidable.

Little change was observed in $T(r)$ in the solid regions for additional calculations involving $\text{reflBe} < 99\%$. Smaller $T(r)$ values were found to occur for a reflBe value of 99.99% ; such reflective properties, however, are beyond the capabilities of modern materials science and were therefore not specifically included in this analysis.

In conclusion to this combination, then, it can be said that if it were possible to isolate radiation as the only mode of heat transfer, the silica wall would most probably retain its integrity without the need for any cooling, as far as the 50 kWth, 250 atm configuration is concerned. The silica wall calculated bulk temperature is 2,260 K, somewhat above the silica melting temperature of 1,873 K [Ultramet, 1992]. As it stands, the wall could be cooled internally to maintain its temperature below melting.

The solid moderator/reflector region would be subject to very high heat fluxes even for the case of only radiative heat transfer. Since today's materials science can produce reflective coatings with up to 99% reflection fractions, reflection of the incident radiative heat flux, by itself, would not be sufficient to maintain the solid region's temperature below melting. An active cooling method, such as film cooling, for example, would be needed to achieve the necessary ΔT prior to the solid region. The listing of GNRATR-1D output files for Combination II is given in Appendix E.2.



10.8.1.3. Combination III

The temperature distribution for configuration III is shown in Figure 10.39. It can be seen that, with radiative heat transfer switched off, a noticeable temperature drop occurs in both the buffer gas and especially the propellant. This is due to finite heat transfer coefficients in the buffer gas and propellant. The temperature drop in the silica wall is very small, of course, due primarily to the thickness being only 0.5 cm and a relatively high thermal conductivity [Incropera and DeWitt, 1992]. For this combination, the variation in reflBe is of no consequence to the $T(r)$, due to the radiative heat transfer being switched off.

As part of the analysis of Combination III, a parametric study on the effects of the propellant axial velocity (and therefore the heat transfer coefficient) was carried out, shown in Figure 10.40. It can be seen that the propellant temperature is a direct function of the axial velocity; a decrease in axial velocity results in an increase in the thermal resistance of the propellant region, which brings about a significant temperature drop across the propellant channel, as evidenced by the 0.1 m/s case.

Decreasing the propellant axial velocity could effectively achieve a desired low temperature in the moderator/reflector region, thus avoiding melting; such a procedure, however, would also reduce the bulk propellant temperature and the associated specific impulse, thereby eliminating the original motivation for developing GCR technology. The data shown in Figure 10.40, however, do indicate toward the most effective method of inducing a large enough temperature drop adjacent to the moderator/reflector region to prevent it from melting: film cooling. A scenario for possible film cooling of the solid region will be presented in Chapter 12. The listing of GNRATR-1D output files for Combination III is given in Appendix E.3.

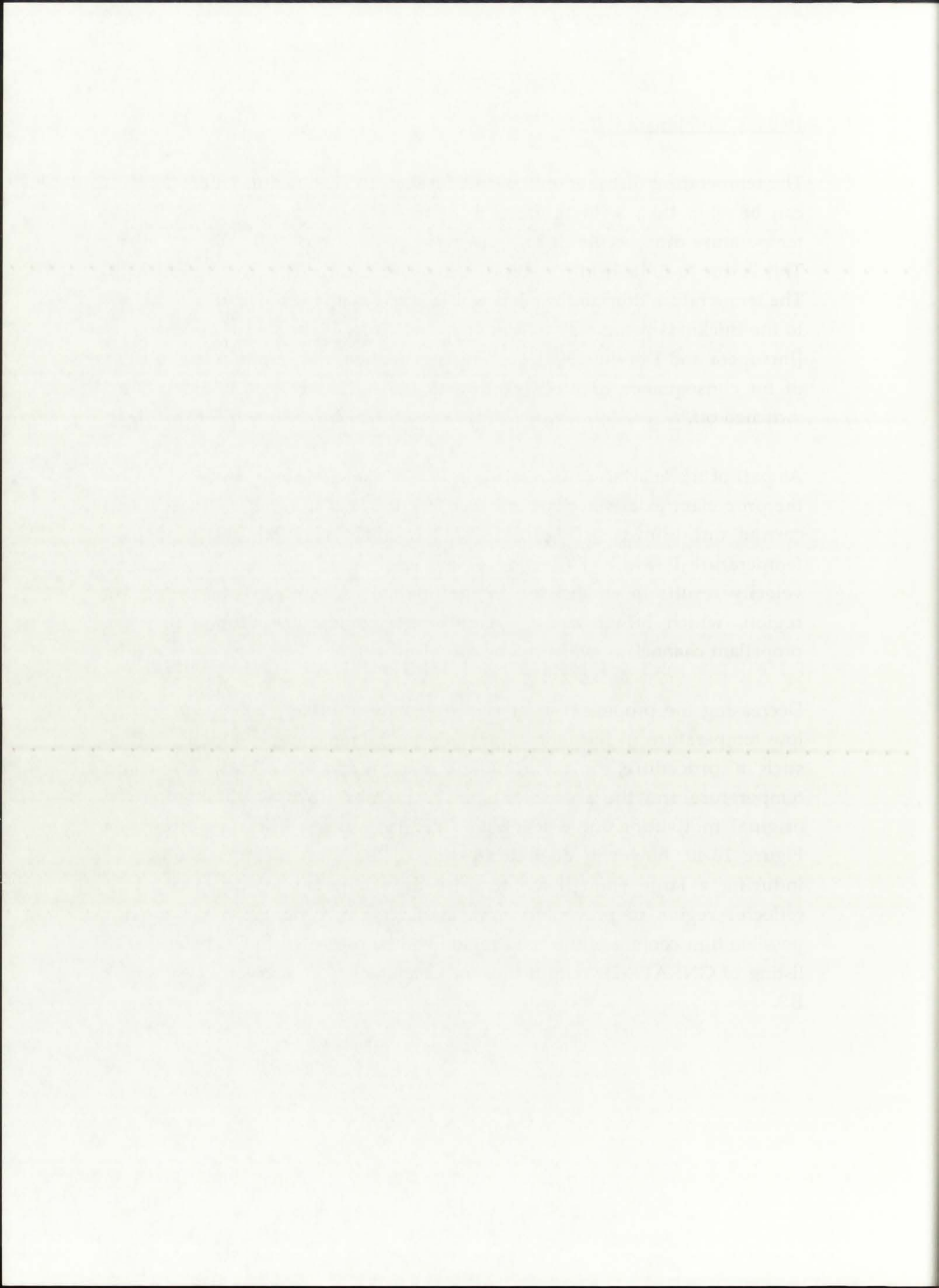
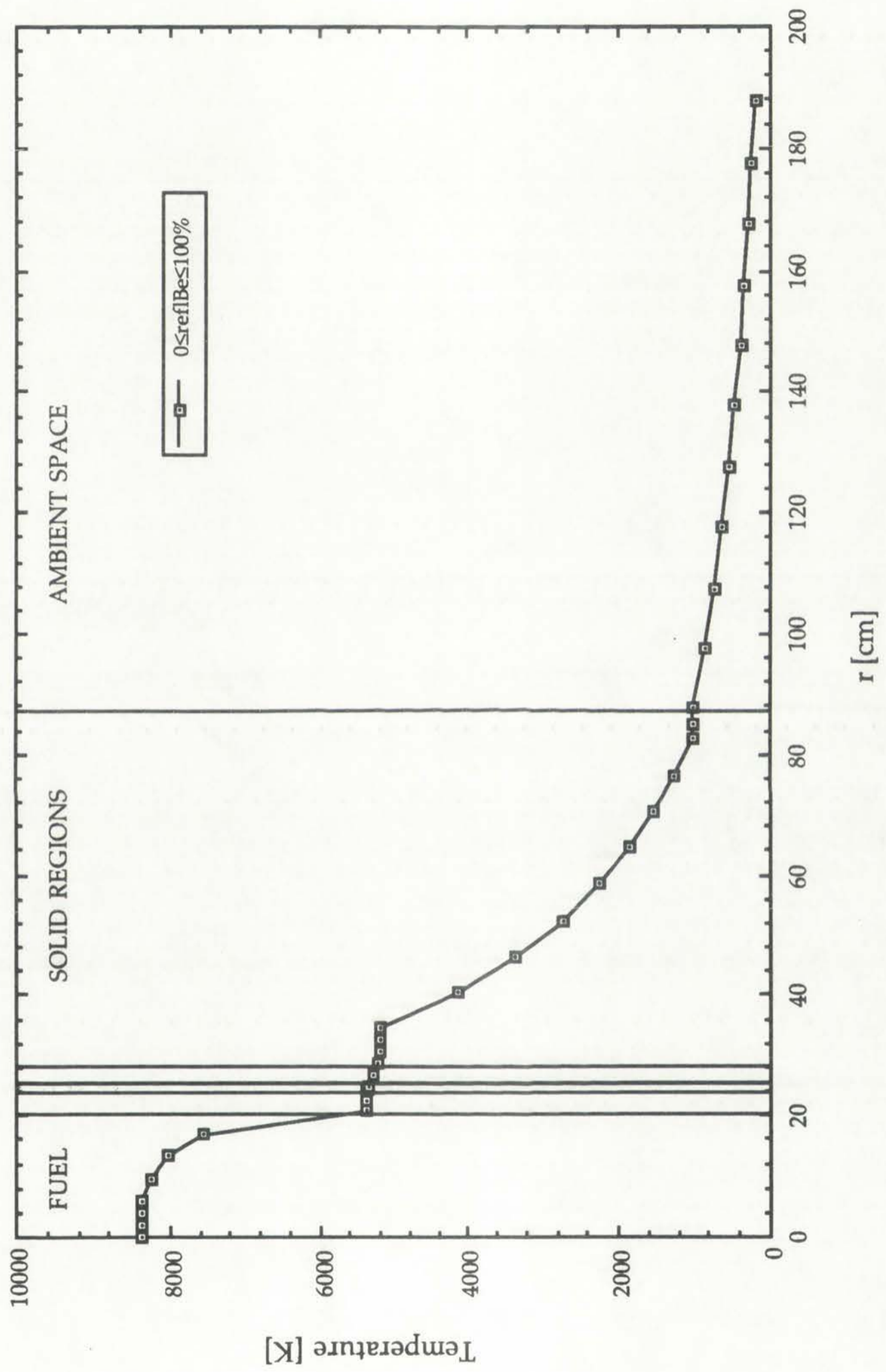


Figure 10.39: $T(r)$ for Combination III.



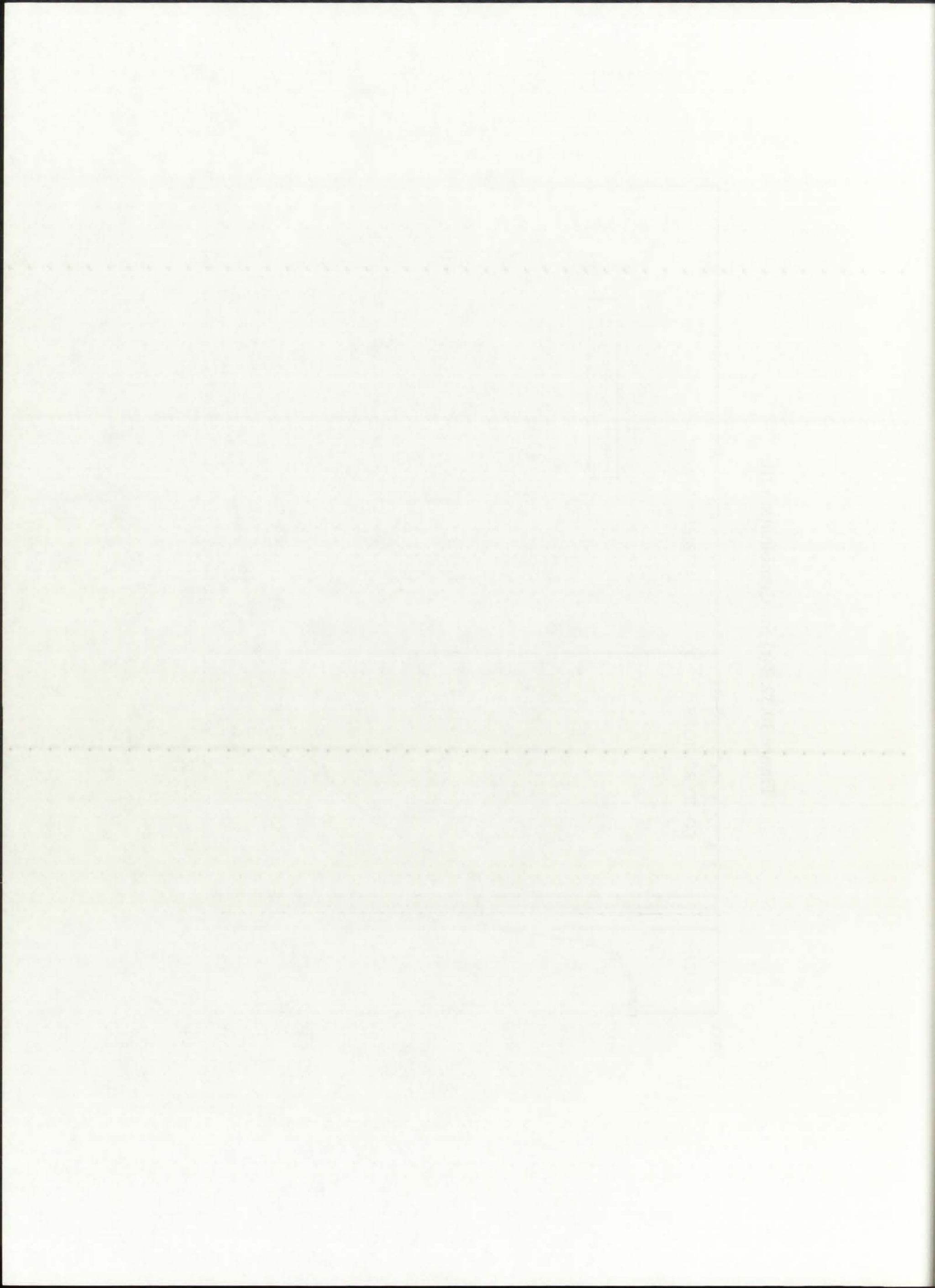
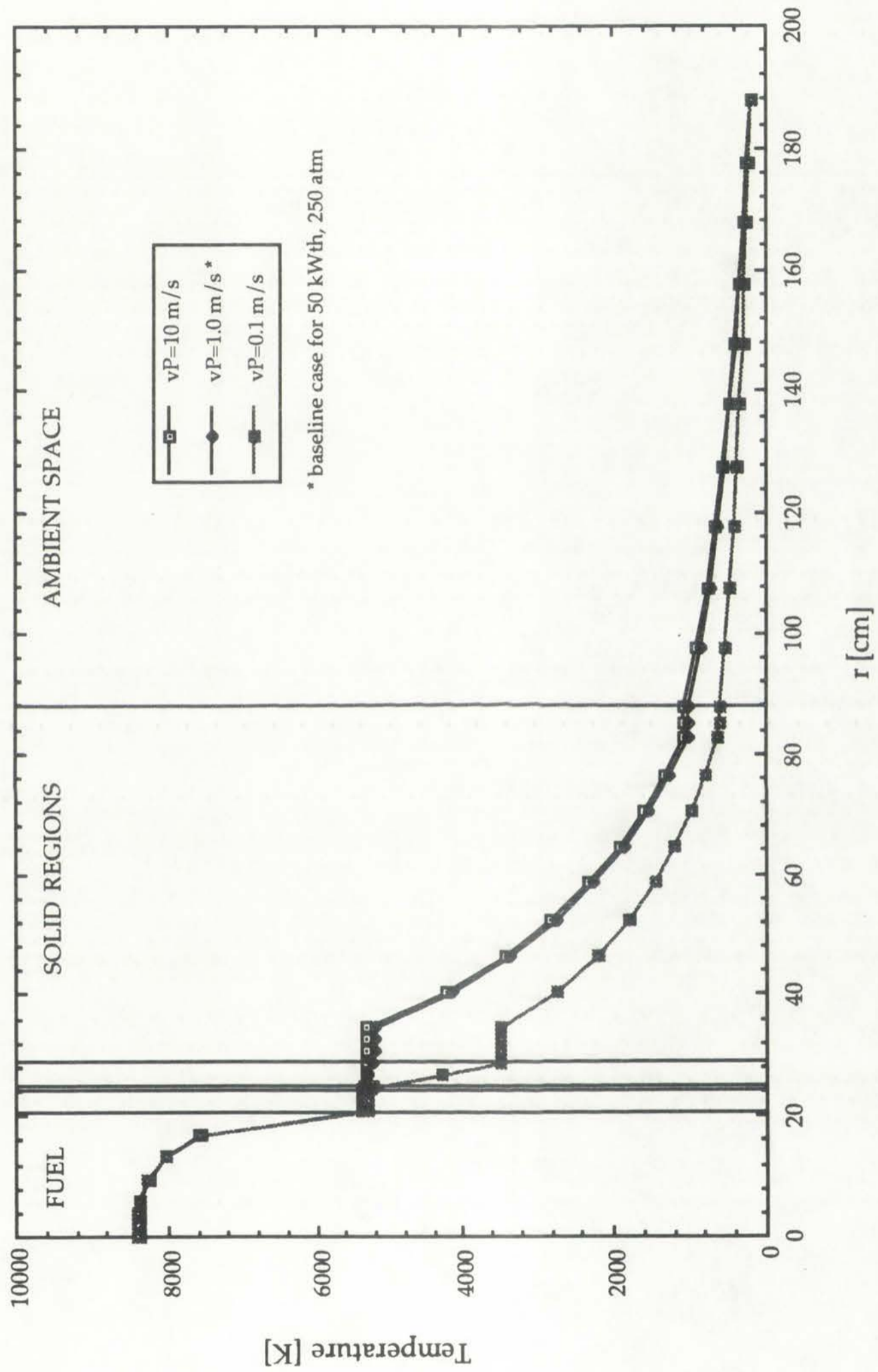
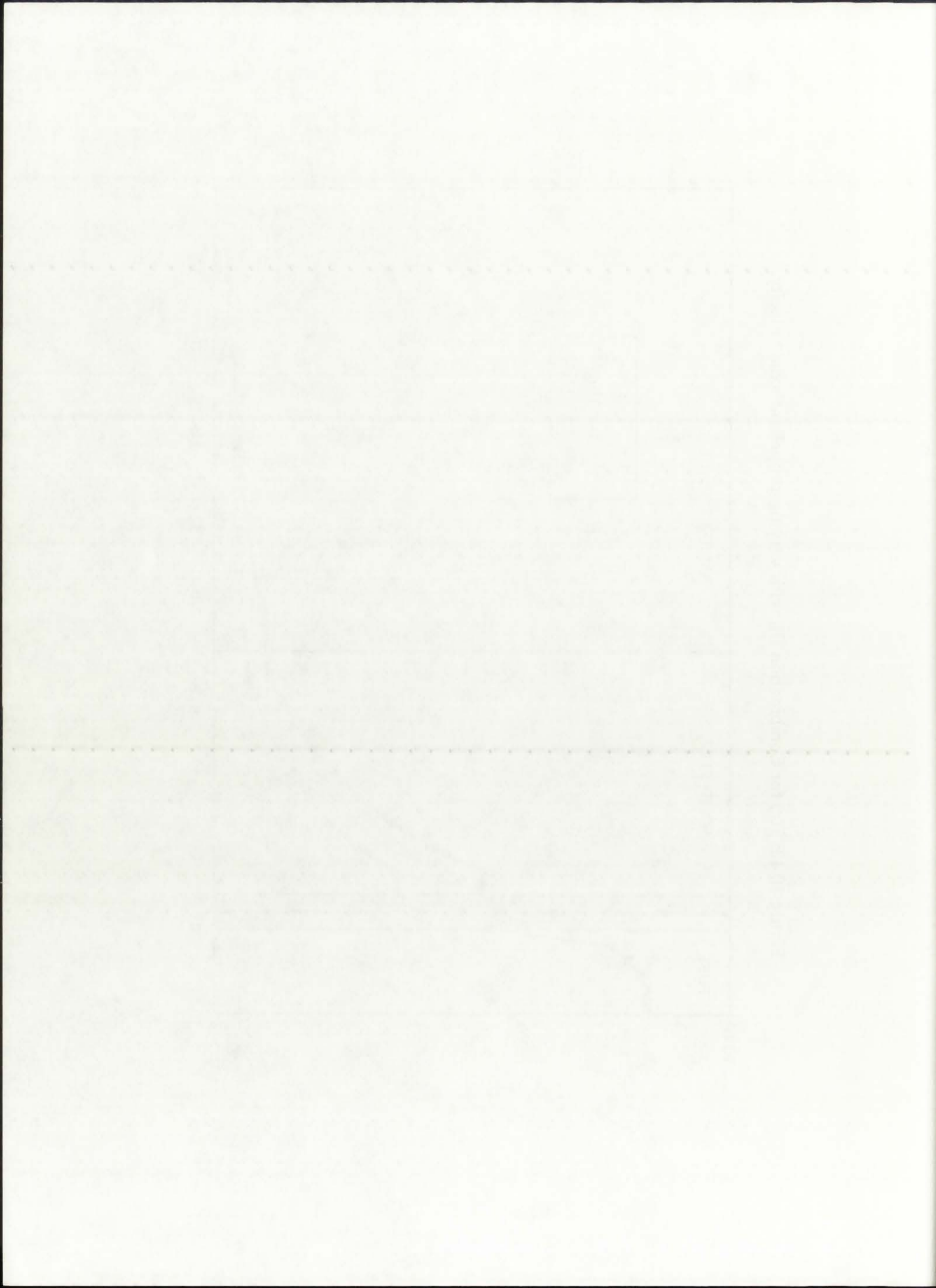


Figure 10.40: $T(r)$ for Combination III, with varying propellant axial velocity.





10.8.2. Effects of Fuel Temperature on k_{eff}

The main motivating factor for this analysis was the desire to quantify the effects of fuel temperature on k_{eff} , as GCR concepts are specifically intended to operate over a wide range of temperatures. The work with TRANSX and generation of temperature-dependent cross-sections provided the capability to perform such an analysis; thus, a baseline case was set up using the 50 kWth, 250 atm configuration with ENDF/B-V cross-sections. All non-fuel materials were set at a reference 300 K temperature so as to remove any temperature-dependent neutronics effects. The fuel, consisting of 96% enriched uranium, was then processed with TRANSX for temperatures of 300 K, 8,000 K, 10,000 K, 20,000 K, 40,000 K, and 60,000 K. Only the temperature of the fuel was varied; all other parameters in TRANSX and ONEDANT were held constant.

As was mentioned previously at the beginning of Section 10.8, a positive Doppler coefficient of reactivity was expected for the fuel, since it is comprised primarily of U-235. The k_{eff} values calculated by ONEDANT are shown in Figure 10.41. There does indeed seem to be a slight, but noticeable, positive reactivity coefficient for the fuel. The effect is very slight up to about 20,000 K, but seems to increase for higher temperatures, at a rate of approximately $1.62 \cdot 10^{-6}$ [1/K]. Such an effect, of course, would be insignificant for non-GCR reactors, which both operate at and are exposed to much lower fuel temperatures. The magnitude of the fuel temperature coefficient is in agreement with an estimate of 10^{-6} - 10^{-7} [1/K] proposed by [Diaz *et al.*, 1991].

The results obtained as part of the fuel temperature effects analysis indicate a potential positive Doppler coefficient of reactivity associated with the fuel. This effect could be beneficial in designing critical high-temperature GCR engines, as it could compensate up to a point for the significant negative fuel density coefficient, which was evident in the comparison of the k_{eff} values of the 500 MWth, 5 MWth, and 50 kWth configurations. The scope of the fuel temperature effects analysis presented here is limited, though, and could serve as a starting point for future, more detailed, analyses. The TRANSX and ONEDANT input files can be found in Appendix F.1 and F.2, respectively.

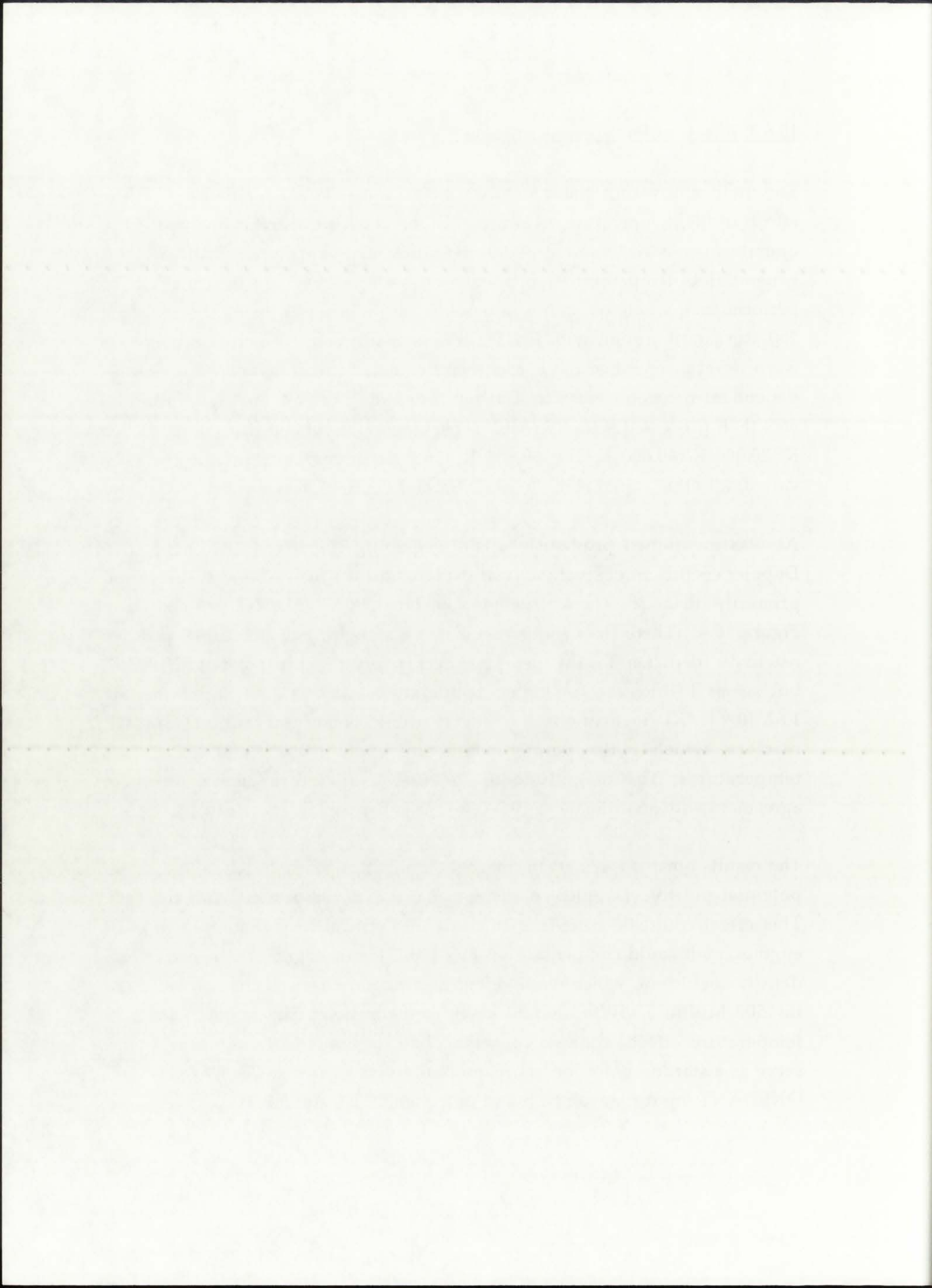
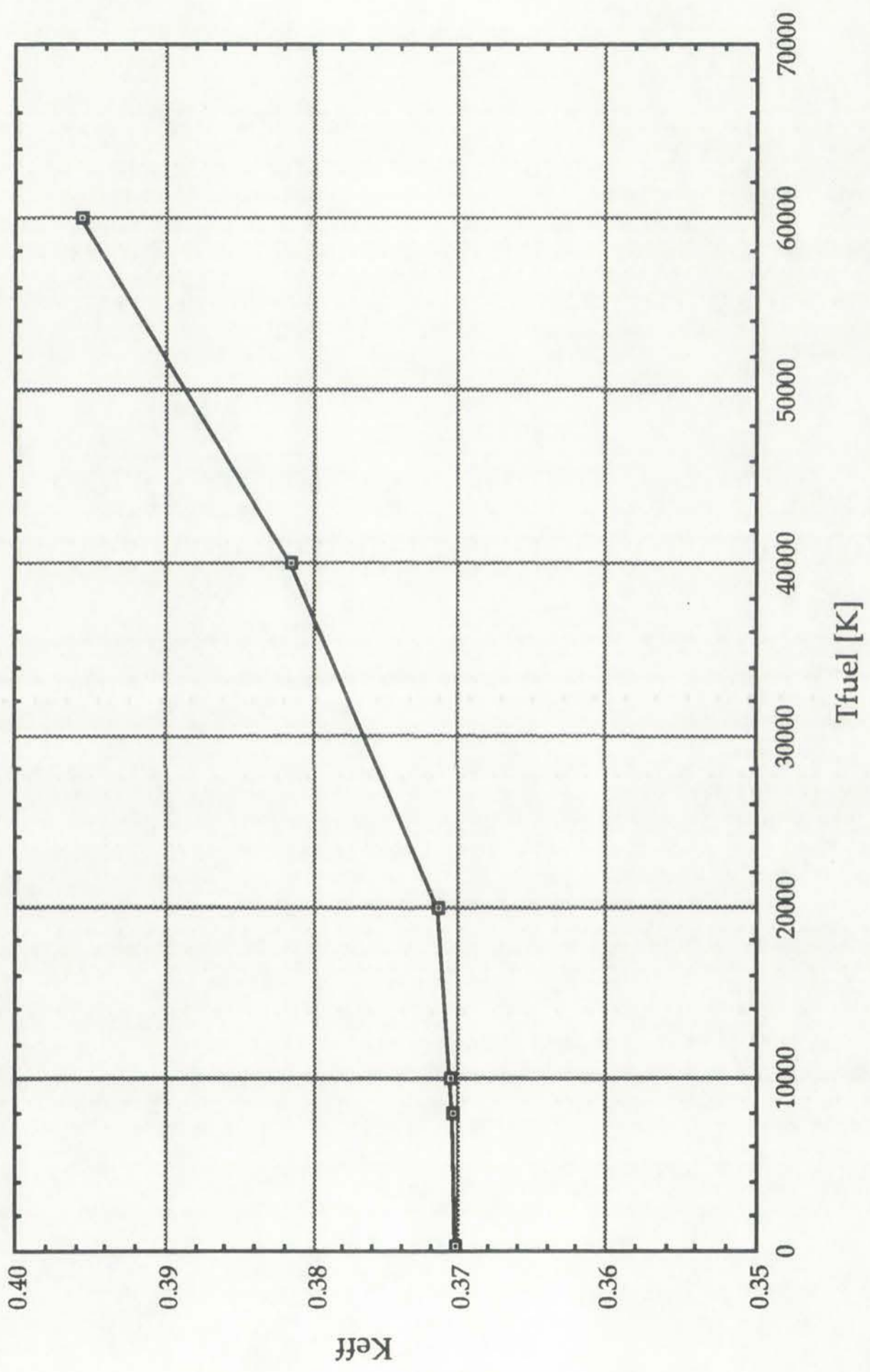


Figure 10.41: Effect of fuel temperature on the Keff of the rocket engine.

(TEST CASE = baseline configuration of 50 kWth, 250 atm based on ENDF/B-V data)



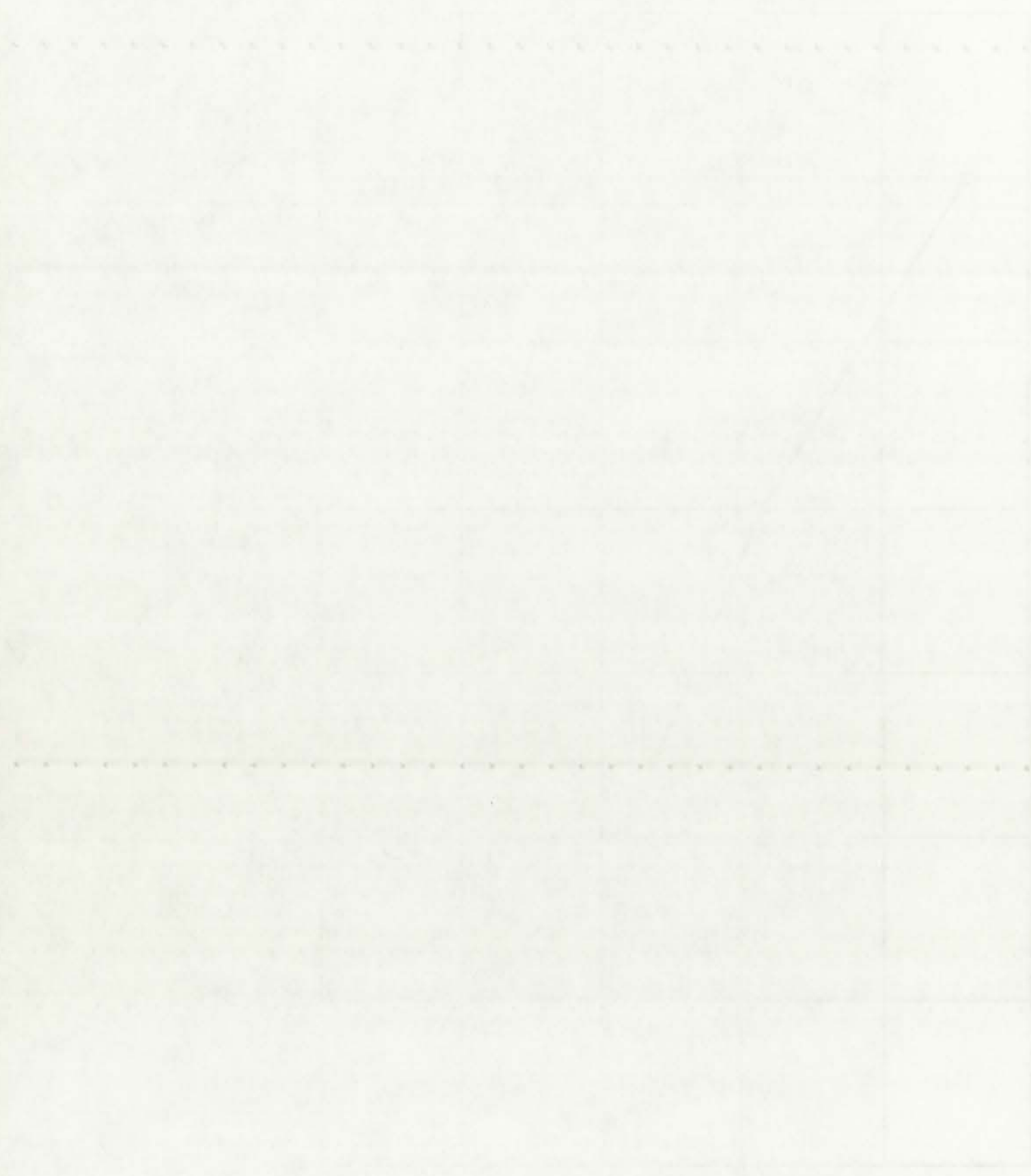


Figure 1: A graph showing a linear relationship between x and y. The line passes through the origin (0,0) and the point (4,4).

10.9. Accuracy of the (r) Geometry Model and Associated Assumptions

A major concern posed during the development of the (r) geometry model was the accuracy of the one-dimensional approximation to the true (r- θ) layout of the unit-cell NLB engine. As was previously shown in Figure 4.1, the segmented propellant channel was effectively "smeared" to convert it into (r) geometry. Such an approximation would necessarily involve a certain loss of accuracy, as θ -dependence would be neglected. The concern centered around the accuracy of the volumetric heat generation rate $Qg'''(r)$ and the neutron flux $\Phi(r)$.

An additional question posed following completion of the neutronics analysis in (r) geometry was the configuration at which criticality ($k_{eff}=1.000$) would be achieved. All three thermal power configurations analyzed in this Dissertation indicated a significantly subcritical system, with the highest k_{eff} being equal to 0.4498 (50 kWth, 250 atm). Even though the unit-cell NLB engine was initially proposed as a GCR test-bed and thus relied on external flux to achieve criticality, it would be interesting to know the conditions for which the unit-cell engine would be critical by itself.

The last concern regarding the thermalhydraulics model was related to the potential neutron and gamma energy deposition in the silica wall and the moderator/reflector region, and its effect on both the uncooled $T(r)$ in those regions as well as any necessary cooling scheme intended for those regions.

10.9.1. (r- θ) Analysis of $Qg'''(r)$

To ascertain the accuracy of the one-dimensional (r)-geometry model used in this Dissertation, a full two-dimensional (r- θ) model, with all dimensions conserved, was created and analyzed with the TWODANT code for the 50 kWth, $p=250$ atm configuration. Due to the existent bi-axial symmetry of the unit-cell engine, a 90° "slice" was analyzed, with reflective boundaries imposed on both the top and bottom. The $Qg'''(r)$ was requested at 8 intervals

10.2. Accuracy of the 1-Dimensional and 2-Dimensional Models

The major concern during the development of the 1-D geometry model was the accuracy of the one-dimensional approximation to the two-dimensional layout of the uncooled ILL engine. As was previously shown in figure 4.1, the labelled propellant channel was relatively confined to convert it into 1-D geometry. Such an approximation would necessarily involve a certain loss of accuracy, as a dependent would be neglected. The concern centred around the accuracy of the volumetric heat generation rate $Q_v''''(r)$ and the engine law (14).

An additional question posed following completion of the numerical analysis in 1-D geometry was the configuration at which criticality (see 1.00) would be achieved. All three distinct power configurations analysed in the literature indicated a significantly subcritical system with the highest k_{eff} being equal to 0.4498 (see 2.00 and 2.01). Even though the uncooled ILL engine was initially proposed as a GCR test-bed and thus relied on external heat to achieve criticality, it would be interesting to know the conditions for which the uncooled engine would be critical by itself.

The last concern regarding the thermally-driven model was related to the potential errors and biases arising from the use of the 1-D model. The moderator reflector region, and its effect on both the uncooled (1-D) and the uncooled (2-D) as well as necessary cooling scheme intended for these regions.

10.3. 1-D Analysis of $Q_v''''(r)$

To ascertain the accuracy of the one-dimensional 1-D geometry model used in the literature, a full two-dimensional (2-D) model, with all conditions converted, was created and analysed with the TWODANT code for the 30 MW, p=300 atm configuration. Due to the extent of axial symmetry of the uncooled engine, a 90° slice was analysed with reflective boundaries imposed on both the top and bottom. The $Q_v''''(r)$ was reported at 8 intervals

in the (r)-direction, and also at 8 intervals of 11.25° in the θ -direction, between $\theta=0^\circ$ (midpoint in the beryllium) and $\theta=90^\circ$ (midpoint in the hydrogen).

The behavior of $Qg'''(r)$ for the Hansen-Roach and ENDF/B-V libraries is shown in Figures 10.42 and 10.43, respectively. Parameter $th=1$ corresponds to $\theta=0^\circ$; parameter $th=8$ corresponds to $\theta=90^\circ$. For the purposes of comparison, the $Qg'''(r)$ for both the (r)-geometry model used in this Dissertation (with H_2 facing the fuel), as well as for a "swapped" (r)-geometry model with beryllium facing the fuel, are included in the figures. With ten plots sharing one graph, it is cluttered; however, the intent of this particular investigation and comparison was to investigate the accuracy of using the one-dimensional (r)-geometry approximation. It can be determined by observation of Figures 10.42 and 10.43 that the maximum deviation between the ten plots has an upper bound of 10%. In conclusion, then, it can be said that the accuracy of the (r)-geometry model is sufficient to provide good insight into the behavior of $Qg'''(r)$ and, derived from it, $T(r)$ in the engine.

10.9.2. (r- θ) Analysis of the Neutron Flux $\Phi(r)$

An (r- θ) analysis of the neutron flux $\Phi(r)$ was conducted to be able to ascertain with confidence the effect of the low-temperature beryllium moderator on k_{eff} . The goal of the analysis was to quantify the fraction of the total neutron flux lying in the 0.006 eV range; if the fraction were small, then the scattering cutoff of beryllium would not really matter and another moderator material (without the cutoff property) could just as well be used.

The analysis was done with both Hansen-Roach and ENDF/B-V libraries. The neutron energy range was split into three broad groups: fast, thermal, and subthermal, as shown below:

<u>Broad Group</u>	<u>Energy Range</u>
I	0.1 - ∞ eV
II	0.01 - 0.1 eV
III	0.00001 - 0.01 eV

in the intermediate and fast fission regions (0.1-10 MeV) is the difference between the number of neutrons produced in the fission and the number of neutrons lost in the system.

The behavior of ρ_{eff} for the Hanson-Ross and BND(BV) theories is shown in figures 10-11 and 10-12 respectively. Figure 10-11 shows ρ_{eff} versus β for the Hanson-Ross model and in the Discussion (with H-R) the ρ_{eff} for both the (-) asymptotic model and in the Discussion (with H-R) being the first, as well as for a "weighted" (-) asymptotic model with feedback being the first, as indicated in the figure. With the first starting one group, it is observed, however, the limit of the particular investigation and comparison was to investigate the accuracy of using the one-dimensional (-) asymptotic approximation. It can be determined by observation of figures 10-11 and 10-12 that the maximum deviation between the two plots has an upper bound of 10%. In conclusion, then, it can be said that the accuracy of the (-) asymptotic model is sufficient to provide good insight into the behavior of ρ_{eff} and control time τ_c in the region.

10-2.1 Analysis of the Hanson-Ross (H-R)

An (-) analysis of the neutron flux $\Phi(t)$ was conducted to be able to ascertain with confidence the effect of the intermediate-cerium moderator on the system. The point of the analysis was to provide the behavior of the total neutron flux $\Phi(t)$ in the 0-100 μ sec range if the reactor were small than the scattering length of cerium would not really matter and another moderator material (without the cerium property) could just as well be used.

The analysis was done with both Hanson-Ross and BND(BV) theories. The neutron energy range was split into three broad groups: fast thermal and subthermal as shown below. It was assumed that the neutron spectrum

Energy Group	Energy Range
I	0.1 - 10 eV
II	1.01 - 0.1 eV
III	0.0001 - 0.01 eV

Figure 10.42: Comparison of (r-theta) slice $Qg'''(r)$ vs. 1-D (r)-geometry approximation. (Hansen-Roach library data)

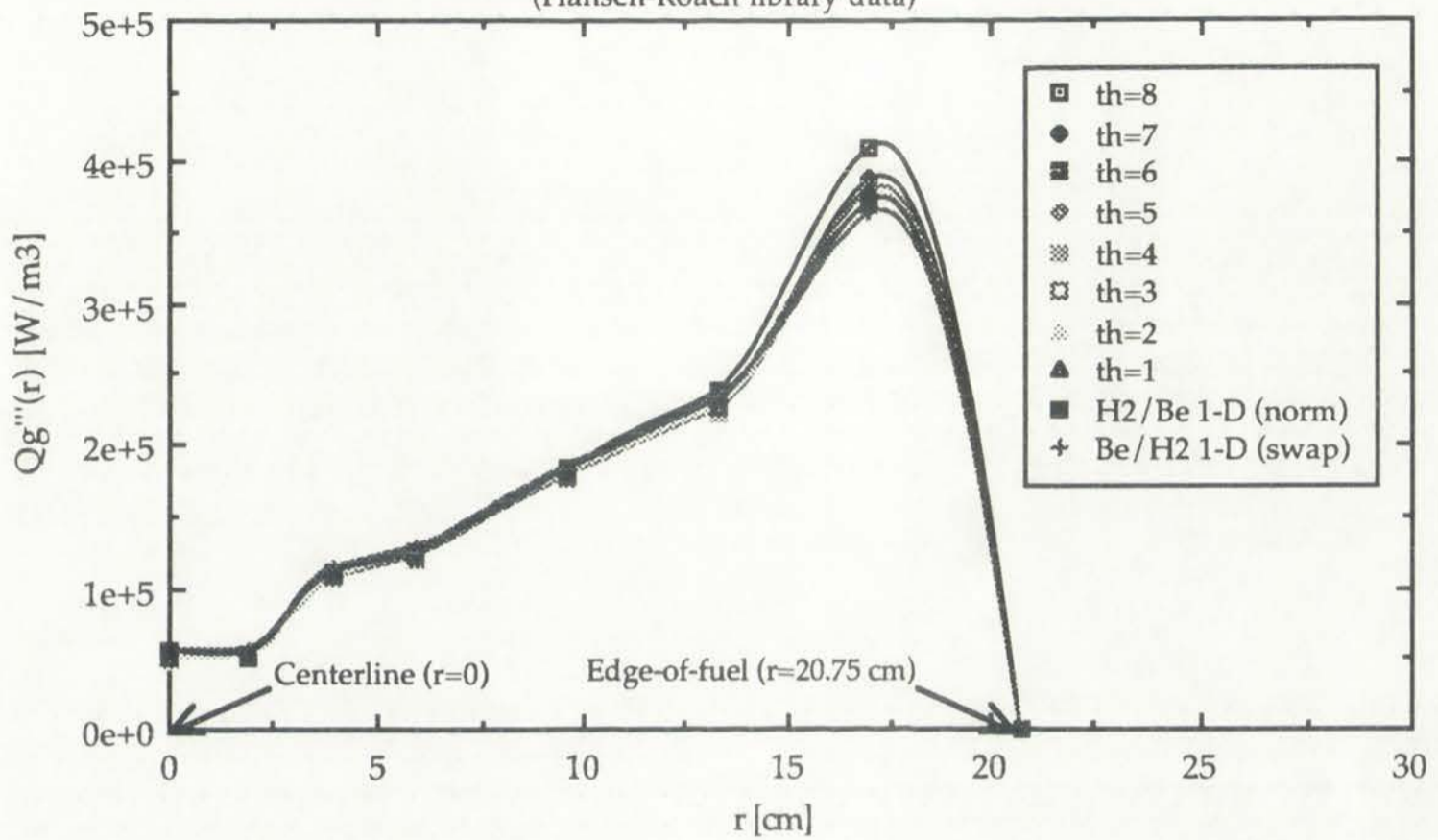
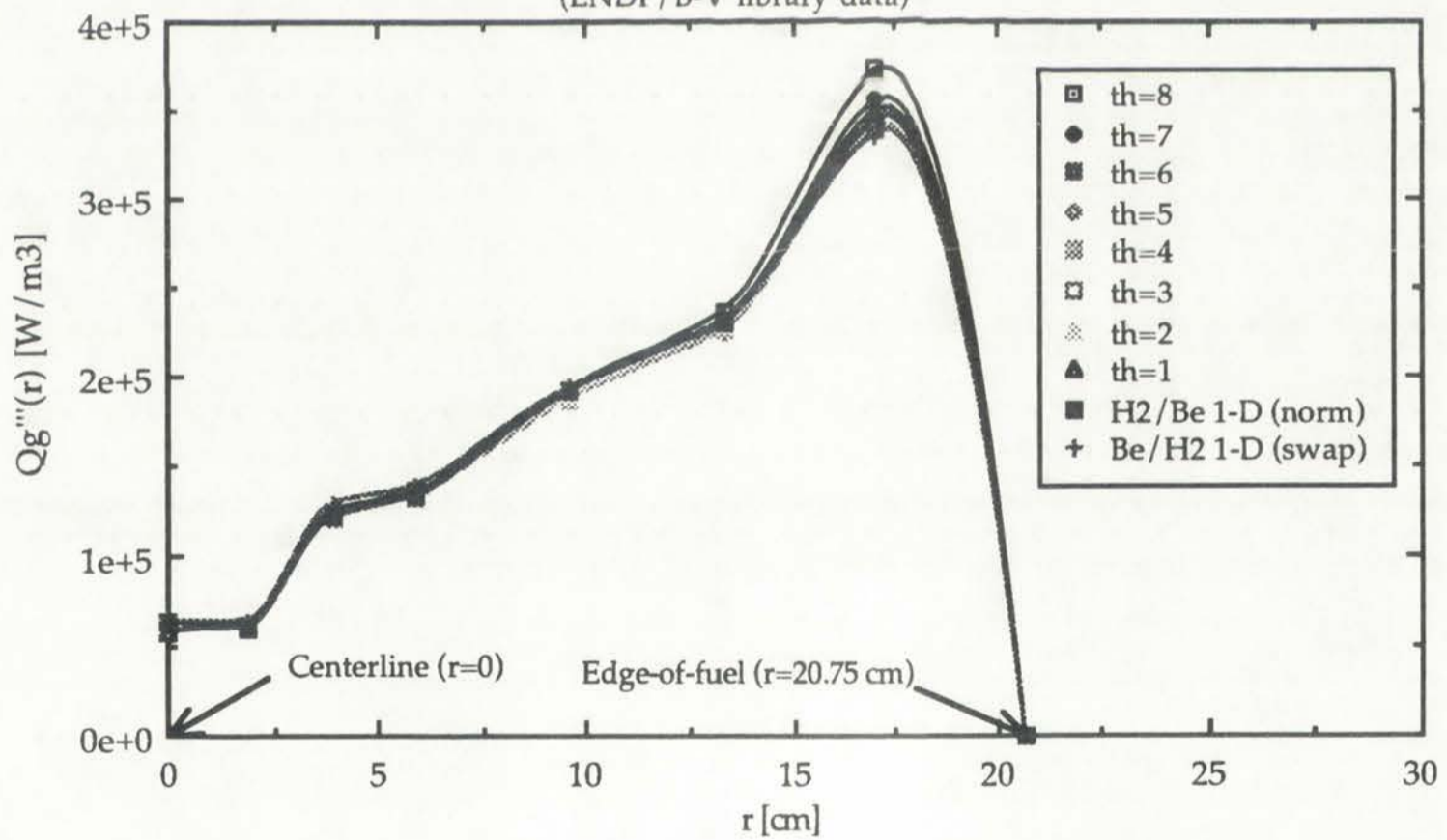
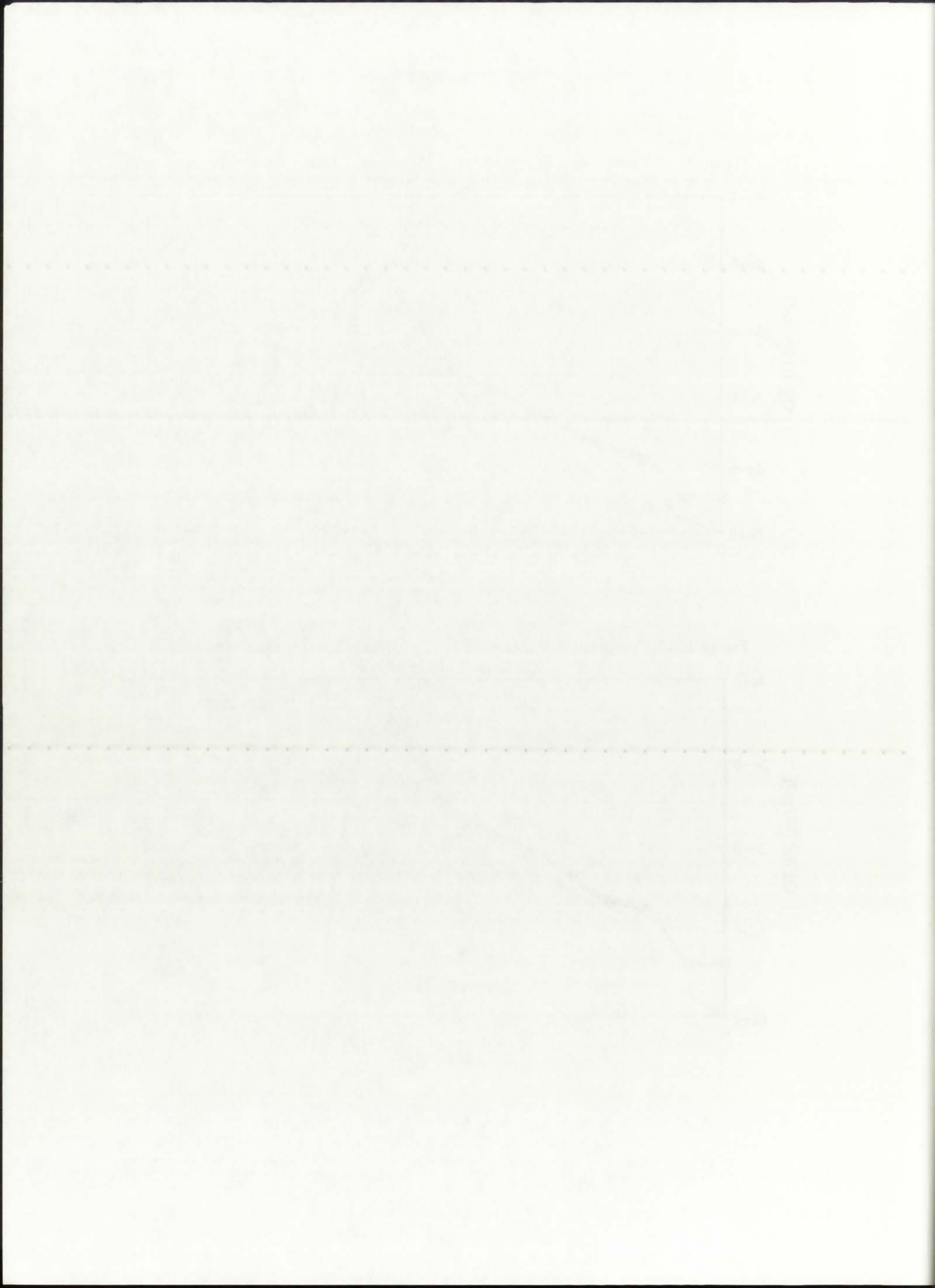


Figure 10.43: Comparison of (r-theta) slice $Qg'''(r)$ vs 1-D (r) geometry approximation. (ENDF/B-V library data)





With TWODANT, the fluxes were collapsed from 16 groups (Hansen-Roach) and 69 groups (ENDF/B-V) to the three broad groups. Naturally, since Hansen-Roach has a lower limit of 0.025 eV, only two broad groups were actually present for the Hansen-Roach part of the analysis.

The fluxes were obtained at 27 radial locations across the engine, and also at $\theta=0^\circ$ (midpoint in the beryllium) and at $\theta=90^\circ$ (midpoint in the hydrogen). The data was plotted in four graphs (midpoint in beryllium for Hansen-Roach and ENDF/B-V, and midpoint in hydrogen for Hansen-Roach and ENDF/B-V). For the ENDF/B-V case, the ratio of the subthermal (Group III) to total flux was calculated for both the midpoint in the beryllium and midpoint in the hydrogen; it is shown in Figure 10.44. As can be seen, the maximum ratio is approximately 0.02 and occurs in the D₂O reflector. Thus, it can be concluded that the bulk of the thermalization occurs in the thick reflector region, and that the beryllium moderator plays no significant role in the thermalization process. The occurrence of a 0.006 eV scattering cutoff in beryllium does not seem to influence the subthermal neutron population, nor does it increase the k_{eff} of the system.

10.9.3. Neutron and Gamma Energy Deposition

The thermalhydraulics analysis conducted as part of this Dissertation work did not specifically take into account neutron/gamma energy deposition in the silica wall and moderator/reflector region, nor did it quantify their effects. Rather, it was assumed that 176 MeV, out of the 198 MeV recoverable energy per fission, was deposited within the fuel [El-Wakil, 1981]. The remainder, carried out of the fuel by gammas and neutrons, could ultimately be deposited in the moderator/reflector. Therefore, it had been implicitly assumed that approximately 11% of the total thermal power would need to be accounted for in whatever cooling scheme would be decided on for the NLB engine. Energy deposition in the silica wall is more crucial, due to constraints on internal cooling of the very thin wall. Neutron energy deposition in silica is negligible, due to the virtual transparency of silica to neutrons ($\sigma_{a,\text{Si}}=0.08$ b, $\sigma_{a,\text{O}}=0.00018$ b) [El-Wakil, 1981].

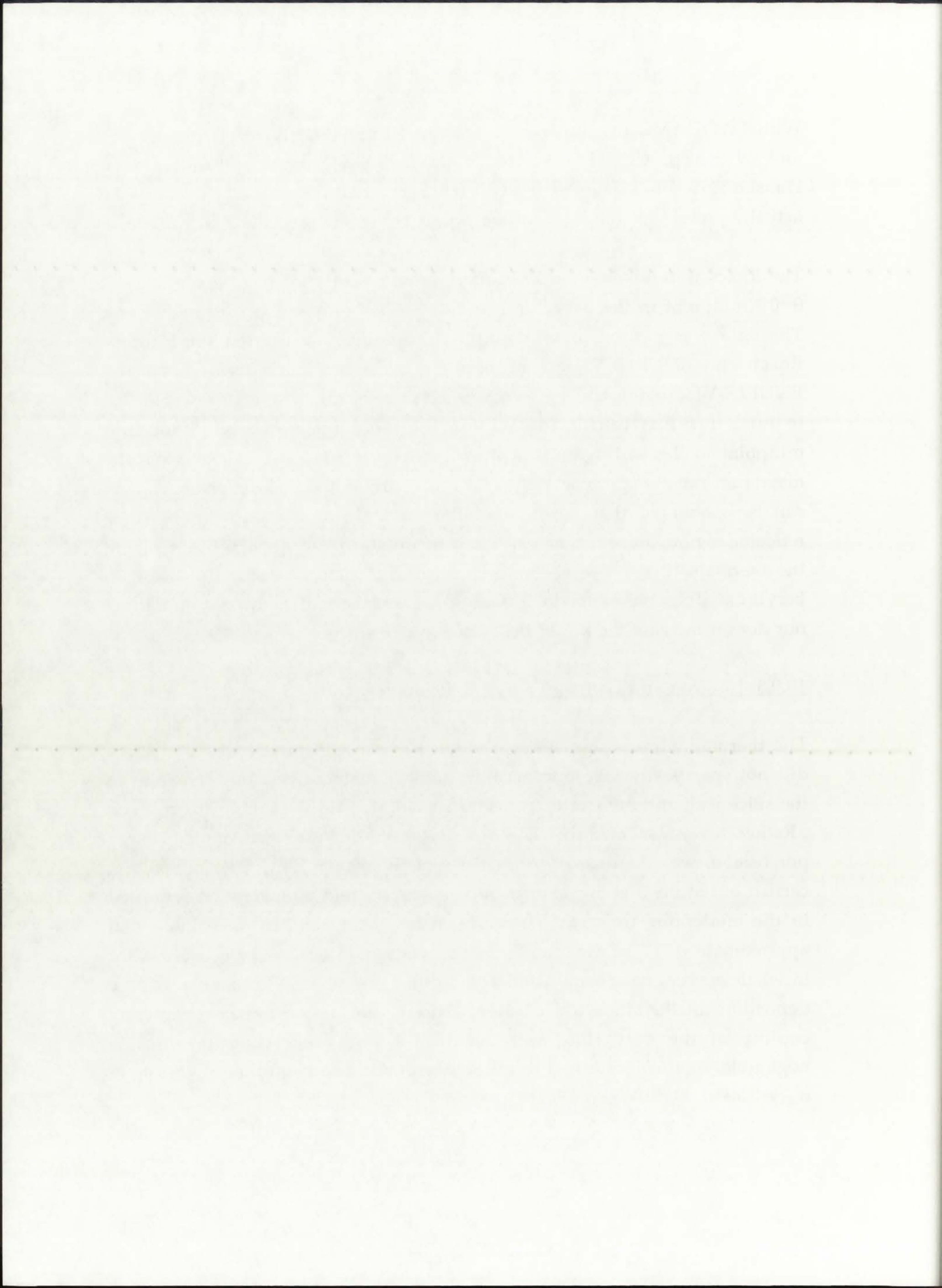
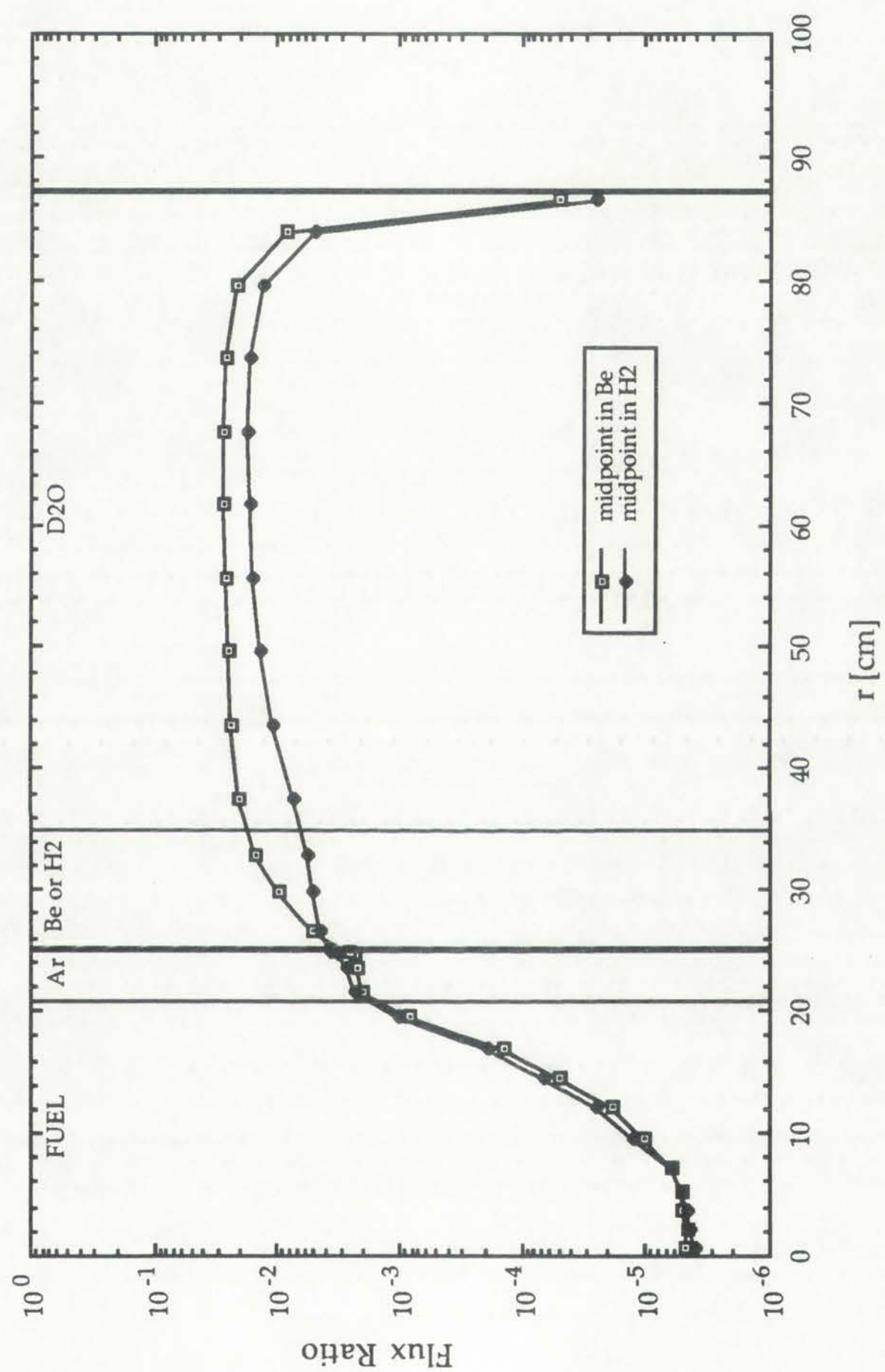
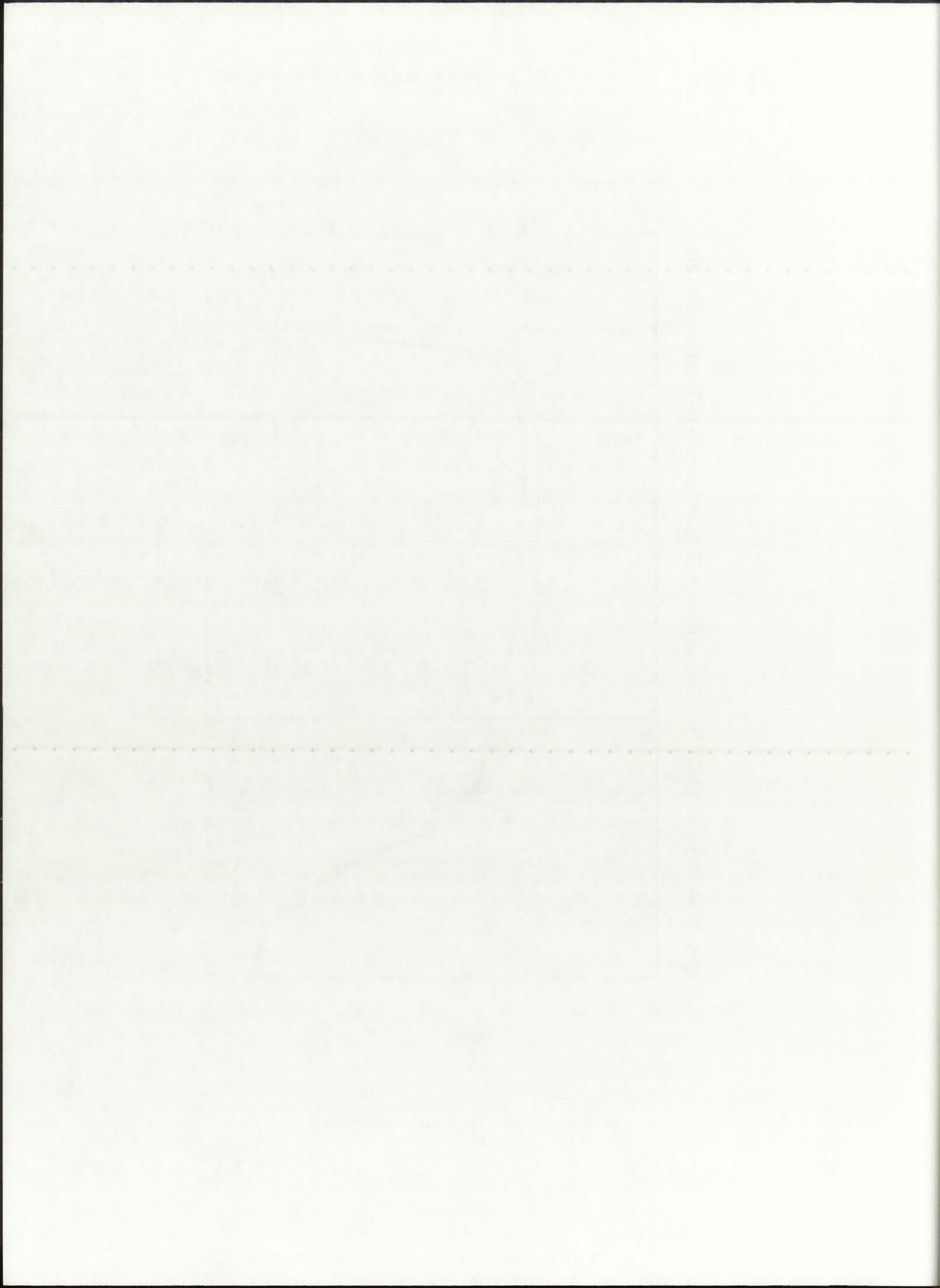


Figure 10.44: Ratio of ENDF/B-V Broad Group III (subthermal)-to-Total neutron flux.





For gammas, however, the average mass attenuation coefficient is approximately 0.15 cm^{-1} ; in 0.49 cm of wall, then, approximately 7% of the incident gamma flux is absorbed. That ultimately results in a value of 0.5% of the total thermal power deposited in the silica wall due to nuclear radiation. For the 50 kWth, 5 MWth, and 500 MWth configurations, then, approximately 250 W, 25 kW, and 2.5 MW are deposited in the wall. These values comprise only a small fraction of the total energy deposited in the wall by *thermal* radiation; as will be shown in Chapter 11, the latter contribution ranges from approximately 1.45 kW for the 50 kWth, 250 atm configuration to 438 MW for the 500 MWth, 1,000 atm configuration. An effective cooling scheme devised to remove thermal radiation energy would also take care of the small incremental energy deposited by *nuclear* radiation.

10.9.4. Criticality Search

A criticality search, based on the 50 kWth configuration, was performed to determine the operating pressure needed to achieve $k_{\text{eff}}=1.000$. The search was performed separately for the Hansen-Roach and ENDF/B-V cross-section libraries; for each library, separate searches were conducted for both the 1-D (r)-geometry model used in this Dissertation, as well as a full 2-D (r- θ) model which took into account the segmented propellant channels of the engine.

The behavior of k_{eff} vs. operating pressure is shown in Figure 10.45. As can be seen, criticality is achieved at 18,000 atm using Hansen-Roach data and at 19,000 atm using the ENDF/B-V data. Such pressures are, for all practical purposes, unfeasible and would require an extremely massive pressure vessel. Thus, from the standpoint of achieving criticality in the unit-cell NLB engine, two alternatives exist: (1) for terrestrial testing and proof-of-concept of the unit-cell, a driver reactor, such as the ACRR, could be used to provide the additional neutron flux (corresponding to the initial UARL plans for the unit-cell), or (2) for reliance on the unit-cell as a standalone rocket engine, a thorough re-design would be necessary. As was discussed previously in this Chapter, the greatest impact on increasing k_{eff} would come from increasing either the fuel volume, fuel pressure, or both.

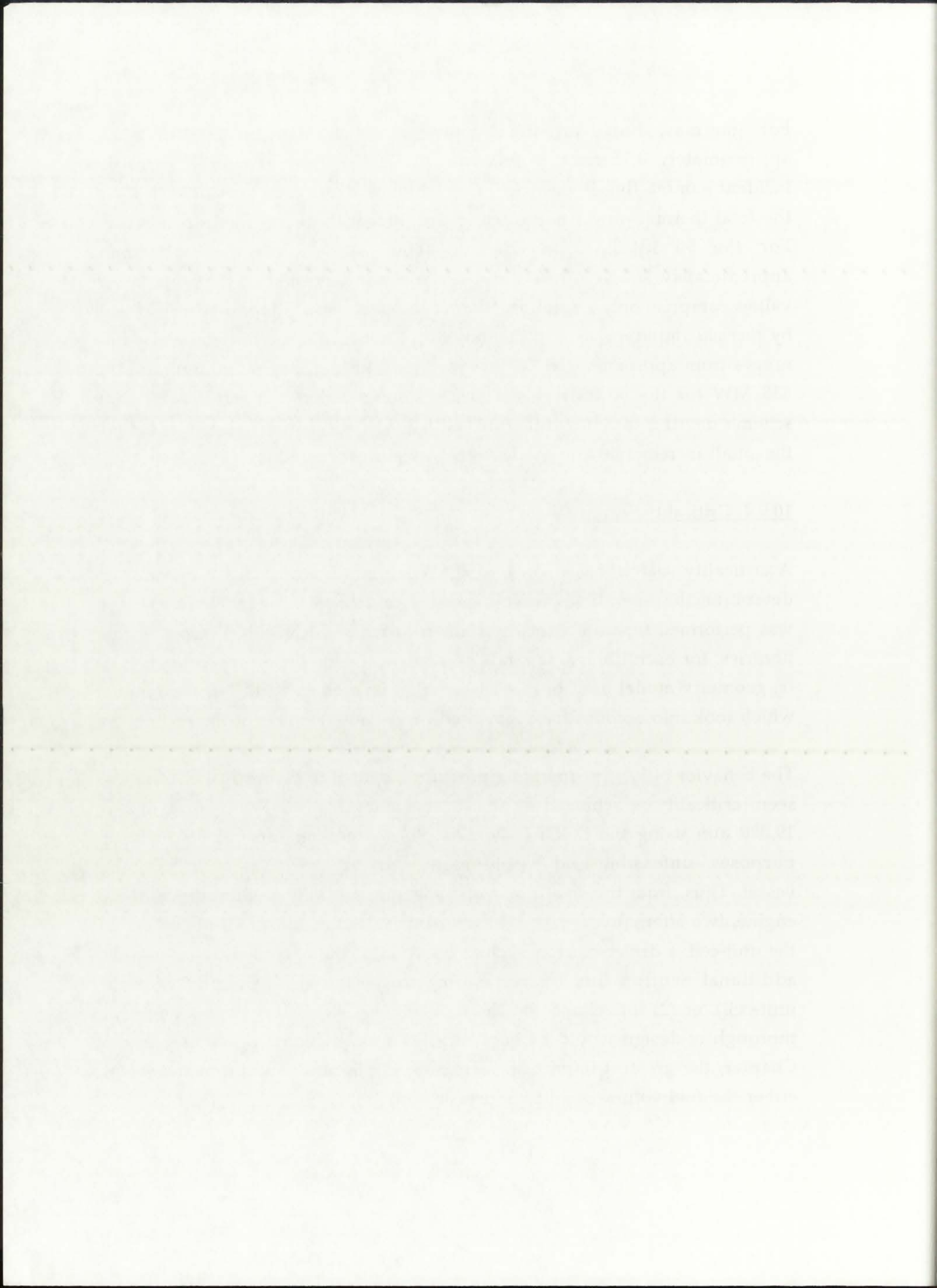
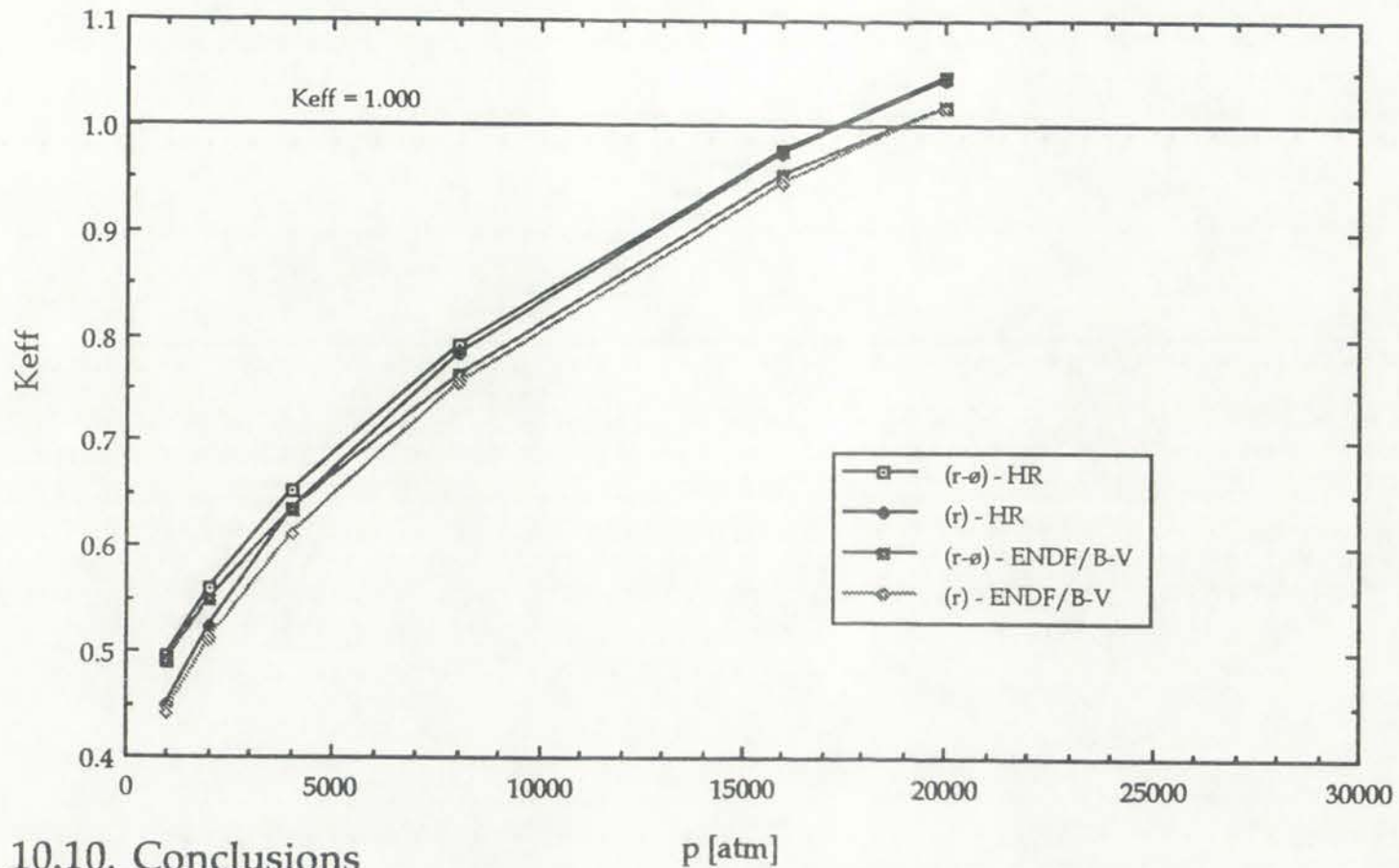


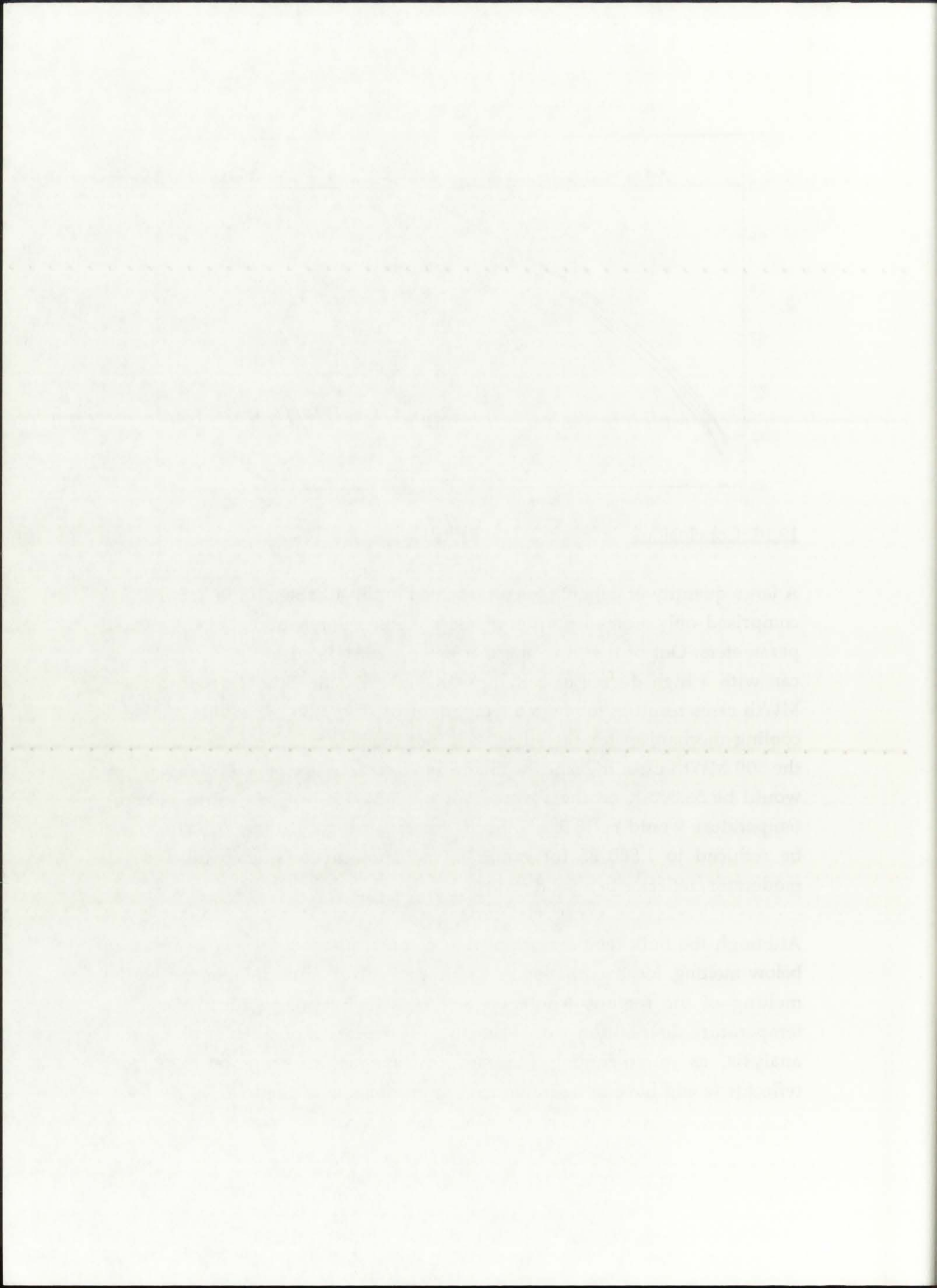
Figure 10.45: Search for criticality: 50 kWth configuration



10.10. Conclusions

A large quantity of data has been presented in this Chapter, and even that has comprised only a small portion of the possible combinations of NLB-related parameters. Out of the three thermal powers considered in this analysis, one can with a high degree of certainty conclude that the 500 MWth and the 5 MWth cases result in too high a temperature distribution to provide a feasible cooling mechanism for the silica wall and moderator/reflector regions. For the 500 MWth case, the silica wall and moderator/reflector liner temperature would be 56,000 K on the average; for the 5 MWth case, the corresponding temperature would be 18,000 K. Such temperatures are too large to effectively be reduced to 1,800 K, for example, to maintain the silica wall and the moderator/reflector in a solid state.

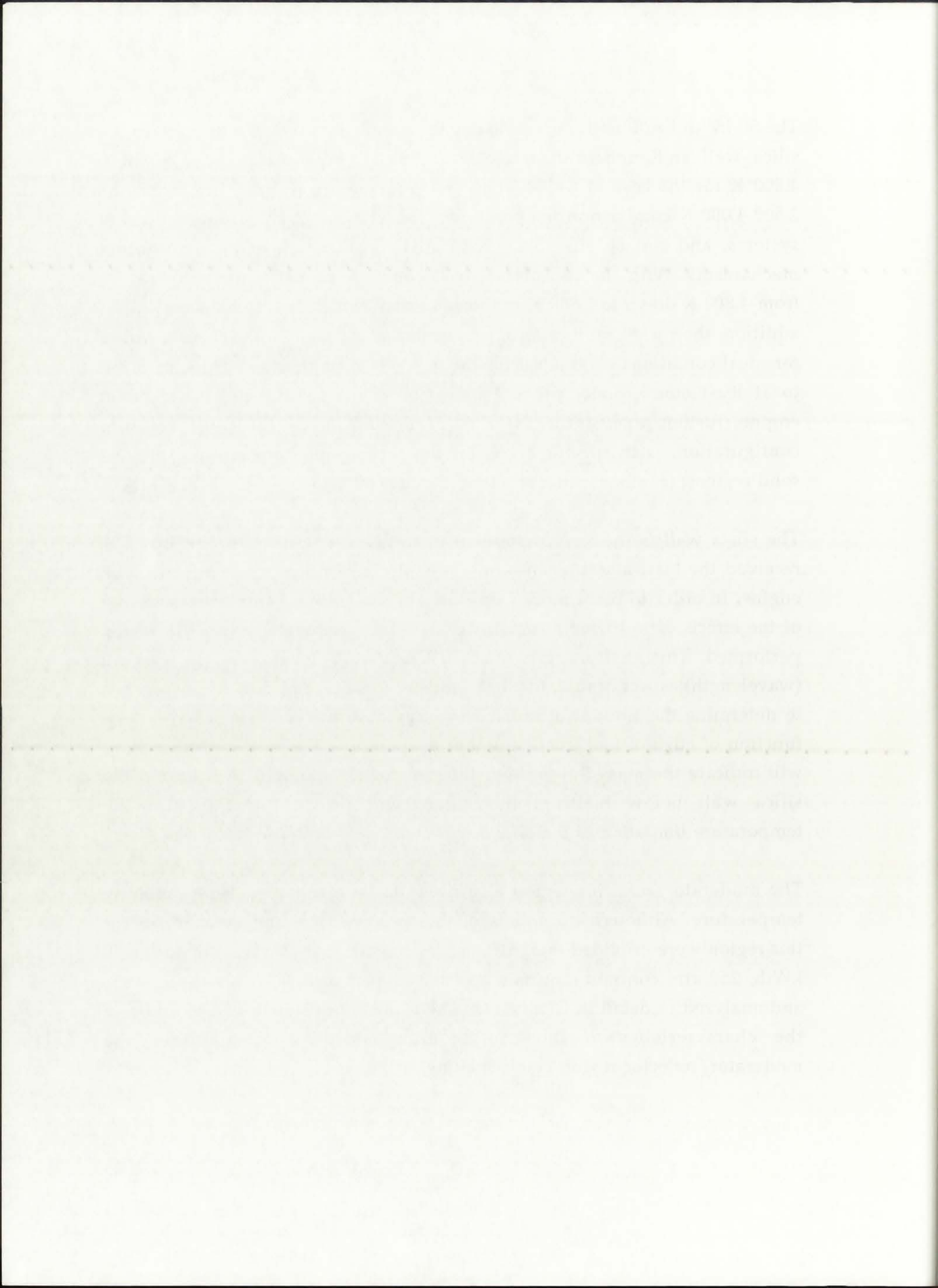
Although the bulk temperature of the regions could possibly be reduced to below melting, localized hot-spots would probably be unavoidable and partial melting of the regions would ensue. An actual representation of such a temperature distribution would necessarily require a detailed (r-θ) thermal analysis, as micro-cooling channels interspersed in the moderator and reflector would have to be introduced to maximize heat removal.



The 50 kWth configuration is probably the only truly feasible option, with the silica wall and moderator/reflector *uncooled* temperature approximately 4,800 K for the case of $p=250$ atm. This temperature is quite similar to the 2,500-4,000 K combustion temperatures characteristic of chemical propulsion systems, and can be effectively reduced by application of proper cooling mechanisms. With the use of internal cooling, a reduction in temperature from 4,800 K down to 1,800 K in the silica wall could feasibly be achieved. In addition, the rocket performance parameters, most notably the thrust, would for ideal conditions be greatest for the 50 kWth configuration. Thus, in order to at least conceptually prove the feasibility of the unit-cell NLB rocket engine, further analysis needs to be performed on the 50 kWth, 250 atm configuration, with specific focus on the cooling mechanisms for the two solid regions: (1) silica wall, and (2) moderator/reflector.

The silica wall is the key component of the NLB engine, and one that has received the least attention in terms of analytical studies involving the NLB engine. In order to place more emphasis on, and gain a better understanding of the effects of radiative heat transfer in silica, a separate analysis has been performed. This analysis, presented in Chapter 11, focuses on the spectral (wavelength) aspect of radiative heat transfer in silica. The goal of the work is to determine the amount of radiative energy absorbed in the silica wall as a function of edge-of-fuel (fuel emission) temperature. The results of this work will indicate the mass flow rate of internal coolant required to maintain the silica wall below melting; this, then, will provide insight into the temperature limitation of the NLB engine with respect to the silica wall.

The moderator/reflector region also needs to be maintained below melting temperature. Although no details on the proposed cooling mechanism for this region were provided by UARL, a film cooling analysis focusing on the 50 kWth, 250 atm configuration is suggested as part of this Dissertation work, and analyzed in detail in Chapter 12. The results of this analysis will indicate the characteristics of the cooling film necessary to maintain the moderator/reflector region below melting.



CHAPTER 11

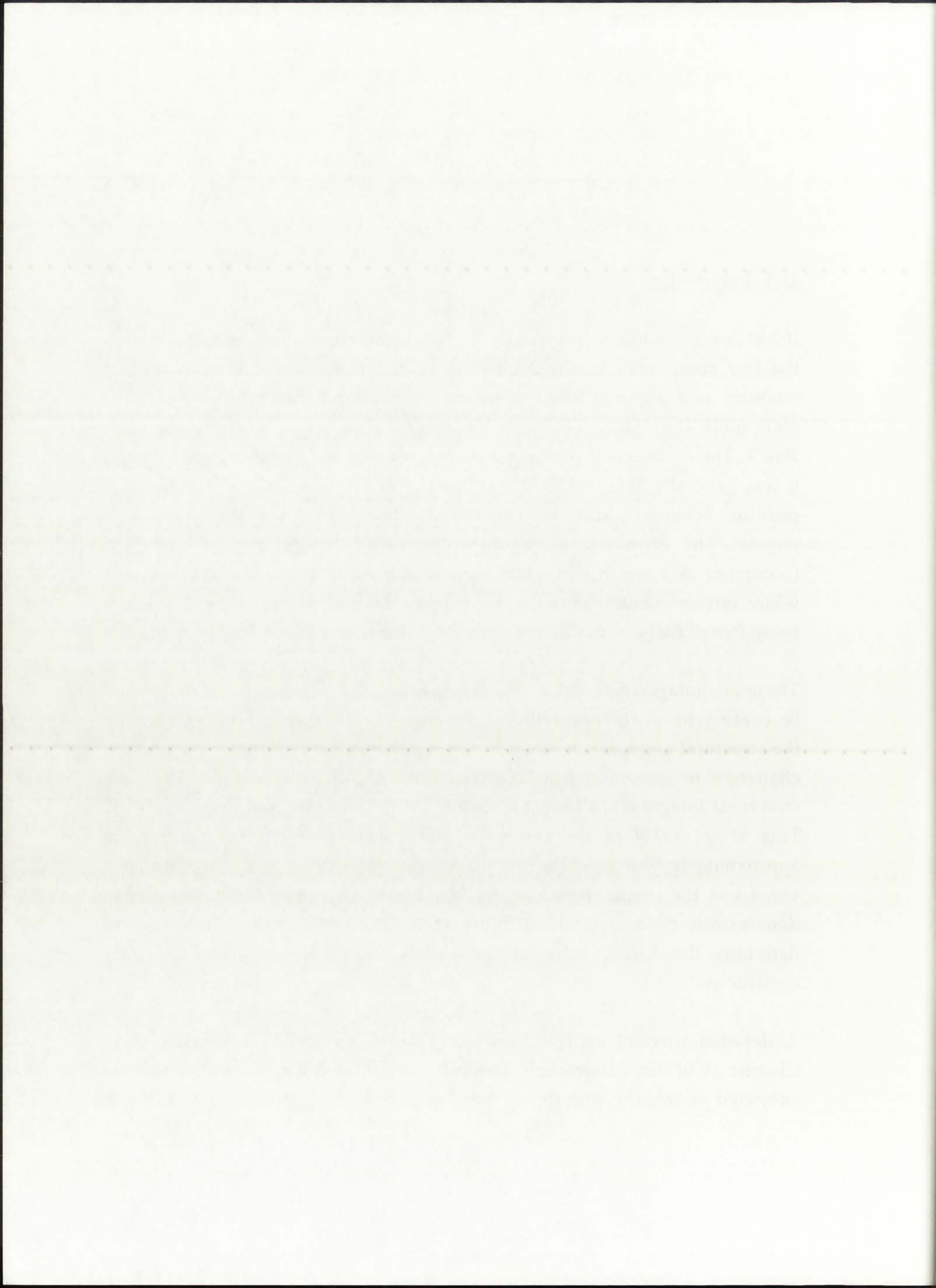
SPECTRAL ANALYSIS OF RADIATIVE HEAT TRANSFER IN THE SILICA WALL

11.1. Introduction

It has been mentioned previously in this Dissertation that the silica wall is the key component of the NLB engine. Inclusion of a solid transmitting medium as a physical barrier between the fuel and the propellant was the main motivating factor behind the then-innovative NLB concept in the early 1960's. The existence of such a barrier led to the term "closed-cycle GCR" and it was generally accepted that the closed-cycle NLB engine could potentially provide economic and environmental advantages over the open-cycle engine. The economic advantages involved elimination of fuel loss (occurring as a result of fuel/propellant mixing in the open-cycle engine), while environmental advantages centered around the propellant exhaust being free of fuel and fission products [McLafferty and Bauer, 1967].

These advantages inherent to the closed-cycle NLB engine, of course, would be contingent on the feasibility of the engine in the first place. Maintaining the structural and thermal integrity of the silica wall is potentially the greatest challenge in demonstrating the feasibility of the NLB engine. The wall structural integrity has been discussed briefly [Schwenk and Franklin, 1970; Tam *et al.*, 1970] in the context of the shear stress of the silica being approximately 0.66 atm. The thermal integrity, however, has generally been viewed as the crucial aspect of the design [Mensing *et al.*, 1990]. In order to demonstrate the potential feasibility of the NLB engine, it is necessary to determine the thermal behavior of the silica wall for the proposed operating conditions.

A detailed thermal analysis, including the silica wall, was presented in Chapter 10 of this Dissertation. The analysis indicated that the wall would be subjected to melting due to combined radiative/convective heat transfer. It



was thus decided to perform a detailed thermal analysis focusing on the radiative heat transfer through the silica wall. Such an analysis would provide insight into the necessary cooling requirements for the more complex portion of the heat transfer; it would then be a simple matter to perform, as part of some future work, an analysis of the film cooling requirements to minimize convective heat transfer to the wall from the buffer gas and propellant.

11.2. Methodology of Analysis

Due to the strong wavelength dependence of radiative heat transfer, spectral variation was incorporated into the radiative heat transfer analysis presented here. The spectral analysis focused on determining the fraction of radiative heat flux originating from the fuel that will be absorbed in the wall. In most NLB-related publications, the wall was termed "transparent" or "transmitting," connoting that only a negligible fraction of the emitted radiative heat flux would be absorbed in the wall. As heat absorption in the wall is a key issue in the feasibility of the whole NLB concept, the goal of this research was to quantify as accurately as possible the thermal absorption in the wall.

The methodology of analysis involved determining the spectral, hemispherical radiative emissive power (i.e., radiative heat flux per unit wavelength) of the fuel as a function of radiation wavelength and fuel temperature. Using a known spectral transmission profile of the silica wall, it is possible to quantify the fraction of emissive power that is emitted below the transmission cutoff (TC) of the silica - in effect, the fraction that is emitted in the wavelength range for which the silica exhibits almost 0% transmission. This fraction of the emissive power becomes absorbed by the silica wall and results in a proportional increase in the wall temperature. It is thus possible to determine the wall temperature on the basis of fuel emissive power and the silica spectral transmission profile.

was then decided to perform a detailed thermal analysis focusing on the radiative heat transfer through the silica wall. Such an analysis would provide insight into the necessary cooling requirements for the more complex portion of the heat transfer it would then be a simple matter to perform, as part of some future work, an analysis of the film cooling requirements to maintain effective heat transfer to the wall from the boiler gas and combustion.

11.2 Methodology of Analysis

For the study, a 1-D energy balance of radiative heat transfer, spectral variation was incorporated into the radiative heat transfer analysis presented here. The spectral analysis focused on determining the fraction of radiative heat flux originating from the fuel side will be absorbed in the wall. In gas side radiative heat transfer, the wall was treated as "transparent" or "nonparticipating," assuming that only a negligible fraction of the emitted radiative heat flux would be absorbed in the wall. As heat absorption in the wall is a key issue in the feasibility of the whole HLB concept, the goal of this research was to quantify as accurately as possible the thermal absorption in the wall.

The methodology of analysis involved determining the spectral radiative heat flux and radiative emission power (i.e., radiative heat flux per unit wavelength) of the fuel as a function of radiative wavelength, and fuel temperature (using a known spectral transmission profile of the silica wall, it is possible to quantify the fraction of radiative power that is emitted below the transmission cutoff (λ_c) of the silica - in effect, the fraction that is emitted in the wavelength range for which the silica exhibits almost 0% transmission. The fraction of the radiative power becomes absorbed by the silica wall and results in a proportional increase in the wall temperature. It is thus possible to determine the wall temperature on the basis of that radiative power and the silica spectral transmission profile.

11.3. Spectral Radiative Heat Transfer Theory

The radiative emissive power of the gaseous fuel in the NLB engine can be closely approximated by blackbody emissive power; the similar thermo-optical properties of the two media have been discussed in [Kesten and Krascella, 1966] and [Schwenk and Franklin, 1970]. This similarity is due to the negligible reflectivity and transmissivity, and very large absorptivity of the fuel. The correlation of blackbody thermal radiation to emissive power was first derived by Max Planck; [Incropera and DeWitt, 1990; and Siegel and Howell, 1992] state that the radiative spectral, hemispherical emissive power is described by Planck's Law:

$$e_{\lambda}(\lambda, T) = \frac{2\pi C_1}{\lambda^5 (e^{C_2/\lambda T} - 1)} , \quad (11.1)$$

where λ and T correspond to the radiation wavelength and the fuel emission temperature, respectively. The constants C_1 and C_2 are equal to $0.595522e8$ [$W\text{-}\mu\text{m}^4/\text{m}^2\text{-sr}$] and $14,387.69$ [$\mu\text{m}\text{-K}$], respectively. The behavior of $e_{\lambda}(\lambda, T)$ is illustrated in numerous radiative heat transfer texts; the temperatures considered, however, are less than $10,000$ K, which comprises the low-end of the proposed GCR operating temperature range. A short computer program, called WVLENABS, was therefore developed as part of this analysis to calculate $e_{\lambda}(\lambda, T)$ for a temperature range of $5,000$ K to $300,000$ K. The variation of $e_{\lambda}(\lambda, T)$ with wavelength and temperature is shown in Figure 11.1. The listing of the program, along with the output, is given in Appendix G.

For a given fuel emission temperature T , it is possible to find the wavelength λ_{max} where the emissive power $e_{\lambda}(\lambda, T)$ reaches a maximum. This correlation, known as Wien's Displacement Law, has the form:

$$\lambda_{\text{max}} = \frac{C_3}{T} , \quad (11.2)$$

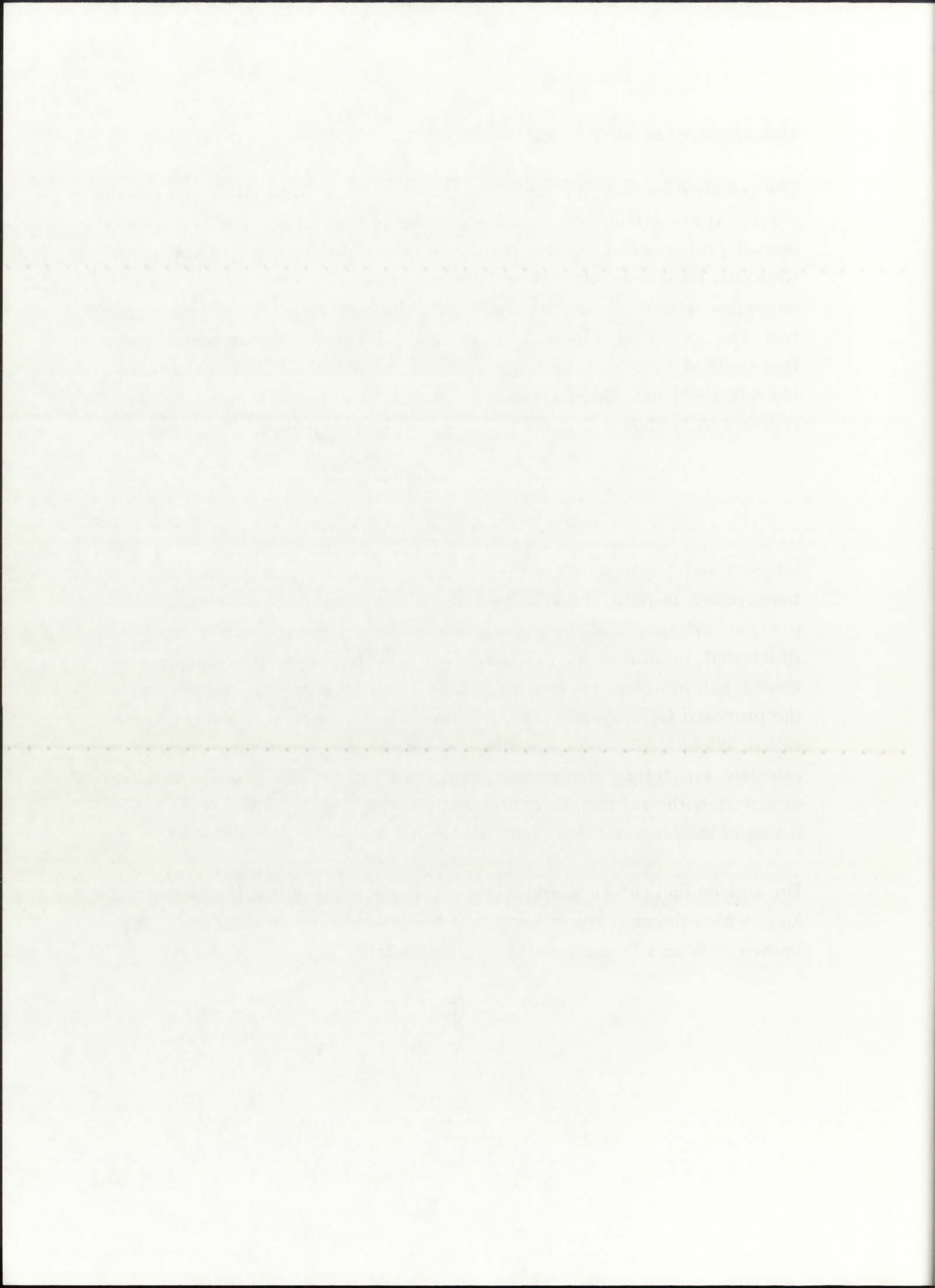
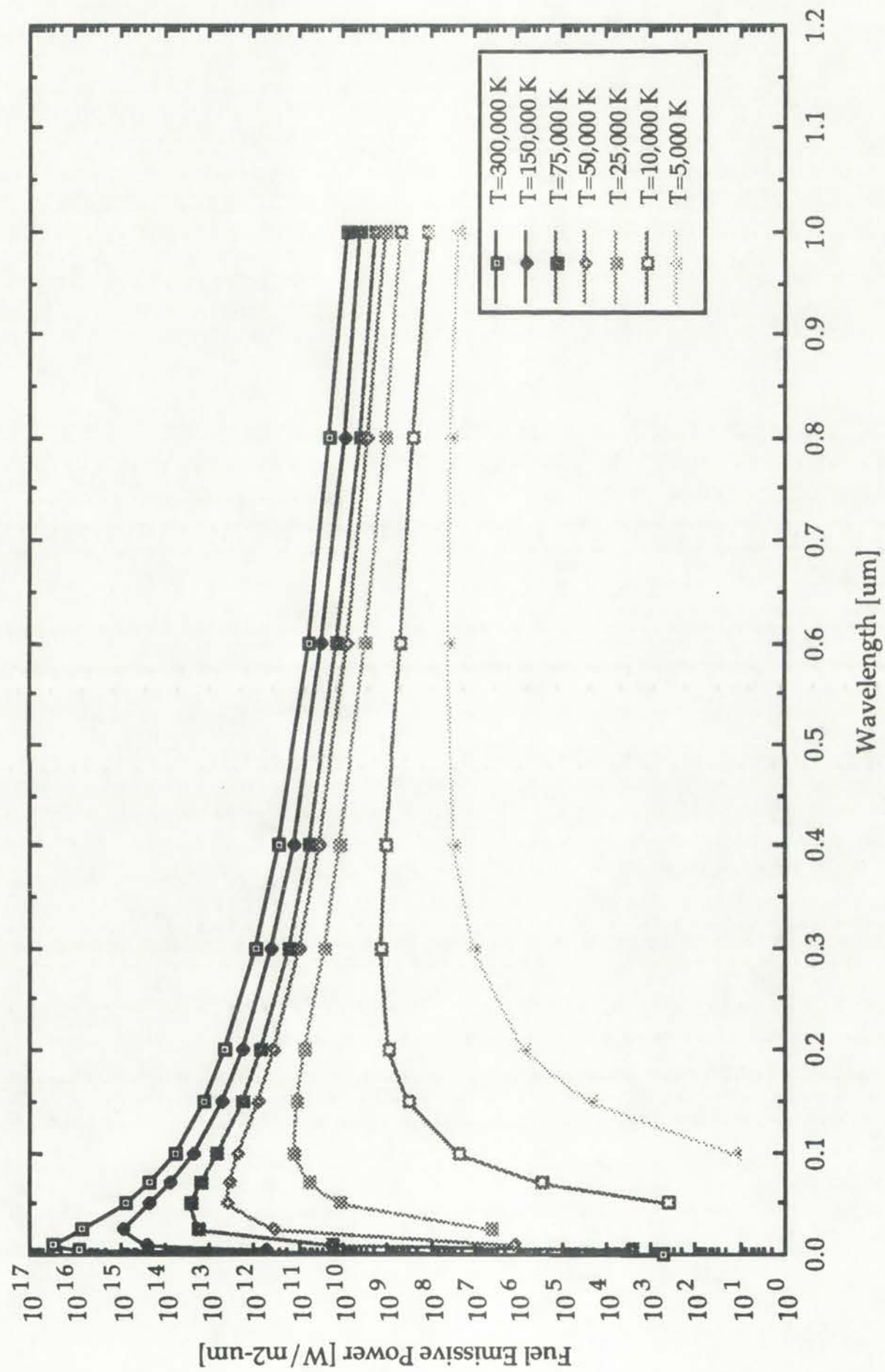
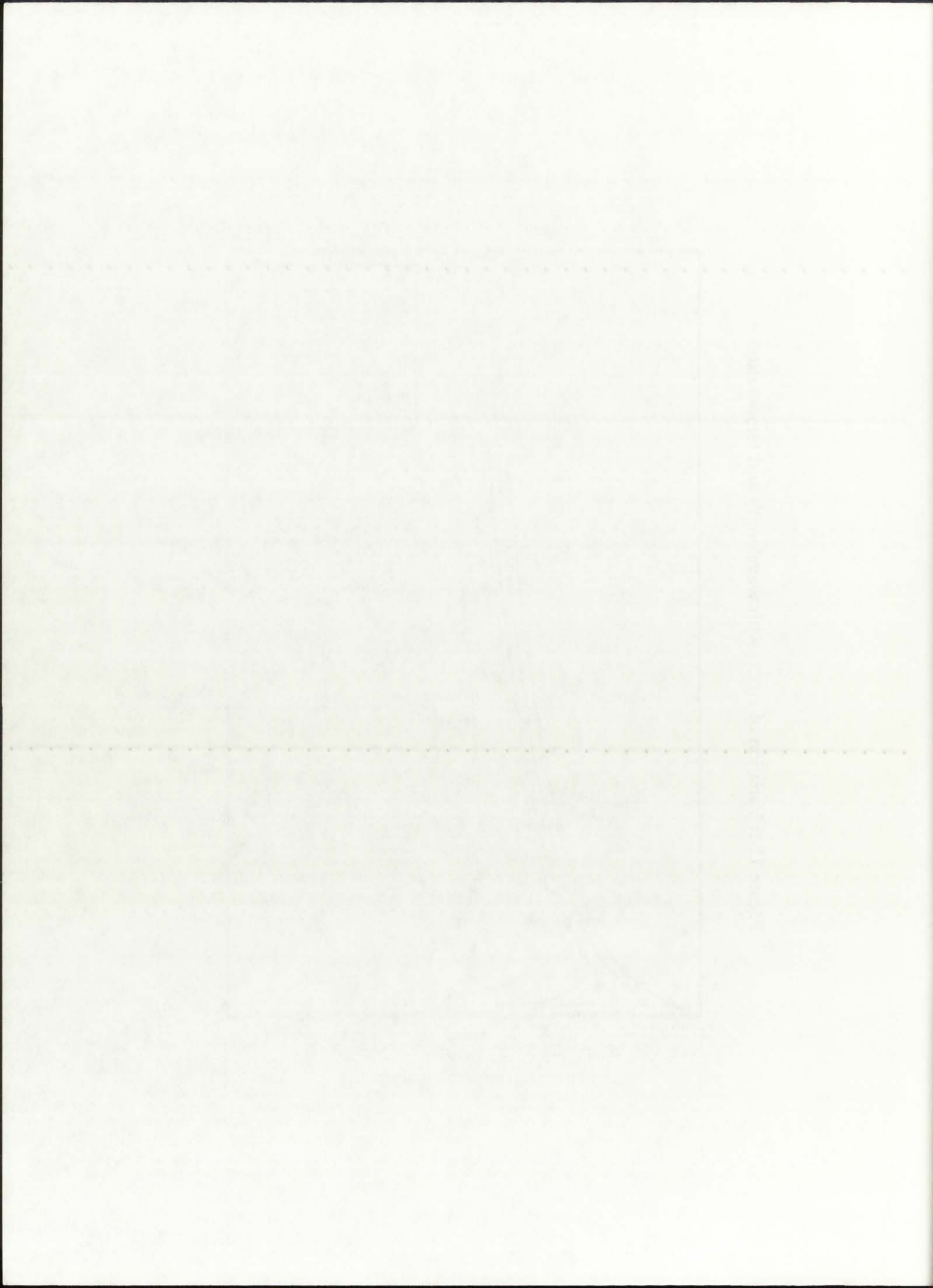


Figure 11.1: Variation of $e_{\lambda}(\lambda, T)$ with wavelength and temperature.





where the constant C_3 has a value of 2,897.8 [$\mu\text{m}\cdot\text{K}$]. As it is related to the maximum of the emissive power curve, Wien's Displacement Law is obtained by setting the wavelength-differential of Planck's Law (eqn. 11.1) equal to zero. An important observation stemming from Wien's Displacement Law is that the wavelength at which the maximum $e_\lambda(\lambda, T)$ is achieved shifts toward shorter wavelengths as the temperature increases. In practical terms, a higher fuel emission temperature causes $e_\lambda(\lambda, T)$ to shift toward shorter wavelengths; this feature will prove to be crucial in determining the thermal behavior of the silica wall. Program WVLENABS calculates the value of λ_{max} for the temperature range 5,000-300,000 K; the variation of λ_{max} with temperature is shown in Figure 11.2. It can be seen that for temperatures of 10,000 K or higher, the value of λ_{max} occurs in the far ultraviolet (UV) region (i.e., below 0.300 μm or 300 nm) where silica-based compounds begin to lose their transmissive properties [Harris *et al.*, 1970; Incropera and DeWitt, 1990; Heraeus-Amersil Co., 1993].

It can be seen from the above discussion that as the fuel emission temperature increases, a greater and greater fraction of the total emissive power lies below a set wavelength. For an extreme condition of infinite emission temperature, $T \approx \infty$, the emissive power would be concentrated at $\lambda = 0$ μm .

11.3.1. The Transmission Cutoff (TC)

The set wavelength mentioned in the preceding paragraph is, for the purposes of radiative transmission through media, referred to as the Transmission Cutoff (TC). By the nature of their atomic structure, "transmitting" media are characterized by a wavelength range in which they provide almost 100% transmission of the incident electromagnetic radiation. Household glass, for instance, has a transmission range that corresponds to the wavelength range of visible light: 0.400-0.700 μm (400-700 nm) [Incropera and DeWitt, 1990]. Outside of that transmission range, glass has negligible transmissivity and absorbs all incident radiation.

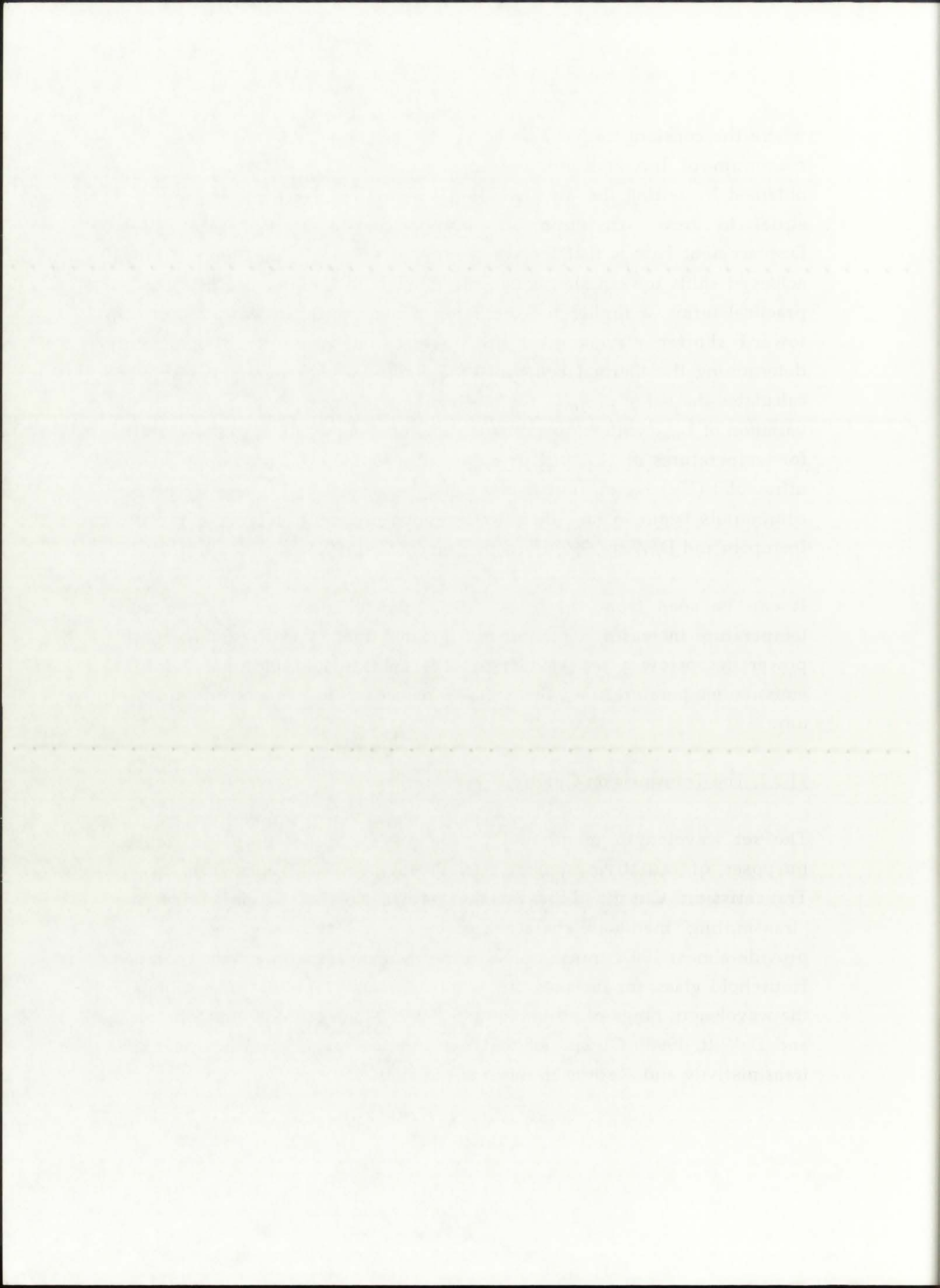


Figure 11.2: Variation of λ_{\max} with temperature.

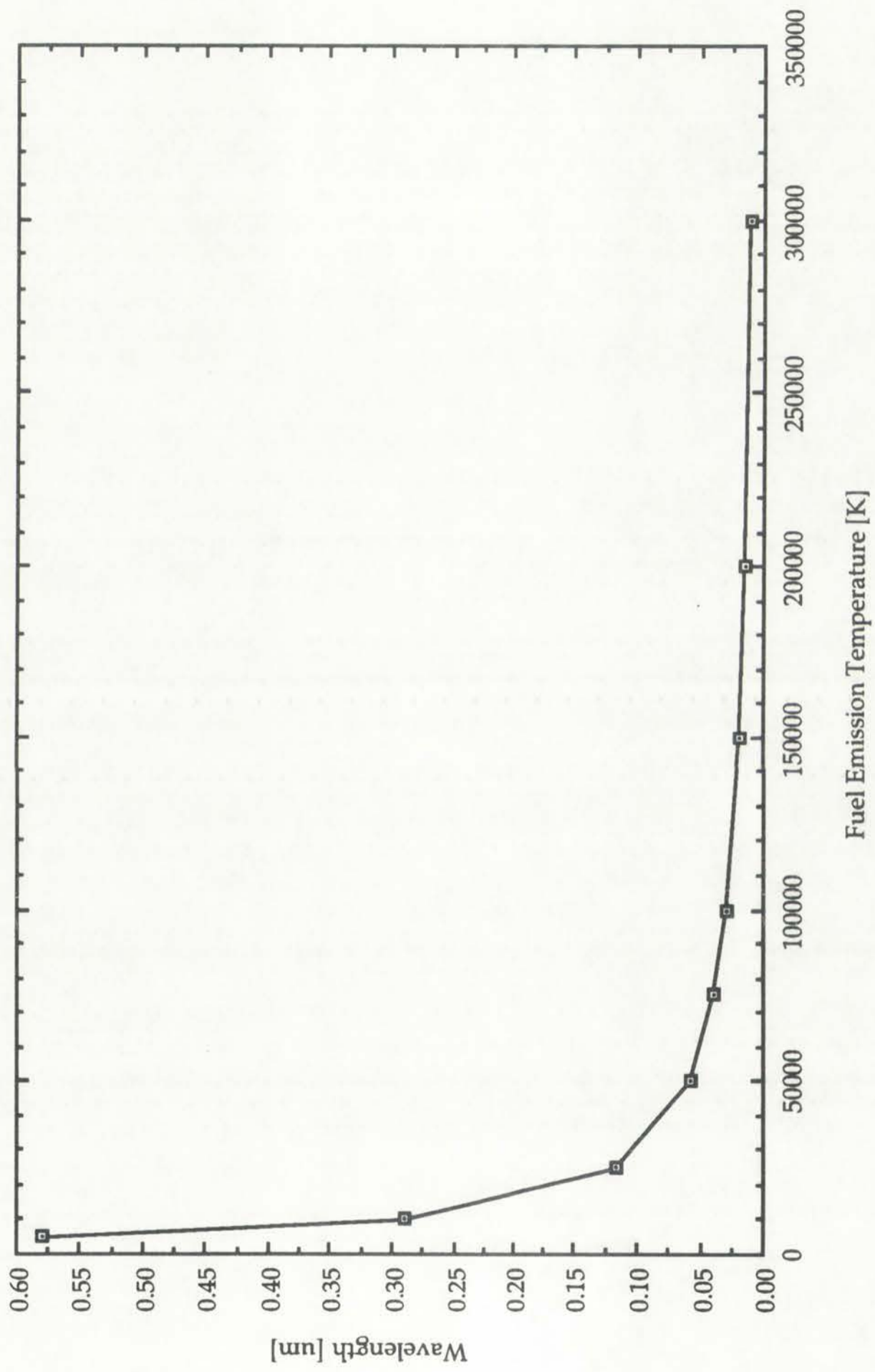




Figure 1: St. Anthony's years with no surgery

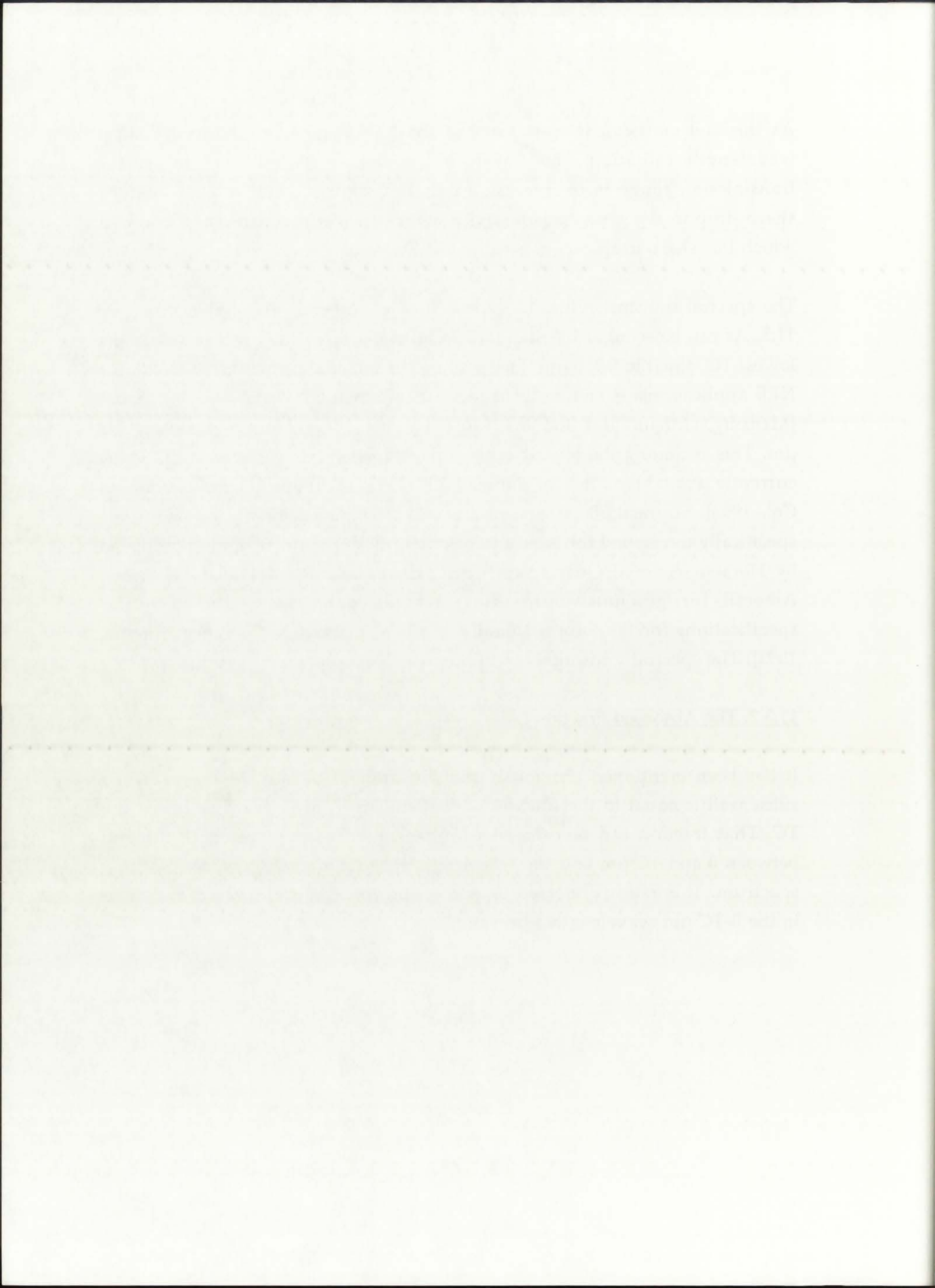
As the fuel emission temperatures of the NLB engine result in very short wavelength radiation, the lower, ultraviolet, end ($\lambda < 0.400 \mu\text{m}$) of the transmission range is of interest. At the UV end is where a characteristic sharp drop in the glass transmissivity occurs; the approximate wavelength at which this sharp drop occurs is called the TC value.

The spectral transmissivities of several glass compounds are shown in Figure 11.3. As can be seen, of the standard industrial glasses, low iron glass has the lowest TC, equal to $0.350 \mu\text{m}$. Fused silica, the material proposed by UARL for NLB applications, is shown to have a TC less than $0.200 \mu\text{m}$; a recent paper [Mensing, Latham, and Roman, 1990] identifies a TC for fused silica of $0.182 \mu\text{m}$. This is among the lowest achievable values of TC. The lowest TC value currently available is that of Suprasil 300 silica: $0.170 \mu\text{m}$ [Heraeus-Amersil Co., 1993]. Suprasil 300 is one of a family of high-purity silica compounds specifically developed for laser and electro-optic applications, and is produced by Heraeus-Amersil Quartzglass Corp.; the author is indebted to Heraeus-Amersil for graciously providing detailed data sheets and technical specifications for the Suprasil family of silica compounds [Heraeus-Amersil, 1993]. The spectral transmissivity of Suprasil 300 is shown in Figure 11.4.

11.3.2. The Absorbed Fraction (AF)

It has been mentioned previously that the amount of heat deposited in the silica wall is equal to the fraction of fuel emissive power that lies below the TC. That fraction can be calculated as the ratio of the wavelength integral between 0 and TC μm and the wavelength integral across the whole emitting spectrum. This ratio is referred to as the Absorbed Fraction (AF) of radiation in the 0-TC μm wavelength interval:

$$AF_{0\text{-TC } \mu\text{m}} = \frac{\int_0^{\text{TC}} e_{\lambda} d\lambda}{\int_0^{\infty} e_{\lambda} d\lambda} \quad (11.3)$$



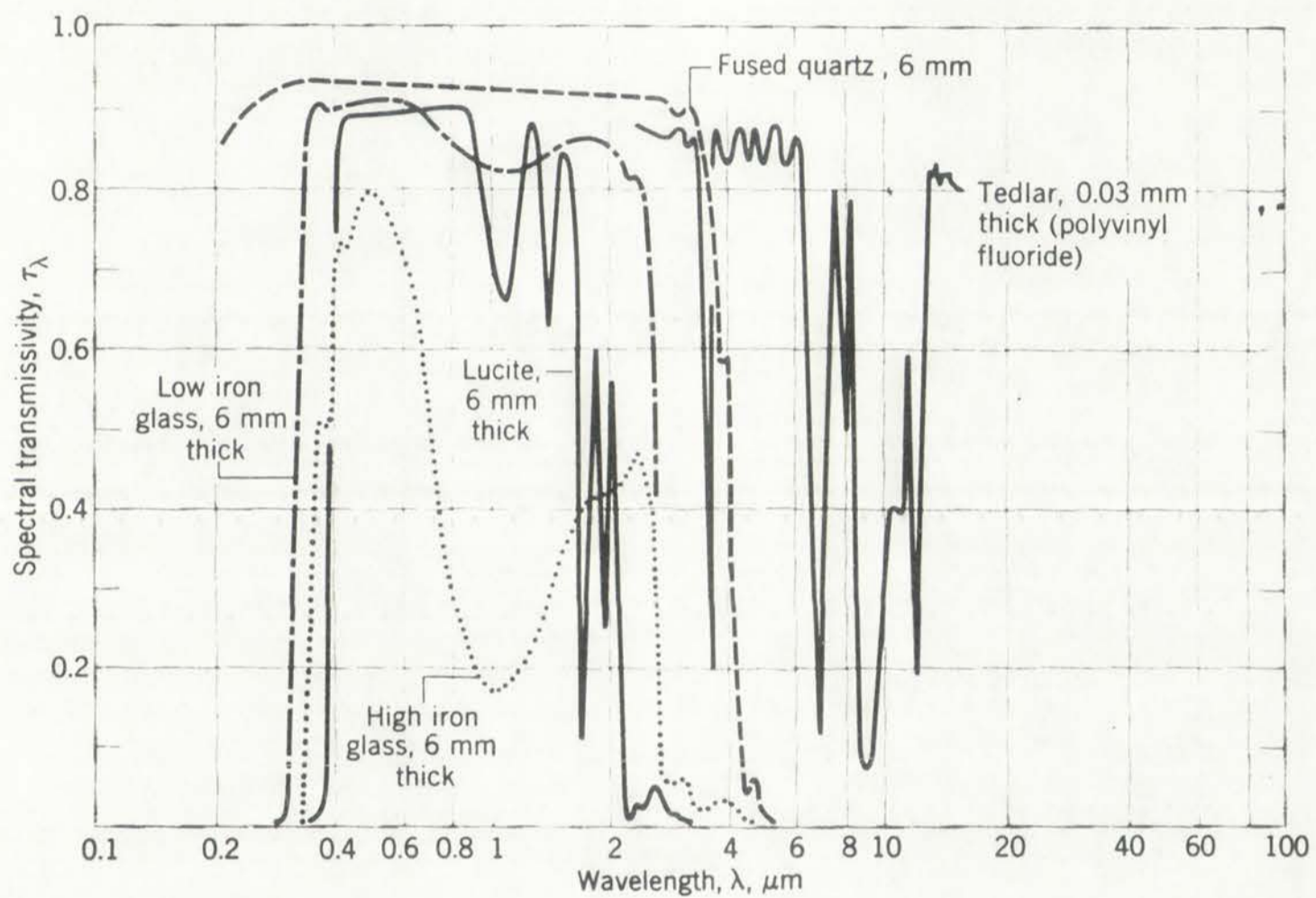


Figure 11.3: Spectral transmissivities of several glass compounds [Incropera and DeWitt, 1990].

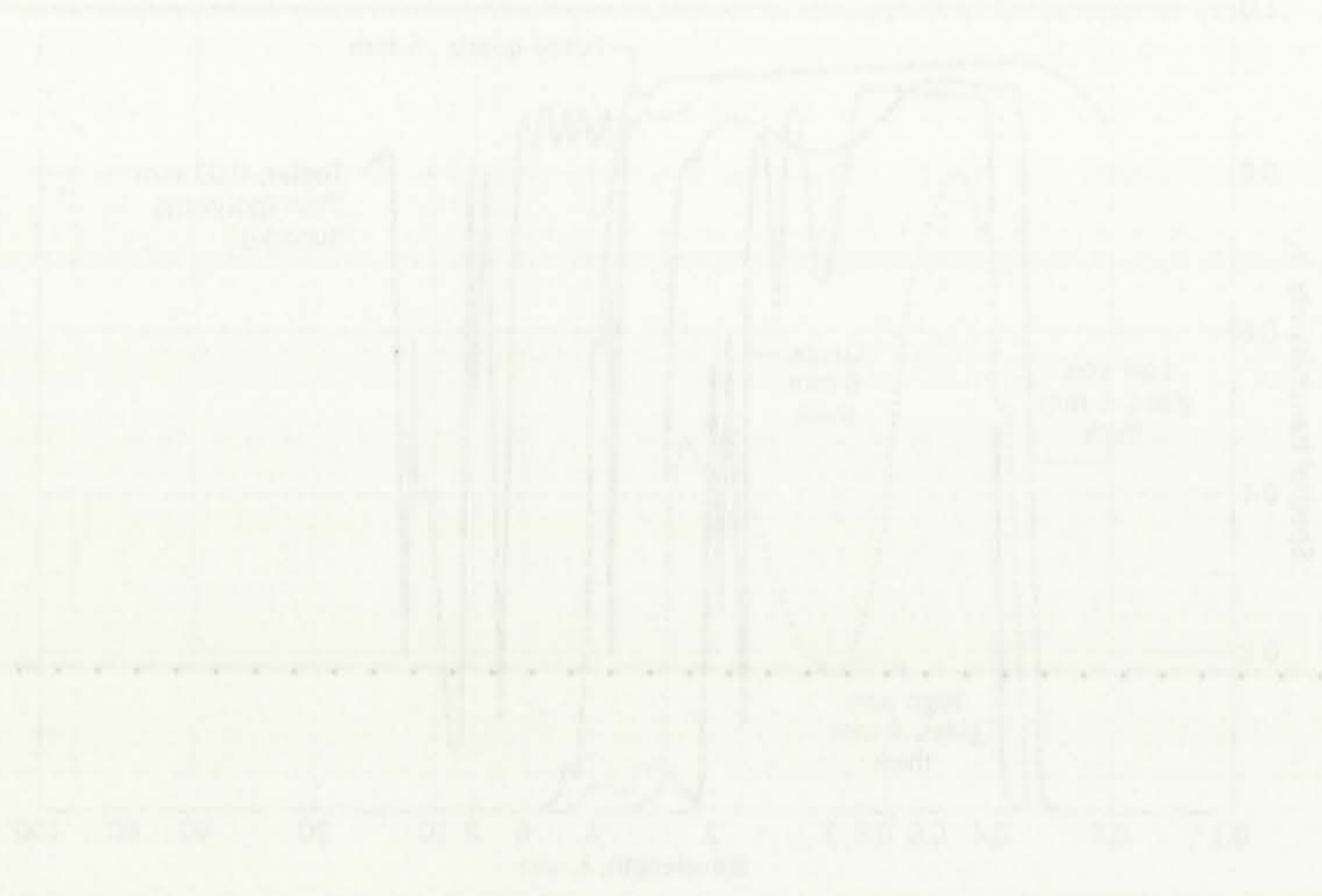


Figure 11.3: Spectral transmission of several glass compounds (Jacobsen and DeWitt, 1990)

SUPRASIL 300

Full Spectrum Low-OH Fused Silica

TYPICAL APPLICATIONS

UV to IR broad spectrum applications such as spectrophotometer and detector windows.

Ultra-low-absorption IR windows.

DESCRIPTION

Suprasil 300 offers the widest optical transmission with its range closely approaching the theoretical fundamental limits for fused silica.

It has an extremely low OH-content of less than 1 ppm, allowing useful optical transmission in the IR up to about 3.6 μm . Also, it is produced from high purity SiCl_4 by chemical reaction in the vapor phase to yield a synthetic quartzglass with less than 10 ppb of total metallic impurities. This allows the useful transmission to extend into the deep UV down to about 180 nm.

In addition, Suprasil 300 is practically free from bubbles and is totally free from inclusions. The material may show striae. Therefore optical homogeneity is not specified.

BUBBLES AND INCLUSIONS

Better than Bubble Class 0; i.e., the average bubble cross section within the volume is $\leq 0.03 \text{ mm}^2/100 \text{ cm}^3$. Maximum bubble size 0.2 mm diameter for pieces less than 6 kg. Zero inclusions.

OH - CONTENT

$< 1 \text{ ppm}$.

SIZE RANGE

Available up to 690 mm diameter and 50 kg.

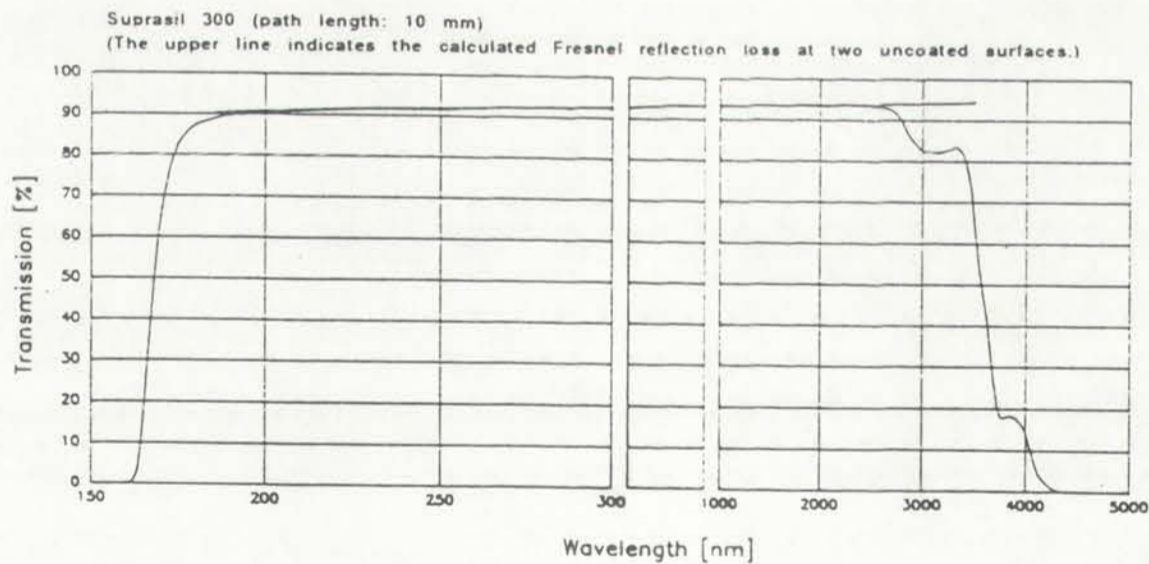
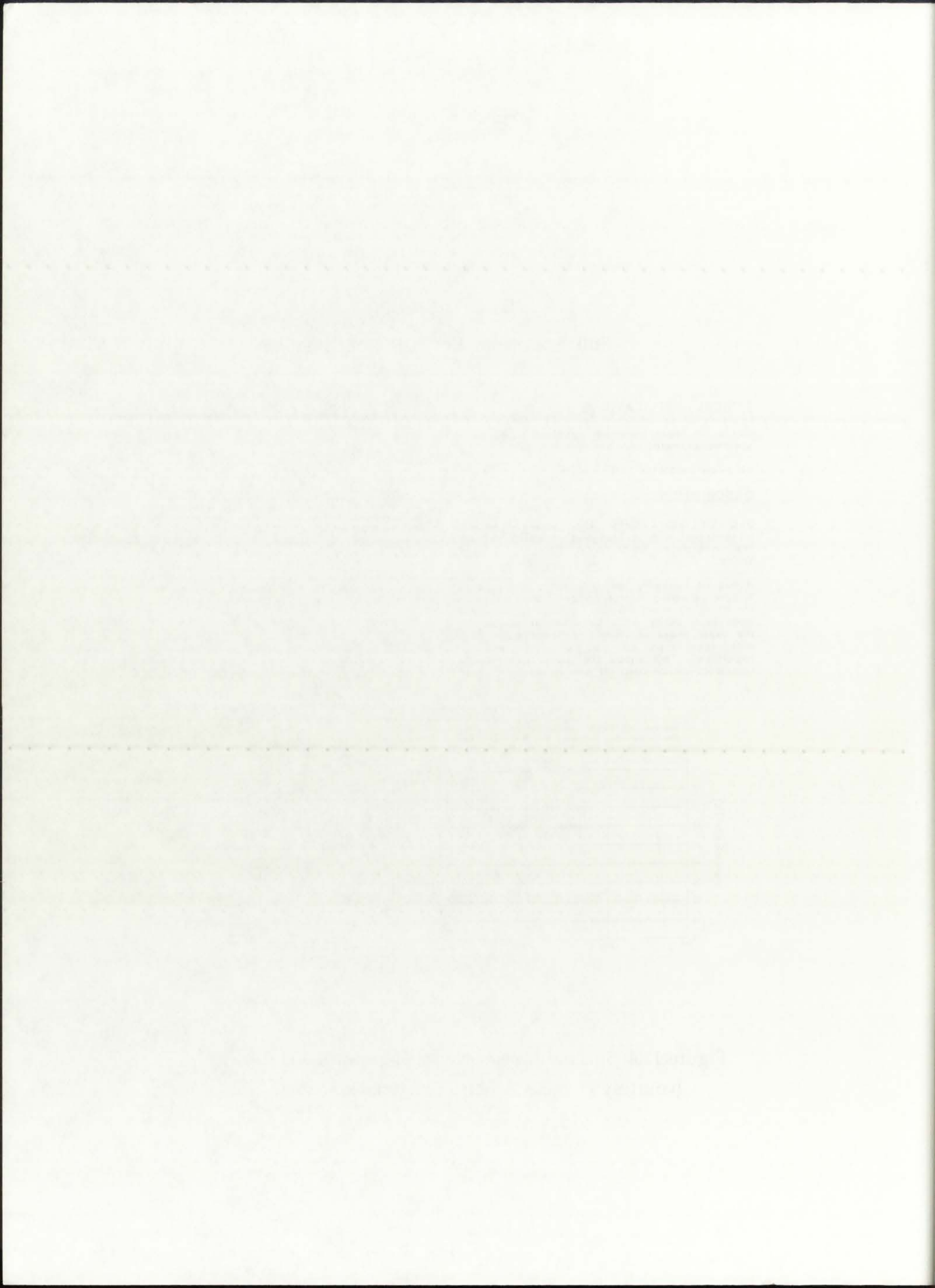


Figure 11.4: Spectral transmissivity of Suprasil 300 silica
[courtesy Heraeus-Amersil Quartzglass Corp.]



For a given fuel emission temperature and silica wall TC, then, the AF can be calculated by ratioing two integrals of the spectral, hemispherical emissive power.

The AF was calculated for fifteen temperatures between 5,000 K and 300,000 K, and for three silica compounds: industrial glass (TC=0.350 μm), fused silica (TC=0.182 μm), and Suprasil 300 (TC=0.170 μm). The numerical integration and calculation of AF was performed with MATHEMATICA for the Macintosh [Wolfram, 1991]. The calculated AF values as a function of fuel emission temperature and wall TC are presented in Figure 11.5. The values are also summarized in Table 11.1 for each of the seven temperatures. The MATHEMATICA calculation printouts are enclosed in Appendix H.

From the data in Figure 11.5 and Table 11.1, it can be seen that industrial glass is a very poor transmission candidate for fuel emission temperatures associated with the NLB engine. Even fused silica and Suprasil 300 are characterized by AF values of around 90% for fuel emission temperatures $\geq 50,000$ K. For temperatures $\geq 100,000$ K, all three silica compounds have $\text{AF} \approx 100\%$. These results indicate that a very large fraction of the heat flux emitted by the fuel gets absorbed in the silica wall, due to the limited transmission range of the silica. To minimize thermal absorption in the silica wall, then, it is necessary to limit the fuel emission temperature.

11.3.3. Silica Wall Temperature

With a calculated absorbed fraction (AF) of the radiative heat flux, it is possible to determine the silica wall mean temperature that would result from a respective AF. Neglecting geometry effects, since the edge-of-fuel and the wall are only approximately 3 cm apart, the following approximate relation between the steady-state emitted and absorbed flux, the AF, and the wall and fuel temperature can be derived:

$$\frac{Q_{\text{abs}}}{Q_{\text{emit}}} \approx \text{AF} \approx \left(\frac{T_w}{T_{\text{eof}}}\right)^4, \quad (11.4)$$

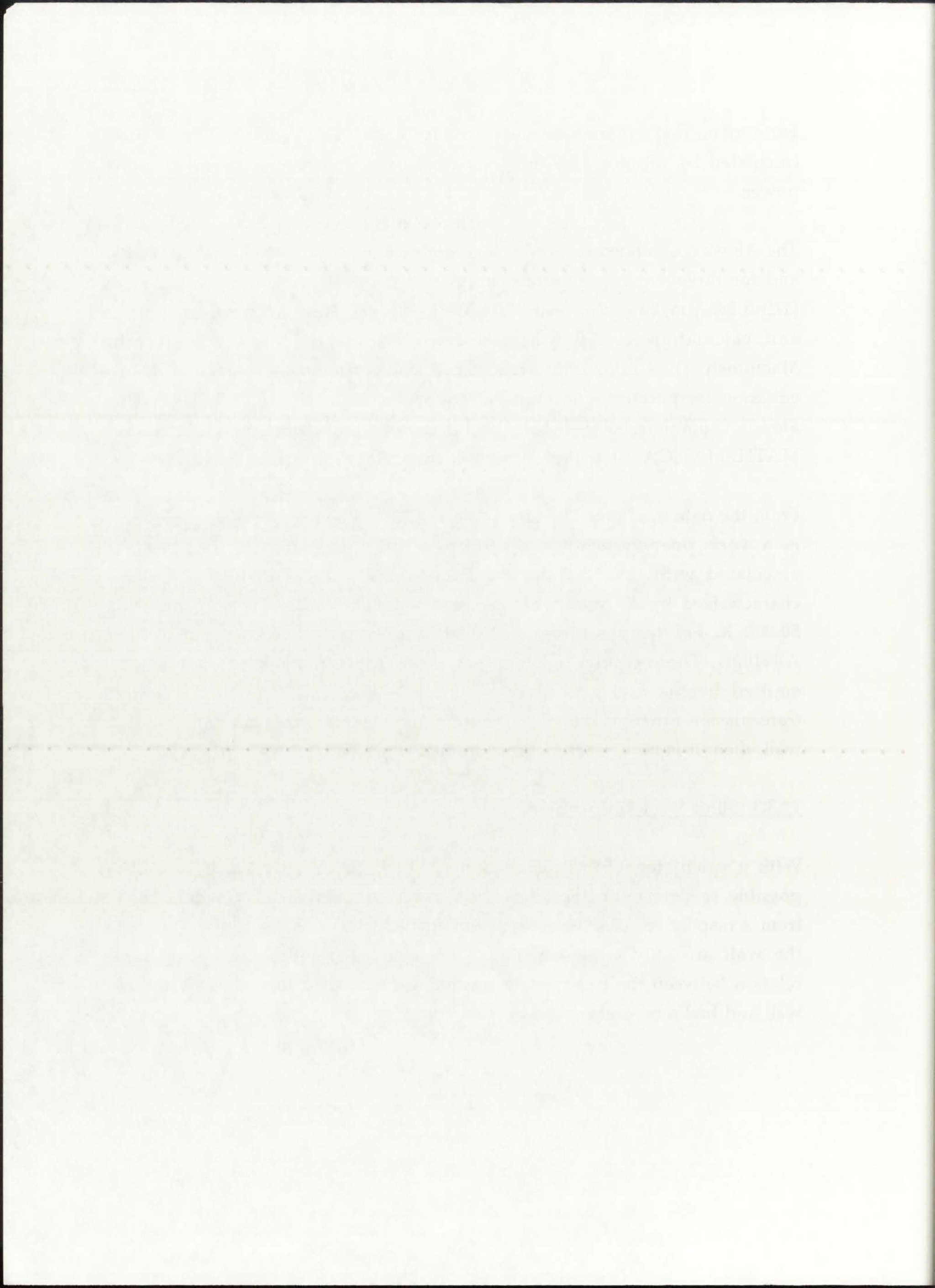
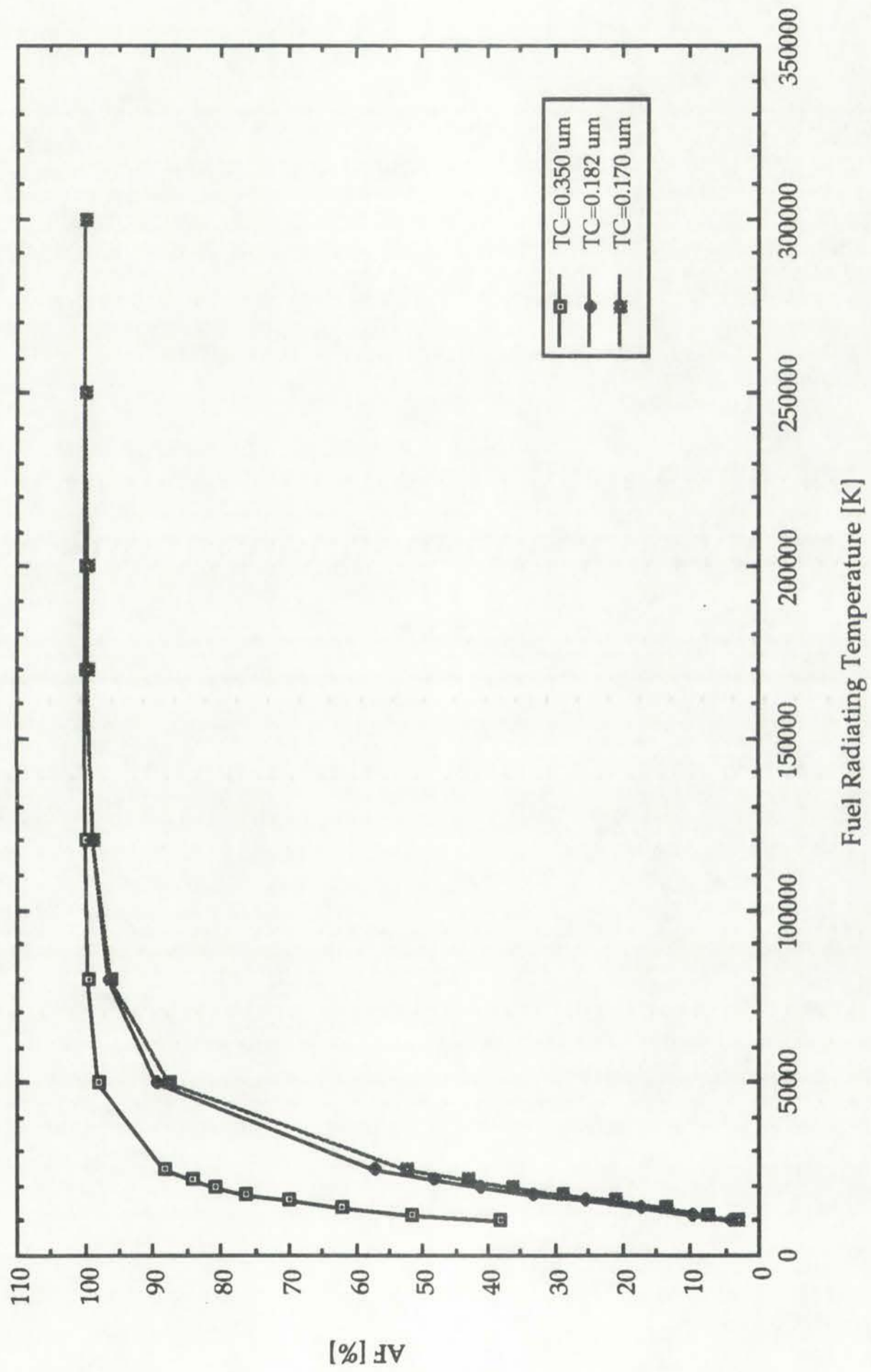


Figure 11.5: Calculated AF values for three silica compounds.



LIBRARY OF THE UNIVERSITY OF TORONTO

TABLE 11.1
 Calculated AF values for three silica compounds.

Fuel Emission Temperature [K]	Industrial Glass (TC=0.350 μm)	Fused Silica (TC=0.182 μm)	Suprasil 300 (TC=0.170 μm)
10,000	38.3 %	4.2 %	2.9 %
12,000	51.6 %	9.8 %	7.3 %
14,000	62.1 %	17.2 %	13.6 %
16,000	70.1 %	25.3 %	21.0 %
18,000	76.2 %	33.5 %	28.7 %
20,000	80.8 %	41.2 %	36.2 %
22,000	84.4 %	48.2 %	43.2 %
25,000	88.3 %	57.2 %	52.4 %
50,000	97.9 %	89.3 %	87.5 %
80,000	99.4 %	96.6 %	96.0 %
120,000	99.8 %	98.8 %	98.6 %
170,000	99.9 %	99.6 %	99.5 %
200,000	99.96 %	99.73 %	99.67 %
250,000	99.98 %	99.86 %	99.83 %
300,000	99.99%	99.91 %	99.90 %

TABLE III

Calculated ΔF values for three other compounds.

Temperature (K)	Calculated ΔF (kcal/mole)	Calculated ΔF (kcal/mole)	Calculated ΔF (kcal/mole)
1000	20.5	20.5	20.5
1200	21.2	21.2	21.2
1400	21.8	21.8	21.8
1600	22.4	22.4	22.4
1800	23.0	23.0	23.0
2000	23.6	23.6	23.6
2200	24.2	24.2	24.2
2400	24.8	24.8	24.8
2600	25.4	25.4	25.4
2800	26.0	26.0	26.0
3000	26.6	26.6	26.6
3200	27.2	27.2	27.2
3400	27.8	27.8	27.8
3600	28.4	28.4	28.4
3800	29.0	29.0	29.0
4000	29.6	29.6	29.6
4200	30.2	30.2	30.2
4400	30.8	30.8	30.8
4600	31.4	31.4	31.4
4800	32.0	32.0	32.0
5000	32.6	32.6	32.6
5200	33.2	33.2	33.2
5400	33.8	33.8	33.8
5600	34.4	34.4	34.4
5800	35.0	35.0	35.0
6000	35.6	35.6	35.6
6200	36.2	36.2	36.2
6400	36.8	36.8	36.8
6600	37.4	37.4	37.4
6800	38.0	38.0	38.0
7000	38.6	38.6	38.6
7200	39.2	39.2	39.2
7400	39.8	39.8	39.8
7600	40.4	40.4	40.4
7800	41.0	41.0	41.0
8000	41.6	41.6	41.6
8200	42.2	42.2	42.2
8400	42.8	42.8	42.8
8600	43.4	43.4	43.4
8800	44.0	44.0	44.0
9000	44.6	44.6	44.6
9200	45.2	45.2	45.2
9400	45.8	45.8	45.8
9600	46.4	46.4	46.4
9800	47.0	47.0	47.0
10000	47.6	47.6	47.6

where T_w and T_{eof} correspond to the mean wall temperature [K] and the edge-of-fuel temperature [K], respectively. The mean silica wall temperature can thus be expressed in terms of the AF and the edge-of-fuel temperature as:

$$T_w = \sqrt[4]{AF} T_{eof} \quad (11.5)$$

A short computer program, called SIWALL, was developed to determine the wall temperature as a function of edge-of-fuel temperature and AF. The calculated wall temperatures are shown in Figure 11.6 and presented in tabular format in Table 11.2. A listing of the SIWALL program is given in Appendix I.

It can be seen from Figure 11.6 and Table 11.2 that, for $T_{eof} \geq 20,000$ K, the silica wall temperature T_w is very close to T_{eof} . This is due to the very large AF associated with such temperatures. The trend, of course, is most pronounced for industrial glass, but is also significant for fused silica and Suprasil 300.

11.3.4. Internal Cooling Mass Flow Rate

An added feature incorporated into the SIWALL program is the ability to estimate the amount of internal cooling that would be needed to maintain the silica wall below its melting temperature. Equating the absorbed heat flux to the amount of energy removed by a flowing coolant:

$$Q_{abs} = \dot{m}_c C_{p,c} (T_w - T_{melt}) \quad (11.6)$$

it becomes possible to estimate the amount of coolant flow needed to reduce the wall temperature from the calculated value of T_w to just below the melting temperature T_{melt} , which for fused silica (and Suprasil 300) is 1,883 K [CRC, 1990].

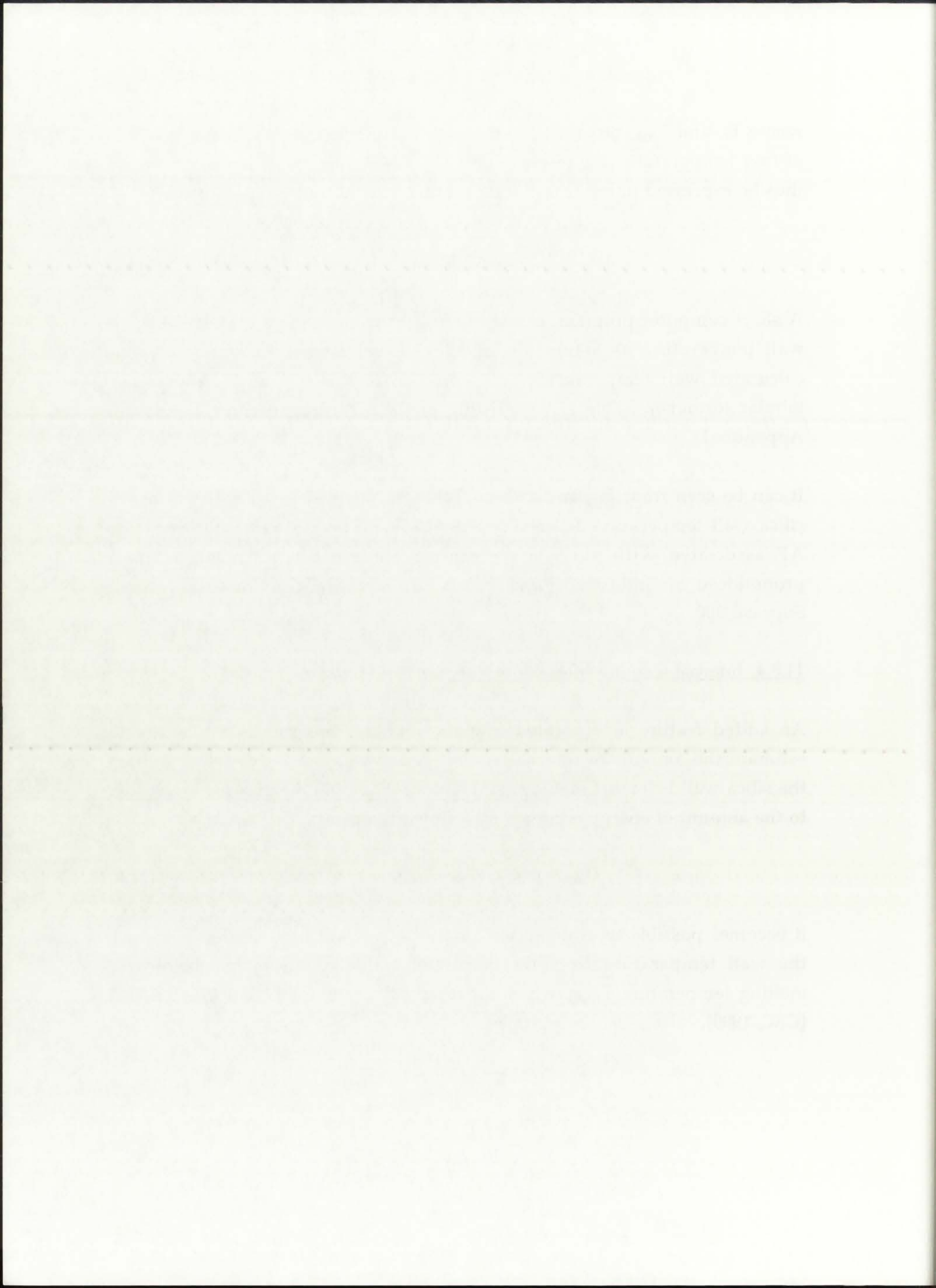
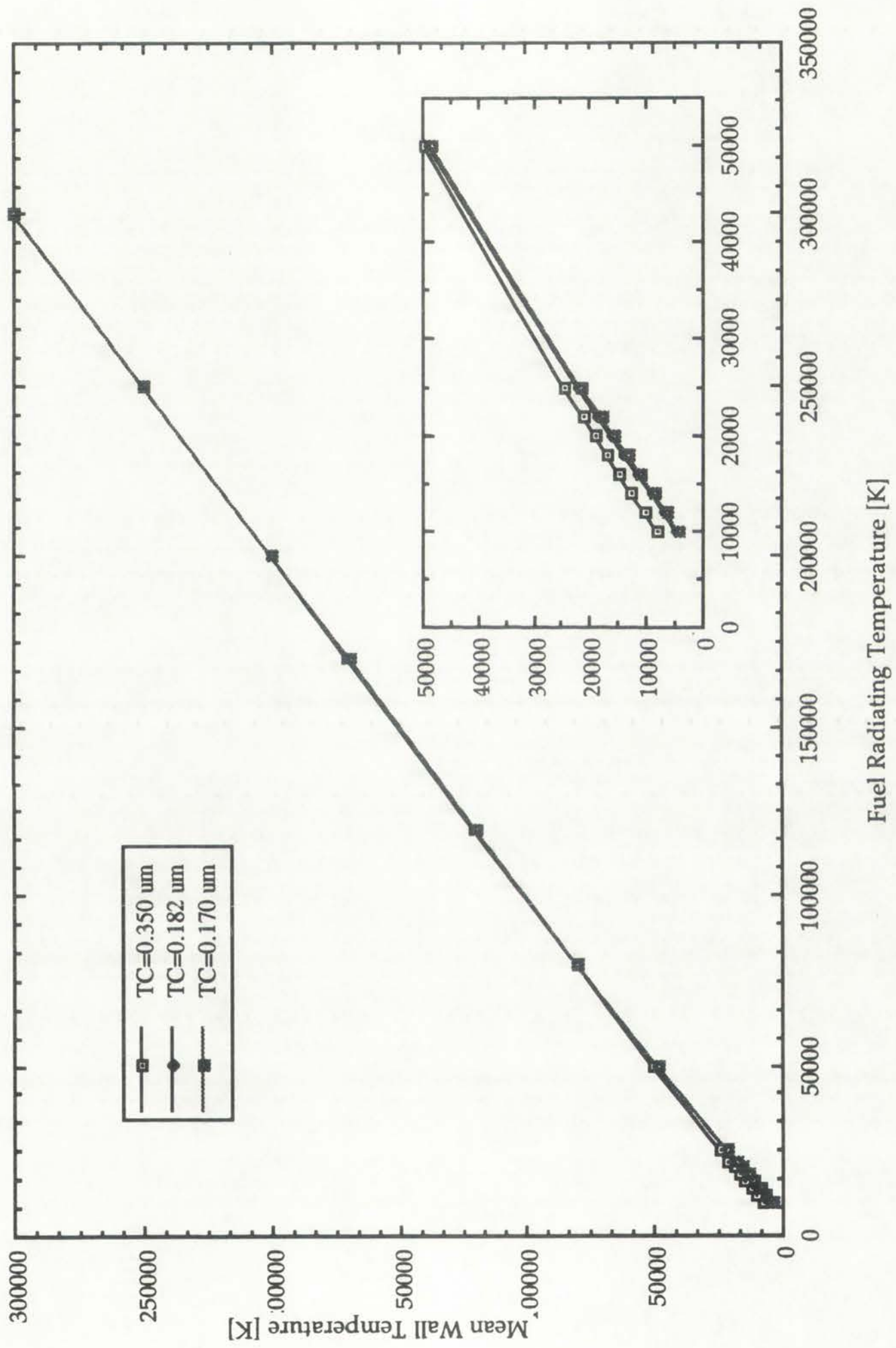
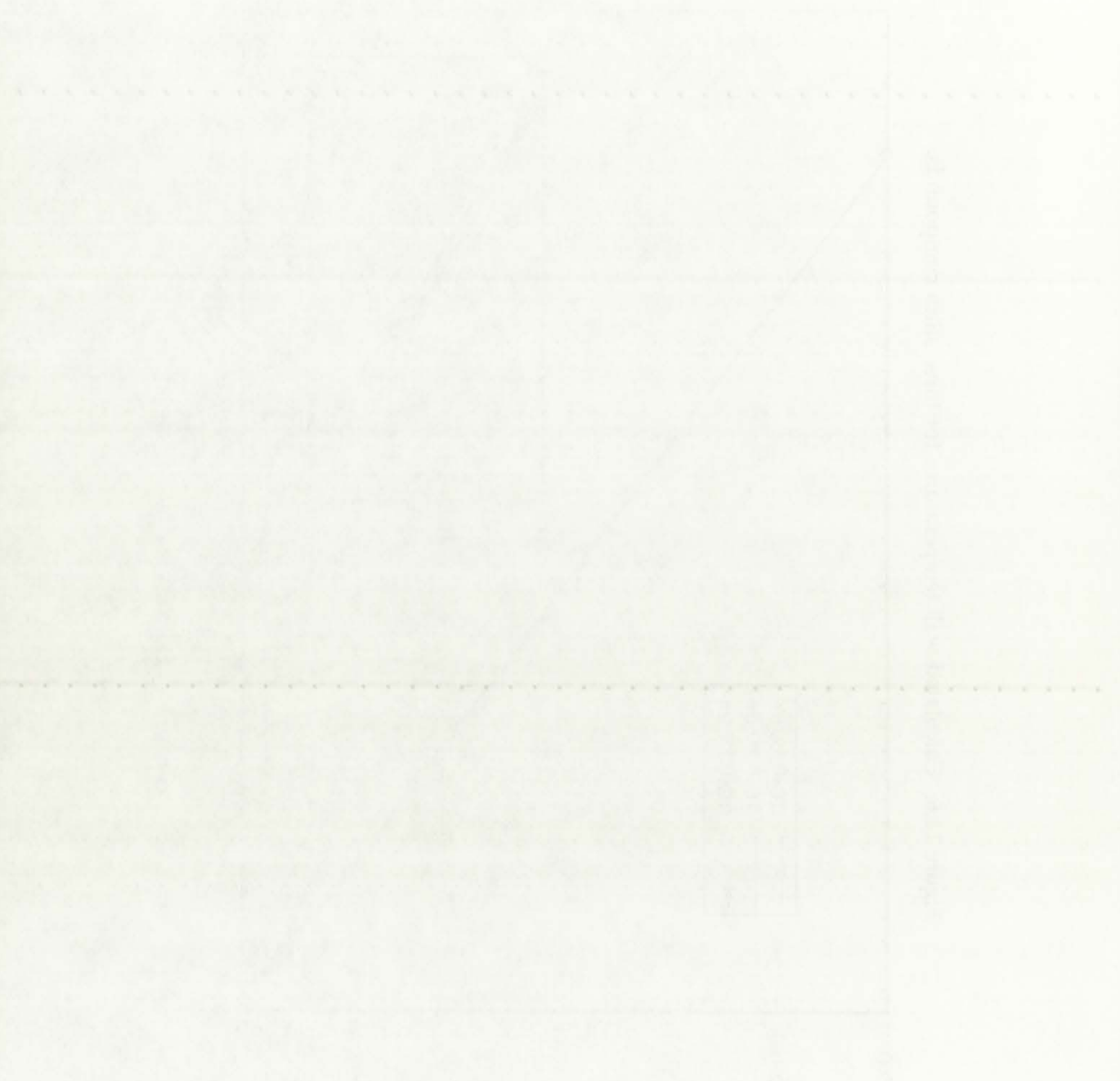


Figure 11.6: Calculated wall temperatures for three silica compounds.



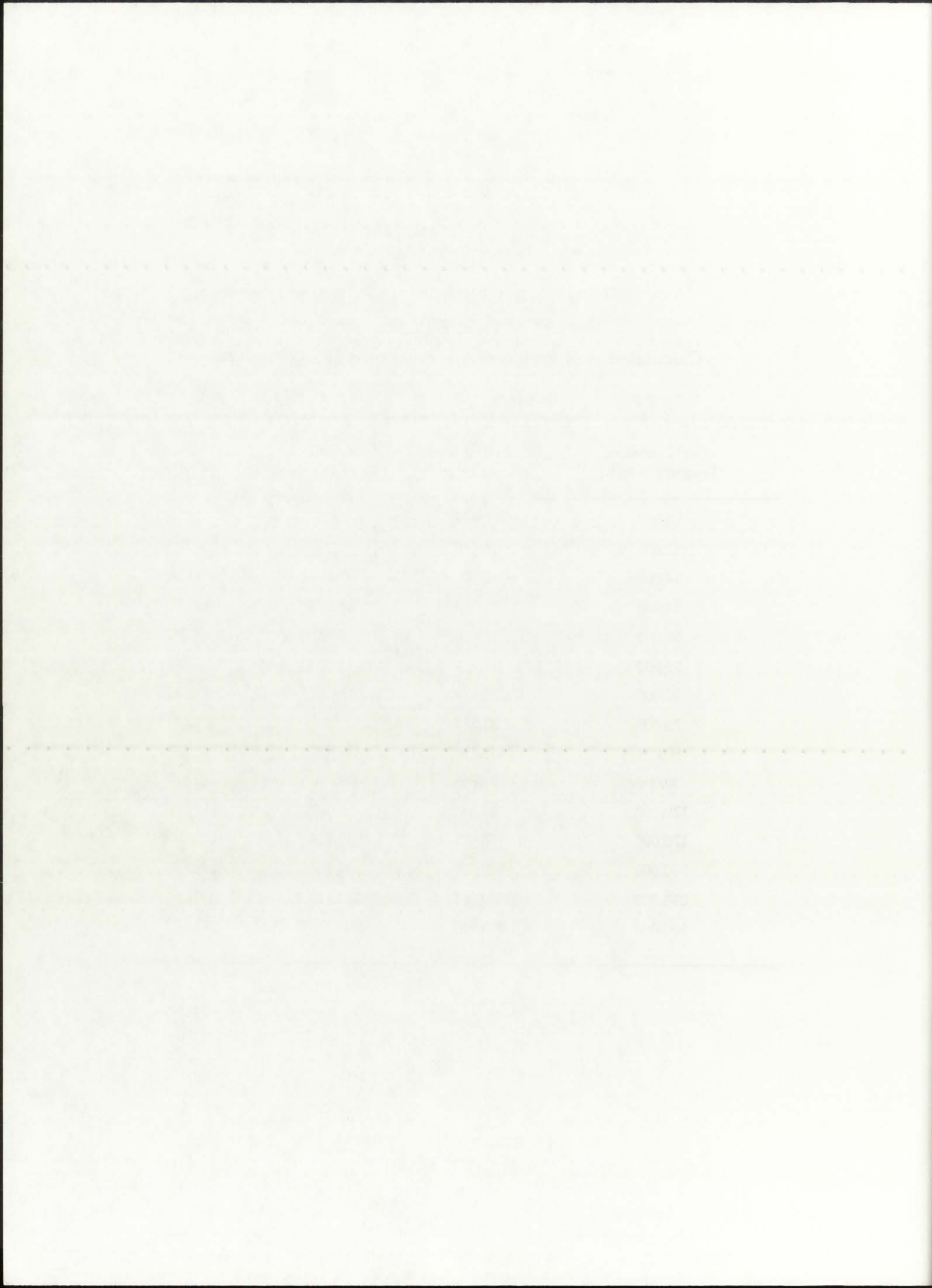
Blank header area with faint horizontal lines.



Blank footer area with faint horizontal lines.

TABLE 11.2
 Calculated wall temperatures for three silica compounds.

Fuel Emission Temperature [K]	Industrial Glass (TC=0.350 μm)	Fused Silica (TC=0.182 μm)	Suprasil 300 (TC=0.170 μm)
10,000	7,866	4,520	4,110
12,000	10,170	6,713	6,239
14,000	12,427	9,012	8,504
16,000	14,640	11,350	10,829
18,000	16,816	13,692	13,172
20,000	18,962	16,020	15,510
22,000	21,084	18,327	17,832
25,000	21,274	21,740	24,231
50,000	49,739	48,602	48,352
80,000	79,885	79,319	79,187
120,000	119,945	119,657	119,587
170,000	169,971	169,816	169,777
200,000	199,979	199,863	199,834
250,000	249,986	249,910	249,891
300,000	299,989	299,935	299,921



The internal wall coolant was taken to be hydrogen, coming from the secondary hydrogen (H₂(II)) tank as shown previously in Figure 2.4. The coolant mass flow rate can be expressed from eqn. (11.6) as:

$$\dot{m}(\text{H}_2) = \frac{Q_{\text{abs}}}{C_p(\text{H}_2)(T_w - T_{\text{melt}})} \quad (11.7)$$

It is important to note here that Q_{abs} denotes heat flux [W/m²]. Therefore, the coolant mass flow $\dot{m}'(\text{H}_2)$ is in units of mass per unit time, per unit wall surface area undergoing heat flux absorption [kg/s-m² of wall].

The coolant mass flow rates required for maintaining the wall below melting temperature are presented in Figure 11.7 and in Table 11.3. It can be seen that the required flow rates are very large, even per unit wall surface area. Using dimensions given previously in Figures 3.1 and 3.2, the mean radial location of the wall is 0.247 m and the total length is 1.827 m; with a 40% annular segment taken for the wall, the total surface area of the wall exposed to the heat flux is 1.134 m². It is thus necessary to multiply the data in Table 11.3 by a factor of 1.134 to obtain the total coolant mass flow in [kg/s] for the silica wall.

Analysis of the data presented in Table 11.3 indicates that coolant mass flow rates of 10-100 kg/s are required for 15,000 ≤ T_{eof} ≤ 25,000 K, 100-1,000 kg/s for 25,000 ≤ T_{eof} ≤ 60,000 K, and greater than 1,000 kg/s for T_{eof} ≥ 60,000 K. To ascertain the feasibility of such mass flow rates, it must be remembered that the total thickness of the wall as proposed by UARL was only 4.9 mm, and that the shear stress of silica is 0.66 atm. Thus, to maintain the structural integrity of the wall (i.e., prevent wall shatter), the pressure head due to the internal coolant must be balanced by the applied external (buffer gas and propellant) pressure:

$$P_{\text{cool}} \leq P + \tau_{\text{wall}} \quad (11.8)$$

where P_{cool} and P denote the coolant and operating pressure, respectively, and τ_{wall} corresponds to the wall shear stress.

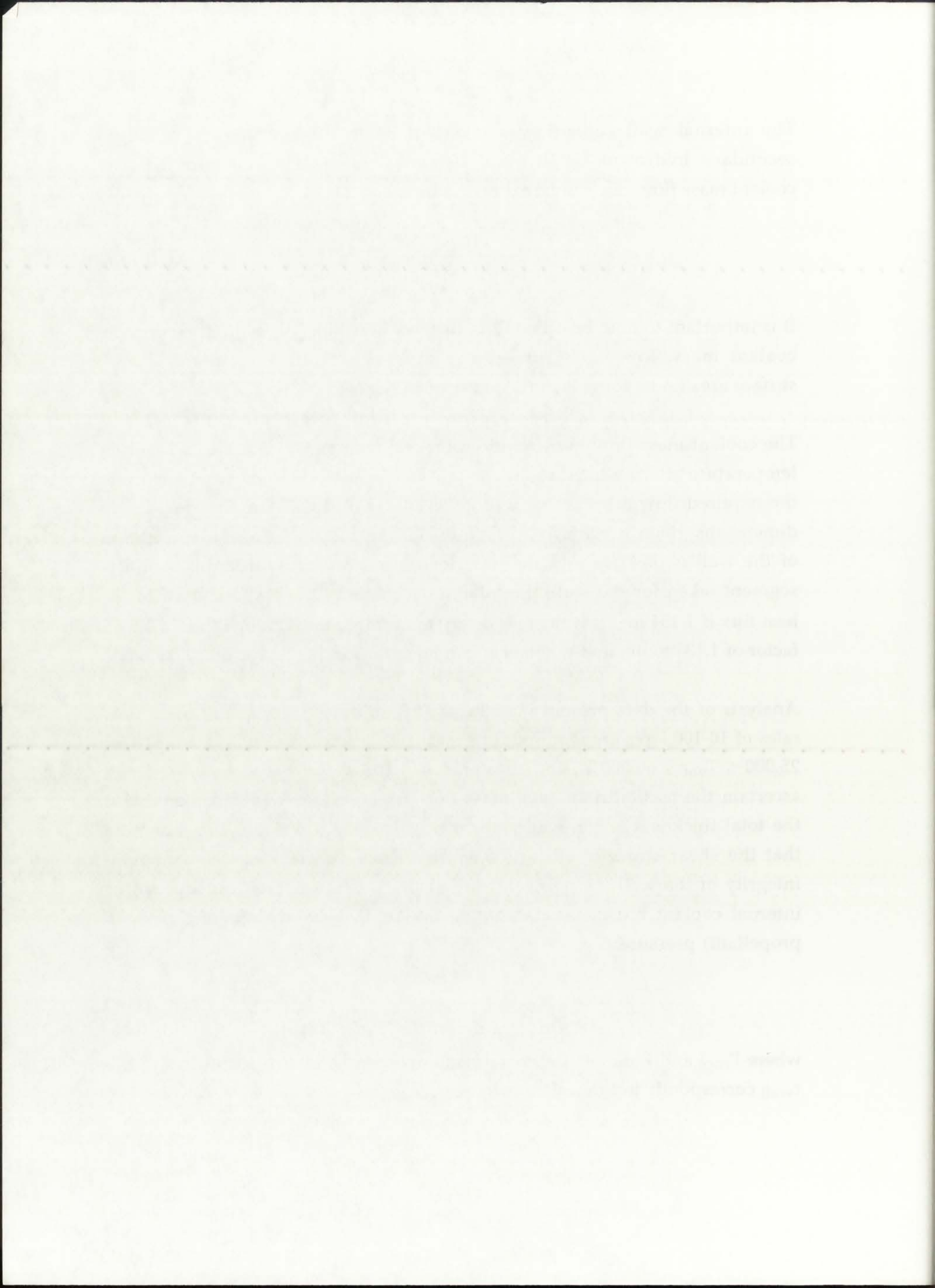
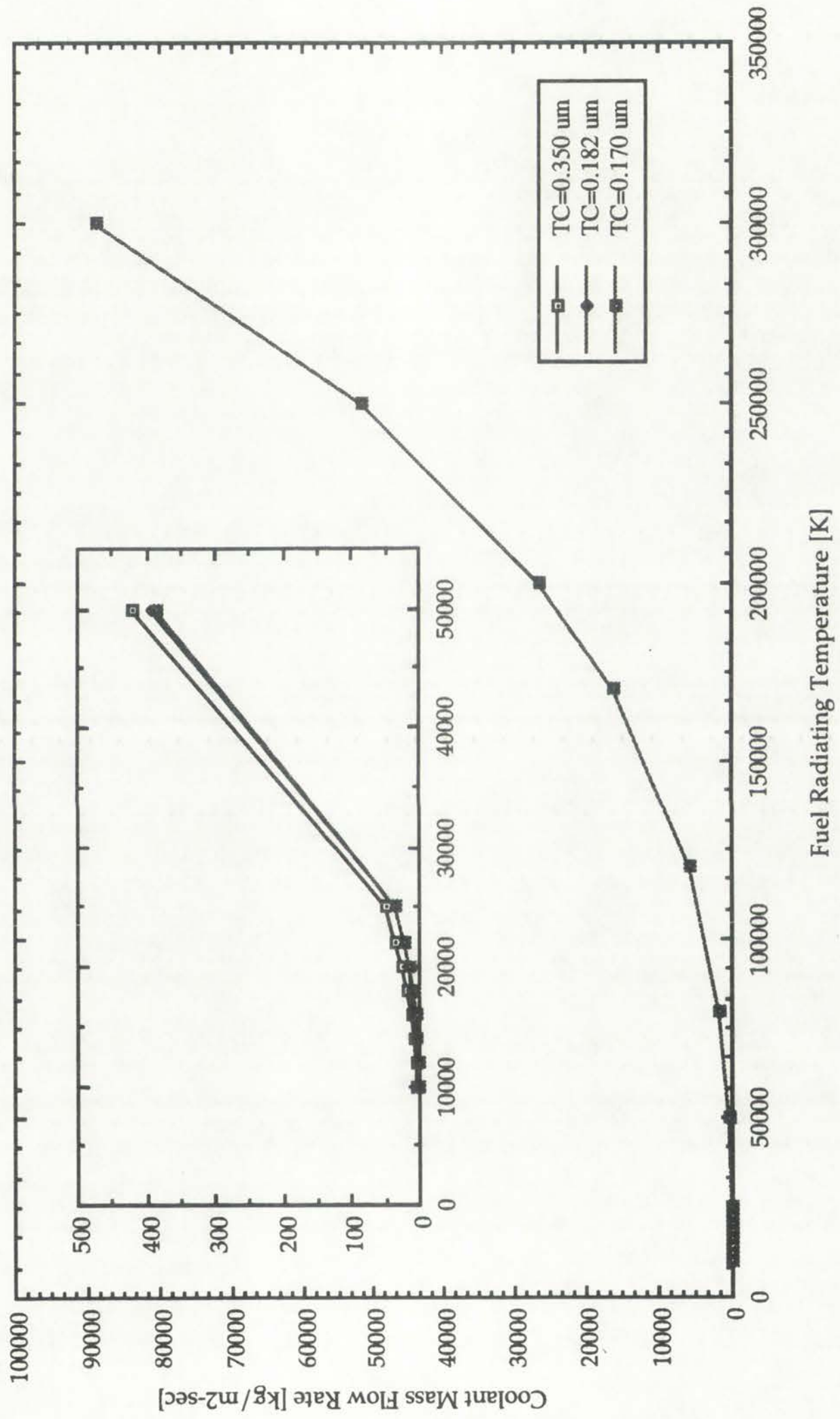


Figure 11.7: Required coolant mass flow rates for the three silica compounds.



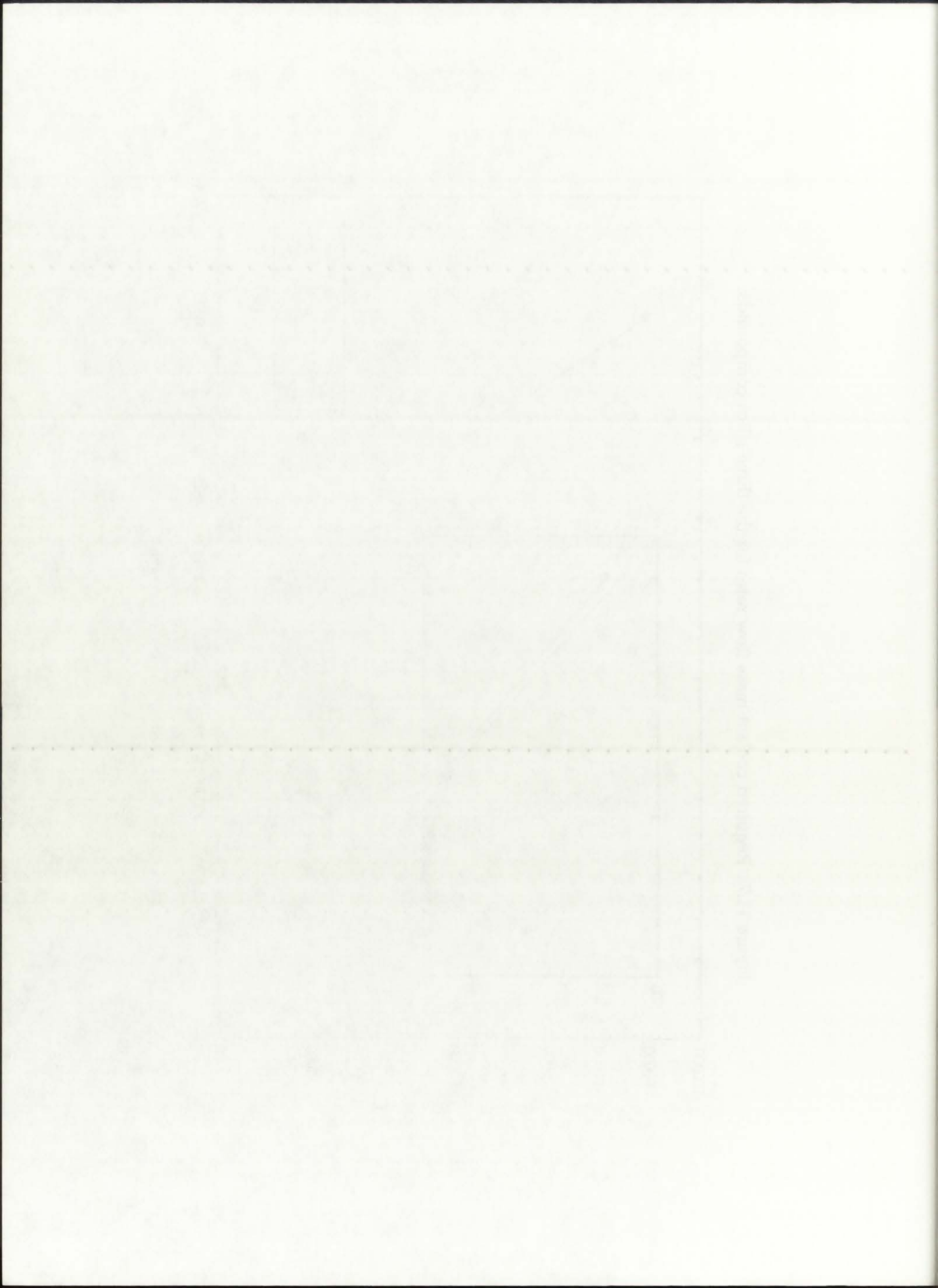
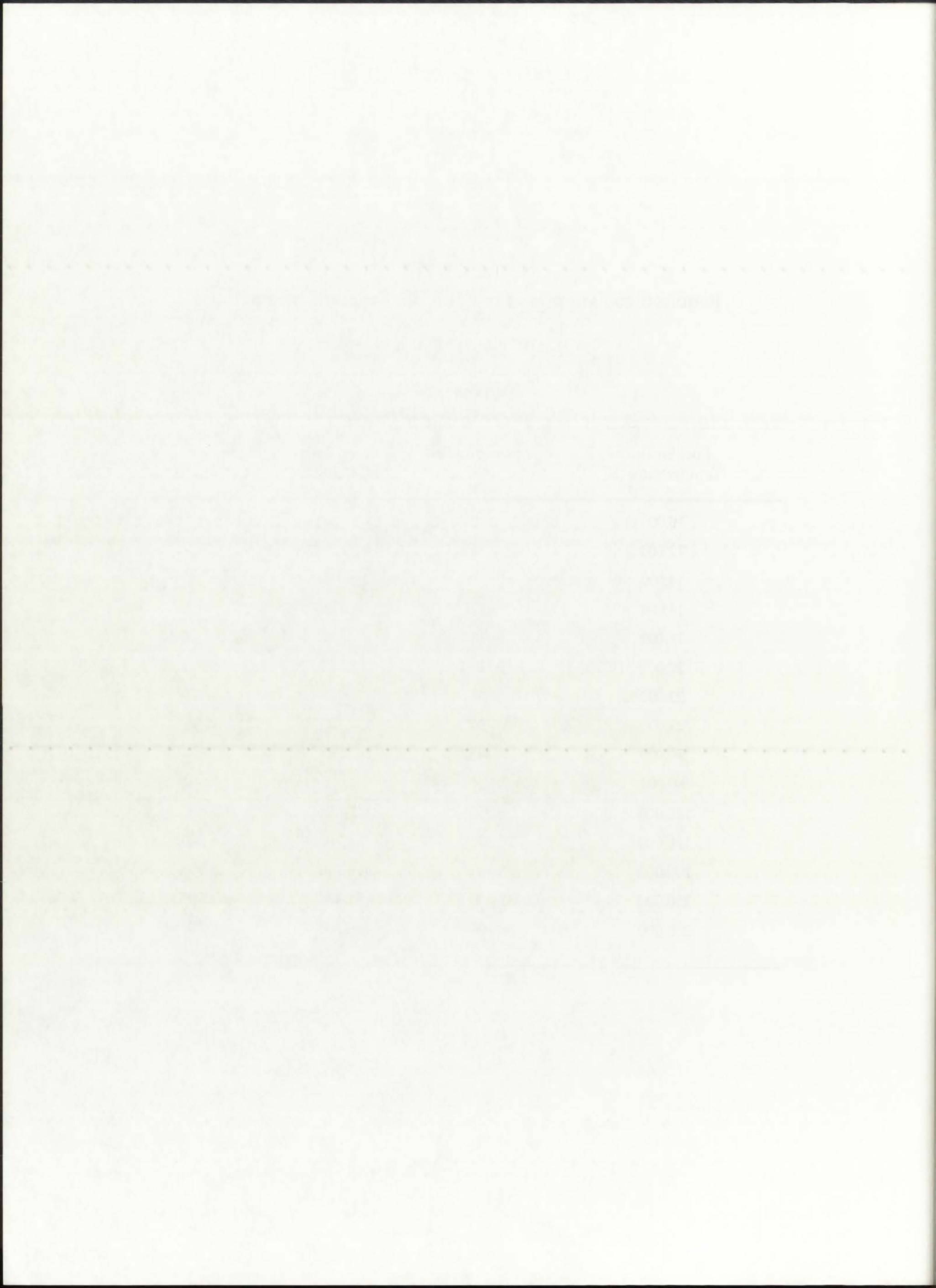


TABLE 11.3
 Required coolant mass flow rates for three silica compounds.

[kg/s-m² of wall]

Fuel Emission Temperature [K]	Industrial Glass (TC=0.350 μm)	Fused Silica (TC=0.182 μm)	Suprasil 300 (TC=0.170 μm)
10,000	2.0	0.5	0.4
12,000	4.2	1.4	1.1
14,000	7.4	3.0	2.6
16,000	12	5.7	5.0
18,000	18	9.7	8.7
20,000	25	15	14
22,000	34	22	21
25,000	50	37	35
50,000	418	390	384
80,000	1,710	1,670	1,660
120,000	5,730	5,680	5,670
170,000	16,200	16,200	16,200
200,000	26,400	26,300	26,300
250,000	51,400	51,400	51,400
300,000	88,700	88,700	88,700



The expression for the pressure head of the internal coolant can be derived from the general Bernoulli equation, according to [Gieck and Gieck, 1990]:

$$P_{\text{cool}} = \frac{1}{2} \frac{\rho v^2}{C_v^2}, \quad (11.9)$$

where C_v corresponds to the coolant velocity coefficient. This same expression can be modified by introducing the equation of continuity, and rearranging to solve for the coolant mass flow rate:

$$\dot{m}_{\text{max}} = \sqrt{2P_{\text{cool}}\rho A_{\text{cs}}^2 C_v^2}, \quad (11.10)$$

where A_{cs} denotes the cross-sectional area to coolant flow [m^2].

For the 50 kWth, $p=250$ atm configuration, applying eqn. (11.10) yields a maximum feasible \dot{m}' equal to 19.5 kg/s. Using Table 11.3 as a reference, this indicates a maximum feasible T_{eof} equal to 17,000 K for the case of industrial glass, and a maximum feasible T_{eof} of 20,000 K for the case of Suprasil 300.




Eqn. (11.10) indicates that there is a direct correlation between the operating pressure (as, for all practical purposes, $P_{\text{cool}} \approx P$) and the maximum feasible internal coolant mass flow rate. Thus, for an increase in operating pressure, greater internal coolant flow rates could theoretically be sustained within the silica wall, as the pressure head would be balanced out by the external pressure. Table 11.4 indicates the relationship between increasing operating pressure and increasing maximum sustainable T_{eof} . As can be seen, for T_{eof} greater than 25,000 K, operating pressures far in excess of 1,000 atm would be required to provide the internal coolant mass flow rates necessary to remove the energy deposited by thermal radiation. Thus, it can be concluded that $T_{\text{eof}} \approx 25,000$ K is the upper limit on overall NLB performance, based on the internal cooling requirements of the silica wall. At this point in time, the author is not familiar with any feasible means of cooling that could successfully provide the required heat removal for $T_{\text{eof}} \approx 25,000$ K.

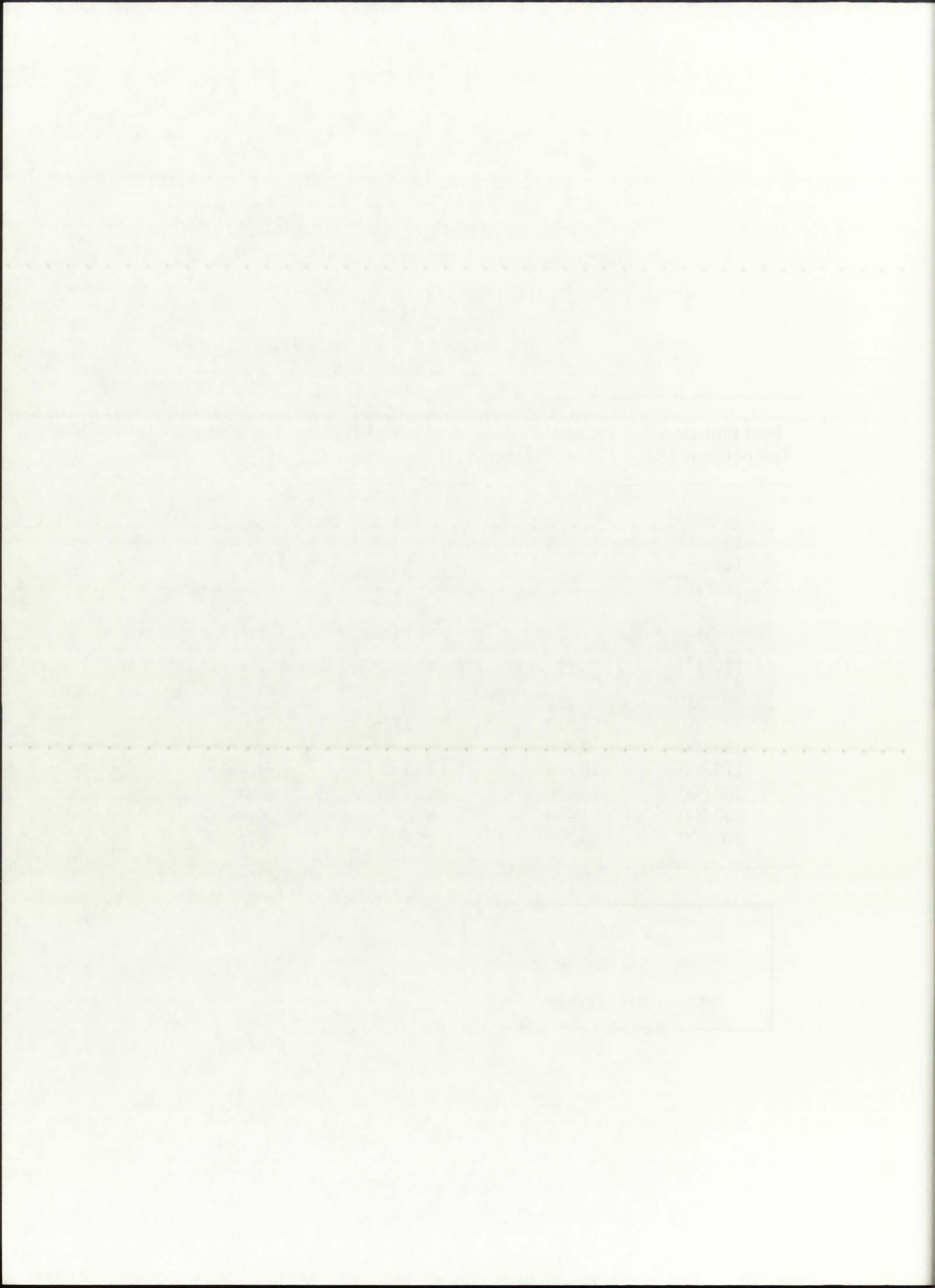
The experiment was conducted in the laboratory of the Department of Psychology, University of California, Los Angeles, California. The subjects were 12 male college students who were paid for their participation. The experiment was designed to investigate the effects of a specific treatment on the dependent variable. The independent variable was the treatment condition, which was either the control group or the experimental group. The dependent variable was the score on the test, which was measured at two different time points. The results of the experiment showed that the experimental group performed significantly better than the control group on the test. This finding suggests that the treatment had a positive effect on the dependent variable. The implications of these findings are discussed in the conclusion of the paper.

TABLE 11.4
Maximum feasible coolant mass flow rates.

required internal cooling mass flow rate \dot{m}
[kg/s-m² of wall]

Fuel Emission Temperature [K]	Industrial Glass (TC=0.350 mm)	Fused Siilica (TC=0.182 mm)	Suprasil 300 (TC=0.170 mm)
10,000	2.0	0.5	0.4
12,000	4.2	1.4	1.1
14,000	7.4	3.0	2.6
16,000	12	5.7	5.0
18,000	18	9.7	8.7
20,000	25	15	14
22,000	34	22	21
25,000	50	37	35
50,000	418	390	384
80,000	1,710	1,670	1,660
120,000	5,730	5,680	5,670
170,000	16,200	16,200	16,200
200,000	26,400	26,300	26,300
250,000	51,400	51,400	51,400
300,000	88,700	88,700	88,700

	P = 250 atm
	P = 500 atm
	P = 1,000 atm



11.4. Conclusions

The spectral analysis of the radiative heat transfer into the silica wall provides detailed insight into the silica wall temperature as a function of fuel temperature. Using spectral transmissivity data, it can be concluded that $T_w \approx T_{eof}$ for $T_{eof} \geq 25,000$ K, even for the best transmitting silica compound available today. Therefore, raising the fuel temperature above 25,000 K results in an almost 1:1 increase in the mean wall temperature. The large amounts of heat absorbed in the wall must be removed if the wall is to remain solid; a possible mode of heat removal is circulation of the secondary hydrogen through the wall. The coolant mass flow rates required to maintain the wall temperature at $\leq 1,883$ K, however, become prohibitively large for $T_{eof} \geq 25,000$ K. Thus, from the standpoint of the integrity of the silica wall, operation of the NLB engine at $T_{eof} \geq 25,000$ K would be, for all practical purposes, impossible. In light of the magnitude of the required internal coolant mass flow rates, a range of $20,000 \text{ K} \leq T_{eof} \leq 25,000 \text{ K}$ would most probably comprise the upper feasibility limit. This temperature range corresponds roughly to the range associated with the 50 kWth configuration as discussed in detail in Chapter 10.

The results pertaining to the silica wall temperature presented in this Chapter are in line with the more general $T(r)$ results presented in Chapter 10. Both indicate that the upper feasibility limit with respect to the unit-cell NLB rocket engine is associated closely with the conditions found in the 50 kWth configuration. The contribution of the work presented in this Chapter is linked with the determination of the upper feasibility limit as imposed by the silica wall; as has been shown, $T_{eof} \approx 25,000$ K can be considered an upper feasibility limit. Based on this conclusion, it can be stated that the original UARL unit-cell NLB engine, with a proposed fuel temperature of 8,333 K, would almost certainly be feasible with respect to thermal and structural integrity of the silica wall. For such a (relatively) low fuel temperature, the internal coolant mass flow rate requirements would be minimal (<1.0 kg/s).

The first part of the report is devoted to a general
 description of the country and its resources. It
 is followed by a detailed account of the
 various industries and occupations of the
 people. The third part of the report
 contains a list of the principal towns and
 villages, with a description of their
 buildings and other interesting features.
 The fourth part of the report is a
 list of the principal rivers and streams,
 with a description of their course and
 the nature of the soil through which they
 flow. The fifth part of the report is a
 list of the principal mountains and hills,
 with a description of their height and
 the nature of the soil on which they
 stand. The sixth part of the report is a
 list of the principal lakes and ponds,
 with a description of their size and
 the nature of the soil on which they
 stand. The seventh part of the report is a
 list of the principal forests, with a
 description of the various kinds of trees
 which grow in them. The eighth part of
 the report is a list of the principal
 minerals, with a description of their
 nature and the way in which they are
 obtained. The ninth part of the report is
 a list of the principal animals, with a
 description of their habits and the way
 in which they are used. The tenth part
 of the report is a list of the principal
 plants, with a description of their
 nature and the way in which they are
 used. The eleventh part of the report is
 a list of the principal birds, with a
 description of their habits and the way
 in which they are used. The twelfth part
 of the report is a list of the principal
 insects, with a description of their
 nature and the way in which they are
 used. The thirteenth part of the report
 is a list of the principal reptiles and
 amphibians, with a description of their
 nature and the way in which they are
 used. The fourteenth part of the report
 is a list of the principal fishes, with a
 description of their habits and the way
 in which they are used. The fifteenth part
 of the report is a list of the principal
 shells, with a description of their
 nature and the way in which they are
 used. The sixteenth part of the report
 is a list of the principal fossils, with a
 description of their nature and the way
 in which they are used. The seventeenth
 part of the report is a list of the
 principal minerals, with a description of
 their nature and the way in which they
 are used. The eighteenth part of the
 report is a list of the principal
 animals, with a description of their
 habits and the way in which they are
 used. The nineteenth part of the report
 is a list of the principal plants, with a
 description of their nature and the way
 in which they are used. The twentieth
 part of the report is a list of the
 principal birds, with a description of
 their habits and the way in which they
 are used. The twenty-first part of the
 report is a list of the principal insects,
 with a description of their nature and
 the way in which they are used. The
 twenty-second part of the report is a
 list of the principal reptiles and
 amphibians, with a description of their
 nature and the way in which they are
 used. The twenty-third part of the
 report is a list of the principal fishes,
 with a description of their habits and
 the way in which they are used. The
 twenty-fourth part of the report is a
 list of the principal shells, with a
 description of their nature and the way
 in which they are used. The twenty-fifth
 part of the report is a list of the
 principal fossils, with a description of
 their nature and the way in which they
 are used.

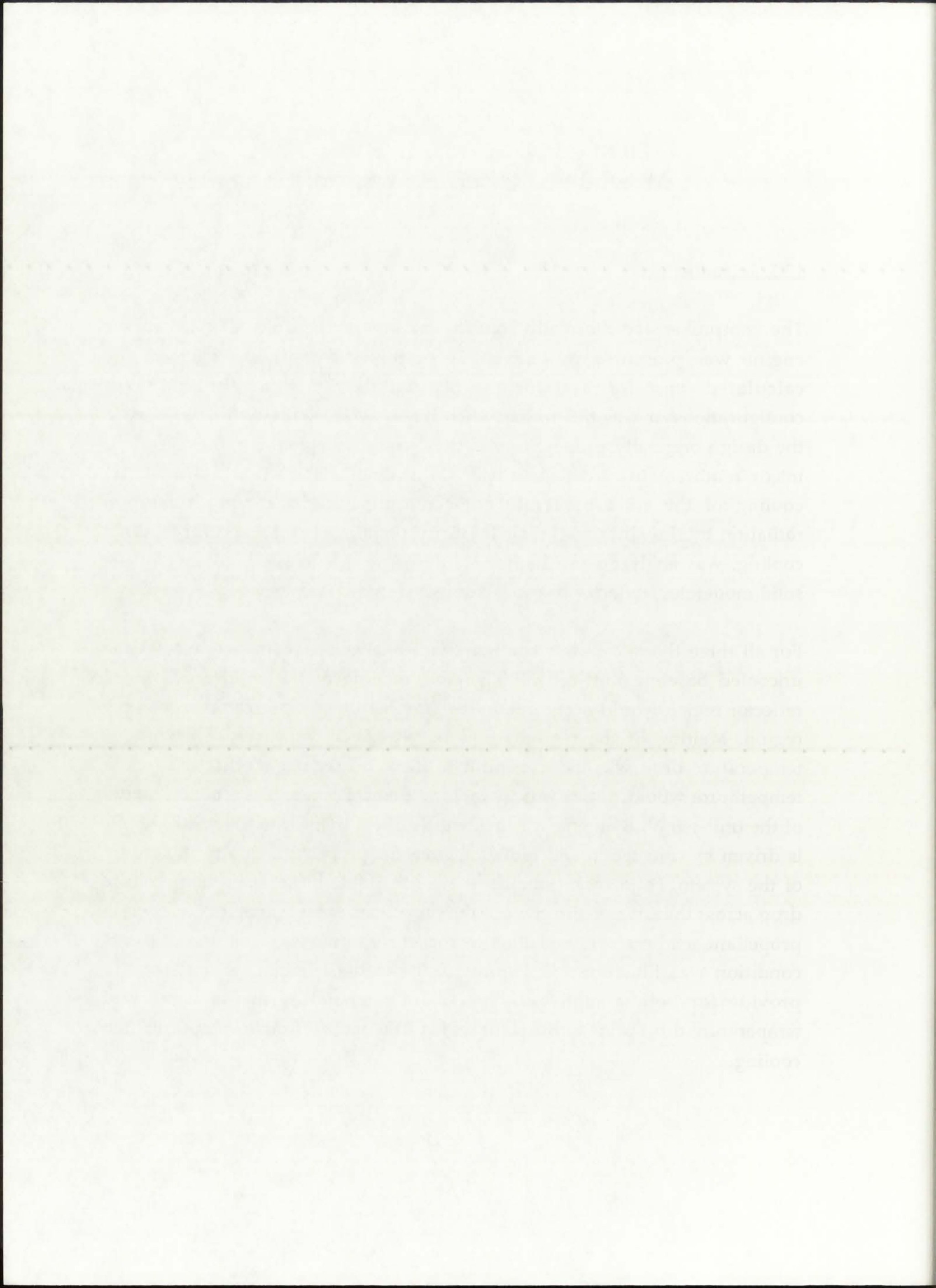
CHAPTER 12

FILM COOLING ANALYSIS OF THE MODERATOR/REFLECTOR REGIONS

12.1. Introduction

The comprehensive thermalhydraulics analysis of the unit-cell NLB rocket engine was presented in Chapter 10 of this Dissertation. Based on the calculated *uncooled* $T(r)$ for the 500 MWth, 5 MWth, and 50 kWth configurations, it was determined that the 50 kWth configuration, closest to the design originally proposed by UARL, would be potentially feasible. Two major requirements were identified: (1) cooling of the silica wall, and (2) cooling of the solid moderator/reflector region. Absorption of thermal radiation by the silica wall, and the corresponding requirement for internal cooling, was analyzed in Chapter 11; the issue of successful cooling of the solid moderator/reflector region is addressed in this Chapter.

For all three thermal power configurations analyzed in conjunction with the uncooled baseline unit-cell NLB engine, melting of the solid moderator/reflector region would occur due to the very high temperatures present in the region. Melting of the region could be prevented, however, if a suitable temperature drop was induced prior to the solid regions so that the region temperature would not exceed its melting point. From analysis of the layout of the unit-cell NLB engine, it is evident that heat transfer to the solid regions is driven by convection and radiation from the propellant. Due to the nature of the system, i.e. a rocket engine, it is undesirable to induce a temperature drop across the entire r -direction of the propellant, since a drastic reduction in propellant temperature, and thus in rocket performance, would result; this condition was illustrated in Figure 10.40 and the adjoining discussion. To provide for both a high bulk propellant temperature and a significant temperature drop prior to the solid regions, the most effective solution is film cooling.



Heat transfer by film cooling is defined as injection along the axial wall surface of a bleed liquid or cool gas propellant, thus forming a boundary layer of much lower temperature than that of the adjacent propellant [Sutton, 1992]. To minimize the detrimental effects of film cooling on rocket performance, it is advisable to maintain as thin as possible the radial thickness of the film.

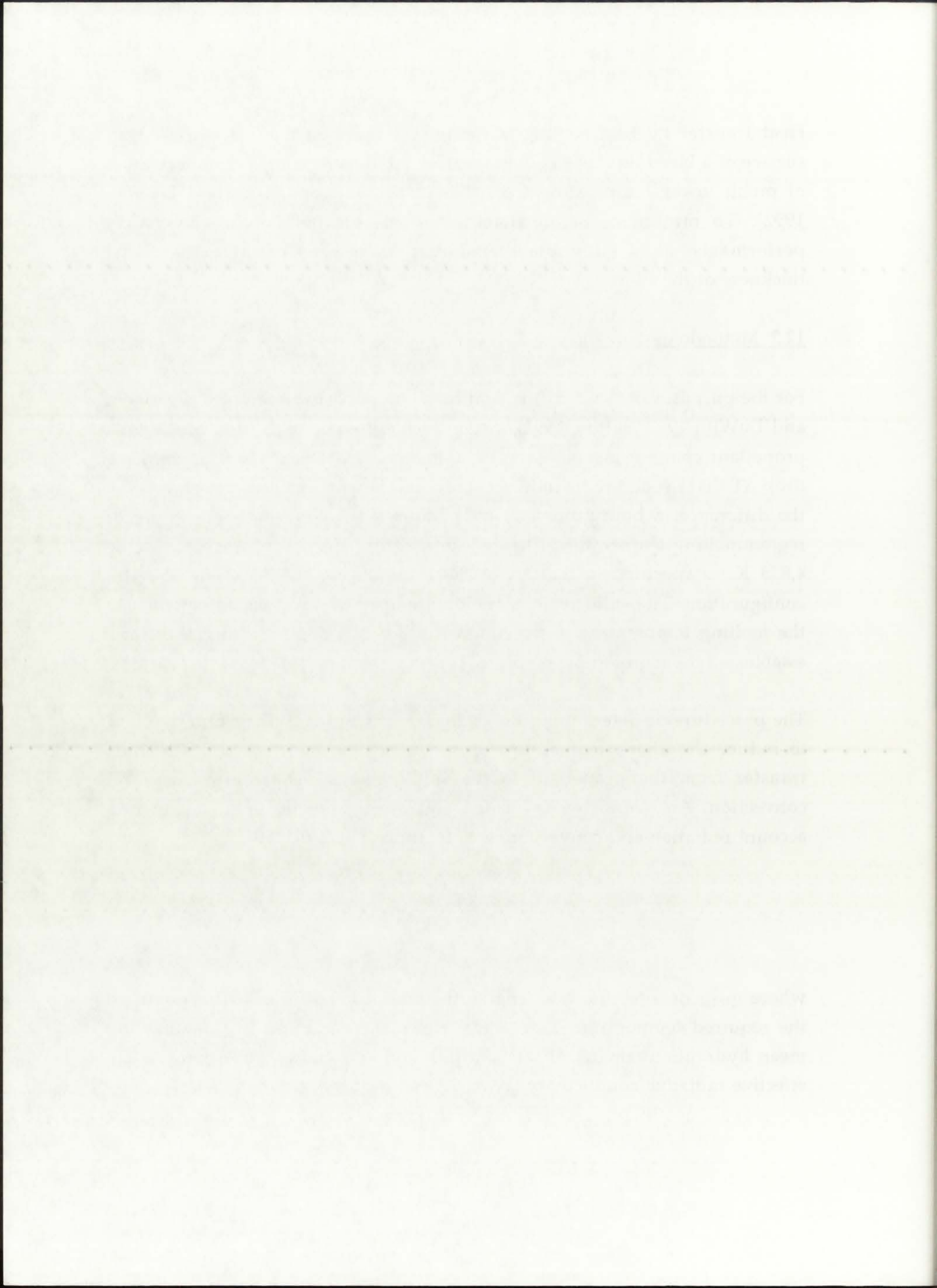
12.2. Methodology of Analysis

For the purposes of this analysis, and based on published examples [Incropera and DeWitt, 1992; Sutton, 1992], a film thickness equal to 1/10-th of the total propellant channel mean hydraulic diameter was chosen. The temperature drop ΔT that needed to be induced across the cooling film was determined by the difference in bulk propellant temperature and solid moderator/reflector region melting temperature. The bulk propellant temperature was taken to be 4,833 K, as specified in the GNRATR-1D results for the 50 kWth, 250 atm configuration. The solid regions' melting temperature was set to be equal to the melting temperature of beryllium: 1,278 K [CRC, 1990]. This, therefore, established the required $\Delta T = 3,555$ K.

The procedure of determining the characteristics of the cooling film required to induce the above temperature drop focused on the two modes of heat transfer from the propellant to the solid regions: (1) radiation, and (2) convection. An overall energy balance across the cooling film, taking into account radiation and convection, has the form [El-Wakil, 1981]:

$$\dot{q}_{\text{total}} = \frac{A_{\text{lm}} \Delta T}{\frac{1}{h_f} + \frac{D_{\text{Hf}}}{k_{\text{rad}}}} \quad (12.1)$$

where q_{total} denotes the total engine thermal power [W], ΔT corresponds to the required temperature drop across the film of 3,555 K, D_{Hf} denotes the mean hydraulic diameter of the film [m], and k_{rad} and h_f correspond to the effective radiative conductivity [W/m-K] and heat transfer coefficient [W/m²-



K] of the film, respectively. The parameter A_{lm} corresponds to the logarithmic mean surface area [m²] of the film [El-Wakil, 1981], and is the result of expansion of the surface area in cylindrical co-ordinates. For this analysis, since D_{Hf} is very small compared to the overall radial dimensions of both the propellant channel and the engine, the logarithmic mean area was taken to be equal to the arithmetic mean area, as suggested by El-Wakil:

$$A_{lm} \approx A_m = 2 \left[\frac{R_{in} + R_{out}}{2} \right] \pi L, \quad (12.2)$$

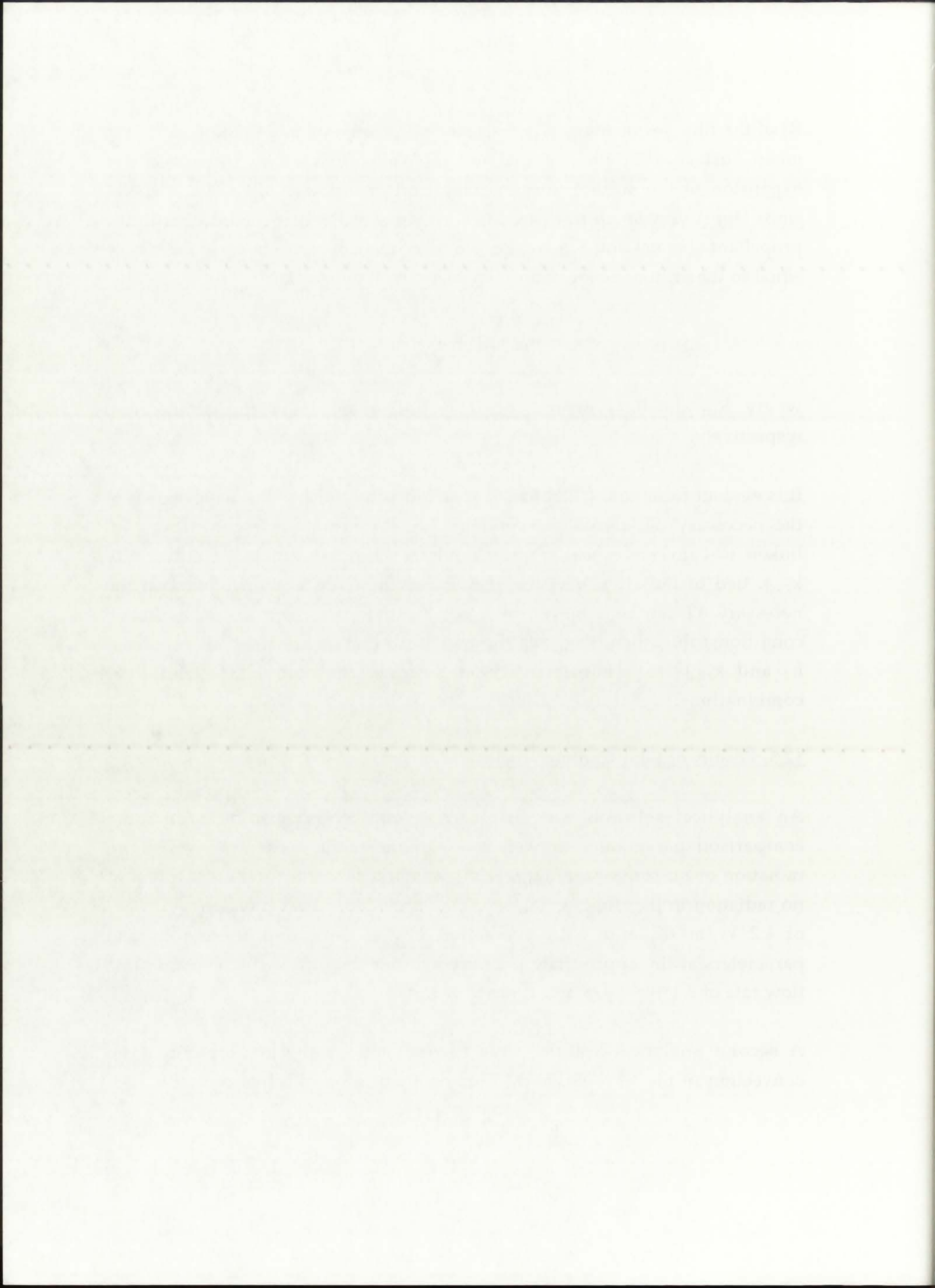
where R_{in} and R_{out} denote the inner and outer radius [m] of the film, respectively.

It is evident from eqn. (12.1) that two factors can influence the achievement of the necessary ΔT across the cooling film: the heat transfer coefficient h_f , linked to convective heat transfer, and the effective radiative conductivity k_{rad} , tied to radiative heat transfer. It can therefore be concluded that the necessary ΔT can be achieved by a combination of convective and radiative conditions; this, then, suggests the need for a parametric analysis involving h_f and k_{rad} to quantitatively determine the convective/radiative combinations.

12.3. Results of Film Cooling Analysis

An analytical solution was first carried out, in order to provide some comparison parameters as well as to delineate the extreme cases of no radiation or no convection. Eqn. (12.1) was first solved for the assumption of no radiation in the film, i.e. $k_{rad} \approx \infty$. This provided a heat transfer coefficient of 4.2 W/m²-K, and with evaluation of the associated thermophysical parameters at the appropriate pressure and temperature, a film coolant mass flow rate of $6.4 \cdot 10^{-8}$ kg/s and velocity of $3.5 \cdot 10^{-6}$ m/s.

A second analytical solution was carried out for the assumption of no convection in the film, i.e. $h_f \approx \infty$. This resulted in an effective radiative heat



transfer coefficient equal to 0.016 W/m-K which, with the usage of a mean radiating film temperature, translated to a Rosseland mean opacity of approximately $530,000 \text{ m}^{-1}$. This is an extremely high opacity, especially considering that the highest opacity of uranium is approximately $200,000 \text{ m}^{-1}$ [Parks, 1968].

The two extreme cases solved analytically provided the bounds for the coupled convective/radiative parametric analysis. The actual parametric analysis was carried out with the aid of a FORTRAN program, called FILMCOOL, developed as part of this research work. A listing of the FILMCOOL program is provided in Appendix J.

The independent variable was chosen to be the film opacity a_R ; a total of 16 opacities were analyzed, ranging from $528,700 \text{ m}^{-1}$ down to 0.00001 m^{-1} . FILMCOOL determined the heat transfer coefficient, mass flow rate, and velocity that would, in combination with each of the given opacities, induce the required ΔT across the film coolant channel. The obtained relationship between a_R , h_f , m_f , and v_f is given in Table 12.1 and in Figures 12.1, 12.2, and 12.3.

In summary, the data presented in Table 12.1 indicates all the possible combinations of convective and radiative parameters in the film that could potentially induce the required temperature drop of $3,555 \text{ K}$. For the specific case of the 50 kWth , 250 atm configuration of the unit-cell NLB rocket engine, one particular convective/ radiative combination exists: this combination is characterized by the opacity at the mean film temperature, $T_{f,avg}=3,056 \text{ K}$, which is approximately equal to 12.0 m^{-1} . With a set film opacity, going back to Table 12.1 indicates that the corresponding required film heat transfer coefficient and mass flow rate is $4.227 \text{ W/m}^2\text{-K}$ and $6.421 \cdot 10^{-8} \text{ kg/s}$, respectively.

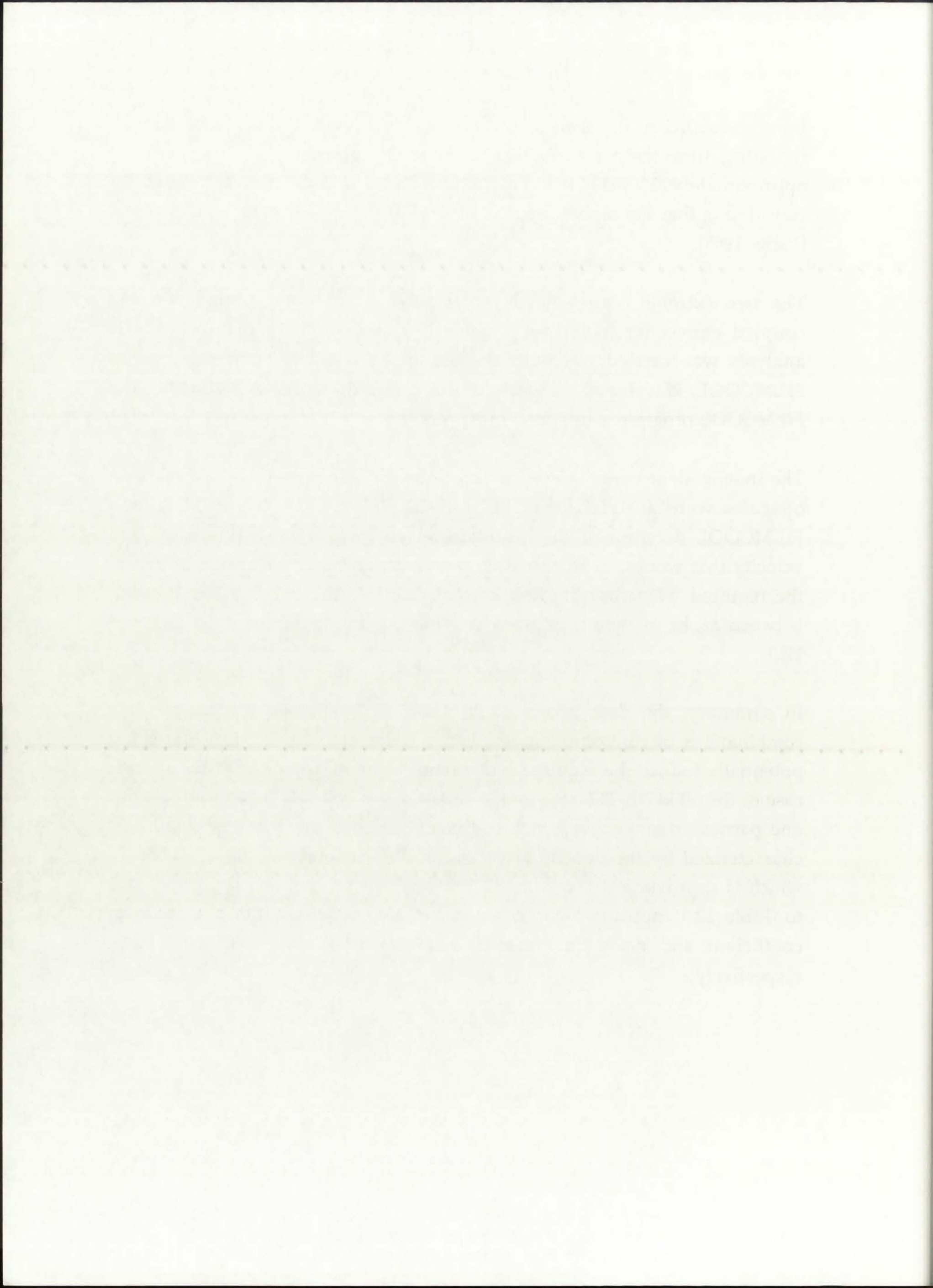


TABLE 12.1
 Parametric analysis of the film cooling parameters for 50 kWth, 250 atm

a_R [m^{-1}]	k_{rad} [W/m-K]	h_f [W/m ² -K]	m_f [kg/s]	v_f [m/s]
5.288e5	1.632e-2	∞	∞	∞
5.287e5	1.632e-2	8.198e7	8.264e1	4.504e3
5.287e5	1.632e-2	2.316e6	9.574e-1	5.218e1
5.000e5	1.725e-2	7.779e1	2.448e-6	1.334e-4
3.250e5	2.654e-2	1.097e1	2.115e-7	1.153e-5
1.500e5	5.751e-2	5.901	9.743e-8	5.310e-6
7.500e4	1.150e-1	4.925	7.774e-8	4.237e-6
2.500e4	3.451e-1	4.437	6.821e-8	3.718e-6
5.000e3	1.725e0	4.267	6.497e-8	3.541e-6
1.000e3	8.626e0	4.235	6.436e-8	3.507e-6
2.000e2	4.313e1	4.228	6.424e-8	3.501e-6
5.000e1	1.725e2	4.227	6.421e-8	3.500e-6
1.000e1	8.626e2	4.227	6.421e-8	3.499e-6
1.000e0	8.626e3	4.227	6.421e-8	3.499e-6
1.000e-1	8.626e4	4.227	6.421e-8	3.499e-6
1.000e-3	8.626e6	4.227	6.421e-8	3.499e-6
1.000e-5	8.626e8	4.227	6.421e-8	3.499e-6
0	∞	4.227	6.421e-8	3.499e-6

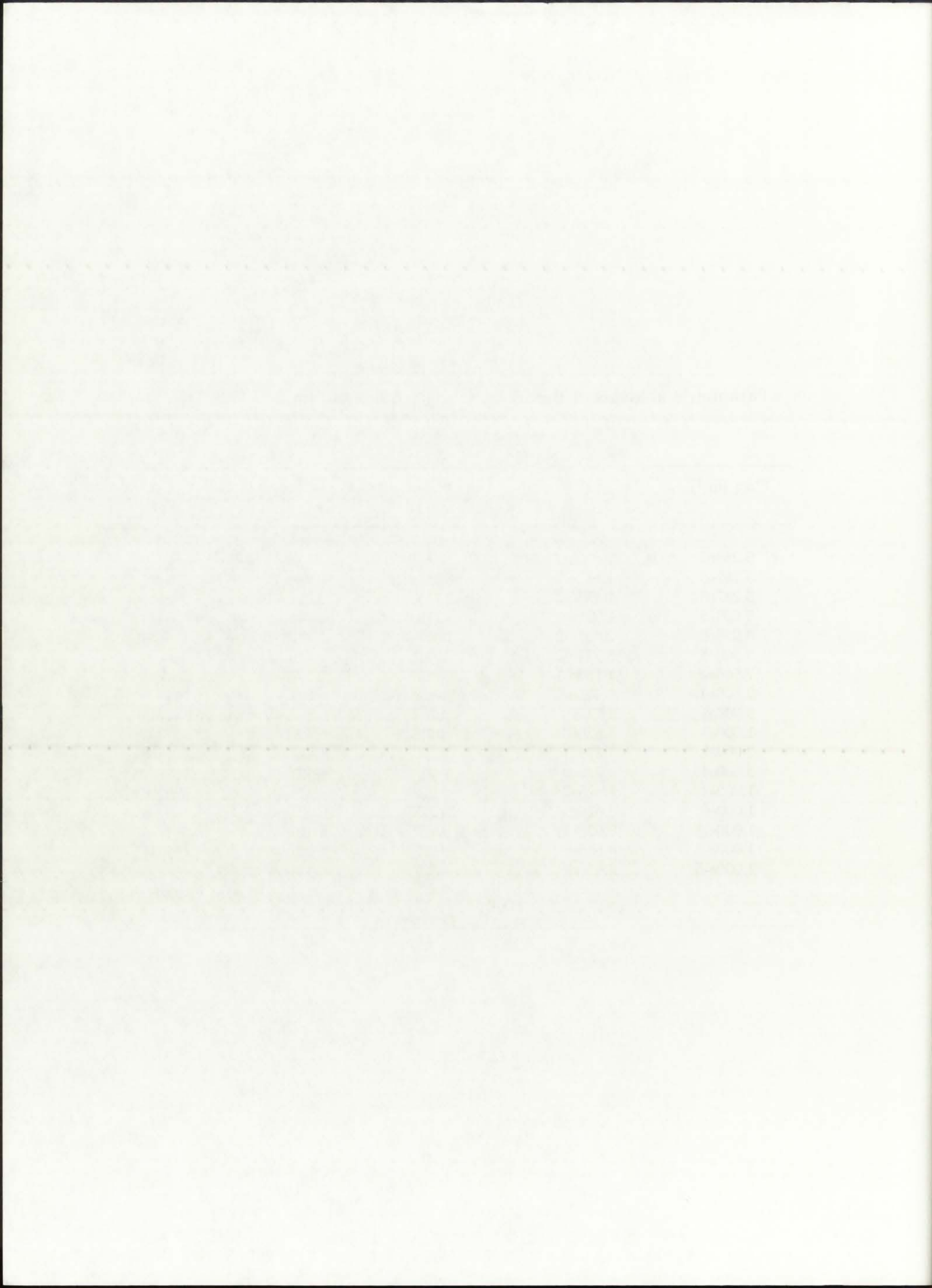
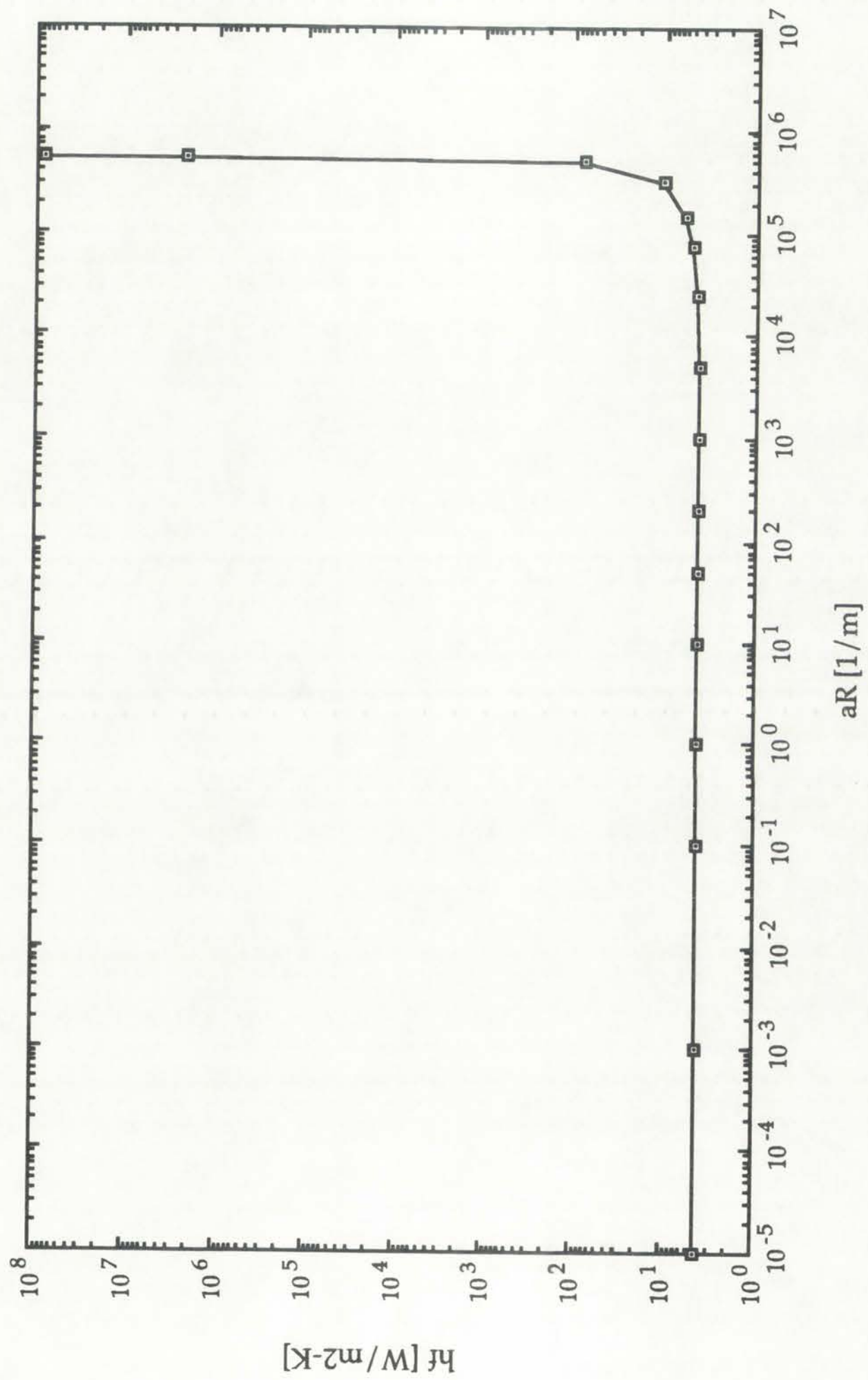


Figure 12.1: Interdependence of film heat transfer coefficient and Rosseland mean opacity.



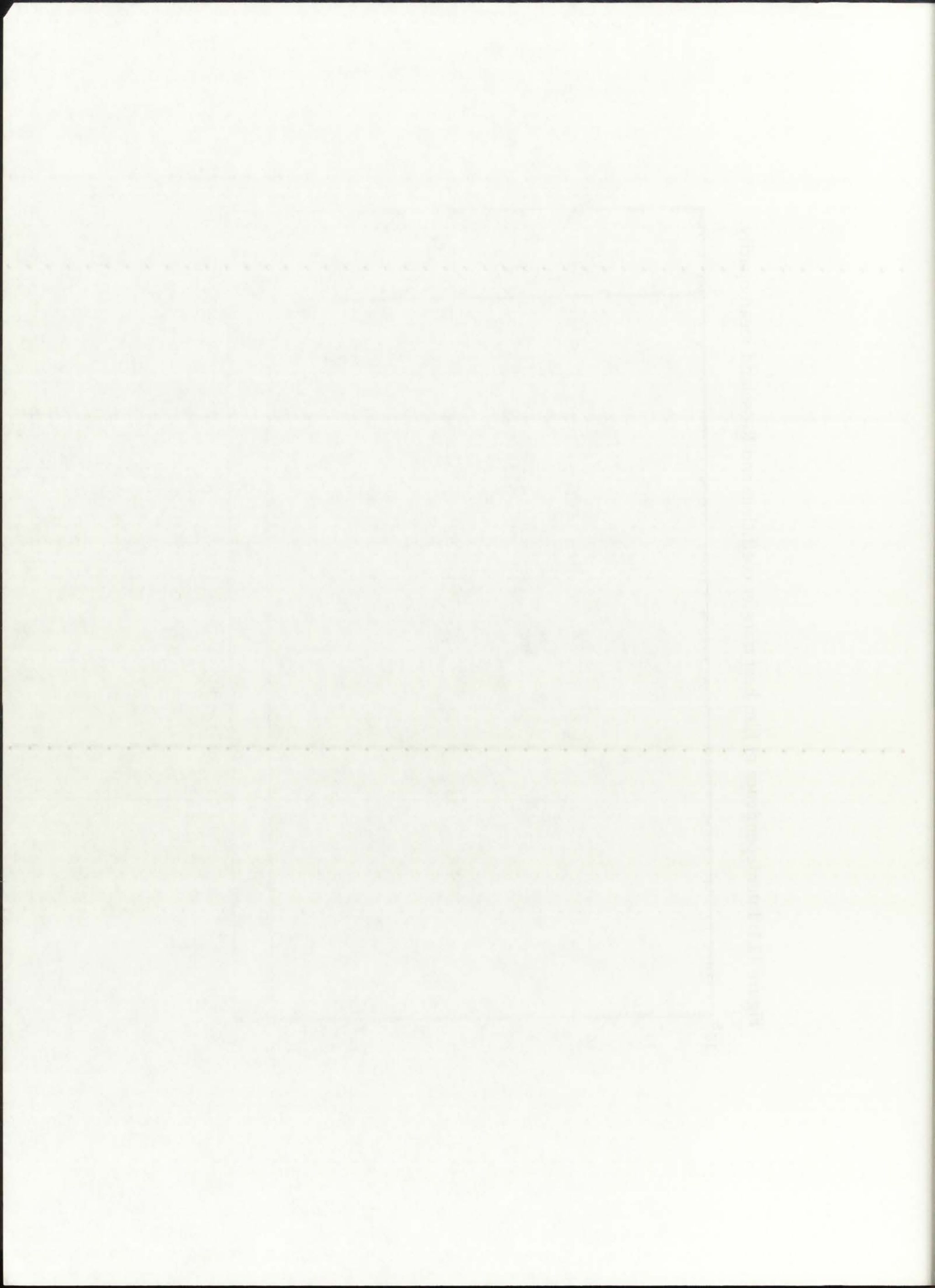
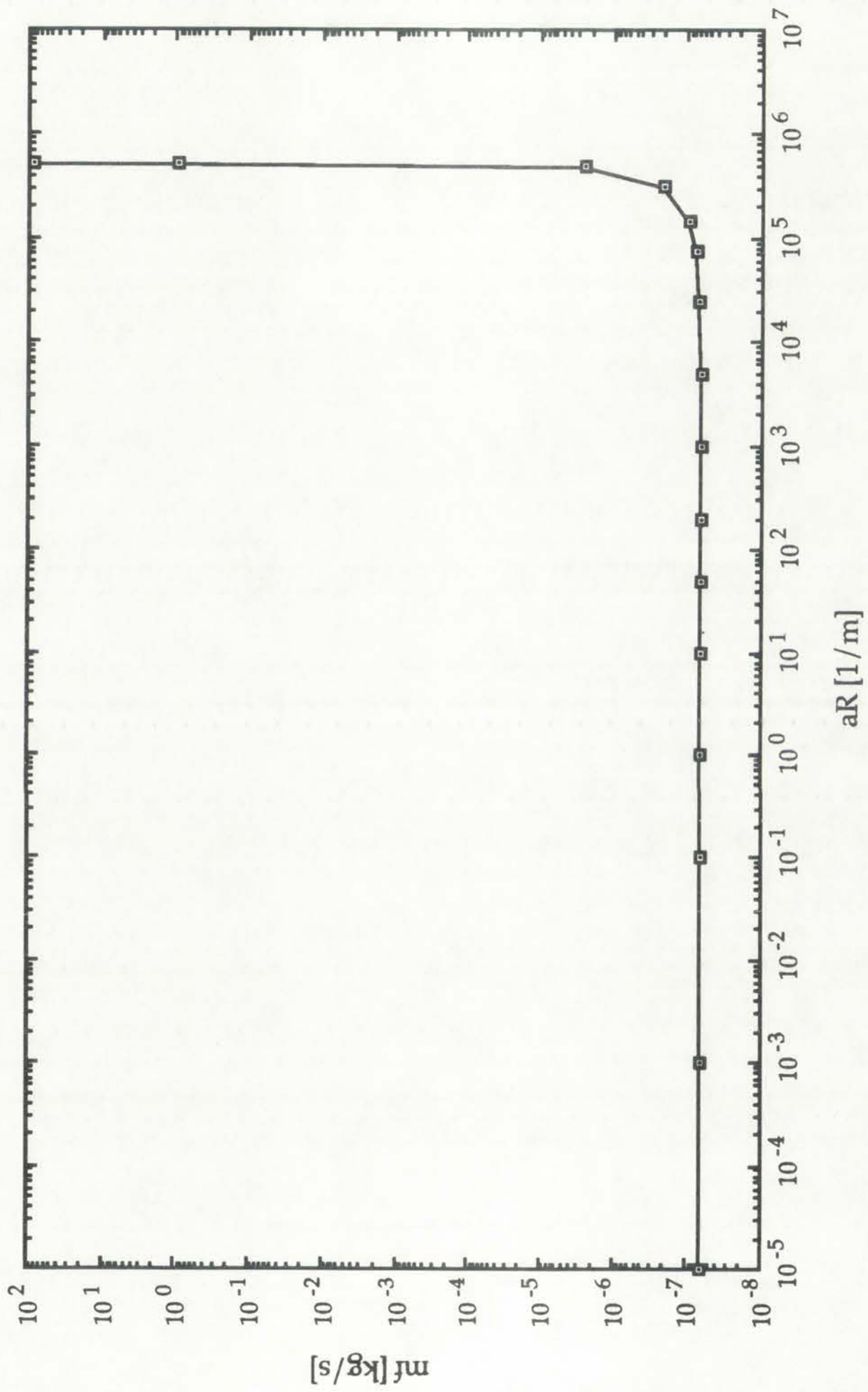
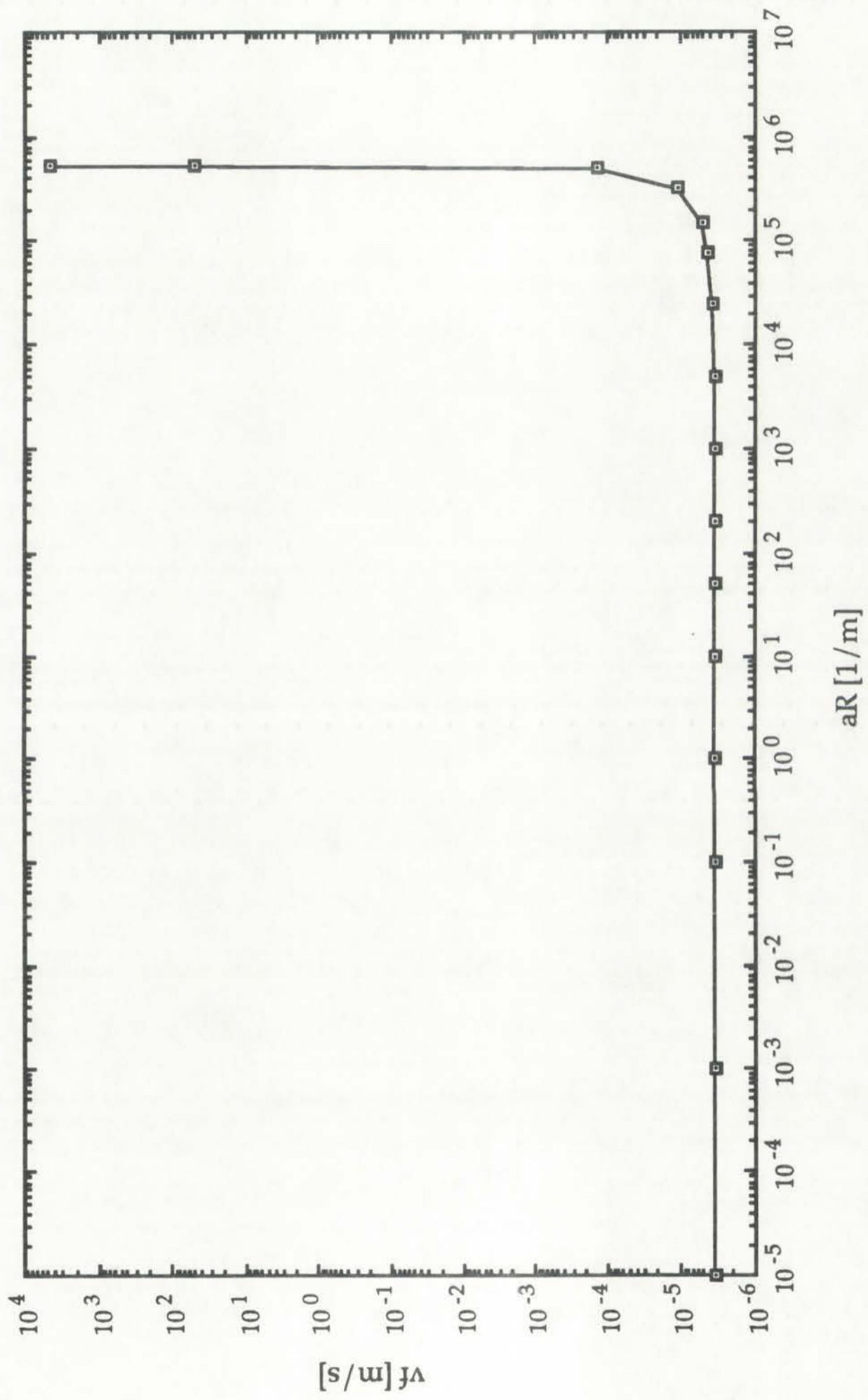


Figure 12.2: Interdependence of film mass flow rate and Rosseland mean opacity.



Journal of the American Medical Association (JAMA)

Figure 12.3: Interdependence of film axial velocity and Rosseland mean opacity.



THE UNIVERSITY OF CHICAGO LIBRARY

12.4. Conclusions

Based on the results presented in this Chapter, it can be concluded that film cooling of the solid moderator/reflector region of the unit-cell NLB rocket engine can be achieved for the 50 kWth, $p=250$ atm configuration. To induce a temperature drop ΔT of 3,555 K, equal to the difference between the bulk propellant temperature and the beryllium melting temperature, in a cooling film with a mean hydraulic diameter of approximately 0.8 cm, would require a film mass flow rate of approximately $6.4 \cdot 10^{-8}$ kg/s. The associated film heat transfer coefficient would then be $4.2 \text{ W/m}^2\text{-K}$ and the film velocity would be $3.5 \cdot 10^{-6}$ m/s.

classical the metal present in the liquid it can be considered that the cooling of the solid medium (reflected region of the wall cell) is a process that can be treated by the 1D heat conduction. To obtain a temperature drop $\Delta T = 100^\circ\text{C}$ and a distance $x = 10^{-3}\text{m}$ a coefficient temperature and the position melting temperature in a cooling film with a new hydraulic diameter of approximately 0.8 cm would require a film mass flow rate of approximately 0.4 kg/s . The standard film heat transfer coefficient would then be $4.2\text{ W/m}^2\text{K}$ and the film velocity would be 0.1 m/s .

... ..

... ..

... ..

... ..

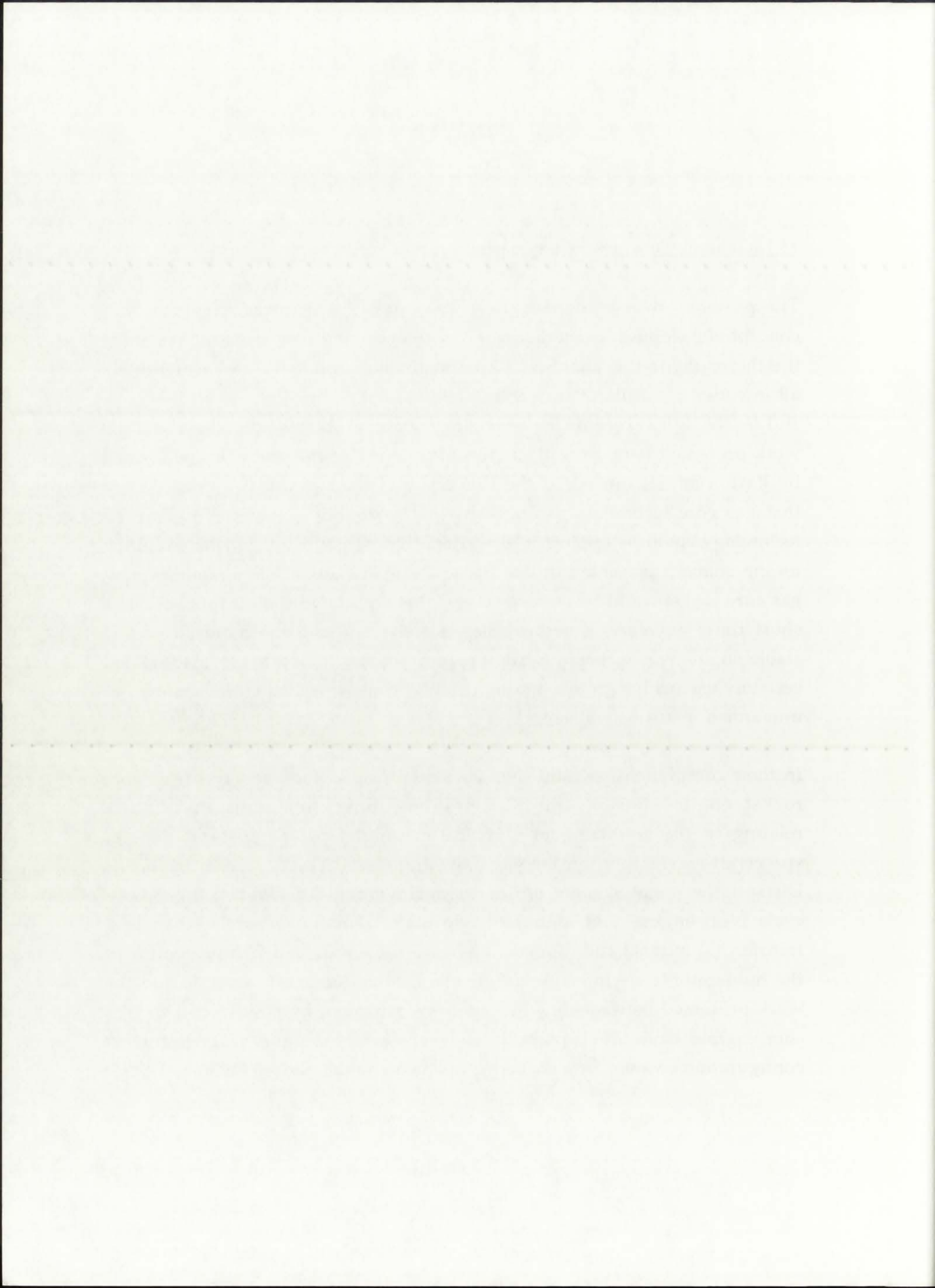
... ..

CHAPTER 13 CONCLUSIONS

13.1. General Conclusions on Feasibility

The previous twelve chapters have been devoted to introducing the NLB concept, developing the methodology of analysis, and discussing the results of the thermalhydraulic analysis. A compendium of results has been presented, all intended to facilitate answering one question: is the unit-cell NLB engine, and indirectly gas core rocket technology, feasible? At this point, based on the work presented here, as well as on contemporary open-cycle work performed by Poston and Kammash at the University of Michigan, it is almost certain that gas core technology *is* feasible; what is doubtful, however, is that the technology could be applied to the extent that was initially envisioned. Based on the analysis presented in this Dissertation, the author has no doubt that a gas core rocket could be developed and that a prototype could function for a short time; however, a neutronically steady-state and thermomechanically stable engine would most probably require significant additional analysis and certainly exhaustive ground testing before it could be relied on for manned or unmanned space propulsion.

In their comprehensive fluid dynamics modeling of the open cycle gas core rocket engine, Poston and Kammash identified numerous instabilities relating to the maintaining of a critical configuration and the influence of spacecraft acceleration on the gas flow. The research work presented in this Dissertation focused more on the thermalhydraulic behavior of the closed-cycle NLB engine, and identified two major requirements related to heat transfer: (1) internal and film cooling of the silica wall, and (2) film cooling of the moderator/reflector region. Both the Poston/Kammash analysis and the work presented here identified *engineering* problems. In other words, the gas core engines have problems in the development phase, and, in their current configurations, would be a challenge to operate in the desired fashion.

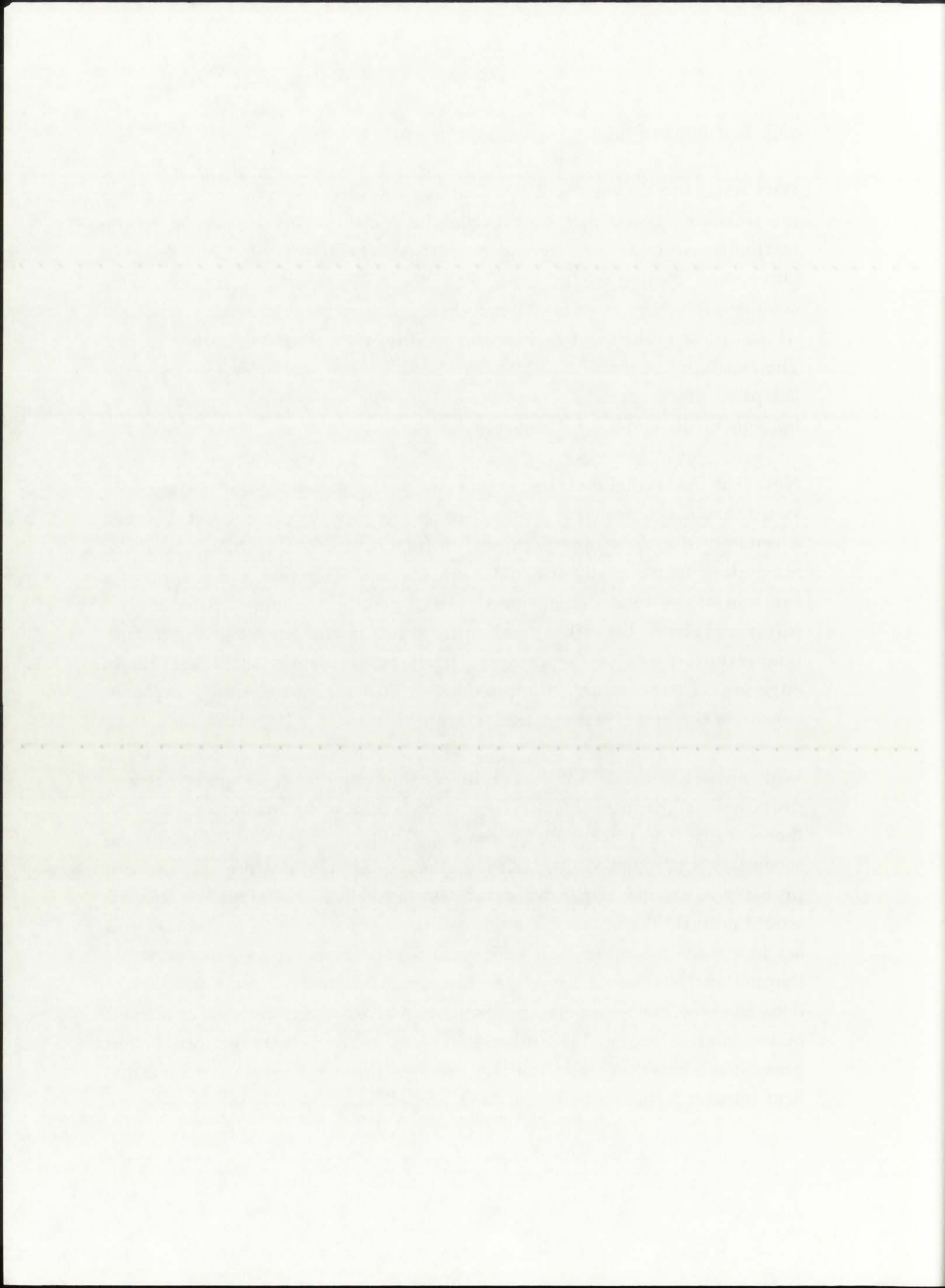


13.2. Feasibility of the Unit-Cell NLB Concept

With respect to the results of this Dissertation work, it can be concluded that the feasibility issues of the unit-cell NLB rocket engine are similar to the feasibility issues of the more conventional, chemical propulsion systems. Other than cooling of the silica wall, the NLB rocket requires the same cooling mechanism as does a chemical rocket, namely the provision of a large ΔT just prior to the solid regions surrounding the central combustion cavity. The feasibility of the unit-cell NLB rocket has been shown by the results of Chapters 10, 11, and 12, which also provide suggested mechanisms to implement the cooling requirements.

Now that the feasibility of the engine has been demonstrated, it must also be stated that, based primarily on the thermal integrity of the engine, it is almost a certainty that a definite performance limitation exists, in the form of the maximum feasible edge-of-fuel temperature. The fuel temperature, a function of the total thermal power and operating pressure of the engine, influences both the silica wall and solid moderator/reflector region temperature. Based on the analysis performed in Chapter 10, 11, and 12, an edge-of-fuel temperature of approximately 20,000-25,000 K would probably constitute the upper performance limit of the unit-cell NLB rocket engine.

With respect to the 50 kWth, 250 atm configuration of the engine that was proposed as the baseline, its feasibility is easily demonstrated, at least theoretically. The silica wall, for example, could be internally cooled by the secondary hydrogen coolant circuit; the required mass flow rate would probably be around 1 kg/s, as was shown in Chapter 11. The internal coolant would mitigate the unavoidable thermal radiation absorption in the wall and act to reduce the mean wall temperature below melting. A more detailed thermal analysis would have to be performed on the wall itself, in order to determine the exact temperature distribution across the entire wall as a result of the internal cooling. The internal coolant, by itself, would probably not prevent the outer edges of the wall from melting as a result of convective heat transfer from the buffer gas and propellant. Therefore, film cooling on

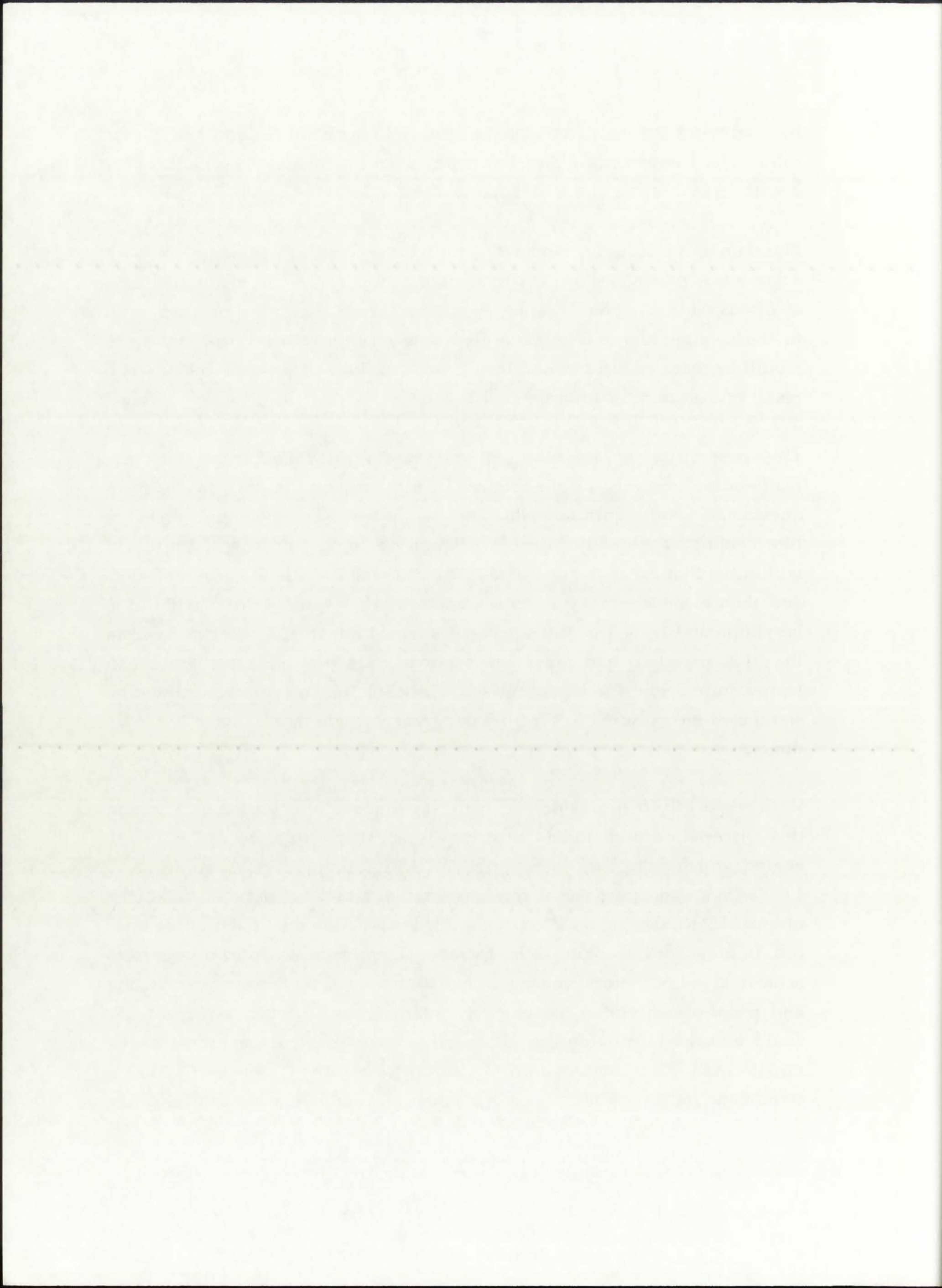


both edges of the wall would be necessary to maintain the entire wall in a solid state. The procedure for film cooling would be similar in concept to that discussed in Chapter 12 for the solid moderator/reflector region.

Maintaining of the solid moderator/reflector region below melting could be achieved by passing a film coolant along the propellant/solid region interface, as discussed in Chapter 12. Thus, to achieve the necessary temperature drop in the cooling film, a film mass flow rate of approximately 6.4×10^{-8} kg/s would be required. This would then prevent melting of the solid regions as a result of heat transfer from the fuel.

The possibility of maintaining the moderator/reflector at the low temperature proposed by the original UARL designers, on the other hand, is questionable and requires detailed analysis. In light of the potential success of film cooling, it might be possible to induce a significant temperature drop within the film, so as to get a moderator/reflector temperature around 300 K, and then to incorporate numerous coolant channels interspersed within the beryllium and D₂O. The coolant channels would flow primary hydrogen from the 20 K main tank and could possibly reduce the beryllium and D₂O mean temperature below 100 K as proposed. This scenario, however, would require significant modification to the NLB design and would have to include a two-dimensional analysis in the (r- θ) plane of the engine.

With respect to its neutronics behavior, the unit-cell NLB engine analyzed in this Dissertation is definitely subcritical. This stems from the design of the engine, which dates back to the original UARL concept proposed in the early 1970's. Since the purpose of this Dissertation was to analyze in detail the original UARL design, no attempt was made to modify the design of the unit-cell. In order for the engine to be operational, however, it will be necessary to achieve $k_{\text{eff}}=1.000$, most probably in one of two ways: (1) for terrestrial testing and proof-of-concept of the unit-cell, a driver reactor, such as the ACRR, could be used to provide the additional neutron flux (corresponding to the initial UARL plans for the unit-cell), or (2) for reliance on the unit-cell as a standalone rocket engine, a thorough re-design would be necessary. Since the



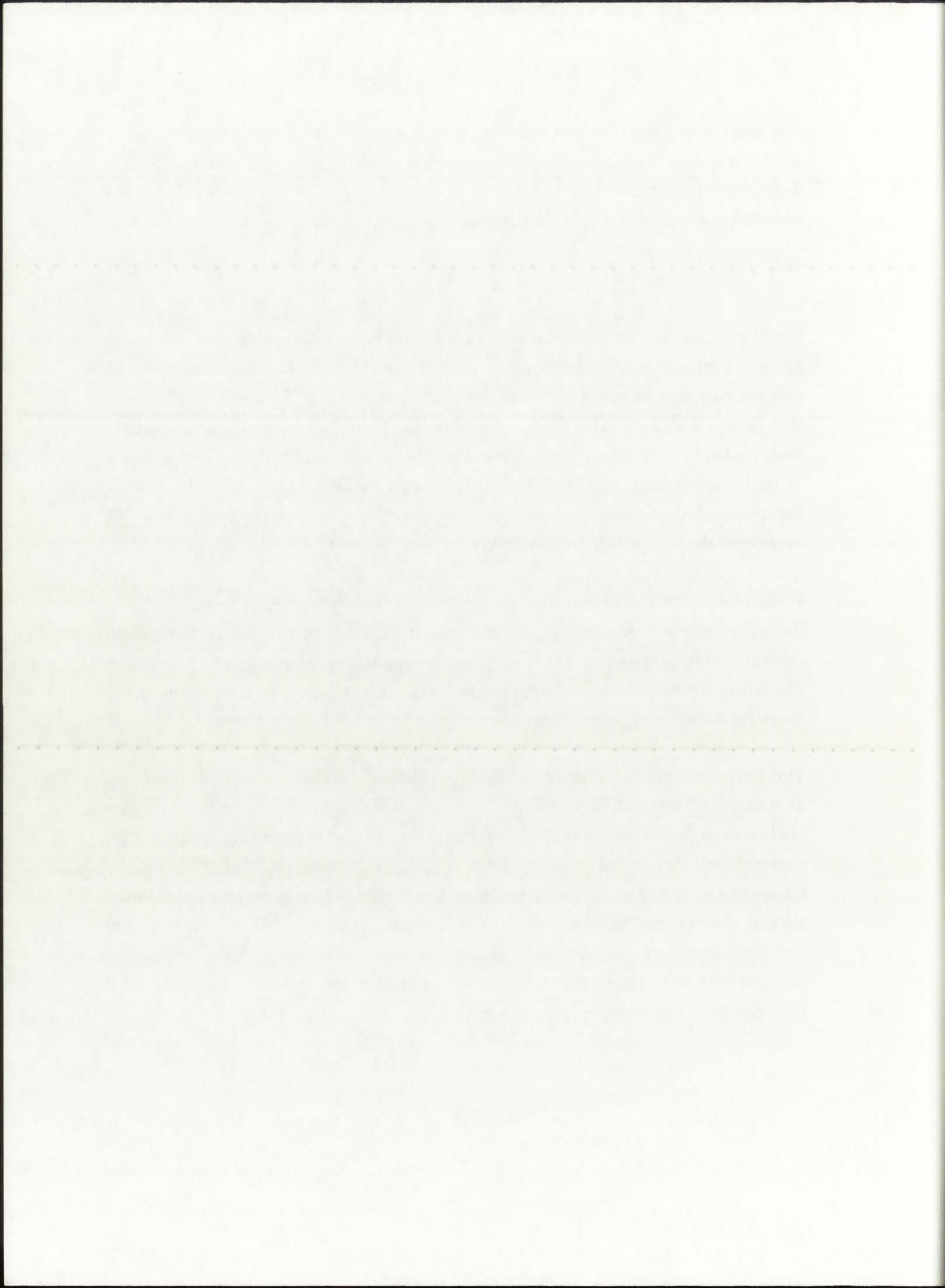
k_{eff} analysis, performed in Chapter 10 for each of the three thermal power configurations, indicated that the unit-cell engine is over-moderated, a redesign of the engine should focus on increasing the fuel volume and/or density, and on optimizing the fuel-to-moderator ratio.

13.3. Conclusions

On the basis of the above discussions, it can be concluded that the NLB engine, and gas core technology in general, is feasible provided a number of engineering issues are addressed. Overall, however, it does not seem likely that gas core technology can feasibly provide the very high operating temperatures once thought possible. For the case of the NLB engine, an edge-of-fuel temperature of 20,000-25,000 K is most probably the upper limit; with the original design maintained, this would translate to a thermal power of approximately 50 kWth or possibly somewhat higher.

With respect to the neutronics behavior, the fuel density was found to have the most impact on the k_{eff} of the system. Thus, to provide steady-state critical reactor operation, the NLB engine would require either an increase in operating pressure to well beyond 1,000 atm or a redesign of the engine with, most probably, a significant increase in the fuel region dimensions.

The performance parameters of the unit-cell NLB engine are not as beneficial as was once believed. In terms of thrust and specific impulse, the NLB engine is closest in performance to NEP systems; the latter, however, are much better understood and more feasible with today's technology. As was stated in Chapter 10, the specific impulse of an electrothermal engine can potentially exceed that of the NLB engine. It would thus be problematic to conclude on the true merit of gas core technology; at least with the current proposed designs, the propulsion characteristics do not provide significant benefits over non-gas core technology.



CHAPTER 14 RECOMMENDATIONS FOR FUTURE WORK

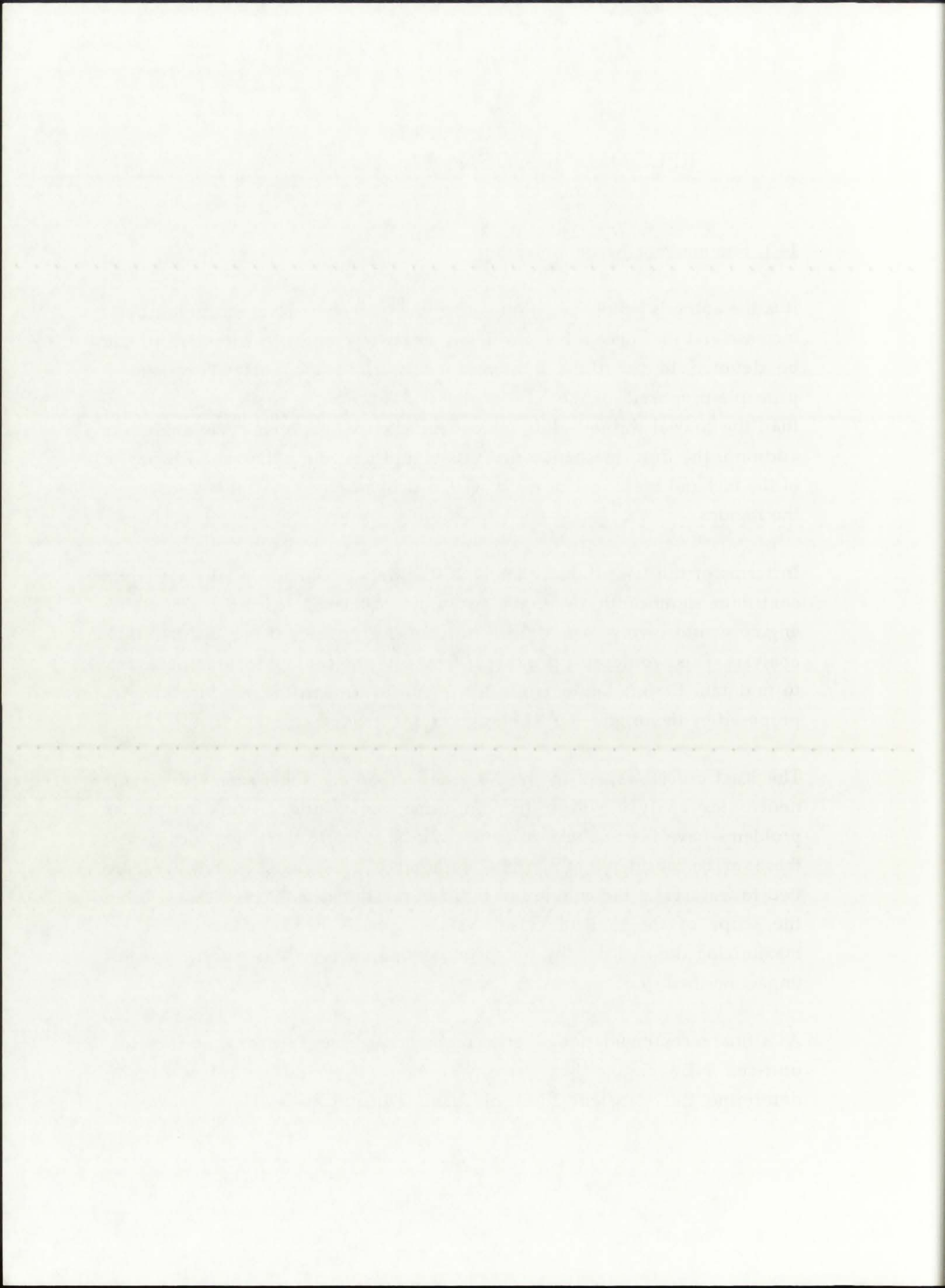
14.1. Summary of Recommendations

It is the author's belief that, if interest in the NLB engine were to significantly increase and the concept be considered for space propulsion, attention should be devoted to the fluid dynamics analysis, as the vortex-confinement principle proposed for the NLB engine is a much more challenging problem than the coaxial through-flow which characterizes the open-cycle engine. In addition, the fluid mechanics analysis would determine the actual behavior of the fuel and buffer gas flows as well as delineate the physical boundaries of the regions.

In terms of the heat transfer analysis, the only additional work that could contribute significantly to the understanding of the characteristics of the NLB engine would involve a multi-dimensional (2-D in $(r-\theta)$ or $(r-z)$ or even 3-D) analysis. This would also provide insight into the cooling scheme necessary to maintain the moderator/reflector region in the low-temperature state as proposed by the original UARL designers.

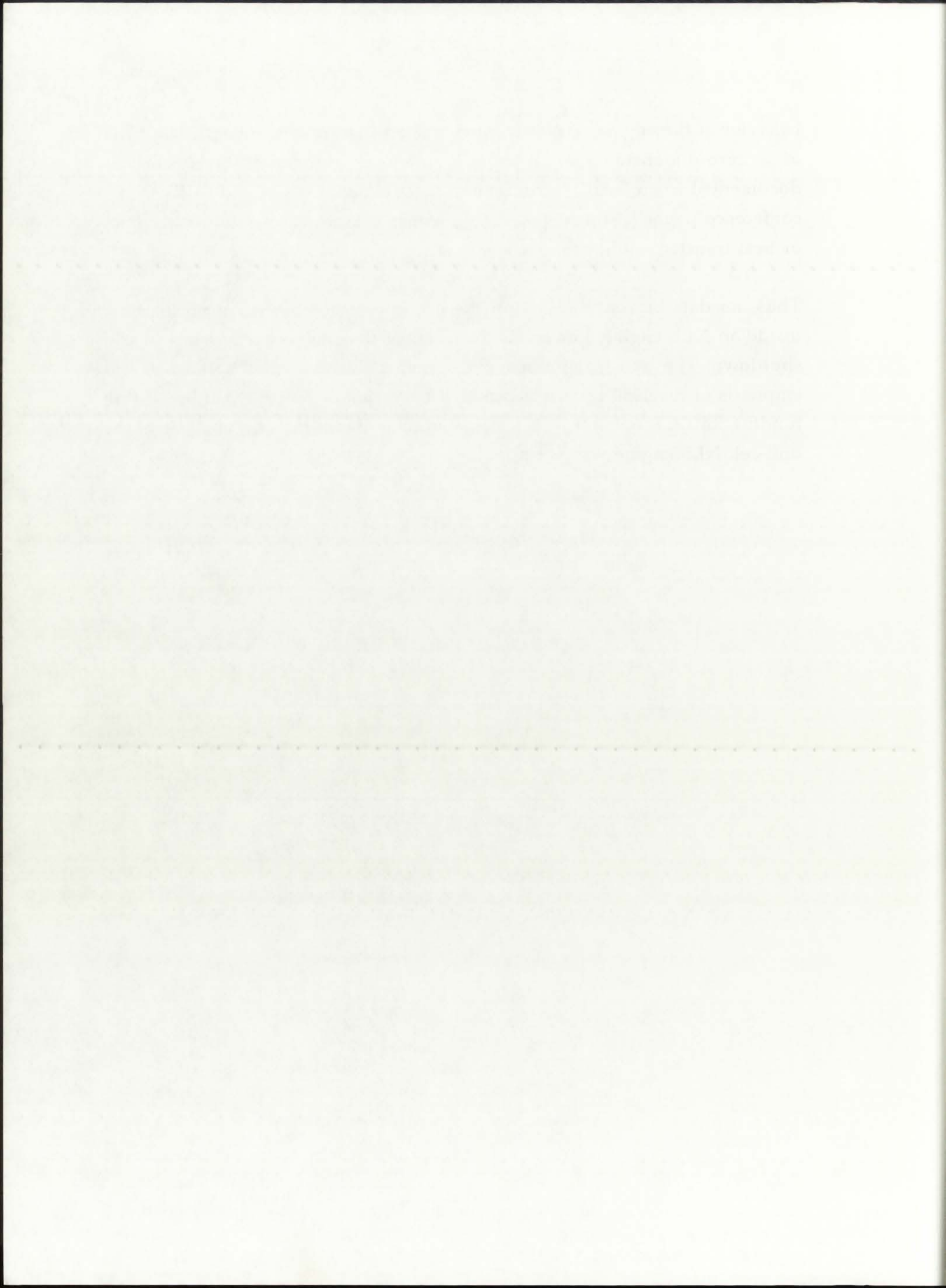
The least crucial aspect of the NLB engine, at this time, seems to be the neutronics analysis. Once the fluid mechanics and thermalhydraulics problems have been solved, attention can be given to the neutronics issues; these can be considered of marginal importance at this point, as they are more tied to features of the engine rather than crucial feasibility problems. Within the scope of the neutronics analysis, emphasis needs to be placed on maximizing the fuel density for given configuration, as this has the greatest impact on the k_{eff} of the system.

As a final recommendation, after a comprehensive steady-state analysis of the unit-cell NLB engine has been performed, it would be interesting to determine the transient fluid mechanics, heat transfer, and neutronics

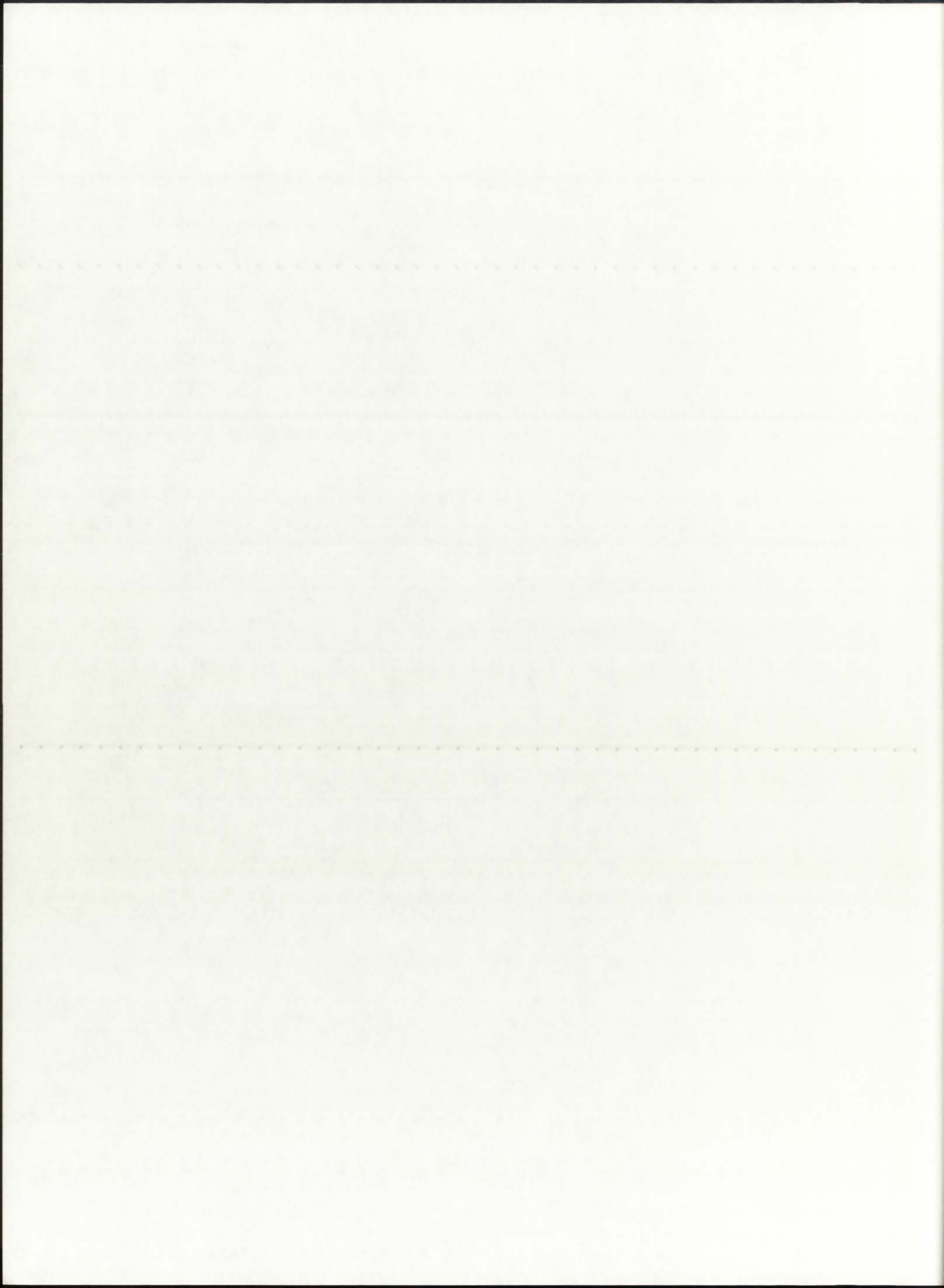


behavior of the engine. The only work related to transient behavior consisted of a zero-dimensional analysis of the effects of reactivity insertion as documented in an UARL technical report [Bauer *et al.*, 1970] and restated in a conference paper [Latham *et al.*, 1970], which was not tied to fluid mechanics or heat transfer conditions.

Thus, no data currently exists on the procedure to achieve the vortex flow inside an NLB engine, nor on the behavior of the engine during startup and shutdown. The transient phases of the engine were assumed solveable, and emphasis of the 1960's work was placed on "proof-of-concept" studies. As all funding for GCR research was terminated in 1973, no transient analysis of the unit-cell NLB engine was performed.



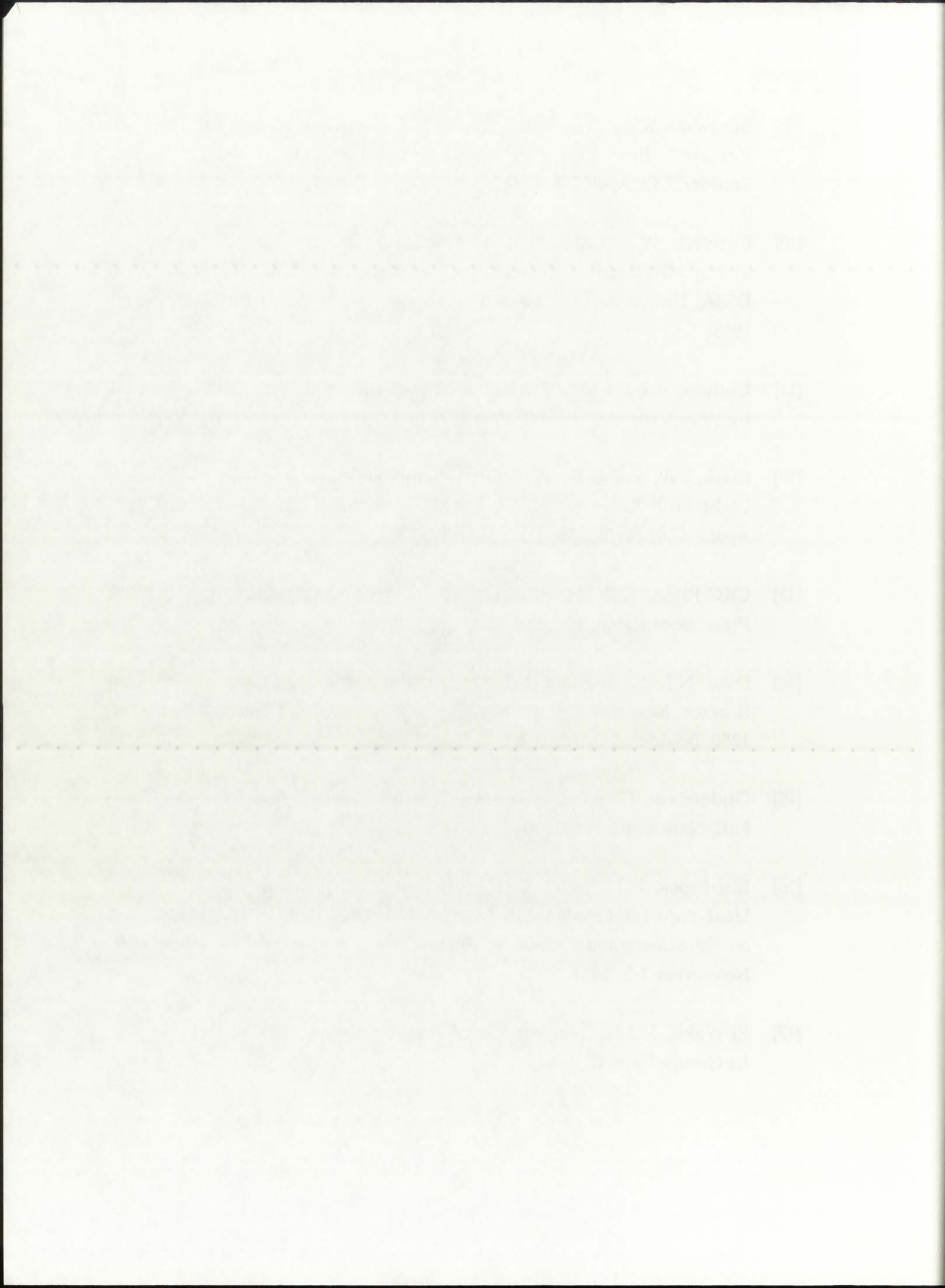
REFERENCES



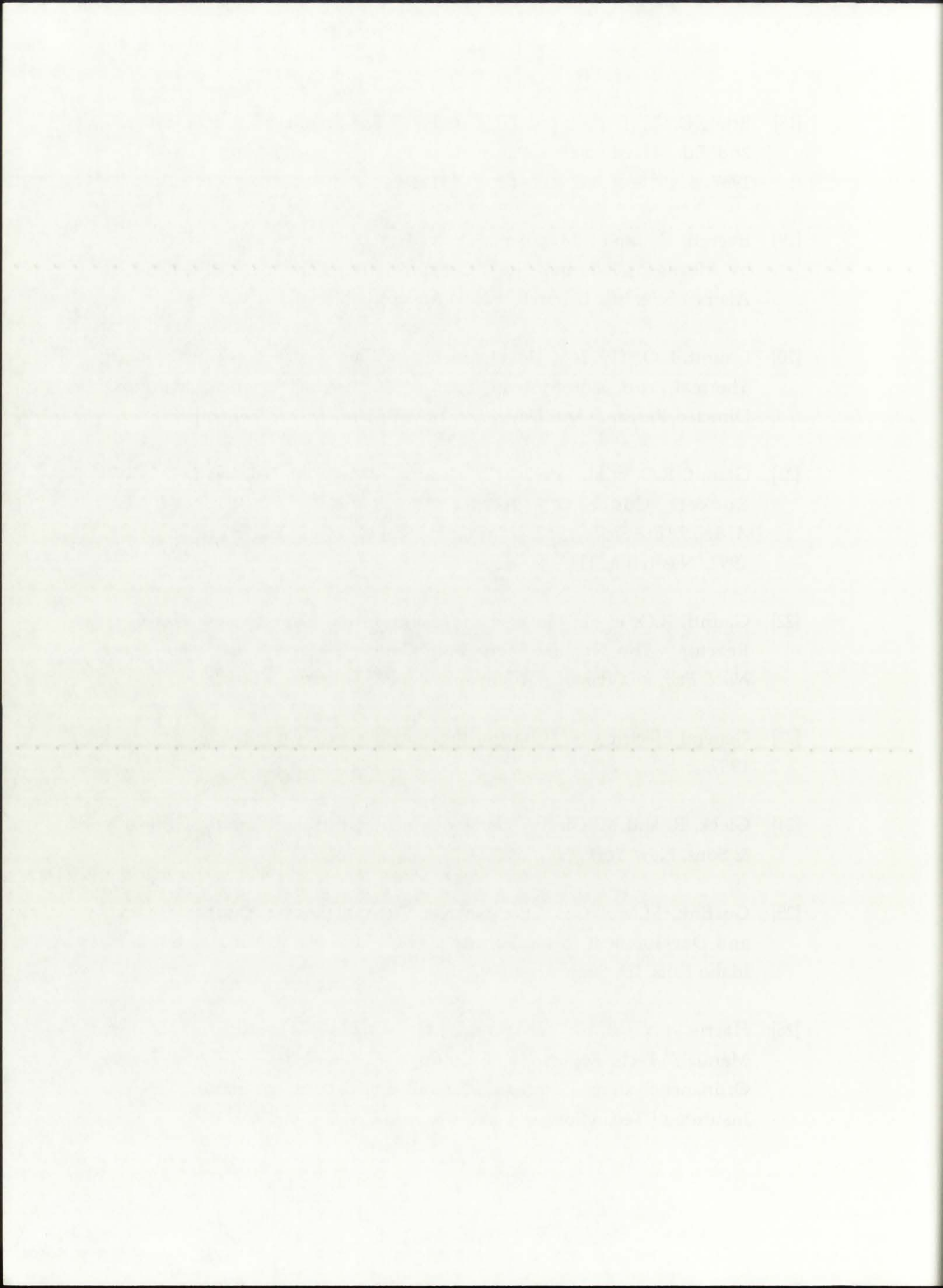
- [1] Alperin, M. and Sutton, G.P., "Advanced Propulsion Systems," Pergamon Press, New York, NY, 1959.
- [2] Angelo, J. and D. Buden, "Space Nuclear Power," Orbit Book Co., Malabar, FL, 1985.
- [3] Bauer, H.E., R.J. Rodgers, and T.S. Latham, "Analytical Studies of Start-up and Dynamic Response Characteristics of the Nuclear Light Bulb Engine," Technical Report J-910900-5, United Aircraft Research Laboratories, East Hartford, CT, September 1970.
- [4] Bennett, C.O. and J.E. Myers, "Momentum, Heat, and Mass Transfer," 3rd Ed., McGraw-Hill Book Co., New York, NY, 1982.
- [5] Bennett, G.L., "Nuclear Thermal Propulsion Program Overview," *Nucl. Therm. Propul. Jt. NASA/DOE/ DOD Workshop*, Cleveland, OH, July 10-12, 1990.
- [6] Bennett, G.L. et al., "Prelude to the Future: A Brief History of Nuclear Thermal Propulsion in the United States," *Crit. Rev. of Space Nucl. Power and Propulsion*, M.S. El-Genk, Ed., American Institute of Physics Press, 1994.
- [7] Bogart, D. and E. Lantz, "Nuclear Physics of Solid-Core Gas-Cooled Rocket Propulsion Reactors," *Proc. NASA-Univ. Conf. on the Science and Technol. of Space Explor.*, NASA SP-11, Chicago, IL, November 1-3, 1962.
- [8] Borowski, S.K., "Nuclear Thermal Rocket Baseline Design - Rover/NERVA," *Nucl. Therm. Propul. Jt. NASA/DOE/ DOD Workshop*, Cleveland, OH, July 10-12, 1990.

Faint, illegible text, possibly bleed-through from the reverse side of the page. The text is arranged in several paragraphs separated by horizontal lines. The content is mostly illegible due to low contrast and blurring.

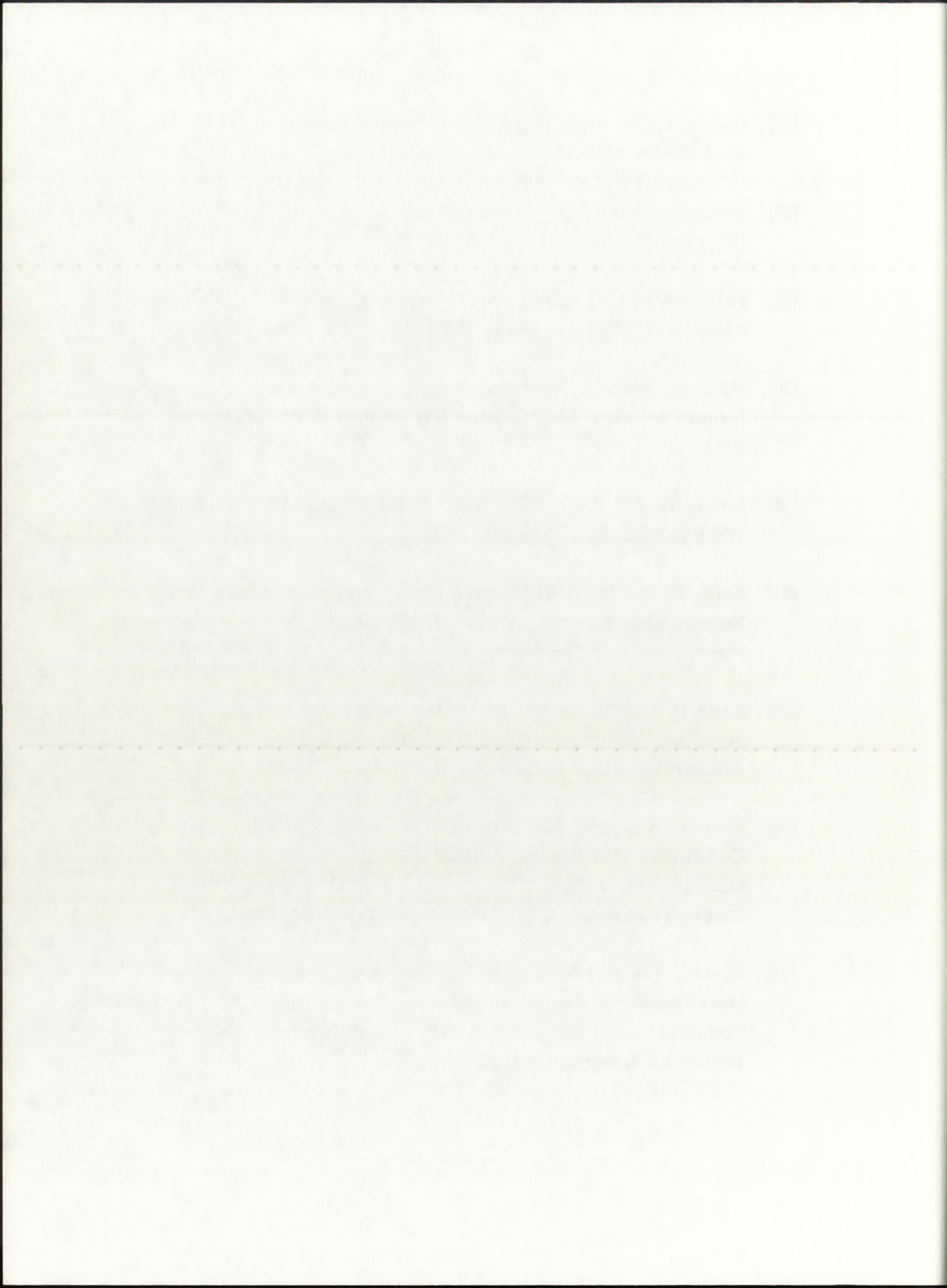
- [9] Borowski, S.K., "The LeRC Open-Cycle Gas Core Rocket Program - A Review," *Proc. Gas Core Nucl. Rocket Workshop*, LA-UR-91-1250, Boulder, CO, April 2-3, 1991.
- [10] Burwell, W., "Calculated Temperature Distributions in a Vortex-Stabilized Gaseous Nuclear Rocket Engine," Technical Report UAR-D53A, United Aircraft Research Laboratories, East Hartford, CT, March 1965.
- [11] Chilton, A.B. et al., "Principles of Radiation Shielding," Prentice-Hall Inc., Englewood Cliffs, NJ, 1984.
- [12] Clark, J.W. and G.H. McLafferty, "Summary of Research on the Nuclear Light Bulb Reactor," NASA SP-236, *Proc. Symp. Res. Uran. Plas. Tech. Appl.*, Gainesville, FL, January 7-8, 1970.
- [13] CRC Press, "CRC Handbook of Chemistry and Physics," 71st Ed., CRC Press, Boca Raton, FL, 1990-91.
- [14] Diaz, N.J., S. Anghaie, E.T. Dugan, and I. Maya, "Status of Gas Core Reactor Research," *Proc. Gas Core Nucl. Rocket Workshop*, LA-UR-91-1250, Boulder, CO, April 2-3, 1991.
- [15] Duderstadt, J. and E. Hamilton, "Nuclear Reactor Analysis," McGraw-Hill, New York, NY, 1990.
- [16] Ellerbrock, H.H., J.N.B. Livingood, and D.M. Straight, "Fluid-Flow and Heat-Transfer Problems in Nuclear Rockets," *Proc. NASA-Univ. Conf. on the Science and Technol. of Space Explor.*, NASA SP-11, Chicago, IL, November 1-3, 1962.
- [17] El-Wakil, M.M., "Nuclear Heat Transport," American Nuclear Society, La Grange Park, IL, 1981.



- [18] Etter, D.M., "Structured FORTRAN 77 For Engineers and Scientists," 2nd Ed., The Benjamin/Cummings Publishing Co., Menlo Park, CA, 1987.
- [19] Everett, C.J. and S.M. Ulam, "On a Method of Propulsion of Projectiles by Means of External Nuclear Explosions," Report LAMS-1955, Los Alamos Scientific Laboratory, Los Alamos, NM, August 1955.
- [20] Gauntt, R.O., (1992a), "Development of a Closed-cycle Gas Core Nuclear Thermal Propulsion System," Sandia National Laboratories Laboratory Directed Research and Development (LDRD) Proposal, September 1992.
- [21] Gauntt, R.O. et al., (1992b) "In-Reactor Tests of the Nuclear Light Bulb Rocket Concept," AIAA Paper No. 92-3816, *Proc. AIAA/SAE/ASME/ASEE 28th Joint Propul. Conf. and Exh.*, July 6-9, 1992, Nashville, TN.
- [22] Gauntt, R.O. et al., "In-Reactor Testing of the Closed Cycle Gas Core Reactor - The Nuclear Light Bulb Concept," *Proc. 10th Symp. Space Nucl. Pwr. and Propul.*, Albuquerque, NM, January 10-14, 1993.
- [23] General Electric Co., "Chart of the Nuclides," GE Co., Schenectady, NY, 1989.
- [24] Gieck, R. and M. Gieck, "Handbook of Engineering Formulas," J.Wiley & Sons, New York, NY, 1990.
- [25] Gurfink, M.M., "Gas Core Nuclear Thermal Rocket Engine Research and Development in the Former USSR," EGG-NE-10391, EG&G Idaho, Idaho Falls, ID, September 1992.
- [26] Harris, J.N., E.A. Welsh, and J.H. Murphy, "Fused Silica Design Manual," Tech. Report No. 4, Contract # N00017-70-C-4438 with Naval Ordnance Systems Command, Engineering Experiment Station, Georgia Institute of Technology, Atlanta, GA, June 1972.



- [27] Helms, I., "A Look at Alternative Propulsion Systems," *Proc. Gas Core Nucl. Rocket Workshop*, LA-UR-91-1250, Boulder, CO, April 2-3, 1991.
- [28] Heraeus-Amersil Corporation, "Quartz Glass for Optics - Data and Properties," Heraeus-Amersil Inc., Duluth, GA, 1993.
- [29] Hill, P. and C. Peterson, "Mechanics and Thermodynamics of Propulsion," Addison-Wesley Publishing Co., Reading, MA, 1965.
- [30] Hill, P. and C. Peterson, "Mechanics and Thermodynamics of Propulsion," 2nd Ed., Addison-Wesley Publishing Co., Reading, MA, 1992.
- [31] Incropera, F.P. and D.P. DeWitt, "Introduction to Heat Transfer," John Wiley & Sons, New York, NY, 1990.
- [32] Kelm, S. and W. Peschka, "Radiation Transport in a Uranium Plasma Reactor with Reflecting Walls," NASA SP-236, *Proc. Symp. Res. Uran. Plasmas and their Tech. Appl.*, Gainesville, FL, January 7-8, 1970.
- [33] Kendall, J.S., "Investigation of Gaseous Nuclear Rocket Technology - Summary Technical Report," Technical Report L-910905-13, United Aircraft Research Laboratories, East Hartford, CT, September 1972.
- [34] Kesten, A.S. and R.B. Kinney, "Theoretical Effect of Changes in Constituent Opacities on Radiant Heat Transfer in a Vortex-Stabilized Gaseous Nuclear Rocket," Technical Report D-910092-5, United Aircraft Research Laboratories, East Hartford, CT, September 1965.
- [35] Kesten, A.S. and N.L. Krascella, "Theoretical Investigation of Radiant Heat Transfer in the Fuel Region of a Gaseous Nuclear Rocket Engine," Technical Report E-910092-9, United Aircraft Research Laboratories, East Hartford, CT, September 1966.



- [36] Kinney, R.B., "Theoretical Effect of Seed Opacity and Turbulence on Temperature Distributions in the Propellant Region of a Vortex-Stabilized Gaseous Nuclear Rocket," Technical Report E-910092-8, United Aircraft Research Laboratories, East Hartford, CT, September 1966.
- [37] Krascella, N.L., "Theoretical Investigation of Spectral Opacities of Hydrogen and Nuclear Fuel," Technical Documentary Report RTD-TDR-63-1101, United Aircraft Research Laboratories, East Hartford, CT, November 1963.
- [38] Krascella, N.L., "Theoretical Investigation of the Radiant Emission Spectrum from the Fuel Region of a Nuclear Light Bulb Engine," Technical Report H-910092-12, United Aircraft Research Laboratories, East Hartford, CT, October 1969.
- [39] Krascella, N.L., "Analytical Study of the Spectral Radiant Flux Emitted from the Fuel Region of a Nuclear Light Bulb Engine," Technical Report J-910904-1, United Aircraft Research Laboratories, East Hartford, CT, September 1970.
- [40] Krascella, N.L., "Spectral Absorption Coefficients of Helium and Neon Buffer Gases and Nitric Oxide-Oxygen Seed Gas Mixture," Technical Report K-910904-2, United Aircraft Research Laboratories, East Hartford, CT, September 1971.
- [41] Krascella, N.L., "Spectral Absorption Coefficients of Argon and Silicon and Spectral Reflectivity of Aluminum," Technical Report L-910904-3, United Aircraft Research Laboratories, East Hartford, CT, September 1972.
- [42] Lamarsh, J.R., "Introduction to Nuclear Engineering," 2nd Ed., Addison-Wesley Publishing Co., Reading, MA, 1983.

[15] Kinsley, J.A. "Theoretical Study of Seed Quality and Temperature-Responsive Characteristics in the Proximal Region of a Vapor-Phase Evaporator." Technical Report R-1000-2, United Aircraft Research Laboratories, East Hartford, CT, September 1955.

[16] Kinsley, J.A. "Theoretical Investigation of Spectral Properties of Hydrogen and Nitrogen Fuel." Technical Document Report RTR-65-1101, United Aircraft Research Laboratories, East Hartford, CT, November 1953.

[17] Kinsley, J.A. "Theoretical Investigation of the Radiation Emission Spectrum from the Fuel Region of a Nuclear Light Bulb Engine." Technical Report R-1000-11, United Aircraft Research Laboratories, East Hartford, CT, October 1955.

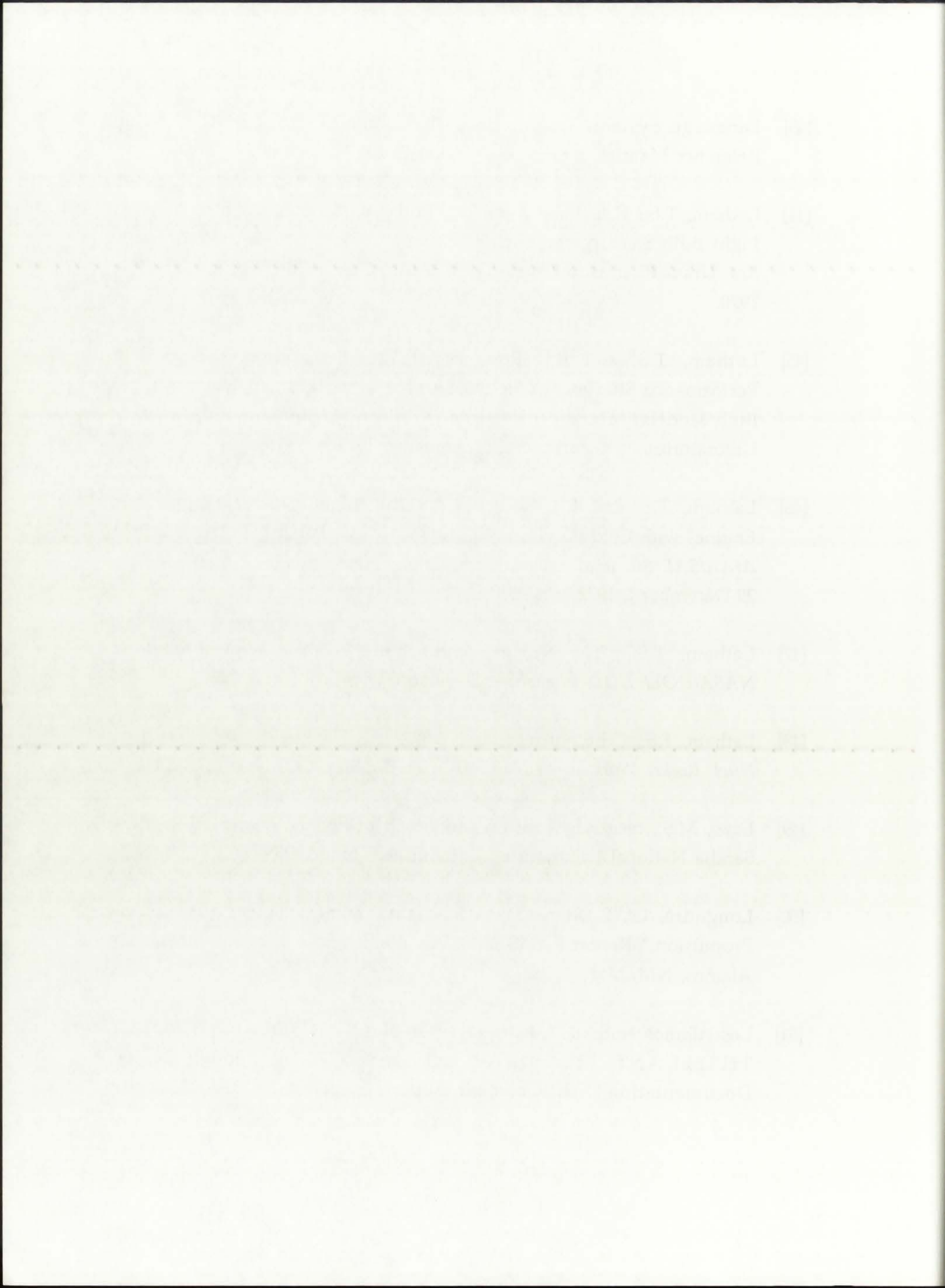
[18] Kinsley, J.A. "Analytical Study of the Spectral Radiation Flux Density from the Fuel Region of a Nuclear Light Bulb Engine." Technical Report R-1000-11, United Aircraft Research Laboratories, East Hartford, CT, September 1955.

[19] Kinsley, J.A. "Spectral Properties of Hydrogen and Nitrogen Fuel." Report R-1000-11, United Aircraft Research Laboratories, East Hartford, CT, September 1955.

[20] Kinsley, J.A. "Spectral Properties of Hydrogen and Nitrogen Fuel." Report R-1000-11, United Aircraft Research Laboratories, East Hartford, CT, September 1955.

[21] Laminar, J.K. "Introduction to Nuclear Engineering," 2nd Ed., Addison-Wesley Publishing Co., Reading, MA, 1963.

- [43] Language Systems Corporation, "Language Systems FORTRAN 3.0 Reference Manual," Language Systems Corp., Herndon, VA, 1992.
- [44] Latham, T.S., H.E. Bauer, and R.J. Rodgers, "Investigation of Nuclear Light Bulb Startup and Engine Dynamics," NASA SP-236, *Proc. Symp. Res. Uran. Plasmas and their Tech. Appl.*, Gainesville, FL, January 7-8, 1970.
- [45] Latham, T.S. and R.J. Rodgers, (1972a) "Analytical Design and Performance Studies of Nuclear Furnace Tests of Small Nuclear Light Bulb Models," Technical Report L-910900-17, United Aircraft Research Laboratories, East Hartford, CT, September 1972.
- [46] Latham, T.S. and R.J. Rodgers, (1972b) "Small Nuclear Light Bulb Engines with Cold Beryllium Reflectors," AIAA Paper No. 72-1093, *Proc. AIAA/SAE 8th Joint Propul. Spec. Conf.*, New Orleans, LA, November 29-December 1, 1972.
- [47] Latham, T.S., "The Nuclear Light Bulb," *Nucl. Therm. Propul. Jt. NASA/DOE/ DOD Workshop*, Cleveland, OH, July 10-12, 1990.
- [48] Latham, T.S., "The Nuclear Light Bulb," LA-UR-91-1250, *Proc. Gas Core Nucl. Rocket Workshop*, LA-UR-91-1250, Boulder, CO, April 2-3, 1991.
- [49] Lazo, M.S., research work on processing of ENDF/VI and NJOY data, Sandia National Laboratories, unpublished, June 1993.
- [50] Longmire, C., F. Reines, and S. Ulam, "Some Schemes for Nuclear Propulsion," Report LAMS-2186, Los Alamos Scientific Laboratory, Los Alamos, NM, March 1958.
- [51] Los Alamos National Laboratory, "ONEDANT, TWODANT, TWOHEX, THREEDANT, TWODANT/GQ and ORION Code System Documentation," Unpublished Report prepared by X-6 Radiation



- Transport Group, Los Alamos National Laboratory, Los Alamos, NM, 1993.
- [52] McFarlane, R., "NJOY Nuclear Cross-Section Processing System, Version 91.38," Unpublished Report, Los Alamos National Laboratory, Los Alamos, NM, May 1992.
- [53] McFarlane, R., "TRANSX2: A Nuclear Processing System for MATXS Files," Unpublished Report, Los Alamos National Laboratory, Los Alamos, NM, December 1993.
- [54] McLafferty, G.H., "Summary of Investigations of a Vortex-Stabilized Gaseous Nuclear Rocket Concept," Technical Documentary Report RTD-TDR-63-1097, United Aircraft Research Laboratories, East Hartford, CT, November 1963.
- [55] McLafferty, G.H. and H.E. Bauer, "Studies of Specific Nuclear Light Bulb and Open-Cycle Vortex-Stabilized Gaseous Nuclear Rocket Engines," Technical Report F-910093-37, United Aircraft Research Laboratories, East Hartford, CT, September 1967.
- [56] Mensing, A., T. Latham, and W. Roman, "Gas Core Nuclear Rocket Technology - Revisited," AIAA Paper No. 90-3790, *Proc. AIAA Space Prog. and Technq. Conf.*, September 25-28, Huntsville, AL, 1990.
- [57] Morley, N.J., "Thermalhydraulic Analysis of the Pellet-Bed Reactor," Ph.D. Dissertation, University of New Mexico, Albuquerque, NM, December 1993.
- [58] Motloch, C., R. Bennett, R. Johnson, and B. Schnitzler, "Gas Core Reactor R&D at INEL," *Proc. Gas Core Nucl. Rocket Workshop*, LA-UR-91-1250, Boulder, CO, April 2-3, 1991.

Transport Group for Alaska National Laboratory, Los Alamos, NM
1961

[20] McLaughlin, R. "NJOY Nuclear Cross-Section Processing System,"
Version 1.88, Unpublished Report for Alaska National Laboratory,
Los Alamos, NM, May 1981.

[21] McLaughlin, R. "TRANSX: A Nuclear Processing System for MATX
Files," Unpublished Report for Alaska National Laboratory, Los
Alamos, NM, December 1981.

[22] McLaughlin, G.H. "Summary of Investigations in a Vapor-Scattered
Gasoline Nuclear Rocket Concept," Technical Document, Report
STD-TDR 63-107, United States Research Laboratories, East Hartford,
CT, December 1963.

[23] McLaughlin, G.H. and H.E. Wiser, "Studies of Spectral Nuclear Light Bulbs
and Open-Cycle Vapor-Scattered Gasoline Nuclear Rocket Engines,"
Technical Report F-81002-7, United States Research Laboratories,
East Hartford, CT, September 1967.

[24] Minton, A. "Laser and X-Ray Sources for Nuclear Rocket
Technology - Research," AIAA Paper No. 80-270, June AIAA 80th
Propulsion Conference, September 22-26, Huntsville, AL, 1980.

[25] Mohr, W.J. "Thermodynamic Analysis of the Rocket-Bed Reactor,"
Ph.D. Dissertation, University of New Mexico, Albuquerque, NM,
December 1967.

[26] Mottel, C., R. Bennett, R. Johnson, and R. Schmittler, "Gas Core
Reactor Bed at INEL," Final Gas Core Reactor Workshop, LA-UR-
81-104, Lockheed CO, April 2-3, 1981.

- [59] Munson, B.R., D.F. Young, and T.H. Okiishi, "Fundamentals of Fluid Mechanics," J. Wiley & Sons, New York, NY, 1990.
- [60] O'Dell et al., "Revised User's Manual for ONEDANT: A Code Package for One-Dimensional, Diffusion-Accelerated, Neutral-Particle Transport," LA-9184-M, Los Alamos National Laboratory, Los Alamos, NM, December 1989.
- [61] Parks, D.E., et al., "Optical Constants of Uranium Plasma," NASA CR-72348/GA-8244, Gulf General Atomic Inc., San Diego, CA, February 2, 1968.
- [62] Patch, R.W., "Status of Opacity Calculations for Application to Uranium-Fueled Gas-Core Reactors," NASA SP-236, *Proc. Symp. Res. Uran. Plasmas and their Tech. Appl.*, Gainesville, FL, January 7-8, 1970.
- [63] Penner, S.S., "Advanced Propulsion Techniques," Pergamon Press, Oxford, England, 1961.
- [64] Poston, D.I. and T. Kammash, "Heat Transfer Model for an Open-Cycle Gas Core Nuclear Rocket" *Proc. 9th Symp. Space Nucl. Pwr. and Propul.*, Albuquerque, NM, January 11-14, 1992.
- [65] Poston, D.I. and T. Kammash, (1994a) "A Comprehensive Thermal-hydraulic Model of an Open-Cycle Gas Core Nuclear Rocket," *Proc. 11th Symp. Space Nucl. Pwr. and Propul.*, Albuquerque, NM, January 11-14, 1994.
- [66] Poston, D.I. and T. Kammash, (1994b) "Hydrodynamic Fuel Containment in an Open-Cycle Gas Core Nuclear Rocket," *Proc. 11th Symp. Space Nucl. Pwr. and Propul.*, Albuquerque, NM, January 11-14, 1994.

[97] Mamon, G.L., G.L. Yehou, and L.L. Gittel. *Thermodynamics of Fluids*. McGraw-Hill, New York, 1960.

[98] O'Neil, J.R. *Advanced User's Manual for ONCART: A Code Package for One-Dimensional, Diffusion-Reaction, Neutral-Particle Transport*. NASA-SP-70-103, NASA Langley Research Center, Hampton, VA, December 1969.

[99] Pitzer, D.E. et al. "Optical Constants of Uranium Fluoride". NASA CR 72548 (CR-824). Goddard Space Flight Center, San Diego, CA, February 1, 1970.

[100] Price, R.W. *Statistical Quality Calculations for Applications to Reactor-Cooled Gas-Core Reactors*. NASA SP-734, Goddard Space Flight Center, Hampton, VA, July 1970.

[101] Pruefer, S.P. *Advanced Population Techniques*. Pergamon Press, Oxford, England, 1961.

[102] Poston, D.L. and T. Kaminaga. "Heat Transfer Model for an Open-Cycle Gas Core Nuclear Reactor". *Proc. 9th Space Reactor Fuel and Propulsion Conference*, Albuquerque, NM, January 11-14, 1974.

[103] Poston, D.L. and T. Kaminaga. (1974a). "A Comparative Thermal-Hydraulic Model of an Open-Cycle Gas Core Nuclear Reactor". *Proc. 11th Space Reactor Fuel and Propulsion Conference*, Albuquerque, NM, January 11-14, 1974.

[104] Poston, D.L. and T. Kaminaga. (1974b). "Hydrodynamic Fuel Distribution in an Open-Cycle Gas Core Nuclear Reactor". *Proc. 11th Space Reactor Fuel and Propulsion Conference*, Albuquerque, NM, January 11-14, 1974.

- [67] Pruvost, N.R. and M.L. Prueitt, "The Hansen-Roach Cross-Sections," LALP-88-20, Los Alamos National Laboratory, Los Alamos, NM, October 1988.
- [68] Ragsdale, R.G., "Relationship Between Engine Parameters and the Fuel Mass Contained in An Open-Cycle Gas-Core Reactor," NASA SP-236, *Proc. Symp. Res. Uran. Plasmas and their Tech. Appl.*, Gainesville, FL, January 7-8, 1970.
- [69] Ragsdale, R., "Open-Cycle Gas Core Nuclear Rockets," *Nucl. Therm. Propul. Jt. NASA/DOE/ DOD Workshop*, Cleveland, OH, July 10-12, 1990.
- [70] Randol, A.G., R.T. Schneider, and C.D. Kylstra, "Boiling Point of Uranium," NASA SP-236, *Proc. Symp. Res. Uran. Plasmas and their Tech. Appl.*, Gainesville, FL, January 7-8, 1970.
- [71] Riggs, J.B., "An Introduction to Numerical Methods for Chemical Engineers," Texas Tech University Press, Lubbock, TX, 1988.
- [72] Rodgers, R.J., T.S. Latham, and H.E. Bauer, "Analytical Studies of Nuclear Light Bulb Engine Radiant Heat Transfer and Performance Characteristics," Technical Report K-910900-10, United Aircraft Research Laboratories, East Hartford, CT, September 1971.
- [73] Rodgers, R.J. and T.S. Latham, "Analytical Design and Performance Studies of the Nuclear Light Bulb Engine," Technical Report L-910900-16, United Aircraft Research Laboratories, East Hartford, CT, September 1972.
- [74] Rom, F.E. and R.G. Ragsdale, "Advanced Concepts for Nuclear Rocket Propulsion," *Proc. NASA-Univ. Conf. on the Science and Technol. of Space Explor.*, NASA SP-11, Chicago, IL, November 1-3, 1962.

[The page contains extremely faint, illegible text, likely bleed-through from the reverse side of the document. The text is too light to transcribe accurately.]

- [75] Schnitzler, B.G., "Gas Core Reactors for Direct Nuclear Propulsion," *Proc. 4th Symp. Space Nucl. Pwr. and Propul.*, Albuquerque, NM, January 11-14, 1988.
- [76] Schwenk, F.C. and C.E. Franklin, "Comparison of Closed-Cycle and Open-Cycle Systems," NASA SP-236, *Proc. Symp. Res. Uran. Plasmas and their Tech. Appl.*, Gainesville, FL, January 7-8, 1970.
- [77] Siegel, R. and J.R. Howell, "Thermal Radiation Heat Transfer," 3rd Ed., Hemisphere Publishing Corporation, Washington, DC, 1992.
- [78] Sparrow, E.M. and R.D. Cess, "Radiation Heat Transfer," Augmented Ed., Hemisphere Publishing Corp., Washington, DC, 1978.
- [79] Sutton, G.P., "Rocket Propulsion Elements - An Introduction to the Engineering of Rockets," 6th Ed., John Wiley & Sons, New York, NY, 1992.
- [80] Tabor, D., "Gases, Liquids, and Solids and Other States of Matter," 3rd Ed., Cambridge Univ. Press, Cambridge, Gt. Britain, 1991.
- [81] Tam, C.K.W., D.B. Goracke, and W.S. Lewellen, "Stability Considerations for a Transparent Wall in a Gaseous Nuclear Rocket," NASA SP-236, *Proc. Symp. Res. Uran. Plasmas and their Tech. Appl.*, Gainesville, FL, January 7-8, 1970.
- [82] Tanner, J.E., "Improved Gas-Core Propulsion Model," *Proc. 11th Symp. Space Nucl. Pwr. and Propul.*, Albuquerque, NM, January 11-14, 1994.
- [83] Thom, K., R.T. Schneider, and F.C. Schwenk, "Physics and Potentials of Fissioning Plasmas for Space Power and Propulsion," *Proc. Internat. Astronaut. Federat. XXVth Congress*, Amsterdam, Netherlands, 30 September - 5 October, 1974.

1. Introduction

2. Methodology

3. Results

4. Discussion

5. Conclusion

6. References

7. Appendix

8. Acknowledgments

9. Contact Information

10. Author Biographies

11. Declaration of Interest

12. Funding Sources

13. Data Availability

14. Ethics Approval

15. Supplementary Materials

16. Correspondence

17. Peer Review

18. Publication History

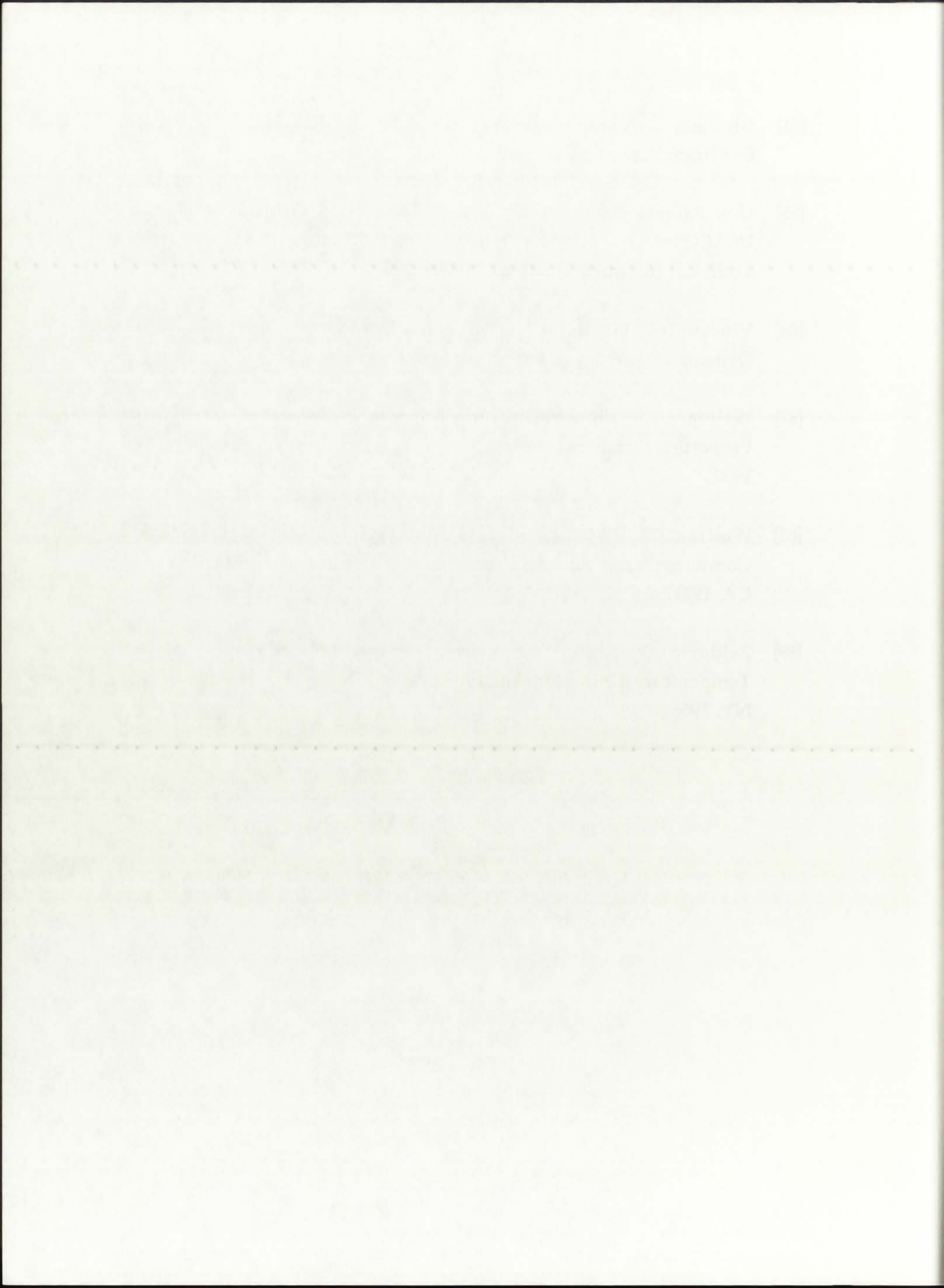
19. Copyright

20. Terms and Conditions

21. Disclaimer

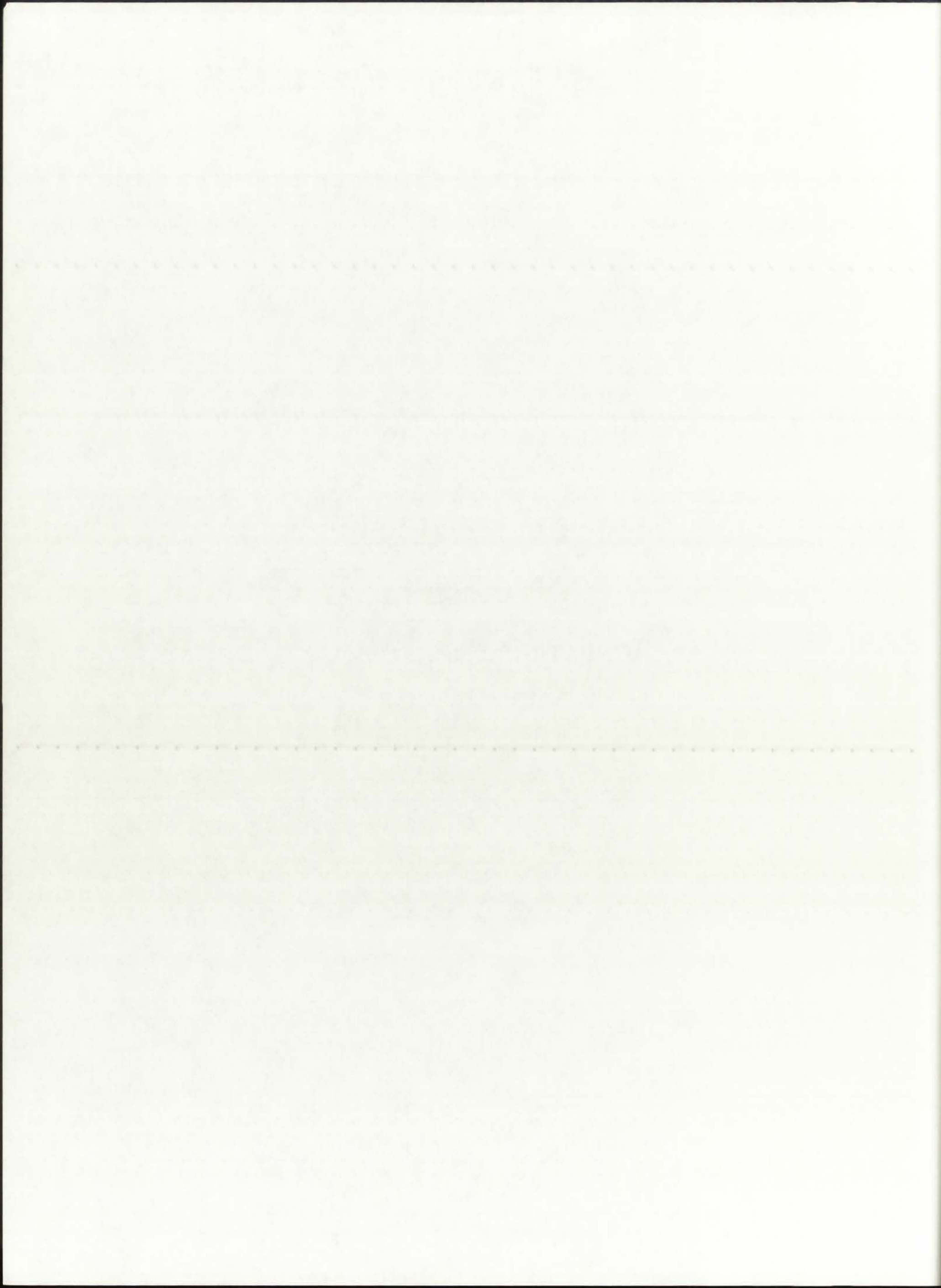
22. Final Remarks

- [84] Ultramet Corporation, "Advanced Materials - CVD/CVI," Corporate Brochure, Pacoima, CA, 1992.
- [85] U.S. Atomic Energy Commission, "Nuclear Propulsion for Space," USAEC booklet, "Understanding the Atom" series, USAEC Division of Technical Information Extension, Oak Ridge, TN, May 1967.
- [86] Vincenti, W.G. and C.H. Kruger, "Introduction to Physical Gas Dynamics," J. Wiley & Sons, New York, NY, 1965.
- [87] Walton, J.T., "NBS+-PH2: National Bureau of Standards Parahydrogen Properties Database," NASA Lewis Research Center, Cleveland, OH, 1992.
- [88] Wolfram, S., "Mathematica: A System for Doing Mathematics by Computer," 2nd Ed., Addison-Wesley Publishing Co., Redwood City, CA, 1991.
- [89] Zeldovich, Ya.B. and Yu.P. Raizer, "Physics of Shock Waves and High-Temperature Hydrodynamic Phenomena," Academy Press, New York, NY, 1966.



APPENDIX A

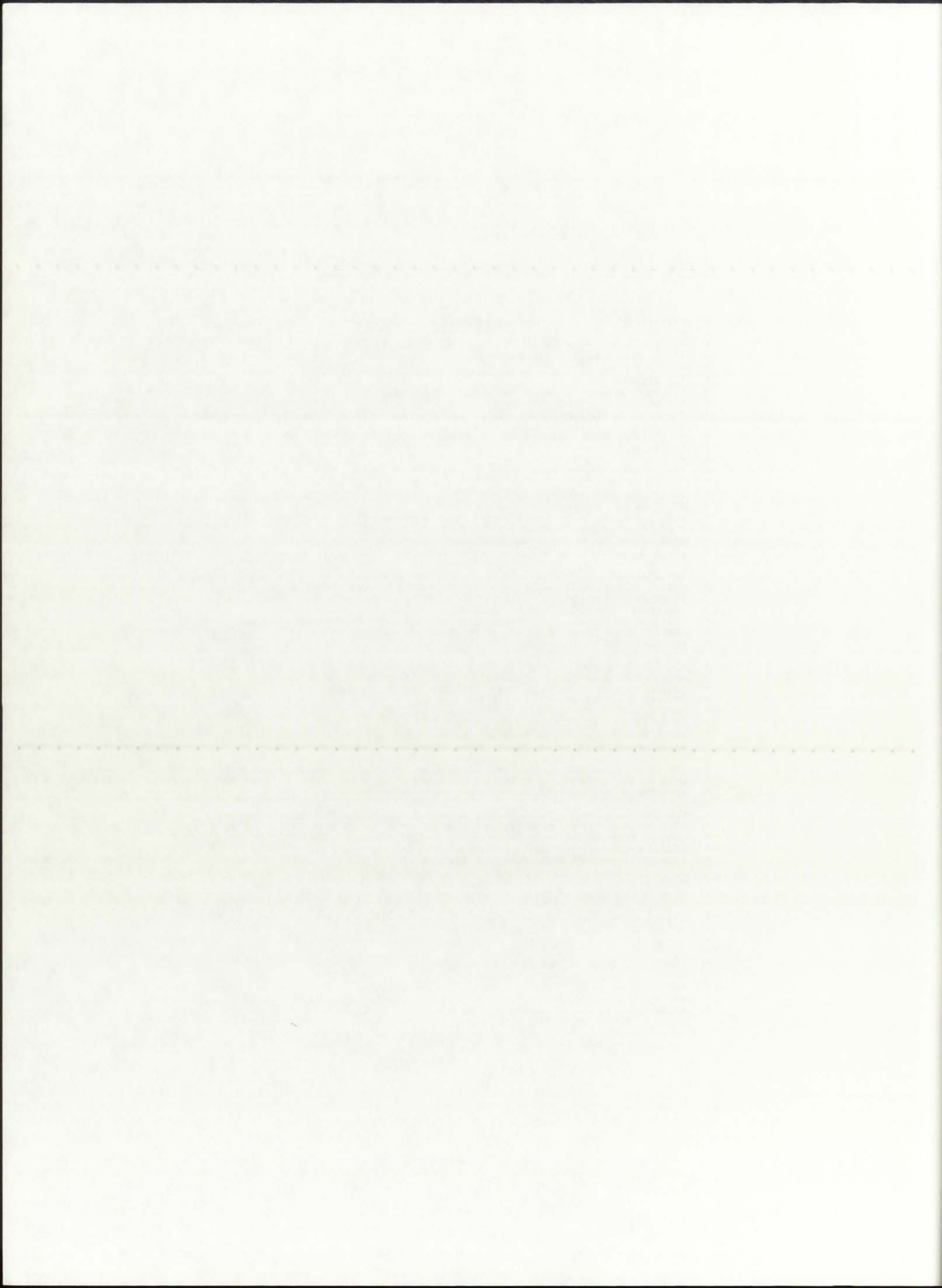
GNRATR-1D.f Source Code Listing



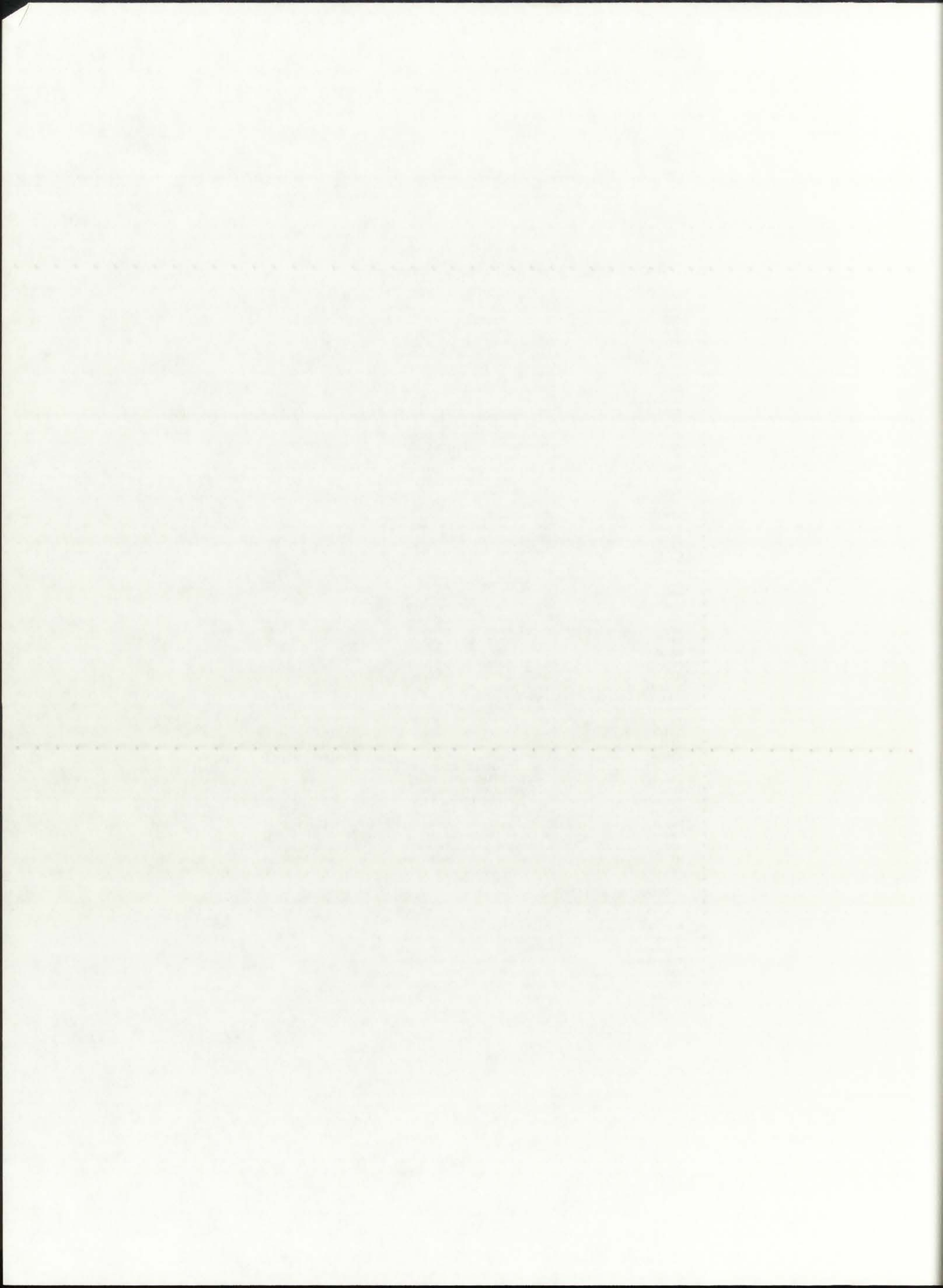
```

*
* *****
* *
* * Gas-Core Nuclear Rocket Analysis by Thermal Radiation * *
* * in One Dimension: GNRATR-1D * *
* *
* * Vojislav Banjac * *
* * Department of Chemical and Nuclear Engineering * *
* * University of New Mexico * *
* * Albuquerque, NM 87131 * *
* *
* * Date of First Compilation: November 1, 1993 * *
* * Version 1.2 * *
* *
* *****
*
* GNRATR-1D is a steady-state, one-dimensional heat transfer code
* designed for analyzing the Nuclear Light Bulb (NLB) gaseous core
* rocket engine. It uses a finite-difference numerical solution to
* the diffusion approximation of the radiation transport equation,
* along with convection, conduction, and generation, to determine
* the temperature distribution in the r-direction.
*
* The analysis method relies on an energy balance equation at each
* node. A Gauss-Seidel iteration scheme is used to accelerate the
* numerical convergence. A detailed discussion of the methodology
* and applicable theory can be found in the Dissertation based on
* this code: Banjac, V.: "Thermalhydraulics Analysis of the Unit
* -Cell Nuclear Light Bulb Gas Core Rocket Engine," University of
* New Mexico, Albuquerque, NM.
*
* The GNRATR-1D code allows for the "switching on and off" of the
* modes of heat transfer in the buffer gas, silica wall, and pro-
* pellant regions. This feature allows the user to determine the
* effects on temperature of radiative, convective, and conductive
* heat transfer. For example, by alternately switching off conve-
* ction in the buffer gas and propellant, the user can determine
* which heat transfer mode has the greatest effect on the silica
* wall temperature.
*
* The code is designed to be user-modifiable, and all pertinent
* data can be varied. On the basis of converged T(r) distribution,
* the code determines applicable rocket performance parameters.
*
* The code consists of 7 modules: program MAIN and subroutines RMO,
* HTCP, HTCGB, ROCKET, HYDROGEN, and TRANSMIT. The subroutines are
* used to provide MAIN with the appropriate thermophysical proper-
* ties for use in the model. The subroutines are explained in the
* subroutine headers as part of this listing.
*
* DATE OF FIRST COMPILATION: November 1, 1993
* DATE OF LAST MODIFICATION: November 15, 1994
*
* -----
* DEFINITION OF VARIABLES USED IN GNRATR-1D:
* -----
*
* aRrF ..... Fuel/Buffer gas RMO ..... [1/m]
* aRBG ..... Buffer gas RMO ..... [1/m]
* aRF ..... Fuel RMO ..... [1/m]
* aRP ..... Propellant RMO ..... [1/m]
* aRSiW ..... Silica wall RMO ..... [1/m]

```



*	dArF	Fuel/BG node thickness	[m]
*	dAS	Ambient space node thickness	...	[m]
*	dBG	BG node thickness	[m]
*	dBe	Beryllium node thickness	[m]
*	dD	Heavy water node thickness	[m]
*	dF	Fuel region node thickness	[m]
*	dP	Propellant node thickness	[m]
*	dSiW	Silica wall node thickness	[m]
*	dSS	Stainless steel node thickness	..	[m]
*	Dhydraul	Propellant hydraulic diameter	..	[m]
*	eps	User convergence criterion	
*	epsAS	Convergence test in amb. space	..	
*	epsBe	Convergence test in beryllium	..	
*	epsF	convergence test in fuel	
*	F	Rocket engine ideal thrust	[N]
*	hBG	Buffer gas heat transfer coeff	..	[W/m2-K]
*	hP	Propellant heat transfer coeff	..	[W/m2-K]
*	h(i)	heat transfer coeff at node i	..	[W/m2-K]
*	i	r-dimension nodal point	
*	itr	iteration counter	
*	iters	User max. no. of iterations	
*	jtr	Auxiliary counter	
*	kcond_	Thermal conductivity of _	[W/m-K]
*	kradAS	Eff. rad. conductivity of AS	...	[W/m-K]
*	nArF	No. of nodes in region ArF	
*	nAS	No. of nodes in region AS	
*	nBe	No. of nodes in region Be	
*	nBG	No. of nodes in region BG	
*	nD	No. of nodes in region D	
*	nF	No. of nodes in region F	
*	nP	No. of nodes in region P	
*	nSiW	No. of nodes in region SiW	
*	nSS	No. of nodes in region SS	
*	n_	Cumulative no. of nodes to _	...	
*	ntotal	Total number of nodes	
*	nnodes	(same as ntotal)	
*	nprntr	Auxiliary counter	
*	P	Engine operating pressure	[atm]
*	Qg(i)	Volum. heat gen. rate at i	[W/m3]
*	r(i)	radial position of i	[m]
*	sigma	Stefan-Boltzmann constant	[W/m2-k4]
*	t_	Total thickness of region _	[m]
*	T(i,itr)	Iteration temperature at i	[K]
*	Tbuffer	Buffer gas mean temperature	[K]
*	Tchamber	Exit channel temperature	[K]
*	Tprop	Propellant mean temperature	[K]
*	Twall	Silica wall mean temperature	...	[K]
*	Taux	Auxiliary temperature	[K]
*	vBG	Buffer gas axial velocity	[m/s]
*	vP	Propellant channel ex. vel.	[m/s]
*	Vexit	Ideal nozzle exit velocity	[m/s]
*					
*	SPECIAL VARIABLES:				
*	-----				
*					
*	Nonodes	No test nodes converged		
*	Onodes	One out of three test nodes converged		
*	Twonodes	Two out of three test nodes converged		
*	Threenodes	All three test nodes converged		
*	rad	Radiation heat transfer present		
*	BGconv	Convection present in buffer gas		
*	Pconv	Convection present in propellant		
*					




```

* -----
* -----

      program GNRATR_1D

      integer i,itr, iters, jtr, nprntr, nArF, nF, nBG, nSiW, nP, nBe, nD, nSS,
>      nAS, n1, n2, n3, n4, n5, n6, n7, n8, n9, ntotal, nnodes

      real  aArF, aRF, aRBG, aRSiW, aRP, kcondBe, kcondD, kcondSS, kcondSiW,
>      kradAS, eps, epsF, epsBe, epsAS, tArF, tF, tBG, tSiW, tP, tBe, tD,
>      tSS, tAS, dArF, dF, dBG, dSiW, dP, dBe, dD, dSS, dAS, Dhydraul, vP,
>      vBG, hP, hBG, T(50,2300), Tchamber, P, Tprop, Twall, Tbuffer

      double precision Qg(50), r(50), krad(50), h(50), reflBe, trnsmBe,
>      sigma, Vexit, F, Isp, Taux

      character*9 Nonodes, Onenodes, Twonodes, Threenodes
      character*5 BGSiWPr, BGc, Pc

      logical rad, BGconv, Pconv

* Open the Comprehensive and Summary Output Data Files.
* -----

      open(unit=11, file='GNRATR-1D.DAT', status='new')
      open(unit=12, file='1D.DAT', status='new')

* Set the region thicknesses of the regions in the model [meters].
* -----

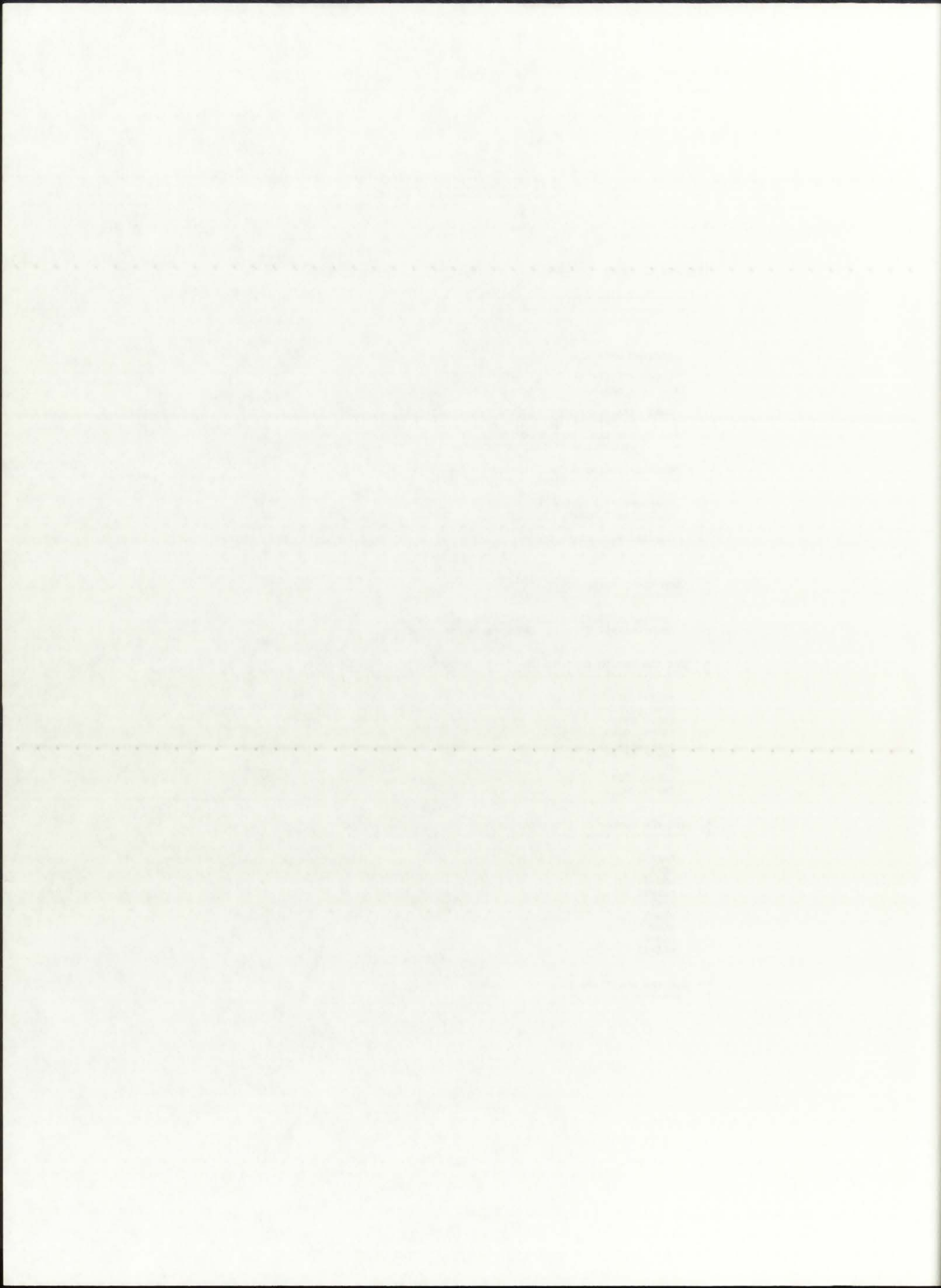
      tArF=0.06
      tF=0.1475
      tBG=0.037
      tSiW=0.0049
      tP=0.0424
      tBe=0.0578
      tD=0.48
      tSS=0.0508
      tAS=1.00

* Set the number of intervals in each region of the model.
* -----

      nArF=3
      nF=4
      nBG=2
      nSiW=2
      nP=2
      nBe=3
      nD=8
      nSS=2
      nAS=10

* Set the auxiliary interval number counters for easy tracking.
* -----

```



```
n1=nAS
n2=n1+nSS
n3=n2+nD
n4=n3+nBe
n5=n4+nP
n6=n5+nSiW
n7=n6+nBG
n8=n7+nF
n9=n8+nArF
ntotal=n9
```

* Set the total regions widths Δr [meters].

*

```
dArF=tArF/nArF
dF=tF/nF
DBG=tBG/nBG
dSiW=tSiW/nSiW
dP=tP/nP
dBe=tBe/nBe
dD=tD/nD
dSS=tSS/nSS
dAS=tAS/nAS
```

* Set the max. thermal conductivities of the solid regions [W/mK].

*

```
kradAS=0.022
kcondSS=34.0
kcondD=0.37
kcondBe=78.7
kcondSiW=4.00
```

* Set the total number of iterations for this run (maximum=2,300).

*

```
iters=xxxx
```

* Set the fraction of heat flux reflected off the Al-liner and the fraction incident on the edge-of-fuel node.

*

```
reflBe=x.xxx
trnsmBe=1.000-reflBe
```

* Set the total engine operating pressure [atm].

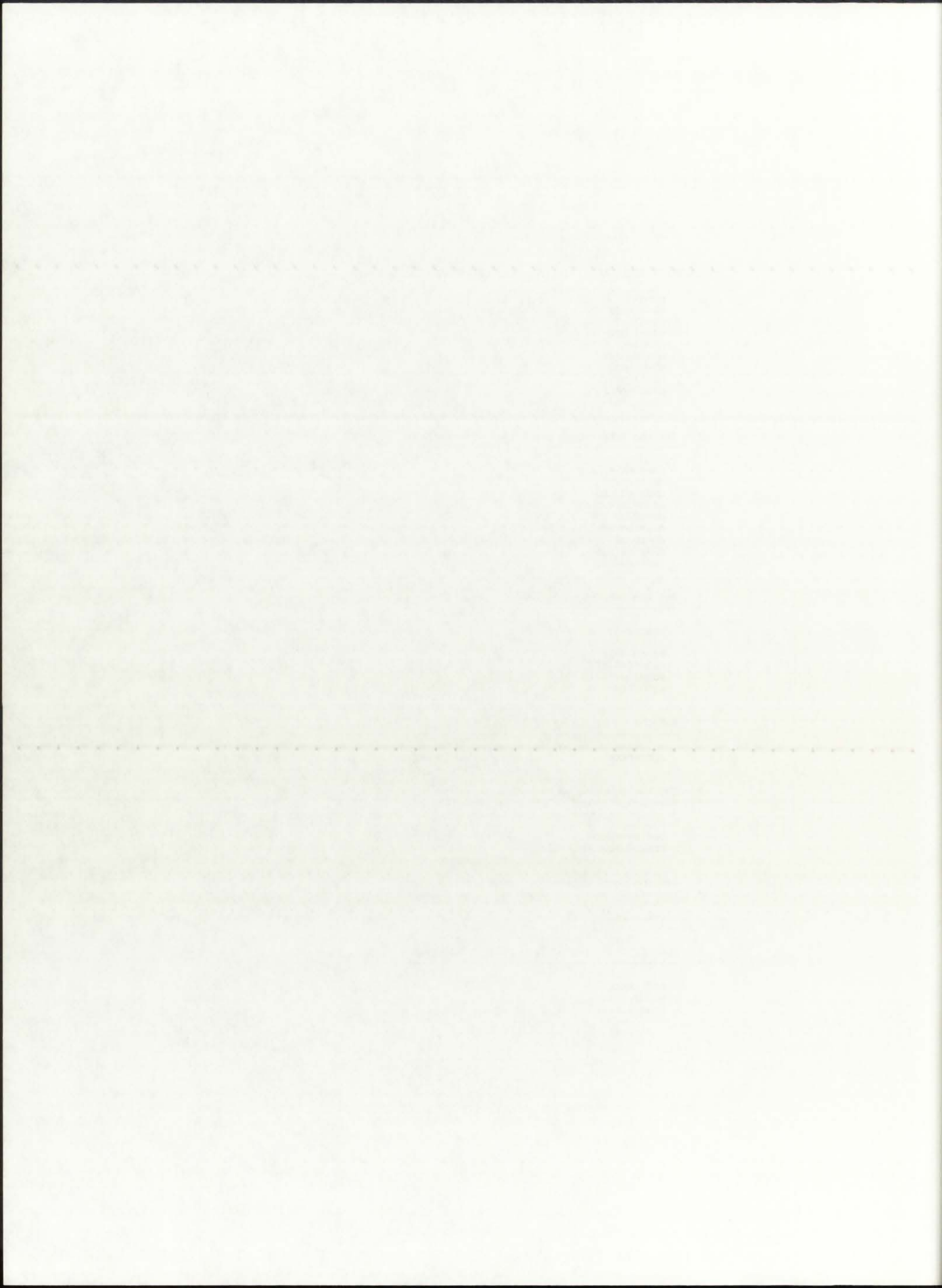
*

```
P=xxxx.x
```

* Specify which region is subject to which mode of heat transfer.

*

```
rad=.xxxx.
BGconv=.xxxx.
Pconv=.xxxx.
```



```
      if((.not.rad).and.(.not.BGconv).and.(.not.Pconv)) then
        write(6,8001)
8001    format(//,2x,'Sorry, you MUST specify at least ONE mode of heat',
>      ' transfer in the propellant and/or buffer gas regions!',/)
        stop
      endif

      if(rad) then
        BGSiWPr='.on.'
      else
        BGSiWPr='.off.'
      endif
      if(BGconv) then
        BGc='.on.'
      else
        BGc='.off.'
      endif
      if(Pconv) then
        Pc='.on.'
      else
        Pc='.off.'
      endif

* Set the inlet flow conditions and parameters. These values are
* needed only if BGconv=.true. and Pconv=.true. were specified.
* -----

      Dhydraul=0.0848
      vP=1.000
      vBG=20.00

* Specification of the three convergence labels.
* -----

      Nonodes = '** 0 **'
      Onenodes = '** 1 **'
      Twonodes = '** 2 **'
      Threenodes = '** 3 **'

* Specify the Stefan-Boltzmann Constant [W/m2-K4].
* -----

      sigma=5.67e-8

* Specify the initial iteration step counter for 0-th iteration.
* -----

      itr=1

* Specify the constant outer boundary temperature [T(1,t)=200 K].
* -----

      do 10 jtr=1, iters
        T(1,jtr)=200.
10    continue
```

MEMORANDUM FOR THE RECORD

On 10/10/54, the following information was received from the [redacted] regarding the [redacted] of [redacted] in [redacted] on [redacted].

The [redacted] was [redacted] by [redacted] and [redacted] on [redacted]. The [redacted] was [redacted] and [redacted] on [redacted]. The [redacted] was [redacted] and [redacted] on [redacted].

The [redacted] was [redacted] by [redacted] and [redacted] on [redacted]. The [redacted] was [redacted] and [redacted] on [redacted]. The [redacted] was [redacted] and [redacted] on [redacted].

The [redacted] was [redacted] by [redacted] and [redacted] on [redacted]. The [redacted] was [redacted] and [redacted] on [redacted]. The [redacted] was [redacted] and [redacted] on [redacted].

The [redacted] was [redacted] by [redacted] and [redacted] on [redacted]. The [redacted] was [redacted] and [redacted] on [redacted]. The [redacted] was [redacted] and [redacted] on [redacted].

```

* Specify the initial temperature distribution (for itr=1) [K].
* -----
* a) Solid regions, wholly dependent on the incoming heat flux.
  do 11 i=2,n1
    T(i,1)=T(i-1,1)+1.
11  continue

  do 12 i=n1+1,n4+1
    T(i,1)=T(i-1,1)+1.
12  continue

* b) Non-fuel radiative regions, with relatively flat profile.
*
*   do 13 i=n4+2,n7+1
*     T(i,1)=xxxxx.x
*13  continue

* c) Fuel region, characterized by an almost-constant profile.
*
*   do 14 i=n7+2,n8+1
*     T(i,1)=xxxxx.x
*14  continue

* d) Fuel/BG Mix. region, also with an almost-constant profile.
*
*   do 15 i=n8+2,ntotal+1
*     T(i,1)=xxxxx.x
*15  continue

* simple method, with linearly increasing initial distribution.
  do 13 i=n4+2,n8+1
    T(i,1)=T(i-1,1)+xxxxx.
13  continue

  do 14 i=n8+2,ntotal+1
    T(i,1)=T(i-1,1)-xxxxx.
14  continue

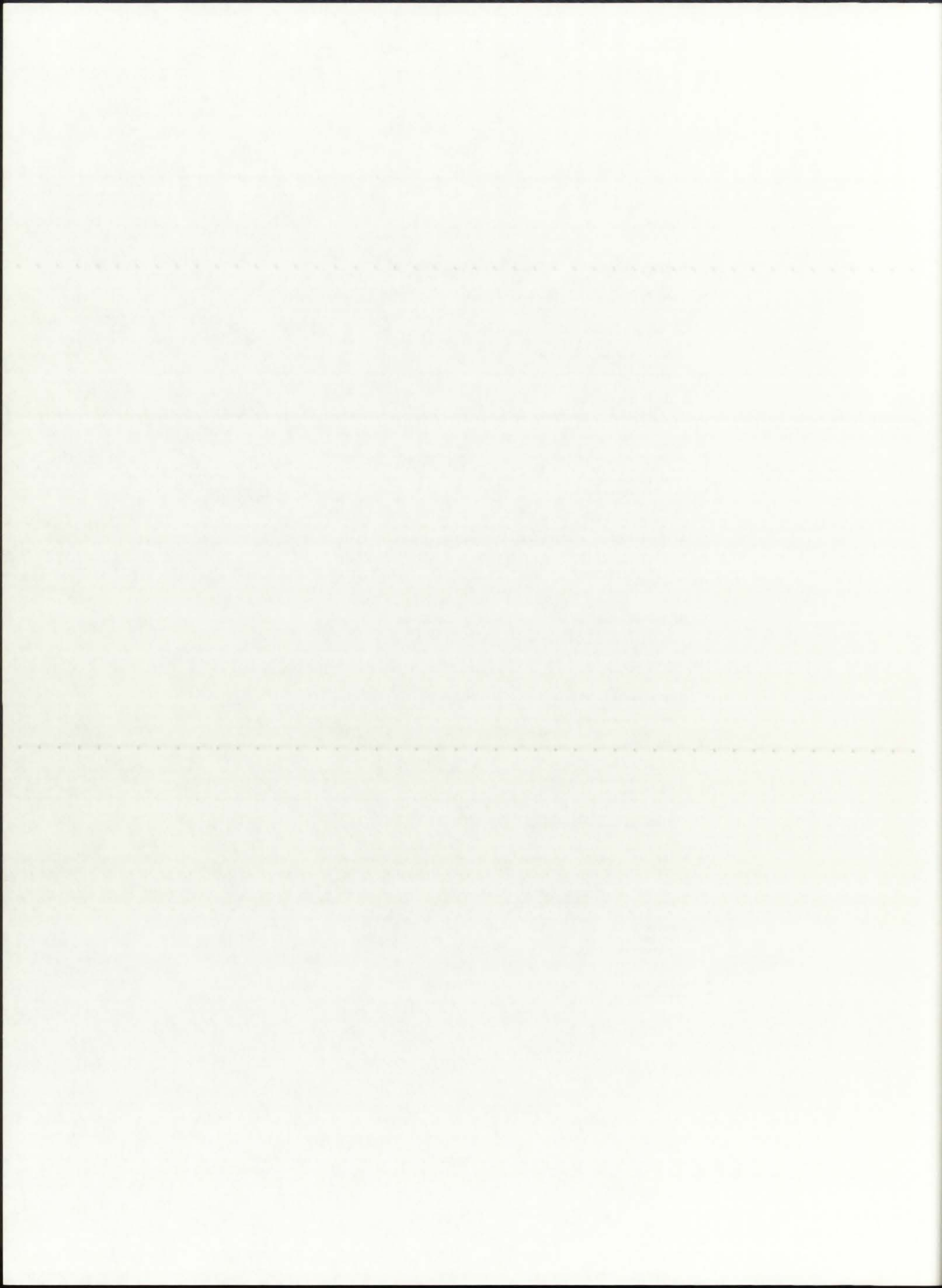
  T(ntotal+2,1)=T(ntotal,1)

* Write the header title into the output files and underline.
* -----

  write(6,16) (nprntr,nprntr=ntotal+1,1,-1)
  write(11,16) (nprntr,nprntr=ntotal+1,1,-1)
16  format(/,2x,' itr ',2x,37(' T(',I3,') ',2x),'Nodes Converged:')
  write(6,17)
  write(11,17)
17  format(2x,5('-',),2x,37(8('-',),2x),16('-',))

* Write the initial temperature distribution [K].
* -----

```




```

      write(6,18)itr,(T(nprntr,1),nprntr=ntotal+1,1,-1),Nonodes
      write(11,18)itr,(T(nprntr,1),nprntr=ntotal+1,1,-1),Nonodes
18   format(/,2x,I5,2x,37(F8.1,2x),4x,A9)

```

```

*   Specify the volumetric heat generation rates at each of the fuel
*   bearing nodes: [all units in W/m3]
*   -----

```

```

*       starting node ==> i=(n7+1) (interface of BG & F)
*       ending node   ==> i=(n9+1) (1D model centerline)

```

```

*   Set all non-fuel nodes equal to zero.
*   -----

```

```

      do 20 i=1,n7
        Qg(i)=0.0
20   continue

```

```

*   OPTION A: Specify the local node generation rates individually.
*   -----

```

```

      Qg(30)=x.xxxex
      Qg(31)=x.xxxex
      Qg(32)=x.xxxex
      Qg(33)=x.xxxex
      Qg(34)=x.xxxex
      Qg(35)=x.xxxex
      Qg(36)=x.xxxex
      Qg(37)=x.xxxex

```

```

*   OPTION B: Specify a zone-averaged generation rate for the fuel.
*   -----

```

```

      do 21 i=n7+1,n9+1
        Qg(i)=x.xxxex
*21  continue

```

```

*   Correct for the reflected heat flux toward the edge-of-fuel.
*   -----

```

```

      Qg(n7+1)=(1.000+reflBe)*Qg(n7+1)

```

```

*   Specify the outer radius of the model: r(1)=r(rocket)+tAS [m].
*   -----

```

```

      r(1)=0.876+1.000

```

```

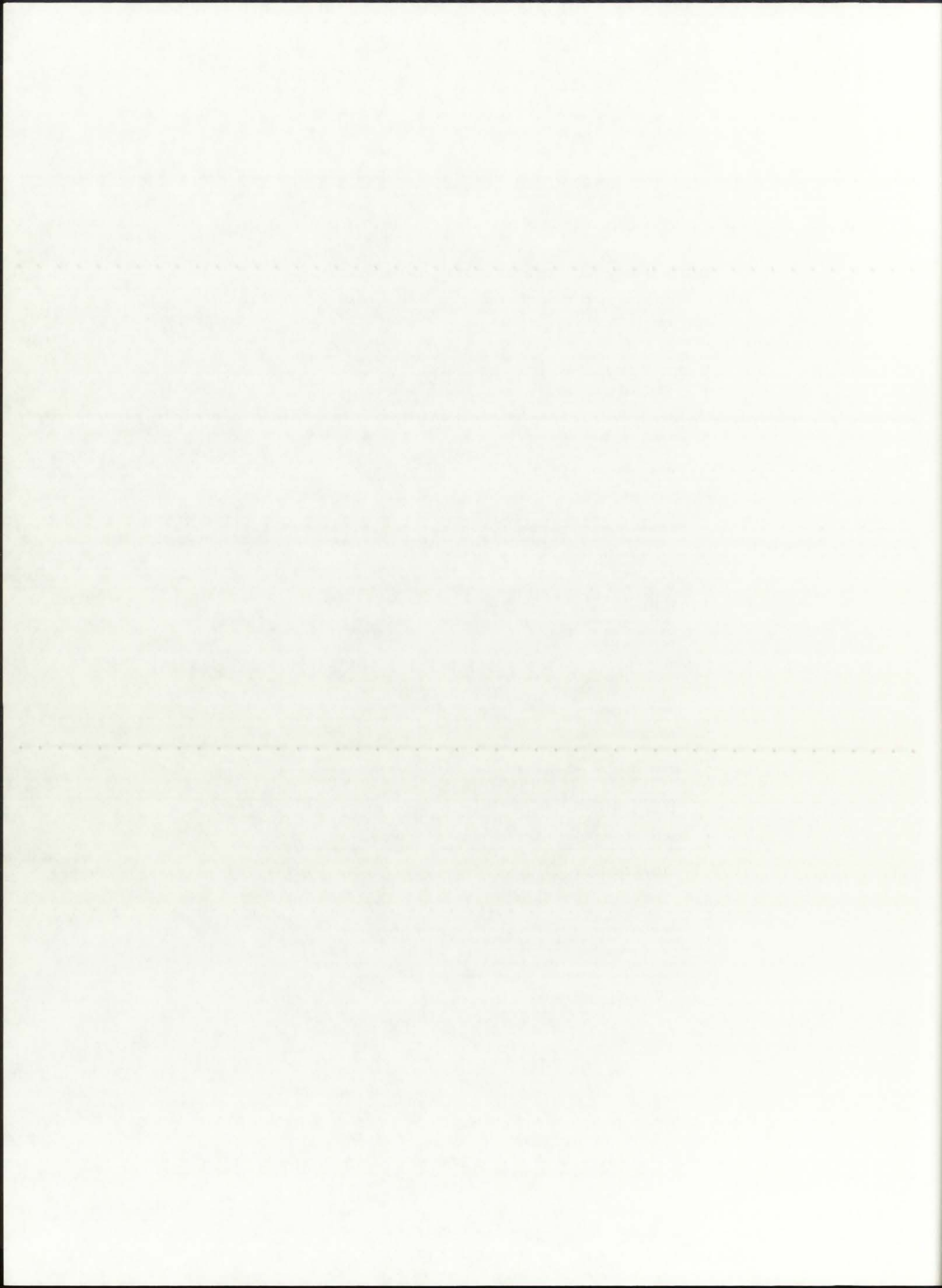
*   =====
*   =====
*   THIS IS WHERE THE MAIN ITERATIVE T(r) CALCULATION LOOP STARTS.
*   =====
*   =====

```

```

100  itr=itr+1

```



```

* First loop => ambient space nodes
* -----

do 101 i=2,n1
  r(i)=r(i-1)-dAS
  r(i+1)=r(i)-dAS
  T(i,itr)=(kradAS*r(i-1)*T(i-1,itr)+kradAS*r(i+1)*T(i+1,
> itr-1))/(kradAS*r(i-1)+kradAS*r(i+1))+0.0
101 continue

* First interface => ambient space/stainless steel pressure vessel
* -----

r(n1+2)=r(n1+1)-dSS
T(n1+1,itr)=(dSS*kradAS*r(n1)*T(n1,itr)+dAS*kcondSS*r(n1+2)*
> T(n1+2,itr-1))/(dSS*kradAS*r(n1)+dAS*kcondSS*
> r(n1+2))

* Second loop => stainless steel pressure vessel nodes
* -----

do 102 i=n1+2,n2
  r(i+1)=r(i)-dSS
  T(i,itr)=(kcondSS*r(i-1)*T(i-1,itr)+kcondSS*r(i+1)*T(i+1,itr-1))
> /(kcondSS*r(i-1)+kcondSS*r(i+1))
102 continue

* Second interface => stainless steel/heavy water reflector
* -----

r(n2+2)=r(n2+1)-dD
T(n2+1,itr)=(dD*kcondSS*r(n2)*T(n2,itr)+dSS*kcondD*r(n2+2)*
> T(n2+2,itr-1))/(dD*kcondSS*r(n2)+dSS*kcondD*r(n2+2))

* Third loop => heavy water nodes
* -----

do 103 i=n2+2,n3
  r(i+1)=r(i)-dD
  T(i,itr)=(kcondD*r(i-1)*T(i-1,itr)+kcondD*r(i+1)*T(i+1,itr-1))
> /(kcondD*r(i-1)+kcondD*r(i+1))
103 continue

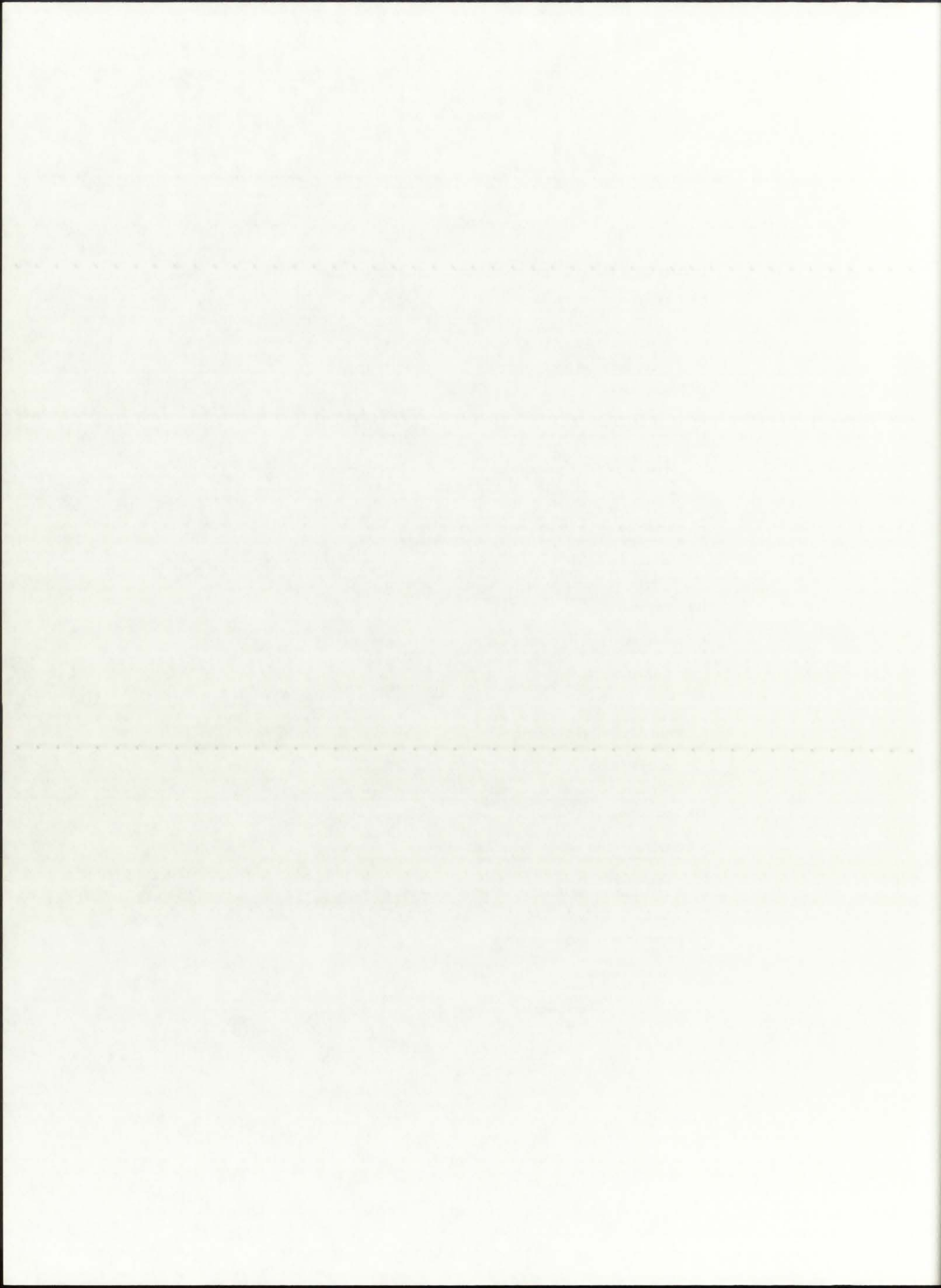
* Third interface => heavy water reflector/beryllium moderator
* -----

r(n3+2)=r(n3+1)-dBe
T(n3+1,itr)=(dBe*kcondD*r(n3)*T(n3,itr)+dD*kcondBe*r(n3+2)*
> T(n3+2,itr-1))/(dBe*kcondD*r(n3)+dD*kcondBe*r(n3+2))

* Fourth loop => beryllium nodes
* -----

do 104 i=n3+2,n4
  r(i+1)=r(i)-dBe
  T(i,itr)=(kcondBe*r(i-1)*T(i-1,itr)+kcondBe*r(i+1)*T(i+1,itr-1))
> /(kcondBe*r(i-1)+kcondBe*r(i+1))

```



104 continue

* Fourth interface => beryllium moderator/hydrogen propellant
 * -----

```

if((rad).and.(Pconv)) then
  r(n4+2)=r(n4+1)-dP
  Taux=T(n4+2,itr-1)
  call RMO(Taux,P,aRP,aRSiW,aRBG,aRF,aRrF)
  krad(n4+2)=16.*sigma*(T(n4+2,itr-1))**3./(3.*aRP)
  call HTCP(Taux,P,Dhydraul,vP,hP)
  h(n4+2)=hP
  T(n4+1,itr)=(dP*kcondBe*r(n4)*T(n4,itr)+(trnsmBe*dBe*krad(n4+2)*r(n4+2)
> +dBe*dP*h(n4+2)*r(n4+2))*T(n4+2,itr-1))/(dP*kcondBe*r(n4)
> +(trnsmBe*dBe*krad(n4+2)*r(n4+2)+dBe*dP*h(n4+2)*r(n4+2)))
elseif((rad).and.(.not.Pconv)) then
  r(n4+2)=r(n4+1)-dP
  Taux=T(n4+2,itr-1)
  call RMO(Taux,P,aRP,aRSiW,aRBG,aRF,aRrF)
  krad(n4+2)=16.*sigma*(T(n4+2,itr-1))**3./(3.*aRP)
  T(n4+1,itr)=(dP*kcondBe*r(n4)*T(n4,itr)+trnsmBe*dBe*krad(n4+2)*r(n4+2)
> *T(n4+2,itr-1))/(dP*kcondBe*r(n4)+trnsmBe*dBe*krad(n4+2)*r(n4+2))
elseif((.not.rad).and.(Pconv)) then
  r(n4+2)=r(n4+1)-dP
  Taux=T(n4+2,itr-1)
  call HTCP(Taux,P,Dhydraul,vP,hP)
  h(n4+2)=hP
  T(n4+1,itr)=(dP*kcondBe*r(n4)*T(n4,itr)+dBe*dP*h(n4+2)*r(n4+2)*T(n4+2,
> itr-1))/(dP*kcondBe*r(n4)+dBe*dP*h(n4+2)*r(n4+2))
else
  write(6,9001)
9001 format(//,2x,'Incorrect specification of heat transfer in propellant')
  stop
endif

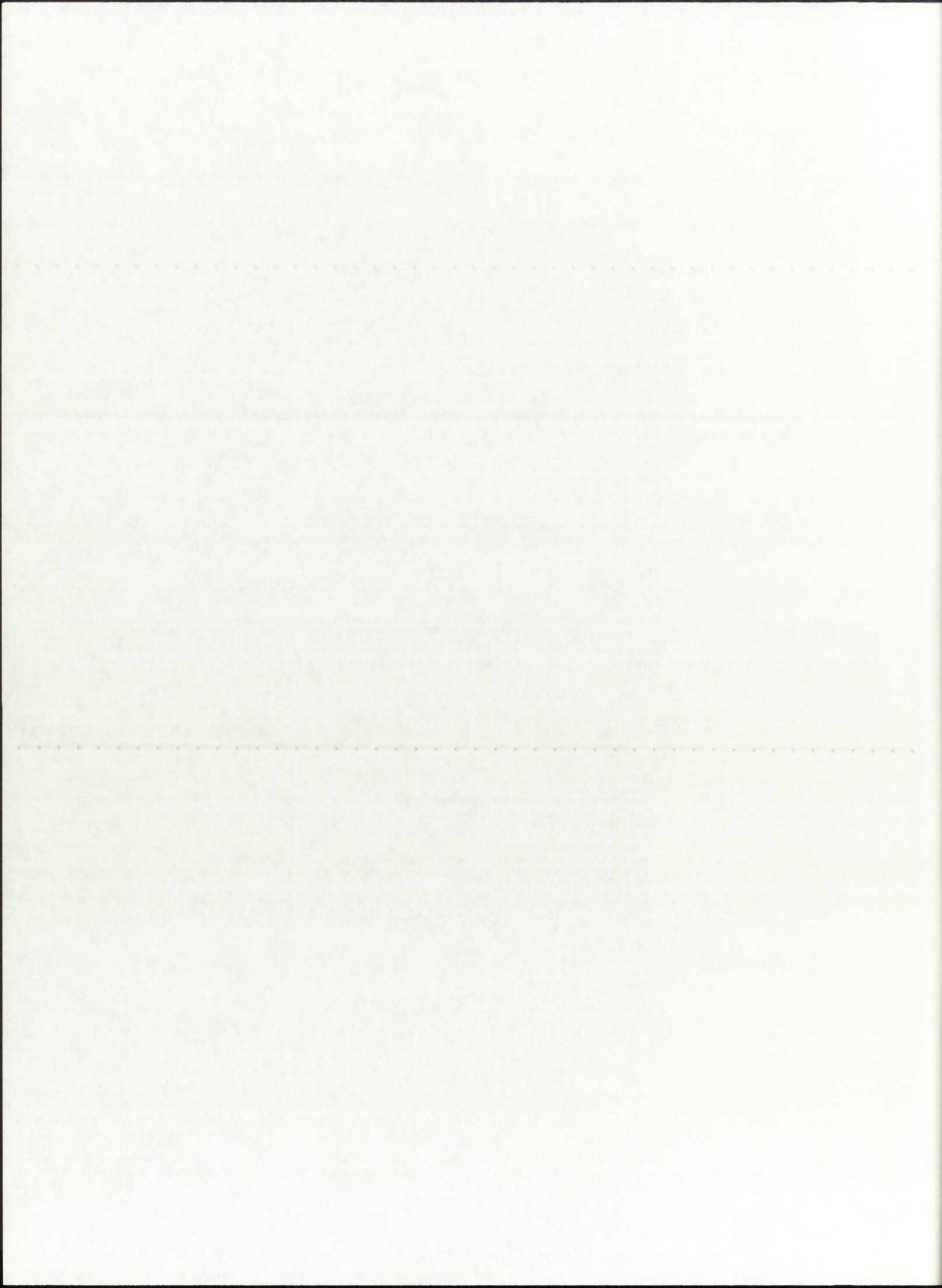
```

* Fifth loop => hydrogen nodes
 * -----

```

if((rad).and.(Pconv)) then
  do 105 i=n4+2,n5
    r(i+1)=r(i)-dP
    Taux=T(i-1,itr)
    call RMO(Taux,P,aRP,aRSiW,aRBG,aRF,aRrF)
    krad(i-1)=16.*sigma*(T(i-1,itr))**3./(3.*aRP)
    call HTCP(Taux,P,Dhydraul,vP,hP)
    h(i-1)=hP
    Taux=T(i+1,itr-1)
    call RMO(Taux,P,aRP,aRSiW,aRBG,aRF,aRrF)
    krad(i+1)=16.*sigma*(T(i+1,itr-1))**3./(3.*aRP)
    call HTCP(Taux,P,Dhydraul,vP,hP)
    h(i+1)=hP
    T(i,itr)=((krad(i-1)*r(i-1)+h(i-1)*r(i-1)*dP)*T(i-1,itr)+(krad(i+1)
> *r(i+1)+h(i+1)*r(i+1)*dP)*T(i+1,itr-1))/((krad(i-1)*r(i-1)
> +h(i-1)*r(i-1)*dP)+(krad(i+1)*r(i+1)+h(i+1)*r(i+1)*dP))
105 continue
elseif((rad).and.(.not.Pconv)) then
  do 1105 i=n4+2,n5
    r(i+1)=r(i)-dP
    Taux=T(i-1,itr)
    call RMO(Taux,P,aRP,aRSiW,aRBG,aRF,aRrF)
    krad(i-1)=16.*sigma*(T(i-1,itr))**3./(3.*aRP)

```



```

    Taux=T(i+1,itr-1)
    call RMO(Taux,P,aRP,aRSiW,aRBG,aRF,aRrF)
    krad(i+1)=16.*sigma*(T(i+1,itr-1))**3./(3.*aRP)
    T(i,itr)=(krad(i-1)*r(i-1)*T(i-1,itr)+krad(i+1)*r(i+1)*T(i+1,itr-1))
>      /(krad(i-1)*r(i-1)+krad(i+1)*r(i+1))
2105  continue
    elseif((.not.rad).and.(Pconv)) then
    do 2105 i=n4+2,n5
        r(i+1)=r(i)-dP
        Taux=T(i-1,itr)
        call HTCP(Taux,P,Dhydraul,vP,hP)
        h(i-1)=hP
        Taux=T(i+1,itr-1)
        call HTCP(Taux,P,Dhydraul,vP,hP)
        h(i+1)=hP
        T(i,itr)=(h(i-1)*r(i-1)*dP*T(i-1,itr)+h(i+1)*r(i+1)*dP*T(i+1,itr-1))
>      /(h(i-1)*r(i-1)*dP+h(i+1)*r(i+1)*dP)
2105  continue
    else
    write(6,9002)
9002  format(//,2x,'Incorrect specification of heat transfer in propellant')
    stop
    endif

```

```

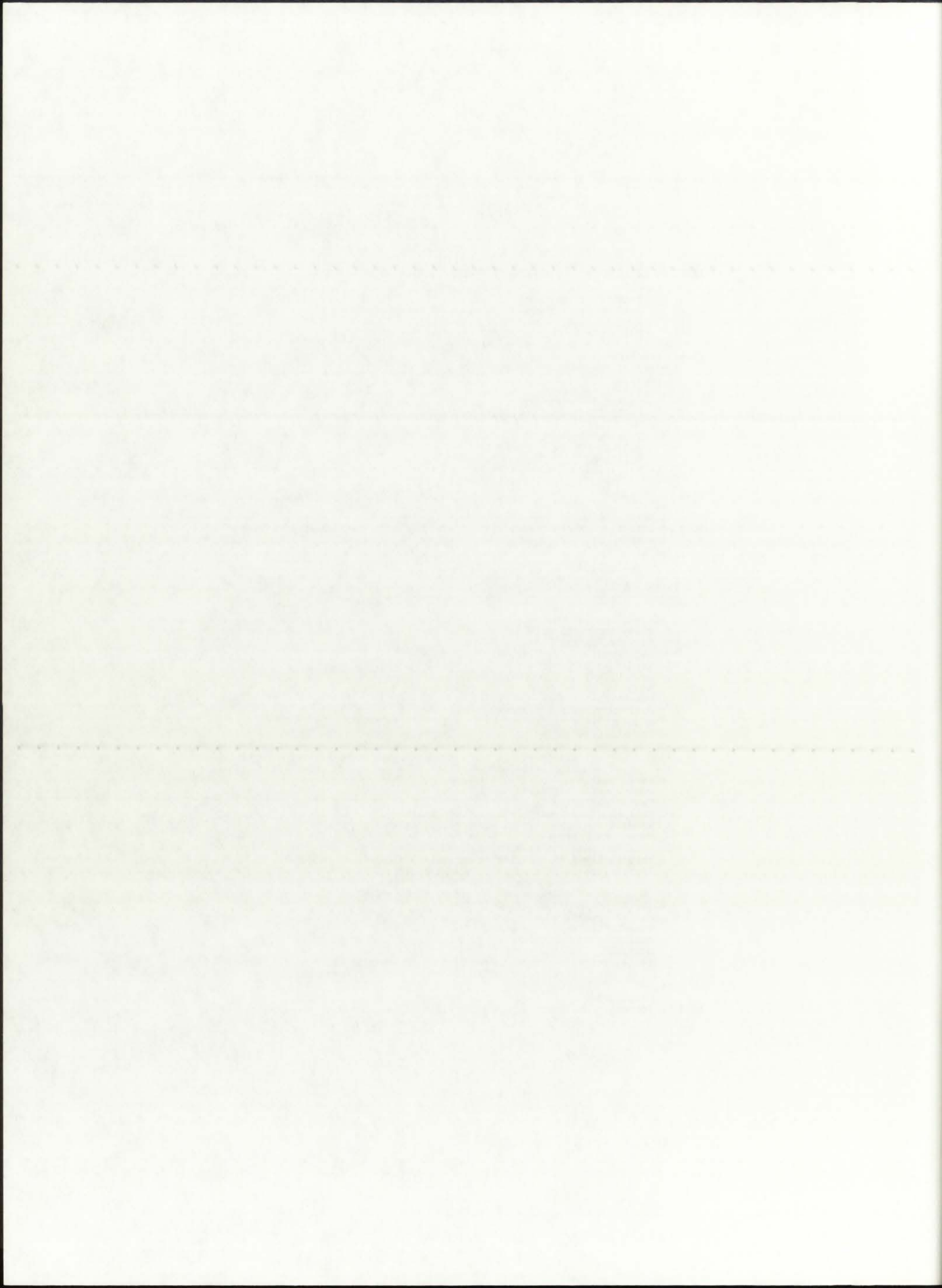
* Fifth interface => hydrogen propellant/silicon wall
* -----

```

```

    if((rad).and.(Pconv)) then
    r(n5+2)=r(n5+1)-dSiW
    Taux=T(n5,itr)
    call RMO(Taux,P,aRP,aRSiW,aRBG,aRF,aRrF)
    krad(n5)=16.*sigma*(T(n5,itr))**3./(3.*aRP)
    call HTCP(Taux,P,Dhydraul,vP,hP)
    h(n5)=hP
    Taux=T(n5+2,itr-1)
    call RMO(Taux,P,aRP,aRSiW,aRBG,aRF,aRrF)
    krad(n5+2)=16.*sigma*(T(n5+2,itr-1))**3./(3.*aRSiW)
    T(n5+1,itr)=(dSiW*krad(n5)*r(n5)+dP*dSiW*h(n5)*r(n5))*T(n5,itr)+(dP*
>      krad(n5+2)*r(n5+2)+dP*kcondSiW*r(n5+2))*T(n5+2,itr-1)/((
>      dSiW*krad(n5)*r(n5)+dP*dSiW*h(n5)*r(n5)+(dP*krad(n5+2)*
>      r(n5+2)+dP*kcondSiW*r(n5+2)))
    elseif((rad).and.(.not.Pconv)) then
    r(n5+2)=r(n5+1)-dSiW
    Taux=T(n5,itr)
    call RMO(Taux,P,aRP,aRSiW,aRBG,aRF,aRrF)
    krad(n5)=16.*sigma*(T(n5,itr))**3./(3.*aRP)
    Taux=T(n5+2,itr-1)
    call RMO(Taux,P,aRP,aRSiW,aRBG,aRF,aRrF)
    krad(n5+2)=16.*sigma*(T(n5+2,itr-1))**3./(3.*aRSiW)
    T(n5+1,itr)=(dSiW*krad(n5)*r(n5)*T(n5,itr)+(dP*krad(n5+2)*r(n5+2)+dP
>      *kcondSiW*r(n5+2))*T(n5+2,itr-1)/(dSiW*krad(n5)*r(n5)+
>      (dP*krad(n5+2)*r(n5+2)+dP*kcondSiW*r(n5+2)))
    elseif((.not.rad).and.(Pconv)) then
    r(n5+2)=r(n5+1)-dSiW
    Taux=T(n5,itr)
    call HTCP(Taux,P,Dhydraul,vP,hP)
    h(n5)=hP
    T(n5+1,itr)=(dP*dSiW*h(n5)*r(n5)*T(n5,itr)+dP*kcondSiW*r(n5+2)*T(n5+2,
>      itr-1))/(dP*dSiW*h(n5)*r(n5)+dP*kcondSiW*r(n5+2))
    else
    write(6,9003)
9003  format(//,2x,'Incorrect specification of heat transfer in silica wall')

```




```

    stop
  endif

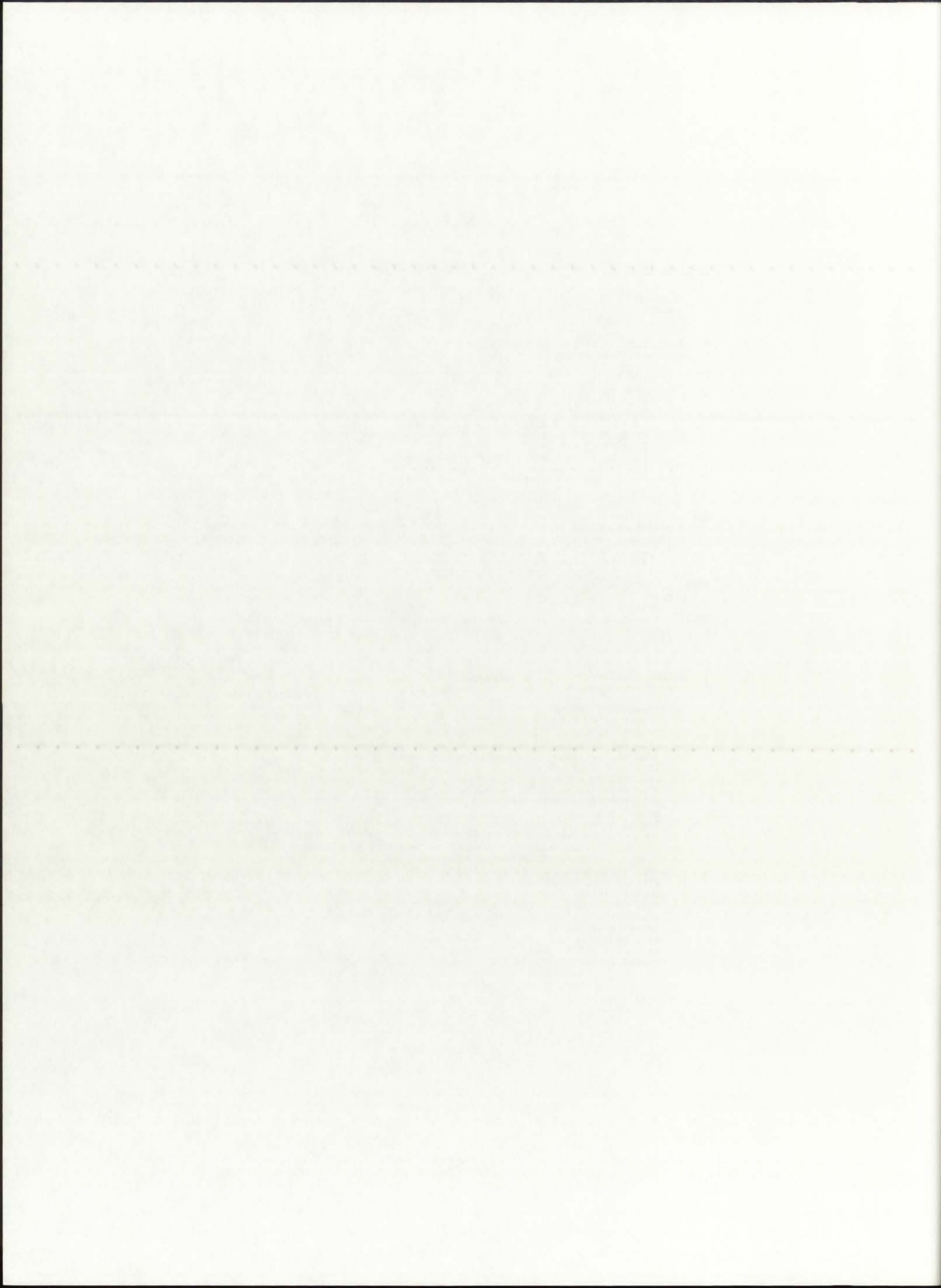
* Sixth loop => silicon nodes
* -----

  if(rad) then
    do 106 i=n5+2,n6
      r(i+1)=r(i)-dSiW
      Taux=T(i-1,itr)
      call RMO(Taux,P,aRP,aRSiW,aRBG,aRF,aRARF)
      krad(i-1)=16.*sigma*(T(i-1,itr))**3./(3.*aRSiW)
      Taux=T(i+1,itr-1)
      call RMO(Taux,P,aRP,aRSiW,aRBG,aRF,aRARF)
      krad(i+1)=16.*sigma*(T(i+1,itr-1))**3./(3.*aRSiW)
      T(i,itr)=(krad(i-1)*r(i-1)+kcondSiW*r(i-1))*T(i-1,itr)+(krad(i+1)*
> r(i+1)+kcondSiW*r(i+1))*T(i+1,itr-1)/(krad(i-1)*r(i-1)+
> kcondSiW*r(i-1)+krad(i+1)*r(i+1)+kcondSiW*r(i+1))
106    continue
    elseif(.not.rad) then
      do 1106 i=n5+2,n6
        r(i+1)=r(i)-dSiW
        T(i,itr)=(kcondSiW*r(i-1)*T(i-1,itr)+kcondSiW*r(i+1)*T(i+1,itr-1))/
> (kcondSiW*r(i-1)+kcondSiW*r(i+1))
1106    continue
    else
      write(6,9004)
9004    format(//,2x,'Incorrect specification of heat transfer in silica wall')
      stop
    endif

* Sixth interface => silicon wall/buffer gas
* -----

  if((rad).and.(BGconv)) then
    r(n6+2)=r(n6+1)-dBG
    Taux=T(n6,itr)
    call RMO(Taux,P,aRP,aRSiW,aRBG,aRF,aRARF)
    krad(n6)=16.*sigma*(T(n6,itr))**3./(3.*aRSiW)
    Taux=T(n6+2,itr-1)
    call RMO(Taux,P,aRP,aRSiW,aRBG,aRF,aRARF)
    krad(n6+2)=16.*sigma*(T(n6+2,itr-1))**3./(3.*aRBG)
    call HTCBG(Taux,P,Dhydraul,vBG,hBG)
    h(n6+2)=hBG
    T(n6+1,itr)=((DBG*krad(n6)*r(n6)+DBG*kcondSiW*r(n6))*T(n6,itr)+(dSiW*
> krad(n6+2)*r(n6+2)+dSiW*dBG*h(n6+2)*r(n6+2))*T(n6+2,itr-1))
> /((DBG*krad(n6)*r(n6)+DBG*kcondSiW*r(n6))+dSiW*krad(n6+2)*
> r(n6+2)+dSiW*dBG*h(n6+2)*r(n6+2))
  elseif((rad).and.(.not.BGconv)) then
    r(n6+2)=r(n6+1)-dBG
    Taux=T(n6,itr)
    call RMO(Taux,P,aRP,aRSiW,aRBG,aRF,aRARF)
    krad(n6)=16.*sigma*(T(n6,itr))**3./(3.*aRSiW)
    Taux=T(n6+2,itr-1)
    call RMO(Taux,P,aRP,aRSiW,aRBG,aRF,aRARF)
    krad(n6+2)=16.*sigma*(T(n6+2,itr-1))**3./(3.*aRBG)
    T(n6+1,itr)=((DBG*krad(n6)*r(n6)+DBG*kcondSiW*r(n6))*T(n6,itr)+dSiW*
> krad(n6+2)*r(n6+2)*T(n6+2,itr-1))/(DBG*krad(n6)*r(n6)+DBG
> *kcondSiW*r(n6)+dSiW*krad(n6+2)*r(n6+2))
  elseif((.not.rad).and.(BGconv)) then
    r(n6+2)=r(n6+1)-dBG

```



```

    Taux=T(n6+2,itr-1)
    call HTCDBG(Taux,P,Dhydraul,vBG,hBG)
    h(n6+2)=hBG
    T(n6+1,itr)=(dBG*kcondSiW*r(n6)*T(n6,itr)+dSiW*dBG*h(n6+2)*r(n6+2)*
>      T(n6+2,itr-1))/(dBG*kcondSiW*r(n6)+dSiW*dBG*h(n6+2)*r(n6+2))
    else
    write(6,9005)
9005  format(//,2x,'Incorrect specification of heat transfer in buffer gas')
    stop
    endif

```

```

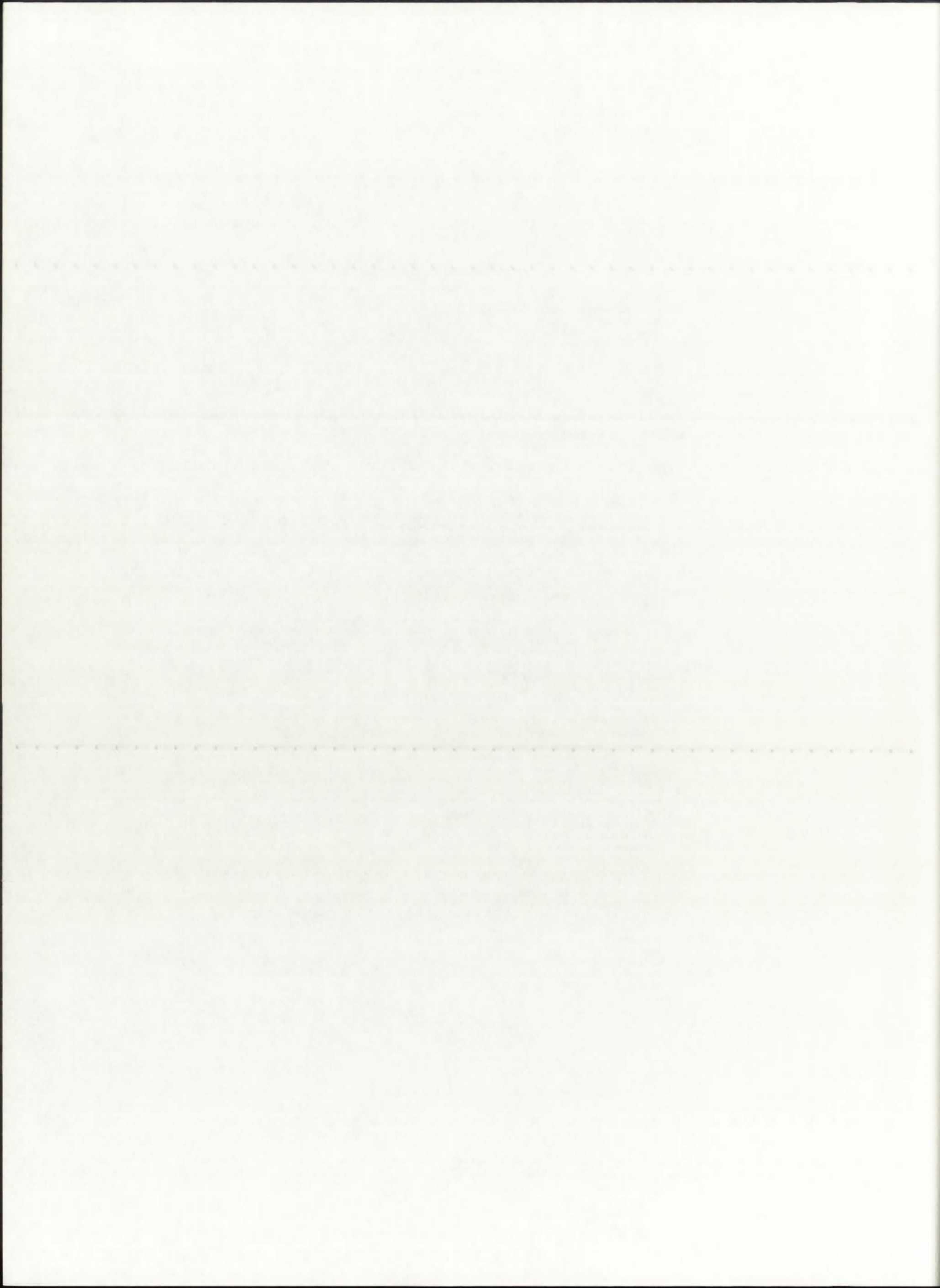
* Seventh loop => buffer gas nodes
* -----

```

```

    if((rad).and.(BGconv)) then
    do 107 i=n6+2,n7
    r(i+1)=r(i)-dBG
    Taux=T(i-1,itr)
    call RMO(Taux,P,aRP,aRSiW,aRBG,aRF,aRrF)
    krad(i-1)=16.*sigma*(T(i-1,itr))**3./(3.*aRBG)
    call HTCDBG(Taux,P,Dhydraul,vBG,hBG)
    h(i-1)=hBG
    Taux=T(i+1,itr-1)
    call RMO(Taux,P,aRP,aRSiW,aRBG,aRF,aRrF)
    krad(i+1)=16.*sigma*(T(i+1,itr-1))**3./(3.*aRBG)
    call HTCDBG(Taux,P,Dhydraul,vBG,hBG)
    h(i+1)=hBG
    T(i,itr)=(krad(i-1)*r(i-1)+h(i-1)*r(i-1)*dBG)*T(i-1,itr)+(krad(i
>      +1)*r(i+1)+h(i+1)*r(i+1)*dBG)*T(i+1,itr-1)/((krad(i-1)
>      *r(i-1)+h(i-1)*r(i-1)*dBG)+(krad(i+1)*r(i+1)+h(i+1)*r(i
>      +1)*dBG))
107  continue
    elseif((rad).and.(.not.BGconv)) then
    do 1107 i=n6+2,n7
    r(i+1)=r(i)-dBG
    Taux=T(i-1,itr)
    call RMO(Taux,P,aRP,aRSiW,aRBG,aRF,aRrF)
    krad(i-1)=16.*sigma*(T(i-1,itr))**3./(3.*aRBG)
    Taux=T(i+1,itr-1)
    call RMO(Taux,P,aRP,aRSiW,aRBG,aRF,aRrF)
    krad(i+1)=16.*sigma*(T(i+1,itr-1))**3./(3.*aRBG)
    T(i,itr)=(krad(i-1)*r(i-1)*T(i-1,itr)+krad(i+1)*r(i+1)*T(i+1,itr-1))
>      /(krad(i-1)*r(i-1)+krad(i+1)*r(i+1))
1107 continue
    elseif((.not.rad).and.(BGconv)) then
    do 2107 i=n6+2,n7
    r(i+1)=r(i)-dBG
    Taux=T(i-1,itr)
    call HTCDBG(Taux,P,Dhydraul,vBG,hBG)
    h(i-1)=hBG
    Taux=T(i+1,itr-1)
    call HTCDBG(Taux,P,Dhydraul,vBG,hBG)
    h(i+1)=hBG
    T(i,itr)=(h(i-1)*r(i-1)*dBG*T(i-1,itr)+h(i+1)*r(i+1)*dBG*T(i+1,itr-1
>      ))/(h(i-1)*r(i-1)*dBG+h(i+1)*r(i+1)*dBG)
2107 continue
    else
    write(6,9006)
9006  format(//,2x,'Incorrect specification of heat transfer in buffer gas')
    stop
    endif

```



```

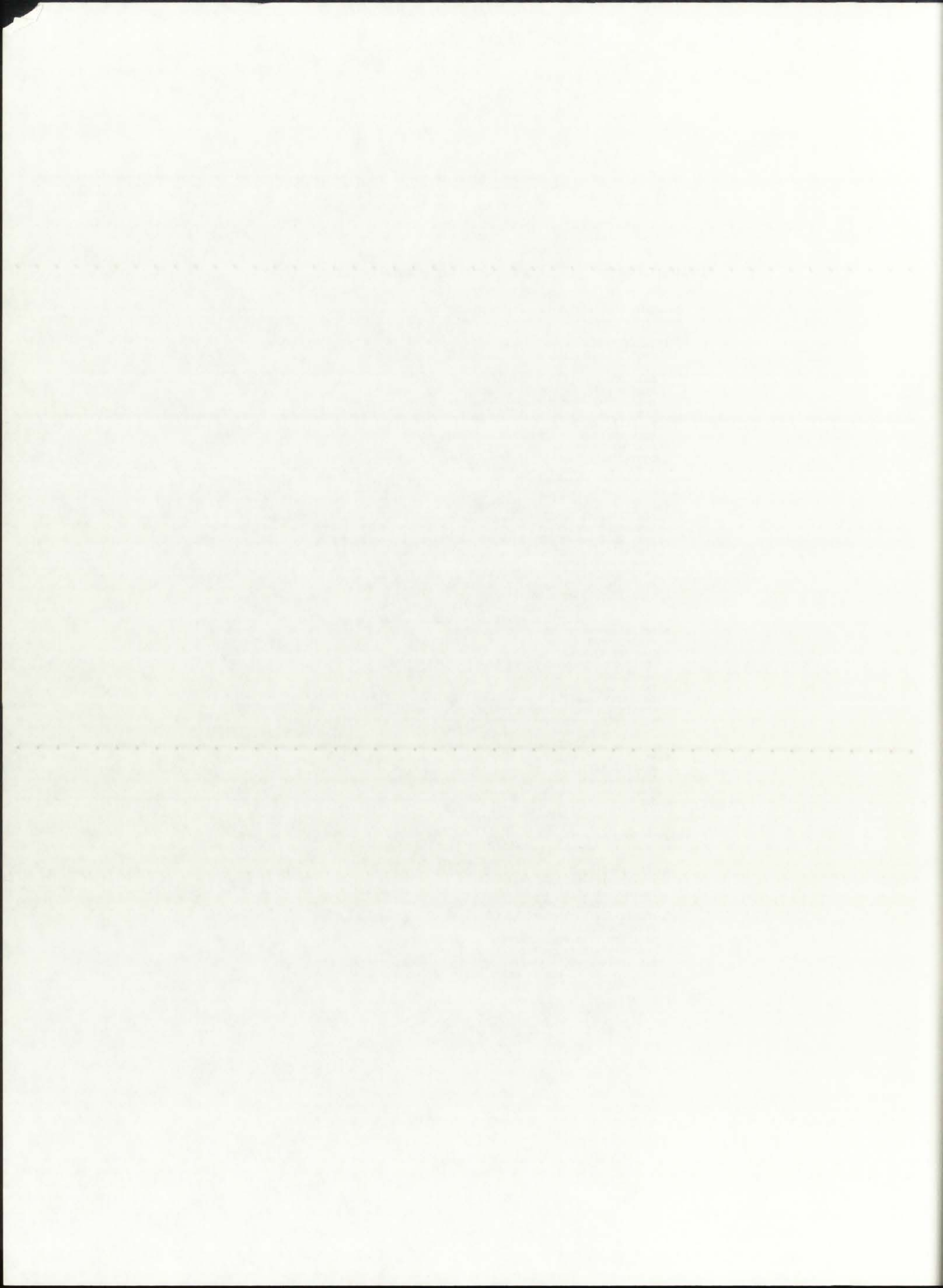
* Seventh interface => buffer gas/fuel
* -----

if((rad).and.(BGconv)) then
  r(n7+2)=r(n7+1)-dF
  Taux=T(n7,itr)
  call RMO(Taux,P,aRP,aRSiW,aRBG,aRF,aRrF)
  krad(n7)=16.*sigma*(T(n7,itr))**3./(3.*aRBG)
  call HTCBG(Taux,P,Dhydraul,vBG,hBG)
  h(n7)=hBG
  Taux=T(n7+2,itr-1)
  call RMO(Taux,P,aRP,aRSiW,aRBG,aRF,aRrF)
  krad(n7+2)=16.*sigma*(T(n7+2,itr-1))**3./(3.*aRF)
  T(n7+1,itr)=(dF*krad(n7)*r(n7)+dBG*dF*h(n7)*r(n7))*T(n7,itr)+dBG*
> krad(n7+2)*r(n7+2)*T(n7+2,itr-1)+Qg(n7+1)*r(n7+1)*dF*dBG
> *(dF+dBG)/2./((dF*krad(n7)*r(n7)+dBG*dF*h(n7)*r(n7))+
> dBG*krad(n7+2)*r(n7+2))
elseif((rad).and.(.not.BGconv)) then
  r(n7+2)=r(n7+1)-dF
  Taux=T(n7,itr)
  call RMO(Taux,P,aRP,aRSiW,aRBG,aRF,aRrF)
  krad(n7)=16.*sigma*(T(n7,itr))**3./(3.*aRBG)
  Taux=T(n7+2,itr-1)
  call RMO(Taux,P,aRP,aRSiW,aRBG,aRF,aRrF)
  krad(n7+2)=16.*sigma*(T(n7+2,itr-1))**3./(3.*aRF)
  T(n7+1,itr)=(dF*krad(n7)*r(n7)*T(n7,itr)+dBG*krad(n7+2)*r(n7+2)*
> T(n7+2,itr-1)+Qg(n7+1)*r(n7+1)*dF*dBG*(dF+dBG)/2./
> (dF*krad(n7)*r(n7)+dBG*krad(n7+2)*r(n7+2))
elseif((.not.rad).and.(BGconv)) then
  r(n7+2)=r(n7+1)-dF
  Taux=T(n7,itr)
  call HTCBG(Taux,P,Dhydraul,vBG,hBG)
  h(n7)=hBG
  Taux=T(n7+2,itr-1)
  call RMO(Taux,P,aRP,aRSiW,aRBG,aRF,aRrF)
  krad(n7+2)=16.*sigma*(T(n7+2,itr-1))**3./(3.*aRF)
  T(n7+1,itr)=(dBG*dF*h(n7)*r(n7)*T(n7,itr)+dBG*krad(n7+2)*r(n7+2)*
> T(n7+2,itr-1)+Qg(n7+1)*r(n7+1)*dF*dBG*(dF+dBG)/2./
> (dBG*dF*h(n7)*r(n7)+dBG*krad(n7+2)*r(n7+2))
else
  write(6,9007)
9007  format(//,2x,'Incorrect specification of heat transfer in fuel')
  stop
endif

* Eighth loop => fuel nodes
* -----

do 108 i=n7+2,n8
  r(i+1)=r(i)-dF
  Taux=T(i-1,itr)
  call RMO(Taux,P,aRP,aRSiW,aRBG,aRF,aRrF)
  krad(i-1)=16.*sigma*(T(i-1,itr))**3./(3.*aRF)
  Taux=T(i+1,itr-1)
  call RMO(Taux,P,aRP,aRSiW,aRBG,aRF,aRrF)
  krad(i+1)=16.*sigma*(T(i+1,itr-1))**3./(3.*aRF)
  T(i,itr)=(krad(i-1)*r(i-1)*T(i-1,itr)+krad(i+1)*r(i+1)*
> T(i+1,itr-1)+dF**2.*Qg(i)*r(i))/(krad(i-1)*r(i-1)
> +krad(i+1)*r(i+1))
108  continue

```



```

* Eighth interface => fuel/buffer gas & fuel mixture
* -----

r(n8+2)=r(n8+1)-dArF
Taux=T(n8,itr)
call RMO(Taux,P,aRP,aRSiW,aRBG,aRF,aRrArF)
krad(n8)=16.*sigma*(T(n8,itr))**3./(3.*aRrArF)
Taux=T(n8+2,itr-1)
call RMO(Taux,P,aRP,aRSiW,aRBG,aRF,aRrArF)
krad(n8+2)=16.*sigma*(T(n8+2,itr-1))**3./(3.*aRrArF)
T(n8+1,itr)=(dArF*krad(n8)*r(n8)*T(n8,itr)+dF*krad(n8+2)*
> r(n8+2)*T(n8+2,itr-1)+Qg(n8+1)*r(n8+1)*dArF*dF*(dArF
> +dF)/2.)/(dArF*krad(n8)*r(n8)+dF*krad(n8+2)*r(n8+2))

* Ninth loop => buffer gas & fuel mixture
* -----

do 109 i=n8+2,ntotal
  r(i+1)=r(i)-dArF
  if(r(i+1).lt.0.0000) then
    r(i+1)=0.0
  endif
  Taux=T(i-1,itr)
  call RMO(Taux,P,aRP,aRSiW,aRBG,aRF,aRrArF)
  krad(i-1)=16.*sigma*(T(i-1,itr))**3./(3.*aRrArF)
  Taux=T(i+1,itr-1)
  call RMO(Taux,P,aRP,aRSiW,aRBG,aRF,aRrArF)
  krad(i+1)=16.*sigma*(T(i+1,itr-1))**3./(3.*aRrArF)
  T(i,itr)=(krad(i-1)*r(i-1)*T(i-1,itr)+krad(i+1)*r(i+1)*
> T(i+1,itr-1)+dArF**2.*Qg(i)*r(i))/(krad(i-1)*r(i-1)
> +krad(i+1)*r(i+1))
109 continue

* Ninth Interface => Centerline node
* -----

r(ntotal+2)=r(ntotal+1)+dArF
Taux=T(ntotal,itr)
call RMO(Taux,P,aRP,aRSiW,aRBG,aRF,aRrArF)
krad(ntotal)=16.*sigma*(T(ntotal,itr))**3./(3.*aRrArF)
Taux=T(ntotal+2,itr-1)
call RMO(Taux,P,aRP,aRSiW,aRBG,aRF,aRrArF)
krad(ntotal+2)=16.*sigma*(T(ntotal+2,itr-1))**3./(3.*aRrArF)
T(ntotal+1,itr)=(krad(ntotal)*r(ntotal)*T(ntotal,itr)+krad(ntotal
> +2)*r(ntotal+2)*T(ntotal+2,itr-1))/(krad(ntotal)*
> r(ntotal)+krad(ntotal+2)*r(ntotal+2))

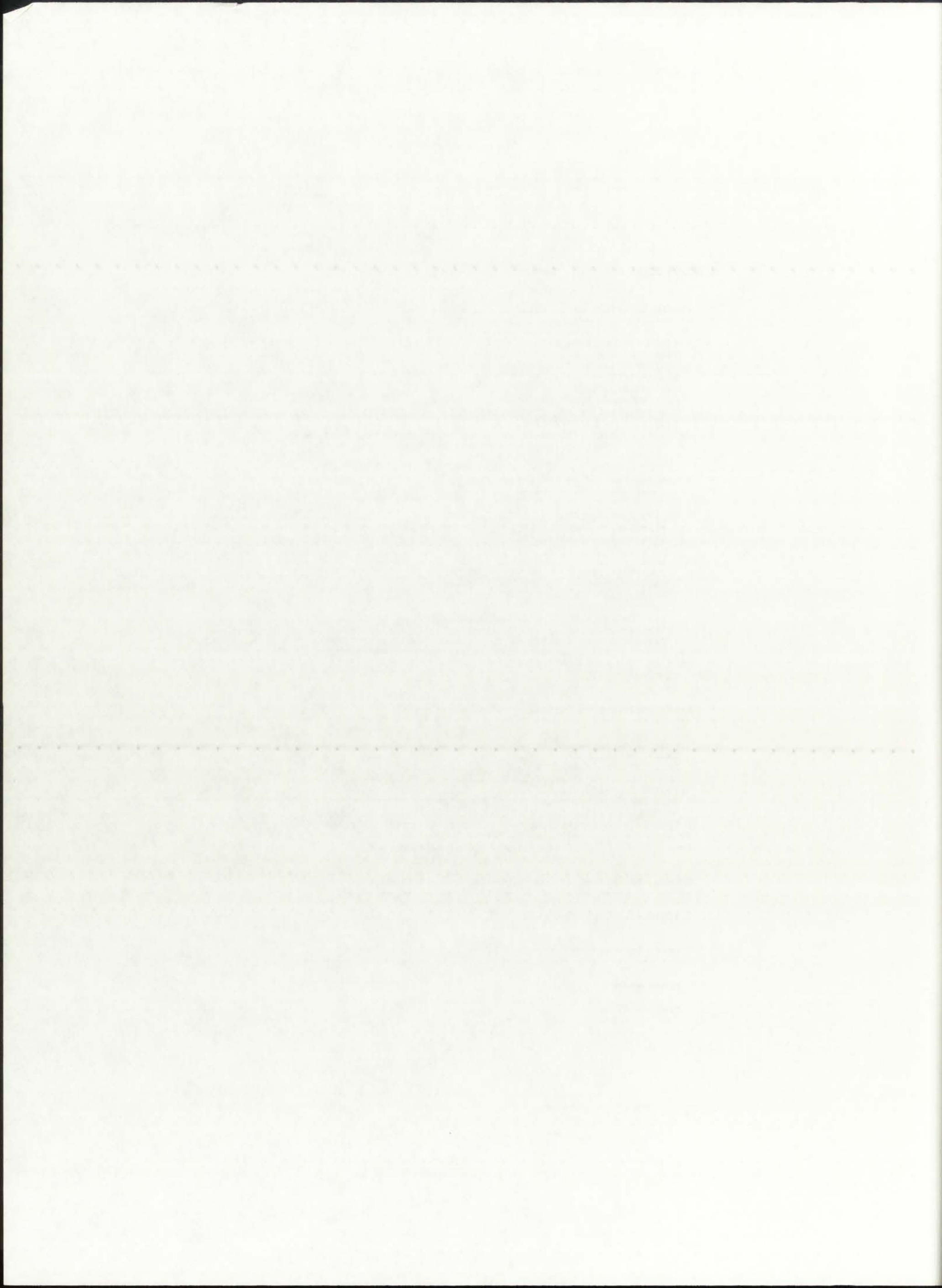
* Update the (ntotal+2) node opposite the centerline node
* -----

T(ntotal+2,itr)=T(ntotal,itr)

* Specify convergence criteria - 1 fuel node,1 Be node,1 AS node
* -----

eps=x.xxxxx
epsF=abs(T(n8,itr)-T(n8,itr-1))

```




```

      epsBe=abs(T(n4,itr)-T(n4,itr-1))
      epsAS=abs(T(n2,itr)-T(n2,itr-1))

* Check for iteration convergence in select fuel, Be, and AS nodes;
* Write calculated temperature distribution for (itr)-th iteration.
* -----

      if((epsF.le.eps).and.(epsBe.le.eps).and.(epsAS.le.eps)) then
        write(6,200)itr,(T(nprntr,itr),nprntr=ntotal+1,1,-1),Threenodes
        write(11,200)itr,(T(nprntr,itr),nprntr=ntotal+1,1,-1),Threenodes
200      format(/,2x,I5,2x,37(F8.1,2x),4x,A9)
        goto 999
      elseif(((epsF.le.eps).and.(epsBe.le.eps)).or.((epsBe.le.eps).and.
>      (epsAS.le.eps)).or.((epsF.le.eps).and.(epsAS.le.eps)))
>      then
        write(6,201)itr,(T(nprntr,itr),nprntr=ntotal+1,1,-1),Twonodes
        write(11,201)itr,(T(nprntr,itr),nprntr=ntotal+1,1,-1),Twonodes
201      format(/,2x,I5,2x,37(F8.1,2x),4x,A9)
      elseif((epsF.le.eps).or.(epsBe.le.eps).or.(epsAS.le.eps)) then
        write(6,202)itr,(T(nprntr,itr),nprntr=ntotal+1,1,-1),Onenodes
        write(11,202)itr,(T(nprntr,itr),nprntr=ntotal+1,1,-1),Onenodes
202      format(/,2x,I5,2x,37(F8.1,2x),4x,A9)
      else
        write(6,203)itr,(T(nprntr,itr),nprntr=ntotal+1,1,-1),Nonodes
        write(11,203)itr,(T(nprntr,itr),nprntr=ntotal+1,1,-1),Nonodes
203      format(/,2x,I5,2x,37(F8.1,2x),4x,A9)
      endif

* Fall-back in case of infinite loop for non-convergence.
* -----

      if(itr.ge.iters) then
        write(6,204)
        write(11,204)
204      format(/,2x,'WARNING: Some nodes may not have converged !!',/)
        GOTO 999
      endif

      goto 100

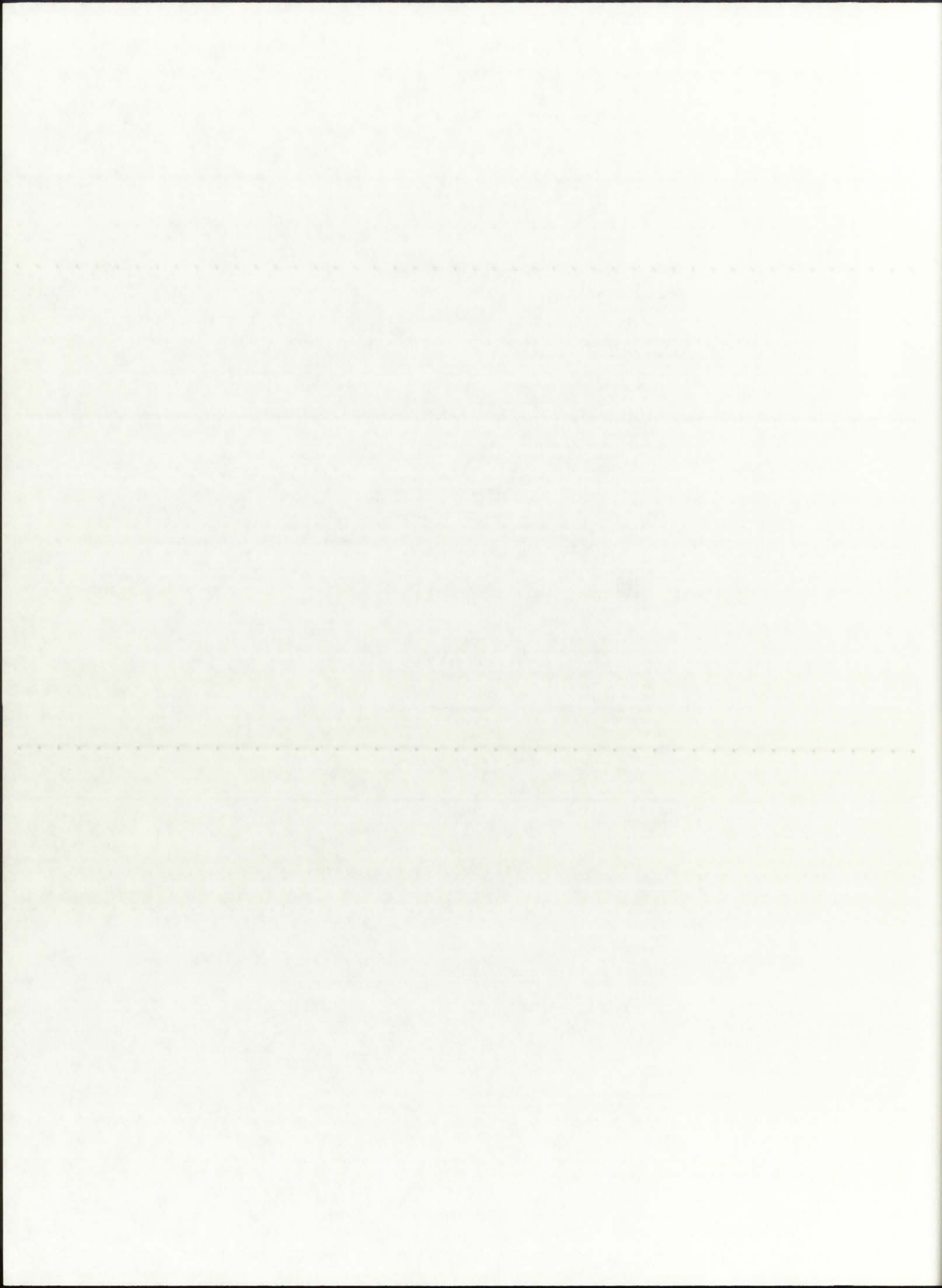
* =====
* End of the main loop - exit for the program in case of full convergence.
* =====

* Correct for the temperatures in the regions where only radiative heat
* transfer has been selected, by determining the transmission fraction.
* -----

999  Tprop=T(25,itr)
      Twall=T(27,itr)
      Tbuffer=T(29,itr)

      if((.not.BGconv).or.(.not.Pconv)) then
        call TRANSMIT(P,tP,tSiW,tBG,BGconv,Pconv,Tprop,Twall,Tbuffer)
        if((.not.BGconv).and.(.not.Pconv)) then
          do 10001 i=n4+2,n5

```



```

      T(i,itr)=Tprop
10001  continue
      do 10002 i=n5+1,n6+1
          T(i,itr)=Twall
10002  continue
      do 10003 i=n6+2,n7
          T(i,itr)=Tbuffer
10003  continue
      elseif(.not.Pconv) then
      do 10004 i=n4+2,n5
          T(i,itr)=Tprop
10004  continue
      elseif(.not.BGconv) then
      do 10005 i=n6+2,n7
          T(i,itr)=Tbuffer
10005  continue
      endif
  endif
endif

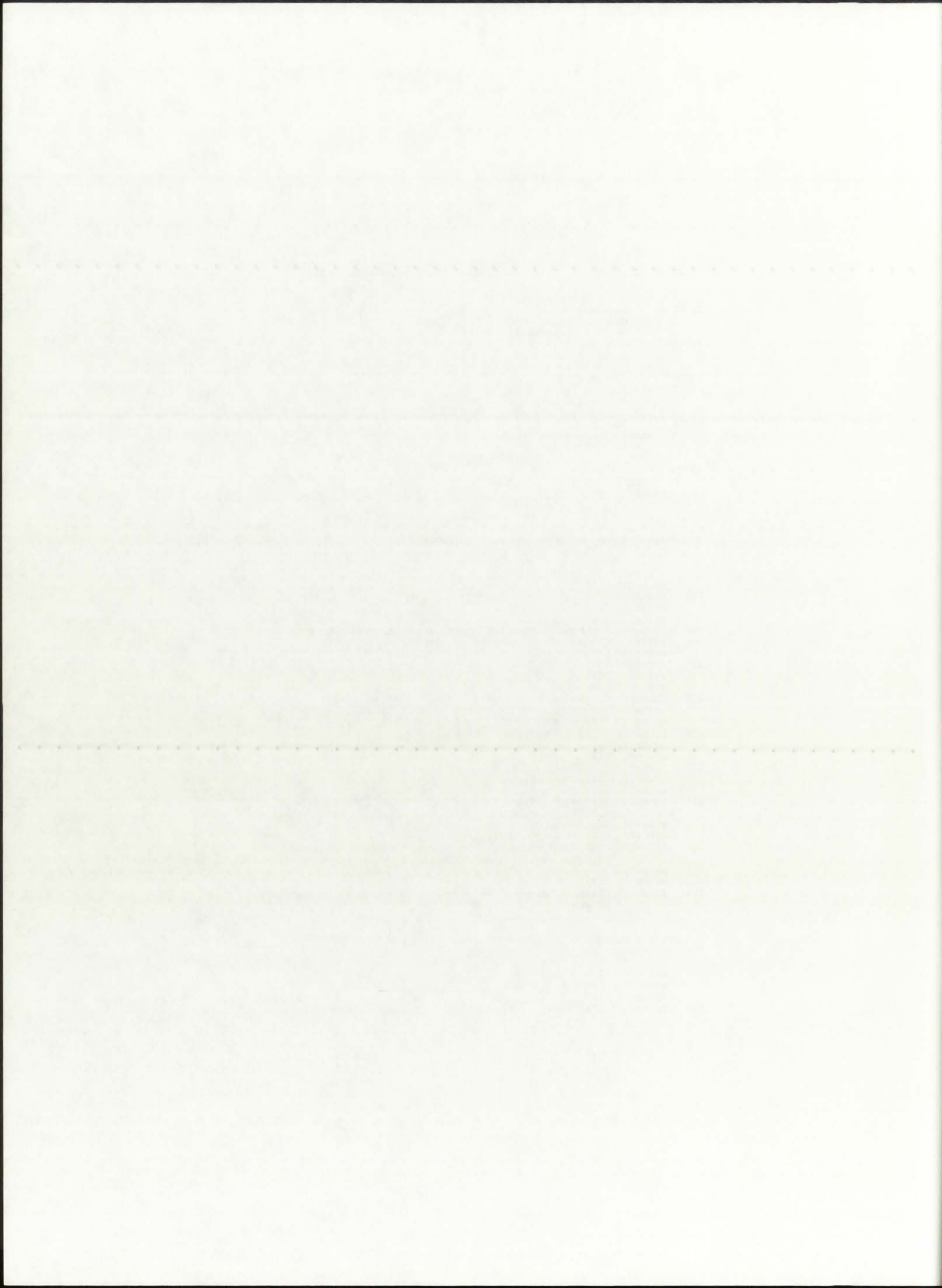
*   Write out the converged results separately.
*   -----

      write(6,205)
      write(11,205)
205  format(/,2x,7x,37(8('-',2x),/,2x,7x,37(8('-',2x))
      write(6,206)
      write(11,206)
206  format(/,2x,'Final Converged Temperature Distribution in Model:')
      write(6,207) (T(nprntr,itr),nprntr=ntotal+1,1,-1)
      write(11,207) (T(nprntr,itr),nprntr=ntotal+1,1,-1)
207  format(/,2x,7x,37(F8.1,2x),' [K] ')
      write(6,208)
      write(11,208)
208  format(/,2x,'Radial Distance from Model Centerline @ r = 0.0 cm:')
      write(6,209) ((r(nprntr)*100.),nprntr=ntotal+1,1,-1)
      write(11,209) ((r(nprntr)*100.),nprntr=ntotal+1,1,-1)
209  format(/,2x,7x,37(F8.3,2x),' [cm] ')
      write(6,210)
      write(11,210)
210  format(/,2x,37(8('*',2x),/,2x,37(8('*',2x))
      write(6,211) (ntotal+1),eps
      write(11,211) (ntotal+1),eps
211  format(/,2x,'Completed Run of GNRATR-1D: Total Nodes Analyzed = '
>      ,I4,' ==> Convergence to within ',F7.5,' [K] Achieved!')
      write(6,212) itr
      write(11,212) itr
212  format(/,2x,'Total Number of Convergence Iterations Required for',
>      ' This Run (itr) = ',I4,' !')
      write(6,213)
      write(11,213)
213  format(/,2x,'A Summary of the Converged Results for this Run is',
>      ' Located in File "1-D.DAT"',//)

*   Write a summary of the converged results in the C.DAT file.
*   -----

      write(6,214)
      write(11,214)
      write(12,214)
214  format(/,2x,'==== SUMMARY OF CONVERGED VALUES ====',//)

```



```

write(6,215)reflBe,P
write(11,215)reflBe,P
write(12,215)reflBe,P
215 format(2x,'This Case Executed for: REFLBe = ',F7.5,/,2x,
> 24x,'Pressure = ',F6.1,' atm')
write(6,216)BGSiWPr,BGc,Pc
write(11,216)BGSiWPr,BGc,Pc
write(12,216)BGSiWPr,BGc,Pc
216 format(/,2x,'Modes of Heat Transfer: Radiation in BG,SiW,',
> ' and P = ',A5,/,37x,'Convection in BG = ',A5,/,38x,
> 'Convection in P = ',A5,/)
write(6,217)
write(11,217)
write(12,217)
217 format(/,2x,' i ',5x,' r(i) ',4x,' T(i) ',5x,' Qg(i) ')
write(6,218)
write(11,218)
write(12,218)
218 format(2x,5('-',),4x,7('-',),4x,7('-',),3x,10('-',),/)

do 300 nprntr=ntotal+1,1,-1
write(6,219)nprntr,r(nprntr),T(nprntr,itr),Qg(nprntr)
write(11,219)nprntr,r(nprntr),T(nprntr,itr),Qg(nprntr)
write(12,219)nprntr,r(nprntr),T(nprntr,itr),Qg(nprntr)
219 format(3x,I3,3x,F8.3,2x,F10.1,2x,E11.4)
300 continue

* Determine the rocket engine parameters for the "exit" conditions.
* -----

write(6,301)
write(11,301)
write(12,301)
301 format(11(/),2x,'==== ROCKET ENGINE PARAMETERS ====',/)

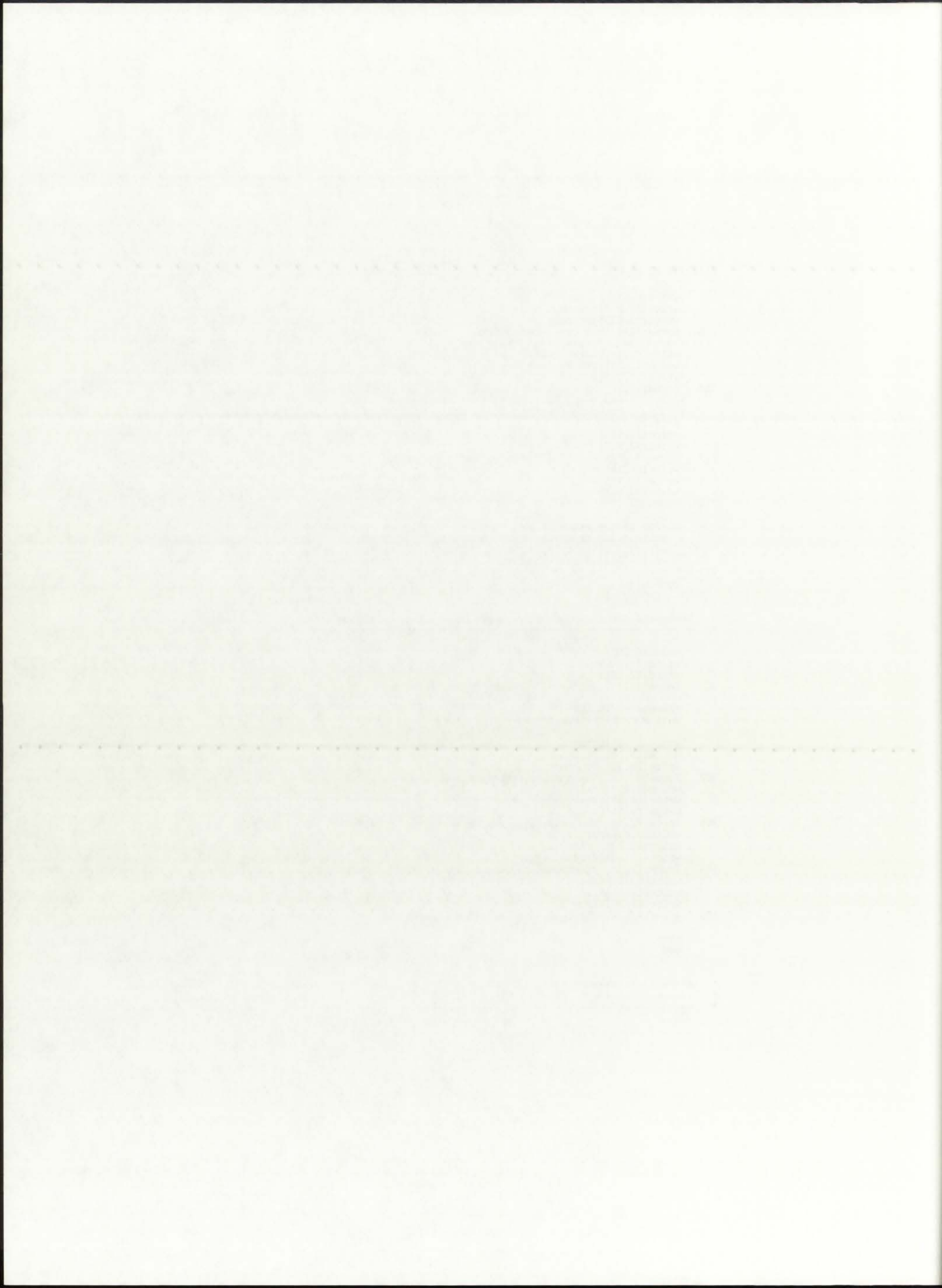
Tchamber=T(25,itr)
call ROCKET(Tchamber,P,tP,vP,Vexit,F,Isp)

write(6,302)Tchamber
write(11,302)Tchamber
write(12,302)Tchamber
302 format(/,2x,'The chamber temperature is: ',8x,F8.1,' K')
write(6,303)Vexit
write(11,303)Vexit
write(12,303)Vexit
303 format(/,2x,'The calculated exit velocity is: ',3x,F8.1,' m/s')
write(6,304)F/1000.
write(11,304)F/1000.
write(12,304)F/1000.
304 format(/,2x,'The calculated thrust is: ',7x,F10.1,' kN')
write(6,305)Isp
write(11,305)Isp
write(12,305)Isp
305 format(/,2x,'The calculated specific impulse is: ',F7.1,' s',/)

stop
end

* =====
* ===== THE END OF THE MAIN PROGRAM =====
* =====

```



```

* -----
* -----  SUBROUTINE Rosseland Mean Opacity (RMO)  -----
* -----
* Subroutine RMO calculates the temperature-dependent Rosseland
* Mean Opacity, aR [1/m], for the five regions subject to radia-
* tion heat transfer. A 16-group RMO library structure is used,
* with an effective temperature range of 3,500 K - 110,000 K. A
* set of 3 operating pressures can be used: 250,500,& 1,000 atm.
*
* UNITS:  aRP      .....   [1/m]   (Propellant RMO)
*         aRSiW   .....   [1/m]   (Silicon Wall RMO)
*         aRBG    .....   [1/m]   (Buffer Gas RMO)
*         aRF     .....   [1/m]   (Fuel RMO)
*         aRArF   .....   [1/m]   (Argon/Fuel Mixture RMO)
*         T       .....   [K]    (local node temperature)
*         P       .....   [atm]  (operating pressure)

```

```
subroutine RMO(T, P, aRP, aRSiW, aRBG, aRF, aRArF)
```

```
real T, P, aRP, aRSiW, aRBG, aRF, aRArF
```

```
if (P.eq.250.0) then
```

```
  if (T.le.3500.) then
```

```
    aRP=12.0
    aRSiW=10.0
    aRBG=2.0e-4
    aRF=150000.
    aRArF=75000.
```

```
  elseif (T.le.5000.) then
```

```
    aRP=20.0
    aRSiW=10.0
    aRBG=2.0e-4
    aRF=150365.
    aRArF=75182.5
```

```
  elseif (T.le.6500.) then
```

```
    aRP=25.0
    aRSiW=10.0
    aRBG=2.0e-4
    aRF=153025.
    aRArF=76512.5
```

```
  elseif (T.le.8000.) then
```

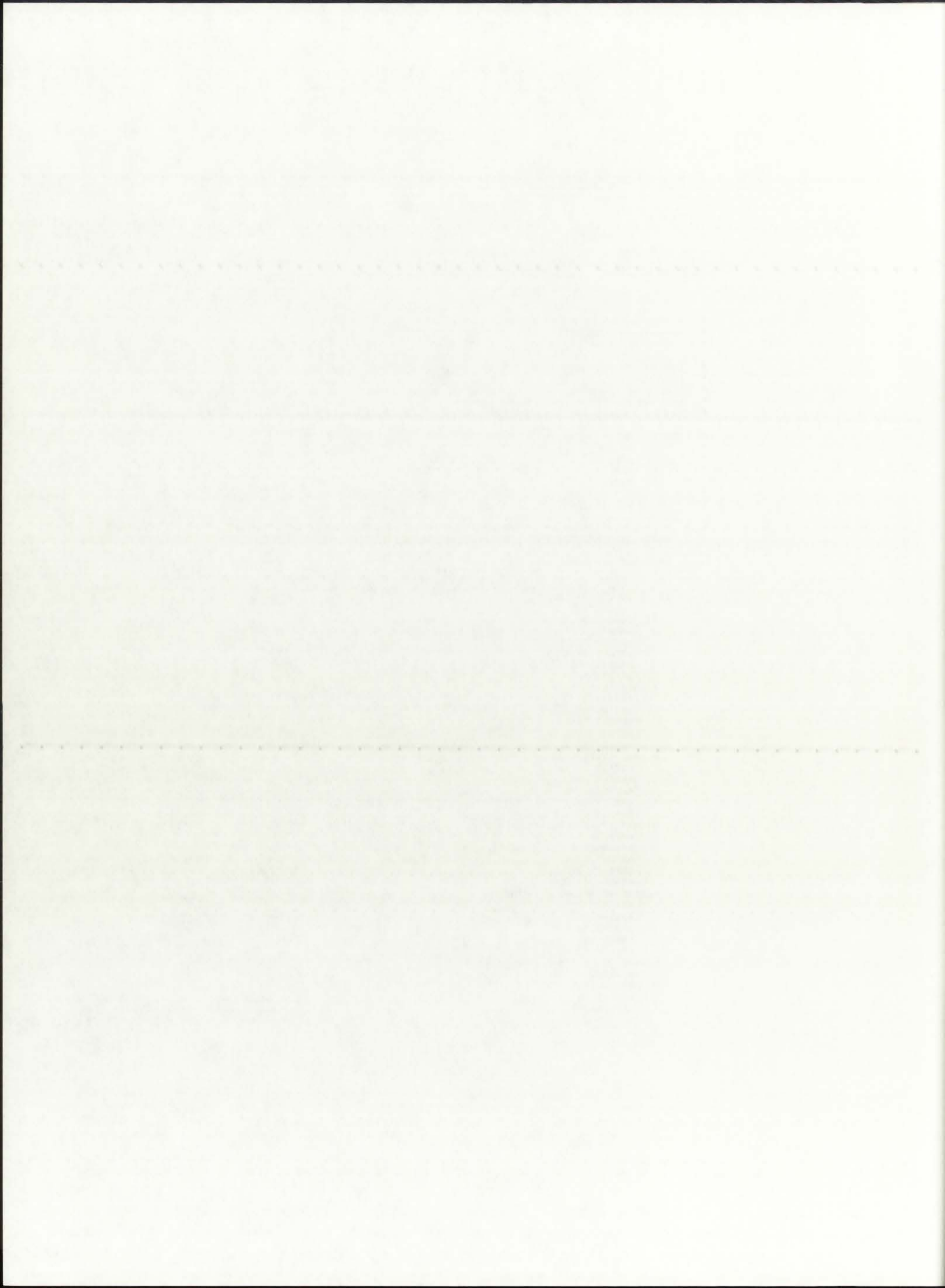
```
    aRP=100.0
    aRSiW=10.0
    aRBG=2.0e-4
    aRF=169621.
    aRArF=84810.5
```

```
  elseif (T.le.10000.) then
```

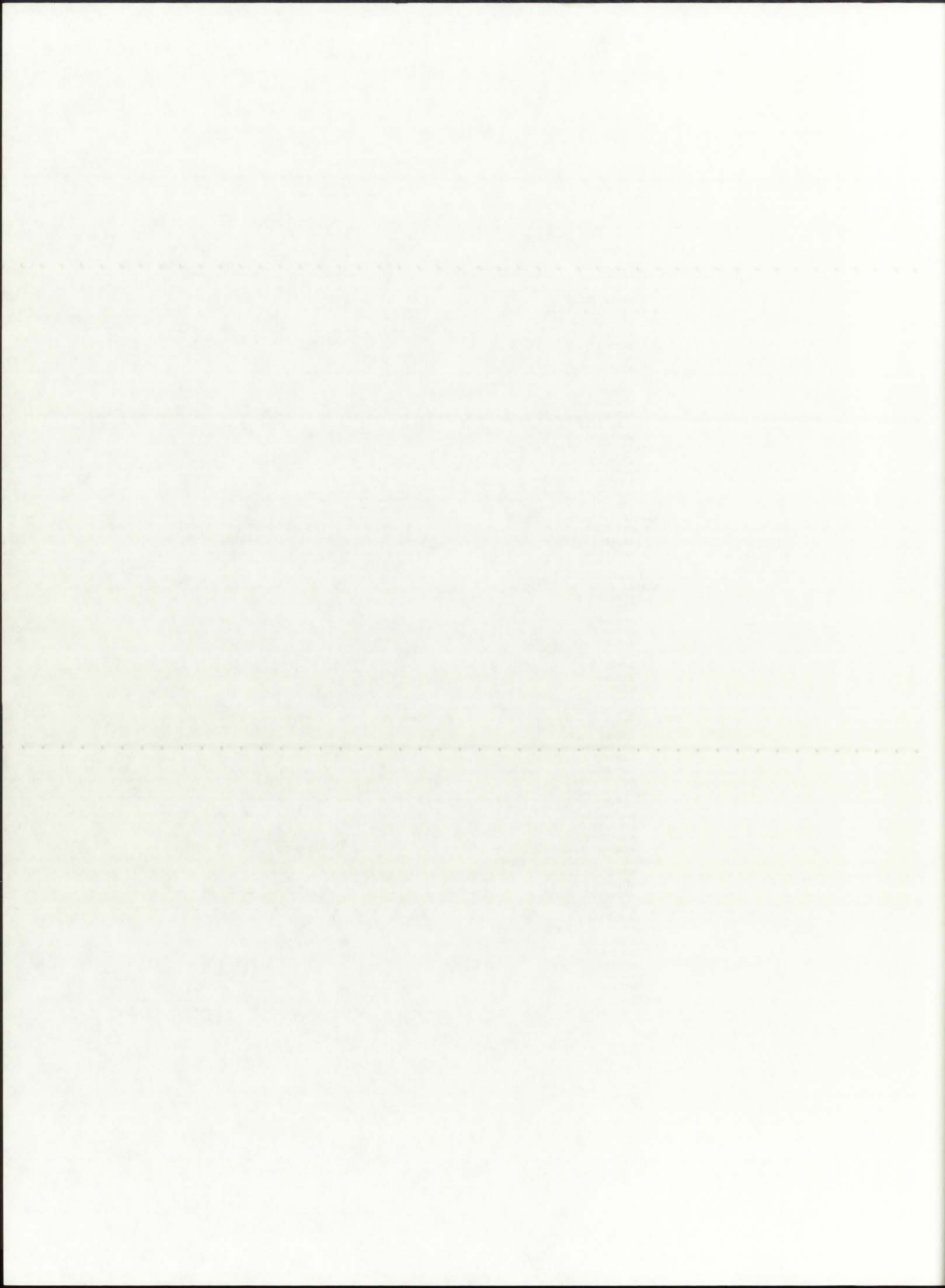
```
    aRP=400.0
    aRSiW=10.0
    aRBG=2.0e-4
    aRF=191006.
    aRArF=95503.
```

```
  elseif (T.le.13000.) then
```

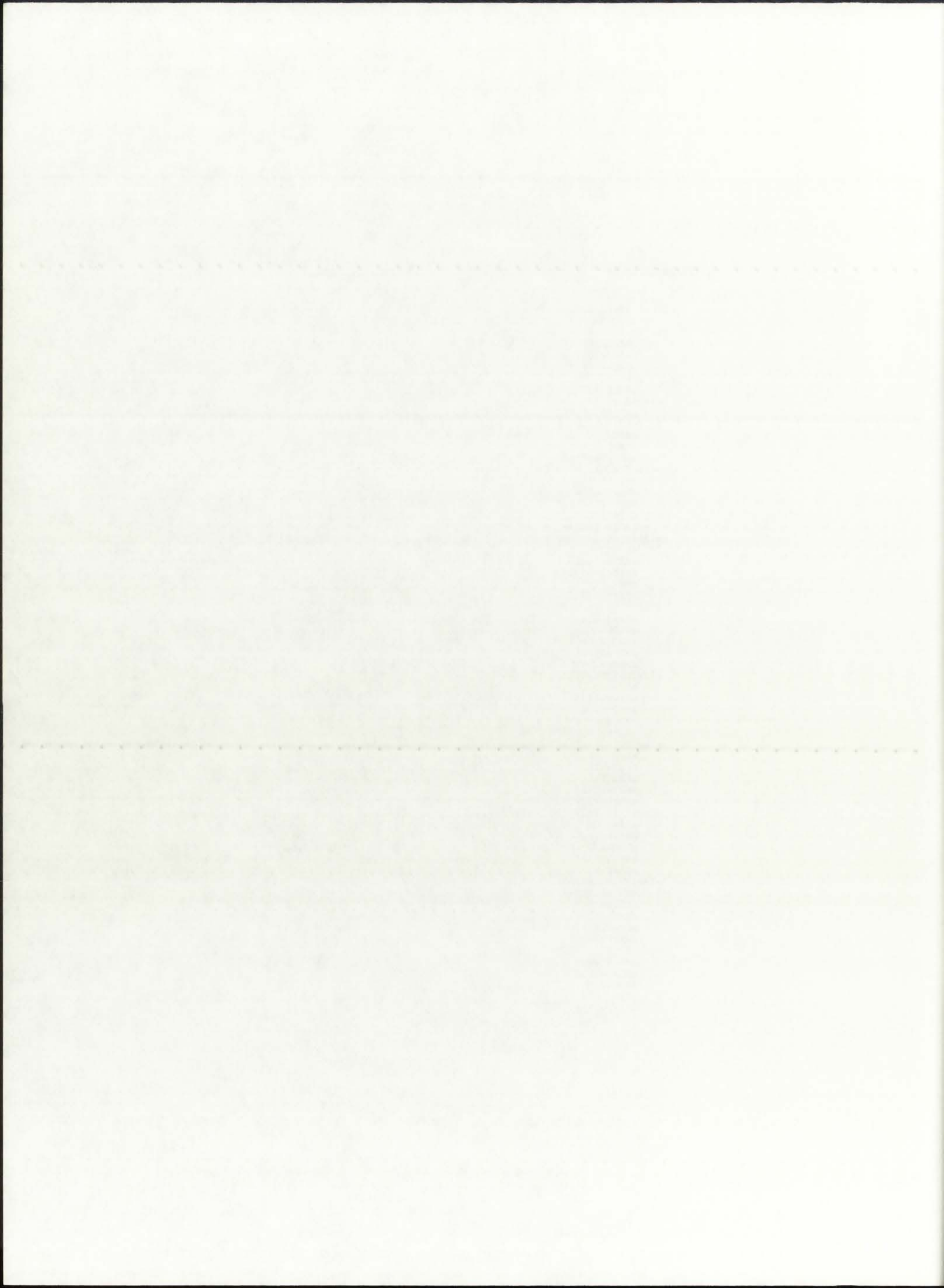
```
    aRP=800.0
    aRSiW=10.0
    aRBG=1.0e-3
    aRF=188307.
```




```
aRrF=94153.5
elseif (T.le.16000.) then
  aRP=2000.0
  aRSiW=10.0
  aRBG=1.0e-2
  aRF=141483.
  aRrF=70741.5
elseif (T.le.20000.) then
  aRP=5000.0
  aRSiW=10.0
  aRBG=0.2
  aRF=79146.
  aRrF=39573.
elseif (T.le.25000.) then
  aRP=6500.0
  aRSiW=10.0
  aRBG=1.0
  aRF=41629.5
  aRrF=20814.8
elseif (T.le.30000.) then
  aRP=5100.0
  aRSiW=10.0
  aRBG=4.0
  aRF=25044.5
  aRrF=12522.3
elseif (T.le.40000.) then
  aRP=2000.0
  aRSiW=10.0
  aRBG=10.0
  aRF=15889.
  aRrF=7944.5
elseif (T.le.50000.) then
  aRP=110.0
  aRSiW=10.0
  aRBG=10.0
  aRF=8934.
  aRrF=4467.
elseif (T.le.70000.) then
  aRP=28.0
  aRSiW=10.0
  aRBG=10.0
  aRF=4968.
  aRrF=2484.
elseif (T.le.90000.) then
  aRP=5.0
  aRSiW=10.0
  aRBG=10.0
  aRF=2103.5
  aRrF=1051.7
elseif (T.le.110000.) then
  aRP=2.0
  aRSiW=10.0
  aRBG=10.0
  aRF=641.5
  aRrF=320.8
elseif (T.gt.110000.) then
  aRP=0.001
  aRSiW=10.0
  aRBG=10.0
  aRF=0.001
  aRrF=0.001
endif
```

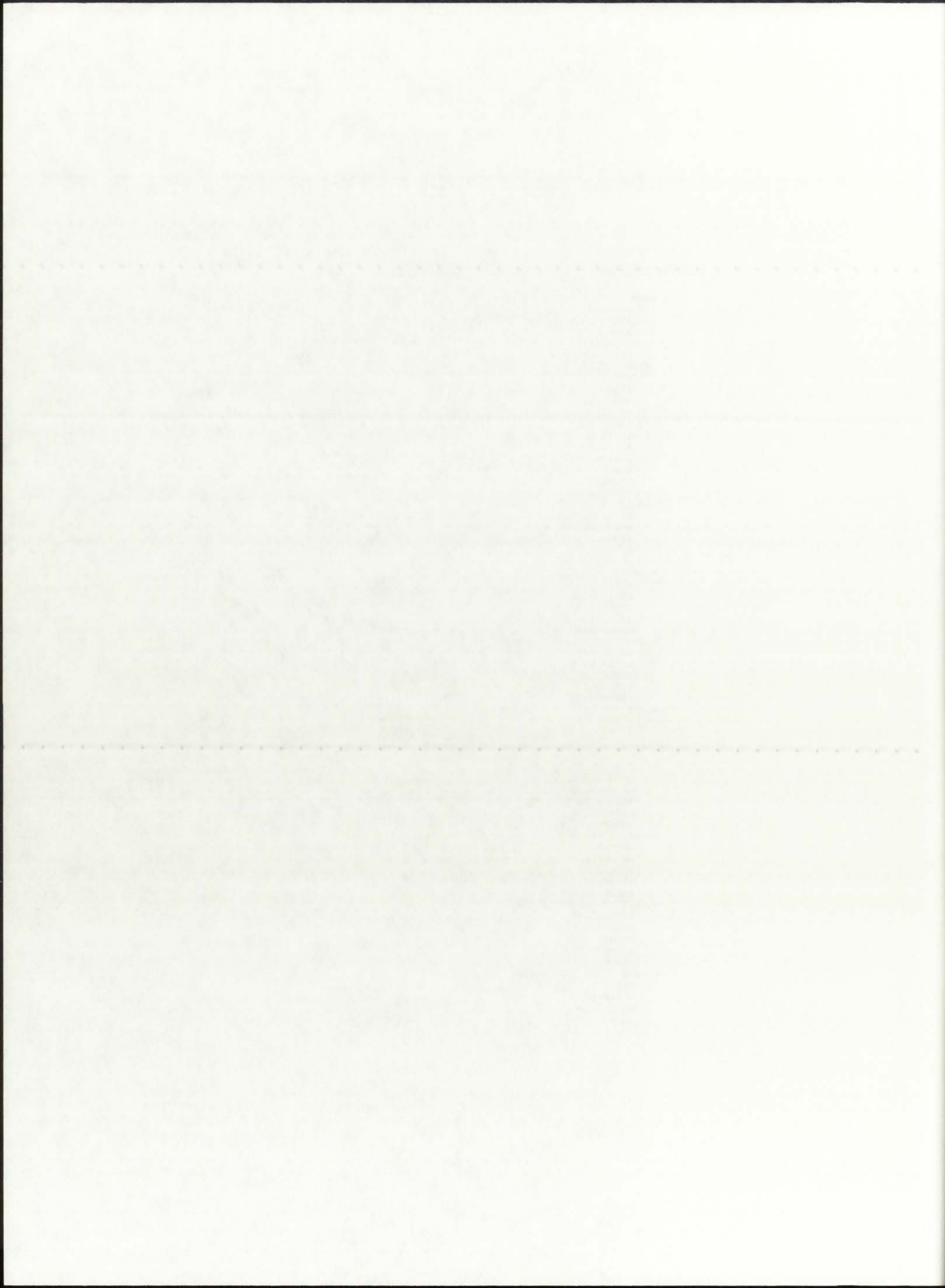


```
elseif (P.eq.500.0) then
  if (T.le.3500.) then
    aRP=12.0
    aRSiW=10.0
    aRBG=2.0e-4
    aRF=300000.
    aRArF=150000.
  elseif (T.le.5000.) then
    aRP=20.0
    aRSiW=10.0
    aRBG=2.0e-4
    aRF=317179.
    aRArF=158590.
  elseif (T.le.6500.) then
    aRP=25.0
    aRSiW=10.0
    aRBG=2.0e-4
    aRF=361672.
    aRArF=180836.
  elseif (T.le.8000.) then
    aRP=100.0
    aRSiW=10.0
    aRBG=2.0e-4
    aRF=380994.
    aRArF=190497.
  elseif (T.le.10000.) then
    aRP=400.0
    aRSiW=10.0
    aRBG=2.0e-4
    aRF=419345.
    aRArF=209673.
  elseif (T.le.13000.) then
    aRP=800.0
    aRSiW=10.0
    aRBG=1.0e-3
    aRF=406855.
    aRArF=203428.
  elseif (T.le.16000.) then
    aRP=2000.0
    aRSiW=10.0
    aRBG=1.0e-2
    aRF=245437.
    aRArF=122719.
  elseif (T.le.20000.) then
    aRP=5000.0
    aRSiW=10.0
    aRBG=0.2
    aRF=127958.
    aRArF=63979.
  elseif (T.le.25000.) then
    aRP=6500.0
    aRSiW=10.0
    aRBG=1.0
    aRF=72616.
    aRArF=36308.
  elseif (T.le.30000.) then
    aRP=5100.0
    aRSiW=10.0
    aRBG=4.0
    aRF=47974.
    aRArF=23987.
```

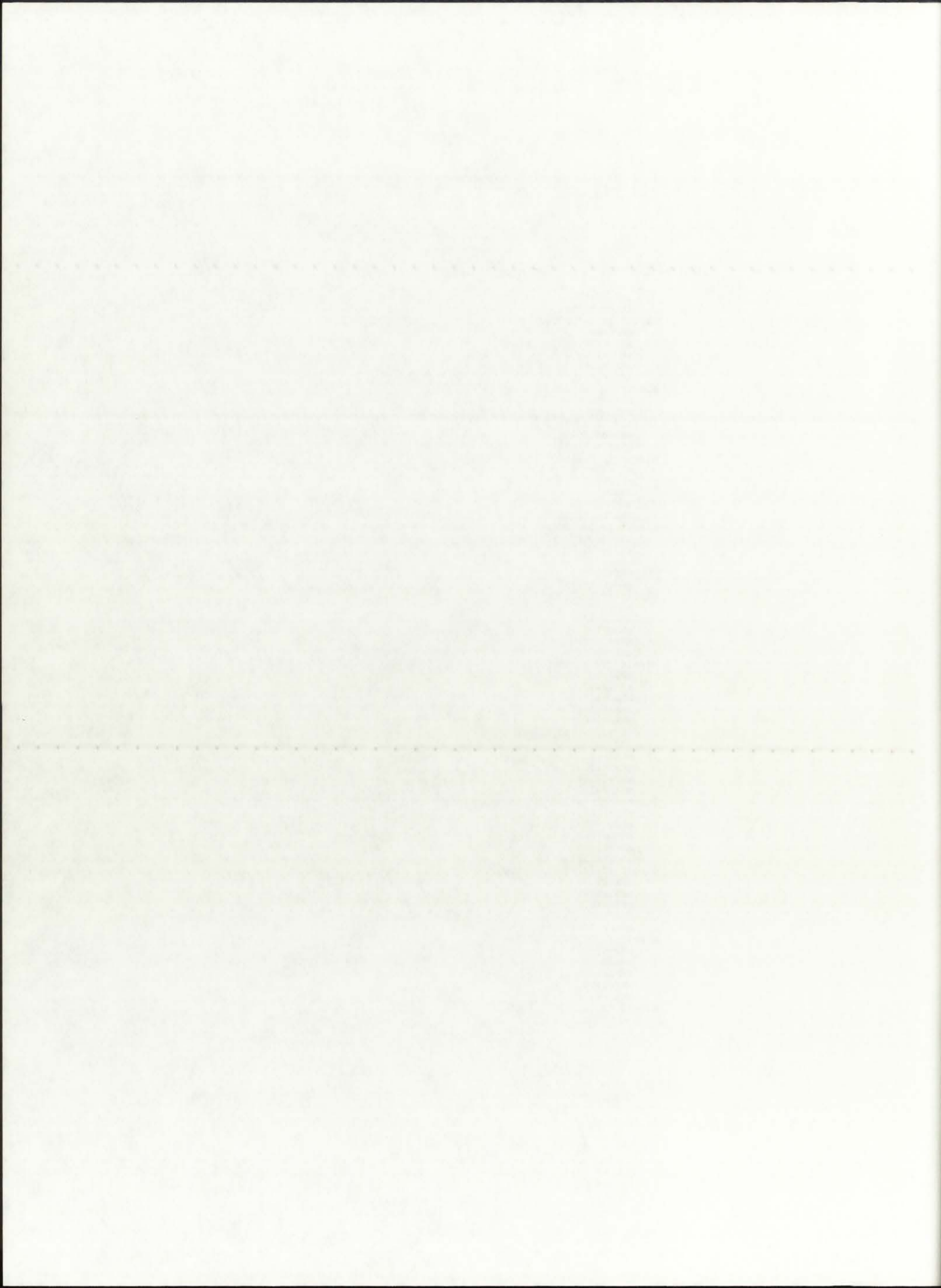


```
elseif (T.le.40000.) then
  aRP=2000.0
  aRSiW=10.0
  aRBG=10.0
  aRF=27478.
  aRArF=13739.
elseif (T.le.50000.) then
  aRP=110.0
  aRSiW=10.0
  aRBG=10.0
  aRF=17300.
  aRArF=8650.
elseif (T.le.70000.) then
  aRP=28.0
  aRSiW=10.0
  aRBG=10.0
  aRF=8193.
  aRArF=4097.
elseif (T.le.90000.) then
  aRP=5.0
  aRSiW=10.0
  aRBG=10.0
  aRF=3302.
  aRArF=1651.
elseif (T.le.110000.) then
  aRP=2.0
  aRSiW=10.0
  aRBG=10.0
  aRF=1087.
  aRArF=544.
elseif (T.gt.110000.) then
  aRP=0.001
  aRSiW=10.0
  aRBG=10.0
  aRF=0.01
  aRArF=0.01
endif
```

```
elseif (P.eq.1000.0) then
  if (T.le.3500.) then
    aRP=12.0
    aRSiW=10.0
    aRBG=2.0e-4
    aRF=610000.
    aRArF=305000.
  elseif (T.le.5000.) then
    aRP=20.0
    aRSiW=10.0
    aRBG=2.0e-4
    aRF=664097.
    aRArF=332050.
  elseif (T.le.6500.) then
    aRP=25.0
    aRSiW=10.0
    aRBG=2.0e-4
    aRF=675232.
    aRArF=337616.
  elseif (T.le.8000.) then
    aRP=100.0
    aRSiW=10.0
    aRBG=2.0e-4
```



```
aRF=774375.  
aRrF=387188.  
elseif (T.le.10000.) then  
aRP=400.0  
aRSiW=10.0  
aRBG=2.0e-4  
aRF=862540.  
aRrF=431270.  
elseif (T.le.13000.) then  
aRP=800.0  
aRSiW=10.0  
aRBG=1.0e-3  
aRF=863362.  
aRrF=431681.  
elseif (T.le.16000.) then  
aRP=2000.0  
aRSiW=10.0  
aRBG=1.0e-2  
aRF=592118.  
aRrF=296059.  
elseif (T.le.20000.) then  
aRP=5000.0  
aRSiW=10.0  
aRBG=0.2  
aRF=335920.  
aRrF=167960.  
elseif (T.le.25000.) then  
aRP=6500.0  
aRSiW=10.0  
aRBG=1.0  
aRF=180099.  
aRrF=90050.  
elseif (T.le.30000.) then  
aRP=5100.0  
aRSiW=10.0  
aRBG=4.0  
aRF=112421.  
aRrF=56211.  
elseif (T.le.40000.) then  
aRP=2000.0  
aRSiW=10.0  
aRBG=10.0  
aRF=67224.  
aRrF=33612.  
elseif (T.le.50000.) then  
aRP=110.0  
aRSiW=10.0  
aRBG=10.0  
aRF=42450.  
aRrF=21225.  
elseif (T.le.70000.) then  
aRP=28.0  
aRSiW=10.0  
aRBG=10.0  
aRF=20096.  
aRrF=10048.  
elseif (T.le.90000.) then  
aRP=5.0  
aRSiW=10.0  
aRBG=10.0  
aRF=9494.  
aRrF=4747.  
elseif (T.le.110000.) then
```




```

      aRP=2.0
      aRSIW=10.0
      aRBG=10.0
      aRF=3486.
      aRARF=1743.
    elseif (T.gt.110000.) then
      aRP=0.001
      aRSIW=10.0
      aRBG=10.0
      aRF=0.01
      aRARF=0.01
    endif
  endif

  return
end

```

```

* ----- *
* - SUBROUTINE Heat Transfer Coefficient - Propellant (HTCP) - *
* ----- *

```

```

* Subroutine HTCP calculates the heat transfer coefficient of the
* hydrogen propellant gas as a function of propellant temperature
* and physical properties. A 16-group physical property library
* structure is used, with an effective range of 3,000 - 30,000 K.
* All the physical properties were obtained from the "NBS_ph2.f"
* program by James T. Walton (NASA LeRC, 7/1992), either directly
* or by linear interpolation and extrapolation.

```

```

* UNITS: rho      ..... [kg/m3]      (mass density)
*         [Pr]     ..... unitless     (Prandtl number)
*         mu       ..... [kg/m-s]     (viscosity)
*         k        ..... [W/m-K]     (thermal conductivity)
*         Dhydraul ..... [m]         (mean hydraulic diameter)
*         vP       ..... [m/s]       (propellant ax. velocity)
*         hP       ..... [W/m2-K]    (heat trans. coefficient)
*         Taux     ..... [K]         (bulk temperature)
*         P        ..... [atm]      (operating pressure)

```

```
subroutine HTCP(Taux, P, Dhydraul, vP, hP)
```

```
real Taux, P, Dhydraul, vP, rho, mu, Pr, k, hP
```

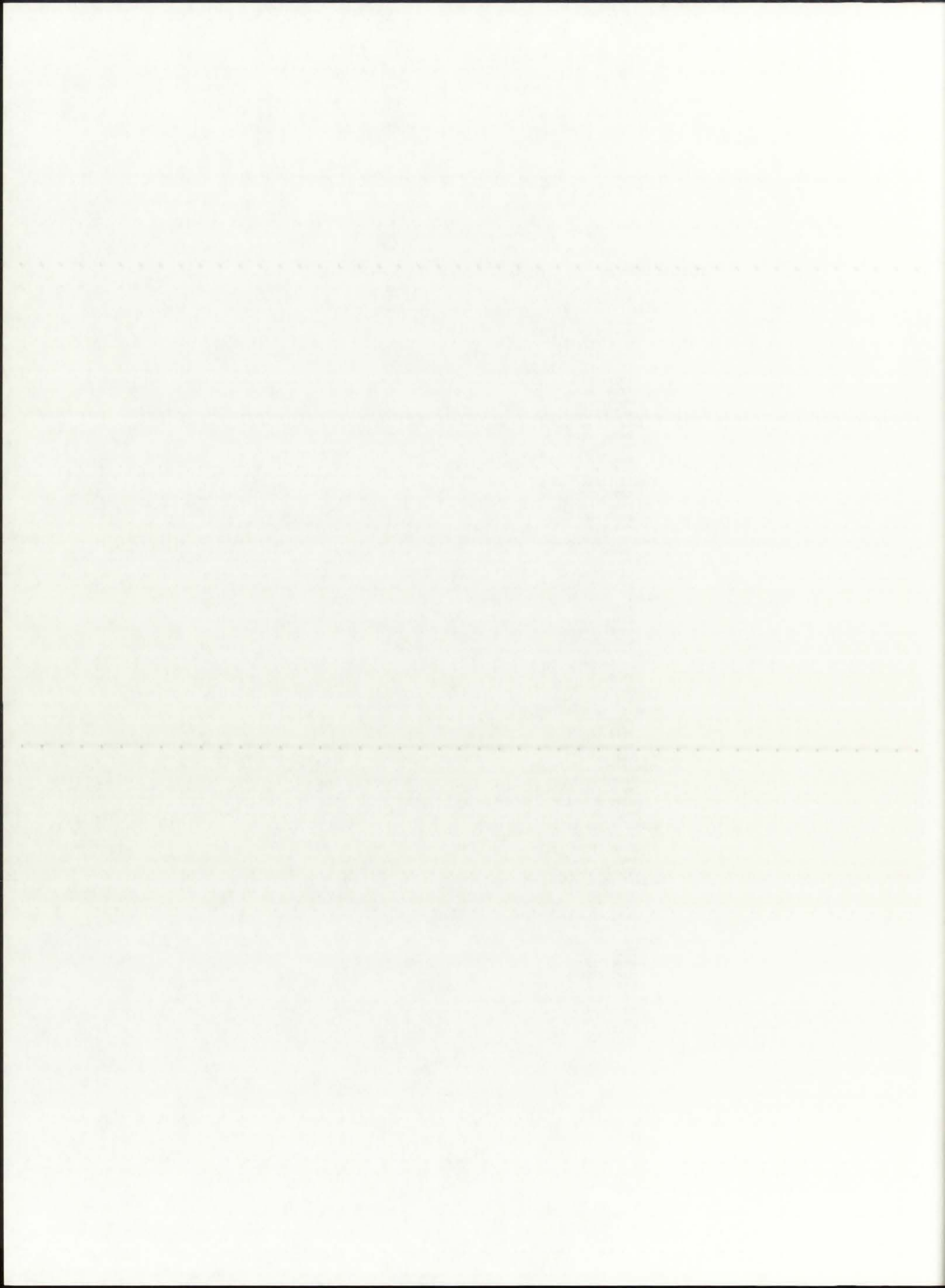
```

if (P.eq.250.0) then
  if (Taux.le.3000.0) then
    rho=2.6100
    Pr=0.5940
    mu=3.080e-5
    k=1.000
  elseif (Taux.le.4000.0) then
    rho=1.9568
    Pr=0.6160
    mu=4.281e-5
    k=1.512
  elseif (Taux.le.5000.0) then
    rho=1.4274
    Pr=0.6385
    mu=5.277e-5

```

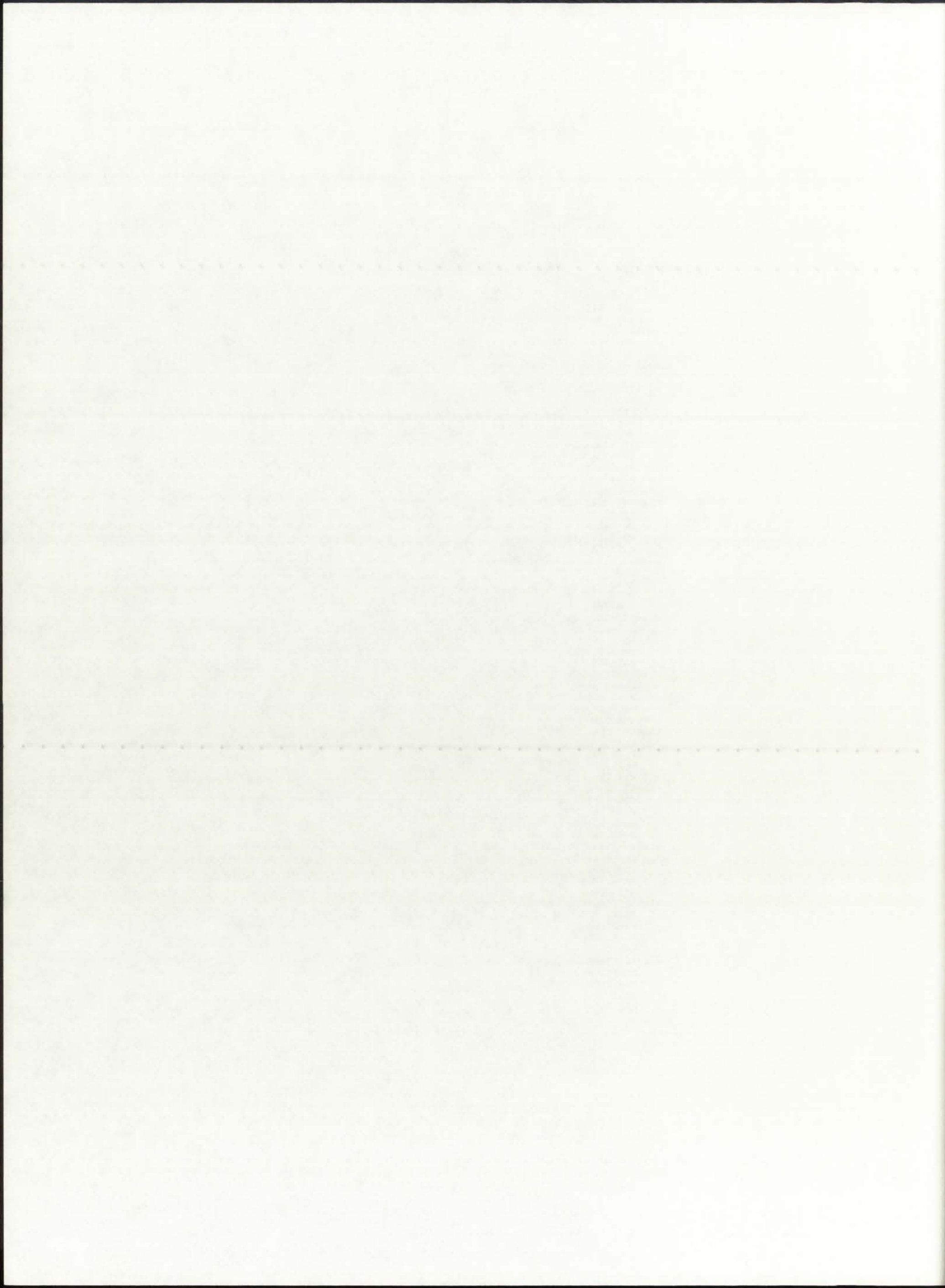


```
      k=3.253
elseif (Taux.le.6000.0) then
  rho=1.0018
  Pr=0.6706
  mu=6.052e-5
  k=6.384
elseif (Taux.le.7000.0) then
  rho=0.6802
  Pr=0.7594
  mu=6.637e-5
  k=7.867
elseif (Taux.le.8000.0) then
  rho=0.4948
  Pr=0.8175
  mu=7.133e-5
  k=6.038
elseif (Taux.le.9000.0) then
  rho=0.3998
  Pr=0.7979
  mu=7.668e-5
  k=4.158
elseif (Taux.le.10000.0) then
  rho=0.3438
  Pr=0.7611
  mu=8.226e-5
  k=3.358
elseif (Taux.le.12000.0) then
  rho=0.3045
  Pr=0.7588
  mu=8.778e-5
  k=3.120
elseif (Taux.le.14000.0) then
  rho=0.2500
  Pr=0.7500
  mu=9.800e-5
  k=2.860
elseif (Taux.le.16000.0) then
  rho=0.2080
  Pr=0.7416
  mu=1.080e-4
  k=2.749
elseif (Taux.le.18000.0) then
  rho=0.1650
  Pr=0.7330
  mu=1.195e-4
  k=2.666
elseif (Taux.le.20000.0) then
  rho=0.1250
  Pr=0.7300
  mu=1.32e-4
  k=2.530
elseif (Taux.le.25000.0) then
  rho=0.0830
  Pr=0.7250
  mu=1.430e-4
  k=2.440
elseif (Taux.le.30000.0) then
  rho=0.0050
  Pr=0.7150
  mu=1.720e-4
  k=2.240
elseif (Taux.gt.30000.0) then
  rho=0.0010
```



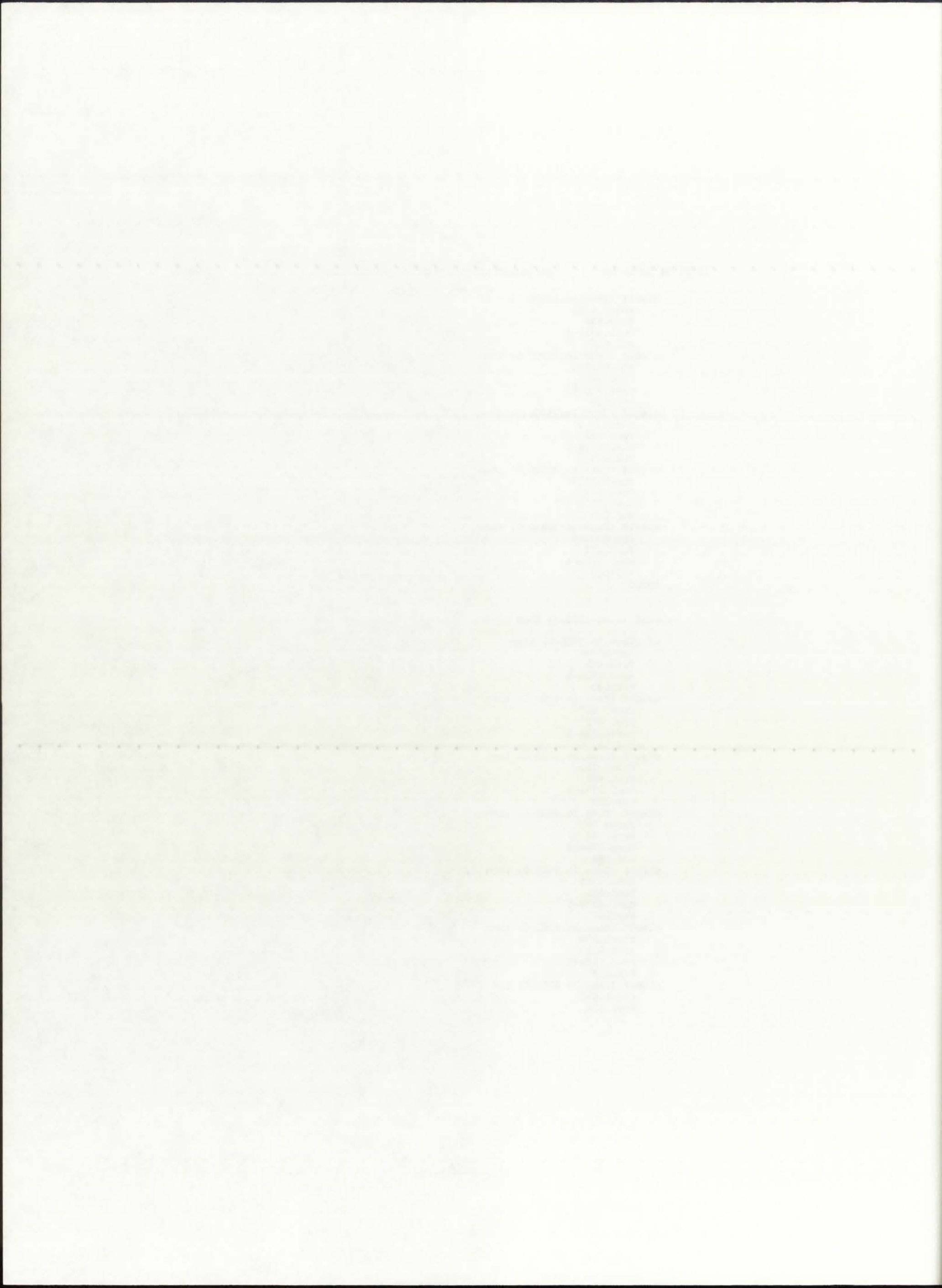
```
Pr=0.7050
mu=2.010e-4
k=2.040
endif
```

```
elseif (P.eq.500.0) then
  if (Taux.le.3000.0) then
    rho=4.97
    Pr=0.519
    mu=3.080e-5
    k=1.000
  elseif (Taux.le.4000.0) then
    rho=3.9136
    Pr=0.539
    mu=4.281e-5
    k=1.512
  elseif (Taux.le.5000.0) then
    rho=2.8548
    Pr=0.559
    mu=5.277e-5
    k=3.253
  elseif (Taux.le.6000.0) then
    rho=2.0036
    Pr=0.587
    mu=6.052e-5
    k=6.384
  elseif (Taux.le.7000.0) then
    rho=1.3604
    Pr=0.664
    mu=6.637e-5
    k=7.867
  elseif (Taux.le.8000.0) then
    rho=0.9897
    Pr=0.715
    mu=7.133e-5
    k=6.038
  elseif (Taux.le.9000.0) then
    rho=0.7995
    Pr=0.698
    mu=7.668e-5
    k=4.158
  elseif (Taux.le.10000.0) then
    rho=0.6877
    Pr=0.715
    mu=8.226e-5
    k=3.358
  elseif (Taux.le.12000.0) then
    rho=0.6090
    Pr=0.698
    mu=8.778e-5
    k=3.120
  elseif (Taux.le.14000.0) then
    rho=0.5200
    Pr=0.666
    mu=9.800e-5
    k=2.860
  elseif (Taux.le.16000.0) then
    rho=0.4600
    Pr=0.664
    mu=1.080e-4
    k=2.749
```



```
elseif (Taux.le.18000.0) then
  rho=0.4100
  Pr=0.656
  mu=1.195e-4
  k=2.666
elseif (Taux.le.20000.0) then
  rho=0.3800
  Pr=0.649
  mu=1.32e-4
  k=2.530
elseif (Taux.le.25000.0) then
  rho=0.3600
  Pr=0.642
  mu=1.430e-4
  k=2.440
elseif (Taux.le.30000.0) then
  rho=0.3500
  Pr=0.639
  mu=1.720e-4
  k=2.240
elseif (Taux.gt.30000.0) then
  rho=0.0010
  Pr=0.617
  mu=2.010e-4
  k=2.040
endif
```

```
elseif (P.eq.1000.0) then
  if (Taux.le.3000.0) then
    rho=9.930
    Pr=0.455
    mu=3.080e-5
    k=1.000
  elseif (Taux.le.4000.0) then
    rho=7.827
    Pr=0.472
    mu=4.281e-5
    k=1.512
  elseif (Taux.le.5000.0) then
    rho=5.710
    Pr=0.489
    mu=5.277e-5
    k=3.253
  elseif (Taux.le.6000.0) then
    rho=4.007
    Pr=0.513
    mu=6.052e-5
    k=6.384
  elseif (Taux.le.7000.0) then
    rho=2.721
    Pr=0.581
    mu=6.637e-5
    k=7.867
  elseif (Taux.le.8000.0) then
    rho=1.979
    Pr=0.611
    mu=7.133e-5
    k=6.038
  elseif (Taux.le.9000.0) then
    rho=1.599
    Pr=0.626
```



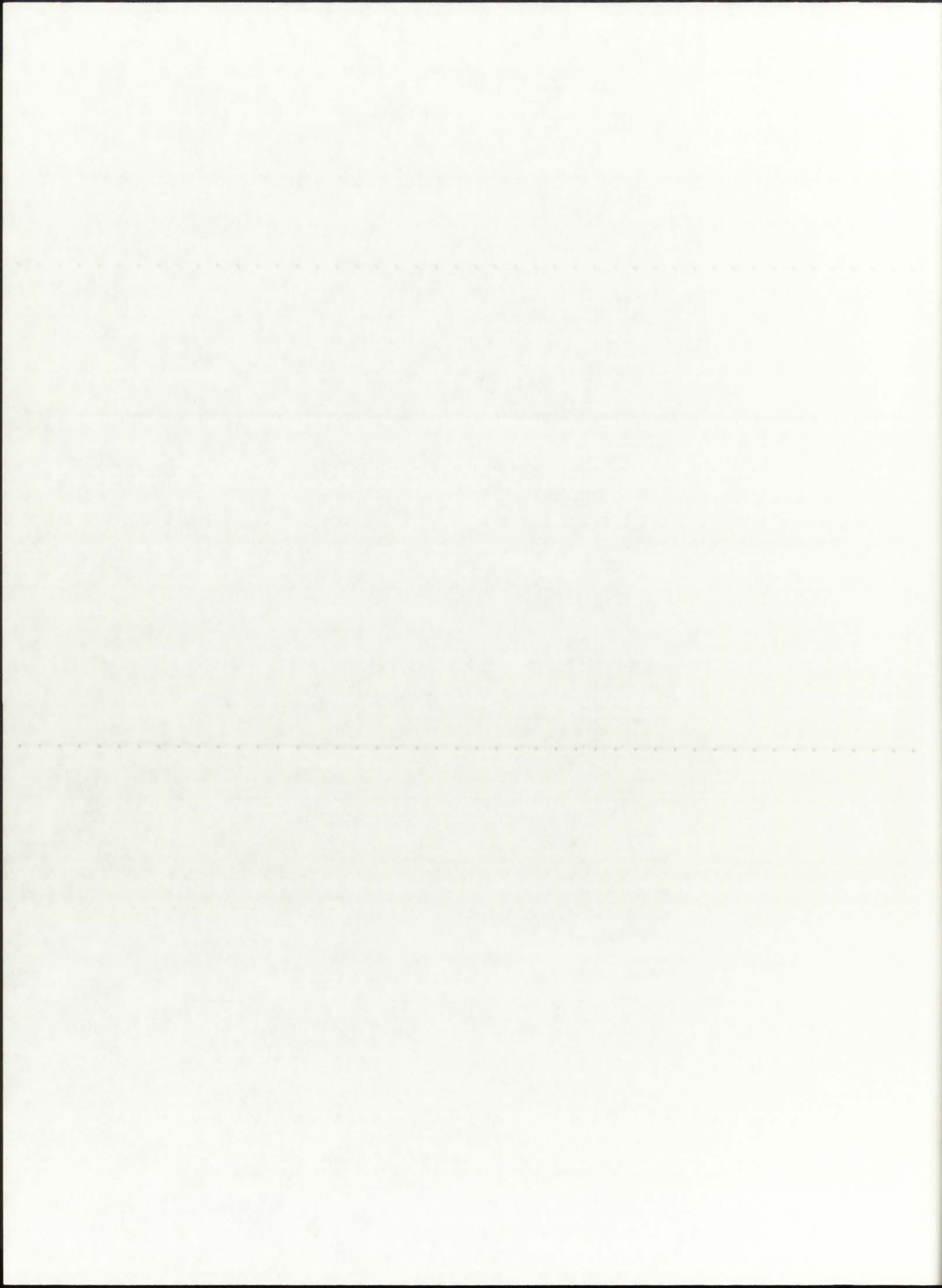

```
mu=7.668e-5
k=4.158
elseif (Taux.le.10000.0) then
rho=1.375
Pr=0.611
mu=8.226e-5
k=3.358
elseif (Taux.le.12000.0) then
rho=1.218
Pr=0.583
mu=8.778e-5
k=3.120
elseif (Taux.le.14000.0) then
rho=1.040
Pr=0.581
mu=9.800e-5
k=2.860
elseif (Taux.le.16000.0) then
rho=0.920
Pr=0.574
mu=1.080e-4
k=2.749
elseif (Taux.le.18000.0) then
rho=0.820
Pr=0.568
mu=1.195e-4
k=2.666
elseif (Taux.le.20000.0) then
rho=0.760
Pr=0.561
mu=1.32e-4
k=2.530
elseif (Taux.le.25000.0) then
rho=0.720
Pr=0.559
mu=1.430e-4
k=2.440
elseif (Taux.le.30000.0) then
rho=0.700
Pr=0.555
mu=1.720e-4
k=2.240
elseif (Taux.gt.30000.0) then
rho=0.0010
Pr=0.540
mu=2.010e-4
k=2.040
endif
endif

Re=rho*vP*Dhydraul/mu
Nu=0.023*(Re)**(4.0/5.0)*(Pr)**0.4
hP=Nu*k/Dhydraul

return
end
```

*

*



```

* - SUBROUTINE Heat Transfer Coefficient - BufferGas (HTCBG) - *
* ----- *
* Subroutine HTCBG calculates the heat transfer coefficient of the
* argon buffer gas as a function of buffer gas temperature and its
* physical properties. A 16-group library structure is used, with
* an effective range of 3,000 K - 30,000 K. All the physical data
* were obtained from the NBS_ph2.f program by modeling argon with
* hydrogen gas. This is valid since both gases exhibit almost ide-
* ntical properties at such high temperatures [CRC, 1991].
*
* UNITS: rho ..... [kg/m3] (mass density)
*         [Pr] ..... unitless (Prandtl number)
*         mu ..... [kg/m-s] (viscosity)
*         k ..... [W/m-K] (thermal conductivity)
*         Dhydraul ..... [m] (mean hydraulic diameter)
*         vBG ..... [m/s] (buffer gas ax. velocity)
*         hBG ..... [W/m2-K] (heat trans. coefficient)
*         Taux ..... [K] (bulk temperature)
*         P ..... [atm] (operating pressure)

```

```
subroutine HTCBG(Taux,P,Dhydraul,vBG,hBG)
```

```
real Taux,P,Dhydraul,vBG,rho,mu,Pr,k,hBG
```

```
if (P.eq.250.0) then
```

```
  if (Taux.le.3000.0) then
```

```
    rho=52.200
    Pr=0.5940
    mu=3.080e-5
    k=1.000
```

```
  elseif (Taux.le.4000.0) then
```

```
    rho=39.136
    Pr=0.6160
    mu=4.281e-5
    k=1.512
```

```
  elseif (Taux.le.5000.0) then
```

```
    rho=28.548
    Pr=0.6385
    mu=5.277e-5
    k=3.253
```

```
  elseif (Taux.le.6000.0) then
```

```
    rho=20.036
    Pr=0.6706
    mu=6.052e-5
    k=6.384
```

```
  elseif (Taux.le.7000.0) then
```

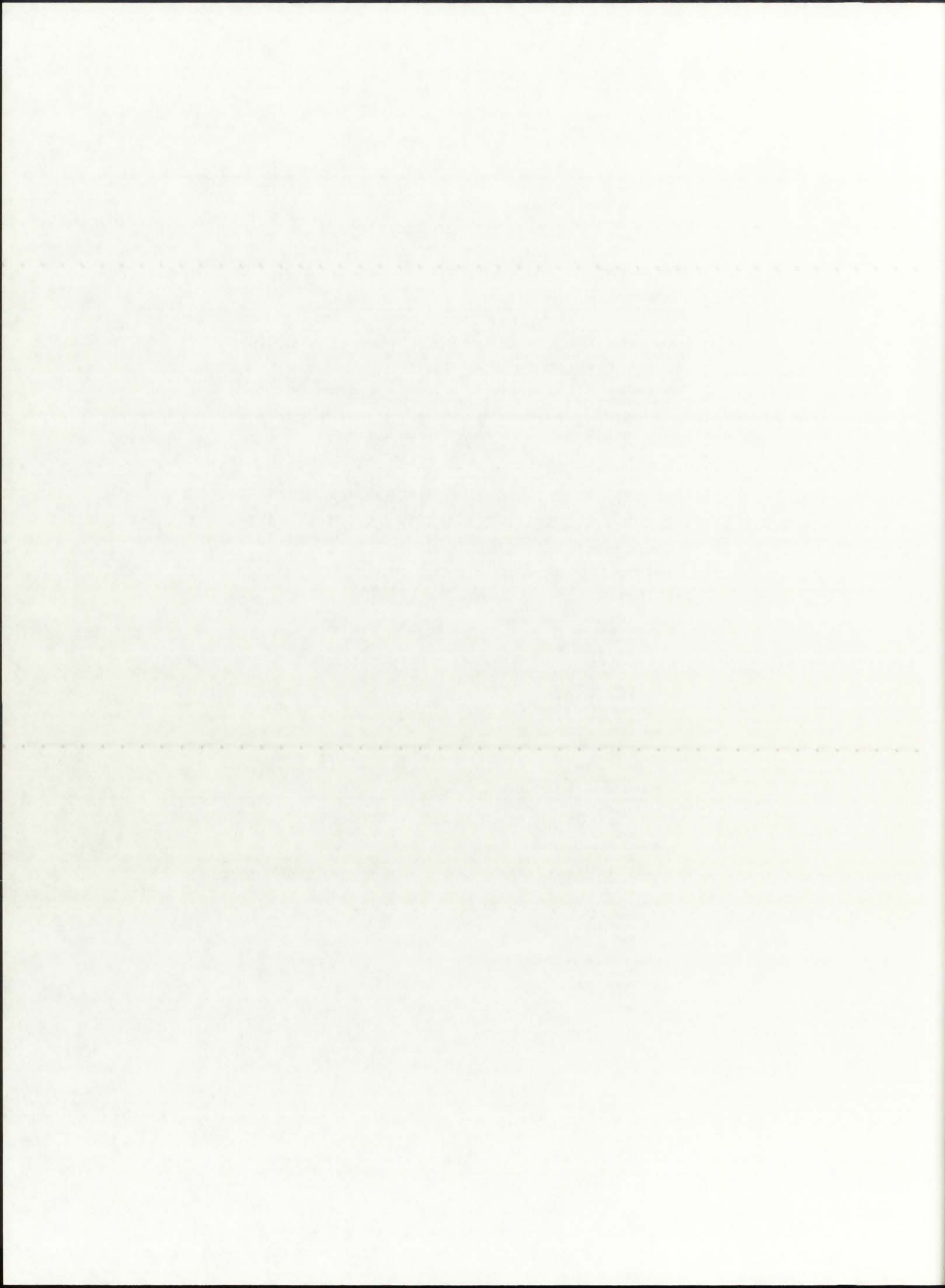
```
    rho=13.604
    Pr=0.7594
    mu=6.637e-5
    k=7.867
```

```
  elseif (Taux.le.8000.0) then
```

```
    rho=9.896
    Pr=0.8175
    mu=7.133e-5
    k=6.038
```

```
  elseif (Taux.le.9000.0) then
```

```
    rho=7.996
    Pr=0.7979
    mu=7.668e-5
    k=4.158
```



```
elseif (Taux.le.10000.0) then
  rho=6.876
  Pr=0.7611
  mu=8.226e-5
  k=3.358
elseif (Taux.le.12000.0) then
  rho=6.090
  Pr=0.7588
  mu=8.778e-5
  k=3.120
elseif (Taux.le.14000.0) then
  rho=5.000
  Pr=0.7500
  mu=9.800e-5
  k=2.860
elseif (Taux.le.16000.0) then
  rho=4.160
  Pr=0.7416
  mu=1.080e-4
  k=2.749
elseif (Taux.le.18000.0) then
  rho=3.300
  Pr=0.7330
  mu=1.195e-4
  k=2.666
elseif (Taux.le.20000.0) then
  rho=2.500
  Pr=0.7300
  mu=1.32e-4
  k=2.530
elseif (Taux.le.25000.0) then
  rho=1.660
  Pr=0.7250
  mu=1.430e-4
  k=2.440
elseif (Taux.le.30000.0) then
  rho=0.100
  Pr=0.7150
  mu=1.720e-4
  k=2.240
elseif (Taux.gt.30000.0) then
  rho=0.02
  Pr=0.7050
  mu=2.010e-4
  k=2.040
endif

elseif (P.eq.500.0) then
  if (Taux.le.3000.0) then
    rho=99.40
    Pr=0.519
    mu=3.080e-5
    k=1.000
  elseif (Taux.le.4000.0) then
    rho=78.272
    Pr=0.539
    mu=4.281e-5
    k=1.512
  elseif (Taux.le.5000.0) then
    rho=57.096
    Pr=0.559
```

1944 1 10 1000 1000
1000 1000
1000 1000
1000 1000

1944 1 10 1000 1000
1000 1000
1000 1000
1000 1000

1944 1 10 1000 1000
1000 1000
1000 1000
1000 1000

1944 1 10 1000 1000
1000 1000
1000 1000
1000 1000

1944 1 10 1000 1000
1000 1000
1000 1000
1000 1000

1944 1 10 1000 1000
1000 1000
1000 1000
1000 1000

1944 1 10 1000 1000
1000 1000
1000 1000
1000 1000

1944 1 10 1000 1000
1000 1000
1000 1000
1000 1000

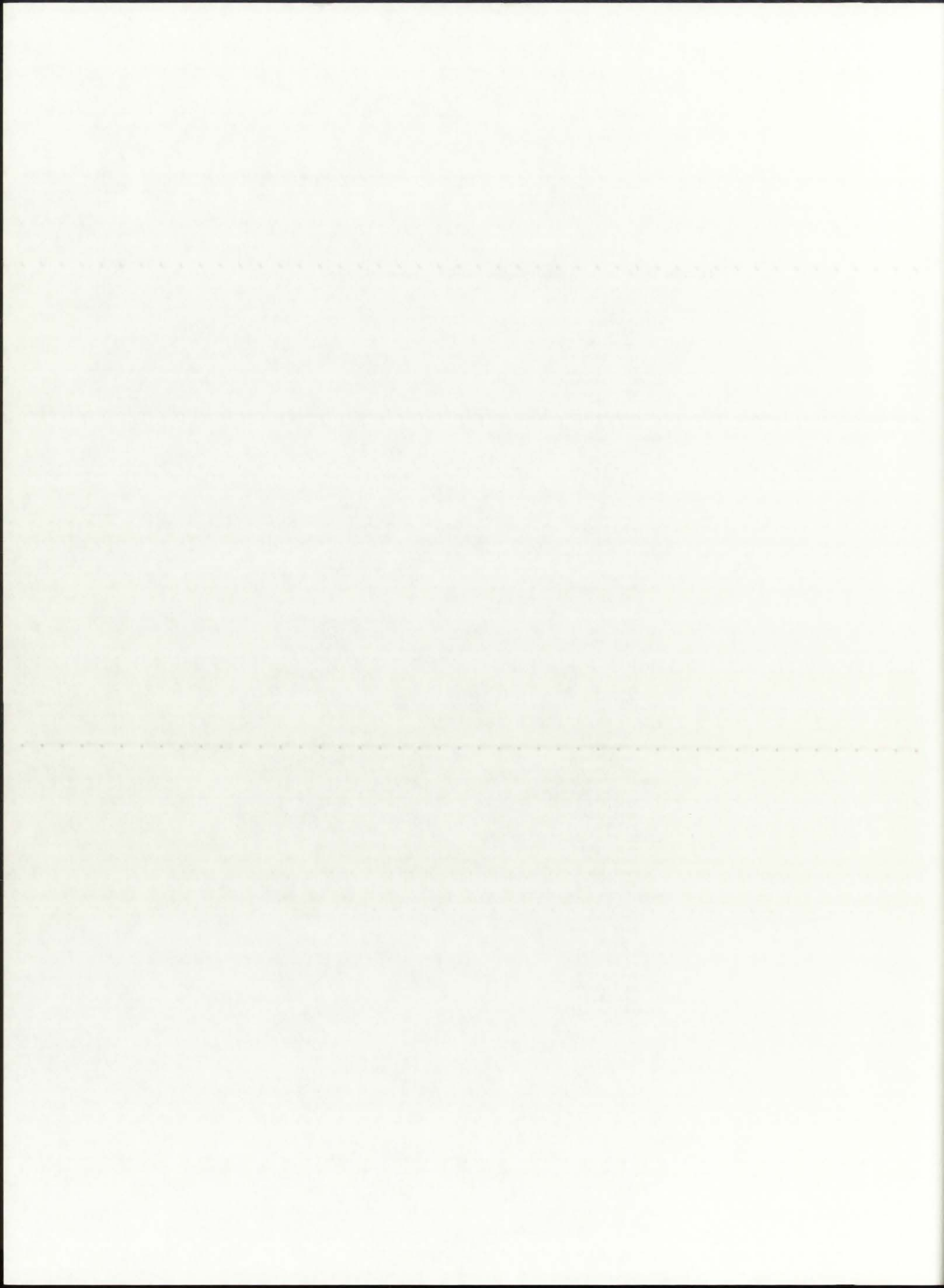
1944 1 10 1000 1000
1000 1000
1000 1000
1000 1000

1944 1 10 1000 1000
1000 1000
1000 1000
1000 1000

1944 1 10 1000 1000
1000 1000
1000 1000
1000 1000

1944 1 10 1000 1000
1000 1000
1000 1000
1000 1000

```
mu=5.277e-5
k=3.253
elseif (Taux.le.6000.0) then
rho=40.072
Pr=0.587
mu=6.052e-5
k=6.384
elseif (Taux.le.7000.0) then
rho=27.208
Pr=0.664
mu=6.637e-5
k=7.867
elseif (Taux.le.8000.0) then
rho=19.794
Pr=0.715
mu=7.133e-5
k=6.038
elseif (Taux.le.9000.0) then
rho=15.990
Pr=0.698
mu=7.668e-5
k=4.158
elseif (Taux.le.10000.0) then
rho=13.754
Pr=0.715
mu=8.226e-5
k=3.358
elseif (Taux.le.12000.0) then
rho=12.180
Pr=0.698
mu=8.778e-5
k=3.120
elseif (Taux.le.14000.0) then
rho=10.40
Pr=0.666
mu=9.800e-5
k=2.860
elseif (Taux.le.16000.0) then
rho=0.4600
Pr=0.664
mu=1.080e-4
k=2.749
elseif (Taux.le.18000.0) then
rho=9.200
Pr=0.656
mu=1.195e-4
k=2.666
elseif (Taux.le.20000.0) then
rho=7.600
Pr=0.649
mu=1.32e-4
k=2.530
elseif (Taux.le.25000.0) then
rho=7.200
Pr=0.642
mu=1.430e-4
k=2.440
elseif (Taux.le.30000.0) then
rho=7.000
Pr=0.639
mu=1.720e-4
k=2.240
elseif (Taux.gt.30000.0) then
```




```
    rho=0.020
    Pr=0.617
    mu=2.010e-4
    k=2.040
endif
```

```
elseif (P.eq.1000.0) then
```

```
  if (Taux.le.3000.0) then
    rho=198.60
    Pr=0.455
    mu=3.080e-5
    k=1.000
```

```
  elseif (Taux.le.4000.0) then
    rho=156.54
    Pr=0.472
    mu=4.281e-5
    k=1.512
```

```
  elseif (Taux.le.5000.0) then
    rho=114.20
    Pr=0.489
    mu=5.277e-5
    k=3.253
```

```
  elseif (Taux.le.6000.0) then
    rho=80.14
    Pr=0.513
    mu=6.052e-5
    k=6.384
```

```
  elseif (Taux.le.7000.0) then
    rho=54.420
    Pr=0.581
    mu=6.637e-5
    k=7.867
```

```
  elseif (Taux.le.8000.0) then
    rho=39.580
    Pr=0.611
    mu=7.133e-5
    k=6.038
```

```
  elseif (Taux.le.9000.0) then
    rho=31.980
    Pr=0.626
    mu=7.668e-5
    k=4.158
```

```
  elseif (Taux.le.10000.0) then
    rho=27.500
    Pr=0.611
    mu=8.226e-5
    k=3.358
```

```
  elseif (Taux.le.12000.0) then
    rho=24.360
    Pr=0.583
    mu=8.778e-5
    k=3.120
```

```
  elseif (Taux.le.14000.0) then
    rho=20.800
    Pr=0.581
    mu=9.800e-5
    k=2.860
```

```
  elseif (Taux.le.16000.0) then
    rho=18.400
    Pr=0.574
    mu=1.080e-4
```

100-1000
100-1000
100-1000
100-1000
100-1000

100-1000
100-1000

100-1000
100-1000
100-1000
100-1000
100-1000

100-1000
100-1000
100-1000
100-1000
100-1000

100-1000
100-1000
100-1000
100-1000
100-1000

100-1000
100-1000
100-1000
100-1000
100-1000

100-1000
100-1000
100-1000
100-1000
100-1000

100-1000
100-1000
100-1000
100-1000
100-1000

```

      k=2.749
    elseif (Taux.le.18000.0) then
      rho=16.400
      Pr=0.568
      mu=1.195e-4
      k=2.666
    elseif (Taux.le.20000.0) then
      rho=15.200
      Pr=0.561
      mu=1.32e-4
      k=2.530
    elseif (Taux.le.25000.0) then
      rho=14.400
      Pr=0.559
      mu=1.430e-4
      k=2.440
    elseif (Taux.le.30000.0) then
      rho=14.000
      Pr=0.555
      mu=1.720e-4
      k=2.240
    elseif (Taux.gt.30000.0) then
      rho=0.020
      Pr=0.540
      mu=2.010e-4
      k=2.040
    endif
  endif

```

```
endif
```

```
Re=rho*vBG*Dhydraul/mu
```

```
Nu=0.023*(Re)**(4.0/5.0)*(Pr)**0.4
```

```
hBG=Nu*k/Dhydraul
```

```
return
end
```

```

* ----- *
* ----- SUBROUTINE Rocket Performance Data (ROCKET) ----- *
* ----- *
* Subroutine ROCKET calculates the propellant exit velocity (Vexit),
* thrust (F), and specific impulse (Isp) based on the given chamber
* temperature and other thermophysical properties of the propellant.
*
* UNITS: Acsexit ..... [m2] (Propellant flow cs area)
* Alpha ..... (hydrogen dissociation fraction)
* go ..... [m/s2] (acceleration of gravity)
* h ..... [J-s] (Planck's constant)
* k ..... [J/K] (Boltzmann's constant)
* matom ..... [kg] (hydrogen atom mass)
* Mwh ..... [g/gmol] (at. mass of hydrogen)
* Mwh2 ..... [g/gmol] (mol. mass of hydrogen)
* Mwhydro ..... [g/gmol] (hydrogen component mass)
* Mwprop ..... [g/gmol] (propellant mol. mass)
* Mwwhat ..... [g/gmol] (tungsten seed mol. mass)
* pi ..... (3.14159)
* Pressure ..... [Pa] (prop. total pressure)
* R ..... [J/gmol-K] (univ. gas constant)

```

1967
1968
1969
1970
1971
1972
1973
1974
1975
1976
1977
1978
1979
1980
1981
1982
1983
1984
1985
1986
1987
1988
1989
1990
1991
1992
1993
1994
1995
1996
1997
1998
1999
2000
2001
2002
2003
2004
2005
2006
2007
2008
2009
2010
2011
2012
2013
2014
2015
2016
2017
2018
2019
2020
2021
2022
2023
2024
2025
2026
2027
2028
2029
2030

```

*      Rpin      ..... [m] (propellant inner radius)
*      Rpout     ..... [m] (propellant outer radius)
*      Tchamber  ..... [K] (propellant chamber temp)
*      ThetaD   ..... [K] (character. dissociation temp)
*      ThetaR   ..... [K] (character. rotation temp)
*      ThetaV   ..... [K] (character. vibration temp)
*      Qelatom  ..... (at. electr. partit. funct)
*      Qelmolec ..... (mol.electr. partit. funct)
*      vP       ..... [m/s] (ax. exit channel velocity)
*      X        ..... (aux. dissociation variable)

```

```
subroutine ROCKET(Tchamber,P,tP,vP,Vexit,F,Isp)
```

```
real vP,go,h,k,matom,MwH,MwH2,MwWnat,pi,P,Pressure,R,Rpin,Rpout,ThetaD,
> ThetaR,ThetaV,Qelatom,Qelmolec,Tchamber,tP,gamexit,rhoexit,Acsexit
```

```
double precision X,Vexit,F,Isp,alpha,Mwhydro,Mwprop,mexit
```

```
* Specify the pertinent constants.
```

```
*
```

```

go=9.807
h=6.6262e-34
k=1.3806e-23
matom=1.67e-27
MwH=1.008
MwH2=2.016
MwWnat=183.85
pi=3.14156
Pressure=P*101325.0
R=8.314
Rpin=0.2494
Rpout=0.2918
ThetaD=51956.0
ThetaR=85.7
ThetaV=5980.0
Qelatom=2.0
Qelmolec=4.0

```

```
* Determine the dissociating variable X.
```

```
*
```

```

X=exp(-ThetaD/Tchamber)/(2.0*Pressure)*(((pi*matom*k*Tchamber)/
> (h**2.0))**(1.5)*k*ThetaR*(1.0-exp(-ThetaV/Tchamber))*(Qelatom
> **2.0/Qelmolec))

```

```
* Determine the dissociation fraction ALPHA.
```

```
*
```

```
alpha=(X/(1.0+X))**0.5
```

```

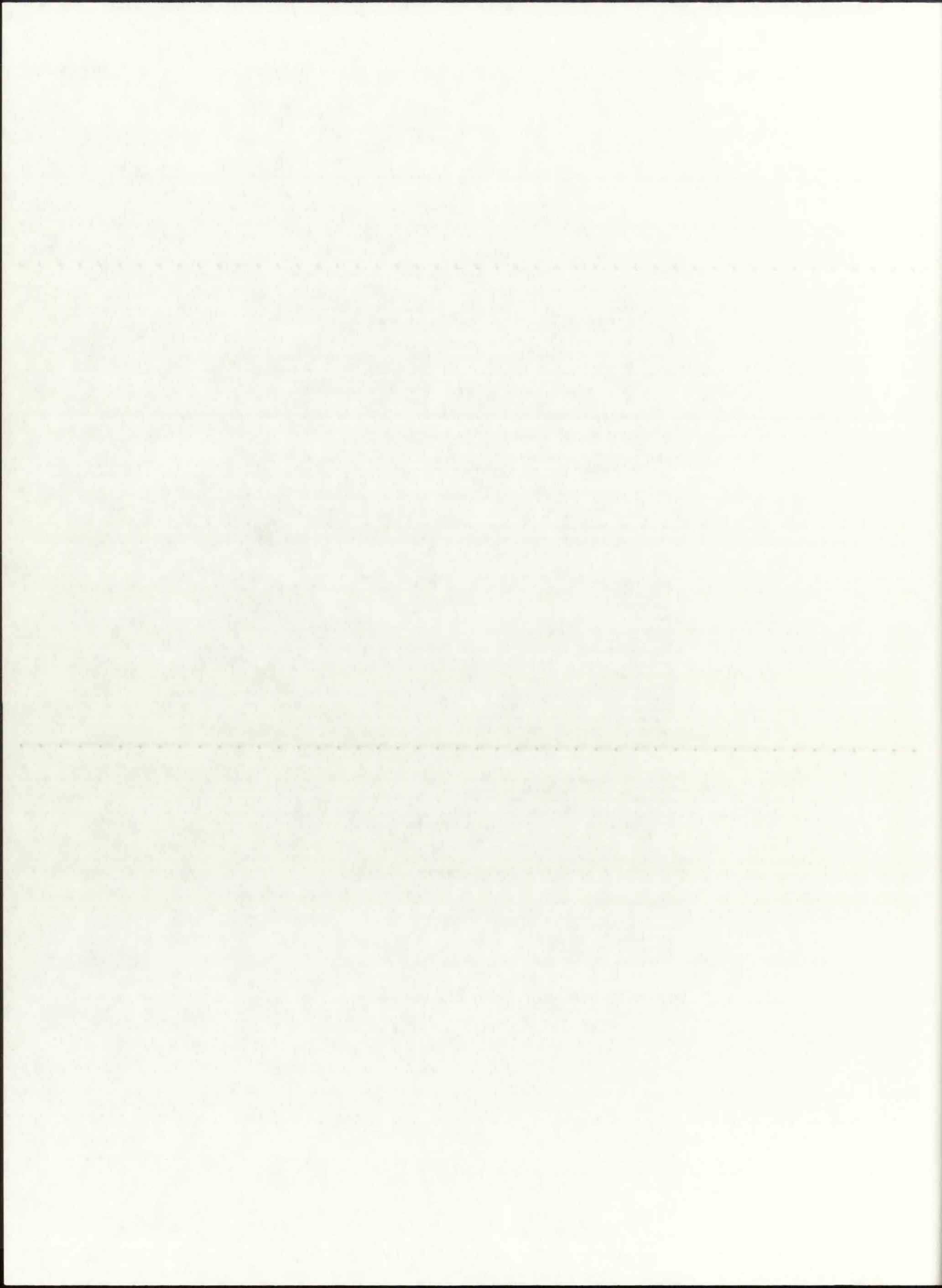
write(6,701)alpha
write(11,701)alpha
write(12,701)alpha

```

```
701 format(2x,'The H2 dissociation fraction is: ',4x,F6.4,')
```

```
* Calculate the Mw of the partially-dissociated hydrogen.
```

```
*
```



```
Mwhydro=alpha*MwH+(1.0-alpha)*MwH2

write(6,702)Mwhydro
write(11,702)Mwhydro
write(12,702)Mwhydro
702  format(2x,'The H2 average molecular weight is: ',F7.4,' g/gmol',/)

* Calculate the total Mw of the propellant (H2 and Tungsten seed).
* -----

Mwprop=0.97*Mwhydro+0.03*MwWnat

write(6,703)Mwprop
write(11,703)Mwprop
write(12,703)Mwprop
703  format(2x,'The propellant molecular weight is: ',F7.4,' g/gmol',/)

* Determine the specific heat ratio and the density at Tchamber.
* -----

call HYDROGEN(Tchamber,P,gamexit,rhoexit)

* Calculate the propellant exit velocity [m/s].
* -----

Vexit=((2.0*gamexit*R*Tchamber*1000.0)/((gamexit-1.0)*Mwprop))**0.5

* Determine the cross-sectional area to propellant flow [m2].
* -----

Acsexit=(Rpout**2.0-Rpin**2.0)*pi

write(6,704)Acsexit
write(11,704)Acsexit
write(12,704)Acsexit
704  format(2x,'The cross-sectional flow area is: ',3x,F6.4,' m2',/)

* Determine the propellant mass flow at the exit [kg/s].
* -----

mexit=Acsexit*vP*rhoexit

write(6,705)mexit
write(11,705)mexit
write(12,705)mexit
705  format(2x,'The propellant mass flow rate is: ',x,F8.2,' kg/s',/)

* Calculate the thrust [N] and specific impulse [s].
* -----

F=mexit*Vexit
Isp=F/(mexit*go)

return
end
```

Faint header text at the top of the page, possibly containing a title or reference number.

Section header text, possibly a title for a specific part of the document.

Text block containing several lines of faint, illegible characters.

Text block containing several lines of faint, illegible characters.

Text block containing several lines of faint, illegible characters.

Section header text, possibly a title for a specific part of the document.

Text block containing several lines of faint, illegible characters.

Text block containing several lines of faint, illegible characters.

Text block containing several lines of faint, illegible characters.

Section header text, possibly a title for a specific part of the document.

Text block containing several lines of faint, illegible characters.

Text block containing several lines of faint, illegible characters.

Text block containing several lines of faint, illegible characters.

Section header text, possibly a title for a specific part of the document.

Text block containing several lines of faint, illegible characters.

Text block containing several lines of faint, illegible characters.

Text block containing several lines of faint, illegible characters.

Section header text, possibly a title for a specific part of the document.

Text block containing several lines of faint, illegible characters.

Text block containing several lines of faint, illegible characters.

Text block containing several lines of faint, illegible characters.

Section header text, possibly a title for a specific part of the document.

Text block containing several lines of faint, illegible characters.


```

* ----- SUBROUTINE Hydrogen Propulsion Data (HYDROGEN) ----- *
*
* Subroutine HYDROGEN determines the hydrogen propellant specific
* heat ratio (gamma) and the density (rho) for a given propellant
* temperature and pressure. These are provided by ROCKET.
*
* UNITS: rho          ..... [kg/m3] (propellant mass density)
*         gamma       ..... (specific heat ratio)
*         Tchamber    ..... [K]   (propellant chamber temp)
*         P           ..... [atm] (operating pressure)

```

```
subroutine HYDROGEN(Tchamber,P,gamexit,rhoexit)
```

```
real gamma,gamexit,rho,rhoexit,Tchamber,P
```

```
if (P.eq.250.0) then
```

```
  if (Tchamber.le.3000.0) then
```

```
    rho=2.6100
```

```
    gamma=1.260
```

```
  elseif (Tchamber.le.4000.0) then
```

```
    rho=1.9568
```

```
    gamma=1.205
```

```
  elseif (Tchamber.le.5000.0) then
```

```
    rho=1.4274
```

```
    gamma=1.211
```

```
  elseif (Tchamber.le.6000.0) then
```

```
    rho=1.0018
```

```
    gamma=1.255
```

```
  elseif (Tchamber.le.7000.0) then
```

```
    rho=0.6802
```

```
    gamma=1.284
```

```
  elseif (Tchamber.le.8000.0) then
```

```
    rho=0.4948
```

```
    gamma=1.322
```

```
  elseif (Tchamber.le.9000.0) then
```

```
    rho=0.3998
```

```
    gamma=1.420
```

```
  elseif (Tchamber.le.10000.0) then
```

```
    rho=0.3438
```

```
    gamma=1.511
```

```
  elseif (Tchamber.le.12000.0) then
```

```
    rho=0.3045
```

```
    gamma=1.548
```

```
  elseif (Tchamber.le.14000.0) then
```

```
    rho=0.2500
```

```
    gamma=1.566
```

```
  elseif (Tchamber.le.16000.0) then
```

```
    rho=0.2080
```

```
    gamma=1.585
```

```
  elseif (Tchamber.le.18000.0) then
```

```
    rho=0.1650
```

```
    gamma=1.599
```

```
  elseif (Tchamber.le.20000.0) then
```

```
    rho=0.1250
```

```
    gamma=1.610
```

```
  elseif (Tchamber.le.25000.0) then
```

```
    rho=0.0830
```

UNITED STATES DEPARTMENT OF THE INTERIOR

BUREAU OF LAND MANAGEMENT

OFFICE OF THE ASSISTANT ATTORNEY GENERAL
WASHINGTON, D. C. 20540

MEMORANDUM FOR THE ASSISTANT ATTORNEY GENERAL
FROM THE BUREAU OF LAND MANAGEMENT
SUBJECT: [Illegible]

DATE: [Illegible]

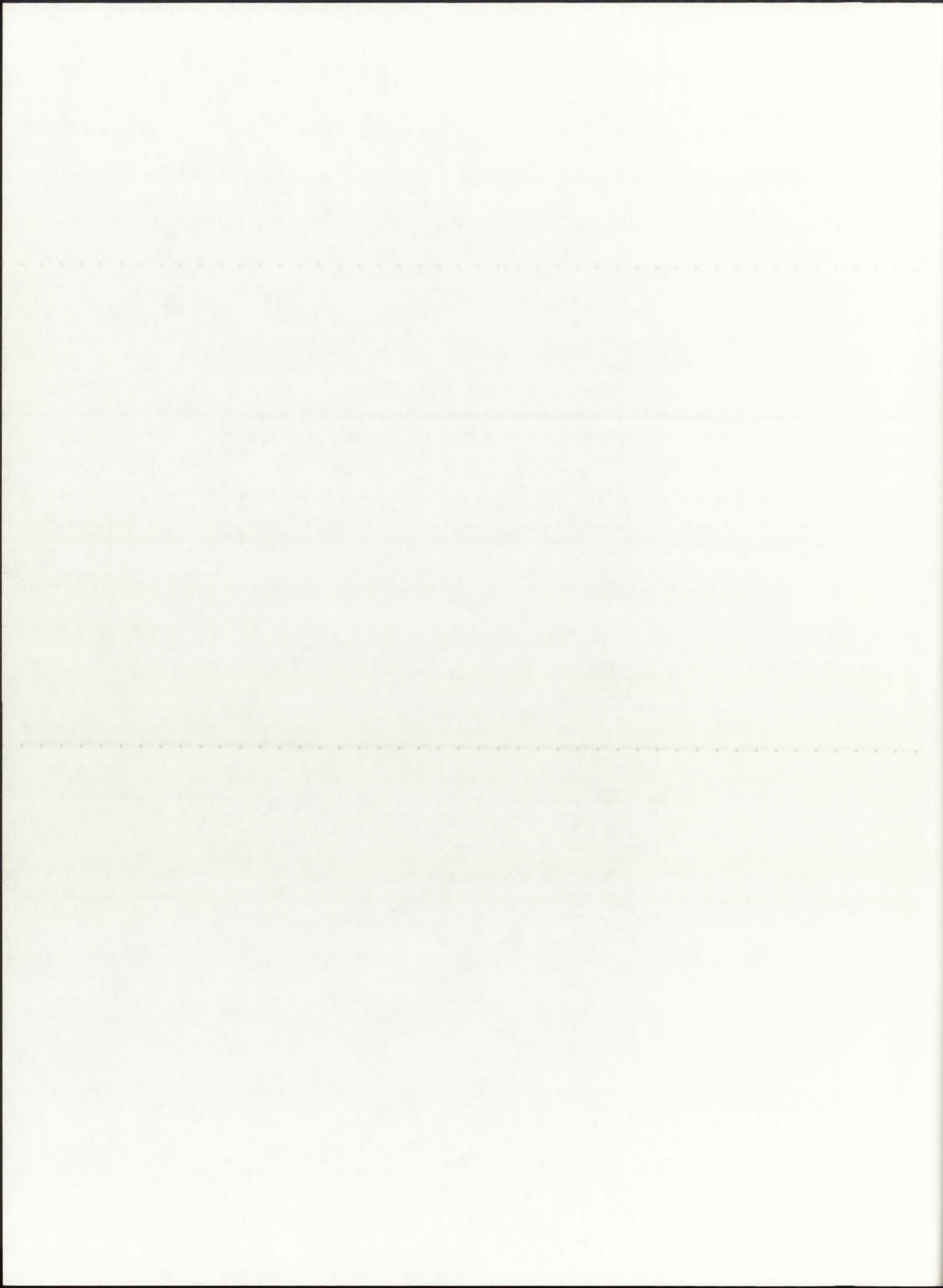
BY: [Illegible]

- 1. [Illegible]
- 2. [Illegible]
- 3. [Illegible]
- 4. [Illegible]
- 5. [Illegible]
- 6. [Illegible]
- 7. [Illegible]
- 8. [Illegible]
- 9. [Illegible]
- 10. [Illegible]
- 11. [Illegible]
- 12. [Illegible]
- 13. [Illegible]
- 14. [Illegible]
- 15. [Illegible]
- 16. [Illegible]
- 17. [Illegible]
- 18. [Illegible]
- 19. [Illegible]
- 20. [Illegible]
- 21. [Illegible]
- 22. [Illegible]
- 23. [Illegible]
- 24. [Illegible]
- 25. [Illegible]
- 26. [Illegible]
- 27. [Illegible]
- 28. [Illegible]
- 29. [Illegible]
- 30. [Illegible]
- 31. [Illegible]
- 32. [Illegible]
- 33. [Illegible]
- 34. [Illegible]
- 35. [Illegible]
- 36. [Illegible]
- 37. [Illegible]
- 38. [Illegible]
- 39. [Illegible]
- 40. [Illegible]
- 41. [Illegible]
- 42. [Illegible]
- 43. [Illegible]
- 44. [Illegible]
- 45. [Illegible]
- 46. [Illegible]
- 47. [Illegible]
- 48. [Illegible]
- 49. [Illegible]
- 50. [Illegible]

```
    gamma=1.616
  elseif (Tchamber.le.30000.0) then
    rho=0.0050
    gamma=1.620
  elseif (Tchamber.gt.30000.0) then
    rho=0.0010
    gamma=1.630
  endif

elseif (P.eq.500.0) then

  if (Tchamber.le.3000.0) then
    rho=4.070
    gamma=1.260
  elseif (Tchamber.le.4000.0) then
    rho=3.9136
    gamma=1.205
  elseif (Tchamber.le.5000.0) then
    rho=2.8548
    gamma=1.211
  elseif (Tchamber.le.6000.0) then
    rho=2.0036
    gamma=1.255
  elseif (Tchamber.le.7000.0) then
    rho=1.3604
    gamma=1.284
  elseif (Tchamber.le.8000.0) then
    rho=0.9897
    gamma=1.322
  elseif (Tchamber.le.9000.0) then
    rho=0.7995
    gamma=1.420
  elseif (Tchamber.le.10000.0) then
    rho=0.6877
    gamma=1.511
  elseif (Tchamber.le.12000.0) then
    rho=0.6090
    gamma=1.548
  elseif (Tchamber.le.14000.0) then
    rho=0.5200
    gamma=1.566
  elseif (Tchamber.le.16000.0) then
    rho=0.4600
    gamma=1.585
  elseif (Tchamber.le.18000.0) then
    rho=0.4100
    gamma=1.599
  elseif (Tchamber.le.20000.0) then
    rho=0.3800
    gamma=1.610
  elseif (Tchamber.le.25000.0) then
    rho=0.3600
    gamma=1.616
  elseif (Tchamber.le.30000.0) then
    rho=0.3500
    gamma=1.620
  elseif (Tchamber.gt.30000.0) then
    rho=0.0010
    gamma=1.630
  endif
endif
```

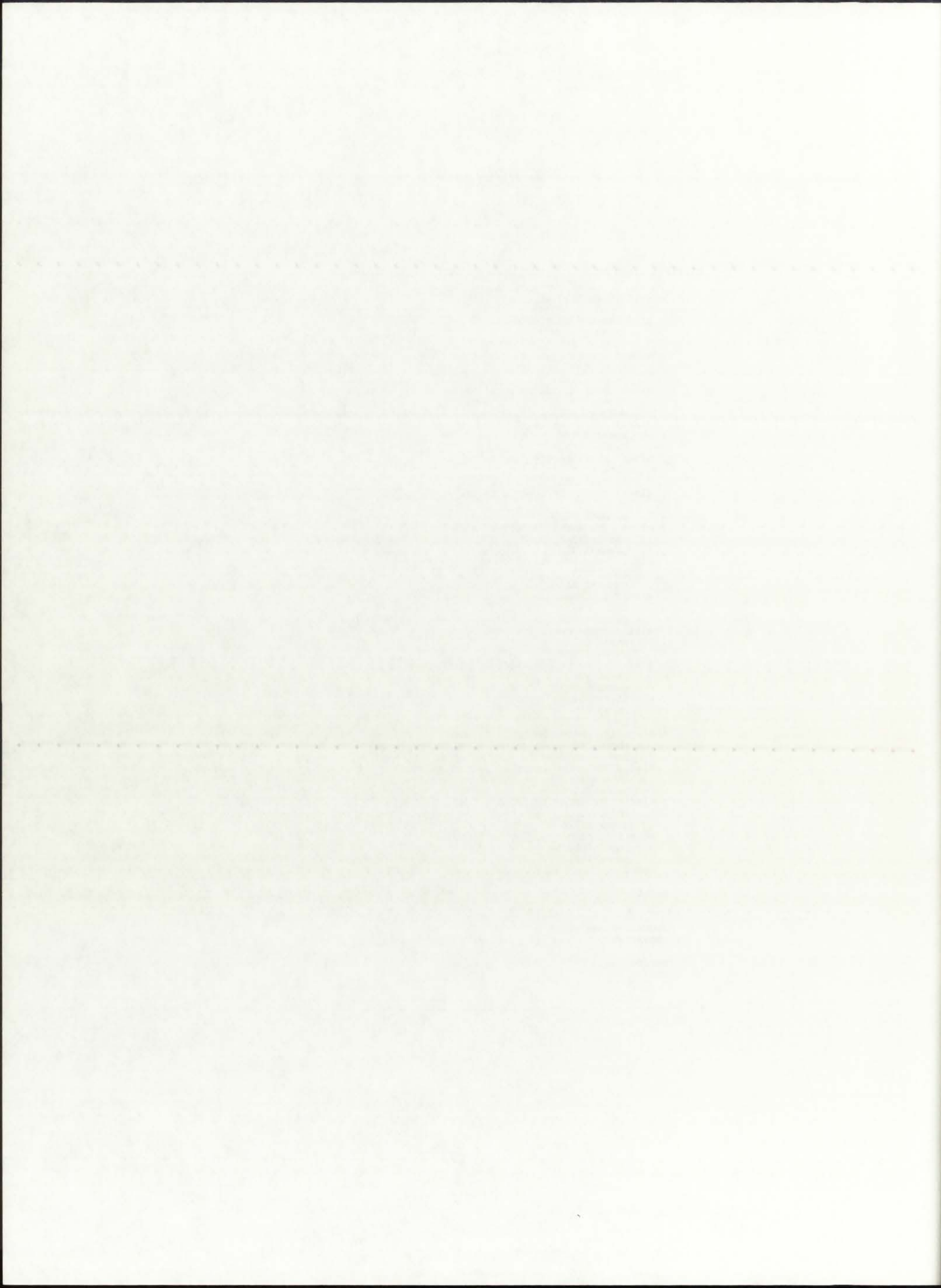


```
elseif (P.eq.1000.0) then
  if (Tchamber.le.3000.0) then
    rho=9.930
    gamma=1.260
  elseif (Tchamber.le.4000.0) then
    rho=7.827
    gamma=1.205
  elseif (Tchamber.le.5000.0) then
    rho=5.710
    gamma=1.211
  elseif (Tchamber.le.6000.0) then
    rho=4.007
    gamma=1.255
  elseif (Tchamber.le.7000.0) then
    rho=2.721
    gamma=1.284
  elseif (Tchamber.le.8000.0) then
    rho=1.979
    gamma=1.322
  elseif (Tchamber.le.9000.0) then
    rho=1.599
    gamma=1.420
  elseif (Tchamber.le.10000.0) then
    rho=1.375
    gamma=1.511
  elseif (Tchamber.le.12000.0) then
    rho=1.218
    gamma=1.548
  elseif (Tchamber.le.14000.0) then
    rho=1.040
    gamma=1.566
  elseif (Tchamber.le.16000.0) then
    rho=0.920
    gamma=1.585
  elseif (Tchamber.le.18000.0) then
    rho=0.820
    gamma=1.599
  elseif (Tchamber.le.20000.0) then
    rho=0.760
    gamma=1.610
  elseif (Tchamber.le.25000.0) then
    rho=0.720
    gamma=1.616
  elseif (Tchamber.le.30000.0) then
    rho=0.700
    gamma=1.620
  elseif (Tchamber.gt.30000.0) then
    rho=0.0010
    gamma=1.630
  endif
endif

gamexit=gamma
rhoexit=rho

return
end
```

* ----- *



```

* ----- SUBROUTINE Transmission Fraction (TRANSMIT) ----- *
* ----- *
* Subroutine TRANSMIT determines the bulk temperature of a gaseous
* region, in which only radiation is present, by correcting the
* diffusion-approximated temperature for that region. The method
* of transmission fractions is used to determine the temperature.
*
* UNITS: Tprop      ..... [K] (propellant temperature)
*        Twall      ..... [K] (silica wall temperature)
*        Tbuffer    ..... [K] (buffer gas temperature)
*        TFP        ..... (propellant trans. fract.)
*        TFSiW      ..... (silica wall trans. fract.)
*        TFBG       ..... (buffer gas trans. fract.)
*
subroutine TRANSMIT(P,tP,tSiW,tBG,BGconv,Pconv,Tprop,Twall,Tbuffer)

real aRrF,aRf,aRBG,aRbuffer,aRSiW,aRsiwall,aRP,aRprop,P,tP,tSiW,
> tBG,Tprop,Twall,Tbuffer,TFBG,TFSiW,TFP

logical BGconv,Pconv

call RMO(Tprop,P,aRprop,aRSiW,aRBG,aRf,aRrF)
call RMO(Twall,P,aRP,aRsiwall,aRBG,aRf,aRrF)
call RMO(Tbuffer,P,aRP,aRSiW,aRbuffer,aRf,aRrF)

if((.not.BGconv).and(.not.Pconv)) then
  TFBG=exp(-aRbuffer*tBG)
  Tbuffer=Tbuffer*(1.0-TFBG)**0.25
  TFSiW=exp(-aRsiwall*tSiW)
  Twall=Twall*(1.0-TFSiW)**0.25
  TFP=exp(-aRprop*tP)
  Tprop=Tprop*(1.0-TFP)**0.25
elseif(.not.BGconv) then
  TFBG=exp(-aRbuffer*tBG)
  Tbuffer=Tbuffer*(1-TFBG)**0.25
elseif(.not.Pconv) then
  TFP=exp(-aRprop*tP)
  Tprop=Tprop*(1.0-TFP)**0.25
else
  write(6,8999)
8999  format(//,2x,'There is an error in subroutine TRANSMIT!')
endif

return
end

* ----- *
* ----- *
* ----- *
* ===== *

```

THE UNIVERSITY OF CHICAGO
DEPARTMENT OF CHEMISTRY
5800 S. UNIVERSITY AVENUE
CHICAGO, ILLINOIS 60637

RECEIVED
JAN 15 1964
BY
DR. J. H. GOLDSTEIN

FROM
DR. J. H. GOLDSTEIN
5800 S. UNIVERSITY AVENUE
CHICAGO, ILLINOIS 60637

RE: [Illegible]

[Illegible text]

[Illegible text]

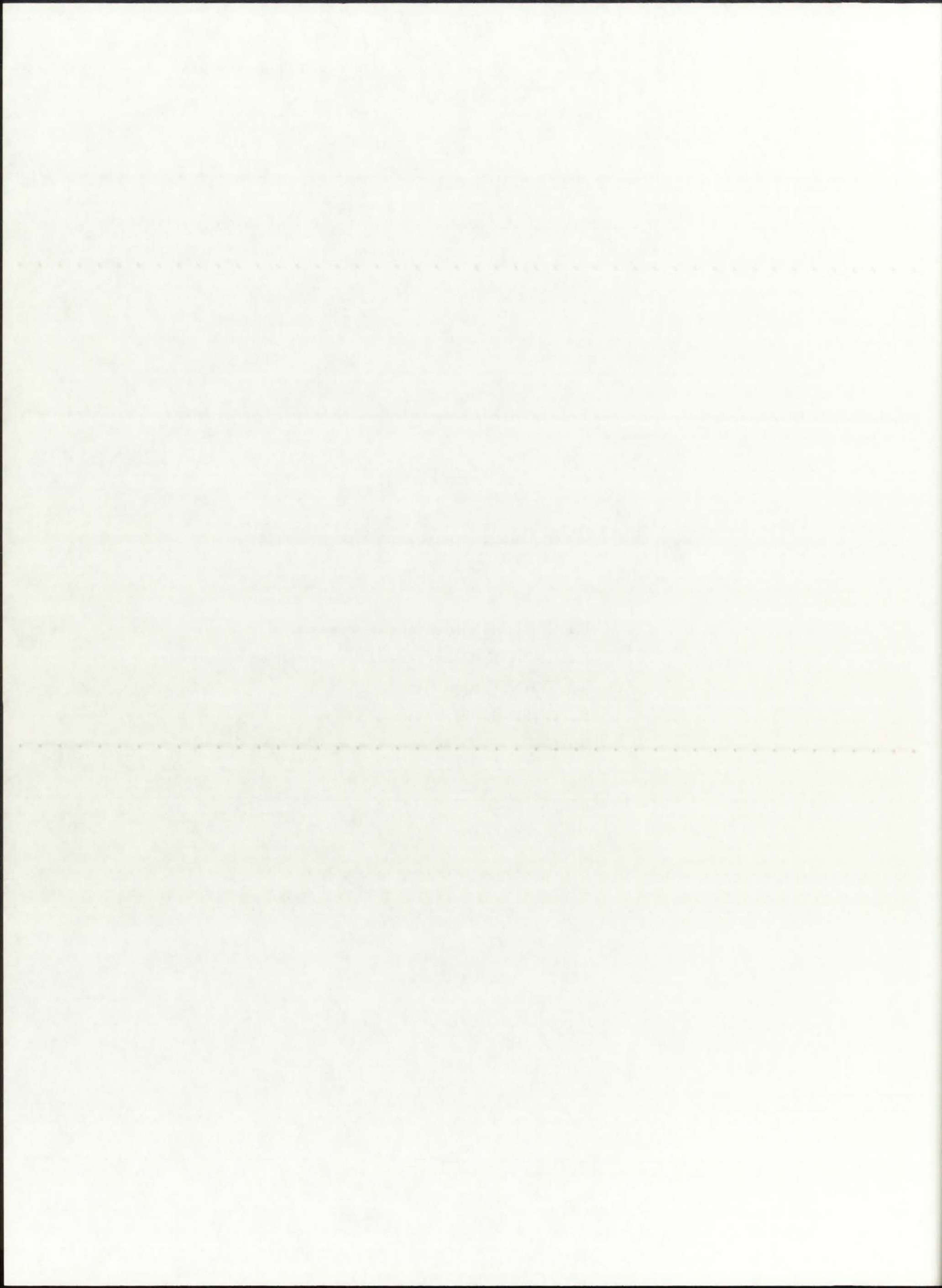
[Illegible text]

[Illegible text]

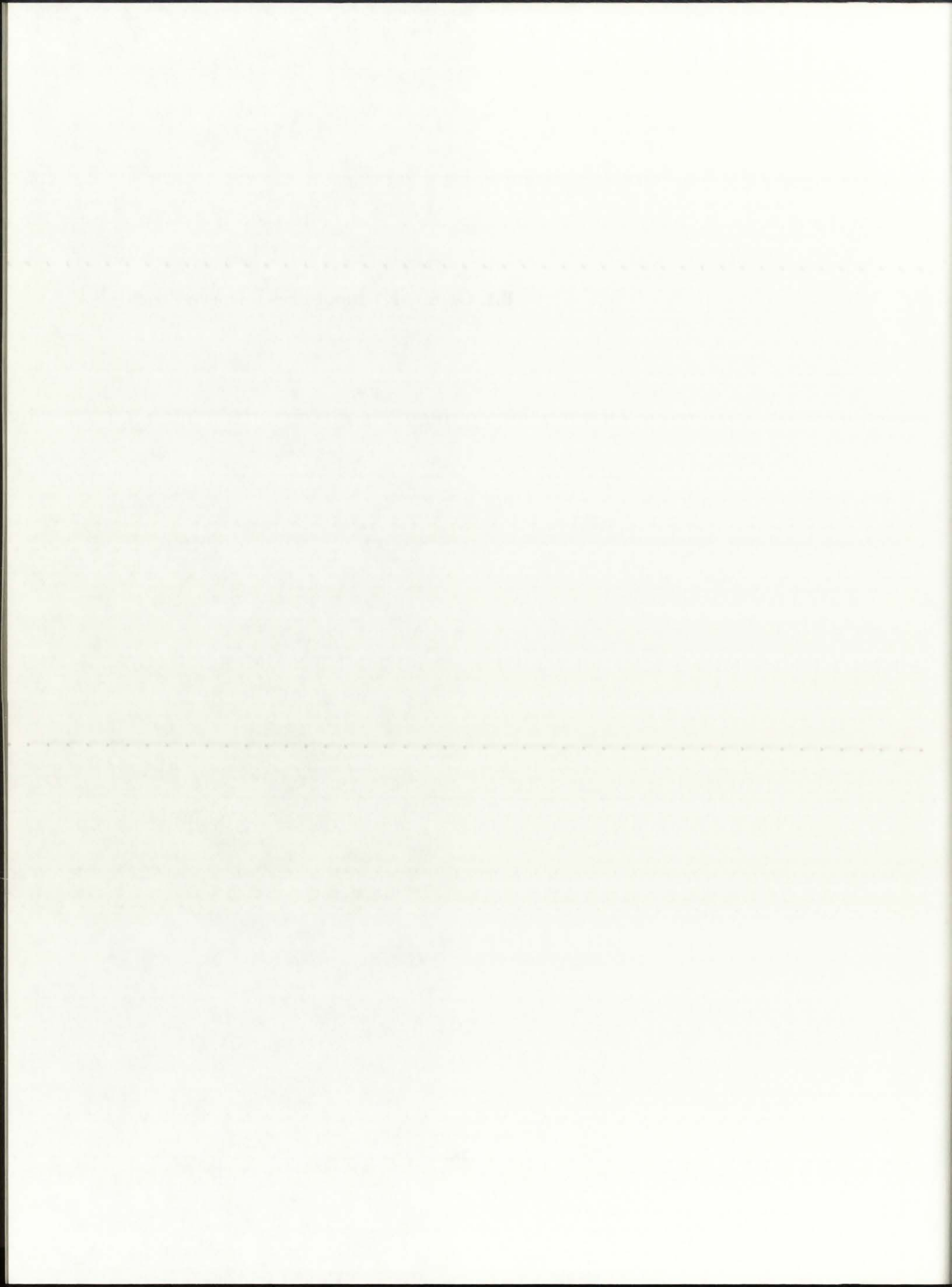
APPENDIX B

500 MWth Case: Input and Output Files

- B.1: ONEDANT Input Files (Hansen-Roach)
- B.2: GNRATR-1D Summary Output Files (Hansen-Roach)
- B.3: TRANSX Input Files (ENDF/B-V)
- B.4: ONEDANT Input Files (ENDF/B-V)
- B.5: GNRATR-1D Summary Output Files (ENDF/B-V)



B.1. ONEDANT Input Files (Hansen-Roach)



```

2 0 0
unit-cell rocket engine - 500 MWth Configuration - P=250 atm
search for Q(r) and keff, based on T(r) from GNRATR-1D code
/
/***** block i *****/
  igeom=cylinder ngroup=16 isn=4 niso=118 mt=10
  nzone=10 im=10 it=29 idimen=1
  t
/
/***** block ii *****/
  xmesh=0.0,6.0,13.375,20.75,24.45,24.94,28.80,34.58,
        58.58,82.58,87.66
  xints=4,3,3,2,2,2,3,4,4,2
  zones=1,2,3,4,5,6,7,8,9,10
  t
/
/***** block iii (cross sections) *****/
  lib=bxslib balxs=1 maxord=1 ihm=10 iht=4 ihs=5
  ifido=0 ititl=1 edname=fiss
  t
/
/***** block iv (mixing) *****/
  matls=mix      "sulfur"      2.5590e-5
                "235-yr"      2.5823e-6
                "u238y"       1.9443e-7;
  uranI  "235-yr"      5.1646e-6
                "u238y"       3.8886e-7;
  uranII "235-yr"      5.1646e-6
                "u238y"       3.8886e-7;
  argon  "sulfur"      5.1190e-5;
  silica "si"          2.666e-2
                "o16"         5.332e-2;
  hydro  "h"           1.0156e-4;
  beryl  "be"          1.236e-1;
  hvywI  "d"           1.894e-2
                "o16"         9.470e-3;
  hvywII "d"           1.894e-2
                "o16"         9.470e-3;
  steel  "fe"          8.486e-2;

  assign=mixture mix 1.0;
                fuelI uranI 1.0;
                fuelII uranII 1.0;
                buffer argon 1.0;
                siwall silica 1.0;
                propel hydro 1.0;
                bemodr beryl 1.0;
                reflI hvywI 1.0;
                reflII hvywII 1.0;
                pvessl steel 1.0;

  t
/
/***** block v (solver) *****/
  ievt=1 isct=1 ibr=0 fluxp=1 bhgt=182.73
  t
/
/***** block vi (edits) *****/
  pted=1 zned=1
  icoll=16; igrped=3
  edxs=n-fiss resdnt=1 power=2.736 mevper=176 rzflux=1
/

```

THE UNIVERSITY OF CHICAGO
DEPARTMENT OF CHEMISTRY

RESEARCH REPORT NO. 100

BY J. H. GOLDSTEIN

1954

PHYSICAL CHEMISTRY

THEORY OF THE Raman EFFECT

IN DIATOMIC MOLECULES

Order	Frequency	Intensity
0	ν_0	0
1	$\nu_0 \pm \nu_1$	I_1
2	$\nu_0 \pm 2\nu_1$	I_2
3	$\nu_0 \pm 3\nu_1$	I_3
4	$\nu_0 \pm 4\nu_1$	I_4
5	$\nu_0 \pm 5\nu_1$	I_5
6	$\nu_0 \pm 6\nu_1$	I_6
7	$\nu_0 \pm 7\nu_1$	I_7
8	$\nu_0 \pm 8\nu_1$	I_8
9	$\nu_0 \pm 9\nu_1$	I_9
10	$\nu_0 \pm 10\nu_1$	I_{10}

11
12
13
14
15
16
17
18
19
20

21
22
23
24
25
26
27
28
29
30

31
32
33
34
35
36
37
38
39
40

41
42
43
44
45
46
47
48
49
50

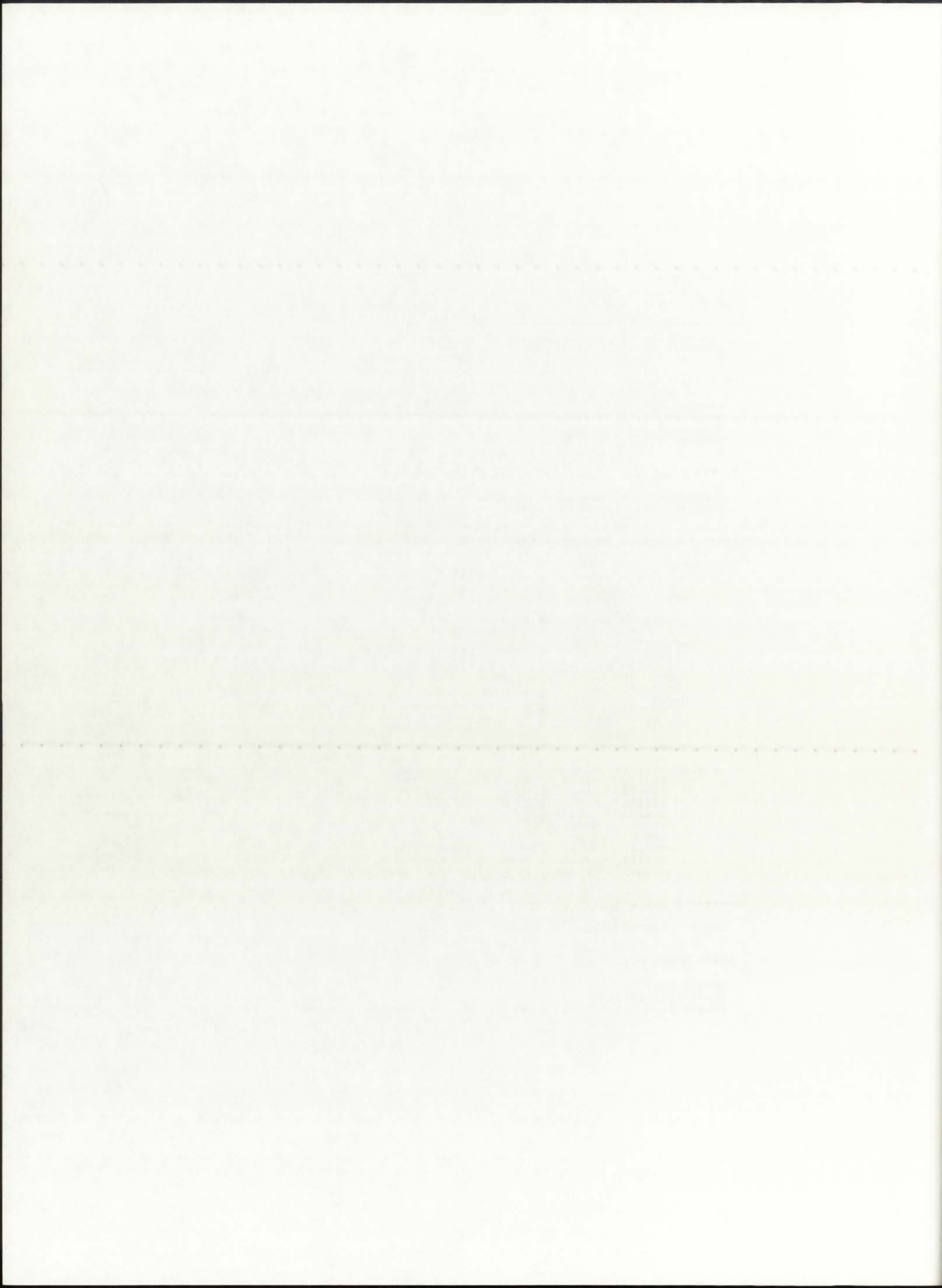
51
52
53
54
55
56
57
58
59
60

```

2 0 0
unit-cell rocket engine - 500 MWth Configuration - P=500 atm
search for Q(r) and keff, based on T(r) from GNRATR-1D code
/
/***** block i *****/
igeom=cylinder ngroup=16 isn=4 niso=118 mt=10
nzone=10 im=10 it=29 idimen=1
t
/
/***** block ii *****/
xmesh=0.0,6.0,13.375,20.75,24.45,24.94,28.80,34.58,
58.58,82.58,87.66
xints=4,3,3,2,2,2,3,4,4,2
zones=1,2,3,4,5,6,7,8,9,10
t
/
/***** block iii (cross sections) *****/
lib=bxslib balxs=1 maxord=1 ihm=10 iht=4 ihs=5
ifido=0 ititl=1 edname=fiss
t
/
/***** block iv (mixing) *****/
matls=mix      "sulfur"      5.1190e-5
                "235-yr"      3.4510e-6
                "u238y"       2.5984e-7;
uranI          "235-yr"      6.9020e-6
                "u238y"       5.1968e-7;
uranII         "235-yr"      6.9020e-6
                "u238y"       5.1968e-7;
argon          "sulfur"      1.0240e-4;
silica         "si"          2.666e-2
                "o16"         5.332e-2;
hydro          "h"           2.0312e-4;
beryl          "be"          1.236e-1;
hvywI          "d"           1.894e-2
                "o16"         9.470e-3;
hvywII         "d"           1.894e-2
                "o16"         9.470e-3;
steel          "fe"          8.486e-2;

assign=mixture mix 1.0;
                fuelI uranI 1.0;
                fuelII uranII 1.0;
                buffer argon 1.0;
                siwall silica 1.0;
                propel hydro 1.0;
                bemodr beryl 1.0;
                reflI hvywI 1.0;
                reflII hvywII 1.0;
                pvessl steel 1.0;
t
/
/***** block v (solver) *****/
ievts=1 isct=1 ibr=0 fluxp=1 bhgt=182.73
t
/
/***** block vi (edits) *****/
pted=1 zned=1
icoll=16; igrped=3
edxs=n-fiss resdnt=1 power=2.736 mevper=176 rzflux=1
/

```




```

2 0 0
unit-cell rocket engine - 500 MWth Configuration - P=1000 atm
search for Q(r) and keff, based on T(r) from GNRATR-1D code
/
/***** block i *****/
igeom=cylinder ngroup=16 isn=4 niso=118 mt=10
nzone=10 im=10 it=29 idimen=1
t
/
/***** block ii *****/
/
xmesh=0.0,6.0,13.375,20.75,24.45,24.94,28.80,34.58,
58.58,82.58,87.66
xints=4,3,3,2,2,2,3,4,4,2
zones=1,2,3,4,5,6,7,8,9,10
t
/
/***** block iii (cross sections) *****/
/
lib=bxslib balxs=1 maxord=1 ihm=10 iht=4 ihs=5
ifido=0 ititl=1 edname=fiss
t
/
/***** block iv (mixing) *****/
/
matls=mix      "sulfur"      1.0240e-4
               "235-yr"      5.0099e-6
               "u238y"       3.7722e-7;
uranI  "235-yr"      1.0020e-5
               "u238y"       7.5443e-7;
uranII "235-yr"      1.0020e-5
               "u238y"       7.5443e-7;
argon  "sulfur"      2.0480e-4;
silica "si"          2.666e-2
               "o16"         5.332e-2;
hydro  "h"           4.0624e-4;
beryl  "be"          1.236e-1;
hvywI  "d"           1.894e-2
               "o16"         9.470e-3;
hvywII "d"           1.894e-2
               "o16"         9.470e-3;
steel  "fe"          8.486e-2;
/
assign=mixture mix 1.0;
               fuelI uranI 1.0;
               fuelII uranII 1.0;
               buffer argon 1.0;
               siwall silica 1.0;
               propel hydro 1.0;
               bemodr beryl 1.0;
               reflI hvywI 1.0;
               reflII hvywII 1.0;
               pvessl steel 1.0;
t
/
/***** block v (solver) *****/
/
ievt=1 isct=1 ibr=0 fluxp=1 bhgt=182.73
t
/
/***** block vi (edits) *****/
/
pted=1 zned=1
icoll=16; igrped=3
edxs=n-fiss resdnt=1 power=2.736 mevper=176 rzflux=1
/

```

THE UNIVERSITY OF CHICAGO
DEPARTMENT OF CHEMISTRY

RESEARCH REPORT
NO. 1000

BY
J. H. GOLDSTEIN

AND
M. L. HUGGINS

DEPARTMENT OF CHEMISTRY
UNIVERSITY OF CHICAGO

CHICAGO, ILLINOIS
1955

Year	Volume	Page
1955	1	1-10
1956	2	11-20
1957	3	21-30
1958	4	31-40
1959	5	41-50
1960	6	51-60
1961	7	61-70
1962	8	71-80
1963	9	81-90
1964	10	91-100
1965	11	101-110
1966	12	111-120
1967	13	121-130
1968	14	131-140
1969	15	141-150
1970	16	151-160
1971	17	161-170
1972	18	171-180
1973	19	181-190
1974	20	191-200
1975	21	201-210
1976	22	211-220
1977	23	221-230
1978	24	231-240
1979	25	241-250
1980	26	251-260
1981	27	261-270
1982	28	271-280
1983	29	281-290
1984	30	291-300
1985	31	301-310
1986	32	311-320
1987	33	321-330
1988	34	331-340
1989	35	341-350
1990	36	351-360
1991	37	361-370
1992	38	371-380
1993	39	381-390
1994	40	391-400
1995	41	401-410
1996	42	411-420
1997	43	421-430
1998	44	431-440
1999	45	441-450
2000	46	451-460
2001	47	461-470
2002	48	471-480
2003	49	481-490
2004	50	491-500
2005	51	501-510
2006	52	511-520
2007	53	521-530
2008	54	531-540
2009	55	541-550
2010	56	551-560
2011	57	561-570
2012	58	571-580
2013	59	581-590
2014	60	591-600
2015	61	601-610
2016	62	611-620
2017	63	621-630
2018	64	631-640
2019	65	641-650
2020	66	651-660
2021	67	661-670
2022	68	671-680
2023	69	681-690
2024	70	691-700
2025	71	701-710
2026	72	711-720
2027	73	721-730
2028	74	731-740
2029	75	741-750
2030	76	751-760
2031	77	761-770
2032	78	771-780
2033	79	781-790
2034	80	791-800
2035	81	801-810
2036	82	811-820
2037	83	821-830
2038	84	831-840
2039	85	841-850
2040	86	851-860
2041	87	861-870
2042	88	871-880
2043	89	881-890
2044	90	891-900
2045	91	901-910
2046	92	911-920
2047	93	921-930
2048	94	931-940
2049	95	941-950
2050	96	951-960
2051	97	961-970
2052	98	971-980
2053	99	981-990
2054	100	991-1000

RESEARCH REPORT
NO. 1000

B.2. GNRATR-1D Summary Output Files (Hansen-Roach)

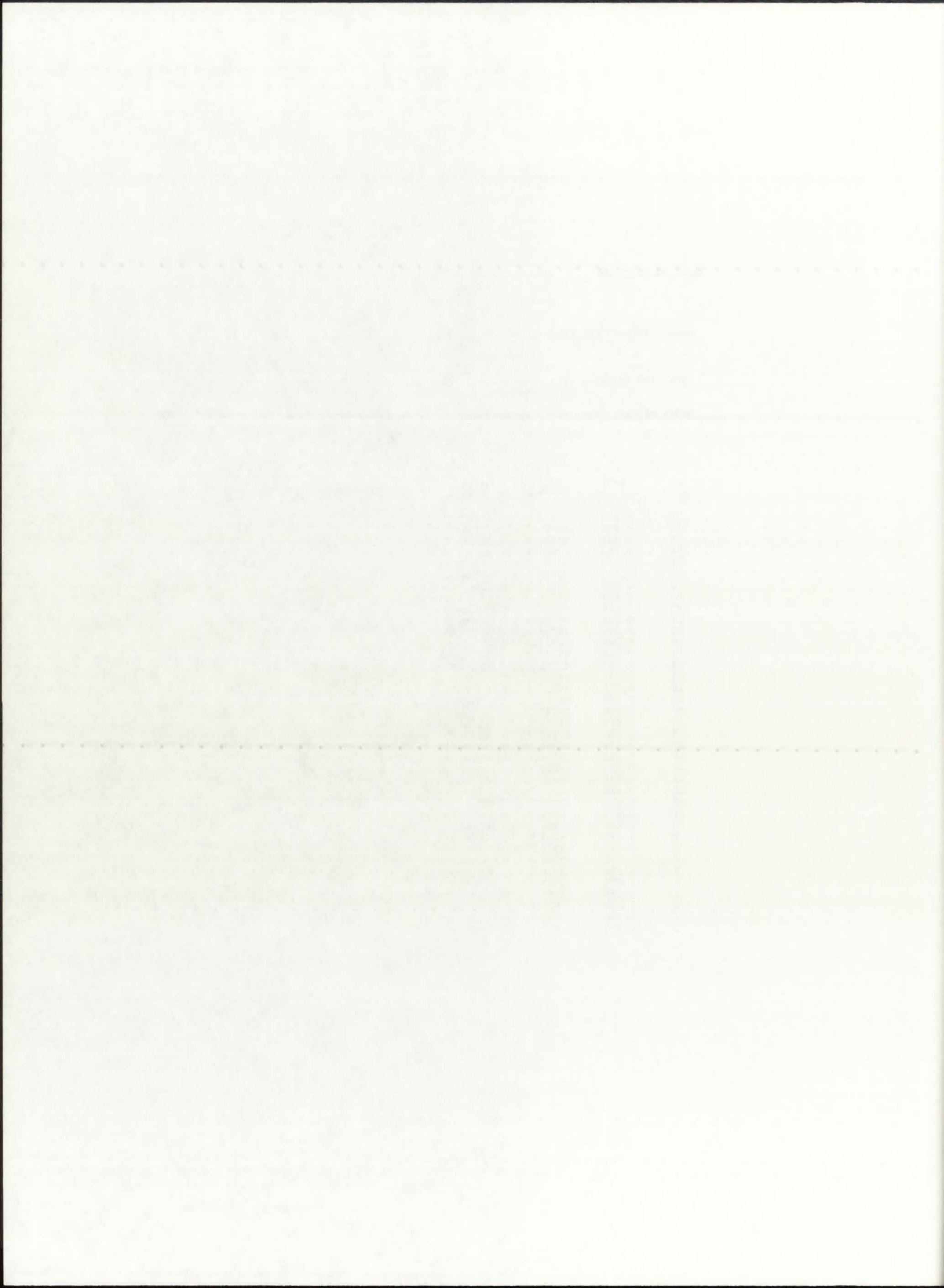
THE CHINA DAILY SUMMARY (Output File: Hksum-0000)

==== SUMMARY OF CONVERGED VALUES ====

This Case Executed for: REFLBe = 0.00000
 Pressure = 250.0 atm

Modes of Heat Transfer: Radiation in BG, SiW, and P = .on.
 Convection in BG = .on.
 Convection in P = .on.

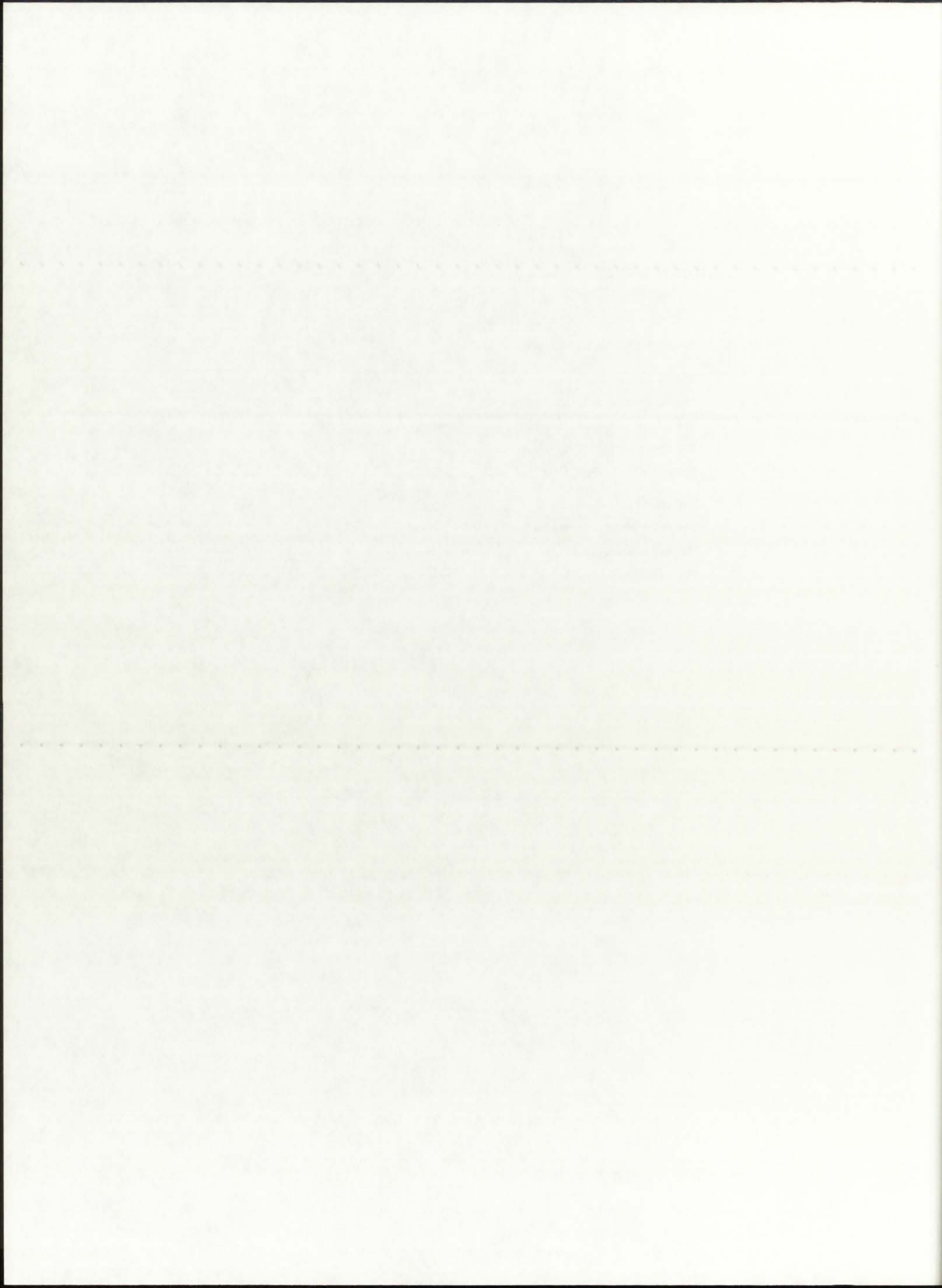
i	r(i)	T(i)	Qg(i)
37	0.000	83970.7	0.1049E+10
36	0.019	83970.7	0.1043E+10
35	0.039	83884.4	0.2079E+10
34	0.059	83621.9	0.2089E+10
33	0.096	81980.8	0.2102E+10
32	0.133	79037.5	0.2120E+10
31	0.170	74010.0	0.2144E+10
30	0.207	46756.8	0.0000E+00
29	0.225	46756.8	0.0000E+00
28	0.244	46756.8	0.0000E+00
27	0.246	46756.8	0.0000E+00
26	0.249	46756.8	0.0000E+00
25	0.268	46756.8	0.0000E+00
24	0.287	46756.8	0.0000E+00
23	0.307	46732.7	0.0000E+00
22	0.326	46711.4	0.0000E+00
21	0.345	46692.6	0.0000E+00
20	0.405	36640.5	0.0000E+00
19	0.465	29181.4	0.0000E+00
18	0.525	23427.4	0.0000E+00
17	0.585	18854.9	0.0000E+00
16	0.645	15134.8	0.0000E+00
15	0.705	12050.4	0.0000E+00
14	0.765	9452.5	0.0000E+00
13	0.825	7235.7	0.0000E+00
12	0.851	7226.5	0.0000E+00
11	0.876	7221.9	0.0000E+00
10	0.976	5859.4	0.0000E+00
9	1.076	4753.7	0.0000E+00
8	1.176	3838.9	0.0000E+00
7	1.276	3069.9	0.0000E+00
6	1.376	2414.5	0.0000E+00
5	1.476	1849.5	0.0000E+00
4	1.576	1357.5	0.0000E+00
3	1.676	925.0	0.0000E+00
2	1.776	541.9	0.0000E+00
1	1.876	200.0	0.0000E+00



==== ROCKET ENGINE PARAMETERS ====

The H2 dissociation fraction is: 0.9992
The H2 average molecular weight is: 1.0088 g/gmol
The propellant molecular weight is: 6.4940 g/gmol
The cross-sectional flow area is: 0.0721 m²
The propellant mass flow rate is: 0.00 kg/s

The chamber temperature is: 46756.8 K
The calculated exit velocity is: 17599.8 m/s
The calculated thrust is: 0.0 kN
The calculated specific impulse is: 1794.6 s

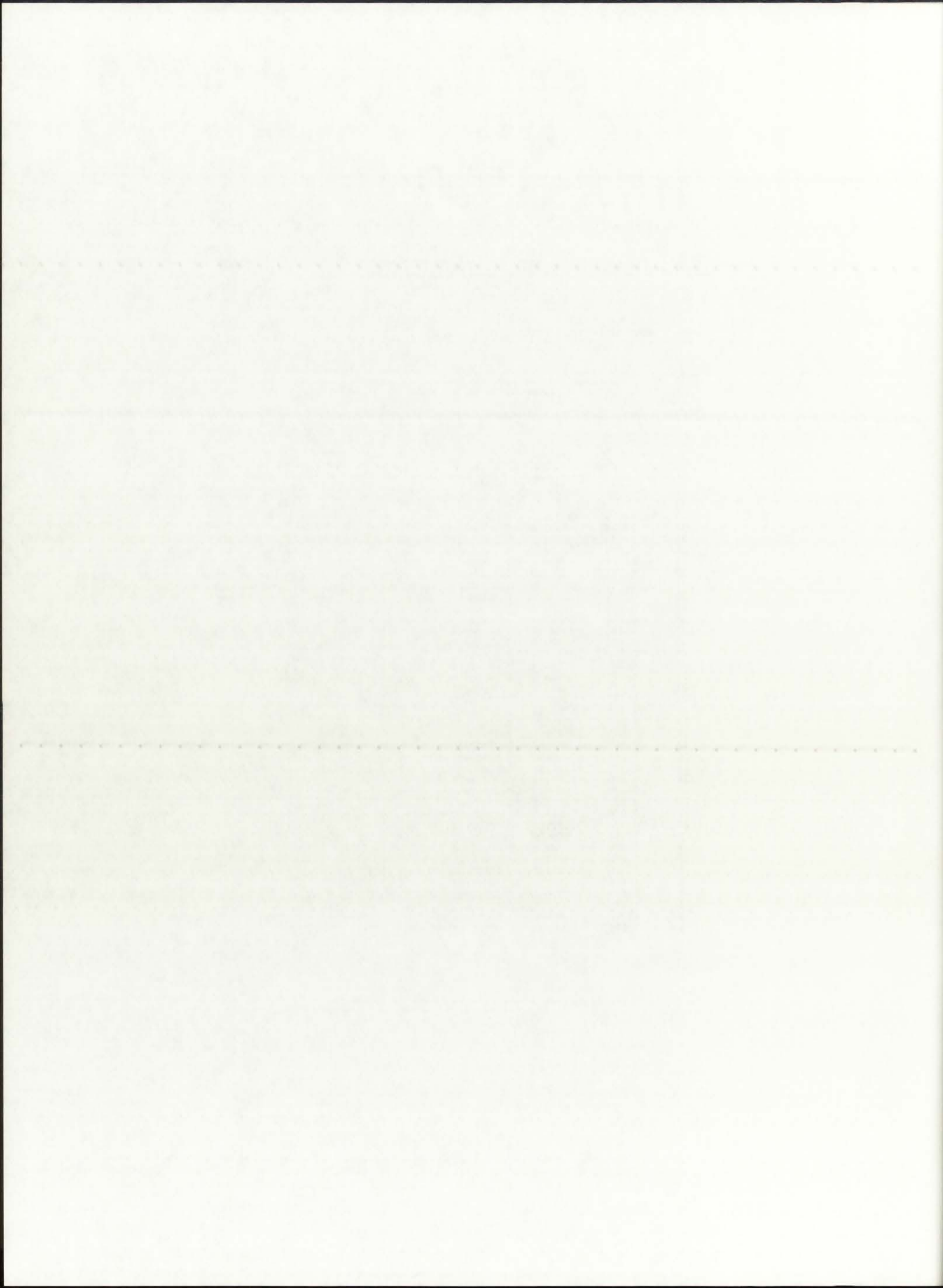


==== SUMMARY OF CONVERGED VALUES ====

This Case Executed for: REFLBe = 0.00000
 Pressure = 500.0 atm

Modes of Heat Transfer: Radiation in BG, SiW, and P = .on.
 Convection in BG = .on.
 Convection in P = .on.

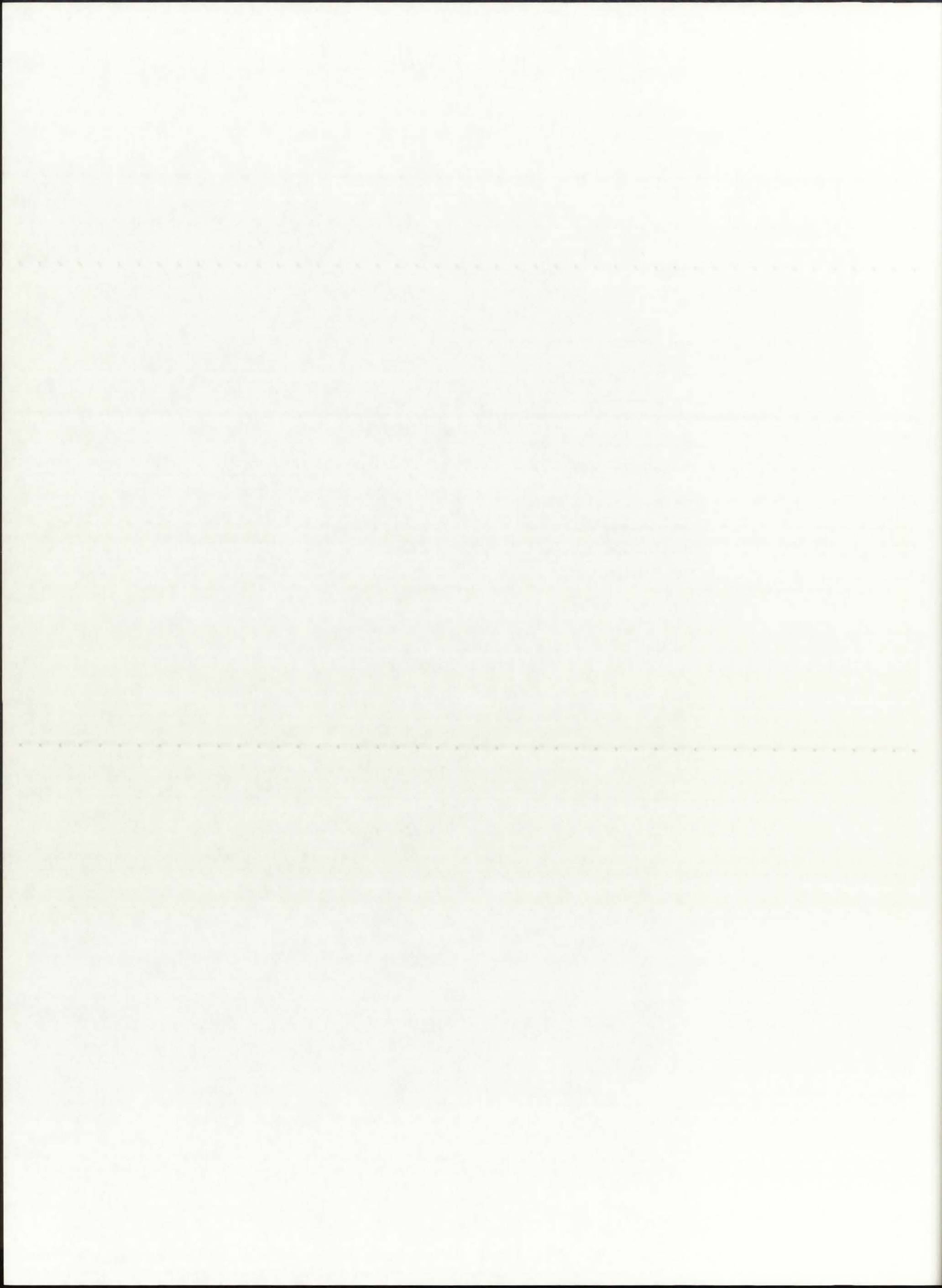
i	r(i)	T(i)	Qg(i)
-----	-----	-----	-----
37	0.000	99891.5	0.1046E+10
36	0.019	99891.5	0.1038E+10
35	0.039	99789.5	0.2071E+10
34	0.059	99478.8	0.2083E+10
33	0.096	97536.0	0.2100E+10
32	0.133	94047.9	0.2123E+10
31	0.170	88084.9	0.2154E+10
30	0.207	55573.4	0.0000E+00
29	0.225	55573.4	0.0000E+00
28	0.244	55573.4	0.0000E+00
27	0.246	55573.4	0.0000E+00
26	0.249	55573.4	0.0000E+00
25	0.268	55573.4	0.0000E+00
24	0.287	55573.4	0.0000E+00
23	0.307	55544.8	0.0000E+00
22	0.326	55519.5	0.0000E+00
21	0.345	55497.1	0.0000E+00
20	0.405	43540.9	0.0000E+00
19	0.465	34668.9	0.0000E+00
18	0.525	27825.0	0.0000E+00
17	0.585	22386.4	0.0000E+00
16	0.645	17961.7	0.0000E+00
15	0.705	14292.9	0.0000E+00
14	0.765	11203.0	0.0000E+00
13	0.825	8566.3	0.0000E+00
12	0.851	8555.3	0.0000E+00
11	0.876	8549.9	0.0000E+00
10	0.976	6929.7	0.0000E+00
9	1.076	5614.9	0.0000E+00
8	1.176	4527.1	0.0000E+00
7	1.276	3612.6	0.0000E+00
6	1.376	2833.3	0.0000E+00
5	1.476	2161.5	0.0000E+00
4	1.576	1576.4	0.0000E+00
3	1.676	1062.1	0.0000E+00
2	1.776	606.5	0.0000E+00
1	1.876	200.0	0.0000E+00



==== ROCKET ENGINE PARAMETERS ====

The H2 dissociation fraction is: 0.9988
The H2 average molecular weight is: 1.0092 g/gmol
The propellant molecular weight is: 6.4944 g/gmol
The cross-sectional flow area is: 0.0721 m²
The propellant mass flow rate is: 0.00 kg/s

The chamber temperature is: 55573.4 K
The calculated exit velocity is: 19187.0 m/s
The calculated thrust is: 0.0 kN
The calculated specific impulse is: 1956.5 s

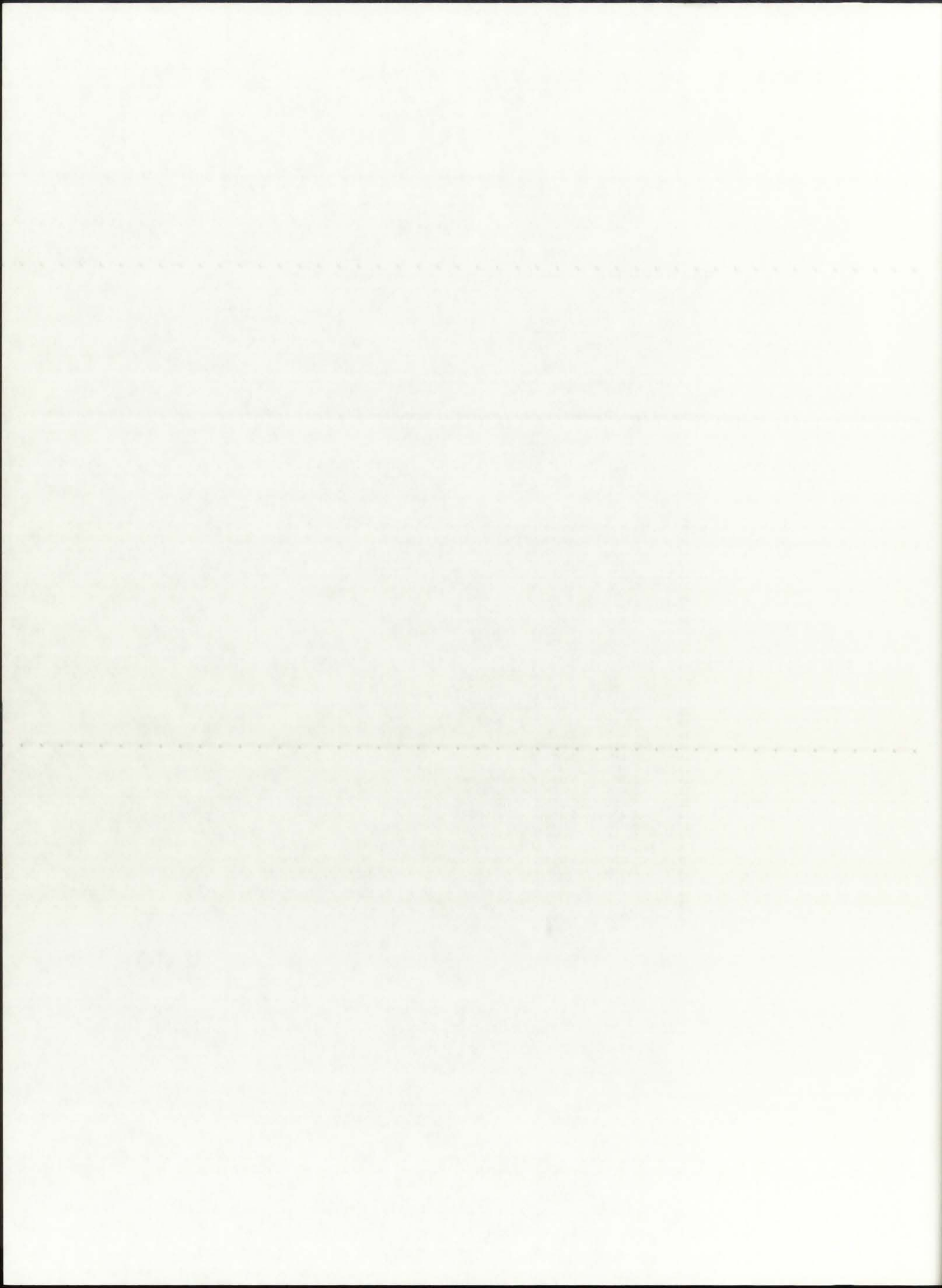


==== SUMMARY OF CONVERGED VALUES ====

This Case Executed for: REFLBe = 0.00000
 Pressure = 1000.0 atm

Modes of Heat Transfer: Radiation in BG, SiW, and P = .on.
 Convection in BG = .on.
 Convection in P = .on.

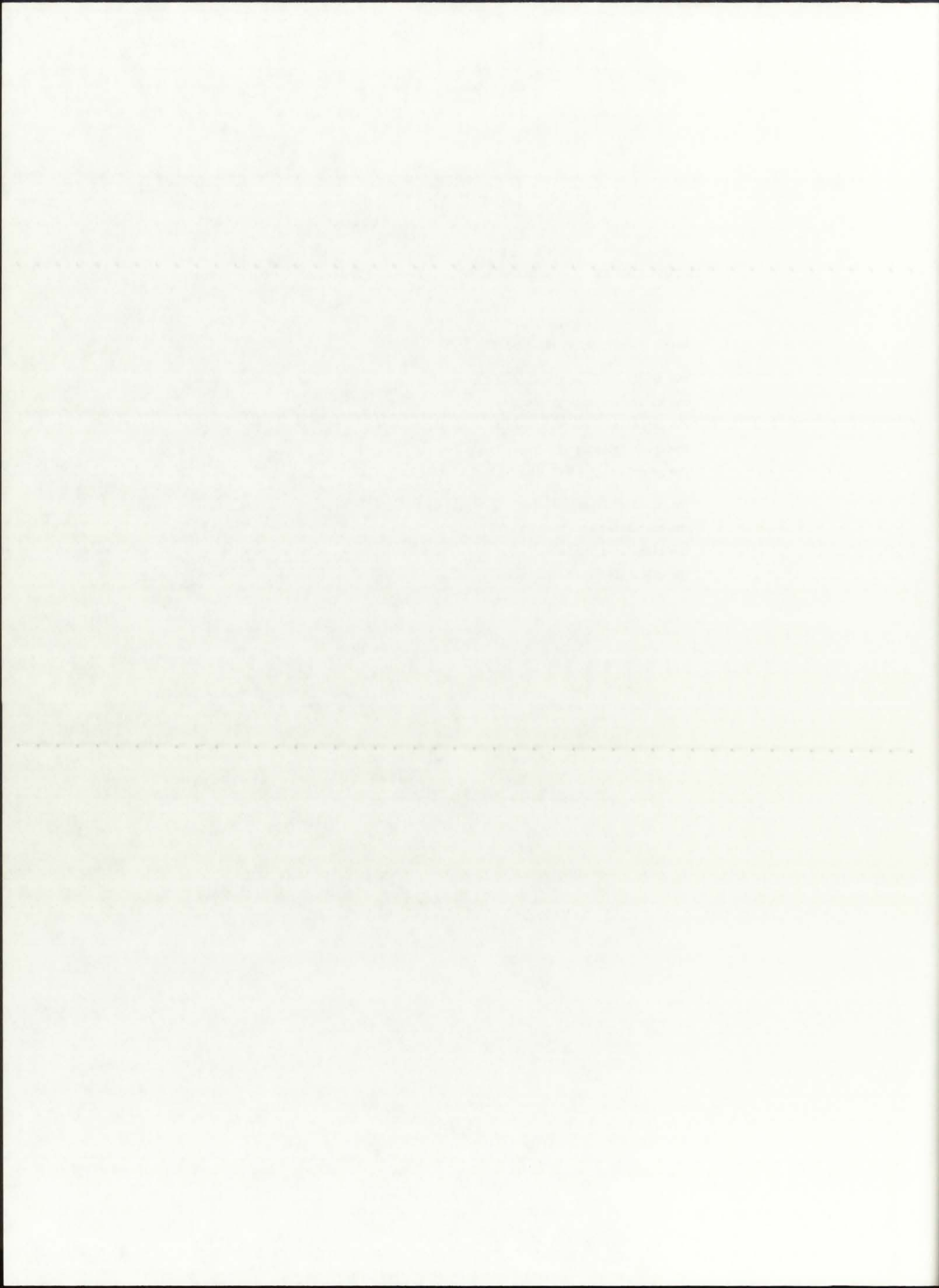
i	r(i)	T(i)	Qg(i)
37	0.000	119360.1	0.1039E+10
36	0.019	119360.1	0.1031E+10
35	0.039	119239.3	0.2056E+10
34	0.059	118871.9	0.2074E+10
33	0.096	116569.5	0.2097E+10
32	0.133	112429.0	0.2129E+10
31	0.170	105339.4	0.2173E+10
30	0.207	66320.1	0.0000E+00
29	0.225	66320.1	0.0000E+00
28	0.244	66320.1	0.0000E+00
27	0.246	66320.1	0.0000E+00
26	0.249	66320.1	0.0000E+00
25	0.268	66320.1	0.0000E+00
24	0.287	66320.1	0.0000E+00
23	0.307	66285.9	0.0000E+00
22	0.326	66255.7	0.0000E+00
21	0.345	66228.9	0.0000E+00
20	0.405	51951.9	0.0000E+00
19	0.465	41357.7	0.0000E+00
18	0.525	33185.3	0.0000E+00
17	0.585	26690.9	0.0000E+00
16	0.645	21407.3	0.0000E+00
15	0.705	17026.4	0.0000E+00
14	0.765	13336.7	0.0000E+00
13	0.825	10188.1	0.0000E+00
12	0.851	10175.1	0.0000E+00
11	0.876	10168.6	0.0000E+00
10	0.976	8234.3	0.0000E+00
9	1.076	6664.6	0.0000E+00
8	1.176	5365.9	0.0000E+00
7	1.276	4274.2	0.0000E+00
6	1.376	3343.8	0.0000E+00
5	1.476	2541.7	0.0000E+00
4	1.576	1843.2	0.0000E+00
3	1.676	1229.2	0.0000E+00
2	1.776	685.3	0.0000E+00
1	1.876	200.0	0.0000E+00



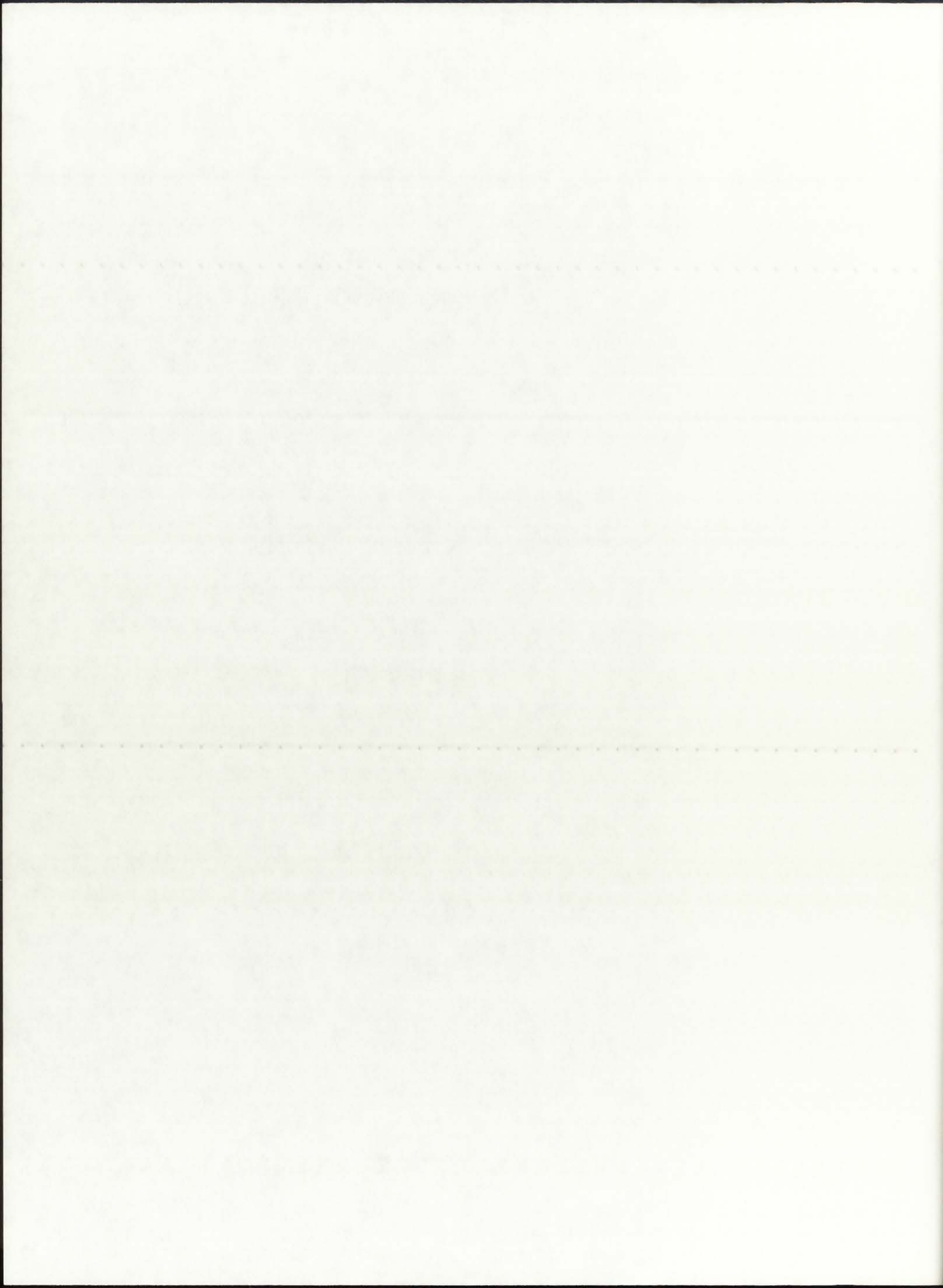
==== ROCKET ENGINE PARAMETERS ====

The H2 dissociation fraction is: 0.9981
The H2 average molecular weight is: 1.0099 g/gmol
The propellant molecular weight is: 6.4951 g/gmol
The cross-sectional flow area is: 0.0721 m²
The propellant mass flow rate is: 0.00 kg/s

The chamber temperature is: 66320.1 K
The calculated exit velocity is: 20959.1 m/s
The calculated thrust is: 0.0 kN
The calculated specific impulse is: 2137.2 s



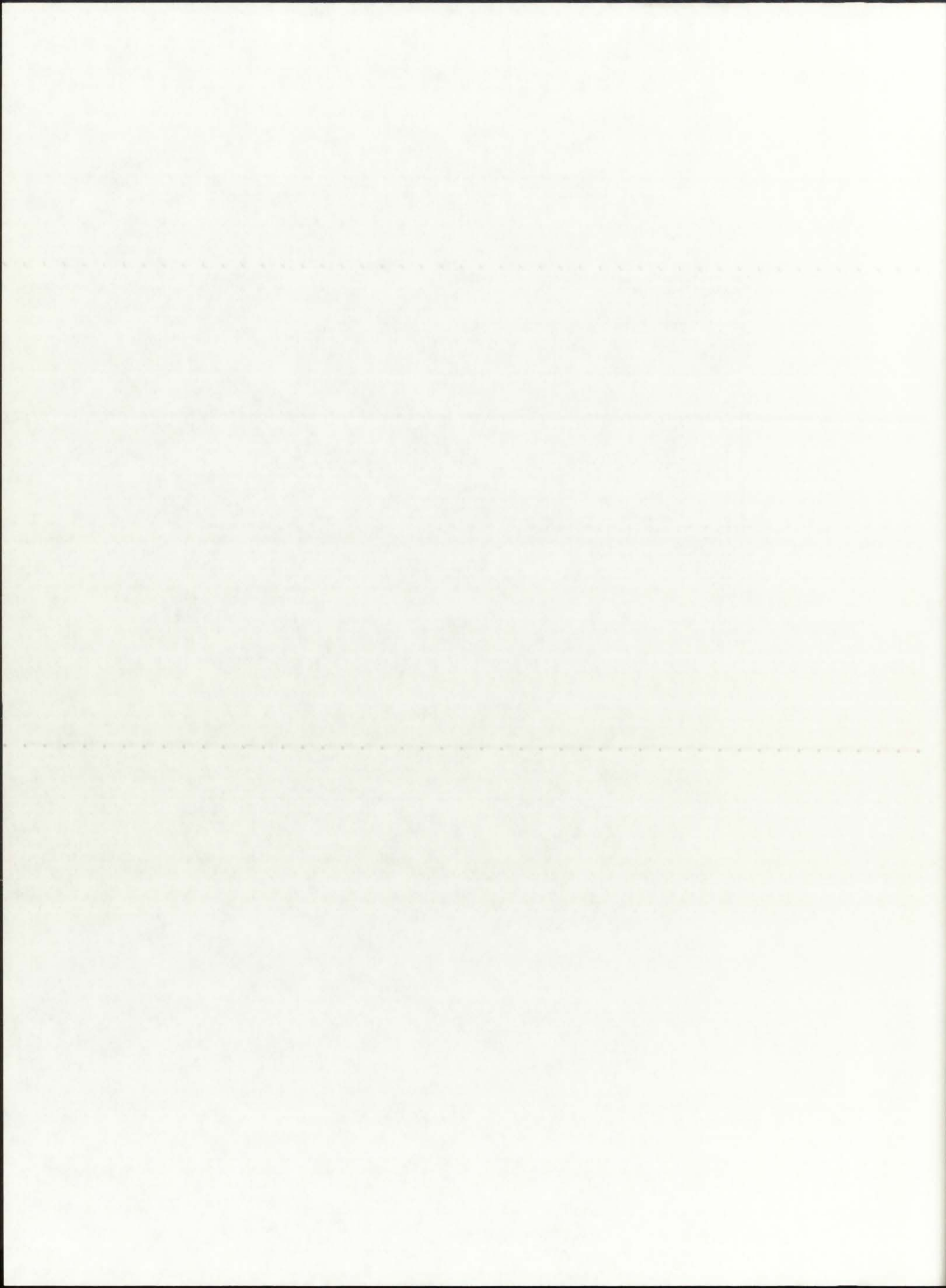
B.3. TRANSX Input Files (ENDF/B-V)



```

*Unit-cell NLB Engine 500MWth P=250 atm input file
*mtx7ey* *isotxs*/
1 6 0 1 1 1 0 2 0 0/
69 2 93 20 8 8 9 9 9/
*enru* *hydr* *deut* *oxgn* *bery* *ar* *si* *fe*
*enru* 70000. 1./
*hydr* 46000. 1./
*deut* 300. 1./
*oxgn* 300. 1./
*bery* 300. 1./
*ar* 46000. 1./
*si* 300. 1./
*fe* 300. 1./
1 1 *u235* 0.96 1.e+10 42 *free*/
1 1 *u238* 0.04 1.e+10 42 *free*/
2 2 *h1* 1.0 1.e+10 42 *free*/
3 3 *h2* 1.0 1.e+10 42 *d2o*/
4 4 *o16* 1.0 1.e+10 42 *free*/
5 5 *be9* 1.0 1.e+10 42 *be* *be$/
6 6 *arnat* 1.0 1.e+10 42 *free*/
7 7 *sinat* 1.0 1.e+10 42 *free*/
8 8 *fenat* 1.0 1.e+10 42 *free*/
*strpl* *sngam* *sfis* *chiso* *snalf* *snp* *sn2n* *snd* *snt*/
1 *trd*/
2 *ng*/
3 *nftot*/
4 *chi*/
5 *na*/
6 *np*/
7 *n2n*/
8 *nd*/
9 *nt*/
*stop*

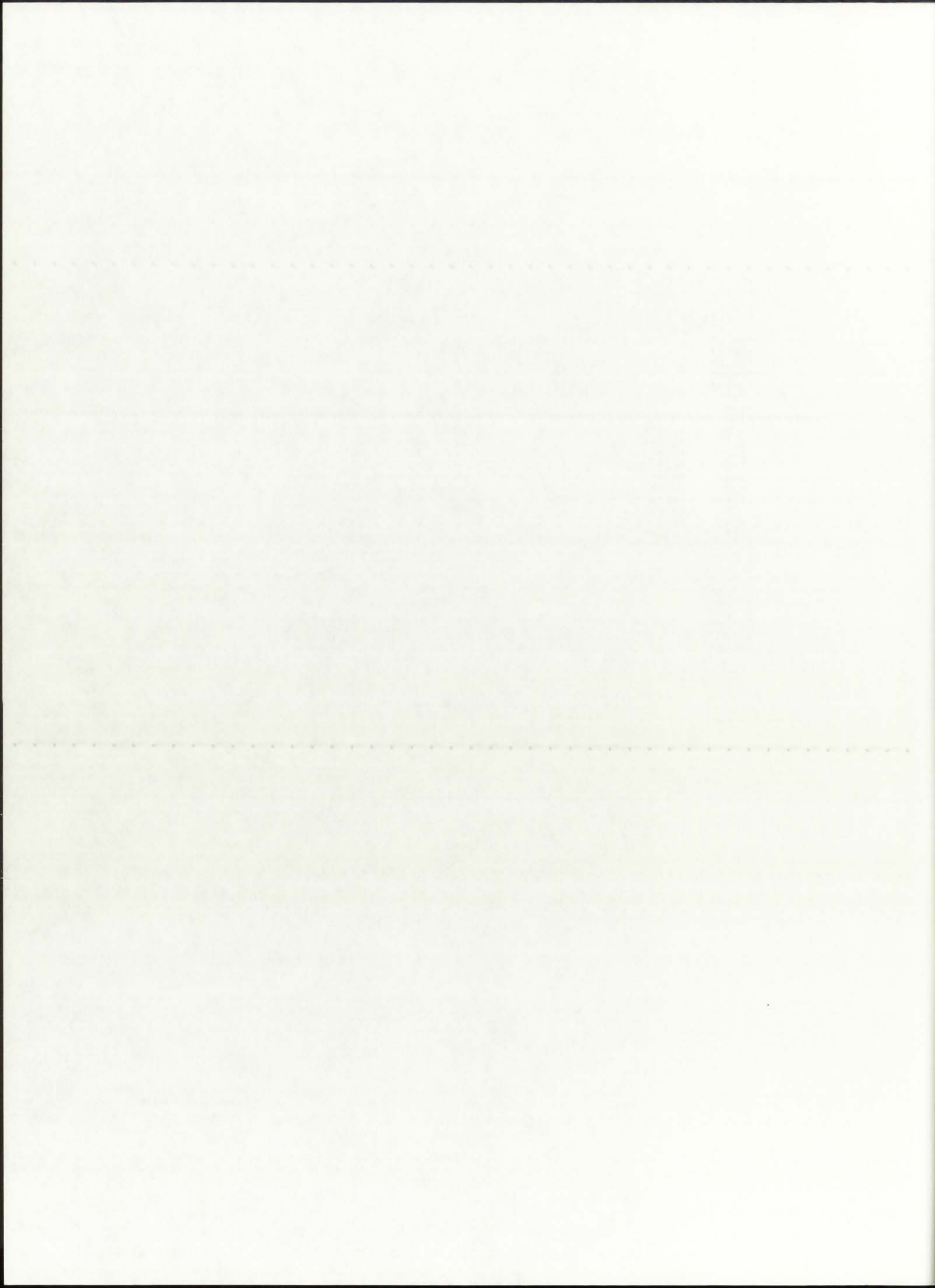
```



```

*Unit-cell NLB Engine 500MWth P=500 atm input file
*mtx7ey* *isotxs*/
1 6 0 1 1 1 0 2 0 0/
69 2 93 20 8 8 9 9 9/
*enru* *hydr* *deut* *oxgn* *bery* *ar* *si* *fe*
*enru* 90000. 1./
*hydr* 55000. 1./
*deut* 300. 1./
*oxgn* 300. 1./
*bery* 300. 1./
*ar* 55000. 1./
*si* 300. 1./
*fe* 300. 1./
1 1 *u235* 0.96 1.e+10 42 *free*/
1 1 *u238* 0.04 1.e+10 42 *free*/
2 2 *h1* 1.0 1.e+10 42 *free*/
3 3 *h2* 1.0 1.e+10 42 *d2o*/
4 4 *ol6* 1.0 1.e+10 42 *free*/
5 5 *be9* 1.0 1.e+10 42 *be* *be$*/
6 6 *arnat* 1.0 1.e+10 42 *free*/
7 7 *sinat* 1.0 1.e+10 42 *free*/
8 8 *fenat* 1.0 1.e+10 42 *free*/
*strpl* *sngam* *sfis* *chiso* *snalf* *snp* *sn2n* *snd* *snt*/
1 *trd*/
2 *ng*/
3 *nftot*/
4 *chi*/
5 *na*/
6 *np*/
7 *n2n*/
8 *nd*/
9 *nt*/
*stop*

```



```

*Unit-cell NLB Engine 500MWth P=1000 atm input file
*mtx7ey* *isotxs*/
1 6 0 1 1 1 0 2 0 0/
69 2 93 20 8 8 9 9 9/
*enru* *hydr* *deut* *oxgn* *bery* *ar* *si* *fe*
*enru* 110000. 1./
*hydr* 66000. 1./
*deut* 300. 1./
*oxgn* 300. 1./
*bery* 300. 1./
*ar* 66000. 1./
*si* 300. 1./
*fe* 300. 1./
1 1 *u235* 0.96 1.e+10 42 *free*/
1 1 *u238* 0.04 1.e+10 42 *free*/
2 2 *h1* 1.0 1.e+10 42 *free*/
3 3 *h2* 1.0 1.e+10 42 *d2o*/
4 4 *o16* 1.0 1.e+10 42 *free*/
5 5 *be9* 1.0 1.e+10 42 *be* *be$/
6 6 *arnat* 1.0 1.e+10 42 *free*/
7 7 *sinat* 1.0 1.e+10 42 *free*/
8 8 *fenat* 1.0 1.e+10 42 *free*/
*strpl* *sngam* *sfis* *chiso* *snalf* *snp* *sn2n* *snd* *snt*/
1 *trd*/
2 *ng*/
3 *nftot*/
4 *chi*/
5 *na*/
6 *np*/
7 *n2n*/
8 *nd*/
9 *nt*/
*stop*

```

STATE OF CALIFORNIA

COUNTY OF LOS ANGELES

IN SENATE

January 1, 1900

REPORT

OF THE

COMMISSIONERS OF THE LAND OFFICE

FOR THE YEAR 1899

AND

THE PROCEEDINGS OF THE

LAND OFFICE

FOR THE YEAR 1899

AND

THE PROCEEDINGS OF THE

LAND OFFICE

FOR THE YEAR 1899

AND

THE PROCEEDINGS OF THE

LAND OFFICE

FOR THE YEAR 1899

AND

THE PROCEEDINGS OF THE

LAND OFFICE

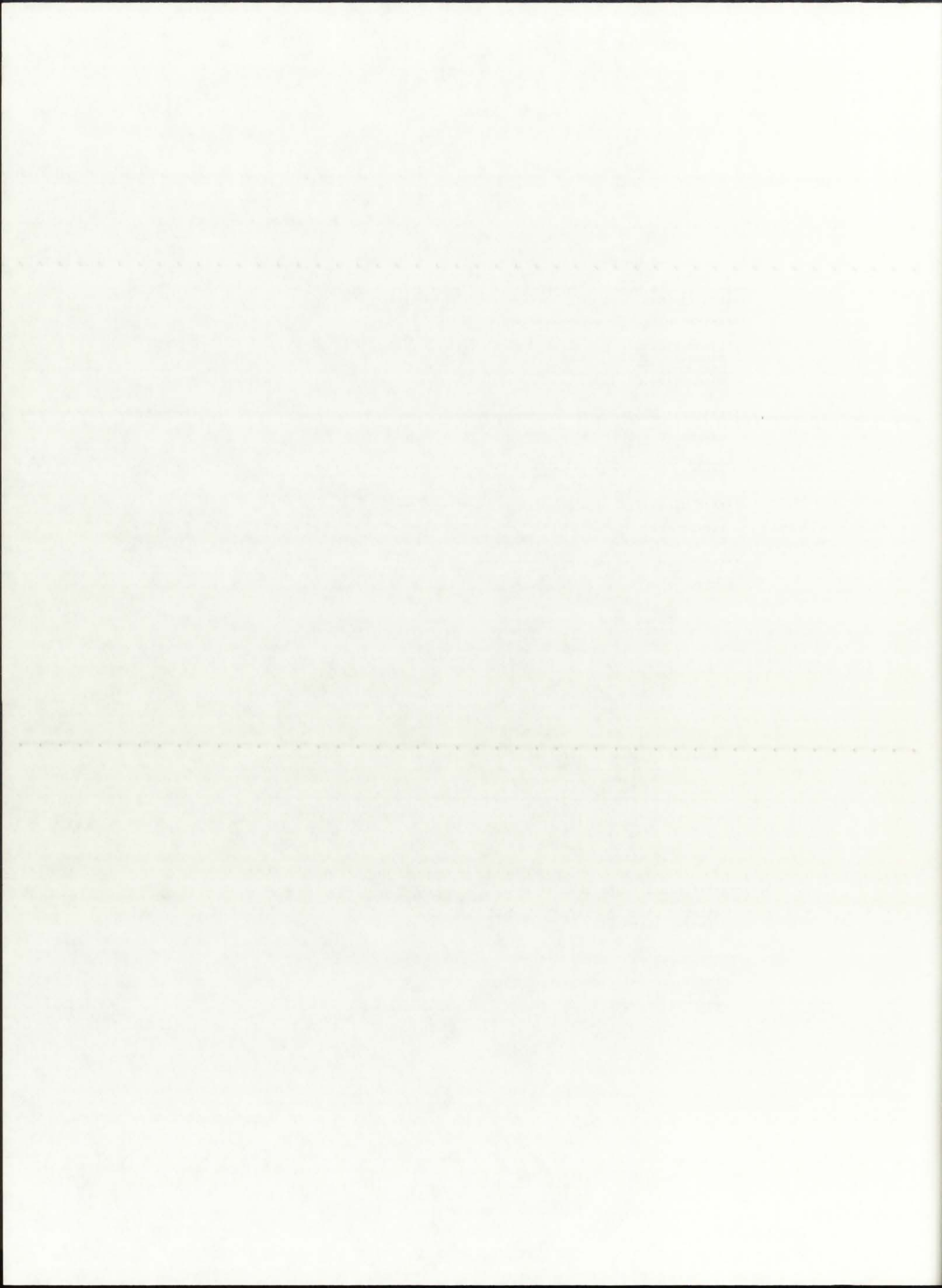
B.4. ONEDANT Input Files (ENDF/B-V)

8.4. CONDENSANT INPUT (ENRDR 8-V)

```

2 0 0
unit-cell NLB engine - 500MWth, P=250 atm, ENDF-VI library
search for Q(r) and keff, based on T(r) from GNRATR-1D code
/
/***** block i *****/
/
  igeom=cylinder  ngroup=69  isn=8  niso=8  mt=10
  nzone=10  im=10  it=29
  maxlcm=500000
  maxscm=100000
  t
/
/***** block ii *****/
/
  xmesh=0.0,6.0,13.375,20.75,24.45,24.94,28.80,34.58,
        58.58,82.58,87.66
  xints=4 3 3 2 2 2 3 4 4 2
  zones=1 2 3 4 5 6 7 8 9 10
  t
/
/***** block iii (cross sections) *****/
/
  lib=isotxs
  t
/
/***** block iv (mixing) *****/
/
  matls=  mixtr  ar      2.5590e-5
         enru   2.5823e-6;
         fuel1  enru   5.1646e-6;
         fuel2  enru   5.1646e-6;
         buffr  ar     5.1190e-5;
         sio2   si     2.6660e-2
         oxgn   5.3320e-2;
         prop   hydr   1.0156e-4;
         bemod  bery   1.2360e-1;
         d2o1   deut   1.8940e-2
         oxgn   9.4700e-3;
         d2o2   deut   1.8940e-2
         oxgn   9.4700e-3;
         steel  fe     8.4860e-2;
/
  assign= 1  mixtr  1.0;
         2  fuel1  1.0;
         3  fuel2  1.0;
         4  buffr  1.0;
         5  sio2   1.0;
         6  prop   1.0;
         7  bemod  1.0;
         8  d2o1   1.0;
         9  d2o2   1.0;
        10  steel  1.0;
  t
/
/***** block v (solver) *****/
/
  ievt=1  isct=1  ibr=0  fluxp=1  bhgt=182.73
  oitm=30  iitm=100
  t
/
/***** block vi (edits) *****/
/
  pted=1  zned=1  icoll=69;  igrped=3
  edxs=n-fiss
  resdnt=1  mevper=176.0  power=2.736  rzflux=1
/

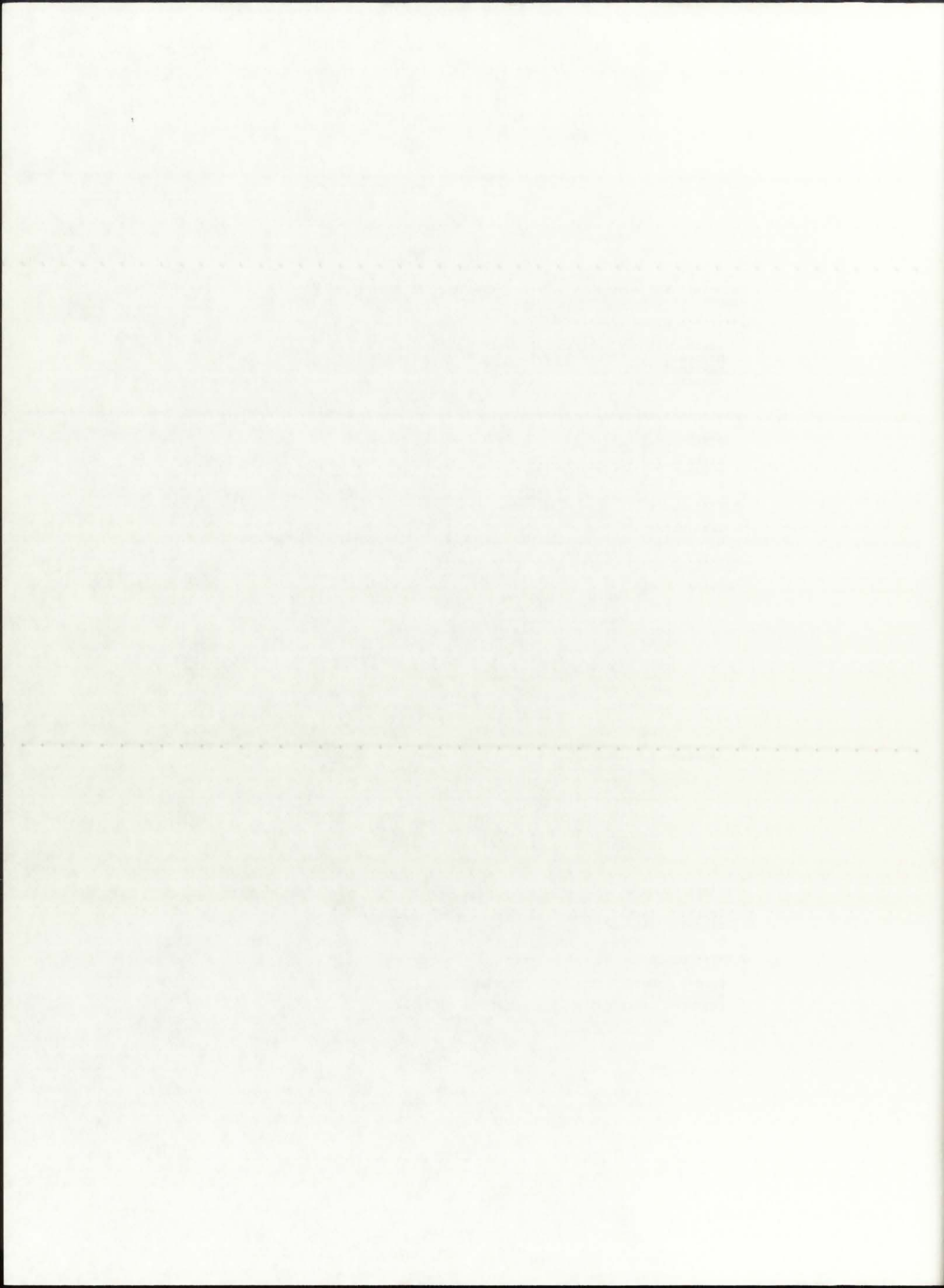
```



```

2 0 0
unit-cell NLB engine - 500MWth, P=500 atm, ENDF-VI library
search for Q(r) and keff, based on T(r) from GNRATR-1D code
/
/***** block i *****/
/
igeom=cylinder ngroup=69 isn=8 niso=8 mt=10
nzone=10 im=10 it=29
maxlcm=500000
maxscm=100000
t
/
/***** block ii *****/
/
xmesh=0.0,6.0,13.375,20.75,24.45,24.94,28.80,34.58,
58.58,82.58,87.66
xints=4 3 3 2 2 2 3 4 4 2
zones=1 2 3 4 5 6 7 8 9 10
t
/
/***** block iii (cross sections) *****/
/
lib=isotxs
t
/
/***** block iv (mixing) *****/
/
matls= mixtr ar 5.1190e-5
enru 3.4510e-6;
fuel1 enru 6.9020e-6;
fuel2 enru 6.9020e-6;
buffr ar 1.0240e-4;
sio2 si 2.6660e-2
oxgn 5.3320e-2;
prop hydr 2.0312e-4;
bemod bery 1.2360e-1;
d2o1 deut 1.8940e-2
oxgn 9.4700e-3;
d2o2 deut 1.8940e-2
oxgn 9.4700e-3;
steel fe 8.4860e-2;
/
assign= 1 mixtr 1.0;
2 fuel1 1.0;
3 fuel2 1.0;
4 buffr 1.0;
5 sio2 1.0;
6 prop 1.0;
7 bemod 1.0;
8 d2o1 1.0;
9 d2o2 1.0;
10 steel 1.0;
t
/
/***** block v (solver) *****/
/
ievt=1 isct=1 ibr=0 fluxp=1 bhgt=182.73
oitm=30 iitm=100
t
/
/***** block vi (edits) *****/
/
pted=1 zned=1 icoll=69; igrped=3
edxs=n-fiss
resdnt=1 mevper=176.0 power=2.736 rzflux=1
/

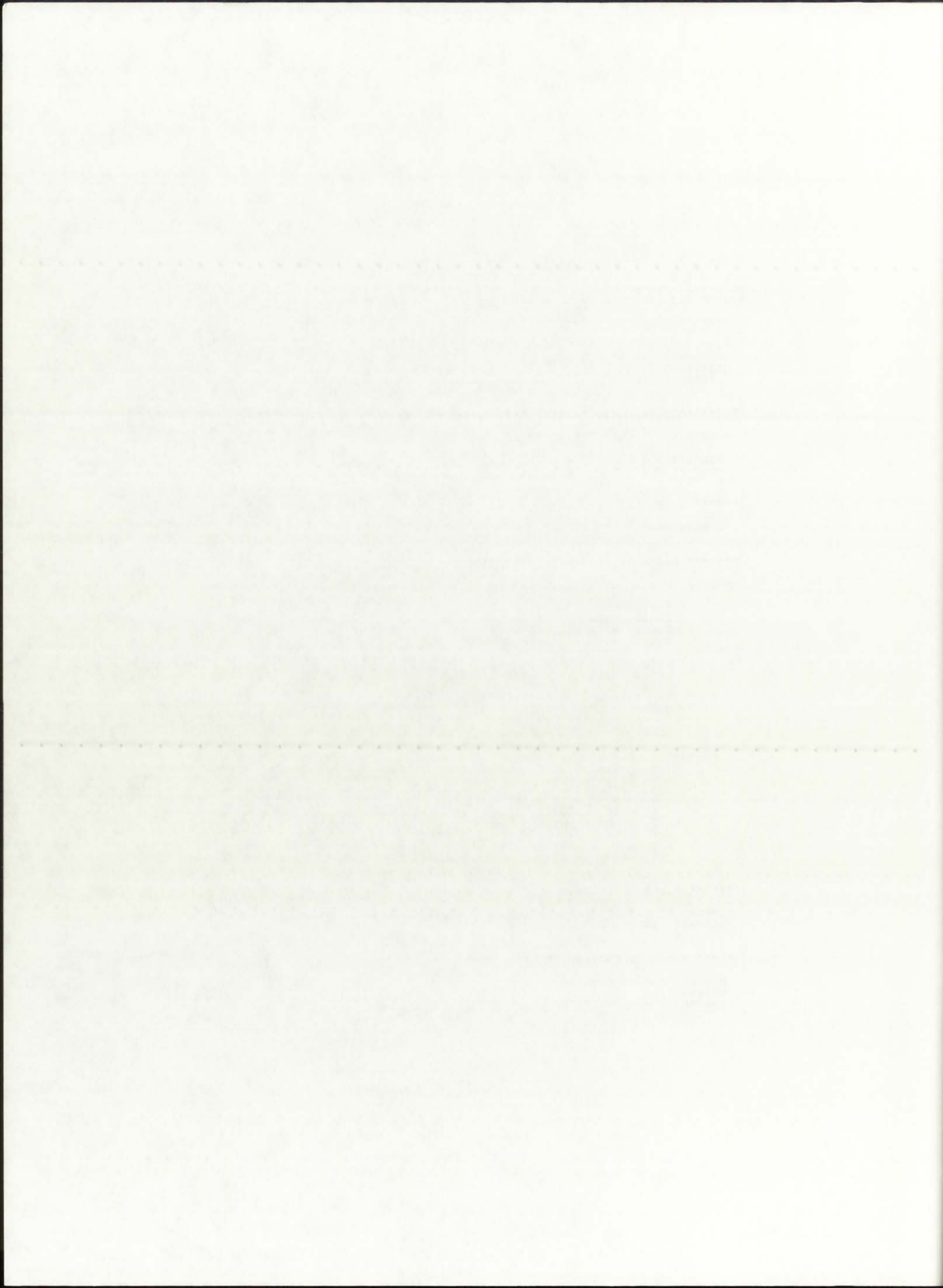
```



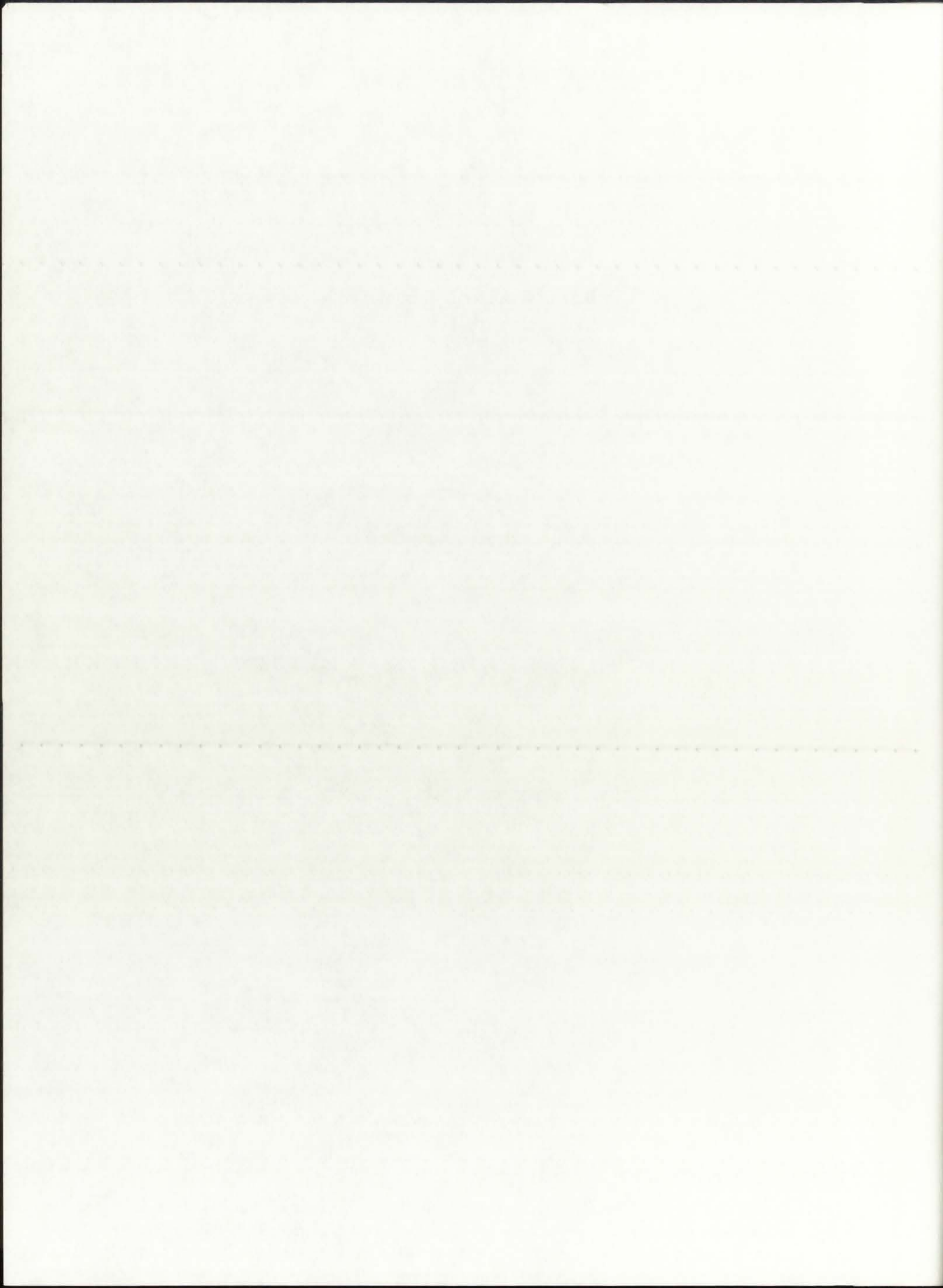
```

2 0 0
unit-cell NLB engine - 500MWth, P=1000 atm, ENDF-VI library
search for Q(r) and keff, based on T(r) from GNRATR-1D code
/
/***** block i *****/
/
  igeom=cylinder ngroup=69 isn=8 niso=8 mt=10
  nzone=10 im=10 it=29
  maxlcm=500000
  maxscm=100000
  t
/
/***** block ii *****/
/
  xmesh=0.0,6.0,13.375,20.75,24.45,24.94,28.80,34.58,
        58.58,82.58,87.66
  xints=4 3 3 2 2 2 3 4 4 2
  zones=1 2 3 4 5 6 7 8 9 10
  t
/
/***** block iii (cross sections) *****/
/
  lib=isotxs
  t
/
/***** block iv (mixing) *****/
/
  matls=  mixtr  ar    1.0240e-4
         enru   5.0099e-6;
         fuel1  enru   1.0020e-5;
         fuel2  enru   1.0020e-5;
         buffr  ar    2.0480e-4;
         sio2   si    2.6660e-2
         oxgn   5.3320e-2;
         prop   hydr  4.0624e-4;
         bemod  bery  1.2360e-1;
         d2o1   deut  1.8940e-2
         oxgn   9.4700e-3;
         d2o2   deut  1.8940e-2
         oxgn   9.4700e-3;
         steel  fe    8.4860e-2;
/
  assign= 1  mixtr  1.0;
         2  fuel1  1.0;
         3  fuel2  1.0;
         4  buffr  1.0;
         5  sio2   1.0;
         6  prop   1.0;
         7  bemod  1.0;
         8  d2o1   1.0;
         9  d2o2   1.0;
        10  steel  1.0;
  t
/
/***** block v (solver) *****/
/
  ievt=1  isct=1 ibr=0 fluxp=1 bhgt=182.73
  oitm=30 iitm=100
  t
/
/***** block vi (edits) *****/
/
  pted=1 zned=1 icoll=69; igrped=3
  edxs=n-fiss
  resdnt=1 mevper=176.0 power=2.736 rzflux=1
/

```



B.5. GNRATR-1D Summary Output Files (ENDF/B-V)

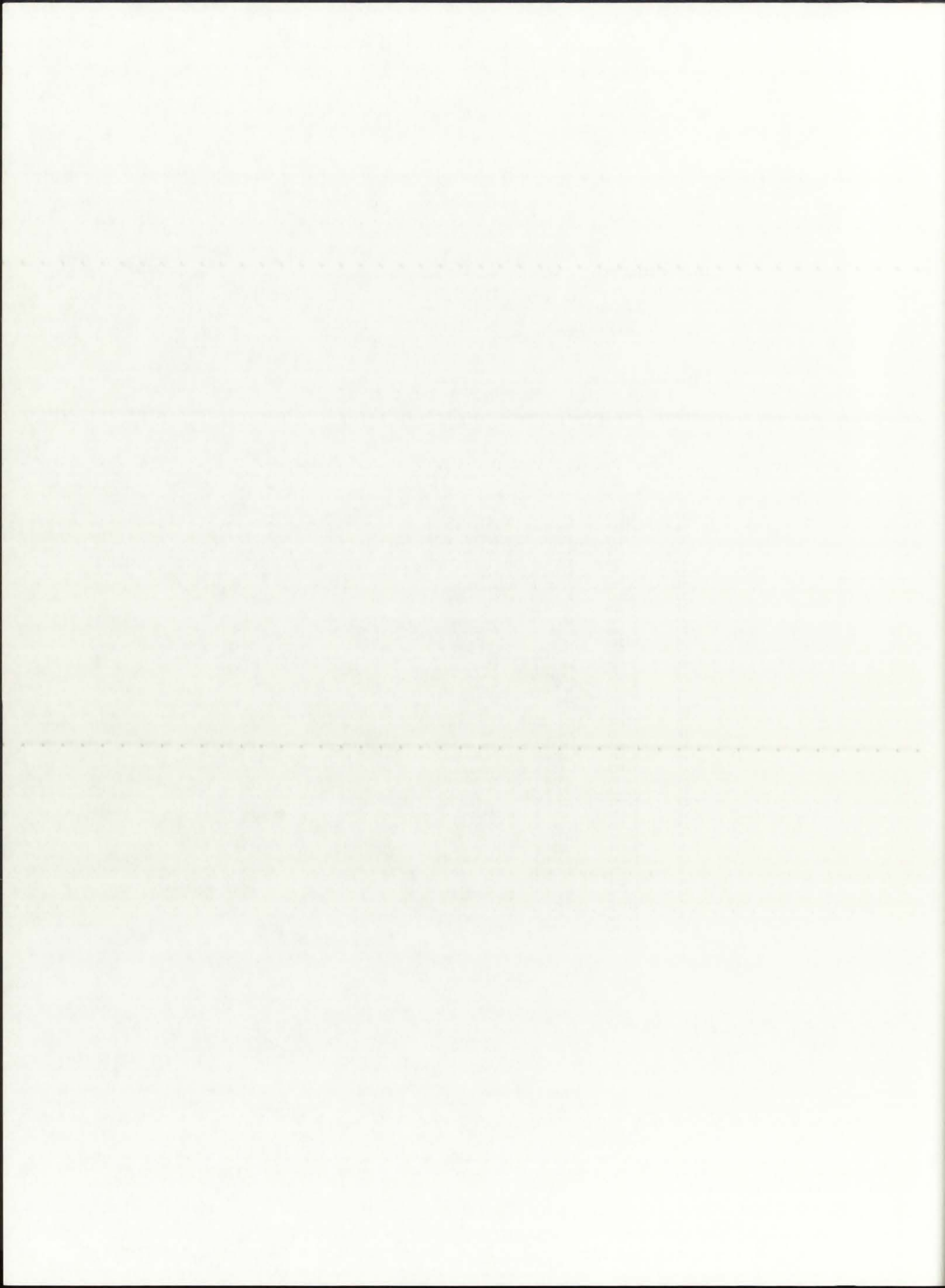


==== SUMMARY OF CONVERGED VALUES ====

This Case Executed for: REFLBe = 0.00000
 Pressure = 250.0 atm

Modes of Heat Transfer: Radiation in BG, SiW, and P = .on.
 Convection in BG = .on.
 Convection in P = .on.

i	r(i)	T(i)	Qg(i)
37	0.000	83970.4	0.1046E+10
36	0.019	83970.4	0.1042E+10
35	0.039	83884.2	0.2077E+10
34	0.059	83621.9	0.2087E+10
33	0.096	81982.5	0.2100E+10
32	0.133	79042.6	0.2119E+10
31	0.170	74021.2	0.2149E+10
30	0.207	46756.8	0.0000E+00
29	0.225	46756.8	0.0000E+00
28	0.244	46756.8	0.0000E+00
27	0.246	46756.8	0.0000E+00
26	0.249	46756.8	0.0000E+00
25	0.268	46756.8	0.0000E+00
24	0.287	46756.8	0.0000E+00
23	0.307	46732.7	0.0000E+00
22	0.326	46711.4	0.0000E+00
21	0.345	46692.6	0.0000E+00
20	0.405	36640.5	0.0000E+00
19	0.465	29181.4	0.0000E+00
18	0.525	23427.4	0.0000E+00
17	0.585	18854.9	0.0000E+00
16	0.645	15134.8	0.0000E+00
15	0.705	12050.4	0.0000E+00
14	0.765	9452.5	0.0000E+00
13	0.825	7235.7	0.0000E+00
12	0.851	7226.5	0.0000E+00
11	0.876	7221.9	0.0000E+00
10	0.976	5859.4	0.0000E+00
9	1.076	4753.7	0.0000E+00
8	1.176	3838.9	0.0000E+00
7	1.276	3069.9	0.0000E+00
6	1.376	2414.5	0.0000E+00
5	1.476	1849.5	0.0000E+00
4	1.576	1357.5	0.0000E+00
3	1.676	925.0	0.0000E+00
2	1.776	541.9	0.0000E+00
1	1.876	200.0	0.0000E+00



==== ROCKET ENGINE PARAMETERS ====

The H2 dissociation fraction is: 0.9992
The H2 average molecular weight is: 1.0088 g/gmol
The propellant molecular weight is: 6.4940 g/gmol
The cross-sectional flow area is: 0.0721 m2
The propellant mass flow rate is: 0.00 kg/s

The chamber temperature is: 46756.8 K
The calculated exit velocity is: 17599.8 m/s
The calculated thrust is: 0.0 kN
The calculated specific impulse is: 1794.6 s

Faint, illegible text at the top of the page, possibly a header or introductory paragraph.

Main body of faint, illegible text, appearing to be several lines of a document or report.

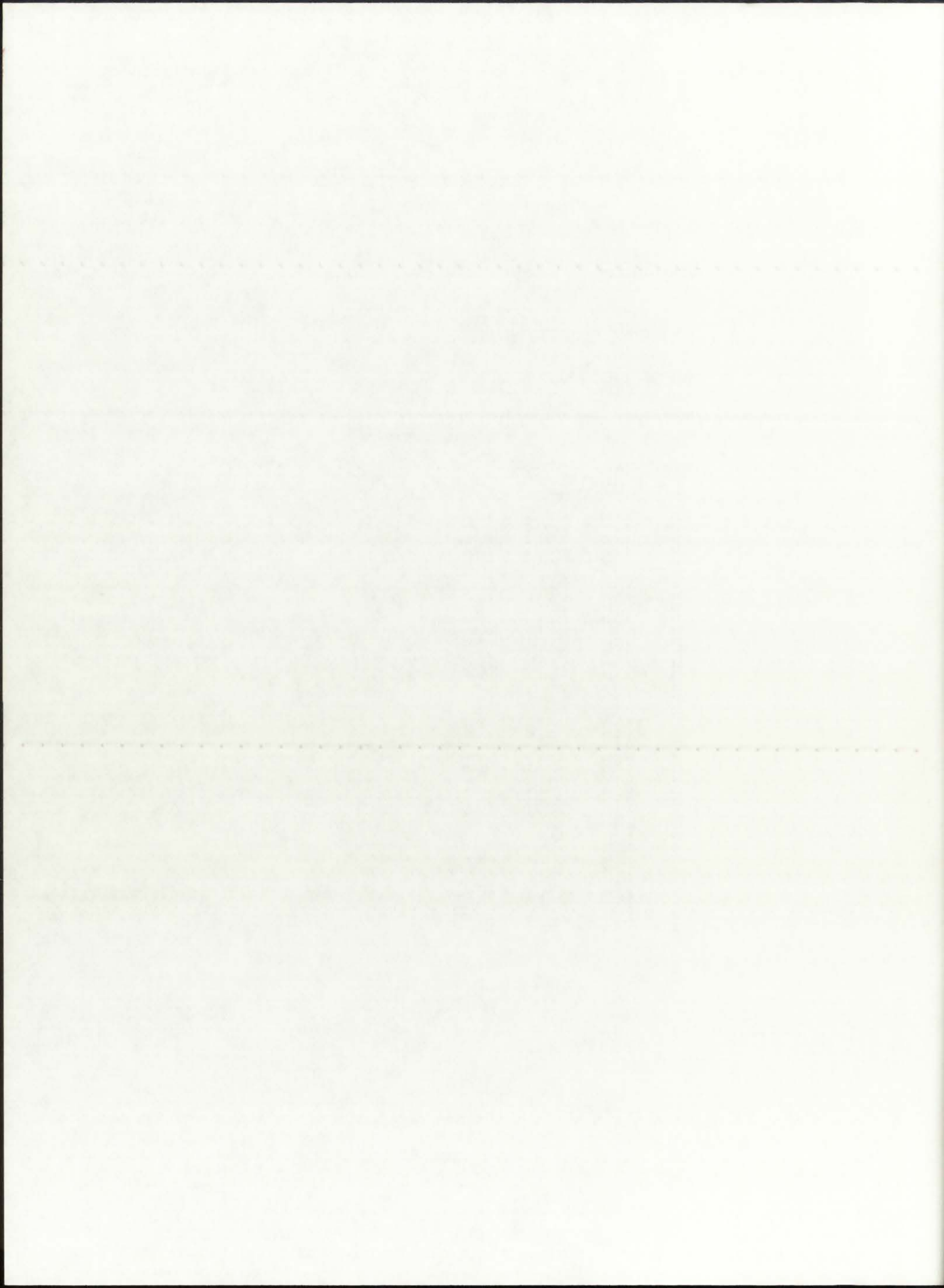
Large block of faint, illegible text occupying the lower half of the page.

==== SUMMARY OF CONVERGED VALUES ====

This Case Executed for: REFLBe = 0.00000
 Pressure = 500.0 atm

Modes of Heat Transfer: Radiation in BG, SiW, and P = .on.
 Convection in BG = .on.
 Convection in P = .on.

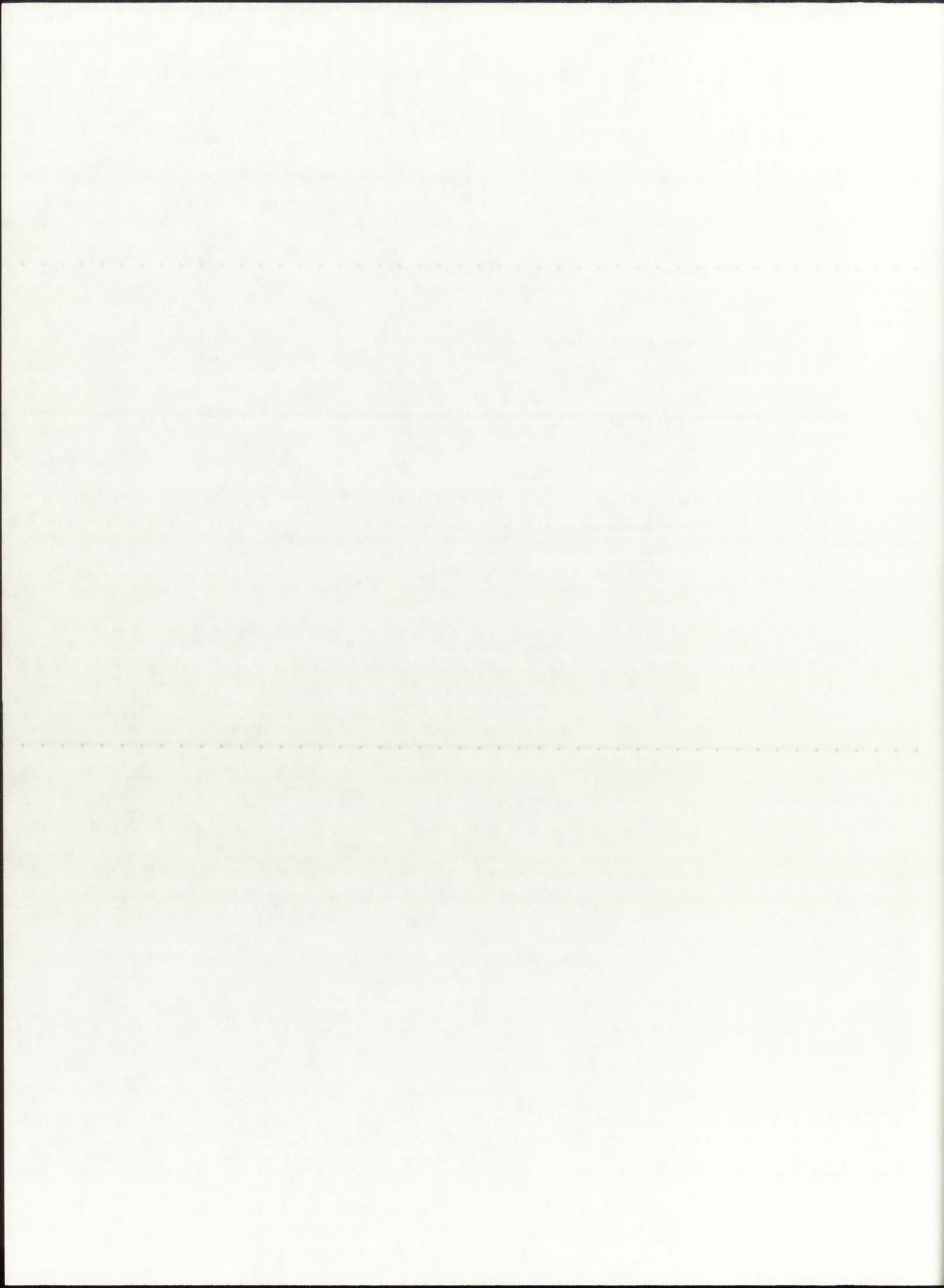
i	r(i)	T(i)	Qg(i)
37	0.000	99897.2	0.1043E+10
36	0.019	99897.2	0.1038E+10
35	0.039	99795.2	0.2069E+10
34	0.059	99484.9	0.2082E+10
33	0.096	97543.7	0.2099E+10
32	0.133	94058.6	0.2122E+10
31	0.170	88102.4	0.2159E+10
30	0.207	55573.4	0.0000E+00
29	0.225	55573.4	0.0000E+00
28	0.244	55573.4	0.0000E+00
27	0.246	55573.4	0.0000E+00
26	0.249	55573.4	0.0000E+00
25	0.268	55573.4	0.0000E+00
24	0.287	55573.4	0.0000E+00
23	0.307	55544.8	0.0000E+00
22	0.326	55519.5	0.0000E+00
21	0.345	55497.1	0.0000E+00
20	0.405	43540.9	0.0000E+00
19	0.465	34668.9	0.0000E+00
18	0.525	27825.0	0.0000E+00
17	0.585	22386.4	0.0000E+00
16	0.645	17961.7	0.0000E+00
15	0.705	14292.9	0.0000E+00
14	0.765	11203.0	0.0000E+00
13	0.825	8566.3	0.0000E+00
12	0.851	8555.3	0.0000E+00
11	0.876	8549.9	0.0000E+00
10	0.976	6929.7	0.0000E+00
9	1.076	5614.9	0.0000E+00
8	1.176	4527.1	0.0000E+00
7	1.276	3612.6	0.0000E+00
6	1.376	2833.3	0.0000E+00
5	1.476	2161.5	0.0000E+00
4	1.576	1576.4	0.0000E+00
3	1.676	1062.1	0.0000E+00
2	1.776	606.5	0.0000E+00
1	1.876	200.0	0.0000E+00



==== ROCKET ENGINE PARAMETERS ====

The H2 dissociation fraction is: 0.9988
The H2 average molecular weight is: 1.0092 g/gmol
The propellant molecular weight is: 6.4944 g/gmol
The cross-sectional flow area is: 0.0721 m²
The propellant mass flow rate is: 0.00 kg/s

The chamber temperature is: 55573.4 K
The calculated exit velocity is: 19187.0 m/s
The calculated thrust is: 0.0 kN
The calculated specific impulse is: 1956.5 s



==== SUMMARY OF CONVERGED VALUES ====

This Case Executed for: REFLBe = 0.00000
 Pressure = 1000.0 atm

Modes of Heat Transfer: Radiation in BG, SiW, and P = .on.
 Convection in BG = .on.
 Convection in P = .on.

i	r(i)	T(i)	Qg(i)
37	0.000	119354.1	0.1038E+10
36	0.019	119354.1	0.1031E+10
35	0.039	119233.3	0.2055E+10
34	0.059	118865.9	0.2073E+10
33	0.096	116564.3	0.2095E+10
32	0.133	112427.0	0.2127E+10
31	0.170	105345.1	0.2177E+10
30	0.207	66320.1	0.0000E+00
29	0.225	66320.1	0.0000E+00
28	0.244	66320.1	0.0000E+00
27	0.246	66320.1	0.0000E+00
26	0.249	66320.1	0.0000E+00
25	0.268	66320.1	0.0000E+00
24	0.287	66320.1	0.0000E+00
23	0.307	66285.9	0.0000E+00
22	0.326	66255.7	0.0000E+00
21	0.345	66228.9	0.0000E+00
20	0.405	51951.9	0.0000E+00
19	0.465	41357.7	0.0000E+00
18	0.525	33185.3	0.0000E+00
17	0.585	26690.9	0.0000E+00
16	0.645	21407.3	0.0000E+00
15	0.705	17026.4	0.0000E+00
14	0.765	13336.7	0.0000E+00
13	0.825	10188.1	0.0000E+00
12	0.851	10175.1	0.0000E+00
11	0.876	10168.6	0.0000E+00
10	0.976	8234.3	0.0000E+00
9	1.076	6664.6	0.0000E+00
8	1.176	5365.9	0.0000E+00
7	1.276	4274.2	0.0000E+00
6	1.376	3343.8	0.0000E+00
5	1.476	2541.7	0.0000E+00
4	1.576	1843.2	0.0000E+00
3	1.676	1229.2	0.0000E+00
2	1.776	685.3	0.0000E+00
1	1.876	200.0	0.0000E+00

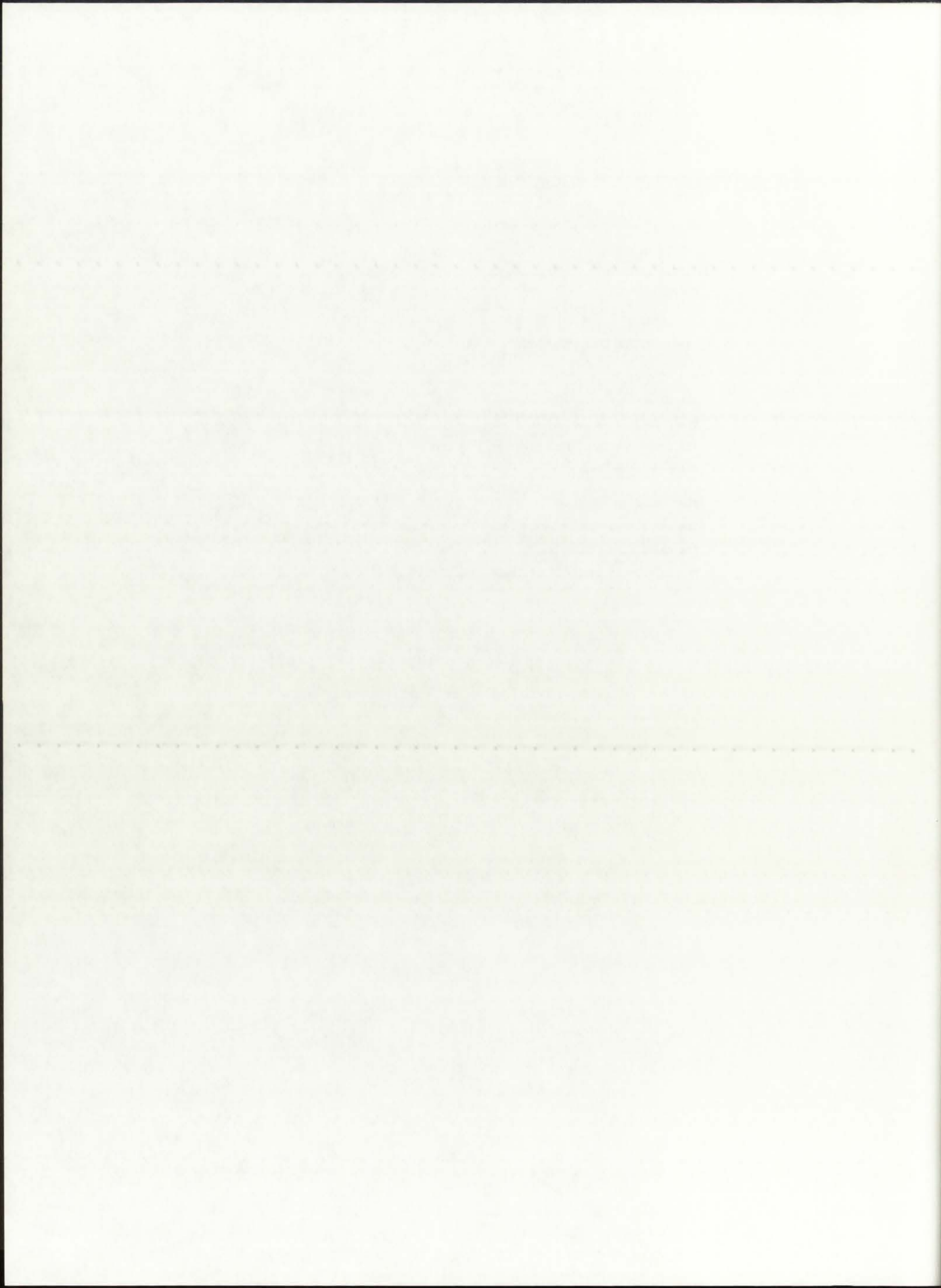
1917
 THE STATE OF TEXAS
 DEPARTMENT OF COMMERCE
 BUREAU OF STATISTICS

Commodity	1916	1917
Wheat	1,200,000	1,300,000
Corn	800,000	900,000
Soybeans	500,000	600,000
Cotton	300,000	400,000
Oats	200,000	250,000
Rye	100,000	150,000
Buckwheat	50,000	75,000
Barley	40,000	60,000
Triticum	30,000	45,000
Speltz	20,000	30,000
Millet	10,000	15,000
Broomcorn	5,000	7,500
Other grains	10,000	15,000
Total	2,975,000	3,337,500

==== ROCKET ENGINE PARAMETERS ====

The H2 dissociation fraction is: 0.9981
The H2 average molecular weight is: 1.0099 g/gmol
The propellant molecular weight is: 6.4951 g/gmol
The cross-sectional flow area is: 0.0721 m²
The propellant mass flow rate is: 0.00 kg/s

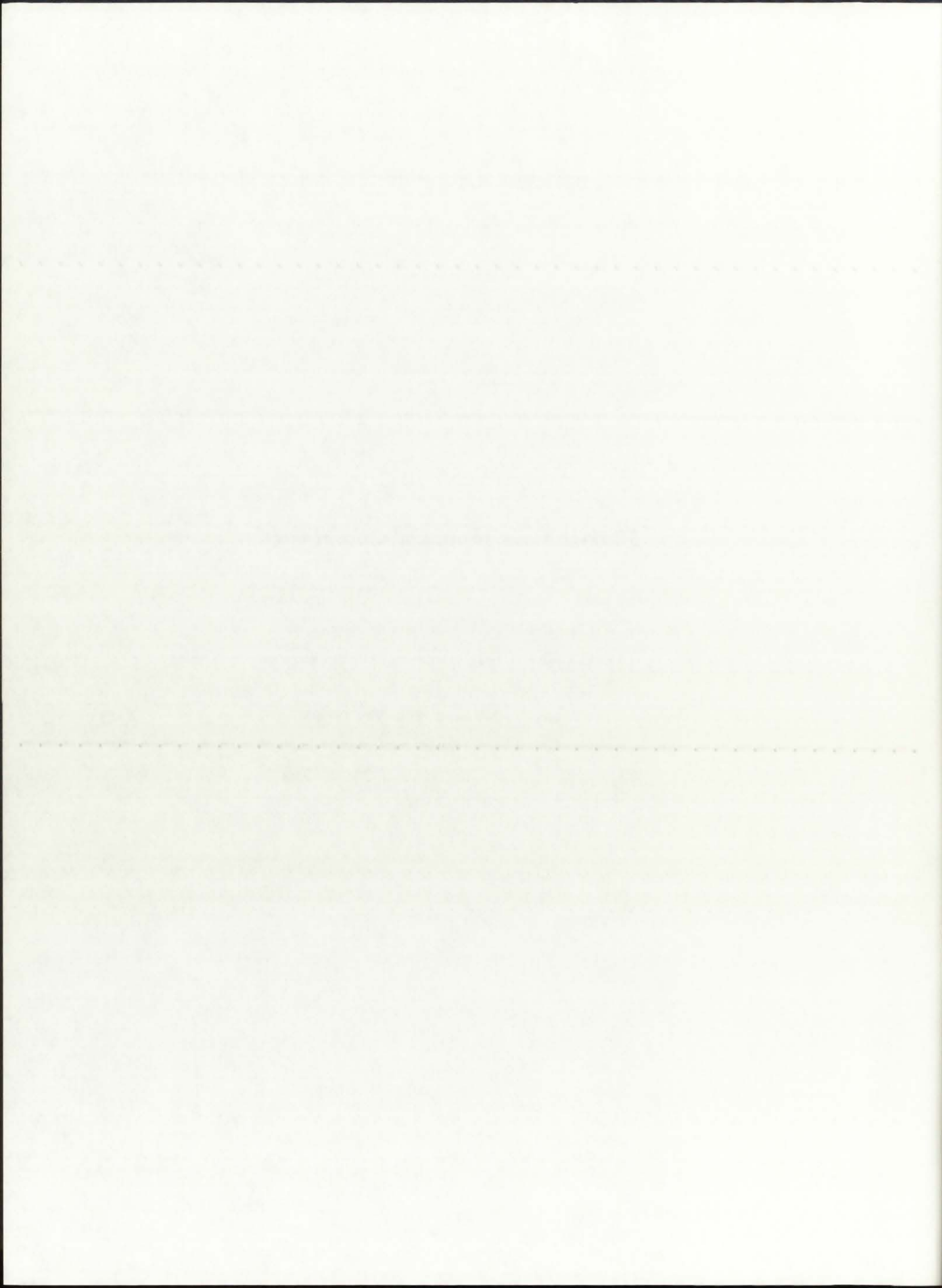
The chamber temperature is: 66320.1 K
The calculated exit velocity is: 20959.1 m/s
The calculated thrust is: 0.0 kN
The calculated specific impulse is: 2137.2 s



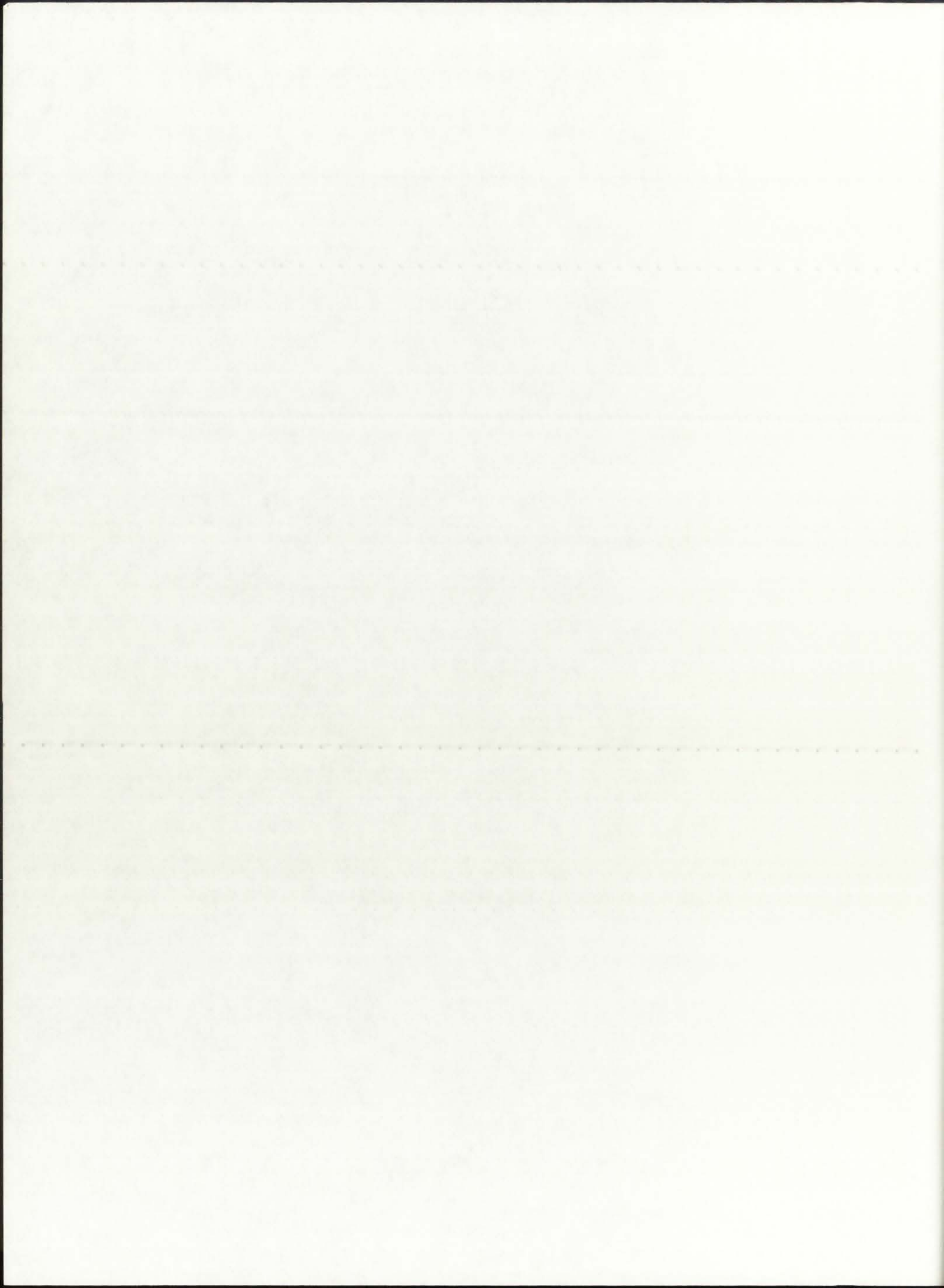
APPENDIX C

5 MWth Case: Input and Output Files

- C.1: ONEDANT Input Files (Hansen-Roach)
- C.2: GNRATR-1D Summary Output Files (Hansen-Roach)
- C.3: TRANSX Input Files (ENDF/B-V)
- C.4: ONEDANT Input Files (ENDF/B-V)
- C.5: GNRATR-1D Summary Output Files (ENDF/B-V)



C.1. ONEDANT Input Files (Hansen-Roach)

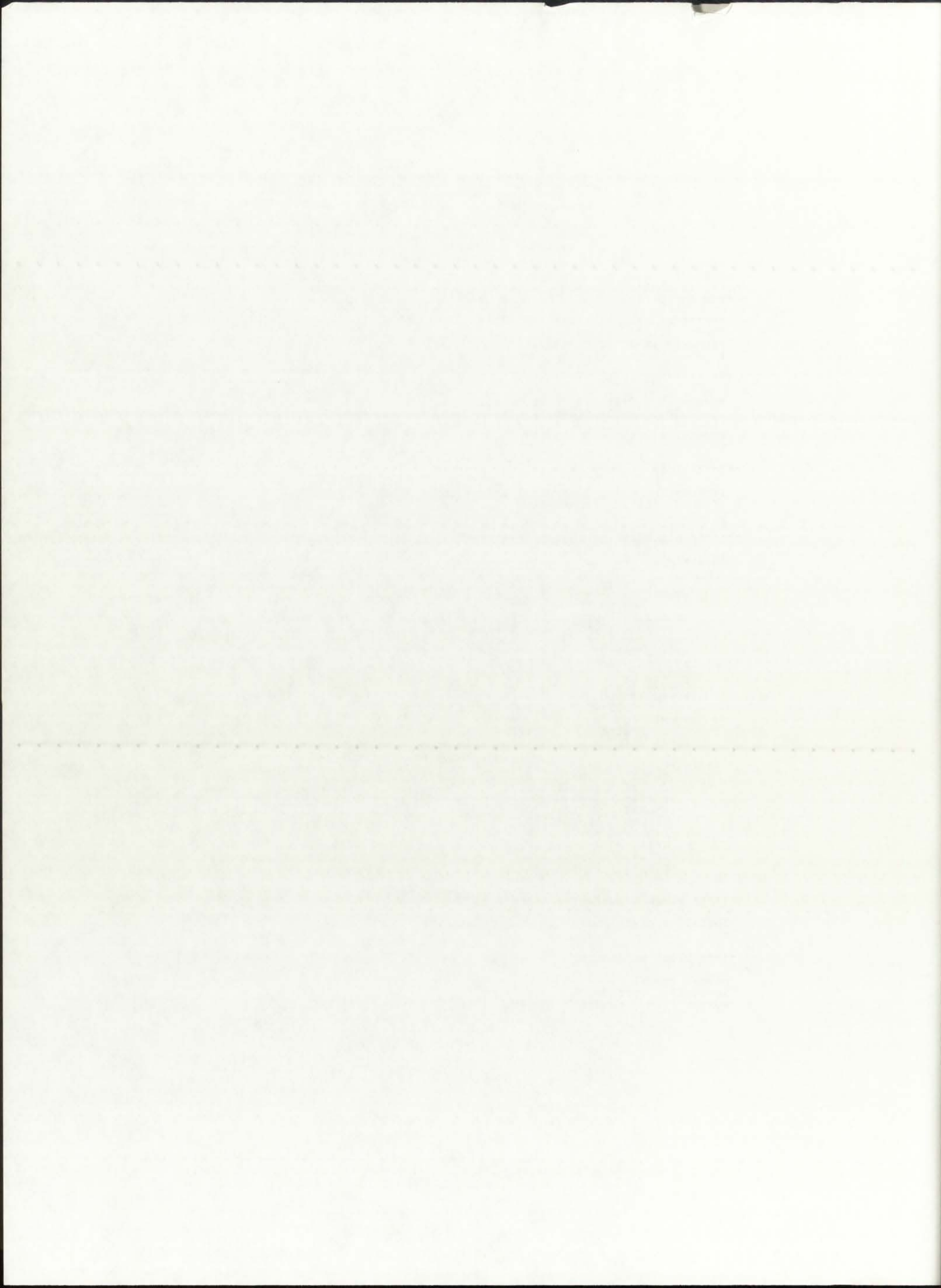


```

2 0 0
unit-cell rocket engine - 5 MWth Configuration - P=250 atm
search for Q(r) and keff, based on T(r) from GNRATR-1D code
/
/***** block i *****/
  igeom=cylinder  ngroup=16  isn=4  niso=118  mt=10
  nzone=10  im=10  it=29  idimen=1
  t
/
/***** block ii *****/
/
  xmesh=0.0,6.0,13.375,20.75,24.45,24.94,28.80,34.58,
        58.58,82.58,87.66
  xints=4,3,3,2,2,2,3,4,4,2
  zones=1,2,3,4,5,6,7,8,9,10
  t
/
/***** block iii (cross sections) *****/
/
  lib=bxslib  balxs=1  maxord=1  ihm=10  iht=4  ihs=5
  ifido=0  ititl=1  edname=fiss
  t
/
/***** block iv (mixing) *****/
/
  matls=mix
    "sulfur"      2.6350e-5
    "235-yr"     1.5292e-5
    "u238y"      1.1514e-6;
  uranI  "235-yr"  3.0583e-5
    "u238y"      2.3027e-6;
  uranII "235-yr"  3.0583e-5
    "u238y"      2.3027e-6;
  argon  "sulfur"  6.9260e-5;
  silica "si"      2.6666e-2
    "o16"        5.332e-2;
  hydro  "h"       1.3740e-4;
  beryl  "be"      1.236e-1;
  hvywI  "d"       1.894e-2
    "o16"        9.470e-3;
  hvywII "d"       1.894e-2
    "o16"        9.470e-3;
  steel  "fe"      8.486e-2;

  assign=mixture  mix  1.0;
    fuelI  uranI  1.0;
    fuelII uranII 1.0;
    buffer argon  1.0;
    siwall silica 1.0;
    propel hydro  1.0;
    bemodr beryl  1.0;
    reflI  hvywI  1.0;
    reflII hvywII 1.0;
    pvessl steel  1.0;
  t
/
/***** block v (solver) *****/
/
  ievt=1  isct=1 ibr=0  fluxp=1  bhgt=182.73
  t
/
/***** block vi (edits) *****/
/
  pted=1  zned=1
  icoll=16;  igrped=3
  edxs=n-fiss  resdnt=1  power=2.736e-2  mevper=176  rzflux=1
/

```

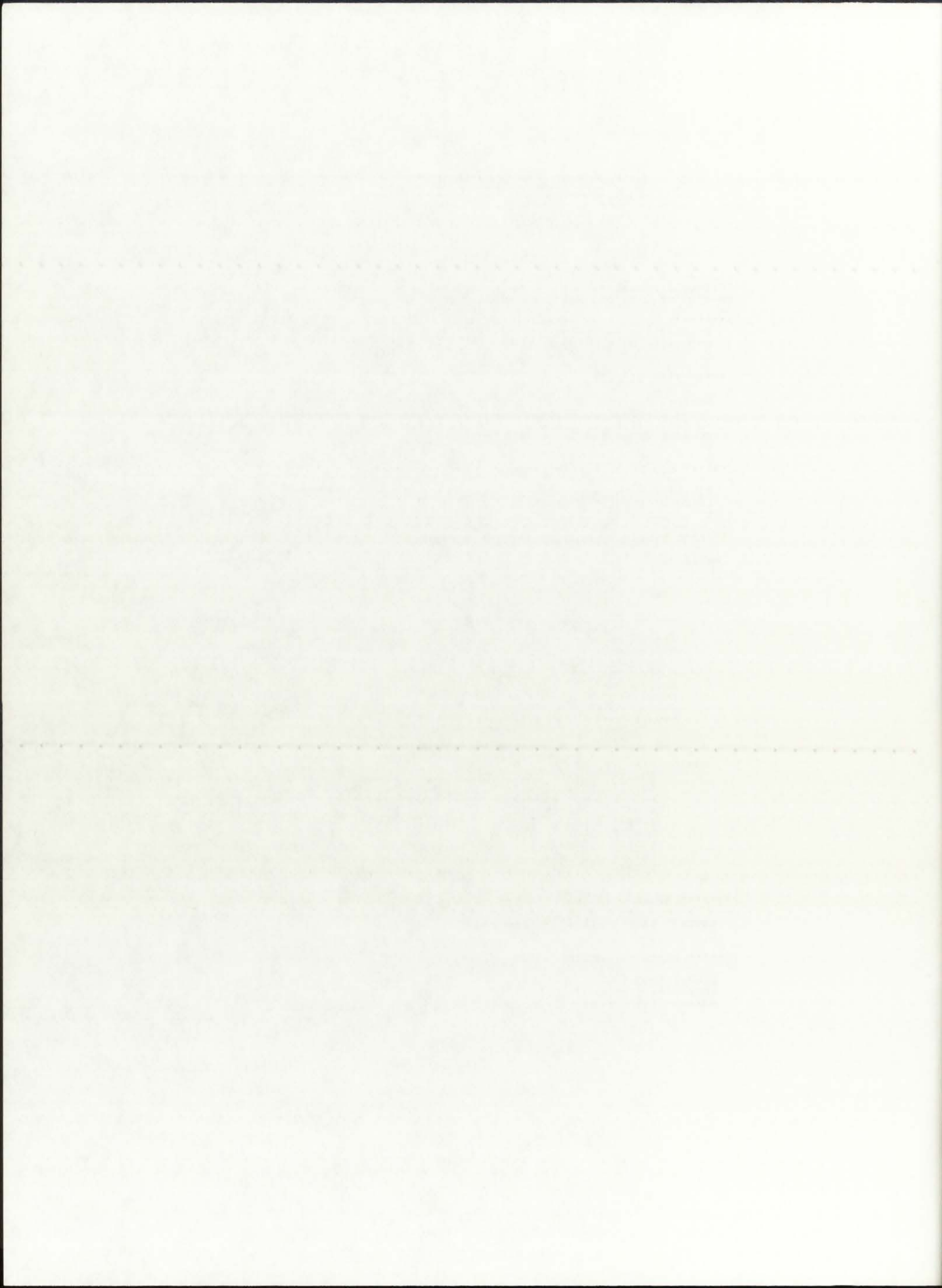


```

2 0 0
unit-cell rocket engine - 5 MWth Configuration - P=500 atm
search for Q(r) and keff, based on T(r) from GNRATR-1D code
/
/***** block i *****/
  igeom=cylinder  ngroup=16  isn=4  niso=118  mt=10
  nzone=10  im=10  it=29  idimen=1
t
/
/***** block ii *****/
/
  xmesh=0.0,6.0,13.375,20.75,24.45,24.94,28.80,34.58,
        58.58,82.58,87.66
  xints=4,3,3,2,2,2,3,4,4,2
  zones=1,2,3,4,5,6,7,8,9,10
t
/
/***** block iii (cross sections) *****/
/
  lib=bxslib  balxs=1  maxord=1  ihm=10  iht=4  ihs=5
  ifido=0  ititl=1  edname=fiss
t
/
/***** block iv (mixing) *****/
/
  matls=mix      "sulfur"      5.1190e-5
                "235-yr"      2.3871e-5
                "u238y"      1.7974e-6;
  uranI  "235-yr"      4.7743e-5
                "u238y"      3.5948e-6;
  uranII "235-yr"      4.7743e-5
                "u238y"      3.5948e-6;
  argon  "sulfur"      1.1900e-4;
  silica "si"          2.666e-2
                "o16"        5.332e-2;
  hydro  "h"           2.3900e-4;
  beryl  "be"          1.236e-1;
  hvywI  "d"           1.894e-2
                "o16"        9.470e-3;
  hvywII "d"           1.894e-2
                "o16"        9.470e-3;
  steel  "fe"          8.486e-2;

  assign=mixture  mix  1.0;
                fuelI uranI 1.0;
                fuelII uranII 1.0;
                buffer argon 1.0;
                siwall silica 1.0;
                propel hydro 1.0;
                bemodr beryl 1.0;
                reflI hvywI 1.0;
                reflII hvywII 1.0;
                pvessl steel 1.0;
t
/
/***** block v (solver) *****/
/
  ievt=1  isct=1 ibr=0  fluxp=1  bhgt=182.73
t
/
/***** block vi (edits) *****/
/
  pted=1  zned=1
  icoll=16;  igrped=3
  edxs=n-fiss  resdnt=1  power=2.736e-2  mevper=176  rzflux=1
/

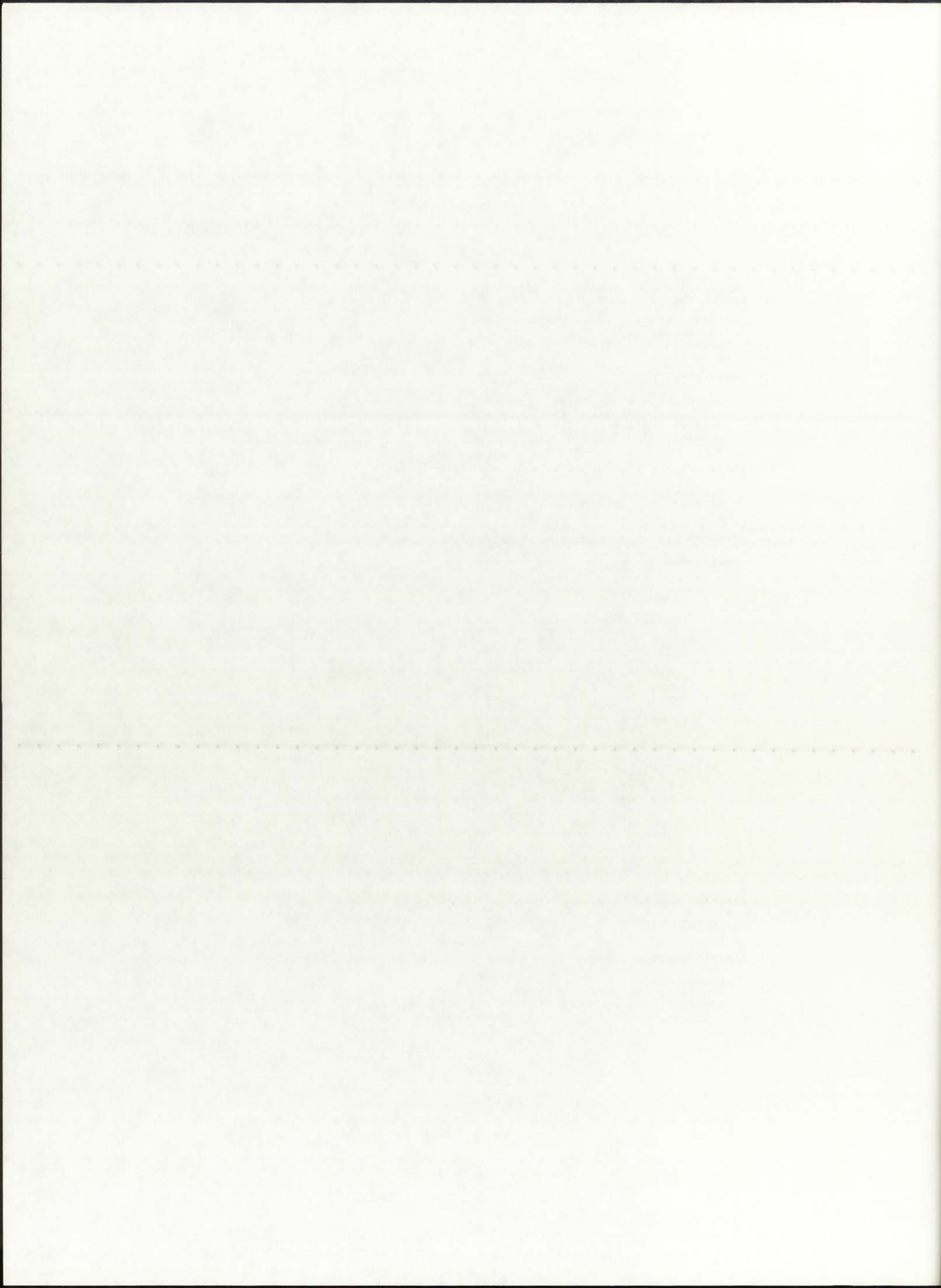
```



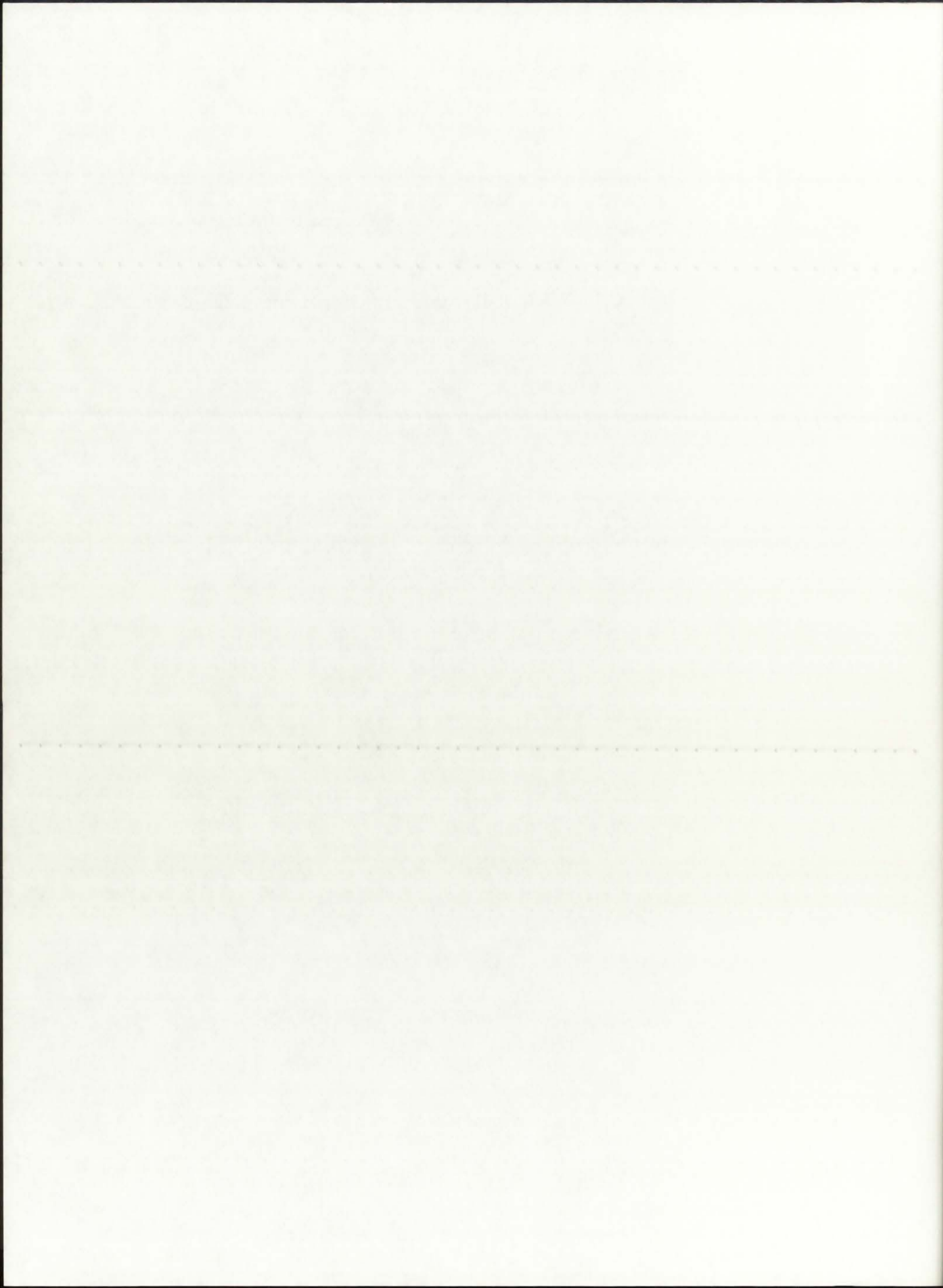
```

2 0 0
unit-cell rocket engine - 5 MWth Configuration - P=1000 atm
search for Q(r) and keff, based on T(r) from GNRATR-1D code
/
/***** block i *****/
  igeom=cylinder ngroup=16 isn=4 niso=118 mt=10
  nzone=10 im=10 it=29 idimen=1
  t
/
/***** block ii *****/
/
  xmesh=0.0,6.0,13.375,20.75,24.45,24.94,28.80,34.58,
        58.58,82.58,87.66
  xints=4,3,3,2,2,2,3,4,4,2
  zones=1,2,3,4,5,6,7,8,9,10
  t
/
/***** block iii (cross sections) *****/
/
  lib=bxslib balxs=1 maxord=1 ihm=10 iht=4 ihs=5
  ifido=0 ititl=1 edname=fiss
  t
/
/***** block iv (mixing) *****/
/
  matls=mix      "sulfur"      1.0240e-4
                "235-yr"      4.0460e-5
                "u238y"       3.0464e-6;
  uranI  "235-yr"      8.0920e-5
                "u238y"       6.0928e-6;
  uranII "235-yr"      8.0920e-5
                "u238y"       6.0928e-6;
  argon  "sulfur"      1.0840e-4;
  silica "si"          2.666e-2
                "o16"         5.332e-2;
  hydro  "h"           4.3013e-4;
  beryl  "be"          1.236e-1;
  hvywI  "d"           1.894e-2
                "o16"         9.470e-3;
  hvywII "d"           1.894e-2
                "o16"         9.470e-3;
  steel  "fe"          8.486e-2;
/
  assign=mixture mix 1.0;
                fuelI uranI 1.0;
                fuelII uranII 1.0;
                buffer argon 1.0;
                siwall silica 1.0;
                propel hydro 1.0;
                bemodr beryl 1.0;
                reflI hvywI 1.0;
                reflII hvywII 1.0;
                pvessl steel 1.0;
  t
/
/***** block v (solver) *****/
/
  ievt=1 isct=1 ibr=0 fluxp=1 bhgt=182.73
  t
/
/***** block vi (edits) *****/
/
  pted=1 zned=1
  icoll=16; igrped=3
  edxs=n-fiss resdnt=1 power=2.736e-2 mevper=176 rzflux=1
/

```



C.2. GNRATR-1D Summary Output Files (Hansen-Roach)

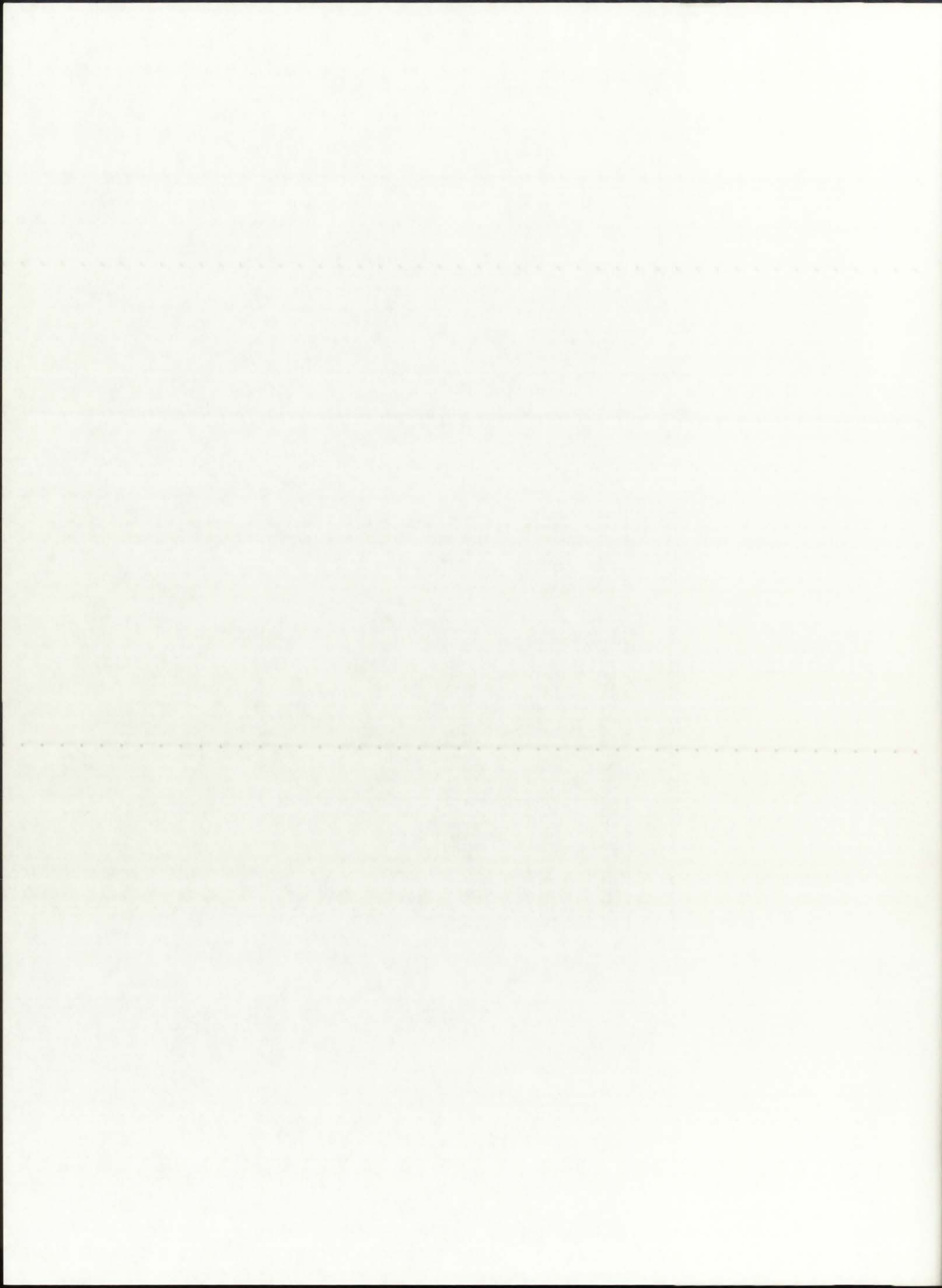


==== SUMMARY OF CONVERGED VALUES . ====

This Case Executed for: REFLBe = 0.00000
 Pressure = 250.0 atm

Modes of Heat Transfer: Radiation in BG, SiW, and P = .on.
 Convection in BG = .on.
 Convection in P = .on.

i	r(i)	T(i)	Qg(i)
-----	-----	-----	-----
37	0.000	26598.0	0.9984E+07
36	0.019	26598.0	0.9840E+07
35	0.039	26572.4	0.1964E+08
34	0.059	26494.4	0.2014E+08
33	0.096	26001.2	0.2077E+08
32	0.133	25102.1	0.2164E+08
31	0.170	23539.6	0.2288E+08
30	0.207	14902.8	0.0000E+00
29	0.225	14902.8	0.0000E+00
28	0.244	14902.8	0.0000E+00
27	0.246	14902.8	0.0000E+00
26	0.249	14902.8	0.0000E+00
25	0.268	14902.8	0.0000E+00
24	0.287	14902.8	0.0000E+00
23	0.307	14895.2	0.0000E+00
22	0.326	14888.5	0.0000E+00
21	0.345	14882.5	0.0000E+00
20	0.405	11709.7	0.0000E+00
19	0.465	9355.3	0.0000E+00
18	0.525	7539.1	0.0000E+00
17	0.585	6095.8	0.0000E+00
16	0.645	4921.6	0.0000E+00
15	0.705	3948.0	0.0000E+00
14	0.765	3128.0	0.0000E+00
13	0.825	2428.3	0.0000E+00
12	0.851	2425.4	0.0000E+00
11	0.876	2424.0	0.0000E+00
10	0.976	1992.5	0.0000E+00
9	1.076	1642.3	0.0000E+00
8	1.176	1352.5	0.0000E+00
7	1.276	1109.0	0.0000E+00
6	1.376	901.4	0.0000E+00
5	1.476	722.5	0.0000E+00
4	1.576	566.6	0.0000E+00
3	1.676	429.6	0.0000E+00
2	1.776	308.3	0.0000E+00
1	1.876	200.0	0.0000E+00



==== ROCKET ENGINE PARAMETERS ====

The H2 dissociation fraction is: 0.9831
The H2 average molecular weight is: 1.0251 g/gmol
The propellant molecular weight is: 6.5098 g/gmol
The cross-sectional flow area is: 0.0721 m²
The propellant mass flow rate is: 0.01 kg/s

The chamber temperature is: 14902.8 K
The calculated exit velocity is: 10155.6 m/s
The calculated thrust is: 0.2 kN
The calculated specific impulse is: 1035.5 s

Faint, illegible text at the top of the page, possibly a header or title area.

Main body of faint, illegible text, appearing to be several lines of a document or report.

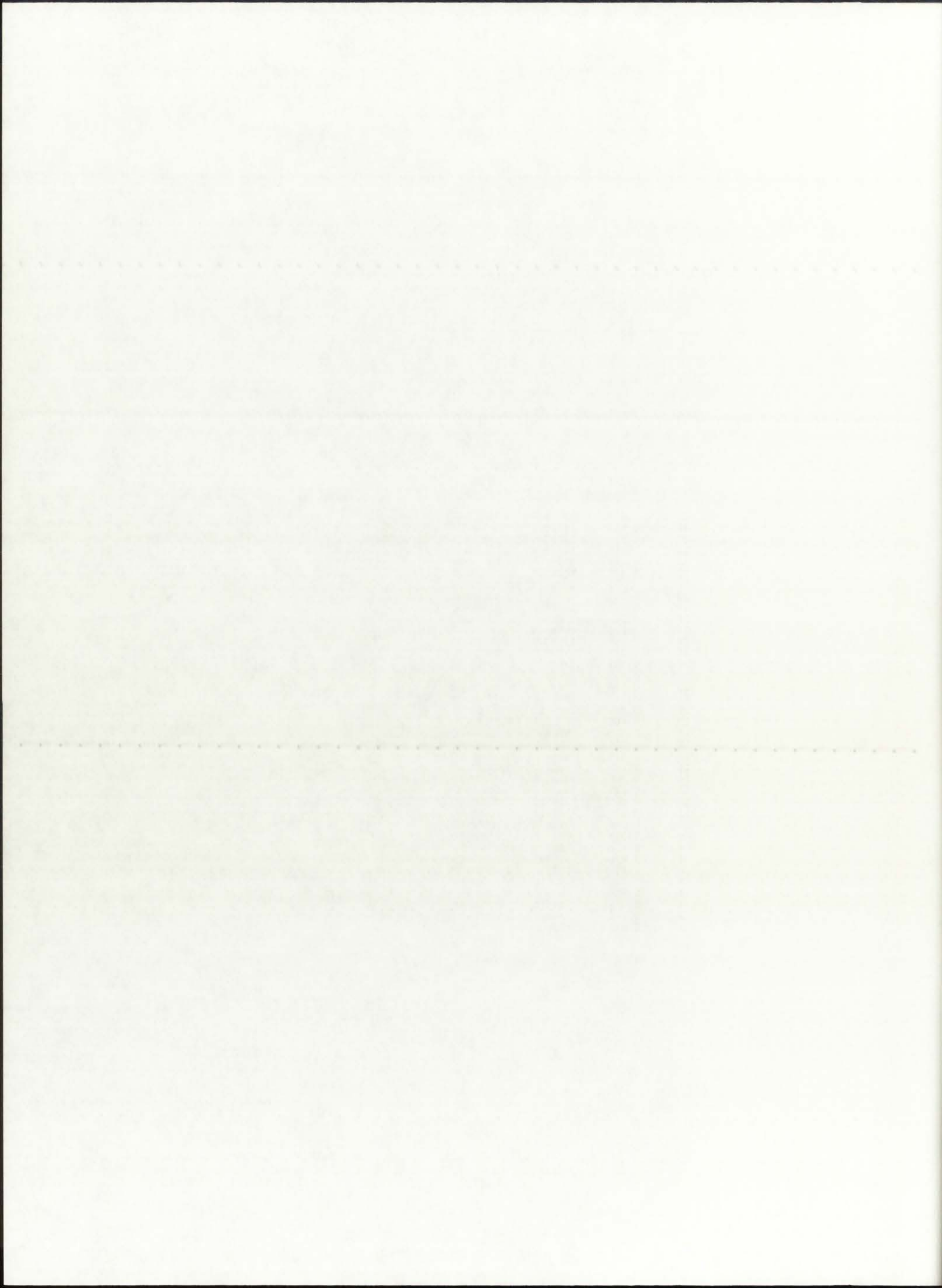
Large section of faint, illegible text at the bottom of the page, possibly a conclusion or footer.

==== SUMMARY OF CONVERGED VALUES ====

This Case Executed for: REFLBe = 0.00000
 Pressure = 500.0 atm

Modes of Heat Transfer: Radiation in BG, SiW, and P = .on.
 Convection in BG = .on.
 Convection in P = .on.

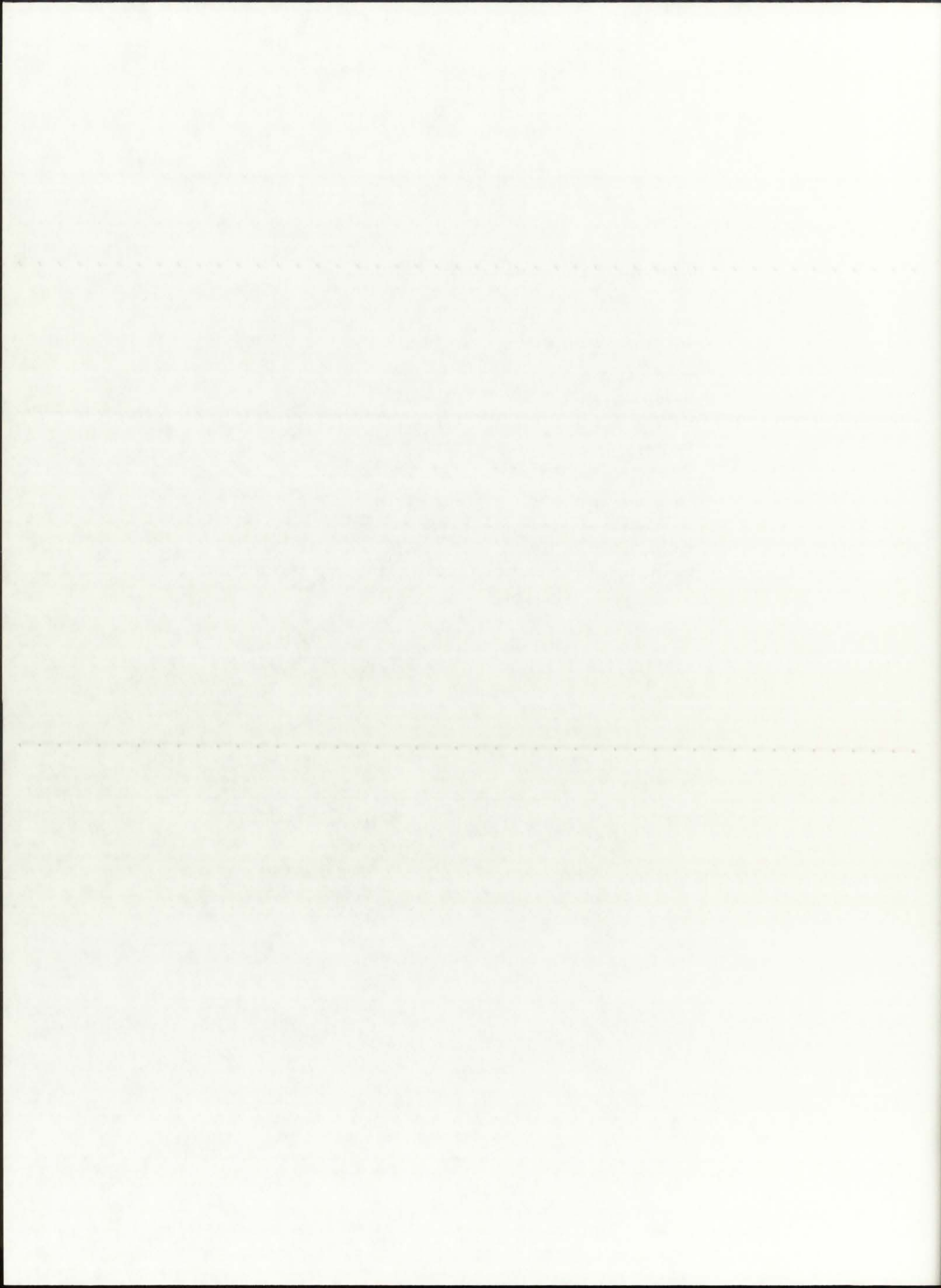
i	r(i)	T(i)	Qg(i)
37	0.000	31726.3	0.9587E+07
36	0.019	31726.3	0.9418E+07
35	0.039	31697.4	0.1883E+08
34	0.059	31609.4	0.1962E+08
33	0.096	31047.3	0.2057E+08
32	0.133	30012.1	0.2193E+08
31	0.170	28196.0	0.2396E+08
30	0.207	17688.7	0.0000E+00
29	0.225	17688.7	0.0000E+00
28	0.244	17688.7	0.0000E+00
27	0.246	17688.7	0.0000E+00
26	0.249	17688.7	0.0000E+00
25	0.268	17688.7	0.0000E+00
24	0.287	17688.7	0.0000E+00
23	0.307	17679.7	0.0000E+00
22	0.326	17671.7	0.0000E+00
21	0.345	17664.6	0.0000E+00
20	0.405	13890.1	0.0000E+00
19	0.465	11089.3	0.0000E+00
18	0.525	8928.7	0.0000E+00
17	0.585	7211.7	0.0000E+00
16	0.645	5814.9	0.0000E+00
15	0.705	4656.7	0.0000E+00
14	0.765	3681.2	0.0000E+00
13	0.825	2848.8	0.0000E+00
12	0.851	2845.3	0.0000E+00
11	0.876	2843.6	0.0000E+00
10	0.976	2330.7	0.0000E+00
9	1.076	1914.4	0.0000E+00
8	1.176	1570.0	0.0000E+00
7	1.276	1280.5	0.0000E+00
6	1.376	1033.8	0.0000E+00
5	1.476	821.0	0.0000E+00
4	1.576	635.8	0.0000E+00
3	1.676	473.0	0.0000E+00
2	1.776	328.7	0.0000E+00
1	1.876	200.0	0.0000E+00



==== ROCKET ENGINE PARAMETERS ====

The H2 dissociation fraction is: 0.9826
The H2 average molecular weight is: 1.0255 g/gmol
The propellant molecular weight is: 6.5103 g/gmol
The cross-sectional flow area is: 0.0721 m2
The propellant mass flow rate is: 0.03 kg/s

The chamber temperature is: 17688.7 K
The calculated exit velocity is: 10982.0 m/s
The calculated thrust is: 0.3 kN
The calculated specific impulse is: 1119.8 s

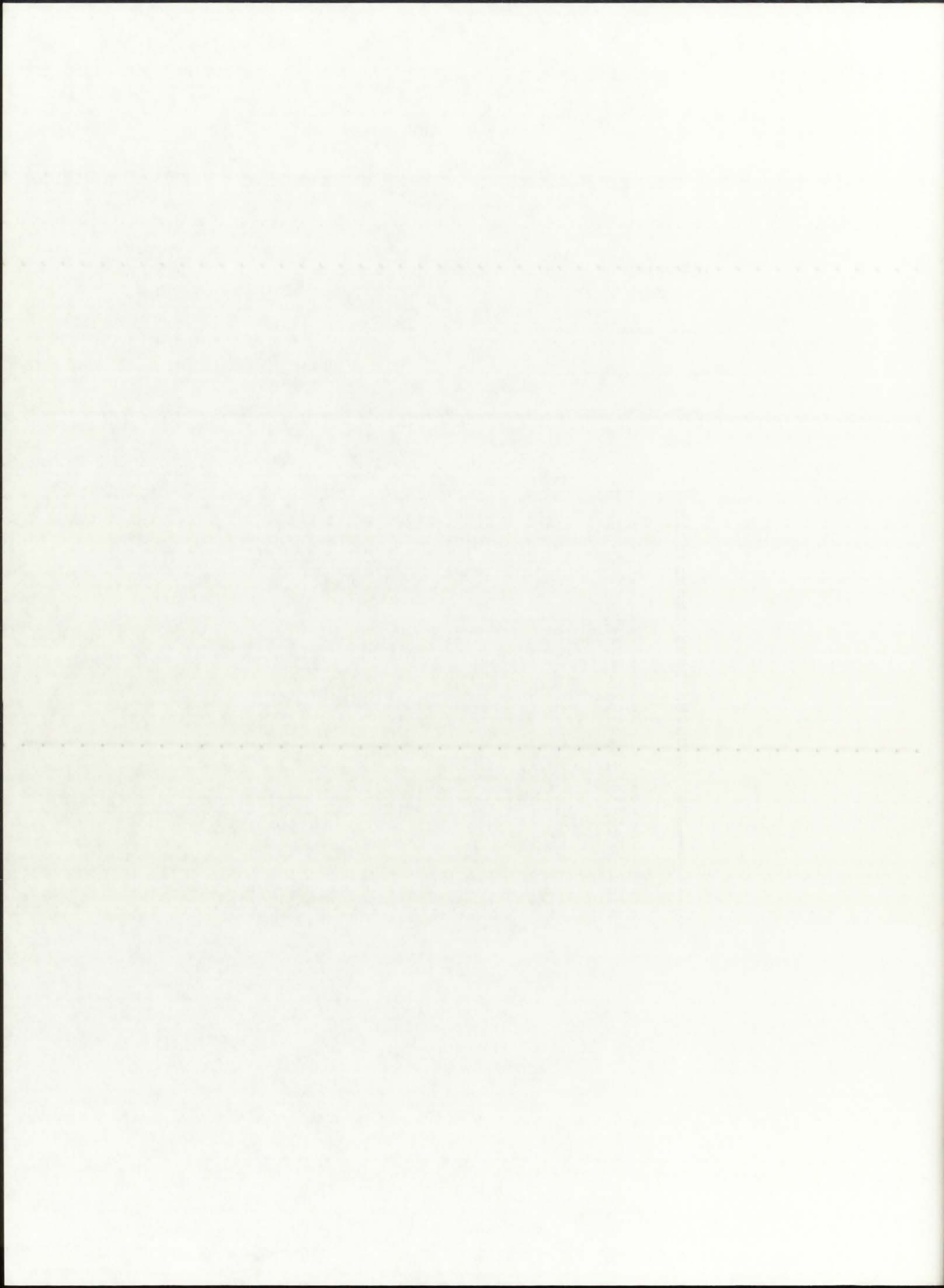


==== SUMMARY OF CONVERGED VALUES ====

This Case Executed for: REFLBe = 0.00000
 Pressure = 1000.0 atm

Modes of Heat Transfer: Radiation in BG, SiW, and P = .on.
 Convection in BG = .on.
 Convection in P = .on.

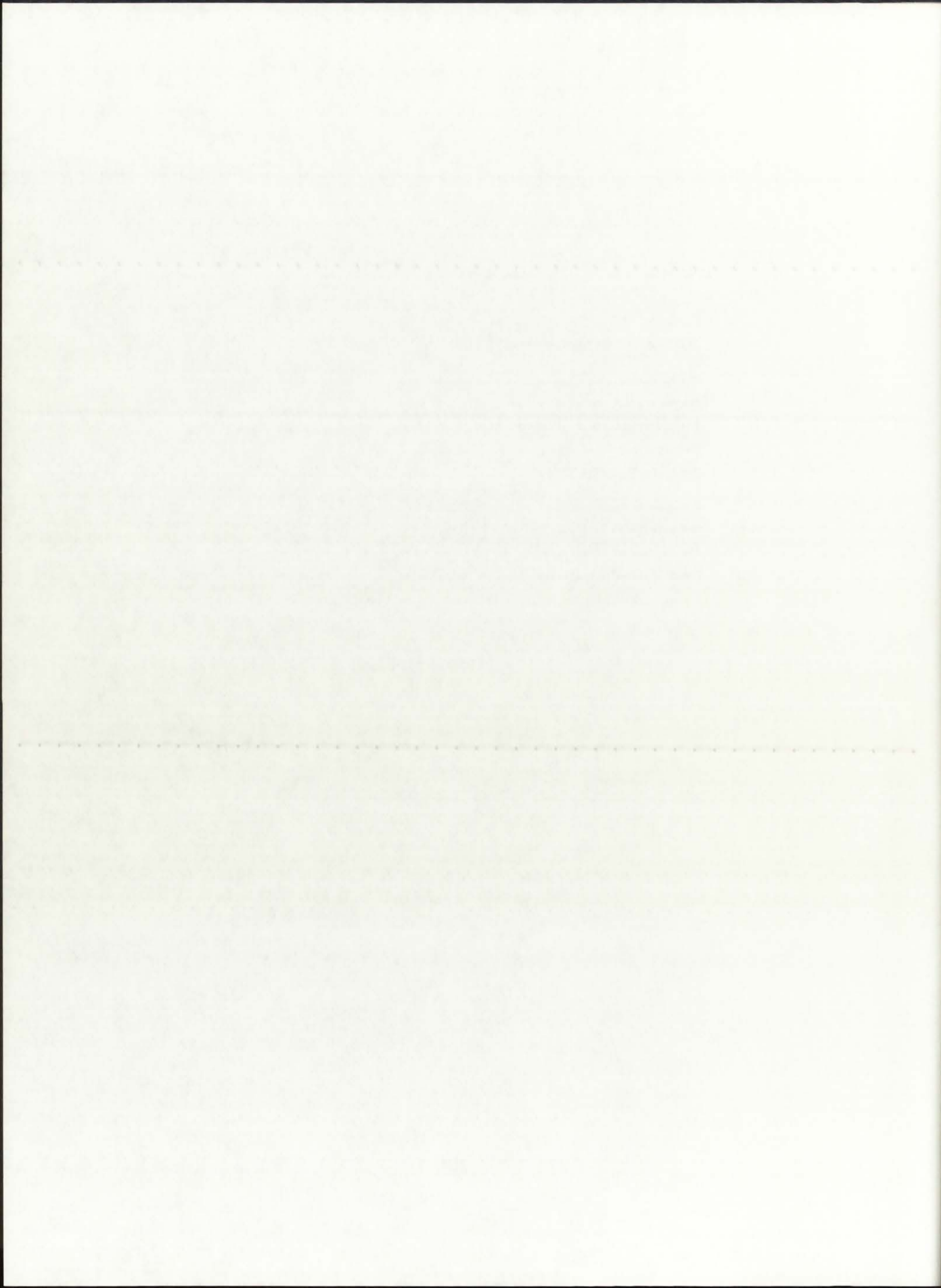
i	r(i)	T(i)	Qg(i)
37	0.000	38097.4	0.8739E+07
36	0.019	38097.4	0.8566E+07
35	0.039	38066.5	0.1726E+08
34	0.059	37972.0	0.1856E+08
33	0.096	37356.4	0.2011E+08
32	0.133	36198.5	0.2243E+08
31	0.170	34126.3	0.2617E+08
30	0.207	21084.5	0.0000E+00
29	0.225	21084.5	0.0000E+00
28	0.244	21084.5	0.0000E+00
27	0.246	21084.5	0.0000E+00
26	0.249	21084.5	0.0000E+00
25	0.268	21084.5	0.0000E+00
24	0.287	21084.5	0.0000E+00
23	0.307	21073.7	0.0000E+00
22	0.326	21064.1	0.0000E+00
21	0.345	21055.7	0.0000E+00
20	0.405	16547.8	0.0000E+00
19	0.465	13202.8	0.0000E+00
18	0.525	10622.4	0.0000E+00
17	0.585	8571.9	0.0000E+00
16	0.645	6903.6	0.0000E+00
15	0.705	5520.4	0.0000E+00
14	0.765	4355.4	0.0000E+00
13	0.825	3361.3	0.0000E+00
12	0.851	3357.2	0.0000E+00
11	0.876	3355.1	0.0000E+00
10	0.976	2742.9	0.0000E+00
9	1.076	2246.1	0.0000E+00
8	1.176	1835.1	0.0000E+00
7	1.276	1489.5	0.0000E+00
6	1.376	1195.1	0.0000E+00
5	1.476	941.2	0.0000E+00
4	1.576	720.1	0.0000E+00
3	1.676	525.8	0.0000E+00
2	1.776	353.6	0.0000E+00
1	1.876	200.0	0.0000E+00



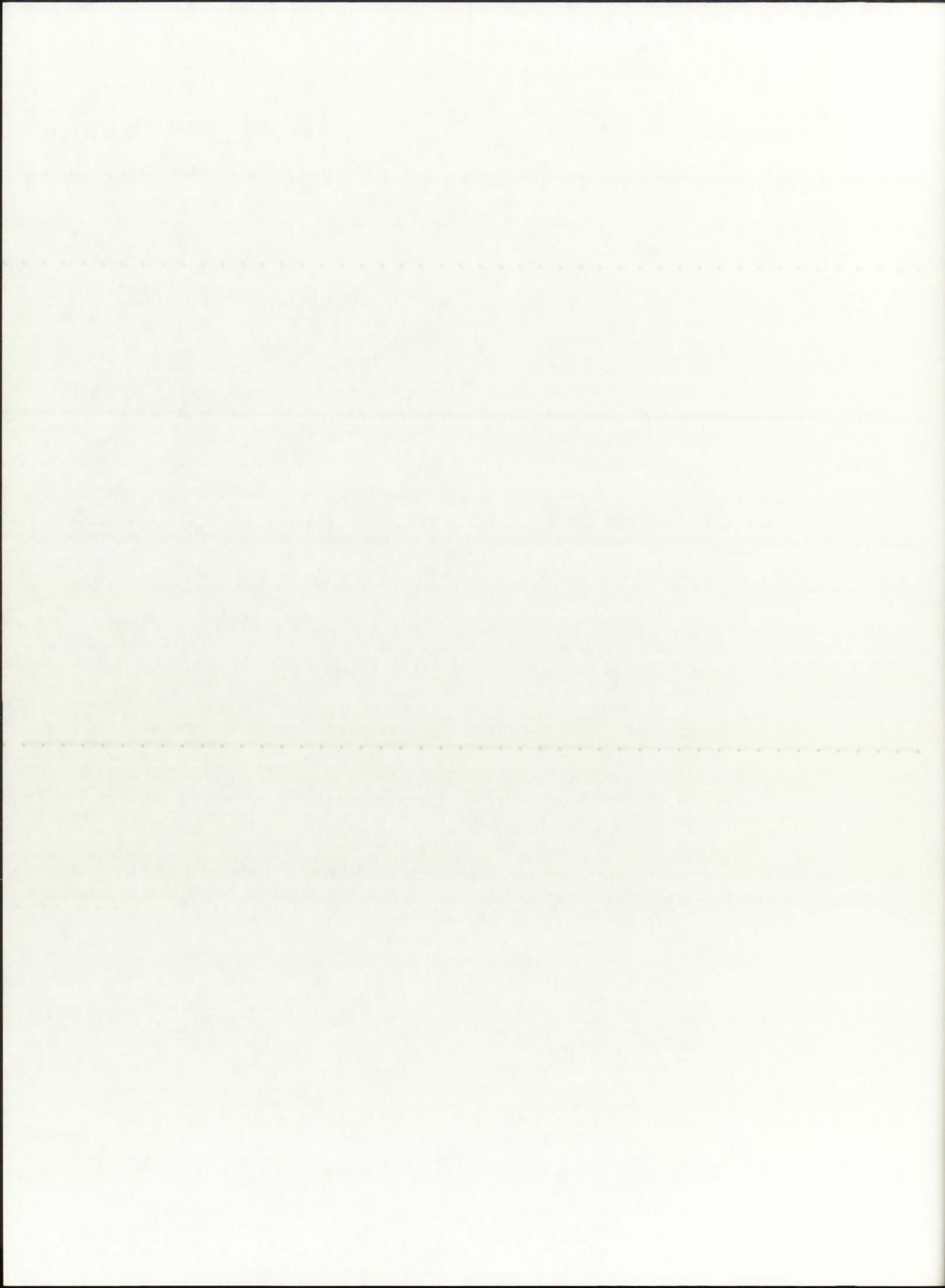
==== ROCKET ENGINE PARAMETERS ====

The H2 dissociation fraction is: 0.9807
The H2 average molecular weight is: 1.0275 g/gmol
The propellant molecular weight is: 6.5121 g/gmol
The cross-sectional flow area is: 0.0721 m2
The propellant mass flow rate is: 0.05 kg/s

The chamber temperature is: 21084.5 K
The calculated exit velocity is: 11884.2 m/s
The calculated thrust is: 0.6 kN
The calculated specific impulse is: 1211.8 s



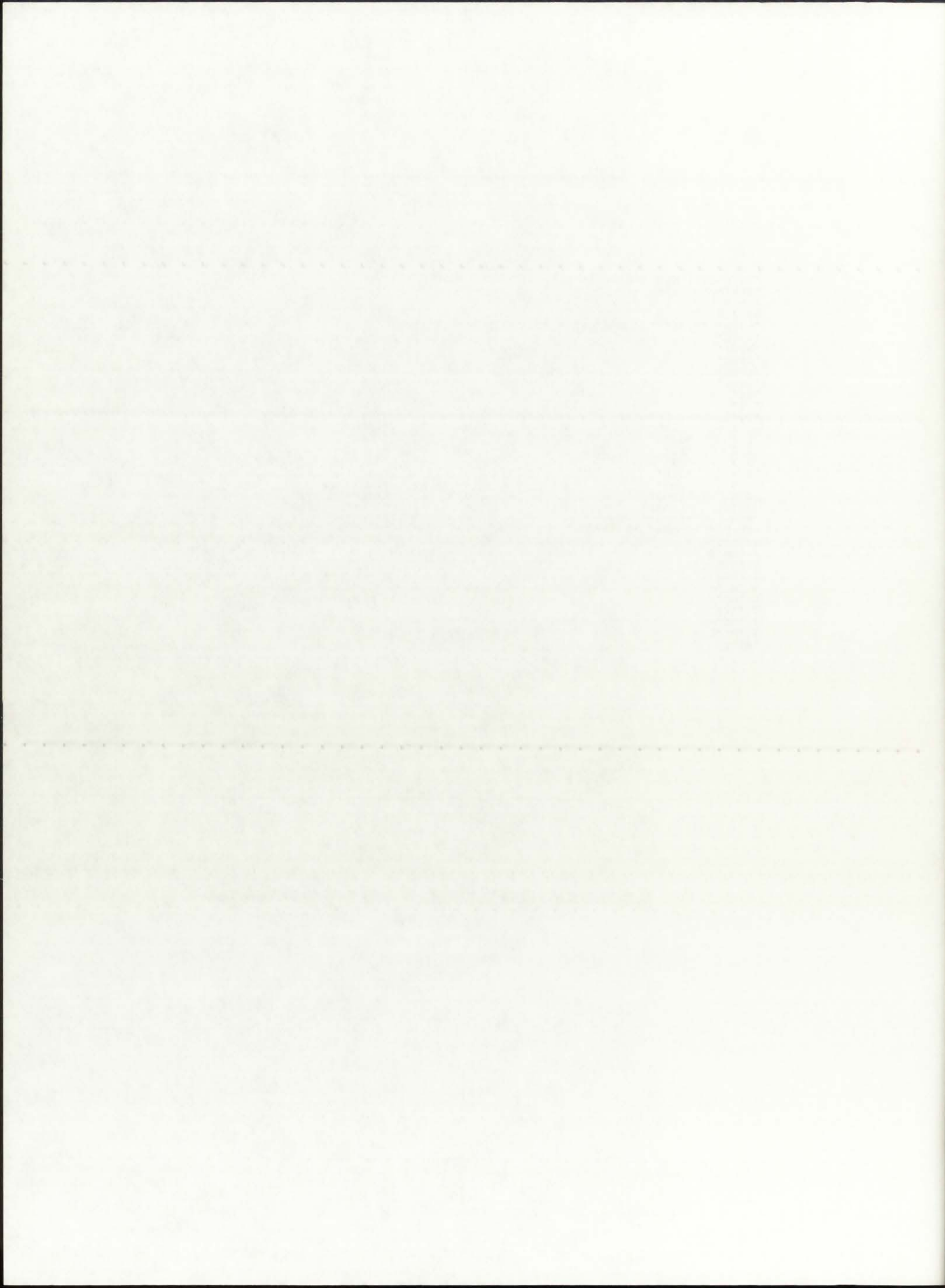
C.3. TRANSX Input Files (ENDF/B-V)




```

*Unit-cell NLB Engine 5MWth P=250 atm input file
*mtx7ey* *isotxs*/
1 6 0 1 1 1 0 2 0 0/
69 2 93 20 8 8 9 9 9/
*enru* *hydr* *deut* *oxgn* *bery* *ar* *si* *fe*
*enru* 25000. 1./
*hydr* 14000. 1./
*deut* 300. 1./
*oxgn* 300. 1./
*bery* 300. 1./
*ar* 14000. 1./
*si* 300. 1./
*fe* 300. 1./
1 1 *u235* 0.96 1.e+10 42 *free*/
1 1 *u238* 0.04 1.e+10 42 *free*/
2 2 *h1* 1.0 1.e+10 42 *free*/
3 3 *h2* 1.0 1.e+10 42 *d2o*/
4 4 *o16* 1.0 1.e+10 42 *free*/
5 5 *be9* 1.0 1.e+10 42 *be* *be$/
6 6 *arnat* 1.0 1.e+10 42 *free*/
7 7 *sinat* 1.0 1.e+10 42 *free*/
8 8 *fenat* 1.0 1.e+10 42 *free*/
*strpl* *sngam* *sfis* *chiso* *snalf* *snp* *sn2n* *snd* *snt*/
1 *trd*/
2 *ng*/
3 *nftot*/
4 *chi*/
5 *na*/
6 *np*/
7 *n2n*/
8 *nd*/
9 *nt*/
*stop*

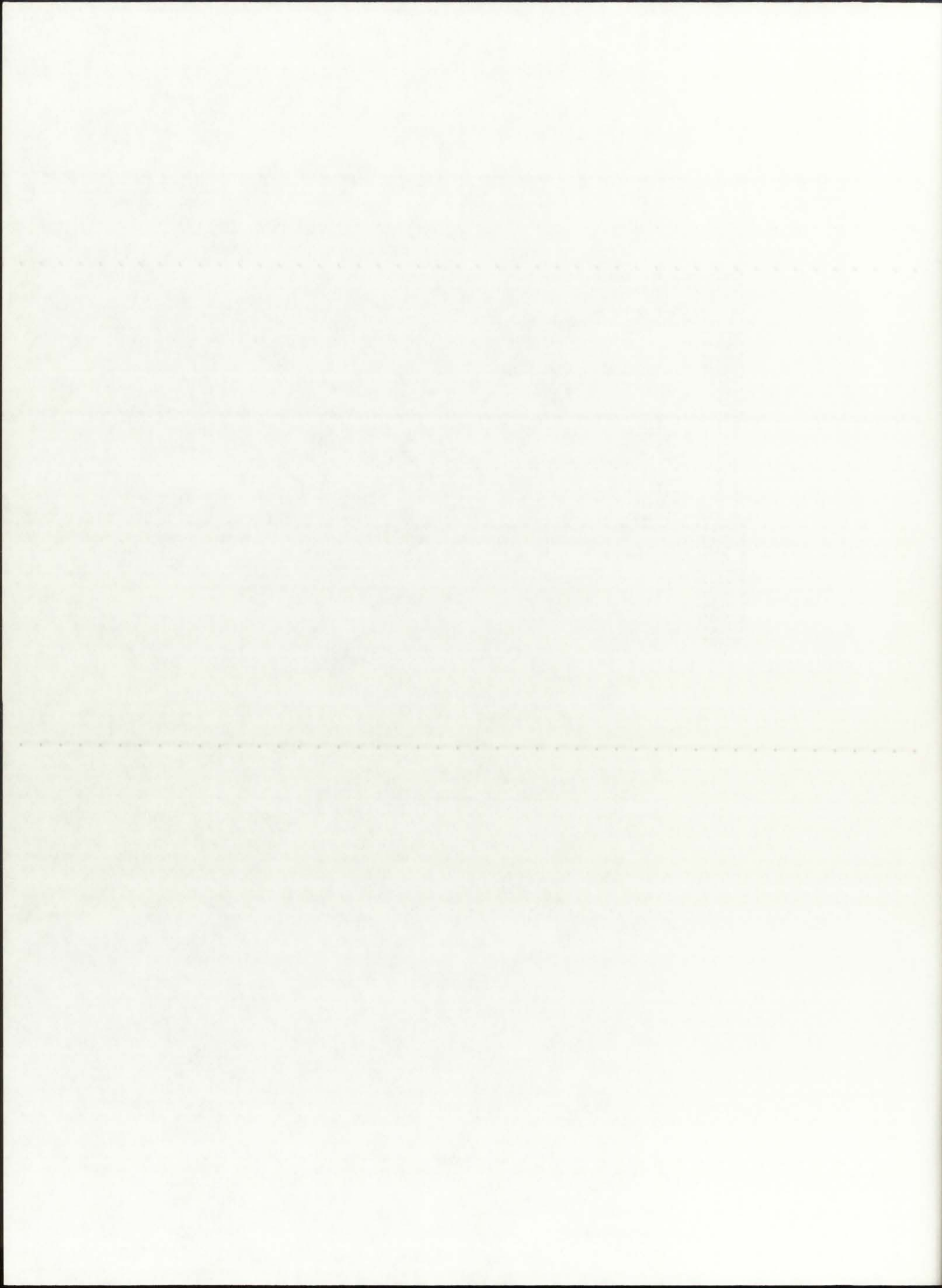
```



```

*Unit-cell NLB Engine 5MWth P=500 atm input file
*mtx7ey* *isotxs*/
1 6 0 1 1 1 0 2 0 0/
69 2 93 20 8 8 9 9 9/
*enru* *hydr* *deut* *oxgn* *bery* *ar* *si* *fe*
*enru*          30000.          1./
*hydr*          17000.          1./
*deut*           300.           1./
*oxgn*           300.           1./
*bery*           300.           1./
*ar*            17000.          1./
*si*             300.           1./
*fe*             300.           1./
1 1      *u235*          0.96      1.e+10 42  *free*/
1 1      *u238*          0.04      1.e+10 42  *free*/
2 2      *h1*            1.0       1.e+10 42  *free*/
3 3      *h2*            1.0       1.e+10 42  *d2o*/
4 4      *o16*           1.0       1.e+10 42  *free*/
5 5      *be9*           1.0       1.e+10 42  *be* *be$/
6 6      *arnat*         1.0       1.e+10 42  *free*/
7 7      *sinat*         1.0       1.e+10 42  *free*/
8 8      *fenat*         1.0       1.e+10 42  *free*/
*strpl* *sngam* *sfis* *chiso* *snalf* *snp* *sn2n* *snd* *snt*/
1 *trd*/
2 *ng*/
3 *nftot*/
4 *chi*/
5 *na*/
6 *np*/
7 *n2n*/
8 *nd*/
9 *nt*/
*stop*

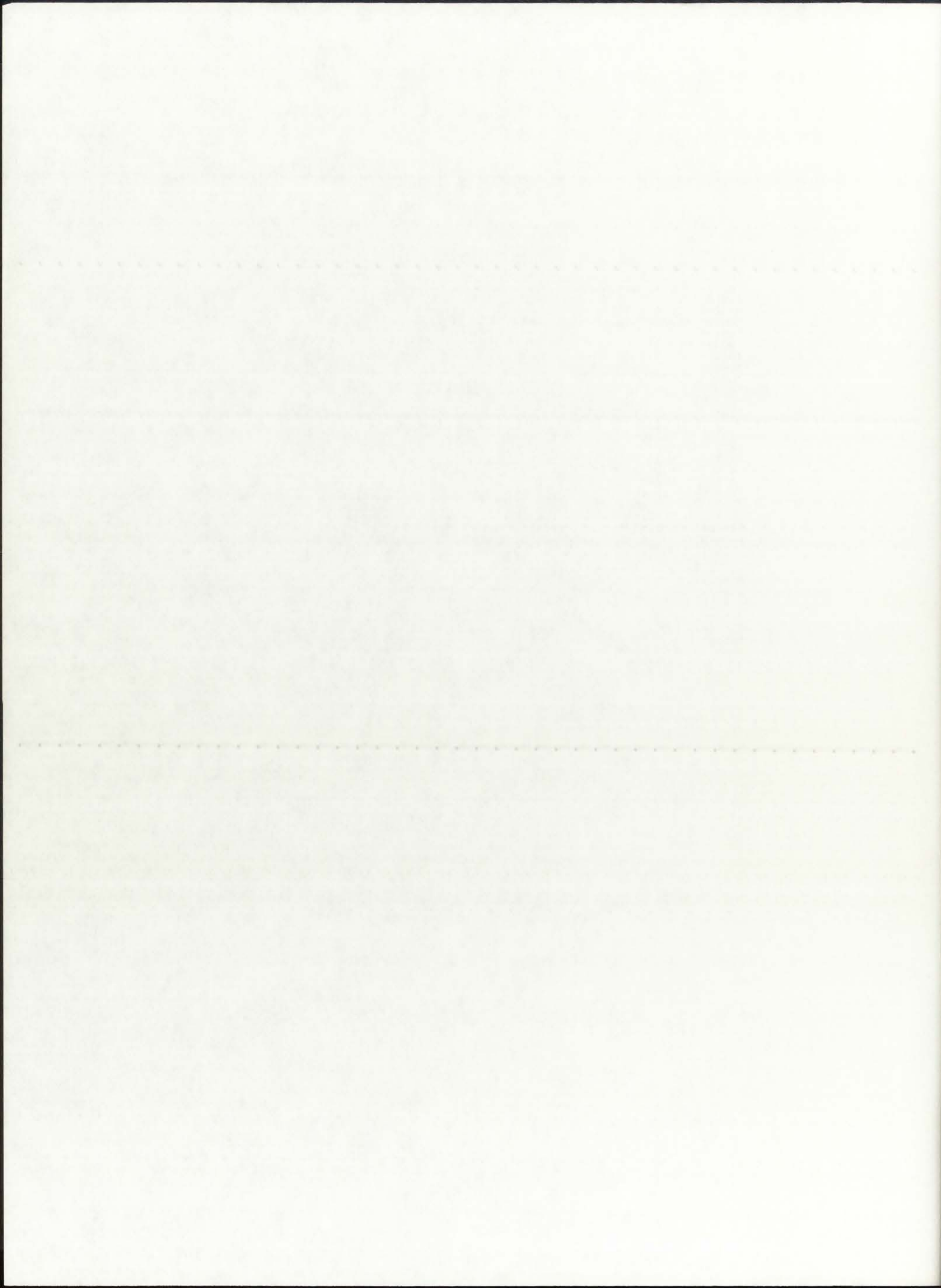
```



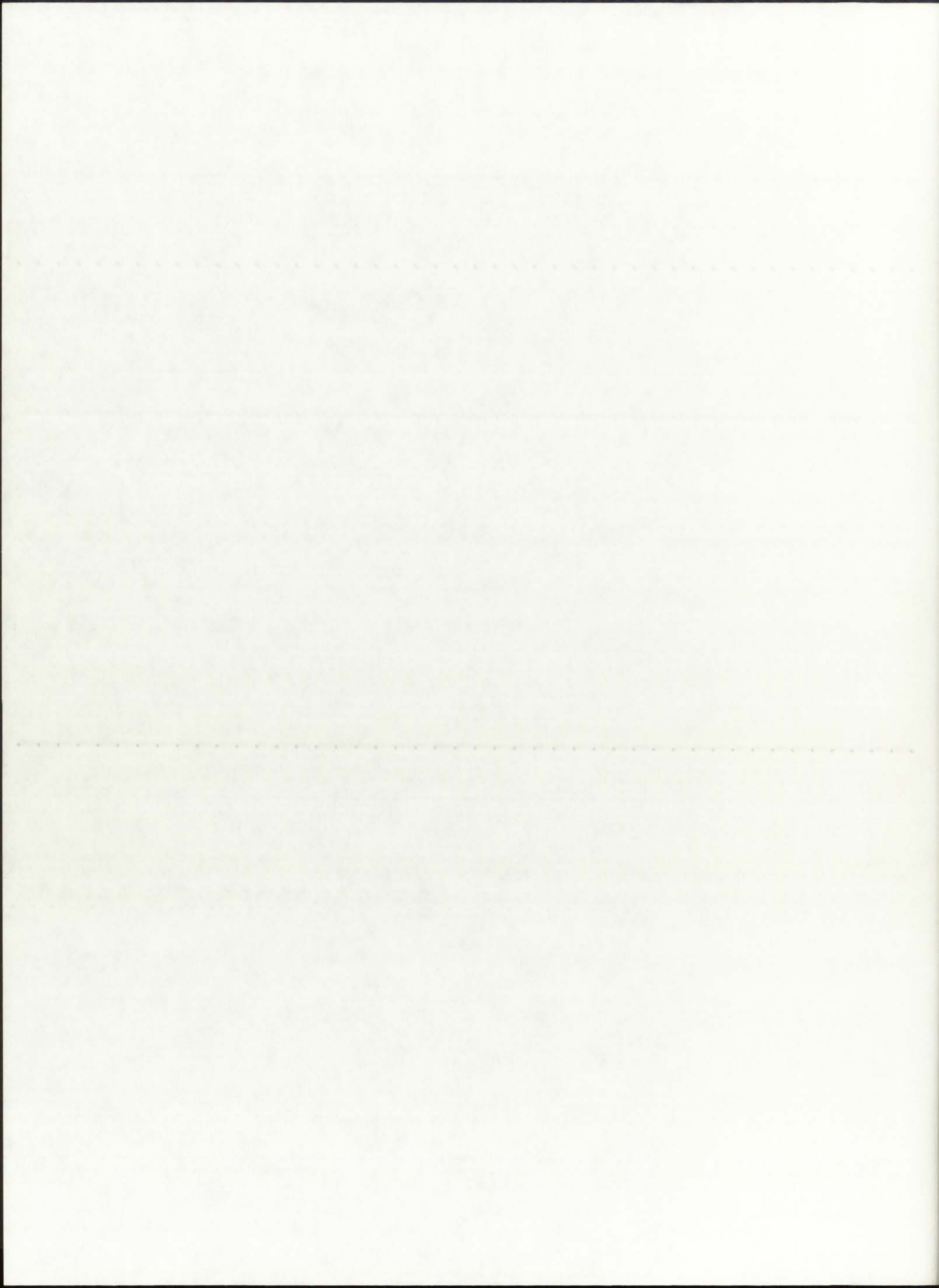
```

*Unit-cell NLB Engine 5MWth P=1000 atm input file
*mtx7ey* *isotxs*/
1 6 0 1 1 1 0 2 0 0/
69 2 93 20 8 8 9 9 9/
*enru* *hydr* *deut* *oxgn* *bery* *ar* *si* *fe*
*enru* 36000. 1./
*hydr* 21000. 1./
*deut* 300. 1./
*oxgn* 300. 1./
*bery* 300. 1./
*ar* 21000. 1./
*si* 300. 1./
*fe* 300. 1./
1 1 *u235* 0.96 1.e+10 42 *free*/
1 1 *u238* 0.04 1.e+10 42 *free*/
2 2 *h1* 1.0 1.e+10 42 *free*/
3 3 *h2* 1.0 1.e+10 42 *d2o*/
4 4 *ol6* 1.0 1.e+10 42 *free*/
5 5 *be9* 1.0 1.e+10 42 *be* *be$*/
6 6 *arnat* 1.0 1.e+10 42 *free*/
7 7 *sinat* 1.0 1.e+10 42 *free*/
8 8 *fenat* 1.0 1.e+10 42 *free*/
*strpl* *sngam* *sfis* *chiso* *snalf* *snp* *sn2n* *snd* *snt*/
1 *trd*/
2 *ng*/
3 *nftot*/
4 *chi*/
5 *na*/
6 *np*/
7 *n2n*/
8 *nd*/
9 *nt*/
*stop*

```



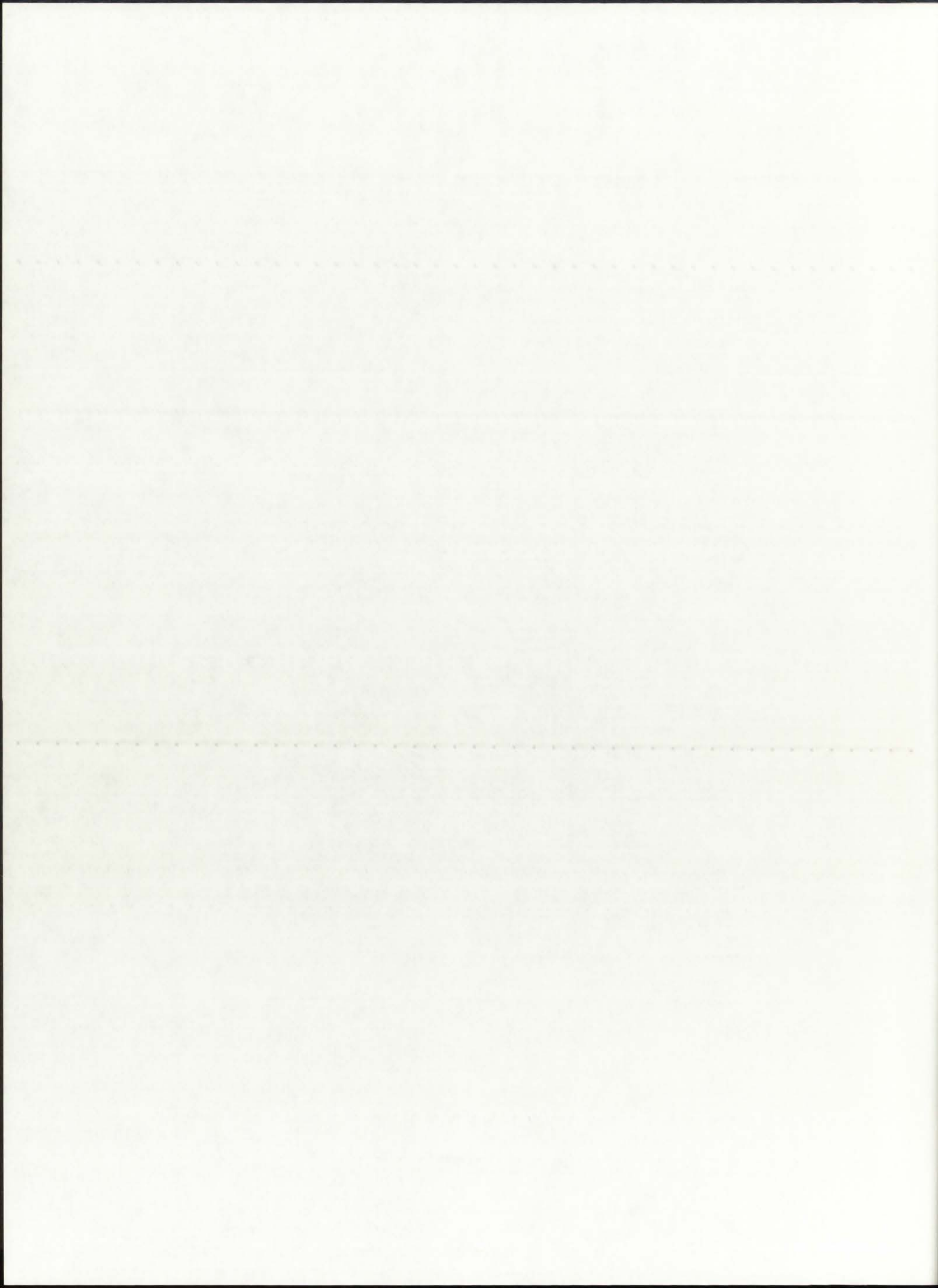
C.4. ONEDANT Input Files (ENDF/B-V)




```

2 0 0
unit-cell NLB engine - 5MWth, P=250 atm, ENDF-VI library
search for Q(r) and keff, based on T(r) from GNRATR-1D code
/
/***** block i *****/
/
  igeom=cylinder ngroup=69 isn=8 niso=8 mt=10
  nzone=10 im=10 it=29
  maxlcm=500000
  maxscm=100000
  t
/
/***** block ii *****/
/
  xmesh=0.0,6.0,13.375,20.75,24.45,24.94,28.80,34.58,
        58.58,82.58,87.66
  xints=4 3 3 2 2 2 3 4 4 2
  zones=1 2 3 4 5 6 7 8 9 10
  t
/
/***** block iii (cross sections) *****/
/
  lib=isotxs
  t
/
/***** block iv (mixing) *****/
/
  matls= mixtr ar      2.3650e-5
          enru      1.5292e-5;
          fuel1 enru  3.0583e-5;
          fuel2 enru  3.0583e-5;
          buffr ar    6.9260e-5;
          sio2  si    2.6660e-2
          oxgn      5.3320e-2;
          prop  hydr  1.3740e-4;
          bemod bery  1.2360e-1;
          d2o1 deut  1.8940e-2
          oxgn      9.4700e-3;
          d2o2 deut  1.8940e-2
          oxgn      9.4700e-3;
          steel fe   8.4860e-2;
/
  assign= 1 mixtr 1.0;
          2 fuel1 1.0;
          3 fuel2 1.0;
          4 buffr 1.0;
          5 sio2  1.0;
          6 prop  1.0;
          7 bemod 1.0;
          8 d2o1  1.0;
          9 d2o2  1.0;
          10 steel 1.0;
  t
/
/***** block v (solver) *****/
/
  ievt=1 isct=1 ibr=0 fluxp=1 bhgt=182.73
  oitm=30 iitm=100
  t
/
/***** block vi (edits) *****/
/
  pted=1 zned=1 icoll=69; igrped=3
  edxs=n-fiss
  resdnt=1 mevper=176.0 power=0.02736 rzflux=1
/

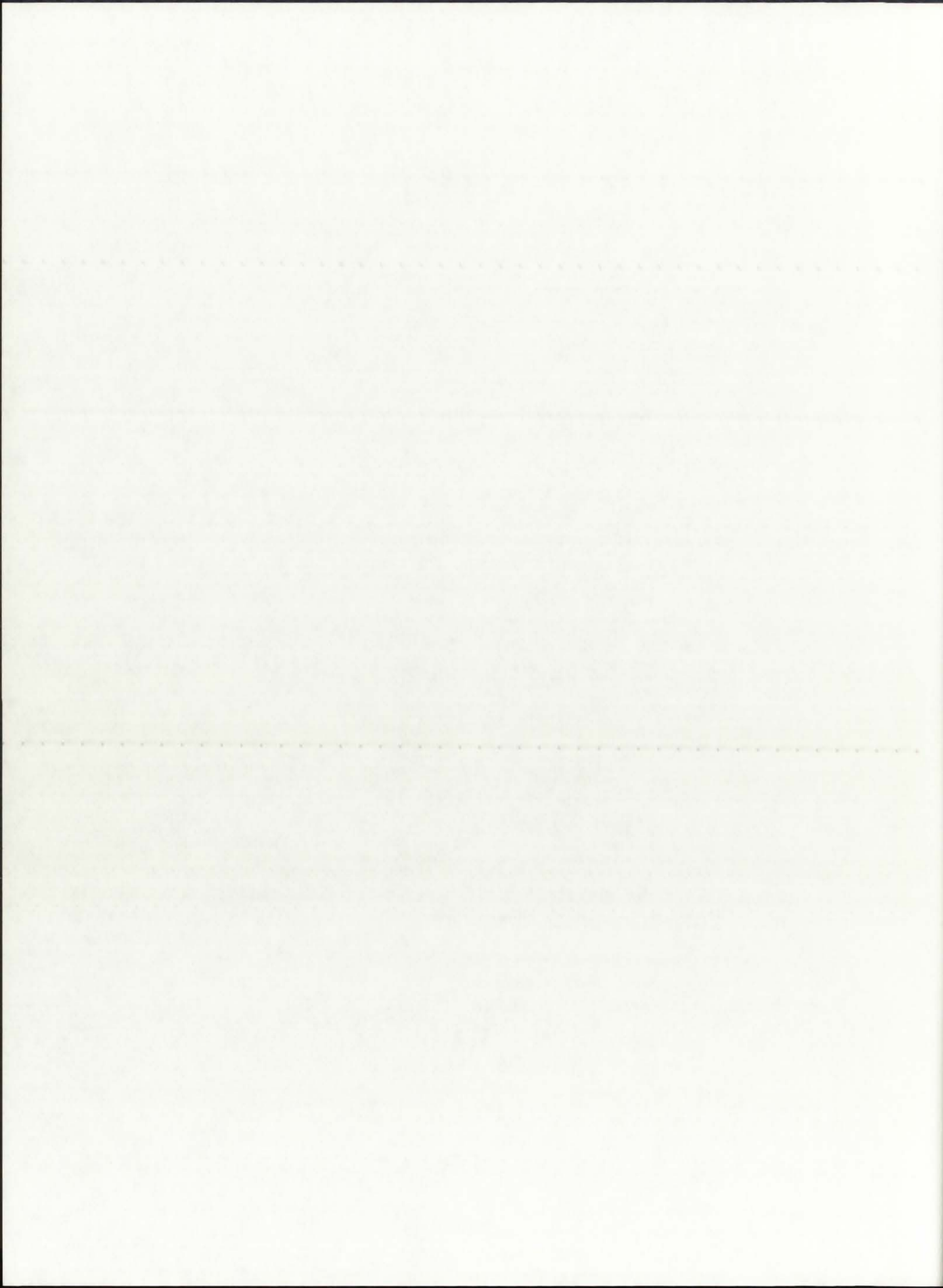
```



```

2 0 0
unit-cell NLB engine - 5MWth, P=500 atm, ENDF-VI library
search for Q(r) and keff, based on T(r) from GNRATR-1D code
/
/***** block i *****/
/
  igeom=cylinder ngroup=69 isn=8 niso=8 mt=10
  nzone=10 im=10 it=29
  maxlcm=500000
  maxscm=100000
  t
/
/***** block ii *****/
/
  xmesh=0.0,6.0,13.375,20.75,24.45,24.94,28.80,34.58,
        58.58,82.58,87.66
  xints=4 3 3 2 2 2 3 4 4 2
  zones=1 2 3 4 5 6 7 8 9 10
  t
/
/***** block iii (cross sections) *****/
/
  lib=isotxs
  t
/
/***** block iv (mixing) *****/
/
  matls= mixtr ar      5.1190e-5
          enru      2.3871e-5;
          fuel1 enru  4.7743e-5;
          fuel2 enru  4.7743e-5;
          buffr ar    1.1900e-4;
          sio2  si    2.6660e-2
          oxgn   5.3320e-2;
          prop  hydr  2.3900e-4;
          bemod bery  1.2360e-1;
          d2o1  deut  1.8940e-2
          oxgn   9.4700e-3;
          d2o2  deut  1.8940e-2
          oxgn   9.4700e-3;
          steel fe    8.4860e-2;
/
  assign= 1 mixtr 1.0;
          2 fuel1 1.0;
          3 fuel2 1.0;
          4 buffr 1.0;
          5 sio2  1.0;
          6 prop  1.0;
          7 bemod 1.0;
          8 d2o1  1.0;
          9 d2o2  1.0;
          10 steel 1.0;
  t
/
/***** block v (solver) *****/
/
  ievt=1 isct=1 ibr=0 fluxp=1 bhgt=182.73
  oitm=30 iitm=100
  t
/
/***** block vi (edits) *****/
/
  pted=1 zned=1 icoll=69; igrped=3
  edxs=n-fiss
  resdnt=1 mevper=176.0 power=0.02736 rzflux=1
/

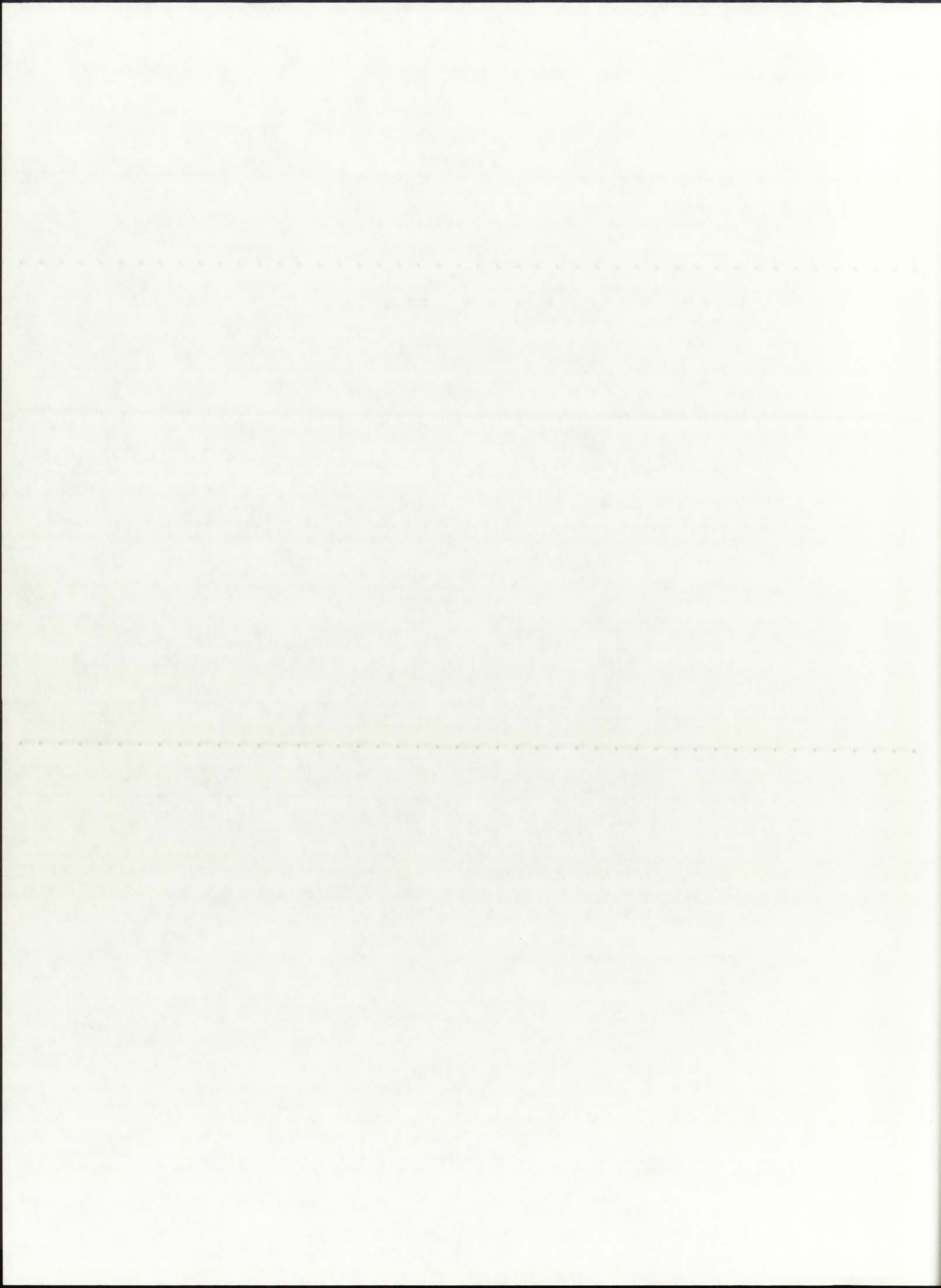
```



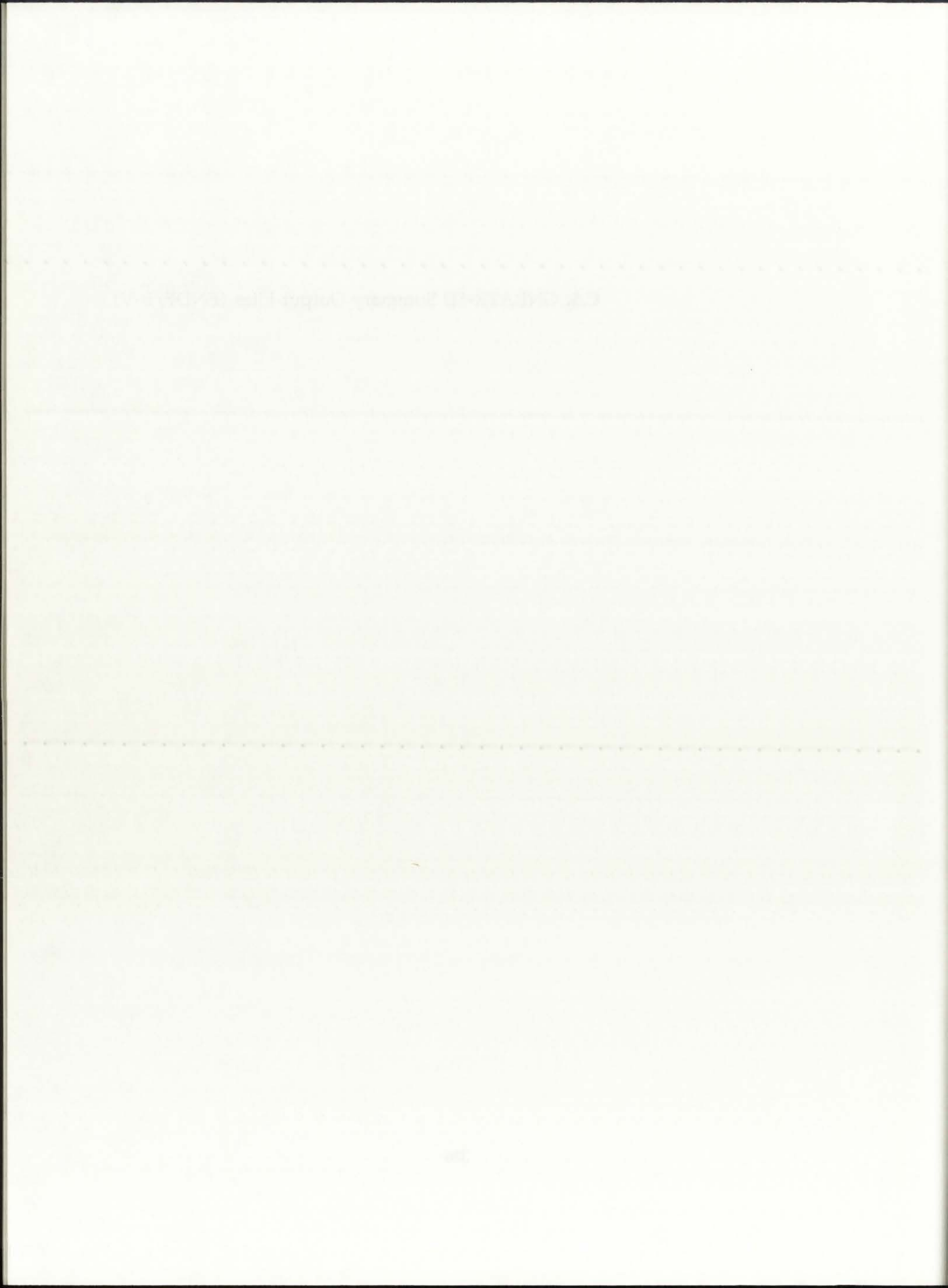
```

2 0 0
unit-cell NLB engine - 5MWth, P=1000 atm, ENDF-VI library
search for Q(r) and keff, based on T(r) from GNRATR-1D code
/
/***** block i *****/
/
  igeom=cylinder ngroup=69 isn=8 niso=8 mt=10
  nzone=10 im=10 it=29
  maxlcm=500000
  maxscm=100000
  t
/
/***** block ii *****/
/
  xmesh=0.0,6.0,13.375,20.75,24.45,24.94,28.80,34.58,
        58.58,82.58,87.66
  xints=4 3 3 2 2 2 3 4 4 2
  zones=1 2 3 4 5 6 7 8 9 10
  t
/
/***** block iii (cross sections) *****/
/
  lib=isotxs
  t
/
/***** block iv (mixing) *****/
/
  matls= mixtr ar 1.0240e-4
          enru 4.0460e-5;
          fuell enru 8.0920e-5;
          fuel2 enru 8.0920e-5;
          buffr ar 1.0840e-4;
          sio2 si 2.6660e-2
          oxgn 5.3320e-2;
          prop hydr 4.3013e-4;
          bemod bery 1.2360e-1;
          d2o1 deut 1.8940e-2
          oxgn 9.4700e-3;
          d2o2 deut 1.8940e-2
          oxgn 9.4700e-3;
          steel fe 8.4860e-2;
/
  assign= 1 mixtr 1.0;
          2 fuell 1.0;
          3 fuel2 1.0;
          4 buffr 1.0;
          5 sio2 1.0;
          6 prop 1.0;
          7 bemod 1.0;
          8 d2o1 1.0;
          9 d2o2 1.0;
          10 steel 1.0;
  t
/
/***** block v (solver) *****/
/
  ievt=1 isct=1 ibr=0 fluxp=1 bhgt=182.73
  oitm=30 iitm=100
  t
/
/***** block vi (edits) *****/
/
  pted=1 zned=1 icoll=69; igrped=3
  edxs=n-fiss
  resdnt=1 mevper=176.0 power=0.02736 rzflux=1
/

```



C.5. GNRATR-1D Summary Output Files (ENDF/B-V)

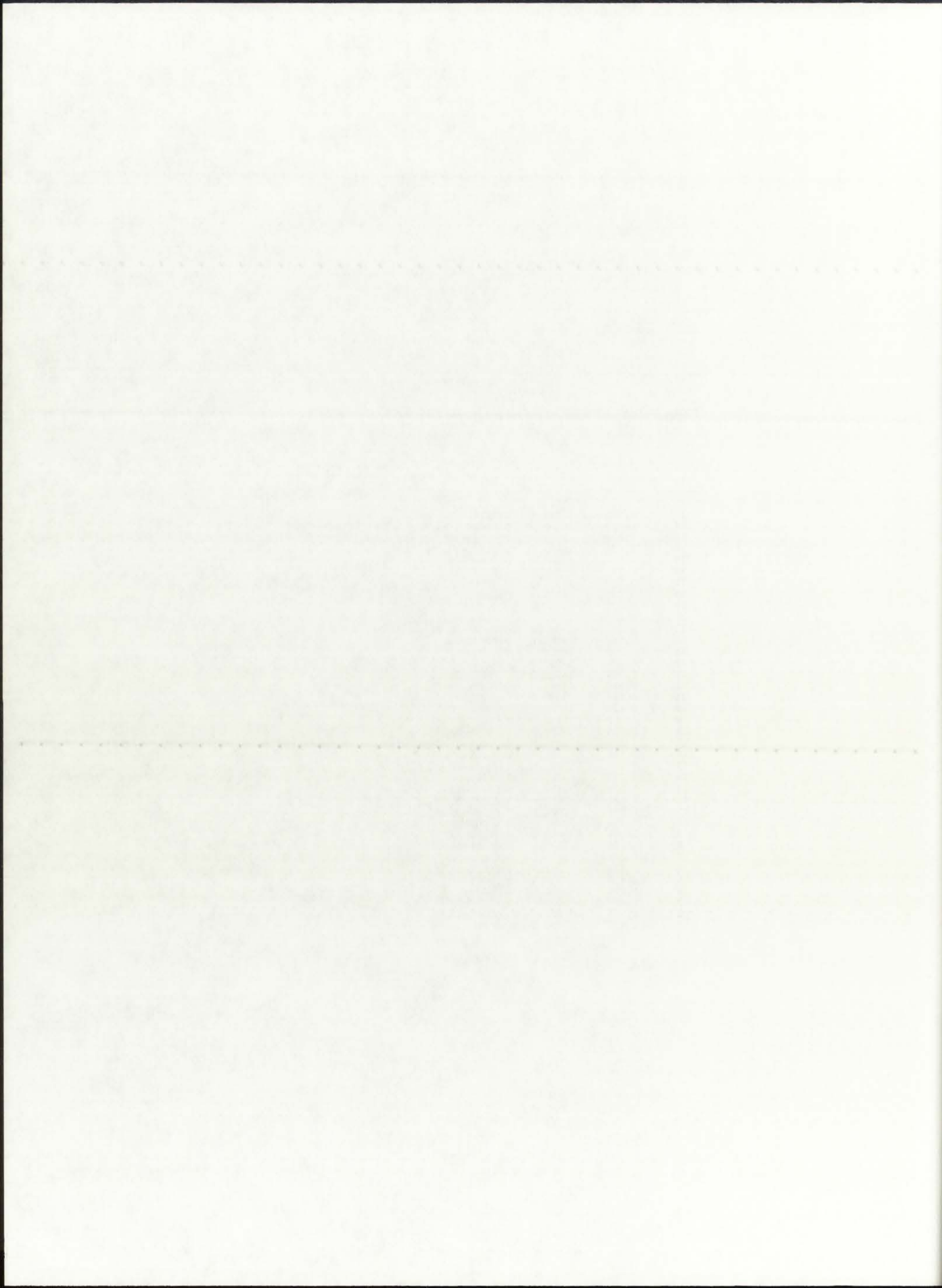


==== SUMMARY OF CONVERGED VALUES ====

This Case Executed for: REFLBe = 0.00000
 Pressure = 250.0 atm

Modes of Heat Transfer: Radiation in BG, SiW, and P = .on.
 Convection in BG = .on.
 Convection in P = .on.

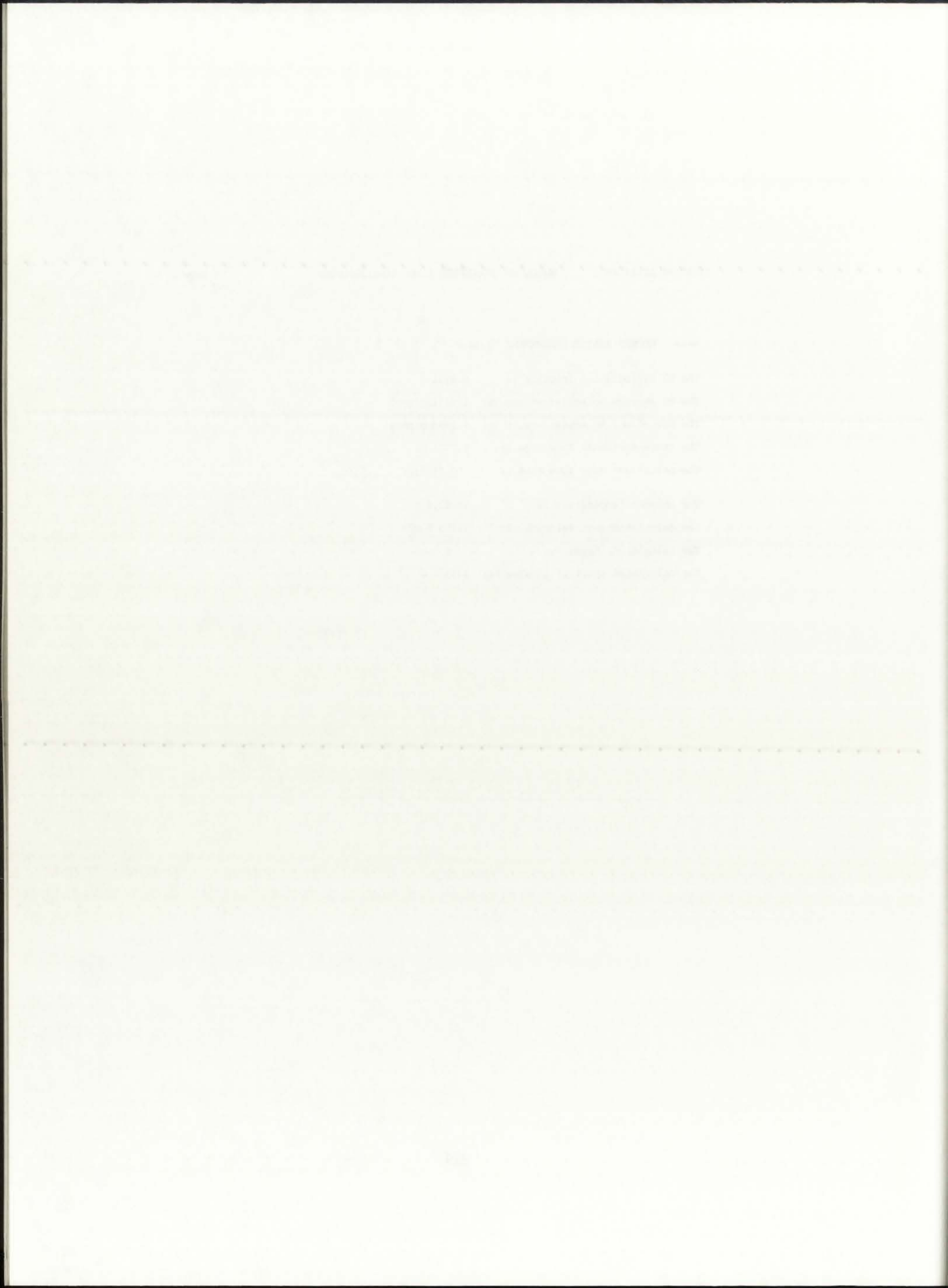
i	r(i)	T(i)	Qg(i)
37	0.000	26593.8	0.9978E+07
36	0.019	26593.8	0.9882E+07
35	0.039	26568.0	0.1967E+08
34	0.059	26489.9	0.2015E+08
33	0.096	25995.9	0.2074E+08
32	0.133	25096.9	0.2156E+08
31	0.170	23537.9	0.2295E+08
30	0.207	14902.8	0.0000E+00
29	0.225	14902.8	0.0000E+00
28	0.244	14902.8	0.0000E+00
27	0.246	14902.8	0.0000E+00
26	0.249	14902.8	0.0000E+00
25	0.268	14902.8	0.0000E+00
24	0.287	14902.8	0.0000E+00
23	0.307	14895.2	0.0000E+00
22	0.326	14888.5	0.0000E+00
21	0.345	14882.5	0.0000E+00
20	0.405	11709.7	0.0000E+00
19	0.465	9355.3	0.0000E+00
18	0.525	7539.1	0.0000E+00
17	0.585	6095.8	0.0000E+00
16	0.645	4921.6	0.0000E+00
15	0.705	3948.0	0.0000E+00
14	0.765	3128.0	0.0000E+00
13	0.825	2428.3	0.0000E+00
12	0.851	2425.4	0.0000E+00
11	0.876	2424.0	0.0000E+00
10	0.976	1992.5	0.0000E+00
9	1.076	1642.3	0.0000E+00
8	1.176	1352.5	0.0000E+00
7	1.276	1109.0	0.0000E+00
6	1.376	901.4	0.0000E+00
5	1.476	722.5	0.0000E+00
4	1.576	566.6	0.0000E+00
3	1.676	429.6	0.0000E+00
2	1.776	308.3	0.0000E+00
1	1.876	200.0	0.0000E+00



==== ROCKET ENGINE PARAMETERS ====

The H2 dissociation fraction is: 0.9831
The H2 average molecular weight is: 1.0251 g/gmol
The propellant molecular weight is: 6.5098 g/gmol
The cross-sectional flow area is: 0.0721 m²
The propellant mass flow rate is: 0.01 kg/s

The chamber temperature is: 14902.8 K
The calculated exit velocity is: 10155.6 m/s
The calculated thrust is: 0.2 kN
The calculated specific impulse is: 1035.5 s

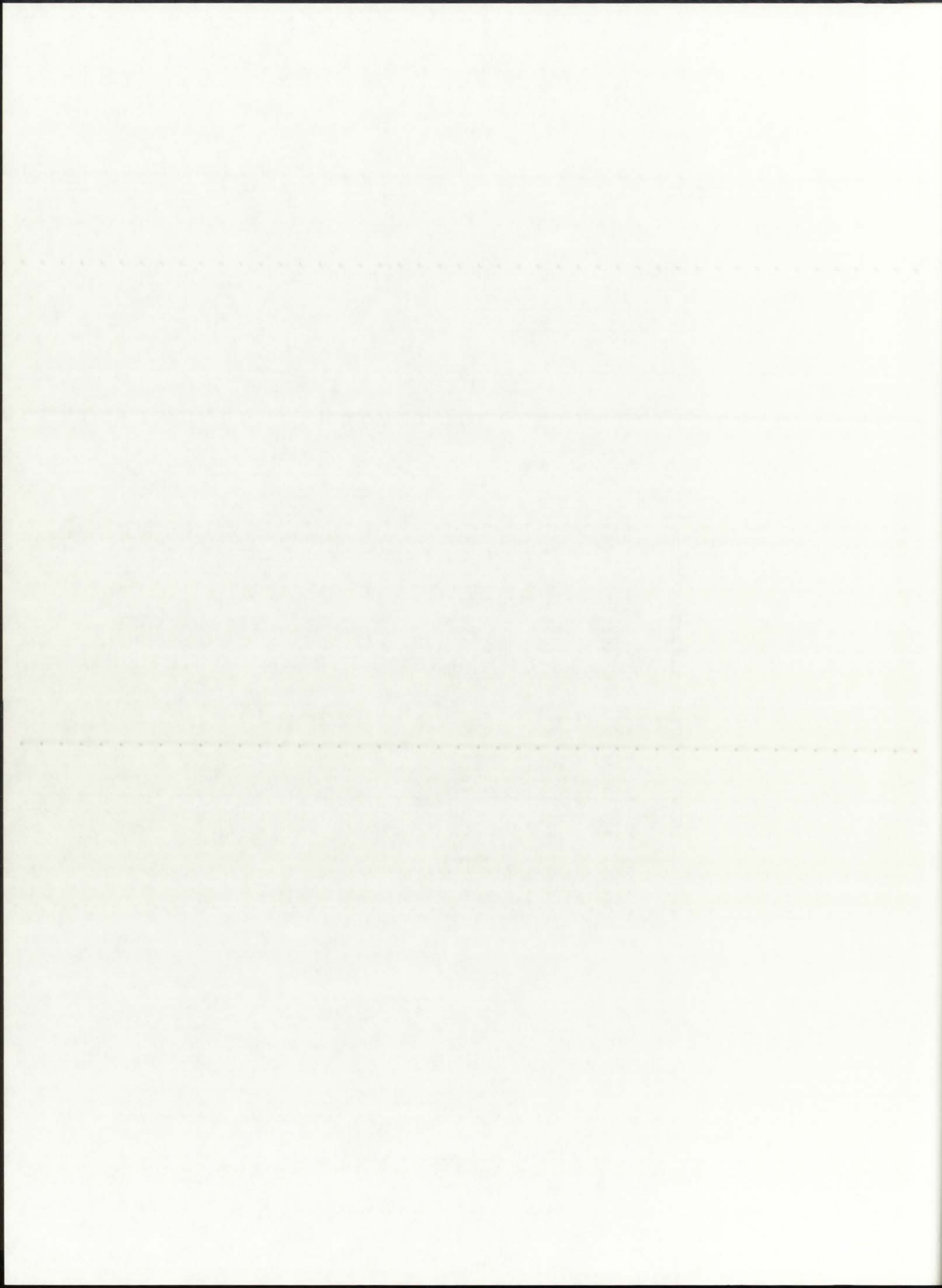


==== SUMMARY OF CONVERGED VALUES ====

This Case Executed for: REFLBe = 0.00000
 Pressure = 1000.0 atm

Modes of Heat Transfer: Radiation in BG, SiW, and P = .on.
 Convection in BG = .on.
 Convection in P = .on.

i	r(i)	T(i)	Qg(i)
37	0.000	38011.5	0.9039E+07
36	0.019	38011.5	0.8922E+07
35	0.039	37979.2	0.1787E+08
34	0.059	37880.5	0.1889E+08
33	0.096	37245.5	0.2018E+08
32	0.133	36064.0	0.2202E+08
31	0.170	33976.8	0.2566E+08
30	0.207	21084.5	0.0000E+00
29	0.225	21084.5	0.0000E+00
28	0.244	21084.5	0.0000E+00
27	0.246	21084.5	0.0000E+00
26	0.249	21084.5	0.0000E+00
25	0.268	21084.5	0.0000E+00
24	0.287	21084.5	0.0000E+00
23	0.307	21073.7	0.0000E+00
22	0.326	21064.1	0.0000E+00
21	0.345	21055.7	0.0000E+00
20	0.405	16547.8	0.0000E+00
19	0.465	13202.8	0.0000E+00
18	0.525	10622.4	0.0000E+00
17	0.585	8571.9	0.0000E+00
16	0.645	6903.6	0.0000E+00
15	0.705	5520.4	0.0000E+00
14	0.765	4355.4	0.0000E+00
13	0.825	3361.3	0.0000E+00
12	0.851	3357.2	0.0000E+00
11	0.876	3355.1	0.0000E+00
10	0.976	2742.9	0.0000E+00
9	1.076	2246.1	0.0000E+00
8	1.176	1835.1	0.0000E+00
7	1.276	1489.5	0.0000E+00
6	1.376	1195.1	0.0000E+00
5	1.476	941.2	0.0000E+00
4	1.576	720.1	0.0000E+00
3	1.676	525.8	0.0000E+00
2	1.776	353.6	0.0000E+00
1	1.876	200.0	0.0000E+00



==== ROCKET ENGINE PARAMETERS ====

The H2 dissociation fraction is: 0.9807
The H2 average molecular weight is: 1.0275 g/gmol
The propellant molecular weight is: 6.5121 g/gmol
The cross-sectional flow area is: 0.0721 m²
The propellant mass flow rate is: 0.05 kg/s

The chamber temperature is: 21084.5 K
The calculated exit velocity is: 11884.2 m/s
The calculated thrust is: 0.6 kN
The calculated specific impulse is: 1211.8 s

THE UNIVERSITY OF CHICAGO

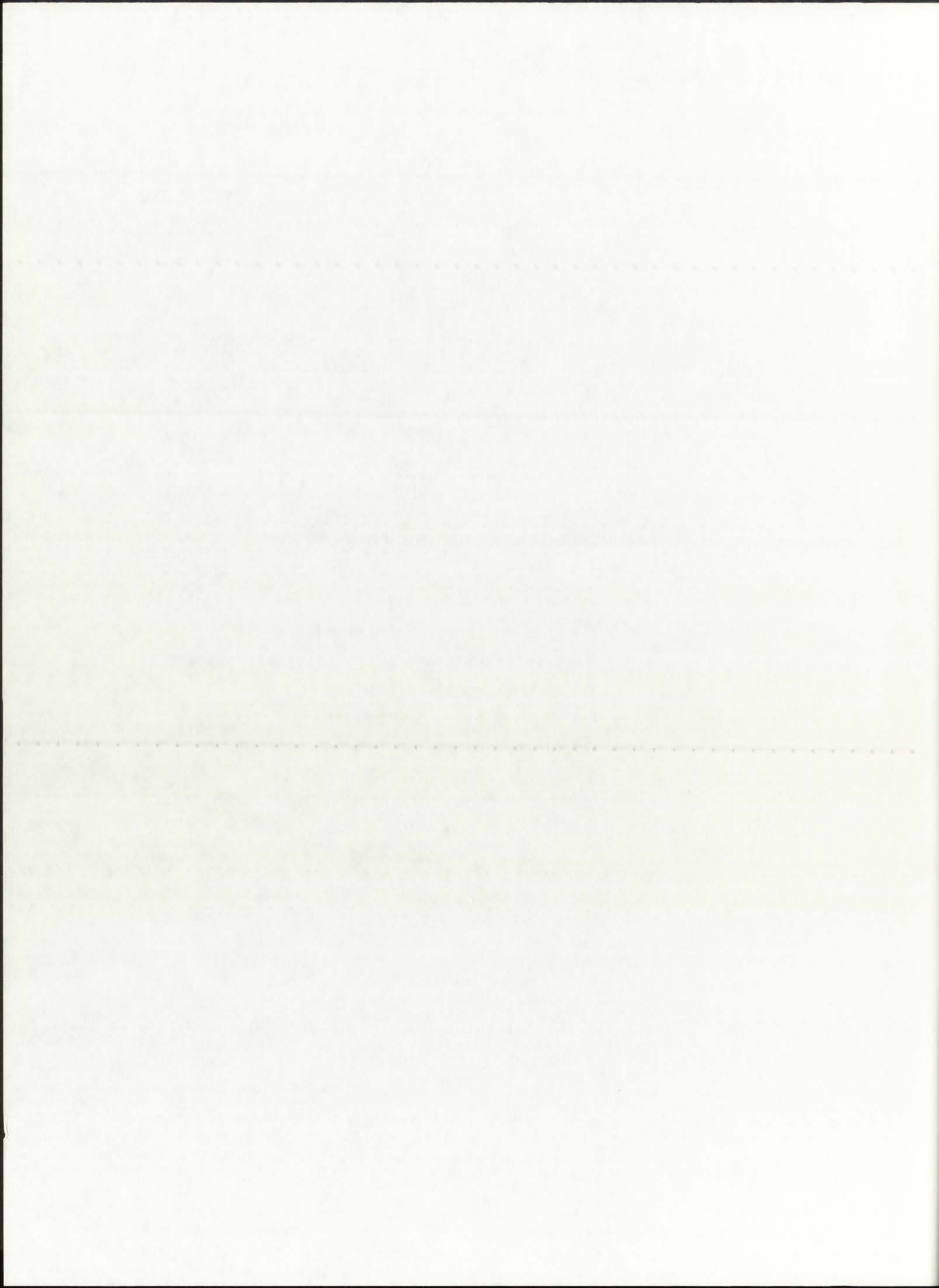
PH.D. THESIS

BY

APPENDIX D

50 kWth Case: Input and Output Files

- D.1: ONEDANT Input Files (Hansen-Roach)
- D.2: GNRATR-1D Summary Output Files (Hansen-Roach)
- D.3: TRANSX Input Files (ENDF/B-V)
- D.4: ONEDANT Input Files (ENDF/B-V)
- D.5: GNRATR-1D Summary Output Files (ENDF/B-V)



D.1. ONEDANT Input Files (Hansen-Roach)

DEPARTMENT OF THE ARMY

1

1

1

1

1

1

1

1

1

1

1

1

1

1

1

1

1

1

1

1

1

1

1

1

1

1

1

1

1

1

1

1

1

1

1

1

1

1

1

1

1

1

1

1

1

1

```

2 0 0
unit-cell rocket engine - 50 kWth Configuration - P=250 atm
search for Q(r) and keff, based on T(r) from GNRATR-1D code
/
***** block i *****
  igeom=cylinder ngroup=16 isn=4 niso=118 mt=10
  nzone=10 im=10 it=29 idimen=1
  t
/
***** block ii *****
/
  xmesh=0.0,6.0,13.375,20.75,24.45,24.94,28.80,34.58,
        58.58,82.58,87.66
  xints=4,3,3,2,2,2,3,4,4,2
  zones=1,2,3,4,5,6,7,8,9,10
  t
/
***** block iii (cross sections) *****
/
  lib=bxslib balxs=1 maxord=1 ihm=10 iht=4 ihs=5
  ifido=0 ititl=1 edname=fiss
  t
/
***** block iv (mixing) *****
/
  matls=mix      "sulfur"      6.0220e-5
                 "235-yr"      1.0382e-4
                 "u238y"       7.8167e-6;
  uranI          "235-yr"      2.0763e-4
                 "u238y"       1.5633e-5;
  uranII         "235-yr"      2.6123e-4
                 "u238y"       1.9669e-5;
  argon          "sulfur"      3.0110e-4;
  silica         "si"         2.666e-2
                 "o16"         5.332e-2;
  hydro          "h"          5.9847e-4;
  beryl          "be"         1.236e-1;
  hvywI          "d"          1.894e-2
                 "o16"         9.470e-3;
  hvywII         "d"          1.894e-2
                 "o16"         9.470e-3;
  steel          "fe"         8.486e-2;
/
  assign=mixture mix 1.0;
                 fuelI uranI 1.0;
                 fuelII uranII 1.0;
                 buffer argon 1.0;
                 siwall silica 1.0;
                 propel hydro 1.0;
                 bemodr beryl 1.0;
                 reflI hvywI 1.0;
                 reflII hvywII 1.0;
                 pvessl steel 1.0;
  t
/
***** block v (solver) *****
/
  ievt=1 isct=1 ibr=0 fluxp=1 bhgt=182.73
  t
/
***** block vi (edits)
/
  pted=1 zned=1
  icoll=16; igrped=3
  edxs=n-fiss resdnt=1 power=2.736e-4 mevper=176 rzflux=1
/

```

.....
.....
.....
.....
.....
.....
.....
.....
.....
.....

.....
.....
.....
.....
.....
.....
.....
.....
.....
.....
.....
.....
.....
.....
.....
.....

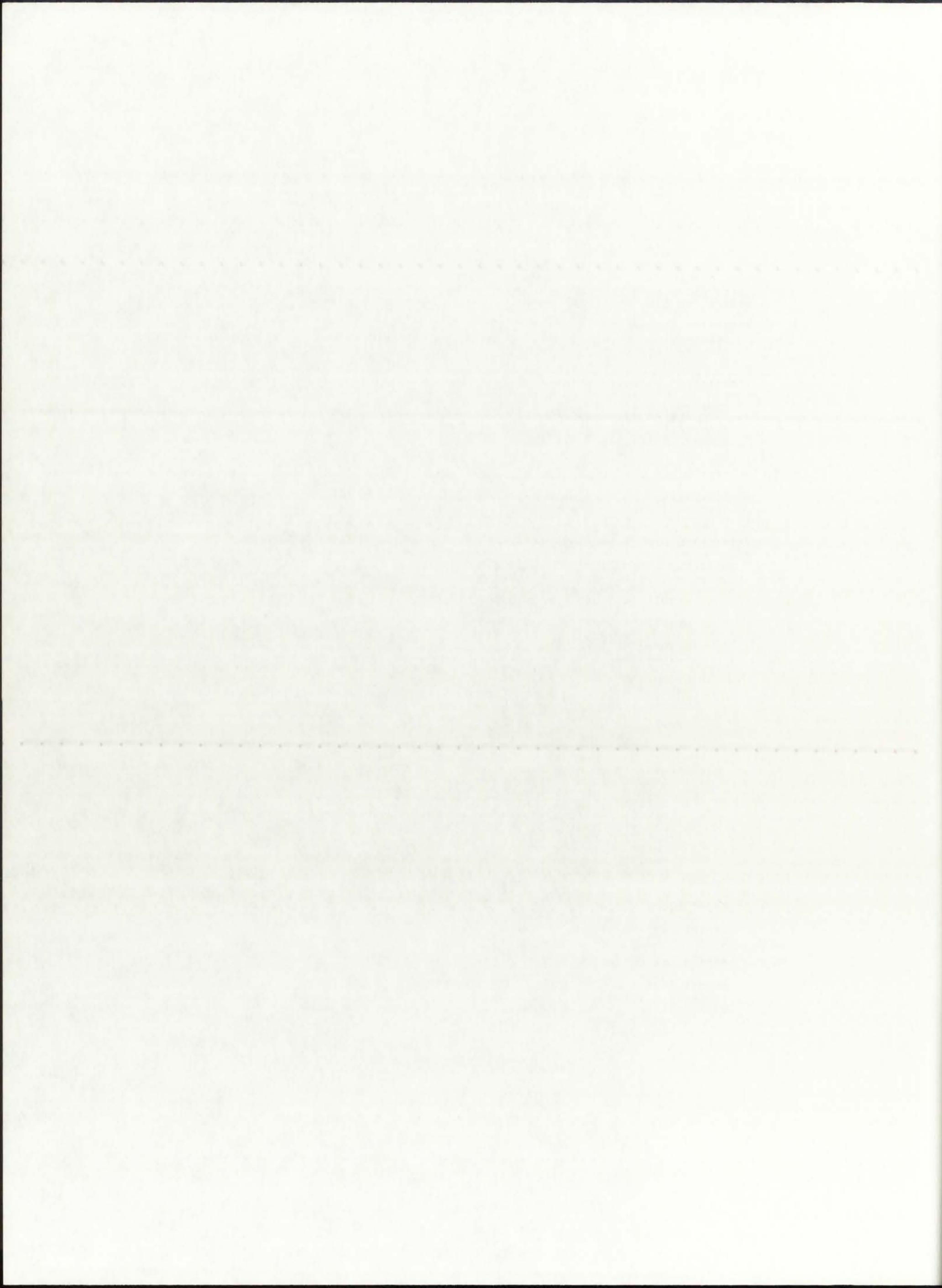
.....
.....
.....
.....
.....
.....
.....
.....
.....
.....

.....
.....
.....
.....
.....
.....
.....
.....

```

2 0 0
unit-cell rocket engine - 50 kWth Configuration - P=500 atm
search for Q(r) and keff, based on T(r) from GNRATR-1D code
/
/***** block i *****/
igeom=cylinder ngroup=16 isn=4 niso=118 mt=10
nzone=10 im=10 it=29 idimen=1
t
/
/***** block ii *****/
xmesh=0.0,6.0,13.375,20.75,24.45,24.94,28.80,34.58,
58.58,82.58,87.66
xints=4,3,3,2,2,2,3,4,4,2
zones=1,2,3,4,5,6,7,8,9,10
t
/
/***** block iii (cross sections) *****/
lib=bxslib balxs=1 maxord=1 ihm=10 iht=4 ihs=5
ifido=0 ititl=1 edname=fiss
t
/
/***** block iv (mixing) *****/
matls=mix      "sulfur"      9.1690e-5
              "235-yr"      1.7850e-4
              "u238y"       1.3440e-5;
uranI        "235-yr"      3.5700e-4
              "u238y"       2.6880e-5;
uranII       "235-yr"      4.1902e-4
              "u238y"       3.1550e-5;
argon        "sulfur"      4.1000e-4;
silica       "si"          2.666e-2
              "o16"        5.332e-2;
hydro        "h"           8.1246e-4;
beryl        "be"          1.236e-1;
hvywI        "d"           1.894e-2
              "o16"        9.470e-3;
hvywII       "d"           1.894e-2
              "o16"        9.470e-3;
steel        "fe"          8.486e-2;
/
assign=mixture mix 1.0;
              fuelI uranI 1.0;
              fuelII uranII 1.0;
              buffer argon 1.0;
              siwall silica 1.0;
              propel hydro 1.0;
              bemodr beryl 1.0;
              reflI hvywI 1.0;
              reflII hvywII 1.0;
              pvessl steel 1.0;
t
/
/***** block v (solver) *****/
ievt=1 isct=1 ibr=0 fluxp=1 bhgt=182.73
t
/
/***** block vi (edits) *****/
pted=1 zned=1
icoll=16; igrped=3
edxs=n-fiss resdnt=1 power=2.736e-4 mevper=176 rzflux=1
/

```



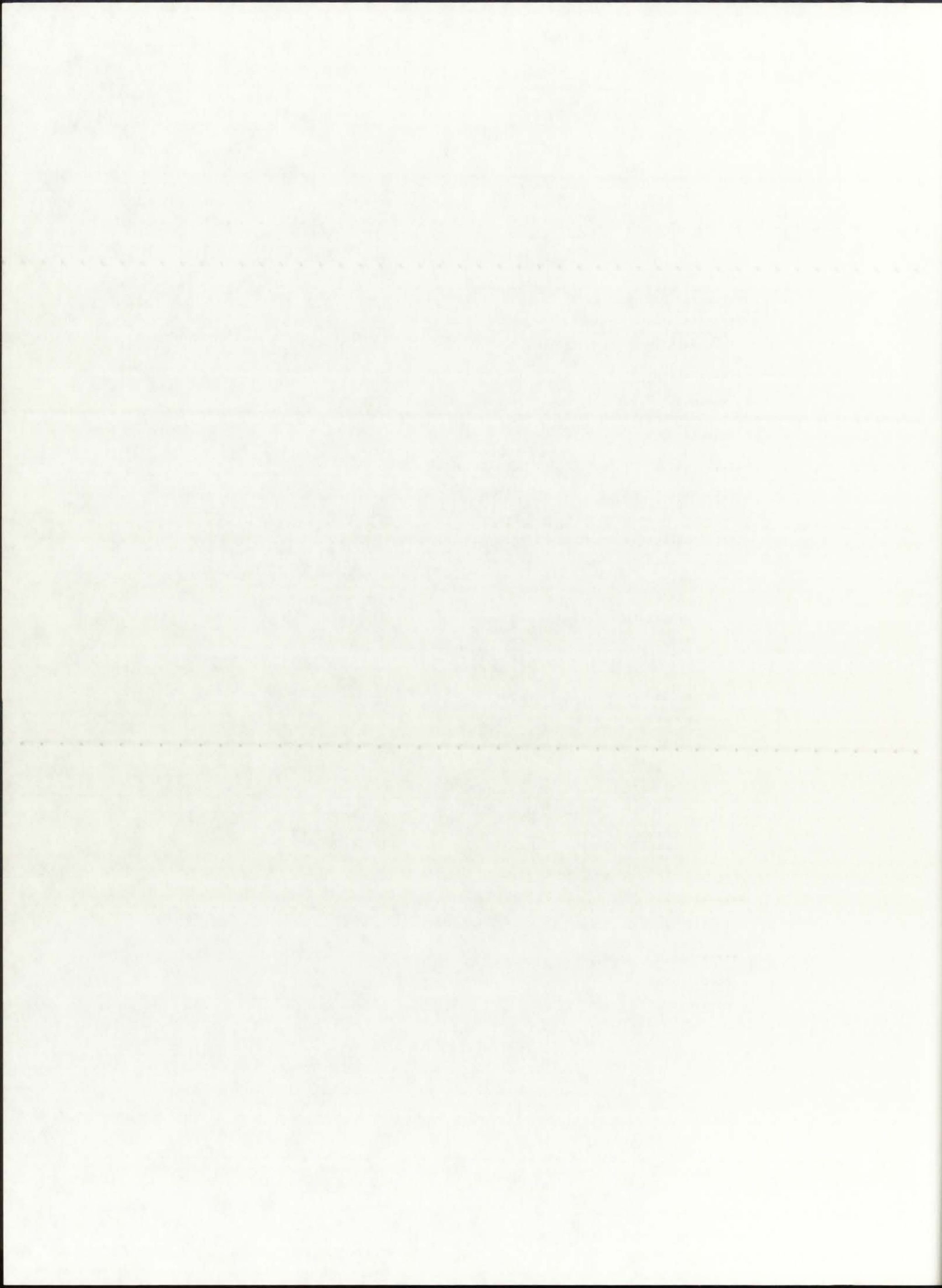

```

2 0 0
unit-cell rocket engine - 50 kwth Configuration - P=1000 atm
search for Q(r) and keff, based on T(r) from GNRATR-1D code
/
/***** block i *****/
  igeom=cylinder  ngroup=16  isn=4  niso=118  mt=10
  nzone=10  im=10  it=29  idimen=1
  t
/
/***** block ii *****/
/
  xmesh=0.0,6.0,13.375,20.75,24.45,24.94,28.80,34.58,
        58.58,82.58,87.66
  xints=4,3,3,2,2,2,3,4,4,2
  zones=1,2,3,4,5,6,7,8,9,10
  t
/
/***** block iii (cross sections) *****/
/
  lib=bxslib  balxs=1  maxord=1  ihm=10  iht=4  ihs=5
  ifido=0  ititl=1  edname=fiss
  t
/
/***** block iv (mixing) *****/
/
  matls=mix
    "sulfur"      1.5660e-4
    "235-yr"     2.7370e-4
    "u238y"      2.0608e-5;
  uranI  "235-yr"  5.4740e-4
    "u238y"      4.1216e-5;
  uranII "235-yr"  6.5607e-4
    "u238y"      4.9398e-5;
  argon  "sulfur"  6.8888e-4;
  silica "si"      2.666e-2
    "o16"        5.332e-2;
  hydro  "h"       1.3663e-3;
  beryl  "be"      1.236e-1;
  hvywI  "d"       1.894e-2
    "o16"        9.470e-3;
  hvywII "d"       1.894e-2
    "o16"        9.470e-3;
  steel  "fe"      8.486e-2;

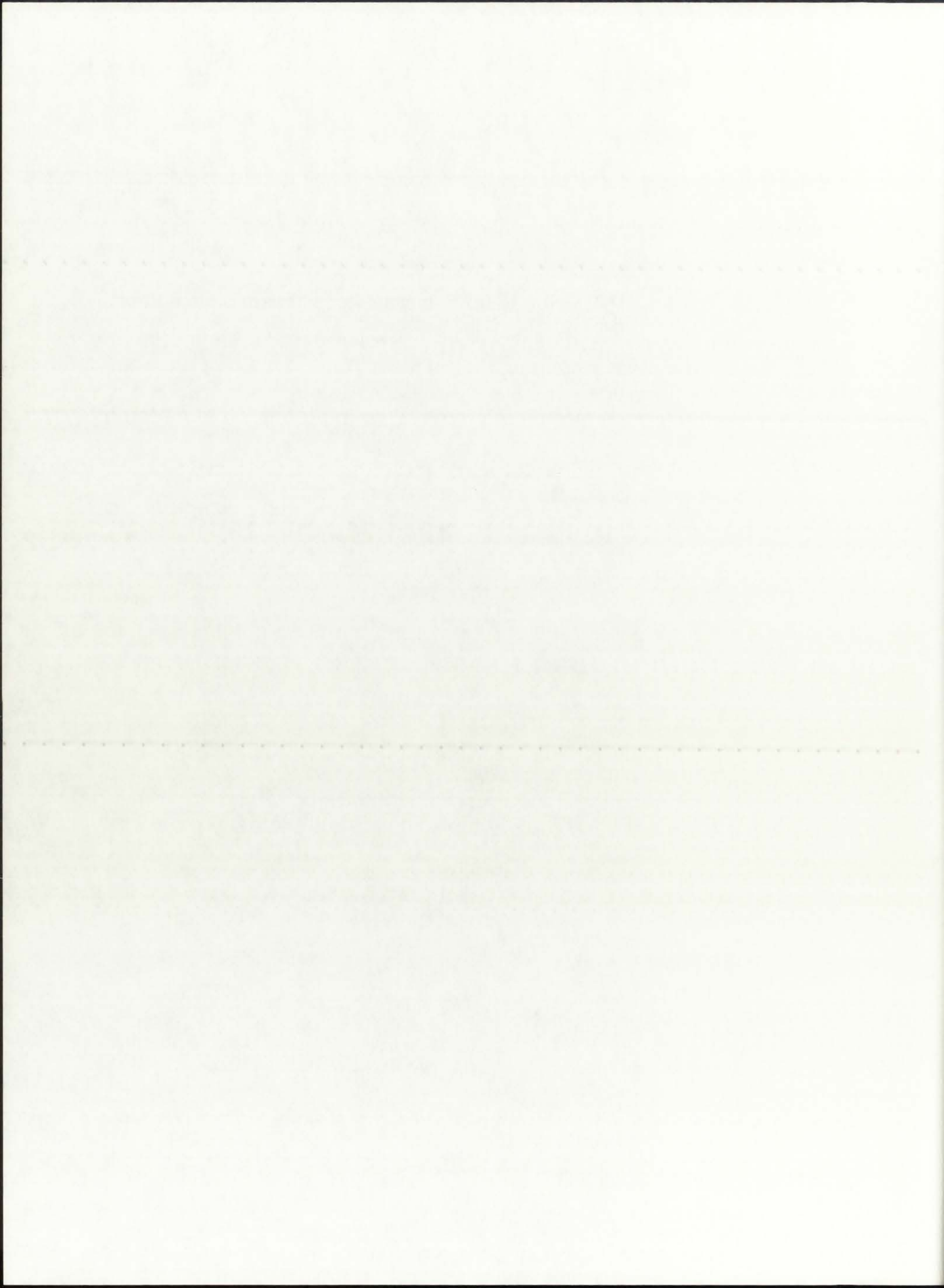
  assign=mixture  mix  1.0;
    fuelI  uranI  1.0;
    fuelII uranII 1.0;
    buffer argon  1.0;
    siwall silica 1.0;
    propel hydro  1.0;
    bemodr beryl  1.0;
    reflI  hvywI  1.0;
    reflII hvywII 1.0;
    pvessl steel  1.0;

  t
/
/***** block v (solver) *****/
/
  ievt=1  isct=1  ibr=0  fluxp=1  bhgt=182.73
  t
/
/***** block vi (edits) *****/
/
  pted=1  zned=1
  icoll=16;  igrped=3
  edxs=n-fiss  resdnt=1  power=2.736e-4  mevper=176  rzflux=1
/

```



D.2. GNRATR-1D Summary Output Files (Hansen-Roach)

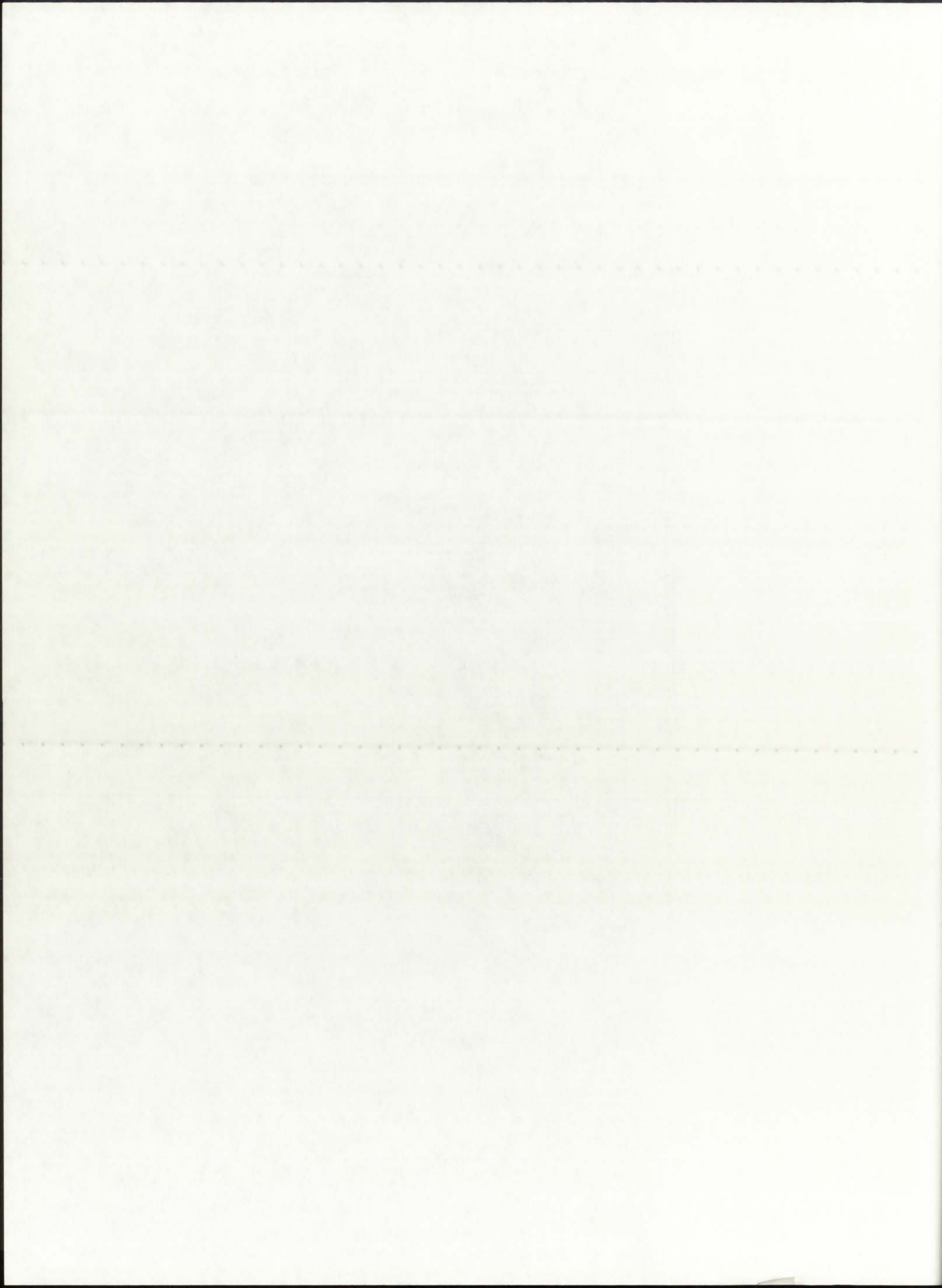


==== SUMMARY OF CONVERGED VALUES ====

This Case Executed for: REFLBe = 0.00000
 Pressure = 250.0 atm

Modes of Heat Transfer: Radiation in BG, SiW, and P = .on.
 Convection in BG = .on.
 Convection in P = .on.

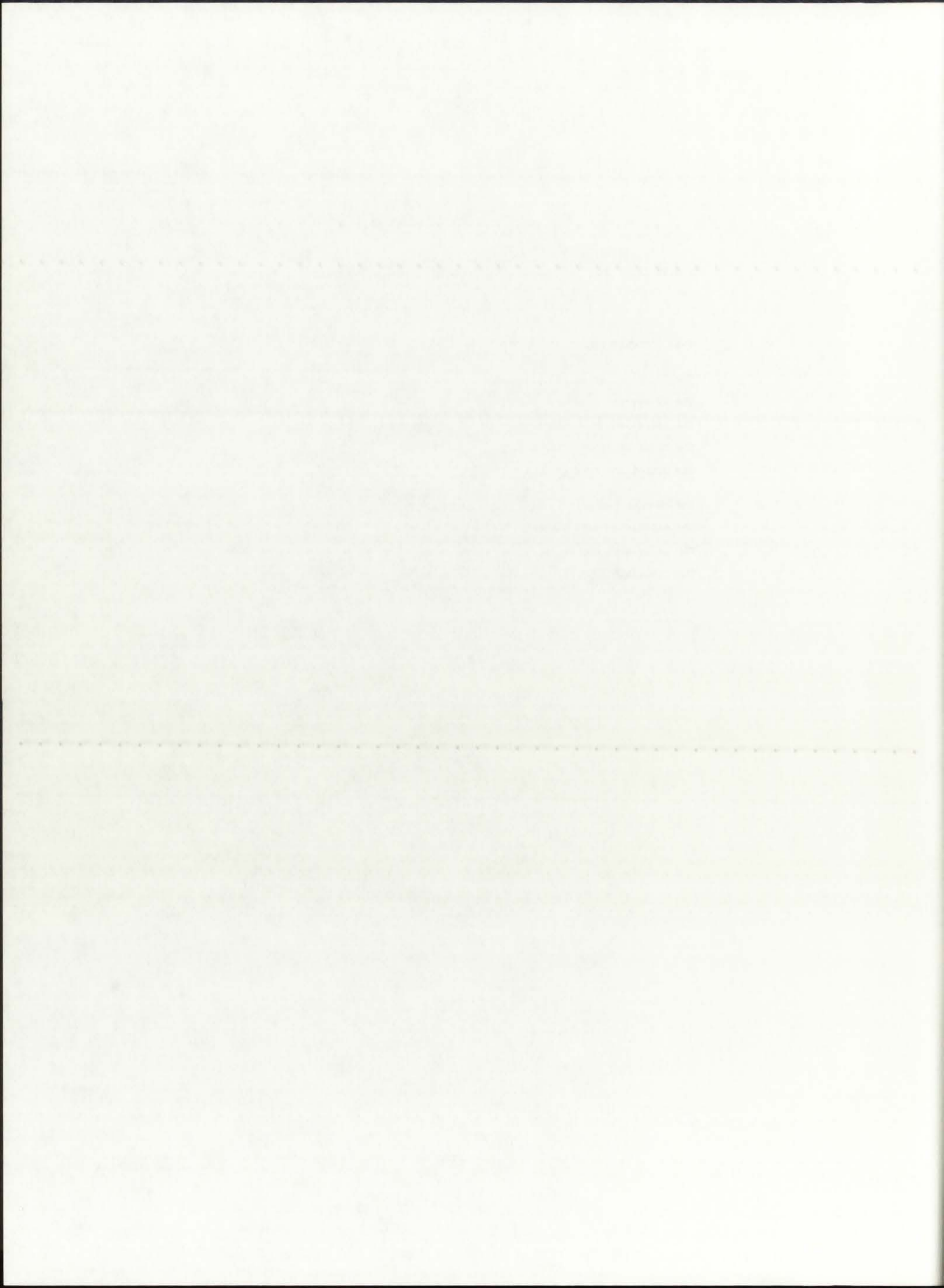
i	r(i)	T(i)	Qg(i)
37	0.000	8604.3	0.5447E+05
36	0.019	8604.3	0.5370E+05
35	0.039	8600.2	0.1110E+06
34	0.059	8587.3	0.1244E+06
33	0.096	8502.2	0.1816E+06
32	0.133	8305.7	0.2326E+06
31	0.170	7920.8	0.3729E+06
30	0.207	4833.2	0.0000E+00
29	0.225	4833.2	0.0000E+00
28	0.244	4833.2	0.0000E+00
27	0.246	4833.2	0.0000E+00
26	0.249	4833.1	0.0000E+00
25	0.268	4833.1	0.0000E+00
24	0.287	4833.0	0.0000E+00
23	0.307	4830.6	0.0000E+00
22	0.326	4828.5	0.0000E+00
21	0.345	4826.6	0.0000E+00
20	0.405	3828.4	0.0000E+00
19	0.465	3087.7	0.0000E+00
18	0.525	2516.3	0.0000E+00
17	0.585	2062.3	0.0000E+00
16	0.645	1692.8	0.0000E+00
15	0.705	1386.5	0.0000E+00
14	0.765	1128.6	0.0000E+00
13	0.825	908.4	0.0000E+00
12	0.851	907.5	0.0000E+00
11	0.876	907.1	0.0000E+00
10	0.976	769.9	0.0000E+00
9	1.076	658.6	0.0000E+00
8	1.176	566.4	0.0000E+00
7	1.276	489.0	0.0000E+00
6	1.376	423.0	0.0000E+00
5	1.476	366.1	0.0000E+00
4	1.576	316.6	0.0000E+00
3	1.676	273.0	0.0000E+00
2	1.776	234.4	0.0000E+00
1	1.876	200.0	0.0000E+00



==== ROCKET ENGINE PARAMETERS ====

The H2 dissociation fraction is: 0.0891
The H2 average molecular weight is: 1.9262 g/gmol
The propellant molecular weight is: 7.3839 g/gmol
The cross-sectional flow area is: 0.0721 m²
The propellant mass flow rate is: 0.10 kg/s

The chamber temperature is: 4833.1 K
The calculated exit velocity is: 7903.5 m/s
The calculated thrust is: 0.8 kN
The calculated specific impulse is: 805.9 s



==== SUMMARY OF CONVERGED VALUES ====

This Case Executed for: REFLBe = 0.00000
 Pressure = 500.0 atm

Modes of Heat Transfer: Radiation in BG, SiW, and P = .on.
 Convection in BG = .on.
 Convection in P = .on.

i	r(i)	T(i)	Qg(i)
37	0.000	10251.8	0.5118E+05
36	0.019	10251.8	0.5085E+05
35	0.039	10247.2	0.1052E+06
34	0.059	10232.7	0.1171E+06
33	0.096	10138.1	0.1597E+06
32	0.133	9933.0	0.2069E+06
31	0.170	9542.2	0.4224E+06
30	0.207	5717.0	0.0000E+00
29	0.225	5717.0	0.0000E+00
28	0.244	5717.0	0.0000E+00
27	0.246	5717.0	0.0000E+00
26	0.249	5717.0	0.0000E+00
25	0.268	5717.0	0.0000E+00
24	0.287	5716.9	0.0000E+00
23	0.307	5714.1	0.0000E+00
22	0.326	5711.5	0.0000E+00
21	0.345	5709.3	0.0000E+00
20	0.405	4520.2	0.0000E+00
19	0.465	3637.9	0.0000E+00
18	0.525	2957.2	0.0000E+00
17	0.585	2416.3	0.0000E+00
16	0.645	1976.3	0.0000E+00
15	0.705	1611.4	0.0000E+00
14	0.765	1304.1	0.0000E+00
13	0.825	1041.9	0.0000E+00
12	0.851	1040.8	0.0000E+00
11	0.876	1040.2	0.0000E+00
10	0.976	877.2	0.0000E+00
9	1.076	744.9	0.0000E+00
8	1.176	635.5	0.0000E+00
7	1.276	543.4	0.0000E+00
6	1.376	465.0	0.0000E+00
5	1.476	397.4	0.0000E+00
4	1.576	338.5	0.0000E+00
3	1.676	286.8	0.0000E+00
2	1.776	240.9	0.0000E+00
1	1.876	200.0	0.0000E+00

STATE OF TEXAS

COMMISSIONERS OF THE GENERAL LAND OFFICE

LAND OFFICE

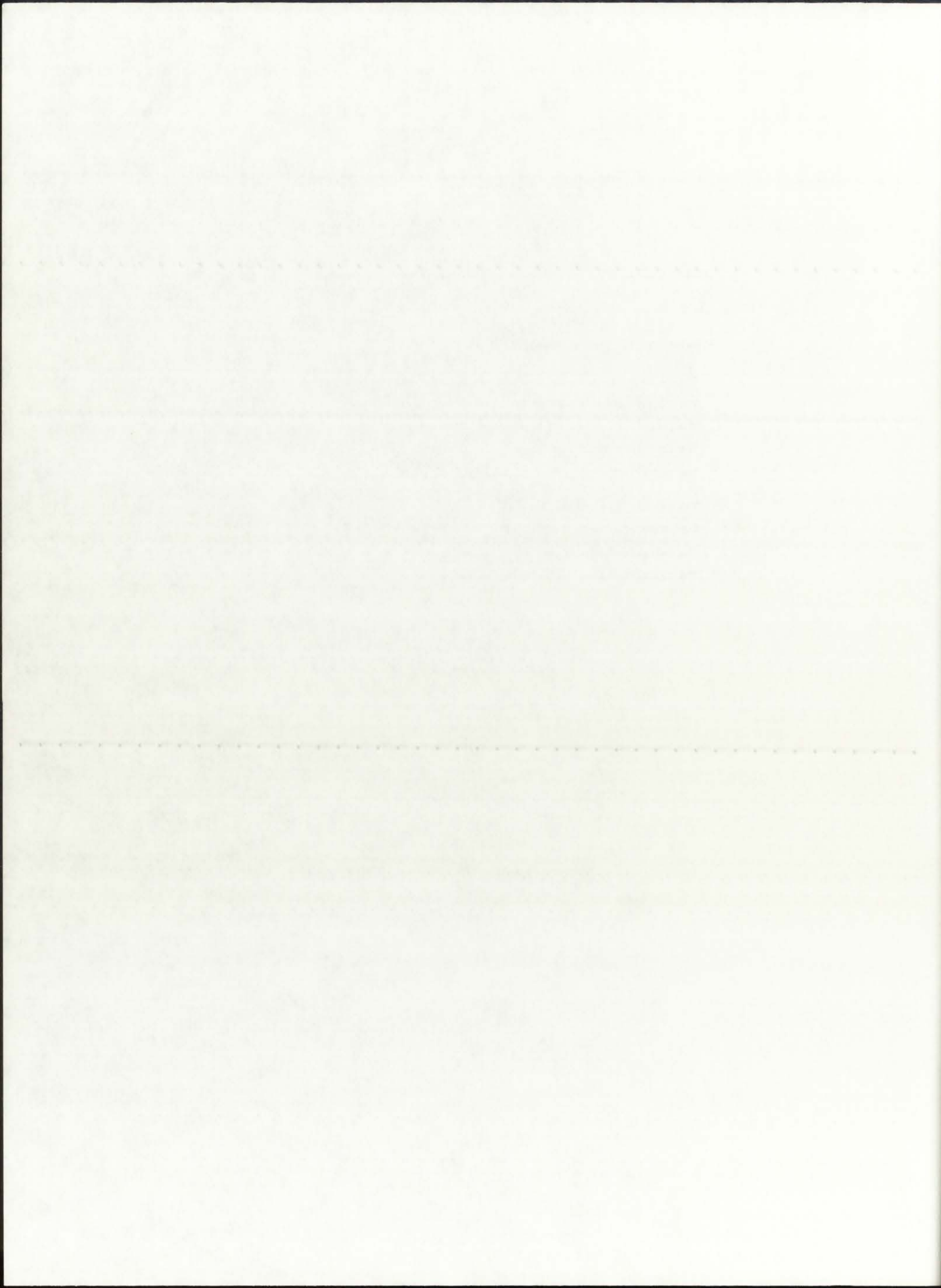
Section 10, Act of September 1, 1907, as amended.

SECTION	ACRES	AMOUNT
Section 10	1.000	100.00
Section 11	1.000	100.00
Section 12	1.000	100.00
Section 13	1.000	100.00
Section 14	1.000	100.00
Section 15	1.000	100.00
Section 16	1.000	100.00
Section 17	1.000	100.00
Section 18	1.000	100.00
Section 19	1.000	100.00
Section 20	1.000	100.00
Section 21	1.000	100.00
Section 22	1.000	100.00
Section 23	1.000	100.00
Section 24	1.000	100.00
Section 25	1.000	100.00
Section 26	1.000	100.00
Section 27	1.000	100.00
Section 28	1.000	100.00
Section 29	1.000	100.00
Section 30	1.000	100.00
Section 31	1.000	100.00
Section 32	1.000	100.00
Section 33	1.000	100.00
Section 34	1.000	100.00
Section 35	1.000	100.00
Section 36	1.000	100.00
Section 37	1.000	100.00
Section 38	1.000	100.00
Section 39	1.000	100.00
Section 40	1.000	100.00
Section 41	1.000	100.00
Section 42	1.000	100.00
Section 43	1.000	100.00
Section 44	1.000	100.00
Section 45	1.000	100.00
Section 46	1.000	100.00
Section 47	1.000	100.00
Section 48	1.000	100.00
Section 49	1.000	100.00
Section 50	1.000	100.00
Section 51	1.000	100.00
Section 52	1.000	100.00
Section 53	1.000	100.00
Section 54	1.000	100.00
Section 55	1.000	100.00
Section 56	1.000	100.00
Section 57	1.000	100.00
Section 58	1.000	100.00
Section 59	1.000	100.00
Section 60	1.000	100.00
Section 61	1.000	100.00
Section 62	1.000	100.00
Section 63	1.000	100.00
Section 64	1.000	100.00
Section 65	1.000	100.00
Section 66	1.000	100.00
Section 67	1.000	100.00
Section 68	1.000	100.00
Section 69	1.000	100.00
Section 70	1.000	100.00
Section 71	1.000	100.00
Section 72	1.000	100.00
Section 73	1.000	100.00
Section 74	1.000	100.00
Section 75	1.000	100.00
Section 76	1.000	100.00
Section 77	1.000	100.00
Section 78	1.000	100.00
Section 79	1.000	100.00
Section 80	1.000	100.00
Section 81	1.000	100.00
Section 82	1.000	100.00
Section 83	1.000	100.00
Section 84	1.000	100.00
Section 85	1.000	100.00
Section 86	1.000	100.00
Section 87	1.000	100.00
Section 88	1.000	100.00
Section 89	1.000	100.00
Section 90	1.000	100.00
Section 91	1.000	100.00
Section 92	1.000	100.00
Section 93	1.000	100.00
Section 94	1.000	100.00
Section 95	1.000	100.00
Section 96	1.000	100.00
Section 97	1.000	100.00
Section 98	1.000	100.00
Section 99	1.000	100.00
Section 100	1.000	100.00

==== ROCKET ENGINE PARAMETERS ====

The H2 dissociation fraction is: 0.1555
The H2 average molecular weight is: 1.8592 g/gmol
The propellant molecular weight is: 7.3189 g/gmol
The cross-sectional flow area is: 0.0721 m²
The propellant mass flow rate is: 0.14 kg/s

The chamber temperature is: 5717.0 K
The calculated exit velocity is: 7995.2 m/s
The calculated thrust is: 1.2 kN
The calculated specific impulse is: 815.3 s



==== SUMMARY OF CONVERGED VALUES ====

This Case Executed for: REFLBe = 0.00000
Pressure = 1000.0 atm

Modes of Heat Transfer: Radiation in BG, SiW, and P = .on.
Convection in BG = .on.
Convection in P = .on.

i	r(i)	T(i)	Qg(i)
37	0.000	12265.2	0.5147E+05
36	0.019	12265.2	0.5123E+05
35	0.039	12259.6	0.1044E+06
34	0.059	12242.6	0.1112E+06
33	0.096	12134.9	0.1500E+06
32	0.133	11906.4	0.1895E+06
31	0.170	11485.1	0.4492E+06
30	0.207	6791.1	0.0000E+00
29	0.225	6791.1	0.0000E+00
28	0.244	6791.1	0.0000E+00
27	0.246	6791.1	0.0000E+00
26	0.249	6791.1	0.0000E+00
25	0.268	6791.1	0.0000E+00
24	0.287	6791.0	0.0000E+00
23	0.307	6787.6	0.0000E+00
22	0.326	6784.6	0.0000E+00
21	0.345	6781.9	0.0000E+00
20	0.405	5360.9	0.0000E+00
19	0.465	4306.4	0.0000E+00
18	0.525	3493.0	0.0000E+00
17	0.585	2846.6	0.0000E+00
16	0.645	2320.7	0.0000E+00
15	0.705	1884.7	0.0000E+00
14	0.765	1517.4	0.0000E+00
13	0.825	1204.0	0.0000E+00
12	0.851	1202.7	0.0000E+00
11	0.876	1202.1	0.0000E+00
10	0.976	1007.6	0.0000E+00
9	1.076	849.9	0.0000E+00
8	1.176	719.3	0.0000E+00
7	1.276	609.6	0.0000E+00
6	1.376	516.1	0.0000E+00
5	1.476	435.4	0.0000E+00
4	1.576	365.2	0.0000E+00
3	1.676	303.5	0.0000E+00
2	1.776	248.8	0.0000E+00
1	1.876	200.0	0.0000E+00

1950
 1951
 1952
 1953
 1954
 1955
 1956
 1957
 1958
 1959
 1960
 1961
 1962
 1963
 1964
 1965
 1966
 1967
 1968
 1969
 1970
 1971
 1972
 1973
 1974
 1975
 1976
 1977
 1978
 1979
 1980
 1981
 1982
 1983
 1984
 1985
 1986
 1987
 1988
 1989
 1990
 1991
 1992
 1993
 1994
 1995
 1996
 1997
 1998
 1999
 2000
 2001
 2002
 2003
 2004
 2005
 2006
 2007
 2008
 2009
 2010
 2011
 2012
 2013
 2014
 2015
 2016
 2017
 2018
 2019
 2020
 2021
 2022
 2023
 2024
 2025
 2026
 2027
 2028
 2029
 2030
 2031
 2032
 2033
 2034
 2035
 2036
 2037
 2038
 2039
 2040
 2041
 2042
 2043
 2044
 2045
 2046
 2047
 2048
 2049
 2050

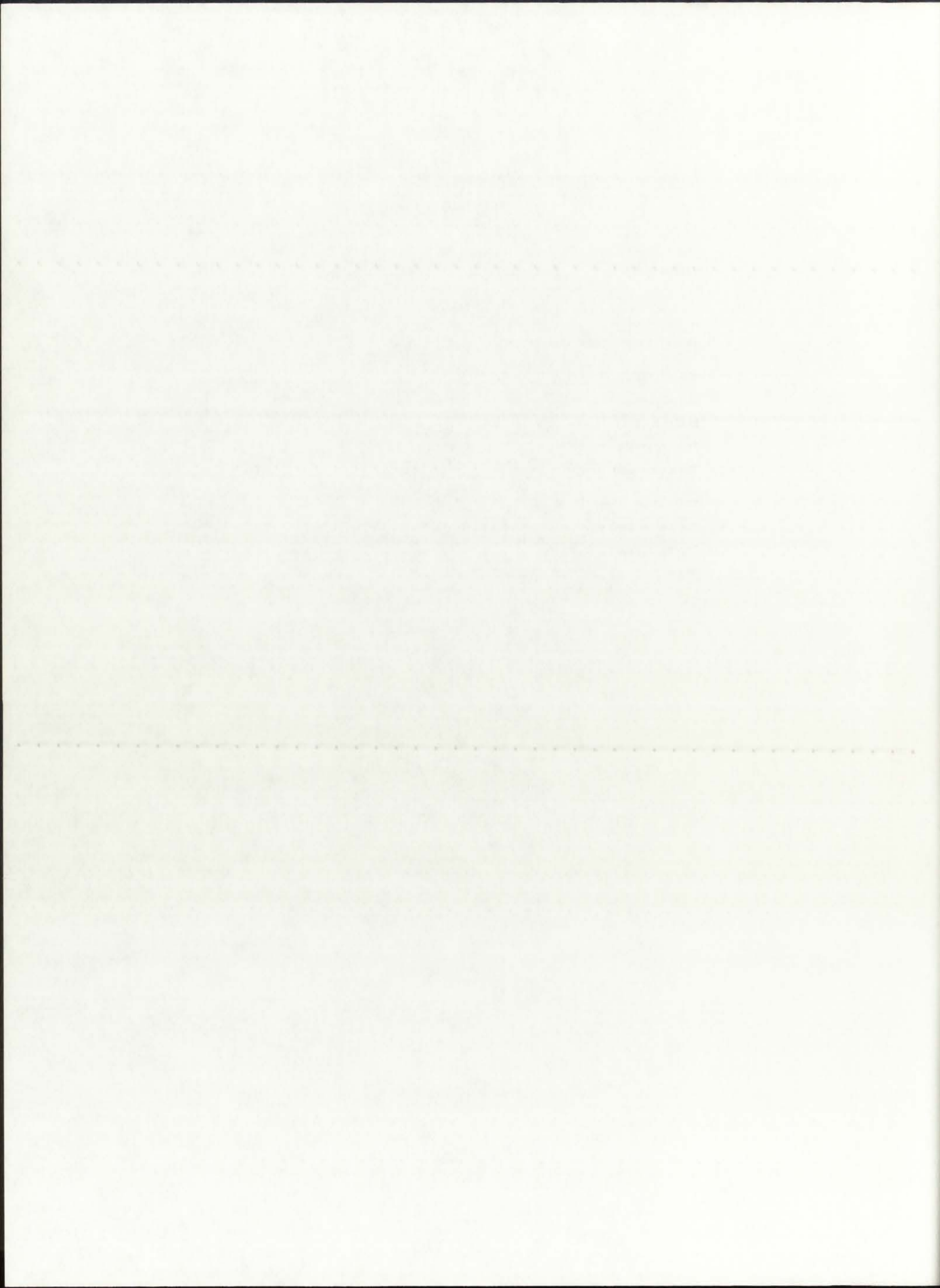
1950
 1951
 1952
 1953
 1954
 1955
 1956
 1957
 1958
 1959
 1960
 1961
 1962
 1963
 1964
 1965
 1966
 1967
 1968
 1969
 1970
 1971
 1972
 1973
 1974
 1975
 1976
 1977
 1978
 1979
 1980
 1981
 1982
 1983
 1984
 1985
 1986
 1987
 1988
 1989
 1990
 1991
 1992
 1993
 1994
 1995
 1996
 1997
 1998
 1999
 2000
 2001
 2002
 2003
 2004
 2005
 2006
 2007
 2008
 2009
 2010
 2011
 2012
 2013
 2014
 2015
 2016
 2017
 2018
 2019
 2020
 2021
 2022
 2023
 2024
 2025
 2026
 2027
 2028
 2029
 2030
 2031
 2032
 2033
 2034
 2035
 2036
 2037
 2038
 2039
 2040
 2041
 2042
 2043
 2044
 2045
 2046
 2047
 2048
 2049
 2050

Year	1950	1951	1952	1953	1954	1955	1956	1957	1958	1959	1960	1961	1962	1963	1964	1965	1966	1967	1968	1969	1970	1971	1972	1973	1974	1975	1976	1977	1978	1979	1980	1981	1982	1983	1984	1985	1986	1987	1988	1989	1990	1991	1992	1993	1994	1995	1996	1997	1998	1999	2000	2001	2002	2003	2004	2005	2006	2007	2008	2009	2010	2011	2012	2013	2014	2015	2016	2017	2018	2019	2020	2021	2022	2023	2024	2025	2026	2027	2028	2029	2030	2031	2032	2033	2034	2035	2036	2037	2038	2039	2040	2041	2042	2043	2044	2045	2046	2047	2048	2049	2050
1950	1950	1951	1952	1953	1954	1955	1956	1957	1958	1959	1960	1961	1962	1963	1964	1965	1966	1967	1968	1969	1970	1971	1972	1973	1974	1975	1976	1977	1978	1979	1980	1981	1982	1983	1984	1985	1986	1987	1988	1989	1990	1991	1992	1993	1994	1995	1996	1997	1998	1999	2000	2001	2002	2003	2004	2005	2006	2007	2008	2009	2010	2011	2012	2013	2014	2015	2016	2017	2018	2019	2020	2021	2022	2023	2024	2025	2026	2027	2028	2029	2030	2031	2032	2033	2034	2035	2036	2037	2038	2039	2040	2041	2042	2043	2044	2045	2046	2047	2048	2049	2050

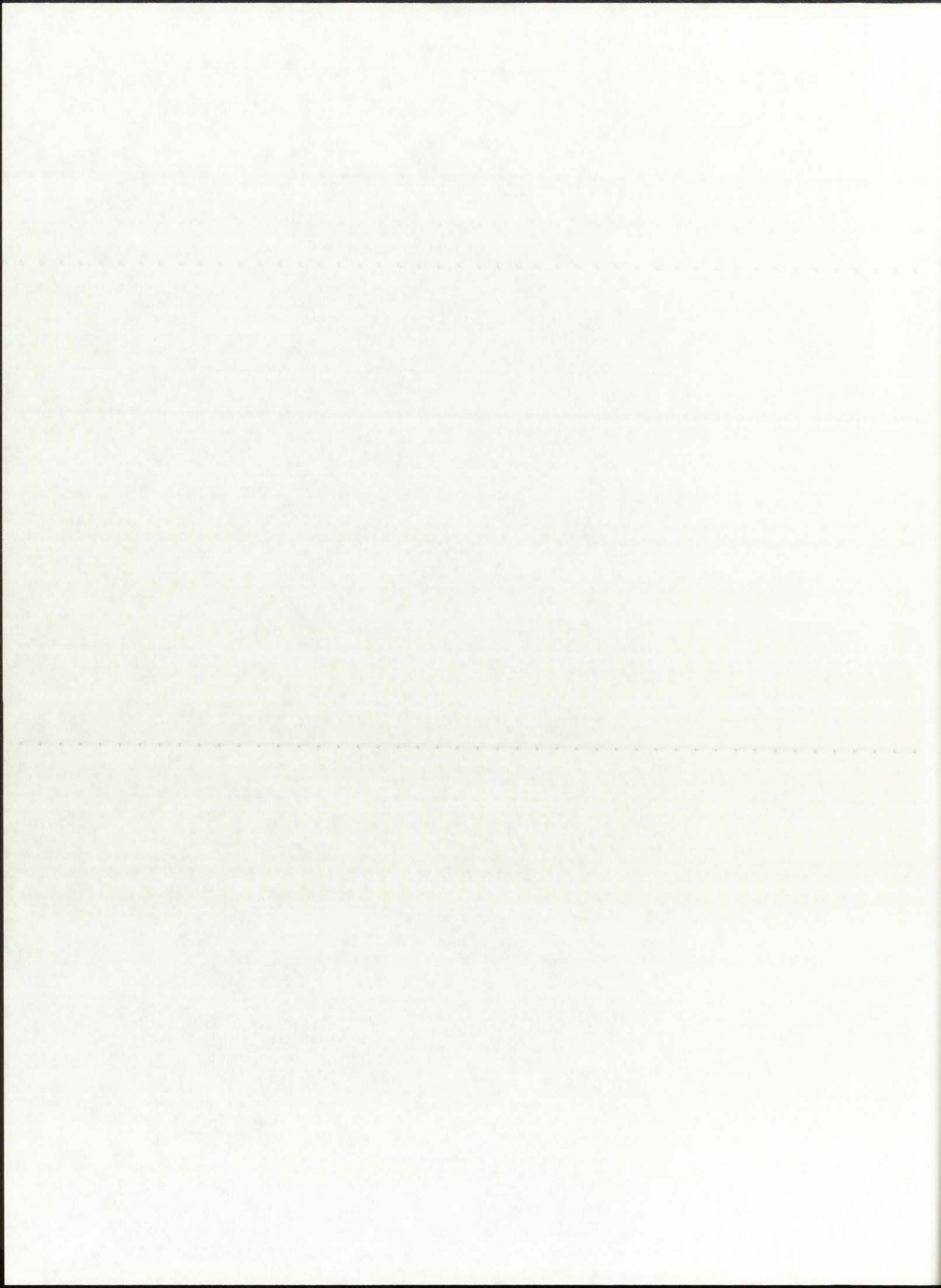
==== ROCKET ENGINE PARAMETERS ====

The H2 dissociation fraction is: 0.2397
The H2 average molecular weight is: 1.7743 g/gmol
The propellant molecular weight is: 7.2366 g/gmol
The cross-sectional flow area is: 0.0721 m²
The propellant mass flow rate is: 0.20 kg/s

The chamber temperature is: 6791.1 K
The calculated exit velocity is: 8399.3 m/s
The calculated thrust is: 1.6 kN
The calculated specific impulse is: 856.5 s



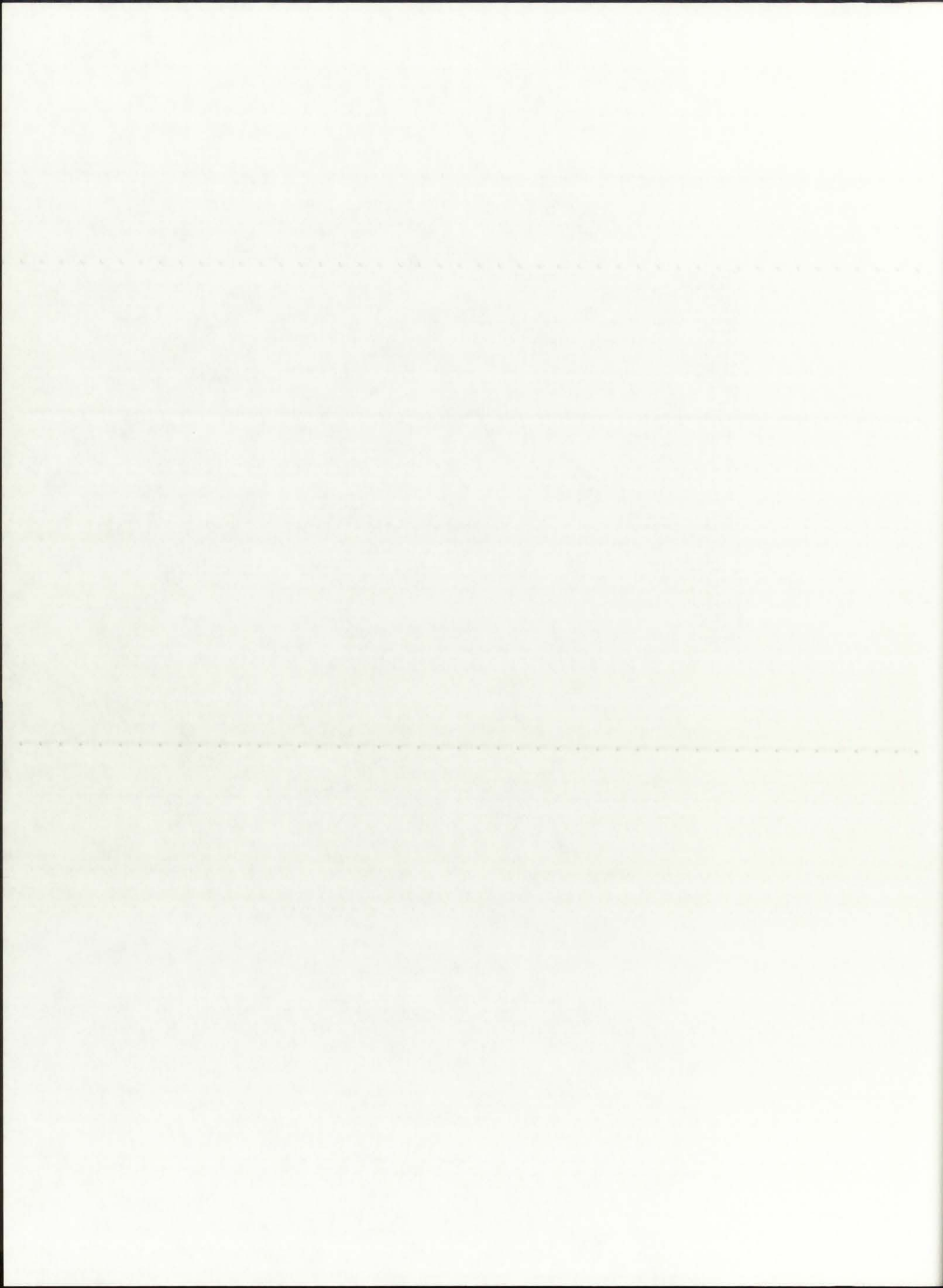
D.3. TRANSX Input Files (ENDF/B-V)



```

*Unit-cell NLB Engine 50kWth P=250 atm input file
*mtx7ey* *isotxs*/
1 6 0 1 1 1 0 2 0 0/
69 2 93 20 8 8 9 9 9/
*enru* *hydr* *deut* *oxgn* *bery* *ar* *si* *fe*
*enru*          8000.          1./
*hydr*          4800.          1./
*deut*           300.          1./
*oxgn*           300.          1./
*bery*           300.          1./
*ar*            4800.          1./
*si*             300.          1./
*fe*             300.          1./
1 1      *u235*          0.96      1.e+10 42  *free*/
1 1      *u238*          0.04      1.e+10 42  *free*/
2 2      *h1*            1.0       1.e+10 42  *free*/
3 3      *h2*            1.0       1.e+10 42  *d2o*/
4 4      *o16*           1.0       1.e+10 42  *free*/
5 5      *be9*            1.0       1.e+10 42  *be* *be$*/
6 6      *arnat*          1.0       1.e+10 42  *free*/
7 7      *sinat*          1.0       1.e+10 42  *free*/
8 8      *fenat*          1.0       1.e+10 42  *free*/
*strpl* *sngam* *sfis* *chiso* *snalf* *snp* *sn2n* *snd* *snt*/
1 *trd*/
2 *ng*/
3 *nftot*/
4 *chi*/
5 *na*/
6 *np*/
7 *n2n*/
8 *nd*/
9 *nt*/
*stop*

```



```

*Unit-cell NLB Engine 50kWth P=500 atm input file
*mtx7ey* *isotxs*/
1 6 0 1 1 1 0 2 0 0/
69 2 93 20 8 8 9 9 9/
*enru* *hydr* *deut* *oxgn* *bery* *ar* *si* *fe*
*enru*          9500.          1./
*hydr*          5700.          1./
*deut*           300.          1./
*oxgn*           300.          1./
*bery*           300.          1./
*ar*             5700.          1./
*si*             300.          1./
*fe*             300.          1./
1 1      *u235*          0.96      1.e+10 42  *free*/
1 1      *u238*          0.04      1.e+10 42  *free*/
2 2      *h1*           1.0        1.e+10 42  *free*/
3 3      *h2*           1.0        1.e+10 42  *d2o*/
4 4      *o16*          1.0        1.e+10 42  *free*/
5 5      *be9*          1.0        1.e+10 42  *be* *be$*/
6 6      *arnat*        1.0        1.e+10 42  *free*/
7 7      *sinat*        1.0        1.e+10 42  *free*/
8 8      *fenat*        1.0        1.e+10 42  *free*/
*strpl* *sngam* *sfis* *chiso* *snalf* *snp* *sn2n* *snd* *snt*/
1 *trd*/
2 *ng*/
3 *nftot*/
4 *chi*/
5 *na*/
6 *np*/
7 *n2n*/
8 *nd*/
9 *nt*/
*stop*

```

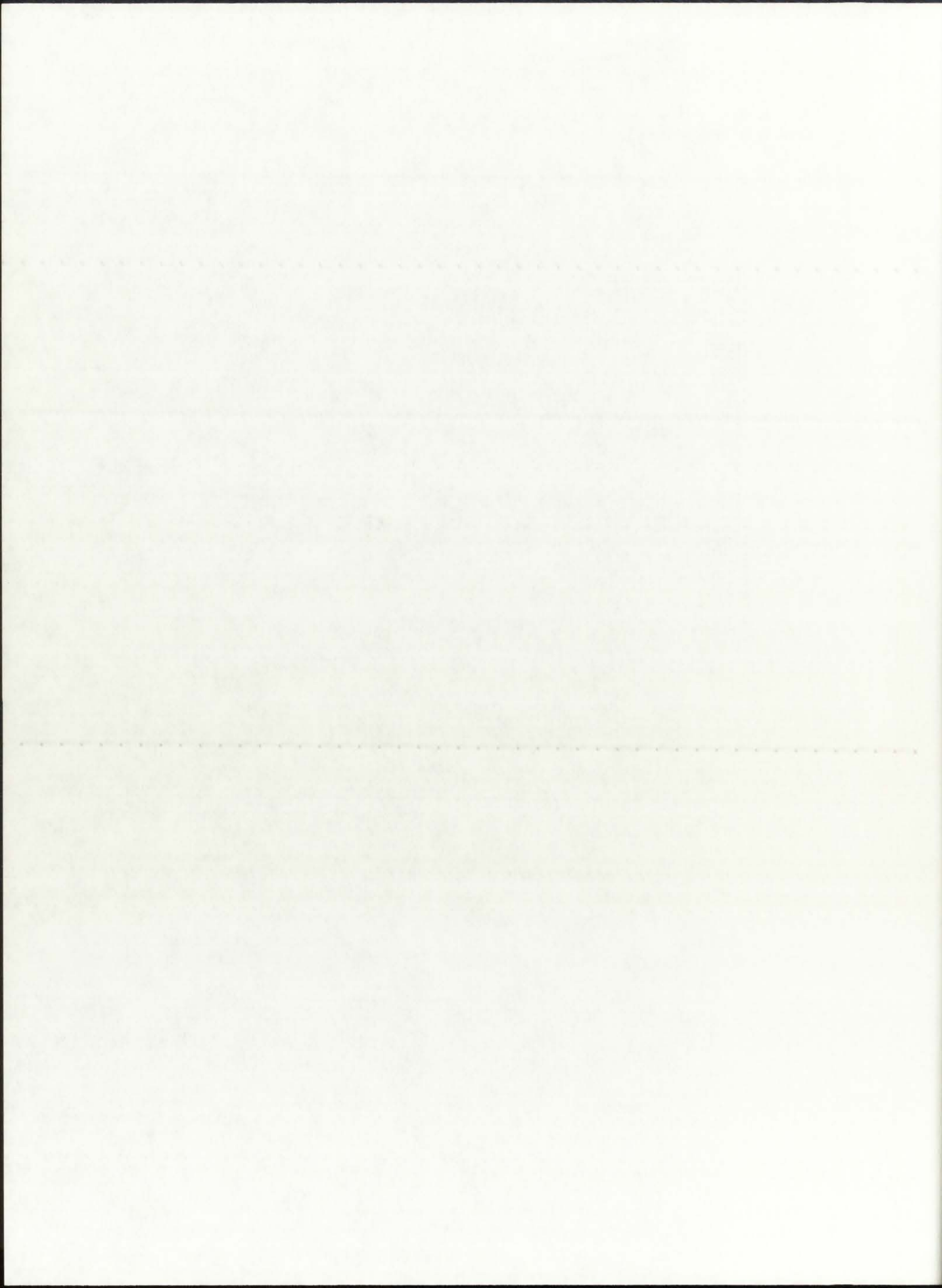
STATE OF CALIFORNIA
COUNTY OF LOS ANGELES
OFFICE OF THE COUNTY CLERK

NOTICE OF PUBLIC HEARING
ON THE APPLICATION OF
[Name] FOR
[Type of License]

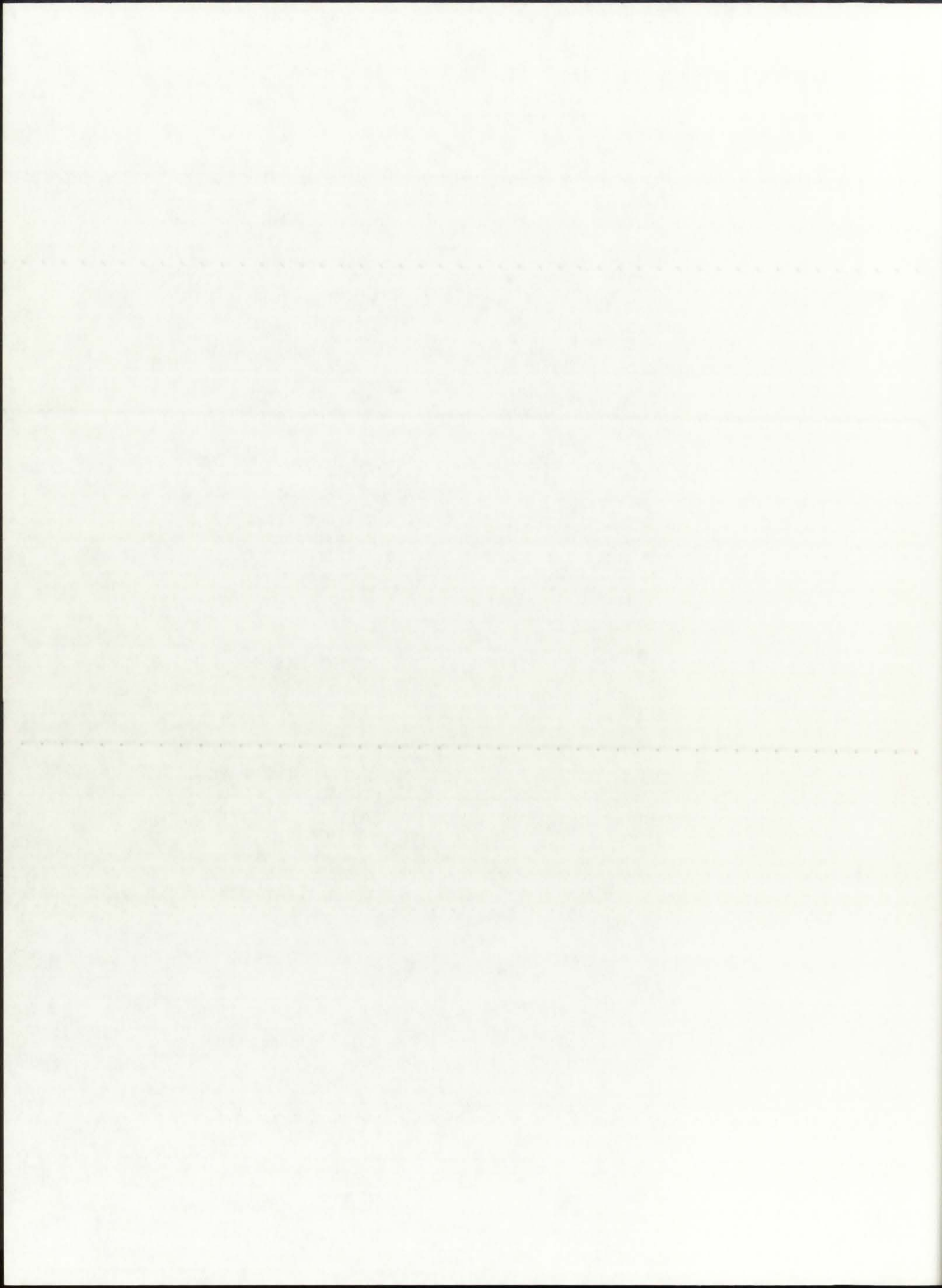
```

*Unit-cell NLB Engine 50kWth P=1000 atm input file
*mtx7ey* *isotxs*/
1 6 0 1 1 1 0 2 0 0/
69 2 93 20 8 8 9 9 9/
*enru* *hydr* *deut* *oxgn* *bery* *ar* *si* *fe*
*enru* 11400. 1./
*hydr* 6700. 1./
*deut* 300. 1./
*oxgn* 300. 1./
*bery* 300. 1./
*ar* 6700. 1./
*si* 300. 1./
*fe* 300. 1./
1 1 *u235* 0.96 1.e+10 42 *free*/
1 1 *u238* 0.04 1.e+10 42 *free*/
2 2 *h1* 1.0 1.e+10 42 *free*/
3 3 *h2* 1.0 1.e+10 42 *d2o*/
4 4 *o16* 1.0 1.e+10 42 *free*/
5 5 *be9* 1.0 1.e+10 42 *be* *be$/
6 6 *arnat* 1.0 1.e+10 42 *free*/
7 7 *sinat* 1.0 1.e+10 42 *free*/
8 8 *fenat* 1.0 1.e+10 42 *free*/
*strpl* *sngam* *sfis* *chiso* *snalf* *snp* *sn2n* *snd* *snt*/
1 *trd*/
2 *ng*/
3 *nftot*/
4 *chi*/
5 *na*/
6 *np*/
7 *n2n*/
8 *nd*/
9 *nt*/
*stop*

```



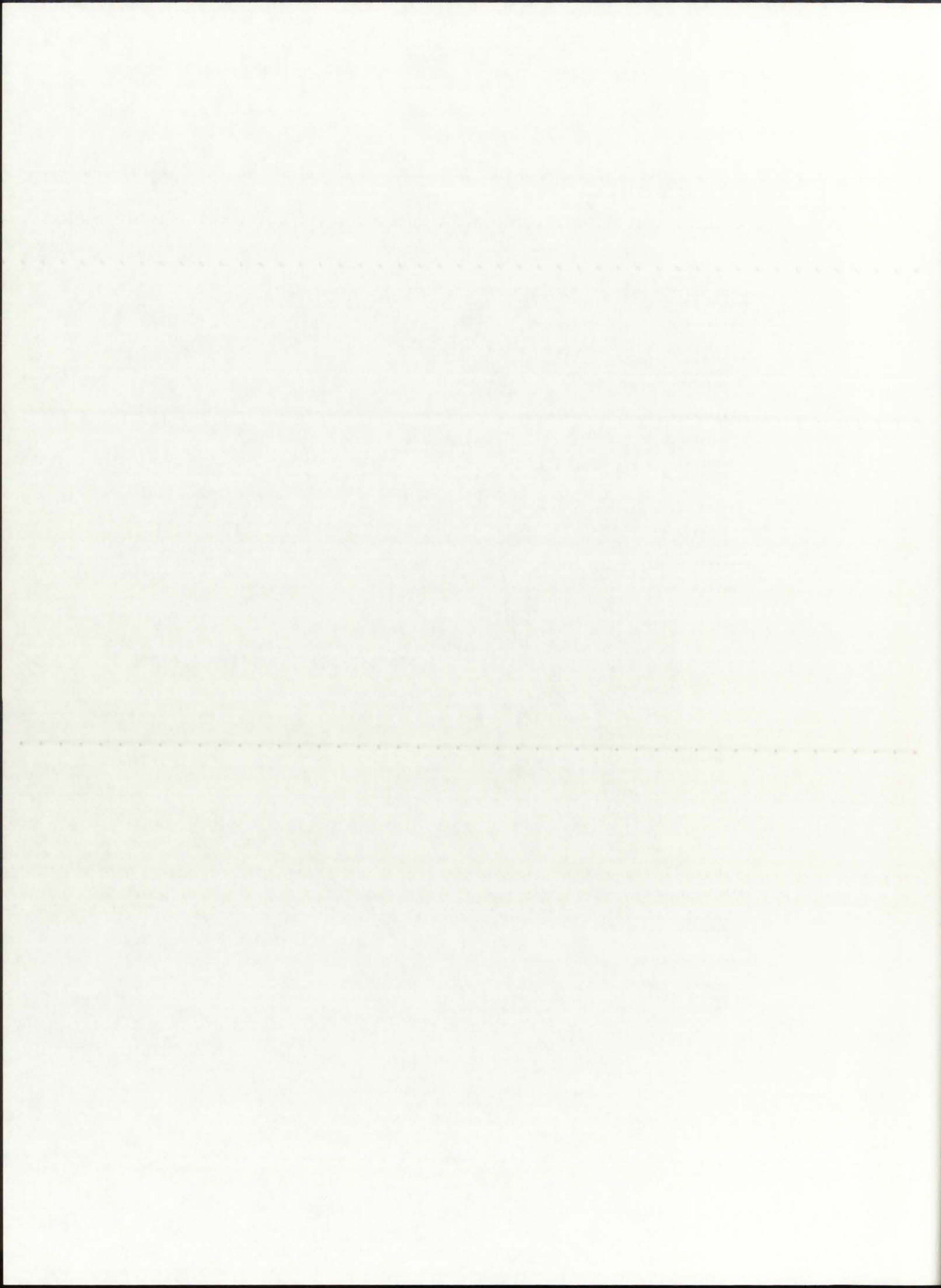
D.4. ONEDANT Input Files (ENDF/B-V)



```

2 0 0
unit-cell NLB engine - 50kWth, P=250 atm, ENDF-VI library
search for Q(r) and keff, based on T(r) from GNRATR-1D code
/
***** block i *****
/
  igeom=cylinder  ngroup=69  isn=8  niso=8  mt=10
  nzone=10  im=10  it=29
  maxlcm=500000
  maxscm=100000
  t
/
***** block ii *****
/
  xmesh=0.0,6.0,13.375,20.75,24.45,24.94,28.80,34.58,
        58.58,82.58,87.66
  xints=4 3 3 2 2 2 3 4 4 2
  zones=1 2 3 4 5 6 7 8 9 10
  t
/
***** block iii (cross sections) *****
/
  lib=isotxs
  t
/
***** block iv (mixing) *****
/
  matls=  mixtr  ar      6.0220e-5
         fuel1  enru    1.0382e-4;
         fuel2  enru    2.0763e-4;
         buffr  ar      3.0110e-4;
         sio2   si      2.6660e-2;
         prop   oxgn    5.3320e-2;
         bemod  hydr    5.9847e-4;
         d2o1   bery    1.2360e-1;
         d2o1   deut    1.8940e-2;
         d2o1   oxgn    9.4700e-3;
         d2o2   deut    1.8940e-2;
         d2o2   oxgn    9.4700e-3;
         steel  fe      8.4860e-2;
/
  assign= 1  mixtr  1.0;
         2  fuel1  1.0;
         3  fuel2  1.0;
         4  buffr  1.0;
         5  sio2   1.0;
         6  prop   1.0;
         7  bemod  1.0;
         8  d2o1   1.0;
         9  d2o2   1.0;
        10  steel  1.0;
  t
/
***** block v (solver) *****
/
  ievt=1  isct=1  ibr=0  fluxp=1  bhgt=182.73
  oitm=30  itm=100
  t
/
***** block vi (edits) *****
/
  pted=1  zned=1  icoll=69;  igrped=3
  edxs=n-fiss
  resdnt=1  mevper=176.0  power=0.0002736  rzflux=1
/

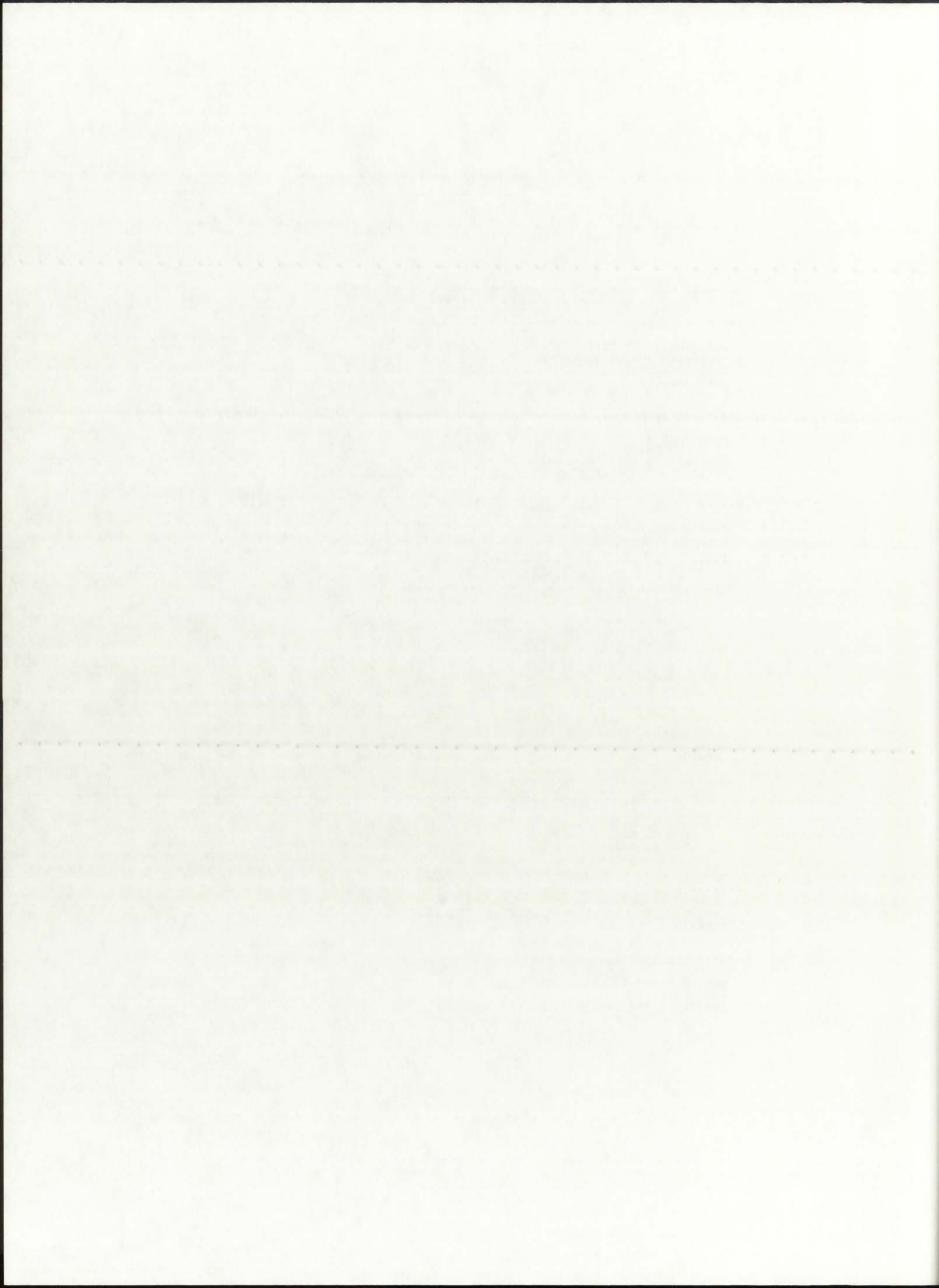
```



```

2 0 0
unit-cell NLB engine - 50kWth, P=500 atm, ENDF-VI library
search for Q(r) and keff, based on T(r) from GNRATR-1D code
/
/***** block i *****/
/
  igeom=cylinder ngroup=69 isn=8 niso=8 mt=10
  nzone=10 im=10 it=29
  maxlcm=500000
  maxscm=100000
  t
/
/***** block ii *****/
/
  xmesh=0.0,6.0,13.375,20.75,24.45,24.94,28.80,34.58,
        58.58,82.58,87.66
  xints=4 3 3 2 2 2 3 4 4 2
  zones=1 2 3 4 5 6 7 8 9 10
  t
/
/***** block iii (cross sections) *****/
/
  lib=isotxs
  t
/
/***** block iv (mixing) *****/
/
  mats=  mixtr  ar      9.1690e-5
        enru    1.7850e-4;
        fuel1  enru    3.5700e-4;
        fuel2  enru    4.1902e-4;
        buffr  ar      4.1000e-4;
        sio2   si      2.6660e-2;
        oxgn   oxgn    5.3320e-2;
        prop   hydr    8.1246e-4;
        bemod  bery    1.2360e-1;
        d2o1   deut    1.8940e-2;
        oxgn   oxgn    9.4700e-3;
        d2o2   deut    1.8940e-2;
        oxgn   oxgn    9.4700e-3;
        steel  fe      8.4860e-2;
/
  assign= 1  mixtr  1.0;
         2  fuel1  1.0;
         3  fuel2  1.0;
         4  buffr  1.0;
         5  sio2   1.0;
         6  prop   1.0;
         7  bemod  1.0;
         8  d2o1   1.0;
         9  d2o2   1.0;
        10  steel  1.0;
  t
/
/***** block v (solver) *****/
/
  ievt=1  isct=1  ibr=0  fluxp=1  bhgt=182.73
  oitm=30  iitm=100
  t
/
/***** block vi (edits) *****/
/
  pted=1  zned=1  icoll=69;  igrped=3
  edxs=n-fiss
  resdnt=1  mevper=176.0  power=0.0002736  rzflux=1
/

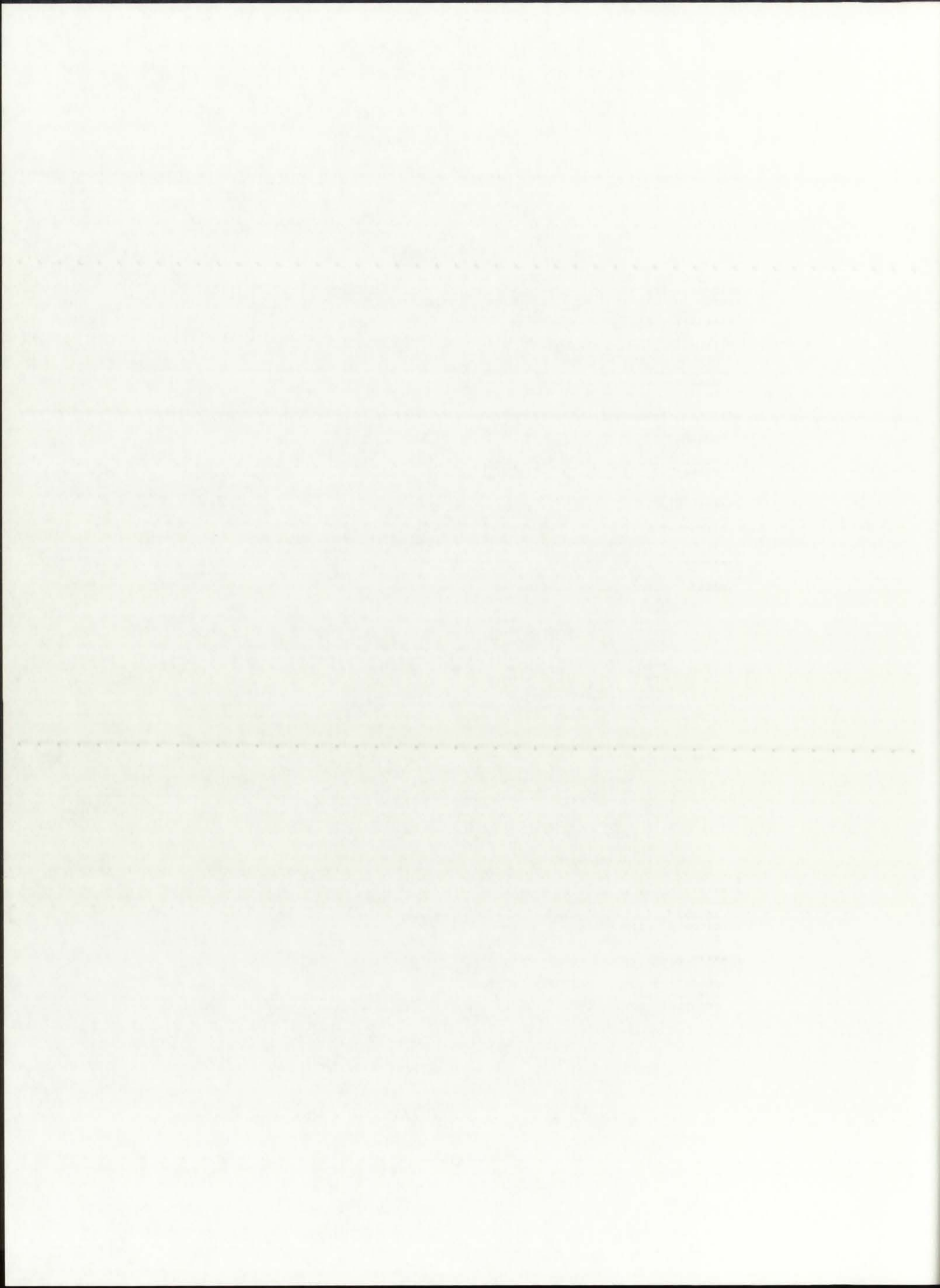
```



```

2 0 0
unit-cell NLB engine - 50kWth, P=1000 atm, ENDF-VI library
search for Q(r) and keff, based on T(r) from GNRATR-1D code
/
/***** block i *****/
/
  igeom=cylinder  ngroup=69  isn=8  niso=8  mt=10
  nzone=10  im=10  it=29
  maxlcm=500000
  maxscm=100000
  t
/
/***** block ii *****/
/
  xmesh=0.0,6.0,13.375,20.75,24.45,24.94,28.80,34.58,
        58.58,82.58,87.66
  xints=4 3 3 2 2 2 3 4 4 2
  zones=1 2 3 4 5 6 7 8 9 10
  t
/
/***** block iii (cross sections) *****/
/
  lib=isotxs
  t
/
/***** block iv (mixing) *****/
/
  matls=  mixtr  ar      1.5660e-4
         enru    2.7370e-4;
         fuel1  enru    5.4740e-4;
         fuel2  enru    6.5607e-4;
         buffr  ar      6.8888e-4;
         sio2   si      2.6660e-2;
         oxgn   oxgn    5.3320e-2;
         prop   hydr    1.3663e-3;
         bemod  bery    1.2360e-1;
         d2o1   deut    1.8940e-2;
         oxgn   oxgn    9.4700e-3;
         d2o2   deut    1.8940e-2;
         oxgn   oxgn    9.4700e-3;
         steel  fe      8.4860e-2;
/
  assign= 1  mixtr  1.0;
         2  fuel1  1.0;
         3  fuel2  1.0;
         4  buffr  1.0;
         5  sio2   1.0;
         6  prop   1.0;
         7  bemod  1.0;
         8  d2o1   1.0;
         9  d2o2   1.0;
        10  steel  1.0;
  t
/
/***** block v (solver) *****/
/
  ievt=1  isct=1  ibr=0  fluxp=1  bhgt=182.73
  oitm=30  iitm=100
  t
/
/***** block vi (edits) *****/
/
  pted=1  zned=1  icoll=69;  igrped=3
  edxs=n-fiss
  resdnt=1  mevper=176.0  power=0.0002736  rzflux=1
/

```



D.5. GNRATR-1D Summary Output Files (ENDF/B-V)

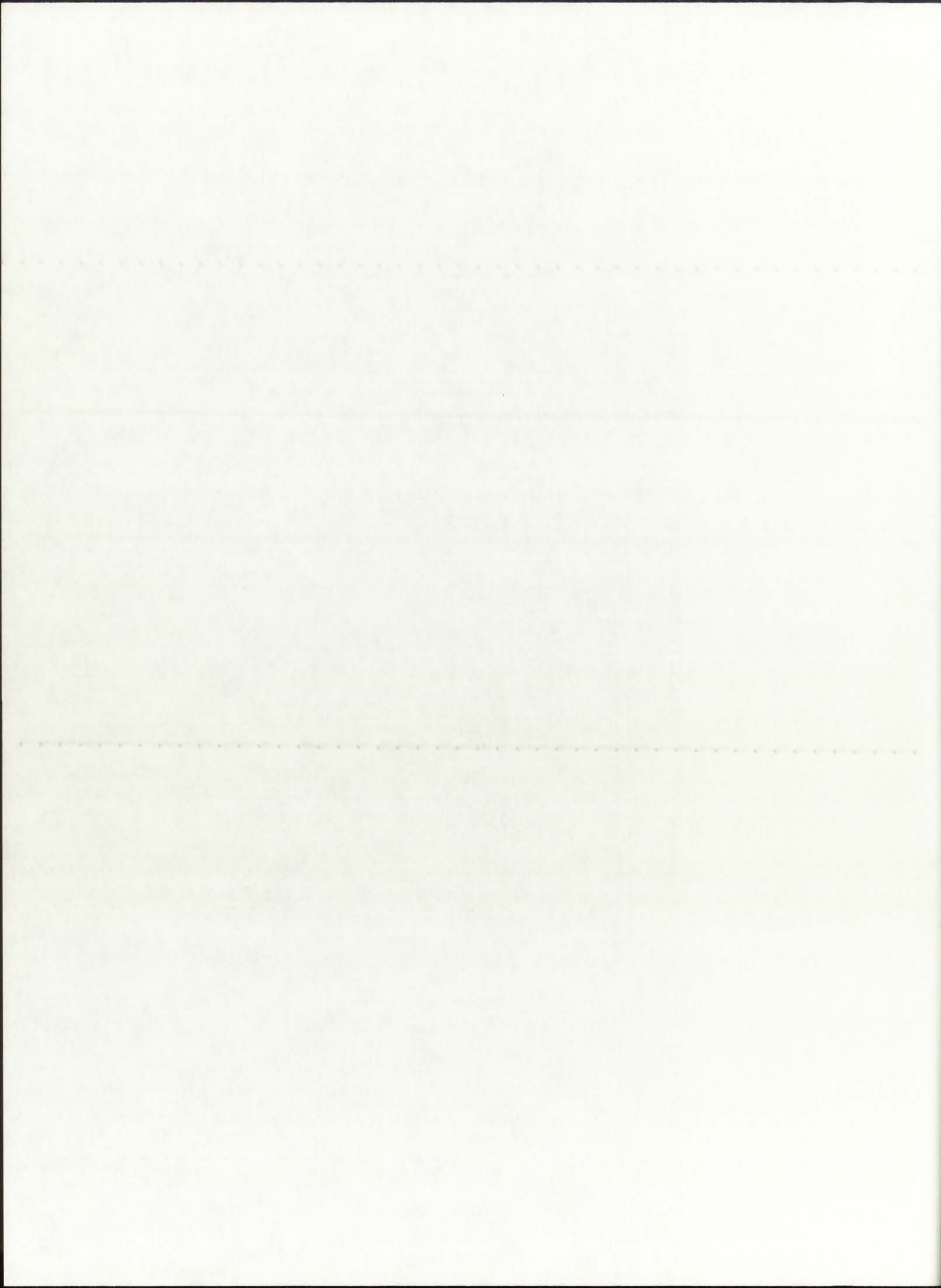
U.S. CHARITABLE SUMMARY OUTPUT FORM (1977)

==== SUMMARY OF CONVERGED VALUES ====

This Case Executed for: REFLBe = 0.00000
Pressure = 250.0 atm

Modes of Heat Transfer: Radiation in BG, SiW, and P = .on.
Convection in BG = .on.
Convection in P = .on.

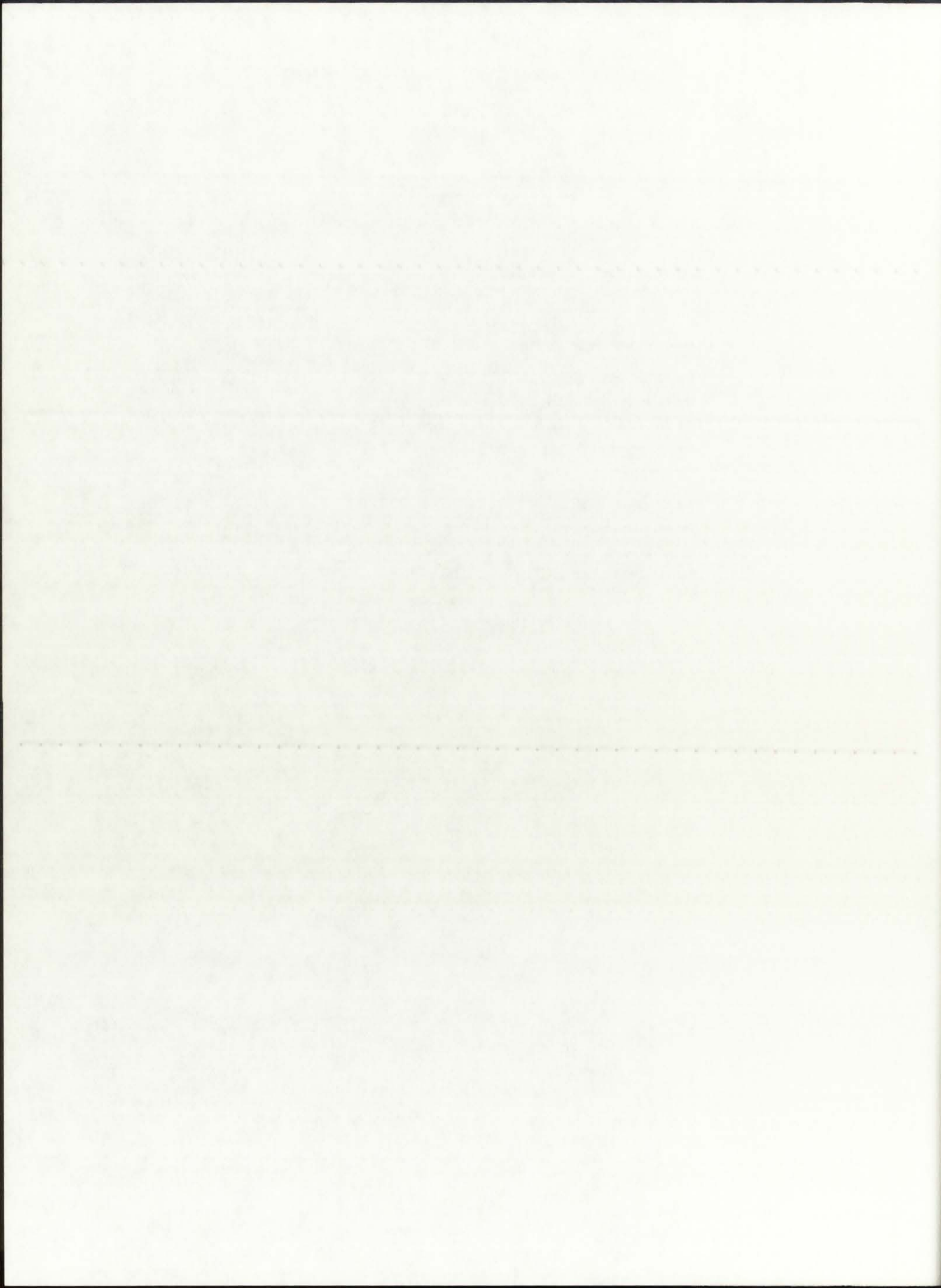
i	r(i)	T(i)	Qg(i)
37	0.000	8559.5	0.6274E+05
36	0.019	8559.5	0.6194E+05
35	0.039	8554.6	0.1255E+06
34	0.059	8539.8	0.1358E+06
33	0.096	8444.1	0.1920E+06
32	0.133	8228.3	0.2300E+06
31	0.170	7820.5	0.3447E+06
30	0.207	4833.2	0.0000E+00
29	0.225	4833.2	0.0000E+00
28	0.244	4833.2	0.0000E+00
27	0.246	4833.2	0.0000E+00
26	0.249	4833.1	0.0000E+00
25	0.268	4833.1	0.0000E+00
24	0.287	4833.0	0.0000E+00
23	0.307	4830.6	0.0000E+00
22	0.326	4828.5	0.0000E+00
21	0.345	4826.6	0.0000E+00
20	0.405	3828.4	0.0000E+00
19	0.465	3087.7	0.0000E+00
18	0.525	2516.3	0.0000E+00
17	0.585	2062.3	0.0000E+00
16	0.645	1692.8	0.0000E+00
15	0.705	1386.5	0.0000E+00
14	0.765	1128.6	0.0000E+00
13	0.825	908.4	0.0000E+00
12	0.851	907.5	0.0000E+00
11	0.876	907.1	0.0000E+00
10	0.976	769.9	0.0000E+00
9	1.076	658.6	0.0000E+00
8	1.176	566.4	0.0000E+00
7	1.276	489.0	0.0000E+00
6	1.376	423.0	0.0000E+00
5	1.476	366.1	0.0000E+00
4	1.576	316.6	0.0000E+00
3	1.676	273.0	0.0000E+00
2	1.776	234.4	0.0000E+00
1	1.876	200.0	0.0000E+00



==== ROCKET ENGINE PARAMETERS ====

The H2 dissociation fraction is: 0.0891
The H2 average molecular weight is: 1.9262 g/gmol
The propellant molecular weight is: 7.3839 g/gmol
The cross-sectional flow area is: 0.0721 m2
The propellant mass flow rate is: 0.10 kg/s

The chamber temperature is: 4833.1 K
The calculated exit velocity is: 7903.5 m/s
The calculated thrust is: 0.8 kN
The calculated specific impulse is: 805.9 s

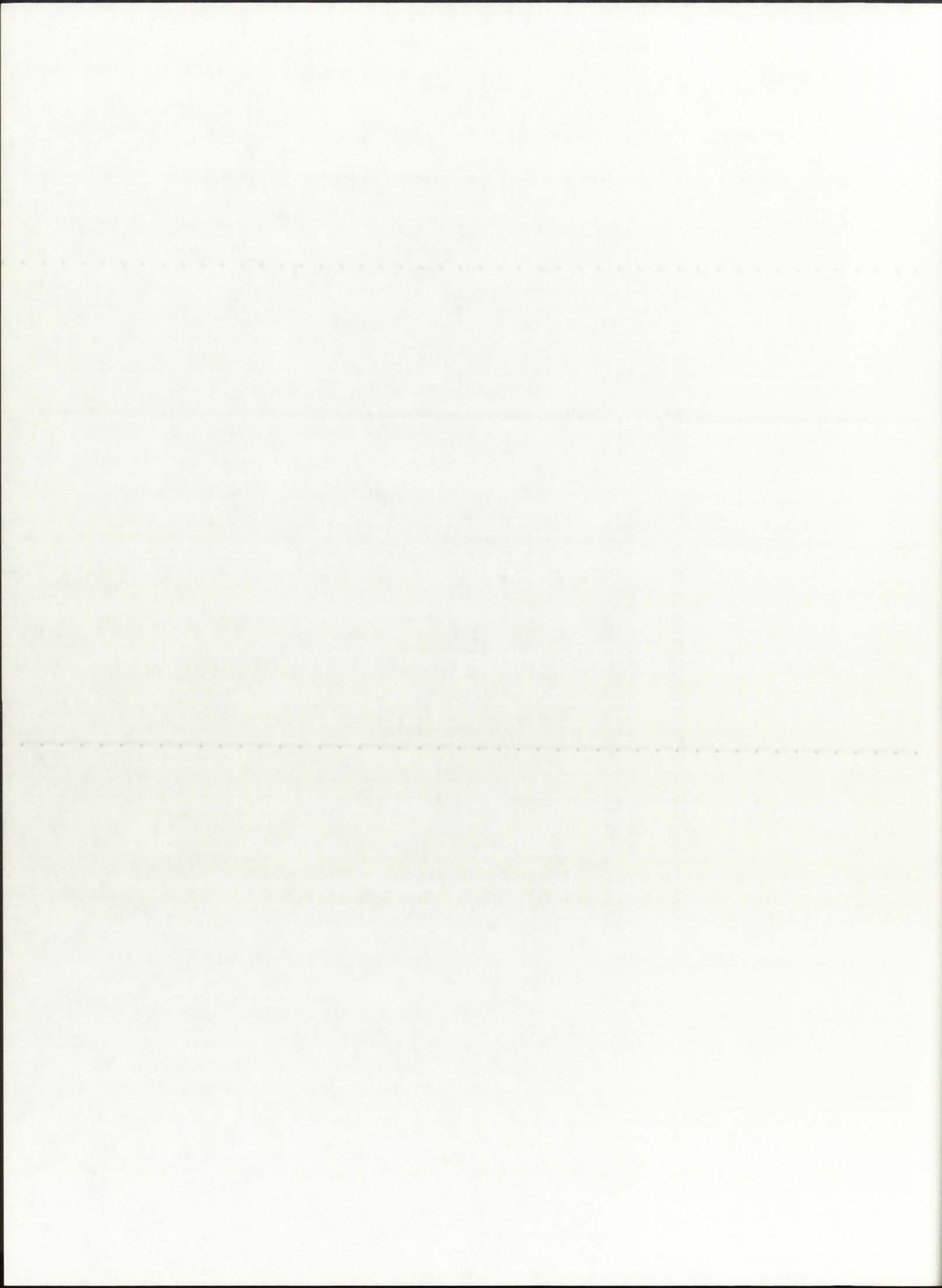


==== SUMMARY OF CONVERGED VALUES ====

This Case Executed for: REFLBe = 0.00000
 Pressure = 500.0 atm

Modes of Heat Transfer: Radiation in BG, SiW, and P = .on.
 Convection in BG = .on.
 Convection in P = .on.

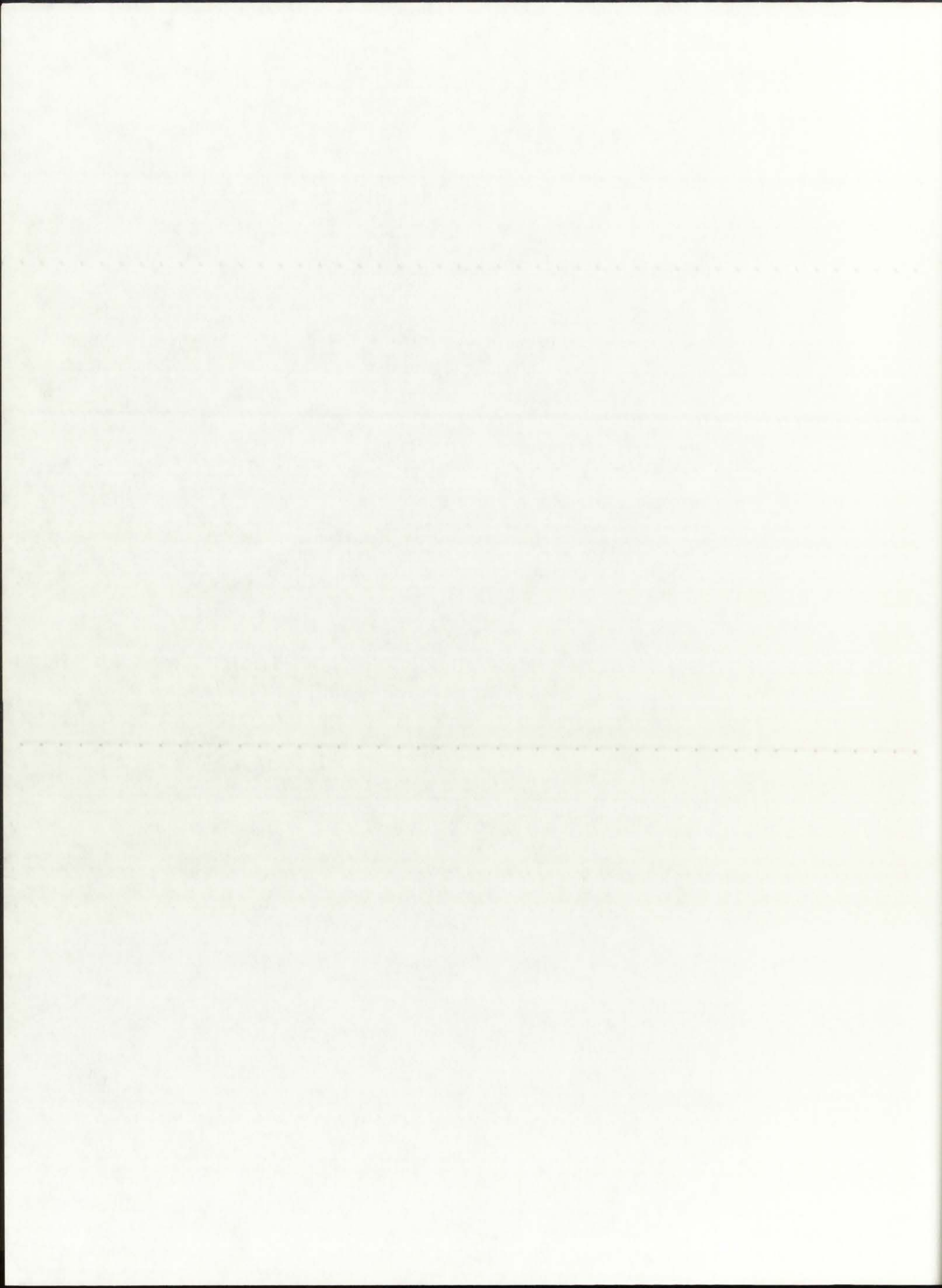
i	r(i)	T(i)	Qg(i)
37	0.000	10211.8	0.5751E+05
36	0.019	10211.8	0.5705E+05
35	0.039	10206.6	0.1170E+06
34	0.059	10190.3	0.1289E+06
33	0.096	10084.1	0.1749E+06
32	0.133	9853.4	0.2180E+06
31	0.170	9417.3	0.3815E+06
30	0.207	5717.0	0.0000E+00
29	0.225	5717.0	0.0000E+00
28	0.244	5717.0	0.0000E+00
27	0.246	5717.0	0.0000E+00
26	0.249	5717.0	0.0000E+00
25	0.268	5717.0	0.0000E+00
24	0.287	5716.9	0.0000E+00
23	0.307	5714.1	0.0000E+00
22	0.326	5711.5	0.0000E+00
21	0.345	5709.3	0.0000E+00
20	0.405	4520.2	0.0000E+00
19	0.465	3637.9	0.0000E+00
18	0.525	2957.2	0.0000E+00
17	0.585	2416.3	0.0000E+00
16	0.645	1976.3	0.0000E+00
15	0.705	1611.4	0.0000E+00
14	0.765	1304.1	0.0000E+00
13	0.825	1041.9	0.0000E+00
12	0.851	1040.8	0.0000E+00
11	0.876	1040.2	0.0000E+00
10	0.976	877.2	0.0000E+00
9	1.076	744.9	0.0000E+00
8	1.176	635.5	0.0000E+00
7	1.276	543.4	0.0000E+00
6	1.376	465.0	0.0000E+00
5	1.476	397.4	0.0000E+00
4	1.576	338.5	0.0000E+00
3	1.676	286.8	0.0000E+00
2	1.776	240.9	0.0000E+00
1	1.876	200.0	0.0000E+00



==== ROCKET ENGINE PARAMETERS ====

The H2 dissociation fraction is: 0.1555
The H2 average molecular weight is: 1.8592 g/gmol
The propellant molecular weight is: 7.3189 g/gmol
The cross-sectional flow area is: 0.0721 m2
The propellant mass flow rate is: 0.14 kg/s

The chamber temperature is: 5717.0 K
The calculated exit velocity is: 7995.2 m/s
The calculated thrust is: 1.2 kN
The calculated specific impulse is: 815.3 s

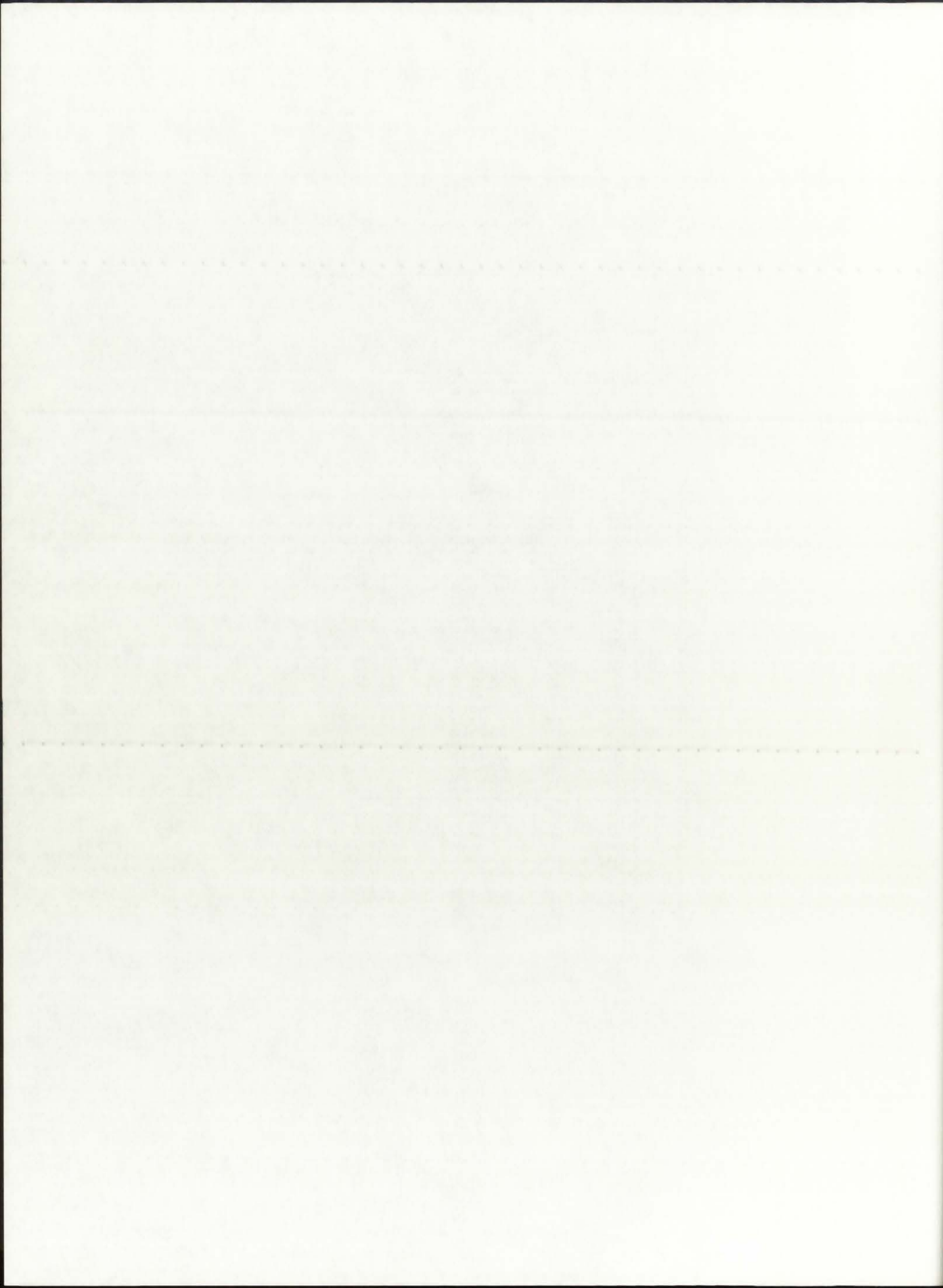


==== SUMMARY OF CONVERGED VALUES ====

This Case Executed for: REFLBe = 0.00000
 Pressure = 1000.0 atm

Modes of Heat Transfer: Radiation in BG, SiW, and P = .on.
 Convection in BG = .on.
 Convection in P = .on.

i	r(i)	T(i)	Qg(i)
37	0.000	12247.5	0.5350E+05
36	0.019	12247.5	0.5327E+05
35	0.039	12241.7	0.1091E+06
34	0.059	12223.8	0.1185E+06
33	0.096	12108.9	0.1624E+06
32	0.133	11859.6	0.2040E+06
31	0.170	11393.9	0.4178E+06
30	0.207	6791.1	0.0000E+00
29	0.225	6791.1	0.0000E+00
28	0.244	6791.1	0.0000E+00
27	0.246	6791.1	0.0000E+00
26	0.249	6791.1	0.0000E+00
25	0.268	6791.1	0.0000E+00
24	0.287	6791.0	0.0000E+00
23	0.307	6787.6	0.0000E+00
22	0.326	6784.6	0.0000E+00
21	0.345	6781.9	0.0000E+00
20	0.405	5360.9	0.0000E+00
19	0.465	4306.4	0.0000E+00
18	0.525	3493.0	0.0000E+00
17	0.585	2846.6	0.0000E+00
16	0.645	2320.7	0.0000E+00
15	0.705	1884.7	0.0000E+00
14	0.765	1517.4	0.0000E+00
13	0.825	1204.0	0.0000E+00
12	0.851	1202.7	0.0000E+00
11	0.876	1202.1	0.0000E+00
10	0.976	1007.6	0.0000E+00
9	1.076	849.9	0.0000E+00
8	1.176	719.3	0.0000E+00
7	1.276	609.6	0.0000E+00
6	1.376	516.1	0.0000E+00
5	1.476	435.4	0.0000E+00
4	1.576	365.2	0.0000E+00
3	1.676	303.5	0.0000E+00
2	1.776	248.8	0.0000E+00
1	1.876	200.0	0.0000E+00



==== ROCKET ENGINE PARAMETERS ====

The H2 dissociation fraction is: 0.2397
The H2 average molecular weight is: 1.7743 g/gmol
The propellant molecular weight is: 7.2366 g/gmol
The cross-sectional flow area is: 0.0721 m2
The propellant mass flow rate is: 0.20 kg/s

The chamber temperature is: 6791.1 K
The calculated exit velocity is: 8399.3 m/s
The calculated thrust is: 1.6 kN
The calculated specific impulse is: 856.5 s

Faint, illegible text at the top of the page, possibly a header or title.

THE UNIVERSITY OF CHICAGO
DEPARTMENT OF CHEMISTRY
5800 S. UNIVERSITY AVENUE
CHICAGO, ILLINOIS 60637
TEL: 773-936-3700
WWW.CHEM.UCHICAGO.EDU

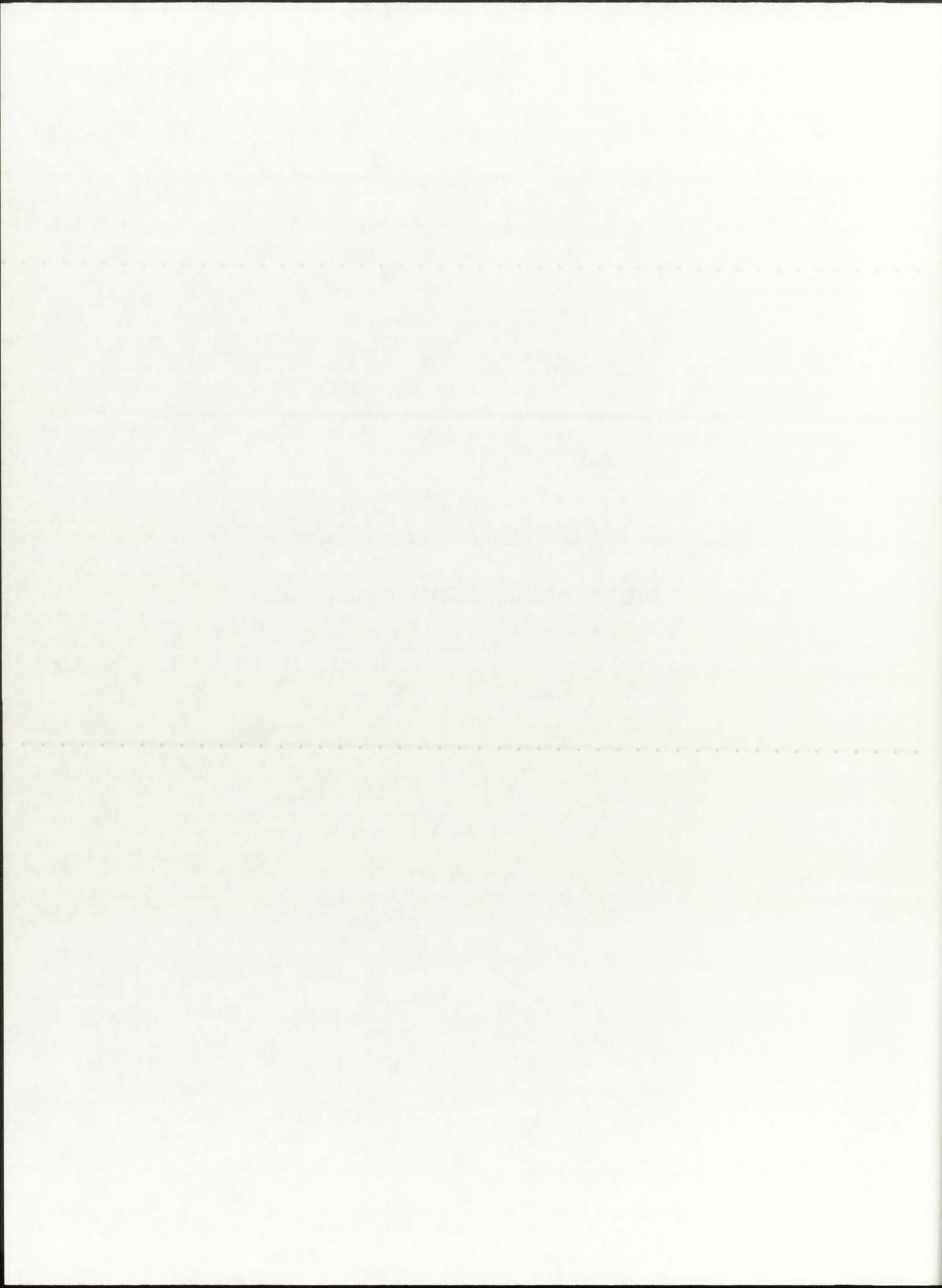
APPENDIX E

50 kWth, 250 atm Baseline Configuration

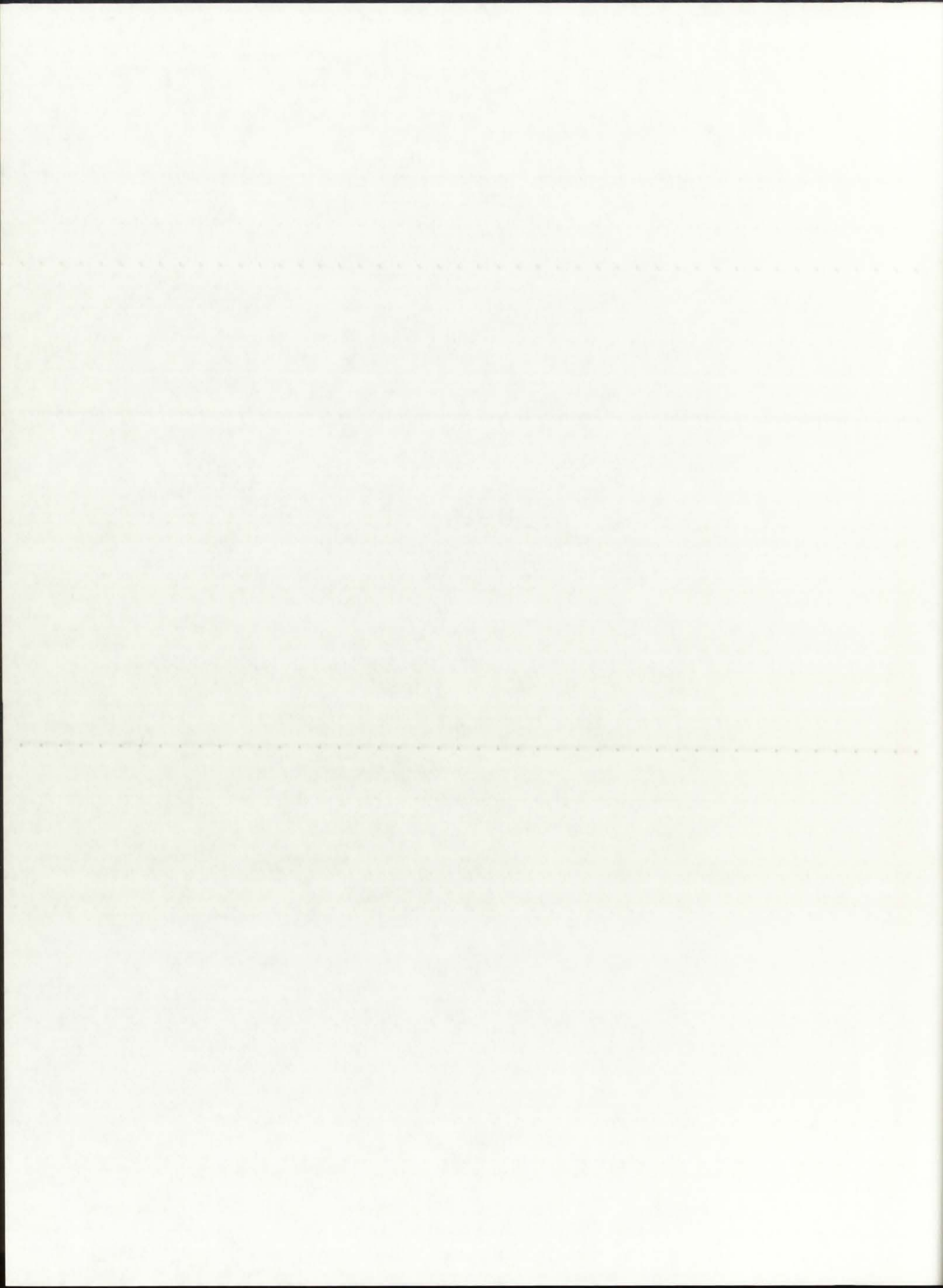
E.1: Combination I

E.2: Combination II

E.3: Combination III



E.1. Combination I

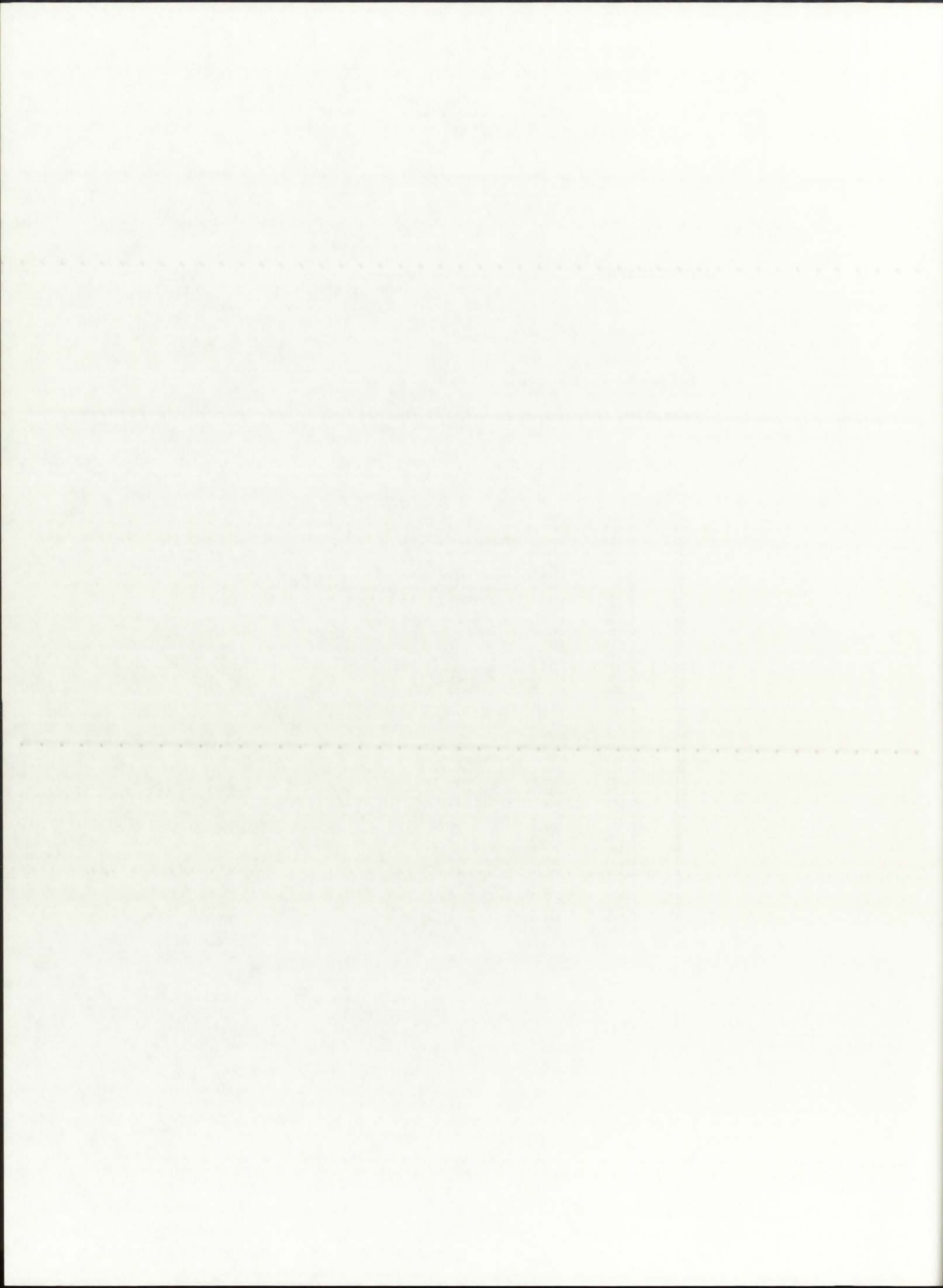


==== SUMMARY OF CONVERGED VALUES ====

This Case Executed for: REFLBe = 0.00000
 Pressure = 250.0 atm

Modes of Heat Transfer: Radiation in BG, SiW, and P = .on.
 Convection in BG = .on.
 Convection in P = .on.

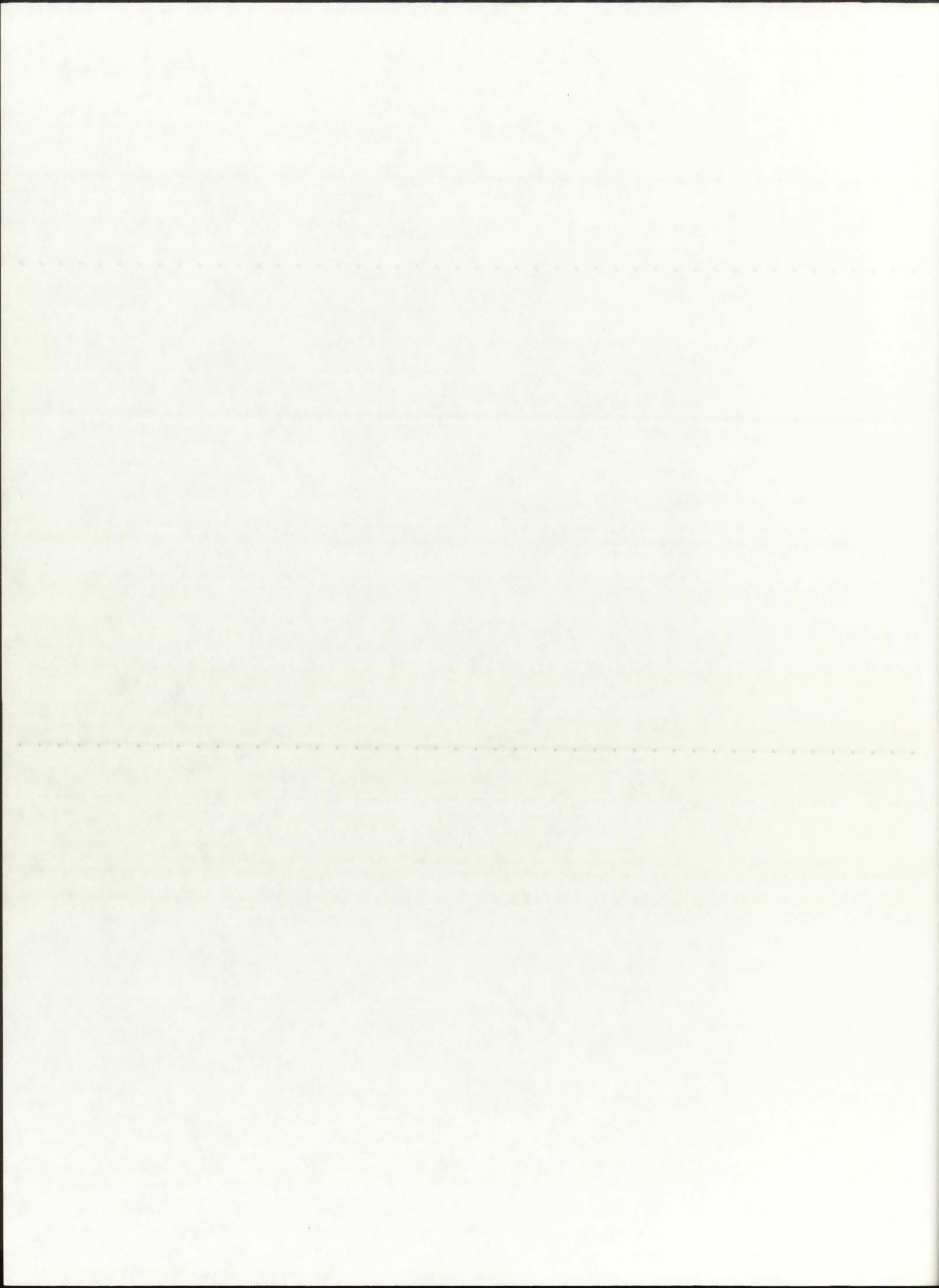
i	r(i)	T(i)	Qg(i)
37	0.000	8559.5	0.6274E+05
36	0.019	8559.5	0.6195E+05
35	0.039	8554.6	0.1255E+06
34	0.059	8539.8	0.1358E+06
33	0.096	8444.1	0.1920E+06
32	0.133	8228.3	0.2300E+06
31	0.170	7820.5	0.3447E+06
30	0.207	4833.2	0.0000E+00
29	0.225	4833.2	0.0000E+00
28	0.244	4833.2	0.0000E+00
27	0.246	4833.2	0.0000E+00
26	0.249	4833.1	0.0000E+00
25	0.268	4833.1	0.0000E+00
24	0.287	4833.0	0.0000E+00
23	0.307	4830.4	0.0000E+00
22	0.326	4828.2	0.0000E+00
21	0.345	4826.2	0.0000E+00
20	0.405	3771.7	0.0000E+00
19	0.465	2989.2	0.0000E+00
18	0.525	2385.6	0.0000E+00
17	0.585	1906.0	0.0000E+00
16	0.645	1515.7	0.0000E+00
15	0.705	1192.2	0.0000E+00
14	0.765	919.6	0.0000E+00
13	0.825	687.1	0.0000E+00
12	0.851	686.1	0.0000E+00
11	0.876	685.7	0.0000E+00
10	0.976	591.0	0.0000E+00
9	1.076	514.2	0.0000E+00
8	1.176	450.8	0.0000E+00
7	1.276	397.7	0.0000E+00
6	1.376	352.4	0.0000E+00
5	1.476	313.4	0.0000E+00
4	1.576	279.6	0.0000E+00
3	1.676	249.8	0.0000E+00
2	1.776	223.5	0.0000E+00
1	1.876	200.0	0.0000E+00



==== ROCKET ENGINE PARAMETERS ====

The H2 dissociation fraction is: 0.0891
The H2 average molecular weight is: 1.9262 g/gmol
The propellant molecular weight is: 7.3839 g/gmol
The cross-sectional flow area is: 0.0721 m²
The propellant mass flow rate is: 0.10 kg/s

The chamber temperature is: 4833.1 K
The calculated exit velocity is: 7903.5 m/s
The calculated thrust is: 0.8 kN
The calculated specific impulse is: 805.9 s

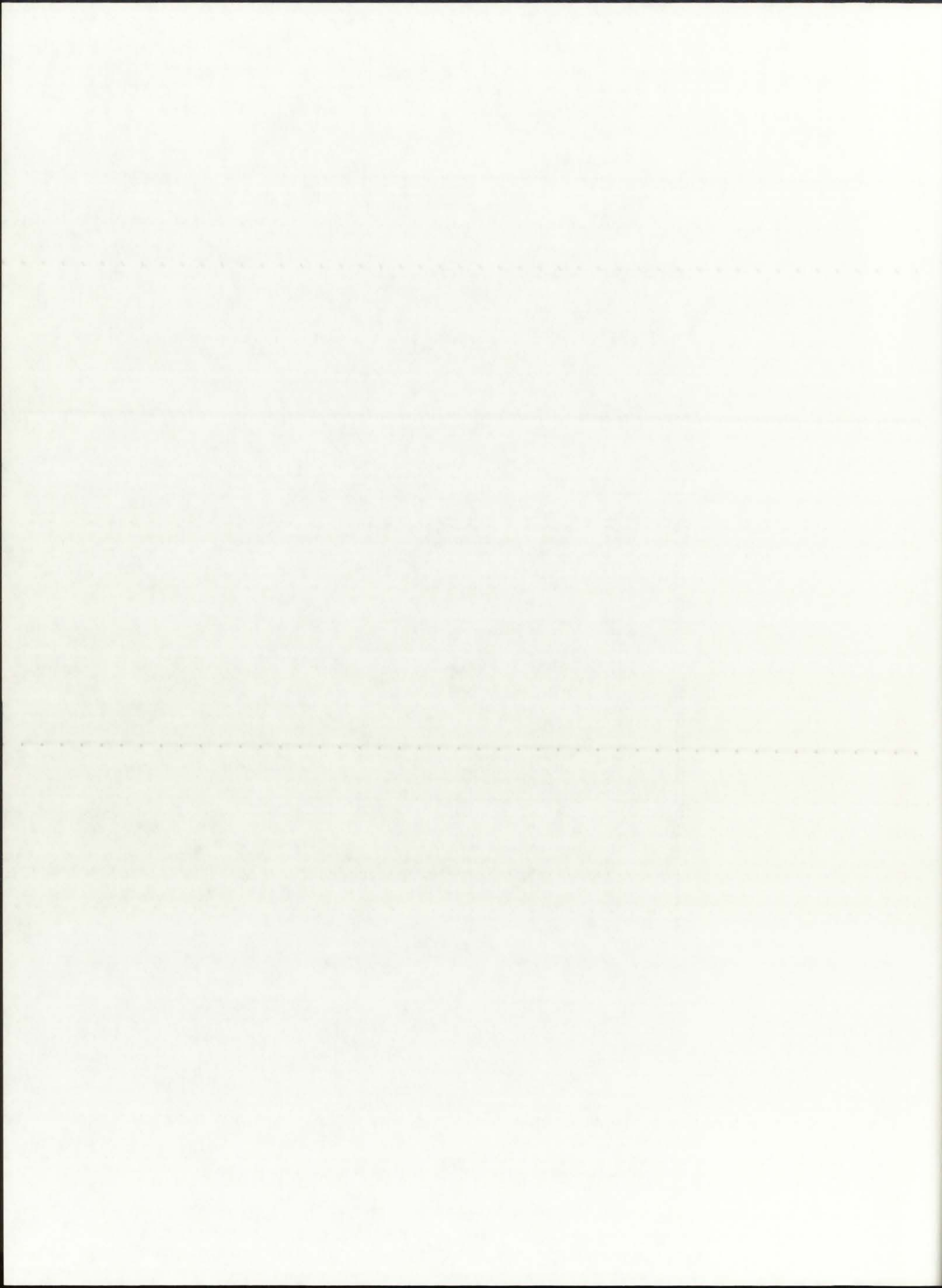


==== SUMMARY OF CONVERGED VALUES ====

This Case Executed for: REFLBe = 0.99000
 Pressure = 250.0 atm

Modes of Heat Transfer: Radiation in BG, SiW, and P = .on.
 Convection in BG = .on.
 Convection in P = .on.

i	r(i)	T(i)	Qg(i)
37	0.000	8559.6	0.6274E+05
36	0.019	8559.6	0.6195E+05
35	0.039	8554.7	0.1255E+06
34	0.059	8539.9	0.1358E+06
33	0.096	8444.2	0.1920E+06
32	0.133	8228.4	0.2300E+06
31	0.170	7820.6	0.3447E+06
30	0.207	4833.0	0.0000E+00
29	0.225	4833.0	0.0000E+00
28	0.244	4833.0	0.0000E+00
27	0.246	4832.1	0.0000E+00
26	0.249	4831.2	0.0000E+00
25	0.268	4823.6	0.0000E+00
24	0.287	4817.0	0.0000E+00
23	0.307	4814.4	0.0000E+00
22	0.326	4812.2	0.0000E+00
21	0.345	4810.2	0.0000E+00
20	0.405	3757.5	0.0000E+00
19	0.465	2976.4	0.0000E+00
18	0.525	2373.8	0.0000E+00
17	0.585	1895.0	0.0000E+00
16	0.645	1505.4	0.0000E+00
15	0.705	1182.4	0.0000E+00
14	0.765	910.3	0.0000E+00
13	0.825	678.2	0.0000E+00
12	0.851	677.2	0.0000E+00
11	0.876	676.7	0.0000E+00
10	0.976	583.8	0.0000E+00
9	1.076	508.4	0.0000E+00
8	1.176	446.2	0.0000E+00
7	1.276	394.0	0.0000E+00
6	1.376	349.6	0.0000E+00
5	1.476	311.3	0.0000E+00
4	1.576	278.1	0.0000E+00
3	1.676	248.9	0.0000E+00
2	1.776	223.0	0.0000E+00
1	1.876	200.0	0.0000E+00



==== ROCKET ENGINE PARAMETERS ====

The H2 dissociation fraction is: 0.0881
The H2 average molecular weight is: 1.9272 g/gmol
The propellant molecular weight is: 7.3849 g/gmol
The cross-sectional flow area is: 0.0721 m2
The propellant mass flow rate is: 0.10 kg/s

The chamber temperature is: 4823.6 K
The calculated exit velocity is: 7895.2 m/s
The calculated thrust is: 0.8 kN
The calculated specific impulse is: 805.1 s

Faint, illegible text at the top of the page, possibly a header or introductory paragraph.

Main body of faint, illegible text, appearing to be several lines of a document or list.

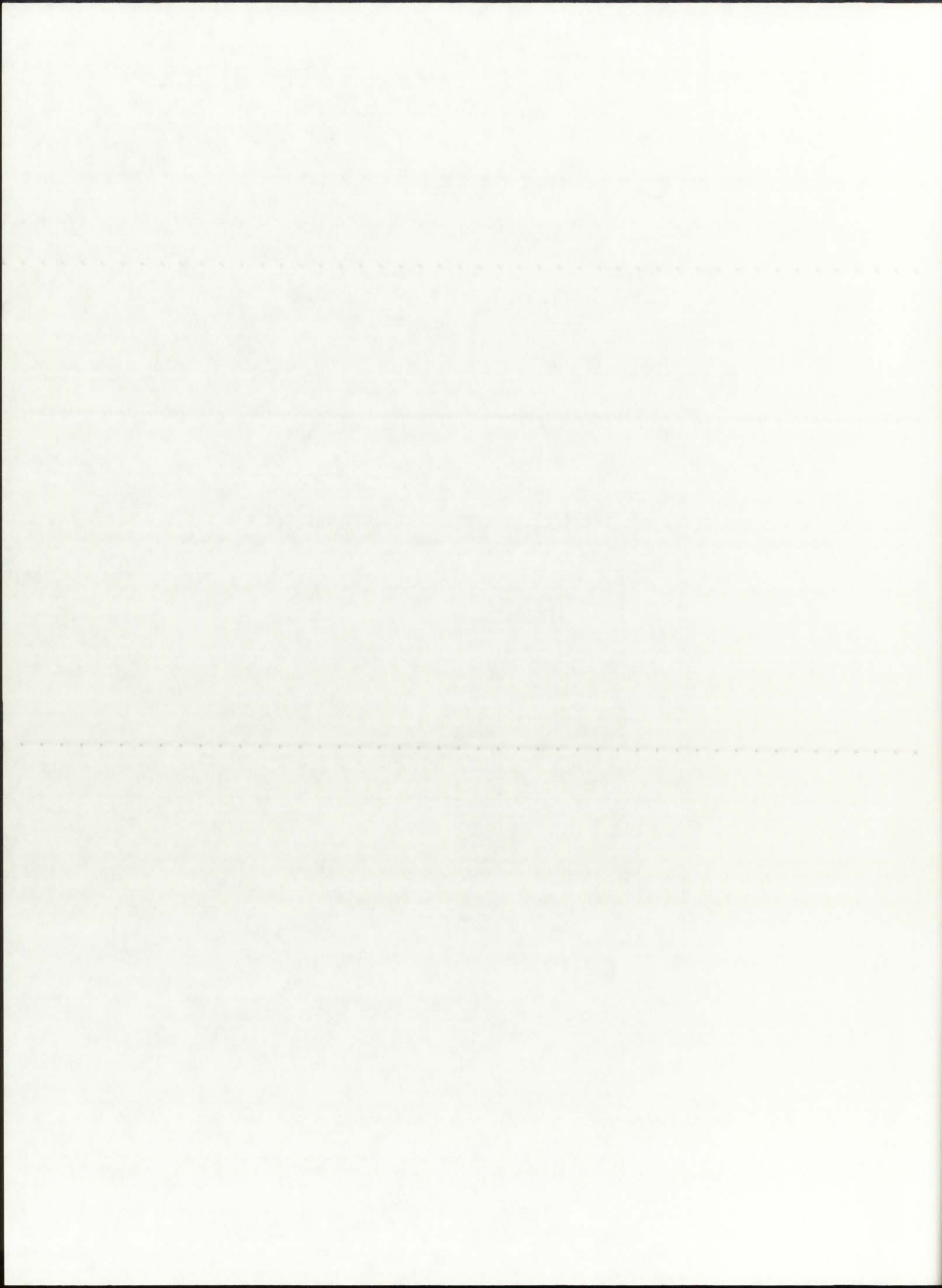
A horizontal line of faint, illegible text, possibly a separator or a specific entry.

==== SUMMARY OF CONVERGED VALUES ====

This Case Executed for: REFLBe = 1.00000
 Pressure = 250.0 atm

Modes of Heat Transfer: Radiation in BG, SiW, and P = .on.
 Convection in BG = .on.
 Convection in P = .on.

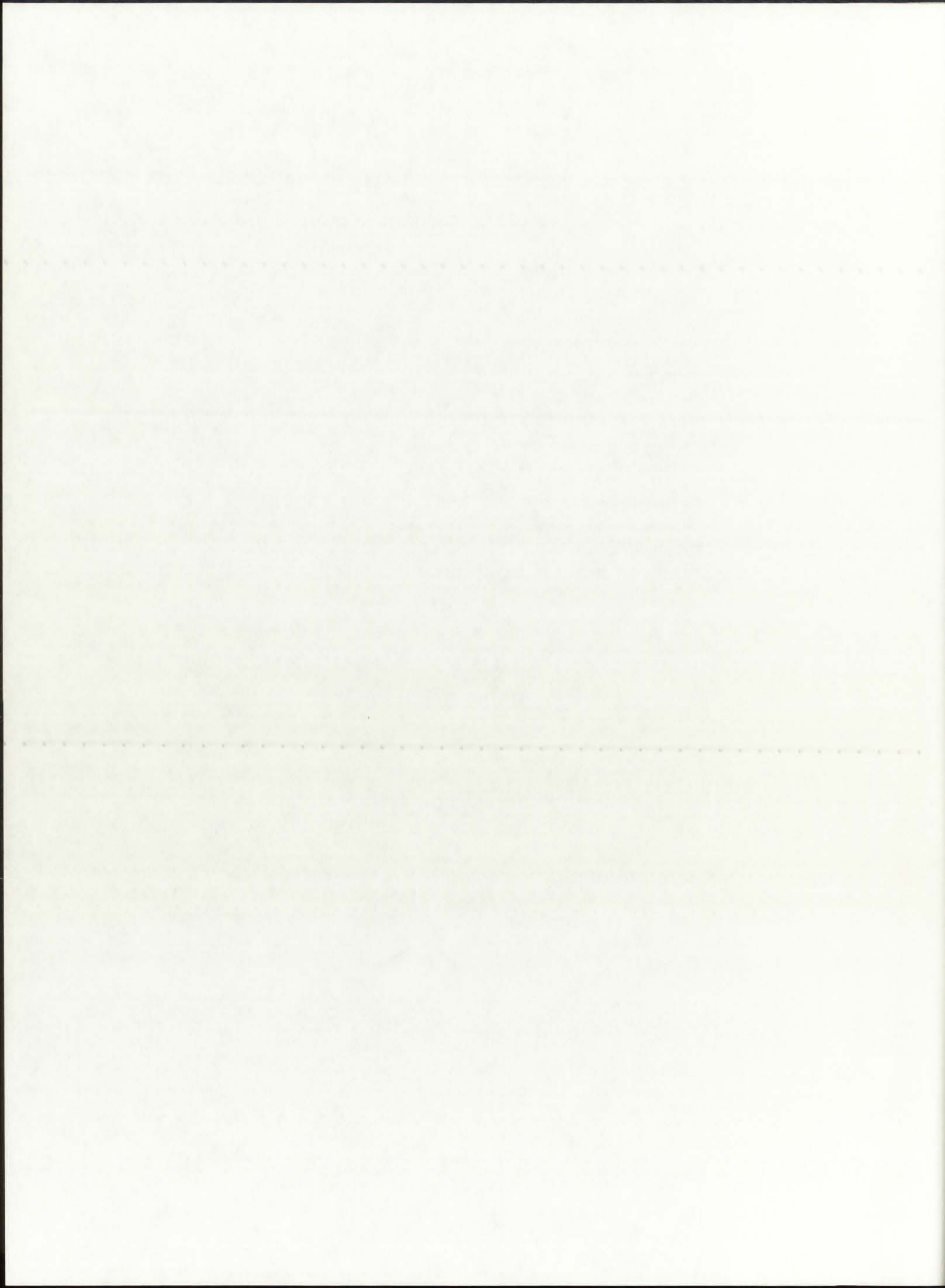
i	r(i)	T(i)	Qg(i)
37	0.000	8560.0	0.6274E+05
36	0.019	8560.0	0.6195E+05
35	0.039	8555.2	0.1255E+06
34	0.059	8540.3	0.1358E+06
33	0.096	8444.7	0.1920E+06
32	0.133	8228.9	0.2300E+06
31	0.170	7821.2	0.3447E+06
30	0.207	4832.2	0.0000E+00
29	0.225	4832.2	0.0000E+00
28	0.244	4832.2	0.0000E+00
27	0.246	4827.4	0.0000E+00
26	0.249	4822.7	0.0000E+00
25	0.268	4780.8	0.0000E+00
24	0.287	4742.7	0.0000E+00
23	0.307	4740.1	0.0000E+00
22	0.326	4737.9	0.0000E+00
21	0.345	4735.9	0.0000E+00
20	0.405	3694.2	0.0000E+00
19	0.465	2921.3	0.0000E+00
18	0.525	2325.0	0.0000E+00
17	0.585	1851.2	0.0000E+00
16	0.645	1465.7	0.0000E+00
15	0.705	1146.1	0.0000E+00
14	0.765	876.9	0.0000E+00
13	0.825	647.2	0.0000E+00
12	0.851	646.2	0.0000E+00
11	0.876	645.8	0.0000E+00
10	0.976	558.7	0.0000E+00
9	1.076	488.3	0.0000E+00
8	1.176	430.1	0.0000E+00
7	1.276	381.2	0.0000E+00
6	1.376	339.7	0.0000E+00
5	1.476	304.0	0.0000E+00
4	1.576	272.9	0.0000E+00
3	1.676	245.6	0.0000E+00
2	1.776	221.5	0.0000E+00
1	1.876	200.0	0.0000E+00



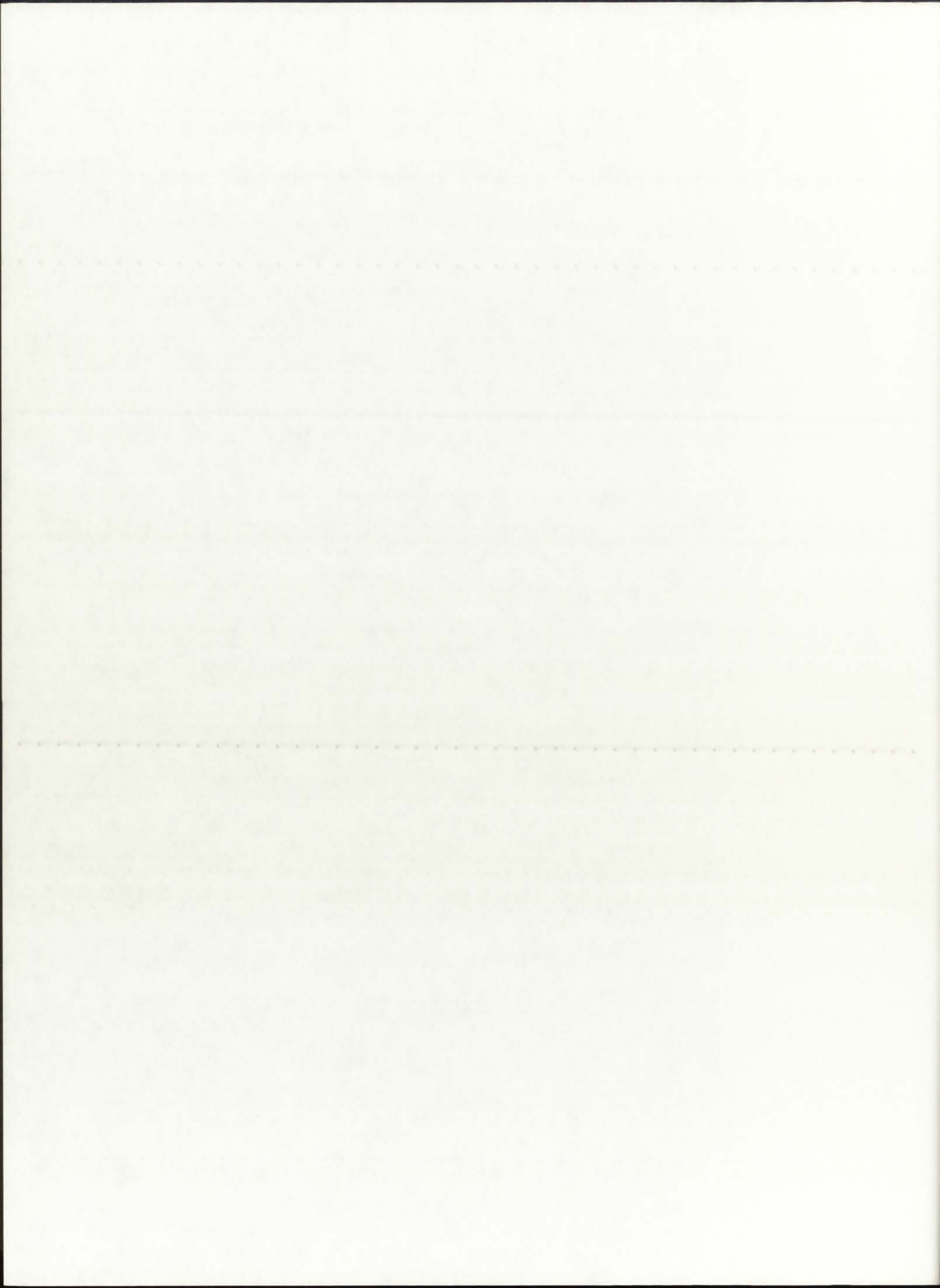
==== ROCKET ENGINE PARAMETERS ====

The H2 dissociation fraction is: 0.0836
The H2 average molecular weight is: 1.9317 g/gmol
The propellant molecular weight is: 7.3893 g/gmol
The cross-sectional flow area is: 0.0721 m²
The propellant mass flow rate is: 0.10 kg/s

The chamber temperature is: 4780.8 K
The calculated exit velocity is: 7857.8 m/s
The calculated thrust is: 0.8 kN
The calculated specific impulse is: 801.2 s



E.2. Combination II

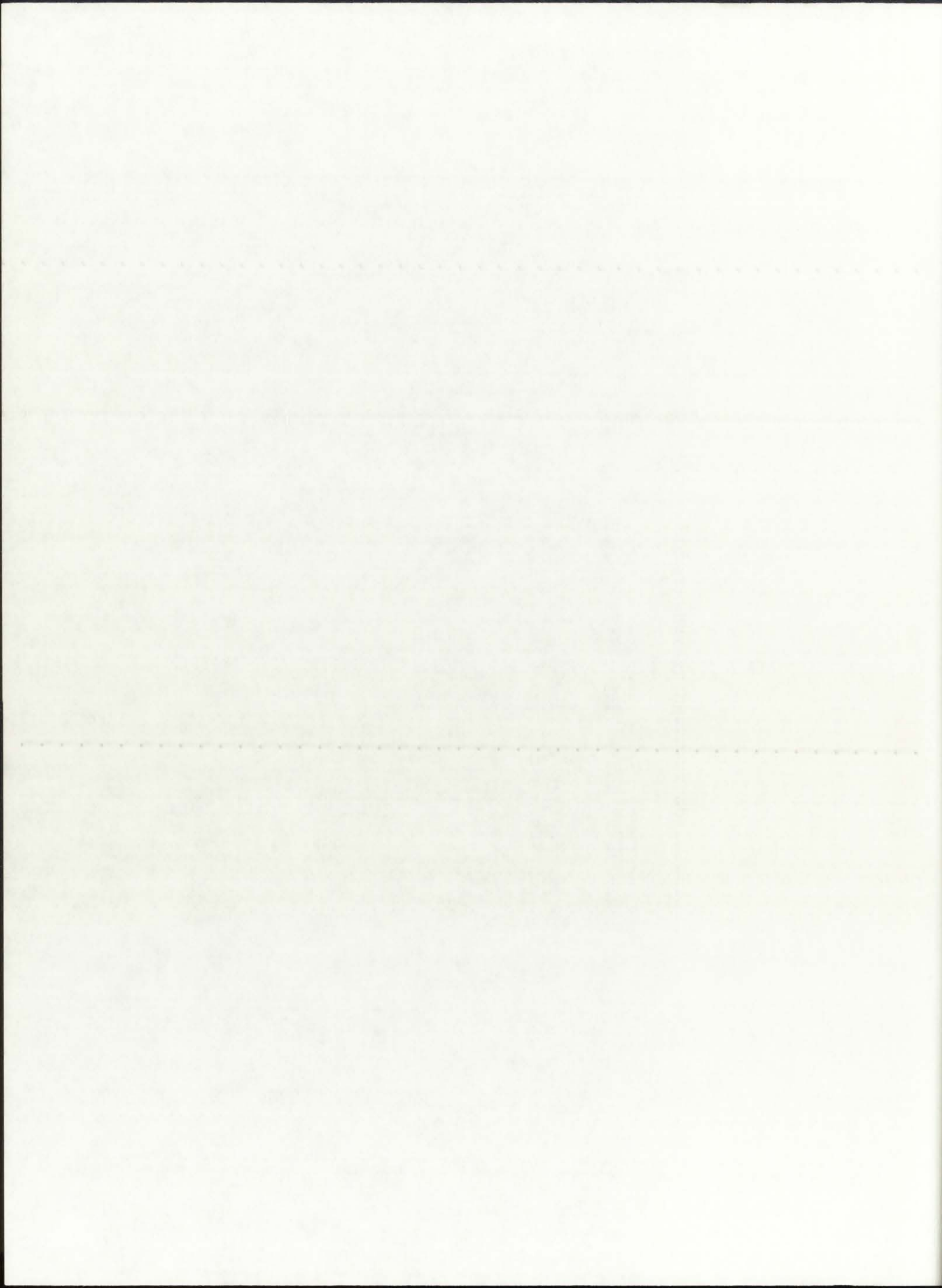


==== SUMMARY OF CONVERGED VALUES ====

This Case Executed for: REFLBe = 0.00000
 Pressure = 250.0 atm

Modes of Heat Transfer: Radiation in BG, SiW, and P = .on.
 Convection in BG = .off.
 Convection in P = .off.

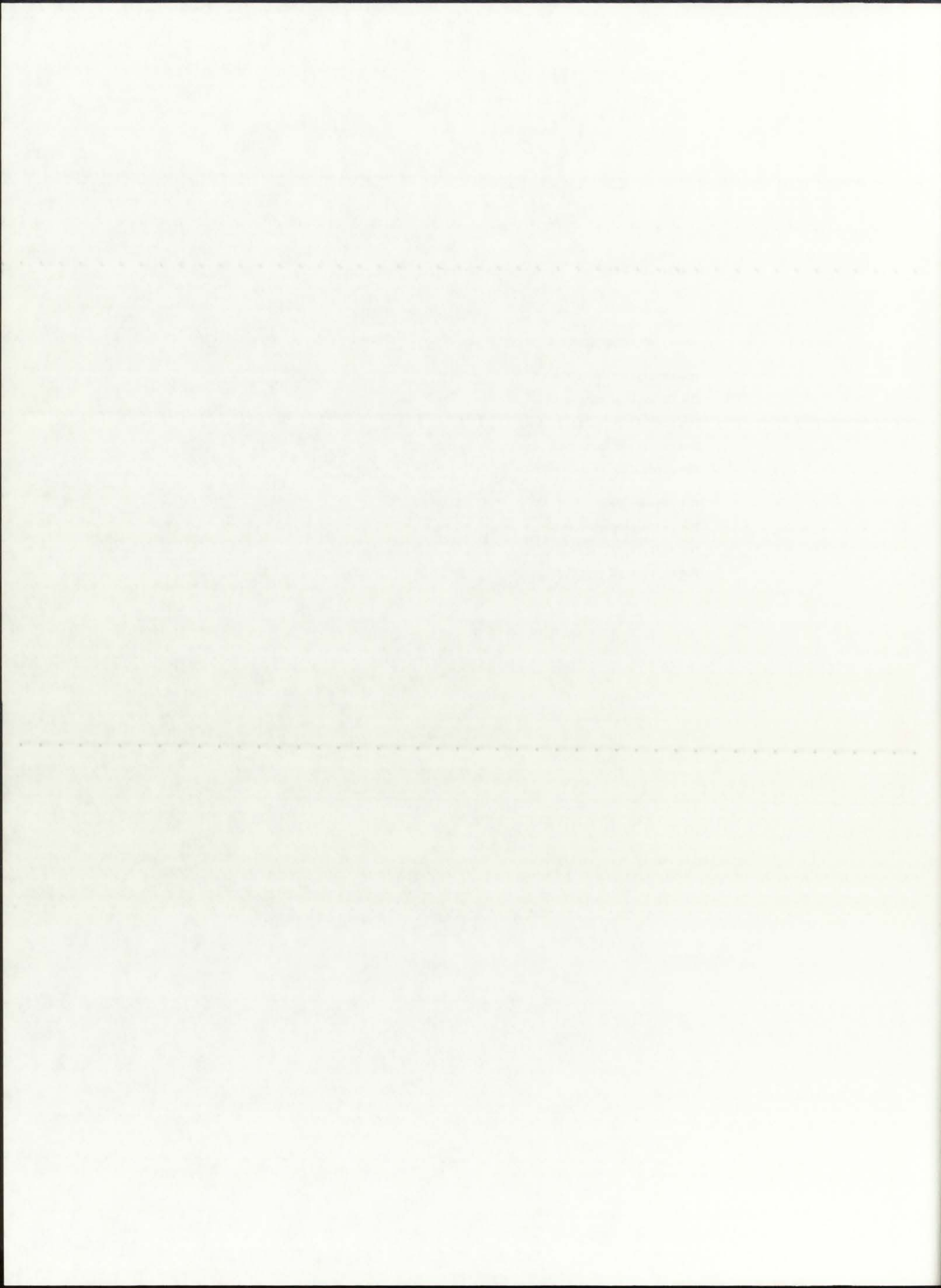
i	r(i)	T(i)	Qg(i)
37	0.000	8559.5	0.6274E+05
36	0.019	8559.5	0.6195E+05
35	0.039	8554.6	0.1255E+06
34	0.059	8539.8	0.1358E+06
33	0.096	8444.1	0.1920E+06
32	0.133	8228.3	0.2300E+06
31	0.170	7820.5	0.3447E+06
30	0.207	4833.2	0.0000E+00
29	0.225	252.0	0.0000E+00
28	0.244	2260.1	0.0000E+00
27	0.246	2260.1	0.0000E+00
26	0.249	2260.1	0.0000E+00
25	0.268	4139.0	0.0000E+00
24	0.287	4833.0	0.0000E+00
23	0.307	4830.4	0.0000E+00
22	0.326	4828.2	0.0000E+00
21	0.345	4826.2	0.0000E+00
20	0.405	3771.7	0.0000E+00
19	0.465	2989.3	0.0000E+00
18	0.525	2385.6	0.0000E+00
17	0.585	1906.0	0.0000E+00
16	0.645	1515.7	0.0000E+00
15	0.705	1192.2	0.0000E+00
14	0.765	919.6	0.0000E+00
13	0.825	687.1	0.0000E+00
12	0.851	686.1	0.0000E+00
11	0.876	685.7	0.0000E+00
10	0.976	591.0	0.0000E+00
9	1.076	514.2	0.0000E+00
8	1.176	450.8	0.0000E+00
7	1.276	397.7	0.0000E+00
6	1.376	352.4	0.0000E+00
5	1.476	313.4	0.0000E+00
4	1.576	279.6	0.0000E+00
3	1.676	249.8	0.0000E+00
2	1.776	223.5	0.0000E+00
1	1.876	200.0	0.0000E+00



==== ROCKET ENGINE PARAMETERS ====

The H2 dissociation fraction is: 0.0335
The H2 average molecular weight is: 1.9822 g/gmol
The propellant molecular weight is: 7.4382 g/gmol
The cross-sectional flow area is: 0.0721 m2
The propellant mass flow rate is: 0.10 kg/s

The chamber temperature is: 4139.0 K
The calculated exit velocity is: 7287.3 m/s
The calculated thrust is: 0.7 kN
The calculated specific impulse is: 743.1 s



==== SUMMARY OF CONVERGED VALUES ====

This Case Executed for: REFLBe = 0.99000
 Pressure = 250.0 atm

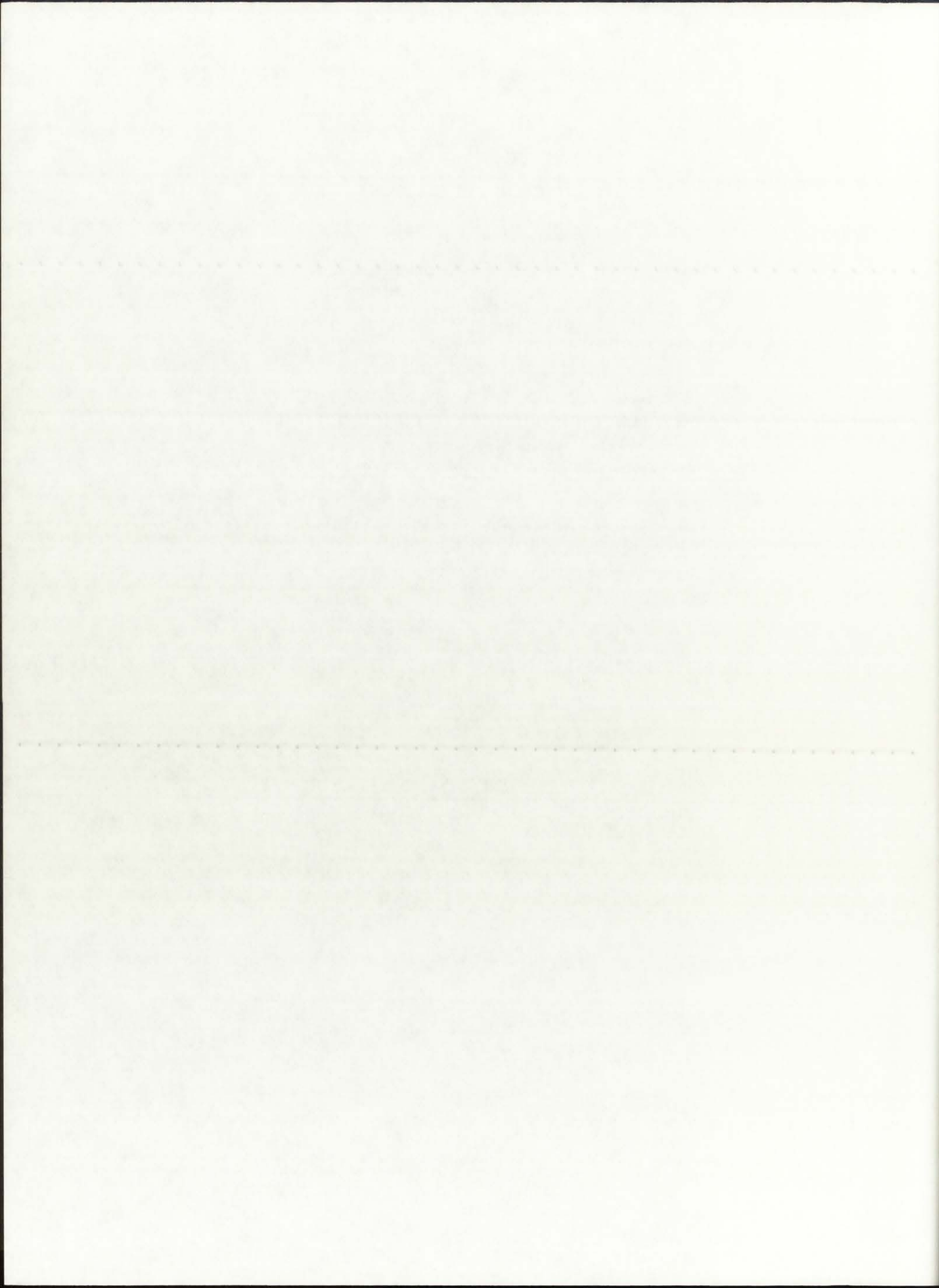
Modes of Heat Transfer: Radiation in BG,SiW, and P = .on.
 Convection in BG = .off.
 Convection in P = .off.

i	r(i)	T(i)	Qg(i)
37	0.000	8559.6	0.6274E+05
36	0.019	8559.6	0.6195E+05
35	0.039	8554.7	0.1255E+06
34	0.059	8539.9	0.1358E+06
33	0.096	8444.2	0.1920E+06
32	0.133	8228.4	0.2300E+06
31	0.170	7820.6	0.3447E+06
30	0.207	4833.0	0.0000E+00
29	0.225	252.0	0.0000E+00
28	0.244	2259.5	0.0000E+00
27	0.246	2259.5	0.0000E+00
26	0.249	2259.5	0.0000E+00
25	0.268	4129.2	0.0000E+00
24	0.287	4813.5	0.0000E+00
23	0.307	4811.0	0.0000E+00
22	0.326	4808.8	0.0000E+00
21	0.345	4806.8	0.0000E+00
20	0.405	3754.4	0.0000E+00
19	0.465	2973.5	0.0000E+00
18	0.525	2371.1	0.0000E+00
17	0.585	1892.4	0.0000E+00
16	0.645	1502.9	0.0000E+00
15	0.705	1180.0	0.0000E+00
14	0.765	908.0	0.0000E+00
13	0.825	676.0	0.0000E+00
12	0.851	675.0	0.0000E+00
11	0.876	674.5	0.0000E+00
10	0.976	582.0	0.0000E+00
9	1.076	507.0	0.0000E+00
8	1.176	445.0	0.0000E+00
7	1.276	393.1	0.0000E+00
6	1.376	348.9	0.0000E+00
5	1.476	310.8	0.0000E+00
4	1.576	277.7	0.0000E+00
3	1.676	248.6	0.0000E+00
2	1.776	222.9	0.0000E+00
1	1.876	200.0	0.0000E+00

==== ROCKET ENGINE PARAMETERS ====

The H2 dissociation fraction is: 0.0330
The H2 average molecular weight is: 1.9827 g/gmol
The propellant molecular weight is: 7.4388 g/gmol
The cross-sectional flow area is: 0.0721 m²
The propellant mass flow rate is: 0.10 kg/s

The chamber temperature is: 4129.2 K
The calculated exit velocity is: 7278.4 m/s
The calculated thrust is: 0.7 kN
The calculated specific impulse is: 742.2 s

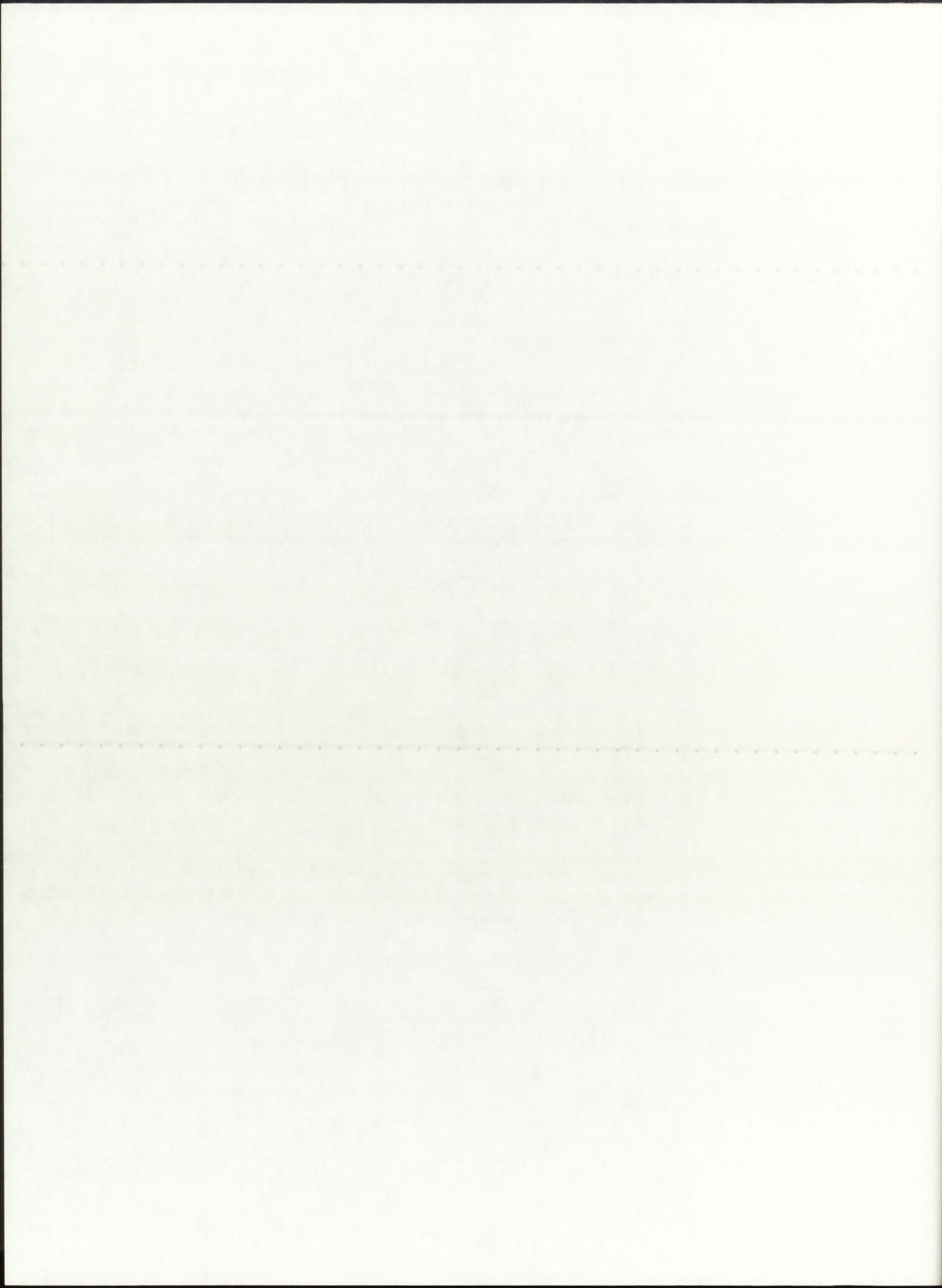


==== SUMMARY OF CONVERGED VALUES ====

This Case Executed for: REFLBe = 1.00000
 Pressure = 250.0 atm

Modes of Heat Transfer: Radiation in BG, SiW, and P = .on.
 Convection in BG = .off.
 Convection in P = .off.

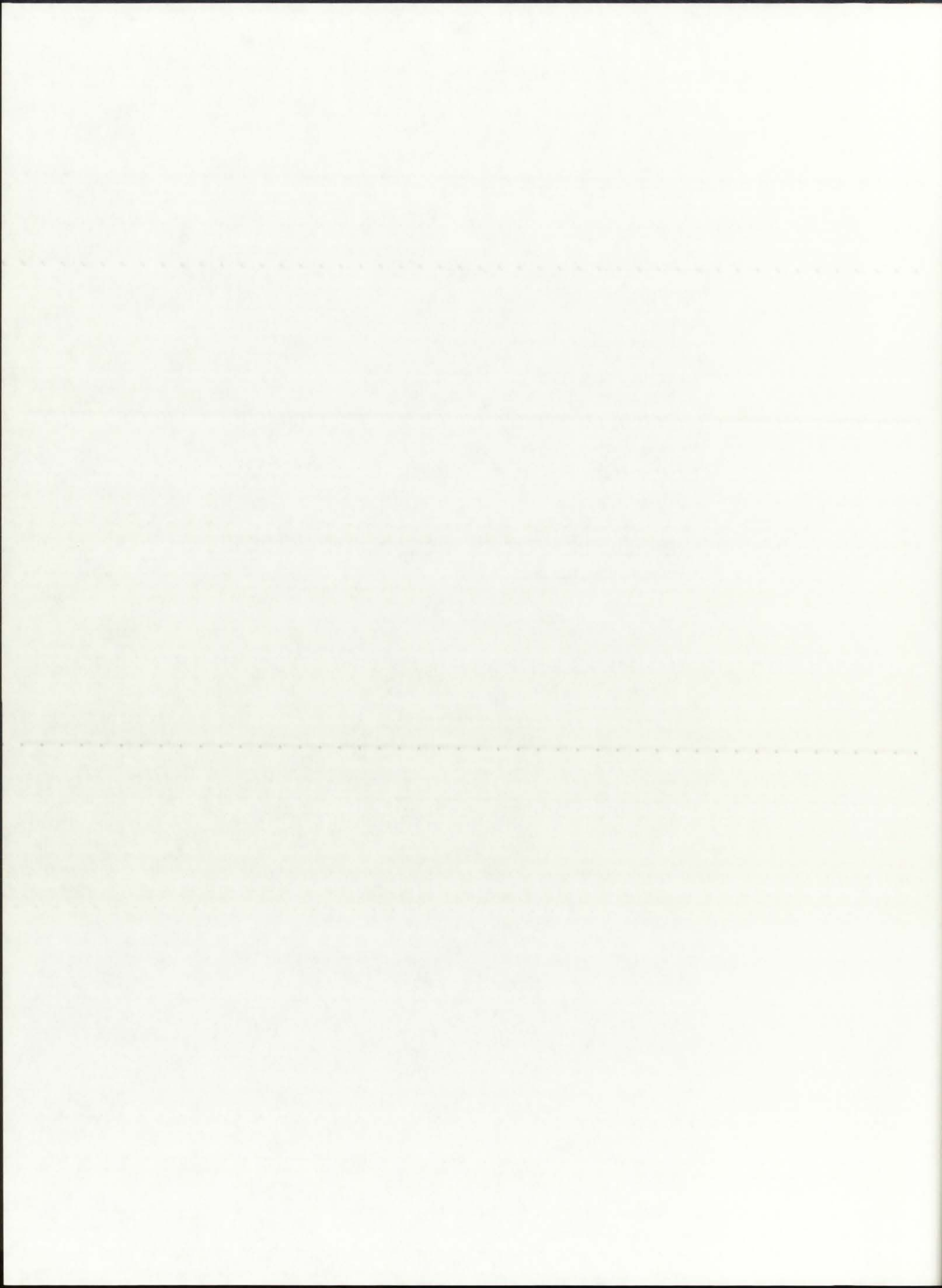
i	r(i)	T(i)	Qg(i)
37	0.000	8559.5	0.6274E+05
36	0.019	8559.5	0.6195E+05
35	0.039	8554.6	0.1255E+06
34	0.059	8539.8	0.1358E+06
33	0.096	8444.1	0.1920E+06
32	0.133	8228.3	0.2300E+06
31	0.170	7820.5	0.3447E+06
30	0.207	4833.2	0.0000E+00
29	0.225	252.0	0.0000E+00
28	0.244	2260.1	0.0000E+00
27	0.246	2260.1	0.0000E+00
26	0.249	2260.1	0.0000E+00
25	0.268	4138.6	0.0000E+00
24	0.287	220.3	0.0000E+00
23	0.307	220.3	0.0000E+00
22	0.326	220.3	0.0000E+00
21	0.345	220.3	0.0000E+00
20	0.405	218.3	0.0000E+00
19	0.465	216.7	0.0000E+00
18	0.525	215.6	0.0000E+00
17	0.585	214.7	0.0000E+00
16	0.645	213.9	0.0000E+00
15	0.705	213.3	0.0000E+00
14	0.765	212.8	0.0000E+00
13	0.825	212.3	0.0000E+00
12	0.851	212.3	0.0000E+00
11	0.876	212.3	0.0000E+00
10	0.976	209.9	0.0000E+00
9	1.076	208.0	0.0000E+00
8	1.176	206.4	0.0000E+00
7	1.276	205.1	0.0000E+00
6	1.376	203.9	0.0000E+00
5	1.476	202.9	0.0000E+00
4	1.576	202.0	0.0000E+00
3	1.676	201.3	0.0000E+00
2	1.776	200.6	0.0000E+00
1	1.876	200.0	0.0000E+00



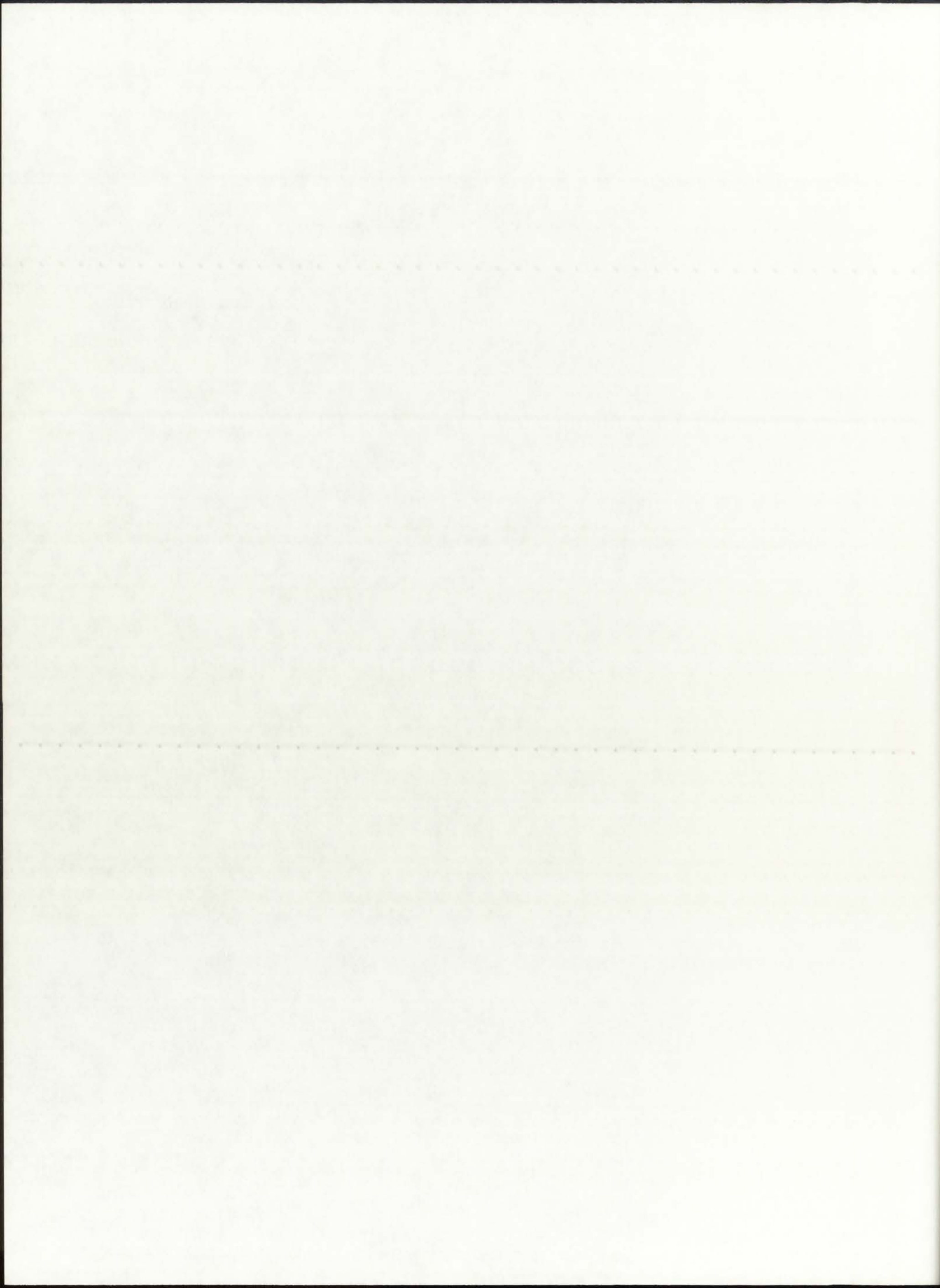
==== ROCKET ENGINE PARAMETERS ====

The H2 dissociation fraction is: 0.0335
The H2 average molecular weight is: 1.9822 g/gmol
The propellant molecular weight is: 7.4383 g/gmol
The cross-sectional flow area is: 0.0721 m2
The propellant mass flow rate is: 0.10 kg/s

The chamber temperature is: 4138.6 K
The calculated exit velocity is: 7286.9 m/s
The calculated thrust is: 0.7 kN
The calculated specific impulse is: 743.0 s



E.3. Combination III

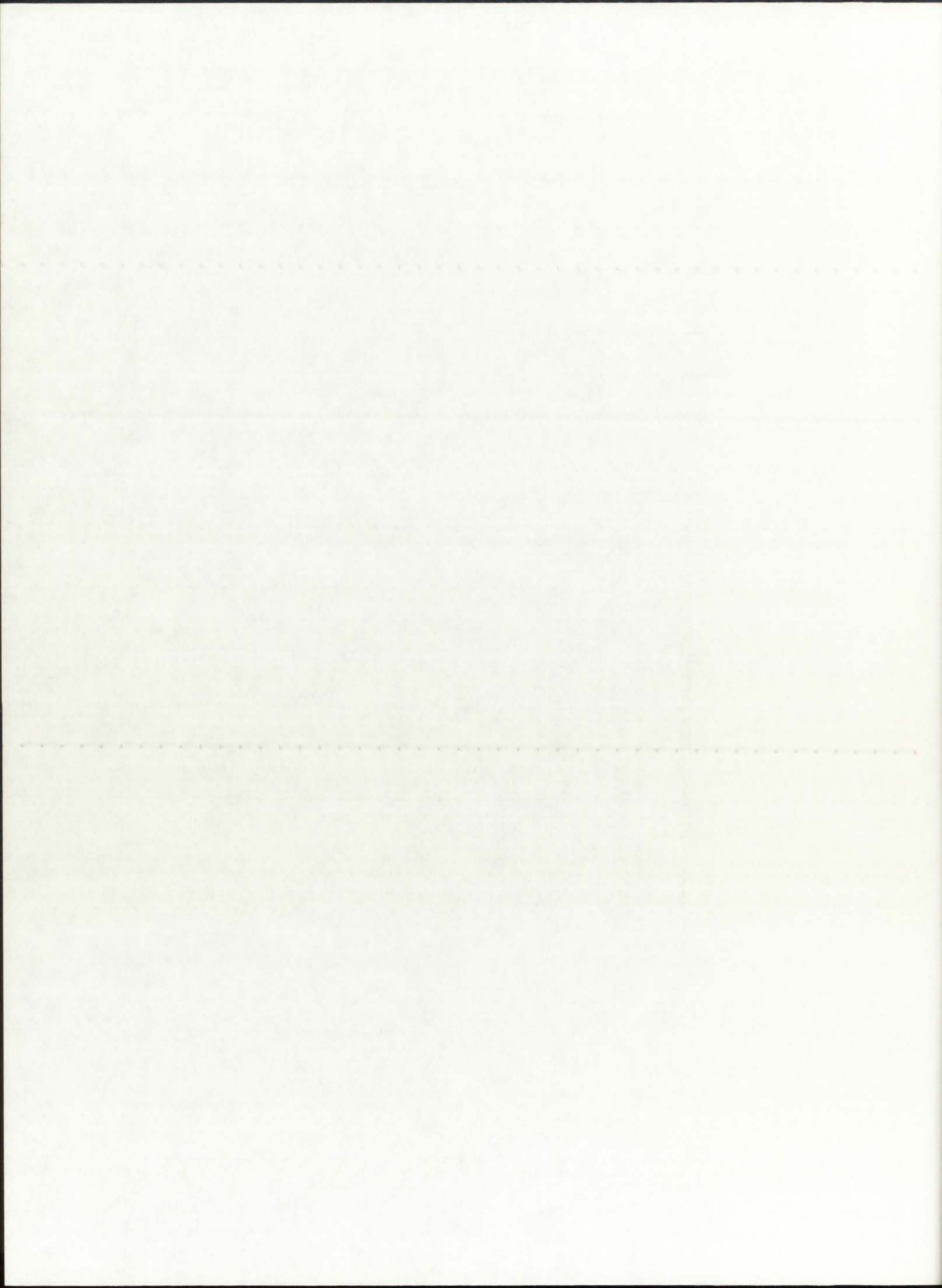


==== SUMMARY OF CONVERGED VALUES ====

This Case Executed for: REFLBe = 0.00000
 Pressure = 250.0 atm

Modes of Heat Transfer: Radiation in BG, SiW, and P = .off.
 Convection in BG = .on.
 Convection in P = .on.

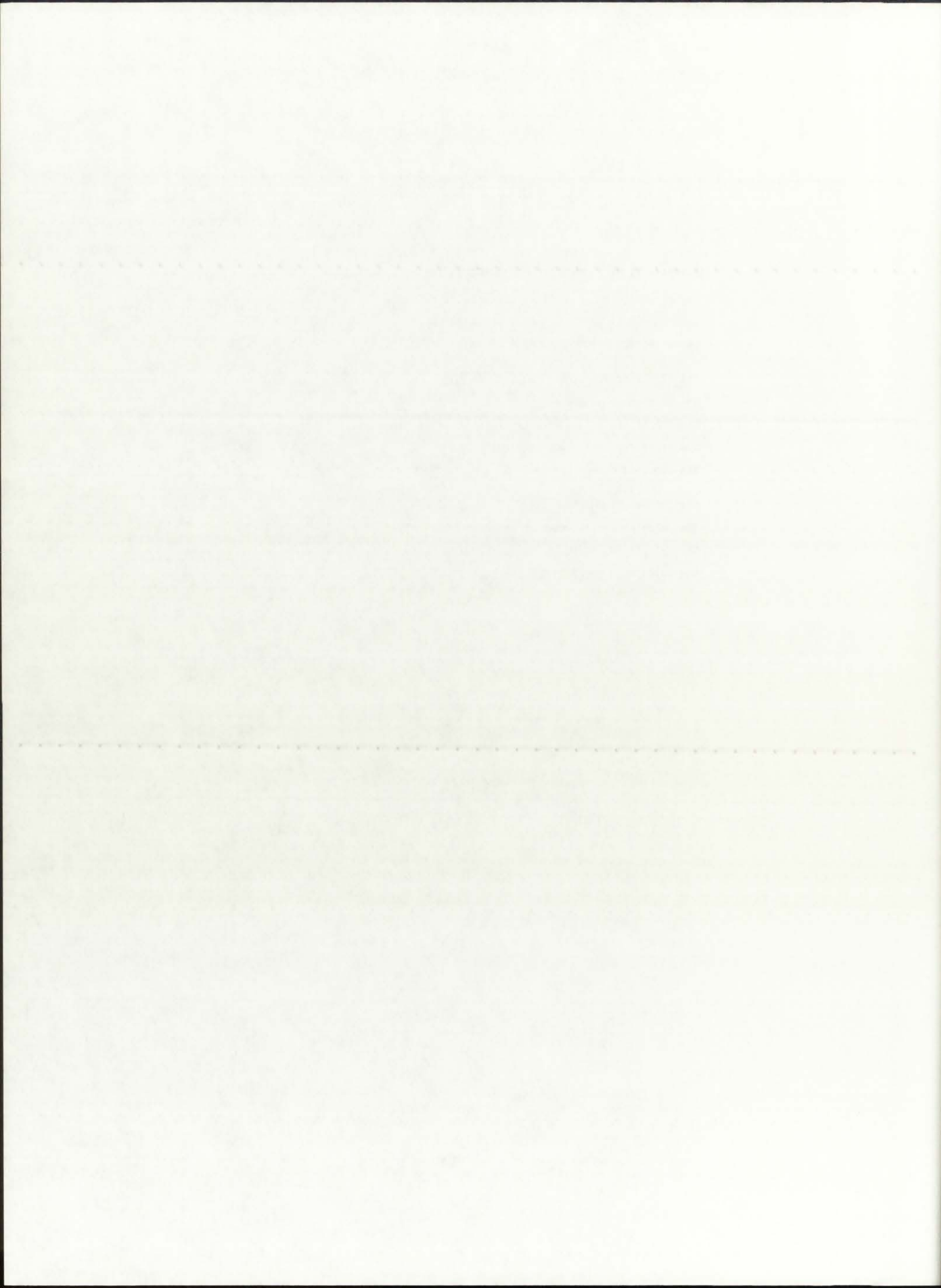
i	r(i)	T(i)	Qg(i)
37	0.000	8375.5	0.6274E+05
36	0.019	8375.5	0.6195E+05
35	0.039	8370.3	0.1255E+06
34	0.059	8354.4	0.1358E+06
33	0.096	8251.8	0.1920E+06
32	0.133	8018.3	0.2300E+06
31	0.170	7566.3	0.3447E+06
30	0.207	5397.5	0.0000E+00
29	0.225	5391.0	0.0000E+00
28	0.244	5385.9	0.0000E+00
27	0.246	5370.0	0.0000E+00
26	0.249	5354.8	0.0000E+00
25	0.268	5283.3	0.0000E+00
24	0.287	5221.9	0.0000E+00
23	0.307	5217.8	0.0000E+00
22	0.326	5214.6	0.0000E+00
21	0.345	5212.1	0.0000E+00
20	0.405	4141.0	0.0000E+00
19	0.465	3346.4	0.0000E+00
18	0.525	2733.8	0.0000E+00
17	0.585	2247.1	0.0000E+00
16	0.645	1851.3	0.0000E+00
15	0.705	1523.3	0.0000E+00
14	0.765	1247.1	0.0000E+00
13	0.825	1011.4	0.0000E+00
12	0.851	1010.4	0.0000E+00
11	0.876	1009.9	0.0000E+00
10	0.976	852.9	0.0000E+00
9	1.076	725.4	0.0000E+00
8	1.176	619.9	0.0000E+00
7	1.276	531.2	0.0000E+00
6	1.376	455.6	0.0000E+00
5	1.476	390.4	0.0000E+00
4	1.576	333.6	0.0000E+00
3	1.676	283.7	0.0000E+00
2	1.776	239.5	0.0000E+00
1	1.876	200.0	0.0000E+00



==== ROCKET ENGINE PARAMETERS ====

The H2 dissociation fraction is: 0.1461
The H2 average molecular weight is: 1.8687 g/gmol
The propellant molecular weight is: 7.3281 g/gmol
The cross-sectional flow area is: 0.0721 m²
The propellant mass flow rate is: 0.07 kg/s

The chamber temperature is: 5283.3 K
The calculated exit velocity is: 7681.2 m/s
The calculated thrust is: 0.6 kN
The calculated specific impulse is: 783.2 s

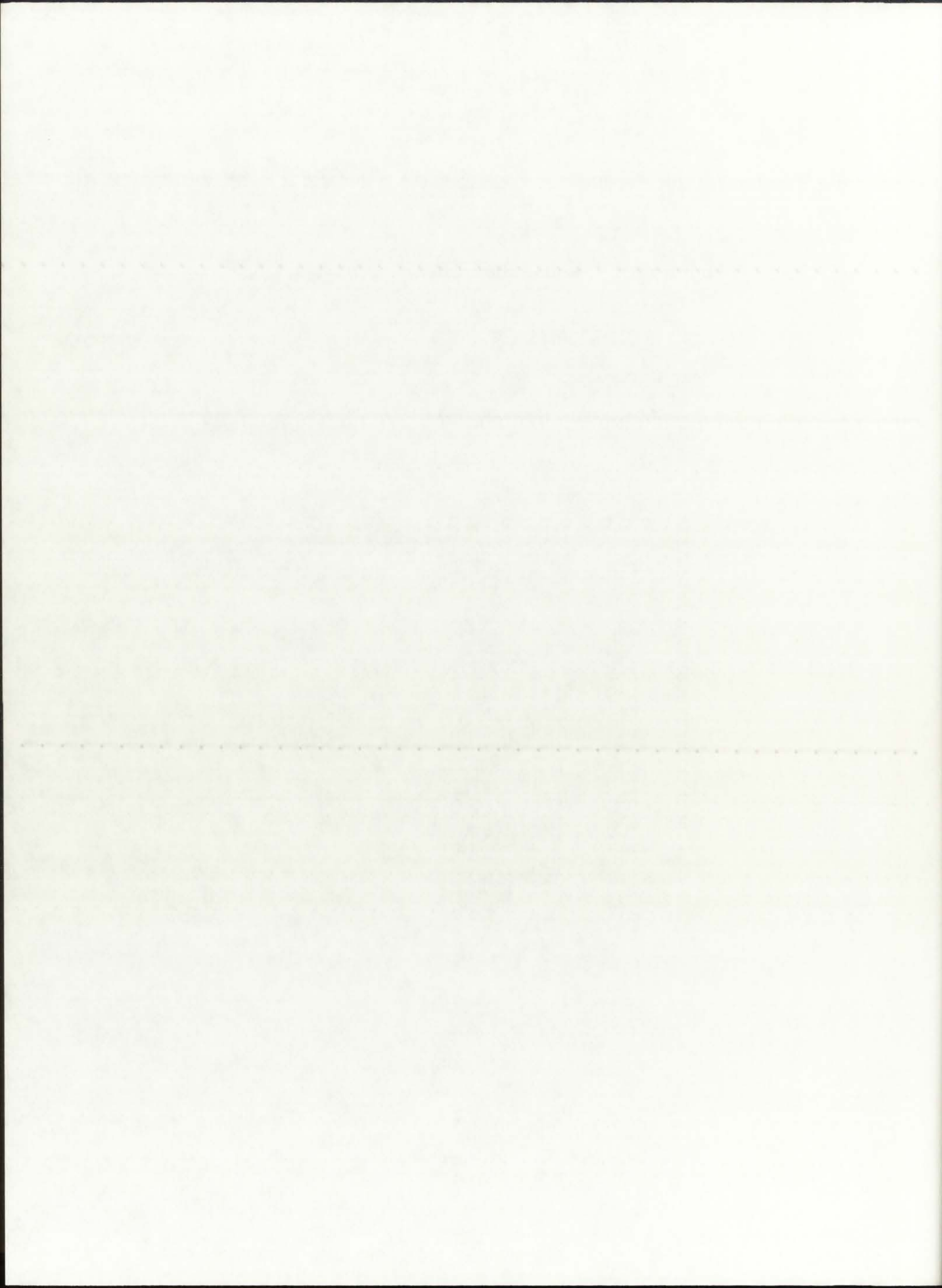


==== SUMMARY OF CONVERGED VALUES ====

This Case Executed for: REFLBe = 0.00000
 Pressure = 250.0 atm

Modes of Heat Transfer: Radiation in BG, SiW, and P = .off.
 Convection in BG = .on.
 Convection in P = .on.

i	r(i)	T(i)	Qg(i)
37	0.000	8393.3	0.6274E+05
36	0.019	8393.3	0.6195E+05
35	0.039	8388.2	0.1255E+06
34	0.059	8372.4	0.1358E+06
33	0.096	8270.4	0.1920E+06
32	0.133	8038.7	0.2300E+06
31	0.170	7591.2	0.3447E+06
30	0.207	5290.1	0.0000E+00
29	0.225	5283.1	0.0000E+00
28	0.244	5277.5	0.0000E+00
27	0.246	5260.1	0.0000E+00
26	0.249	5243.3	0.0000E+00
25	0.268	4294.8	0.0000E+00
24	0.287	3474.0	0.0000E+00
23	0.307	3469.4	0.0000E+00
22	0.326	3466.2	0.0000E+00
21	0.345	3464.0	0.0000E+00
20	0.405	2735.5	0.0000E+00
19	0.465	2195.5	0.0000E+00
18	0.525	1779.5	0.0000E+00
17	0.585	1449.2	0.0000E+00
16	0.645	1180.8	0.0000E+00
15	0.705	958.5	0.0000E+00
14	0.765	771.4	0.0000E+00
13	0.825	611.8	0.0000E+00
12	0.851	611.1	0.0000E+00
11	0.876	610.8	0.0000E+00
10	0.976	530.9	0.0000E+00
9	1.076	466.1	0.0000E+00
8	1.176	412.6	0.0000E+00
7	1.276	367.6	0.0000E+00
6	1.376	329.3	0.0000E+00
5	1.476	296.3	0.0000E+00
4	1.576	267.5	0.0000E+00
3	1.676	242.3	0.0000E+00
2	1.776	219.9	0.0000E+00
1	1.876	200.0	0.0000E+00



==== ROCKET ENGINE PARAMETERS ====

The H2 dissociation fraction is: 0.0429
The H2 average molecular weight is: 1.9727 g/gmol
The propellant molecular weight is: 7.4291 g/gmol
The cross-sectional flow area is: 0.0721 m2
The propellant mass flow rate is: 0.01 kg/s

The chamber temperature is: 4294.8 K
The calculated exit velocity is: 7427.7 m/s
The calculated thrust is: 0.1 kN
The calculated specific impulse is: 757.4 s

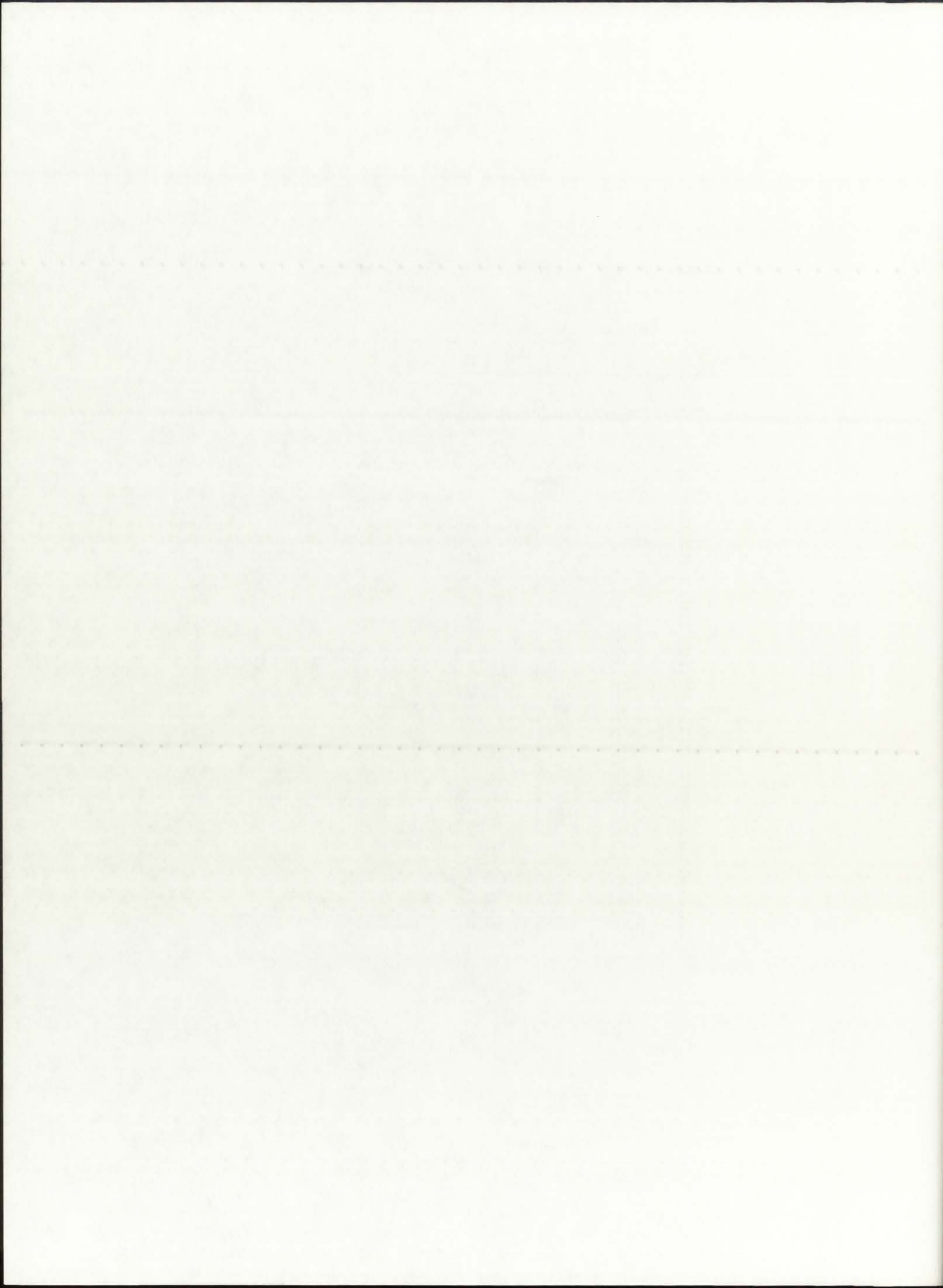
THE UNIVERSITY OF CHICAGO
DEPARTMENT OF CHEMISTRY
5800 S. UNIVERSITY AVENUE
CHICAGO, ILLINOIS 60637
TEL: 773-936-3700
WWW.CHEM.UCHICAGO.EDU

==== SUMMARY OF CONVERGED VALUES ====

This Case Executed for: REFLBe = 0.00000
 Pressure = 250.0 atm

Modes of Heat Transfer: Radiation in BG, SiW, and P = .off.
 Convection in BG = .on.
 Convection in P = .on.

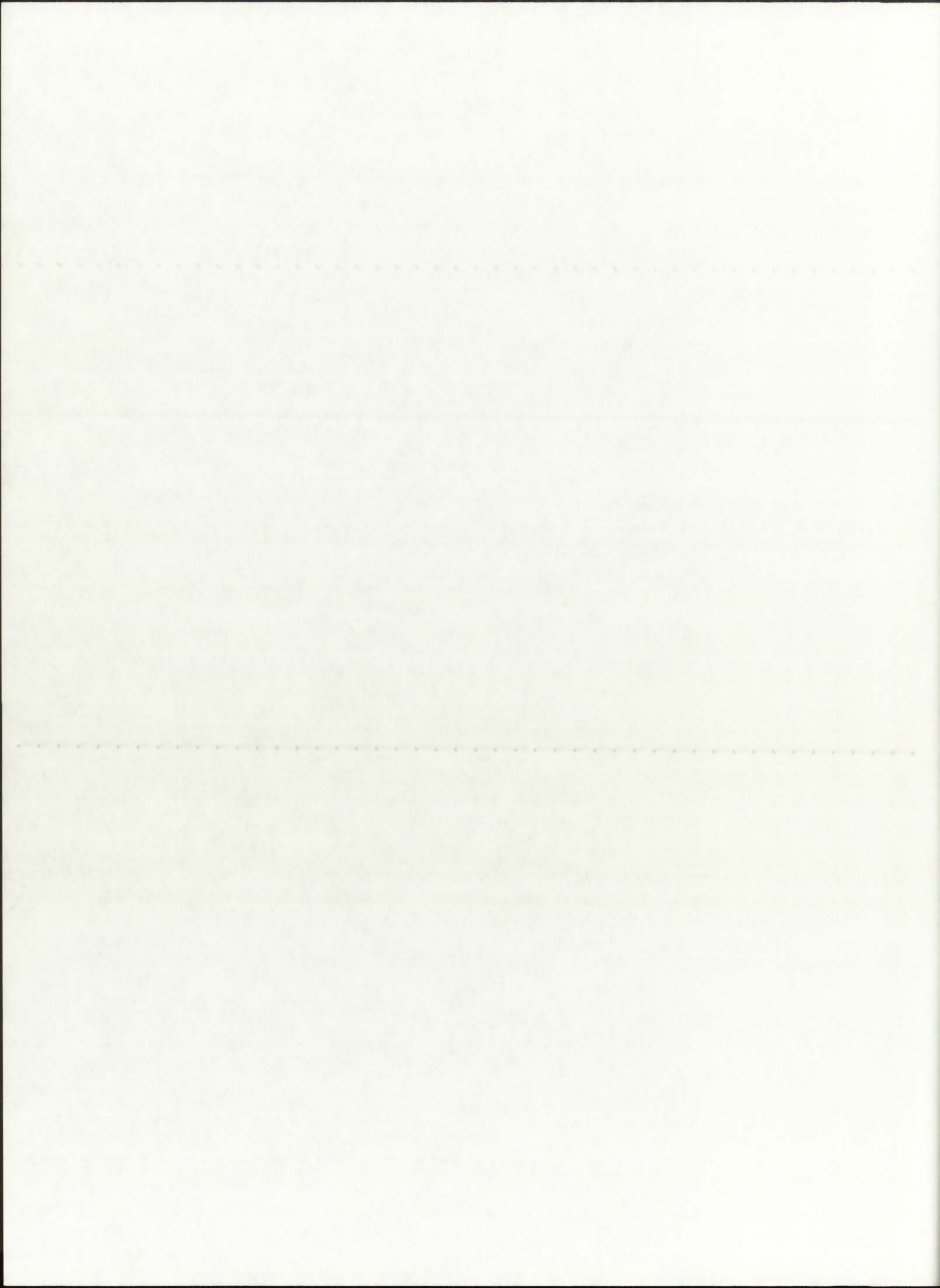
i	r(i)	T(i)	Qg(i)
37	0.000	8376.5	0.6274E+05
36	0.019	8376.5	0.6195E+05
35	0.039	8371.3	0.1255E+06
34	0.059	8355.4	0.1358E+06
33	0.096	8252.8	0.1920E+06
32	0.133	8019.5	0.2300E+06
31	0.170	7567.8	0.3447E+06
30	0.207	5389.8	0.0000E+00
29	0.225	5383.3	0.0000E+00
28	0.244	5378.1	0.0000E+00
27	0.246	5361.9	0.0000E+00
26	0.249	5346.4	0.0000E+00
25	0.268	5334.9	0.0000E+00
24	0.287	5325.2	0.0000E+00
23	0.307	5321.3	0.0000E+00
22	0.326	5318.2	0.0000E+00
21	0.345	5315.8	0.0000E+00
20	0.405	4232.4	0.0000E+00
19	0.465	3428.8	0.0000E+00
18	0.525	2809.1	0.0000E+00
17	0.585	2316.9	0.0000E+00
16	0.645	1916.5	0.0000E+00
15	0.705	1584.6	0.0000E+00
14	0.765	1305.2	0.0000E+00
13	0.825	1066.8	0.0000E+00
12	0.851	1065.8	0.0000E+00
11	0.876	1065.3	0.0000E+00
10	0.976	897.6	0.0000E+00
9	1.076	761.5	0.0000E+00
8	1.176	648.8	0.0000E+00
7	1.276	554.0	0.0000E+00
6	1.376	473.2	0.0000E+00
5	1.476	403.6	0.0000E+00
4	1.576	342.8	0.0000E+00
3	1.676	289.5	0.0000E+00
2	1.776	242.2	0.0000E+00
1	1.876	200.0	0.0000E+00



==== ROCKET ENGINE PARAMETERS ====

The H2 dissociation fraction is: 0.1538
The H2 average molecular weight is: 1.8610 g/gmol
The propellant molecular weight is: 7.3207 g/gmol
The cross-sectional flow area is: 0.0721 m²
The propellant mass flow rate is: 0.72 kg/s

The chamber temperature is: 5334.9 K
The calculated exit velocity is: 7722.5 m/s
The calculated thrust is: 5.6 kN
The calculated specific impulse is: 787.4 s

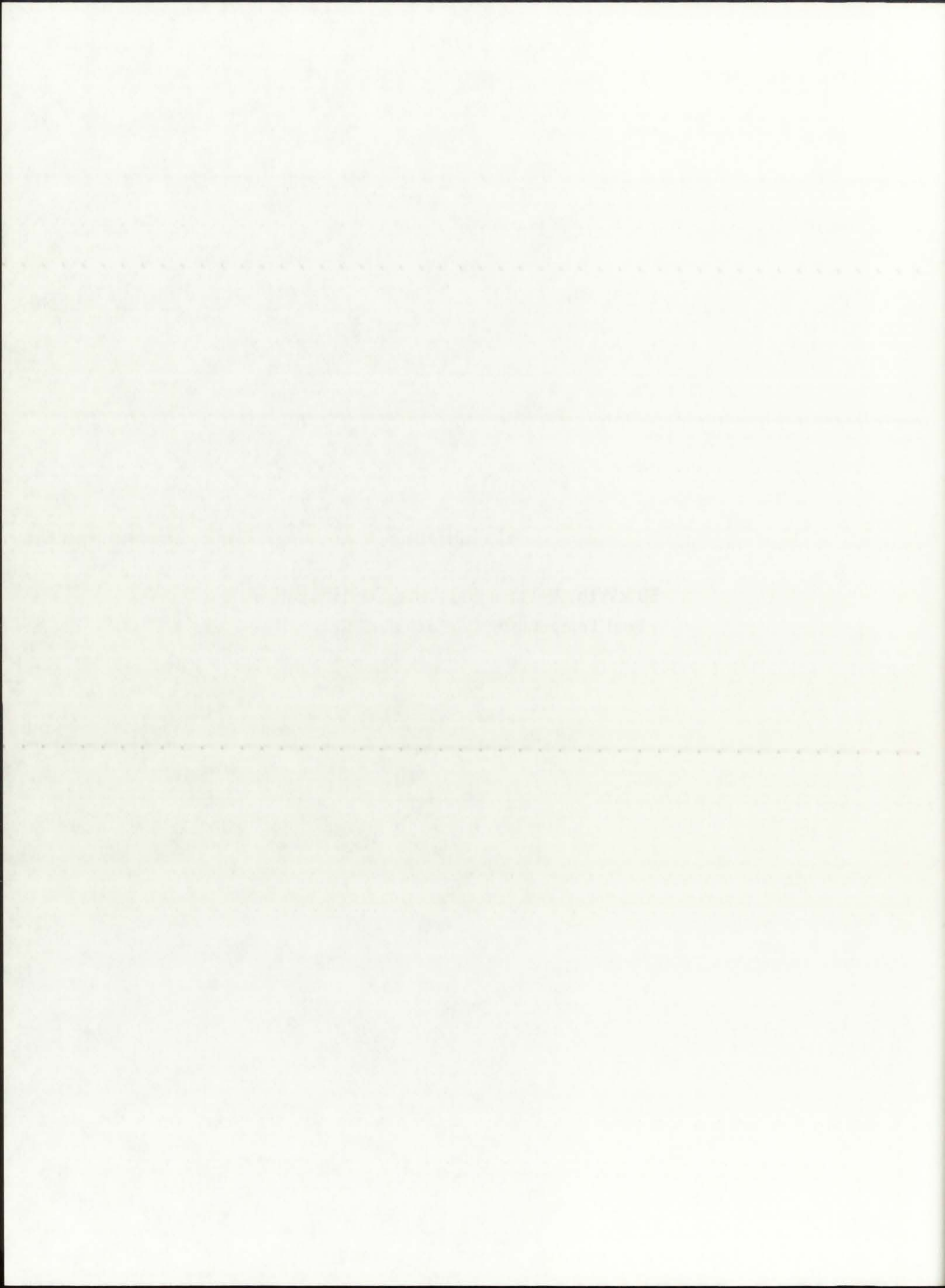


APPENDIX F

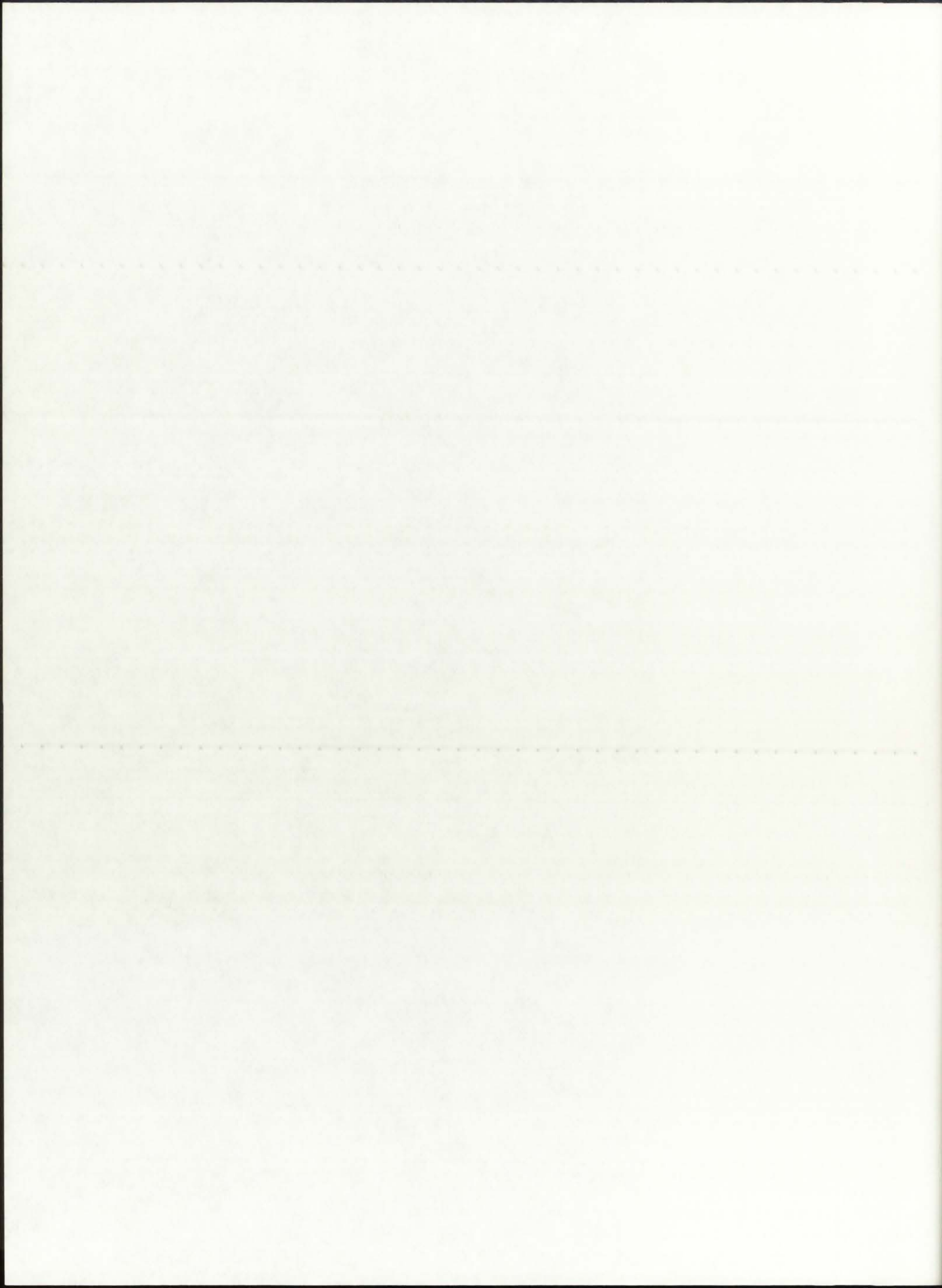
50 kWth, 250 atm Baseline Configuration - Fuel Temperature Coefficient of Reactivity -

F.1: TRANSX Input Files

F.2: ONEDANT Input File



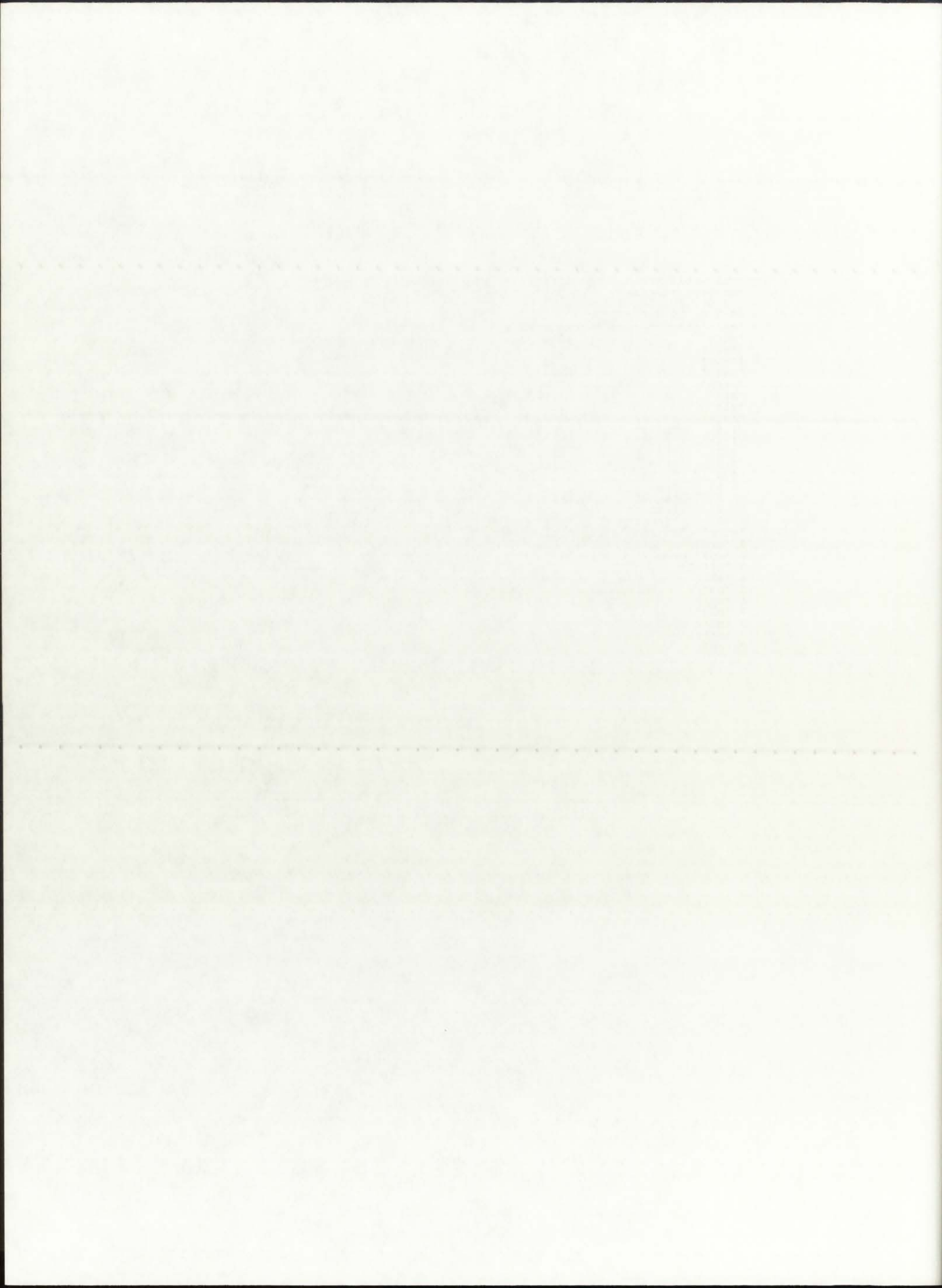
F.1. TRANSX Input Files



```

*Unit-cell NLB Engine: effects of Tfuel on keff: Tfuel=8,000 K
*mtx7ey* *isotxs*/
1 6 0 1 1 1 0 2 0 0/
69 2 93 20 8 8 9 9 9/
*enru* *hydr* *deut* *oxgn* *bery* *ar* *si* *fe*
*enru* 8000. 1./
*hydr* 300. 1./
*deut* 300. 1./
*oxgn* 300. 1./
*bery* 300. 1./
*ar* 300. 1./
*si* 300. 1./
*fe* 300. 1./
1 1 *u235* 0.96 1.e+10 42 *free*/
1 1 *u238* 0.04 1.e+10 42 *free*/
2 2 *h1* 1.0 1.e+10 42 *free*/
3 3 *h2* 1.0 1.e+10 42 *d2o*/
4 4 *o16* 1.0 1.e+10 42 *free*/
5 5 *be9* 1.0 1.e+10 42 *be* *be$*/
6 6 *arnat* 1.0 1.e+10 42 *free*/
7 7 *sinat* 1.0 1.e+10 42 *free*/
8 8 *fenat* 1.0 1.e+10 42 *free*/
*strpl* *sngam* *sfis* *chiso* *snalf* *snp* *sn2n* *snd* *snt*/
1 *trd*/
2 *ng*/
3 *nftot*/
4 *chi*/
5 *na*/
6 *np*/
7 *n2n*/
8 *nd*/
9 *nt*/
*stop*

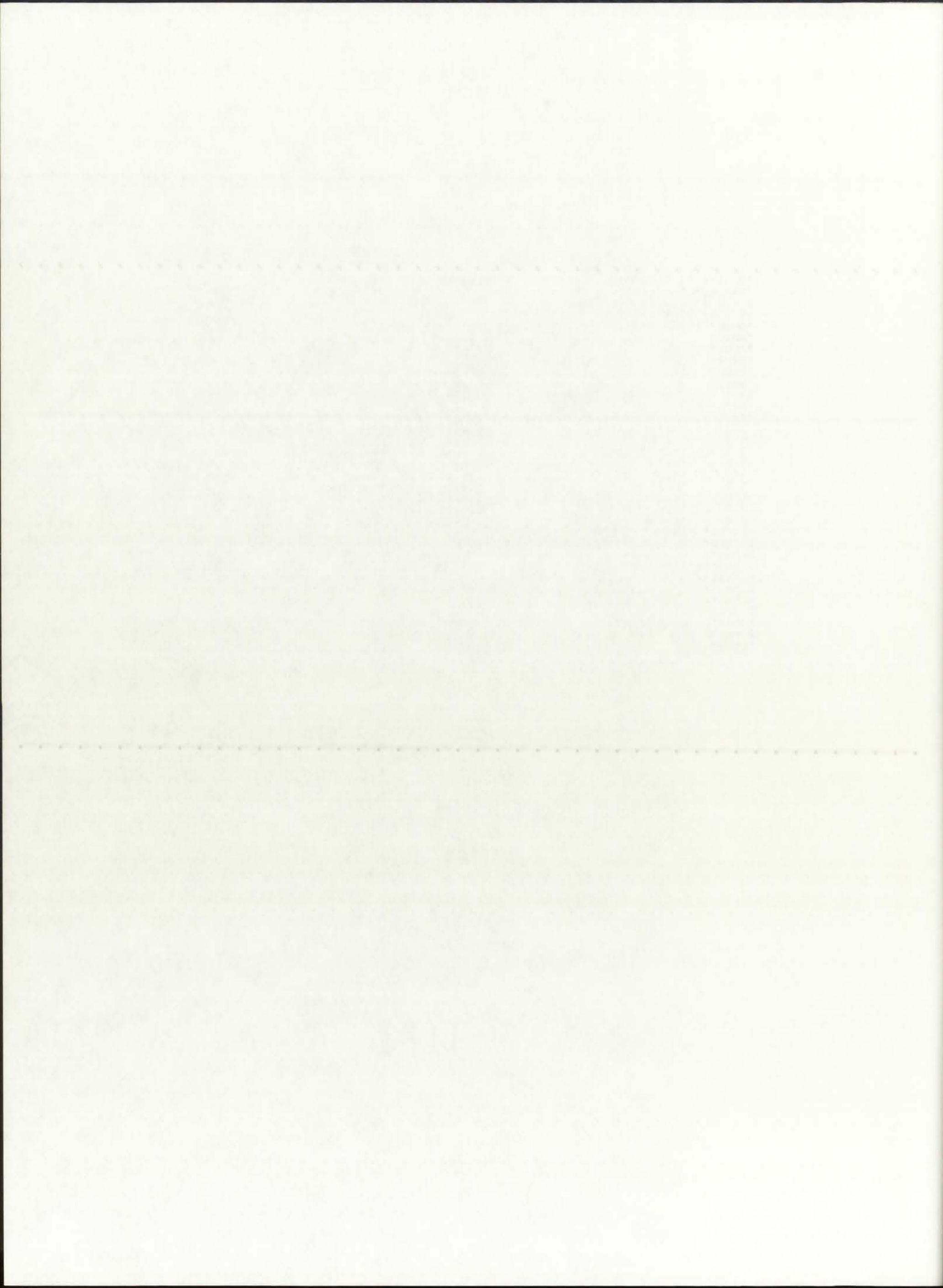
```




```

*Unit-cell NLB Engine: effects of Tfuel on keff: Tfuel=10,000 K
*mtx7ey* *isotxs*/
1 6 0 1 1 1 0 2 0 0/
69 2 93 20 8 8 9 9 9/
*enru* *hydr* *deut* *oxgn* *bery* *ar* *si* *fe*
*enru* 10000. 1./
*hydr* 300. 1./
*deut* 300. 1./
*oxgn* 300. 1./
*bery* 300. 1./
*ar* 300. 1./
*si* 300. 1./
*fe* 300. 1./
1 1 *u235* 0.96 1.e+10 42 *free*/
1 1 *u238* 0.04 1.e+10 42 *free*/
2 2 *h1* 1.0 1.e+10 42 *free*/
3 3 *h2* 1.0 1.e+10 42 *d2o*/
4 4 *o16* 1.0 1.e+10 42 *free*/
5 5 *be9* 1.0 1.e+10 42 *be* *be$*/
6 6 *arnat* 1.0 1.e+10 42 *free*/
7 7 *sinat* 1.0 1.e+10 42 *free*/
8 8 *fenat* 1.0 1.e+10 42 *free*/
*strpl* *sngam* *sfis* *chiso* *snalf* *snp* *sn2n* *snd* *snt*/
1 *trd*/
2 *ng*/
3 *nftot*/
4 *chi*/
5 *na*/
6 *np*/
7 *n2n*/
8 *nd*/
9 *nt*/
*stop*

```



*Unit-cell NLB Engine: effects of Tfuel on keff: Tfuel=20,000 K

mtx7ey *isotxs*/

1 6 0 1 1 1 0 2 0 0/

69 2 93 20 8 8 9 9 9/

enru *hydr* *deut* *oxgn* *bery* *ar* *si* *fe*

enru 20000. 1./

hydr 300. 1./

deut 300. 1./

oxgn 300. 1./

bery 300. 1./

ar 300. 1./

si 300. 1./

fe 300. 1./

1 1 *u235* 0.96 1.e+10 42 *free*/

1 1 *u238* 0.04 1.e+10 42 *free*/

2 2 *h1* 1.0 1.e+10 42 *free*/

3 3 *h2* 1.0 1.e+10 42 *d2o*/

4 4 *o16* 1.0 1.e+10 42 *free*/

5 5 *be9* 1.0 1.e+10 42 *be* *be\$*/

6 6 *arnat* 1.0 1.e+10 42 *free*/

7 7 *sinat* 1.0 1.e+10 42 *free*/

8 8 *fenat* 1.0 1.e+10 42 *free*/

strpl *sngam* *sfis* *chiso* *snalf* *snp* *sn2n* *snd* *snt*/

1 *trd*/

2 *ng*/

3 *nftot*/

4 *chi*/

5 *na*/

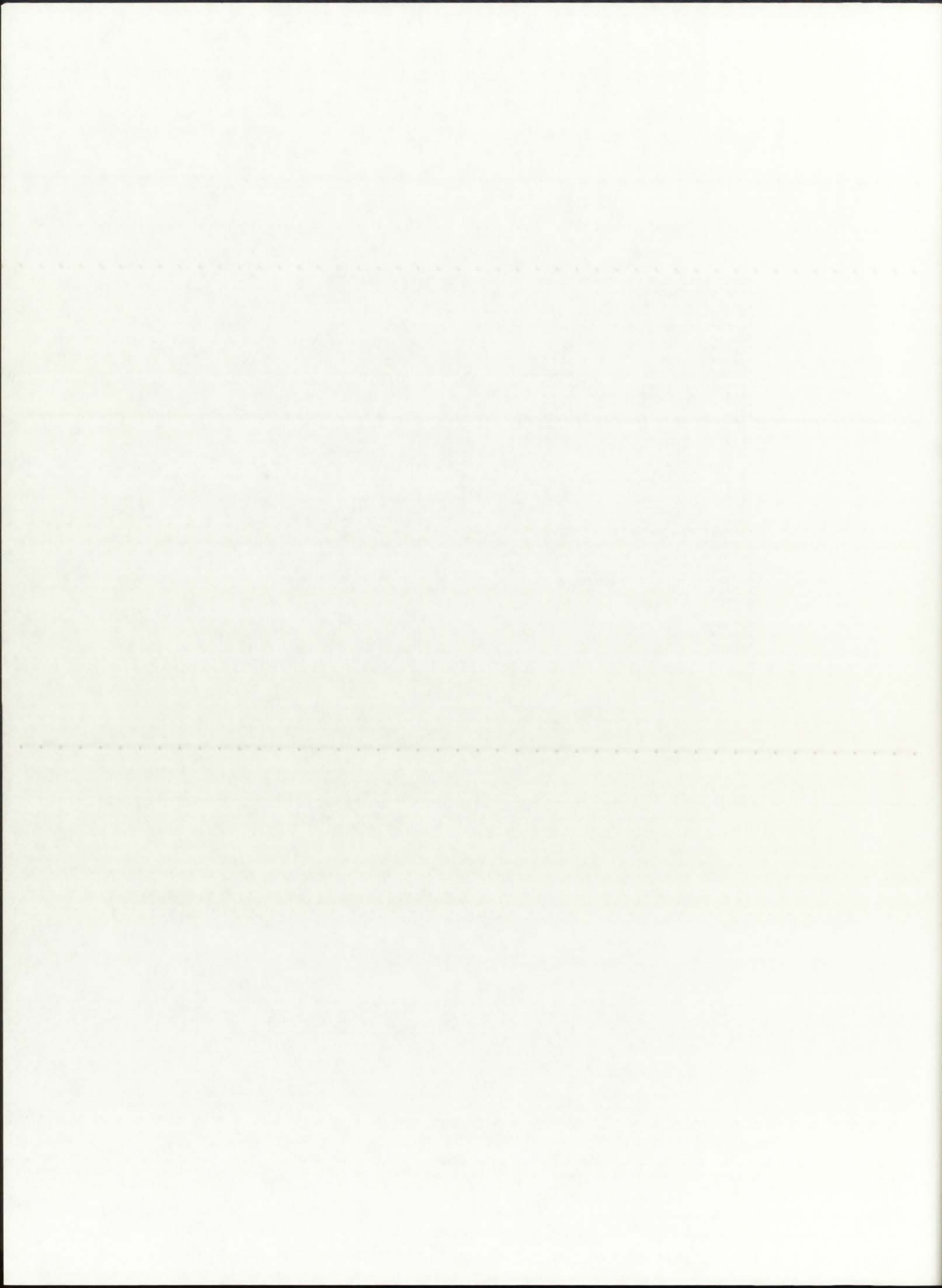
6 *np*/

7 *n2n*/

8 *nd*/

9 *nt*/

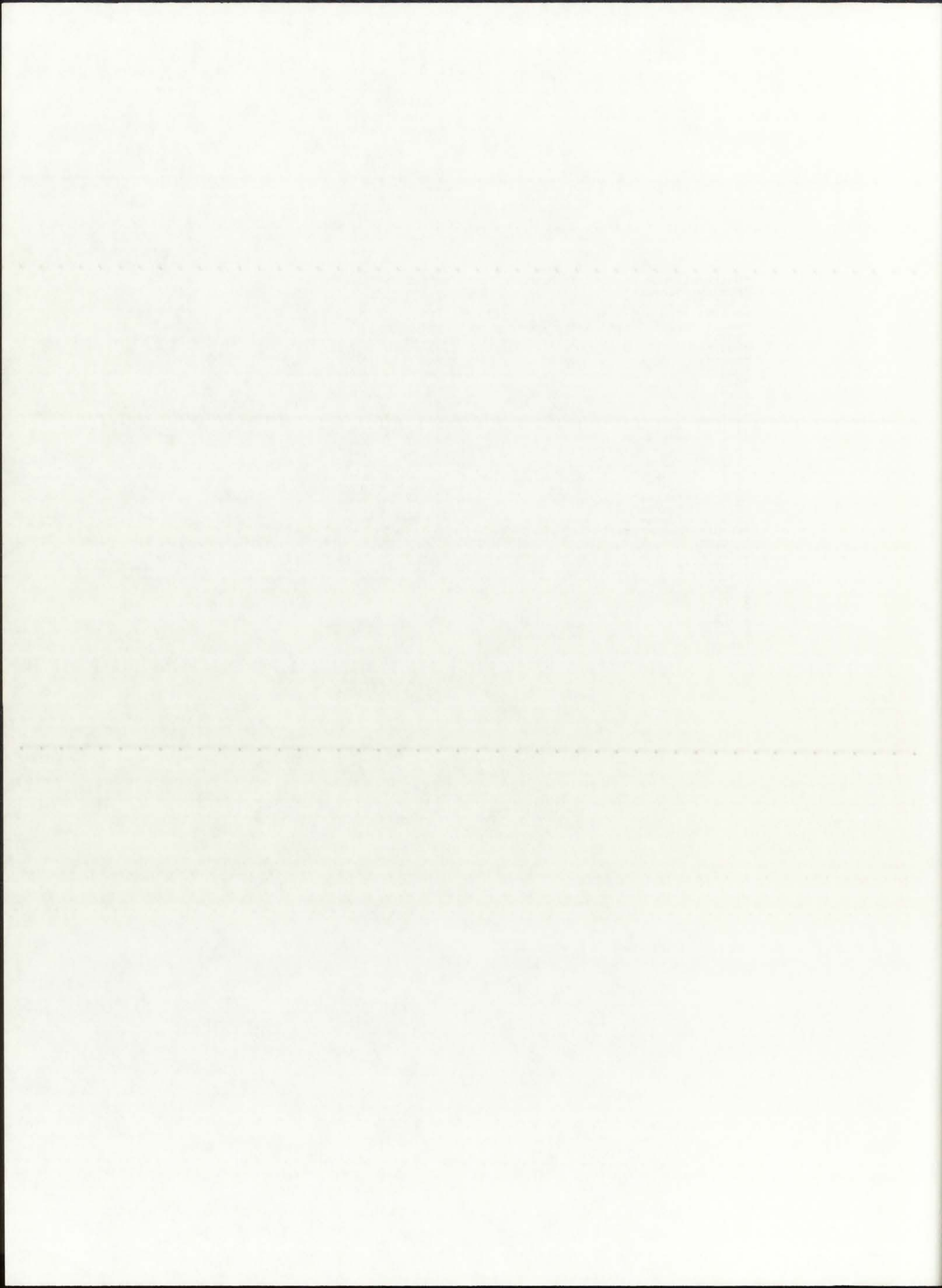
stop



```

*Unit-cell NLB Engine: effects of Tfuel on keff: Tfuel=40,000 K
*mtx7ey* *isotxs*/
1 6 0 1 1 1 0 2 0 0/
69 2 93 20 8 8 9 9 9/
*enru* *hydr* *deut* *oxgn* *bery* *ar* *si* *fe*
*enru* 40000. 1./
*hydr* 300. 1./
*deut* 300. 1./
*oxgn* 300. 1./
*bery* 300. 1./
*ar* 300. 1./
*si* 300. 1./
*fe* 300. 1./
1 1 *u235* 0.96 1.e+10 42 *free*/
1 1 *u238* 0.04 1.e+10 42 *free*/
2 2 *h1* 1.0 1.e+10 42 *free*/
3 3 *h2* 1.0 1.e+10 42 *d2o*/
4 4 *o16* 1.0 1.e+10 42 *free*/
5 5 *be9* 1.0 1.e+10 42 *be* *be$*/
6 6 *arnat* 1.0 1.e+10 42 *free*/
7 7 *sinat* 1.0 1.e+10 42 *free*/
8 8 *fenat* 1.0 1.e+10 42 *free*/
*strpl* *sngam* *sfis* *chiso* *snalf* *snp* *sn2n* *snd* *snt*/
1 *trd*/
2 *ng*/
3 *nftot*/
4 *chi*/
5 *na*/
6 *np*/
7 *n2n*/
8 *nd*/
9 *nt*/
*stop*

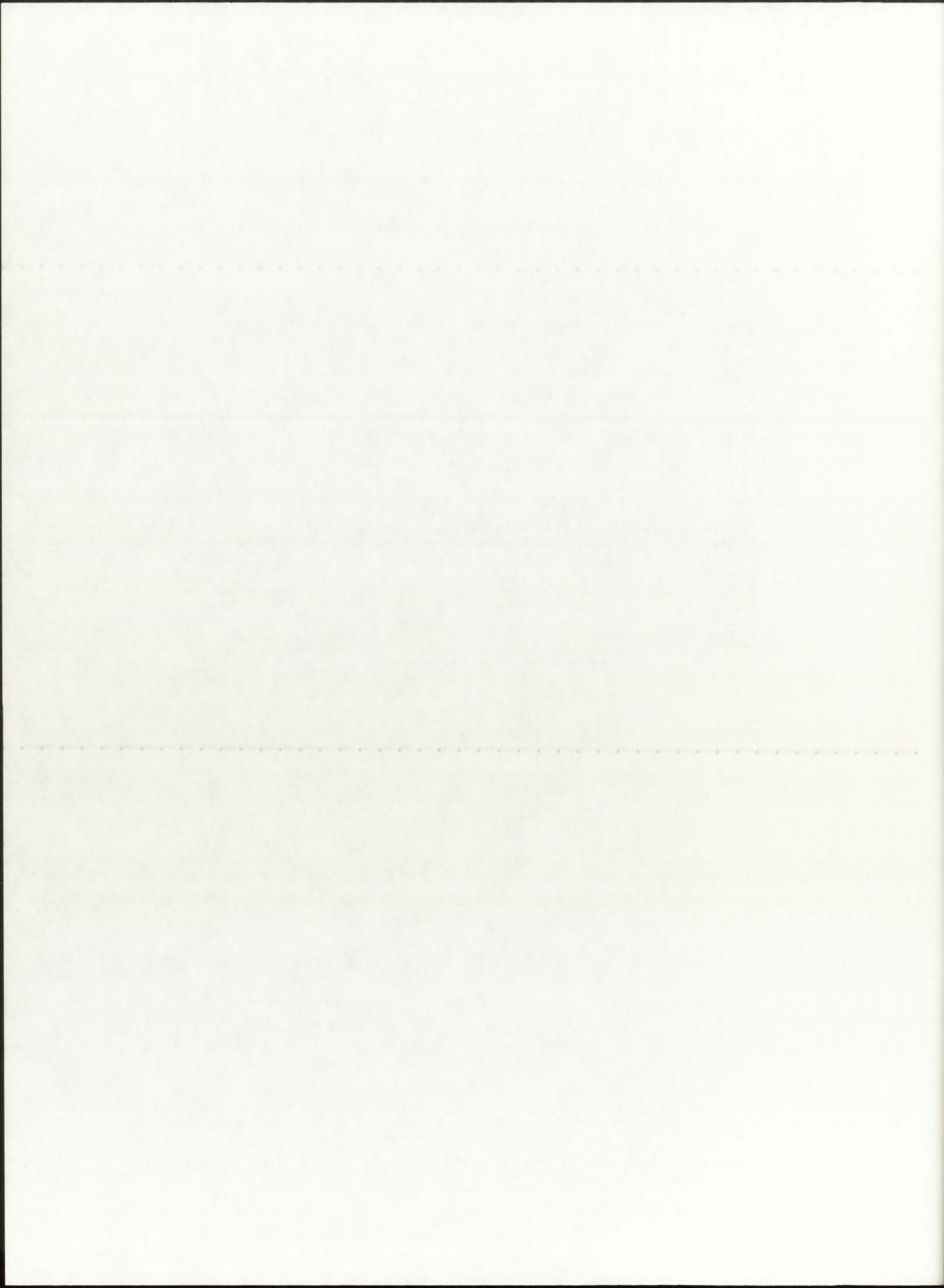
```



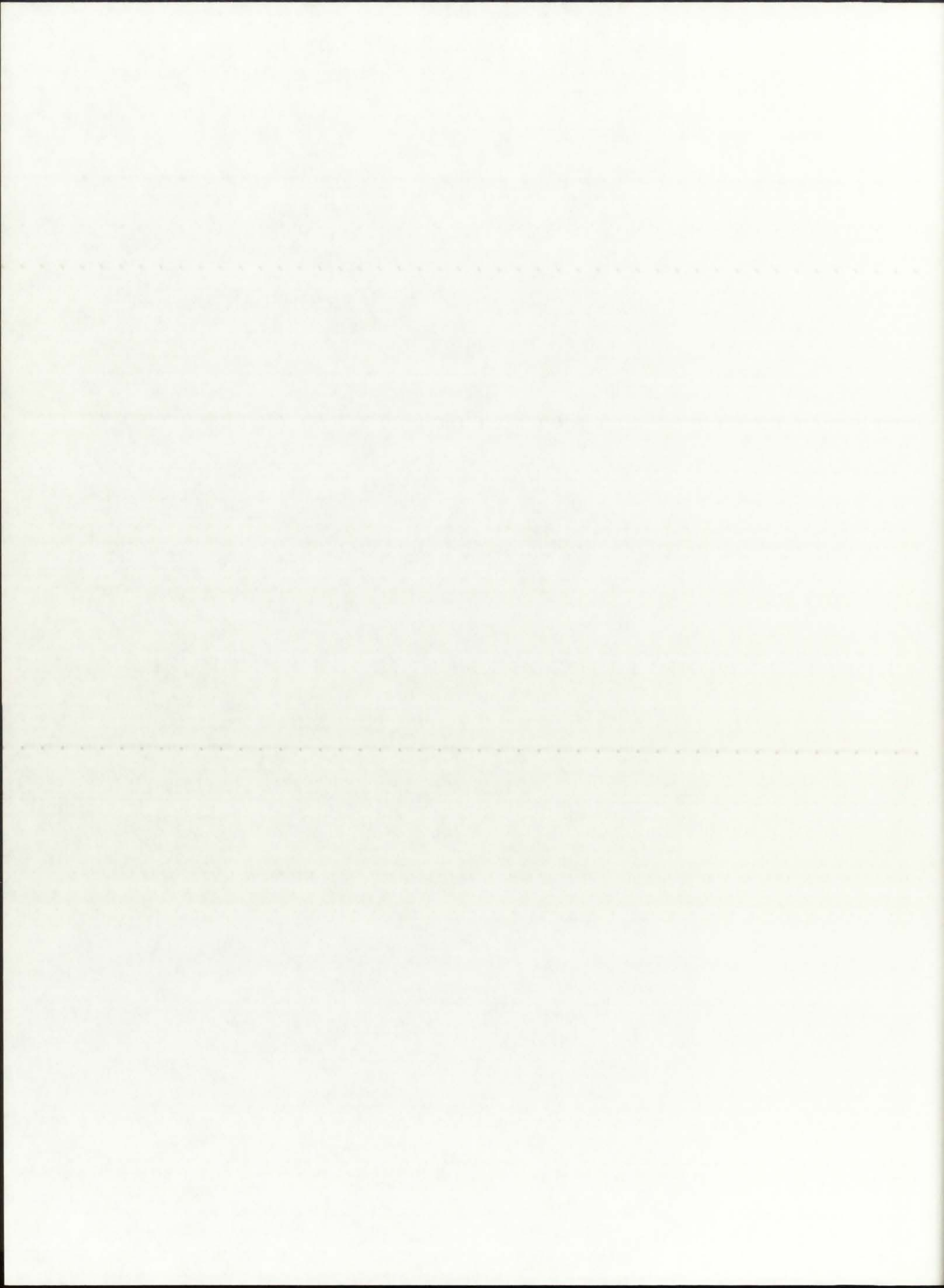
```

*Unit-cell NLB Engine: effects of Tfuel on keff: Tfuel=60,000 K
*mtx7ey* *isotxs*/
1 6 0 1 1 1 0 2 0 0/
69 2 93 20 8 8 9 9 9/
*enru* *hydr* *deut* *oxgn* *bery* *ar* *si* *fe*
*enru* 60000. 1./
*hydr* 300. 1./
*deut* 300. 1./
*oxgn* 300. 1./
*bery* 300. 1./
*ar* 300. 1./
*si* 300. 1./
*fe* 300. 1./
1 1 *u235* 0.96 1.e+10 42 *free*/
1 1 *u238* 0.04 1.e+10 42 *free*/
2 2 *h1* 1.0 1.e+10 42 *free*/
3 3 *h2* 1.0 1.e+10 42 *d2o*/
4 4 *o16* 1.0 1.e+10 42 *free*/
5 5 *be9* 1.0 1.e+10 42 *be* *be$/
6 6 *arnat* 1.0 1.e+10 42 *free*/
7 7 *sinat* 1.0 1.e+10 42 *free*/
8 8 *fenat* 1.0 1.e+10 42 *free*/
*strpl* *sngam* *sfis* *chiso* *snalf* *snp* *sn2n* *snd* *snt*/
1 *trd*/
2 *ng*/
3 *nftot*/
4 *chi*/
5 *na*/
6 *np*/
7 *n2n*/
8 *nd*/
9 *nt*/
*stop*

```



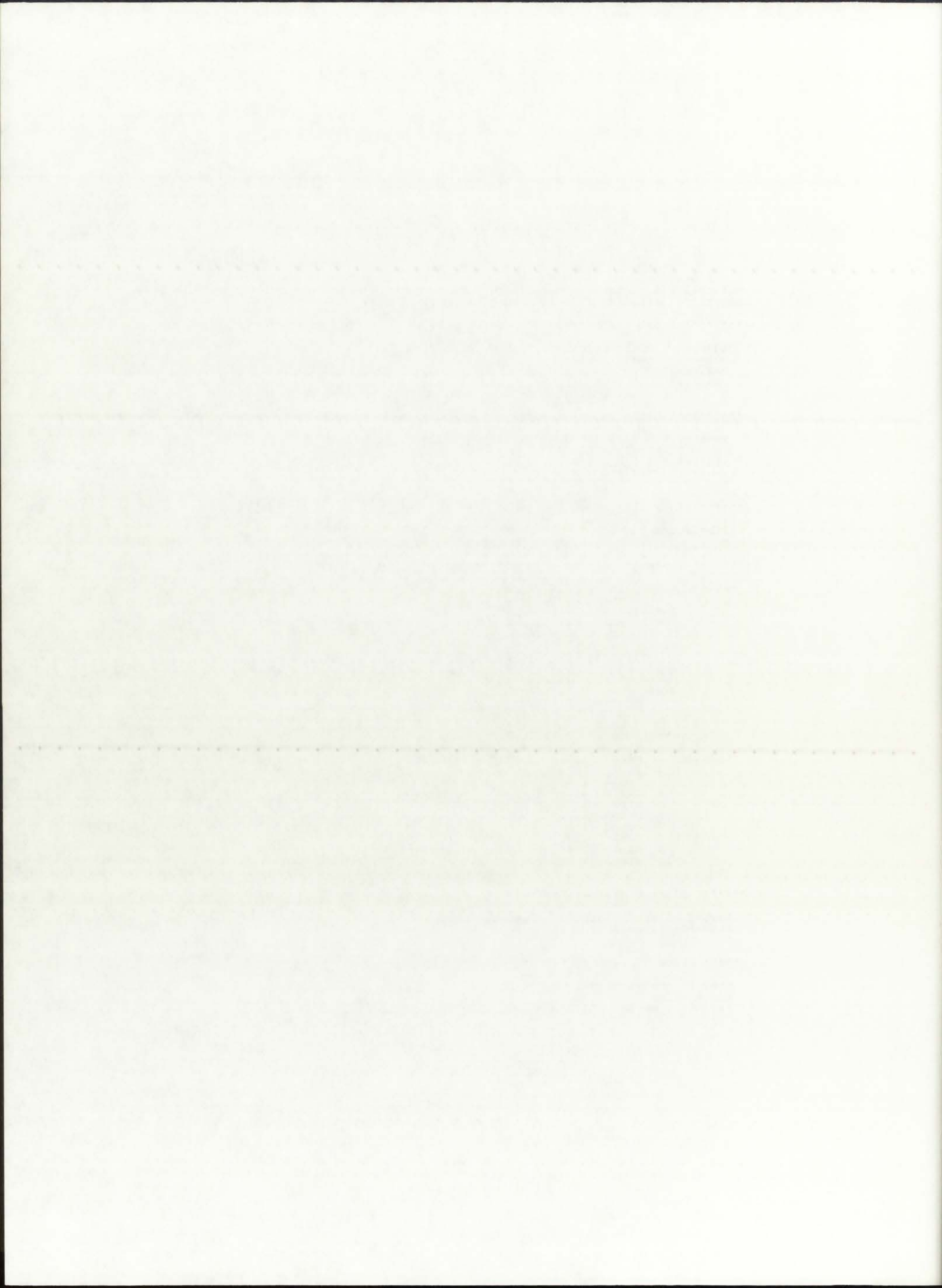
F.2. ONEDANT Input File



```

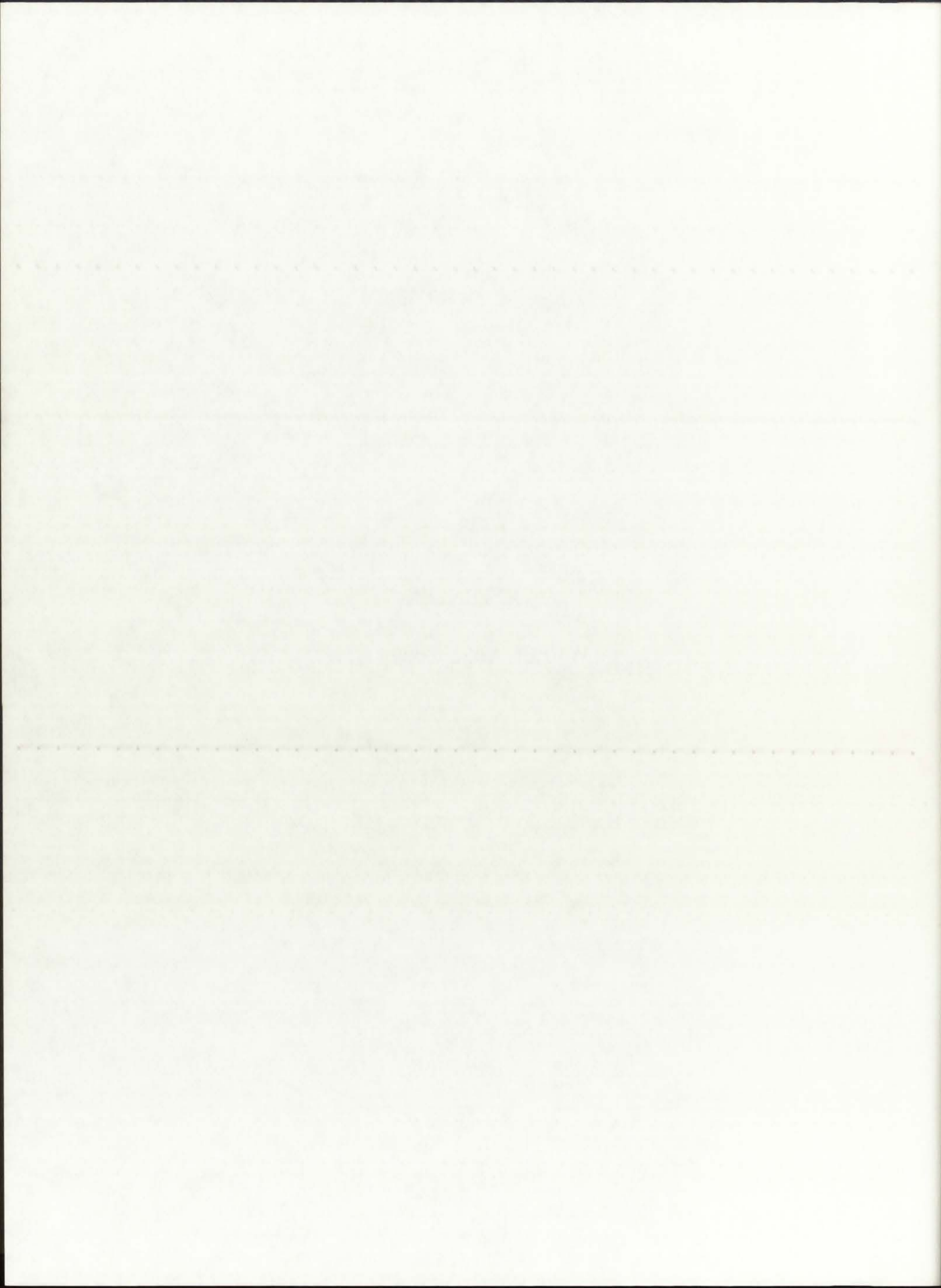
2 0 0
unit-cell NLB engine - 50kWth, P=250 atm, ENDF-VI library
analysis of effects of increasing Tfuel ONLY on keff
/
/***** block i *****/
/
  igeom=cylinder  ngroup=69  isn=8  niso=8  mt=10
  nzone=10  im=10  it=29
  maxlcm=500000
  maxscm=100000
  t
/
/***** block ii *****/
/
  xmesh=0.0,6.0,13.375,20.75,24.45,24.94,28.80,34.58,
        58.58,82.58,87.66
  xints=4 3 3 2 2 2 3 4 4 2
  zones=1 2 3 4 5 6 7 8 9 10
  t
/
/***** block iii (cross sections) *****/
/
  lib=isotxs
  t
/
/***** block iv (mixing) *****/
/
  matls=  mixtr  ar      6.0220e-5
         fuel1  enru    1.0382e-4;
         fuel2  enru    2.0763e-4;
         buffr  ar      3.0110e-4;
         sio2   si      2.6660e-2
         prop   oxgn    5.3320e-2;
         bemod  bery    1.2360e-1;
         d2o1   deut    1.8940e-2
         d2o2   oxgn    9.4700e-3;
         steel  fe      8.4860e-2;
/
  assign= 1  mixtr  1.0;
         2  fuel1  1.0;
         3  fuel2  1.0;
         4  buffr  1.0;
         5  sio2   1.0;
         6  prop   1.0;
         7  bemod  1.0;
         8  d2o1   1.0;
         9  d2o2   1.0;
        10  steel  1.0;
  t
/
/***** block v (solver) *****/
/
  ievt=1  isct=1  ibr=0  fluxp=1  bhgt=182.73
  oitm=30  iitm=100
  t
/
/***** block vi (edits) *****/
/
  pted=1  zned=1  icoll=69;  igrped=3
  edxs=n-fiss
  resdnt=1  mevper=176.0  power=0.0002736  rzflux=1
/

```



APPENDIX G

WVLENABS.f Code Listing



```

* PROGRAM Wvlenabs.f
*
* This program calculates the blackbody emissive power as a function of
* wavelength and temperature. The emissive power is in [W/m2-um]. The
* temperature is varied from 10,000 K to 300,000 K, and the wavelength
* is varied from 1 nm to 8,000 nm. The objective of this analysis is to
* determine the portion of heat flux that gets emitted in the very low
* wavelengths for higher temperatures.
*
* Created: December 10, 1993

      program WvLENABS

      real lambda(14),Temp(9),lambmax(9)
      double precision Elb(9)
      integer i,j,k

      open(unit=11,file='wvlenabs.dat',status='new')

* The optical constants and their units:
* -----
*
*      C1 ..... [W-um4/m2-sr]
*      C2 ..... [um-K]
*      C3 ..... [um-K]

      C1=0.595522e+8
      C2=14387.69
      C3=2897.8

* Temperature data for determination of emissive power:
* -----

      data Temp/5.0e3,10.0e3,25.0e3,50.0e3,75.0e3,100.0e3,150.0e3,
>          200.0e3,300.0e3/

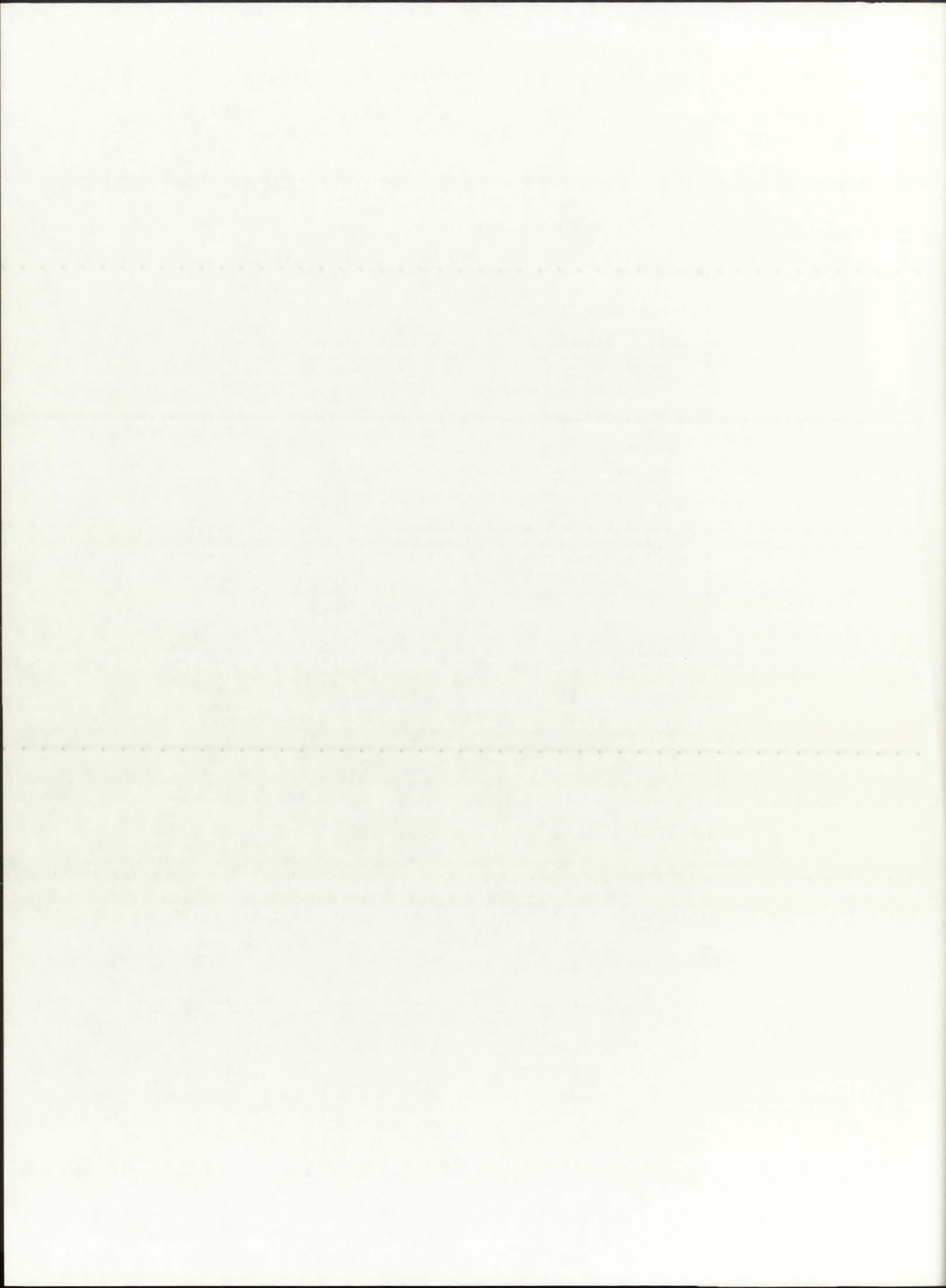
      data lambda/0.001,0.005,0.010,0.025,0.050,0.070,0.100,
>          0.150,0.200,0.300,0.400,0.600,0.800,1.000/

      write(6,100)(k,k=1,9)
      write(11,100)(k,k=1,9)
100  format(/,2x,'WV [um]',3x,9('T (',I1,') ',2x),/)

      do 10 i=1,14
      do 20 j=1,9
          Elb(j)=(2.0*3.14156*C1)/(lambda(i)**5.0*(exp(C2/(lambda(i)
>          *Temp(j)))-1.0))
20  > continue
      write(6,101)lambda(i),(Elb(k),k=i,9)
      write(11,101)lambda(i),(Elb(k),k=1,9)
101  format(2x,F7.4,3x,9(E9.3,2x))
10  continue

      do 30 i=1,9
          lambmax(i)=C3/Temp(i)

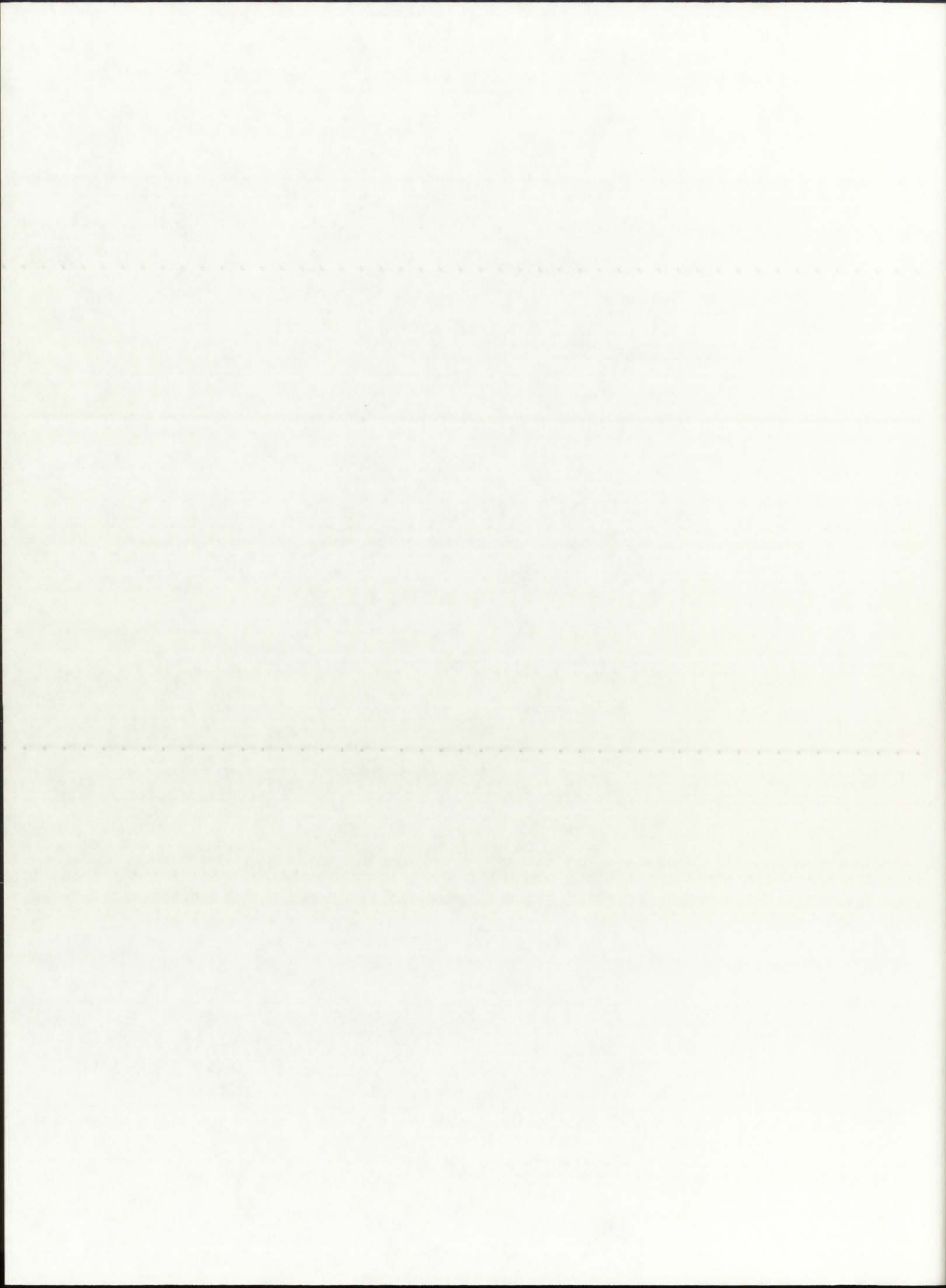
```



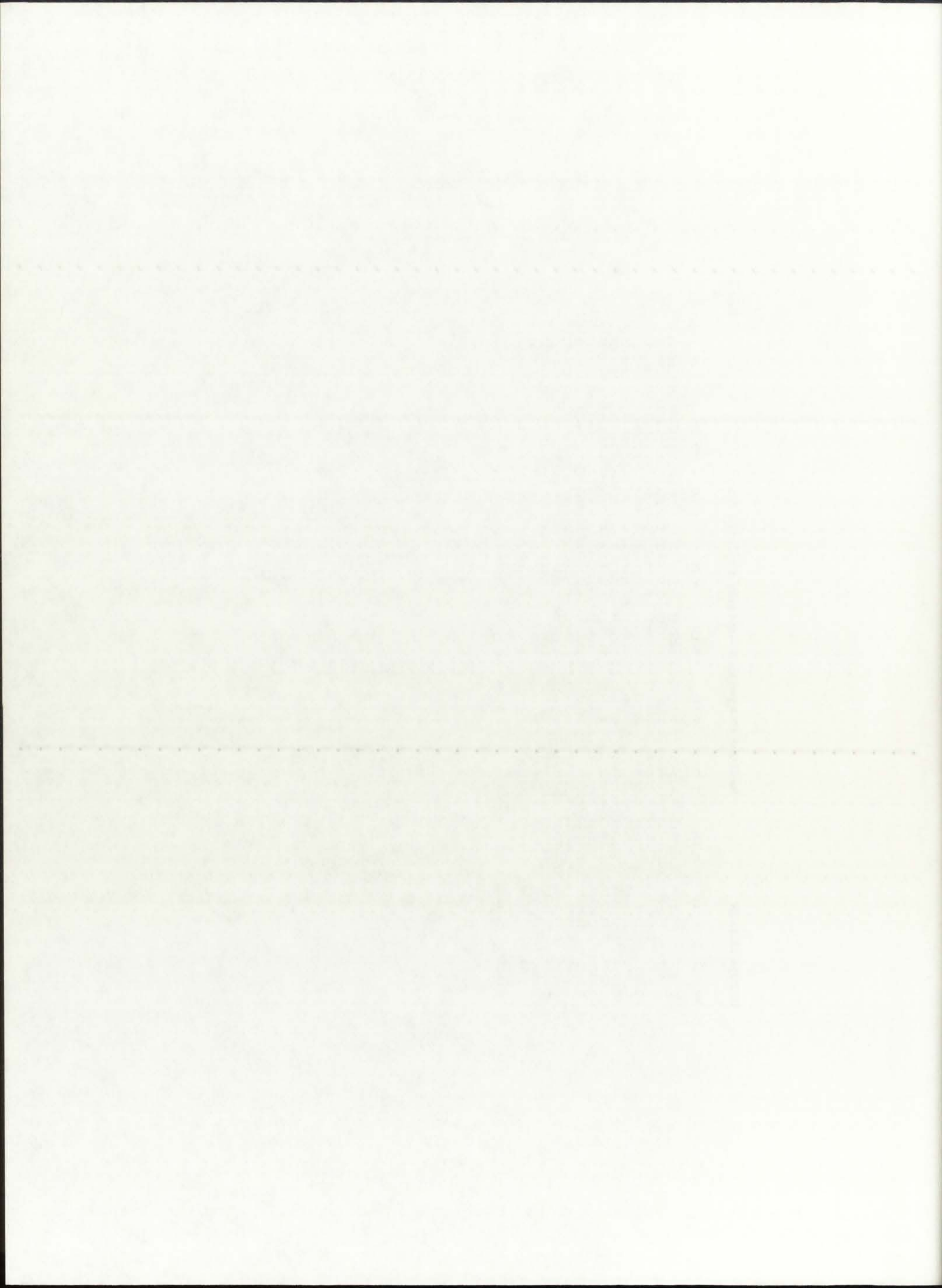

```
30  continue

      write(6,102)(lambmax(i),i=1,9)
      write(11,102)(lambmax(i),i=1,9)
102  format(/,2x,'lambmax:',2x,9(F9.5,2x))

      stop
      end
```

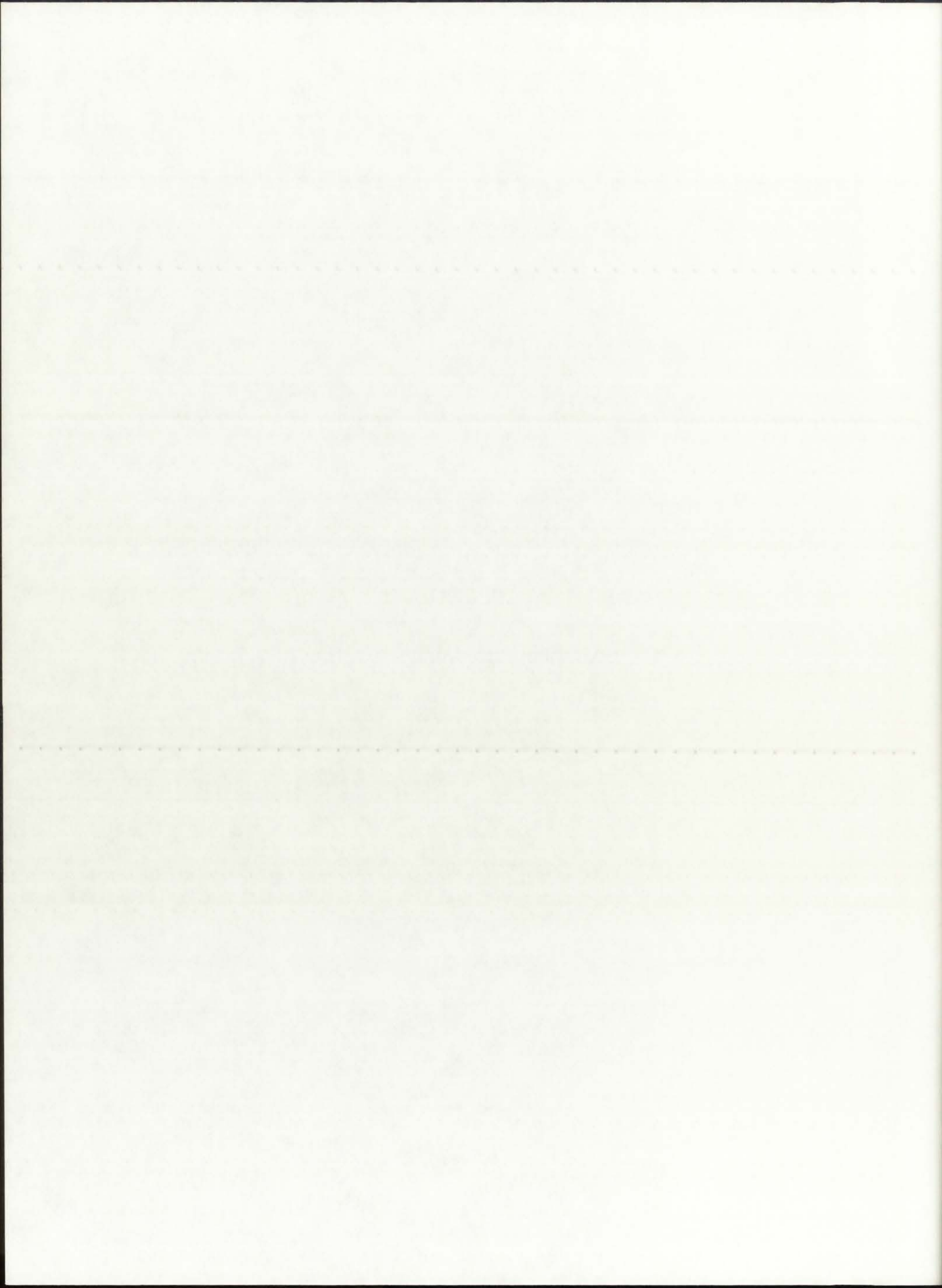


WV [um]	T (1)	T (2)	T (3)	T (4)	T (5)	T (6)	T (7)	T (8)	T (9)
0.0010	0.000E+00	0.000E+00	0.430-226	0.401-101	0.182E-59	0.122E-38	0.825E-18	0.214E-07	0.556E+03
0.0050	0.138-229	0.128-104	0.123E-29	0.121E-04	0.260E+04	0.381E+08	0.558E+12	0.676E+14	0.818E+16
0.0100	0.401-106	0.122E-43	0.379E-06	0.119E+07	0.174E+11	0.211E+13	0.256E+15	0.281E+16	0.312E+17
0.0250	0.394E-33	0.389E-08	0.385E+07	0.384E-12	0.178E+14	0.122E+15	0.844E+15	0.228E+16	0.659E+16
0.0500	0.121E-09	0.381E+03	0.120E+11	0.380E-13	0.264E+14	0.714E+14	0.206E+15	0.372E+15	0.744E+15
0.0700	0.312E-03	0.264E+06	0.599E+11	0.371E-13	0.154E+14	0.327E+14	0.758E+14	0.124E+15	0.226E+15
0.1000	0.119E+02	0.211E+08	0.119E+12	0.223E+13	0.644E+13	0.116E+14	0.232E+14	0.355E+14	0.608E+14
0.1500	0.230E+05	0.336E+09	0.109E+12	0.848E-12	0.190E+13	0.306E+13	0.550E+13	0.801E+13	0.131E+14
0.2000	0.660E+06	0.879E+09	0.697E+11	0.364E-12	0.726E+12	0.111E+13	0.190E+13	0.270E+13	0.431E+13
0.3000	0.105E+08	0.128E+10	0.265E+11	0.957E+11	0.172E+12	0.250E+12	0.409E+12	0.568E+12	0.888E+12
0.4000	0.275E+08	0.103E+10	0.114E+11	0.347E+11	0.594E+11	0.844E+11	0.135E+12	0.185E+12	0.287E+12
0.6000	0.401E+08	0.481E+09	0.299E+10	0.782E+10	0.128E+11	0.178E+11	0.278E+11	0.378E+11	0.578E+11
0.8000	0.322E+08	0.227E+09	0.108E+10	0.264E+10	0.421E+10	0.580E+10	0.896E+10	0.121E+11	0.185E+11
1.0000	0.223E+08	0.116E+09	0.481E+09	0.112E+10	0.177E+10	0.242E+10	0.372E+10	0.502E+10	0.762E+10
lambmax:	0.57956	0.28978	0.11591	0.05796	0.03864	0.02898	0.01932	0.01449	0.00966



APPENDIX H

Mathematica Analysis Listing



```
NIntegrate[(2 3.14156 C1)/(x^5 (Exp[C2/(x T)] - 1)), {x, 10^-3, 0.350}]
```

```
2.17129 10^8
```

```
totQ=5.67044 10^8  
fractQ=2.17129 10^8
```

```
Qabsfr=fractQ/totQ
```

```
0.382914
```

```
-----  
-----  
Second Calculation: T=25,000 K  
-----  
-----
```

```
C1=0.595522 10^8  
C2=14387.69  
T=25.0 10^3
```

```
NIntegrate[(2 3.14156 C1)/(x^5 (Exp[C2/(x T)] - 1)), {x, 10^-3, 10^3}]
```

```
2.21502 10^10
```

```
NIntegrate[(2 3.14156 C1)/(x^5 (Exp[C2/(x T)] - 1)), {x, 10^-3, 0.170}]
```

```
1.16159 10^10
```

```
totQ=2.21502 10^10  
fractQ=1.16159 10^10
```

```
Qabsfr=fractQ/totQ
```

```
0.524415
```

```
NIntegrate[(2 3.14156 C1)/(x^5 (Exp[C2/(x T)] - 1)), {x, 10^-3, 0.182}]
```

```
1.26667 10^10
```

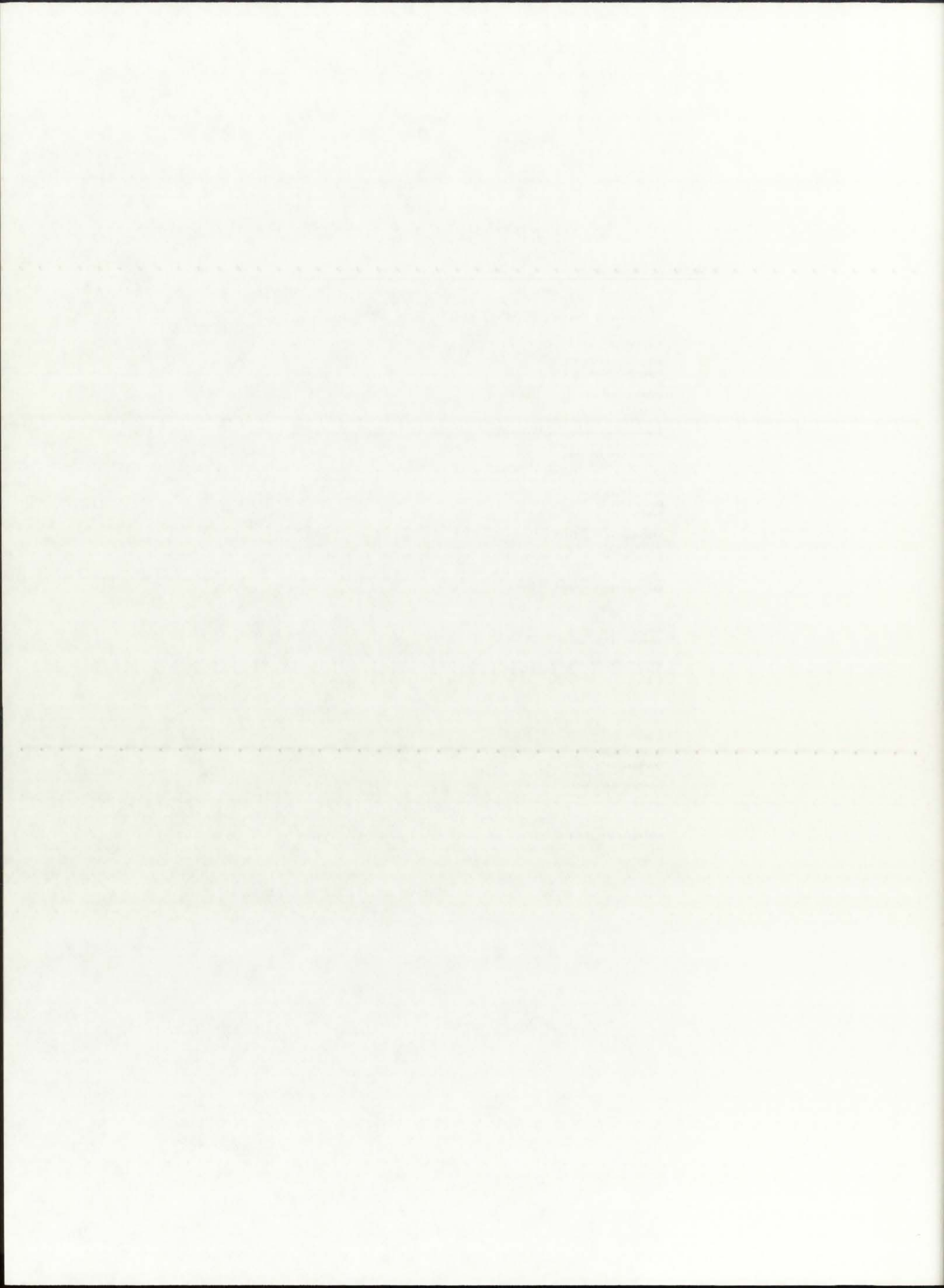
```
totQ=2.21502 10^10  
fractQ=1.26667 10^10
```

```
Qabsfr=fractQ/totQ
```

```
0.571855
```

```
NIntegrate[(2 3.14156 C1)/(x^5 (Exp[C2/(x T)] - 1)), {x, 10^-3, 0.350}]
```

```
1.95499 10^10
```




```
totQ=2.21502 10^10
fractQ=1.95499 10^10
```

```
Qabsfr=fractQ/totQ
```

```
0.882606
```

```
-----
Third Calculation: T=50,000 K
-----
```

```
C1=0.595522 10^8
C2=14387.69
T=50.0 10^3
```

```
NIntegrate[(2 3.14156 C1)/(x^5 (Exp[C2/(x T)] - 1)), {x, 10^-3, 10^3}]
```

```
3.54403 10^11
```

```
NIntegrate[(2 3.14156 C1)/(x^5 (Exp[C2/(x T)] - 1)), {x, 10^-3, 0.170}]
```

```
3.0995 10^11
```

```
totQ=3.54403 10^11
fractQ=3.0995 10^11
```

```
Qabsfr=fractQ/totQ
```

```
0.874569
```

```
NIntegrate[(2 3.14156 C1)/(x^5 (Exp[C2/(x T)] - 1)), {x, 10^-3, 0.182}]
```

```
3.16402 10^11
```

```
totQ=3.54403 10^11
fractQ=3.16402 10^11
```

```
Qabsfr=fractQ/totQ
```

```
0.892775
```

```
NIntegrate[(2 3.14156 C1)/(x^5 (Exp[C2/(x T)] - 1)), {x, 10^-3, 0.350}]
```

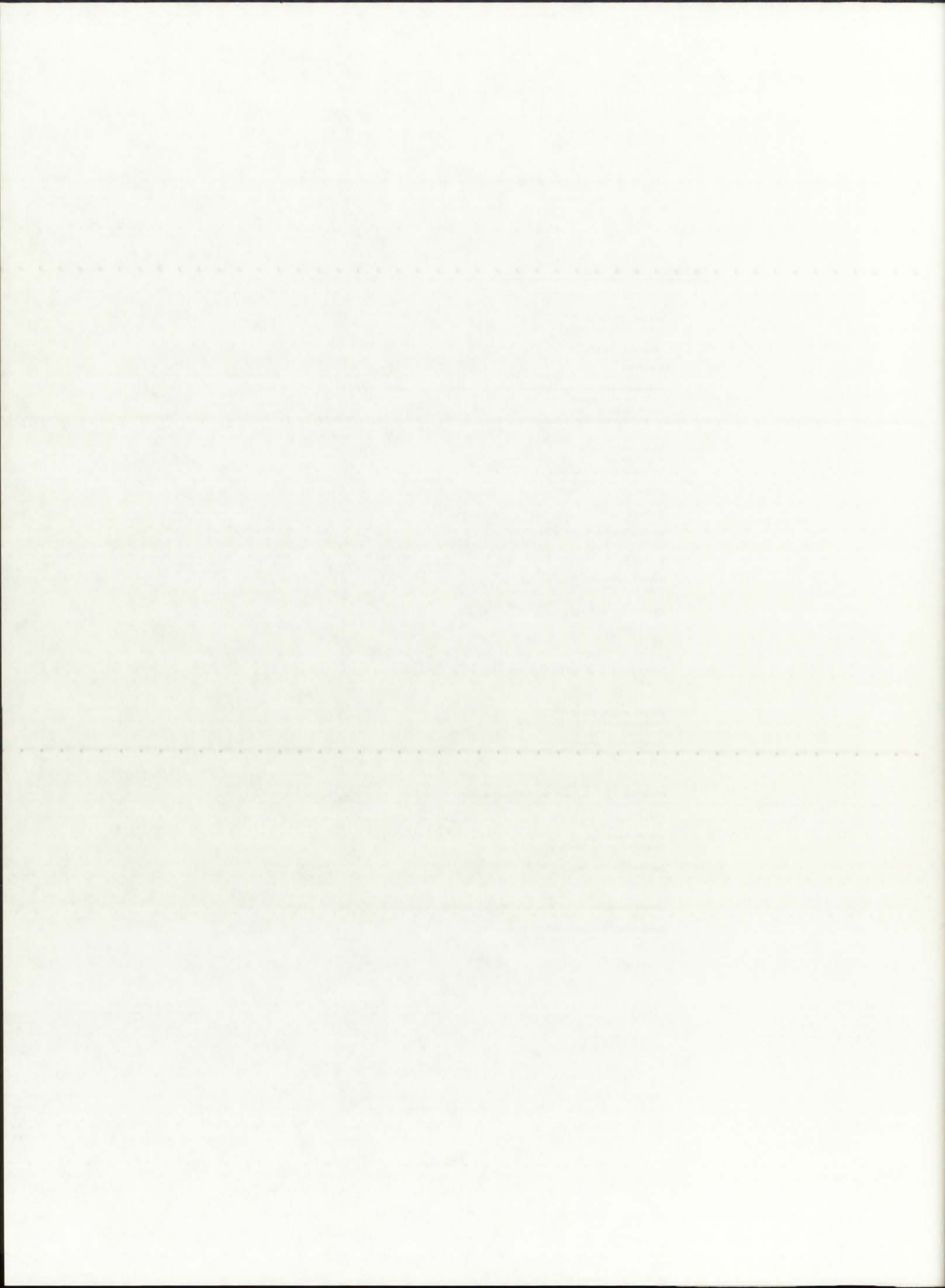
```
3.47071 10^11
```

```
totQ=3.54403 10^11
fractQ=3.47071 10^11
```

```
Qabsfr=fractQ/totQ
```

```
0.979312
```

```
-----
Fourth Calculation: T=80,000 K
-----
```



```
C1=0.595522 10^8
C2=14387.69
T=80.0 10^3

NIntegrate[(2 3.14156 C1)/(x^5 (Exp[C2/(x T)] - 1)), {x, 10^-3, 10^3}]
2.32261 10^12

NIntegrate[(2 3.14156 C1)/(x^5 (Exp[C2/(x T)] - 1)), {x, 10^-3, 0.170}]
2.22966 10^12
totQ=2.32261 10^12
fractQ=2.22966 10^12
Qabsfr=fractQ/totQ
0.95998

NIntegrate[(2 3.14156 C1)/(x^5 (Exp[C2/(x T)] - 1)), {x, 10^-3, 0.182}]
2.24465 10^12
totQ=2.32261 10^12
fractQ=2.24465 10^12
Qabsfr=fractQ/totQ
0.966434

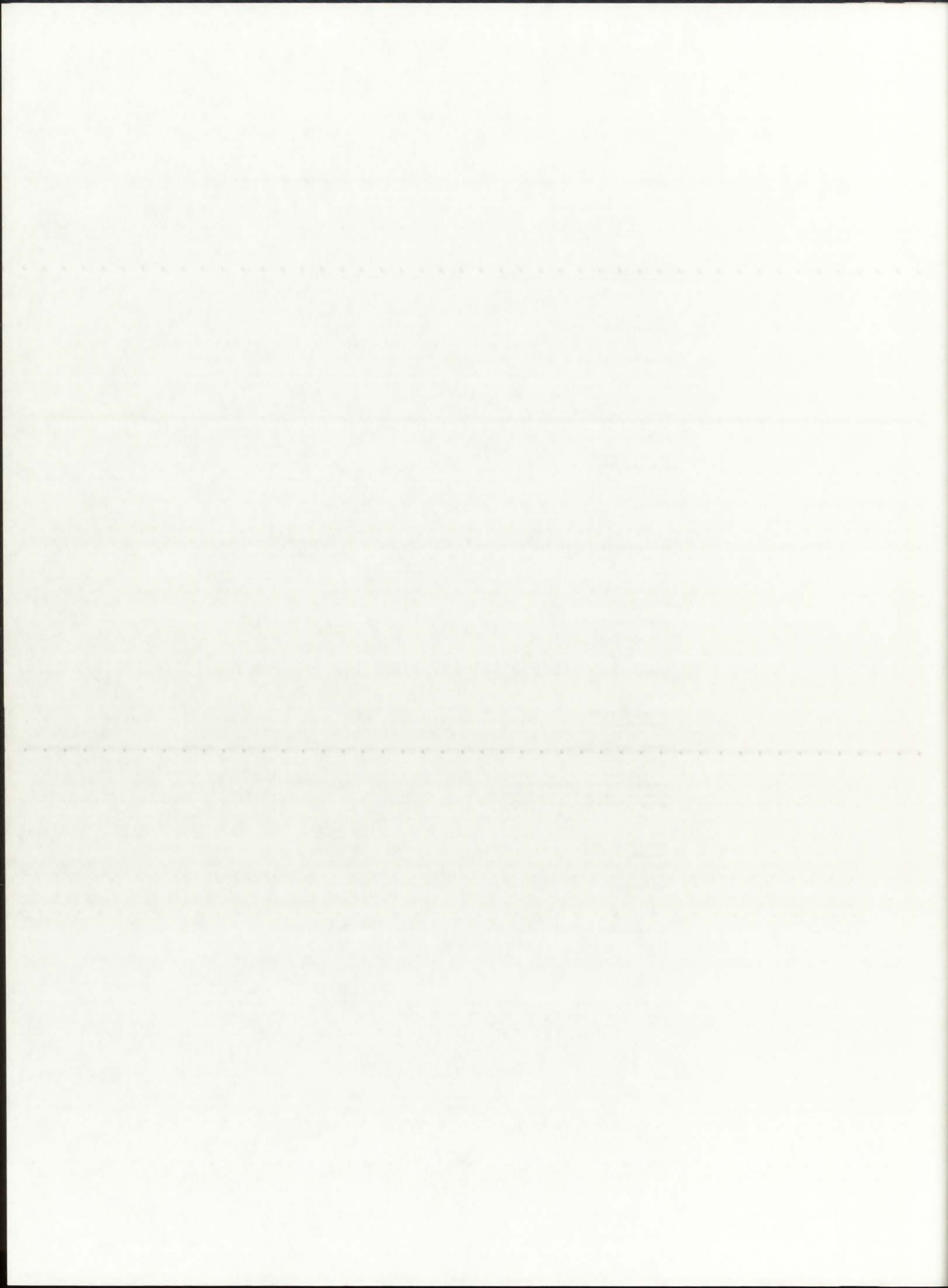
NIntegrate[(2 3.14156 C1)/(x^5 (Exp[C2/(x T)] - 1)), {x, 10^-3, 0.350}]
2.30934 10^12
totQ=2.32261 10^12
fractQ=2.30934 10^12
Qabsfr=fractQ/totQ
0.994287

=====
Fifth Calculation: T=120,000 K
=====

C1=0.595522 10^8
C2=14387.69
T=120.0 10^3

NIntegrate[(2 3.14156 C1)/(x^5 (Exp[C2/(x T)] - 1)), {x, 10^-3, 10^3}]
1.17582 10^13

NIntegrate[(2 3.14156 C1)/(x^5 (Exp[C2/(x T)] - 1)), {x, 10^-3, 0.170}]
1.15973 10^13
```



```
totQ=1.17582 10^13
fractQ=1.15973 10^13

Qabsfr=fractQ/totQ

0.986316
```

```
NIntegrate[(2 3.14156 C1)/(x^5 (Exp[C2/(x T)] - 1)), {x, 10^-3, 0.182}]
```

```
1.16246 10^13
```

```
totQ=1.17582 10^13
fractQ=1.16246 10^13
```

```
Qabsfr=fractQ/totQ
```

```
0.988638
```

```
NIntegrate[(2 3.14156 C1)/(x^5 (Exp[C2/(x T)] - 1)), {x, 10^-3, 0.350}]
```

```
1.17369 10^13
```

```
totQ=1.17582 10^13
fractQ=1.17369 10^13
```

```
Qabsfr=fractQ/totQ
```

```
0.998188
```

```
-----
Sixth Calculation: T=170,000 K
-----
```

```
C1=0.595522 10^8
C2=14387.69
T=170.0 10^3
```

```
NIntegrate[(2 3.14156 C1)/(x^5 (Exp[C2/(x T)] - 1)), {x, 10^-3, 10^3}]
```

```
4.736 10^13
```

```
NIntegrate[(2 3.14156 C1)/(x^5 (Exp[C2/(x T)] - 1)), {x, 10^-3, 0.170}]
```

```
4.71125 10^13
```

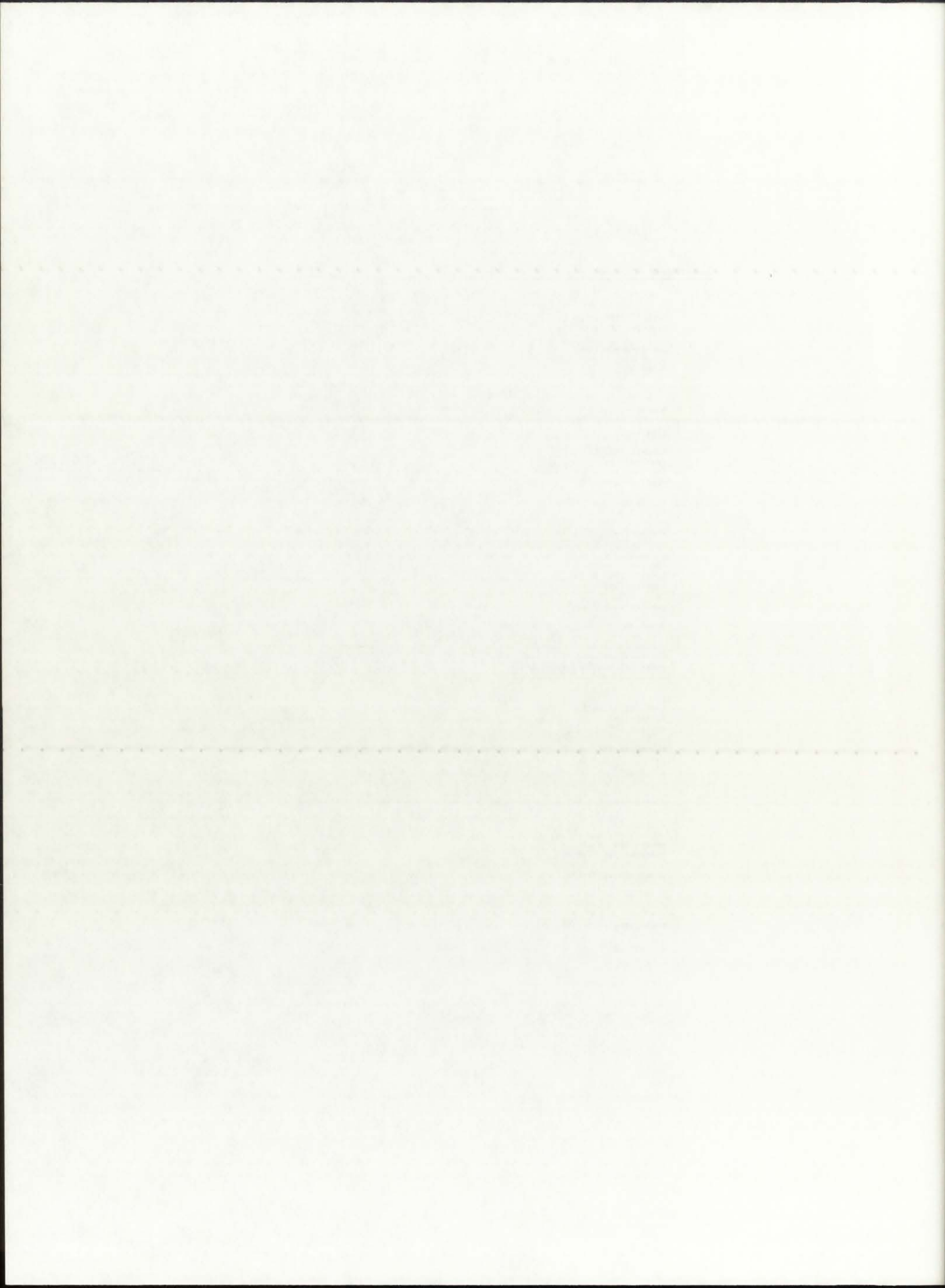
```
totQ=4.736 10^13
fractQ=4.71125 10^13
```

```
Qabsfr=fractQ/totQ
```

```
0.994774
```

```
NIntegrate[(2 3.14156 C1)/(x^5 (Exp[C2/(x T)] - 1)), {x, 10^-3, 0.182}]
```

```
4.71557 10^13
```



```
totQ=4.736 10^13
fractQ=4.71557 10^13

Qabsfr=fractQ/totQ

0.995686

NIntegrate[(2 3.14156 C1)/(x^5 (Exp[C2/(x T)] - 1)), {x, 10^-3, 0.350}]

4.73288 10^13

totQ=4.736 10^13
fractQ=4.73288 10^13

Qabsfr=fractQ/totQ

0.999341

-----
Seventh Calculation: T=200,000 K
-----

C1=0.595522 10^8
C2=14387.69
T=200.0 10^3

NIntegrate[(2 3.14156 C1)/(x^5 (Exp[C2/(x T)] - 1)), {x, 10^-3, 10^3}]

9.07271 10^13

NIntegrate[(2 3.14156 C1)/(x^5 (Exp[C2/(x T)] - 1)), {x, 10^-3, 0.170}]

9.04271 10^13

totQ=9.07271 10^13
fractQ=9.04271 10^13

Qabsfr=fractQ/totQ

0.996693

NIntegrate[(2 3.14156 C1)/(x^5 (Exp[C2/(x T)] - 1)), {x, 10^-3, 0.182}]

9.04799 10^13

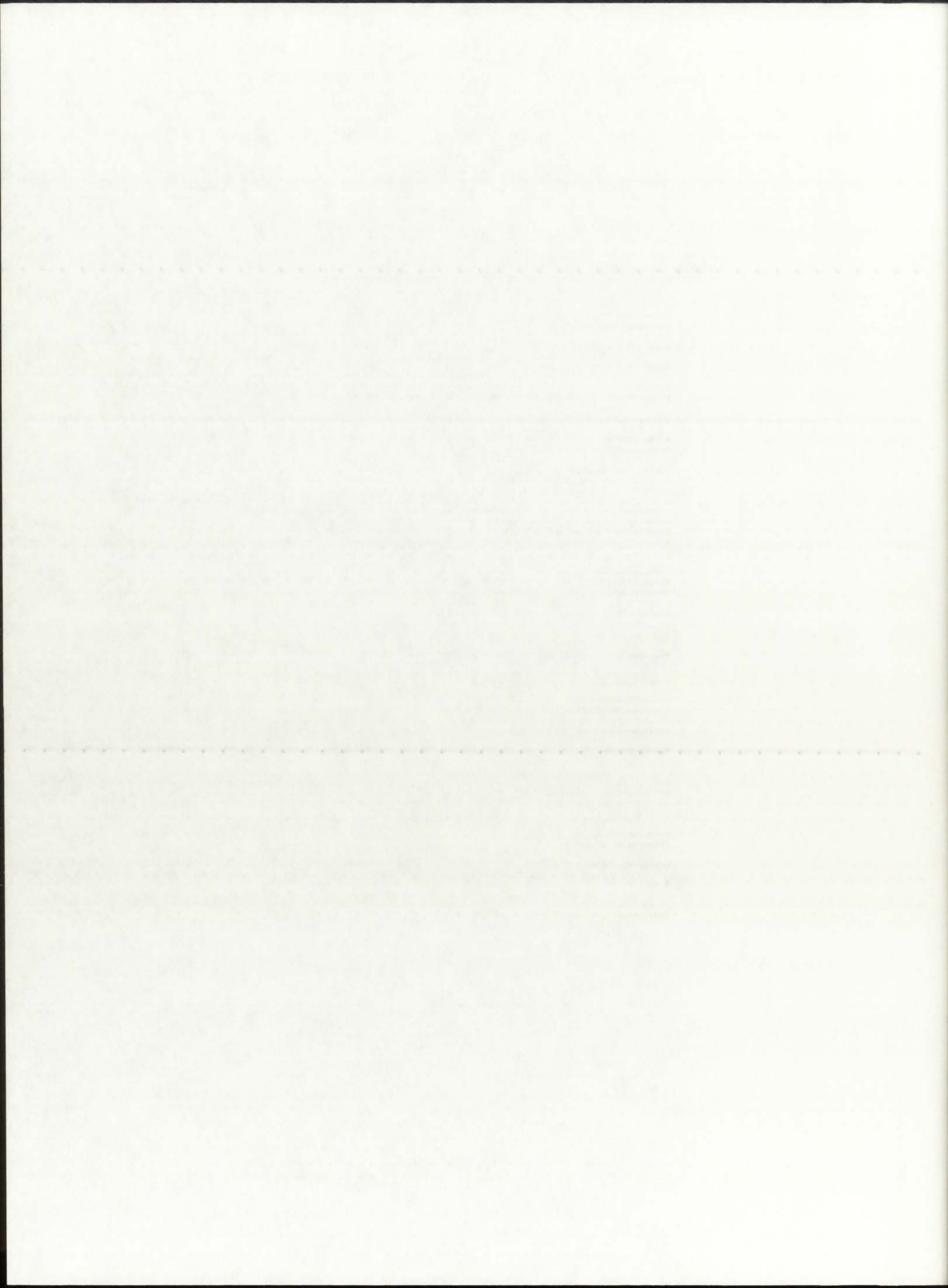
totQ=9.07271 10^13
fractQ=9.04799 10^13

Qabsfr=fractQ/totQ

0.997275

NIntegrate[(2 3.14156 C1)/(x^5 (Exp[C2/(x T)] - 1)), {x, 10^-3, 0.350}]

9.06897 10^13
```




```
totQ=9.07271 10^13
fractQ=9.06897 10^13
```

```
Qabsfr=fractQ/totQ
```

```
0.999588
```

```
-----
Eighth Calculation: T=250,000 K
-----
```

```
C1=0.595522 10^8
```

```
C2=14387.69
```

```
T=250.0 10^3
```

```
NIntegrate[(2 3.14156 C1)/(x^5 (Exp[C2/(x T)] - 1)), {x, 10^-3, 10^3}]
```

```
2.215 10^14
```

```
NIntegrate[(2 3.14156 C1)/(x^5 (Exp[C2/(x T)] - 1)), {x, 10^-3, 0.170}]
```

```
2.21114 10^14
```

```
totQ=2.215 10^14
```

```
fractQ=2.21114 10^14
```

```
Qabsfr=fractQ/totQ
```

```
0.998257
```

```
NIntegrate[(2 3.14156 C1)/(x^5 (Exp[C2/(x T)] - 1)), {x, 10^-3, 0.182}]
```

```
2.21183 10^14
```

```
totQ=2.215 10^14
```

```
fractQ=2.21183 10^14
```

```
Qabsfr=fractQ/totQ
```

```
0.998569
```

```
NIntegrate[(2 3.14156 C1)/(x^5 (Exp[C2/(x T)] - 1)), {x, 10^-3, 0.350}]
```

```
2.21454 10^14
```

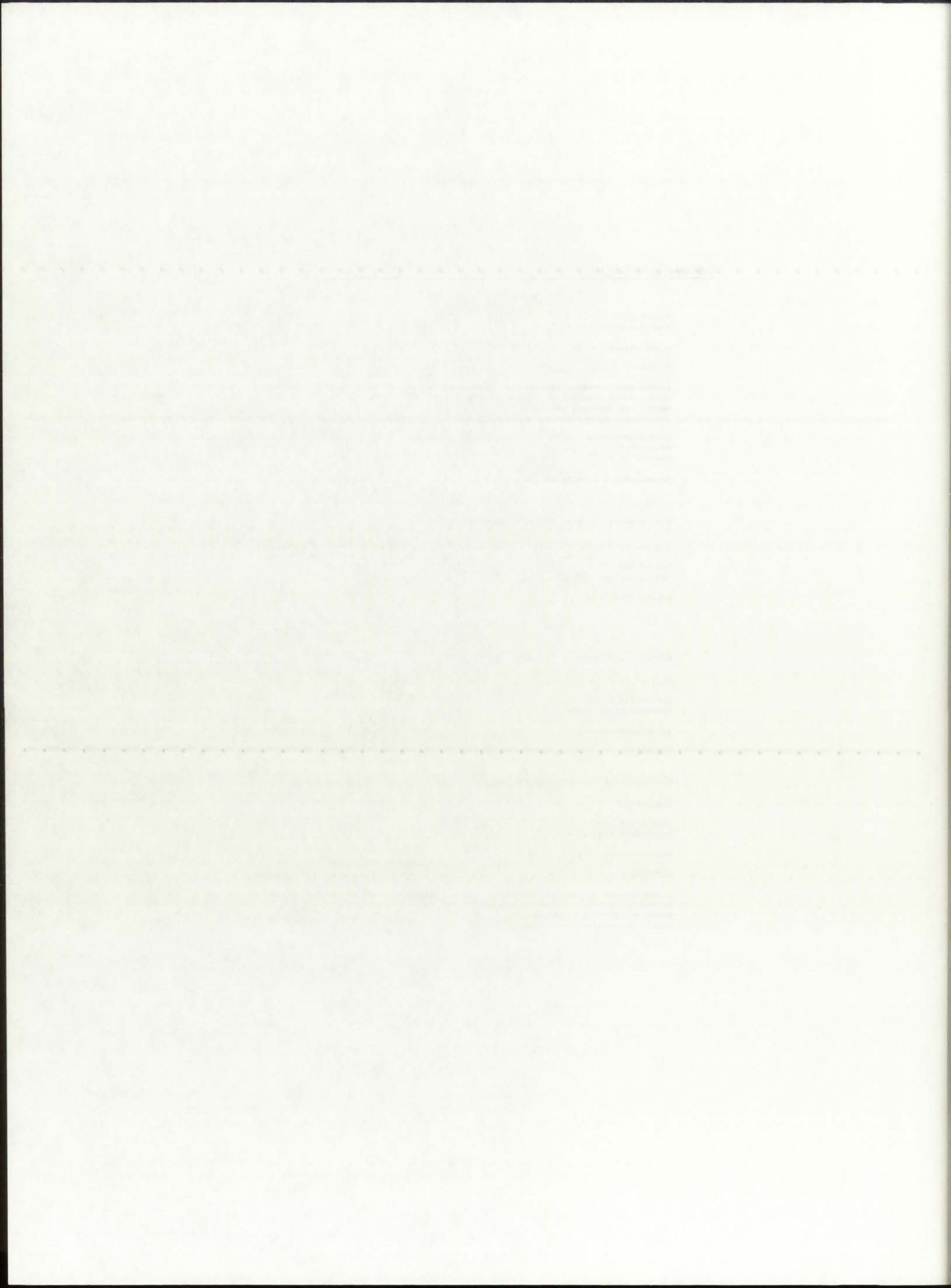
```
totQ=2.215 10^14
```

```
fractQ=2.21454 10^14
```

```
Qabsfr=fractQ/totQ
```

```
0.999792
```

```
-----
Ninth Calculation: T=300,000 K
-----
```



```
C1=0.595522 10^8
C2=14387.69
T=300.0 10^3

NIntegrate[(2 3.14156 C1)/(x^5 (Exp[C2/(x T)] - 1)), {x, 10^-3, 10^3}]

4.5931 10^14

NIntegrate[(2 3.14156 C1)/(x^5 (Exp[C2/(x T)] - 1)), {x, 10^-3, 0.170}]

4.58831 10^14

totQ=4.5931 10^14
fractQ=4.58831 10^14

Qabsfr=fractQ/totQ

0.998957

NIntegrate[(2 3.14156 C1)/(x^5 (Exp[C2/(x T)] - 1)), {x, 10^-3, 0.182}]

4.58916 10^14

totQ=4.5931 10^14
fractQ=4.58916 10^14

Qabsfr=fractQ/totQ

0.999142

NIntegrate[(2 3.14156 C1)/(x^5 (Exp[C2/(x T)] - 1)), {x, 10^-3, 0.350}]

4.59248 10^14

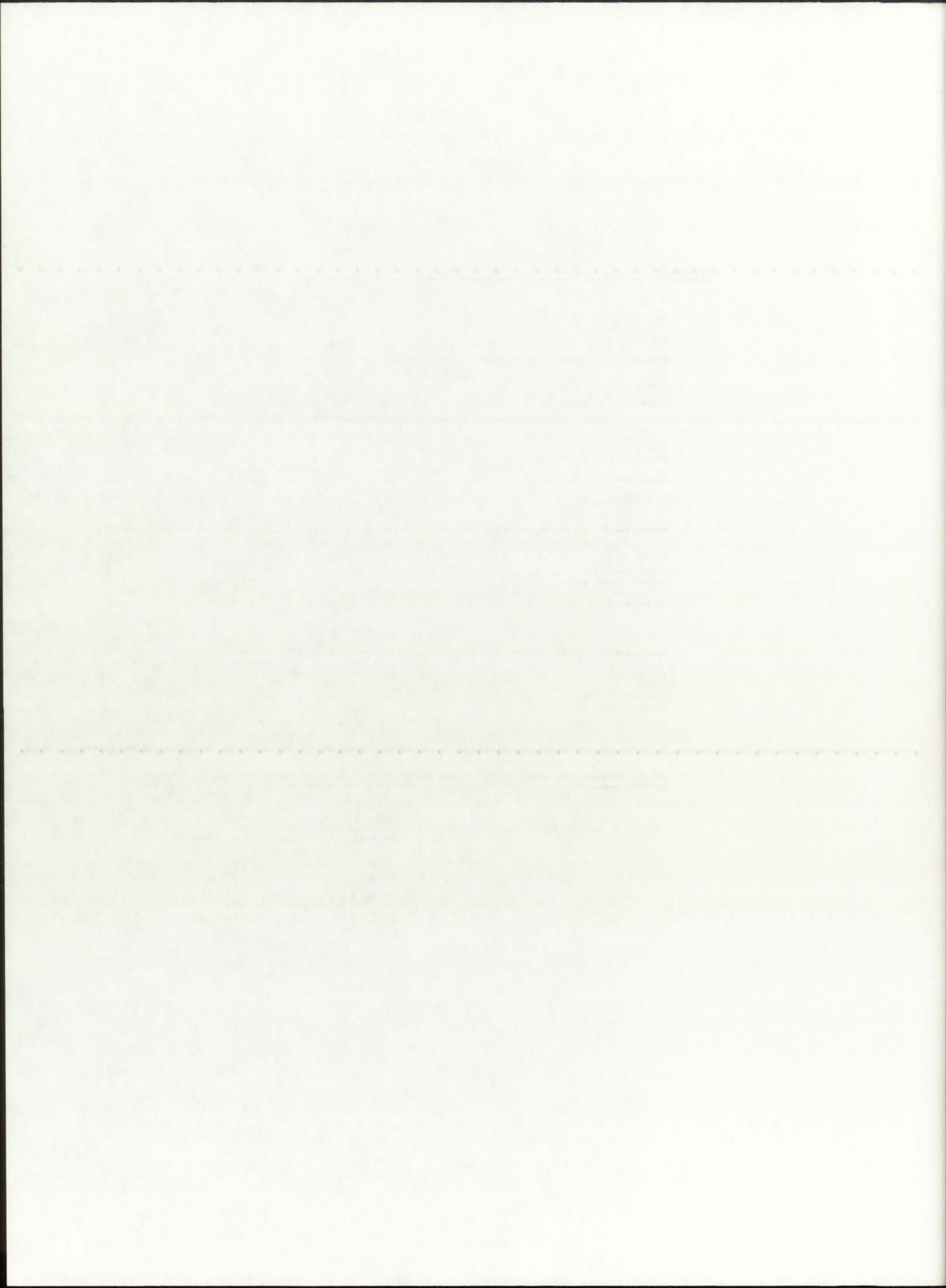
totQ=4.5931 10^14
fractQ=4.59248 10^14

Qabsfr=fractQ/totQ

0.999865
```

```
*****
*****

TESTING: Integration from negative infinity to infinity. Result will be meaningless
         since there is no such thing as a negative wavelength
```



```

NIntegrate[(2 3.14156 C1)/(x^5 (Exp[C2/(x T)] - 1)), {x, -Infinity, Infinity}]

General::ovfl: Overflow occurred in computation.

NIntegrate::slwcon: Numerical integration converging too slowly; suspect one of the following:
singularity, oscillatory integrand, or insufficient WorkingPrecision.

General::ovfl: Overflow occurred in computation.

NIntegrate::ncvb: NIntegrate failed to converge to prescribed accuracy after 7 recursive bisections
near x = -4.36999 10-57 .
0.

```

```

=====
=====

```

ADDITIONAL CALCULATIONS TO DETERMINE Qabsfr BETWEEN 10,000 K-25,000 K:

```

=====
=====

```

Temperature=12,000 K

T=12.0 10³

```

NIntegrate[(2 3.14156 C1)/(x^5 (Exp[C2/(x T)] - 1)), {x, 10-3, 103}]

```

1.17582 10⁹

```

NIntegrate[(2 3.14156 C1)/(x^5 (Exp[C2/(x T)] - 1)), {x, 10-3, 0.170}]

```

8.59137 10⁷

```

totQ=1.17582 109
fractQ=8.59137 107

```

```

Qabsfr=fractQ/totQ

```

0.0730671

```

NIntegrate[(2 3.14156 C1)/(x^5 (Exp[C2/(x T)] - 1)), {x, 10-3, 0.182}]

```

1.15166 10⁸

```

totQ=1.17582 109
fractQ=1.15166 108

```

```

Qabsfr=fractQ/totQ

```

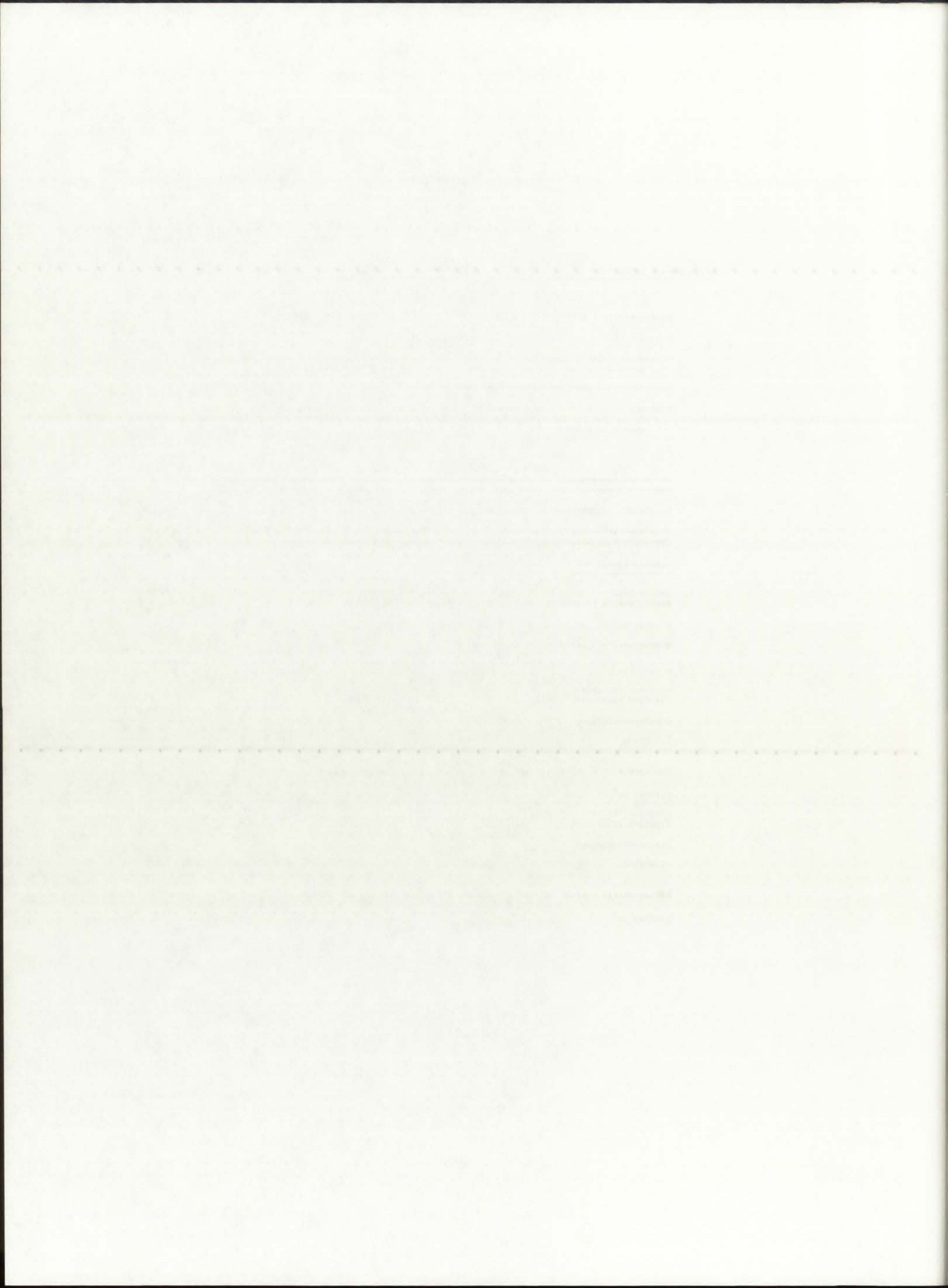
0.0979453

```

NIntegrate[(2 3.14156 C1)/(x^5 (Exp[C2/(x T)] - 1)), {x, 10-3, 0.350}]

```

6.06729 10⁸



```
totQ=1.17582 10^9
fractQ=6.06729 10^8
Qabsfr=fractQ/totQ
0.516005
```

```
-----
Temperature=14,000 K
-----
```

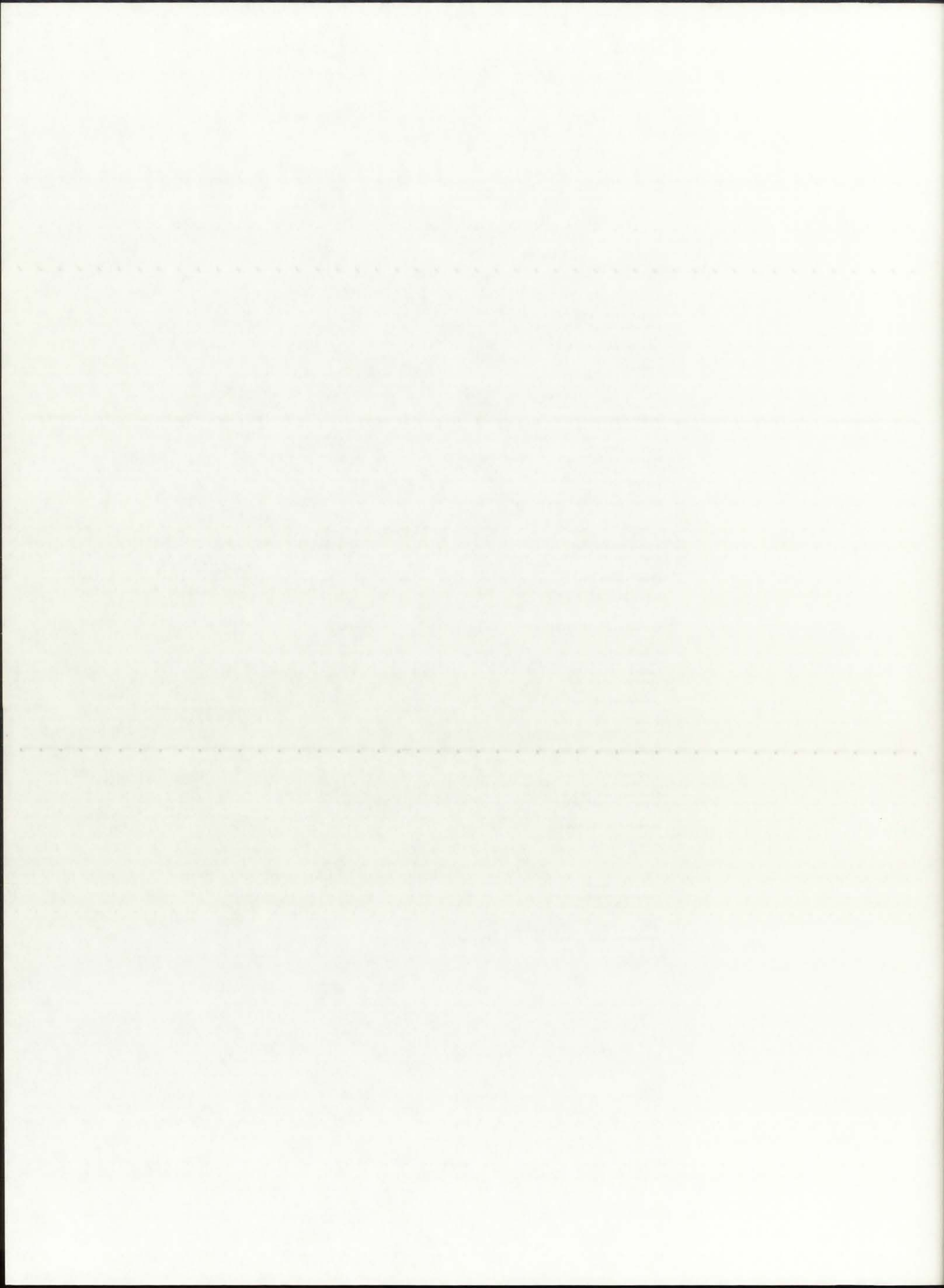
```
T=14.0 10^3
NIntegrate[(2 3.14156 C1)/(x^5 (Exp[C2/(x T)] - 1)), {x, 10^-3, 10^3}]
2.17836 10^9
NIntegrate[(2 3.14156 C1)/(x^5 (Exp[C2/(x T)] - 1)), {x, 10^-3, 0.170}]
2.96557 10^8
totQ=2.17836 10^9
fractQ=2.96557 10^8
Qabsfr=fractQ/totQ
0.136138
```

```
NIntegrate[(2 3.14156 C1)/(x^5 (Exp[C2/(x T)] - 1)), {x, 10^-3, 0.182}]
3.74101 10^8
totQ=2.17836 10^9
fractQ=3.74101 10^8
Qabsfr=fractQ/totQ
0.171735
```

```
NIntegrate[(2 3.14156 C1)/(x^5 (Exp[C2/(x T)] - 1)), {x, 10^-3, 0.350}]
1.35252 10^9
totQ=2.17836 10^9
fractQ=1.35252 10^9
Qabsfr=fractQ/totQ
0.620889
```

```
-----
Temperature=16,000 K
-----
```

```
T=16.0 10^3
NIntegrate[(2 3.14156 C1)/(x^5 (Exp[C2/(x T)] - 1)), {x, 10^-3, 10^3}]
3.71618 10^9
```




```
NIntegrate[(2 3.14156 C1)/(x^5 (Exp[C2/(x T)] - 1)), {x, 10^-3, 0.170}]
```

```
7.79836 10^8
```

```
totQ=3.71618 10^9  
fractQ=7.79836 10^8
```

```
Qabsfr=fractQ/totQ
```

```
0.209849
```

```
NIntegrate[(2 3.14156 C1)/(x^5 (Exp[C2/(x T)] - 1)), {x, 10^-3, 0.182}]
```

```
9.41259 10^8
```

```
totQ=3.71618 10^9  
fractQ=9.41259 10^8
```

```
Qabsfr=fractQ/totQ
```

```
0.253287
```

```
NIntegrate[(2 3.14156 C1)/(x^5 (Exp[C2/(x T)] - 1)), {x, 10^-3, 0.350}]
```

```
2.60513 10^9
```

```
totQ=3.71618 10^9  
fractQ=2.60513 10^9
```

```
Qabsfr=fractQ/totQ
```

```
0.701024
```

```
-----  
Temperature=18,000 K  
-----
```

```
T=18.0 10^3
```

```
NIntegrate[(2 3.14156 C1)/(x^5 (Exp[C2/(x T)] - 1)), {x, 10^-3, 10^3}]
```

```
5.95261 10^9
```

```
NIntegrate[(2 3.14156 C1)/(x^5 (Exp[C2/(x T)] - 1)), {x, 10^-3, 0.170}]
```

```
1.70711 10^9
```

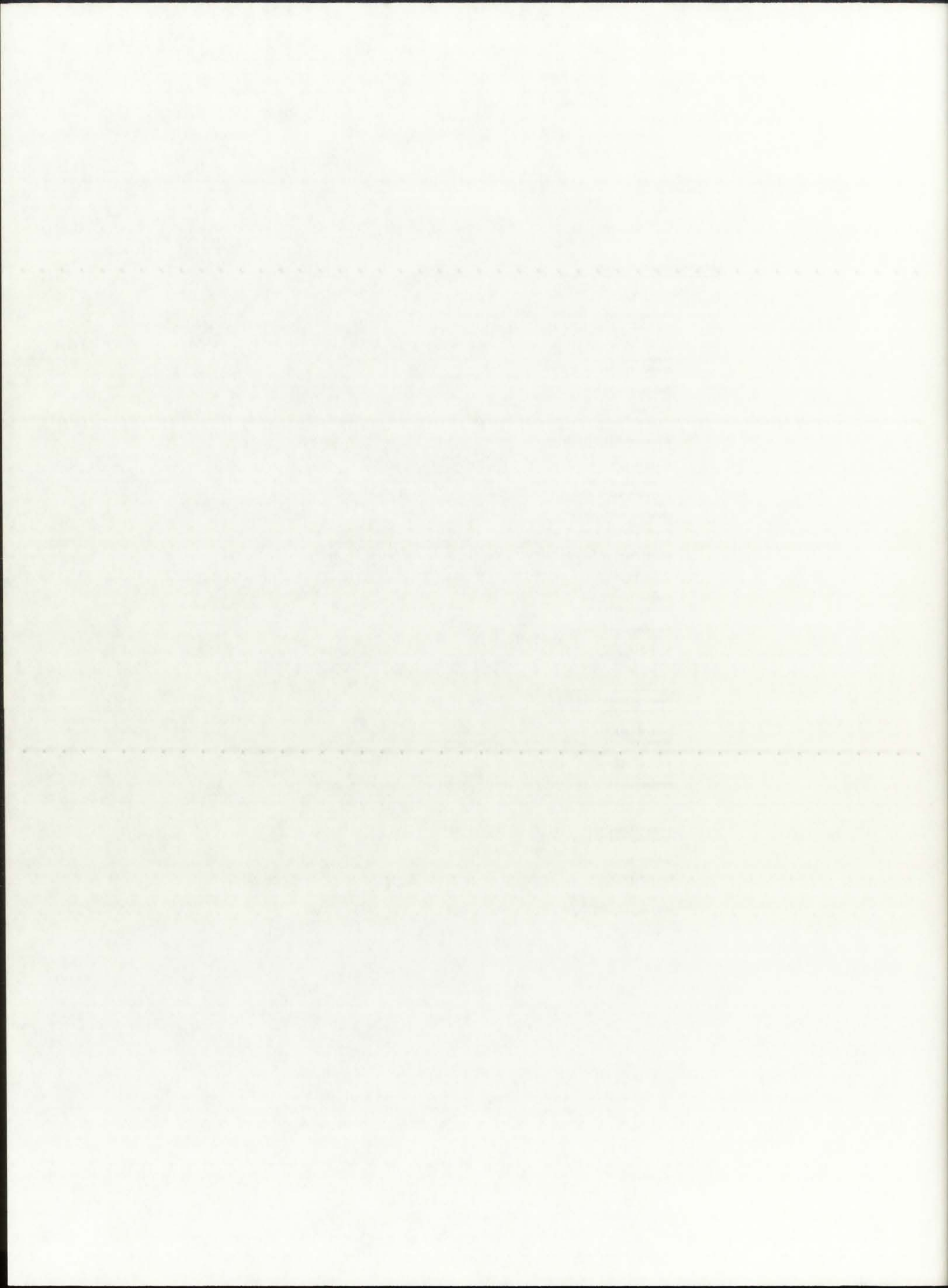
```
totQ=5.95261 10^9  
fractQ=1.70711 10^9
```

```
Qabsfr=fractQ/totQ
```

```
0.286783
```

```
NIntegrate[(2 3.14156 C1)/(x^5 (Exp[C2/(x T)] - 1)), {x, 10^-3, 0.182}]
```

```
1.99329 10^9
```



```
totQ=5.95261 10^9
fractQ=1.99329 10^9

Qabsfr=fractQ/totQ

0.33486

NIntegrate[(2 3.14156 C1)/(x^5 (Exp[C2/(x T)] - 1)), {x, 10^-3, 0.350}]

4.53473 10^9

totQ=5.95261 10^9
fractQ=4.53473 10^9

Qabsfr=fractQ/totQ

0.761805

-----
Temperature=20,000 K
-----

T=20.0 10^3
NIntegrate[(2 3.14156 C1)/(x^5 (Exp[C2/(x T)] - 1)), {x, 10^-3, 10^3}]

9.07271 10^9

NIntegrate[(2 3.14156 C1)/(x^5 (Exp[C2/(x T)] - 1)), {x, 10^-3, 0.170}]

3.2819 10^9

totQ=9.07271 10^9
fractQ=3.2819 10^9

Qabsfr=fractQ/totQ

0.361733

NIntegrate[(2 3.14156 C1)/(x^5 (Exp[C2/(x T)] - 1)), {x, 10^-3, 0.182}]

3.73553 10^9

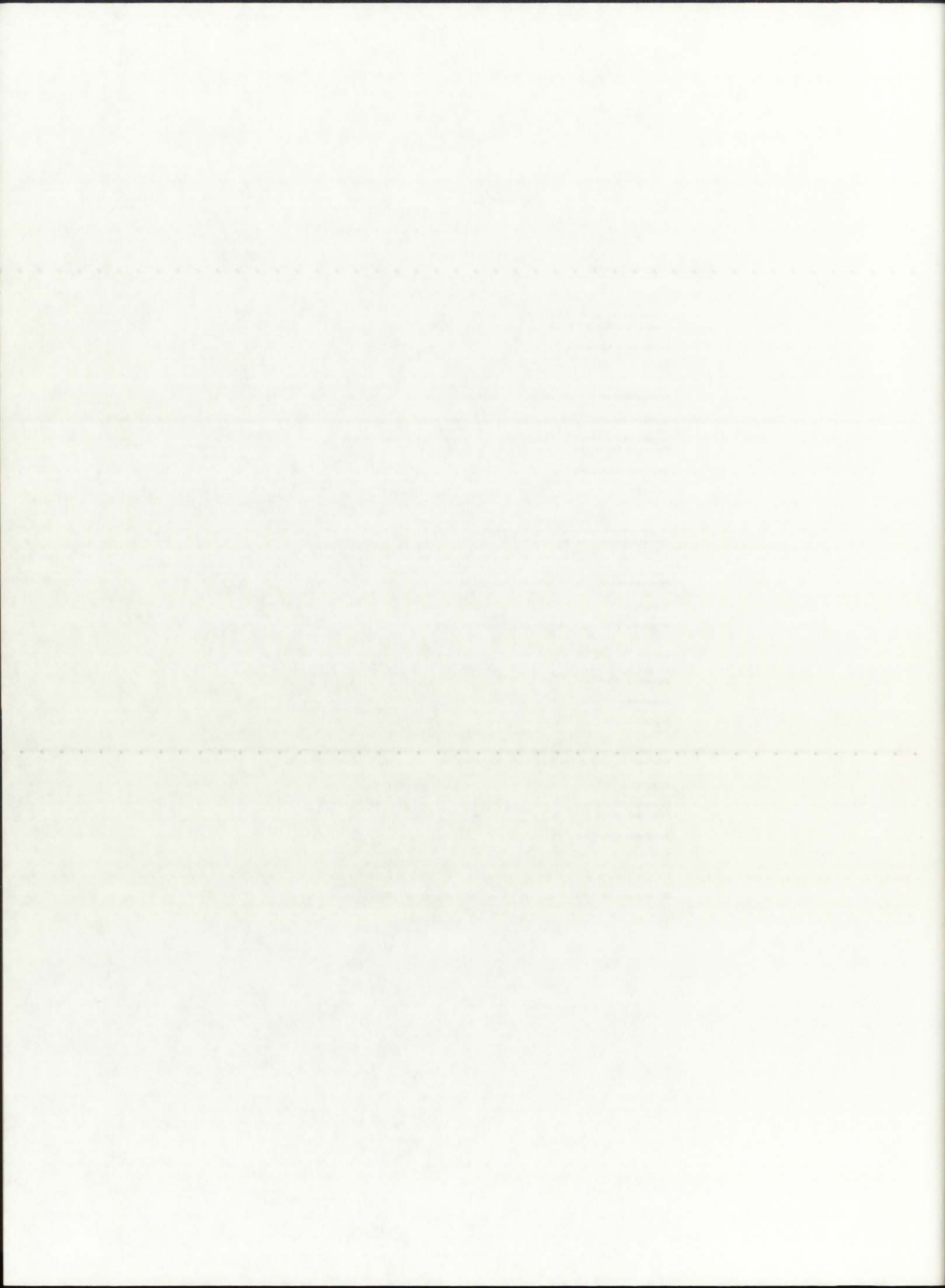
totQ=9.07271 10^9
fractQ=3.73553 10^9

Qabsfr=fractQ/totQ

0.411733

NIntegrate[(2 3.14156 C1)/(x^5 (Exp[C2/(x T)] - 1)), {x, 10^-3, 0.350}]

7.33145 10^9
```



```
totQ=9.07271 10^9  
fractQ=7.33145 10^9
```

```
Qabsfr=fractQ/totQ
```

```
0.808077
```

```
-----  
Temperature=22,000 K  
-----
```

```
T=22.0 10^3
```

```
NIntegrate[(2 3.14156 C1)/(x^5 (Exp[C2/(x T)] - 1)), {x, 10^-3, 10^3}]
```

```
1.328336 1010
```

```
NIntegrate[(2 3.14156 C1)/(x^5 (Exp[C2/(x T)] - 1)), {x, 10^-3, 0.170}]
```

```
5.73413 109
```

```
totQ=1.328336 10^10
```

```
fractQ=5.73413 10^9
```

```
Qabsfr=fractQ/totQ
```

```
0.431678
```

```
NIntegrate[(2 3.14156 C1)/(x^5 (Exp[C2/(x T)] - 1)), {x, 10^-3, 0.182}]
```

```
6.39719 109
```

```
totQ=1.328336 10^10
```

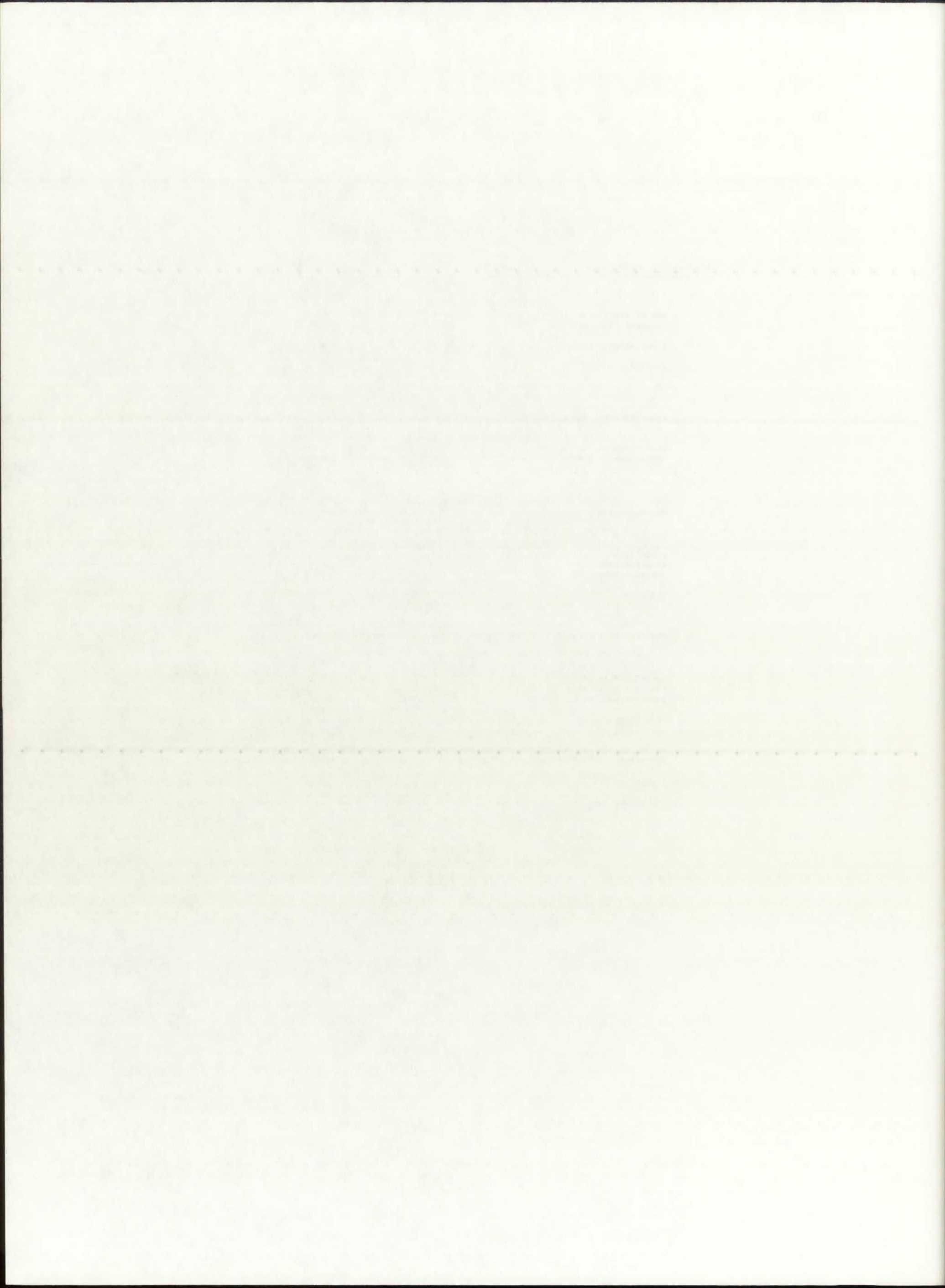
```
fractQ=6.39719 10^9
```

```
Qabsfr=fractQ/totQ
```

```
0.481594
```

```
NIntegrate[(2 3.14156 C1)/(x^5 (Exp[C2/(x T)] - 1)), {x, 10^-3, 0.350}]
```

```
1.12058 1010
```



```
totQ=1.328336 10^10
fractQ=1.12058 10^10
Qabsfr=fractQ/totQ
0.843597
```

```
=====
***** END OF WAVELENGTH ABSORPTION STUDIES *****
=====
```

Date Concluded: December 18, 1993

Data for Qabs/Qtotal (Qabsfr) for the 3 glass materials analyzed here,
as well as calculated approximate propellant temperatures, is located
in the Cricket Graph file "Qabs/Qtot & Tprop. Data".

```
=====
=====
=====
=====
```

Faint, illegible text at the top of the page, possibly a header or title.

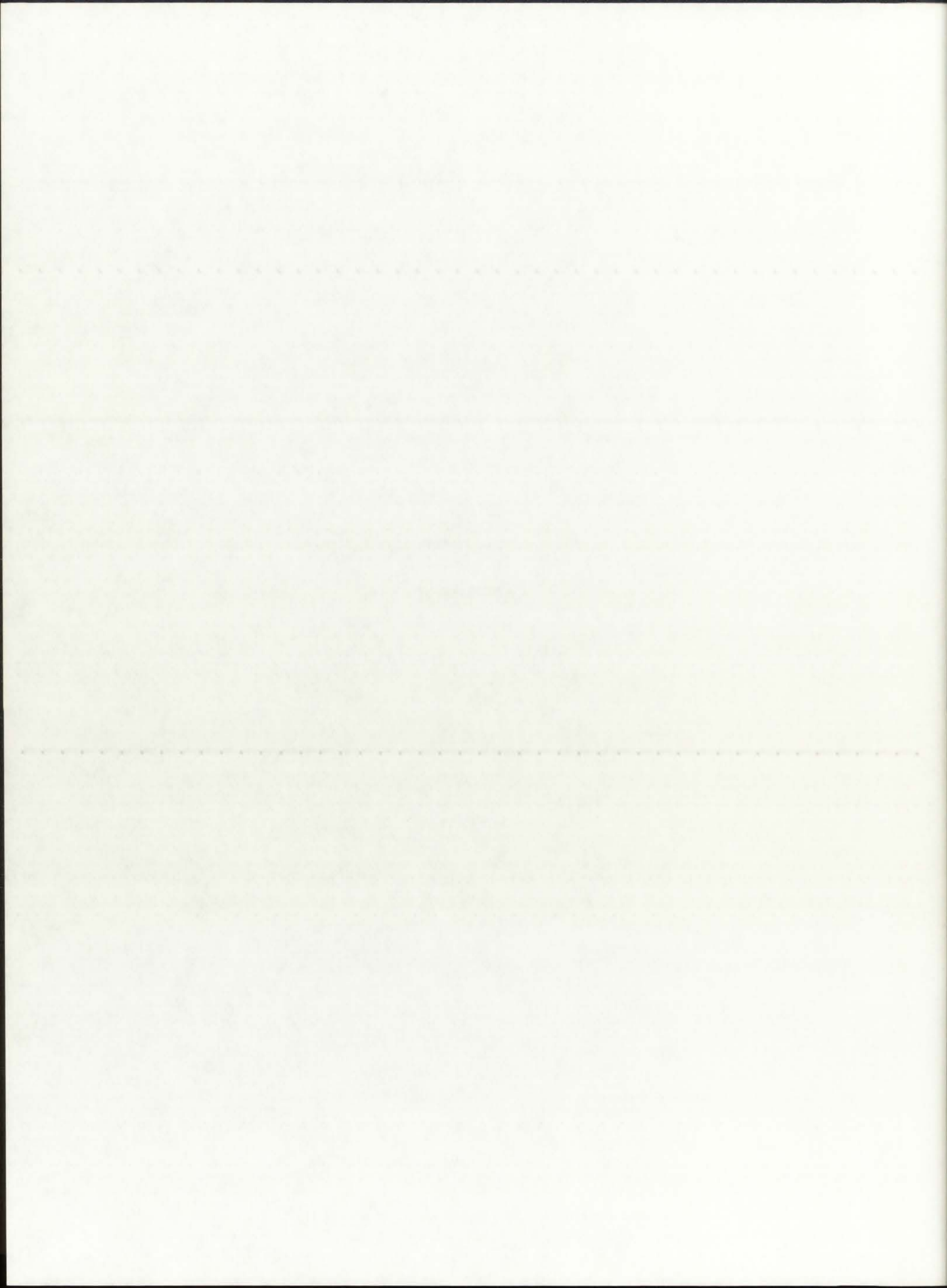
1911
No. 1000
1000

Main body of faint, illegible text, possibly a list or report.

Faint, illegible text at the bottom of the page, possibly a footer or page number.

APPENDIX I

SIWALL.f Code Listing



```

* PROGRAM siwall.f
*
* This program calculates the approximate required mass flow rate of the
* silicon wall coolant (i.e, the secondary hydrogen circuit) that, while
* absorbing the heat flux emitted from the fuel, will maintain the wall
* temperature below the melting point of SiO2: 1873 K.
*
* The resultant mass flow rates are in [kg/s-m2-fuel], and can be multi-
* plied by the radiating surface area of the fuel [m2-fuel] to obtain
* the total required mass flow rate of coolant within the silicon walls.
*
* Created: December 19, 1993

      program SIWALL

      real Tfuel(15),AFSupr(15),AFFSil(15),AFIndG(15),sigma,Tmelt,CpH2
      double precision Qemit(15),QabsSupr(15),QabsFSil(15),QabsIndG(15),
>          TwSupr(15),TwFSil(15),TwIndG(15),mSupr(15),mFSil
>          (15),mIndG(15)
      integer i

      open(unit=11,file='siwall.dat',status='new')

* Temperature data for determination of emissive power:
* -----
      data Tfuel/10.0e3,12.0e3,14.0e3,16.0e3,18.0e3,20.0e3,22.0e3,
>          25.0e3,50.0e3,80.0e3,120.0e3,170.0e3,200.0e3,250.0e3,
>          300.0e3/

      data AFSupr/0.02853,0.07307,0.13614,0.20985,0.28678,0.36173,
>          0.43168,0.52442,0.87457,0.95998,0.98632,0.99477,
>          0.99669,0.99826,0.99896/

      data AFFSil/0.04174,0.09794,0.17174,0.25329,0.33486,0.41173,
>          0.48159,0.57186,0.89278,0.96643,0.98864,0.99569,
>          0.99727,0.99857,0.99914/

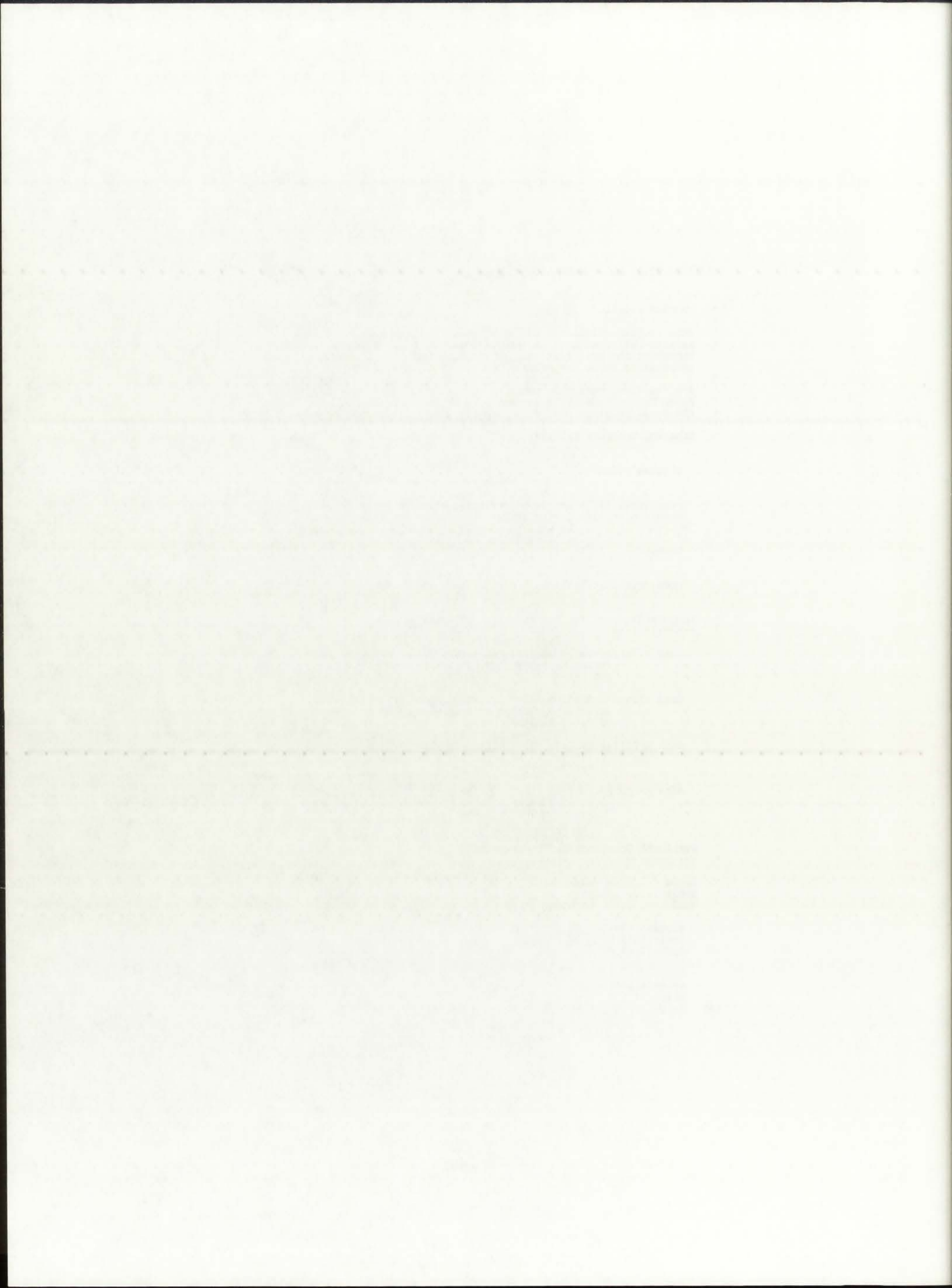
      data AFIndG/0.38291,0.51600,0.62089,0.70102,0.76180,0.80808,
>          0.84360,0.88261,0.97931,0.99429,0.99819,0.99934,
>          0.99959,0.99979,0.99986/

* Pertinent Constants and Their Units:
* -----
* sigma      ..... [W/m2-K4]
* Tmelt      ..... [K]
* CpH2       ..... [J/kg-K]

      sigma=5.67e-8
      Tmelt=1873.0
      CpH2=17360.0

      write(6,100)
      write(11,100)
100  format(/,4x,'Tfuel',5x,'TwSupr',5x,'mSupr',5x,'TwFSil',5x,'mFSil',

```



```
>      5x, 'TwIndG', 5x, 'mIndG', //)

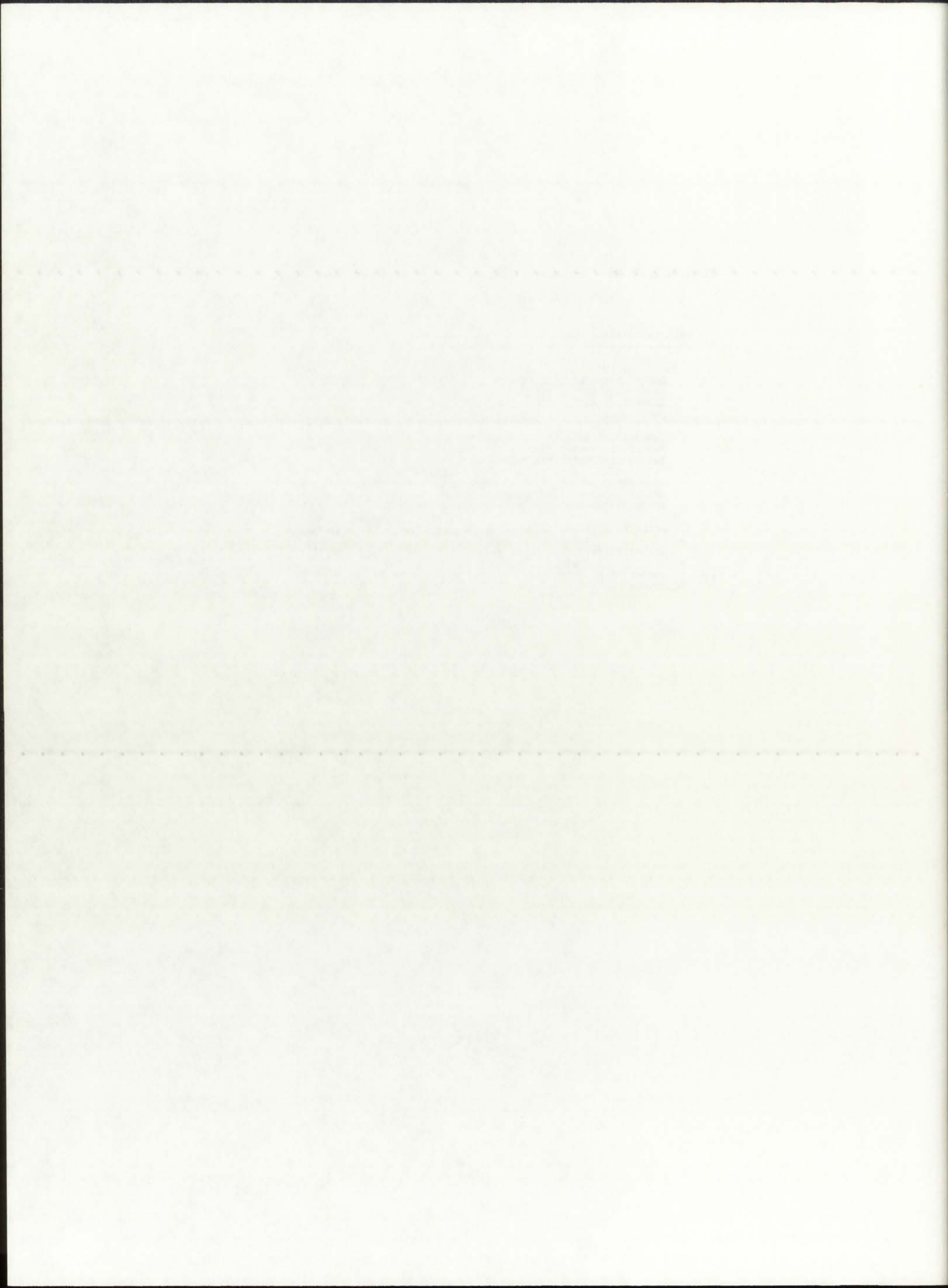
* Main Calculation Loop for Mass Flow Rates:
* -----
do 10 i=1,15
  Qemit(i)=sigma*(Tfuel(i))**4.0
  QabsSupr(i)=AFSupr(i)*Qemit(i)
  QabsFSil(i)=AFFSil(i)*Qemit(i)
  QabsIndG(i)=AFIndG(i)*Qemit(i)

  TwSupr(i)=Tfuel(i)*(AFSupr(i))**0.25
  TwFSil(i)=Tfuel(i)*(AFFSil(i))**0.25
  TwIndG(i)=Tfuel(i)*(AFIndG(i))**0.25

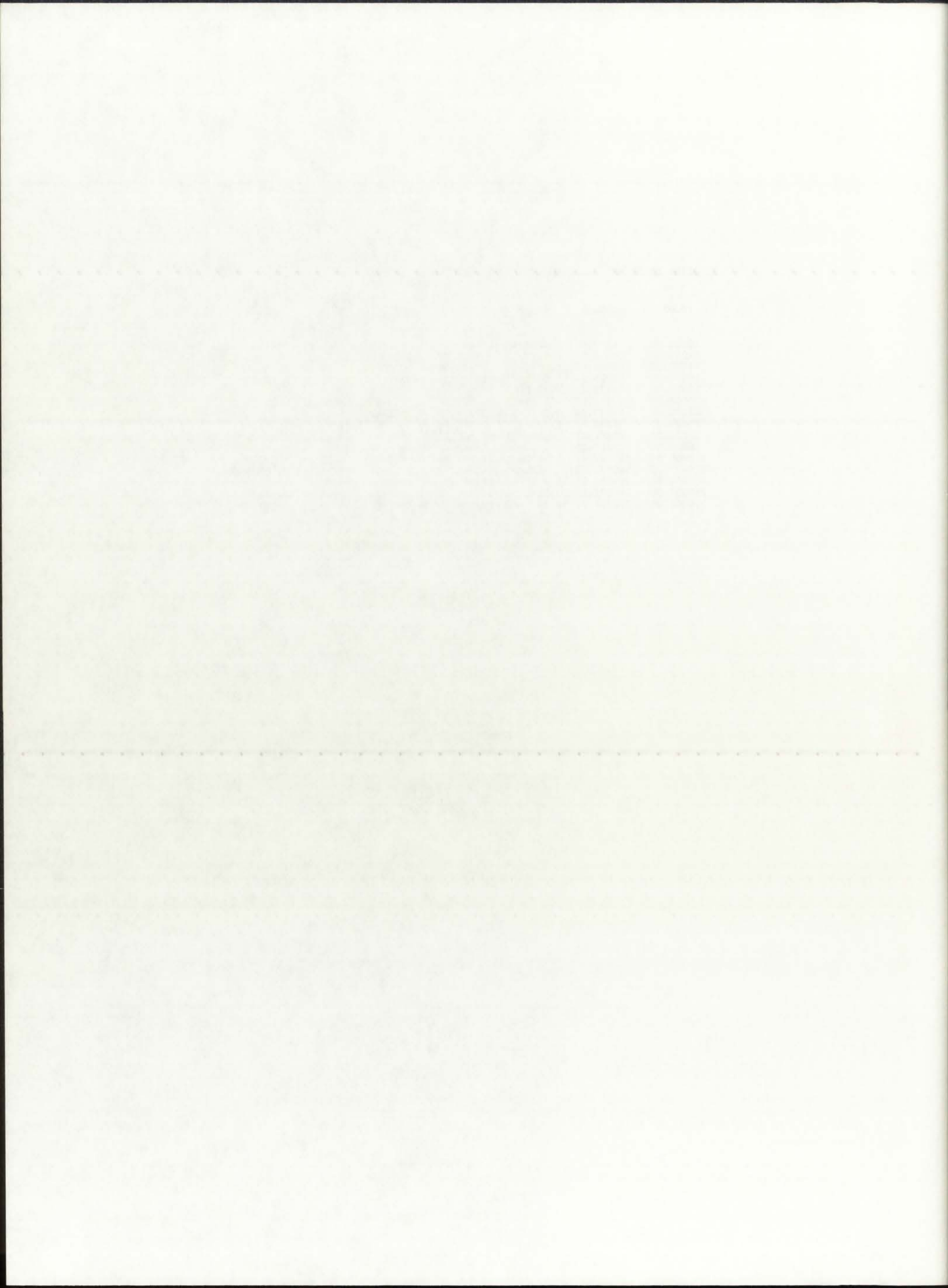
  mSupr(i)=QabsSupr(i)/(CpH2*(TwSupr(i)-Tmelt))
  mFSil(i)=QabsFSil(i)/(CpH2*(TwFSil(i)-Tmelt))
  mIndG(i)=QabsIndG(i)/(CpH2*(TwIndG(i)-Tmelt))

  write(6,101)Tfuel(i),TwSupr(i),mSupr(i),TwFSil(i),mFSil(i),
>      TwIndG(i),mIndG(i)
  write(11,101)Tfuel(i),TwSupr(i),mSupr(i),TwFSil(i),mFSil(i),
>      TwIndG(i),mIndG(i)
101  format(2x,F9.2,3x,3(F9.2,2x,E9.3,2x))
10  continue

stop
end
```

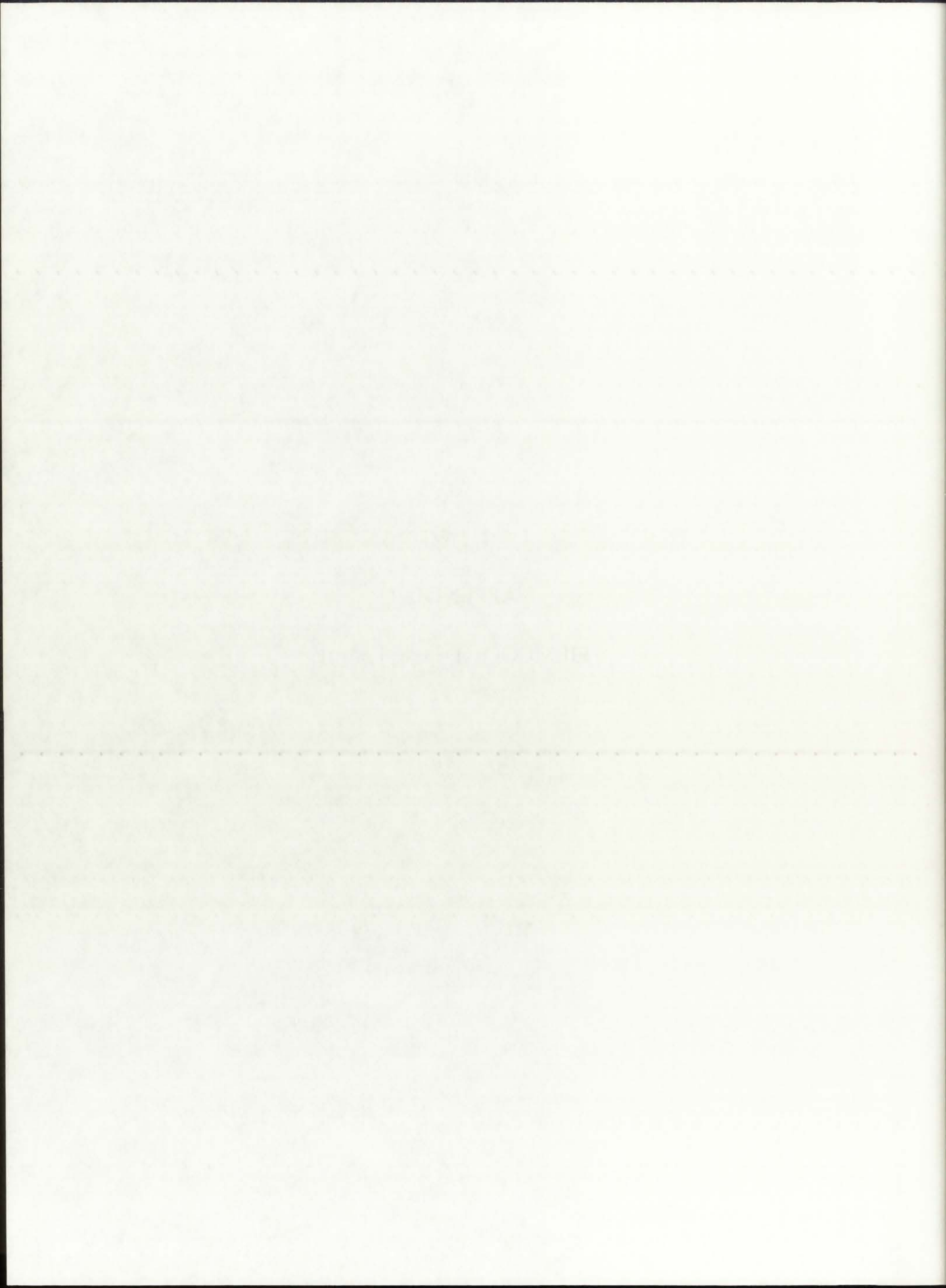


Tfuel	TwSupr	mSupr	TwFSil	mFSil	TwIndG	mIndG
10000.00	4109.84	0.417E+00	4520.00	0.515E+00	7866.37	0.209E+01
12000.00	6239.01	0.113E+01	6713.07	0.137E+01	10170.53	0.421E+01
14000.00	8504.02	0.258E+01	9012.51	0.302E+01	12427.44	0.738E+01
16000.00	10829.22	0.502E+01	11350.75	0.572E+01	14640.39	0.118E+02
18000.00	13172.24	0.870E+01	13692.68	0.971E+01	16816.39	0.175E+02
20000.00	15510.51	0.139E+02	16020.76	0.152E+02	18962.41	0.247E+02
22000.00	17832.54	0.207E+02	18327.03	0.224E+02	21084.19	0.336E+02
25000.00	21274.52	0.345E+02	21740.15	0.367E+02	24231.61	0.504E+02
50000.00	48352.47	0.384E+03	48602.22	0.390E+03	49739.34	0.418E+03
80000.00	79187.30	0.166E+04	79319.98	0.167E+04	79885.55	0.171E+04
120000.00	119587.48	0.567E+04	119657.74	0.568E+04	119945.66	0.573E+04
170000.00	169777.29	0.162E+05	169816.53	0.162E+05	169971.94	0.162E+05
200000.00	199834.29	0.263E+05	199863.36	0.263E+05	199979.50	0.264E+05
250000.00	249891.18	0.514E+05	249910.58	0.514E+05	249986.87	0.514E+05
300000.00	299921.97	0.887E+05	299935.48	0.887E+05	299989.50	0.887E+05



APPENDIX J

FILMCOOL.f Code Listing



```

* PROGRAM Filmcool.f
*
* This program determines the heat transfer properties in the film
* cooling channel adjacent to the solid wall of the NLB engine. The
* film is susceptible to both convection and radiation; parametric
* analysis of the interdependence of opacity and the heat transfer
* coefficient in the film is carried out.
* =====
* For convection ONLY, hf=4.20 [W/m2-K]
* For radiation ONLY, aR=528,728. [1/m]
* =====
*
* Created: November 7, 1994

      program FILMCOOL

      real aR(16),Rf,Rw,pi,L,sigma,Pr,mu,rho,kcond,Tfp,Tfw,Dhf,qtot,
>      Ravg,Asavg,Acs,Tfavg
      double precision krad(16),hf(16),mf(16),vf(16),Nu,Re
      integer i

      open(unit=11,file='filmcool.dat',status='new')

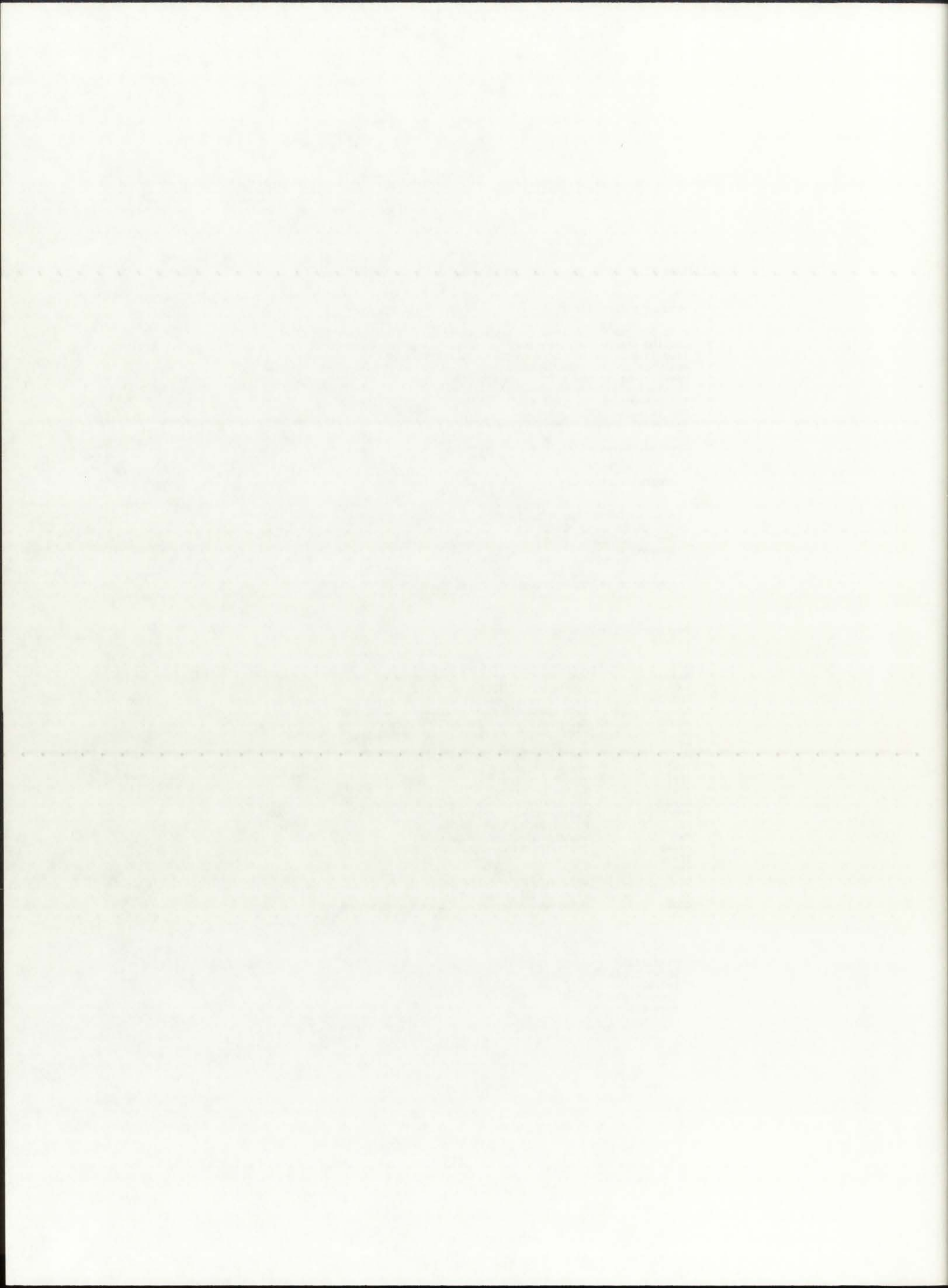
* Pertinent film cooling data (based on 1-D model):
* -----
*
* Acs      ....   cross-sectional area of film channel [m2]
* Asavg    ....   avg. surface area to heat transfer [m2]
* aR       ....   hydrogen RMO @Tfavg and P=250 atm [1/m]
* Dhf      ....   film channel mean hydraulic diameter [m]
* hf       ....   film heat transfer coefficient [W/m2-K]
* kcond    ....   hydrogen thermal conductivity [W/m-K]
* L        ....   total length of propellant channel [m]
* mf       ....   film mass flow rate [kg/s]
* mu       ....   hydrogen viscosity [kg/m-s]
* [Nu]     ....   Nusselt number
* [Pr]     ....   Prandtl number
* [Re]     ....   Reynolds number
* Ravg     ....   average radius of propellant channel [m]
* rho      ....   hydrogen mass density [kg/m3]
* Rf       ....   Film channel inner radius [m]
* Rw       ....   Solid wall inner radius [m]
* sigma    ....   Stefan-Boltzmann constant [W/m2-K4]
* Tfavg    ....   average film channel temperature [K]
* Tfp      ....   propellant-side film temperature [K]
* Tfw      ....   wall-side film temperature [K]
* vf       ....   film velocity [m/s]
* qtot     ....   total thermal power of rocket engine [W]

```

```

pi=3.14159
Dhf=0.00848
L=1.827
sigma=5.67e-8
Pr=0.616

```



```

mu=4.281e-5
rho=2.61
kcond=1.512
Tfp=4833.
Tfw=1278.
Rw=0.29180
Rf=Rw-Dhf
qtot=50.0e+3

Ravg=(Rf+Rw)/2.
Asavg=2.*Ravg*pi*L

Acs=(Rw**2.-Rf**2.)*pi

Tfavg=(Tfp+Tfw)/2.

* RMO data for determination of convective properties:
* -----
data aR/528727.968749,528727.,500000.,325000.,150000.,75000.,25000.,
> 5000.,1000.,200.,50.,10.,1.0,0.1,0.001,0.00001/

write(6,100)
write(11,100)
100 format(/,4x,'aR [1/m]',4x,'krad [W/m-K]',4x,'hf [W/m2-K]',4x,
> 'mf [kg/s]',4x,'vf [m/s]')
write(6,101)
write(11,101)
101 format(3x,10('-'),2x,14('-'),2x,13('-'),2x,11('-'),2x,10('-'),/)

* Calculation loop for radiative/convective dependence:
* -----
do 10 i=1,16
krad(i)=16.0*sigma*Tfavg**3.0/(3.0*aR(i))
hf(i)=1.0/((Asavg*(Tfp-Tfw)/qtot)-Dhf/krad(i))
Nu=hf(i)*Dhf/kcond
Re=(Nu/(0.023*Pr**0.4))**(5./4.)
mf(i)=(Re*pi*mu*Dhf)/4.
vf(i)=mf(i)/(Acs*rho)
write(6,200)aR(i),krad(i),hf(i),mf(i),vf(i)
write(11,200)aR(i),krad(i),hf(i),mf(i),vf(i)
200 format(3x,E10.4,4x,E10.4,5x,E10.4,4x,E10.4,3x,E10.4)
10 continue

* write(6,*)Acs

stop
end

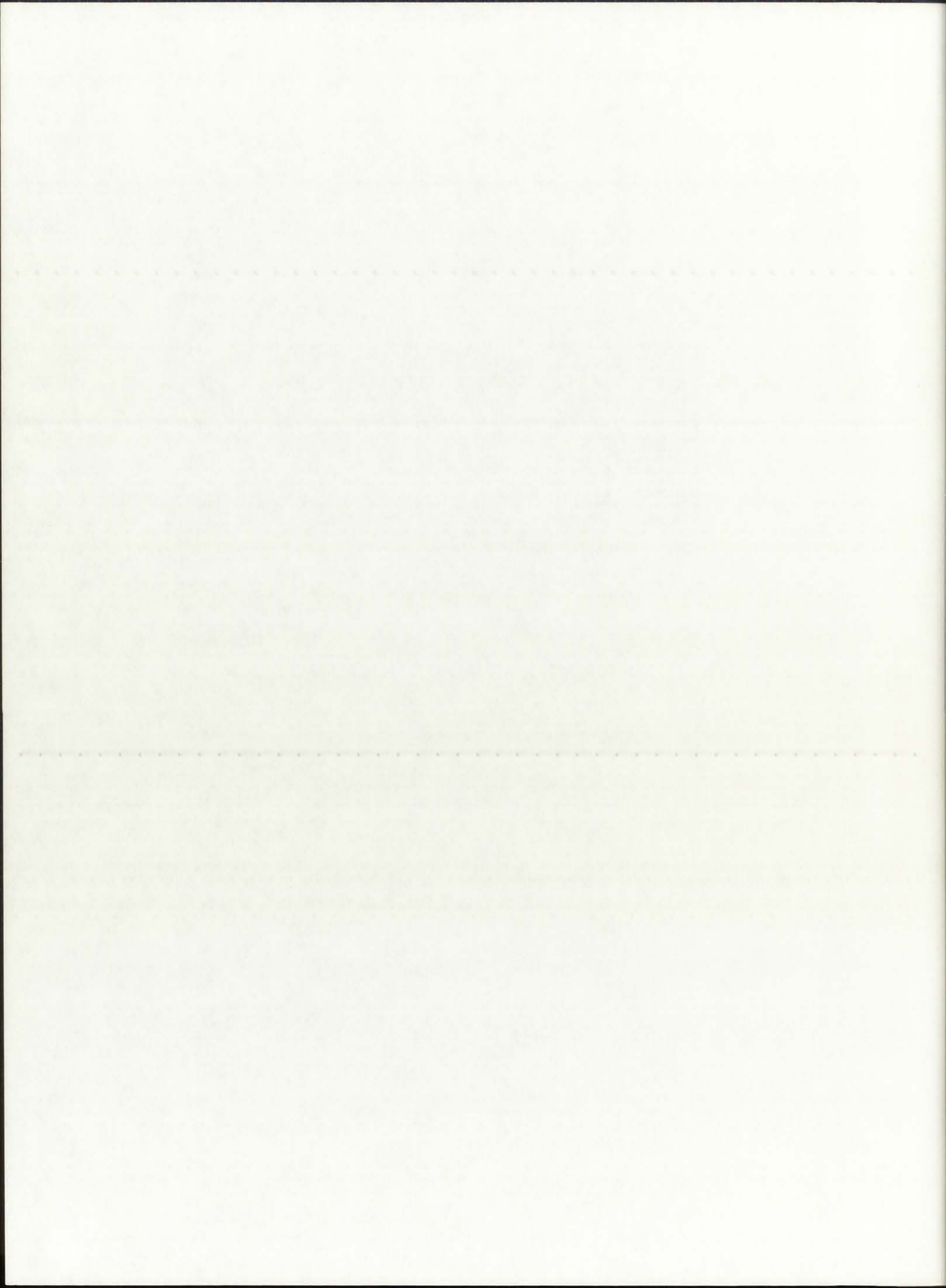
```

1975-1976
1976-1977
1977-1978
1978-1979
1979-1980
1980-1981
1981-1982
1982-1983
1983-1984
1984-1985
1985-1986
1986-1987
1987-1988
1988-1989
1989-1990
1990-1991
1991-1992
1992-1993
1993-1994
1994-1995
1995-1996
1996-1997
1997-1998
1998-1999
1999-2000
2000-2001
2001-2002
2002-2003
2003-2004
2004-2005
2005-2006
2006-2007
2007-2008
2008-2009
2009-2010
2010-2011
2011-2012
2012-2013
2013-2014
2014-2015
2015-2016
2016-2017
2017-2018
2018-2019
2019-2020
2020-2021
2021-2022

1975-1976
1976-1977
1977-1978
1978-1979
1979-1980
1980-1981
1981-1982
1982-1983
1983-1984
1984-1985
1985-1986
1986-1987
1987-1988
1988-1989
1989-1990
1990-1991
1991-1992
1992-1993
1993-1994
1994-1995
1995-1996
1996-1997
1997-1998
1998-1999
1999-2000
2000-2001
2001-2002
2002-2003
2003-2004
2004-2005
2005-2006
2006-2007
2007-2008
2008-2009
2009-2010
2010-2011
2011-2012
2012-2013
2013-2014
2014-2015
2015-2016
2016-2017
2017-2018
2018-2019
2019-2020
2020-2021
2021-2022

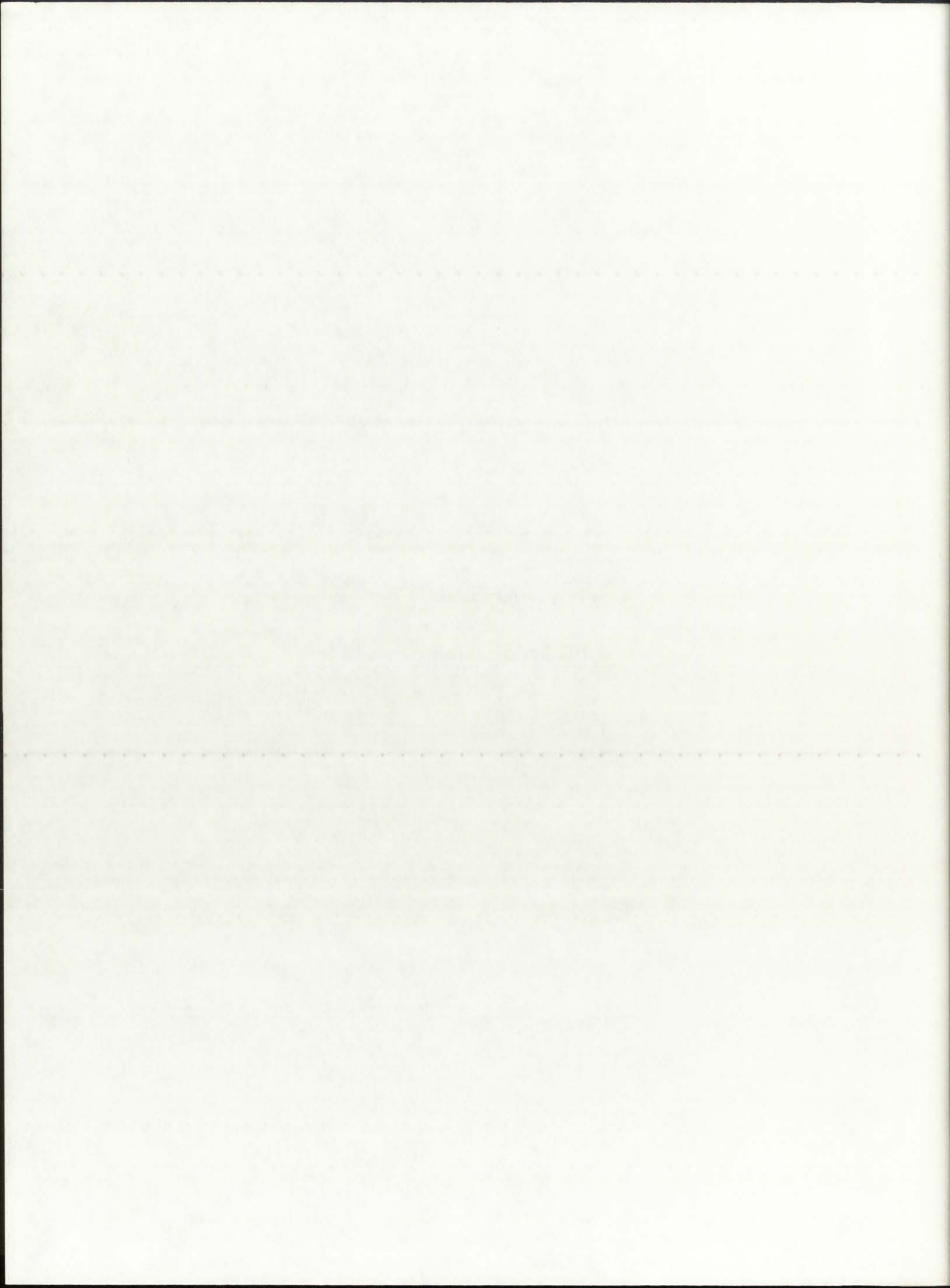
1975-1976
1976-1977
1977-1978
1978-1979
1979-1980
1980-1981
1981-1982
1982-1983
1983-1984
1984-1985
1985-1986
1986-1987
1987-1988
1988-1989
1989-1990
1990-1991
1991-1992
1992-1993
1993-1994
1994-1995
1995-1996
1996-1997
1997-1998
1998-1999
1999-2000
2000-2001
2001-2002
2002-2003
2003-2004
2004-2005
2005-2006
2006-2007
2007-2008
2008-2009
2009-2010
2010-2011
2011-2012
2012-2013
2013-2014
2014-2015
2015-2016
2016-2017
2017-2018
2018-2019
2019-2020
2020-2021
2021-2022

aR [1/m]	krad [W/m-K]	hf [W/m2-K]	mf [kg/s]	vf [m/s]
0.5287E+06	0.1632E-01	0.8198E+08	0.8264E+02	0.4504E+04
0.5287E+06	0.1632E-01	0.2316E+07	0.9574E+00	0.5218E+02
0.5000E+06	0.1725E-01	0.7779E+02	0.2448E-05	0.1334E-03
0.3250E+06	0.2654E-01	0.1097E+02	0.2115E-06	0.1153E-04
0.1500E+06	0.5751E-01	0.5901E+01	0.9743E-07	0.5310E-05
0.7500E+05	0.1150E+00	0.4925E+01	0.7774E-07	0.4237E-05
0.2500E+05	0.3451E+00	0.4437E+01	0.6821E-07	0.3718E-05
0.5000E+04	0.1725E+01	0.4267E+01	0.6497E-07	0.3541E-05
0.1000E+04	0.8626E+01	0.4235E+01	0.6436E-07	0.3507E-05
0.2000E+03	0.4313E+02	0.4228E+01	0.6424E-07	0.3501E-05
0.5000E+02	0.1725E+03	0.4227E+01	0.6421E-07	0.3500E-05
0.1000E+02	0.8626E+03	0.4227E+01	0.6421E-07	0.3499E-05
0.1000E+01	0.8626E+04	0.4227E+01	0.6421E-07	0.3499E-05
0.1000E+00	0.8626E+05	0.4227E+01	0.6421E-07	0.3499E-05
0.1000E-02	0.8626E+07	0.4227E+01	0.6421E-07	0.3499E-05
0.1000E-04	0.8626E+09	0.4227E+01	0.6421E-07	0.3499E-05

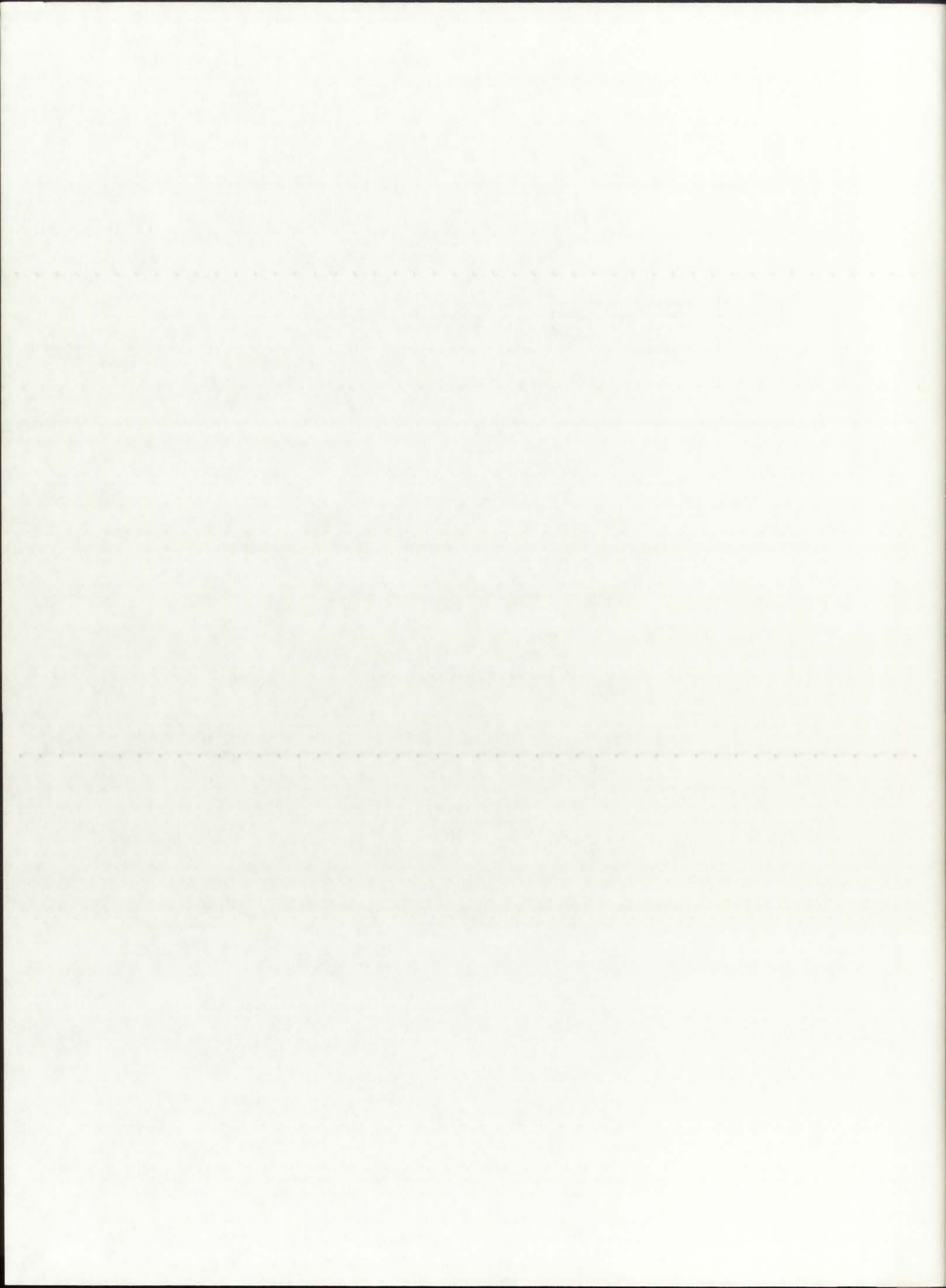


APPENDIX K

BBC code sample input file



```
-1 /input file type=-1 coded (name=text)
1 /output file type=1 binary (name=matxs)
0 /modify flag=0 no modifications (default)
0 /list option=0 not listed
1 /indexing option=1 indexed (name=index)
```



APPENDIX L

TRANSX code sample input file
(room temperature material cross-sections)

APPENDIX I

TRANSX code sample input file
(from temperature control cross-section)

```

nit-cell NLB Rocket Engine room temperature file
itx7ey* *isotxs*/
6 0 1 1 1 0 2 0 0/
2 93 20 8 8 9 9 9/
nru* *hydr* *deut* *oxgn* *bery* *ar* *si* *fe*
nru*          300.          1./
ydr*          300.          1./
leut*         300.          1./
xgn*          300.          1./
ery*          300.          1./
r*            300.          1./
i*            300.          1./
e*            300.          1./
1 *u235*      0.96          1.e+10 42 *free*/
1 *u238*      0.04          1.e+10 42 *free*/
2 *h1*        1.0           1.e+10 42 *free*/
3 *h2*        1.0           1.e+10 42 *d2o*/
4 *o16*       1.0           1.e+10 42 *free*/
5 *be9*       1.0           1.e+10 42 *be* *be$/
6 *arnat*     1.0           1.e+10 42 *free*/
7 *sinat*     1.0           1.e+10 42 *free*/
8 *fenat*     1.0           1.e+10 42 *free*/
trpl* *sngam* *sfis* *chiso* *snalf* *snp* *sn2n* *snd* *snt*/
*trd*/
*ng*/
*nftot*/
*chi*/
*na*/
*np*/
*n2n*/
*nd*/
*nt*/
top*

```

